First Benchmark Workshop on

NUMERICAL ANALYSIS OF DAMS

Bergamo (Italy)
May 28-29, 1991

First Benchmark Workshop

on

NUMERICAL ANALYSIS OF DAMS

Bergamo (Italy)
May 28-29, 1991

organized by

the «ad hoc» Committee on
Computational Aspects of
Dam Analysis and Design

of

CIGB
ICOLD

International Commission on Large Dams
Commission Internationale des Grands Barrages

in cooperation with

ISMES

and

Dam Engineering

FOREWORD

The new ICOLD Committee for Computational Aspects of Dam Analysis and Design, appointed in the 1987 Executive Meeting of Beijing, addressed its attention to the more pressing needs of the dam engineer's profession in this field.

It was apparent that a shift of focus has taken place in the last years. Performing a numerical analysis is, seemingly, easier and easier, insofar as automatic computational tools (powerful hardware at reasonable costs, abundance of efficient software) have taken away the drudgery and length of such tasks.

However, shedding this burden from one's mind, one is more and more aware that computations are only a part of the long road of dam design/analysis. Refined mathematical models, calling for precise values of physical parameters, only highlight our quite wide fringes of uncertainty; deeper and deeper understanding of real behaviour, with all its attending non-linearities and discontinuities, reveal the incompleteness of even the most up-to-date formulations. Besides, the reliability of existing software is too often simply taken for granted, rather than verified.

Last but not least, fitting together the delicate, multi-disciplinary process of "design" with the rigorously specialized job of computational analysis is by no means a trivial matter. Likewise, linking the results of computations to operational decisions is a big jump, and one, moreover, which is not amenable to formalization.

In this context, my personal opinion is that two main points of debate will emerge in the coming years: on one hand, the reliability of dam analysis software (and this topic is addressed by Benchmark Workshops such as the present one); on the other hand, the correct interpretation of computer analysis results in the broader framework of the design process and of the safety appraisal.

In fact, a difficult change of approach is needed (and is partly in the making). From a world of apparently certain rules and formalized knowledge, we are moving with ever increasing awareness to what I would like to call "the rational management of uncertainties". For this, however, not all the proper tools are yet in existence.

If our ad-hoc Committee will succeed in at least initiating a meaningful activity in one, or both, of the above-mentioned problem areas, I think it will have performed a welcome and useful role for dam professionals in general.

The present Benchmark-Workshop was conceived as the first step in a continuing activity of systematic, critical comparison of existing softwares in the several provinces of dam analysis problems. If, as we hope, it will be successfully carried out, it should be followed by a large number of similar B-W.S, to be held on a regular basis under the auspices of ICOLD, as an international forum in which to produce a completely documented set of test-cases and expected results together with confidence bands.

The publication of these results, possibly as Bulletins, or periodic Reports, of ICOLD, would then constitute a permanent reference source - periodically updated when and if necessary - for everyone who is involved in the critical use of computational tools.

Prof. M.A. Fanelli

March 27, 1991

THEME A

"The linear-elastic computation
of a double-curvature concrete arch dam
with its foundation under self-weight,
hydrostatic load, thermal loads"

WRITTEN COMMENT
WILL FOLLOW

	Table of participants			
cod.	Authors	Corporation	Address	Country
p01	Yeh, Cui, Bondi	Harza Eng. Co.	Chicago	USA
p02	Clough, Ghanaat	Univ. of California	Berkeley	USA
p03	Bolognini, Bettinali, Ciccotelli, Meghella	Cise s.p.a.	Milano	I
p04	Promper	Tauernkraftwerke	Salzburg	A
p05	Paul, Tarbox, Shih	Bechtel Co.	S. Francisco	USA
p06	Dungar, Mallick	Colenco	Baden	CH
p07	Onate, Miquel, Buil, Botello	Univ. Polit. de Catalunya	Barcelona	E
p08	Wilson	Univ. of California	Berkeley	USA
p09	Mee, Curtis, Wozniak	Acres Int. ltd	Niagara Falls	CDN
p10	Salmonte Palmeiro	Iberduero s.a.	Madrid	E
p11	Greeves, Taylor, Severn	Univ. of Bristol	Bristol	GB
p12	Zghal, Tardieu, Carrere	Coyne et Bellier	Paris	F
p13	Chopra	Univ. of California	Berkeley	USA
p14	Ruggeri, Palumbo, Mazza`	Ismes s.p.a., Enel/Cris	Bergamo, Milano	I
p15	Koji	Energoproject Co.	Belgrade	YU
p16	Lofti, Naji-Mahelen, Mokhtar, Oroomchi	Mohab Ghodds cons.eng.	Tehran	IR
p17	Bourdarot, Milovanovitch	E.D.F/CNEH	Le Bourget du Lac	F

Participant	STATIC ANALYSIS			THERMAL PERIODIC ANALYSIS	DYNAMIC ANALYSIS	
	Dead weight	Hydr. load	Therm. load		Empty	Full
1	*	*	*	*	*	*
2	*	*	*	—	*	*
3	—	—	—	—	*	*
4	*	*	—	—	—	—
5	*	*	*	*	*	*
6	*	*	*	—	*	*
7	*	*	—	—	*	*
8	—	—	—	—	*	*
9	*	*	*	*	*	*
10	*	*	*	—	*	*
11	—	—	—	—	*	*
12	*	*	*	*	*	*
13	*	*	—	—	*	*
14	*	*	*	*	*	*
15	*	*	—	—	—	—
16	*	*	*	*	*	—
17	*	*	*	*	*	*
TOTAL	17	14	14	10	7	15	14

METHODS AND COMPUTER CODES

Participant	Method	Computer code
1	F.E.M.	SAP IV
2	F.E.M.	EADAP
3	F.E.M.	INDIA-3
4	F.E.M. - T.L.M.	CODCOD
5	F.E.M.	SAP90
6	F.E.M.	EFESYS
7	F.E.M.	___
8	F.E.M.	SAP2000
9	F.E.M.	EADAP
10	F.E.M.	SAP-IBERDUERO
11	F.E.M.	SAPIV-SOLVIA
→ 12	F.E.M.	COQEF3
13	F.E.M.	EACD-3D
14	F.E.M.	FIESTA
14	F.E.M.	___
16	F.E.M.	MADAP
17	F.E.M.	___

NOTES ON THE INPUT DATA ADOPTED

STATIC ANALYSIS

MESH:

10 participants used the proposed mesh without any modification; within these 4 participants used the 8-node linear element and 1 participant used p-version of F.E.M. with both p-level equal to 2 and 6.

4 participants used their own modified mesh.

CONSTRAINTS:

1 participant used springs to model the foundation, which eliminates the f.e. idealization.

NO

ELASTIC PARAMETERS: 1 participant used a Young modulus of $E = 3.00 \times 10^{10}$ N/m^2 in the static analysis.

LOADS:

All the participants defined load conditions exactly as foreseen in the specification.

NOTES ON THE INPUT DATA ADOPTED

THERMAL ANALYSIS

MESH: 10 participants used the proposed mesh without any modification; within these 2 participants used the 8-node linear element and 1 participant used p-version of F.E.M. with p-level equal 6.

ELASTIC PARAMETERS: 1 participant used a Young modulus of $E = 3.00 \times 10^{10}$ N/m^2.

LOADS: All the participants defined load conditions exactly as foreseen in the specification.

NOTES ON THE INPUT DATA ADOPTED

DYNAMIC ANALYSIS

MESH OF THE DAM:

14 participants used the proposed mesh without any modifications

1 participant used a modified mesh

MESH OF THE RESERVOIR:

8 participants used the proposed mesh with incompressible fluid

3 participants used the proposed mesh with compressible fluid

2 participant used added masses

1 participant used a mixed solution F.E. discretization plus a semi analytic formulation

ELASTIC PARAMETER:

1 participant used a Young modulus of $E = 6.00 \times 10^{10}$ for the dam

STATIC-THERMAL AND DYNAMIC ANALYSIS

OUTPUT:

9 participants provided the output exactly as requested in the specification

2 participants computed the results at the Gauss integration points (instead than at nodes)

1 participant provided the results at the centre of the elements

1 participant inverted the x-axis with the y-axis in the reference system

1 participant did not provide the diskette.

STATIC ANALYSIS

SUMMARY OF COMPARISON OF THE RESULTS

- DISPLACEMENTS -

DEAD WEIGHT Vertical displacements					
SUMMARY OF THE COMPARISON OF THE RESULTS (s%=difference from best estimate)					
node		0 =< s =< 2	2 < s =< 5	s > 5	TOTAL
1	Participants	7	2	1	10
	Participants(%)	70,00	20,00	10,00	100
4	Participants	5	3	2	10
	Participants(%)	50,00	30,00	20,00	100
19	Participants	5	3	2	10
	Participants(%)	50,00	30,00	20,00	100
31	Participants	5	3	2	10
	Participants(%)	50,00	30,00	20,00	100
40	Participants	6	1	3	10
	Participants(%)	60,00	10,00	30,00	100
3	Participants	7	2	1	10
	Participants(%)	70,00	20,00	10,00	100
6	Participants	5	3	2	10
	Participants(%)	50,00	30,00	20,00	100
21	Participants	5	3	2	10
	Participants(%)	50,00	30,00	20,00	100
33	Participants	4	3	3	10
	Participants(%)	40,00	30,00	30,00	100
42	Participants	3	3	4	10
	Participants(%)	30,00	30,00	40,00	100

Note :

Two participants provided results for input data strongly modified in respect of the ones indicated in the specifications.

HYDROSTATIC LOAD

Horizontal downstream-upstream displacements

SUMMARY OF THE COMPARISON OF THE RESULTS (s%=difference from best estimate)

node		0 =< s =< 2	2 < s =< 5	s > 5	TOTAL
1	Participants	8	2	1	11
	Participants(%)	72,73	18,18	9,09	100
4	Participants	7	2	2	11
	Participants(%)	63,64	18,18	18,18	100
19	Participants	6	3	2	11
	Participants(%)	54,55	27,27	18,18	100
31	Participants	5	3	3	11
	Participants(%)	45,45	27,27	27,27	100
40	Participants	7	1	3	11
	Participants(%)	63,64	9,09	27,27	100
3	Participants	7	3	1	11
	Participants(%)	63,64	27,27	9,09	100
6	Participants	7	3	1	11
	Participants(%)	63,64	27,27	9,09	100
21	Participants	6	3	2	11
	Participants(%)	54,55	27,27	18,18	100
33	Participants	5	3	3	11
	Participants(%)	45,45	27,27	27,27	100
42	Participants	5	3	3	11
	Participants(%)	45,45	27,27	27,27	100

Note :

Two participants provided results for input data strongly modified in respect of the ones indicated in the specifications.

THERMAL CHANGE

Horizontal downstream-upstream displacements

SUMMARY OF THE COMPARISON OF THE RESULTS (s%=difference from best estimate)

node		0 =< s =< 2	2 < s =< 5	s > 5	TOTAL
1	Participants	5	2	2	9
	Participants(%)	55,56	22,22	22,22	100
4	Participants	5	3	1	9
	Participants(%)	55,56	33,33	11,11	100
19	Participants	5	1	3	9
	Participants(%)	55,56	11,11	33,33	100
31	Participants	2	3	4	9
	Participants(%)	22,22	33,33	44,44	100
40	Participants	9	0	0	9
	Participants(%)	100,00	0,00	0,00	100
3	Participants	4	4	1	9
	Participants(%)	44,44	44,44	11,11	100
6	Participants	5	3	1	9
	Participants(%)	55,56	33,33	11,11	100
21	Participants	5	2	2	9
	Participants(%)	55,56	22,22	22,22	100
33	Participants	2	0	7	9
	Participants(%)	22,22	0,00	77,78	100
42	Participants	9	0	0	9
	Participants(%)	100,00	0,00	0,00	100

Note :

Two participants provided results for input data strongly modified in respect of the ones indicated in the specifications.

SUMMARY OF THE COMPARISON OF THE RESULTS (s%=differ.from best estimate)			
LOADS	$0 \leq s \leq 2$	$2 < s \leq 5$	$s > 5$
DEAD WEIGHT	52,00	26,00	22,00
HYDROSTATIC LOAD	57,27	23,64	19,09
THERMAL CHANGE	56,67	20,00	23,33

STATIC-THERMAL ANALYSIS

GRAPHIC COMPARISON OF THE RESULTS

- DISPLACEMENTS -

Dead weight

Displacement DZ

Cantilever-nodes : 1, 4, 19, 31, 40

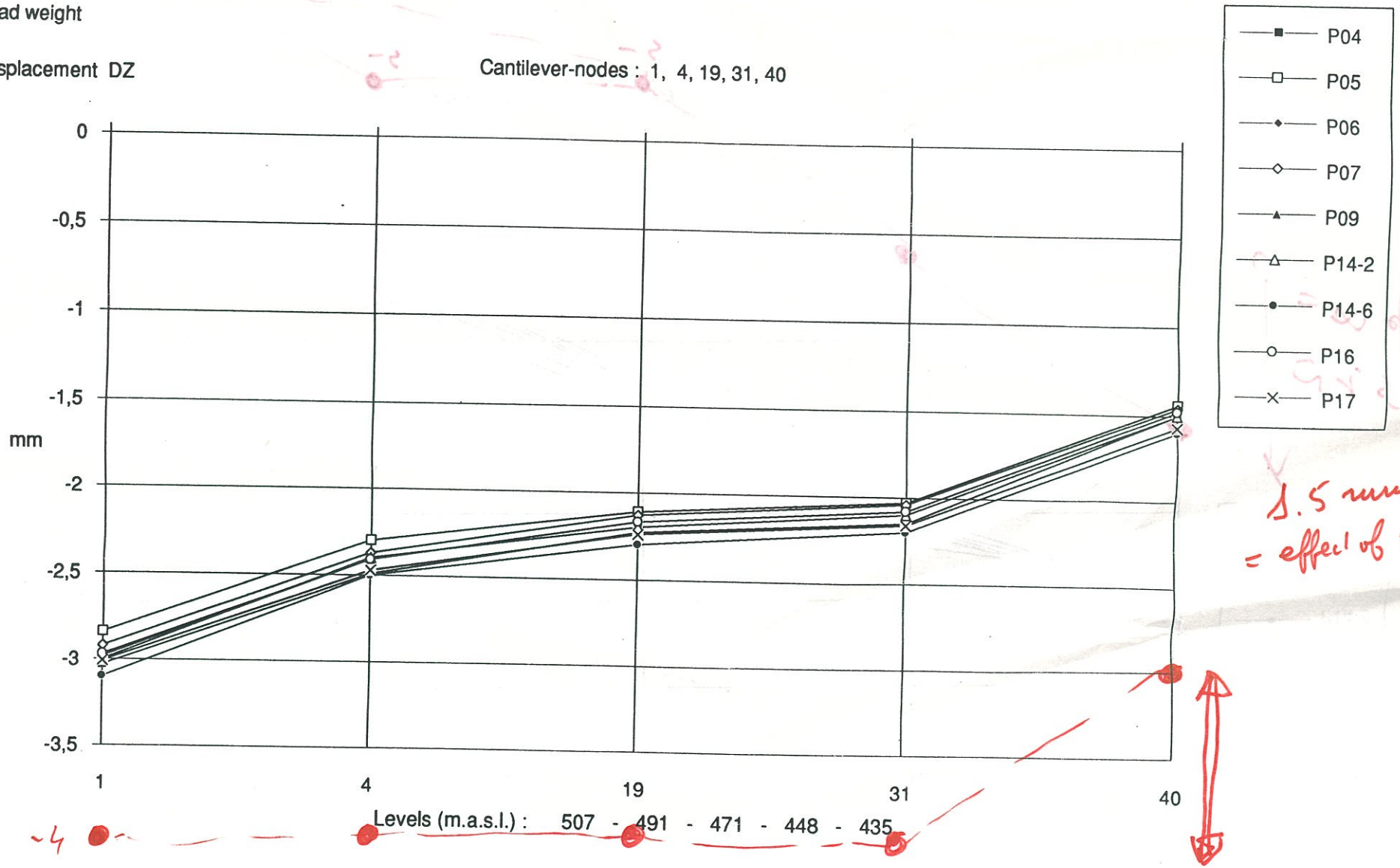

Dead weight

Displacement DZ

Cantilever-nodes : 3, 6, 21, 33, 42

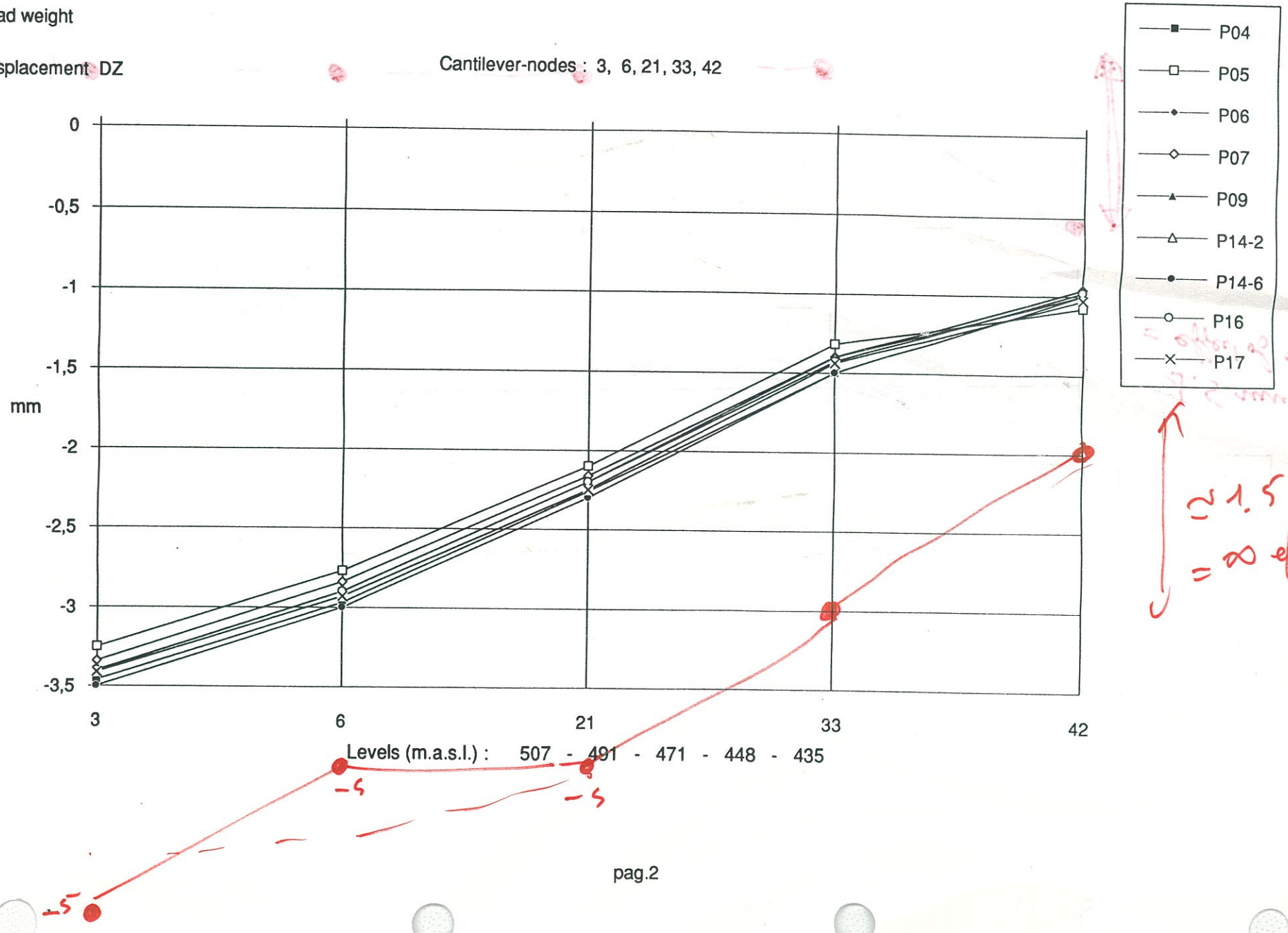

Hydrostatic load

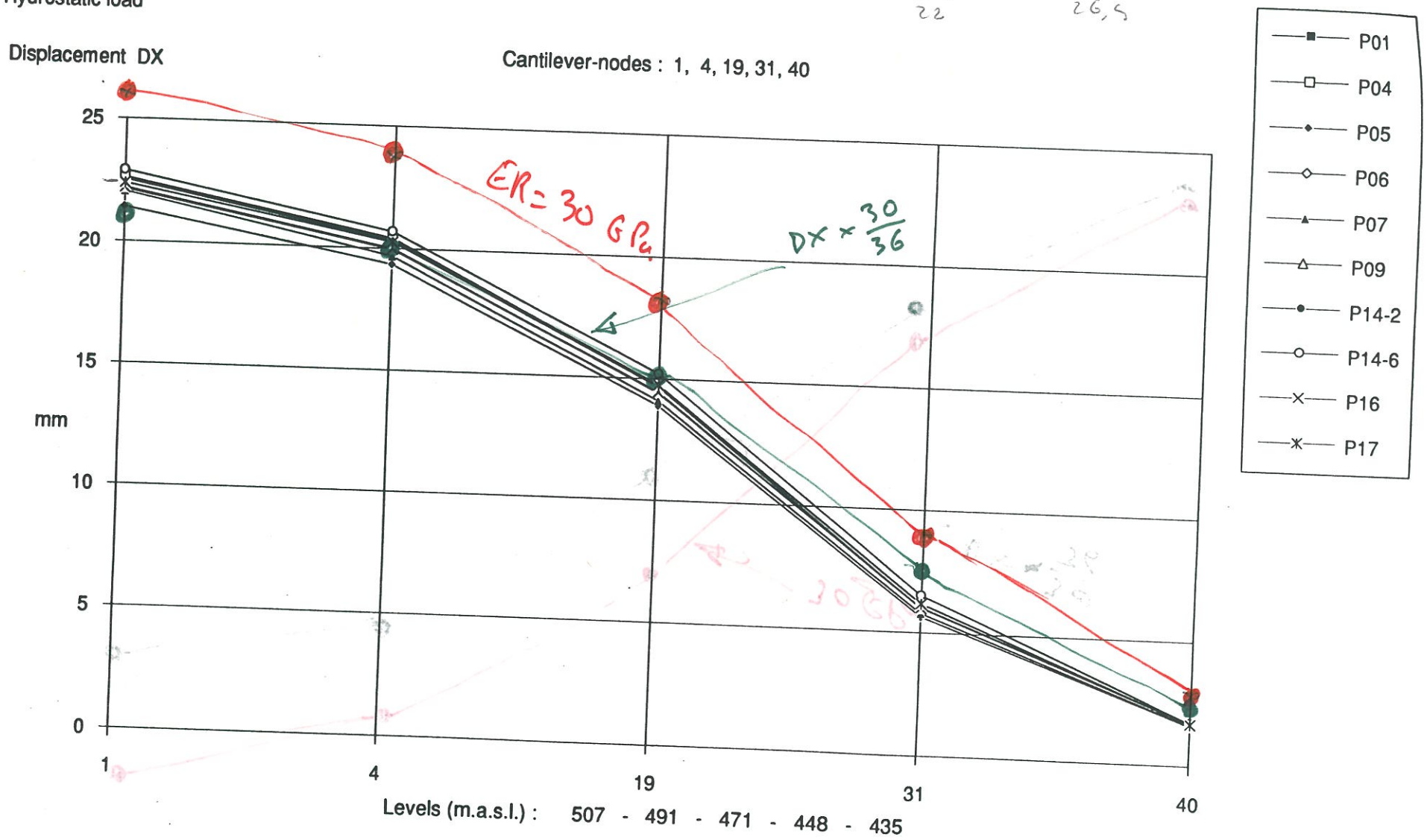

Hydrostatic load

Displacement DX

Cantilever-nodes : 3, 6, 21, 33, 42

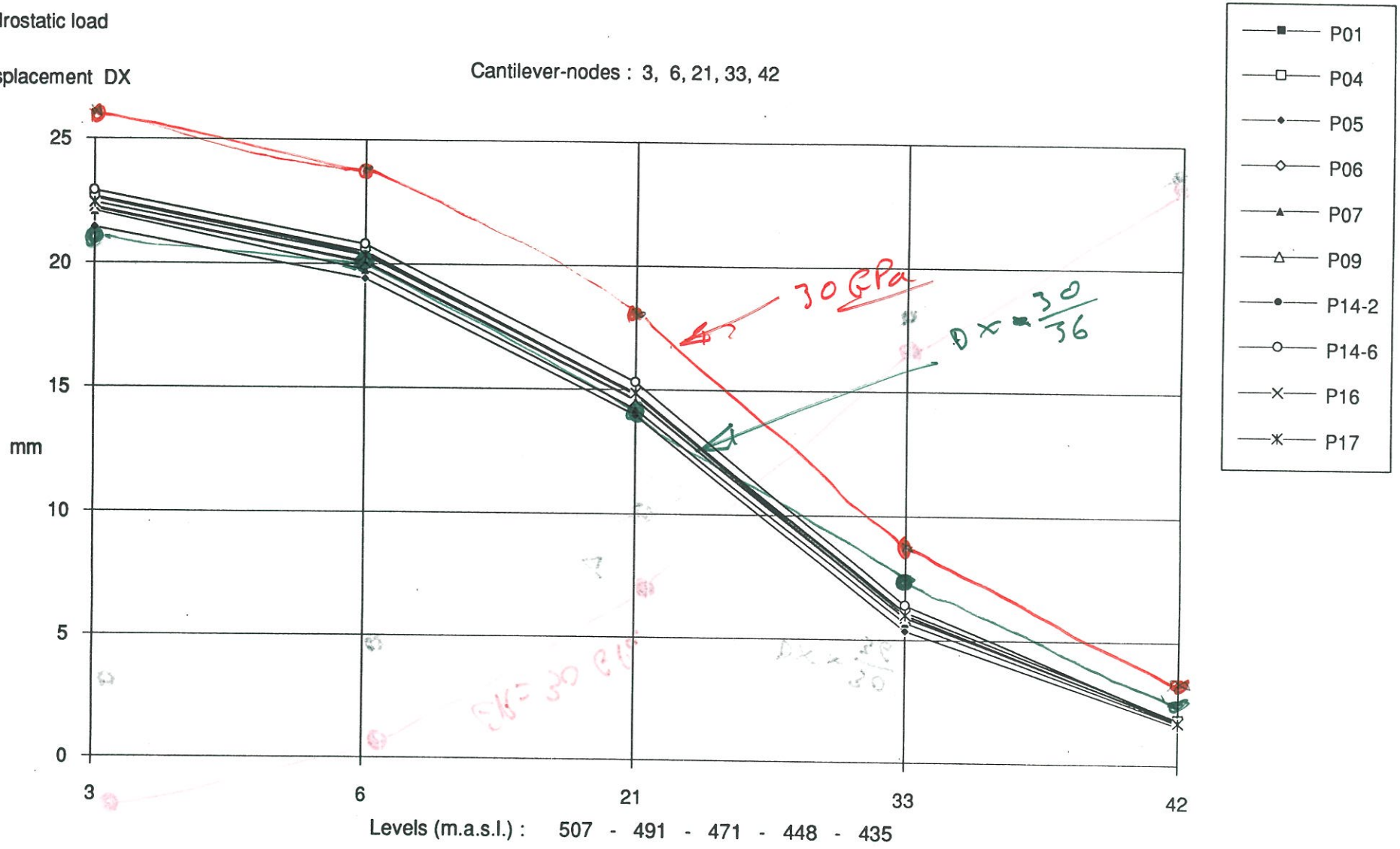

Temperature change

Displacement DX

Cantilever-nodes : 1, 4, 19, 31, 40

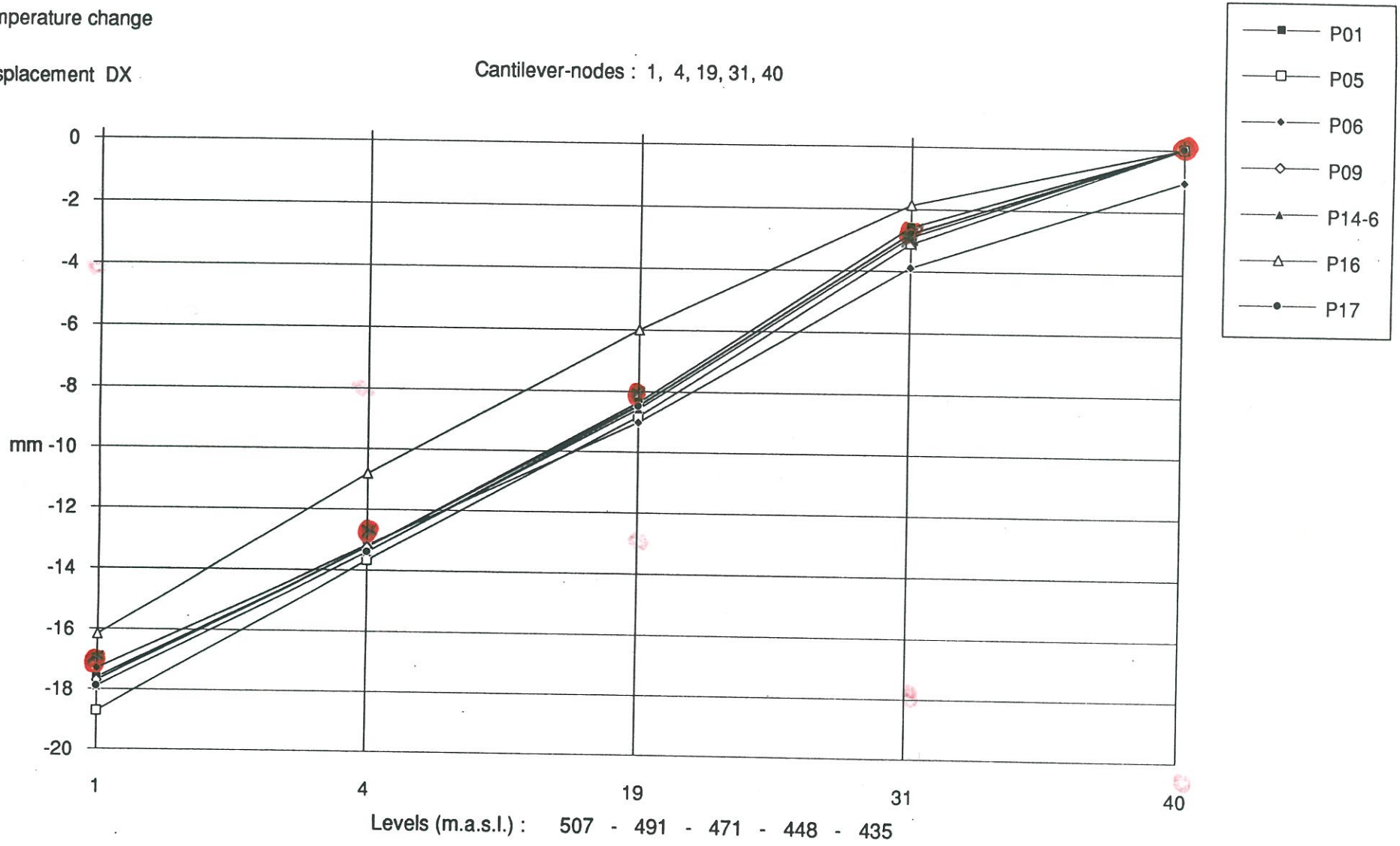

Temperature change

Displacement DX

Cantilever-nodes : 3, 6, 21, 33, 42

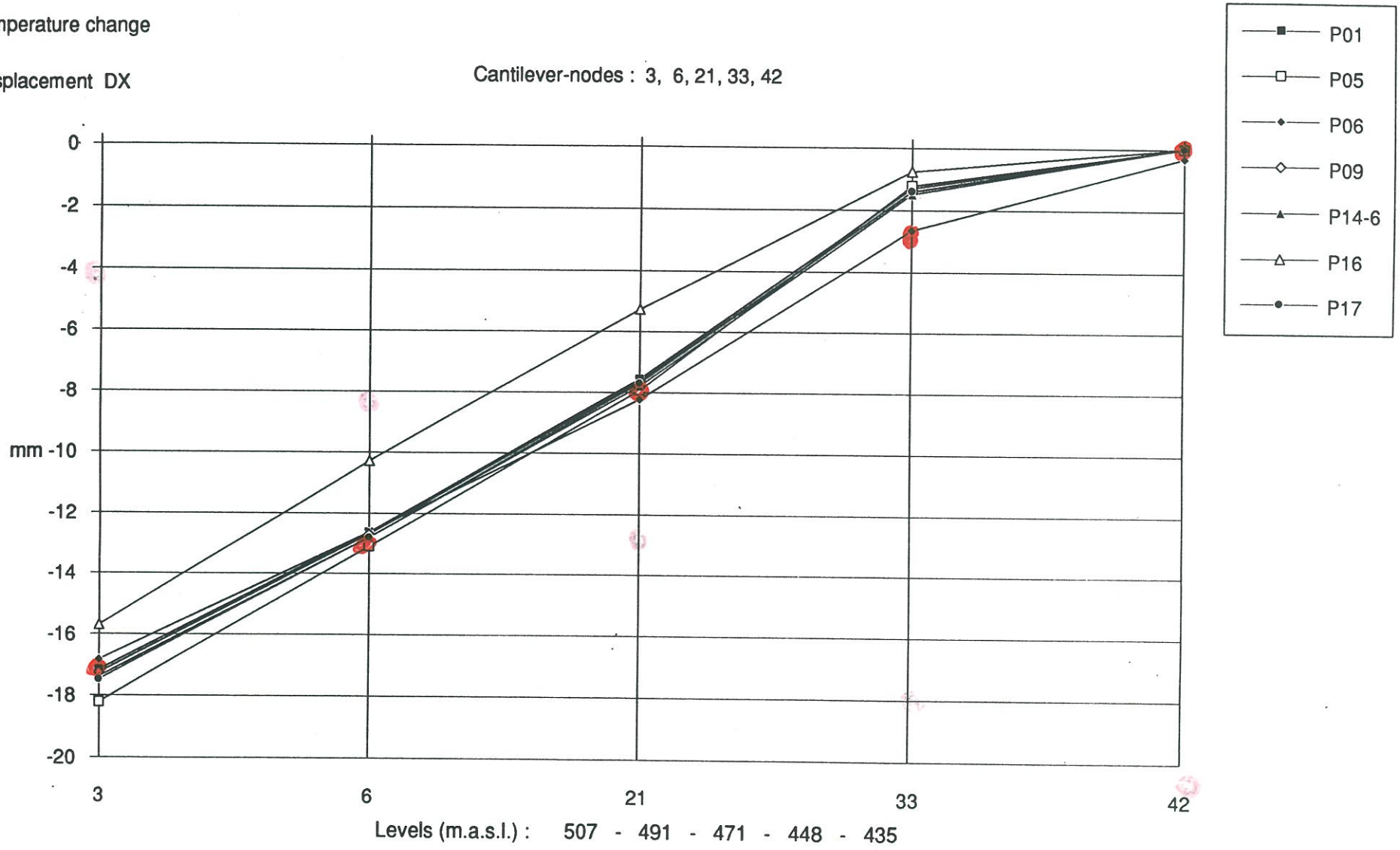

Temperature change

Displacement DZ

Cantilever-nodes : 1, 4, 19, 31, 40

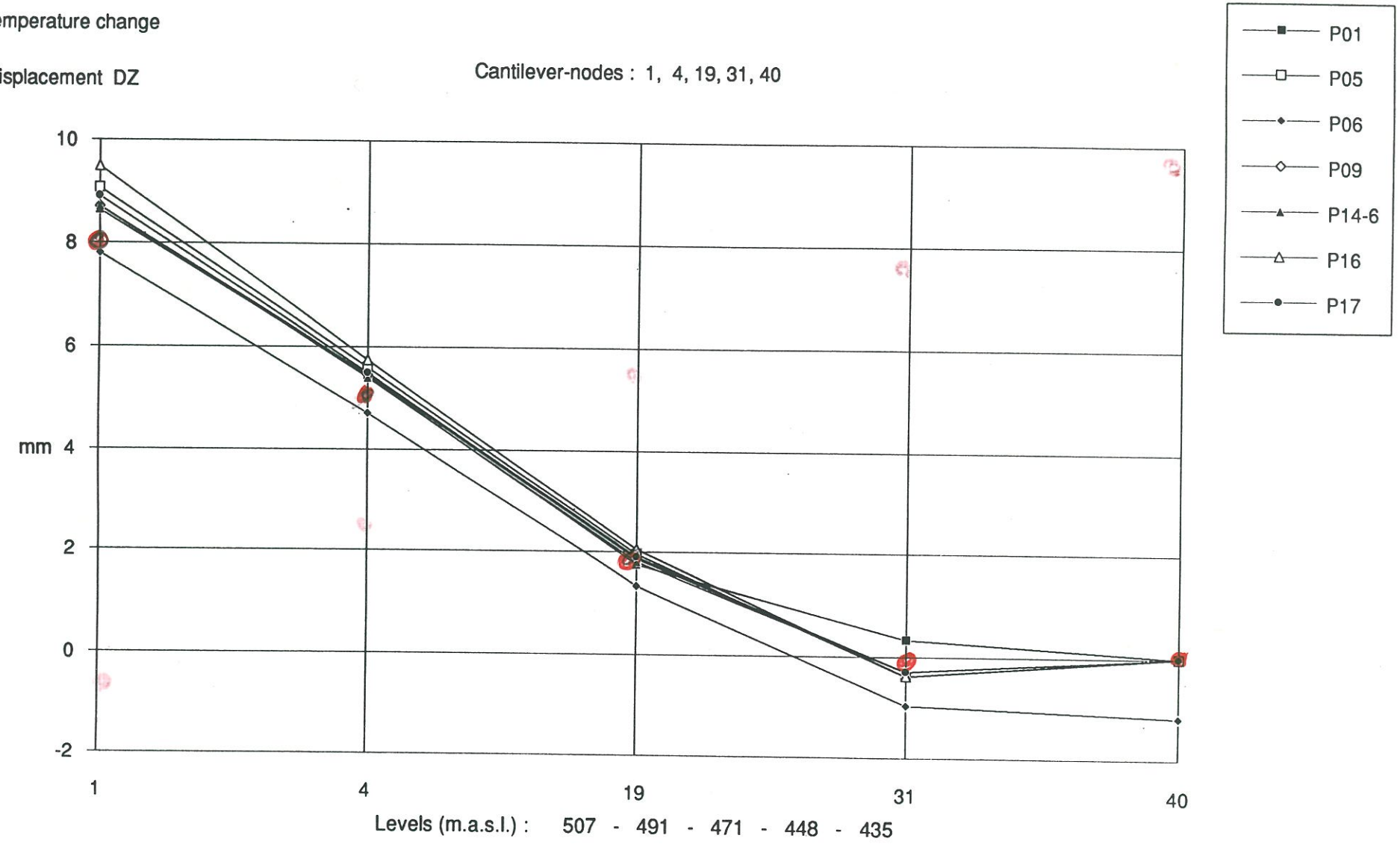

Temperature change

Displacement DZ

Cantilever-nodes : 3, 6, 21, 33, 42

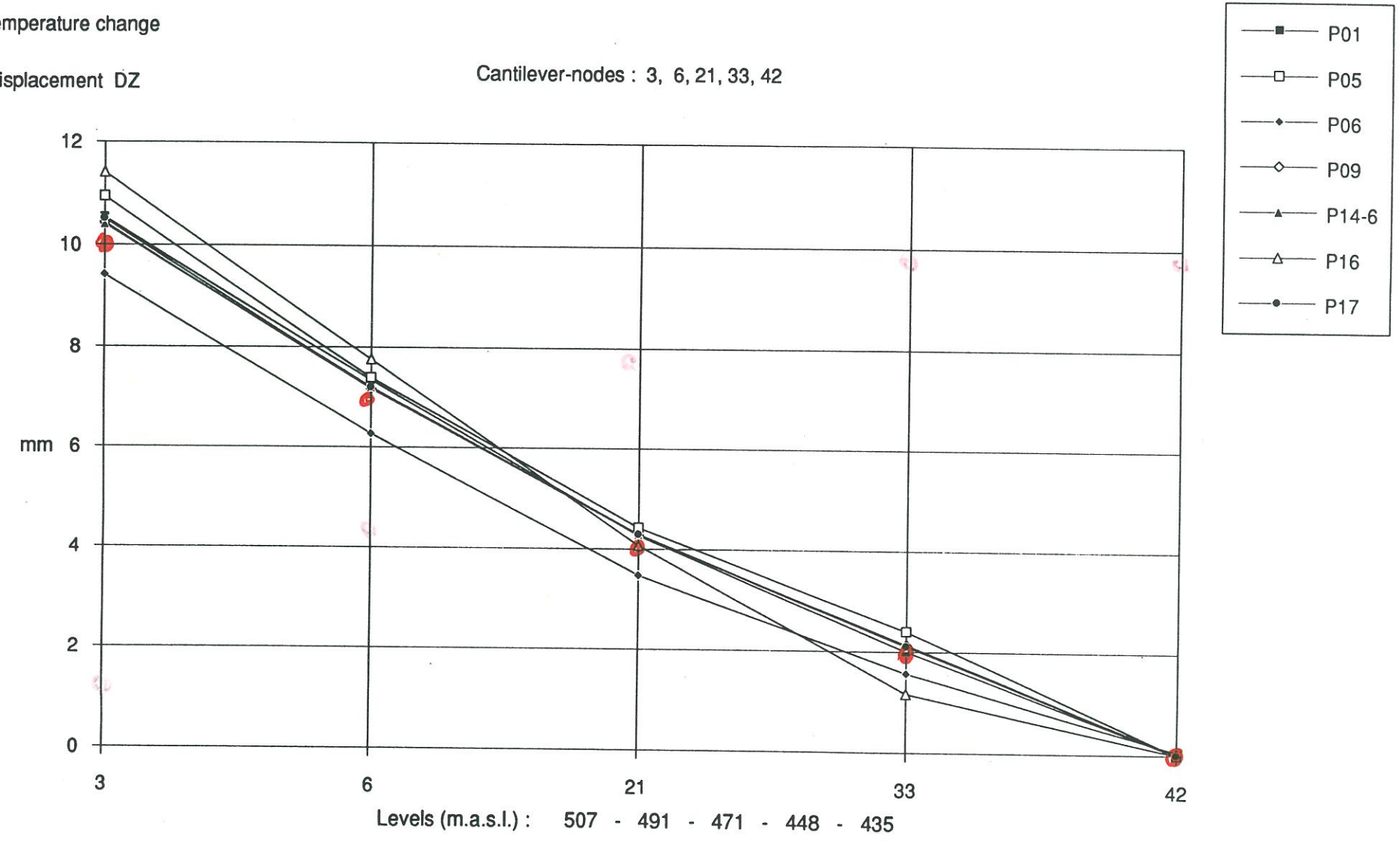

STATIC-THERMAL ANALYSIS

GRAPHIC COMPARISON OF THE RESULTS

- STRESSES -

Dead weight

Principal stress P1

Cantilever-nodes : 1, 4, 19, 31, 40

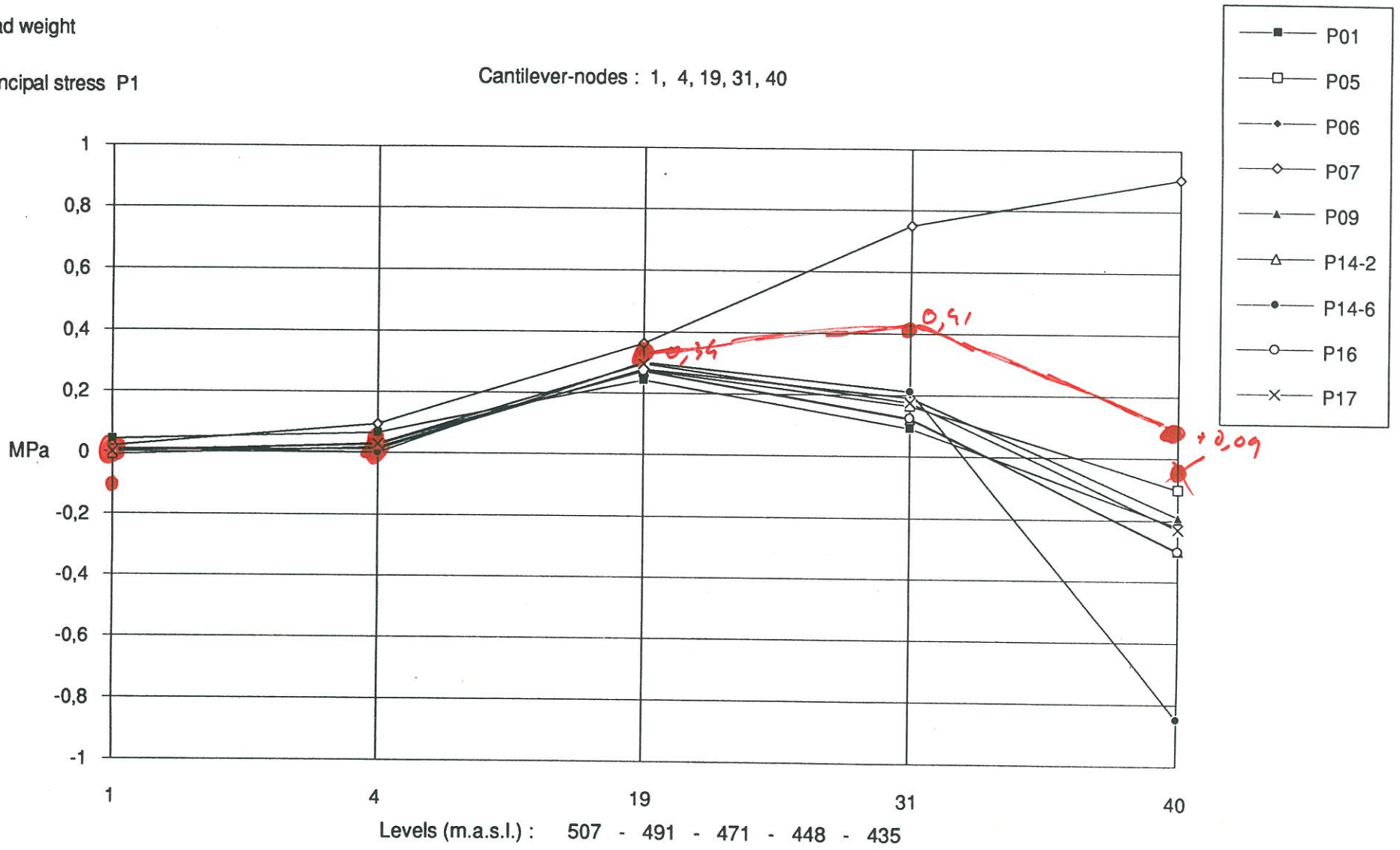

Dead weight

Principal stress P2

Cantilever-nodes : 1, 4, 19, 31, 40

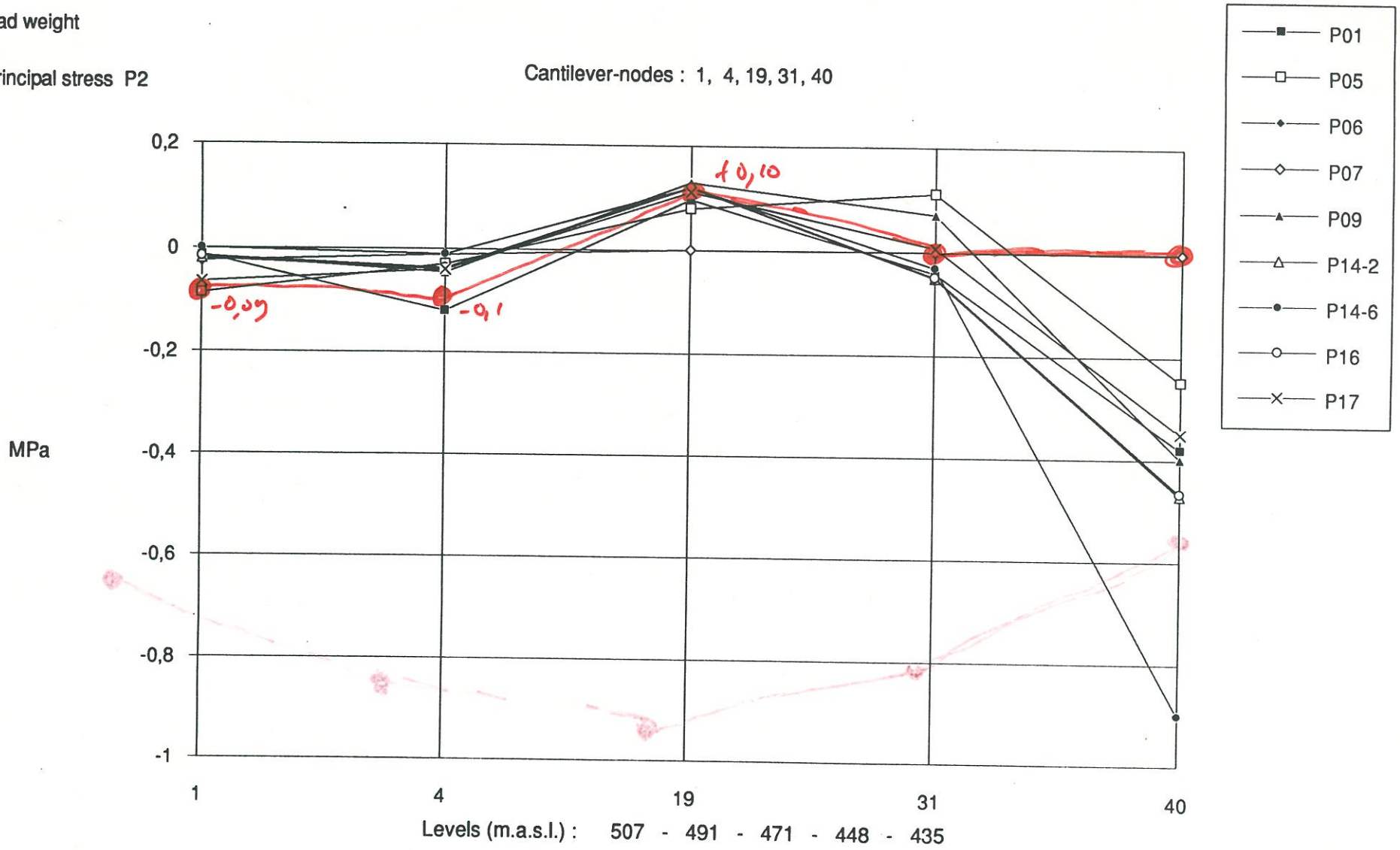

Dead weight

Principal stress P3

Cantilever-nodes : 1, 4, 19, 31, 40

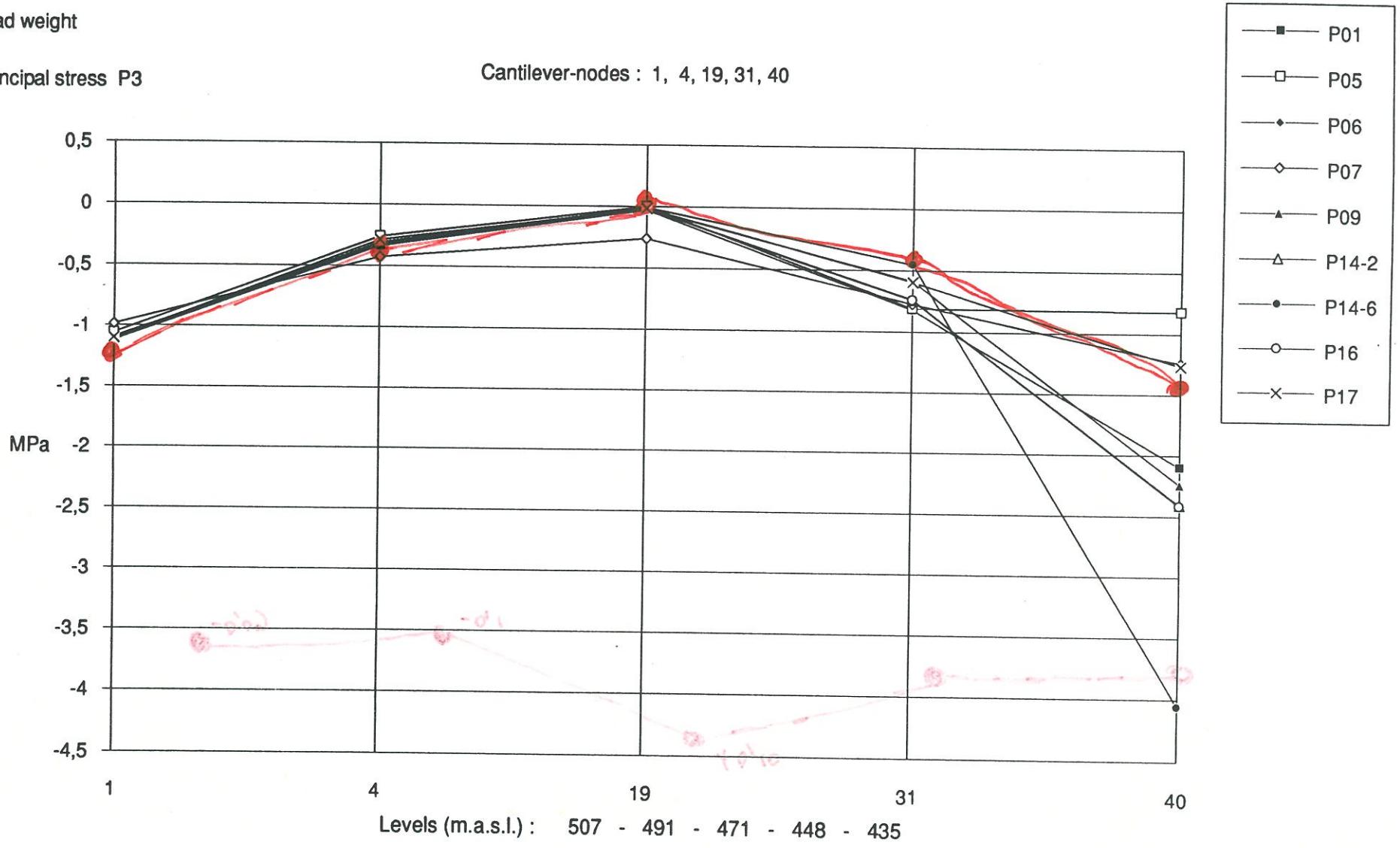

Dead weight

Principal stress P1

Cantilever-nodes : 3, 6, 21, 33, 42

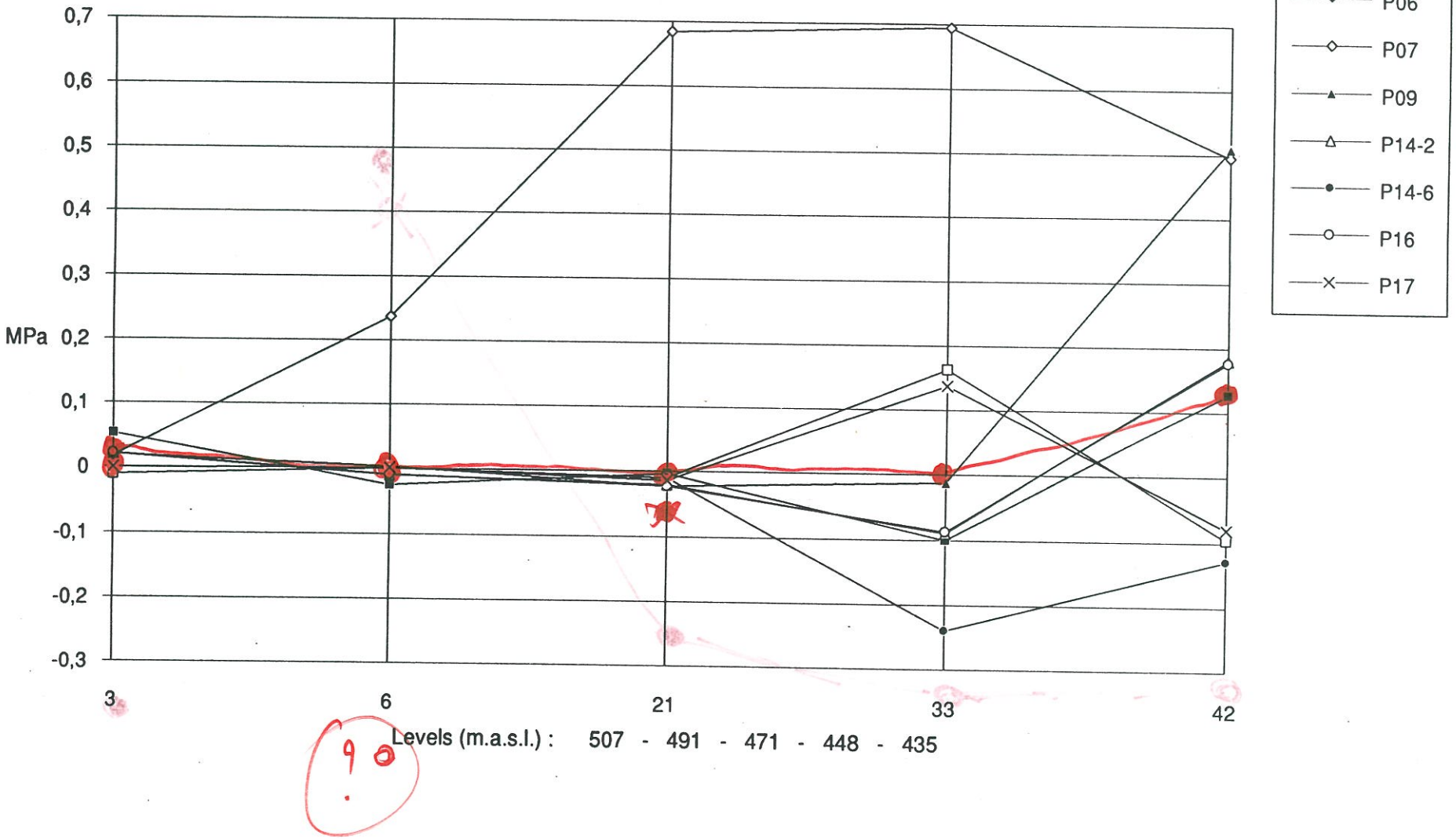

Dead weight

Principal stress P2

Cantilever-nodes : 3, 6, 21, 33, 42

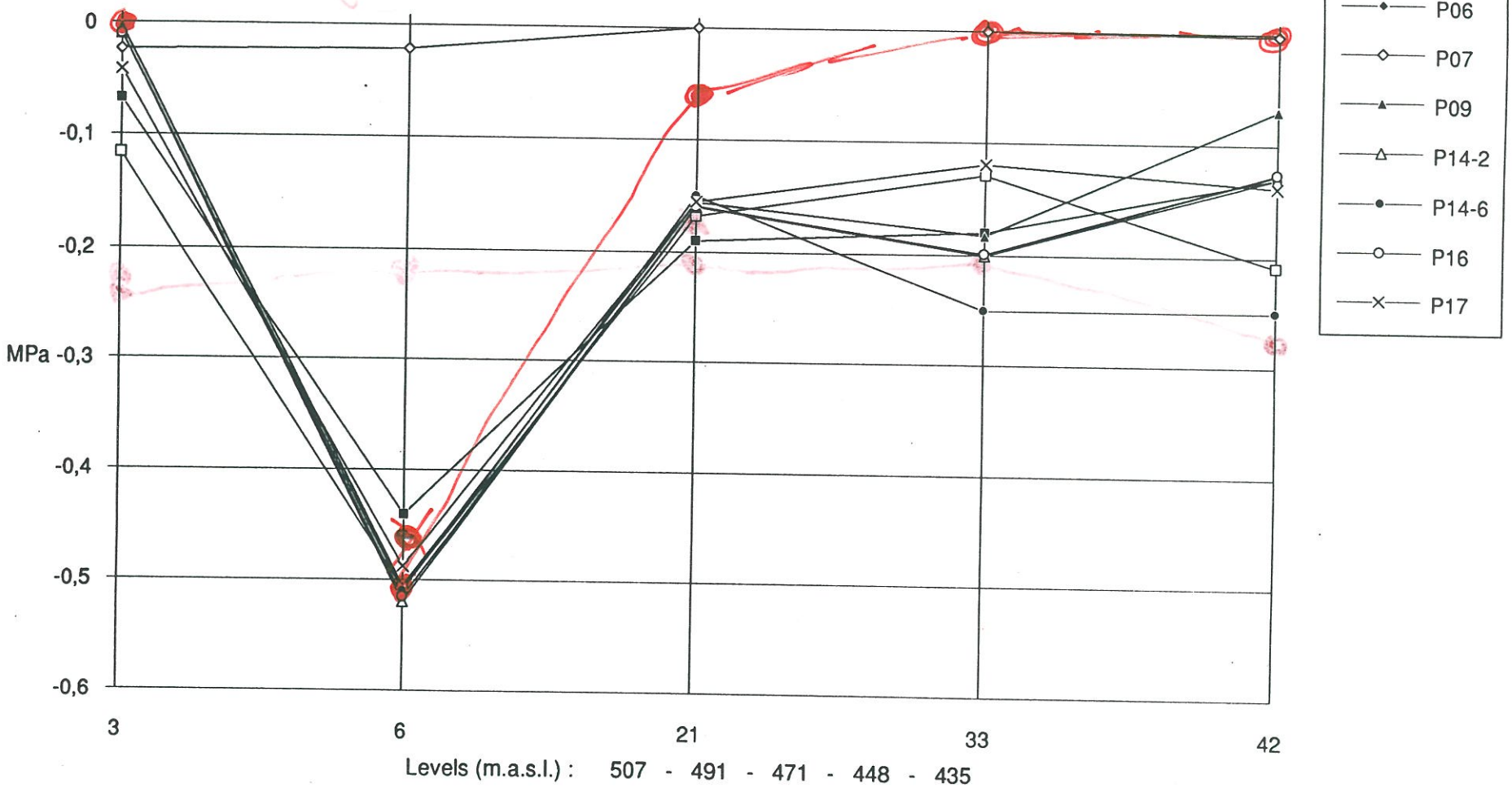

Dead weight

Principal stress P3

Cantilever-nodes : 3, 6, 21, 33, 42

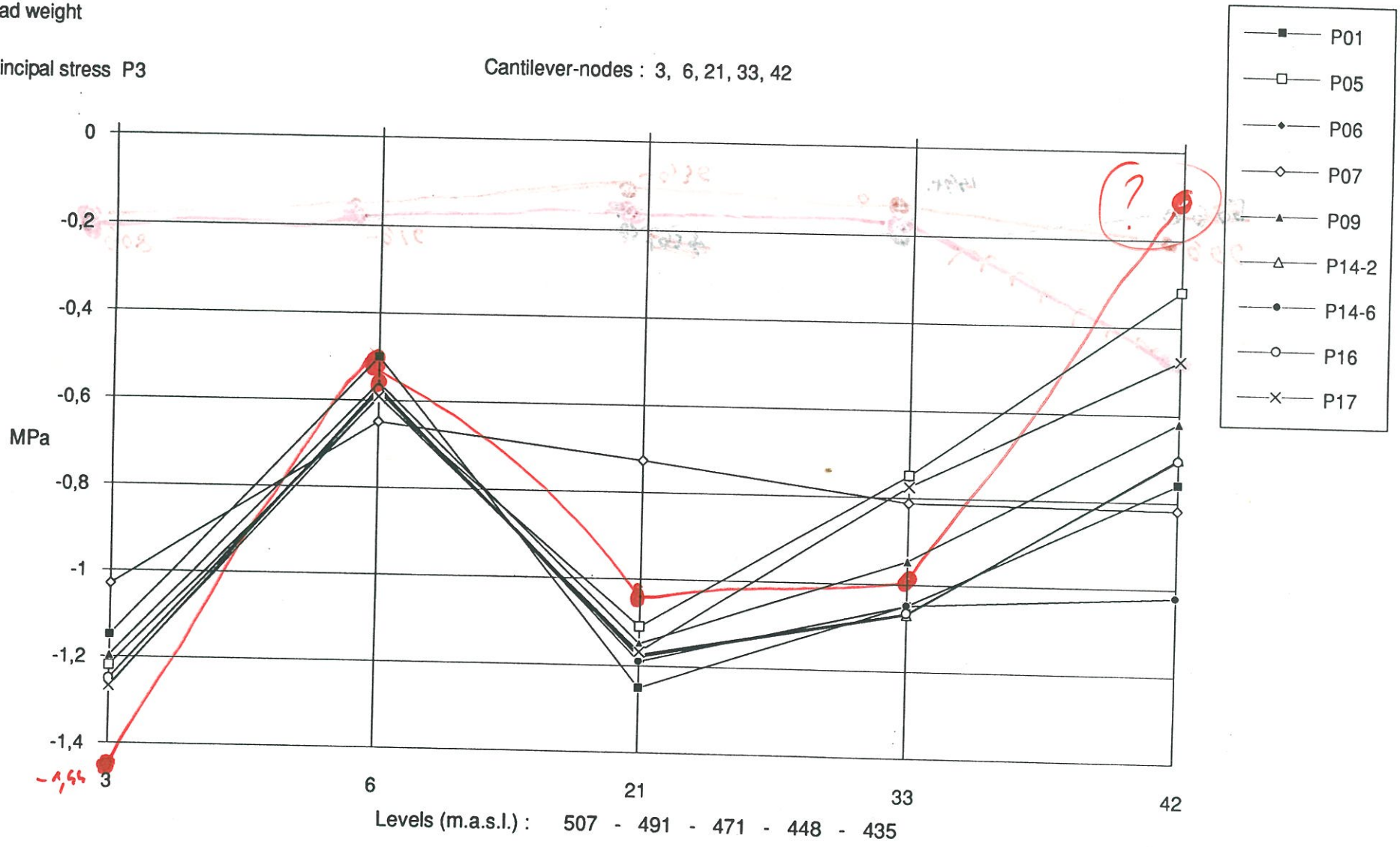

Hydrostatic load

Principal stress P1

Cantilever-nodes : 1, 4, 19, 31, 40

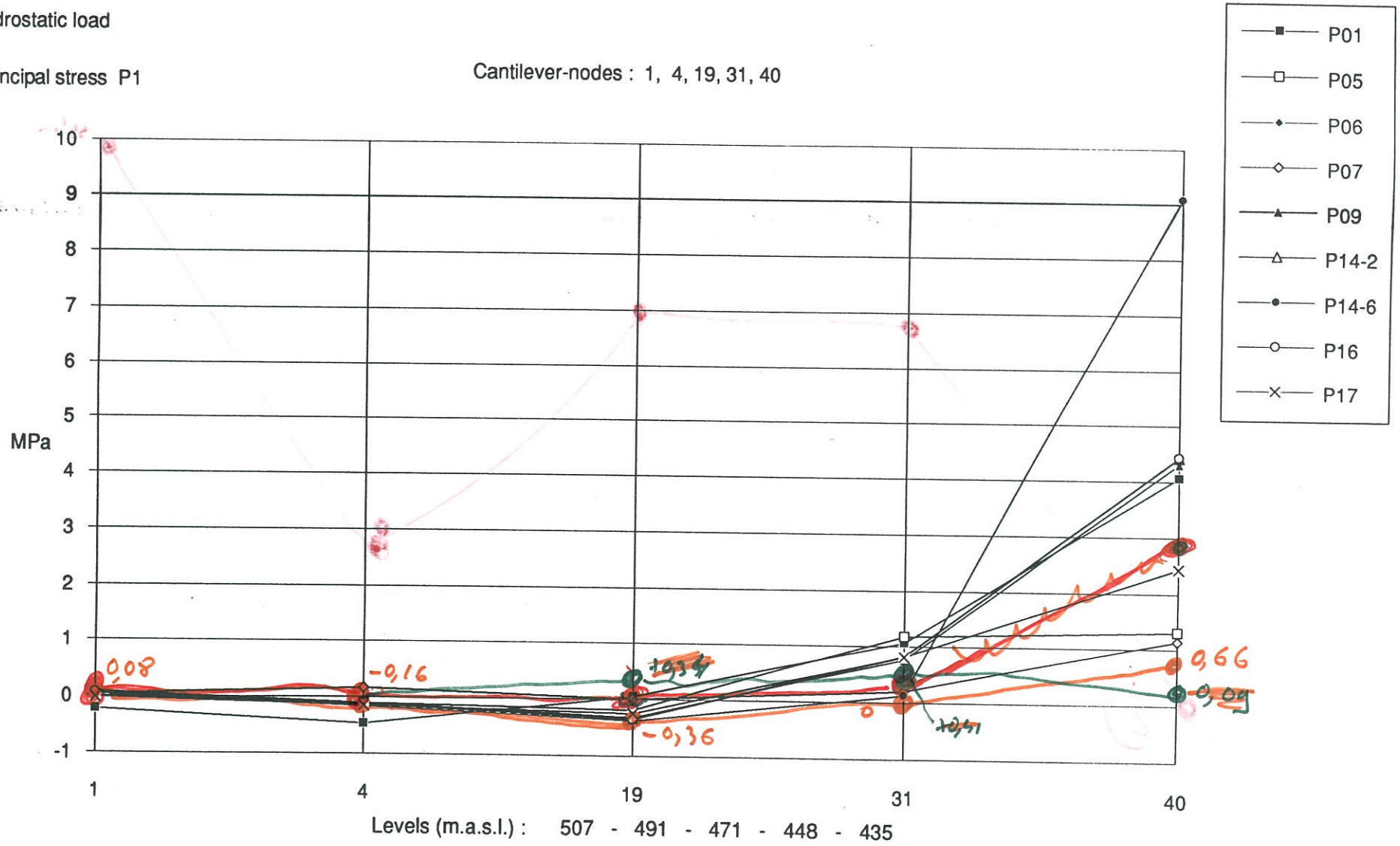

Hydrostatic load

Principal stress P2

Cantilever-nodes : 1, 4, 19, 31, 40

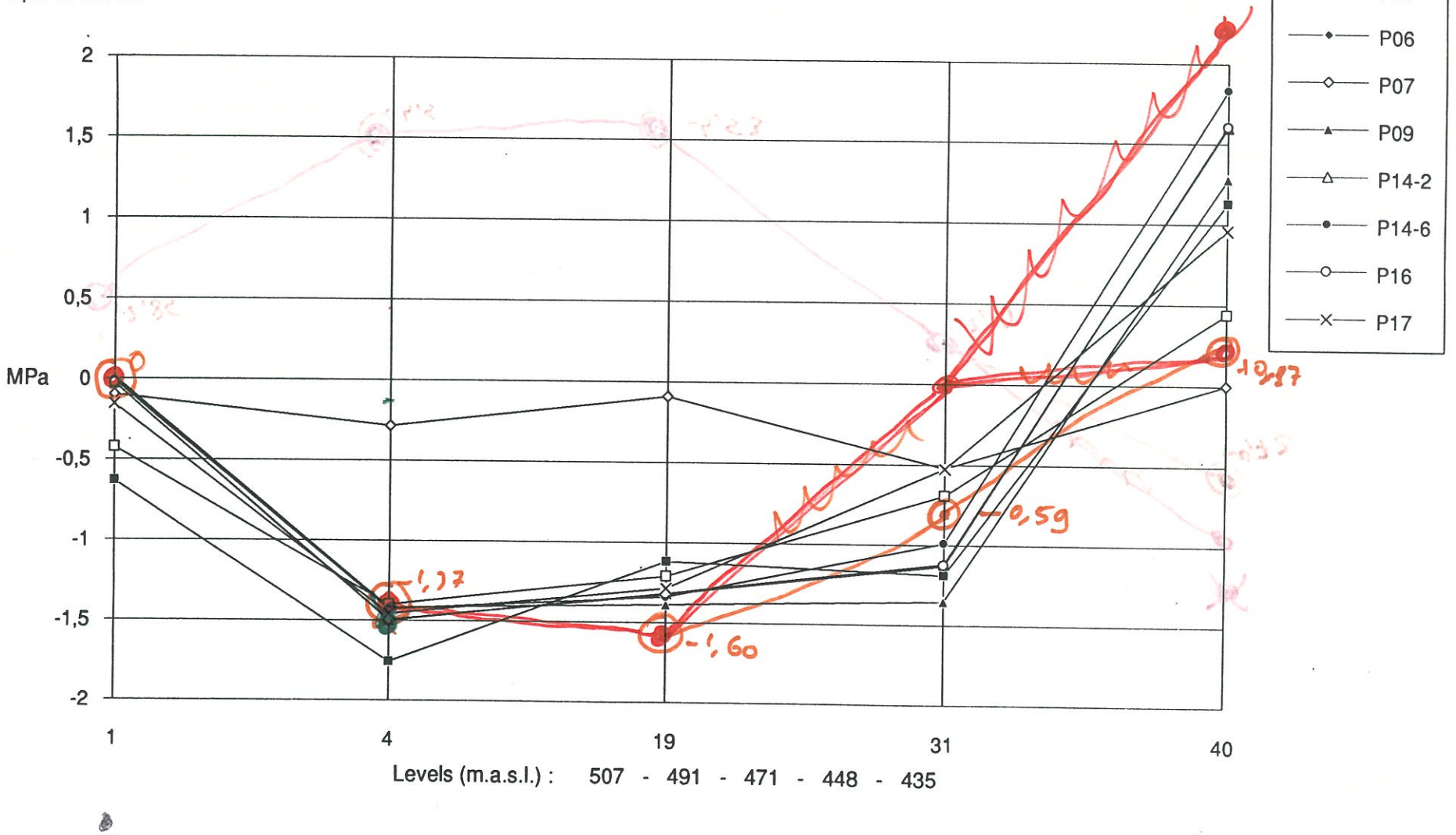

Hydrostatic load

Principal stress P3

Cantilever-nodes : 1, 4, 19, 31, 40

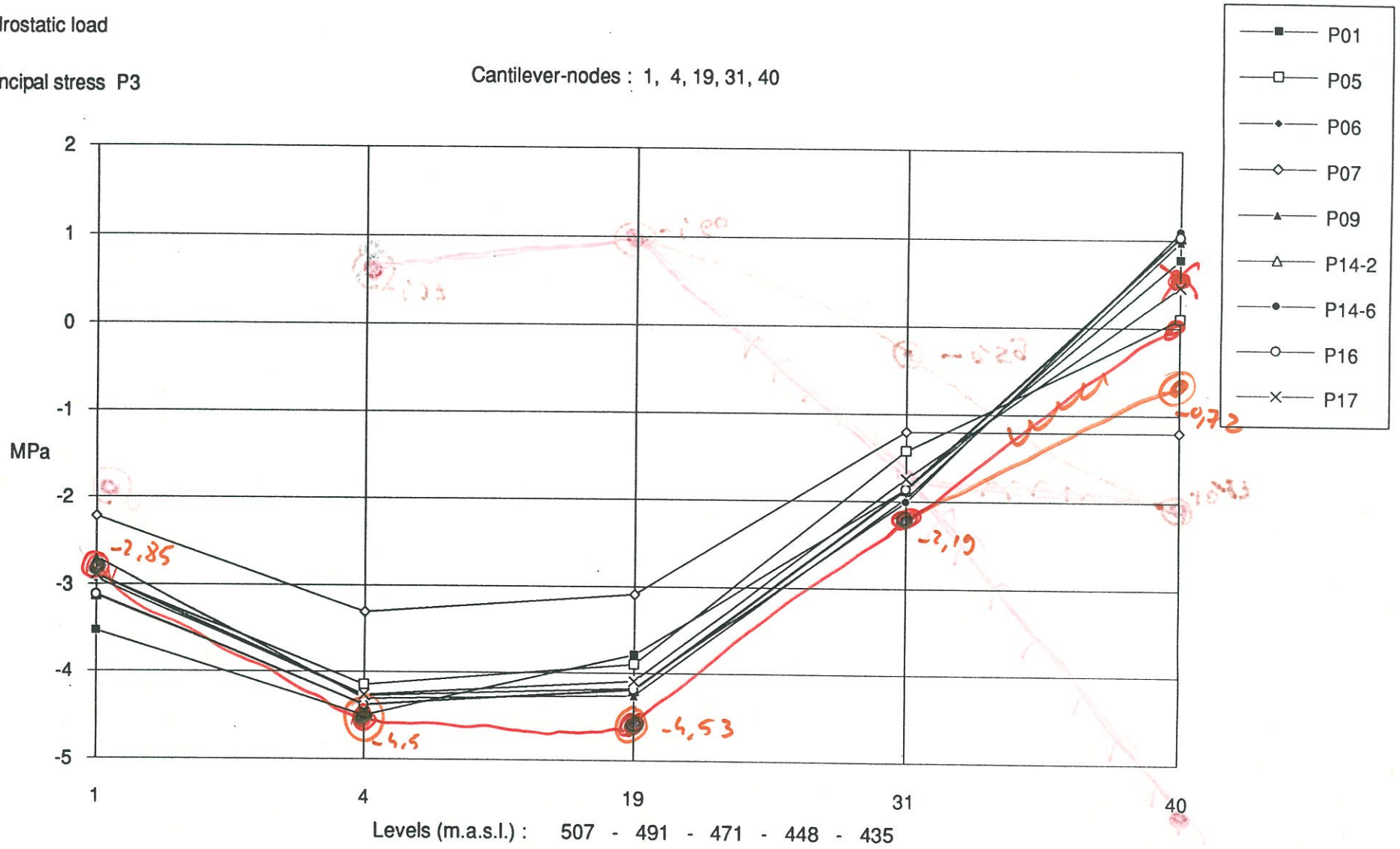

Hydrostatic load

Principal stress P1

Cantilever-nodes : 3, 6, 21, 33, 42

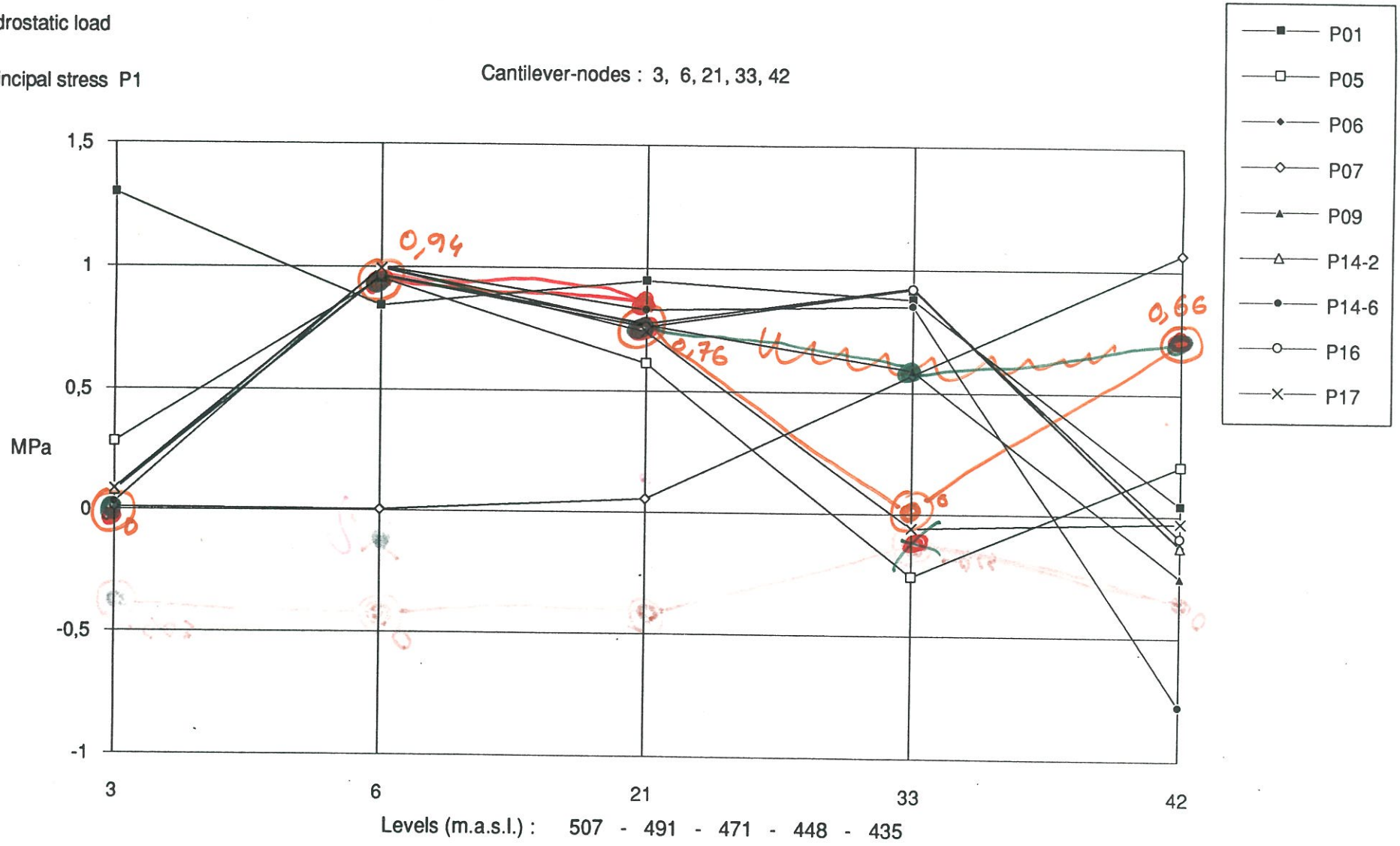

Hydrostatic load

Principal stress P2

Cantilever-nodes : 3, 6, 21, 33, 42

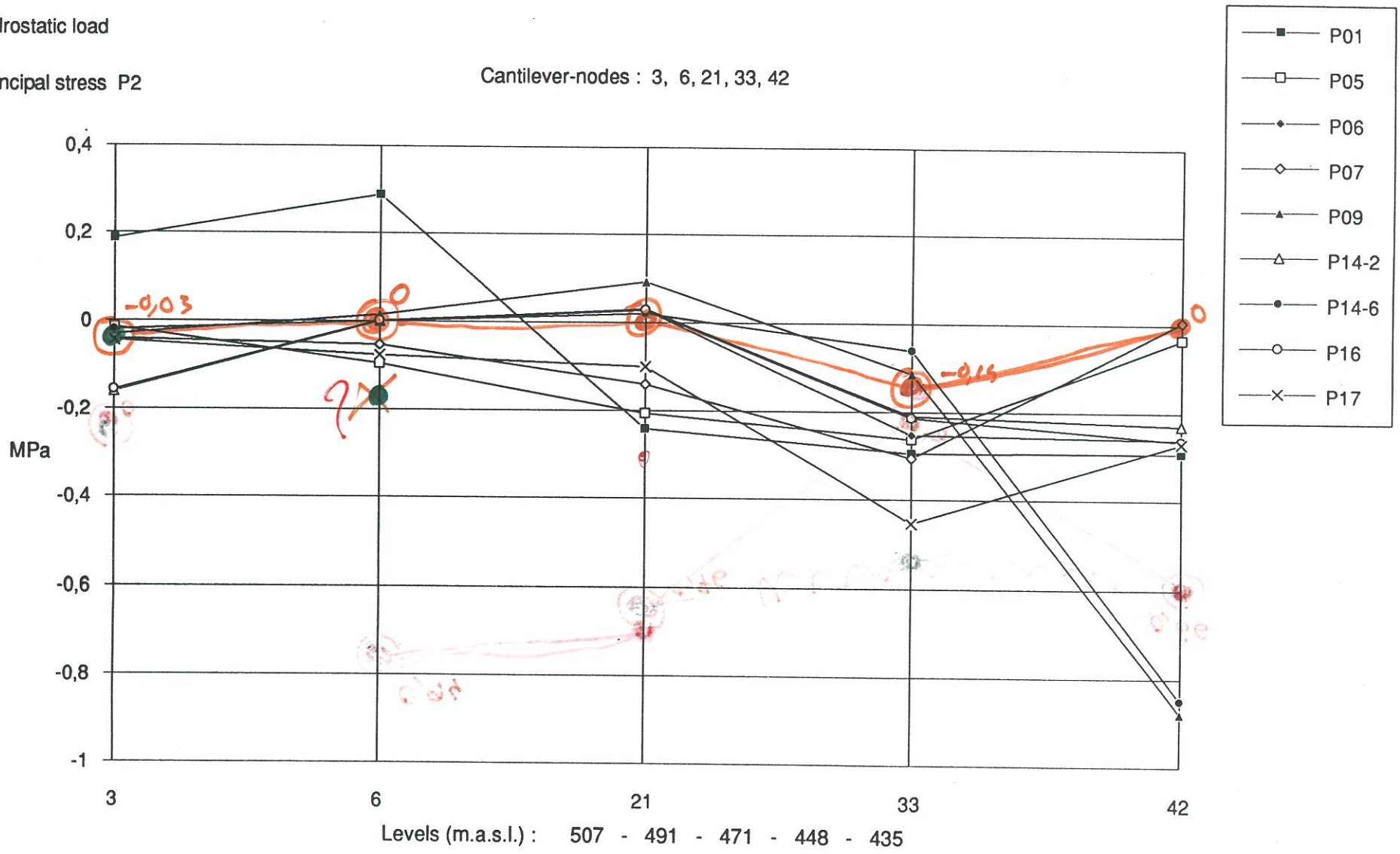

Hydrostatic load

Principal stress P3

Cantilever-nodes : 3, 6, 21, 33, 42

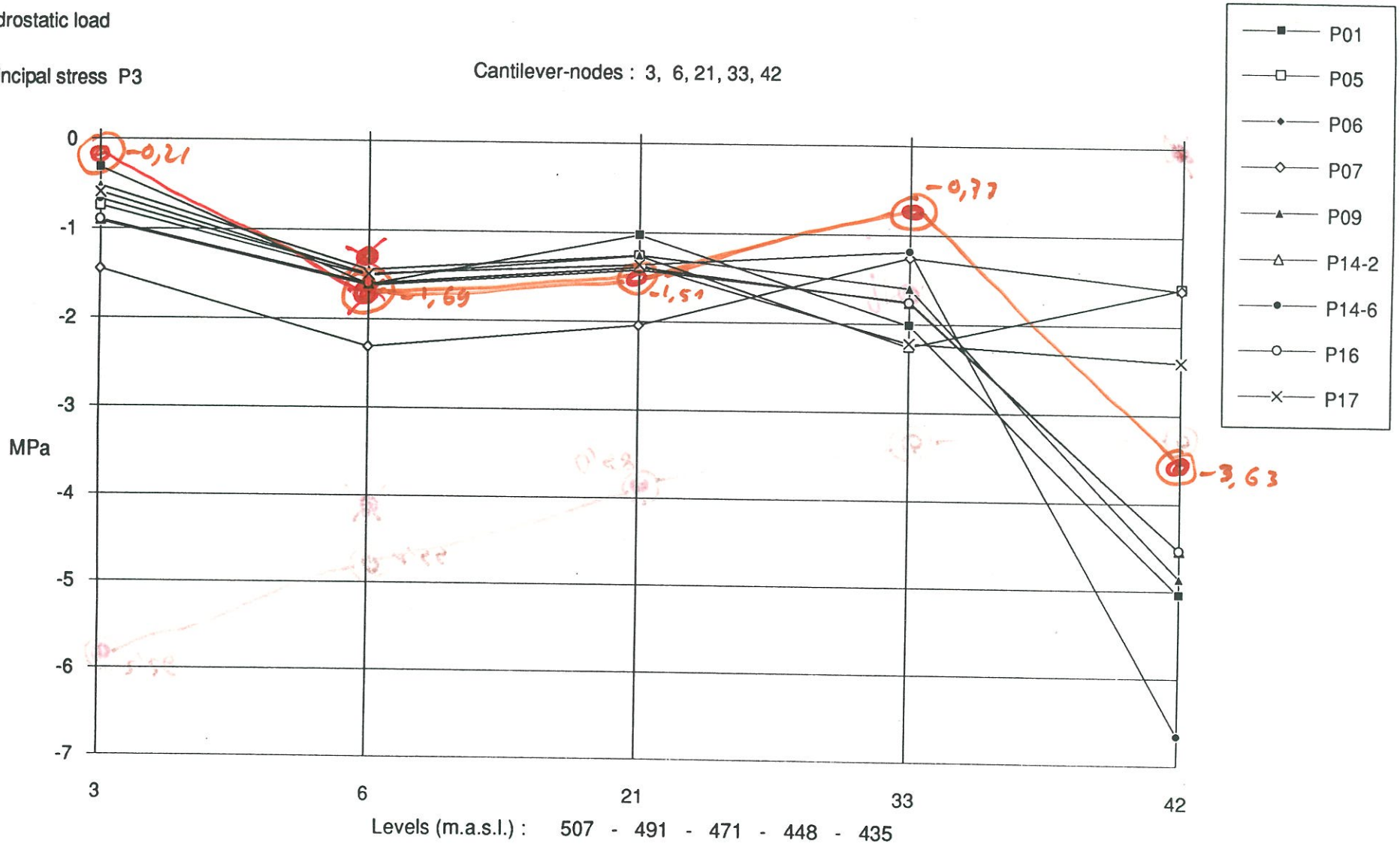

Temperature change

Principal stress P1

Cantilever-nodes : 1, 4, 19, 31, 40

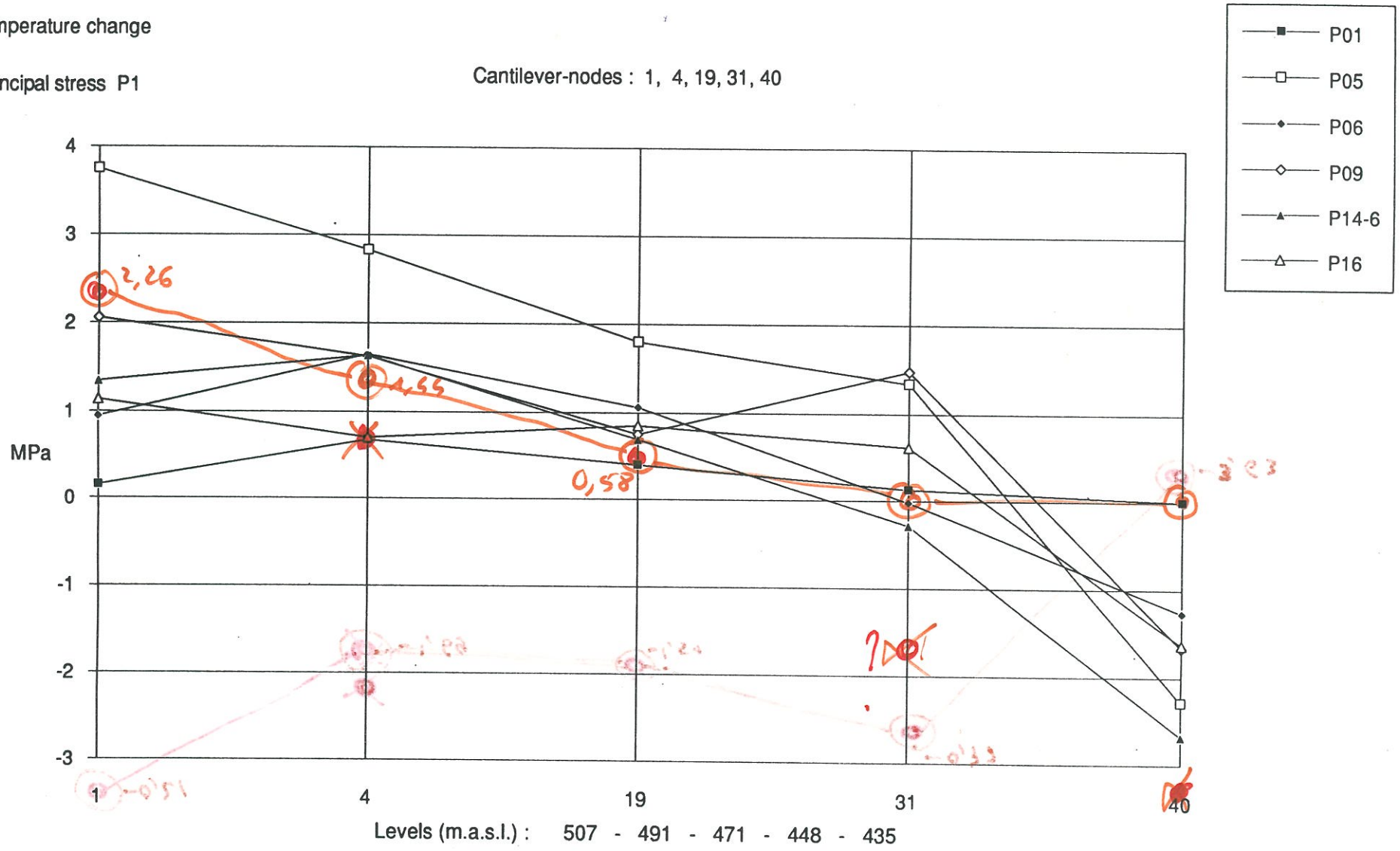

Temperature change

Principal stress P2

Cantilever-nodes : 1, 4, 19, 31, 40

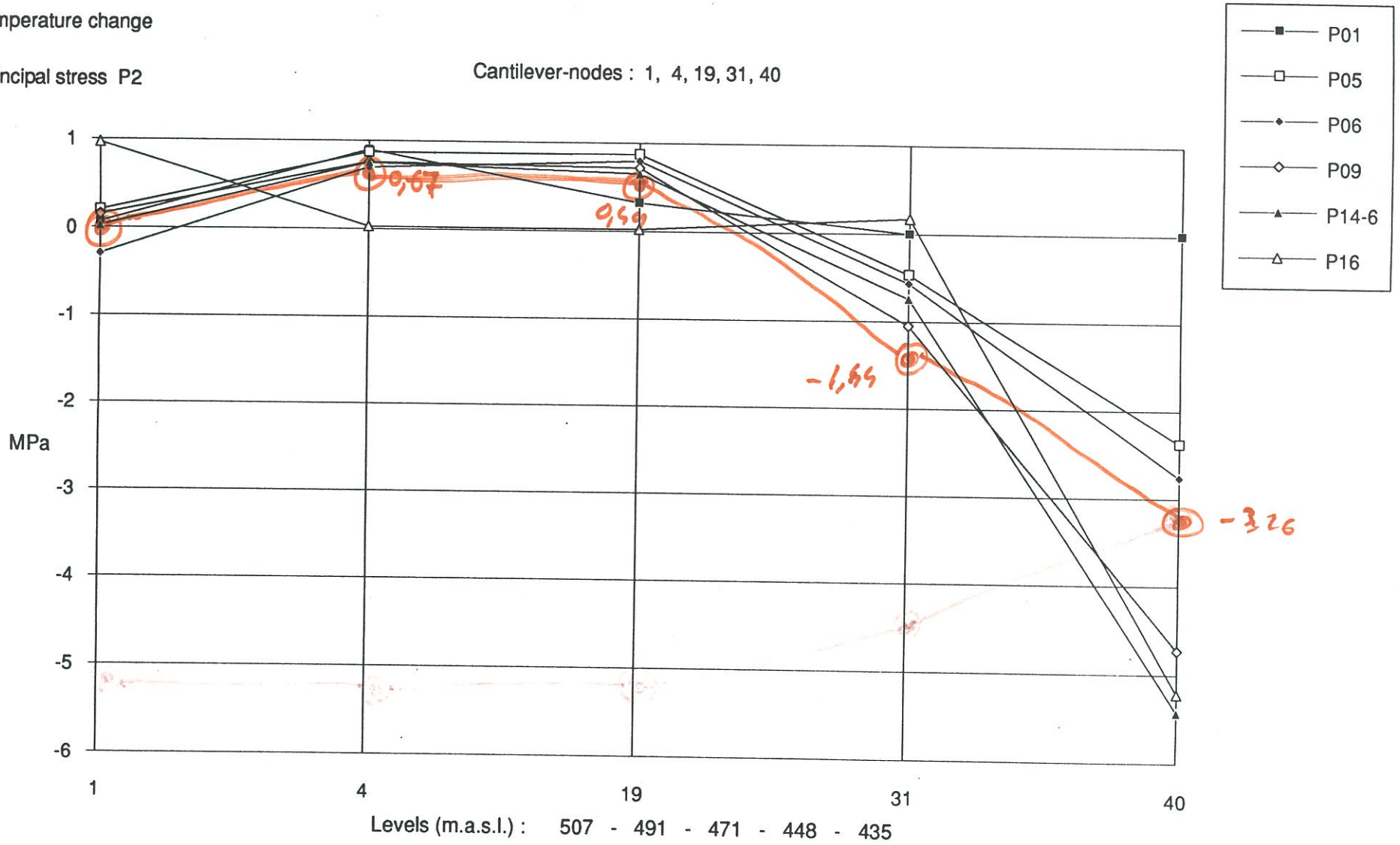

Temperature change

Principal stress P3

Cantilever-nodes : 1, 4, 19, 31, 40

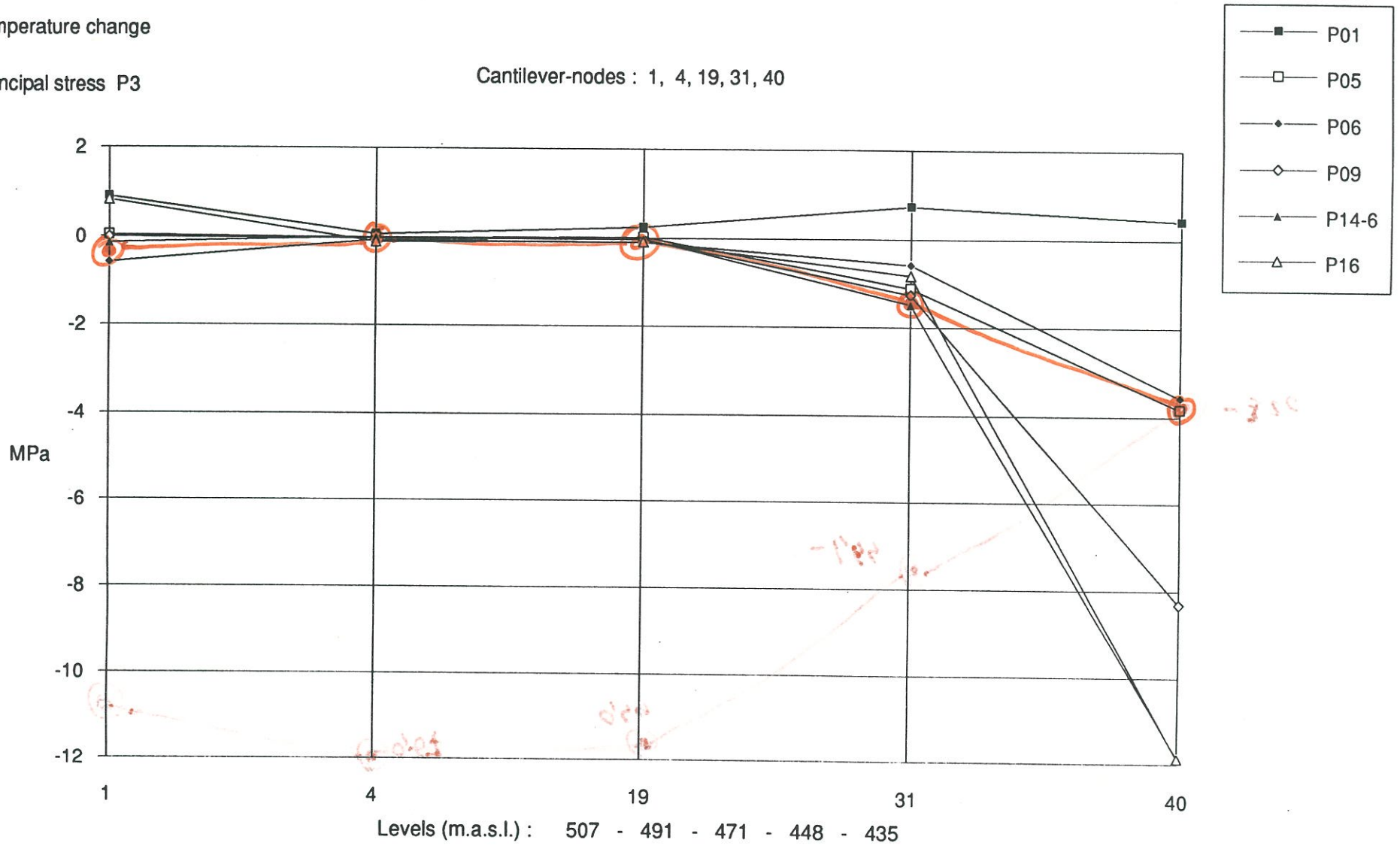

Temperature change

Principal stress P1

Cantilever-nodes : 3, 6, 21, 33, 42

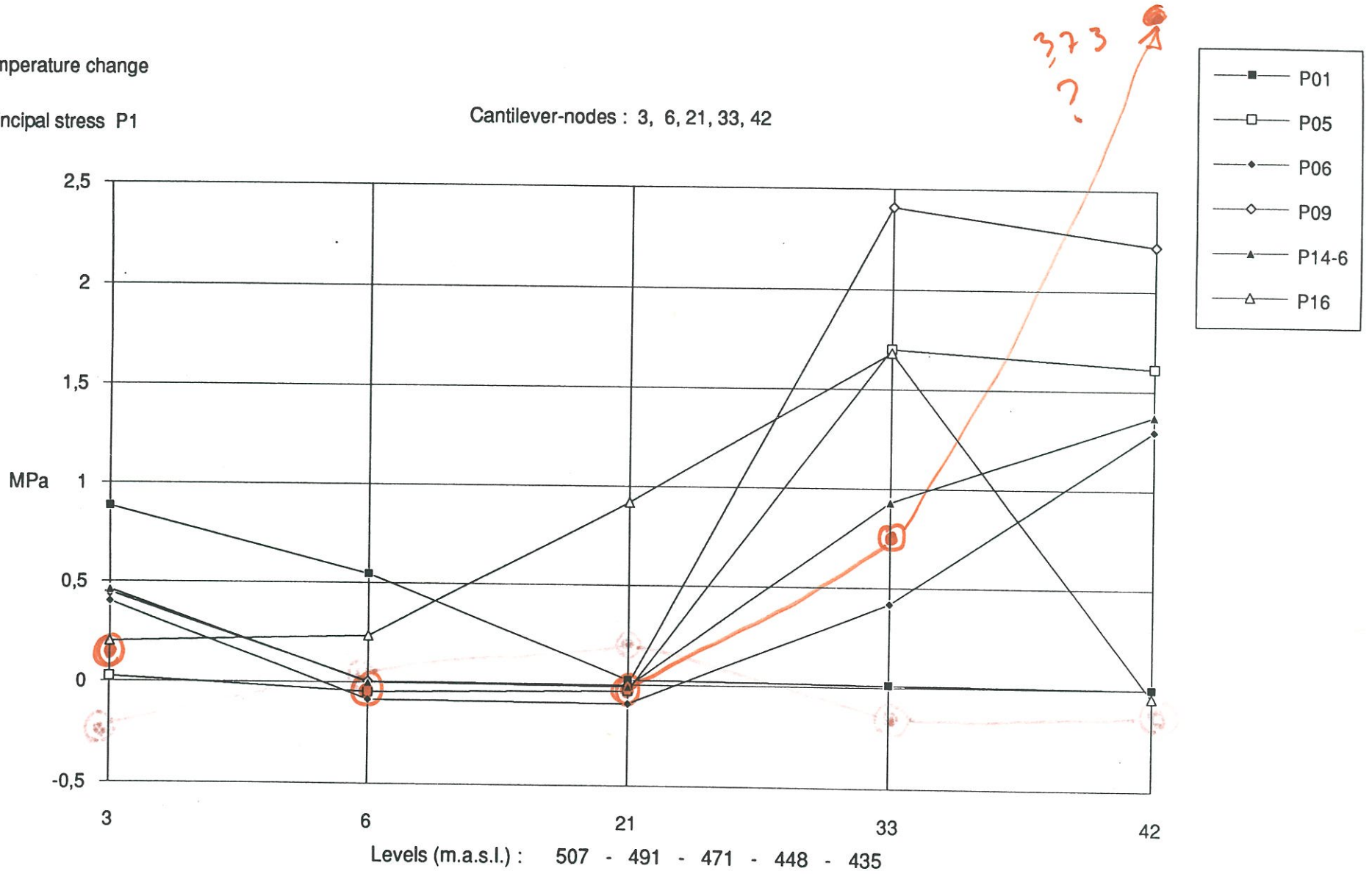

Temperature change

Principal stress P2

Cantilever-nodes : 3, 6, 21, 33, 42

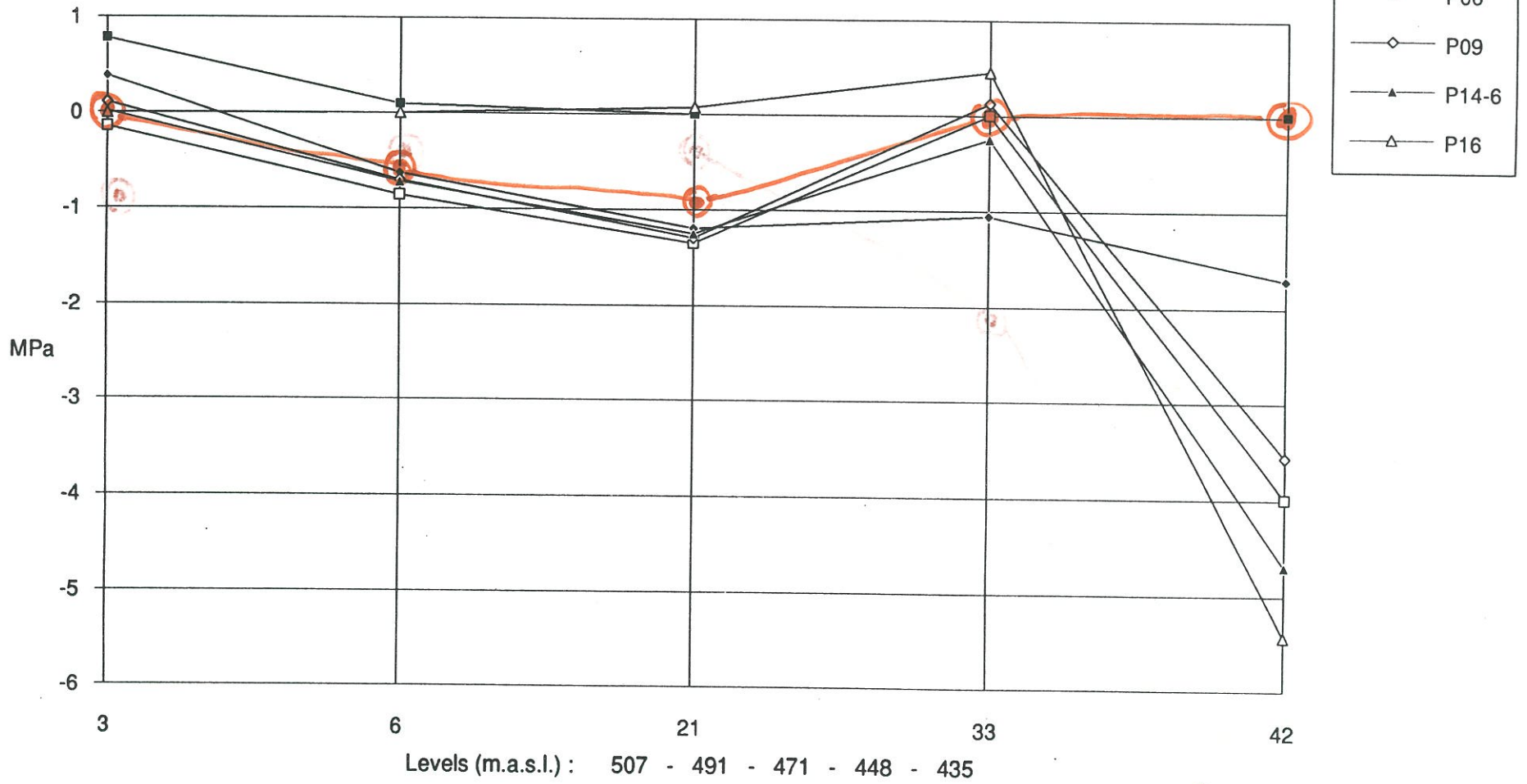

Temperature change

Principal stress P3

Cantilever-nodes : 3, 6, 21, 33, 42

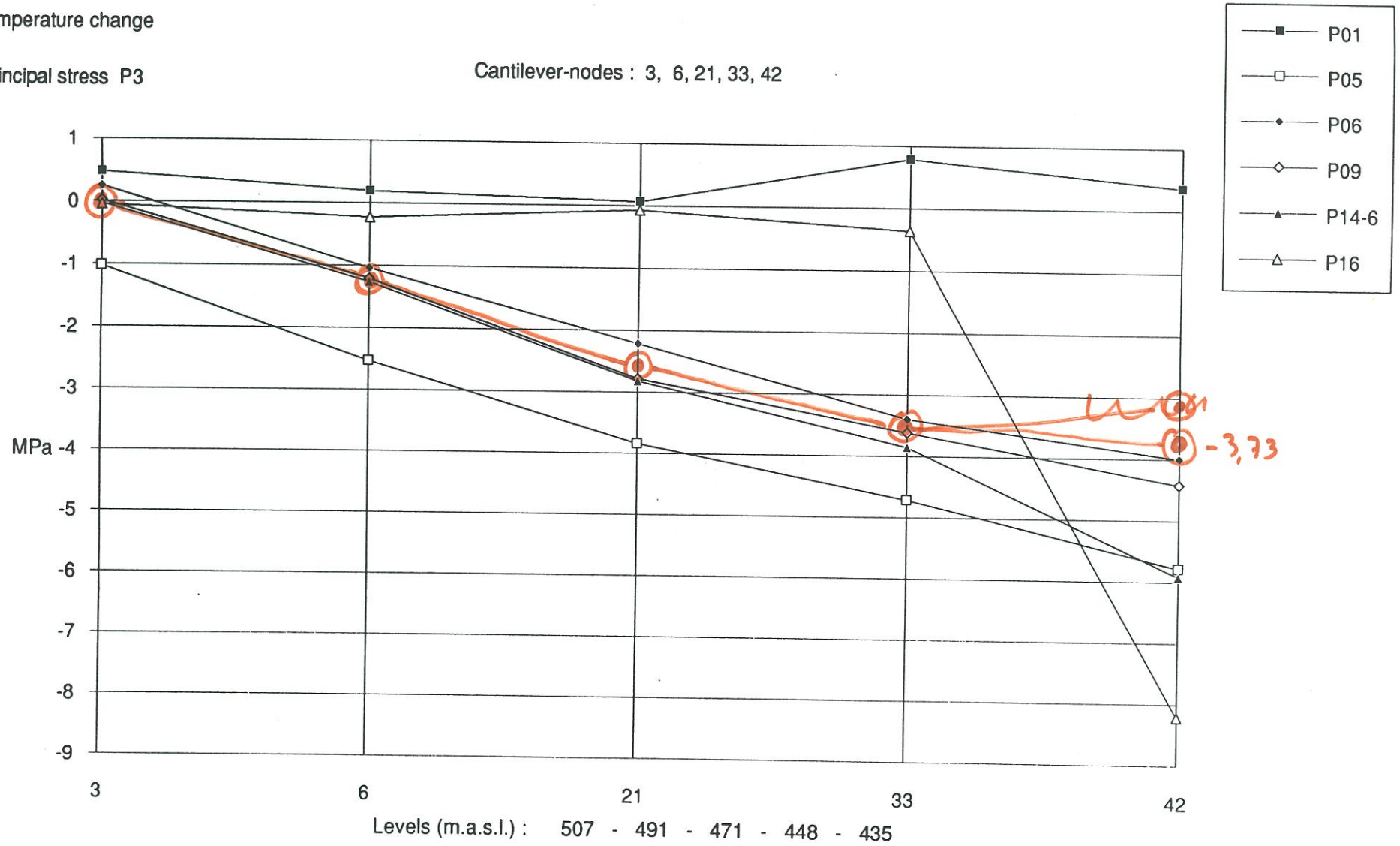

THERMAL PERIODIC ANALYSIS

SUMMARY OF COMPARISON OF THE RESULTS

- TEMPERATURES -

1D TH

THERMAL PERIODIC ANALYSIS Amplitude A (°C)							
node		P A R T I C I P A N T S					
	p01	p05	p09	p12	p14	p16	p17
1	9.943	10.000	10.000	6.900	10.000	10.000	10.000
2	9.943	10.000	10.000	6.900	10.000	10.000	10.000
3	9.943	10.000	10.000	6.900	10.000	10.000	10.000
4	5.620	6.990	7.630	6.900	8.790	7.629	9.490
5	5.620	6.990	7.646	6.900	9.090	7.633	9.730
6	5.620	5.870	5.856	5.900	5.890	5.856	7.160
7	5.620	5.870	5.841	5.900	5.870	5.841	7.160
8	5.620	5.630	5.728	5.900	5.760	5.728	7.150
9	5.620	5.630	5.630	5.900	5.640	5.630	7.130
10	5.620	5.630	5.682	5.900	5.740	5.693	7.060
11	3.481	3.600	3.752	3.900	3.790	3.750	7.120
12	3.481	3.600	3.740	3.900	3.780	3.742	7.130
13	3.481	3.600	3.683	3.900	3.710	3.681	7.140
14	3.481	3.600	4.134	3.900	4.150	4.121	7.460
15	1.774	1.780	1.853	2.100	2.080	1.852	7.150
16	1.774	1.780	1.895	2.100	2.050	1.873	7.160
17	1.774	1.780	2.224	2.100	2.280	2.209	7.440
18	1.584	1.260	1.733	1.400	1.870	1.702	7.830
19	1.584	1.260	1.674	1.400	1.830	1.676	7.810
20	1.584	1.260	1.698	1.400	1.900	2.225	7.840

?

THERMAL PERIODIC ANALYSIS Phase f (rad)							
Node		P A R T I C I P A N T S					
	p01	p05	p09	p12	p14	p16	p17
1	0.000	0.000	0.000	0.350	0.000	0.000	0.000
2	0.000	0.000	0.000	0.350	0.000	0.000	0.000
3	0.000	0.000	0.000	0.350	0.000	0.000	0.000
4	-0.947	-0.624	-0.547	0.350	-0.500	-0.547	-0.030
5	-0.947	-0.624	-0.552	0.350	-0.500	-0.553	-0.020
6	-0.947	-0.925	-0.958	0.350	-1.000	-0.958	-0.190
7	-0.947	-0.925	-0.961	0.710	-1.000	-0.961	-0.190
8	-0.947	-0.968	-0.981	0.710	-1.000	-0.981	-0.190
9	-0.947	-0.968	-1.013	0.710	-1.000	-1.013	-0.190
10	-0.947	-0.968	-1.007	0.710	-1.000	-1.005	-0.200
11	-1.463	-1.442	-1.567	1.540	-1.600	-1.568	-0.190
12	-1.463	-1.442	-1.572	1.540	-1.600	-1.571	-0.190
13	-1.463	-1.442	-1.592	1.540	-1.600	-1.590	-0.190
14	-1.463	-1.442	-1.467	1.540	-1.500	-1.462	-0.160
15	-1.980	-1.872	-2.250	1.990	-2.200	-2.262	-0.190
16	-1.980	-1.872	-2.254	1.990	-2.200	-2.199	-0.190
17	-1.980	-1.872	-2.128	2.200	-2.100	-2.031	-0.170
18	-2.000	-2.044	-2.289	2.200	-2.200	-2.300	-0.130
19	-2.000	-2.044	-2.342	2.200	-2.200	-2.289	-0.140
20	-2.000	-2.044	-2.291	2.200	-2.200	-2.397	-0.130

THERMAL STEADY STATE ANALYSIS									
Temperature T(°C)									
node			P A R T I C I P A N T S						
	p01	p05	p06	p09	p10	p12	p14	p16	p17
1	0.015	0.015	0.015	0.015	0.015	0.013	0.015	0.015	0.015
2	0.015	0.015	0.015	0.015	0.015	0.013	0.015	0.015	0.015
3	0.015	0.015	0.015	0.015	0.015	0.013	0.015	0.015	0.015
4	0.012	0.013	0.015	0.014	0.014	0.013	0.015	0.014	0.014
5	0.012	0.013	0.015	0.014	0.014	0.013	0.015	0.014	0.014
6	0.012	0.012	0.012	0.012	0.012	0.013	0.012	0.012	0.012
7	0.012	0.012	0.012	0.012	0.012	0.013	0.012	0.012	0.012
8	0.012	0.012	0.012	0.012	0.012	0.013	0.012	0.012	0.012
9	0.012	0.012	0.012	0.012	0.012	0.013	0.012	0.012	0.012
10	0.012	0.012	0.012	0.012	0.012	0.013	0.012	0.012	0.012
11	0.012	0.012	0.012	0.012	0.012	0.013	0.012	0.012	0.012
12	0.012	0.012	0.012	0.012	0.012	0.013	0.012	0.012	0.012
13	0.012	0.013	0.012	0.012	0.012	0.013	0.012	0.012	0.012
14	0.012	0.013	0.013	0.013	0.013	0.013	0.013	0.013	0.013
15	0.012	0.012	0.012	0.012	0.012	0.013	0.012	0.012	0.012
16	0.012	0.012	0.012	0.012	0.012	0.013	0.012	0.012	0.012
17	0.012	0.012	0.013	0.013	0.013	0.013	0.013	0.013	0.013
18	0.013	0.013	0.013	0.013	0.013	0.013	0.013	0.013	0.013
19	0.013	0.013	0.013	0.013	0.013	0.013	0.013	0.013	0.013
20	0.013	0.013	0.013	0.013	0.013	0.013	0.013	0.013	0.013

THERMAL PERIODIC ANALYSIS
Amplitude A (°C)

SUMMARY OF THE COMPARISON OF THE RESULTS (s%=difference from best estimate)

NODE		0 <= s =< 2	2 < s =< 5	s > 5	TOTAL
1	Participants	6	0	1	7
	Participants (%)	85.71	0.00	14.29	100
2	Participants	6	0	1	7
	Participants (%)	85.71	0	14.29	100
3	Participants	6	0	1	7
	Participants (%)	85.71	0.00	14.29	100
4	Participants	2	0	5	7
	Participants (%)	28.57	0.00	71.43	100
5	Participants	2	0	5	7
	Participants (%)	28.57	0.00	71.43	100
6	Participants	5	1	1	7
	Participants (%)	71.43	14.29	14.29	100
7	Participants	5	1	1	7
	Participants (%)	71.43	14.29	14.29	100
8	Participants	5	1	1	7
	Participants (%)	71.43	14.29	14.29	100
9	Participants	5	1	1	7
	Participants (%)	71.43	14.29	14.29	100
10	Participants	4	2	1	7
	Participants (%)	57.14	28.57	14.29	100
11	Participants	3	2	2	7
	Participants (%)	42.86	28.57	28.57	100
12	Participants	3	2	2	7
	Participants (%)	42.86	28.57	28.57	100
13	Participants	3	1	3	7
	Participants (%)	42.86	14.29	42.86	100
14	Participants	3	0	4	7
	Participants (%)	42.86	0.00	57.14	100
15	Participants	2	2	3	7
	Participants (%)	28.57	28.57	42.86	100
16	Participants	2	0	5	7
	Participants (%)	28.57	0.00	71.43	100
17	Participants	2	1	4	7
	Participants (%)	28.57	14.29	57.14	100
18	Participants	2	0	5	7
	Participants (%)	28.57	0.00	71.43	100
19	Participants	2	0	5	7
	Participants (%)	28.57	0.00	71.43	100
20	Participants	1	0	6	7
	Participants (%)	14.29	0.00	85.71	100

THERMAL PERIODIC ANALYSIS
Phase f (rad)

SUMMARY OF THE COMPARISON OF THE RESULTS (s%=difference from best estimate)

NODE		0 <= s =< 2	2 < s =< 5	s > 5	TOTAL
1	Participants	7	0	0	7
	Participants (%)	100.00	0.00	0.00	100
2	Participants	7	0	0	7
	Participants (%)	100.00	0.00	0.00	100
3	Participants	7	0	0	7
	Participants (%)	100.00	0.00	0.00	100
4	Participants	2	0	5	7
	Participants (%)	28.57	0.00	71.43	100
5	Participants	2	0	5	7
	Participants (%)	28.57	0.00	71.43	100
6	Participants	3	2	2	7
	Participants (%)	42.86	28.57	28.57	100
7	Participants	3	2	2	7
	Participants (%)	42.86	28.57	28.57	100
8	Participants	4	1	2	7
	Participants (%)	57.14	14.29	28.57	100
9	Participants	3	1	3	7
	Participants (%)	42.86	14.29	42.86	100
10	Participants	3	1	3	7
	Participants (%)	42.86	14.29	42.86	100
11	Participants	2	1	4	7
	Participants (%)	28.57	14.29	57.14	100
12	Participants	3	0	4	7
	Participants (%)	42.86	0.00	57.14	100
13	Participants	3	0	4	7
	Participants (%)	42.86	0.00	57.14	100
14	Participants	4	1	2	7
	Participants (%)	57.14	14.29	28.57	100
15	Participants	2	1	4	7
	Participants (%)	28.57	14.29	57.14	100
16	Participants	2	1	4	7
	Participants (%)	28.57	14.29	57.14	100
17	Participants	2	1	4	7
	Participants (%)	28.57	14.29	57.14	100
18	Participants	2	1	4	7
	Participants (%)	28.57	14.29	57.14	100
19	Participants	1	1	5	7
	Participants (%)	14.29	14.29	71.43	100
20	Participants	1	1	5	7
	Participants (%)	14.29	14.29	71.43	100

THERMAL STEADY STATE ANALYSIS
Temperature T('C)

SUMMARY OF THE COMPARISON OF THE RESULTS (s%-difference from best estimate)

NODE		0 <= s =< 2	2 < s =< 5	s > 5	TOTAL
1	Participants	8	0	1	9
	Participants (%)	88.89	0.00	11.11	100
2	Participants	8	0	1	9
	Participants (%)	88.89	0.00	11.11	100
3	Participants	8	0	1	9
	Participants (%)	88.89	0.00	11.11	100
4	Participants	3	2	4	9
	Participants (%)	33.33	22.22	44.44	100
5	Participants	3	2	4	9
	Participants (%)	33.33	22.22	44.44	100
6	Participants	9	0	0	9
	Participants (%)	100.00	0.00	0.00	100
7	Participants	9	0	0	9
	Participants (%)	100.00	0.00	0.00	100
8	Participants	9	0	0	9
	Participants (%)	100.00	0.00	0.00	100
9	Participants	9	0	0	9
	Participants (%)	100.00	0.00	0.00	100
10	Participants	9	0	0	9
	Participants (%)	100.00	0.00	0.00	100
11	Participants	9	0	0	9
	Participants (%)	100.00	0.00	0.00	100
12	Participants	9	0	0	9
	Participants (%)	100.00	0.00	0.00	100
13	Participants	9	0	0	9
	Participants (%)	100.00	0.00	0.00	100
14	Participants	8	1	0	9
	Participants (%)	88.89	11.11	0.00	100
15	Participants	9	0	0	9
	Participants (%)	100.00	0.00	0.00	100
16	Participants	9	0	0	9
	Participants (%)	100.00	0.00	0.00	100
17	Participants	9	0	0	9
	Participants (%)	100.00	0.00	0.00	100
18	Participants	8	1	0	9
	Participants (%)	88.89	11.11	0.00	100
19	Participants	7	2	0	9
	Participants (%)	77.78	22.22	0.00	100
20	Participants	7	2	0	9
	Participants (%)	77.78	22.22	0.00	100

DYNAMIC ANALYSIS

FUNDAMENTAL FREQUENCIES

SUMMARY OF COMPARISON OF THE RESULTS

Table of frequency values (Hertz)															
Partic.:		p01	p02	p03	p05	p06	p07	p09	p10	p11	p12	p13	p14	p16	p17
Vib.shape:		1	Condition	3.5.1		Rigid	basement		without	water					
	freq														
	1	4,2510	4,2720	4,2960	4,2800	4,2961	4,3190	4,3000	4,3100	4,1750	4,3400	4,3100	4,3020	4,2990	4,3122
	2	4,4520	4,5520	4,5780	4,5600	4,5783	4,4590	4,5800	4,6000	4,4630	4,6200	4,5900	4,5780	4,5810	4,5936
	3	5,5780	5,6740	5,6980	5,6300	5,6985	5,7520	5,7000	5,6900	5,5110	5,7500	5,7200	5,7280	5,7010	5,7059
	4	6,5770	6,6400	6,7180	6,7800	6,7188	6,7800	6,7200	6,8600	6,5020	6,7300	6,7500	6,7110	6,7250	6,7437
	5	8,2820	8,4300	8,5880	8,6000	8,5881	8,6040	8,5900	8,7700	8,2190	8,5600	8,6100	8,6330	8,5970	8,5694
	6	8,9410	9,3010	9,3750	8,9700	9,3758	8,8680	9,3800	9,1900	8,9560	9,5300	9,4600	9,5480	9,3700	9,4161
		2	Condition	3.5.2		Flexible	basement		with	compressible		fluid			
	freq														
	1			3,5755			3,6210		3,1790	3,6180					3,5531
	2			3,7700			3,8120		3,4460	4,2910					3,7555
	3			5,1015			5,1650		4,6940	5,7300					5,0801
	4			6,0910			6,1670		5,3900	6,9680					6,0739
	5			6,4535			6,7640		5,7570	7,3620					6,4526
	6			7,4216			7,9500		6,0340	7,5910					7,4304
		3	Condition	3.5.2		Flexible	basement		with	incompressible		fluid			
	freq														
	1	3,5630	3,4490		3,6300	3,5757		3,6700		3,7120	3,4600	3,5800	3,5700		3,5598
	2	3,6960	3,7310		3,7600	3,7883		3,9100		3,9760	4,7400	3,7900	3,7980		3,7819
	3	5,0640	4,9270		5,1200	5,1166		5,1900		5,1300	7,2000	5,1400	5,1230		5,1031
	4	5,9520	5,8070		6,1200	6,0980		6,1700		6,0520	7,4800	6,1200	6,0750		6,0851
	5	6,8560	6,9000		6,8500	6,9056		7,1400		7,5090	8,5400	7,0300	7,3650		6,9329
	6	7,5250	7,4660		7,8300	7,8749		8,0100		7,8100	8,9200	7,8900	7,9260		7,8969

DYNAMIC ANALYSIS
FUNDAMENTAL FREQUENCIES - CONDITION 1
(Rigid base; no water)

SUMMARY OF THE COMPARISON OF THE RESULTS (s%=difference from best estimate)

FREQ.		0 =< s =< 2	2 < s =< 5	s > 5	TOTAL
1	Participants	13	1	0	14
	Participants(%)	92,86	7,14	0,00	100
2	Participants	11	3	0	14
	Participants(%)	78,57	21,43	0,00	100
3	Participants	12	2	0	14
	Participants(%)	85,71	14,29	0,00	100
4	Participants	11	3	0	14
	Participants(%)	78,57	21,43	0,00	100
5	Participants	11	3	0	14
	Participants(%)	78,57	21,43	0,00	100
6	Participants	10	3	1	14
	Participants(%)	71,43	21,43	7,14	100

DYNAMIC ANALYSIS
FUNDAMENTAL FREQUENCIES - CONDITION 2
(Flexible base; water level 491 m a.s.l. compressible fluid)

SUMMARY OF THE COMPARISON OF THE RESULTS (s%=difference from best estimate)

FREQ.		0 =< s =< 2	2 < s =< 5	s > 5	TOTAL
1	Participants	4	0	1	5
	Participants(%)	80,00	0,00	20,00	100
2	Participants	3	0	2	5
	Participants(%)	60,00	0,00	40,00	100
3	Participants	3	0	2	5
	Participants(%)	60,00	0,00	40,00	100
4	Participants	3	0	2	5
	Participants(%)	60,00	0,00	40,00	100
5	Participants	2	1	2	5
	Participants(%)	40,00	20,00	40,00	100
6	Participants	2	1	2	5
	Participants(%)	40,00	20,00	40,00	100

DYNAMIC ANALYSIS
FUNDAMENTAL FREQUENCIES - CONDITION 3
(Flexible base; water level 491 m.a.s.l. incompressible fluid)

SUMMARY OF THE COMPARISON OF THE RESULTS (s%-difference from best estimate)

FREQ.		0 =< s =< 2	2 < s =< 5	s > 5	TOTAL
1	Participants	6	4	0	10
	Participants(%)	60,00	40,00	0,00	100
2	Participants	6	3	1	10
	Participants(%)	60,00	30,00	10,00	100
3	Participants	8	1	1	10
	Participants(%)	80,00	10,00	10,00	100
4	Participants	7	1	2	10
	Participants(%)	70,00	10,00	20,00	100
5	Participants	6	1	3	10
	Participants(%)	60,00	10,00	30,00	100
6	Participants	7	1	2	10
	Participants(%)	70,00	10,00	20,00	100

DYNAMIC ANALYSIS FUNDAMENTAL FREQUENCIES			
SUMMARY OF THE COMPARISON OF THE RESULTS (s%=differ from best estimate)			
LOADS	$0 \leq s \leq 2$	$2 < s \leq 5$	$s > 5$
CONDITION 1	80,95	17.86	1,19
CONDITION 2	56,67	6,67	36,67
CONDITION 3	66,67	18,33	15,00

Condition 1 : Rigid base; no water.

Condition 2 : Flexible base; water level 491 m.a.s.l. compressible fuid

Condition 3 : Flexible base; water level 491 m.a.s.l. incompress. fluid

STATIC-THERMAL ANALYSIS

TABLES CONTAINING THE COMPLETE SET OF DIFFERENT RESULTS

	Dead weight			Displacement DX							
node	P04	P05	P06	P07	P09			P14-2	P14-6	P16	P17
1	0,7800	0,6660	0,8184	0,8020	0,8190			0,8000	0,6000	0,8210	0,5710
2	0,7900	0,6820	0,8333	0,8170	0,8340			0,8000	0,7000	0,8360	0,5860
3	0,8100	0,6980	0,8489	0,8320	0,8490			0,8000	0,7000	0,8510	0,6020
4	-0,6190	-0,6500	-0,5869	-0,5800	-0,5900			-0,6000	-0,7000	-0,5800	-0,7500
5	-0,6100	-0,6400	-0,5779	-0,5700	-0,5800			-0,6000	-0,7000	-0,5800	-0,7400
6	-0,5980	-0,6300	-0,5653	-0,5600	-0,5600			-0,6000	-0,7000	-0,5600	-0,7300
7	-0,5770	-0,5900	-0,5461	-0,5400	-0,5500			-0,5000	-0,7000	-0,5400	-0,7000
8	-0,5710	-0,5800	-0,5397	-0,5300	-0,5400			-0,5000	-0,7000	-0,5400	-0,6900
9	-0,5620	-0,5700	-0,5294	-0,5200	-0,5300			-0,5000	-0,7000	-0,5300	-0,6800
10	-0,2300	-0,1900	-0,2153	-0,2100	-0,2200			-0,2000	-0,3000	-0,2100	-0,2700
11	-0,2420	-0,1900	-0,2254	-0,2200	-0,2300			-0,2000	-0,3000	-0,2200	-0,2800
12	-0,2460	-0,2000	-0,2285	-0,2200	-0,2300			-0,2000	-0,3000	-0,2300	-0,2900
13	-0,0614	-0,0840	-0,0673	-0,0660	-0,0670			-0,1000	-0,1000	-0,0680	-0,0550
14	-0,0463	-0,0530	-0,0485	-0,0480	-0,0490			0,0000	0,0000	-0,0490	-0,0370
15	-0,0216	-0,0220	-0,0191	-0,0190	-0,0190			0,0000	0,0000	-0,0200	-0,0100
16	-0,1480	-0,1300	-0,1461	-0,1400	-0,1500			-0,1000	-0,2000	-0,1500	-0,1500
17	-0,1400	-0,1100	-0,1357	-0,1300	-0,1400			-0,1000	-0,1000	-0,1400	-0,1300
18	-0,1150	-0,0880	-0,1101	-0,1100	-0,1100			-0,1000	-0,1000	-0,1100	-0,1000
19	-1,3950	-1,3300	-1,3601	-1,3400	-1,3600			-1,4000	-1,5000	-1,3600	-1,4700
20	-1,3970	-1,3200	-1,3618	-1,3400	-1,3600			-1,4000	-1,5000	-1,3600	-1,4800
21	-1,3780	-1,3100	-1,3439	-1,3200	-1,3400			-1,3000	-1,5000	-1,3400	-1,4600
22	-1,2910	-1,2100	-1,2616	-1,2400	-1,2600			-1,3000	-1,4000	-1,2600	-1,3600
23	-1,3000	-1,2100	-1,2705	-1,2500	-1,2700			-1,3000	-1,4000	-1,2700	-1,3700
24	-1,2880	-1,2100	-1,2589	-0,0840	-1,2600			-1,3000	-1,4000	-1,2600	-1,3600
25	-0,4930	-0,5000	-0,5830	-0,5700	-0,5800			-0,6000	-0,7000	-0,5800	-0,6100
26	-0,5170	-0,5400	-0,6257	-0,6100	-0,6300			-0,6000	-0,7000	-0,6200	-0,6600
27	-0,4750	-0,5800	-0,6542	-0,6400	-0,6500			-0,7000	-0,8000	-0,6500	-0,7000
28	-0,0678	-0,0420	-0,0658	-0,0650	-0,0660			-0,1000	-0,1000	-0,0650	-0,0590
29	-0,1010	-0,0720	-0,0999	-0,0980	-0,1000			-0,1000	-0,1000	-0,1000	-0,1100
30	-0,1400	-0,1000	-0,1340	-0,1300	-0,1300			-0,1000	-0,2000	-0,1300	-0,1400
31	-0,6460	-0,5900	-0,6385	-0,6300	-0,6400			-0,6000	-0,8000	-0,6400	-0,7000
32	-0,6410	-0,5200	-0,6226	-0,6100	-0,6200			-0,6000	-0,7000	-0,6200	-0,6700
33	-0,6230	-0,4500	-0,6004	-0,5900	-0,6000			-0,6000	-0,7000	-0,6000	-0,6200
34	-0,5340	-0,4600	-0,5298	-0,5200	-0,5300			-0,5000	-0,6000	-0,5300	-0,5800
35	-0,5350	-0,4200	-0,5261	-0,5200	-0,5300			-0,5000	-0,6000	-0,5300	-0,5700
36	-0,5320	-0,3900	-0,5149	-0,5100	-0,5100			-0,5000	-0,6000	-0,5100	-0,5400
37	-0,0043	0,0459	0,0021	0,0022	0,0019			0,0000	0,0000	0,0019	0,0350
38	-0,0504	-0,0210	-0,0540	-0,0530	-0,0540			-0,1000	-0,1000	-0,0540	-0,0660
39	-0,1270	-0,0880	-0,1180	-0,1200	-0,1200			-0,1000	-0,1000	-0,1200	-0,1200
40	-0,0085	0,0768	0,0073	0,0070	0,0073			0,0000	0,0000	0,0073	0,0514
41	-0,0129	0,0175	0,0011	0,0010	0,0012			0,0000	0,0000	0,0012	-0,0160
42	-0,0719	-0,0420	-0,0534	-0,0520	-0,0530			-0,1000	-0,1000	-0,0530	-0,0610

	Dead weight			Displacement DY							
node	P04	P05	P06	P07	P09			P14-2	P14-6	P16	P17
1	0,0000	0,0000	0,0000	-0,0004	0,0000			0,0000	0,0000	0,0000	0,0000
2	0,0000	0,0000	0,0000	-0,0006	0,0000			0,0000	0,0000	0,0000	0,0000
3	0,0000	0,0000	0,0000	-0,0007	0,0000			0,0000	0,0000	0,0000	0,0000
4	0,0000	0,0000	0,0000	-0,0001	0,0000			0,0000	0,0000	0,0000	0,0000
5	0,0000	0,0000	0,0000	-0,0002	0,0000			0,0000	0,0000	0,0000	0,0000
6	0,0000	0,0000	0,0000	-0,0004	0,0000			0,0000	0,0000	0,0000	0,0000
7	0,1620	-0,1300	-0,1444	-0,1400	-0,1400			-0,1000	-0,1000	-0,1400	-0,1300
8	0,1770	-0,1500	-0,1595	-0,1600	-0,1600			-0,2000	-0,2000	-0,1600	-0,1500
9	0,1930	-0,1800	-0,1756	-0,1700	-0,1800			-0,2000	-0,2000	-0,1800	-0,1800
10	0,4310	-0,4000	-0,4164	-0,4100	-0,4200			-0,4000	-0,4000	-0,4200	-0,4100
11	0,4640	-0,4400	-0,4488	-0,4400	-0,4500			-0,4000	-0,5000	-0,4500	-0,4600
12	0,5000	-0,4800	-0,4843	-0,4800	-0,4800			-0,5000	-0,5000	-0,4800	-0,5000
13	0,5020	-0,4600	-0,4802	-0,4700	-0,4800			-0,5000	-0,5000	-0,4800	-0,5100
14	0,4710	-0,4200	-0,4508	-0,4400	-0,4500			-0,5000	-0,5000	-0,4500	-0,4900
15	0,4480	-0,3900	-0,4293	-0,4200	-0,4300			-0,4000	-0,5000	-0,4300	-0,4700
16	0,1880	-0,1600	-0,1771	-0,1700	-0,1800			-0,2000	-0,2000	-0,1800	-0,1900
17	0,1530	-0,1300	-0,1444	-0,1400	-0,1400			-0,1000	-0,2000	-0,1400	-0,1600
18	0,1190	-0,1000	-0,1139	-0,1100	-0,1100			-0,1000	-0,1000	-0,1100	-0,1200
19	0,0000	0,0000	0,0000	0,0002	0,0000			0,0000	0,0000	0,0000	0,0000
20	0,0000	0,0000	0,0000	0,0001	0,0000			0,0000	0,0000	0,0000	0,0000
21	0,0000	0,0000	0,0000	-0,0001	0,0000			0,0000	0,0000	0,0000	0,0000
22	-0,1100	0,1190	0,1097	0,1080	0,1100			0,1000	0,1000	0,1100	0,1240
23	0,0670	0,0663	0,0678	0,0666	0,0678			0,1000	0,1000	0,0677	0,0775
24	-0,0210	0,0139	0,0230	0,1600	0,0231			0,0000	0,0000	0,0229	0,0273
25	0,2090	0,1010	0,1099	0,1080	0,1100			0,1000	0,1000	0,1100	0,1270
26	0,3000	0,0139	0,0260	0,0254	0,0261			0,0000	0,0000	0,0260	0,0337
27	0,0917	-0,0730	-0,0721	-0,0710	-0,0720			-0,1000	-0,1000	-0,0720	-0,0690
28	0,0824	-0,0660	-0,0742	-0,0730	-0,0740			-0,1000	-0,1000	-0,0740	-0,0800
29	0,0996	-0,0710	-0,0944	-0,0930	-0,0940			-0,1000	-0,1000	-0,0940	-0,1000
30	0,1070	-0,0760	-0,1014	-0,1000	-0,1000			-0,1000	-0,1000	-0,1000	-0,1000
31	0,0000	0,0000	0,0000	0,0003	0,0000			0,0000	0,0000	0,0000	0,0000
32	0,0000	0,0000	0,0000	0,0002	0,0000			0,0000	0,0000	0,0000	0,0000
33	0,0000	0,0000	0,0000	0,0001	0,0000			0,0000	0,0000	0,0000	0,0000
34	-0,1100	0,1250	0,1199	0,1180	0,1200			0,1000	0,1000	0,1200	0,1330
35	-0,0500	0,0462	0,0541	0,0532	0,0541			0,1000	0,1000	0,0541	0,0604
36	0,0197	-0,0330	-0,0096	-0,0094	-0,0096			0,0000	0,0000	-0,0095	-0,0140
37	-0,0450	0,0530	0,0583	0,0575	0,0584			0,1000	0,1000	0,0586	0,0594
38	0,0230	0,0014	-0,0217	-0,0210	-0,0220			0,0000	0,0000	-0,0220	-0,0210
39	0,0804	-0,0500	-0,0668	-0,0660	-0,0670			-0,1000	-0,1000	-0,0670	-0,0740
40	0,0000	0,0001	0,0000	0,0002	0,0000			0,0000	0,0000	0,0000	0,0000
41	0,0000	0,0001	0,0000	0,0002	0,0000			0,0000	0,0000	0,0000	0,0003
42	0,0000	0,0000	0,0000	0,0001	0,0000			0,0000	0,0000	0,0000	0,0011

	Dead weight			Displacement DZ						
node	P04	P05	P06	P07	P09			P14-2	P14-6	P16	P17
1	-3,0300	-2,8400	-2,9751	-2,9200	-2,9800			-3,0000	-3,1000	-2,9700	-3,0100
2	-3,2400	-3,0500	-3,1889	-3,1300	-3,1900			-3,2000	-3,3000	-3,1900	-3,2100
3	-3,4600	-3,2500	-3,4027	-3,3400	-3,4000			-3,4000	-3,5000	-3,4000	-3,4100
4	-2,4900	-2,3000	-2,4103	-2,3700	-2,4100			-2,4000	-2,5000	-2,4100	-2,4700
5	-2,7200	-2,5400	-2,6454	-2,6000	-2,6500			-2,6000	-2,8000	-2,6400	-2,6900
6	-2,9700	-2,7700	-2,8975	-2,8400	-2,9000			-2,9000	-3,0000	-2,9000	-2,9300
7	-2,3800	-2,2200	-2,3197	-2,2800	-2,3200			-2,3000	-2,4000	-2,3200	-2,3700
8	-2,6100	-2,4500	-2,5550	-2,5100	-2,5500			-2,6000	-2,7000	-2,5500	-2,6000
9	-2,8700	-2,6800	-2,8090	-2,7600	-2,8100			-2,8000	-2,9000	-2,8100	-2,8400
10	-1,7400	-1,6100	-1,7015	-1,6700	-1,7000			-1,7000	-1,8000	-1,7000	-1,7400
11	-1,9800	-1,8500	-1,9361	-1,9000	-1,9400			-1,9000	-2,0000	-1,9400	-1,9700
12	-2,2400	-2,0900	-2,1999	-2,1600	-2,2000			-2,2000	-2,3000	-2,2000	-2,2300
13	-0,8500	-0,7800	-0,8395	-0,8200	-0,8400			-0,8000	-0,9000	-0,8400	-0,8400
14	-1,0200	-0,9400	-1,0000	-0,9800	-1,0000			-1,0000	-1,1000	-1,0000	-1,0200
15	-1,2100	-1,0900	-1,1819	-1,1600	-1,1800			-1,2000	-1,2000	-1,1800	-1,2000
16	-0,4000	-0,3600	-0,3892	-0,3800	-0,3900			-0,4000	-0,4000	-0,3900	-0,3800
17	-0,4700	-0,4200	-0,4610	-0,4500	-0,4600			-0,5000	-0,5000	-0,4600	-0,4800
18	-0,5200	-0,4900	-0,5046	-0,5000	-0,5000			-0,5000	-0,5000	-0,5000	-0,5300
19	-2,2300	-2,1100	-2,1693	-2,1300	-2,1700			-2,2000	-2,3000	-2,1700	-2,2400
20	-2,2300	-2,1000	-2,1737	-2,1300	-2,1700			-2,2000	-2,3000	-2,1700	-2,2400
21	-2,2600	-2,1000	-2,2011	-2,1600	-2,2000			-2,2000	-2,3000	-2,2000	-2,2500
22	-2,1600	-2,0400	-2,1027	-2,0600	-2,1000			-2,1000	-2,2000	-2,1000	-2,1700
23	-2,1600	-2,0300	-2,1007	-2,0600	-2,1000			-2,1000	-2,2000	-2,1000	-2,1600
24	-2,1700	-2,0200	-2,1152	-0,7000	-2,1200			-2,1000	-2,2000	-2,1100	-2,1700
25	-1,6800	-1,5500	-1,6020	-1,5700	-1,6000			-1,6000	-1,7000	-1,6000	-1,6600
26	-2,0500	-1,5000	-1,5673	-1,5400	-1,5700			-1,6000	-1,6000	-1,5700	-1,6100
27	-1,4700	-1,4400	-1,4980	-1,4700	-1,5000			-1,5000	-1,6000	-1,5000	-1,5400
28	-0,8200	-0,7800	-0,8066	-0,7900	-0,8100			-0,8000	-0,8000	-0,8100	-0,8300
29	-0,8800	-0,7600	-0,8488	-0,8300	-0,8500			-0,8000	-0,9000	-0,8500	-0,8700
30	-0,7700	-0,7400	-0,7542	-0,7400	-0,7500			-0,8000	-0,8000	-0,7500	-0,7800
31	-2,1500	-2,0300	-2,0766	-2,0400	-2,0800			-2,1000	-2,2000	-2,0800	-2,1600
32	-1,7800	-1,6800	-1,7369	-1,7000	-1,7400			-1,7000	-1,9000	-1,7400	-1,8200
33	-1,5000	-1,3200	-1,4273	-1,4000	-1,4300			-1,4000	-1,5000	-1,4300	-1,4400
34	-2,0100	-1,9100	-1,9506	-1,9100	-1,9500			-2,0000	-2,1000	-1,9500	-2,0400
35	-1,7100	-1,5900	-1,6536	-1,6200	1,6500			-1,7000	-1,8000	-1,6500	-1,7300
36	-1,4100	-1,2800	-1,3548	-1,3300	-1,3500			-1,4000	-1,4000	-1,3500	-1,3800
37	-1,2200	-1,2000	-1,1989	-1,1800	-1,2000			-1,2000	-1,3000	-1,2000	-1,2600
38	-1,2500	-1,0900	-1,1856	-1,1600	-1,1900			-1,2000	-1,3000	-1,1900	-1,2300
39	-0,9800	-0,9700	-0,9477	-0,9300	-0,9500			-0,9000	-1,0000	-0,9500	-0,9800
40	-1,5000	-1,4400	-1,4842	-1,4600	-1,4800			-1,5000	-1,6000	-1,4800	-1,5700
41	-1,3600	-1,2600	-1,3167	-1,2900	-1,3200			-1,3000	-1,4000	-1,3200	-1,4000
42	-1,0000	-1,0800	-0,9767	-0,9600	-0,9800			-1,0000	-1,0000	-0,9800	-1,0300

		Dead weight			Principal stress P1							
node	P01		P05	P06	P07	P09			P14-2	P14-6	P16	P17
1	0,0410		-0,0094	0,0024	0,0182	0,0096			0,0000	0,0100	0,0024	-0,0006
2	0,0103		-0,0100	0,0025	0,0177	0,0029			0,0000	0,0000	0,0024	-0,0007
3	0,0521		-0,0106	0,0211	0,0172	0,0196			0,0200	0,0000	0,0210	-0,0008
4	0,0655		0,0170	0,0264	0,0934	0,0105			0,0300	0,0000	0,0265	0,0286
5	0,0045		0,0086	-0,0081	0,1630	0,0022			-0,0100	0,0000	-0,0081	0,0021
6	-0,0250		0,0002	-0,0090	0,2363	0,0027			-0,0100	0,0000	-0,0090	0,0013
7	0,0436		0,0482	0,0638	0,1069	0,0362			0,0600	0,0400	0,0639	0,0568
8	-0,0400		-0,0042	-0,0063	0,1893	0,0024			-0,0100	0,0000	-0,0063	0,0022
9	0,0498		0,0013	-0,0078	0,2743	0,0032			-0,0100	0,0000	-0,0079	0,0014
10	0,2090		0,2040	0,3234	0,1529	0,2978			0,3200	0,3000	0,3227	0,2874
11	0,0558		-0,0049	0,0163	0,3151	0,0079			0,0200	0,0100	0,0162	0,0088
12	0,0099		-0,0042	-0,0025	0,4777	0,0032			0,0000	0,0100	-0,0026	-0,0078
13	0,4200		0,2200	0,3588	0,2767	0,3395			0,3600	0,3000	0,3582	0,2519
14	0,1940		0,1257	0,1938	0,4676	0,2120			0,1900	0,1900	0,1934	0,2191
15	0,2000		0,1880	0,2105	0,6587	0,2141			0,2100	0,2500	0,2071	0,2269
16	0,4720		0,3280	0,4720	0,3458	0,5625			0,4700	0,6600	0,4214	0,3268
17	0,2730		-0,0368	0,2936	0,4891	0,3204			0,2900	0,3000	0,2944	0,2483
18	0,1340		0,0064	0,1488	0,6438	0,1888			0,1500	0,1300	0,1615	0,1216
19	0,2420		0,2750	0,2715	0,3620	0,2783			0,2700	0,3000	0,2717	0,2962
20	0,0373		-0,0047	0,0809	0,5202	0,0614			0,0800	0,0900	0,0808	0,0887
21	-0,0039		-0,0098	-0,0231	0,6837	-0,0223			-0,0200	-0,0100	-0,0231	-0,0136
22	0,2740		0,2760	0,2865	0,3868	0,2928			0,2900	0,3100	0,2860	0,3045
23	0,1310		-0,0059	0,0954	0,5440	0,0773			0,1000	0,1000	0,0952	0,1031
24	-0,0360		-0,0112	-0,0168	0,5354	-0,0177			-0,0200	0,0100	-0,0167	-0,0140
25	0,2890		0,2260	0,2428	0,5240	0,2554			0,2400	0,2500	0,2459	0,2435
26	0,1500		0,1710	0,1481	0,6547	0,1564			0,1500	0,1700	0,1474	0,1732
27	0,0531		0,1160	0,0757	0,7878	0,0647			0,0800	0,1000	0,0728	0,0921
28	0,1130		1,2900	0,1008	0,6016	0,1740			0,1000	-0,0400	0,1004	0,0654
29	0,1470		1,0870	0,1774	0,6539	0,1804			0,1800	0,2100	0,1652	0,1621
30	0,2700		0,8840	0,3023	0,7244	0,3296			0,3000	0,4400	0,2774	0,2093
31	0,0897		0,1630	0,1227	0,7483	0,1902			0,1200	0,2100	0,1235	0,1746
32	0,0049		0,1630	0,0002	0,7209	0,0221			0,0000	0,0700	0,0012	0,0608
33	-0,1000		0,1630	-0,0880	0,6943	-0,0121			-0,0900	-0,2400	-0,0878	0,1377
34	0,1160		0,1670	0,1177	0,7619	0,1665			0,1200	0,1800	0,1182	0,1936
35	-0,0210		0,1640	-0,0072	0,7257	0,0167			-0,0100	0,0600	-0,0070	0,0732
36	-0,0690		0,1610	-0,0593	0,6919	-0,0022			-0,0600	-0,1500	-0,0596	0,1100
37	-0,0960		2,1300	-0,1294	0,8460	-0,0148			-0,1300	-0,5300	-0,1204	-0,1441
38	-0,0150		1,8450	-0,0016	0,7512	-0,0145			0,0000	0,0300	-0,0132	0,0702
39	0,1290		1,5600	0,1676	0,6743	0,4759			0,1700	0,4100	0,1381	0,1436
40	-0,2200		-0,1010	-0,3029	0,9031	-0,1906			-0,3000	-0,8500	-0,3010	-0,2296
41	-0,2200		-0,0988	-0,2524	0,6927	-0,2343			-0,2500	-0,1000	-0,2514	-0,0938
42	0,1270		-0,0965	0,1776	0,4957	0,5086			0,1800	-0,1300	0,1763	-0,0801

		Dead weight			Principal stress P2							
node	P01		P05	P06	P07	P09			P14-2	P14-6	P16	P17
1	-0,0120		-0,0860	-0,0164	-0,0246	-0,0151			-0,0200	0,0000	-0,0164	-0,0650
2	-0,0130		-0,1010	-0,0110	-0,0242	0,0022			-0,0100	-0,0100	-0,0110	-0,0495
3	-0,0680		-0,1160	-0,0104	-0,0238	-0,0038			-0,0100	-0,0100	-0,0105	-0,0424
4	-0,1200		-0,0298	-0,0373	-0,0111	-0,0459			-0,0400	-0,0100	-0,0373	-0,0401
5	-0,2800		-0,2689	-0,3070	-0,0172	-0,2987			-0,3100	-0,3100	-0,3069	-0,3005
6	-0,4400		-0,5080	-0,5156	-0,0220	-0,5058			-0,5200	-0,5100	-0,5157	-0,4880
7	-0,0540		-0,0096	-0,0210	-0,0326	-0,0185			-0,0200	0,0000	-0,0209	-0,0175
8	-0,2600		-0,1964	-0,2561	-0,0530	-0,2555			-0,2600	-0,2600	-0,2561	-0,2503
9	-0,3900		-0,4410	-0,4526	-0,0692	-0,4452			-0,4500	-0,4500	-0,4526	-0,4435
10	-0,0430		-0,0056	-0,0164	0,0566	-0,0126			-0,0200	0,0100	-0,0165	-0,0068
11	0,0341		-0,1345	-0,0386	0,0111	-0,0401			-0,0400	-0,0400	-0,0387	-0,0362
12	-0,1800		-0,1320	-0,1674	-0,0206	-0,1706			-0,1700	-0,1600	-0,1668	-0,1616
13	0,1630		0,0633	0,1713	0,1370	0,1883			0,1700	0,1400	0,1721	0,1361
14	0,0168		0,0025	-0,0067	0,1336	0,0194			-0,0100	-0,0100	-0,0080	-0,0137
15	-0,0150		0,0049	0,0144	0,1335	0,0404			0,0100	0,0200	0,0126	-0,0224
16	0,0649		-0,0800	0,1344	0,1674	0,2406			0,1300	0,0200	0,0904	0,0197
17	-0,1800		-0,1115	-0,1603	0,1825	-0,1558			-0,1600	-0,0800	-0,1648	-0,0448
18	-0,1600		-0,1150	-0,1687	0,1865	-0,1540			-0,1700	-0,1400	-0,1629	-0,1386
19	0,0967		0,0800	0,1202	0,0007	0,1292			0,1200	0,1200	0,1201	0,1108
20	-0,0490		-0,0440	-0,0029	0,0003	-0,0214			0,0000	-0,0200	-0,0029	-0,0138
21	-0,1900		-0,1680	-0,1589	-0,0001	-0,1554			-0,1600	-0,1500	-0,1592	-0,1553
22	0,0849		0,0344	0,0987	0,0267	0,1039			0,1000	0,0900	0,0985	0,0771
23	0,0333		-0,0488	-0,0021	0,0144	-0,0205			0,0000	-0,0300	-0,0023	-0,0145
24	-0,0970		-0,1320	-0,1397	-0,1242	-0,1377			-0,1400	-0,1300	-0,1397	-0,1346
25	0,1010		0,0327	0,1111	0,0851	0,0728			0,1100	0,0100	0,1120	-0,0009
26	0,0010		0,0246	0,0060	0,0789	0,0104			0,0100	-0,0300	0,0056	-0,0097
27	0,0149		0,0165	0,0308	0,0716	0,0336			0,0300	0,0600	0,0265	-0,0174
28	-0,1200		-0,1520	-0,1323	0,1220	-0,0360			-0,1300	-0,4700	-0,1252	-0,1762
29	-0,1800		-0,1615	-0,1950	0,1534	-0,2045			-0,2000	-0,1200	-0,1994	-0,0563
30	0,0479		-0,1710	-0,0001	0,1681	0,1794			0,0000	-0,1800	-0,0296	-0,1103
31	-0,0410		0,1110	-0,0482	0,0000	0,0716			-0,0500	-0,0300	-0,0489	0,0077
32	-0,0370		-0,0090	-0,0392	0,0000	0,0038			-0,0400	0,0300	-0,0398	0,0000
33	-0,1800		-0,1290	-0,1993	0,0000	-0,1826			-0,2000	-0,2500	-0,1989	-0,1194
34	-0,0650		0,1410	-0,0635	0,0141	0,0229			-0,0600	-0,0500	-0,0628	0,0187
35	-0,0580		0,0510	-0,0525	0,0137	-0,0318			-0,0500	0,0100	-0,0527	0,0034
36	-0,2200		-0,0390	-0,2134	0,0112	-0,2025			-0,2100	-0,2200	-0,2142	-0,1120
37	-0,3600		-0,3720	-0,3859	0,0476	-0,2783			-0,3900	-0,7600	-0,3700	-0,3529
38	-0,2600		-0,3050	-0,2432	0,0842	-0,2839			-0,2400	-0,1700	-0,2538	-0,1102
39	0,0192		-0,2380	0,0998	0,1038	0,2316			0,1000	-0,1600	0,0441	-0,0775
40	-0,3800		-0,2480	-0,4654	-0,0016	-0,3985			-0,4700	-0,9000	-0,4658	-0,3501
41	-0,3100		-0,2285	-0,3734	0,0000	-0,3184			-0,3700	-0,1900	-0,3738	-0,2286
42	-0,1300		-0,2090	-0,1265	-0,0025	-0,0700			-0,1300	-0,2500	-0,1263	-0,1382

FIRST BENCHMARK WORKSHOP

ON

NUMERICAL ANALYSIS OF DAMS

THEME A

LINEAR ELASTIC COMPUTATION OF A

DOUBLE CURVATURE CONCRETE ARCH DAM

Bergamo, May 28-29, 1991

Design tool for arch dams

presented by

Reinhard PROMPER
Tauernkraftwerke A.G.Salzurg
Austria

First Benchmark Workshop
on
Numerical analyses of dams

Bergamo(Italy)
May 28-29,1991

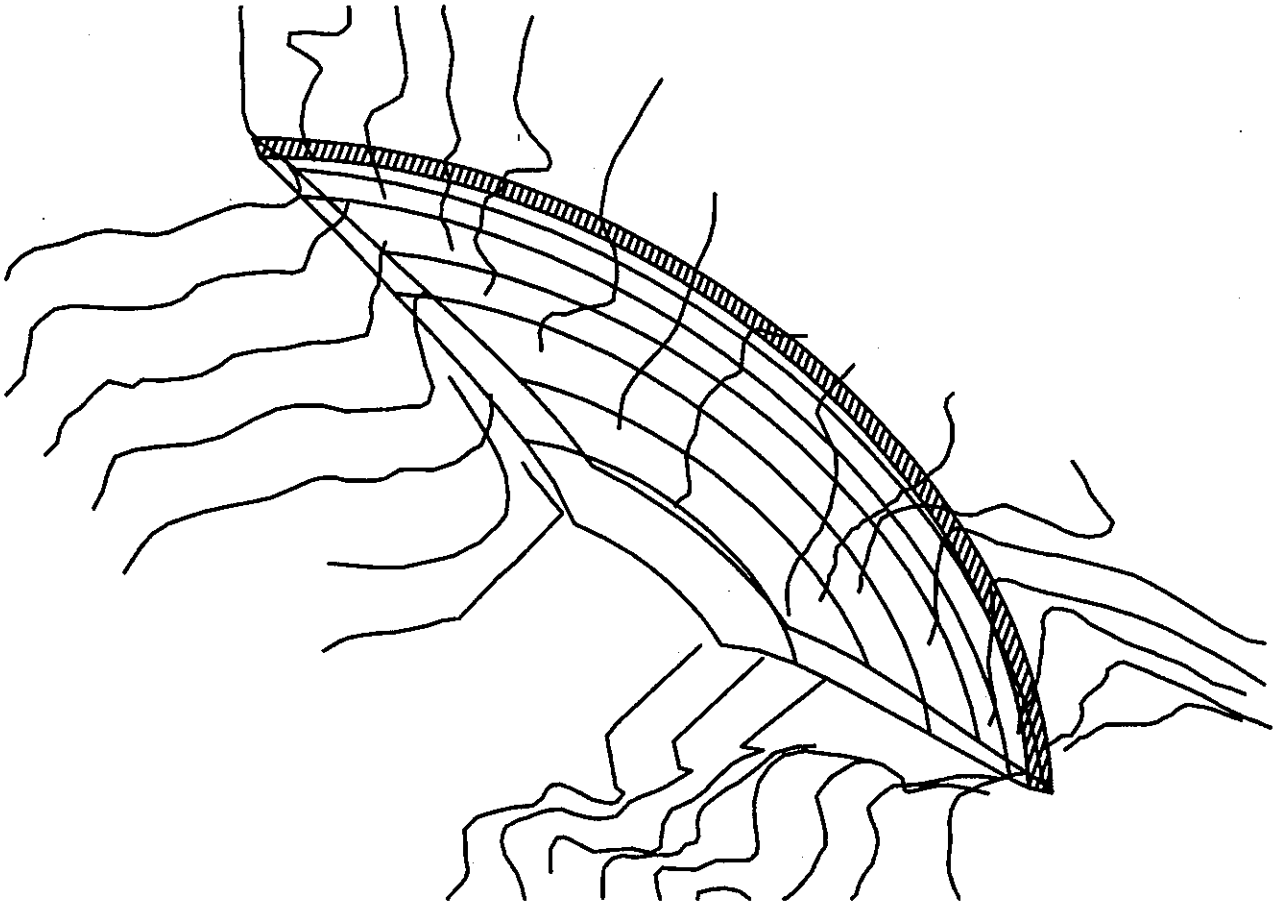

Introduction:

The U.S.Bureau of Reclamation has develloped the famed trial load method (TLM) of analyzing arch dams (1923)/1-3/. Since 1953 the TLM is supplemented by the FE-Method. In the year 1973 a geometrical parameter model was presented /4/ which was based on arces for the horizontal upstream and downstream boundaries of the cross sections. A finite element model was included /7-8/. 1961 a construction tool based on the TLM stresses with conical sections for the horicontal middle axis of the dam was developed by /5 u. 6/.
The new design tool CODCOD (Fig.1) includes now a parametric representation of the horizontal middle axis, with the connection to trial load method and FE-method. Different FE-Modelling tools are available (SDRC-IDEAS-Supertab, ADAP, FIN3D). The results for TLM, ADAP and FIN3D are reported in a identical curved coordinate system and can easily be compared in graphical and numerical form.

Dam Design Tool:

In order that results of different geometrical forms might be compared conveniently a parametrical representation is choosen. Different visualising possibilities are available:

- o ... Parametric diagram form.
- o ... CAD Model.

To put in a new geometry this uniform conical horizontal cross-sections have to be defined using various parameters (Cycles, Ellipses, Hyperboles).

This parameters can be shown in a diagram-form supporting the design by further simple evaluations.

The horizontal cross-sections are used as input for a CAD-Model.
Additional vertical sections are added to this model, which can be situated in the terrain.

Numerical Analyses of the Talvacchia Dam:

Shortform:

- o ... Theme A.
- o ... Type of Software: FEM and Trial Load Method.

The mesh is represented in two ways:

- o ... as MESH-ONE.GEO in symmetrical form and
- o ... as CODCOD geometrie in symmetrical form.

The CODCOD geometry is a good approximation to the given form. The differencies are be shown on Fig.2.
The rock foundation is simulated in the two cases in a very similar form, so that the differencies in the results can be neglected.

The two different computations based on the individual meshes can not be interpreted conveniently without further statements about the different fundamental ideas. To simplify the problem the stresses are shown in the same style due to the load cases "Dead weight" and "Hydrostatic pressure" (Fig.5 - 14). There are realy great differences on the upstream face of the middle cantilever (vertical tensile stresses). This results demonstrates that the influence of the stress distribution is dominating. Different programs act on different stress extrapolations and therefore results on the face can only be compared with the following assumptions:

- o ... Linear stress distribution in the cross section (thickness).
- o ... Integrationtechnic without hourglass effects.
- o ... The surface approximation in all points (not only boundaries) agrees with the geometrie.

Therefore a comparison of different programs with the same theoretical base have to agree in numerical sense. The differences are only situated in the integration technic and the stress extrapolation.

The usefulness of finite element programs in the construction state of a curved concrete dam depends on comparable stress presentation for a parametric study of the construction /9/.

This paper should familiarize you with the difficulties of the interpretation of the results. On the following pages the stress distribution are shown in graphical and numerical form in the middle point of each element.

The results in the form CODCOD have been compared with field messurements and laboratory tests namely on hard rock. In all cases a good agreement has been observed.

References:

/ 1/ UNITES STATES COMMITTEE (USCOLD) ON LARGE DAMS : Current unites states practice for numerical analysis of dams. Part 1. Feb. 1985

/ 2/ INTERNATIONAL COMMISSION ON LARGE DAMS: Report on design criteria.; ICOLD, Mai 1985

/ 3/ DESIGN OF ARCH DAMS: Design manual for concrete arch dams, A water resources technical publication; Bureau of reclamation, Denver Colorado,1977

/ 4/ CLOUGH R. & RAPHAEL J.M. & MOJTAHEDI S.: ADAP, A computer program for static and dynamic analyses of arch dams; U.S. Bureau of Reclamation, Denver, Colerado, EERC Report No. 73-14, June 1972.

/ 5/ WIDMANN R.: Zur Berechnung und wirtschaftlichen Formgebung von Bogengewichtsmauern; Österreichische Ingenieurzeitschrift, 4.Jahrg., Heft 8, p.274-280, 1961

/ 6/ WIDMANN, R.: Zum derzeitigen Stand der Theorie von Gewölbemauern; Österreichische Ingenieur-Zeitschrift, 8. Jahrg., Heft 1, p.18-22, 1965

/ 7/ INTERNATIONAL COMMISSION ON LARGE DAMS: Finite element methods in analysis and design of dams; ICOLD, Bulletin 30, Jänner 1978

/ 8/ MORROW POINT DAM AND POWERPLANT: A water resources technical publication, Technical record of design and construction; United states department of the interior bureau of reclamation, Denver Colorado, Sept. 1983

/ 9/ RESCHER O. J.: Geomechanische Modelluntersuchungen für die Gründung von Talsperren; Rock mechanics 14, 117-166 1981, Springer Verlag

CODCOD ... Construction Design and Computation of dams

CODCOD

CAD - Design

Numerical model for the dam
with convertion to a CADKEY-CAD Program
Graphical presentation of the parametermodel.
With it:
Direct construction in the building site.
Different views can be shown.
Output on plotters and printers
in induvidual layouts.
-
Numerical model for axes: conical sections
Numerical model for the survace : UPBS
Numerical model for the building site: Lines

Element grid

The elementgrid can describe the surface
with predefined precision.
Construction direct as a CAD-Model.
The foundation is generated autometicaly.
Connection of curved dam-elements
with linear foundation elements.
Grid refinement without deformed elements
(special connection method)

Computation with CAD-Model

Curved coordinate system on the surface.
Stresses stabalized by the form functions
and special numerical methods.
Special formed triangles
Computation effort equal trial load method
Precision controled by the residual load
vector and the condition number

Results

Stresses in the form of Trial Load Method
Curved coordinate system related to the dam
Triangle form of the numerical output.
Surface stresses upstream & downstream.
Induvidual views for the deformations.
Axionometrical representations.

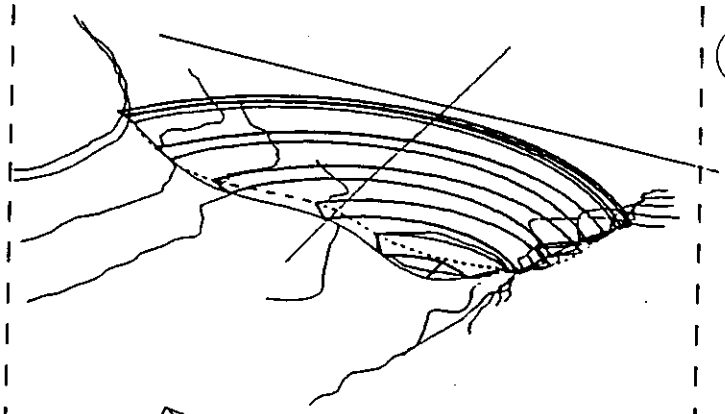

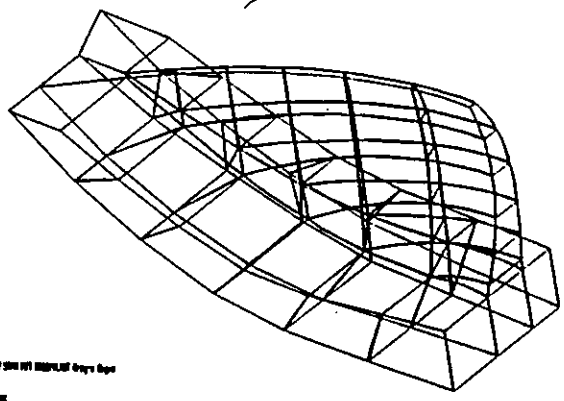

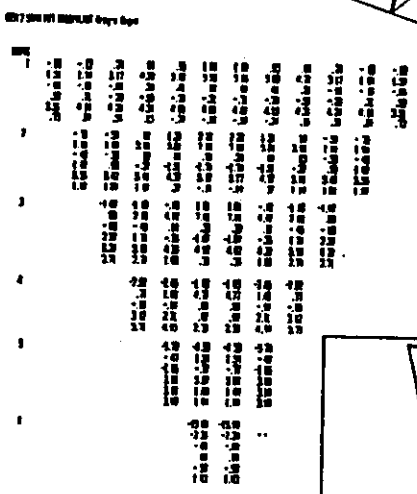

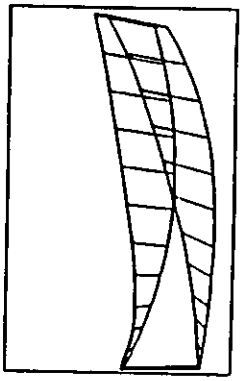

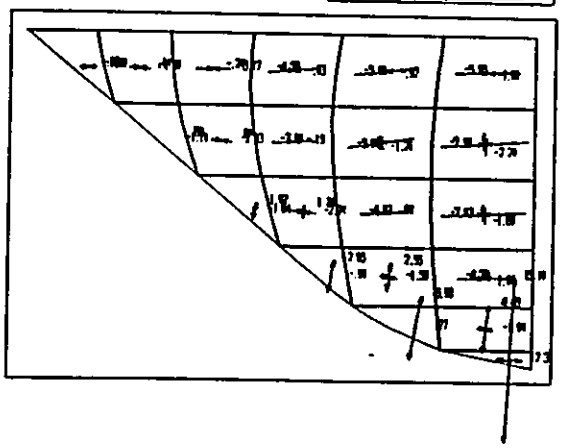

Fig. 1.

Fig. 2

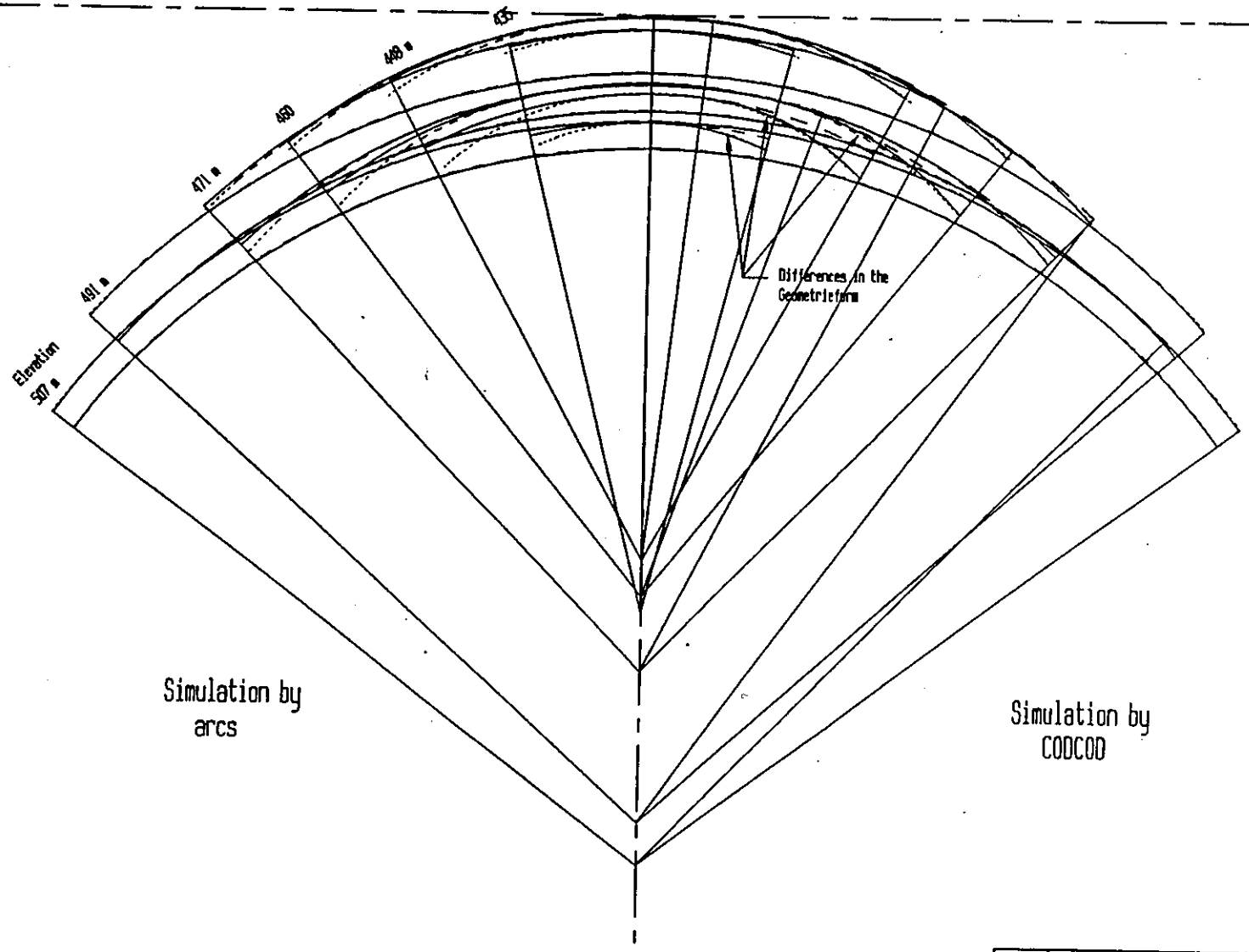

Titel	TALYACCHIA-DAM CODCOD with building form comparison Horizontal sections	Rev.
Scale	Date 10.1.91	Nr

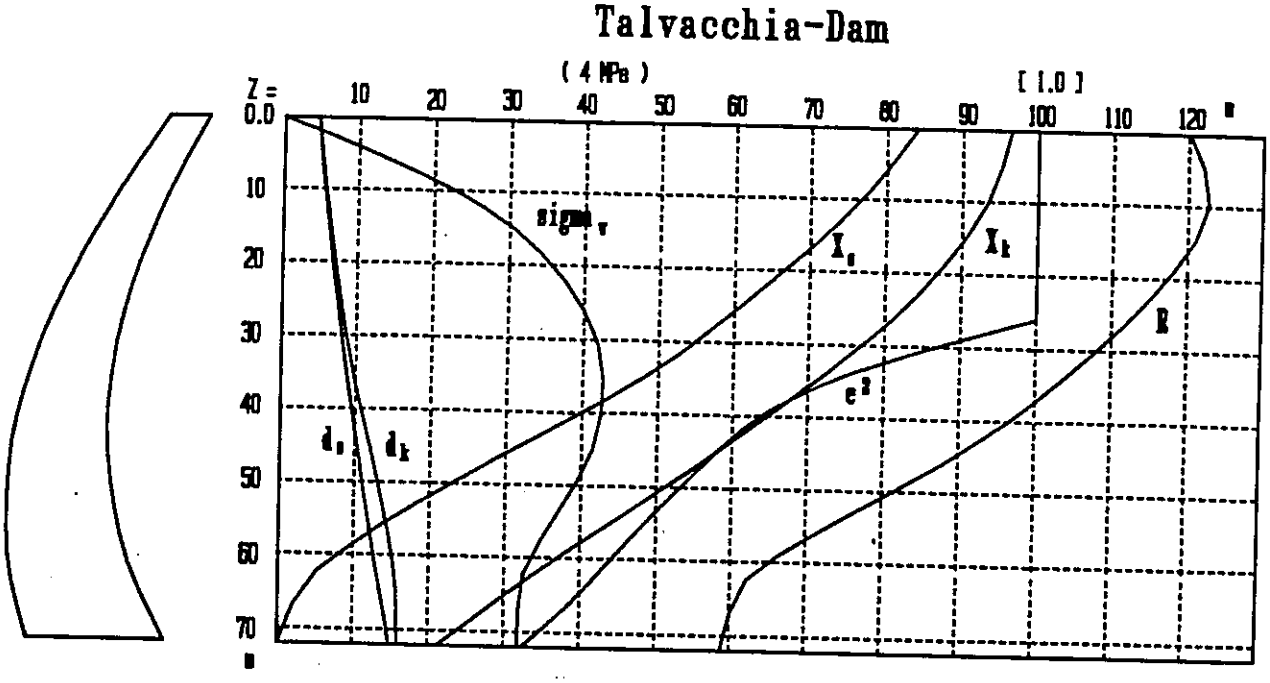

Parameter of the dam (conical form)

Fig. 3

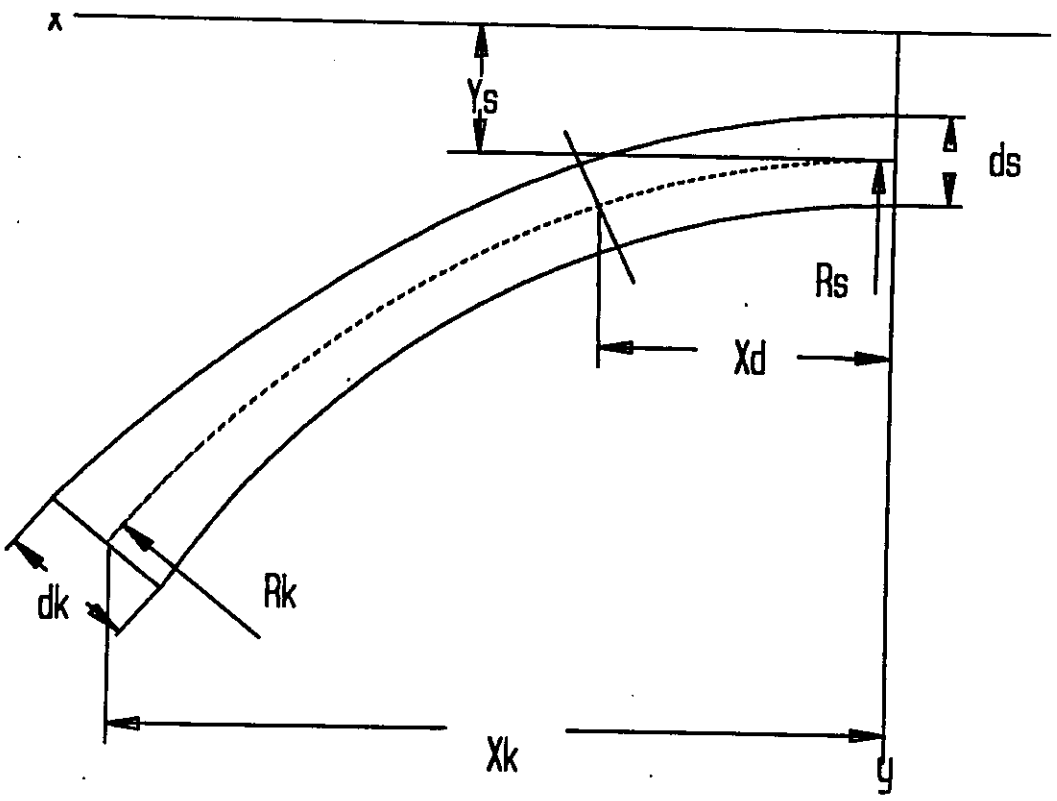

Definition of the parameters

Fig. 4

TALVACHIA-DAM

B E N C H M A R K W O R K S H O P

RESULTS: Principal stresses - upstream face
CASE : Gravity Load (unjointed dam)
PROGRAM: CODCOD

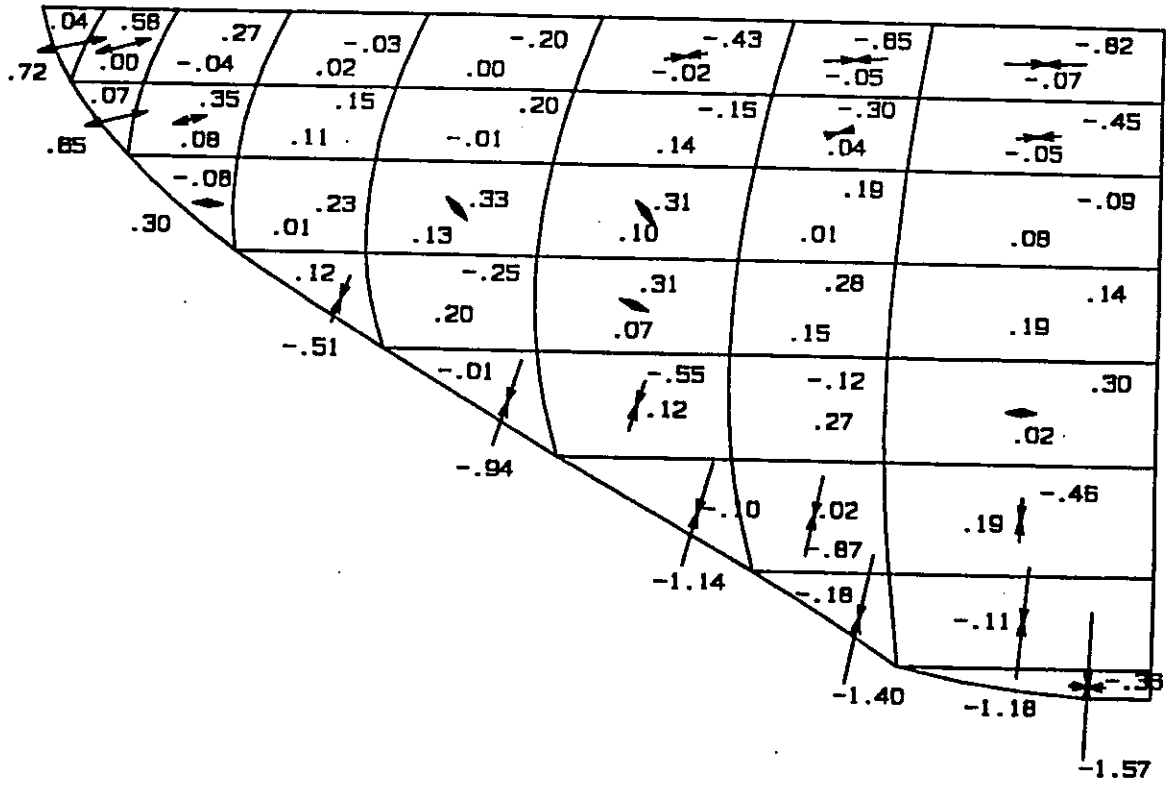

Principal stresses - upstream face

.72251	.58055	.26912	.01605	.00123	-.01584	-.04651	-.06913
.04480	.00387	-.04408	-.02863	-.20308	-.43273	-.64924	-.82303
13.20	16.13	21.98	38.80	-76.25	-81.66	-86.36	-89.11
	.65096	.34771	.15221	.20344	.14262	.03547	-.04813
	.06579	.07955	.11029	-.01063	-.14815	-.30127	-.44820
	15.25	15.38	-40.87	-59.12	-65.19	-75.64	-85.60
		.30162	.22871	.32628	.30736	.19010	.07609
		-.08204	.01269	.12988	.09988	.00941	-.09397
		-2.66	-27.87	-48.12	-53.04	-61.96	-80.00
			.12316	.20068	.30816	.28028	.19415
			-.51082	-.25392	.06812	.14976	.14322
			-20.87	-24.00	-23.53	-23.90	-19.46
σmax				-.00599	.12111	.26926	.30158
σmin				-.94122	-.55010	-.12240	.02445
α				-17.87	-17.24	-8.60	-2.21
					-.09634	.02094	.19001
					-1.14283	-.86807	-.46172
					-15.33	-11.79	-3.88
						-.18349	-.11051
						-1.40239	-1.18345
						-11.34	-4.99
							-.36397
							-1.56832
							-2.17

Fig. 5

TALVACHIA-DAM

B E N C H M A R K W O R K S H O P

RESULTS: Principal stresses - upstream face
CASE : Gravity Load (unjointed dam)
PROGRAM: FIN3D

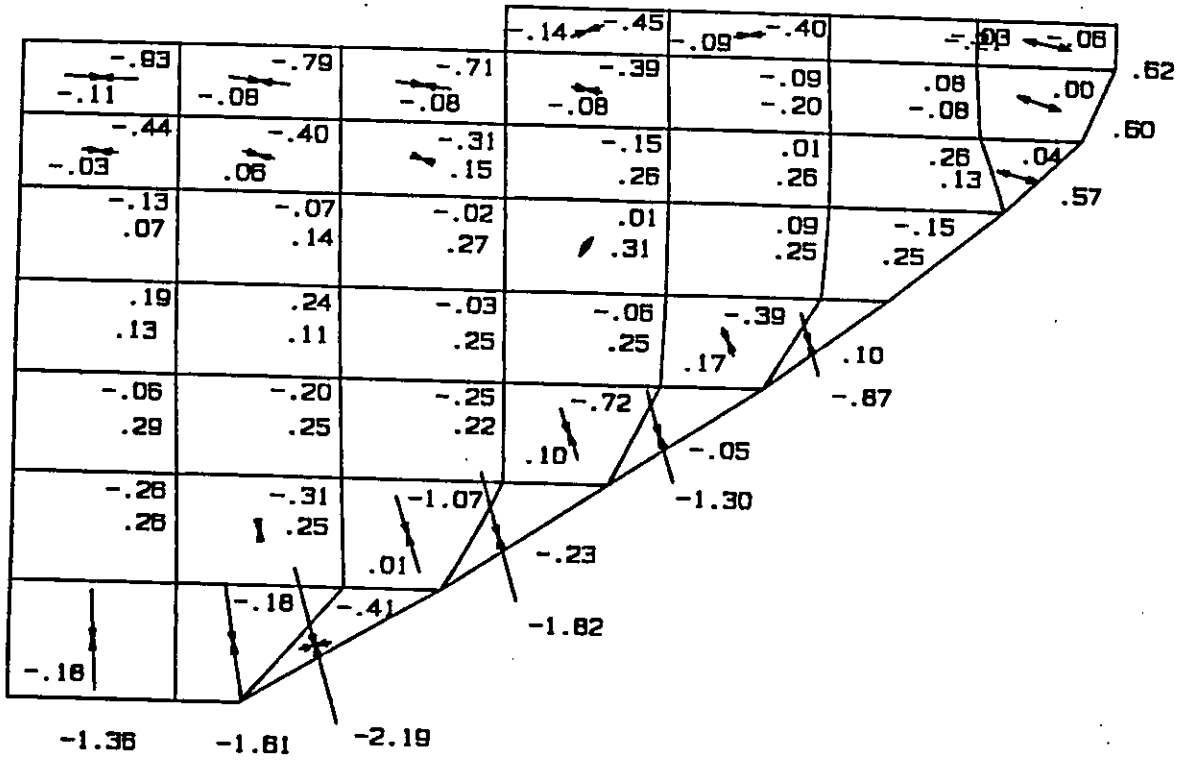

Principal stresses - upstream face

σmax (MPa)			-.08966	-.14001	-.02587	.62491
σmin (MPa)			-.44867	-.40312	-.20828	-.06263
α (°)			-68.00	-83.53	-41.05	-11.00
-.10860	-.08072	-.08294	-.08281	-.08636	.08302	.60311
-.93296	-.79138	-.70774	-.38984	-.19792	-.07873	-.00325
87.98	83.70	83.50	81.13	69.22	-24.56	-16.92
-.03249	.05532	.15146	.25713	.25745	.26126	.56966
-.44493	-.40377	-.30589	-.15231	.00902	.13311	.03613
86.04	76.78	71.39	70.78	73.51	-24.57	-14.92
.06650	.13944	.26650	.30669	.25243	.24999	
-.13404	-.07288	-.01805	.00807	.08729	-.15086	
80.96	66.17	61.28	56.38	51.71	13.16	
.18986	.23802	.24534	.24553	.17494	.09949	
.12843	.10953	-.03035	-.05735	-.39429	-.87223	
23.25	31.37	28.41	27.49	22.43	16.08	
.28505	.24944	.21793	.10235	-.05282		
-.05938	-.19601	-.24725	-.72190	-1.29731		
3.36	10.42	13.39	19.32	16.72		
.26429	.24662	.00599	-.22997			
-.26215	-.31390	-1.07272	-1.82315			
4.77	8.54	17.51	15.86			
.17610	-.17769	-.41369				
-1.36252	-1.60614	-2.18532				
2.72	8.54	15.80				

Fig. 6

TALVACHIA-DAM

B E N C H M A R K W O R K S H O P

RESULTS: Principal stresses - downstream face
CASE : Gravity Load (unjointed dam)
PROGRAM: CODCOD

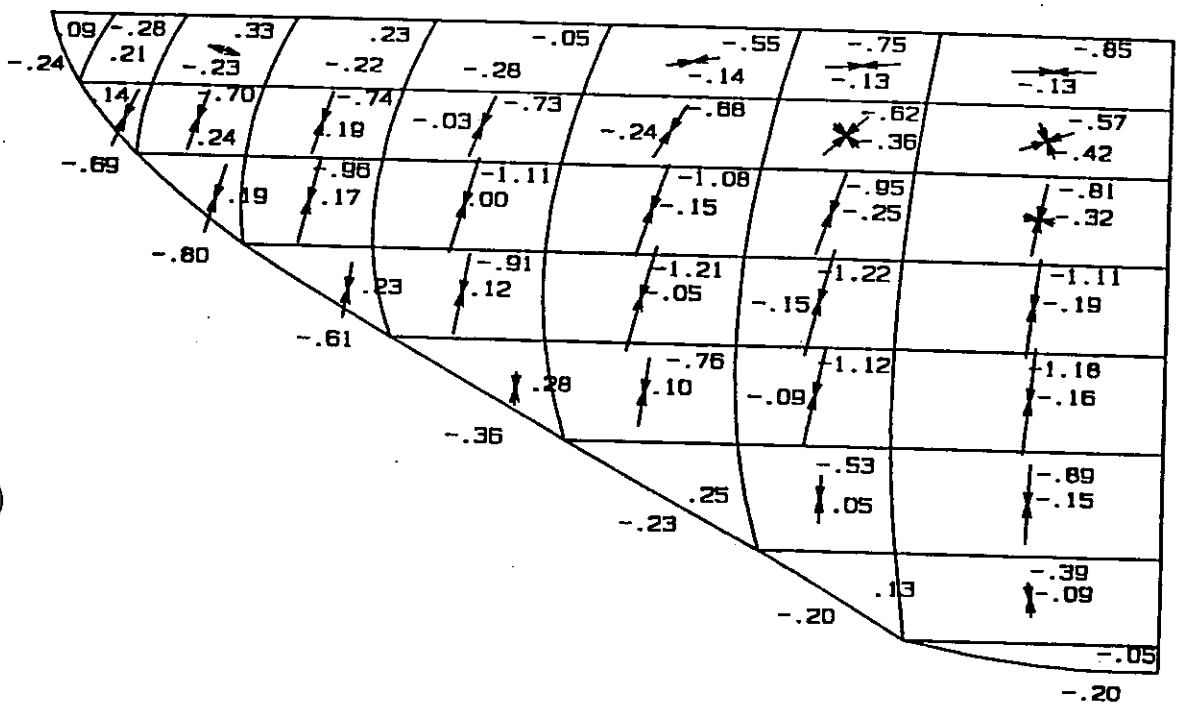

Principal stresses - downstream face

.08964	.20548	.32947	.23132	-.05124	-.13809	-.13453	-.12622
-.24392	-.28143	-.22903	-.22019	-.27581	-.54570	-.75119	-.85057
-25.56	-23.20	-17.92	-20.11	-45.46	-79.18	-85.61	-88.54
	.13915	.23892	.19015	-.02663	-.24255	-.35980	-.41571
	-.68561	-.70384	-.73755	-.72812	-.67744	-.62456	-.57214
	-22.62	-17.47	-17.05	-21.05	-30.15	-44.73	-68.41
		.18699	.17377	.00338	-.15038	-.24900	-.31887
		-.80423	-.95704	-1.1136	-1.0805	-.95360	-.81179
		-15.54	-12.94	-14.95	-17.68	-17.94	-10.18
			.23122	.11872	-.05311	-.14747	-.19337
			-.60842	-.90598	-1.2101	-1.2150	-1.1056
			-8.35	-10.15	-14.18	-13.96	-6.87
σmax				.27509	.09725	-.08516	-.16120
σmin				-.36435	-.76255	-1.1174	-1.1833
α				-2.57	-8.03	-11.11	-5.70
					.25087	.04733	-.15232
					-.22518	-.53197	-.88811
					3.12	-1.35	-2.31
						.12716	-.08921
						-.19508	-.38736
						12.55	6.12
							-.05321
							-.20163
							2.24

Fig. 7

TALVACHIA-DAM
B E N C H M A R K W O R K S H O P

RESULTS: Principal stresses - downstream face
CASE : Gravity Load (unjointed dam)
PROGRAM: FIN3D

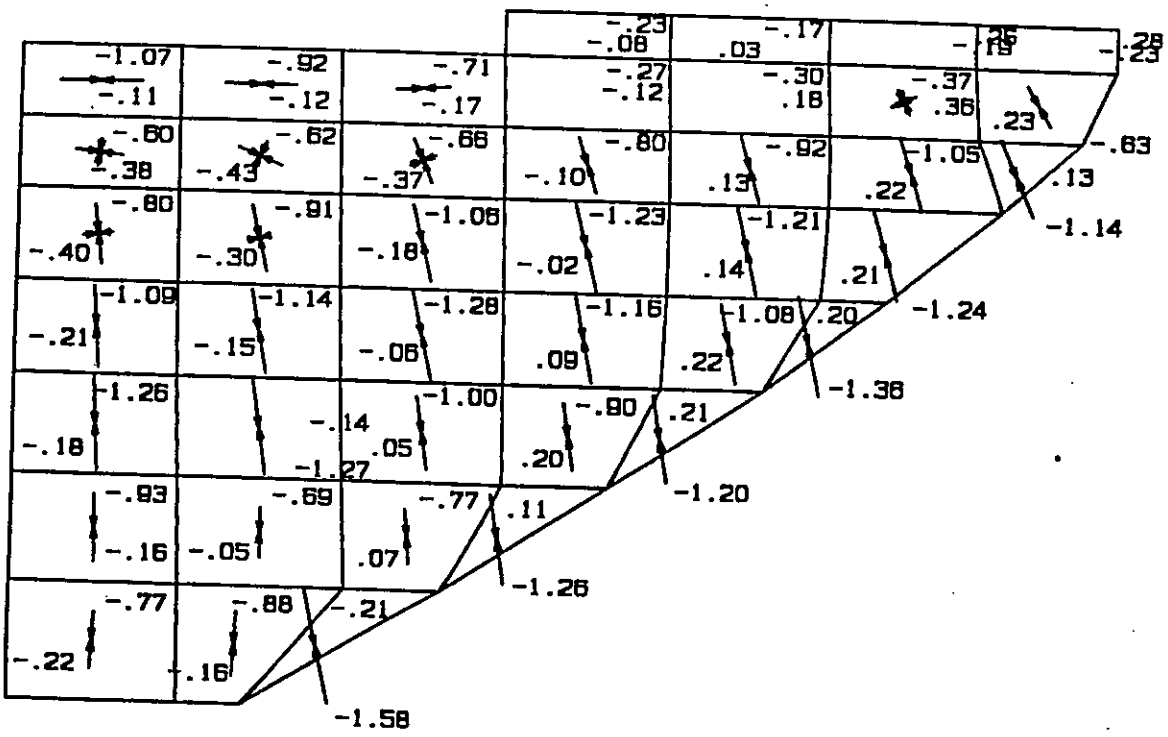

Principal stresses - downstream face

σmax (MPa)			-.08096	.03293	.24764	.27809
σmin (MPa)			-.23185	-.16507	-.18886	-.23112
α (°)			-67.70	37.05	28.49	35.42
-.10769	-.12267	-.17035	-.12358	.18361	.35788	.22687
-1.06629	-.92315	-.71208	-.26994	-.29669	-.37366	-.63158
-89.60	89.72	-85.65	47.89	23.93	25.90	30.41
-.37680	-.43169	-.37473	-.10076	.12817	.22216	.13452
-.59990	-.61764	-.65740	-.80183	-.92188	-1.05488	-1.14152
83.06	66.32	22.59	17.61	16.32	17.65	22.71
-.39564	-.30350	-.18194	-.02412	.13652	.21083	
-.79961	-.90857	-1.06134	-1.23321	-1.21261	-1.24382	
7.29	13.45	13.99	13.97	12.90	15.57	
-.20953	-.14984	-.05998	.09402	.21539	.20119	
-1.09033	-1.13690	-1.28298	-1.16229	-1.08451	-1.36307	
4.36	10.39	12.82	11.28	11.18	12.98	
-.17752	-.14174	.04961	.19696	.20526		
-1.25969	-1.27371	-.99772	-.90108	-1.19560		
2.65	8.16	8.64	8.55	9.36		
-.15852	-.05083	.06786	.11371			
-.93476	-.69367	-.76610	-1.26378			
1.11	.23	4.58	9.10			
-.22140	-.16438	-.20536				
-.76650	-.88086	-1.57573				
-3.20	-2.76	12.30				

Fig. 8

TALVACHIA-DAM

B E N C H M A R K W O R K S H O P

RESULTS: Principal stresses - upstream face
CASE : Waterload
PROGRAM: CODCOD

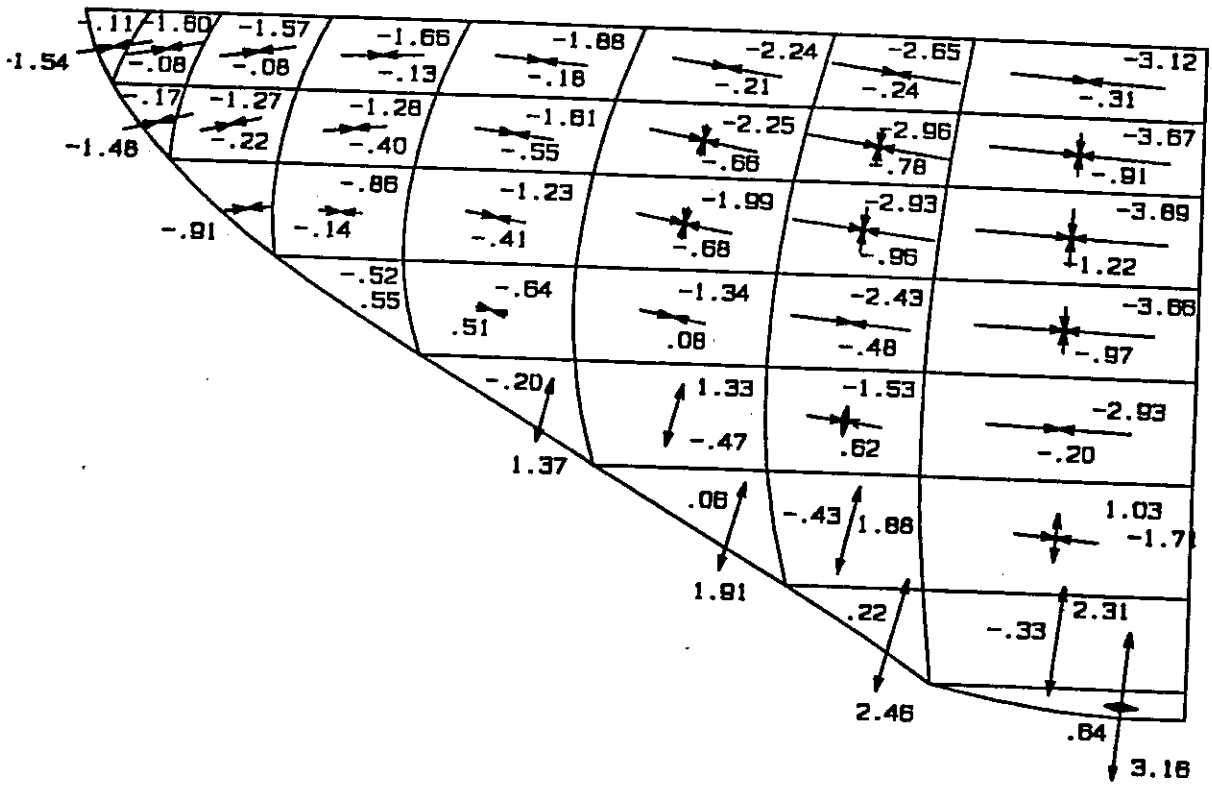

Principal stresses - upstream face

.10610	-.07727	-.07928	-.13175	-.18226	-.21323	-.24496	-.30843
-1.53900	-1.59925	-1.56814	-1.66051	-1.88408	-2.24291	-2.65377	-3.11727
-78.96	-78.71	-81.23	-87.69	85.29	81.68	82.52	86.80
	-.16959	-.21804	-.39694	-.54993	-.65799	-.77749	-.91356
	-1.47647	-1.27403	-1.28253	-1.60725	-2.25116	-2.96255	-3.66783
	-74.73	-75.78	-84.30	83.04	79.40	81.72	86.73
		.00115	-.13847	-.40746	-.67953	-.95887	-1.22195
		-.90569	-.85650	-1.22894	-1.98842	-2.93387	-3.89449
		-83.32	88.00	80.17	79.61	83.09	87.51
			.55328	.50587	.07858	-.48363	-.97156
			-.51746	-.63641	-1.34265	-2.43454	-3.65648
			79.52	76.21	79.26	84.16	88.25
	σmax			1.36613	1.32954	.61601	-.19530
	σmin			-.19999	-.47157	-1.52759	-2.92976
	α			76.46	75.34	82.09	87.76
					1.91344	1.88049	1.03136
					.06153	-.42926	-1.70789
					74.81	77.23	85.37
						2.46138	2.30594
						.22096	-.32843
						75.74	83.49
							3.16476
							.63532
							85.10

Fig. 9

TALVACHIA-DAM

B E N C H M A R K W O R K S H O P

RESULTS: Principal stresses - upstream face
CASE : Waterload
PROGRAM: FIN3D

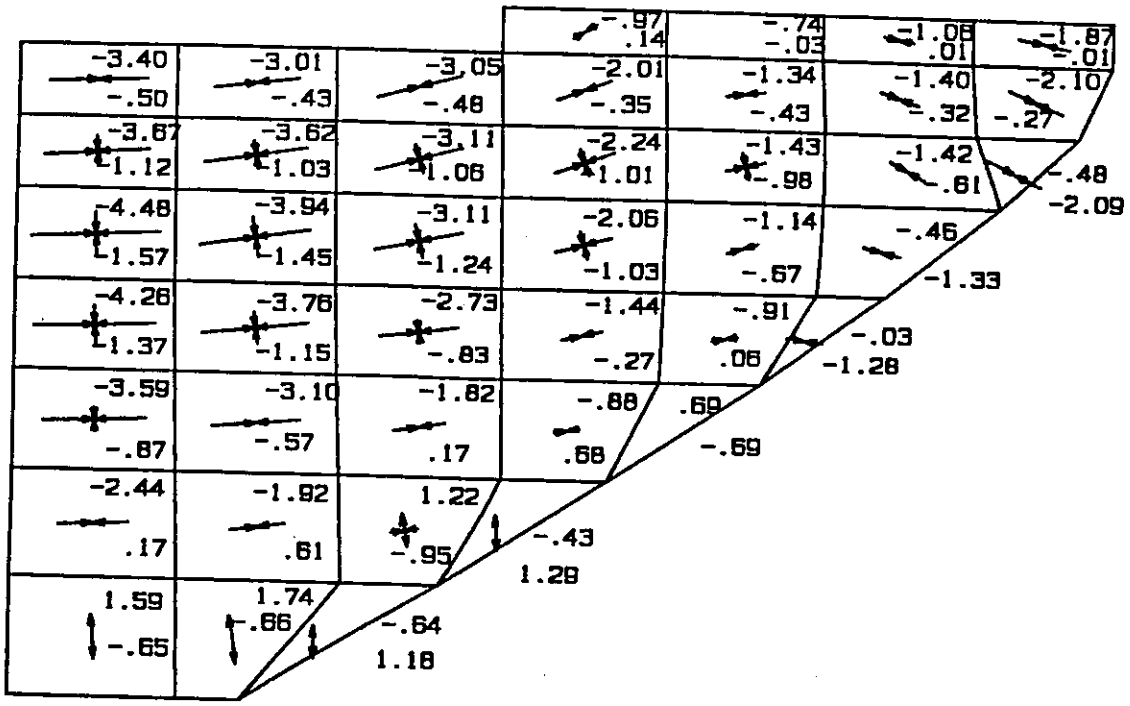

Principal stresses - upstream face

σmax σmin α			.13502 -.96645 -56.98	-.02760 -.73842 -82.81	.00896 -1.06338 78.49	-.00929 -1.86566 78.39
-.49954 -3.39855 -87.76	-.42676 -3.01363 -82.56	-.47883 -3.04922 -74.27	-.35214 -2.01076 -68.40	-.42752 -1.33940 -81.44	-.32130 -1.39859 70.86	-.26906 -2.10019 66.92
-1.12026 -3.66602 -85.54	-1.02632 -3.61855 -80.56	-1.06167 -3.11432 -73.81	-1.01114 -2.23754 -69.78	-.97762 -1.42575 -76.82	-.61099 -1.42209 60.35	-.48072 -2.08669 63.06
-1.56919 -4.48491 -87.11	-1.45029 -3.94456 -80.83	-1.23961 -3.10500 -77.15	-1.02619 -2.05570 -74.83	-.67155 -1.13660 -71.93	-.46024 -1.32849 76.57	
-1.36552 -4.26147 -87.63	-1.15202 -3.75925 -83.40	-.83037 -2.72729 -81.64	-.26997 -1.44136 -75.52	.06375 -.90603 -80.12	-.02722 -1.28453 82.10	
-.87384 -3.59123 -87.66	-.56705 -3.10151 -84.67	.17053 -1.82295 -79.68	.68268 -.87824 -79.29	.69119 -.68880 -87.64		
.16669 -2.44209 -87.14	.61376 -1.92153 -81.46	1.22188 -.95168 -79.32	1.28888 -.43169 -86.49			
1.59430 -.65477 -85.55	1.74128 -.65565 -81.30	1.18294 -.63722 -89.51				

Fig. 10

TALVACHIA-DAM

B E N C H M A R K W O R K S H O P

RESULTS: Principal stresses - downstream face
CASE : Waterload
PROGRAM: CODCOD

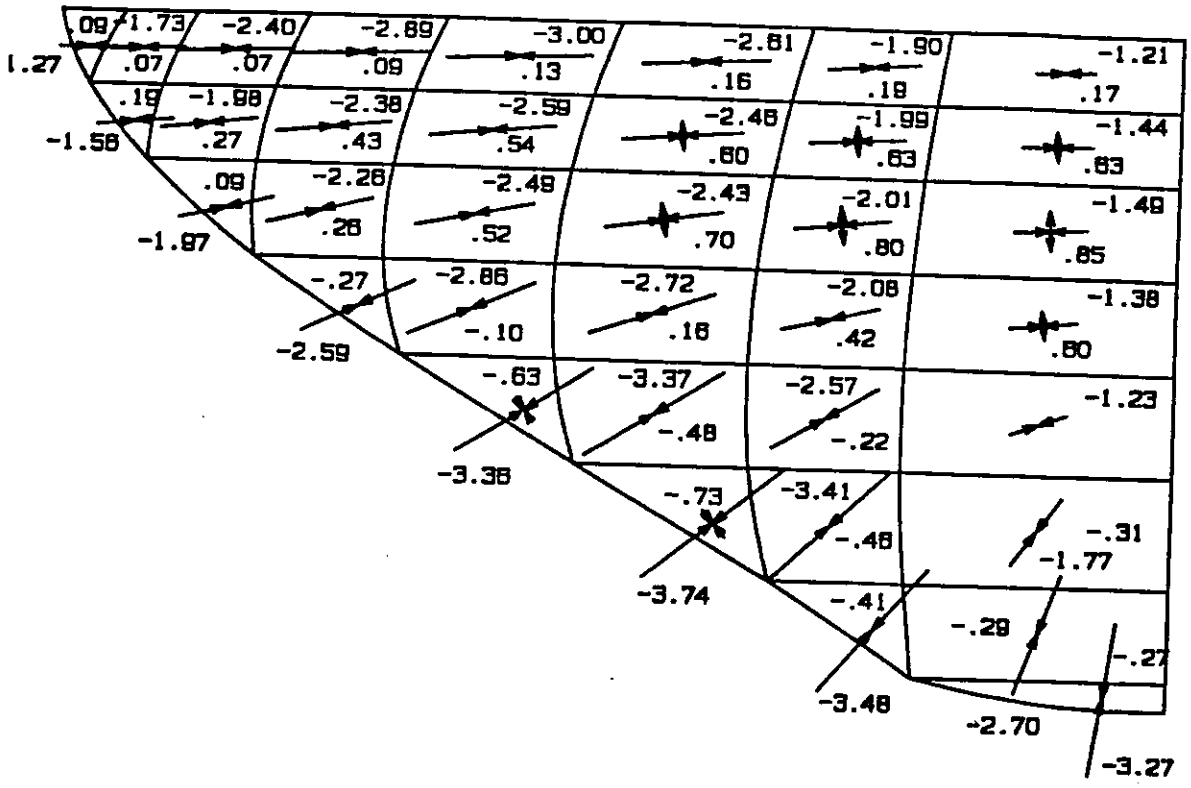

Principal stresses - downstream face

.09125	.07164	.07275	.09028	.12672	.16235	.18779	.17095
-1.26705	-1.72667	-2.39541	-2.88923	-2.99535	-2.61337	-1.90478	-1.21405
-89.55	-88.24	-88.31	-88.12	-87.59	-86.71	-85.65	-86.85
	.18939	.27244	.42503	.53722	.60486	.63422	.62872
	-1.55536	-1.98449	-2.38348	-2.58967	-2.46427	-1.98559	-1.43912
	-84.08	-82.85	-83.62	-84.30	-85.28	-86.22	-88.10
		.09044	.26318	.52088	.69989	.80153	.85011
		-1.96641	-2.25834	-2.49034	-2.43423	-2.01100	-1.49112
		-75.92	-75.76	-77.98	-81.09	-83.92	-87.37
σmax			-.27278	-.10006	.15969	.42069	.60155
σmin			-2.58556	-2.86487	-2.71584	-2.08271	-1.37509
α			-64.47	-66.15	-71.09	-76.54	-83.79
				-.63271	-.48224	-.21655	.00137
				-3.36094	-3.37378	-2.57406	-1.22658
				-57.10	-57.36	-59.51	-69.24
					-.73435	-.46296	-.30842
					-3.73538	-3.41267	-1.76525
					-50.71	-46.31	-35.52
						-.41126	-.28784
						-3.47857	-2.70272
						-40.09	-19.56
							-.26727
							-3.27132
							-8.34

Fig. 11

TALVACHIA-DAM

B E N C H M A R K W O R K S H O P

RESULTS: Principal stresses - downstream face
CASE : Waterload
PROGRAM: FIN3D

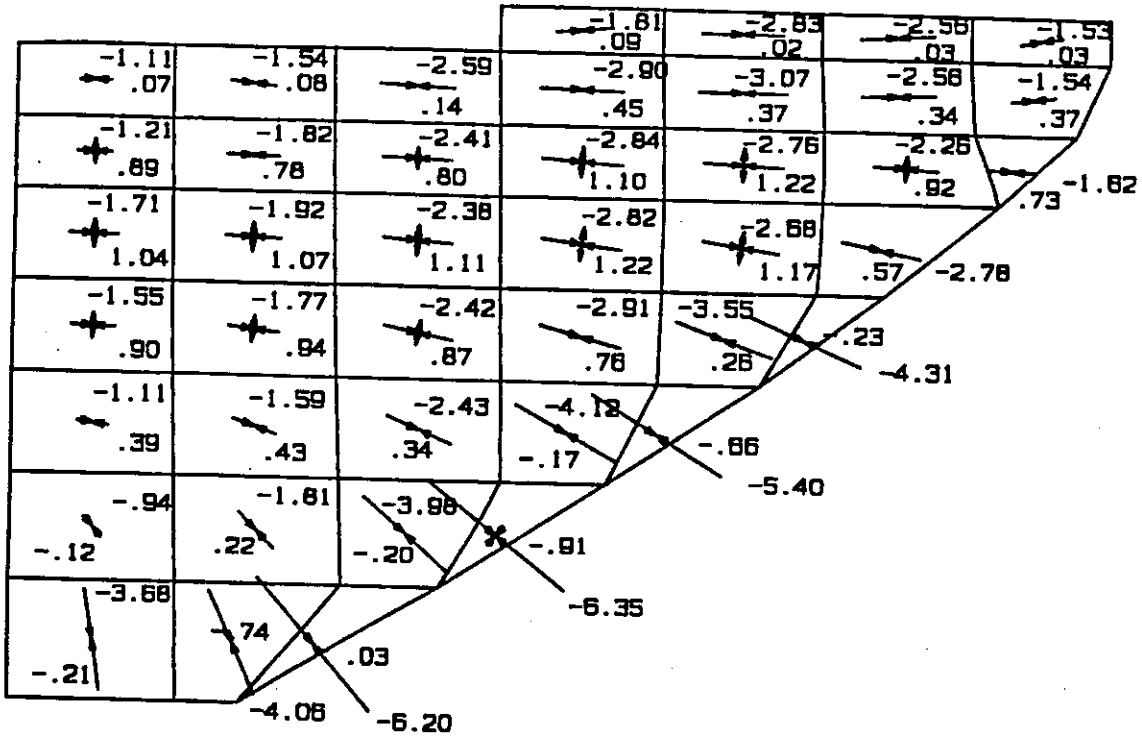

Principal stresses - downstream face

σmax (MPa)			.08620	.01730	.03222	.03015
σmin (MPa)			-1.80664	-2.82937	-2.56127	-1.52737
α (°)			-84.62	-89.90	-86.34	-79.40
.07228	.08055	.14372	.45450	.36686	.33786	.36802
-1.11097	-1.54466	-2.59259	-2.90329	-3.06626	-2.56172	-1.54098
89.08	83.85	87.01	88.62	-89.98	-87.59	-83.94
.89314	.77868	.80085	1.10365	1.22454	.91975	.72929
-1.21328	-1.81652	-2.40571	-2.83679	-2.75998	-2.25585	-1.62213
88.79	88.14	87.49	85.79	87.27	86.57	89.09
1.04220	1.06792	1.11423	1.21795	1.17265	.56742	
-1.71477	-1.91845	-2.38106	-2.82307	-2.67775	-2.78347	
88.55	87.36	85.04	82.19	81.27	78.86	
.89811	.93982	.87359	.76315	.25828	-.22777	
-1.54717	-1.76690	-2.41750	-2.90985	-3.55318	-4.30958	
86.83	83.11	78.69	74.97	69.66	66.31	
.39473	.43327	.34354	-.16581	-.65912		
-1.11049	-1.58812	-2.42876	-4.12451	-5.39842		
81.65	70.35	66.70	60.80	58.07		
-.11531	.22131	-.20431	-.90926			
-.94033	-1.81251	-3.98363	-6.35444			
38.50	42.59	46.92	50.57			
.20531	.02731	-.73862				
-3.68375	-4.06083	-6.20126				
8.42	23.50	39.72				

Fig. 12

TALVACHIA-DAM
B E N C H M A R K W O R K S H O P

RESULTS: Displacements
CASE : Gravity load (unjointed dam)
PROGRAM: FIN3D

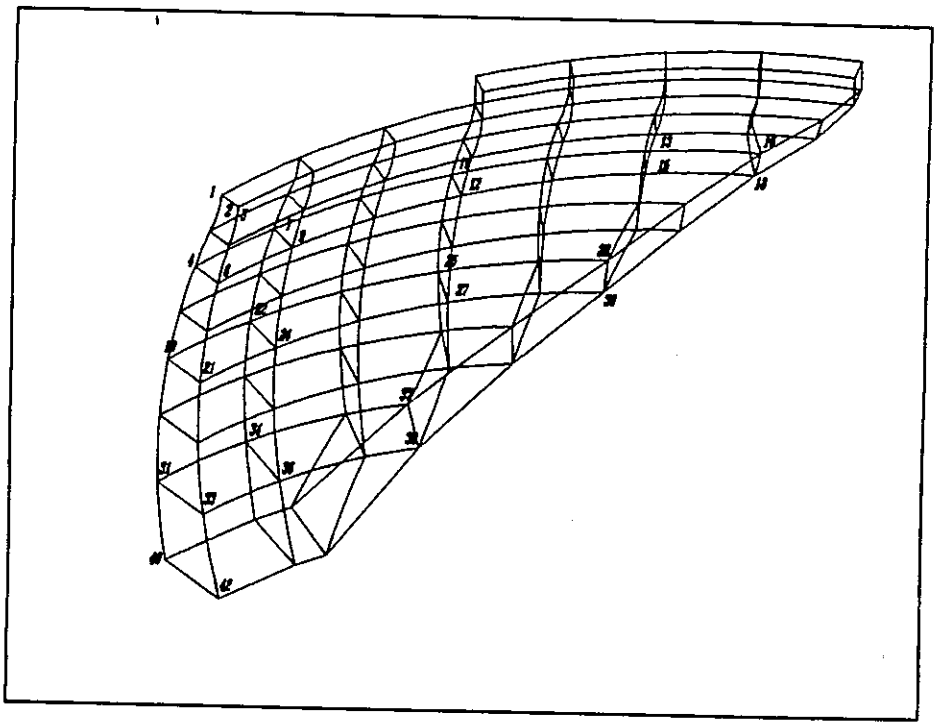

Nr	s (m)	Node	Displ.x (m)	Displ.y (m)	Displ.z (m)
1	0.0	723	0.000000E+00	-7.808826E-04	-3.030259E-03
3	0.0	725	0.000000E+00	-8.074039E-04	-3.455839E-03
4	0.0	737	0.000000E+00	6.190205E-04	-2.488249E-03
6	0.0	739	0.000000E+00	5.982756E-04	-2.973536E-03
7	16.0	639	1.620533E-04	5.767185E-04	-2.378223E-03
9	16.0	641	1.928238E-04	5.620392E-04	-2.867162E-03
10	48.0	450	4.305168E-04	2.297331E-04	-1.741657E-03
12	48.0	452	5.002776E-04	2.462639E-04	-2.244636E-03
13	80.0	226	5.022610E-04	6.138643E-05	-8.535485E-04
15	80.0	228	4.484690E-04	2.155188E-05	-1.207199E-03
16	99.2	158	1.879101E-04	1.477183E-04	-3.954269E-04
18	99.2	154	1.187811E-04	1.154783E-04	-5.182423E-04
19	0.0	751	0.000000E+00	1.395174E-03	-2.232042E-03
21	0.0	753	0.000000E+00	1.378418E-03	-2.259516E-03
22	16.0	653	-1.118231E-04	1.290894E-03	-2.162304E-03
24	16.0	655	-2.077431E-05	1.288048E-03	-2.170697E-03
25	48.0	454	2.086984E-04	4.927194E-04	-1.683094E-03
27	48.0	456	9.166564E-05	4.747210E-04	-1.474179E-03
28	75.0	291	8.240493E-05	6.778433E-05	-8.223985E-04
30	75.0	287	1.067966E-04	1.404648E-04	-7.703525E-04
31	0.0	765	0.000000E+00	6.458662E-04	-2.154439E-03
33	0.0	767	0.000000E+00	6.234635E-04	-1.494955E-03
34	16.0	667	-1.148082E-04	5.341254E-04	-2.013429E-03
36	16.0	669	1.972520E-05	5.318566E-04	-1.410336E-03
37	41.5	480	-4.539846E-05	4.276891E-06	-1.217428E-03
39	41.5	476	8.038332E-05	1.270579E-04	-9.766713E-04
40	0.0	772	0.000000E+00	8.539215E-06	-1.502989E-03
42	0.0	774	0.000000E+00	7.188106E-05	-9.951161E-04

Fig. 13

TALVACHIA-DAM
B E N C H M A R K W O R K S H O P

RESULTS: Displacements
CASE : Waterload
PROGRAM: FIN3D

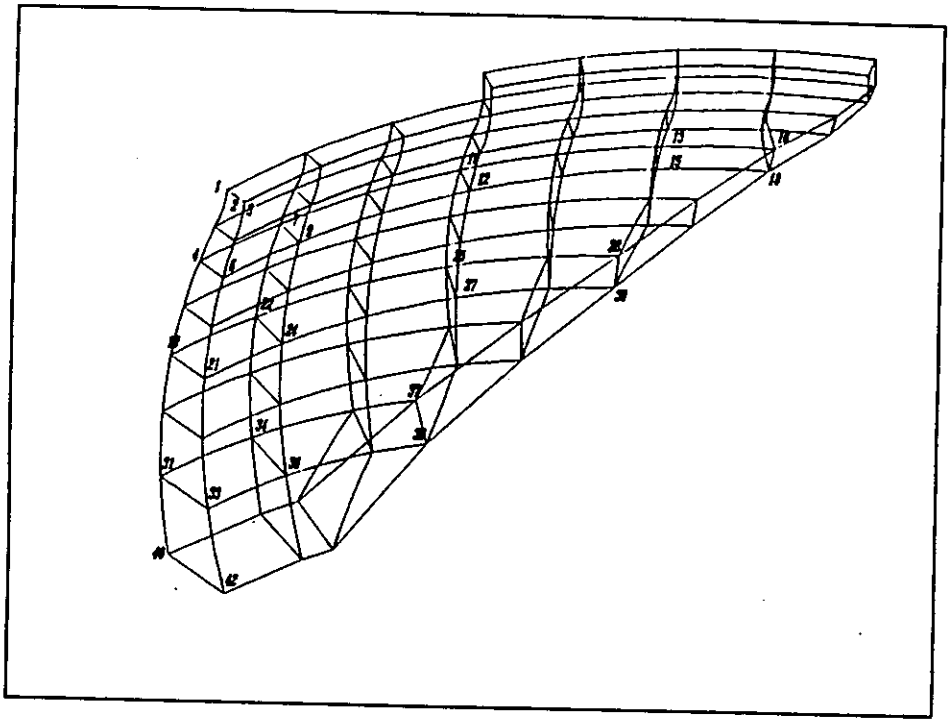

Nr	s (m)	Node	Displ.x (m)	Displ.y (m)	Displ.z (m)
1	0.0	723	0.000000E+00	-2.261866E-02	-6.138632E-04
3	0.0	725	0.000000E+00	-2.265360E-02	-1.175658E-03
4	0.0	737	0.000000E+00	-2.040962E-02	3.108555E-04
6	0.0	739	0.000000E+00	-2.049742E-02	-8.918695E-04
7	16.0	639	1.763604E-03	-1.870989E-02	4.500014E-04
9	16.0	641	6.858645E-04	-1.892786E-02	-6.344828E-04
10	48.0	450	1.920524E-03	-9.069160E-03	5.313394E-04
12	48.0	452	1.931402E-04	-9.895480E-03	6.818432E-05
13	80.0	226	-6.691708E-04	-1.849196E-03	7.478310E-05
15	80.0	228	-1.166582E-03	-2.285618E-03	2.235491E-04
16	99.2	158	-7.383530E-04	-8.684970E-04	-1.423999E-04
18	99.2	154	-7.678961E-04	-8.504618E-04	-1.412253E-05
19	0.0	751	0.000000E+00	-1.470988E-02	2.687766E-03
21	0.0	753	0.000000E+00	-1.482104E-02	-4.050334E-04
22	16.0	653	1.653732E-03	-1.339827E-02	2.540516E-03
24	16.0	655	5.325857E-04	-1.369031E-02	-4.077989E-04
25	48.0	454	2.104554E-03	-8.569482E-03	8.228581E-04
27	48.0	456	1.465989E-03	-5.600480E-03	9.298999E-04
28	75.0	291	-5.565695E-04	-1.221501E-03	1.912221E-04
30	75.0	287	-1.001245E-03	-1.580332E-03	-3.794536E-04
31	0.0	765	0.000000E+00	-6.162909E-03	3.319218E-03
33	0.0	767	0.000000E+00	-6.123330E-03	-9.717662E-04
34	16.0	667	7.760181E-04	-5.320963E-03	2.914292E-03
36	16.0	669	-1.468838E-04	-5.448931E-03	-9.758176E-04
37	41.5	480	1.167084E-04	-1.419268E-03	1.016604E-03
39	41.5	476	-9.093344E-04	-2.063088E-03	-8.003972E-04
40	0.0	772	0.000000E+00	-1.673101E-03	1.814116E-03
42	0.0	774	0.000000E+00	-1.872861E-03	-9.375341E-04

Fig. 14

FIRST BENCHMARK WORKSHOP ON NUMERICAL ANALYSIS OF DAMS
BERGAMO, ITALY
May 28-29, 1991

THEME A: DOUBLE CURVATURE CONCRETE ARCH DAM
TALVACCHIA DAM

STATIC ANALYSIS OF TALVACCHIA DAM AND NEED FOR MORE ACCURATE PENTAHEDRAL ELEMENT

Slobodan B. Kojić, Ph.D., C.E.
Chief Engineer

Energoprojekt Holding - Hydroengineering Co.
B. Lenjina 12, 11070 N. Belgrade, Yugoslavia

STATIC ANALYSIS OF TALVACCHIA DAM AND NEED FOR MORE ACCURATE PENTAHEDRAL ELEMENT

Slobodan B. Kojić, Ph.D., C.E.
Chief Engineer

Energoprojekt Holding - Hydroengineering Co.
B. Lenjina 12, 11070 N. Belgrade, Yugoslavia

ABSTRACT

Talvacchia dam and its foundation are discretized by linear, isoparametric, incompatible 3-D 8-node finite elements. The dam is analyzed for influence of the self weight and hydrostatic pressure. Under those loading conditions, displacements and stresses are computed for the two different ways of the hexahedral element degeneration into prismatic pentahedral elements. Since the degenerated elements are not spatially isotropic their stiffness depends on the way of the element degeneration. Consequently, stresses in the degenerated elements and in the surrounding regular hexahedral elements change according to the way of the element degeneration. Sometimes this stress ambiguity may be important for arch dam design and therefore, more accurate prismatic element is needed.

INTRODUCTION

The arch dam analysis by the most accurate methods and corresponding computer programs is of an extreme importance from the major two reasons: the computed dam safety factor is more reliable and thousands of cubic meters of the concrete can be saved. Today, linear static or dynamic analysis of arch dams can be performed by cheap high speed personal computers. Numerical models with up to 10,000 equations are successfully handled on such computers which sometimes show certain superiority over some main frames. Therefore computer facilities do not make any restrictions regarding the choice of numerical model but one question still remains, how is accurate the method or computer program which we use in our design office?. This First benchmark workshop on numerical analysis of dams will surely answer some of these questions and point out problems to be solved by the time of a future meeting.

An intention of this paper is not to show the results of the analysis obtained by supposed the most accurate type of the finite element (Kojić, et al., 1988), but rather to demonstrate results obtained by the simplest 8-node finite elements and to emphasize that possible different ways of degeneration of the hexahedral elements into 6-node prismatic elements may lead to different dam stiffness. Our practice in arch dam design shows

that this numerical phenomenon can cause, in some cases, significant stress differences and consequently the dam thickness increase or decrease in order to meet concrete allowable stresses. The prismatic degenerated element with six nodes is possible to formulate in such way to maintain its spatial isotropy by applying the appropriate corrections to the interpolation displacement functions. Another possibility for solution of this problem is the application of aerial coordinates. Both ways lead to more accurate prismatic element.

Details of the model and of the analysis of Talvacchia dam are described in the following.

FINITE ELEMENT MODEL OF THE DAM AND RESULTS OF THE ANALYSIS

The body and surrounding foundation of Talvacchia dam are discretized by 84 and 160 3-D 8-node isoparametric finite elements, respectively. The coordinates of the corner nodes and mechanical properties of the dam body and foundation rock are identical to the data given by ICOLD and ISMES, 1990. Formulation of the element stiffness matrix is with incompatible displacement shape functions whose extra degrees of freedom are condensed out at element level (Wilson, et al.,1973). The dam model has 966 active degrees of freedom. The dam is analyzed for two static load conditions: self weight and hydrostatic pressure caused by reservoir water at elevation at 507.0 m. The dam for both load cases is considered as a monolithic, isotropic homogeneous body. The foundation is assumed to be weightless, i.e. only its stiffness participates in the dam response. The finite element model is mostly consisted of the 8-node hexahedral elements and teen 6-node prismatic pentahedral elements located along the dam abutment. The prismatic element is made from the regular 8-node element by collapsing one of its six faces. Such element is not spatially isotropic. For the hexahedral 8-node and degenerated 6-node elements the low order Gauss integration scheme 2x2x2 is used. Since the foundation elements are pretty distorted they are integrated by 3x3x3 integration points in r, s and t directions.

Several possible ways of element degeneration are shown in Fig. 1. The case A is identical to the case C and the case B is identical to the case D. In the cases A and C the subvertical right face is degenerated into upper line and in the cases B and D, the bottom faces is degenerated into the left lower line. Orientation of the element local coordinate system is different for all four cases but that fact is of no consequence on element stiffness. The cases A and B give different stiffness of prismatic degenerated element and therefore different displacement and stress distribution.

For the case A, Tables I and II review displacements of the element corner nodes caused by the dam self weight and hydrostatic pressure, respectively. Tables III and IV show displacements for the case B of element degeneration. It can be seen that difference of the largest node displacement between

TABLE I

TALVACCHIA DAM

DISPLACEMENTS DUE TO DEAD WEIGHT

CASE (A)

Points	s (m)	Displ.x (m)	Displ.y (m)	Displ.z (m)	P1	P2	P3
1	0.0	0.00069	0.00000	-0.00286			
2	0.0						
3	0.0	0.00072	0.00000	-0.00327			
4	0.0	-0.00065	0.00000	-0.00232			
5	0.0						
6	0.0	-0.00063	0.00000	-0.00279			
7	16.0	-0.00059	0.00013	-0.00223			
8	16.0	-0.00057	0.00017	-0.00270			
9	16.0						
10	48.0	-0.00020	0.00040	-0.00163			
11	48.0						
12	48.0	-0.00021	0.00047	-0.00211			
13	80.0	-0.00009	0.00045	-0.00079			
14	80.0						
15	80.0	-0.00003	0.00039	-0.00110			
16	99.2	-0.00013	0.00016	-0.00036			
17	99.2						
18	99.2	-0.00009	0.00010	-0.00048			
19	0.0	-0.00134	0.00000	-0.00211			
20	0.0						
21	0.0	-0.00132	0.00000	-0.00211			
22	16.0	-0.00123	0.00012	-0.00205			
23	16.0						
24	16.0	-0.00122	0.00002	-0.00203			
25	48.0	-0.00052	0.00011	-0.00157			
26	48.0						
27	48.0	-0.00060	0.00007	-0.00145			
28	75.0	-0.00004	0.00006	-0.00077			
29	75.0						
30	75.0	-0.00010	0.00007	-0.00072			
31	0.0	-0.00060	0.00000	-0.00203			
32	0.0						
33	0.0	-0.00046	0.00000	-0.00131			
34	16.0	-0.00047	0.00012	-0.00190			
35	16.0						
36	16.0	-0.00041	0.00002	-0.00128			
37	41.5	0.00005	0.00004	-0.00118			
38	41.5						
39	41.5	-0.00010	0.00005	-0.00096			
40	0.0	0.00007	0.00000	-0.00144			
41	0.0						
42	0.0	-0.00004	0.00000	-0.00106			

TABLE II

TAVLACCHIA DAM

DISPLACEMENTS DUE TO HYDROSTATIC PRESSURE

CASE (A)

Points	s (m)	Displ.x (m)	Displ.y (m)	Displ.z (m)	P1	P2	P3
1	0.0	0.02157	0.00000	-0.00066			
2	0.0						
3	0.0	0.02159	0.00000	-0.00114			
4	0.0	0.01950	0.00000	0.00029			
5	0.0						
6	0.0	0.01955	0.00000	-0.00085			
7	16.0	0.01787	0.00171	0.00034			
8	16.0	0.01808	0.00065	-0.00071			
9	16.0						
10	48.0	0.00850	0.00196	0.00044			
11	48.0						
12	48.0	0.00932	0.00026	-0.00004			
13	80.0	0.00173	-0.00052	0.00004			
14	80.0						
15	80.0	0.00213	-0.00090	0.00011			
16	99.2	0.00075	-0.00064	-0.00016			
17	99.2						
18	99.2	0.00077	-0.00065	-0.00007			
19	0.0	0.01399	0.0000	0.00258			
20	0.0						
21	0.0	0.01406	0.00000	-0.00049			
22	16.0	0.01266	0.00166	0.00244			
23	16.0						
24	16.0	0.01292	0.00050	-0.00049			
25	48.0	0.00511	0.00162	0.00143			
26	48.0						
27	48.0	0.00614	-0.00011	-0.00055			
28	75.0	0.00110	-0.00051	0.00011			
29	75.0						
30	75.0	0.00140	-0.00088	-0.00043			
31	0.0	0.00563	0.00000	0.00324			
32	0.0						
33	0.0	0.00533	0.00000	-0.00106			
34	16.0	0.00478	0.00078	0.00273			
35	16.0						
36	16.0	0.00478	-0.00021	-0.00101			
37	41.5	0.00133	0.00001	0.00076			
38	41.5						
39	41.5	0.00187	-0.00092	-0.00085			
40	0.0	0.00155	0.00000	0.00140			
41	0.0						
42	0.0	0.00161	0.00000	-0.00100			

TABLE III

TALVACCHIA DAM

DISPLACEMENTS DUE TO DEAD WEIGHT

CASE (B)

Points	s (m)	Displ.x (m)	Displ.y (m)	Displ.z (m)	P1	P2	P3
1	0.0	0.00067	0.00000	-0.00285			
2	0.0						
3	0.0	0.00070	0.00000	-0.00327			
4	0.0	-0.00067	0.00000	-0.00231			
5	0.0						
6	0.0	-0.00064	0.00000	-0.00278			
7	16.0	-0.00060	0.00013	-0.00222			
8	16.0	-0.00059	0.00017	-0.00270			
9	16.0						
10	48.0	-0.00020	0.00040	-0.00163			
11	48.0						
12	48.0	-0.00021	0.00048	-0.00211			
13	80.0	-0.00008	0.00047	-0.00080			
14	80.0						
15	80.0	-0.00002	0.00040	-0.00111			
16	99.2	-0.00014	0.00016	-0.00036			
17	99.2						
18	99.2	-0.00009	0.00010	-0.00048			
19	0.0	-0.00136	0.00000	-0.00210			
20	0.0						
21	0.0	-0.00134	0.00000	-0.00210			
22	16.0	-0.00124	-0.00012	-0.00204			
23	16.0						
24	16.0	-0.00123	-0.00002	-0.00203			
25	48.0	-0.00051	-0.00010	-0.00157			
26	48.0						
27	48.0	-0.00059	0.00008	-0.00146			
28	75.0	-0.00004	0.00007	-0.00077			
29	75.0						
30	75.0	-0.00010	0.00008	-0.00074			
31	0.0	-0.00061	0.00000	-0.00203			
32	0.0						
33	0.0	-0.00047	0.00000	-0.00131			
34	16.0	-0.00048	-0.00012	-0.00190			
35	16.0						
36	16.0	-0.00041	0.00003	-0.00127			
37	41.5	0.00005	-0.00004	-0.00118			
38	41.5						
39	41.5	-0.00010	0.00005	-0.00097			
40	0.0	0.00006	0.00000	-0.00144			
41	0.0						
42	0.0	-0.00004	0.00000	-0.00108			

TABLE IV

TALVACCHIA DAM

DISPLACEMENTS DUE TO HYDROSTATIC PRESSURE

CASE (B)

Points	s (m)	Displ.x (m)	Displ.y (m)	Displ.z (m)	P1	P2	P3
1	0.0	0.02147	0.00000	-0.00066			
2	0.0						
3	0.0	0.02148	0.00000	-0.00113			
4	0.0	0.01940	0.00000	0.00028			
5	0.0						
6	0.0	0.01946	0.00000	-0.00085			
7	16.0	0.01778	0.00171	0.00034			
8	16.0	0.01798	0.00064	-0.00071			
9	16.0						
10	48.0	0.00842	0.00195	0.00045			
11	48.0						
12	48.0	0.00924	0.00026	-0.00004			
13	80.0	0.00171	-0.00053	0.00004			
14	80.0						
15	80.0	0.00210	-0.00090	0.00011			
16	99.2	0.00074	-0.00064	-0.00014			
17	99.2						
18	99.2	0.00076	-0.00063	-0.00006			
19	0.0	0.01393	0.00000	0.00256			
20	0.0						
21	0.0	0.01400	0.00000	-0.00049			
22	16.0	0.01259	0.00167	0.00243			
23	16.0						
24	16.0	0.01285	0.00050	-0.00049			
25	48.0	0.00505	0.00161	0.00143			
26	48.0						
27	48.0	0.00605	-0.00011	-0.00055			
28	75.0	0.00112	-0.00053	0.00010			
29	75.0						
30	75.0	0.00142	-0.00091	-0.00041			
31	0.0	0.00562	0.00000	0.00322			
32	0.0						
33	0.0	0.00532	0.00000	-0.00106			
34	16.0	0.00475	0.00080	0.00272			
35	16.0						
36	16.0	0.00475	-0.00022	-0.00101			
37	41.5	0.00132	0.00002	0.00074			
38	41.5						
39	41.5	0.00188	-0.00092	-0.00083			
40	0.0	0.00155	0.00000	0.00139			
41	0.0						
42	0.0	0.00160	0.00000	-0.00100			

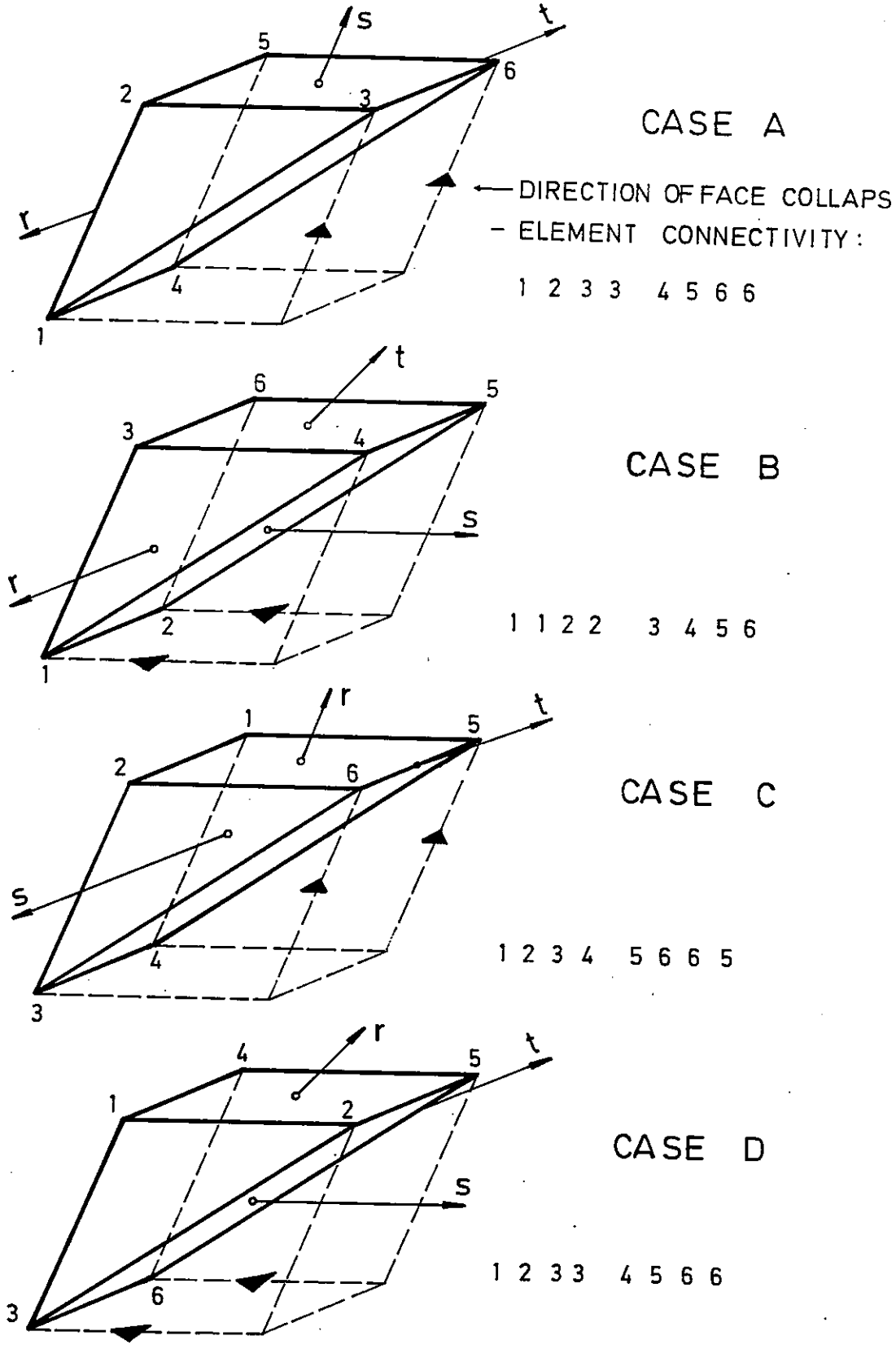

FIG. 1 TALVACCHIA DAM - POSSIBLE WAYS OF ELEMENT DEGENERATION; CASE A - D

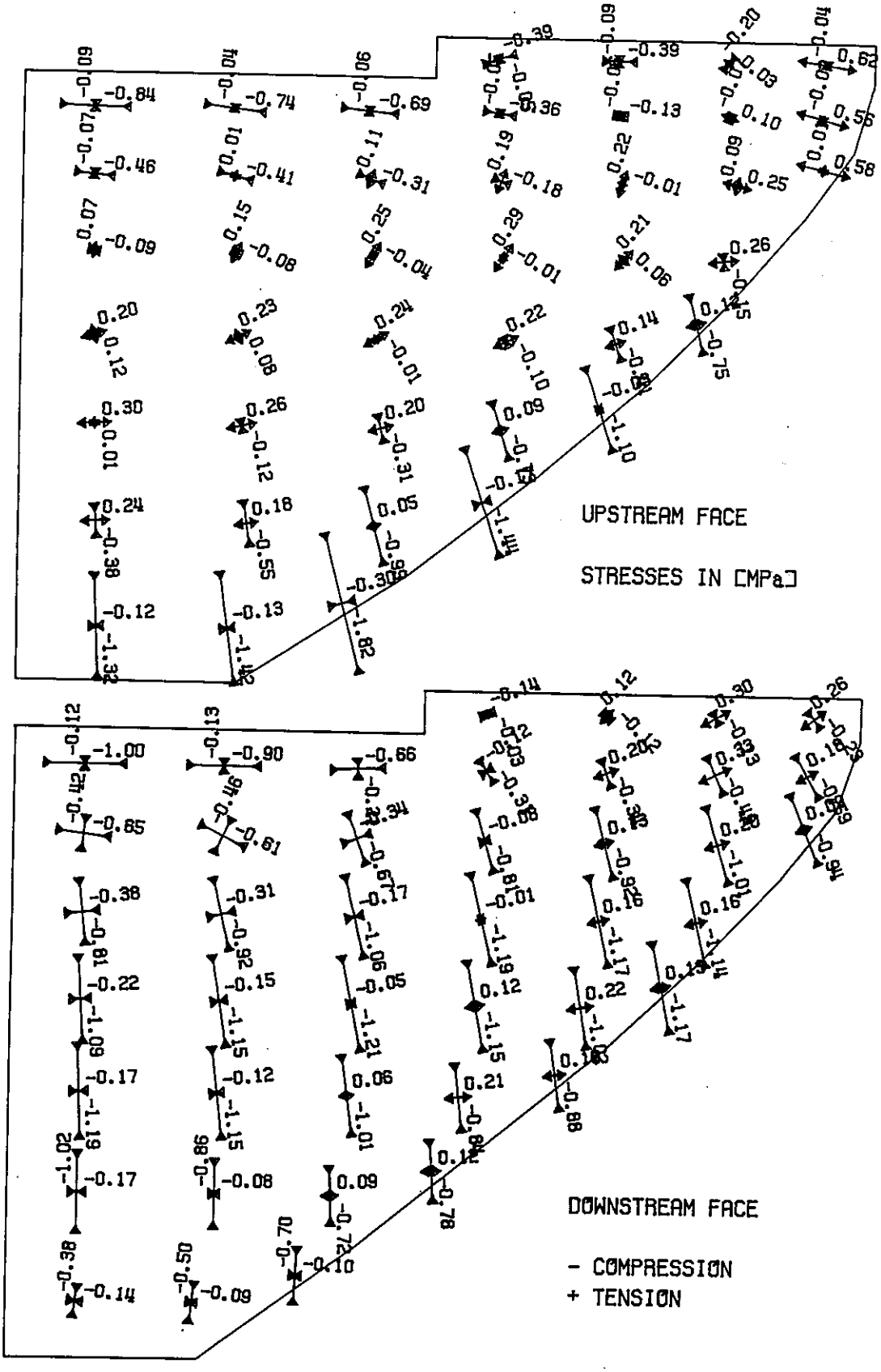

FIG.2 TALVACCHIA DAM - PRINCIPAL STRESSES DUE TO DEAD WEIGHT; CASE A

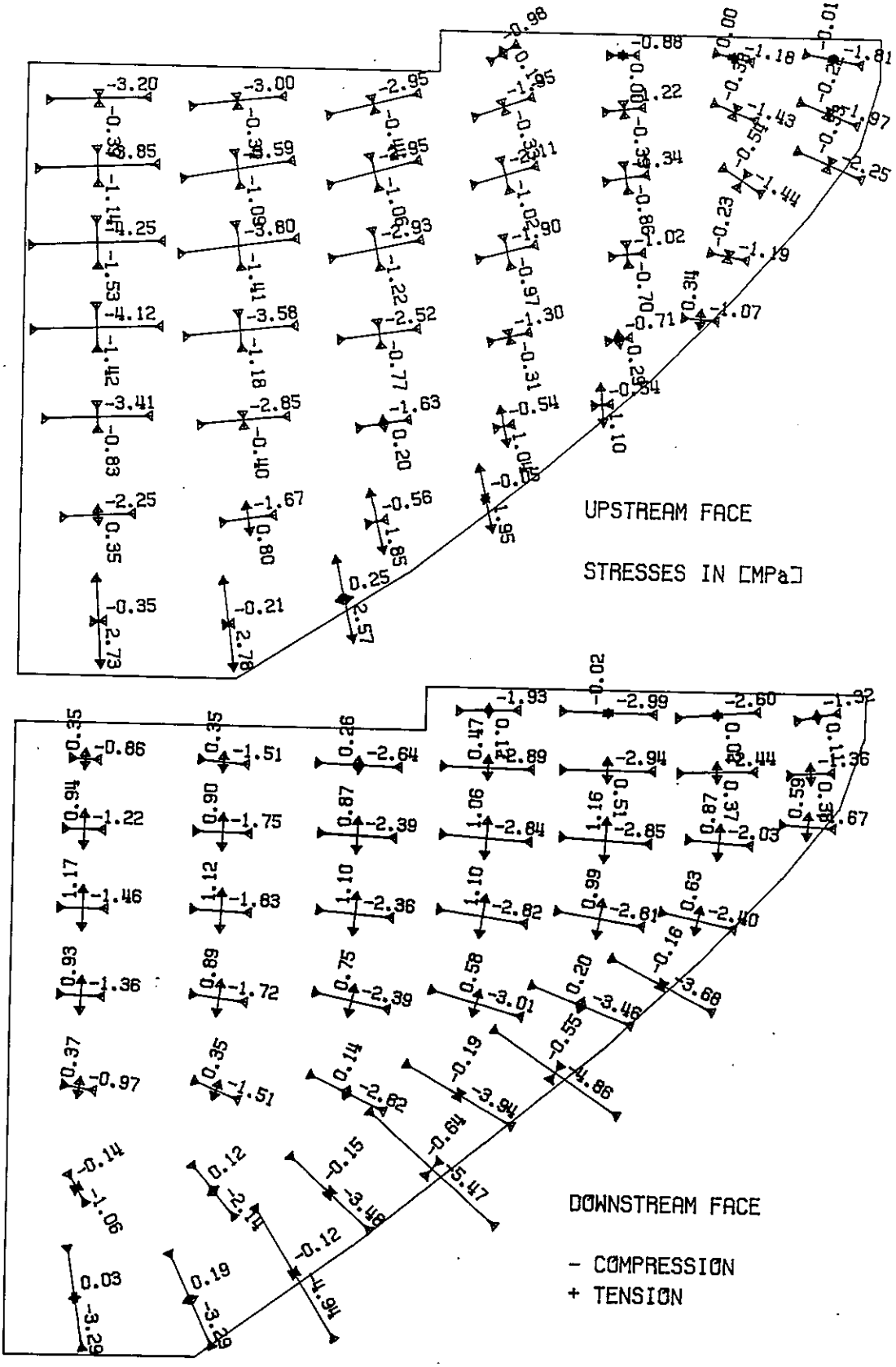

FIG.3 TALVACCHIA DAM - PRINCIPAL STRESSES DUE TO HYDROSTATIC PRESSURE; CASE A

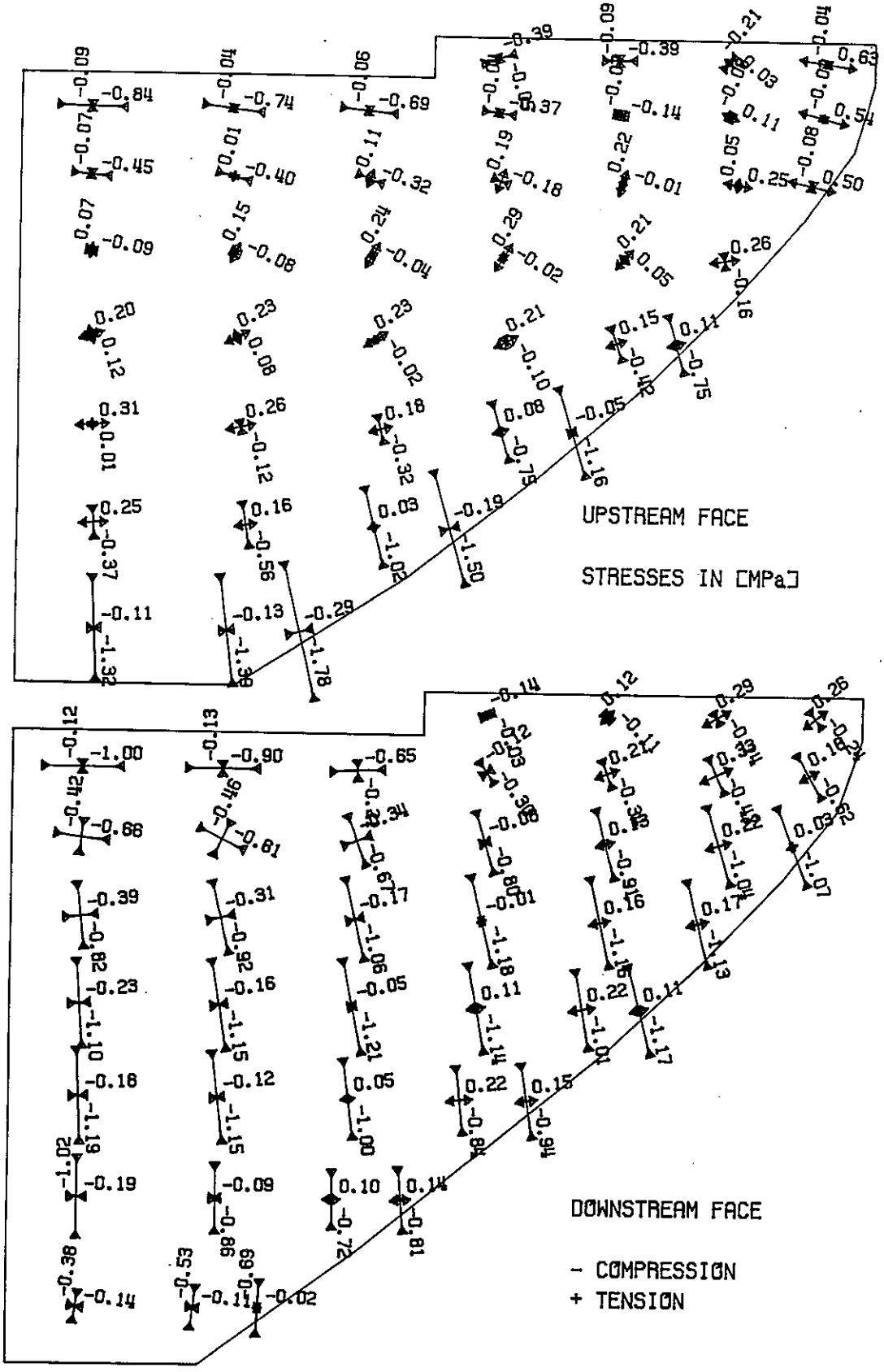

FIG.4 TALVACCHIA DAM - PRINCIPAL STRESSES DUE TØ DEAD WEIGHT; CASE B

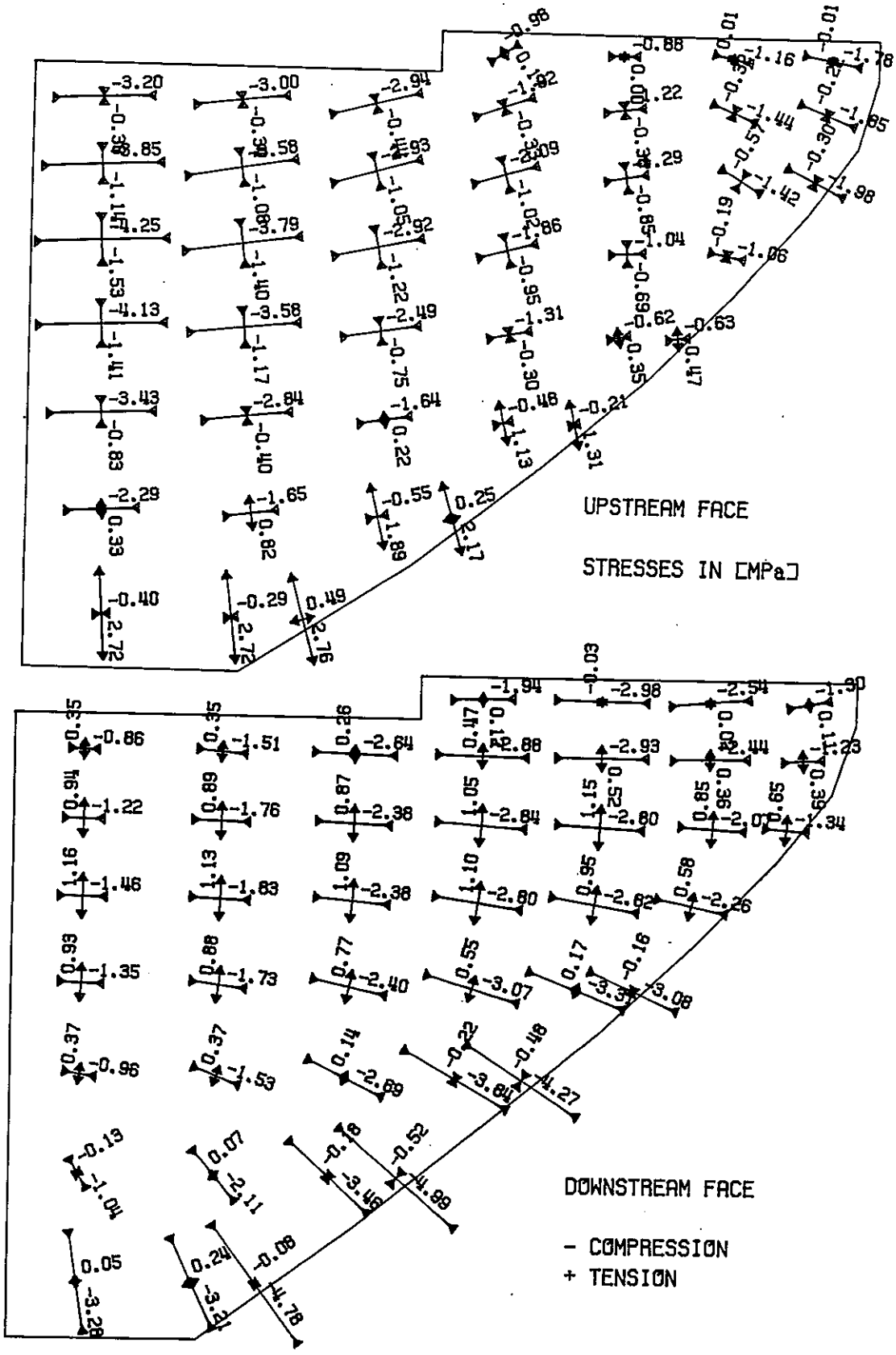

FIG.5 TALVACCHIA DAM - PRINCIPAL STRESSES DUE TØ HYDRØSTATIC PRESSURE; CASE B

the case A and B is about 3% for both load conditions. The principal stresses are computed at the centers of upstream and downstream dam face. For the case A the stresses are shown in Fig. 2 and Fig. 3, and for the case B, those are shown in Fig. 4 and Fig. 5. For the dam self weight (Fig. 2 and Fig. 4), maximum differences of the algebraically largest stresses in the hexahedral elements are about 4% and in the degenerated prismatic elements are about 15%. In the case of hydrostatic pressure (Fig. 3 an Fig. 5) stress differences are in the hexahedral elements about 10% and in the degenerated elements are about 20%. It must be noticed that stress differences in the degenerated elements, for the cases A and B, are not only due to their changed stiffness, but also due to different stress locations on the element faces.

All shown results of the analysis are obtained by the finite element computer program developed in Energoproject Co.. This program possesses specialties for analysis of dams and appurtenant structures. It has its own pre- and post-processing. Talvacchia arch dam, with two load cases, is solved on IBM personal system/2, model 70-386, for 488.90 sec.

CONCLUSION

The results of static analysis of Talvacchia dam loaded by self weight and hydrostatic pressure are reviewed for comparison. The dam and its foundation has been discretized by 3-D 8-node isoparametric, incompatible elements. Some hexahedral elements along the dam abutments are degenerated into spatially non-isotropic prismatic elements. Different ways of element degeneration cause different element stiffness and therefore different displacement and stress distributions. In some cases of the arch dam design, this ambiguity of stress magnitudes can influence dam thickness, i.e. increase or decrease the volume of the dam concrete. Therefore, more accurate prismatic element is required for arch dam analysis.

REFERENCES

1. S. Kojić, M. Trifunac and V. Lee, "Earthquake Response of Arch Dams to Non-uniform Canyon Motion", Report No. 88-03, University of Southern California, Los Angeles, California, 1988.

2. ICOLD, "Data of the Finite Element Model of Talvacchia Dam", ISMES, Bergamo, Italy, 1990.

3. E.L. Wilson, R.L. Taylor, W.P. Doherty and J. Ghaboussi, "Incompatible Displacement Models" in "Numerical and Computer Methods in Structural Mechanics", Academic Press, Inc., New York, 1973.

DYNAMIC ANALYSIS OF ARCH DAMS

Edward L. Wilson

The T. Y. and Margaret Lin
Professor in Engineering
University of California
Berkeley, CA 94720

ABSTRACT

A large number of computer programs which are currently used for the dynamic analysis of concrete arch dams are based on versions of the SAP program which was initially developed by the author in 1970. During the last ten years the new computer programs SAP80, SAP90 and SAP2000 have been developed which are based on new numerical methods and new finite element technology. The programs have very large capacity and operate efficiently on inexpensive personal computer workstations.

The purpose of this paper is to demonstrate the accuracy and versatility of the SAP2000 program when applied to the dynamic analysis of arch dams. A new three dimensional four to eight node solid element, which is used by the program, produces element stresses which are in static equilibrium with the applied loads. This solid element has the ability to model the reservoir as a compressible fluid with radiation boundary conditions. Also, the same element can be used to model the foundation with radiation boundary conditions.

The modeshapes and frequencies of vibration are evaluated using a new subspace iteration technique. The exact eigenvalue solution method is compared with a new Ritz vector algorithm which is approximately 100 times faster than the old subspace iteration approach.

The use of the new elements and numerical methods in the SAP2000 program is illustrated by the selective analyses of the benchmark arch dam.

To be presented at the First Benchmark Workshop on NUMERICAL ANALYSIS OF DAMS, Bergamo, Italy, May 28-29, 1991.

INTRODUCTION

The computer analysis and design of arch dams involve several phases. The various steps can be summarized as follows:

In the case of the design of a new dam the first step, after the selection of the site, is to establish the geometry of the arch dam. In the past, the selection of geometry has been based on experience or on membrane shapes, in equilibrium with hydrostatic loading only, which have been estimated by laboratory experiments or by a special computer program [1]. At the present time there is no formal method to select a shape which is optimum for both hydrostatic and earthquake loading.

Second; the selection of a mathematical model is necessary in order to make an estimation of the displacements and the stresses within the real arch dam. There are major assumptions associated with this phase. Should construction and initial adiabatic thermal stresses be included as initial conditions for the subsequent application of hydrostatic, thermal and dynamic loads? Should the short term and long term creep properties of the concrete be considered? What part of the foundation should be considered in the model? In the case of earthquake loading should the shape of the valley and multiple support excitation be considered? What type of reservoir model should be used for the dynamic response analysis? How many mode shapes should be used in the analysis? Many of the assumptions which must be made in this phase can be studied separately on small models of the structure using hand calculations and different computer programs. Also, existing research papers may be used to estimate the relative importance of the various approximations.

Third; the selection of the computer program, or computer programs, to perform the various analyses is the least important phase of the analysis of an arch dam. A large number of programs exist and, if applied correctly, can be used for this purpose. It must always be remembered, however, that the user of the computer program has the responsibility to verify the accuracy of the program for every different type of application of the program. A fundamental knowledge of the numerical methods used within the programs is essential for the intelligent use of any program. Of course, the verification of a program can be made relatively easy if good plotting options, automatic equilibrium checks and other error estimators exist.

Fourth; the most important phase of the analysis is the interpretation of the results of the mathematical model as it relates to the real physical behavior of the dam. For this reason field measurements must be conducted for static, thermal and dynamic loads in order to check the basic assumptions used to create the mathematical model.

In order that the engineer/dam designer can investigate a large number of designs and loading conditions it is important that the program is very efficient and that the computational cost of an analysis is negligible compared to personal costs. Also, the engineering time associated with data preparation and presentation of results should be minimal if the program is to be used as a design tool. In order that these criteria can be satisfied it is necessary that the program operate on the new generation of personal computer workstations in which the total cost of the computer hardware is less than one month's salary of an engineer.

The purpose of this paper is to summarize some of the fundamentals of finite element technology, as related to three dimensional dam analysis, and to present the details of new numerical methods which make it possible to conduct dynamic response of large dam/foundation/reservoir systems on inexpensive systems. At least one other paper presented in this workshop used SAP90, an earlier version of the SAP2000 program; therefore, a large number of numerical results will not be given in this paper. Emphasis will be placed on the new computational techniques which are now available and the development problems which still must be solved.

THREE DIMENSIONAL FINITE ELEMENTS

Since the development of three dimensional isoparametric elements over thirty years ago considerable experience has been obtained and new elements have been developed. For example, the twenty node three dimensional element [2] has excellent behavior properties if it is rectangular and is subjected to static loads. However, experience with this element has indicated the following disadvantages:

1. The node numbering system is not regular and it is difficult to generate meshes unless a special purpose program is used.

2. The element accuracy is reduced significantly if used in the nonrectangular mode.

3. The lumped mass matrix for the element is poorly conditioned. The use of a consistent mass matrix for the element increases computational effort significantly.

4. The stiffness matrix generated can have a large bandwidth compared to a mesh of lower order elements.

5. The stresses are accurate only at the integration points and special methods must be used to extrapolate the stresses to the nodes and surface of the element.

If should be pointed out that all finite elements used should pass the "patch" test. This test requires that if a group of elements is subjected to boundary displacements which are associated with constant strain conditions the program should produce the appropriate constant stresses. For example, the eight node element which was used in SAP-IV and SAP90 passed the patch test for rectangular geometry only.

Recent research [3] has indicated that the new 4 to 8 node isoparametric three dimensional element has behavior properties which are equal or superior to the 21 node element. Therefore, the computational effort to solve three dimensional solids, such as arch dams, has been significantly reduced. The element has "corrected" incompatible modes which allow the element to pass the patch test for all geometries. Also, the element can be used for material which has a very low shear modulus (Poisson's ratio near 0.5) without locking. Therefore, it can be used to approximate fluid like material. In addition, a force method is used to calculate element stresses directly from element nodal forces which are in exact global equilibrium. This element has been incorporated into the SAP2000 program [4].

DYNAMIC RESPONSE ANALYSIS

One of the most computationally intensive phases of a dynamic response analysis of a large three dimensional structure is the calculation of modeshapes and frequencies. Many of the programs for arch dam analysis use a version of the subspace iteration method which was developed by J. Bathe and the author over twenty years ago. The accuracy and speed of the basic subspace algorithm has been significantly improved [5].

Modeshapes (eigenvectors) are used to transform the dynamic equilibrium equations into a set of uncoupled modal equations which can be integrated with a minimum of numerical effort. It was long assumed that the exact eigenvectors were the most accurate vectors to be used to produce the uncoupled modal equations; however, it has been shown that this is not true [6]. It is possible to generate a set of Ritz vectors, which are mass and stiffness orthogonal, which produce more accurate displacements and stresses in a mode superposition analysis if the same number of vectors are used. Furthermore, the computational effort involved to calculate the Ritz vectors is significantly less than that required to solve the eigenvalue problem. The basic reason why the Ritz vectors are more accurate than the eigenvectors is that the spatial properties of the loads are used to generate the Ritz vectors; whereas, this information is neglected in the solution of the eigenvalue problem. An additional advantage to the use of Ritz vectors is that they can be used to solve wave propagation and foundation response problems [7].

Dams with infinite foundation and reservoir boundary conditions can be approximated with finite (finite element) models if viscous dash pots are added to the boundary of the model. For a finite element model of this type real mode shapes and frequencies do not exist. However, the solution of the coupled model equations in the time domain can be accomplished by a new integration algorithm [8]. The approach is very fast and only involves a small increase in computer time during the numerical integration of the modal equations.

ANALYSIS OF THE BENCHMARK ARCH DAM

The verification of any computer program is to start with the solution of simple problems with theoretical results. A standard set of test problems have evolved over the past several years in order to verify different elements and numerical methods. This verification work started with one paper [9]. At the present time this ongoing verification work is reported in "Benchmark" which is a quarterly newsletter of the National Agency for Finite Element Methods and Standards [10]. While arch dam structures are more complex they are just a special case of the application of three dimensional finite elements.

If a finite element model of an arch dam, subjected to hydrostatic loading, produces a maximum displacement at the crest which is low, compared to a converged solution, then all the other displacements at other points in the dam will also be low. If the element used is a displacement based element and consistent stresses are calculated all significant stresses at all locations will also be low. It is also reasonable to conclude, if there are no errors in the calculation of the total mass of the elements, that the free frequencies will be larger than the converged values. On the other hand, the thermal stresses associated within the stiff finite element model may be larger than the converged values due to thermal locking [3].

In the case of mode shapes, it is of little value to compare plots of mode shapes since mode shapes are not physically or mathematically unique if their frequencies are equal. The mode shapes of a dam associated with the low frequencies, and their participating mass factors, can add important physical incite into the behavior of the dam. However, sets of mode shapes, which are significantly different, can produce almost identical displacements and stresses when used as the basis of a mode superposition time history analysis.

The upstream view of one mesh used for the analysis of the dam is shown in Figure 1. In order to eliminate the number of variables which are introduced the foundation was condidered fixed. The first six frequencies, in cycles per second, were found by the subspace iteration method to be

1	2	3	4	5	6
4.203	4.469	5.776	6.475	8.003	8.807

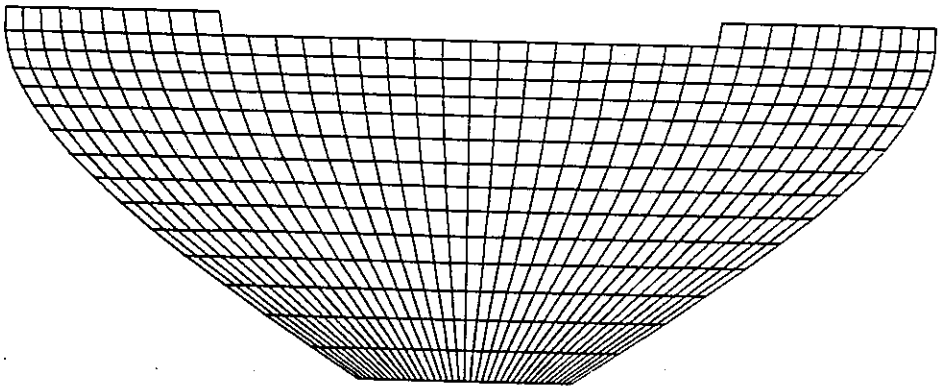

Figure 1. FINITE ELEMENT MODEL OF ARCH DAM

A finite element analysis was also run with two elements in the thickness direction and, as expected, the frequencies were a fraction of one percent smaller. Therefore, it was verified that, for the purpose of evaluating the displacements, one eight node element in the thickness direction (with corrected incompatible modes) is adequate. With respect to stresses, however, the same conclusions cannot be made. At the intersection of the dam and the foundations are points of stress concentrations; therefore, the finer the mesh the larger the values of stress. The problem of interpreting the engineering significance of these large stress concentrations under both static and dynamic loads involves considering local nonlinear material behavior and the creep properties of the concrete. For these reasons no values of stress will be presented in this paper since large tensile stresses exist only in the finite element model and not in the real structure.

The first 24 periods (obtained from an exact eigenvalue analysis) and participating mass in the three different directions are summarized in table 1. The participating mass in a direction indicates the amount of base shear force which would be produced by that mode if a unit base acceleration was applied in that direction. It is a standard requirement in the dynamic analysis of structures that one must include a sufficient number of modes in order to capture at least 90 percent of the mass in the direction of the dynamic load. It is apparent that if only six modes are used in an earthquake analysis of this arch dam a significant error would result.

TABLE 1. FIRST 24 PERIODS and PARTICIPATING MASS

		PARTICIPATING MASS - (percent)					
MODE	EXACT PERIOD(sec)	X-DIR	Y-DIR	Z-DIR	X-SUM	Y-SUM	Z-SUM
1	.23792	.000	9.985	.000	.000	9.985	.000
2	.22376	13.933	.000	.002	13.933	9.985	.002
3	.17313	22.575	.000	.539	36.508	9.985	.541
4	.15443	.000	2.127	.000	36.508	12.112	.541
5	.12448	.387	.000	1.238	36.895	12.112	1.779
6	.11355	18.328	.000	4.925	55.223	12.112	6.704
7	.10055	.000	.007	.000	55.223	12.119	6.704
8	.09397	.000	11.924	.000	55.223	24.043	6.704
9	.08364	.211	.000	.162	55.433	24.043	6.866
10	.07579	2.036	.000	1.073	57.469	24.043	7.940
11	.07168	.000	.992	.000	57.469	25.035	7.940
12	.06634	.000	2.135	.000	57.469	27.171	7.940
13	.06504	3.326	.000	15.793	60.795	27.171	23.733
14	.06158	.644	.000	.000	61.440	27.171	23.733
15	.05948	.000	41.128	.000	61.440	68.299	23.733
16	.05844	.315	.000	.086	61.755	68.299	23.818
17	.05317	.000	.005	.000	61.755	68.304	23.818
18	.05237	.000	2.319	.000	61.755	70.623	23.818
19	.05180	.000	.485	.000	61.755	71.108	23.818
20	.04934	.912	.000	29.726	62.666	71.108	53.545
21	.04664	.067	.000	.002	62.734	71.108	53.547
22	.04558	.003	.000	.036	62.737	71.108	53.583
23	.04423	.067	.000	.209	62.804	71.108	53.791
24	.04348	.000	.068	.000	62.804	71.176	53.791

TABLE 2. PERIODS AND PARTICIPATING MASS FOR RITZ VECTORS

		PARTICIPATING MASS - (percent)					
MODE	approximate PERIOD(sec)	X-DIR	Y-DIR	Z-DIR	X-SUM	Y-SUM	Z-SUM
1	.23792	.000	9.985	.000	.000	9.985	.000
2	.22376	13.933	.000	.002	13.933	9.985	.002
3	.17313	22.575	.000	.539	36.508	9.985	.541
4	.15443	.000	2.127	.000	36.508	12.111	.541
5	.12448	.387	.000	1.238	36.895	12.111	1.779
6	.11355	18.328	.000	4.925	55.223	12.111	6.704
7	.10047	.000	.007	.000	55.223	12.118	6.704
8	.09397	.000	11.928	.000	55.223	24.046	6.704
9	.08364	.211	.000	.162	55.434	24.046	6.866
10	.07579	2.036	.000	1.074	57.469	24.046	7.940
11	.07031	.000	1.893	.000	57.469	25.939	7.940
12	.06504	3.327	.000	15.794	60.796	25.939	23.734
13	.06156	.667	.000	.000	61.463	25.939	23.735
14	.05967	.000	42.551	.000	61.463	68.490	23.735
15	.05824	.290	.000	.090	61.753	68.490	23.825
16	.05010	.000	3.049	.000	61.753	71.539	23.825
17	.04934	.919	.000	29.774	62.672	71.539	53.599
18	.04031	5.863	.000	1.090	68.536	71.539	54.689
19	.03716	3.841	.000	9.464	72.377	71.539	64.153
20	.03444	3.015	.000	.432	75.392	71.539	64.585
21	.03066	1.911	.000	8.110	77.303	71.539	72.695
22	.02942	.000	15.905	.000	77.303	87.443	72.695
23	.02239	5.679	.000	5.387	82.982	87.443	78.082
24	.02018	8.011	.000	9.912	90.994	87.443	87.993

The dynamic properties of the "load dependent Ritz vectors" for the same arch dam finite element model are summarized in Table 2. The vectors were generated using uniform acceleration loads in the three global directions as the starting vectors in the sequential generation algorithm. For this case the first 10 periods are the same as the periods found from the exact eigenvalue solution method. The other Ritz vectors, which are linear combinations of exact eigenvectors, are different; however, their participating masses are considerably larger than the exact eigenvectors. Therefore, for earthquake type of loading the 24 Ritz vectors will produce significantly more accurate results than if the exact eigenvectors are used in a mode superposition analysis.

Not only are the use of Ritz vectors more accurate for this arch dam, the computer time required to calculate the Ritz vectors is significantly less. On a personal computer, with a 20 MHz 80387 coprocessor, the following computer times were required:

Calculation of 24 Exact Eigenvalues	220 minutes and 30 seconds
Calculation of 24 Ritz Vectors	14 minutes and 41 seconds

It also should be pointed out that the subspace algorithm used to calculate the exact eigenvalues is significantly faster than the one which was used in the SAP-IV program. Therefore, during the last 20 years, the computer time required for this phase of a dynamic analysis has been reduced by approximately a factor of 100.

The computer time for the static solution of this problem (552 elements, 1248 nodes, 3228 equations and 4 load conditions) can be summarized as follows:

Read, generate and check input data	2 minutes	20 seconds
Calculation of element stiffnesses	6 minutes	10 seconds
Profile or bandwidth reduction	4 minutes	10 seconds
Formation of equilibrium equations	5 minutes	20 seconds
Solution of equations	6 minutes	50 seconds
Equilibrium check and calculation of reactions	3 minutes	10 seconds
Calculation of element stresses	12 minutes	30 seconds
TOTAL COMPUTER TIME	40 minutes	30 seconds

ANALYSIS OF ARCH DAM AND RESERVOIR

As previously mentioned the eight node solid element has the ability to model materials which have a Poisson's ratio near 0.5. In order to illustrate this option the dam and reservoir was modeled by the mesh shown in Figure 2. The material properties used for the dam and water are summarized as follows:

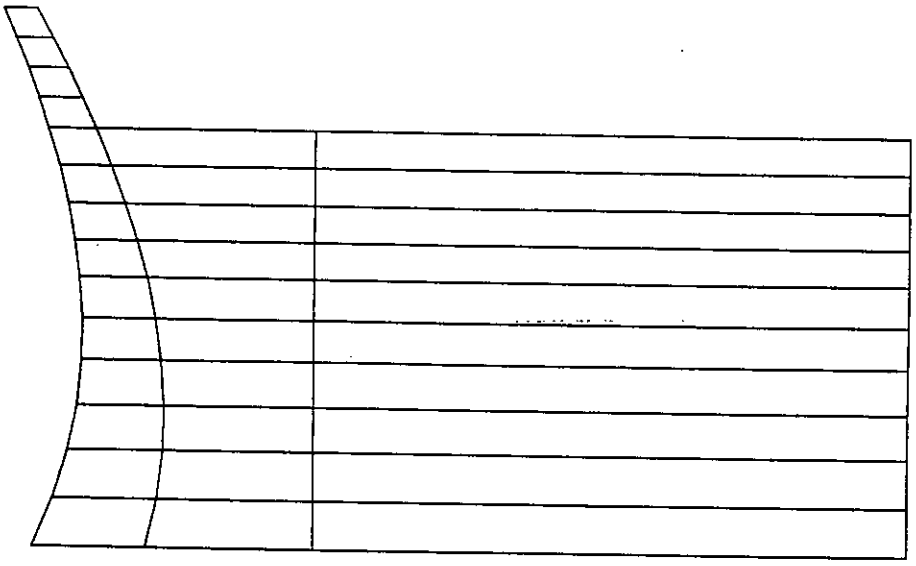

FIGURE 2. FINITE ELEMENT MESH FOR DAM-RESERVOIR

	DAM	WATER
Unit weight	30 kNm^{-3}	10 kNm^{-3}
Possion's Ratio	0.2000	0.4995
Young's Modulus	36 10^6 kNm^{-2}	0.006 10^6 kNm^{-2}
Shear Modulus	15 10^6 kNm^{-2}	0.002 10^6 kNm^{-2}
Bulk Modulus	50 10^6 kNm^{-2}	2.114 10^6 kNm^{-2}
Compression Wave Velocity	4044 ms^{-1}	1440 ms^{-1}

It is apparent that water is not incompressible compared to concrete. In fact, water is a very light weight and soft material compared to concrete. Also, for this arch dam example, the reservoir is at a low elevation. Therefore, we would expect the dam-reservoir interaction effects during earthquake loading to be minimum.

In order to check if the finite element model of the reservoir has fluid like behavior the selfweight displacements of the dam are calculated using a water elevation of 491 meters. The following results were obtained:

Selfweight of dam and surface pressure on upstream face (figure 1)	0.5645 cm
Selfweight of dam-reservoir system (figure 2)	0.5586 cm

Since the difference is less than one percent this example clearly illustrates that the fluid elements are not locking and that the correct pressure is being developed within the fluid model. For this loading the boundary at the right surface was restrained in the upstream direction.

The following approximate frequencies, associated with a Ritz vector analysis, were calculated for the bounded dam-reservoir system:

1	2	3	4	5	6
3.243	3.355	4.840	5.842	6.541	7.226

As expected, these frequencies are lower than the results obtained without the reservoir. It is of interest to note that the added mass of the water has been estimated by a very simple model. A more significant test of this model is if dynamic loads are applied and the results are compared with a more exact method [12].

This model can be used for a dynamic response analysis if radiation boundary conditions are used at the upstream face. Normally these radiation boundary conditions are frequency dependent; however, it has been shown that a system of boundary springs and linear dampers can be used to obtain very accurate results [11]. These boundary condition options exist in SAP2000.

Additional comparative studies are required before this approach can be used. However, this verification can be conducted using two dimensional models [12,13].

FINAL REMARKS

The following list contains the author's opinions with respect to the finite element analysis of arch dams:

1. It is the responsibility of every user to personally verify (benchmark) accuracy of every computer program used for the analysis of dams.

2. Many of the computer programs currently used for the analysis of dams are obsolete with respect to efficient finite elements and numerical methods.

3. A modern program, which has no errors, can still produce poor results if the user is not familiar with basic finite element approximations and is inexperienced with the dynamic behavior of complex solid/fluid/foundation structural systems.

4. The development of more accurate finite elements, the Ritz vector generation algorithm and a more general numerical time integration method allow large dam-reservoir structures to be solved on inexpensive personal computer systems.

5. The comparison of frequencies only, as an indication of the accuracy of a dam reservoir finite element model, is of little or no value in the prediction of the dynamic response of the system.

6. A large number of eigen or Ritz vectors are required to accurately predict the dynamic response of arch dams. The participating mass factors can be used to estimate the number of modes required.

7. A standard two dimensional dam/foundation/reservoir "benchmark" problem, subjected to time history loading, should be established in order to evaluate the different numerical methods which are currently being used.

8. After the two dimensional study is completed a simple, but realistic, model of an arch dam structure can be defined as a "benchmark" problem.

9. The problem of multi-support input ground motion should also be considered for arch dams [14].

REFERENCES

1. P. G. Smith and E. L. Wilson, "Automatic Design of Shell Structures", Journal of the Structural Division, ASCE, Vol. 97. January 1971, pp. 191-201.

2. K. J. Bathe, E. L. Wilson and F. E. Peterson, "SAP IV--A Structural Analysis Program for Static and Dynamic Response of Linear Systems" , UCB/EERC Report No. 73/11, Earthquake Engineering Research Center, University of California, Berkeley, June 1973.

3. E. L. Wilson and A. Ibrahimbegovic, "Use of Incompatible Modes for the Calculation of Element Stiffnesses or Stresses", Finite Elements in Analysis and Design, Vol. 7, 1990, pp. 229-241.

4. E. L. Wilson, "SAP2000 - A General Purpose Computer Program for the Static and Dynamic Analysis of Structures", Structural Analysis Programs, Inc., 1050 Leneve Place, El Cerrito, CA 94530, USA.

5. E. L. Wilson and T. Itoh, "An Eigensolution Strategy for Large Systems", J. Computers and Structures, Vol. 16, No. 1-4, 1983, pp. 259-265.

6. E. L. Wilson, M. Yuan and J. Dickens, "Dynamic Analysis by Direct Superposition of Ritz Vectors", Earthquake Engineering and Structural Dynamics, Vol. 10, 1982.

7. E. L. Wilson and E. P. Bayo, "Use of Ritz Vectors in Wave Propagation and Foundation Response", Earthquake Engineering and Structural Dynamics, Vol. 12, 1984, pp. 499-505.

8. A. Ibrahimbegovic and E. L. Wilson, "Simple Numerical Algorithms for the Mode Superposition Analysis of Linear Structural Systems with Nonproportional Damping", Computers and Structures, Vol. 33, No. 2, pp. 523-531, 1989.

9. R. H. MacNeal and R. L. Harder, "A Proposed Standard Set of Problems to Test Finite Element Accuracy", Finite Elements in Analysis and Design", Vol. pp. 3-20, 1985.

10. "Benchmark", Editor: Dr. George Leckie; NAFEMS, National Engineering Laboratory, East Kilbride, Glasgow G75 0QU.

11. J. P. Wolf, "Consistent Lumped-Parameter Models for Unbounded Soil", Earthquake Engineering and Structural Dynamics", Vol. 20, January 1991.

12. G. Fenves and A. K. Chopra, Earthquake Analysis and Response of Concrete Gravity Dams", Report UCB/EERC-84/10, University of California, Berkeley, CA (1984).

13. A. C. Singhal, "Comparison of Computer Codes for Seismic Analysis of Dams", Computers and Structures, Vol. 38, No. 1., pp 107-112, 1991.

14. S. B. Kojic and M. D. Trifunac, "Earthquake Stresses in Arch Dams", ASCE J. of Eng. Mech., Vol. 117, no.3, March 1990, pp. 532-574.

First Benchmark Workshop on
NUMERICAL ANALYSIS OF DAMS
Bergamo (Italy) May 28-29,1991

The linear dynamic analysis of an arch dam including both incompressible and compressible fluid interaction (theme A)

E.J.Greeves, C.A.Taylor & R.T.Severn
Earthquake Engineering Research Centre
University of Bristol
Department of Civil Engineering
Bristol UK

1.0 Introduction

As part of an initiative stemming from the ICOLD meeting held in Sydney, May 1990, a benchmark conference was devised to help compare all available software used in the analysis and design of dams. It is proposed to use the findings from the conference to produce an ICOLD bulletin concerning this area of work. The paper presented here is concerned only with the dynamic behaviour of the chosen analysis example, the Talvacchia dam, Italy. A series of modal analyses were performed, comparing dry structural response with coupled fluid-structure response, also highlighting the role of fluid compressibility is such analyses.

2.0 Dry Modal Analysis (rigid foundation block)

The first in the specified series of analyses was concerned with obtaining the first six mode shapes and natural frequencies for the dam on a rigid foundation block. This was achieved by simply restraining all nodes which were in contact with the foundation elements.

2.1 Mesh details

The mesh as supplied by the organising committee was used, with no amendments, other than element node re-ordering to satisfy the codes used. The combined dam and foundation mesh is shown in fig.(1). A standard 27 point Gauss integration grid was used for the dam elements.

2.2 Software and algorithms used

Two analyses were performed, one using SAPIV (Bathe et al,1973) and the second using SOLVIA (Solvia Engineering,1989). Both these packages were subsequently used to perform coupled (fluid-structure) modal analyses, hence a comparison of their structural performance was required. The SOLVIA pre-processor (Solvia Engineering,1989) has a bandwidth reduction algorithm based on that proposed by Cuthill and McKee (1969). This scheme determines the optimum equation numbering within the mesh, and does not require costly node re-numbering. In using this method, the bandwidth of this first mesh was minimised to 201 equations, with a total of 1662 equations. The source code for SAPIV was suitably amended to allow the use of this bandwidth optimisation scheme as well.

For both analyses, the Subspace Iteration algorithm was used (Bathe,1971) to determine the first six eigen-pairs. A subspace of 14 base vectors was used for the solution, with a convergence tolerance of 1e-5.

2.3 Modal results

The first six mode shapes are plotted in fig(2). The natural frequencies are tabulated in table (1) for both the SOLVIA and SAPIV analyses. As a check, the SAPIV mesh was re-analysed using 21-noded elements (a centre node was introduced for each element), this giving an insignificant variation in frequencies ($<0.5\%$).

The results as shown, conform with the expected dynamic behaviour of an arch dam. The first mode exhibited is the first anti-symmetric mode, with the first mode containing the second vertical cantilever bending motions appearing as mode 6.

3.0 Coupled Modal Analysis (incompressible fluid formulation)

The second of the specified analyses required the first six eigen-pairs for the coupled dam-foundation-reservoir system. This section considers an incompressible fluid model.

3.1 Fluid formulation

3.1.1 Governing equations - The chosen fluid representation models the hydrodynamic pressure distribution arising in the reservoir due to the dynamic action of the dam. This hydrodynamic pressure distribution is governed by the general wave equation, the general vector form being given by

$$\nabla^T \nabla \varphi = \frac{1}{c^2} \frac{\partial^2 \varphi}{\partial t^2} \quad \ldots\ldots\ldots\ldots\ldots\ldots\ldots\ldots\ldots\ldots \quad [1]$$

φ = hydrodynamic pressure

$$\nabla = \left[\frac{\partial}{\partial x} \frac{\partial}{\partial y} \frac{\partial}{\partial z} \right]$$

c is the wave celerity of the fluid

The solution of this equation is governed by a pair of boundary equations. The first defines the presence of a free surface, ignoring the presence of surface waves. Bustamente (1963) has shown that this assumption leads to insignificant error for civil engineering structures. The boundary condition can be written as

$$\varphi \Big|_{z=h} = 0 \quad \ldots\ldots\ldots\ldots\ldots\ldots\ldots\ldots\ldots\ldots \quad [2]$$

h is the depth of the reservoir

The second boundary condition is concerned with the fluid-solid boundaries. This second condition can be wrtitten as

$$\frac{\partial \varphi}{\partial n} = -\rho a_n \quad \ldots\ldots\ldots\ldots\ldots\ldots\ldots\ldots\ldots\ldots \quad [3]$$

n is the normal direction to the boundary

ρ is the fluid density

a_n is the normal acceleration of the boundary

Obviously for rigid boundaries (canyon sides etc.), the normal acceleration value is zero.

For an incompressible fluid, the wave celerity is assumed to be infinite. This allows us to rewrite eqn.[1] as

$$\nabla^T \nabla \varphi = 0 \quad \ldots\ldots\ldots\ldots\ldots\ldots\ldots\ldots\ldots\ldots \quad [4]$$

which is the form used for this incompressible fluid representation.

3.1.2 Finite element representation of the fluid - One possible technique which can be used for the solution of eqns.[2],[3] and [4] is the finite element method. Other methods have been used, including electrical analogues (Zienkiewicz & Nath,1964), and a closed form solution using a Ritz expansion (Chakrabarti &

Chopra,1971). The finite element method readily allows the use of irregular and arbitrary reservoir geometry, and was adopted in producing a general three dimensional fluid-structure interaction analysis package, SAPIVP (Greeves & Dumanoglu,1989).

In discretising the fluid domain using the finite element technique, the standard assumption concerning the primary nodal variable(pressure) is made

$$\varphi = N p^e \quad \ldots\ldots\ldots\ldots\ldots\ldots\ldots\ldots\ldots\ldots \quad [5]$$

N are the chosen interpolation functions

p^e are the nodal pressure values

This assumption is used to discretise the governing, second order differential equation (eqn. [4]), and boundary conditions [2] and [3] via the weighted residual statement (Zienkiewicz,1977). Substituting eqns.[2], [3] and [4] into this statement gives

$$\int_V (\nabla^T N)(\nabla N)\, dv\, p^e - \int_S N^T \rho\, a_n\, ds = 0 \quad \ldots\ldots\ldots \quad [6]$$

From this we can establish the standard 'stiffness matrix' relation for the fluid domain

$$G\,\mathbf{p} = R \quad \ldots\ldots\ldots\ldots\ldots\ldots\ldots\ldots\ldots\ldots \quad [7]$$

G is the fluid stiffness matrix $= \int_V (\nabla^T N)(\nabla N)\, dv$

R is the fluid load vector $= \int_S N^T \rho\, a_n\, ds$

$\mathbf{p}$ is a vector of fluid nodal pressures

For any known fluid boundary acceleration distribution, the subsequent hydrodynamic pressure distribution can be readily obtained by the use of eqn.[7].

3.2 Coupled eigen-solution algorithm

The standard eigen statement for a general eigen vector can be written as

$$K X_i = \lambda_i M X_i \quad \ldots\ldots\ldots\ldots\ldots\ldots\ldots\ldots\ldots\ldots \quad [8]$$

K is the system stiffness matrix

X_i is the i^{th} eigen-vector

λ_i is the i^{th} eigen-value

M is the system mass matrix

A possible solution algorithm can be developed using inverse iteration to give the fundamental eigen-pair. A typical algorithm would be

1) form a suitable starting iteration vector X_1^0

2) form the product $Y_1^k = M X_1^{k-1}$

3) solve the equation $K X_1^k = Y_1^k$

4) obtain current estimate eigen vale $\lambda_1 = \dfrac{1}{(X_1^k)_{j,max}}$

5) normalise the iteration vector such that $\max \left| (X_1^k)_{j,max} \right| = 1.0$

Steps 2 to 5 are repeated until convergence on the eigen-value is achieved. Higher modes can be simply obtained by orthogonalising the current iteration vector to previous found solutions, or by shifting above these previously found results.

When using an incompressible fluid model to represent fluid-structure interaction, the fluid effects can be represented by an added fluid mass. In doing this, the standard eigen problem of eqn.[8] is recast as

$$K X_i = \lambda_i (M_S + M_F) X_i \quad \ldots\ldots\ldots\ldots\ldots\ldots\ldots\ldots [9]$$

M_S is the solid mass matrix

M_F is the added fluid mass matrix

The algorithm as described in steps 1 to 5 above can still be used, noting that now in step 2, the mass-iteration vector product must now include the additional mass term ie.

$$Y_1^k = M_S X_1^{k-1} + M_F X_1^{k-1} \quad \ldots\ldots\ldots\ldots\ldots\ldots\ldots\ldots [10]$$

Dungar (1978), proposed a novel coupling procedure for evaluating this additional term. The product of added fluid mass and iteration vector is equated to a mass and acceleration product, the result being an equivalent inertial force. This force can be also represented by the hydrodynamic force acting on the upstream face of the dam. Dungars' method involved forming the fluid load vector, based on the current iteration (acceleration) vector, solving for the hydrodynamic pressures in the fluid, and subsequently integrating them over the fluid-structure interface. This is summarised by the two steps given by

$$\mathbf{p}_1^{k-1} = G^{-1} \int_S N^T \rho X_1^{k-1} \, ds$$

$$M_F X_1^{k-1} = \int_S \mathbf{p}_1^{k-1} \, ds \quad \ldots\ldots\ldots\ldots\ldots\ldots\ldots\ldots [11]$$

In this way, the added fluid mass terms are never explicitly derived, the solution procedure being very efficient. It is this algorithm which has been implemented within SAPIVP (Greeves & Dumanoglu,1989).

3.3 Mesh details

The mesh as supplied by the organising committee was used for both dam and foundation, and reservoir. The foundation flexibility was included, but assumed massless as instructed. The fluid mesh was modelled as a substructure, linked by common interface nodes to the dam. The combined dam-foundation-reservoir mesh is shown in fig.(3).

At all the free surface nodes in the fluid, zero pressure conditions were enforced by deflating these nodal degress of freedom. At the far boundary of the reservoir, the pressures were not deflated, thus providing a check on possible mesh truncation errors. For an incompressible fluid, it is unlikely that these will be significant when using a mesh of this extent.

The 20 noded, isoparametric fluid elements employed a standard 27 point Gauss integration grid in their formulation, as did all the solid elements.

3.4 Results

3.4.1 Structual response - The frequencies and corresponding mode shapes are summarised in table (2), the crest displacements for each mode being shown in fig.(4). We note that the modal frequencies have changed, as well as their ordering. As expected all the frequencies have decreased, this decrease varying between 6% and 16%. The most affected mode shape is that containing the second vertical cantilever motions. This is also as expected, due the variation of dam motion along the vertical axis. A simplistic approach would indicate that the additional fluid mass for this mode is of the order of 30 to 40% of the total dam mass, although this does not account for the spatial distribution of this added mass. The eigen-vectors produced by SAPIVP are mass normalised, now including the additional fluid mass effects.

3.4.2 Fluid response - As a by-product of the eigen-solution scheme, the modal fluid pressure distributions are also found. These can be used in subsequent linear response analyses, as can the structural mode shapes, by a suitable combination scheme. The modal pressures also give a useful indication of the combined fluid-structure system behaviour. Pressures at the dam-resrvoir interface are presented in figs.(5) to (7). Several vertical sections were taken at positions of s=-64m, s=-32m, s=0m, s=32m and s=64m. This coordinate scheme refers to Appendix 8 of the instructions, as supplied by the organising committee. The second mode for the coupled model is the second symmetric mode. The pressure distributions clearly reflect this, with these distributions being also symmetric about the centre line of the dam. The peak pressure values occur at the centre line and decrease towards the abutments. This reflects both the decreasing dam acceleration values, and depth of the reservoir, away from the centre line. The third

mode for the system is the first symmetric mode of the dam. Again we see that the pressure distributions are also symmetric about the centre of the dam, now noting that the peak pressure values occur at about s = +/-32m. This is due to the peak dam motions occurring in this region. As a final check, we consider the fifth mode of the coupled system. This is the first mode where the dam is deforming in the second vertical cantilever mode. It is also symmetric about the centre of the dam. We now see that the peak pressure value occurs at about mid reservoir depth, compared with the second mode, where the corresponding peak value occurs at about a quarter of the depth from the free surface. If the reservoir had been deeper we could have expected to have seen both a positive and negative lobe in the pressure distribution.

As a check on possible mesh truncation errors, the decay of hydrodynamic pressures into the reservoir was considered. Fig.(8) shows this decay, away from the upstream face of the dam, for modes two and five. As is clearly shown, the decay is exponential, and the pressures have reached a negligible level at about 150m from the dam. This corresponds to about three times the depth of the reservoir, which is widely regarded as an acceptable limit for the fluid mesh, using an incompressible fluid formulation.

4.0 Coupled modal analysis (compressible fluid formulation)

The effects and siginficance of fluid compressibility on the dynamic response of fluid-structure systems is still under debate. Work by Tanaka & Hudspeth (1988) resinforces ideas put forward earlier by Chopra (1968), that fluid compressibility effects become significant for responses with a frequency greater than the fundamental frequency of the reservoir. Duran and Hall (1988) offer a slighlty different opinion, based on their experimental and thoeretical studies of Morrow Point arch dam. They conclude that fluid compressibility influences the dynamic response of the dam at frequencies greater than 60% of the reservoirs fundamental mode. This agrees well with a theortical study carried out by O'Connor and Boot (1988), which gives a critical frequency of 70% of the reservoir fundamental mode.

Using these later figures, it would seem that some of the first six modes of vibration for the Talvacchia dam may well be influenced by fluid compressibility effects. The way in which fluid effects are currently understood to influence structural behaviour, is by the inclusion of added hydrodynamic damping terms, as well as added fluid mass. For this paper we are only performing undamped, modal analyses, hence complex responses cannot be predicted.

The modal analysis for the coupled dam-foundation-reservoir system is now repeated, using this alternative, compressible fluid model. The mode shapes subsequently presented are standard, mass ortho-normalised as for the previous results.

4.1 Fluid formulation

The element formulation discussed here is based upon that proposed by Wilson and Khalavati (1986) for a novel two dimensional fluid element

4.1.1 Governing fluid equations - We are now concerned with a standard solid element formulation, the stress-strain relationship being used to dictate the performance of the element. The principal element strain term is the bulk strain, which is related to fluid pressure by the bulk modulus term ie.

$$p_v = K \varepsilon_v \quad \ldots\ldots\ldots\ldots\ldots\ldots\ldots\ldots\ldots\ldots\ldots\ldots\ldots\ldots [12]$$

p_v is the bulk stress
K is the bulk modulus of the fluid
ε_v is the bulk strain

We are modelling a perfect, inviscid fluid which is irrotational in nature. We can define 3 rotational or vortex strains for the three dimensional element. These are given by

$$\hat{\varepsilon_x} = \tfrac{1}{2}\left[\frac{\partial v}{\partial z} - \frac{\partial w}{\partial y}\right]$$

$$\hat{\varepsilon_y} = \tfrac{1}{2}\left[\frac{\partial w}{\partial x} - \frac{\partial u}{\partial z}\right]$$

$$\hat{\varepsilon_z} = \tfrac{1}{2}\left[\frac{\partial u}{\partial y} - \frac{\partial v}{\partial x}\right] \quad \ldots\ldots\ldots\ldots\ldots\ldots\ldots\ldots\ldots\ldots [13]$$

x, y and z refer to the carterian directions
u,v and w are the corresponding displacement vectors

To enforce irrotationality for the element, we must assign a very large spring stiffness to these strain terms. These can be thought of as 'watch-spring' type stiffnesses. In doing this, we will of course only approximate the irrotational condition, but choosing large enough spring constants will render the rotational motion frequencies well above the range of interest. The complete stress-strain relationship for the element is therefore.

$$\begin{Bmatrix} \sigma_v \\ \hat{\sigma_x} \\ \sigma_y \\ \hat{\sigma_z} \end{Bmatrix} = \begin{bmatrix} K & 0 & 0 & 0 \\ 0 & K_r & 0 & 0 \\ 0 & 0 & K_r & 0 \\ 0 & 0 & 0 & K_r \end{bmatrix} \begin{Bmatrix} \varepsilon_v \\ \hat{\varepsilon_x} \\ \varepsilon_y \\ \varepsilon_z \end{Bmatrix} \quad \ldots\ldots\ldots\ldots\ldots\ldots\ldots\ldots [14]$$

K_r is the rotational stiffness parameter

To provide the governing fluid equation of motion we shall use an energy approach. The strain energy for the element is given in the standard manner by

$$\pi_1 = \frac{1}{2}\int_v \varepsilon^T D\, \varepsilon dv \quad \ldots\ldots\ldots\ldots\ldots\ldots\ldots\ldots\ldots\ldots [15]$$

Similarly the kinetic energy is given in by the familiar expression

$$\pi_2 = \frac{1}{2}\int_v \mathbf{v}^T M\, \mathbf{v}\, dv \quad \ldots\ldots\ldots\ldots\ldots\ldots\ldots\ldots\ldots\ldots [16]$$

v is a vector of element velocities
M is the element mass matrix

A third possible energy contribution comes from the low frequency fluid sloshing motions. These correspond to overall zero volume modes. This gives the additional energy term

$$\pi_3 = \frac{1}{2}\int_s \mathbf{U_s}^T \rho\, g\, \mathbf{U_s}\, ds \quad \ldots\ldots\ldots\ldots\ldots\ldots\ldots\ldots\ldots\ldots [17]$$

$\mathbf{U_s}$ is a vector of element surface displacements

These terms can be combined in a Lagrangian analysis to derive the equation of motion, as is shown in the next section.

4.1.2 Finite element discretisation - A standard isoparametric formulation is required, ensuring compatibility with standard solid elements (8..27 noded brick element). The strain-displacement matrix is formed using the previously defined stress-strain relationships in eqns. [12] and [13]. The derivatives of the element shape functions with respect to cartesian space are determined by the use of

$$\begin{bmatrix} \frac{\partial}{\partial x} \\ \frac{\partial}{\partial y} \\ \frac{\partial}{\partial z} \end{bmatrix} = \mathbf{J}^{-1} \begin{bmatrix} \frac{\partial}{\partial r} \\ \frac{\partial}{\partial s} \\ \frac{\partial}{\partial t} \end{bmatrix} \quad \ldots\ldots\ldots\ldots\ldots\ldots\ldots\ldots\ldots\ldots [18]$$

r, *s* and *t* refer to the element naturalcoordinate system
J is the Jacobian matrix

The strain-displacement matrix is constructed directly from these terms. Substituting this matrix into the previously found energy component expressions, and using the equivalent matrix terms for eqns.[16] and [17] we obtain the expression

$$\pi = \frac{1}{2}\left[\int_v (B\,u)^T D\,(B\,u)\, dv + \mathbf{v}^T M\, \mathbf{v} + U_s{}^T \rho\, g\, U_s\right] \quad \ldots [19]$$

A direct application of Hamiltons equation yields the discretised equation of motion, given by

$$M\ddot{x} + Kx + S x_s = R \quad \ldots\ldots\ldots\ldots\ldots\ldots\ldots\ldots\ldots\ldots [20]$$

S is the surface stiffness matrix given by eqn.[17]

x_s is the vector of free surface displacements

4.1.3 Integration schemes - Clearly the element formulation includes a penalty requirement, due to the enforced irrotationality of the element. This requires that these strain terms are integrated with a reduced scheme, preventing an overstiff response of the element. In addition, however, the element must also be able to model incompressible fluid behaviour, such as the low frequency sloshing motions described in § 4.1.1. This therefore requires that the bulk strain term is also integrated by a reduced scheme. For an eight noded brick element, a single integration point at the centre of the element would be used, and for 20 to 27 noded arrangements a 2 by 2 by 2 Gauss scheme would be required.

The use of these lower integration orders allows the element to represent the required strain fields, but also has a side effect of rendering a high degree of matrix singularity. For the fluid element, this is further aggravated by there being only 4 independent strain terms per integration point (eqn.[14]), compared with 6 for a standard solid element, with 3 structural strains against 2 fluid strains for a two dimemensional element. For the combined fluid mesh, significant singularity can in some instancesbe retained, even after the imposition of fixed boundary conditions. Such behaviour is generaly restricted to two dimensional meshes. The free-surface stiffnesses introduced by the sloshing behaviour, eqn.[17], control the fluid mesh behaviour during these otherwise singular modes, giving rise to the mechanism by which low frequency sloshing motions can occur.

This tendency for low frequency motions can render the element highly inefficient, since many such low frequency sloshing modes may be required before the required fluid-structure modes are obtained. An alternative approach is to impose a shift on the combined system stiffness matrix to render these unwanted eigen-values negative. As a check, we can consider the stability of the 20 noded element fluid mesh used for this benchmark analysis. There are a total of 1710 fluid nodes, leading to 5130 (1710x3) possible degrees of freedom. A total of 164 degrees of freedom are restrained at the far boundary of the reservoir, leaving 4966 degrees of freedom. There are 363, 20 noded fluid elements each employing a total of 8 (2x2x2) Gauss points. At each Gauss point 4 independent strain relations are introduced. For the assembled fluid mesh this gives a total of 11616 (363x8x4) independent strain relations. This is clearly greater than the unrestrained degrees of freedom present in the fluid mesh (4996), and as such no low frequency sloshing motions would be expected.

A final point should be made concerning the element performance and the chosen integration scheme. Work with the 2 dimensional elements has shown that the use of reduced integration can incur errors of up to 30% in bulk strain modes, which can have a serious effect on the combined system behaviour. Recent work with the Field Consistent technique (Greeves et al.) has shown that significant enhancement in element performance can be obtained over the reduced integration element. Early work with the three dimensional element indicates possible similar enhancement for the 8-noded brick element.

4.2 Mesh details

As for the incompressible fluid analysis performed in § 3, the mesh supplied by the organising committee was used. In this case, however, some additional elements were included to link the fluid to the dam and canyon sides. As stated in § 4.1.1, the fluid is inviscid in nature. This implies that at fluid-solid interfaces only normal forces can be transmitted, there being no tangential component. This condition was enforced by the use of rigid link elements. The dam-reservoir interface nodes were connected by these elements, and the other boundary nodes were constrained to move tangentially to the canyon sides and bottom by the use of these links. At the far end of the reservoir, all nodal degrees of freedom were deflated, effectively forming a reflecting boundary.

The fluid elements were all integrated using an 8 point Gauss grid for both bulk and rotational strain terms. The rotational stiffnesses were chosen to be 1000 times greater than the bulk modulus terms. This value has been found to provide sufficient rotational constraint, without causing numerical instability (Olson & Bathe,1983;Hamdi et al,1978).

The displacement fluid element has been investigated within NONSAP (Bathe et al,1974) allowing the evaluation of both linear and non-linear fluid-structure systems (Greeves & Taylor,1990). Because of the size of the problem considered here, the SOLVIA analysis package was used, a variable noded three dimensional fluid element included in the code. The element, however, did not incorporate the free surface stiffness terms as described in the preceding sections. Although these modes will not be present for this mesh, the code was updated to allow the use of 8-noded brick elements.

As for the previous meshes, a bandwidth minimisation scheme was used by the SOLVIA preprocessor. For this mesh the optimised bandwidth was 1188, there being a total of 8295 equations. The analysis was carried out on an IBM 3090 machine with vector processing facilities.

4.3 Results

We now find the results from the coupled eigen solution to be somewhat different from those found previously. No longer do we find six, well separated and clearly defined mode shapes, but a large number of closely spaced modal responses. Here we see the phenomena of 'multiple system modes', responses where the structure is deforming in the same manner with the fluid displacing differently, the modes occurring at different frequencies. In some instances the frequencies are closely spaced, and in others they are well separated. Some of these multiple frequencies occur at values above the previously found dry responses.

Table (3) groups these modes together to offer an initial comparison with the results found using the incompressible pressure method. In these possible groups, there are some modes which offer a good comparison with the incompressible fluid results, and others which are in considerable variance. We must remember that to classify the mode shapes correctly, the motions of the whole mesh must be considered, including both structure and fluid.

5.0 Discussion of Results

To enable a comparison to be made, and a discussion of the results found using the compressible fluid element, this multiple mode behaviour must be interpreted. As we have stated in the previous section, the fluid motions must also be included in the modal classification. The fluid is a highly flexible domain, and may exhibit many more possible motions than the dam over the frequency range of interest.

There have been several earlier investigations into the dynamic response of arch dam-reservoir systems (Clough & Ghanaat,1986;Fok & Chopra,1985,1987). These studies were interested in establishing the significance of fluid compressibility in this response, and the effects which it has. Both Clough & Ghanaat and Fok & Chopra used compressible pressure fluid models, performing their analyses in the frequency domain. Clough & Ghanaat demonstrated that a general three dimensional fluid domain will possess many pressure resonances, at these resonances the hydrodynamic pressures becoming very large. For complex, three dimensional geometries the form of theses resonances becomes increasingly complex. The first of these fluid resonances is recognised as the fundamental compressive mode of the reservoir.

For the compressible fluid analyses performed here, a displacement type fluid element was used. Because of the reduced integration technique employed in the

element formulation, the fluid element is able to model both incompressible and compressible fluid regimes. To illustrate the significance of this, a modal analysis was repeated for the coupled fluid-structure model, with the dam and foundation now completely restrained. Hence the modal response of the fluid will be obtained. Approximately 30 fluid-only modes were found in the frequency range spanned by the coupled modal analysis, the first of such frequencies occurring at 3.01Hz. This is clearly lower than the fundamental compressive mode of the fluid, which would be expected to have a frequency of between 8 and 10Hz, allowing for the trapezoidal nature of the reservoir.

The presence of the multiple system modes for the compressible modal solution can now be understood in light of this behaviour for the fluid region of the finite element mesh. Figure (9) shows the four coupled system results where the dam deforms in the first antisymmetric mode, covering a frequency range from 3.183Hz to 4.438Hz. The incompressible fluid model predicts this frequency to occur at a frequency of 3.792Hz. Figure (10) shows three fluid-only modes which correspond closely to the fluid behaviour in the coupled dam-reservoir model. There is one mode, however, where the fluid behaviour is not seen in the fluid-only results. This is mode number 5, which has a frequency of 3.618Hz. The good agreement with the incompressible result should be highlighted. For this displacement fluid element analysis, it has been possible to identify three modes where the fluid motions are very similar for both the flexible and rigid dam conditions. For the flexible case the dam deforms in the first antisymmetric mode for each one. It would seem that these fluid-only resonances are driving the dam response, giving an apparent coupled system response. The single mode where this behaviour is not seen corresponds well with the previously found incompressible result, as would be expected since fluid compressibility should not be significant at this frequency. This 'driving' behaviour of the fluid mesh seems to represent a significant drawback in the modal analysis of such three dimensional fluid-structure systems using this technique. For the first antisymmetric mode of the dam it has been possible to seperate such behaviour, but for higher modes it becomes increasingly difficult, and requires considerable effort. Table (4) summarises the results found now after identification of these fluid driven modes. There is poor correspondence in frequency values, in some cases the coupled response occurring at higher values than the original dry modes. Clearly this does not conform with current understanding of fluid-structure interaction. Olson and Bathe (1983) highlighted the difficulties of modelling this type of fluid-structure interaction (category 4 in their original paper) using displacement fluid elements. In their analyses, they used standard integration in the element formulations and concluded that such elements were over-stiff. It would seem that when a reduced integration scheme is used, as here, the element still shows considerable problems, particularly for

modal analyses. It must be reported, however, that workers have successfully used the element in response analyses, El-Aidi & Hall (1988a,b) looked at the nonlinear response of Pine Flat gravity dam, Greeves and Taylor (1990) performed a similar investigation on Koyna dam, and Ahmadi & Osaka (1988) calibrated the response of an arch dam using the three dimensional element against field data. The Authors have not yet found any published data pertaining to a similar modal analysis as carried out here.

6.0 Conclusions

The aims of this paper have been to investigate numerically the fluid-structure interaction effects on the Talvacchia arch dam. The paper has evaluated two different techniques for modelling this interaction, one using an incompressible pressure formulation, and a second using a compressible displacement fluid element.

The results found using the incompressible fluid model compare well with previous similar results, the incremental shifts in modal frequencies consistent with the fairly low water level used in the analysis.

The second analysis was aimed at investigating the influence of fluid compressibility on the response of the coupled system. Instead, it shows an inherent problem in performing modal analyses for fluid-structure systems using this technique. The fluid portion of the mesh appears to drive the response of the dam, leading to coupled system modes where the dam deforms in the same manner but at different frequencies. Such behaviour arises because of the fluids ability to model a wide range of both incompressible and compressible resonances. For some coupled modes it is possible to extract 'genuine' fluid-structure interaction motions, but for others it is not.

7.0 References

Ahmadi,M.T. & Ozaka,Y.O. (1988) *A simple method for the full-scale 3-D dynamic analysis of arch dam* Proceedings of the Ninth World Conference on Earthquake Engineering, **VI**, pp.373-378,Japan, 1988

Bathe,K.J (1971) *Solution methods of large generalised eigenvalue problems in structural engineering* report no. UC SESM 71-20, Civil Engineering Department, University of California, Berkeley, 1971.

Bathe,K.J, Wilson,E.L & Peterson,F.E (1973) *SAPIV A structural analysis program for static and dynamic response of linear systems* report no. EERC 73-11 College of Engineering, University of California, Berkeley, June 1973.

Bustamente,J.I. (1963) *Precision hidrodinamica en presas y depositos* Boletin Sociedad Mexicana de Ingeniera Sismica, 1963

Chakrabarti,P & Chopra,A.K (1973) *Earthquake analysis of gravity dams including hydrodynamic interaction* Earthquake Engineering and Structural Dynamics, **2**, 1973.

Chopra,A.K. (1968) *Earthquake behaviour of reservoir-dam systems* Proceedings American Society of Civil Engineers, EM6, **94**, 1968

Clough,R.W. & Ghanaat,Y. (1986) *Dynamic arch dam-reservoir interaction* Proceedings of the 8th European Conference on Earthquake Engineering, Lisbon, **3**

Cuthill,E.H. & McKee,J.M. (1969) *Reducing the bandwidth of sparse symmetric matrices* Proceedings, Conference Association for Computing Machinery, pp151-172, 1969

Dungar,R (1978) *An efficient method of fluid-structure coupling in the dynamic analysis of structures* International Journal of Numerical Methods in Engineering, **13**, 1978.

Duron,Z.H & Hall,J.F (1988) *Experimental and finite element studies of the forced vibration response of Morrow Point dam* Earthquake Engineering and Structural Dynamics, **16**, 1988.

El-Aidi,B. & Hall,J.F. (1989a) *Nonlinear earthquake response of concrete gravity dams part 1 : modelling* Earthquake Engineering and Structural Dynamics, **18**, 1989

El-Aidi,B. & Hall,J.F. (1989b) *Nonlinear earthquake response of concrete gravity dams part 2 : behaviour* Earthquake Engineering and Structural Dynamics, **18**, 1989

Fok,K.L. & Chopra,A.K. (1985) *Earthquake analysis and response of concrete arch dams* Report no.UCB/EERC-85/07, Earthquake Engineering Research Centre, University of California,Berkeley

Mode number	SAPIV frequency (Hz)	SOLVIA frequency (Hz)
1 - A1 B1	4.193	4.175
2 - S2 B1	4.478	4.463
3 - S1 B1	5.534	5.511
4 - A2 B1	6.530	6.502
5 - S3 B1	8.266	8.229
6 - S2 B2	8.984	8.956

Notes S:symmetric A:antisymmetric B:vertical cantilever bending

Table 1 - Dry modal analysis with rigid foundation block - first 6 modes

Mode number	SAPIV frequency (Hz)	SOLVIA frequency (Hz)
1 - A1 B1	4.193	4.175
2 - S2 B1	4.478	4.463
3 - S1 B1	5.534	5.511
4 - A2 B1	6.530	6.502
5 - S3 B1	8.266	8.229
6 - S2 B2	8.984	8.956

Notes S:symmetric A:antisymmetric B:vertical cantilever bending

Table 1 - Dry modal analysis with rigid foundation block - first 6 modes

Mode number	SAPIV frequency (Hz) dry rigid base	SAPIVP frequency (Hz) coupled
1 - A1 B1	4.193	3.712
2 - S2 B1	4.478	3.976
3 - S1 B1	5.534	5.130
4 - A2 B1	6.530	6.052
5 - S2 B2	8.984	7.509
6 - S3 B1	8.266	7.810

Notes - S:symmetric A:antisymmetric B:vertical cantilever bending

Table 2 - Coupled natural frequencies incompressible fluid - first 6 modes

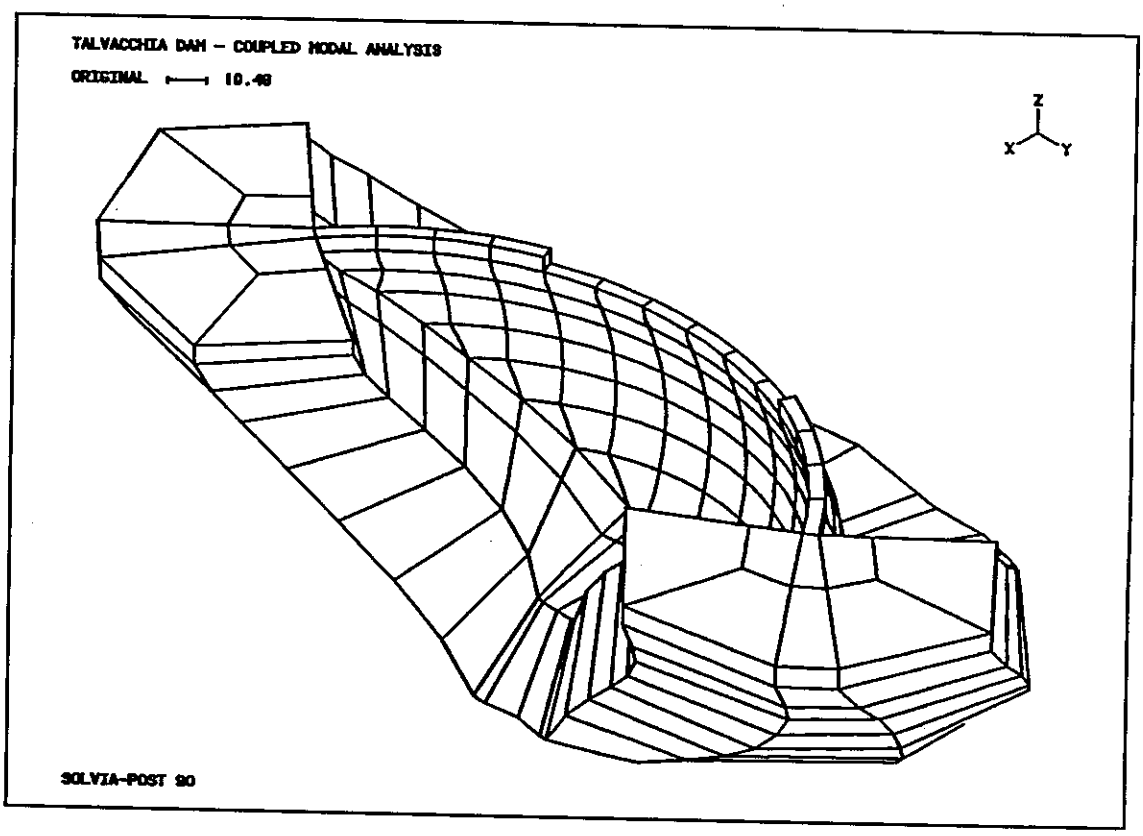

Figure 1 - Dam and foundation mesh

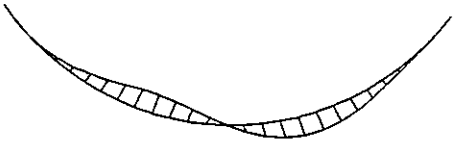

Mode 1 - A1 B1 - 4.193 Hz

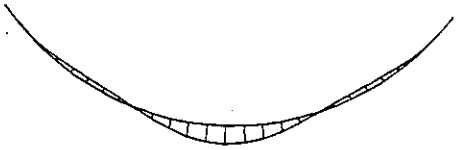

Mode 2 - S2 B1 - 4.478 Hz

Mode 3 - S1 B1 - 5.534 Hz

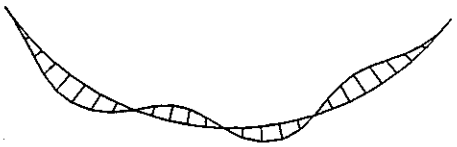

Mode 4 - A2 B1 - 6.530 Hz

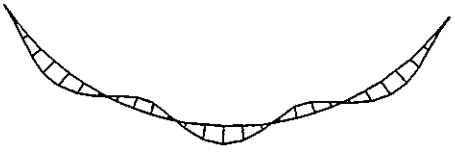

Mode 5 - S3 B1 - 8.266 Hz

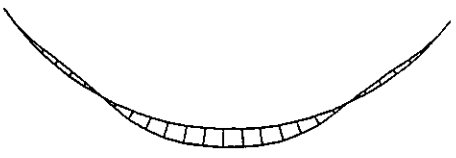

Mode 6 - S2 B2 - 8.984 Hz

Notes - S:symmetric mode A:antisymmetric mode B: vertical cantilever mode

Figure 2 - First 6 dry mode shapes : crest profiles

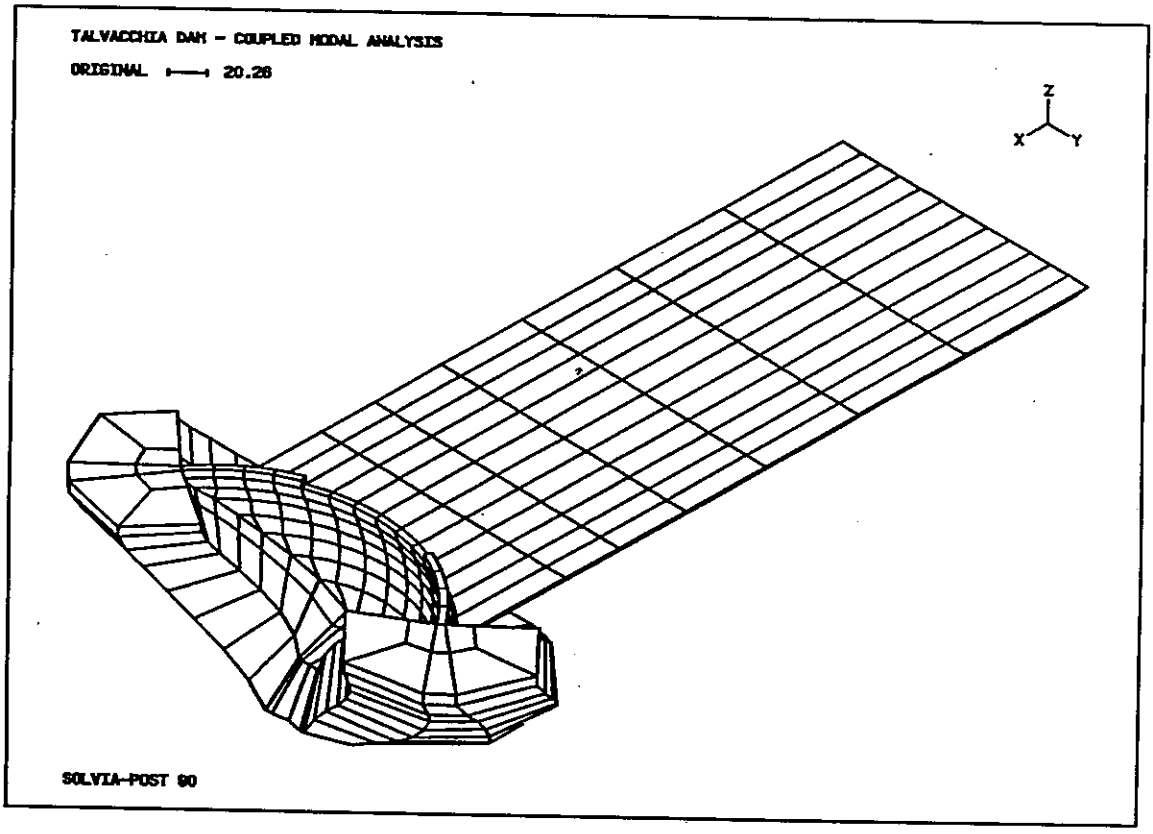

Figure 3 - Coupled dam-foundation-reservoir mesh

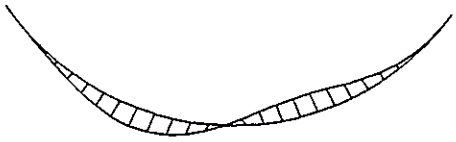

Mode 1 - A1 B1 - 3.712 Hz

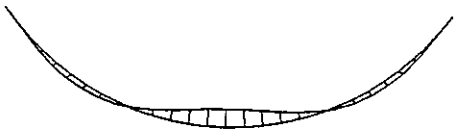

Mode 2 - S2 B1 - 3.976 Hz

Mode 3 - S1 B1 - 5.130 Hz

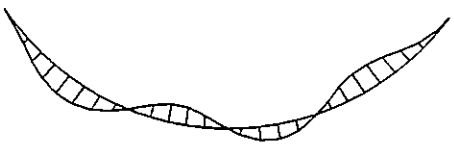

Mode 4 - A2 B1 - 6.052 Hz

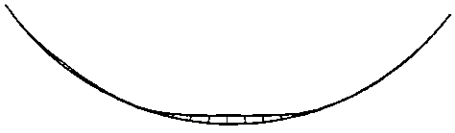

Mode 5 - S2 B2 - 7.509 Hz

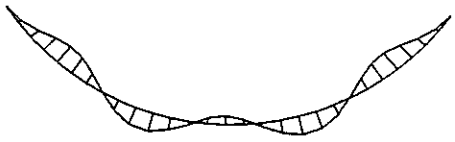

Mode 6 - S3 B1 - 7.810 Hz

Notes - S:symmetric mode A:antisymmetric mode B: vertical cantilever mode

Figure 4 - First 6 coupled mode shapes (SAPIVP) : crest profiles

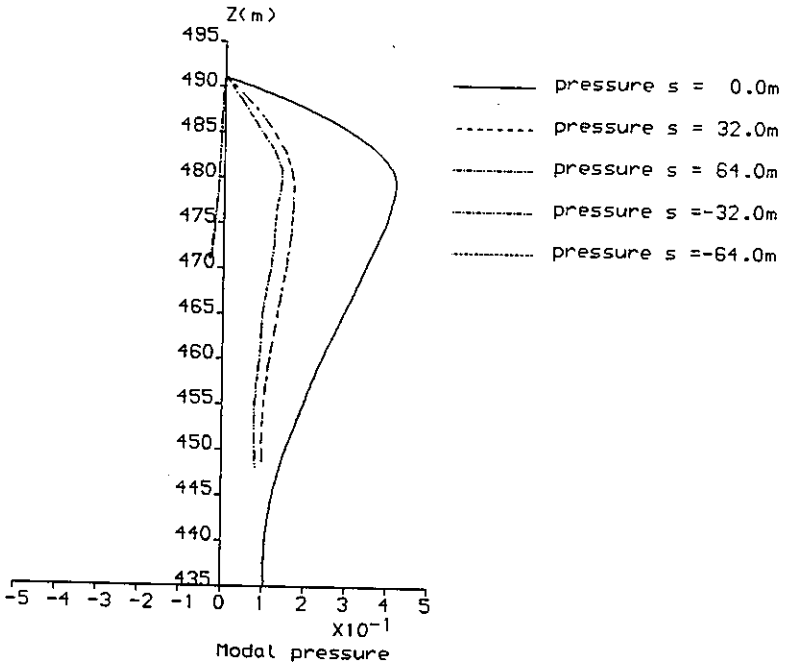

Figure 5 - Interface hydrodynamic pressures for mode 2

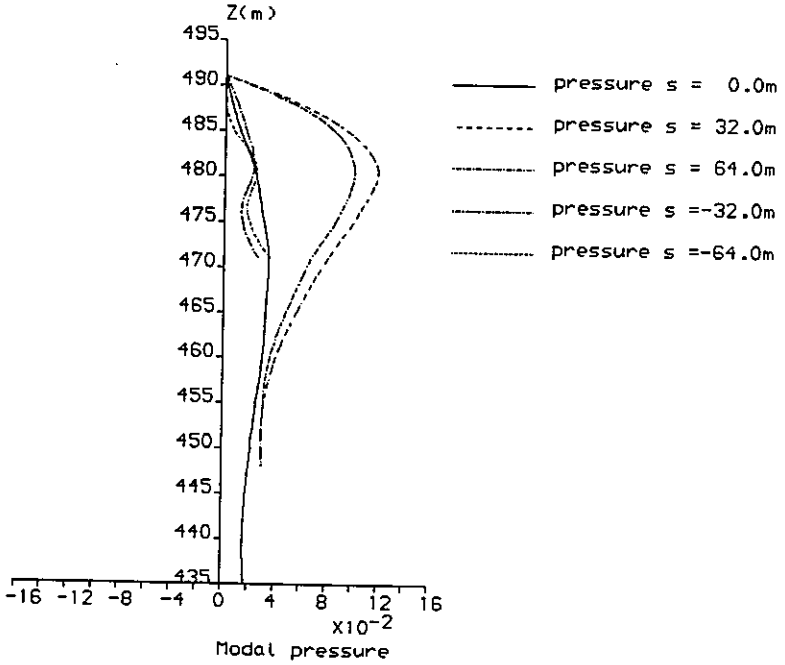

Figure 6 - Interface hydrodynamic pressures for mode 3

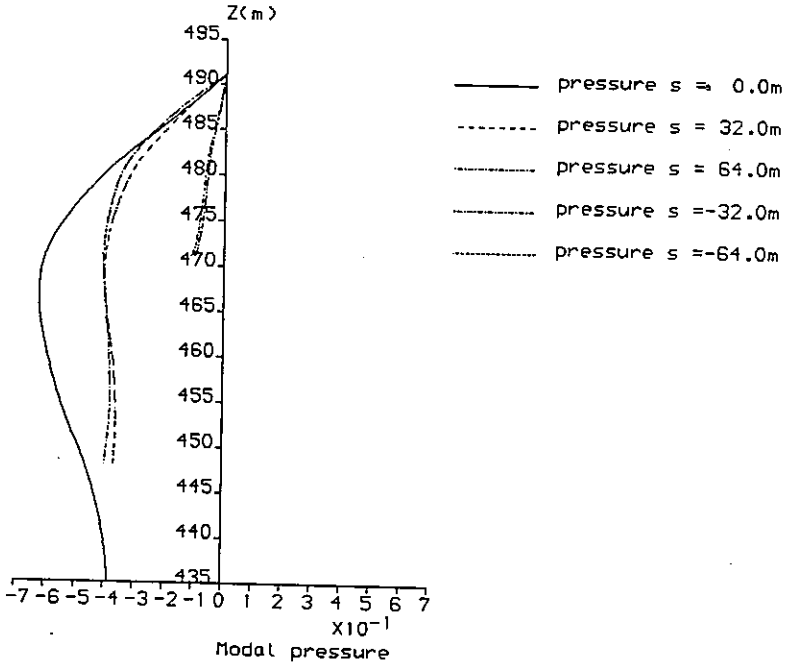

Figure 7 - Interface hydrodynamic pressures for mode 5

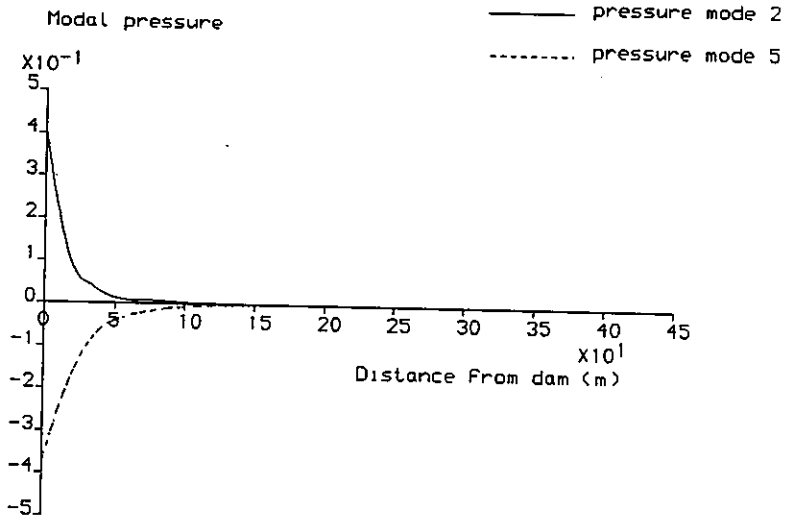

Figure 8 - Decay of hydrodynamic pressures into reservoirfor modes 2 & 5

Mode	SAPIVP frequency (Hz)	SOLVIA frequency (Hz)
1 - A1 B1	3.792	3.183(3) 3.324(4) 3.618(5) 4.438(11)
2 - S2 B1	3.976	4.291 (9) 5.015 (13)
3 - S1 B1	5.130	3.892 (6) 5.730 (15) 6.986 (20)
4 - A2 B1	6.052	4.826 (12) 7.061(21) 7.361(22)
5 - S3 B1	7.810	9.527 (30) 9.644 (31) 9.829 (32)
6 - S2 B2	7.509	7.591 (23) 8.291 (24) 10.10 (34)

Notes A:antisymmetic S:symmetric B:vertical cantilever bending SOLVIA frequencies also indicate mode number (bracketed)

Table 3 - SOLVIA compressible fluid results

Mode	SAPIVP frequency (Hz)	SOLVIA frequency (Hz)
1 - A1 B1	3.792	3.618 (5)
2 - S2 B1	3.976	4.291 (9)
3 - S1 B1	5.130	5.730 (15) 6.968 (20)
4 - A2 B1	6.052	7.361 (22)
5 - S3 B1	7.810	9.644 (31)
6 - S2 B2	7.509	7.591 (23)

Notes A:antisymmetic S:symmetric B:vertical cantilever bending SOLVIA frequencies also indicate mode number (bracketed)

Table 4 - Best estimates of SOLVIA coupled modes using displacement fluid finite element

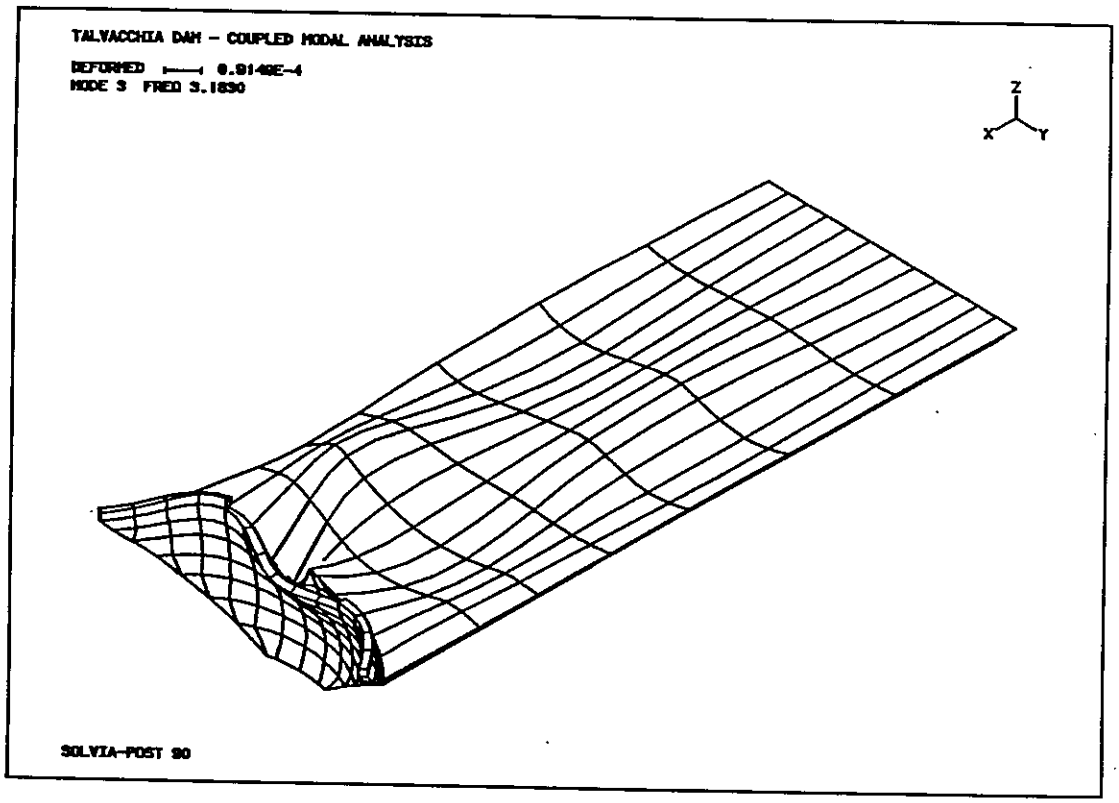

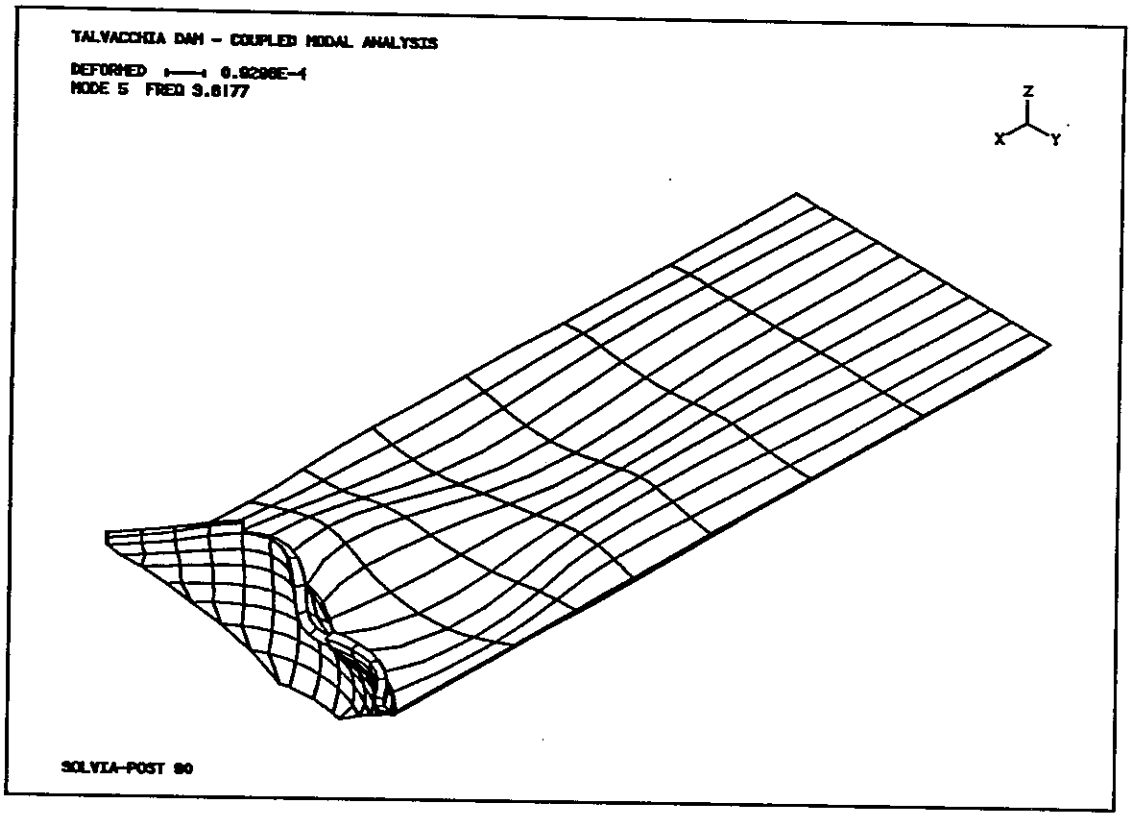

Figure 9 - Coupled system modes containing first antisymmetric motions of the dam

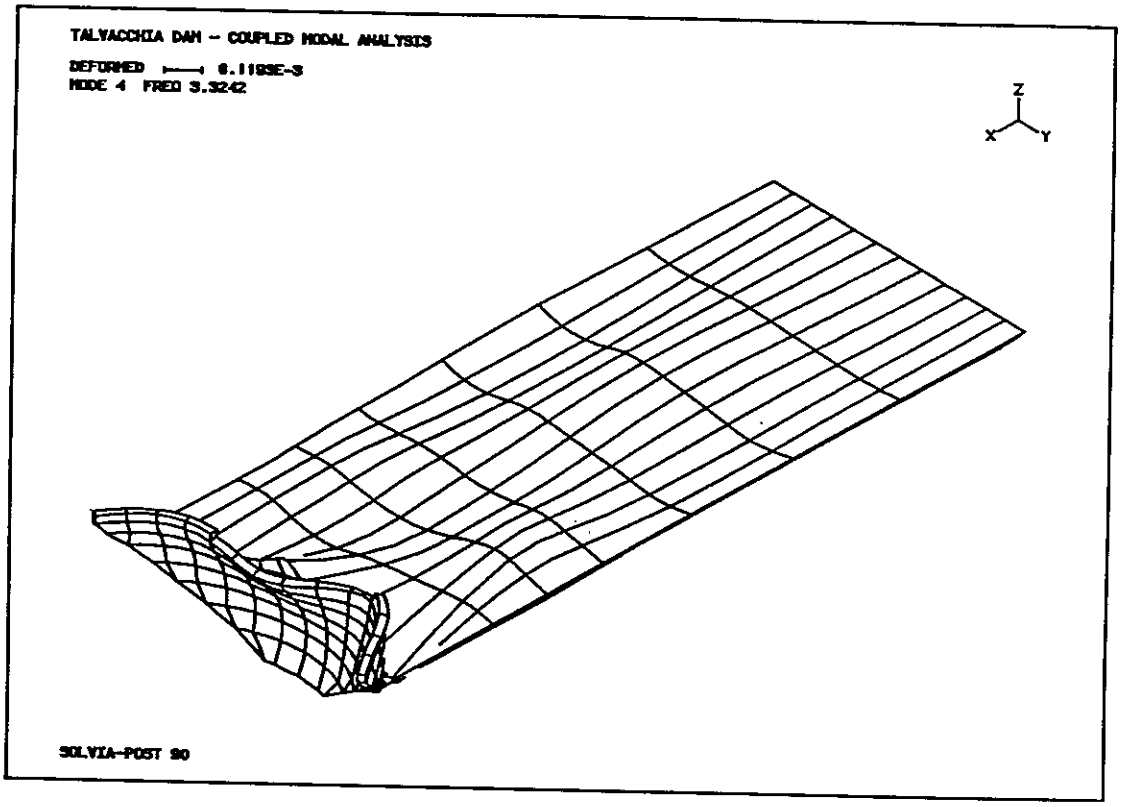

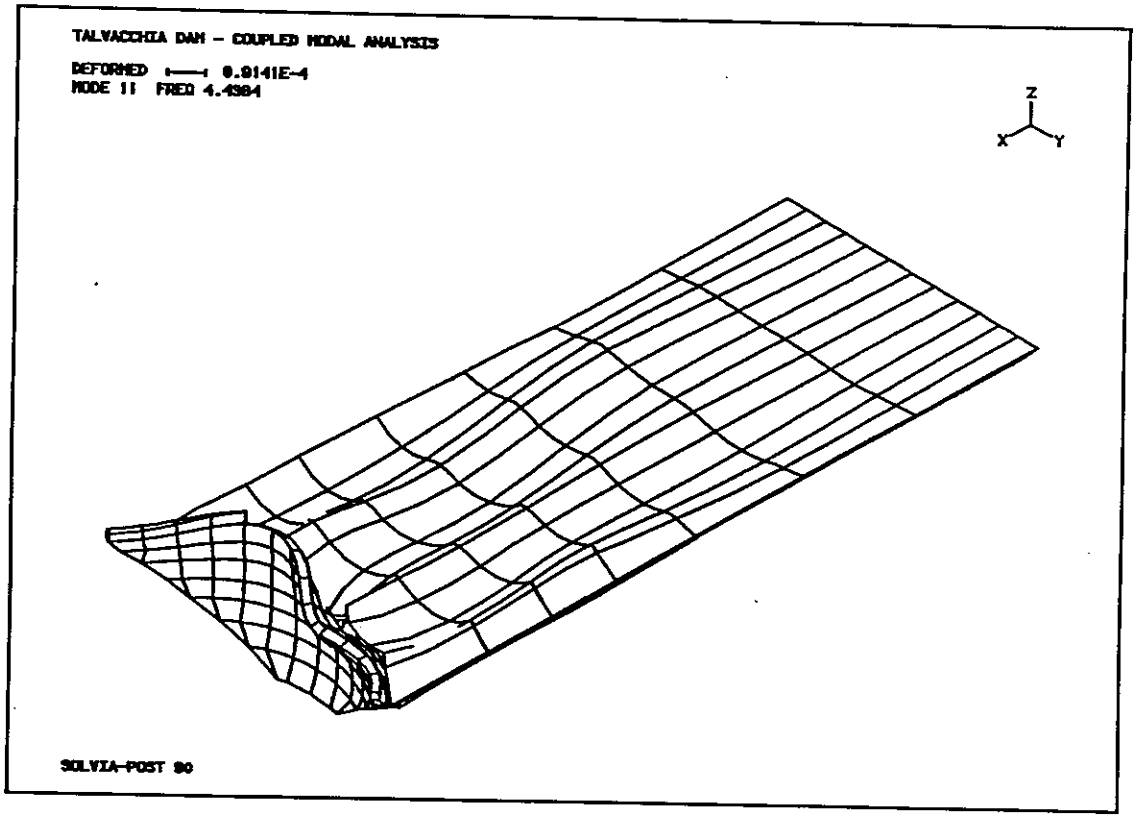

Figure 9 - Coupled system modes containing first antisymmetric motions of the dam

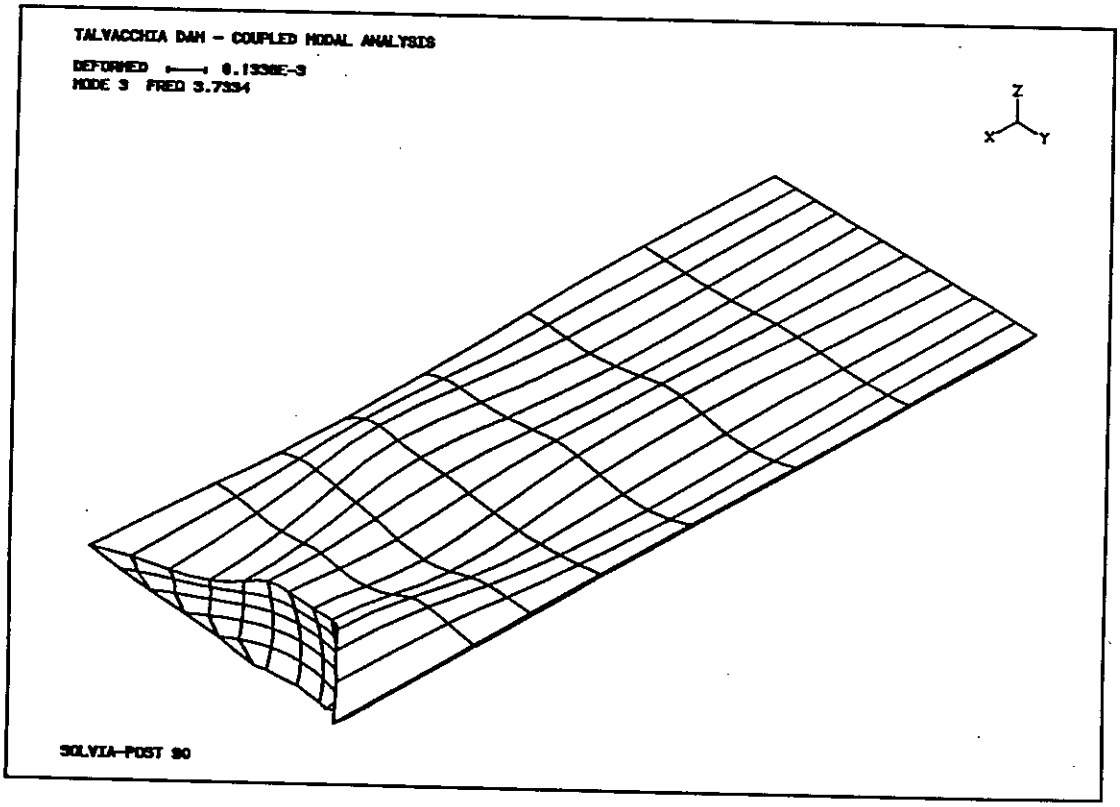

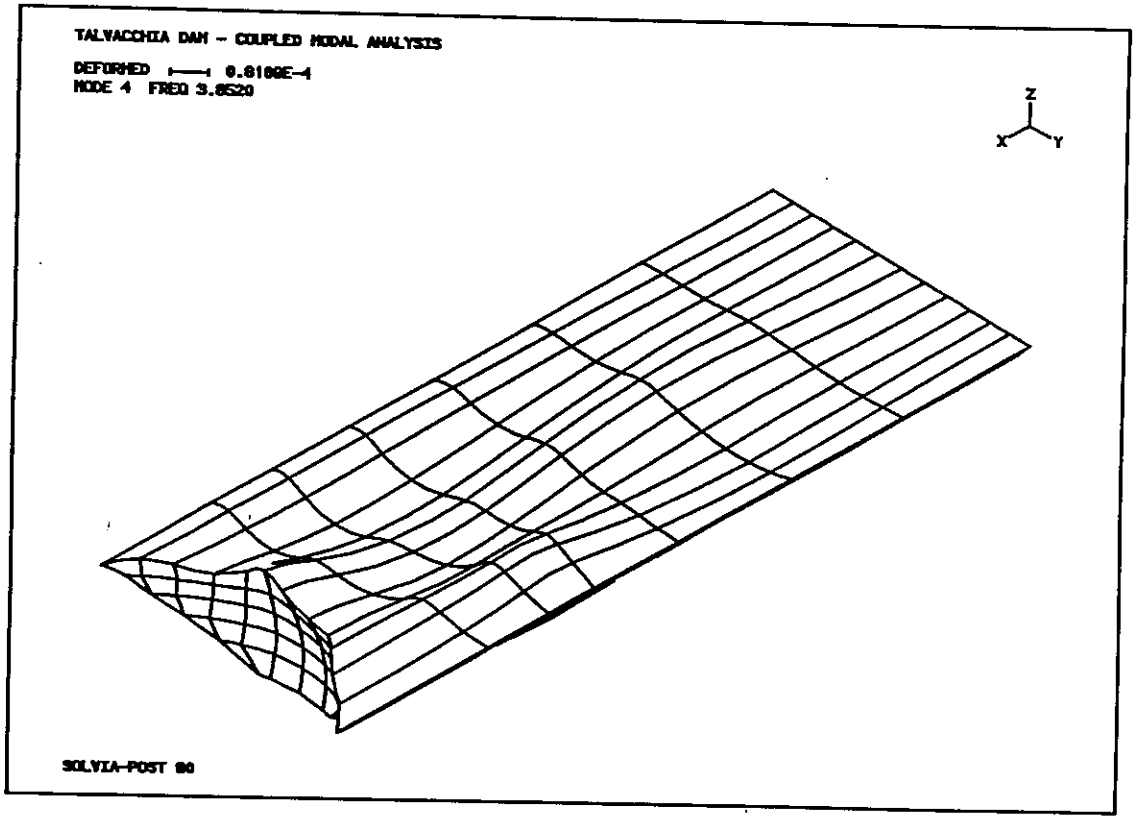

Figure 10 - FLuid-only modes spanning first coupled system mode

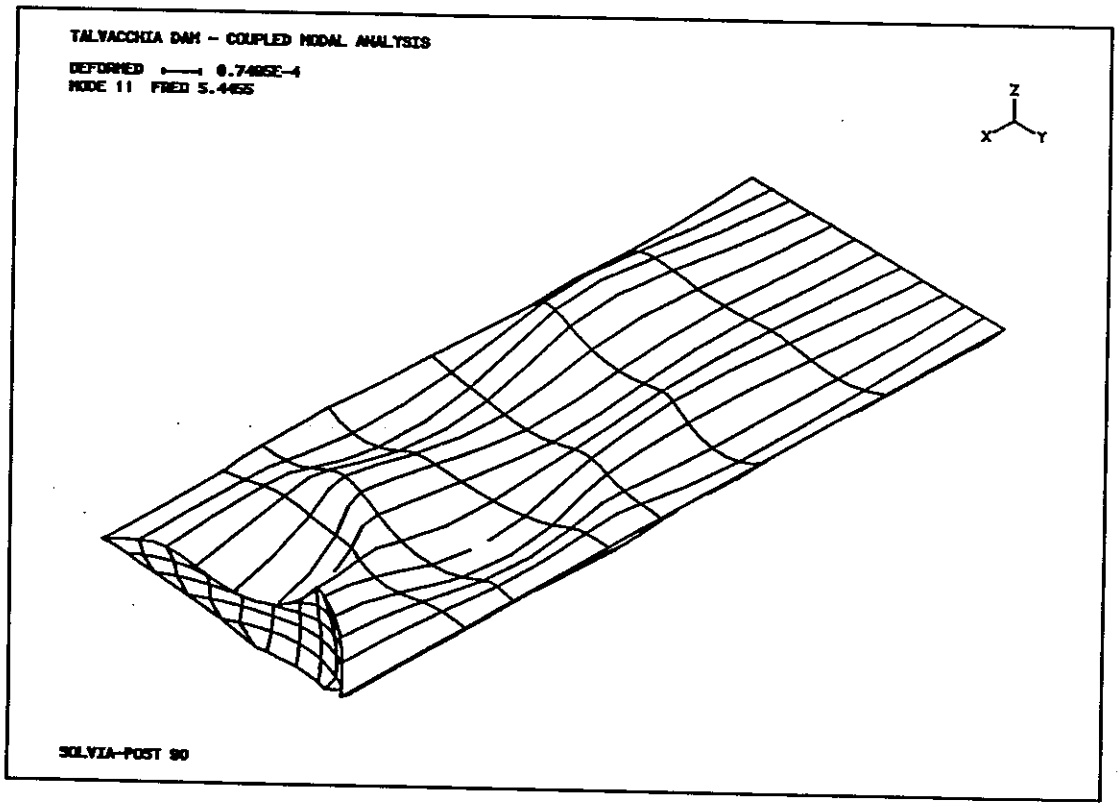

Figure 10 - FLuid-only modes spanning first coupled system mode

FIRST BENCHMARK WORKSHOP ON NUMERICAL ANALYSIS OF DAMS
THEME A: DOUBLE CURVATURE CONCRETE ARCH DAM
TALVACCHIA DAM, ITALY

C. H. YEH, X. CUI AND J. S. BONDI
HARZA ENGINEERING COMPANY
CHICAGO, ILLINOIS USA

1. INTRODUCTION

The rapid development of the numerical analysis since the 1960s drastically changed the method of dam analysis. In particular, the development of the finite element method and the associated analysis programs enable the designers to analyze complex structures with arbitrary boundary conditions under various loading combinations. The term finite element method became well known to engineers just like moment distribution.

The use of computer programs does present one problem. Unlike moment distribution, the result of a computer analysis cannot be verified by checking the calculation sheets. The experience and the understanding of the physical phenomenon of each individual designer become major factors in judging the results of a computer analysis. While experience and knowledge of the problem can detect major errors in results, relatively minor errors are often undetected.

There are two causes for errors in numerical analysis:

- **bugs or limitations of the program**
- **mistakes in input data**

Quality control procedures in checking input data largely eliminate errors caused by mistakes in data preparation. The inherited bugs or limitations of the software are much more difficult to find considering the fact that new programs are

continuously being developed and that many designers use executable codes without seeing source code.

Conscious of this problem in numerical analysis, the ICOLD ad-hoc committee for Computational Aspects of Dam Analysis and Design, in cooperation with ISMES and Dam Engineering, organized this benchmark workshop. A standard problem was formulated and engineers all over the world were invited to analyze it using their own software. The results were required to be presented in a specific format to facilitate comparison. It is hoped that this workshop will serve as a vehicle for designers to validate their software for the analysis of dams.

2. THE DAM AND THE MODEL

The 77m high Talvacchia Dam in Italy was chosen by the Organizing Committee for the benchmark analysis. This is a double curvature symmetric thin arch dam. Two finite element meshes were developed. The first one (Exhibit 1) is for stress and frequency analysis. It consisted of 84 20 node isoparametric elements modelling the dam and 160 elements for the foundation rock. Because of symmetry, only one half of the model was analyzed. The second model is similar to the first one except there are two elements through the thickness of the dam. This one was intended for thermal analysis. Material properties used in the analysis are listed below:

- Young's elastic modules (concrete) $E_c = 3.60\ 10^{10}\ Nm^{-2}$
- Young's elastic modules (rock) $E_r = 1.20\ 10^{10}\ Nm^{-2}$
- Poisson ratio coefficient (concrete) $\nu = 0.20$
- Poisson ratio coefficient (rock) $\nu = 0.16$
- Thermal diffusivity coeff. (concrete) $a = 1.0\ 10^{-6}\ m^2s^{-1}$
- Thermal dilatation coeff. (concrete) $\alpha = 0.7\ 10^{-5}\ °C^{-1}$
- Specific weight (concrete) $\gamma_c = 24{,}000\ Nm^{-3}$
- Specific weight (rock) $\gamma_r = 20{,}000\ Nm^{-3}$
- Specific weight (water) $\gamma_w = 10{,}000\ Nm^{-3}$

3. CASES ANALYZED

3.1 Dead Load. Weight of the concrete was assumed to apply instantaneously on a monolithic dam.

3.2 Water Load. Hydrostatic load was applied only to the upstream face of the dam with water level at 507.0m (crest of spillway).

3.3 Thermal Analysis (Exhibit 2)

3.3.1 Steady-State Case

$T_1 = 15°C$ $T_2 = 10°C$

3.3.2 Periodic Case

$$T_1 = 10°Sin(\omega t)$$

$$T_2 = 5°Sin(\omega t - 0.52)$$

Note: This is a hypothetic case because water temperature cannot be -5°C.

3.4 Thermal Stress. Temperature stress due to steady-state thermal load was computed assuming a 0°C stress free temperature.

3.5 Natural Frequencies and Mode Shapes.

3.5.1 Empty reservoir with rigid foundation.

3.5.2 Flexible foundation with water level at 491.0m.

4. RESULTS OF ANALYSES

Stress calculations were made using program SAPIV (1). This is a general purpose three-dimensional linear structural analysis program developed at the University of California. SAPIV computed stresses in the global coordinates. A post-processing program was used to compute the principal stresses.

4.1 Dead load principal stresses for the 42 nodes identified in Exhibit 3A are presented in Table 1. Nodal stress are the average stresses of the adjacent elements.

4.2 Water load deformation is plotted in Exhibit 4 and principal stresses for the above 42 nodes due to water load are given in Table 2. Cartesian components of displacement are also submitted separately on diskette.

4.3 Two dimensional finite element analysis was made for thermal distribution. The analysis was made for the crown cantilever section. It was assumed that heat transfer in the arch direction is negligible. The computer program used is DETECT (2), also developed at the University of California.

4.4 Thermal stresses of the 42 nodes in Exhibit 3A due to steady-state condition are given in Table 4. These stresses were computed using SAPIV. Thermal load deformation is presented in Exhibit 5.

4.5 Natural frequencies of the first six modes for the empty reservoir and rigid foundation and corresponding mode shapes are presented in Exhibit 6. Numerical value of the mode shapes are submitted separately on a diskette for easy comparison. The mode shapes were normalized such that the maximum component in each mode

has the value of unit. Two analyses were made with symmetric and anti-symmetric boundary conditions on the center plane.

4.6 Reservoir-dam interaction is one of the most difficult problems in arch dam analysis. In this study, the reservoir was modelled by three dimensional fluid element as suggested by the Organizing Committee. The program RSVOIR (3) was used. It assumed that the water is incompressible and that hydrodynamic pressure is negligible at the upstream end of the model. This analysis resulted in a full added mass matrix interconnection all the degrees-of-freedom on the upstream face of the dam.

In addition, a modified Westergaard approach was also considered. The modification recognized the curvature of the dam and that hydrodynamic pressure is normal to the surface of the dam. The foundation rock was assumed to be massless. Mode shape and frequency computation was made using an enhanced version of SAPIV. The original SAPIV assumed a diagonalized mass matrix. The modification enables the program to handle full mass matrix discussed above.

Resulting frequencies for these two types of added mass and associated mode shapes are presented in Exhibits 7 and 8 respectively.

5. DISCUSSION

With the exception of the last case, all analyses above are straight forward and are considered routine operations. Similar results are expected using different computer programs. The last case, coupled analysis of the dam-reservoir

system, is the most interesting part of this benchmark analysis. Up to the 1980s, the most commonly used approach in simulating hydrodynamic effect of the reservoir during earthquake was by added mass based on Westergaard formulation. The wide acceptance of this simple approximate approach was mainly due to the fact that there was no readily available alternative.

In the last few years, modelling the reservoir by finite elements to evaluate the hydrodynamic effect has gradually gained acceptance by the designers world wide. Studies (4) showed that the finite element solution is much closer to the experimental result than the Westergaard formulation.

In this analysis of the Talvacchia Dam, natural frequencies were computed using both the finite element modelling of the reservoir and the Westergaard formulation. Examining Exhibits 7 and 8, it can be seen that these results are very close. This is because the reservoir considered is only about three quarters full and the change of natural frequency due to the presence of the reservoir is nominal. It is anticipated that the difference between these two solution will be more prominent for higher reservoir level.

REFERENCES

1. "SAPIV - A Structural Analysis Program for Static and Dynamic Response of Linear Systems" K. J. Bathe, E. L. Wilson and F. E. Peterson, EERC Report 73-11, University of California, Revised April 1974.

2. "Finite Element Analysis of Nonlinear Heat Transfer Problems" R. M. Polivka, and E. L. Wilson, SESM Report No. 76-2, University of California, June 1976.

3. "Fluid-Structure Interactions: Added Mass Computations for Incompressible Fluid", S. H. Kuo. EERC Report No. 82-09, University of California, August 1982.

4. "Study on Arch Dam - Reservoir Water Interaction under Earthquake Condition" H. Q. Chen, S. Z. Hou and D. W. Yang, Journal of Hydraulic Engineering No. 7, 1989 Beijing.

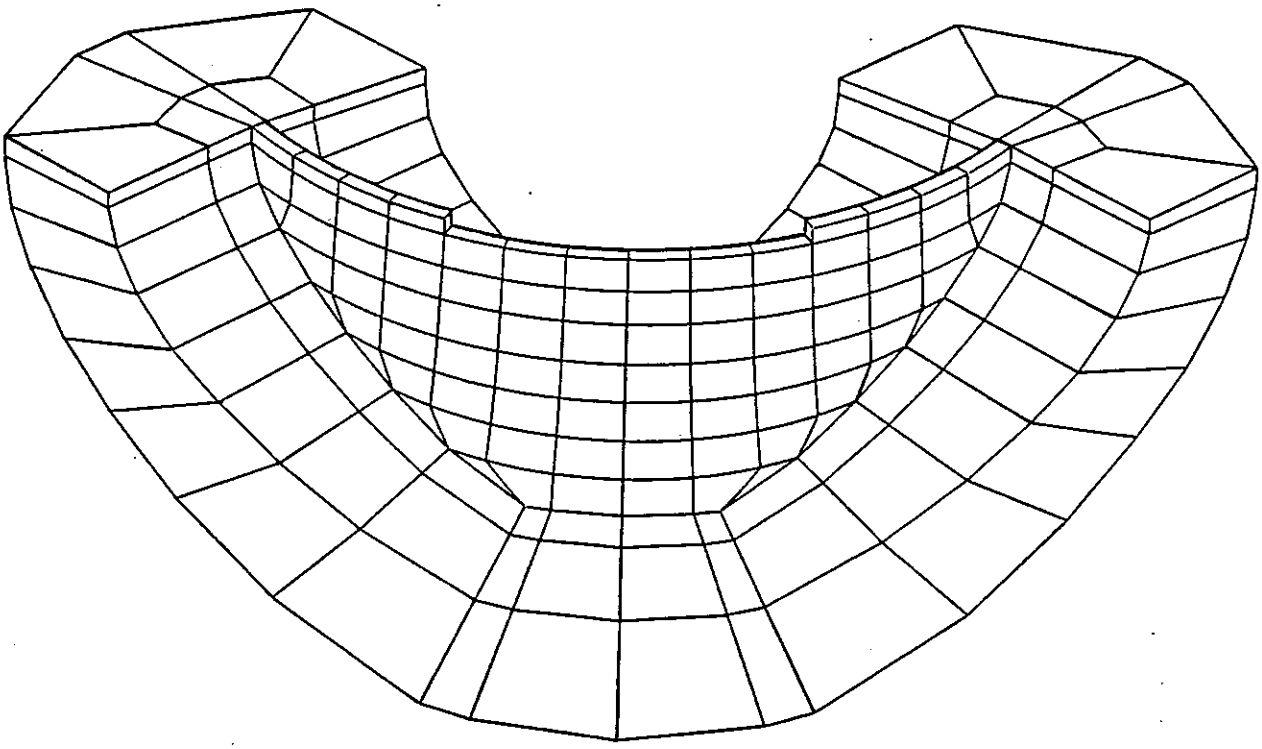

EXHIBIT – 1. Talvacchia Dam. Finite Element Mesh.

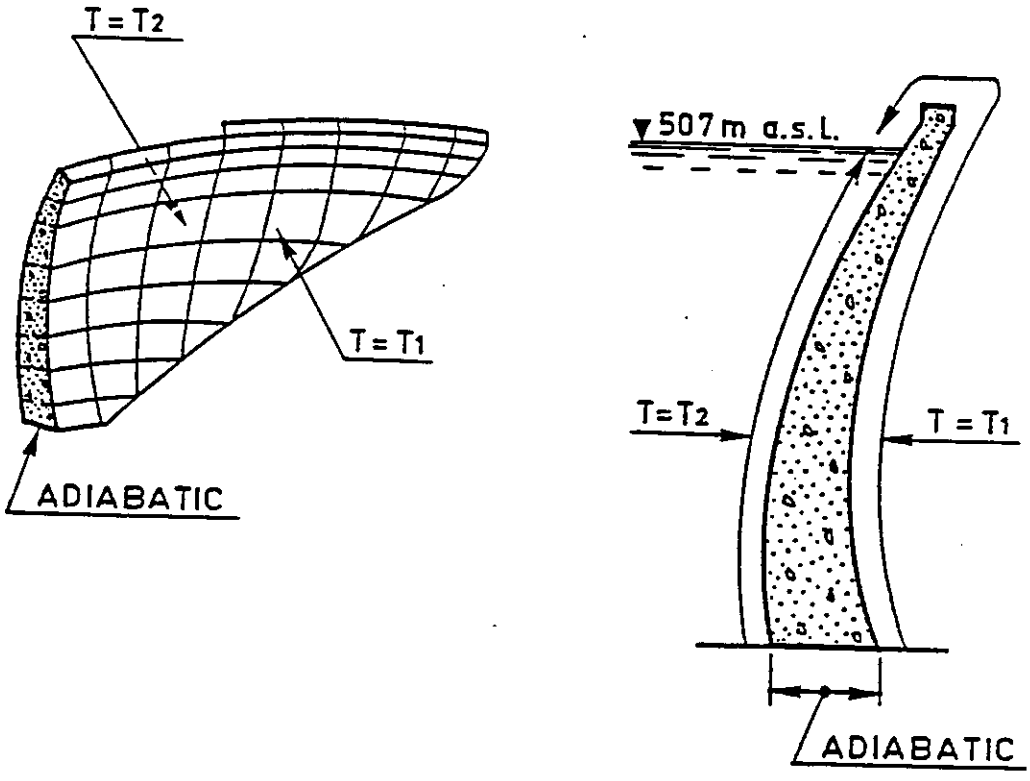

EXHIBIT – 2. Thermal Analysis.

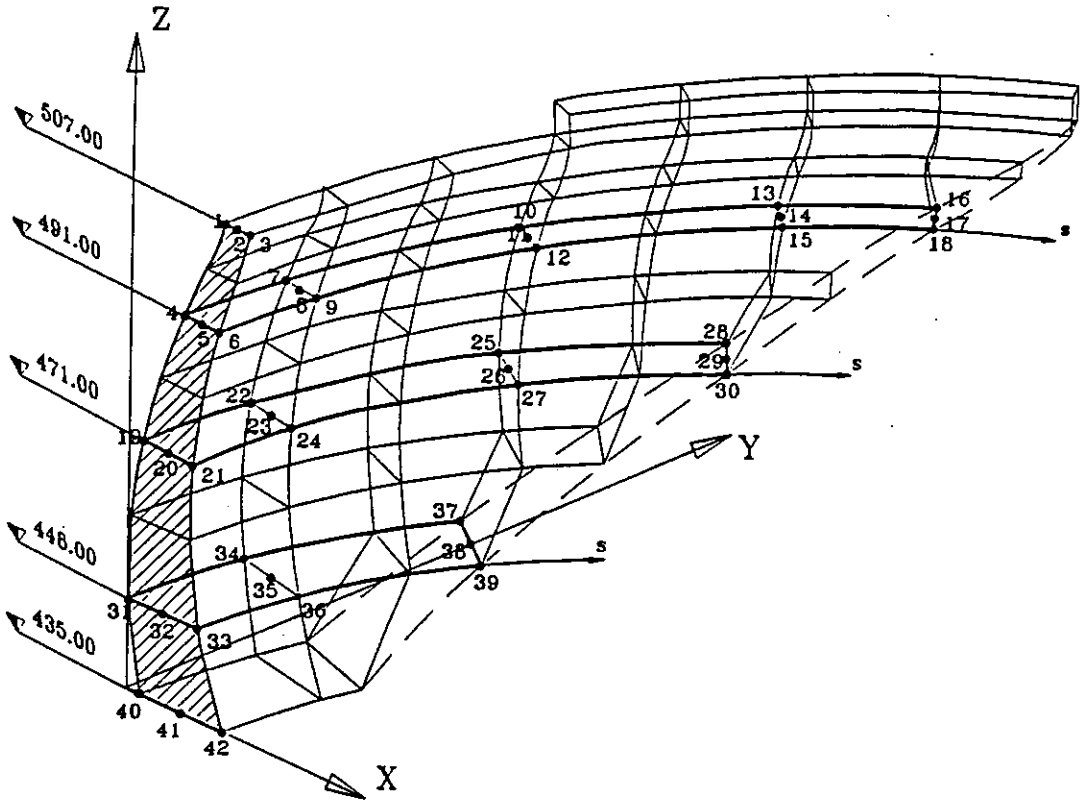

EXHIBIT – 3A. Output Location A.

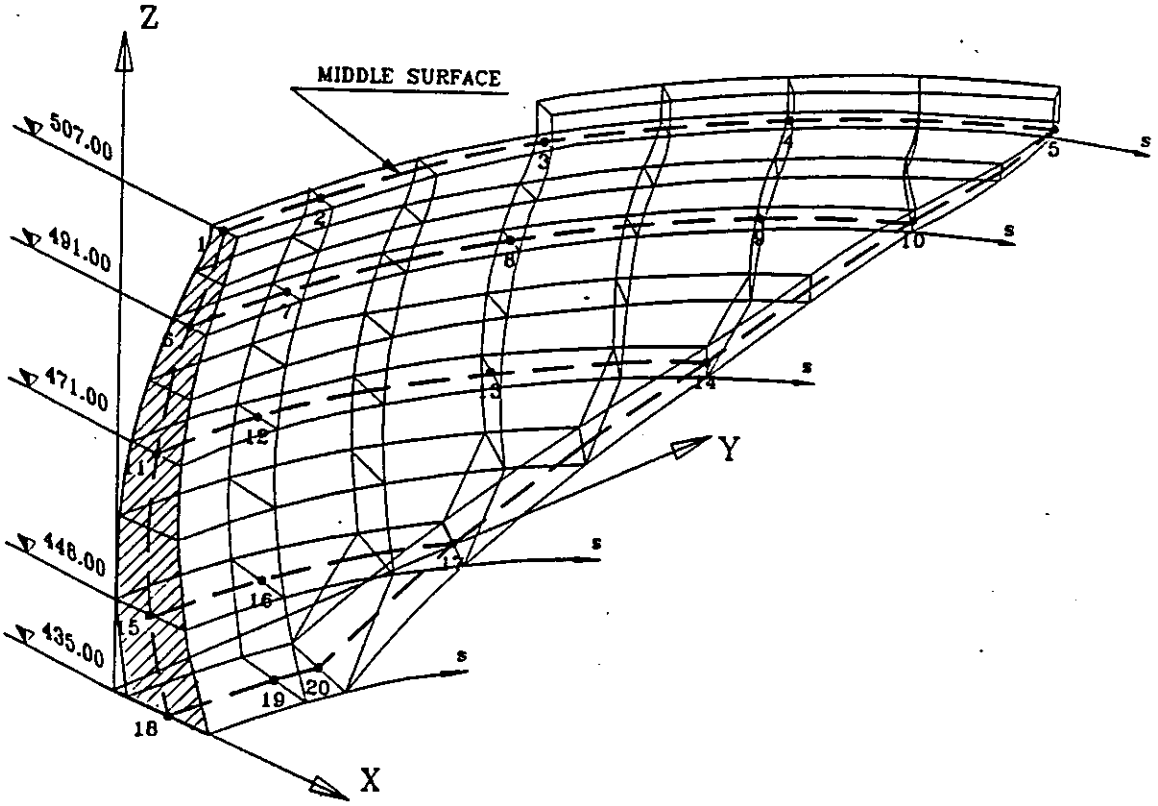

EXHIBIT – 3B. Output Location B.

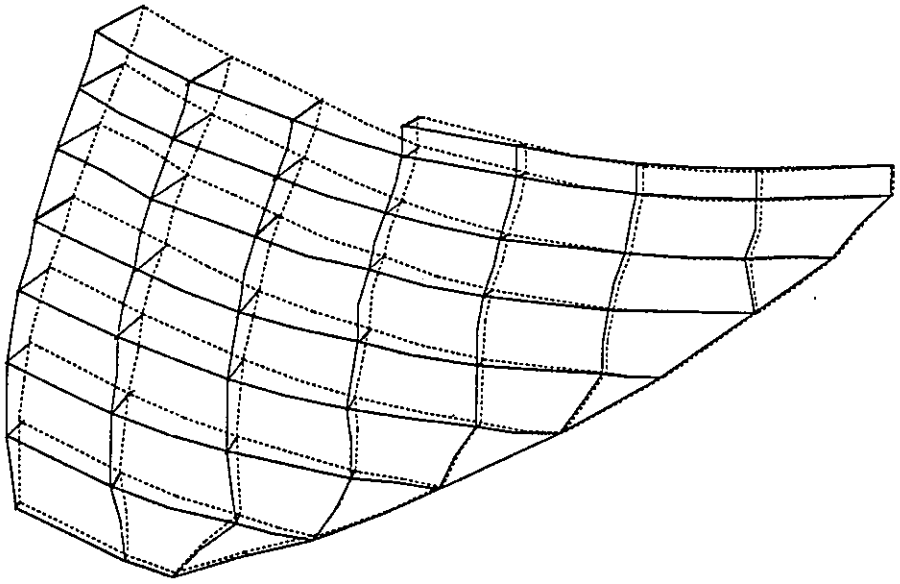

EXHIBIT – 4. Water Load Deformation.

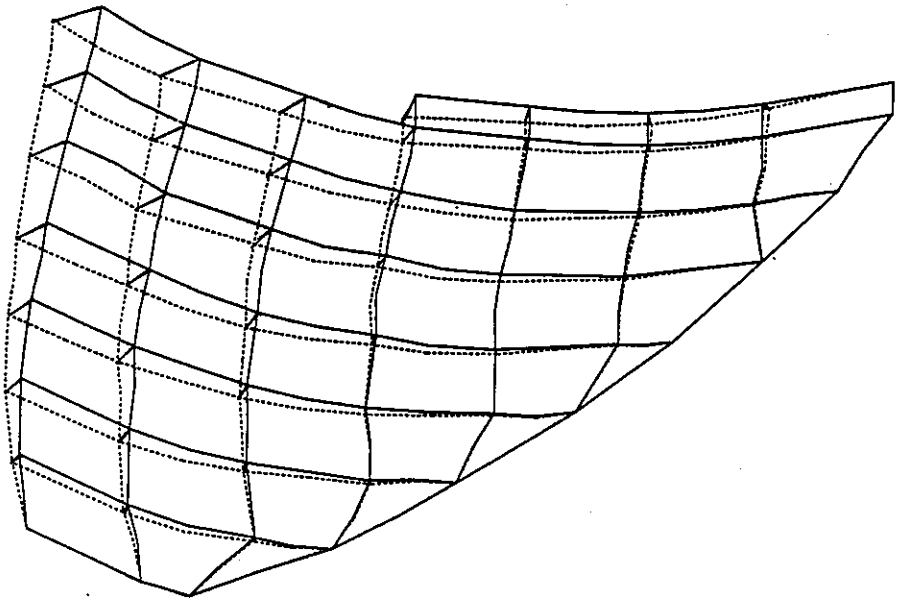

EXHIBIT – 5. Thermal Load Deformation.

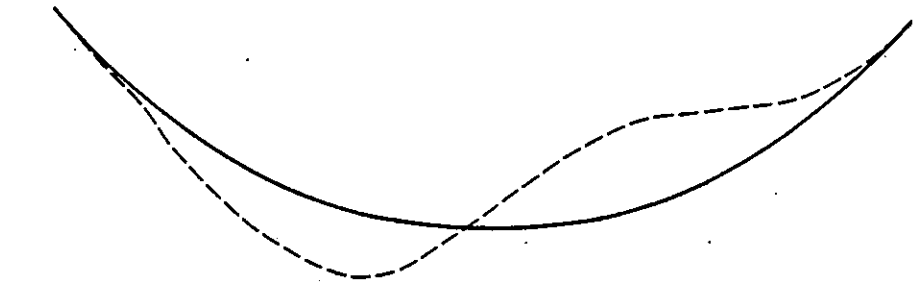

Mode 1 w = 4.251

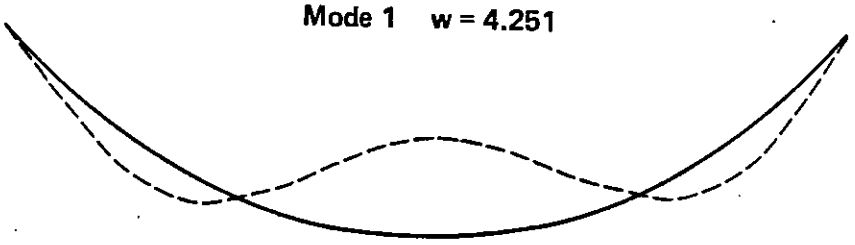

Mode 2 w = 4.452

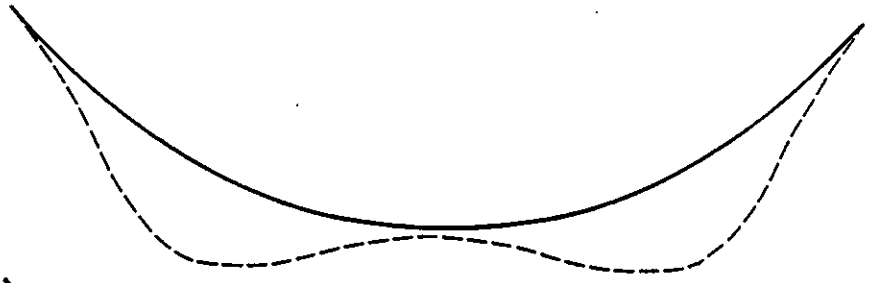

Mode 3 w = 5 578

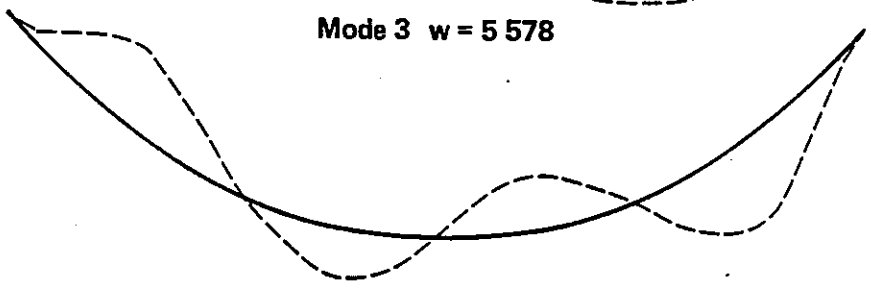

Mode 4 w = 6.577

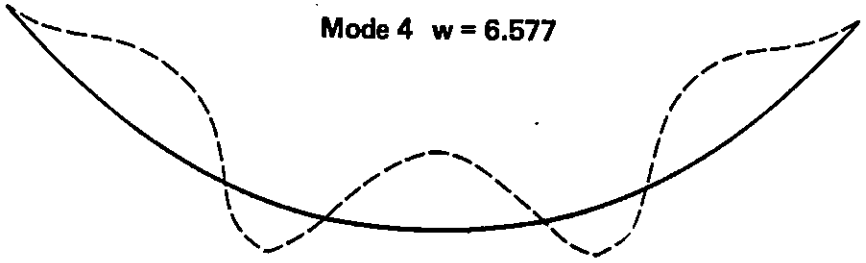

Mode 5 w = 8.282

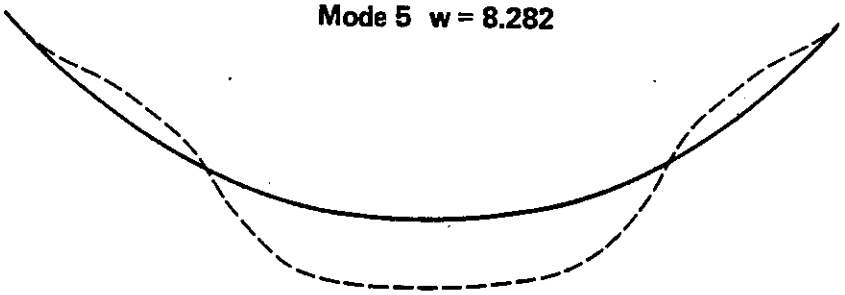

Mode 6 w = 8.941

EXHIBIT — 6. Mode Shape Plot, Rigid Base Empty Reservoir.

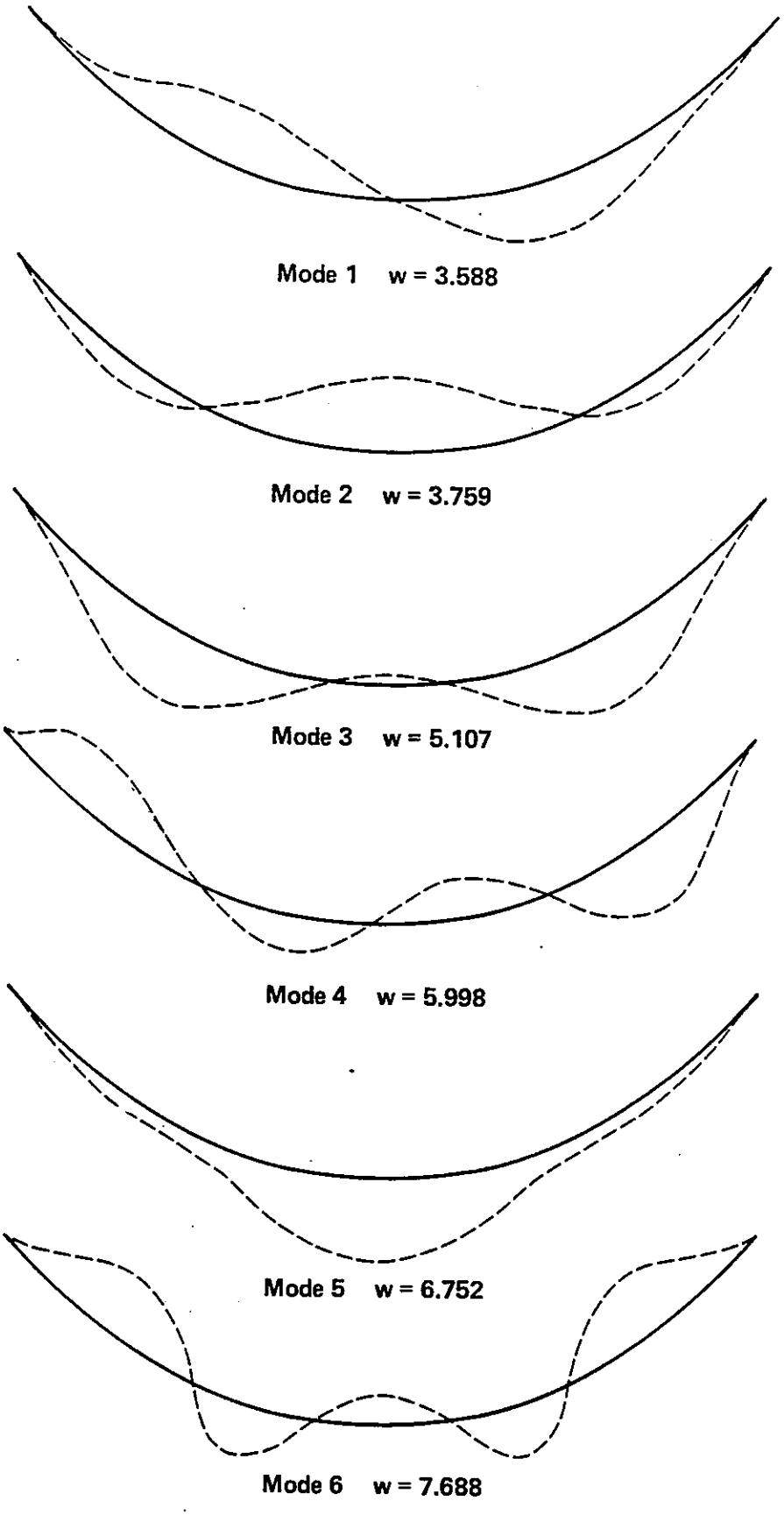

EXHIBIT – 7. Mode Shape Plot, Finite Element Modelling of Reservoir.

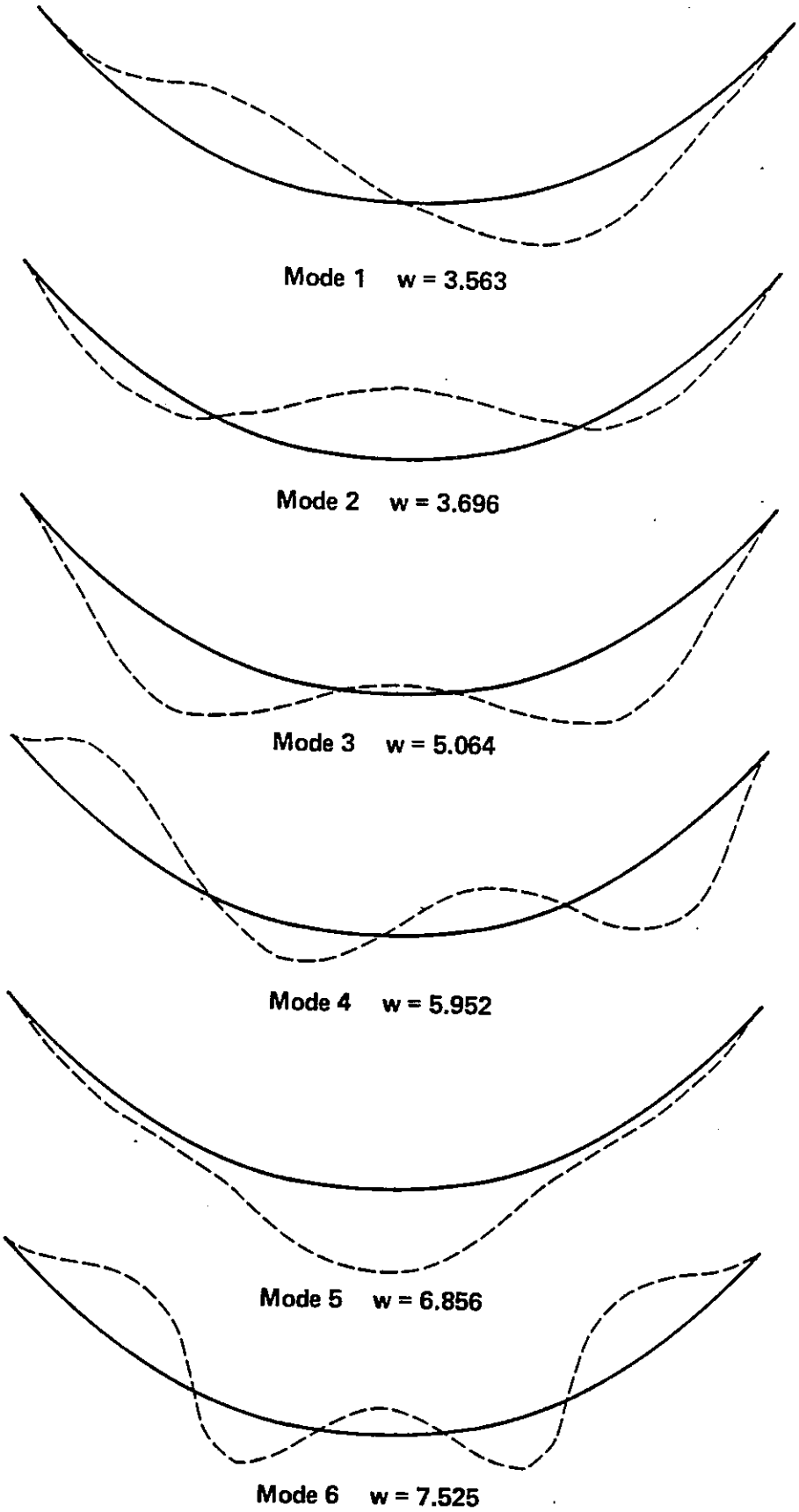

EXHIBIT — 8. Mode Shape Plot, Generalized Westergaard Formulation.

Table 1

Stress Under Dead Weight Load

(MPa)

Point No.	p1	p2	p3
1	0.0410	-0.0119	-1.1174
2	0.0103	-0.0128	-1.1609
3	0.0521	-0.0683	-1.1495
4	0.0655	-0.1242	-0.3429
5	0.0045	-0.2822	-0.3977
6	-0.0251	-0.4411	-0.5000
7	0.0436	-0.0539	-0.2961
8	-0.0397	-0.2554	-0.4429
9	0.0498	-0.3887	-0.6692
10	0.2093	-0.0431	-0.1419
11	0.0558	0.0341	-0.3465
12	0.0099	-0.1798	-0.8731
13	0.4202	0.1625	-0.0491
14	0.1935	0.0168	-0.2975
15	0.2002	-0.0152	-1.0558
16	0.4717	0.0649	-0.3079
17	0.2733	-0.1750	-0.4976
18	0.1335	-0.1648	-1.3666
19	0.2424	0.0967	-0.0330
20	0.0373	-0.0488	-0.5678
21	-0.0039	-0.1923	-1.2512
22	0.2742	0.0849	-0.0571
23	0.1306	0.0333	-0.3482
24	-0.0360	-0.0965	-1.0231
25	0.2890	0.1006	-0.1219
26	0.1502	0.0010	-0.6458
27	0.0531	0.0149	-1.1792
28	0.1128	-0.1194	-1.2890
29	0.1466	-0.1841	-0.5790
30	0.2701	0.0479	-1.1512
31	0.0897	-0.0414	-0.8230
32	0.0049	-0.0369	-0.7657
33	-0.0999	-0.1750	-1.0458
34	0.1156	-0.0646	-0.8154
35	-0.0207	-0.0576	-0.7852
36	-0.0694	-0.2222	-0.9110
37	-0.0957	-0.3645	-2.3820
38	-0.0149	-0.2587	-0.6980
39	0.1290	0.0192	-0.9741
40	-0.2207	-0.3824	-2.0957
41	-0.2240	-0.3054	-0.9175
42	0.1271	-0.1315	-0.7602

Table 2

Stress Under Hydrostatic Load

(MPa)

Point No.	p1	p2	p3
1	-0.2273	-0.6350	-3.5372
2	0.2746	0.0149	-1.6355
3	1.2992	0.1869	-0.3183
4	-0.4670	-1.7552	-4.4997
5	-0.0900	-0.4144	-2.8830
6	0.8409	0.2877	-1.6084
7	-0.3079	-1.3194	-3.5824
8	0.0003	-0.2399	-2.7379
9	0.9375	0.0214	-1.7449
10	0.3379	-0.7806	-2.0689
11	-0.1270	-0.5091	-2.7428
12	0.9063	-0.0047	-3.0032
13	-0.2408	-0.9115	-1.1305
14	-0.0041	-0.1042	-1.6443
15	1.0654	0.1157	-2.3941
16	-0.3309	-0.5713	-2.5533
17	0.0102	-0.4335	-1.6358
18	0.6397	-0.1871	-1.8517
19	0.0438	-1.1179	-3.7909
20	-0.0349	-0.2710	-2.6497
21	0.9490	-0.2425	-1.0291
22	-0.1635	-1.2994	-4.1304
23	-0.2078	-0.5541	-2.9145
24	0.6536	-0.0055	-1.6860
25	0.1338	-0.3592	-1.6481
26	0.2689	-0.2378	-2.0745
27	0.6064	-0.4453	-2.6449
28	0.6585	0.4792	-0.9890
29	0.2942	-0.3642	-1.1262
30	-0.2790	-0.5943	-4.5267
31	1.0601	-1.1884	-1.8634
32	0.7246	-0.8142	-0.9950
33	0.8780	-0.2960	-2.0126
34	1.1733	-0.8427	-1.7332
35	0.5534	-0.5237	-1.0952
36	0.5102	0.1620	-2.3269
37	2.8845	1.3019	0.2617
38	1.1518	0.4536	-0.6498
39	-0.3409	-0.8609	-5.4191
40	4.0628	1.1293	0.7713
41	1.6694	0.6574	-0.7738
42	0.0414	-0.2934	-5.0416

Table 3

Thermal Analyses

Points No.	S.S.A.* Temperature	Periodic Analysis Amplitude+	Phase (Rad)
1	0.15000E+02	0.99427E+01	0.00000E+00
2	0.15000E+02	0.99427E+01	0.00000E+00
3	0.15000E+02	0.99427E+01	0.00000E+00
4	0.12417E+02	0.56195E+01	-0.94680E+00
5	0.12417E+02	0.56195E+01	-0.94680E+00
6	0.12417E+02	0.56195E+01	-0.94680E+00
7	0.12417E+02	0.56195E+01	-0.94680E+00
8	0.12417E+02	0.56195E+01	-0.94680E+00
9	0.12417E+02	0.56195E+01	-0.94680E+00
10	0.12417E+02	0.56195E+01	-0.94680E+00
11	0.12404E+02	0.34809E+01	-0.14632E+01
12	0.12404E+02	0.34809E+01	-0.14632E+01
13	0.12404E+02	0.34809E+01	-0.14632E+01
14	0.12404E+02	0.34809E+01	-0.14632E+01
15	0.12423E+02	0.17738E+01	-0.19796E+01
16	0.12423E+02	0.17738E+01	-0.19796E+01
17	0.12423E+02	0.17738E+01	-0.19796E+01
18	0.13064E+02	0.15843E+01	-0.20000E+01
19	0.13064E+02	0.15843E+01	-0.20000E+01
20	0.13064E+02	0.15843E+01	-0.20000E+01

* S.S.A. Steady-State Analysis
+ Temperature Amplitude °C

Table 4

Stress Under Thermal Load

(MPa)

Point No.	p1	p2	p3
1	3.1508	1.0649	0.8952
2	0.8128	-0.0521	-0.4551
3	0.8829	0.7746	0.4726
4	1.6736	0.8930	0.0694
5	0.2644	0.0471	-0.1264
6	-0.5455	-0.9477	-1.1854
7	1.2980	0.6173	0.2806
8	0.1302	-0.0528	-0.2262
9	0.0428	-0.8121	-1.2224
10	0.4728	-0.5029	-0.7516
11	0.1634	0.1014	-1.1332
12	-0.0522	-0.2758	-1.9852
13	-0.7140	-1.2139	-2.3993
14	-0.1915	-0.8443	-2.9696
15	0.5819	-0.8536	-3.7428
16	-1.1499	-4.0102	-5.8371
17	-0.1710	-4.0912	-4.6407
18	2.6254	-4.2572	-4.5479
19	0.3957	0.3196	-0.2450
20	-0.1194	-0.3070	-1.1557
21	0.2195	-1.3575	-3.0591
22	0.5716	0.3073	-0.2486
23	0.1436	-0.1611	-1.0888
24	-0.2249	-1.1027	-2.8331
25	0.5280	-0.3927	-1.4615
26	0.2265	-0.2198	-2.5751
27	0.9379	0.0510	-3.2312
28	-0.4481	-3.9320	-6.8950
29	0.2010	-3.8791	-4.0944
30	1.6564	-4.7005	-5.5257
31	-0.1269	-0.2989	-2.7353
32	0.2467	-1.3090	-2.7723
33	1.7456	-2.1155	-3.7848
34	-0.2191	-1.4261	-2.2871
35	-0.0074	-1.3790	-3.0386
36	1.0737	-1.5042	-4.3755
37	-0.6116	-4.3411	-8.9026
38	0.1951	-3.9393	-4.3075
39	3.2537	-4.1132	-4.6825
40	-1.1243	-4.2299	-7.4254
41	-0.5938	-4.3308	-4.5988
42	2.7778	-4.0954	-4.3547

BENCHMARK ANALYSIS OF TALVACCHIA DAM USING EADAP

by

Yusof Ghanaat[1] and Ray W. Clough[2]

Introduction

This report describes the Benchmark analysis of Talvacchia Dam using the Enhanced Arch Dam Analysis Program-EADAP[1], and summarizes the essential part of the results that were obtained. EADAP is an extended version of the Arch Dam Analysis Program-ADAP[2] that was developed in 1973 at the University of California, Berkeley for the U.S. Bureau of Reclamation. During subsequent use in a number of arch dam dynamic analysis projects done by the Earthquake Engineering Research Center (EERC) of the University of California, the program was extended and enhanced in several respects: to account for interaction with incompressible reservoir water, to improve the capabilities of the mesh generator, and to add a number of features related to correlation of the analysis with results of forced vibration field tests.

The present enhanced version, EADAP, is distributed at nominal cost by the National Information Service for Earthquake Engineering operated by the EERC. More recently Quest Structures of Emeryville, California, further enhanced the program by the addition of an advanced mesh generator, new analysis features, and pre-and post-processing graphics capabilities. This Graphics-based Dam Analysis Program named GDAP[3] is available from Quest Structures; all plots contained in this report were produced by GDAP.

This report starts with a brief description of EADAP, and then presents the various results specified for the Benchmark Workshop. It closes with a few comments concerning the results required for this Workshop and offers some suggestions with regard to a possible Second Benchmark Workshop.

EADAP Description

EADAP is a special purpose finite element program incorporating the types of elements and analysis procedures used in the original program ADAP, and like that program is designed to provide static and dynamic analyses of concrete arch dams of arbitrary geometry. The dam body is idealized as

---

[1]Principal, Quest Structures, Emeryville, CA

[2]Nishkian Professor of Structural Engineering, Emeritus, University of California, Berkeley, CA

an assemblage of 3D finite elements with nodal points generally arranged along horizontal and vertical planes cut through the dam. The type of element utilized along the foundation rock interface is a form of 16 node isoparametric element called 3DSHEL that uses quadratic geometry and displacement interpolation in the dam face directions but only linear interpolation through the thickness. For regions in the dam body away from the foundation interface, a modified version of this element called THKSHEL is used, in which the 16 outer face nodes are reduced to 8 mid-surface nodes, each having 5 degrees of freedom (three translation and two rotation), it being assumed that the change of thickness is negligible. The program carries out static analyses for gravity loads, hydrostatic pressures, and loads resulting from specified temperature changes; in addition it performs vibration analyses and dynamic response analyses using the mode superposition method.

The foundation block that supports the dam is idealized as an assemblage of 8 node isoparametric "brick" elements having linear geometry and displacement interpolation in all three axes. The foundation mesh is constructed on semi-circular planes cut into the canyon walls in the direction normal to the dam-foundation contact surface. Typically, the radius of each foundation semicircle is equal to the dam height, and its center is located midway between the interface nodes of the section. Figs. 1(a) and 1(b) show the finite element models of the concrete arch and the foundation rock used in the analysis of Talvacchia Dam.

For vibration analysis including dam-reservoir interaction, the reservoir water is modelled as an assemblage of incompressible liquid elements. In general, it is assumed that the reservoir boundary is a cylindrical surface generated by translating the dam-canyon wall interface in the upstream direction. The water nodes match those on the dam face and usually are arranged in successive planes oriented normal to the axis of the cylinder, with the distance between the planes increasing with distance from the dam. For Talvacchia Dam, the reservoir water was modeled by 5 layers of elements that extended upstream a distance five times the water depth,as shown in Fig. 1(c), although experience shows that a set of 3 layers extending upstream three times the reservoir depth is adequate.

When used in a dynamic analysis, the nodal point pressures of the incompressible water elements are used as the unknowns. The bottom and sides of the reservoir are assumed to be rigid, including the vertical plane at the upstream end. Pressures at the interior nodes are eliminated by static condensation so the reservoir water ultimately is represented by the hydrodynamic pressures at the dam face; these are then expressed in terms of consistent added masses which are combined with the mass of the dam

concrete in the dynamic analysis. It is evident in Fig. 1(c) that the level of the reservoir in this analysis is well below the crest of Talvacchia Dam, hence the added mass of the water is relatively unimportant in this case.

Static Loads Considered

Water Pressure: The water load acting at each element node is calculated as the consistent force resulting from water pressure applied to the element face; contributions from all elements having a water face at the node are then combined vectorially to obtain the resultant nodal force.

Temperature: The consistent nodal forces resulting from constraining the element against thermal strains due to the specified nodal temperature changes are calculated element by element, and are then combined vectorially to obtain the nodal temperature loads.

Gravity: To determine the gravity load acting at each dam node, EADAP calculates the consistent force for each element induced by the unit weight of the concrete, and then combines the contributions from all elements attached to the node.

Static Stress Results

Stresses are calculated by EADAP on the upstream and downstream faces of the dam; for the THKSHEL elements the stress points are at the four Gauss quadrature integration points on each face, for the 3DSHEL elements they are at the mid-points of the four edges and at the center of each face. At each stress point for both types of elements these surface stresses are defined with respect to a local axis normal to the dam face, together with two axes tangent to the face--one horizontal and the other perpendicular to the horizontal; thus they represent the arch and cantilever stresses typical of arch dam analysis.

These stress results are depicted by GDAP in two different types of display, each shown on a projected view of the dam face: (1) stress contours, and (2) principal stress vectors plotted from the stress points. Contour plots of the calculated water load stresses are presented in Fig. 2; the arch direction stresses are shown in plots (a) and (b) on the upstream and downstream faces respectively, while the cantilever direction stresses are shown correspondingly in plots (c) and (d). Arch and cantilever

stresses due to the temperature change (shown in Fig. 3e) are presented in the same sequence in plots (a), (b), (c) and (d) of Fig. 3, while the stresses due to the gravity loads are given similarly in plots (a), (b), (c) and (d) of Fig. 4.

These same stress results are also presented in stress vector form, following the same sequence in Figs. 5, 6, and 7; the upstream and downstream faces respectively are shown in plots (a) and (b) of each figure. The advantage of the stress vector plots in portraying the direction of stress flow on the dam faces is clearly evident in these figures; however, it is similarly apparent that the stress contours give a clearer qualitative picture of the stress values pertaining to any specified location.

In addition to these graphic displays, selected items of the calculated stress results are listed in Tables 1, 2, and 3 as described subsequently.

Static Displacements

EADAP evaluates the static displacement components for certain nodes of the finite element mesh: in the case of 3DSHEL elements, translational movements are calculated for all nodes in the three global coordinate directions; but for the THKSHEL elements, these global coordinate translations are calculated only for the mid-surface nodes together with their rotations about the local mid-surface axes. The deflected shapes caused by the water load and the temperature change are shown in Figs. 8(a) and 8(b), respectively. In addition, the values of the translation displacement components calculated at selected nodal points are listed in tables as described in the following section.

Tabulated Static Analysis Results

Static analysis stress results calculated for a selected group of finite element nodes are listed in Tables 1, 2, and 3 for the hydrostatic, thermal, and gravity load cases, respectively. The nodal points to which these results pertain are numbered as shown in Fig. 9(a) taken from the Benchmark Workshop instructions. It may be seen in the tables that the stress data is available only for the nodes at the dam face locations, and that the quantities listed are the two principal surface stress values and their orientation angle. It should be noted that these stresses were not actually calculated for the numbered nodal point locations, but for the point marked on each element with a (+) symbol in Fig. 9(b). As was mentioned earlier, these stress points are at the mid-edge positions for the 3DSHEL elements (those in

contact with the foundation block) and at an integration point near the node for the remaining elements– which are of the THKSHEL type. Furthermore, it is apparent in the tables that the displacements are presented for the nodes on both faces but not at mid-surface of the 3DSHEL elements, while for the THKSHEL elements (the ones not in contact with the foundation rock) only the mid-surface displacements are given.

Vibration Mode Shapes and Frequencies

The vibration properties of the dam-reservoir water-foundation system are evaluated by solving a standard eigen problem involving the mass and stiffness matrices of the system. In the EADAP analysis, the stiffness matrix is assembled by combining the stiffness of the concrete elements of the dam with the stiffness of the foundation rock elements. The mass matrix is assembled by appropriately adding the mass matrices of the concrete dam elements to the added mass matrix of the reservoir water that is in contact with the dam face. The mass of the foundation rock typically is excluded from the vibration analysis.

The system eigen problem is solved by the subspace iteration method for any desired number of vibration mode shapes and frequencies. In this analysis, six modes were calculated for each of the three cases considered: rigid foundation with no reservoir water, flexible foundation with no reservoir water, and flexible foundation with reservoir water. The calculated frequencies for these cases are listed in Table 4.

In addition, the global coordinate displacement components of the first six vibration mode shapes for the case including flexible foundation and reservoir water have been listed in Tables 5(a) through 5(f). The quantities shown are the displacement components for the mid-surface nodes numbered as shown in Fig. 10. Each mode shape has been normalized to provide a unit value for the greatest nodal displacement component. These mode shapes also are plotted in Fig. 11.

Closing Remarks

It is recognized that the fundamental purpose of this workshop is software validation rather than dam engineering; thus the nature of the performance of the dam that may be indicated by the analysis is not of any major interest. However, it is essential that any dam analysis software be effective in

determining whether or not the dam performance is satisfactory; hence the Benchmark comparisons should emphasize results that are most significant in the evaluation of dam performance. It is for this reason that the Benchmark analyses should concentrate on the analysis of surface stresses for the concrete arch--which are closely related to its potential failure mechanism--rather than on global coordinate principal stresses which are not directly related to the material crushing or tensile cracking. Accordingly, only the surface coordinate principal stresses have been presented in this report.

With regard to the dynamic behavior, the vibration mode shapes and frequencies certainly are a fundamental property of the dam-foundation-reservoir water system; however their values actually are immaterial in the evaluation of dam performance. The vibration properties are used differently in time domain analyses of dynamic response as compared with frequency domain procedures, and hence different representations of the vibration properties may be pertinent--especially with regard to the contribution of water compressibility. For this reason, the relative performance of programs with regard to dynamic analysis should be based on comparisons of the predicted dynamic response behavior and not merely on some aspect of vibration analysis. The calculated dynamic response stresses and displacements can be compared directly, regardless of whether the analysis was done in the time domain or the frequency domain and whether or not the compressibility of the water was considered. Consequently, it is easy to judge the relative effectiveness of all types of programs on this basis.

For this reason, it is hoped that a Second Benchmark Workshop will be organized in which a major objective will be to analyze the response of the structure to a specified earthquake excitation. The test earthquake must be selected with care, with due consideration of the dominant ground motion frequencies as compared with the fundamental frequencies of the dam and the reservoir. In fact it probably would be the most effective to consider three different versions of the test earthquake, the two modified versions being time-scaled to reduce and to increase the frequency range of the input waves that supply the majority of the excitation energy.

Other factors of importance in the specified earthquake excitation are the spacial variation of the prescribed free-field earthquake motions and the interaction of the foundation rock with the dynamic response of the dam. However these topics are still in the realm of active research, and it would be premature to consider them in a Benchmark Workshop at this time.

REFERENCES

[1] "EADAP - Enhanced Arch Dam Analysis Program" Report No. UCB/EERC 89/07, by Yusof Ghanaat and Ray W. Clough, Earthquake Engineering Research Center, University of California, Berkeley, November 1989.

[2] "ADAP - A Computer Program for Static and Dynamic Analysis of Arch Dams" Report No. UCB/EERC-73/14, by Ray W. Clough, J. M. Raphael, and S. Mojtahedi, EERC, University of California, Berkeley, June 1973.

[3] "GDAP - Graphics Based Dam Analysis Program," User's Manual by Quest Structures, 2000 Powell Street, Emeryville, CA 94608, April 1990.

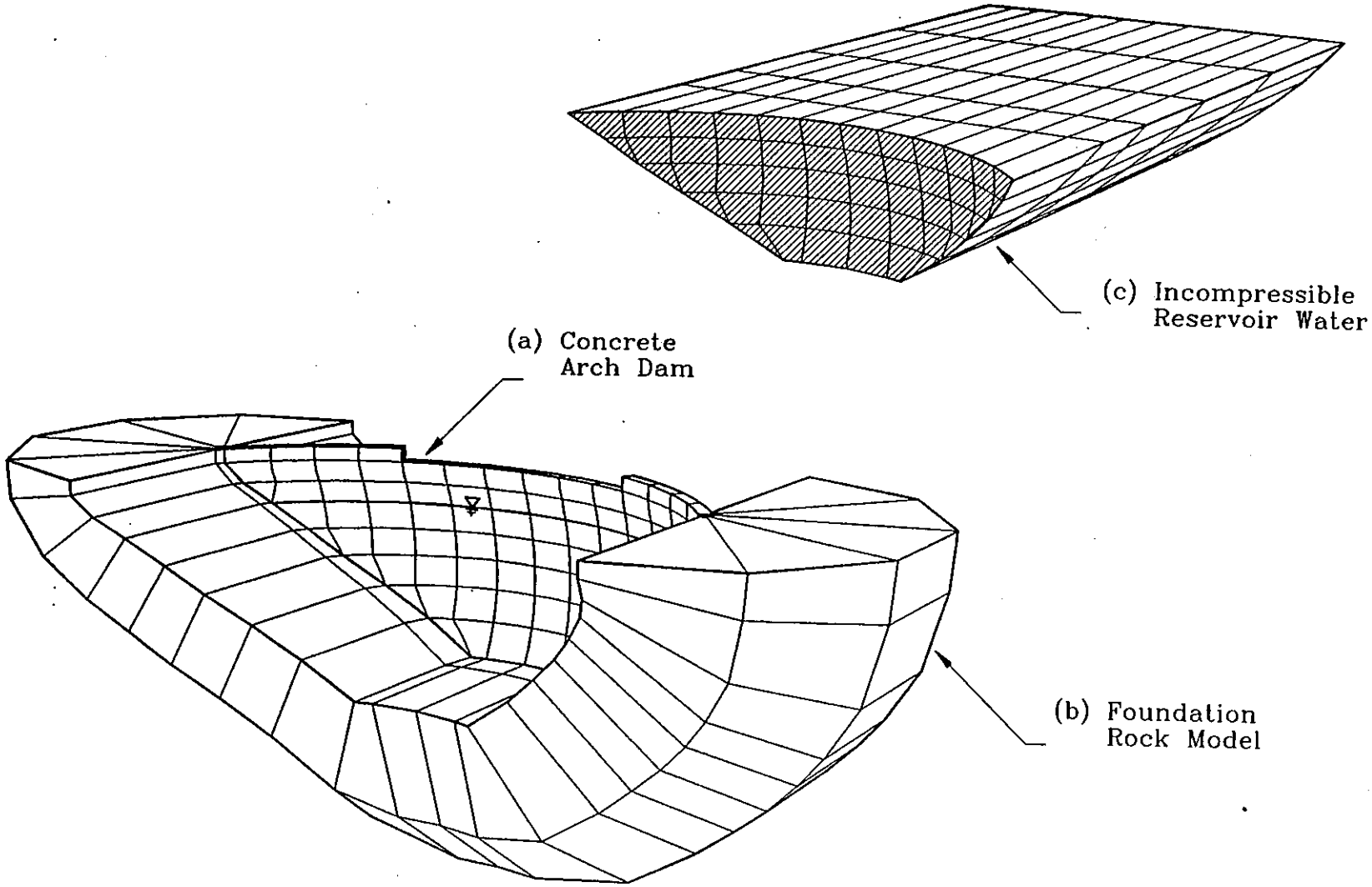

Fig. 1 Finite Element Model of Talvacchia Dam System

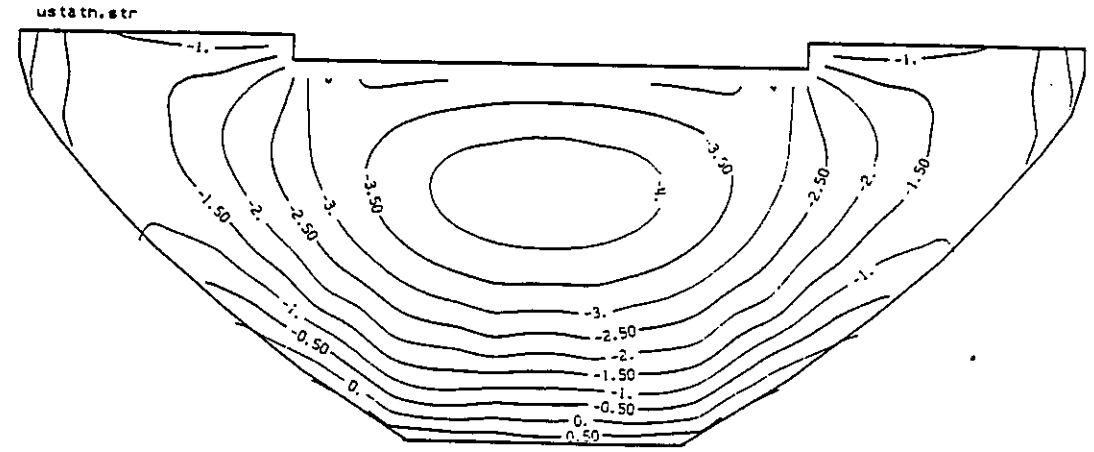

(a) U/S ARCH STRESSES

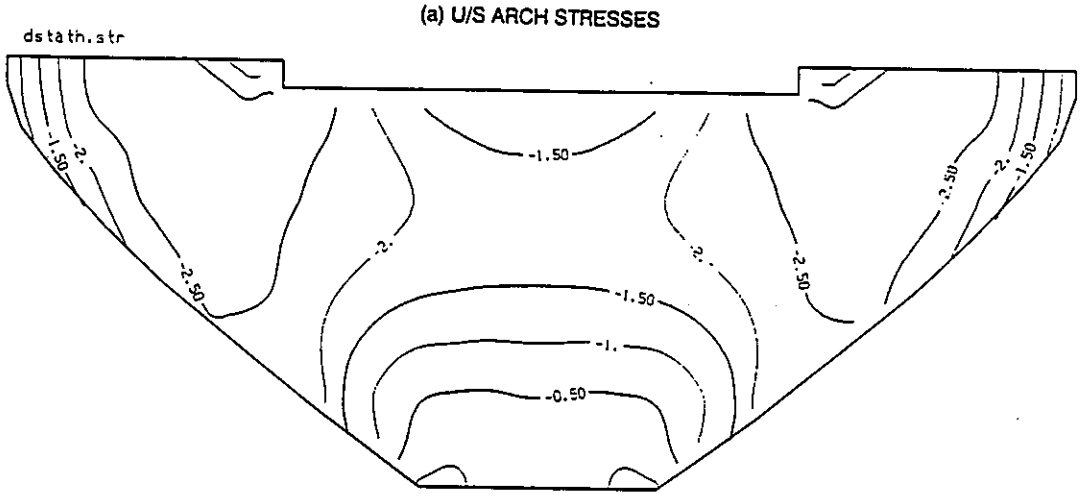

(b) D/S ARCH STRESSES

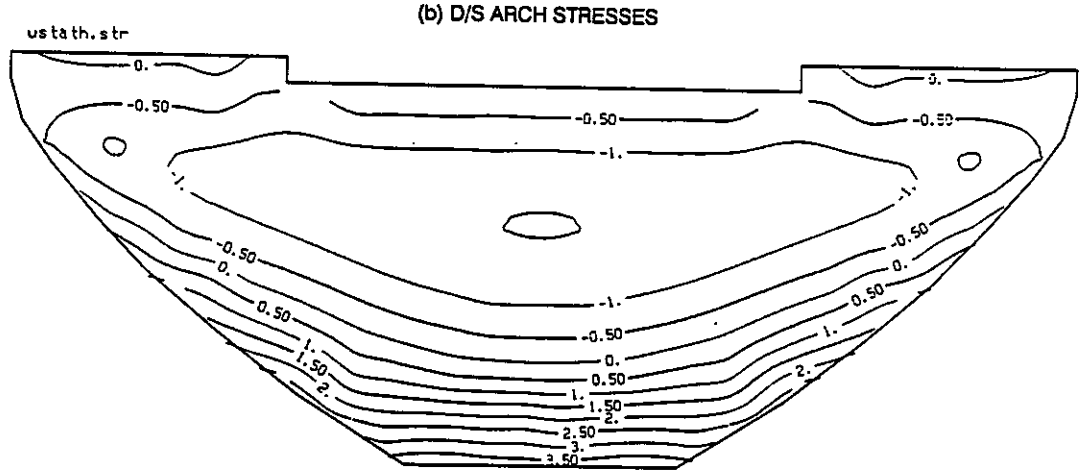

(c) U/S CANTILEVER STRESSES

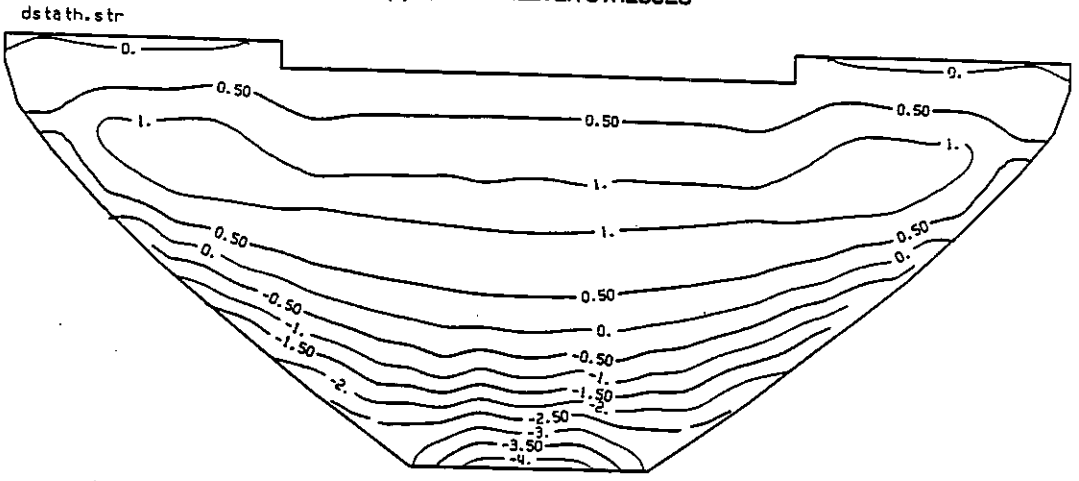

(d) D/S CANTILEVER STRESSES

Fig. 2 Surface Stresses due to Water Load (Megapascals)

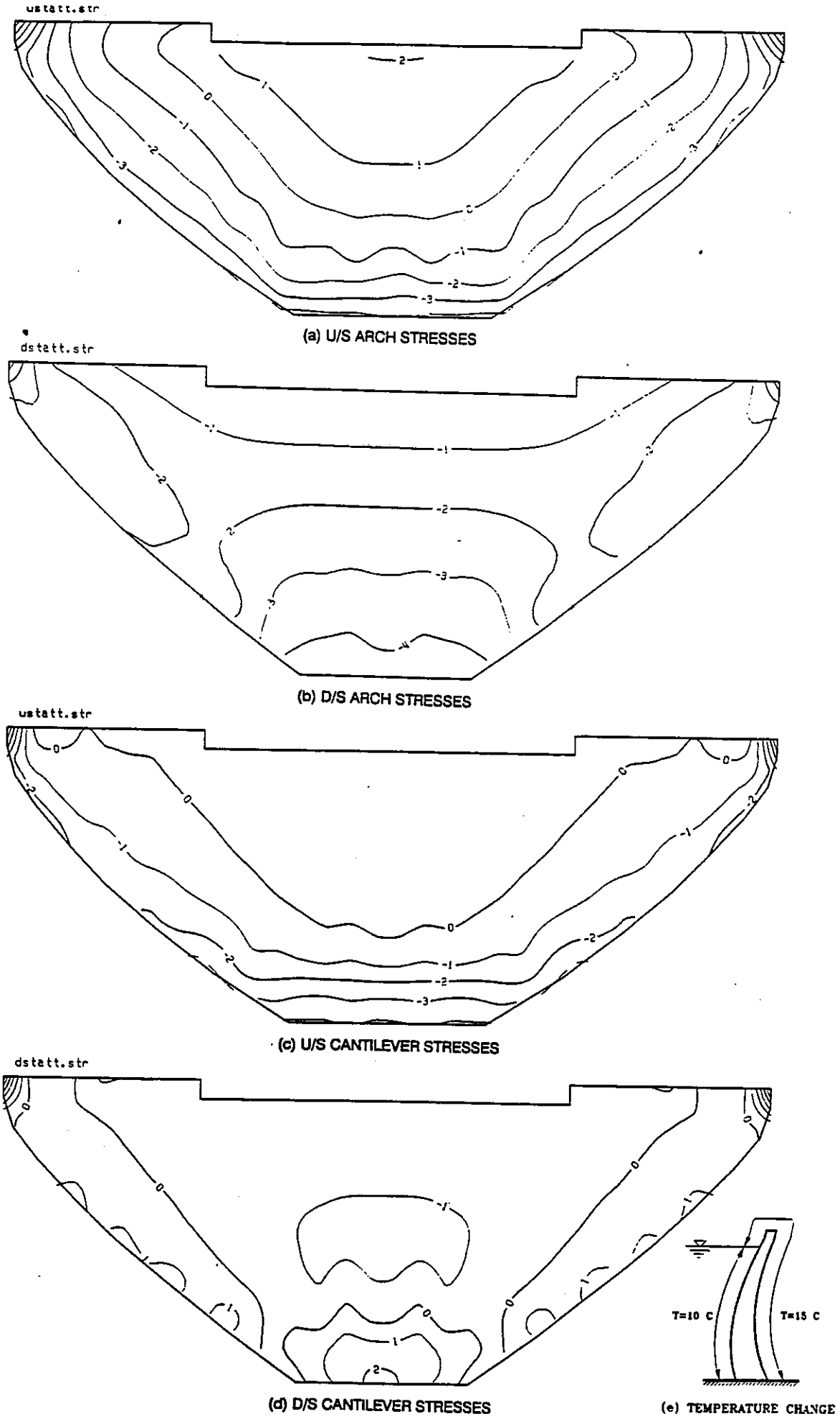

(a) U/S ARCH STRESSES

(b) D/S ARCH STRESSES

(c) U/S CANTILEVER STRESSES

(d) D/S CANTILEVER STRESSES

(e) TEMPERATURE CHANGE

Fig. 3 Surface Stresses due to Temperature Change (Megapascals)

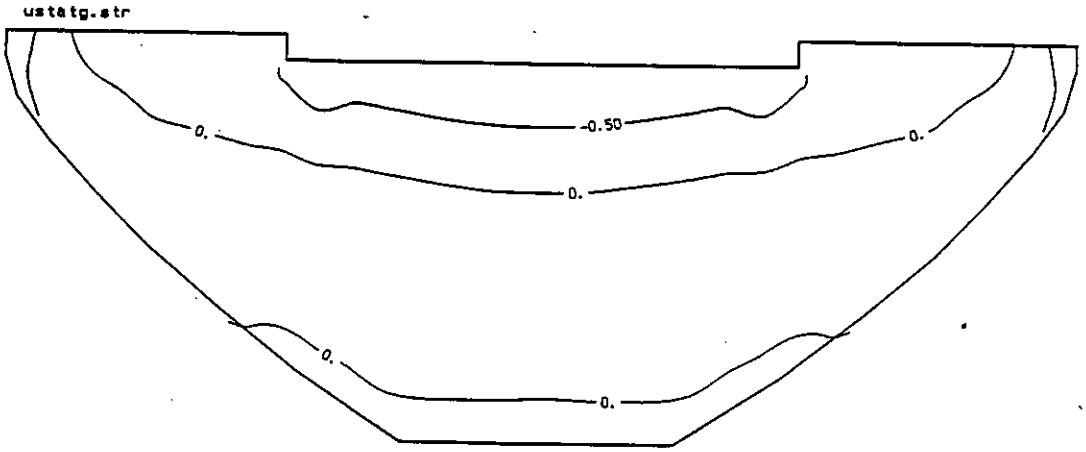

(a) U/S ARCH STRESSES

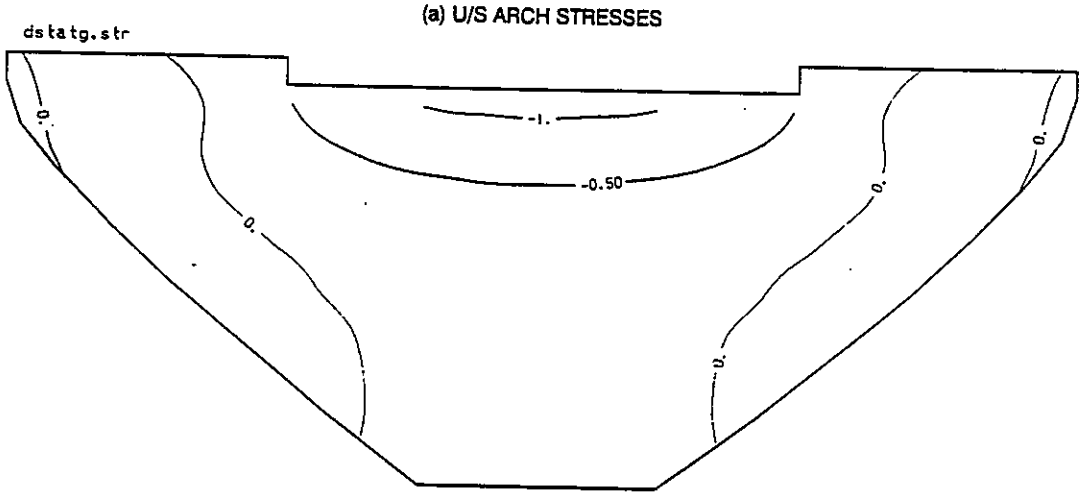

(b) D/S ARCH STRESSES

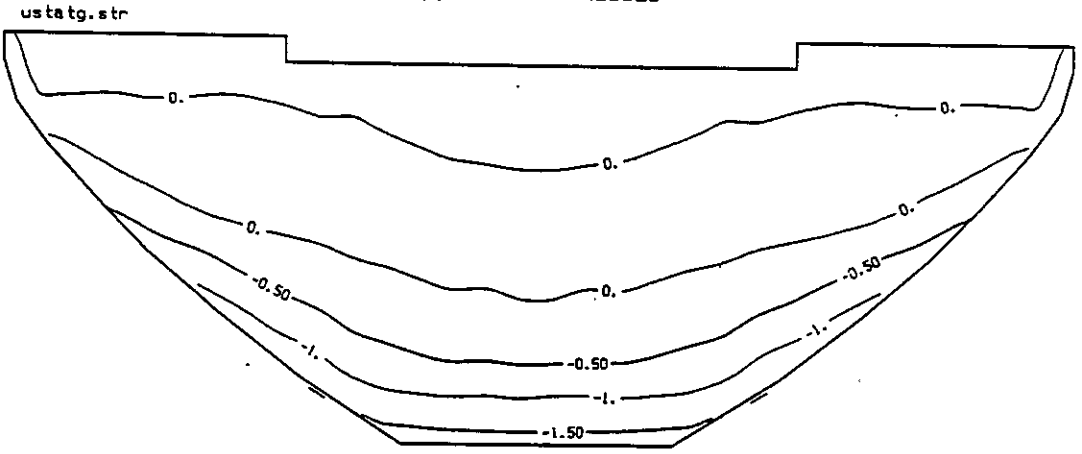

(c) U/S CANTILEVER STRESSES

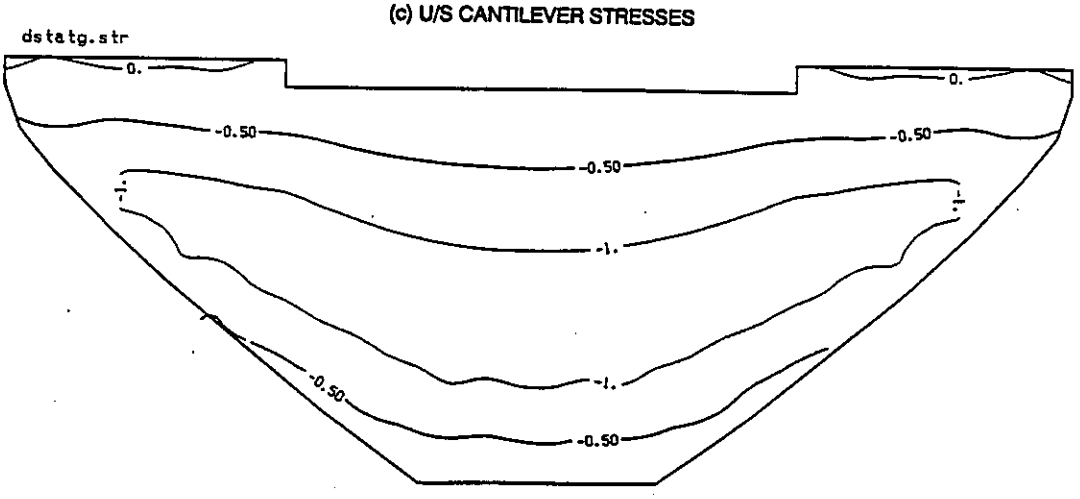

(d) D/S CANTILEVER STRESSES

Fig. 4 Surface Stresses due to Gravity Load (Megapascals)

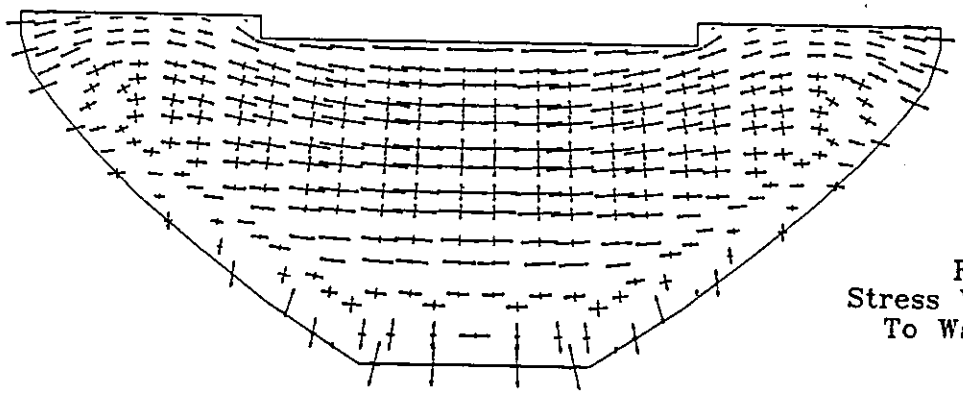

(a) U/S Principal Stresses

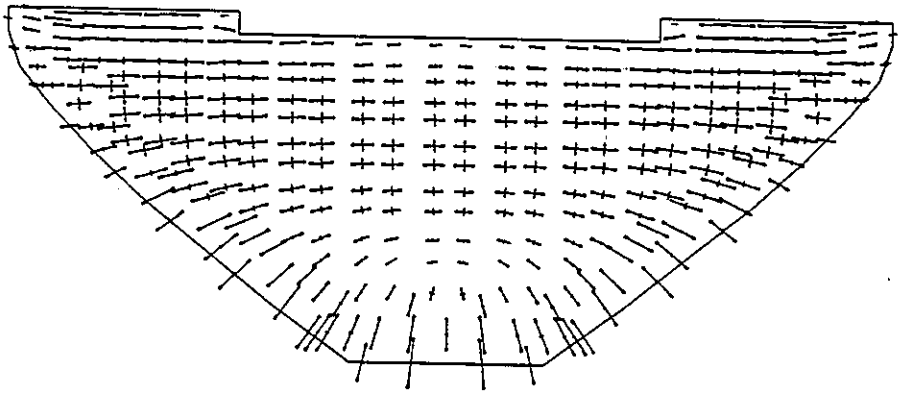

(b) D/S Principal Stresses

Fig. 5
Stress Vectors Due
To Water Load

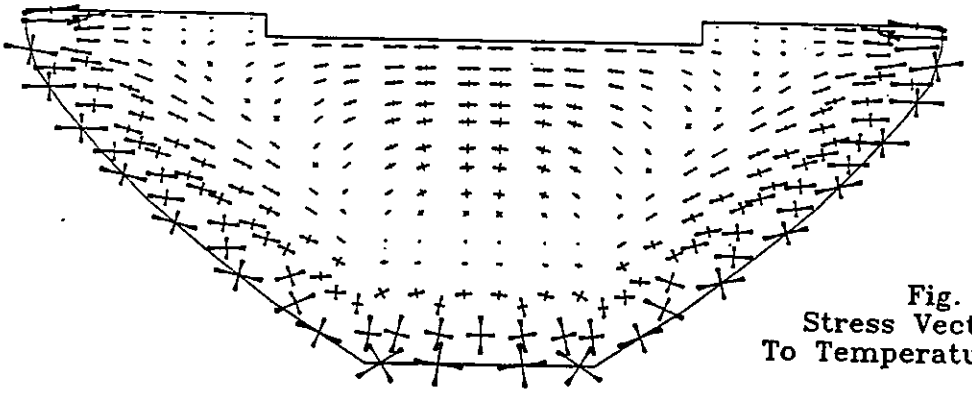

(a) U/S Principal Stresses

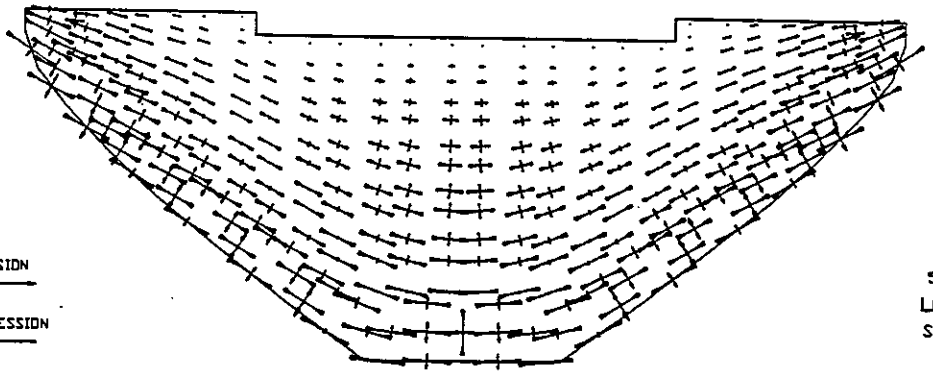

(b) D/S Principal Stresses

Fig. 6
Stress Vectors Due
To Temperature Change

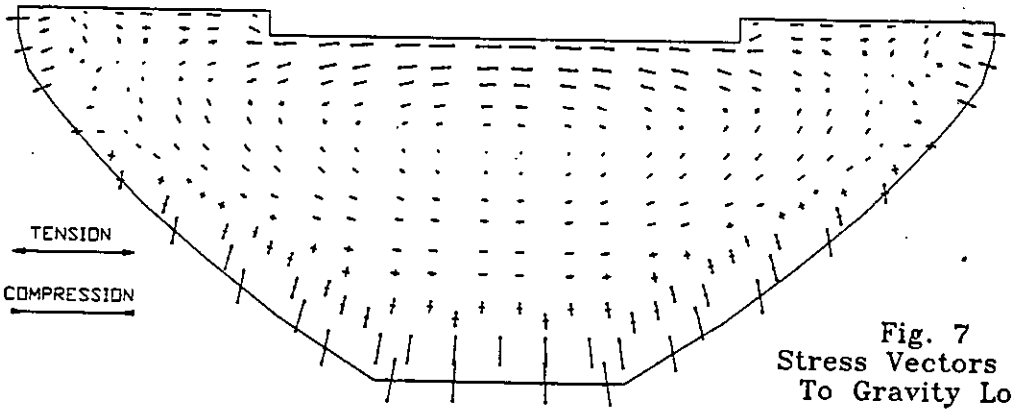

(a) U/S Principal Stresses

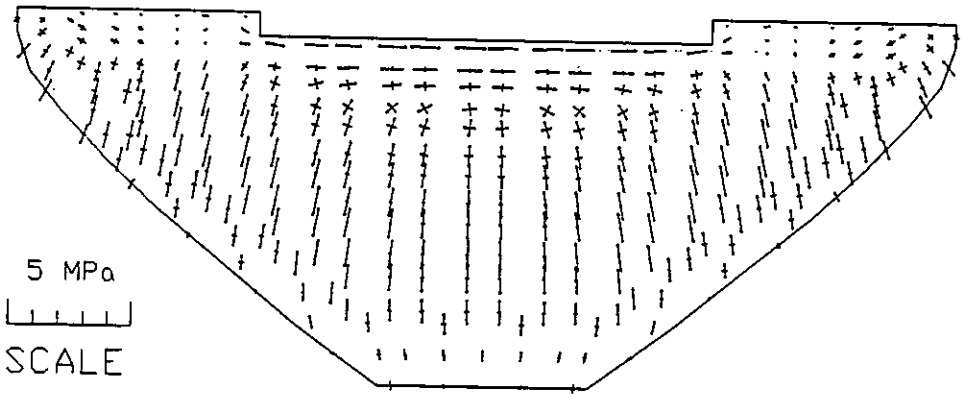

(b) D/S Principal Stresses

Fig. 7
Stress Vectors Due
To Gravity Load

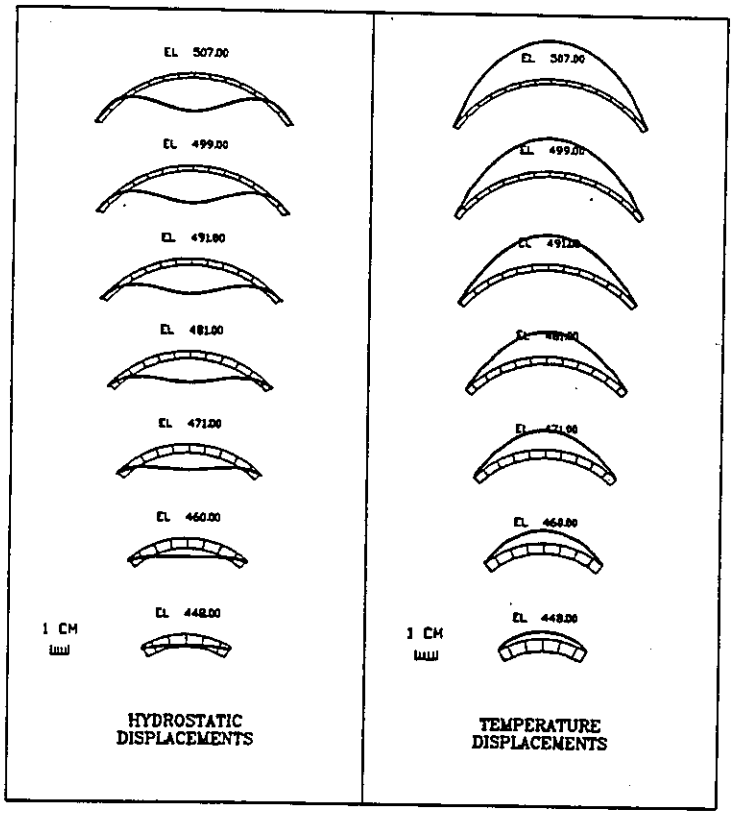

Fig. 8 Deflected Shapes Due To Static Loads

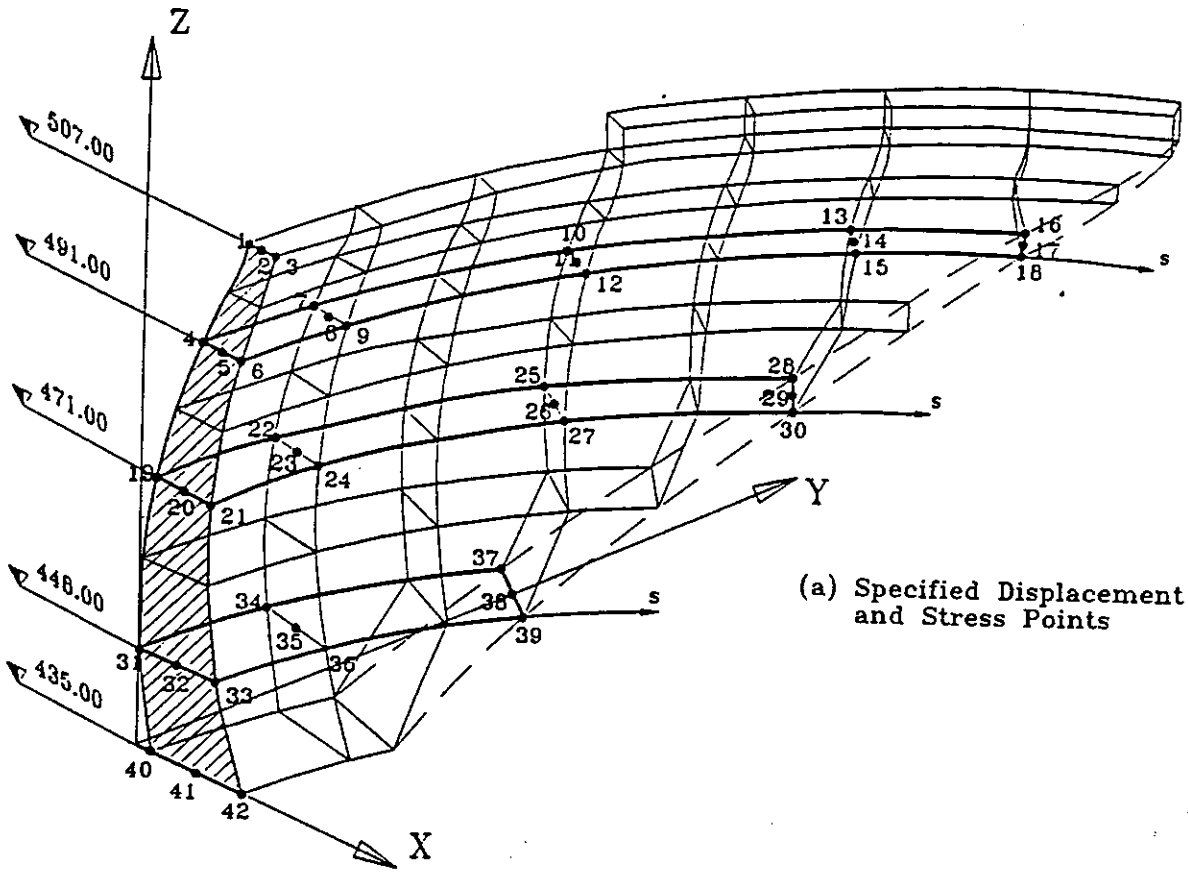

(a) Specified Displacement and Stress Points

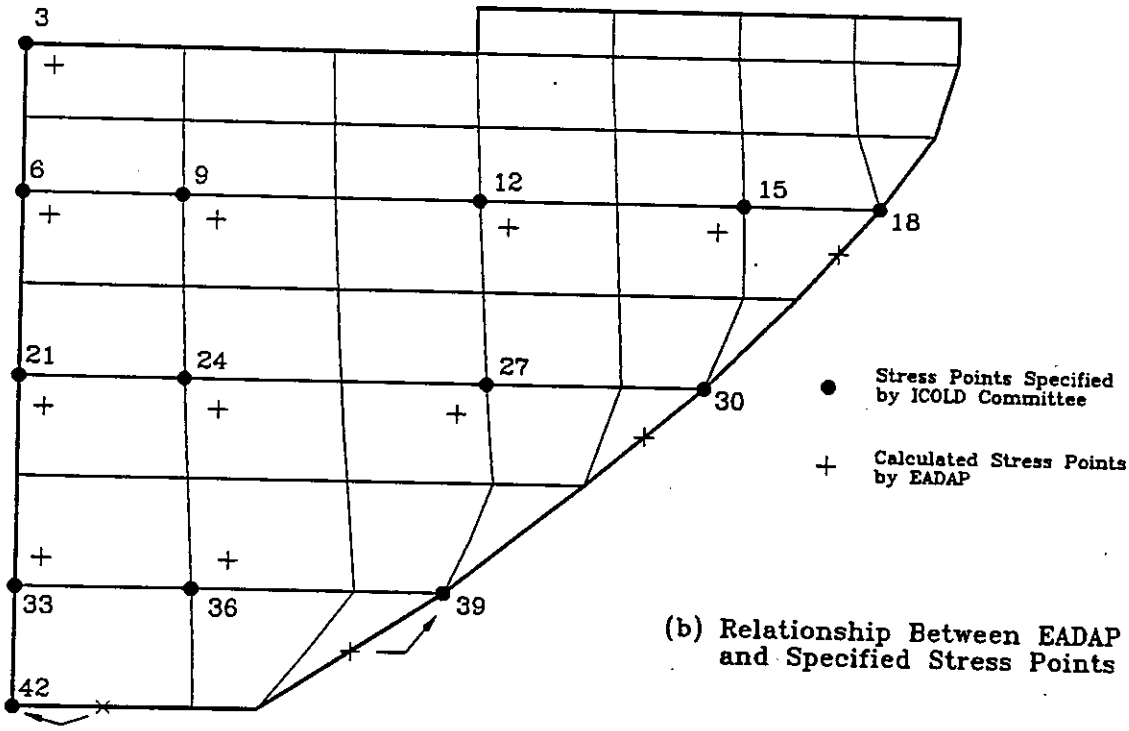

(b) Relationship Between EADAP and Specified Stress Points

Fig. 9 Points at Which Stresses and Displacements Are Tabulated (See Tables 1, 2, and 3)

Table 1 Results due to Water Load

Points	s	Global Displacements			Surface Principal Stresses		
	(m)	X (m)	Y (m)	Z (m)	Major (MPa)	Minor (MPa)	Angle
1	0.0				-0.094	-2.963	89.363
2	0.0	0.221E-01	0.182E-06	-0.553E-03			
3	0.0				0.070	-0.953	-88.699
4	0.0				-1.409	-4.271	88.887
5	0.0	0.201E-01	0.112E-06	0.302E-04			
6	0.0				1.034	-1.749	-89.643
7	16.0				-1.363	-4.060	84.010
8	16.0	0.187E-01	-0.121E-02	0.926E-04			
9	16.0				1.039	-1.945	-88.489
10	48.0				-1.258	-2.603	78.007
11	48.0	0.100E-01	-0.137E-02	0.309E-03			
12	48.0				1.212	-2.672	-84.791
13	80.0	0.223E-02	0.312E-03	0.104E-03	-0.996	-1.335	-81.992
14	80.0						
15	80.0	0.279E-02	0.918E-03	0.126E-03	1.346	-2.560	-83.975
16	99.2	0.807E-03	0.783E-03	-0.117E-03	0.141	-1.550	-74.419
17	99.2						
18	99.2	0.102E-02	0.952E-03	-0.489E-04	0.092	-1.542	-81.194
19	0.0				-1.220	-3.847	89.090
20	0.0	0.148E-01	0.476E-07	0.127E-02			
21	0.0				0.679	-1.401	-88.006
22	16.0				-1.051	-3.589	86.008
23	16.0	0.136E-01	-0.115E-02	0.118E-02			
24	16.0				0.662	-1.517	-80.048
25	48.0	0.614E-02	-0.193E-02	0.164E-02	-0.269	-1.971	85.330
26	48.0						
27	48.0	0.703E-02	-0.106E-03	-0.497E-03	0.500	-2.530	-71.831
28	75.0	0.109E-02	0.524E-03	0.256E-03	1.604	-0.699	-89.625
29	75.0						
30	75.0	0.201E-02	0.117E-02	-0.593E-03	-0.526	-2.902	-52.316
31	0.0	0.623E-02	-0.662E-08	0.350E-02	0.510	-1.841	88.311
32	0.0						
33	0.0	0.586E-02	0.299E-07	-0.837E-03	-0.405	-1.055	-13.728
34	16.0	0.548E-02	-0.797E-03	0.310E-02	0.848	-1.772	83.872
35	16.0						
36	16.0	0.528E-02	0.123E-03	-0.884E-03	0.209	-1.706	-32.270
37	41.5	0.141E-02	-0.324E-04	0.995E-03	2.742	0.538	79.948
38	41.5						
39	41.5	0.256E-02	0.963E-03	-0.975E-03	0.230	-3.522	-34.420
40	0.0	0.183E-02	-0.755E-09	0.169E-02	3.774	0.836	87.276
41	0.0						
42	0.0	0.189E-02	0.961E-08	-0.107E-02	-0.117	-4.418	-6.021

Table 2 Results due to Temperature Change

Points	s	Global Displacements			Surface Principal Stresses		
	(m)	X (m)	Y (m)	Z (m)	Major (MPa)	Minor (MPa)	Angle
1	0.0				2.177	0.068	0.122
2	0.0	-0.176E-01	0.690E-07	0.910E-02			
3	0.0				0.073	-0.045	-1.779
4	0.0				1.537	0.760	2.041
5	0.0	-0.135E-01	0.405E-07	0.605E-02			
6	0.0				-0.786	-1.268	87.452
7	16.0				1.302	0.562	15.728
8	16.0	-0.126E-01	0.146E-02	0.580E-02			
9	16.0				-0.708	-1.314	76.287
10	48.0				0.310	-0.873	54.462
11	48.0	-0.708E-02	0.264E-02	0.403E-02			
12	48.0				0.031	-1.965	63.297
13	80.0	-0.146E-02	0.169E-02	0.889E-03	-0.811	-2.098	74.497
14	80.0						
15	80.0	-0.161E-02	0.552E-03	0.221E-02	1.202	-3.213	65.781
16	99.2	0.000E+00	0.000E+00	0.000E+00	-2.446	-4.490	-89.981
17	99.2	0.000E+00	0.000E+00	0.000E+00			
18	99.2	0.000E+00	0.000E+00	0.000E+00	2.290	-4.366	61.469
19	0.0				0.655	0.624	48.513
20	0.0	-0.894E-02	0.127E-07	0.292E-02			
21	0.0				-1.228	-2.550	85.140
22	16.0				0.517	0.166	39.515
23	16.0	-0.809E-02	0.103E-02	0.276E-02			
24	16.0				-0.839	-2.802	70.305
25	48.0	-0.305E-02	0.199E-02	0.616E-03	-0.644	-1.799	64.680
26	48.0						
27	48.0	-0.257E-02	0.124E-03	0.250E-02	0.933	-2.924	60.477
28	75.0	0.000E+00	0.000E+00	0.000E+00	-2.038	-3.862	74.983
29	75.0	0.000E+00	0.000E+00	0.000E+00			
30	75.0	0.000E+00	0.000E+00	0.000E+00	0.951	-4.338	57.622
31	0.0	-0.347E-02	-0.326E-09	-0.644E-03	-0.715	-1.314	-84.207
32	0.0						
33	0.0	-0.158E-02	0.307E-08	0.231E-02	-0.237	-3.520	86.719
34	16.0	-0.298E-02	0.693E-03	-0.506E-03	-0.930	-1.356	-61.648
35	16.0						
36	16.0	-0.123E-02	-0.159E-03	0.212E-02	-0.068	-3.959	70.981
37	41.5	0.000E+00	0.000E+00	0.000E+00	-2.632	-4.172	67.730
38	41.5	0.000E+00	0.000E+00	0.000E+00			
39	41.5	0.000E+00	0.000E+00	0.000E+00	-0.415	-4.700	60.436
40	0.0	0.000E+00	0.000E+00	0.000E+00	-3.820	-4.269	81.797
41	0.0	0.000E+00	0.000E+00	0.000E+00			
42	0.0	0.000E+00	0.000E+00	0.000E+00	1.400	-4.225	86.756

Table 3 Results due to Gravity Load

Points	s	Surface Principal Stresses		
	(m)	Major (MPa)	Minor (MPa)	Angle
1	0.0	-0.064	-1.033	-89.470
2	0.0			
3	0.0	-0.024	-1.193	89.870
4	0.0	-0.022	-0.233	-85.085
5	0.0			
6	0.0	-0.456	-0.638	-5.783
7	16.0	0.063	-0.207	-66.723
8	16.0			
9	16.0	-0.393	-0.724	-18.150
10	48.0	0.333	-0.055	-59.004
11	48.0			
12	48.0	-0.085	-1.076	-13.499
13	80.0	0.283	0.117	-64.456
14	80.0			
15	80.0	0.179	-1.212	-11.806
16	99.2	0.408	-0.265	3.697
17	99.2			
18	99.2	0.168	-0.782	-20.002
19	0.0	0.314	0.106	-3.236
20	0.0			
21	0.0	-0.122	-1.178	-1.405
22	16.0	0.341	0.053	-12.907
23	16.0			
24	16.0	-0.107	-1.194	-7.662
25	48.0	0.267	-0.211	-18.244
26	48.0			
27	48.0	0.086	-1.133	-10.581
28	75.0	0.146	-1.125	-9.318
29	75.0			
30	75.0	0.140	-0.223	-20.356
31	0.0	0.215	-0.416	-1.544
32	0.0			
33	0.0	-0.111	-0.984	-0.030
34	16.0	0.213	-0.582	-9.514
35	16.0			
36	16.0	-0.132	-0.864	0.708
37	41.5	-0.166	-1.472	-10.542
38	41.5			
39	41.5	-0.117	-0.229	65.830
40	0.0	-0.368	-1.675	-2.346
41	0.0			
42	0.0	-0.016	-0.178	8.104

Table 4 Calculated Vibration Frequencies (Hertz)

MODE NO	RIGID FOUNDATION NO RESERVOIR	FLEXIBLE FOUNDATION NO RESERVOIR	FLEXIBLE FOUNDATION 5-LAYER RESERVOIR
1	4.272	3.642	3.449
2	4.552	4.042	3.731
3	5.674	5.115	4.927
4	6.640	5.925	5.807
5	8.430	7.514	6.900
6	9.301	8.161	7.466

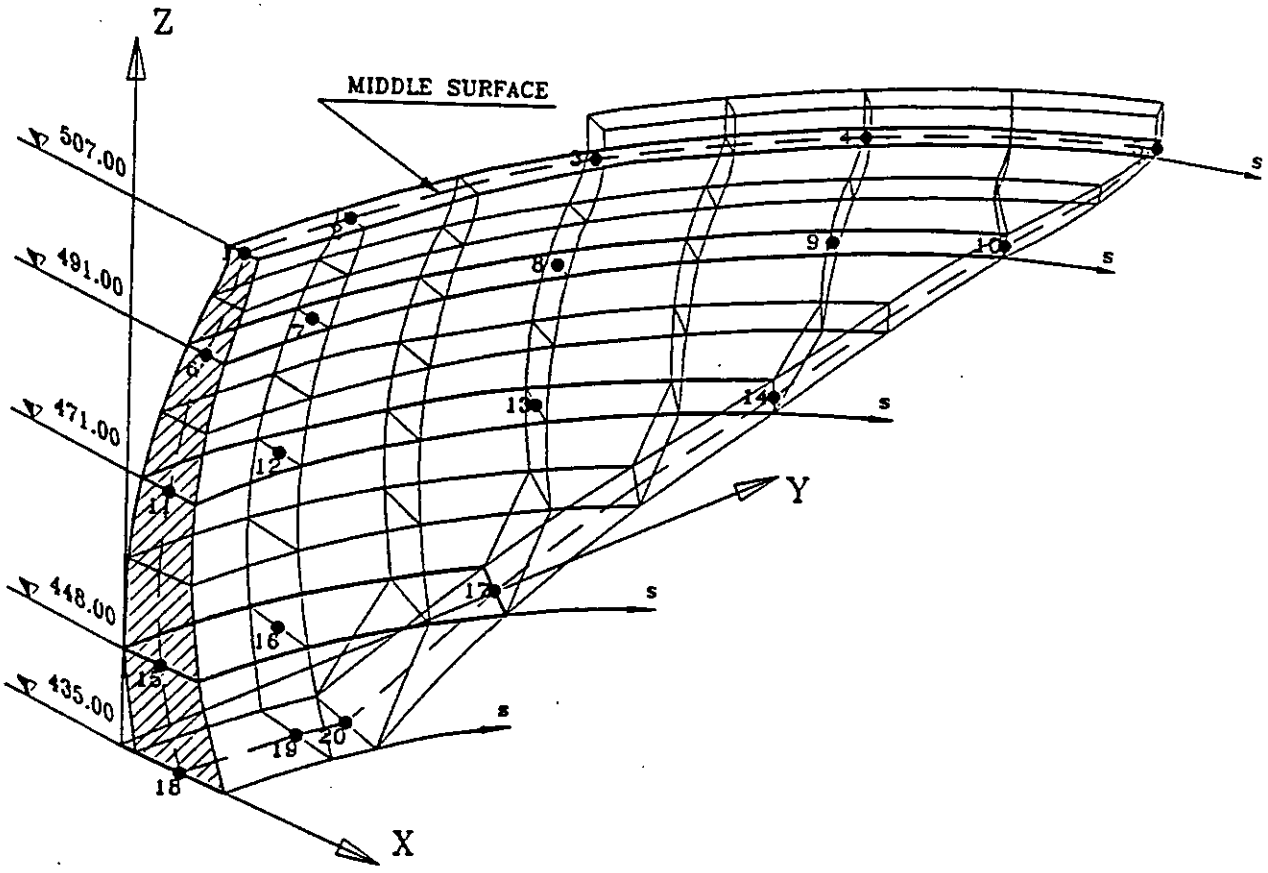

Fig. 10 Points For Which Mode Shape Displacements Are Tabulated

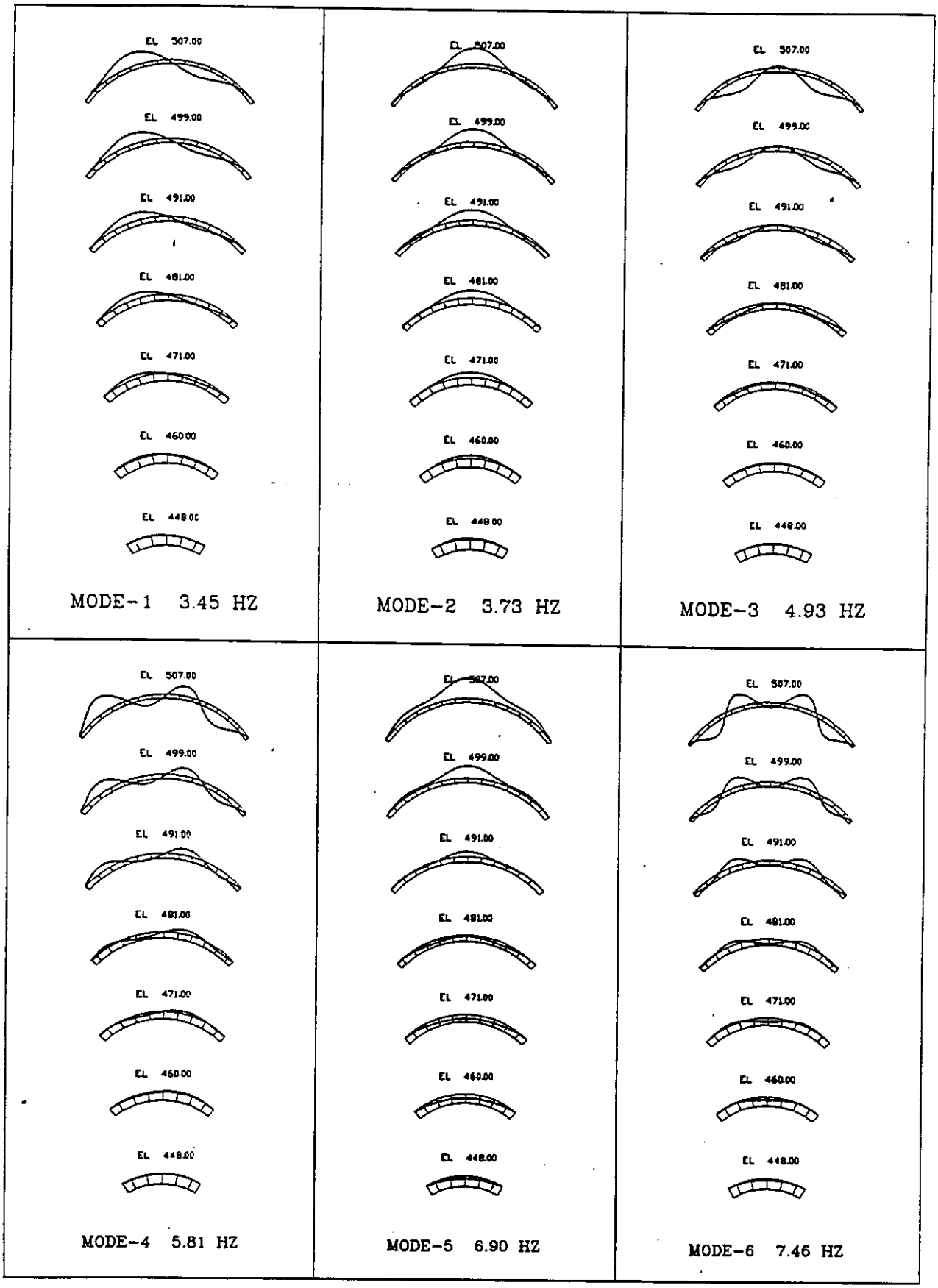

Fig. 11 Vibration Shapes For First Six Modes

Table 5 Vibration Mode Shapes
(Normalized to Maximum Value of Unity)

MODE 1

Points	s	Displ x	Displ y	Displ z
1	0.0	-0.185E-03	-0.359E+00	0.329E-04
2	16.0	0.680E+00	-0.410E+00	-0.146E+00
3	48.0	0.100E+01	-0.513E+00	-0.187E+00
4	80.0	0.299E+00	-0.151E+00	-0.325E-01
5	112.9	0.204E-01	0.174E-01	-0.695E-03
6	0.0	-0.120E-03	-0.247E+00	0.993E-05
7	16.0	0.418E+00	-0.278E+00	-0.483E-01
8	48.0	0.598E+00	-0.331E+00	-0.345E-01
9	80.0	0.157E+00	-0.975E-01	0.119E-01
10	99.2	0.237E-01	0.823E-02	0.187E-02
11	0.0	-0.581E-04	-0.119E+00	-0.624E-05
12	16.0	0.186E+00	-0.135E+00	0.172E-01
13	48.0	0.214E+00	-0.138E+00	0.368E-01
14	75.0	0.316E-01	-0.105E-01	0.663E-02
15	0.0	-0.153E-04	-0.424E-01	-0.655E-05
16	16.0	0.410E-01	-0.452E-01	0.207E-01
17	41.5	0.192E-01	-0.255E-01	0.188E-01
18	0.0	-0.290E-05	-0.222E-01	-0.297E-05
19	16.0	0.444E-02	-0.206E-01	0.107E-01
20	22.0	0.444E-02	-0.189E-01	0.133E-01

MODE 2

Points	s	Displ x	Displ y	Displ z
1	0.0	-0.100E+01	0.314E-04	0.179E+00
2	16.0	-0.813E+00	0.102E-01	0.133E+00
3	48.0	0.592E-01	-0.188E+00	-0.578E-01
4	80.0	0.203E+00	-0.214E+00	-0.561E-01
5	112.9	0.378E-02	-0.999E-02	-0.252E-02
6	0.0	-0.665E+00	0.222E-04	0.576E-01
7	16.0	-0.553E+00	0.133E-01	0.398E-01
8	48.0	-0.367E-01	-0.890E-01	-0.188E-01
9	80.0	0.683E-01	-0.106E+00	-0.275E-02
10	99.2	0.110E-02	-0.231E-01	0.957E-03
11	0.0	-0.329E+00	0.113E-04	-0.323E-01
12	16.0	-0.276E+00	0.125E-01	-0.298E-01
13	48.0	-0.464E-01	-0.312E-01	-0.788E-02
14	75.0	-0.638E-02	-0.281E-01	0.204E-02
15	0.0	-0.887E-01	0.434E-05	-0.353E-01
16	16.0	-0.726E-01	0.733E-03	-0.282E-01
17	41.5	-0.185E-01	-0.151E-01	-0.256E-02
18	0.0	-0.176E-01	0.236E-05	-0.155E-01
19	16.0	-0.144E-01	-0.338E-02	-0.125E-01
20	22.0	-0.126E-01	-0.500E-02	-0.952E-02

Table 5 Cont'd

MODE 3

Points	s	Displ x	Displ y	Displ z
1	0.0	-0.168E+00	0.220E-05	0.103E+00
2	16.0	0.767E-01	-0.854E-01	0.334E-01
3	48.0	0.100E+01	-0.508E+00	-0.228E+00
4	80.0	0.522E+00	-0.298E+00	-0.949E-01
5	112.9	0.374E-01	0.288E-01	-0.651E-02
6	0.0	-0.320E-01	0.126E-05	0.409E-01
7	16.0	0.912E-01	-0.503E-01	0.162E-01
8	48.0	0.515E+00	-0.242E+00	-0.469E-01
9	80.0	0.237E+00	-0.131E+00	-0.754E-03
10	99.2	0.435E-01	0.163E-01	-0.549E-02
11	0.0	0.492E-01	0.496E-06	0.113E-01
12	16.0	0.870E-01	-0.178E-01	0.116E-01
13	48.0	0.170E+00	-0.669E-01	0.173E-01
14	75.0	0.459E-01	0.539E-02	-0.448E-02
15	0.0	0.291E-01	0.176E-06	0.887E-02
16	16.0	0.337E-01	-0.198E-02	0.102E-01
17	41.5	0.220E-01	0.202E-02	0.480E-02
18	0.0	0.885E-02	0.125E-06	0.369E-02
19	16.0	0.912E-02	0.149E-02	0.419E-02
20	22.0	0.915E-02	0.210E-02	0.401E-02

MODE 4

Points	s	Displ x	Displ y	Displ z
1	0.0	-0.532E-05	0.104E+00	-0.659E-05
2	16.0	-0.853E+00	0.147E+00	0.230E+00
3	48.0	0.384E+00	-0.425E+00	-0.152E+00
4	80.0	0.100E+01	-0.792E+00	-0.248E+00
5	112.9	0.583E-01	0.127E-01	-0.177E-01
6	0.0	-0.180E-04	0.546E-01	-0.164E-05
7	16.0	-0.500E+00	0.836E-01	0.926E-01
8	48.0	-0.363E-03	-0.111E+00	-0.620E-02
9	80.0	0.351E+00	-0.305E+00	-0.135E-01
10	99.2	0.566E-01	-0.287E-01	-0.965E-02
11	0.0	-0.184E-04	0.132E-01	-0.108E-05
12	16.0	-0.197E+00	0.312E-01	0.452E-02
13	48.0	-0.609E-01	-0.102E-01	0.101E-01
14	75.0	0.196E-01	-0.329E-01	0.183E-02
15	0.0	-0.729E-05	-0.192E-02	-0.132E-05
16	16.0	-0.433E-01	0.263E-02	-0.501E-02
17	41.5	-0.210E-01	-0.746E-02	0.965E-02
18	0.0	-0.205E-05	-0.118E-02	-0.136E-06
19	16.0	-0.866E-02	-0.159E-02	0.119E-02
20	22.0	-0.990E-02	-0.229E-02	0.272E-02

Table 5 Cont'd

MODE 5

Points	s	Displ x	Displ y	Displ z
1	0.0	-0.100E+01	0.221E-05	0.445E+00
2	16.0	-0.794E+00	0.932E-01	0.372E+00
3	48.0	-0.185E+00	0.109E+00	0.139E+00
4	80.0	-0.154E+00	0.140E+00	0.672E-01
5	112.9	-0.542E-02	0.386E-02	0.834E-02
6	0.0	-0.265E+00	0.157E-05	0.179E+00
7	16.0	-0.176E+00	0.114E-01	0.150E+00
8	48.0	0.541E-01	-0.203E-01	0.517E-01
9	80.0	-0.199E-01	0.288E-01	0.193E-01
10	99.2	-0.232E-02	0.727E-02	0.992E-02
11	0.0	0.179E+00	0.121E-05	0.408E-01
12	16.0	0.186E+00	-0.261E-01	0.384E-01
13	48.0	0.123E+00	-0.444E-01	0.273E-01
14	75.0	0.185E-01	0.344E-02	0.111E-01
15	0.0	0.126E+00	0.470E-06	0.281E-01
16	16.0	0.114E+00	-0.113E-01	0.259E-01
17	41.5	0.418E-01	0.180E-02	0.959E-02
18	0.0	0.417E-01	0.337E-06	0.741E-02
19	16.0	0.360E-01	0.109E-02	0.740E-02
20	22.0	0.319E-01	0.272E-02	0.657E-02

MODE 6

Points	s	Displ x	Displ y	Displ z
1	0.0	0.469E+00	0.727E-05	-0.997E-01
2	16.0	-0.151E+00	0.110E+00	0.801E-01
3	48.0	-0.658E+00	0.157E+00	0.160E+00
4	80.0	0.100E+01	-0.857E+00	-0.276E+00
5	112.9	0.747E-01	0.612E-02	-0.258E-01
6	0.0	0.451E+00	0.538E-05	-0.770E-01
7	16.0	0.102E+00	0.387E-01	-0.120E-02
8	48.0	-0.436E+00	0.156E+00	0.821E-01
9	80.0	0.281E+00	-0.258E+00	-0.122E-01
10	99.2	0.647E-01	-0.434E-01	-0.131E-01
11	0.0	0.333E+00	0.349E-05	-0.248E-01
12	16.0	0.192E+00	-0.553E-02	-0.151E-01
13	48.0	-0.113E+00	0.586E-01	0.856E-02
14	75.0	0.132E-02	-0.189E-01	0.112E-01
15	0.0	0.124E+00	0.117E-05	-0.146E-02
16	16.0	0.864E-01	-0.278E-02	-0.517E-02
17	41.5	0.782E-02	0.125E-01	-0.203E-02
18	0.0	0.389E-01	0.781E-06	-0.144E-01
19	16.0	0.293E-01	0.473E-02	-0.128E-01
20	22.0	0.229E-01	0.687E-02	-0.118E-01

DYNAMIC ANALYSIS OF ARCH DAM-RESERVOIR SYSTEM

F. Bettinali*, L. Bolognini#, M. Ciccotelli#, M. Meghella*

CISE Tecnologie Innovative Spa - Segrate - Milan - Italy
* ENEL-CRIS - Milan - Italy

1. - INTRODUCTION

The linear elastic dynamic analysis (theme A) of the proposed Talvacchia arch dam-reservoir system is presented.

Suggested finite element models of dam, rock foundation, reservoir and boundary conditions have been used for both the dynamic cases.

A short presentation of the computer code used for the analyses is presented in the following.

2. - COUPLED FLUID-STRUCTURE PROBLEM FORMULATION IN INDIA-3 CODE

The equilibrium equations for dynamic analysis of three-dimensional systems taking into account fluid-structure interaction have been derived following the hypotheses stated below:

- the structure has a linear elastic behaviour;
- fluid velocity field is negligible so that only the pressure field is considered;
- sloshing effects are neglected;

With these assumptions the fluid equilibrium equation is the wave equation:

$$\nabla^2 p = \frac{1}{c^2} \frac{\partial^2 p}{\partial t^2} \qquad (1)$$

where **p** is the pressure field and c is the sound speed.

The boundary surface S is subdivided into four parts S1, S2, S3, S4 and the conditions imposed on these surfaces are:

- free surface S1: $p\big|_{s1} = 0.$
- fluid-structure interface S2: $\frac{1}{\rho_f} \nabla p \cdot n_2 \big|_{s2} = - \ddot{u}_{n2}$

where n_2 is the unit vector normal to S2, ρ_f is the fluid density and $\ddot{u}_{n2}$ is the structure boundary surface acceleration in direction n_2.

- bottom surface S3: $\frac{1}{\rho_f} \nabla p \cdot n_3 \big|_{s3} = - \ddot{u}_{gn3}$

where $\ddot{u}_{gn3}$ is the component of the bottom surface acceleration normal to surface S3;

- upstream surface S4: $\nabla p \cdot \mathbf{n}_4 \big|_{s4} = -\frac{1}{c}\frac{\partial p}{\partial t}\big|_{s4}$

Using Galerkin method for the fluid domain and a classical formulation (Virtual Work based) for the structure, the equilibrium equations take the form:

$$\begin{aligned} &\mathbf{K}_s\mathbf{d} + \mathbf{C}_s\dot{\mathbf{d}} + \mathbf{M}_s\ddot{\mathbf{d}} - \mathbf{H}^T\mathbf{p} = \mathbf{f} \\ &\mathbf{K}_f\mathbf{p} + \frac{1}{c}\mathbf{C}_f\dot{\mathbf{p}} + \frac{1}{c^2}\mathbf{M}_f\ddot{\mathbf{p}} + \rho_f\mathbf{H}\ddot{\mathbf{d}} = \mathbf{g} \end{aligned} \qquad (2)$$

where $\mathbf{d}$ is the displacement vector, $\mathbf{p}$ is the nodal pressure vector and a dot means time derivation.

Previous equations are solved by the computer code INDIA-3, developed at CISE /1/ in the frame of a contract with ENEL-CRIS, by means of the Modal Superposition Method, using the undamped modes of coupled fluid-structure system.

The undamped eigenvalue problem associated to the equations (2) can be reduced to the standard form:

$$\mathbf{K}^* \mathbf{Y} = \mathbf{Y}\,\Omega^{-2} \qquad (3)$$

with the associated normalization condition:

$$\mathbf{Y}^T\mathbf{Y} = \mathbf{I} \qquad (4)$$

being $\mathbf{K}^*$ symmetrical positive definite matrice given by:

$$\mathbf{K}^* = \begin{vmatrix} \mathbf{R}^{-T}(\mathbf{M}_S + \rho_f\mathbf{H}^T\mathbf{K}_f^{-1}\mathbf{H})\mathbf{R}^{-1} & \mathbf{R}^{-T}\mathbf{H}^T\mathbf{K}_f^{-1}\mathbf{S}^T\sqrt{\rho_f}/c \\ \mathbf{S}\mathbf{K}_f^{-1}\mathbf{H}\mathbf{R}^{-1}\sqrt{\rho_f}/c & \mathbf{S}\mathbf{K}_f^{-1}\mathbf{S}^T/c^2 \end{vmatrix}$$

where: $\mathbf{K}_S = \mathbf{R}^T\mathbf{R}$; $\mathbf{M}_f = \mathbf{S}^T\mathbf{S}$

The solution algorithm of the foregoing eigenvalue problem is the Subspace Iteration Method /2/.

INDIA-3 provides the response computation to seismic loads, defined in the form of a response spectrum as well as in the form of acceleration time history. Also the response to any loading time history can be computed.

In order to improve the efficiency of modal analysis the "Missing Modes Correction" technique can be used in the code.

Comparison with experimental results proved the validity of the code /3/, /4/.

3. - PRESENTATION OF RESULTS.

For all the modal shapes presented the normalization factor is the maximum component of the original eigenvectors.

The eigenvectors components reported in the requested format are obtained dividing the original ones by the normalization factor itself.

4. - DAM ON RIGID FOUNDATION WITHOUT WATER.

Tab. 4.1 -

MODE	FREQUENCY (HZ)
1	4.296073E+00
2	4.578230E+00
3	5.698445E+00
4	6.718756E+00
5	8.588079E+00
6	9.375742E+00

Tab. 4.2 -

MODAL SHAPE N. 1

FREQUENCY 4.296073E+00 HZ

NORM.FACTOR 8.552253E-06 NODE 37 COMP. X

Pts.	displ. x	displ. y	displ. z
1	-4.17646E-08	2.59938E-01	-1.46374E-09
2	-6.77232E-01	3.17452E-01	1.73790E-01
3	-8.60451E-01	4.15582E-01	2.03559E-01
4	-1.64833E-01	7.69275E-02	2.54826E-02
5	-1.23131E-07	-1.31045E-07	3.73748E-08
6	1.01867E-07	1.72516E-01	-5.50436E-08
7	-3.71151E-01	2.01449E-01	6.14551E-02
8	-4.49945E-01	2.31621E-01	4.94427E-02
9	-5.95256E-02	3.47551E-02	-4.10820E-03
10	-1.95560E-07	-1.88049E-07	3.31959E-08
11	-4.25098E-08	6.85088E-02	-1.69906E-08
12	-1.28429E-01	7.93553E-02	-5.50984E-03
13	-1.04419E-01	6.46986E-02	-1.31713E-02
14	-2.49932E-07	4.77825E-09	-8.42325E-08
15	-3.83632E-08	1.36532E-02	-8.08907E-09
16	-1.45515E-02	1.36074E-02	-5.45625E-03
17	-1.39945E-07	2.45759E-07	-2.54890E-07
18	-4.81232E-12	2.78177E-07	-7.26913E-12
19	-1.53673E-08	2.21596E-07	-1.16222E-07
20	-2.36464E-08	1.94189E-07	-1.46386E-07

Tab. 4.3 -

MODAL SHAPE N. 2

FREQUENCY 4.578230E+00 HZ

NORM. FACTOR 1.153405E-05 NODE 125 COMP. X

Pts.	displ. x	displ. y	displ. z
1	-9.99367E-01	-8.55042E-08	2.35839E-01
2	-7.88290E-01	2.88704E-02	1.77098E-01
3	1.01248E-01	-1.53584E-01	-5.23164E-02
4	1.41879E-01	-1.30089E-01	-4.20813E-02
5	1.28323E-08	-5.42621E-09	1.26860E-08
6	-5.77581E-01	-6.86894E-08	8.51699E-02
7	-4.64042E-01	1.64358E-02	6.23325E-02
8	8.48668E-03	-6.99718E-02	-1.35797E-02
9	3.95736E-02	-4.92918E-02	-2.48413E-03
10	-1.98626E-08	-1.39525E-07	9.42691E-08
11	-2.14263E-01	-2.74443E-08	-1.13212E-02
12	-1.71141E-01	9.02825E-03	-1.10465E-02
13	-8.50354E-03	-1.84694E-02	-2.95836E-03
14	-5.99650E-08	-2.97506E-07	9.29221E-08
15	-2.85202E-02	-5.80066E-09	-9.47081E-03
16	-2.03842E-02	3.99732E-04	-6.95105E-03
17	-1.35922E-07	-2.27093E-07	-1.92869E-08
18	-1.13650E-07	7.29669E-13	-1.47539E-07
19	-7.57573E-08	-5.62772E-08	-1.10195E-07
20	-6.35723E-08	-6.63313E-08	-9.67274E-08

Tab. 4.4 -

MODAL SHAPE N. 3

FREQUENCY 5.698445E+00 HZ

NORM. FACTOR 8.499251E-06 NODE 38 COMP. X

Pts.	displ. x	displ. y	displ. z
1	-7.67101E-02	-2.50643E-07	1.41432E-02
2	-2.58385E-01	8.45850E-02	6.68317E-02
3	-8.24152E-01	4.09605E-01	2.26078E-01
4	-2.86243E-01	1.69067E-01	6.11782E-02
5	-1.66258E-07	-1.70776E-07	5.80013E-08
6	-3.32048E-02	-1.76392E-07	7.82179E-03
7	-1.15957E-01	4.01661E-02	2.40979E-02
8	-3.46524E-01	1.62676E-01	5.02137E-02
9	-8.61372E-02	5.26983E-02	-1.81710E-03
10	-2.73917E-07	-2.11954E-07	6.65335E-08
11	-5.61237E-03	-5.20527E-08	1.91916E-03
12	-2.63336E-02	7.73549E-03	1.18741E-03
13	-5.77423E-02	2.63411E-02	-5.02136E-03
14	-3.03235E-07	-1.05810E-07	4.15540E-08
15	1.39122E-03	-6.39155E-09	5.69622E-04
16	-4.93165E-04	-1.00888E-04	-1.55997E-04
17	-7.05423E-08	-2.72108E-08	-4.49425E-08
18	2.06159E-08	-8.40680E-14	-1.82663E-09
19	1.09272E-08	-3.77938E-09	-1.10545E-08
20	1.24179E-09	-5.46992E-09	-1.94354E-08

Tab. 4.5 -

MODAL SHAPE N. 4

FREQUENCY 6.718756E+00 HZ

NORM. FACTOR 6.451211E-06 NODE 12 COMP. X

Pts.	displ. x	displ. y	displ. z
1	2.65672E-07	7.51941E-02	-2.02437E-10
2	-6.48618E-01	1.14507E-01	1.78979E-01
3	3.93546E-01	-3.29019E-01	-1.51567E-01
4	5.57719E-01	-4.29812E-01	-1.52332E-01
5	1.95874E-07	1.54035E-07	-4.79325E-08
6	-3.29129E-09	4.21714E-02	9.31934E-08
7	-3.49021E-01	6.35596E-02	6.66598E-02
8	3.53330E-02	-7.57662E-02	-1.70996E-02
9	1.41489E-01	-1.24216E-01	-5.53568E-03
10	2.79223E-07	-5.95000E-08	5.98923E-08
11	4.76556E-09	1.16798E-02	6.67159E-08
12	-1.09906E-01	2.20606E-02	2.97002E-05
13	-2.42967E-02	-1.65479E-03	-6.10403E-04
14	1.29971E-07	-2.28884E-07	6.36018E-08
15	1.76969E-08	1.34260E-03	2.28186E-08
16	-1.22360E-02	2.61526E-03	-2.61993E-03
17	-1.70124E-07	-9.33998E-08	3.74469E-08
18	-2.60924E-12	2.68010E-08	-6.51105E-12
19	-4.57583E-08	8.55853E-09	-7.52541E-09
20	-5.56991E-08	-4.28035E-09	-1.54852E-08

Tab. 4.6 -

MODAL SHAPE N. 5

FREQUENCY 8.588079E+00 HZ

NORM. FACTOR 4.934588E-06 NODE 103 COMP. X

Pts.	displ. x	displ. y	displ. z
1	-1.00000E+00	1.92042E-07	3.86252E-01
2	-3.33440E-01	-1.17127E-02	1.77774E-01
3	3.03121E-01	-1.45998E-02	-1.25124E-02
4	-6.81764E-01	5.80162E-01	2.11612E-01
5	-2.02661E-07	-1.01722E-07	5.38528E-08
6	-3.70533E-01	-1.16390E-08	1.49238E-01
7	-6.32318E-02	-2.84298E-02	7.24989E-02
8	3.35405E-01	-1.13763E-01	-2.79565E-02
9	-1.31424E-01	1.30174E-01	1.20258E-02
10	-2.88209E-07	2.96561E-07	-1.02851E-07
11	-1.51205E-02	-7.15780E-07	2.59530E-02
12	5.64779E-02	-1.70244E-02	2.11750E-02
13	1.08195E-01	-4.61325E-02	9.62169E-03
14	1.69943E-07	2.58719E-07	-8.57638E-08
15	9.75848E-03	-3.72837E-07	7.04586E-03
16	1.39112E-02	-2.99189E-03	7.31870E-03
17	2.94863E-07	5.47434E-09	1.32652E-07
18	6.00413E-08	-6.12934E-12	1.83544E-07
19	6.26242E-08	-5.93630E-09	1.56899E-07
20	7.54839E-08	-1.64130E-08	1.50149E-07

Tab. 4.7 -

MODAL SHAPE N. 6

FREQUENCY 9.375742E+00 HZ

NORM. FACTOR 4.173912E-06 NODE 125 COMP. X

Pts.	displ. x	displ. y	displ. z
1	-9.93629E-01	-2.46812E-06	6.03504E-01
2	-9.63199E-01	1.76961E-01	5.64642E-01
3	-2.10962E-01	1.14252E-01	1.73697E-01
4	2.59343E-01	-1.71226E-01	-5.21162E-02
5	1.85695E-07	1.52762E-07	-4.51060E-08
6	2.64130E-01	-1.86001E-06	1.47803E-01
7	1.88664E-01	-3.28298E-03	1.46558E-01
8	6.75240E-02	-8.38271E-03	6.95959E-02
9	7.48047E-02	-4.75876E-02	6.91641E-03
10	3.22076E-07	1.00855E-07	9.85404E-09
11	5.75008E-01	-3.26810E-07	3.17519E-02
12	4.83088E-01	-5.28815E-02	3.55890E-02
13	1.05970E-01	-2.55565E-02	3.05583E-02
14	4.02010E-07	1.54321E-07	1.44926E-07
15	1.28489E-01	5.14383E-08	2.50447E-02
16	9.83941E-02	-7.88182E-03	2.04421E-02
17	7.53941E-07	3.44995E-07	1.74499E-07
18	8.45154E-07	-1.34047E-12	-1.11677E-08
19	6.08205E-07	1.17671E-07	-4.02399E-09
20	5.05935E-07	1.36303E-07	7.22422E-08

5. - DAM ON FLEXIBLE FOUNDATION, WATER LEVEL 491 m.a.s.l.

The reported results refer to the following hypotheses:

- rock density is assumed to be zero ($\rho_r=0$);
- fluid is considered compressible (c=1440 m/s);
- the fluid boundary condition at the upstream face, opposite to the dam, is assumed to be of full reflection.

We also enclose the drawings of the complete six modal shapes obtained using the post-processor Supertab (I-DEAS) currently connected to INDIA-3.

Tab. 5.1 -

MODE	FREQUENCY (Hz)
1	3.575478E+00
2	3.770009E+00
3	5.101492E+00
4	6.090990E+00
5	6.453512E+00
6	7.421593E+00

Tab. 5.2 -

MODAL SHAPE N. 1

FREQUENCY 3.575478E+00 HZ

NORM. FACTOR 8.803795E-06 NODE 38 COMP. X

Pts.	displ. x	displ. y	displ. z
1	-7.24992E-07	3.09781E-01	1.32762E-06
2	-6.29668E-01	3.58247E-01	1.39798E-01
3	-8.73884E-01	4.39366E-01	1.67877E-01
4	-2.21957E-01	1.01325E-01	2.12575E-02
5	-1.46101E-02	-1.41210E-02	2.42174E-04
6	3.68404E-07	2.12064E-01	8.98309E-07
7	-3.75986E-01	2.40031E-01	4.56611E-02
8	-5.10221E-01	2.78433E-01	3.02668E-02
9	-1.09196E-01	6.40131E-02	-1.31247E-02
10	-1.47750E-02	-1.04632E-02	-2.85777E-03
11	7.79351E-07	1.01227E-01	6.53624E-07
12	-1.60744E-01	1.15015E-01	-1.47747E-02
13	-1.72757E-01	1.12114E-01	-3.19281E-02
14	-1.92857E-02	5.28808E-03	-8.50311E-03
15	4.45489E-07	3.67102E-02	5.13896E-07
16	-3.34707E-02	3.86629E-02	-1.69540E-02
17	-1.27434E-02	2.06856E-02	-1.57002E-02
18	-1.25100E-07	1.97311E-02	9.23044E-08
19	-2.95567E-03	1.77415E-02	-7.93576E-03
20	-2.56570E-03	1.63198E-02	-1.03521E-02

Tab. 5.3 -

MODAL SHAPE N. 2

FREQUENCY 3.770009E+00 HZ

NORM. FACTOR 1.053547E-05 NODE 125 COMP. X

Pts.	displ. x	displ. y	displ. z
1	9.99791E-01	-3.95102E-07	-1.81556E-01
2	8.12961E-01	-1.39710E-02	-1.35345E-01
3	-3.73073E-02	1.71456E-01	5.14473E-02
4	-1.63732E-01	1.84595E-01	4.63215E-02
5	3.21182E-03	5.37275E-03	6.30523E-06
6	6.56700E-01	-2.89439E-07	-5.79387E-02
7	5.46852E-01	-1.46348E-02	-4.03389E-02
8	4.78845E-02	8.08644E-02	1.66136E-02
9	-4.79065E-02	9.12772E-02	1.26046E-04
10	6.95190E-03	1.94928E-02	-4.68701E-03
11	3.24687E-01	-9.98763E-08	3.07175E-02
12	2.73261E-01	-1.25754E-02	2.84008E-02
13	4.91852E-02	3.01348E-02	7.70332E-03
14	1.05419E-02	2.74536E-02	-2.73396E-03
15	8.80374E-02	-1.76171E-08	3.21443E-02
16	7.17171E-02	-1.01989E-04	2.58942E-02
17	1.76138E-02	1.66659E-02	2.38563E-03
18	1.71964E-02	-1.28081E-07	1.19856E-02
19	1.34813E-02	4.56205E-03	9.59654E-03
20	1.10030E-02	6.22987E-03	7.50546E-03

Tab. 5.4 -

MODAL SHAPE N. 3

FREQUENCY 5.101492E+00 HZ

NORM. FACTOR 8.036090E-06 NODE 10 COMP. X

Pts.	displ. x	displ. y	displ. z
1	2.38035E-01	-2.24023E-06	-1.06460E-01
2	1.08076E-03	6.75159E-02	-3.84729E-02
3	-8.39534E-01	4.29896E-01	1.95465E-01
4	-3.88276E-01	2.16272E-01	6.79926E-02
5	-2.27713E-02	-2.05063E-02	9.78800E-04
6	7.98440E-02	-1.67685E-06	-3.91604E-02
7	-3.59053E-02	3.94519E-02	-1.59521E-02
8	-4.16686E-01	1.99275E-01	3.93364E-02
9	-1.65057E-01	8.96482E-02	-4.88791E-03
10	-2.64440E-02	-1.51541E-02	-1.22966E-03
11	-2.04921E-02	-1.05496E-06	-6.04136E-03
12	-5.46770E-02	1.34150E-02	-6.72251E-03
13	-1.28201E-01	5.24486E-02	-1.39484E-02
14	-3.11939E-02	-6.06056E-03	-1.15112E-04
15	-1.93990E-02	-4.93837E-07	-4.24052E-03
16	-2.31557E-02	1.56770E-03	-5.73952E-03
17	-1.54107E-02	-1.77648E-03	-3.39131E-03
18	-6.09281E-03	-2.54404E-07	-9.39963E-04
19	-6.16836E-03	-1.25155E-03	-1.43413E-03
20	-6.15079E-03	-1.60175E-03	-1.63328E-03

Tab. 5.5 -

MODAL SHAPE N. 4

FREQUENCY 6.090990E+00 HZ

NORM. FACTOR 6.511380E-06 NODE 7 COMP. X

Pts.	displ. x	displ. y	displ. z
1	-1.40111E-05	-6.01265E-02	3.80928E-06
2	5.85478E-01	-9.00966E-02	-1.56341E-01
3	-3.54349E-01	3.33509E-01	1.27257E-01
4	-6.43375E-01	5.02359E-01	1.55187E-01
5	-2.16459E-02	-1.34755E-02	2.06091E-03
6	-1.04031E-05	-3.05043E-02	2.25415E-06
7	3.42214E-01	-5.06239E-02	-6.35210E-02
8	-2.77287E-02	8.96718E-02	6.49378E-03
9	-2.11873E-01	1.86973E-01	1.32110E-03
10	-2.30557E-02	1.15613E-02	-4.97085E-03
11	-2.93369E-06	-6.78994E-03	-3.66921E-08
12	1.38794E-01	-1.98307E-02	-4.23644E-03
13	4.36459E-02	7.82613E-03	-9.25398E-03
14	-8.61900E-03	1.98513E-02	-4.04592E-03
15	1.01891E-06	2.65279E-04	-3.54135E-07
16	3.25064E-02	-2.83728E-03	2.14727E-03
17	1.73726E-02	5.06612E-03	-8.65437E-03
18	8.36938E-07	-1.15406E-03	-1.76079E-07
19	7.27543E-03	-4.47752E-04	-2.60400E-03
20	8.13096E-03	2.14587E-04	-3.77029E-03

Tab. 5.6 -

MODAL SHAPE N. 5

FREQUENCY 6.453512E+00 HZ

NORM. FACTOR 6.497299E-06 NODE 125 COMP. X

Pts.	displ. x	displ. y	displ. z
1	-9.96883E-01	1.82536E-06	4.08856E-01
2	-8.56758E-01	1.04859E-01	3.57020E-01
3	-2.93504E-01	1.24197E-01	1.43544E-01
4	-5.89778E-02	3.88487E-02	3.33596E-02
5	-2.47467E-04	-7.68969E-04	2.73022E-03
6	-2.70490E-01	1.69889E-06	1.50134E-01
7	-2.18595E-01	1.91678E-02	1.30257E-01
8	-3.59686E-02	3.57261E-03	5.06155E-02
9	-4.16004E-03	-1.41728E-03	1.56840E-02
10	-8.68229E-04	-2.76168E-03	7.20804E-03
11	1.71517E-01	1.54516E-06	2.01828E-02
12	1.64188E-01	-2.27290E-02	2.01450E-02
13	8.19365E-02	-3.19625E-02	2.01559E-02
14	1.06356E-02	-1.97541E-03	1.24156E-02
15	1.34030E-01	9.58024E-07	1.43569E-02
16	1.17346E-01	-1.11816E-02	1.31332E-02
17	3.92708E-02	3.72647E-03	4.32743E-03
18	4.81837E-02	5.15343E-07	-5.62414E-03
19	4.03656E-02	2.77622E-03	-4.52452E-03
20	3.51075E-02	4.54948E-03	-3.99060E-03

Tab. 5.7 -

MODAL SHAPE N. 6

FREQUENCY 7.421593E+00 HZ

NORM. FACTOR 7.265724E-07 NODE 125 COMP. X

Pts.	displ. x	displ. y	displ. z
1	-9.97905E-01	-1.54447E-05	4.59171E-01
2	-7.24588E-01	8.36788E-02	3.66472E-01
3	-1.03490E-01	1.02433E-01	1.29875E-01
4	-2.31231E-01	2.18669E-01	9.12032E-02
5	-1.70323E-03	2.07657E-03	3.62447E-03
6	-2.12699E-01	-1.33367E-05	1.73531E-01
7	-9.46900E-02	6.89935E-04	1.37853E-01
8	1.36451E-01	-4.13745E-02	4.16635E-02
9	-3.43087E-02	5.17836E-02	1.96866E-02
10	-1.52328E-03	1.12190E-02	5.51156E-03
11	1.85251E-01	-9.21687E-06	4.34029E-02
12	2.03060E-01	-2.79270E-02	4.05007E-02
13	1.48269E-01	-5.04051E-02	2.83318E-02
14	2.11681E-02	7.98035E-03	1.09887E-02
15	9.90014E-02	-4.68032E-06	3.05075E-02
16	9.24692E-02	-8.34552E-03	2.83329E-02
17	3.69917E-02	4.00921E-03	1.03352E-02
18	2.51298E-02	-2.28319E-06	9.62884E-03
19	2.20710E-02	2.38269E-03	8.87086E-03
20	1.99588E-02	3.54775E-03	8.07477E-03

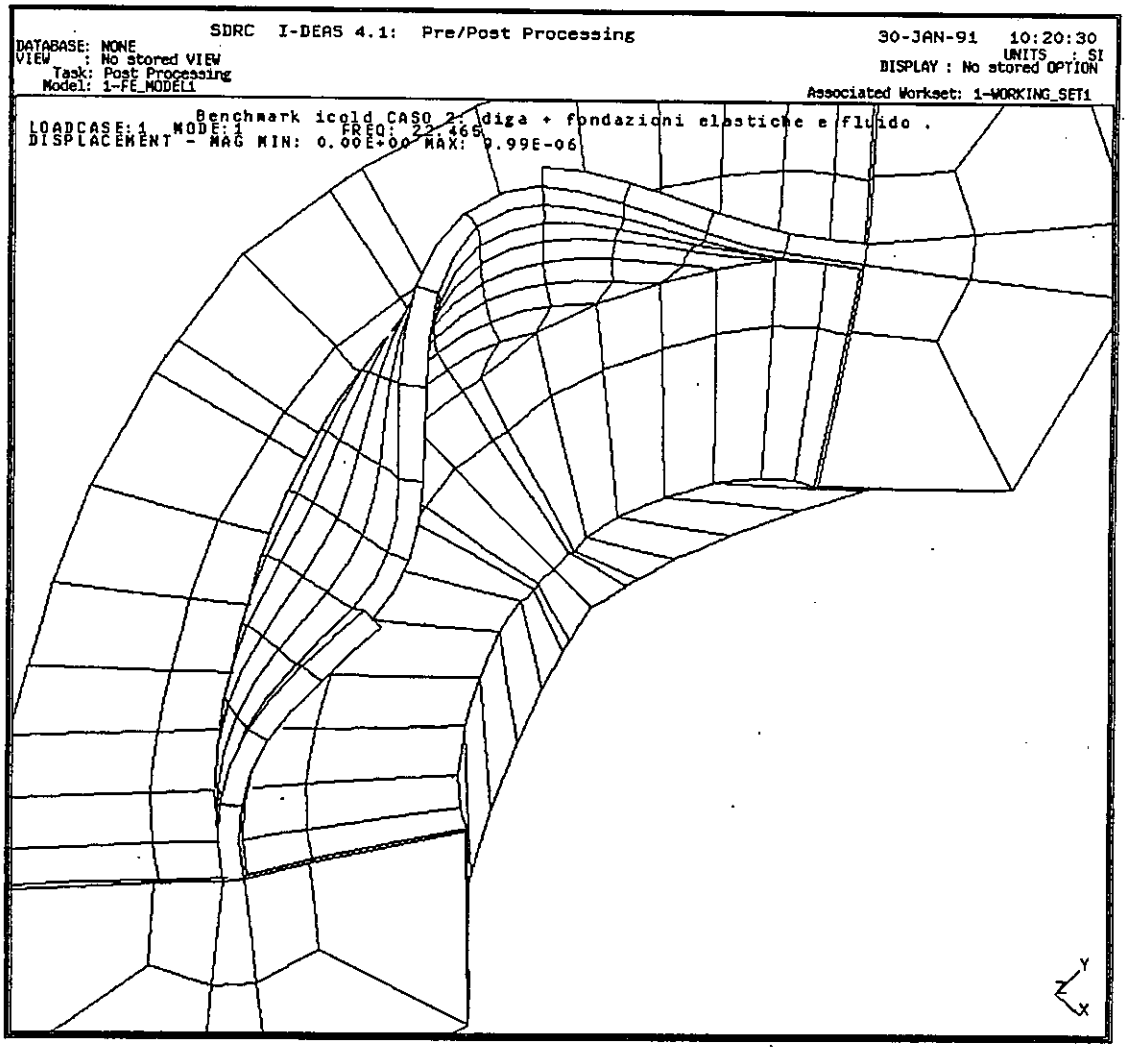
SDRC I-DEAS 4.1: Pre/Post Processing
30-JAN-91 10:20:30
DATABASE: NONE
VIEW : No stored VIEW
Task: Post Processing
Model: 1-FE_MODEL1
UNITS : SI
DISPLAY : No stored OPTION
Associated Workset: 1-WORKING_SET1
Benchmark icold CASO 2: diga + fondazioni elastiche e fluido .
LOADCASE:1 MODE:1 FREQ: 22.465
DISPLACEMENT - MAG MIN: 0.00E+00 MAX: 9.99E-06
Y
Z
X

Fig. 5.1 -

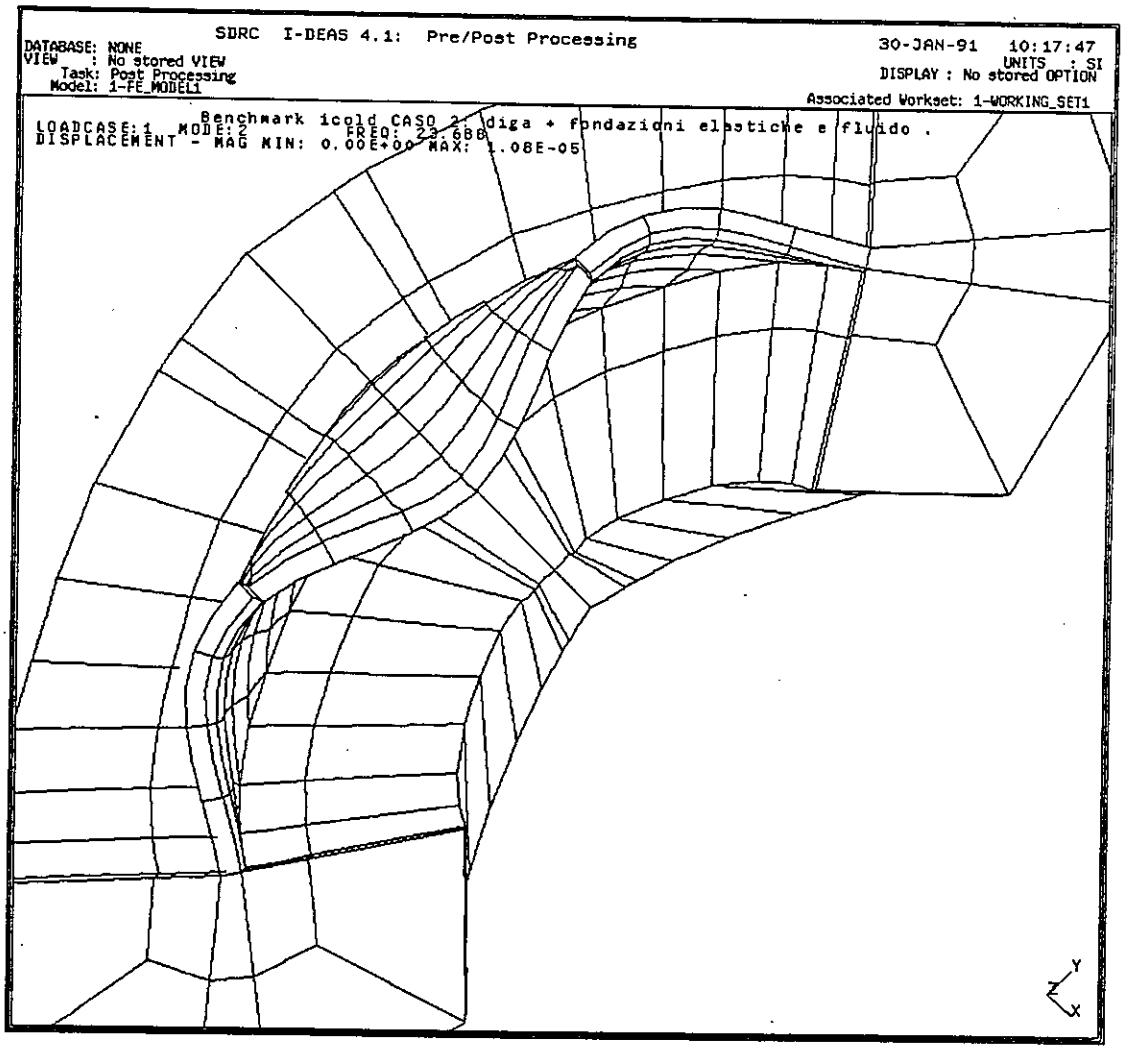
SDRC I-DEAS 4.1: Pre/Post Processing
DATABASE: NONE
VIEW : No stored VIEW
Task: Post Processing
Model: 1-FE_MODEL1
30-JAN-91 10:17:47
UNITS : SI
DISPLAY : No stored OPTION
Associated Workset: 1-WORKING_SET1
Benchmark icold CASO 2 diga + fondazioni elastiche e fluido .
LOADCASE: 1 MODE: 2 FREQ: 23.688
DISPLACEMENT - MAG MIN: 0.00E+00 MAX: 1.08E-05
Y
Z
X

Fig. 5.2 -

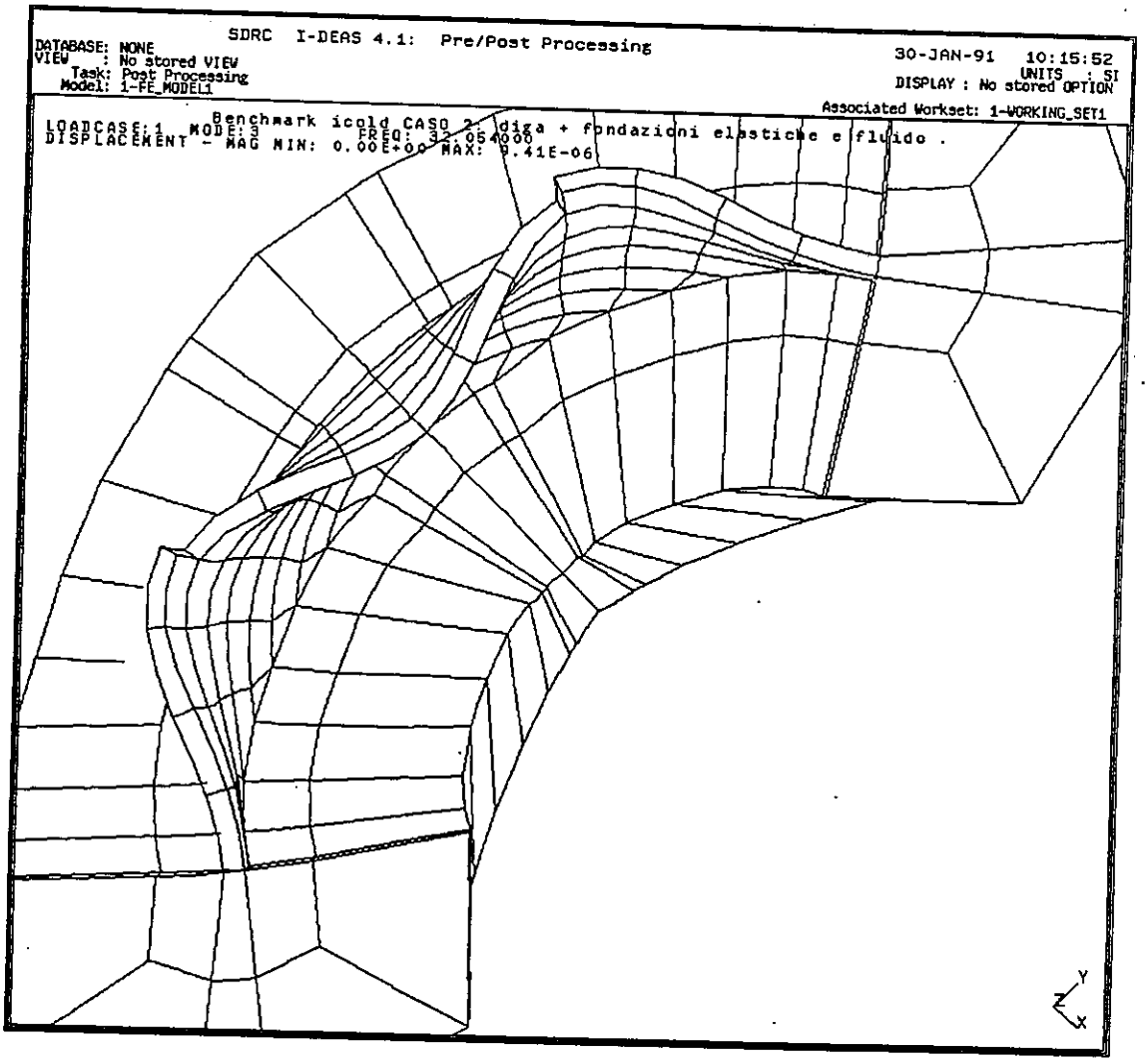
SDRC I-DEAS 4.1: Pre/Post Processing
DATABASE: NONE
VIEW : No stored VIEW
Task: Post Processing
Model: 1-FE_MODEL1
30-JAN-91 10:15:52
UNITS : SI
DISPLAY : No stored OPTION
Associated Workset: 1-WORKING_SET1
LOADCASE:1 MODE:3 FREQ: 32.054000
DISPLACEMENT - MAG MIN: 0.00E+00 MAX: 9.41E-06
Benchmark icold CASO 2: diga + fondazioni elastiche e fluido .
Y
Z
X

Fig. 5.3 -

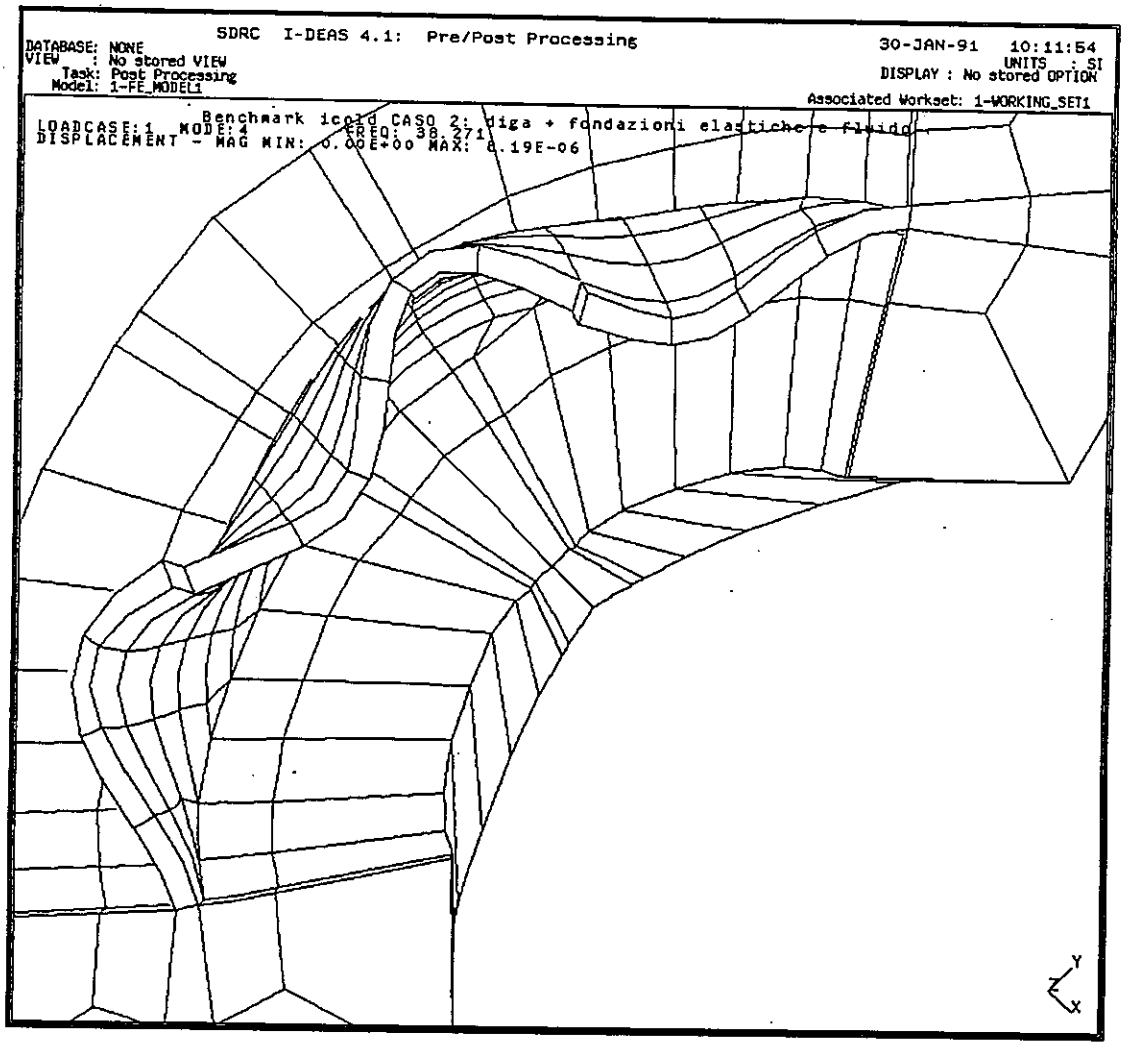
SDRC I-DEAS 4.1: Pre/Post Processing
DATABASE: NONE
VIEW : No stored VIEW
Task: Post Processing
Model: 1-FE_MODEL1
30-JAN-91 10:11:54
UNITS : SI
DISPLAY : No stored OPTION
Associated Workset: 1-WORKING_SET1
Benchmark icold CASO 2: diga + fondazioni elastiche e fluido
LOADCASE:1 MODE:4 FREQ: 38.271
DISPLACEMENT - MAG MIN: 0.00E+00 MAX: 8.19E-06
Y
Z
X

Fig. 5.4 -

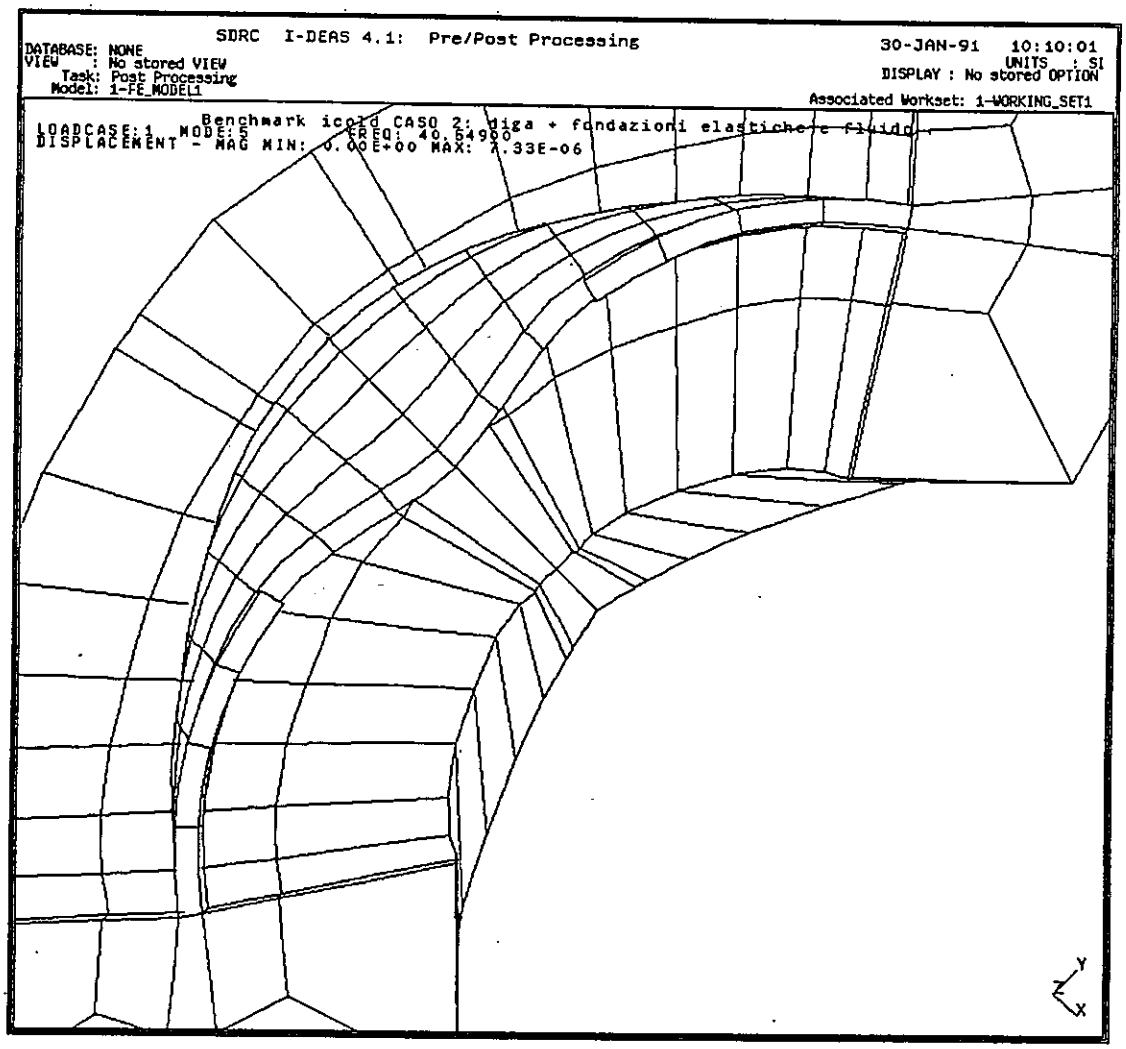
SDRC I-DEAS 4.1: Pre/Post Processing
DATABASE: NONE
VIEW : No stored VIEW
Task: Post Processing
Model: 1-FE_MODEL1
30-JAN-91 10:10:01
UNITS : SI
DISPLAY : No stored OPTION
Associated Workset: 1-WORKING_SET1
Benchmark icold CASO 2: diga + fondazioni elastiche/e fluido
LOADCASE:1 MODE:5 FREQ: 40.64900
DISPLACEMENT - MAG MIN: 0.00E+00 MAX: 7.33E-06
Y
Z
X

Fig. 5.5 -

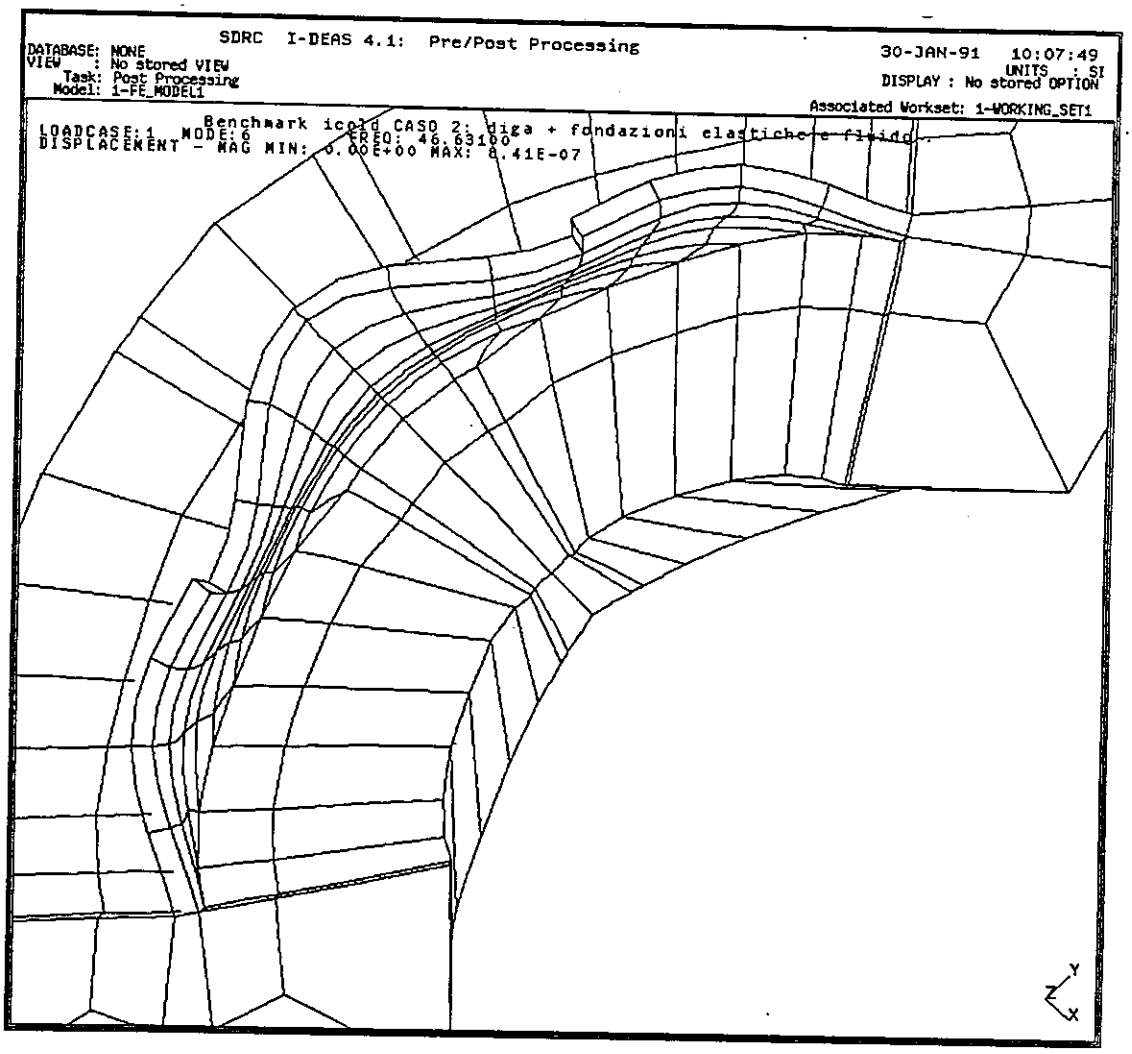
SDRC I-DEAS 4.1: Pre/Post Processing
DATABASE: NONE
VIEW : No stored VIEW
Task: Post Processing
Model: 1-FE_MODEL1
30-JAN-91 10:07:49
UNITS : SI
DISPLAY : No stored OPTION
Associated Workset: 1-WORKING_SET1
Benchmark icold CASO 2: diga + fondazioni elastiche e fluido
LOADCASE:1 MODE:6 FREQ: 46.63100
DISPLACEMENT - MAG MIN: 0.00E+00 MAX: 8.41E-07
Y
Z
X

Fig. 5.6 -

6. - REFERENCES

/1/ Applied Mathematical Section, "INDIA: Computer Code for Dynamic Analysis of Three-dimensional Fluid-structure Coupled Systems"; Report CISE n.- 3123, (1986).

/2/ L. Brusa et al., "Vibration Analysis of Coupled Fluid Structure Systems: a Convenient Computational Approach"; Nuc. Eng. and Des., vol. 70, (1982), pp. 101-106.

/3/ L. Brusa et al., "Experimental and Numerical Evaluation of Vibration Characteristics of Fluid Structure Coupled Systems"; Proc. Num. Meth. for Transient and Coupled Problems, Venice, July 1984, pp. 251-261.

/4/ L. Brusa et al., "Fluid-structure Interaction: Experimental and Numerical Analyses", Proc. Int. Conf. on Computer Methods and Water Resources, Rabat, March 1988.

PC NUMERICAL ANALYSIS OF TALVACCHIA ARCH DAM

by Glenn S. Tarbox[1], Warren J. Paul[2], and Po-Tsung Shih[3]

ABSTRACT

Linear elastic solutions of the static, thermal, and eigenproblems of an arch dam-foundation system were obtained on an AT-compatible 386 PC. The dam and foundation structural model was constructed from 8 node three-dimensional linear brick elements, with a single element representing the entire thickness of the dam. The reservoir model for the computation of added mass was constructed from 16 node quadratic three-dimensional fluid elements and 8 node quadratic fluid-structure interaction surface elements. A reservoir model constructed from 8 node linear three-dimensional fluid elements and 4 node linear interaction elements was also studied. Two-dimensional heat flow models consisting of 4 node linear elements were constructed at the crown cantilever and at the quarter-point of the dam axis, which is the arc at the upstream crest of the crown cantilever.

The static problem was solved for monolithic dead load, hydrostatic reservoir pressure, and steady-state temperatures. The thermal problem was solved for both steady-state and periodic input. The eigenproblem was solved for four cases: dam only fixed at the dam-foundation contact with an empty reservoir, dam plus foundation with an empty reservoir, dam plus foundation with reservoir added mass from a quadratic element reservoir model, and dam plus foundation with reservoir added mass from a linear element reservoir model.

---

[1]Vice President and Manager, Water Resources, Bechtel Corporation, San Francisco, California, USA

[2]Senior Dam Engineering Specialist, Water Resources, Bechtel Corporation, San Francisco, California, USA

[3]Senior Engineer, Bechtel Corporation, San Francisco, California, USA

The analysis results described in this report, used in concert with the results obtained by other Benchmark Workshop participants, will provide a basis for comparing models constructed from linear and quadratic elements, for comparing complete and lumped added mass formulations, and for comparing compressible, incompressible, and classical Westergaard reservoir formulations.

HARDWARE AND SOFTWARE

All computations were performed on a Compaq 386/25e computer which was configured with an Intel 387 math chip, a 32 kilobyte static RAM cache, 16 megabytes of dynamic RAM including a 1 megabyte disk cache, and two IDE hard disks, of 120 megabyte and 212 megabyte size. The operating system was Compaq MS-DOS Version 3.31.

Several computer programs were used. The commercial SAP90 package of programs [1] was used for all structural analyses. Other programs were obtained in Fortran source form from the University of California at Berkeley and modified by the authors. All Fortran programs were compiled with the Lahey extended memory compiler [2]. Bitmapped graphics were produced by SAP90 and vector graphics were produced by original Fortran pre- and post-processors on a Hewlett Packard LaserJet III printer with 3 megabytes of RAM. The original pre- and post-processors used the Laserjet III as an HP-GL/2 vector plotter driven by the PLOT88 Fortran library [3].

The programs obtained from the University of California were the DETECT two-dimensional transient heat flow program [4] and the INCRES dam-reservoir interaction program, a module of the EADAP package [5]. DETECT was used for all thermal analyses. INCRES was modified by the authors in order to compute the lumped added mass used to model dynamic dam-reservoir interaction. All real variables in DETECT and INCRES were compiled as data type REAL*8.

MODEL DETAILS

Material Properties. The material properties used in the finite element models were supplied by the workshop sponsors. They are listed in Table 1 below.

TABLE 1. TALVACCHIA DAM MATERIAL PROPERTIES

Property Name	Symbol	Material	Value
Young's Modulus	E	Concrete	3.60×10^{10} Nm^{-2}
		Rock	1.20×10^{10} Nm^{-2}
Poisson's Ratio	ν	Concrete	0.20
		Rock	0.16
Specific Weight	γ	Concrete	24,000 Nm^{-3}
		Rock	20,000 Nm^{-3}
		Water	10,000 Nm^{-3}
Thermal Diffusivity	h^2	Concrete	1.0×10^{-6} m^2s^{-1}
Thermal Conductivity	k	Concrete	2.0 $Wm^{-1}\,°C^{-1}$
Thermal Dilation	α	Concrete	7.0×10^{-6} $°C^{-1}$
Speed of Sound	c	Water	1440.0 ms^{-1}

Structural Models. Two structural models were used in the various analyses. Both were constructed with a single layer of 8 node solid elements simulating the dam. All rotational degrees of freedom were fixed in both models.

The first model consisted of the concrete arch with all degrees of freedom fixed at the dam-foundation contact (Figure 1). There were 196 nodal points, 84 elements representing the dam, and 462 degrees of freedom. The second model consisted of the 84 solid element concrete dam combined with 160 additional solid elements used to represent the rock foundation (Figure 2). All degrees of freedom at the limiting surfaces of the rock were fixed, with the exception of the top surface. The top surface, which represents the reservoir bottom, canyon walls, and downstream river bed, was left

free in all translational degrees of freedom. The second model contained 966 degrees of freedom.

The node numbers and coordinates distributed by the workshop sponsors were used with the element numbering scheme and element corner node connectivity. The only change to the mesh was that all element middle nodes were eliminated, consistent with the use of linear, rather than quadratic, elements.

The 8 node solid element formulation in SAP90 is isoparametric with nine incompatible bending modes available as an option. The nine incompatible modes were used in all elements except the wedge shaped collapsed elements at the arch abutments. The wedge elements function properly only when all incompatible modes are suppressed. A 2x2x2 numerical integration scheme is used to form the element matrices.

Heat Flow Models. Two-dimensional steady-state and periodic heat flow studies were conducted on two models. Both models were constructed from linear 4 node two-dimensional heat flow elements integrated by 2x2 quadrature. The first model was developed as a vertical section through the crown cantilever of the dam with 48 nodes, 35 elements, and 91 degrees of freedom (Figure 3). The second model consisted of a vertical section taken near the quarter point of the dam axis (Figure 4). This model included 42 nodes, 30 elements, and 79 degrees of freedom. Both thermal models used five heat flow finite elements through the thickness of the dam, with horizontal mesh lines at elevations identical to those in the structural model. The six nodes at each elevation were equally spaced through the thickness. The dam-foundation contact was treated as adiabatic in both models. The prescribed external temperatures were applied to the external model surfaces as step functions for steady-state analysis and as sine wave time histories for periodic analysis.

Reservoir Models. The reservoir was modeled as a body extending upstream for a distance five times the crown cantilever structural height of the dam, which is about 6.4 times the 56 meter partial fill depth of the reservoir (Figure 5). The reservoir surface for dynamic analysis was set at Elevation 491 meters. The reservoir sides and bottom were extended parallel to the line of arch centers and follow the shape of the canyon at the arch abutments. The upstream limit of the reservoir was a vertical plane perpendicular to the line of arch centers. The reservoir bottom, sides, and upstream limit were all treated as reflective boundaries. The free surface at the reservoir top was treated as a zero pressure surface, meaning that surface wave effects were neglected. The reservoir water was treated as an incompressible fluid. Two reservoir models were studied, one that consisted of quadratic elements and another that consisted of linear elements.

The quadratic element reservoir model consisted of 16 node three-dimensional fluid elements, with quadratic surfaces normal to the flow direction and 2x2x2 integration order for quadrature. Special 8 node quadratic curvilinear interface elements with 2x2 integration order for quadrature were used to map the upstream surface of the dam. The top surface of both the reservoir mesh and the interface element mesh was the reservoir surface. The geometry was based on the structural model without foundation, but with the element middle nodes included. Mesh fineness in the flow direction increased near the dam interface. There were 978 fluid nodal points, 163 interface nodal points, 240 three-dimensional fluid elements, and 48 curvilinear interface elements in the quadratic reservoir model. There were 2484 degrees of freedom, which were statically condensed to 489 degrees of freedom on the dam-reservoir interface.

The linear element reservoir model consisted of a mesh identical to the quadratic element model, but with the quadratic 16 node fluid elements replaced by linear 8 node three-dimensional fluid

elements. The quadratic 8 node interface elements were replaced by linear 4 node curvilinear interface elements. The linear element model included 348 fluid nodal points, 58 interface nodal points, 240 three-dimensional fluid elements, and 48 curvilinear interface elements. The model contained 810 degrees of freedom, which were statically condensed to 174 degrees of freedom on the dam-reservoir interface.

STATIC LOADING CONDITIONS

Static analyses were performed for three loading conditions: dead load, reservoir hydrostatic pressure, and steady-state temperature. Each loading condition was analyzed as requested by the workshop sponsors.

Dead Load. Dead load deflections and stresses were computed for the dam plus foundation model. Dead load was considered as the weight of the dam, with the weightless foundation contributing flexibility. The dam was treated as a monolithic body for the purpose of dead load computations.

Hydrostatic Pressure. Deflections and stresses due to reservoir pressure on the dam were computed using the dam plus foundation model. The hydrostatic pressure of the reservoir at Elevation 507 meters was applied as an element surface load to the upstream face of the dam. Hydrostatic load was not applied to the portion of rock foundation that serves as reservoir bottom.

Steady-State Temperature. Temperatures from the steady-state heat flow analyses described later were applied to the nodes of the dam model fixed at the dam-foundation contact. The calculated deflections and stresses were due to the differences between the applied temperatures and the assumed stress-free concrete temperature of 0°C.

THERMAL ANALYSES

Steady-state and periodic heat flow studies were carried out on the two thermal models to calculate temperatures for use in structural analysis. Two-dimensional heat flow studies are acceptable for arch dam analysis because the major heat flow is through the dam between the reservoir and the downstream face.

Actual arch dam temperature profiles exhibit a highly curved shape (Figure 6) that requires several nodes for adequate reproduction, while the structural stress variation through the thickness is nearly the straight line of simple bending theory. This implies that a finer mesh through the thickness of an arch dam is needed for thermal studies than for structural studies.

The results from the crown cantilever and quarter-arc models are essentially identical, with the exception that the quarter-arc model exhibits the effects of air temperature applied to the upstream face above water level. Effective temperatures from the surfaces of each model were obtained by constructing linear profiles with the same area and first moment of area as the curved computed profiles (Figure 6). Steady-state analysis results were applied to the three-dimensional structural mesh in a rational manner. Periodic temperature results from the periodic input prescribed by the workshop sponsors were also calculated for benchmarking. The periodic calculations were made with a period of 365 days, a time step of 1 day, and an output interval of 5 days.

DYNAMIC ANALYSES

Dynamic analysis for the Benchmark Workshop consists of solving the eigenproblem of the structure for the lowest six natural modes of vibration. The empty reservoir eigenproblem was solved for the model of the dam fixed at the foundation contact. The eigenproblem with the reservoir was solved for the model that included the

foundation, which was treated as massless. The dam-reservoir interaction was simulated by providing added mass, calculated using the quadratic element reservoir model, on the upstream face of the dam. The solution of these two eigenproblems completed the studies defined by the workshop sponsors.

Two additional eigenproblems of interest were investigated. The first was the dam plus massless foundation with an empty reservoir. The second was the dam plus massless foundation with the reservoir, which was simulated by upstream face added masses computed using the linear element model.

Added Mass. The representation of fluid-structure dynamic interaction through the placement of added masses on the fluid-structure interface follows naturally from the mathematics of the problem [6]. A special case solution in modern form was first introduced by Westergaard [7]. Physically, the added mass can be viewed as the mass of the volume of fluid that moves with the submerged portion of a vibrating structure. The added mass on a dam can be calculated from the pressures produced by a fluid on a boundary subject to known accelerations. The pressures are computed as the solution to the wave equation:

$$\nabla^2 p - \frac{\ddot{p}}{c^2} = 0 \ .$$

The reservoir water is treated as an incompressible fluid in INCRES, so that the wave equation reduces to the Laplace equation:

$$\nabla^2 p = 0 \ .$$

All reservoir boundaries were treated as reflecting, except for the free surface and the surface at the dam interface. The free surface was treated as a boundary with an enforced pressure of zero, which means that surface wave effects were neglected. The boundary condition at the dam interface was defined so that the spatial pressure gradient in the direction normal to a point on the dam surface is equal and opposite to the acceleration of the dam

along the normal, multiplied by the fluid density. This statement of Newton's second and third laws can be represented as:

$$\frac{\partial p}{\partial n} = -\rho \ddot{s}_n \ .$$

The solution is obtained by using a Galerkin type discretization, with a static condensation to the degrees of freedom corresponding to the dam face.

The output from INCRES is the complete system added mass matrix on the fluid-structure interface, including significant off-diagonal terms. A structural analysis program such as EADAP or special versions of SAP-IV [8] needs specific code to read and properly assemble the complete added mass matrix. This capability is not available in most commercial packages. A module that lumps the complete added mass matrix by scaling the diagonals to the total mass was therefore added to INCRES. Lumped masses can be input as nodal masses to commercial programs such as SAP90. The Benchmark Workshop provides the opportunity to determine whether there are any significant differences between structural results based on lumped and complete added mass matrix representations of arch dam-reservoir interaction.

The results computed with the quadratic element reservoir model were reported on the workshop forms for benchmarking. The middle nodes were eliminated to match the structural mesh after the diagonal lumping process was completed. This was accomplished by proportioning the added mass associated with each middle node degree of freedom between the corresponding element corner node degrees of freedom according to the corner node added mass values.

The final variation tested was the use of linear elements in the reservoir model. The INCRES program uses a serendipity shape function formulation that degenerates from quadratic to linear when the middle nodes are omitted.

Eigenproblem Results. The frequencies corresponding to the first six natural modes for the four eigenproblems solved are listed in Table 2 below.

TABLE 2. TALVACCHIA DAM NATURAL FREQUENCIES (Hertz)

Reservoir:	None	None	Quadratic	Linear
Foundation:	None	Yes	Yes	Yes
Mode 1	4.28	3.81	3.63	3.65
Mode 2	4.56	4.13	3.76	3.79
Mode 3	5.63	5.27	5.12	5.15
Mode 4	6.78	6.29	6.12	6.15
Mode 5	8.60	7.84	6.85	6.87
Mode 6	8.97	8.20	7.83	7.86

The results in Table 2 demonstrate that including the foundation or the reservoir in the model causes significant changes in the computed natural frequencies. Given modern computational tools, it would be imprudent to exclude either from a complete analysis. There is not much difference in results between incompressible reservoir models based on quadratic and linear elements. A comparison between the finite element reservoir solutions and the classical Westergaard solution for added mass was calculated at the crown cantilever and is displayed in Figure 7.

CONCLUSIONS

An analysis of the Talvacchia arch dam for the purpose of benchmarking programs, computers, and modeling techniques was performed. The analysis demonstrated that simple, linear element formulations can yield satisfactory results. Given the convergence properties of such elements with mesh fineness, it is clear that such formulation should produce accurate results.

A dynamic analysis dam-reservoir interaction model based on the lumped added mass method is presented for comparison with results based on complete added mass formulations. The demonstration of a satisfactory level of accuracy by a lumped mass formulation could prove to be of value. It is also worthy to note that a reservoir mesh constructed from linear elements yields essentially the same results as a mesh constructed from quadratic elements.

All computations were performed on an industry standard architecture 386 PC with a 387 math chip. The operating system was MS-DOS. The time necessary to complete a static run was 6 minutes. The time necessary to complete a 2000 time step transient heat flow analysis was about 2½ minutes. The time necessary to compute the added mass with a quadratic element reservoir model was about 12 minutes, which decreased to only about 1 minute when the linear element reservoir model was used. The time necessary to solve the six mode structural eigenproblem including the foundation was about 5½ minutes, which increased to about 7 minutes for a ten mode solution. It is clear that all linear problems involving arch dams can be solved with a comfortable turn-around time on inexpensive personal computers.

We would like to thank the sponsors of the First Benchmark Workshop for the valuable opportunity to exchange results with other professionals in the field of numerical analysis. As a philosophical point, it would prove useful at future workshops to include details such as alternate cantilever dead load analysis and hydrostatic loading on the reservoir bottom in an effort to relate the standard problems to practical applications.

REFERENCES

1. E.L. Wilson and A. Habibullah, SAP90 Users Manual, Computers & Structures Inc., Berkeley, California, USA, 1989.
2. Fortran F77L-EM32 Version 4.00, Lahey Computer Systems, Inc., Incline Village, Nevada, USA, 1991.
3. T.L. Young and M.L. Van Woert, PLOT88 Software Library Reference Manual, 3rd ed., Plotworks, Inc., Ramona, California, USA, 1989.
4. R.M. Polivka and E.L. Wilson, Finite Element Analysis of Nonlinear Heat Transfer Problems, University of California at Berkeley Report No. UC SESM 76-2, USA, 1976.
5. Yusof Ghanaat and Ray W. Clough, EADAP Enhanced Arch Dam Analysis Program User's Manual, University of California at Berkeley Report No. UCB/EERC-89/07, USA, 1989.
6. O.C. Zienkiewicz, The Finite Element Method, 3rd ed., McGraw-Hill Book Company (UK) Limited, Maidenhead, Berkshire, England, UK, 1977.
7. H.M. Westergaard, "Water Pressure on Dams During Earthquakes", Transactions of the American Society of Civil Engineers, Vol. 98, New York, New York, USA, 1933.
8. K.-J. Bathe, E.L. Wilson, and F.E. Peterson, SAP IV, A Structural Analysis Program For Static And Dynamic Response Of Linear Systems, University of California at Berkeley Report No. EERC 73-11, USA, 1973.

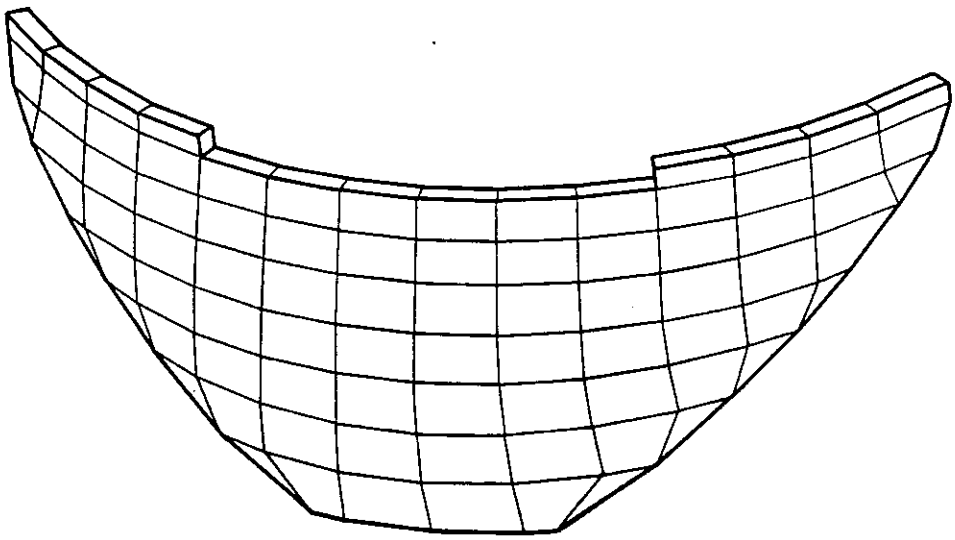

Figure 1.
Finite Element Model
Fixed At Foundation Contact

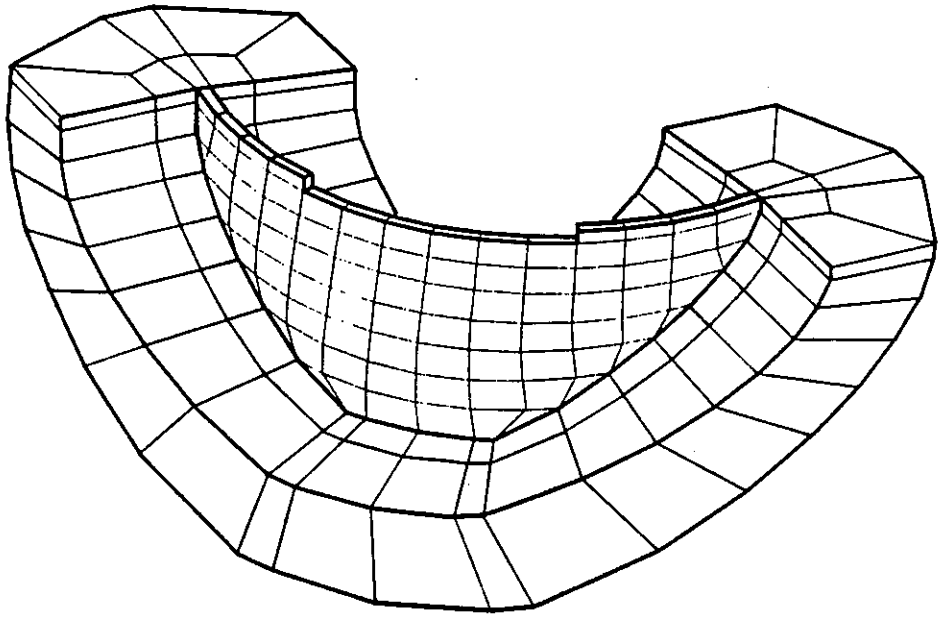

Figure 2.
Finite Element Model
With Foundation

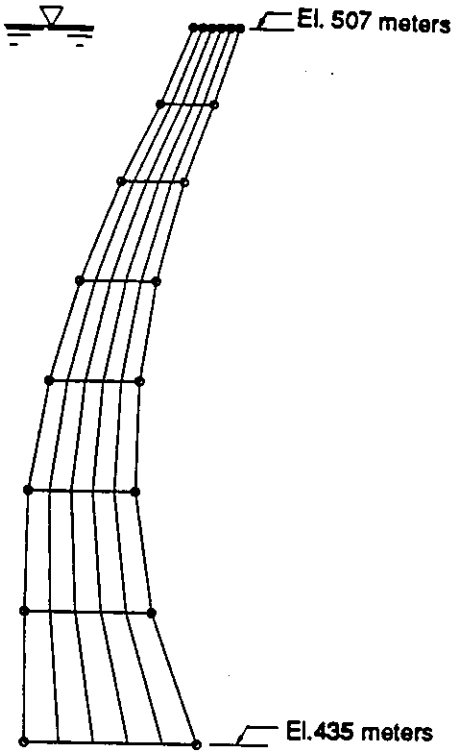

Figure 3.
Crown Cantilever
Heat Flow Model
∘ - Imposed Boundary Temperature Function

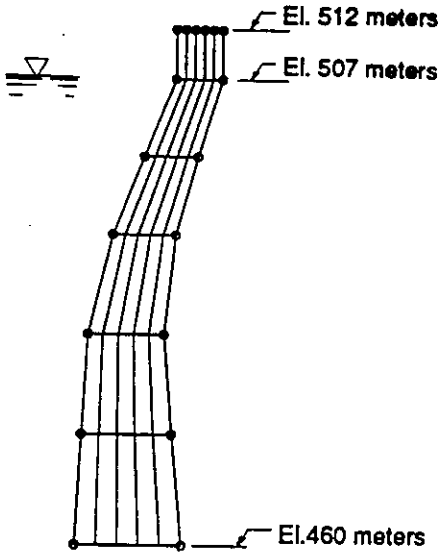

Figure 4.
Heat Flow Model
At Quarter-Arc Point
∘ - Imposed Boundary Temperature Function

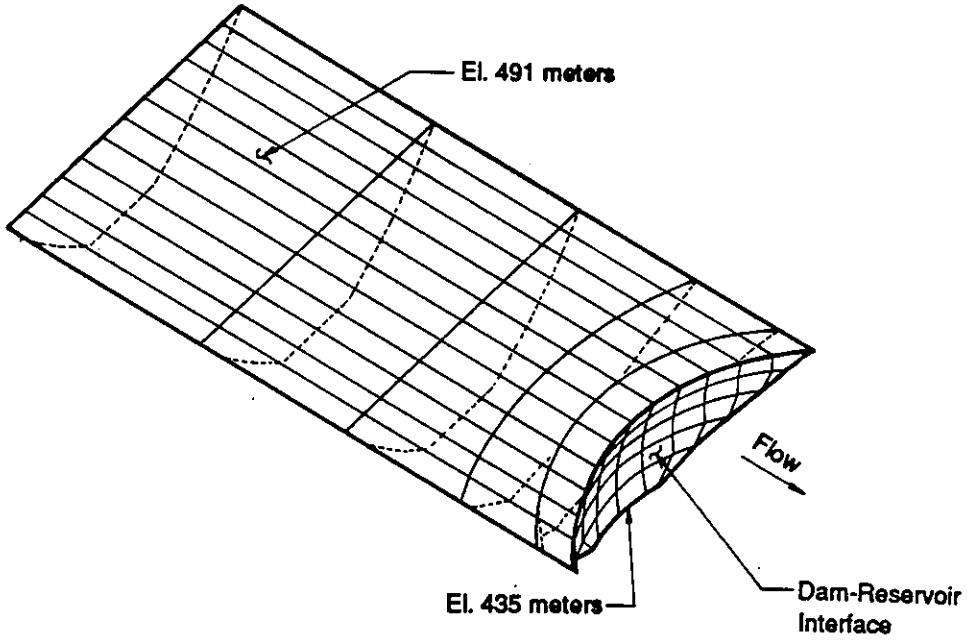

Figure 5.
Finite Element Model
Of Reservoir

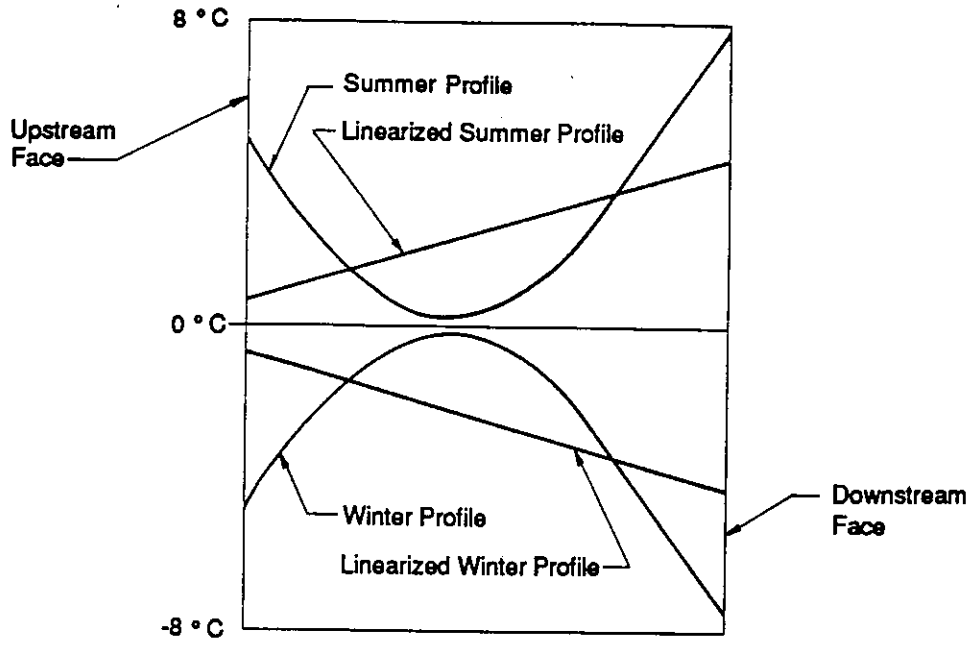

Figure 6.
Typical Summer And Winter
Through Thickness Temperature Profiles
From Periodic Analysis

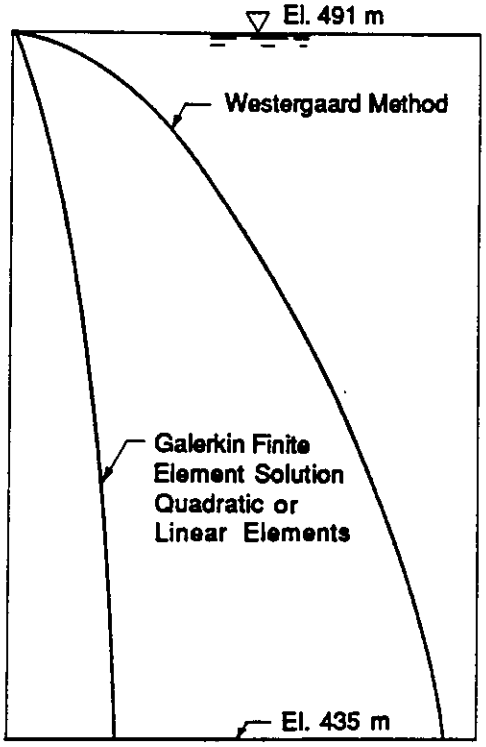

Figure 7.
Normalized Hydrodynamic Pressure
At The Crown Cantilever

Linear-elastic Analysis of a Double-Curvature Arch Dam Using the EFESYS Program

First ICOLD Benchmark Workshop:
Contribution to Theme A

by

R. Dungar,
Colenco Power Consultants Ltd.

May 1991

Abstract

The paper describes the displacement and stress results obtained for the 77m high Talvacchia arch dam, Italy, analysed for a linear-elastic deformation under self-weight, hydrostatic and steady-state temperature loading. Results for the first six eigen-modes are also presented for the case of an incompressible reservoir and including foundation-structure interaction and also for the case of an empty reservoir and with no foundation interaction. The finite element program EFESYS was used and the finite element meshes and other data were as supplied for the benchmark test by the workshop organizing committee.

1 Introduction

By way of introduction the following main points are given for the information contained in this paper:

- The data supplied for the benchmark solution will not be repeated here. It is assumed that the reader is familiar with the details of the benchmark requirements.
- The finite element mesh used to obtain the results for this paper is that provided by the organizers, and is not reproduced here. The mesh is that which contains one element across the dam thickness and which also includes foundation elements.
- In the case of the eigenvalue-vector analyses, two cases are considered: a) the case of structure-foundation-fluid interaction, termed here "full reservoir", and b) the case of an empty reservoir and a dam on a rigid foundation, termed "empty reservoir". In the full reservoir case, the assumption of an incompressible fluid is invoked.
- The EFESYS finite element program was used to obtain all results.

Location Number	Node Number	Temperature (°C)	Location Number	Node Number	Temperature (°C)
1	103	15.1417	11	477	12.3478
2	104	15.1374	12	478	12.3515
3	106	15.0981	13	480	12.3776
4	108	15.0795	14	482	12.5843
5	110	15.0460	15	603	12.2543
6	304	12.3624	16	604	12.3249
7	305	12.3608	17	606	12.6574
8	307	12.3482	18	645	12.7701
9	309	12.3250	19	646	12.7305
10	310	12.2989	20	647	12.7571

Table 1: Temperature results for Steady State Conditions

- A finite element mesh is normally developed for the EFESYS program by using the pre- and post-processing program EMPRESS[1]. However, for the present benchmark solutions, the geometry of the dam was idealized by an appropriate geometry model for reasons of display of post-processing results and the stress results were transformed to principal stresses within the upstream or downstream surface of the finite element mesh before plotting in a projection corresponding approximately to the reference-cylinder projection.

2 Static Analysis

The static load cases required for the benchmark are:

- Selfweight loading applied to the as-built dam,
- Hydrostatic surface loading applied to the water face, and
- Temperature loading.

In the case of temperature loading, either a steady state or transient load case is requested, and here the steady-state case was chosen. The solution to determine the internal temperatures, at the various node points, was obtained by solving the relevant equations for steady-state temperature with the known surface temperatures as boundary conditions, by using the given structural finite element mesh.

The temperature results at the selected node points are given in Table 1.

The results for the self weight, hydrostatic and temperature loadings are presented in Table 2, 3 and 4 respectively and the Figures 1-3 summarized the displacements at elevation 507 (top of the spillway) and the water- and air-face stresses.

[1]EMPRESS is the pre- and post-processing program of EFESYS.

3 Dynamic Analysis

3.1 Methodology

In order to obtain the required eigen-quantities (frequencies and mode shapes) for the first six modes of vibration, the following equation was solved[2]:

$$(\mathbf{K} - \omega_i^2 \mathbf{M})\mathbf{x}_i = \mathbf{0} \tag{1}$$

where $\mathbf{M}$ and $\mathbf{K}$ are the mass and stiffness matrices, respectively, and ω_i the resonant frequency for the ith mode and $\mathbf{x}_i$ the corresponding resonant mode shape. The mass matrix is also given as

$$\mathbf{M} = \mathbf{M}_s + \mathbf{M}_f \tag{2}$$

where $\mathbf{M}_s$ and $\mathbf{M}_f$ are the structural and fluid mass matrices, respectively, the fluid being assumed incompressible. The matrix $\mathbf{M}_f$ is not formed explicitly, but is treated in the eigenvalue solution by the sub-structure process described by Dungar (1978).

The modal vectors are normalized such that the largest component is unity, and the following quantities are also presented in the appropriate tables:

$$M_{g,i} = \mathbf{x}_i^T \mathbf{M} \mathbf{x}_i \tag{3}$$

$$D_{g,r,i} = \mathbf{x}_i^T \mathbf{M} \delta_r \tag{4}$$

where $M_{g,i}$ is the generalized mass for the ith mode and $D_{g,r,i}$ the generalized forcing function for the ith mode and for a unit acceleration in the direction r, the vector δ_r being a vector of 0's and 1's which specifies the direction of earthquake attack for those degrees of freedom in the coordinate direction r.

3.2 Results with Reservoir

The results of the first six resonant frequencies for the case of the dam on its elastic foundation and with the action of the reservoir[3] are presented in Table 5. The results for the respective mode shapes are given in Tables 6-11 for displacement components at the required locations as well as the values of principal stress at the same locations. The respective displacement shapes at elevation 507 (top of spillway) and the corresponding modal stresses are displayed in Figures 4-9.

3.3 Results for no foundation and Empty Reservoir

The results of the first six resonant frequencies for the dam on a rigid foundation and with no reservoir water are presented in Table 12. The results for the respective mode shapes are given in Tables 13-18.

3.4 Results with foundation and Empty Reservoir

For reasons of comparison, the results of the first six resonant frequencies for the dam on a flexible foundation and with no reservoir water are presented in Table 19.

[2]See the solution method presented in §5 for details.

[3]The term "full reservoir" is used in this paper for brevity, although the height of the reservoir in by no means at the height of the spillway.

Mode	1	2	3	4	5	6
Freq.(Hz)	3.5757	3.7883	5.1166	6.0980	6.9056	7.8749
Gen. Mass	25.456	15.410	14.641	16.136	10.160	16.344
$D_{g,x}$	0.0000	-40.661	-38.383	-0.0004	26.117	-9.7617
$D_{g,y}$	32.100	0.0000	0.0000	-9.3763	0.0000	-0.0014
$D_{g,z}$	0.0001	-0.6613	1.8345	-0.0001	9.6211	2.2308

Table 5: Frequencies and Dynamic Values for Full Reservoir

Mode	1	2	3	4	5	6
Freq.(Hz)	4.2961	4.5783	5.6985	6.7188	8.5881	9.3758
Gen. Mass	18.764	9.0840	10.799	13.483	14.104	16.539
$D_{g,x}$	0.0000	-16.299	-22.391	0.0000	2.4442	26.356
$D_{g,y}$	-19.052	0.0000	0.0000	7.4593	0.0000	0.0000
$D_{g,z}$	0.0000	0.18649E	3.5908	0.0000	5.1972	1.1200

Table 12: Frequencies and Dynamic Values for Empty Reservoir

Mode	1	2	3	4	5	6
Freq.(Hz)	3.7689	4.1019	5.2799	6.2263	7.8707	8.3245
Gen. Mass	21.086	11.147	12.887	16.414	9.5504	20.267
$D_{g,x}$	0.0000	-20.893	-28.808	-0.0003	9.3641	27.305
$D_{g,y}$	24.652	0.0000	0.0000	-10.080	0.0002	0.0000
$D_{g,z}$	0.0001	-1.51350	1.8781	0.0000	11.093	15.070

Table 19: Frequencies and Dynamic Values with Foundation and Empty Reservoir

Mode	1	2	3	4	5	6
With foundation	5.40	2.85	3.19	2.10	13.97	5.71
Without foundation	20.25	20.85	11.37	10.18	24.36	19.06

Table 20: Change of Frequency from Case with Full Reservoir (%)

4 Eigenvalue Algorithm using Lanczos Vectors

Solution of the eigenvalue-vector problem was accomplished by using a Lanczos algorithm, which is based on the power and Rayleigh Ritz methods. The eigenvalue problem:

$$(\mathbf{K} - \lambda\mathbf{M})\mathbf{x} = \mathbf{0} \tag{5}$$

is thus transformed to the form:

$$(\mathbf{T} - \theta\mathbf{I})\mathbf{u} = \mathbf{0} \tag{6}$$

where $\theta = 1/\lambda$. Transformation to $\mathbf{T}$ is achieved by applying

$$\mathbf{x} = \mathbf{Q}\mathbf{u} \tag{7}$$

with the addition of the condition

$$\mathbf{Q}^T\mathbf{M}\mathbf{Q} = \mathbf{Q}^T\mathbf{M}^T\mathbf{Q} = \mathbf{I} \tag{8}$$

The vectors $\mathbf{Q} = [\mathbf{q}_1, \mathbf{q}_2, \ldots, \mathbf{q}_n]$ are known as the Lanczos vectors. The matrix $\mathbf{T}$ is of the form

$$\mathbf{T} = \mathbf{Q}^T\mathbf{M}^T\mathbf{K}^{-1}\mathbf{M}\mathbf{Q} = \begin{bmatrix} \alpha_1 & \beta_2 & & & & & \\ \beta_2 & \alpha_2 & \beta_3 & & & & \\ & \beta_3 & \alpha_3 & \beta_4 & & & \\ & & \ddots & \ddots & \ddots & & \\ & & & \ddots & \ddots & \ddots & \\ & & & & \beta_{n-1} & \alpha_{n-1} & \beta_n \\ & & & & & \beta_n & \alpha_n \end{bmatrix} \tag{9}$$

From this a three term recurrence is obtained in order to calculate the coefficients α_i, β_i and the vectors $\mathbf{q}_i$ as

$$\mathbf{K}^{-1}\mathbf{M}\mathbf{q}_i = \beta_i\mathbf{q}_{i-1} + \alpha_i\mathbf{q}_i + \beta_{i+1}\mathbf{q}_{i+1} \tag{10}$$

with $\mathbf{q}_0 = \mathbf{0}$ and $\beta_{n+1} = 0$. All the elements of $\mathbf{T}$ can be calculated and the Lanczos vectors $\mathbf{Q}$ can be calculated by use of the matrix condition of equation (7), from which we obtain, after premultiplying by $\mathbf{q}_i^T\mathbf{M}^T$:

$$\alpha_i = \mathbf{q}_i^T\mathbf{M}^T[\mathbf{K}^{-1}\mathbf{M}\mathbf{q}_i - \beta_i\mathbf{q}_{i-1}] \tag{11}$$

after which the vector

$$\mathbf{r} = \beta_{i+1}\mathbf{q}_{i+1} \tag{12}$$

can be defined from:

$$\mathbf{r} = \mathbf{K}^{-1}\mathbf{M}\mathbf{q}_i - \beta_i\mathbf{q}_{i-1} - \alpha_i\mathbf{q}_i \tag{13}$$

from which β_{i+1} can be found by using the normalization condition of (7), or:

$$\beta_{i+1}^2 = \mathbf{r}^T\mathbf{M}\mathbf{r} \tag{14}$$

after which $\mathbf{q}_{i+1}$ is given from (12)

The algorithm begins by establishing starting values for the vector, $\mathbf{r}$, for which a convenient form is:

$$r_j = \frac{1}{\sqrt{n}} \tag{15}$$

followed by the sequence, for $i = 1, 2, \ldots, s$ where s is the number of Lanczos vectors to be employed in the approximation process, $n_e \leq s \leq n$, and n_e the number of required eigenvalues :

$$\mathbf{p} = \mathbf{M}\mathbf{r} \tag{16}$$

and from (14) and then (12):

$$\beta_2 = \sqrt{\mathbf{p}^T\mathbf{r}} \tag{17}$$

and

$$\mathbf{q}_i = \mathbf{r}/\beta_i \tag{18}$$

$$\mathbf{r} = \mathbf{p} = \mathbf{p}/\beta_i \tag{19}$$

From (11):

$$\mathbf{p} = \mathbf{K}^{-1}\mathbf{p} - \beta_i\mathbf{q}_{i-1} \tag{20}$$

$$\alpha_i = \mathbf{p}^T\mathbf{r} \tag{21}$$

and from (12):

$$\mathbf{r} = \mathbf{q}_{i+1} = \mathbf{p} - \alpha_i\mathbf{q}_i \tag{22}$$

which is then the vector for the next sequence, and the sequence continues until sufficient precision is obtained.

After n_e sequences, the precision is tested by examining the first n_e eigenvalues of the tri-diagonal T matrix, which may easily be reconstructed using the values of α and β, and here the QR algorithm can conveniently be used. Convergence is deemed to have occurred when each eigenvalue is the same as for the previous sequence, to within a specified tolerance.

Due to the fact that normality of vectors $\mathbf{q}_i$ are not completely retained as the sequence progresses, it is prudent to correct for normality by the inclusion of a Gram-Schmid algorithm at the end of each loop in the sequence.

The final step in the complete process is to obtain the eigenvectors of the matrix T, and here again the QR algorithm is again used. These are then post-multiplied by the vectors $\mathbf{q}_i$, i=1...s, to obtain the eigenvectors of the original system.

5 Reference

Dungar R. (1978) An efficient method of fluid-structure coupling in the dynamic analysis of structures. Int. J. of Numerical Methods in Engrg., 13, pp 93 - 107.

Loc Num	Node Num	δ_x (mm)	δ_y (mm)	δ_z (mm)	P_1 (Mpa)	P_2 (MPa)	P_3 (MPa)
1	81	0.8184	0.0000	-2.9751	0.0024	-0.0164	-1.1104
2	103	0.8333	0.0000	-3.1889	0.0025	-0.0110	-1.1801
3	125	0.8489	0.0000	-3.4027	0.0211	-0.0104	-1.2503
4	285	-0.5869	0.0000	-2.4103	0.0264	-0.0373	-0.3169
5	304	-0.5779	0.0000	-2.6454	-0.0081	-0.3070	-0.4175
6	323	-0.5653	0.0000	-2.8975	-0.0090	-0.5156	-0.5761
7	287	-0.5461	-0.1444	-2.3197	0.0638	-0.0210	-0.2848
8	305	-0.5397	-0.1595	-2.5550	-0.0063	-0.2561	-0.4307
9	325	-0.5294	-0.1756	-2.8090	-0.0078	-0.4526	-0.6523
10	291	-0.2153	-0.4164	-1.7015	0.3234	-0.0164	-0.1021
11	307	-0.2254	-0.4488	-1.9361	0.0163	-0.0386	-0.4402
12	329	-0.2285	-0.4843	-2.1999	-0.0025	-0.1674	-0.9749
13	295	-0.0673	-0.4802	-0.8395	0.3588	0.1713	-0.0469
14	309	-0.0485	-0.4508	-1.0000	0.1938	-0.0067	-0.3916
15	333	-0.0191	-0.4293	-1.1819	0.2105	0.0144	-1.1549
16	297	-0.1461	-0.1771	-0.3892	0.4720	0.1344	-0.2866
17	310	-0.1357	-0.1444	-0.4610	0.2936	-0.1603	-0.3690
18	335	-0.1101	-0.1139	-0.5046	0.1488	-0.1687	-1.1822
19	461	-1.3601	0.0000	-2.1693	0.2715	0.1202	-0.0228
20	477	-1.3618	0.0000	-2.1737	0.0809	-0.0029	-0.4589
21	493	-1.3439	0.0000	-2.2011	-0.0231	-0.1589	-1.1753
22	463	-1.2616	0.1097	-2.1027	0.2865	0.0987	-0.0233
23	478	-1.2705	0.0678	-2.1007	0.0954	-0.0021	-0.4837
24	495	-1.2589	0.0230	-2.1152	-0.0168	-0.1397	-1.1914
25	467	-0.5830	0.1099	-1.6020	0.2428	0.1111	-0.2117
26	480	-0.6257	0.0260	-1.5673	0.1481	0.0060	-0.6490
27	499	-0.6542	-0.0721	-1.4980	0.0757	0.0308	-1.1407
28	471	-0.0658	-0.0742	-0.8066	0.1008	-0.1323	-1.5421
29	482	-0.0999	-0.0944	-0.8488	0.1774	-0.1950	-0.6308
30	503	-0.1340	-0.1014	-0.7542	0.3023	-0.0001	-1.0402
31	593	-0.6385	0.0000	-2.0766	0.1227	-0.0482	-0.7390
32	603	-0.6226	0.0000	-1.7369	0.0002	-0.0392	-0.7758
33	613	-0.6004	0.0000	-1.4273	-0.0880	-0.1993	-1.0675
34	595	-0.5298	0.1199	-1.9506	0.1177	-0.0635	-0.8238
35	604	-0.5261	0.0541	-1.6536	-0.0072	-0.0525	-0.7793
36	615	-0.5149	-0.0096	-1.3548	-0.0593	-0.2134	-0.9294
37	599	0.0021	0.0583	-1.1989	-0.1294	-0.3859	-2.4213
38	606	-0.0540	-0.0217	-1.1856	-0.0016	-0.2432	-0.7272
39	619	-0.1180	-0.0668	-0.9477	0.1676	0.0998	-1.0392
40	638	0.0073	0.0000	-1.4842	-0.3029	-0.4654	-2.4146
41	645	0.0011	0.0000	-1.3167	-0.2524	-0.3734	-0.9742
42	652	-0.0534	0.0000	-0.9767	0.1776	-0.1265	-0.7034

Table 2: Results for Selfweight Load

Loc Num	Node Num	δ_x (mm)	δ_y (mm)	δ_z (mm)	P_1 (Mpa)	P_2 (MPa)	P_3 (MPa)
1	81	22.1369	0.0000	-0.5322	0.0541	-0.0300	-3.1088
2	103	22.1692	0.0000	-0.8056	0.1420	-0.0450	-2.0136
3	125	22.1860	0.0000	-1.0892	0.0778	-0.1583	-0.9160
4	285	19.9594	0.0000	0.4461	-0.1245	-1.4975	-4.3789
5	304	20.0139	0.0000	-0.1773	-0.0530	-0.3108	-3.0543
6	323	20.0455	0.0000	-0.7247	0.9658	0.0008	-1.6195
7	287	18.3734	-1.6633	0.4864	-0.1282	-1.4456	-4.2042
8	305	18.4959	-1.1606	-0.0869	-0.0567	-0.2924	-3.0326
9	325	18.6003	-0.6409	-0.5852	0.9700	-0.0020	-1.7951
10	291	8.9614	-1.9205	0.5345	-0.1391	-1.2738	-2.7142
11	307	9.3706	-1.0798	0.2706	-0.0967	-0.2460	-2.5935
12	329	9.7843	-0.2158	0.0737	1.0465	-0.0277	-2.6297
13	295	1.8586	0.6201	0.0818	-0.1574	-0.9292	-1.0548
14	309	2.0707	0.8498	0.1391	0.0203	-0.1214	-1.7033
15	333	2.2964	1.0952	0.2205	1.1336	-0.0501	-2.5049
16	297	0.8556	0.7111	-0.1300	-0.2005	-0.5529	-1.9955
17	310	0.8847	0.7498	-0.0736	-0.0806	-0.4025	-1.5302
18	335	0.8473	0.7289	-0.0110	0.5306	-0.2684	-1.8287
19	461	14.4445	0.0000	2.6825	-0.3508	-1.3258	-4.1894
20	477	14.5210	0.0000	1.1305	-0.1662	-0.4768	-2.9160
21	493	14.5667	0.0000	-0.3838	0.7738	0.0281	-1.4198
22	463	13.1660	-1.6309	2.5304	-0.3224	-1.2084	-3.9566
23	478	13.3285	-1.0930	1.0581	-0.1520	-0.4412	-2.8133
24	495	13.4633	-0.5363	-0.3890	0.7423	-0.0104	-1.5512
25	467	5.6009	-1.6611	1.4976	0.0997	-0.4923	-1.6251
26	480	6.1075	-0.7812	0.5148	0.1898	-0.2964	-2.1194
27	499	6.6036	0.0851	-0.4987	0.5396	-0.2293	-2.8334
28	471	1.2525	0.5031	0.1802	0.9147	0.4224	-1.3313
29	482	1.5245	0.8407	-0.1134	0.3133	-0.5449	-1.4685
30	503	1.5850	0.9525	-0.3715	-0.5733	-0.7101	-4.9836
31	593	6.0020	0.0000	3.3125	0.8069	-1.1331	-1.8568
32	603	5.9001	0.0000	1.1603	0.7314	-0.7281	-0.9620
33	613	5.9140	0.0000	-0.9028	0.9243	-0.2534	-1.7480
34	595	5.1989	-0.7579	2.8882	1.0171	-0.8619	-1.7895
35	604	5.2113	-0.2943	0.9607	0.5715	-0.5190	-1.0416
36	615	5.2903	0.1290	-0.9278	0.5413	0.0724	-2.2045
37	599	1.4958	-0.1480	0.9604	3.0965	1.1055	0.2758
38	606	1.9345	0.5387	-0.0408	0.8185	0.2951	-1.0152
39	619	2.0601	0.8529	-0.7952	-0.5059	-1.3067	-6.1463
40	638	1.6800	0.0000	1.7527	4.4208	1.6074	1.0379
41	645	1.7919	0.0000	0.1015	1.8533	0.6786	-0.4539
42	652	1.8015	0.0000	-0.9229	-0.1271	-0.2626	-4.5407

Table 3: Results for Hydrostatic Load

Loc Num	Node Num	δ_x (mm)	δ_y (mm)	δ_z (mm)	P_1 (Mpa)	P_2 (MPa)	P_3 (MPa)
1	81	-17.3167	-0.0001	7.7958	0.9427	-0.2948	-0.5938
2	103	-17.0945	-0.0001	8.6202	0.6456	0.0260	-0.1113
3	125	-16.8481	-0.0001	9.4202	0.3998	0.3824	0.2485
4	285	-13.1788	0.0000	4.7128	1.6539	0.6915	-0.0712
5	304	-12.9489	-0.0001	5.4945	0.3835	0.1246	-0.1030
6	323	-12.6408	-0.0001	6.2619	-0.0852	-0.6327	-1.0348
7	287	-12.3549	1.7722	4.5484	1.5202	0.6290	-0.0669
8	305	-12.1612	1.4834	5.3345	0.3209	0.1012	-0.1078
9	325	-11.8907	1.1853	6.1087	-0.0839	-0.6282	-1.0378
10	291	-7.0798	3.5491	3.3449	0.6421	-0.0149	-0.1116
11	307	-7.0773	2.9419	4.1415	0.1537	0.0130	-0.6543
12	329	-7.0103	2.3057	4.9449	-0.0781	-0.3482	-1.4418
13	295	-1.3655	2.3770	1.6037	-0.0777	-0.6383	-1.6742
14	309	-1.4541	1.8506	2.1651	0.0381	-0.2432	-2.1662
15	333	-1.5032	1.2784	2.7847	0.4455	-0.2004	-2.8765
16	297	0.4358	0.9673	0.5046	-0.9126	-1.3883	-3.7053
17	310	0.4653	0.7324	0.7275	-0.1324	-1.5637	-3.5599
18	335	0.4979	0.4736	0.8418	1.6280	-1.6263	-3.9073
19	461	-9.0356	0.0000	1.3378	1.0595	0.7901	-0.0983
20	477	-8.7061	0.0000	2.4189	0.0095	-0.0602	-0.4228
21	493	-8.2375	0.0000	3.4780	-0.0947	-1.1945	-2.2081
22	463	-8.2278	1.5172	1.2940	0.9222	0.6140	-0.0811
23	478	-7.9534	1.1230	2.3430	0.0246	-0.0451	-0.6125
24	495	-7.5455	0.7028	3.3822	-0.0771	-1.0509	-2.2677
25	467	-3.2988	2.3766	0.9379	0.2375	-0.3385	-1.1151
26	480	-3.2559	1.6319	1.7498	0.2154	-0.1407	-1.7998
27	499	-3.1391	0.8231	2.5941	0.2231	0.0629	-2.5645
28	471	0.0184	0.9225	0.3697	-0.4484	-1.5674	-3.3351
29	482	0.0211	0.6328	0.7443	-0.2469	-2.0494	-3.3211
30	503	0.1150	0.3649	0.8075	2.0068	-1.8235	-3.6105
31	593	-3.8938	0.0000	-0.9560	-0.0235	-0.5626	-0.5842
32	603	-3.3429	0.0000	0.3187	0.0854	-0.9803	-1.9018
33	613	-2.6451	0.0000	1.5562	0.4174	-1.0537	-3.3980
34	595	-3.3107	0.9611	-0.8015	-0.0497	-0.5124	-0.7549
35	604	-2.8302	0.5681	0.3301	0.0605	-0.9101	-2.0038
36	615	-2.1963	0.1636	1.4724	0.4262	-0.6422	-3.4257
37	599	-0.4810	1.0772	-0.3718	-0.6773	-2.3618	-4.0345
38	606	-0.4637	0.6728	0.2645	-0.4393	-2.3716	-3.3849
39	619	-0.2496	0.3496	0.4928	2.2373	-1.7650	-3.6170
40	638	-1.0733	0.0000	-1.1650	-1.2652	-2.7615	-3.5759
41	645	-0.7825	0.0000	-0.2877	-0.8059	-2.6723	-3.6357
42	652	-0.3211	0.0000	0.0578	1.2951	-1.7101	-4.0023

Table 4: Results for Temperature Load

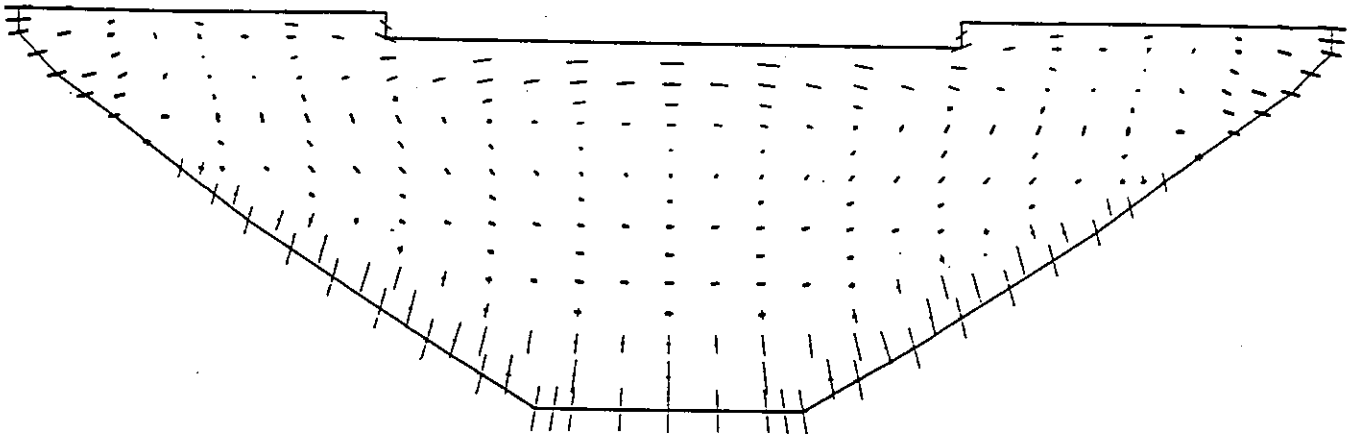

Principal Stress : Upstream Face

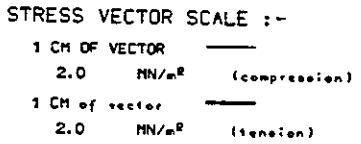

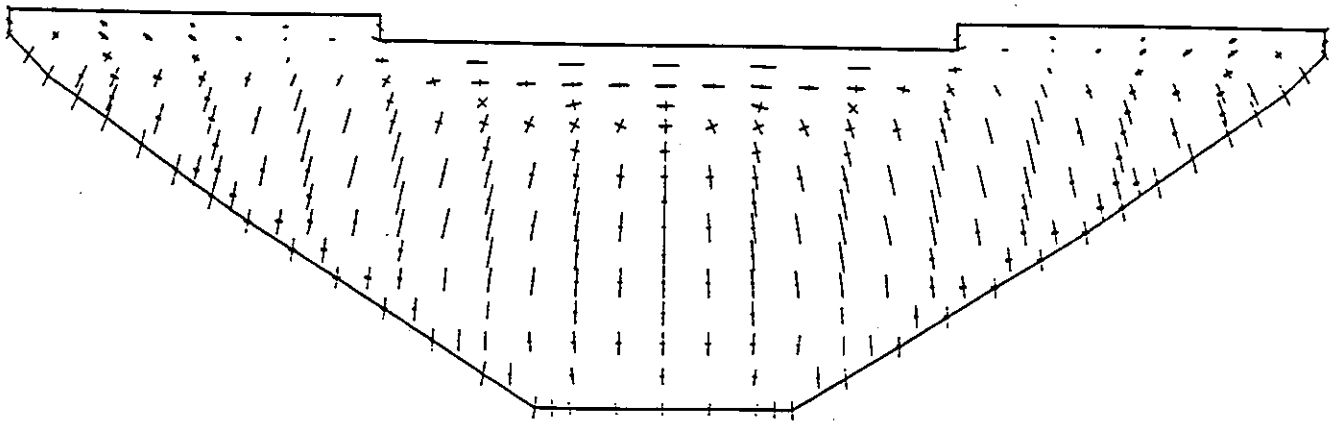

Principal Stress : Downstream Face

Figure 1: Results for Selfweight Load

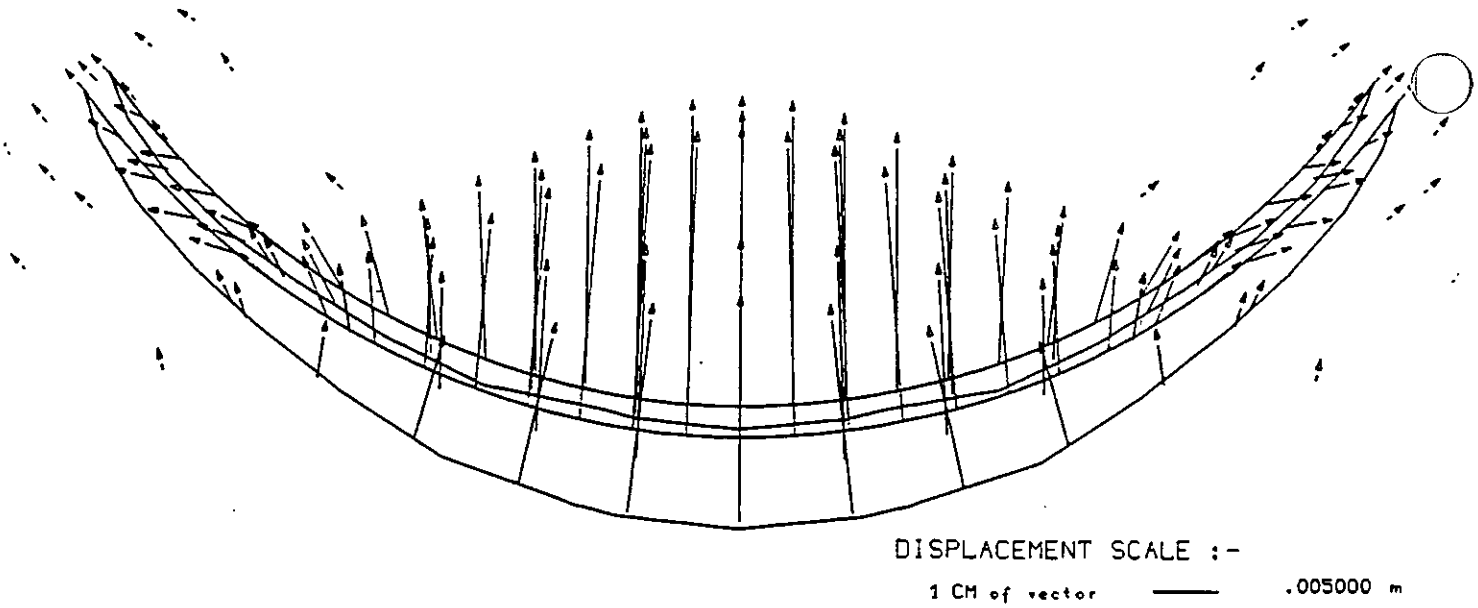

Displaced Section

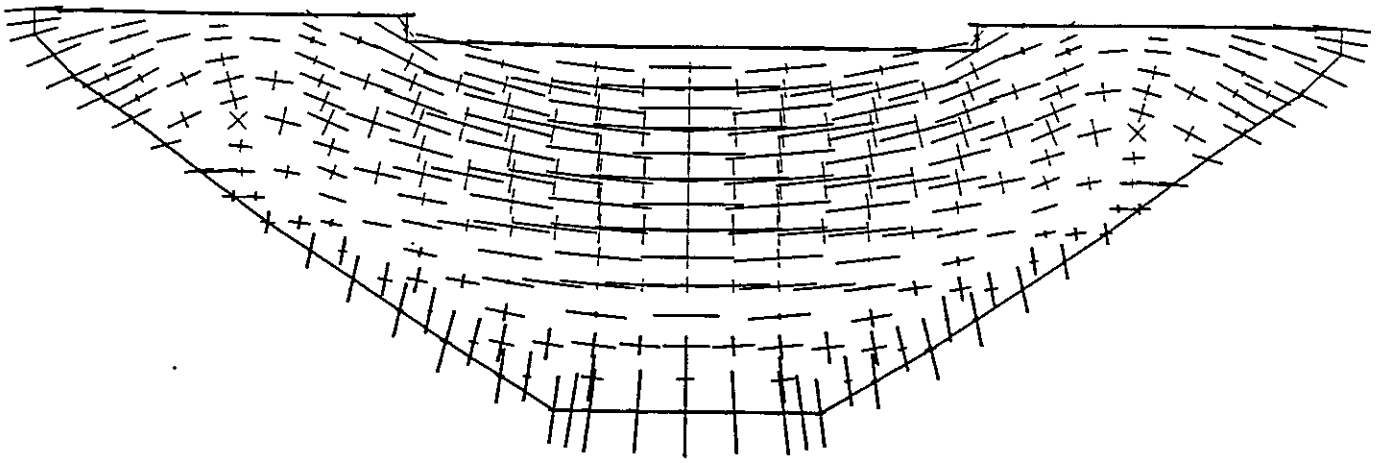

Principal Stress : Upstream Face

STRESS VECTOR SCALE :-
1 CM OF VECTOR
2.0 MN/m² (compression)
1 CM of vector
2.0 MN/m² (tension)

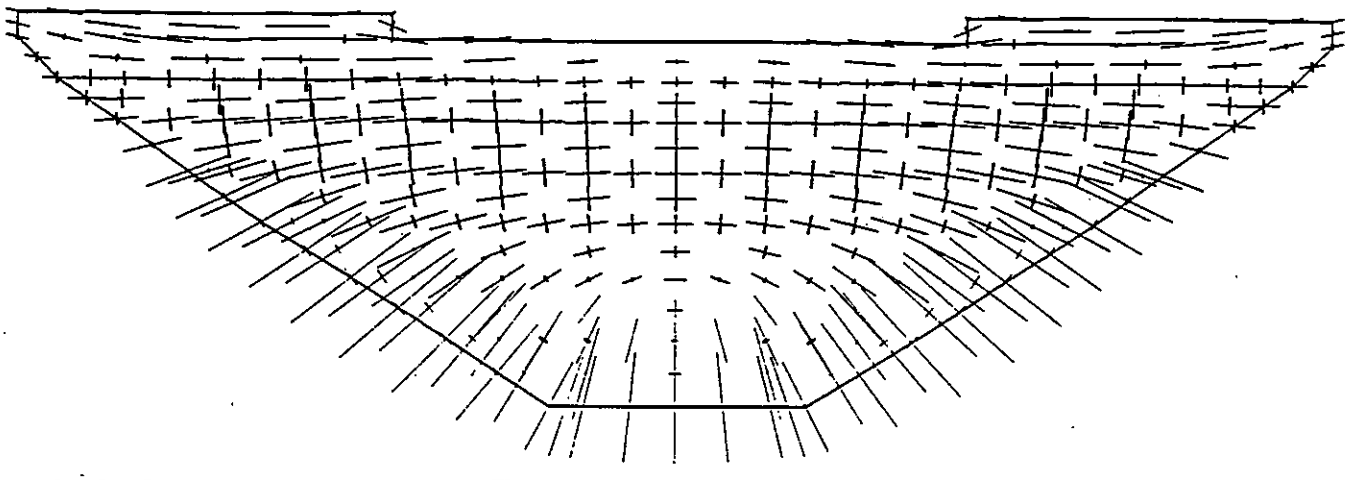

Principal Stress : Downstream Face

Figure 2: Results for Hydrostatic Load

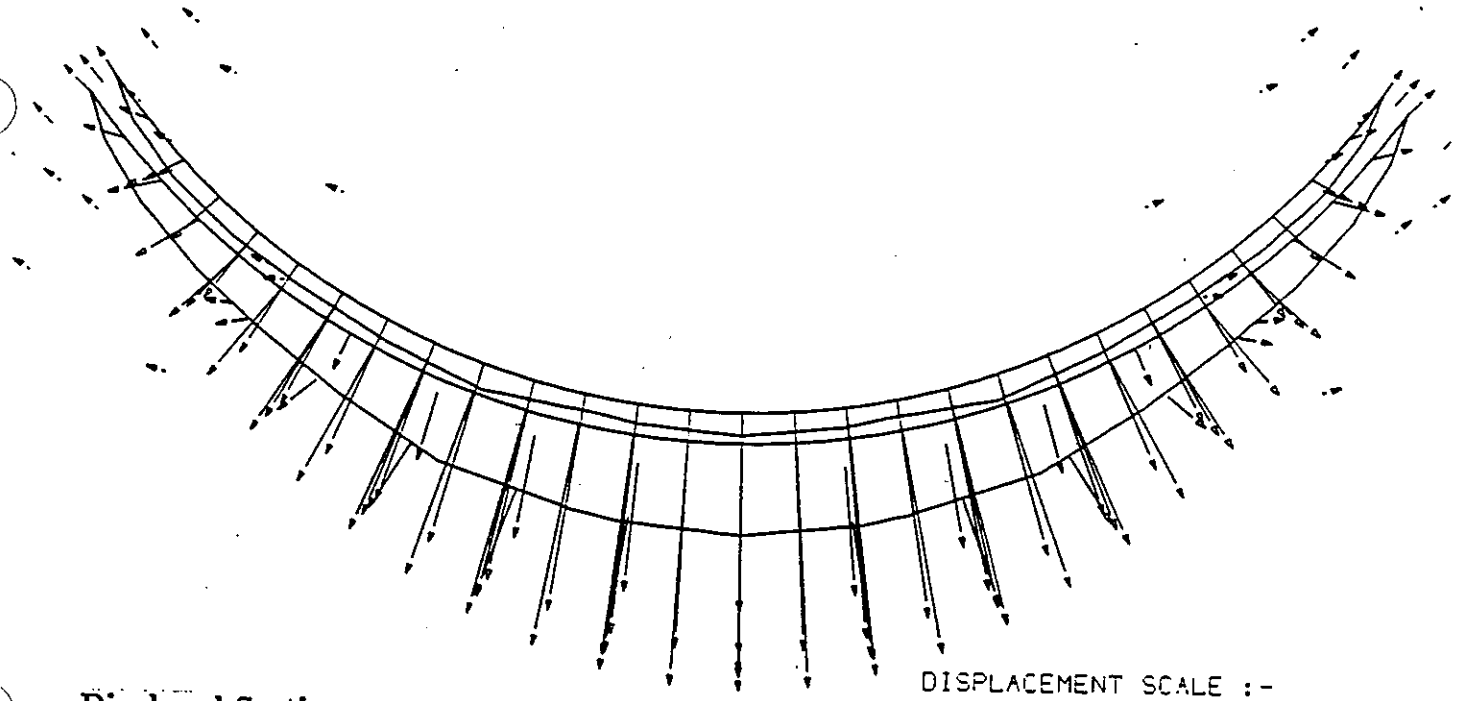

Displaced Section

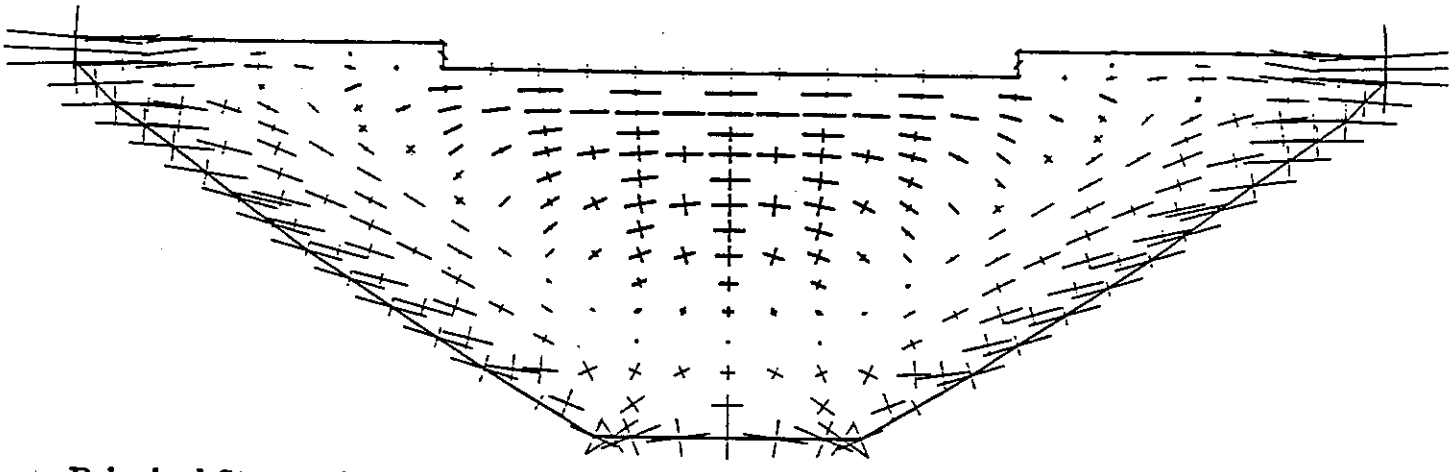

Principal Stress : Upstream Face

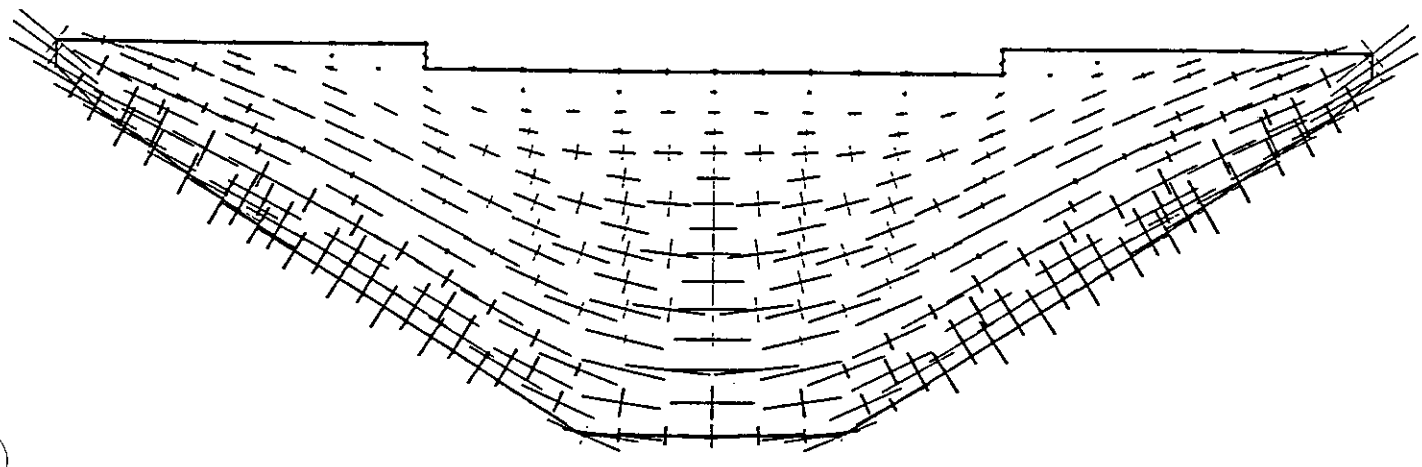

Principal Stress : Downstream Face

Figure 3: Results for Temperature Load

Loc Num	Node Num	δ_x	δ_y	δ_z	P_1	P_2	P_3
1	103	0.00000	0.30974	0.00000	59.0885	0.0000	-59.0883
2	104	-0.62937	0.35820	0.13973	73.3848	3.0556	-27.1815
3	106	-0.87388	0.43945	0.16786	78.9163	11.8922	-3.6656
4	108	-0.22212	0.10147	0.02127	62.8426	0.3928	-3.5603
5	110	-0.01462	-0.01412	0.00024	39.5509	5.8254	-4.3474
6	304	0.00000	0.21204	0.00000	19.3345	0.0000	-19.3346
7	305	-0.37575	0.23999	0.04562	32.0776	-2.2467	-3.9576
8	307	-0.51020	0.27848	0.03025	46.6980	11.2601	-12.3776
9	309	-0.10931	0.06412	-0.01313	13.3027	-1.0068	-20.9707
10	310	-0.01479	-0.01045	-0.00287	8.4910	3.5705	-10.8332
11	477	0.00000	0.10122	0.00000	21.8572	0.0000	-21.8574
12	478	-0.16054	0.11499	-0.01479	25.7343	-2.1300	-14.9840
13	480	-0.17278	0.11217	-0.03194	18.0192	4.4375	-23.3206
14	482	-0.01941	0.00540	-0.00851	11.0794	-9.8855	-21.7120
15	603	0.00000	0.03671	0.00000	14.4249	0.0001	-14.4249
16	604	-0.03338	0.03866	-0.01695	8.0634	-1.6015	-20.3573
17	606	-0.01283	0.02077	-0.01573	-4.2362	-10.9806	-26.4486
18	645	0.00000	0.01973	0.00000	9.2937	0.0002	-9.2917
19	646	-0.00294	0.01775	-0.00795	-4.4188	-8.3804	-19.9119
20	647	-0.00256	0.01634	-0.01037	-1.2054	-8.1981	-18.7648

Table 6: Results for Eigenvector 1: Full Reservoir

Loc Num	Node Num	δ_x	δ_y	δ_z	P_1	P_2	P_3
1	103	-0.99979	0.00000	0.18340	86.1446	2.0304	-0.0512
2	104	-0.81226	0.01416	0.13685	85.8672	-0.0097	-12.0662
3	106	0.04005	-0.17192	-0.05129	43.1012	-2.9616	-16.1056
4	108	0.16471	-0.18448	-0.04624	23.8777	-0.1463	-5.9855
5	110	-0.00304	-0.00521	0.00001	10.4299	0.4598	-0.8764
6	304	-0.65389	0.00000	0.05875	64.9447	7.0036	-4.4241
7	305	-0.54393	0.01444	0.04102	61.7468	5.3789	-4.9816
8	307	-0.04537	-0.08137	-0.01638	32.2445	-1.0858	-1.5084
9	309	0.04859	-0.09121	0.00000	37.2821	-0.0763	-5.2370
10	310	-0.00673	-0.01928	0.00471	45.1748	12.2345	-7.8366
11	477	-0.32037	0.00000	-0.03037	43.6377	5.3258	-7.8550
12	478	-0.26927	0.01220	-0.02806	42.0335	2.9686	-6.9937
13	480	-0.04738	-0.03044	-0.00746	28.3257	-0.0365	-8.2788
14	482	-0.01016	-0.02723	0.00279	30.6216	5.4375	-0.2339
15	603	-0.08566	0.00000	-0.03181	4.4221	3.7866	-19.4026
16	604	-0.06967	-0.00003	-0.02562	8.2162	-1.1123	-14.5745
17	606	-0.01703	-0.01643	-0.00238	9.8992	-3.4959	-13.5008
18	645	-0.01638	0.00000	-0.01203	-7.9986	-17.4250	-25.7300
19	646	-0.01282	-0.00448	-0.00965	-7.3560	-11.3061	-22.3701
20	647	-0.01046	-0.00610	-0.00757	-6.4432	-11.6707	-14.9339

Table 7: Results for Eigenvector 2: Full Reservoir

Loc Num	Node Num	δ_x	δ_y	δ_z	P_1	P_2	P_3
1	103	0.18697	0.00000	-0.09120	86.9507	4.1827	-3.1021
2	104	-0.04064	0.07006	-0.02601	129.9547	6.1659	-20.9989
3	106	-0.84059	0.42582	0.19638	193.0810	22.5610	-0.9419
4	108	-0.38245	0.21059	0.06697	97.7498	3.7907	-6.3690
5	110	-0.02270	-0.02053	0.00104	56.4692	11.4715	-4.0033
6	304	0.05599	0.00000	-0.03367	54.6441	7.5695	-9.1043
7	305	-0.05505	0.04009	-0.01154	64.2916	3.0943	-8.1237
8	307	-0.41632	0.19613	0.03989	76.6903	7.5597	-4.2872
9	309	-0.16281	0.08664	-0.00450	38.3436	-1.2638	-26.3855
10	310	-0.02647	-0.01563	-0.00093	25.5716	7.0859	-20.2853
11	477	-0.02330	0.00000	-0.00641	17.9304	4.8229	-0.4541
12	478	-0.05621	0.01298	-0.00703	21.8382	2.0731	-1.4783
13	480	-0.12629	0.05051	-0.01365	23.3747	3.1677	-8.8270
14	482	-0.03112	-0.00660	0.00023	23.6641	-8.0532	-15.8065
15	603	-0.01689	0.00000	-0.00477	2.1432	1.4147	-2.1941
16	604	-0.02078	0.00117	-0.00613	2.6913	1.2601	-4.0459
17	606	-0.01452	-0.00198	-0.00347	1.8152	-3.7670	-9.6072
18	645	-0.00468	0.00000	-0.00160	0.9185	-4.0620	-6.3991
19	646	-0.00496	-0.00127	-0.00199	-0.6594	-4.4961	-6.5329
20	647	-0.00510	-0.00158	-0.00211	1.2103	-3.5873	-7.4571

Table 8: Results for Eigenvector 3: Full Reservoir

Loc Num	Node Num	δ_x	δ_y	δ_z	P_1	P_2	P_3
1	103	0.00001	0.06191	0.00000	107.0049	0.0001	-107.0041
2	104	-0.59770	0.09307	0.16018	43.4671	-11.6914	-36.8304
3	106	0.34628	-0.33092	-0.12482	30.5460	-26.1623	-256.2810
4	108	0.64578	-0.50495	-0.15575	12.9820	-7.0331	-97.9893
5	110	0.02170	0.01345	-0.00204	-2.6961	-17.1783	-44.6027
6	304	0.00000	0.03145	0.00000	58.9250	-0.0004	-58.9241
7	305	-0.34696	0.05195	0.06467	49.5824	12.5055	-31.9418
8	307	0.02460	-0.08879	-0.00587	28.2749	12.6885	-43.9347
9	309	0.21278	-0.18813	-0.00128	49.1916	0.7909	-41.7622
10	310	0.02314	-0.01182	0.00507	74.4562	18.8509	-52.6060
11	477	0.00000	0.00674	0.00000	22.4732	-0.0001	-22.4729
12	478	-0.13838	0.01970	0.00406	26.8204	9.8030	-7.8237
13	480	-0.04289	-0.00832	0.00913	29.0948	6.9701	-5.0315
14	482	0.00898	-0.02021	0.00409	30.7839	9.2465	-1.5321
15	603	0.00000	-0.00054	0.00000	4.4670	0.0002	-4.4670
16	604	-0.03156	0.00247	-0.00222	5.6672	2.1965	-2.8478
17	606	-0.01680	-0.00524	0.00845	13.6072	-6.0052	-9.6799
18	645	0.00000	0.00085	0.00000	2.3205	0.0000	-2.3192
19	646	-0.00691	0.00018	0.00246	-0.6140	-4.4401	-7.5298
20	647	-0.00773	-0.00044	0.00359	-3.0077	-3.8618	-6.2655

Table 9: Results for Eigenvector 4: Full Reservoir

Loc Num	Node Num	δ_x	δ_y	δ_z	P_1	P_2	P_3
1	103	-0.99702	0.00000	0.44182	288.7652	13.5532	-2.0888
2	104	-0.82024	0.10257	0.37734	256.8790	12.6851	-6.6343
3	106	-0.21645	0.11209	0.14205	106.8116	16.5373	-2.9056
4	108	-0.07936	0.07586	0.04588	18.9687	4.1400	-2.0893
5	110	0.00175	0.00201	0.00300	2.7163	0.0246	-3.4554
6	304	-0.21861	0.00000	0.16239	47.5955	23.5379	-24.4295
7	305	-0.15283	0.01225	0.13828	48.6422	11.0646	-21.7528
8	307	0.03221	-0.01283	0.05167	29.7210	0.5690	-27.0581
9	309	-0.00096	0.00988	0.01823	11.2934	0.2015	-11.2575
10	310	0.00187	0.00283	0.00710	8.0273	-0.5237	-7.7253
11	477	0.21340	0.00000	0.03063	-3.6353	-24.4205	-66.8021
12	478	0.20788	-0.02683	0.02995	-1.6076	-19.9006	-64.6475
13	480	0.11193	-0.03794	0.02595	20.1743	-11.4915	-40.5986
14	482	0.01651	0.00268	0.01310	16.7064	-3.2393	-18.1684
15	603	0.13603	0.00000	0.02287	24.8892	-26.6223	-30.7250
16	604	0.12001	-0.01052	0.02090	22.4616	-18.8373	-31.5272
17	606	0.04139	0.00550	0.00751	27.1888	6.1987	-22.1712
18	645	0.04386	0.00000	0.00007	47.0223	13.8873	-15.3127
19	646	0.03690	0.00336	0.00060	41.6236	12.0403	-11.7263
20	647	0.03231	0.00514	0.00068	21.2869	13.2036	-4.2425

Table 10: Results for Eigenvector 5: Full Reservoir

Loc Num	Node Num	δ_x	δ_y	δ_z	P_1	P_2	P_3
1	103	-0.48178	0.00000	0.13777	5.8565	-21.9669	-25.2109
2	104	0.03430	-0.06637	-0.01148	115.6092	-3.8227	-175.6420
3	106	0.36825	-0.04299	-0.06614	243.2883	27.2948	-55.7673
4	108	-0.76550	0.65094	0.20765	102.2262	17.7220	-8.0096
5	110	-0.02731	-0.01020	0.00336	73.8846	16.3921	4.3499
6	304	-0.37656	0.00000	0.08954	37.5785	33.2766	7.5321
7	305	-0.08950	-0.02686	0.02574	84.5469	14.0516	-64.1955
8	307	0.32353	-0.10992	-0.05074	16.6110	-18.0091	-73.1811
9	309	-0.19641	0.18618	0.00274	44.8676	2.5282	-46.5193
10	310	-0.03048	0.02529	-0.00636	93.4204	-21.5128	-115.1303
11	477	-0.23884	-0.00001	0.03189	51.8455	46.9367	3.7176
12	478	-0.12294	0.00042	0.02282	51.1014	32.5121	-13.6683
13	480	0.11296	-0.05537	-0.00322	6.5764	-13.0025	-34.0647
14	482	0.00647	0.01138	-0.00982	8.0518	-11.4269	-33.7257
15	603	-0.08601	-0.00001	0.01029	25.5985	13.6081	-5.3978
16	604	-0.05589	-0.00088	0.01173	27.2285	3.5927	-2.3343
17	606	0.00187	-0.01355	0.00246	14.8558	4.6081	-5.5161
18	645	-0.02839	0.00000	0.01784	15.8201	-15.1948	-17.6445
19	646	-0.02028	-0.00618	0.01500	16.9352	-4.8982	-16.0569
20	647	-0.01526	-0.00821	0.01323	21.0433	-8.6341	-12.0216

Table 11: Results for Eigenvector 6: Full Reservoir

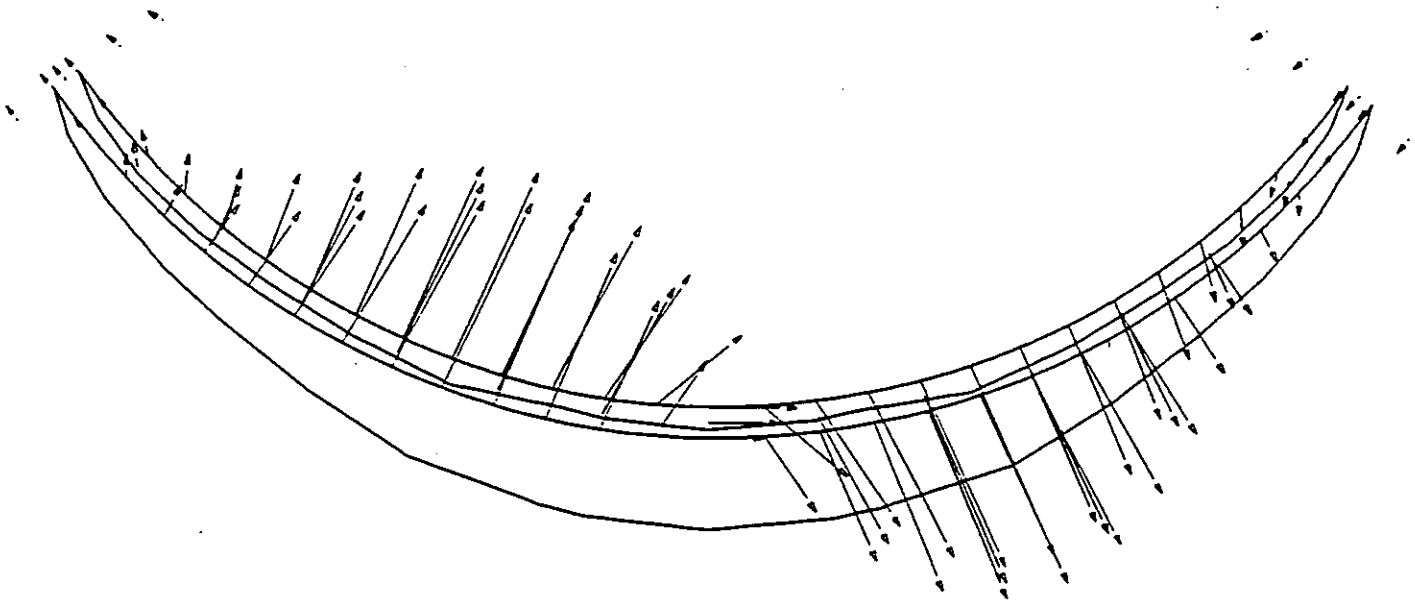

Displaced Section

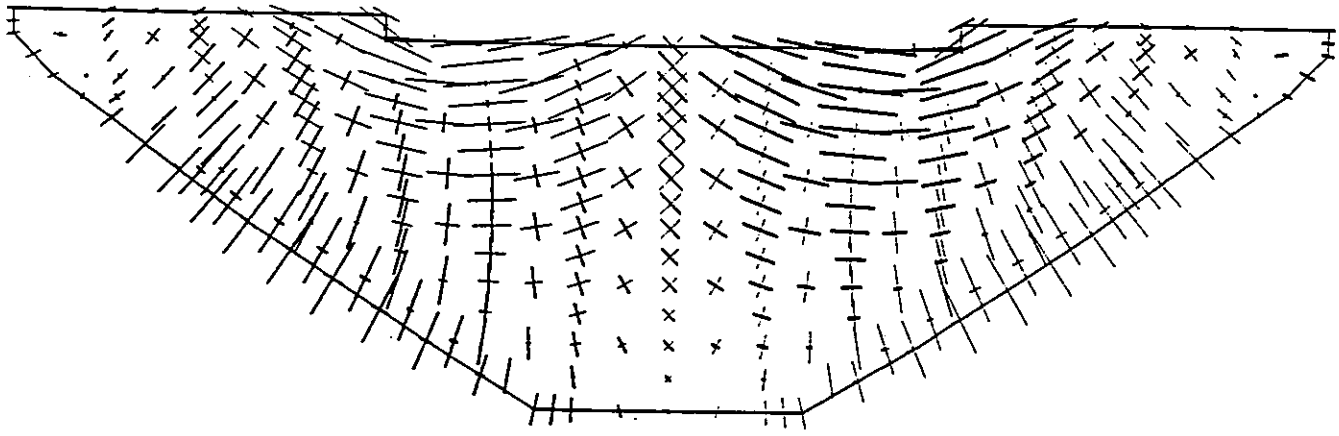

Principal Stress : Upstream Face

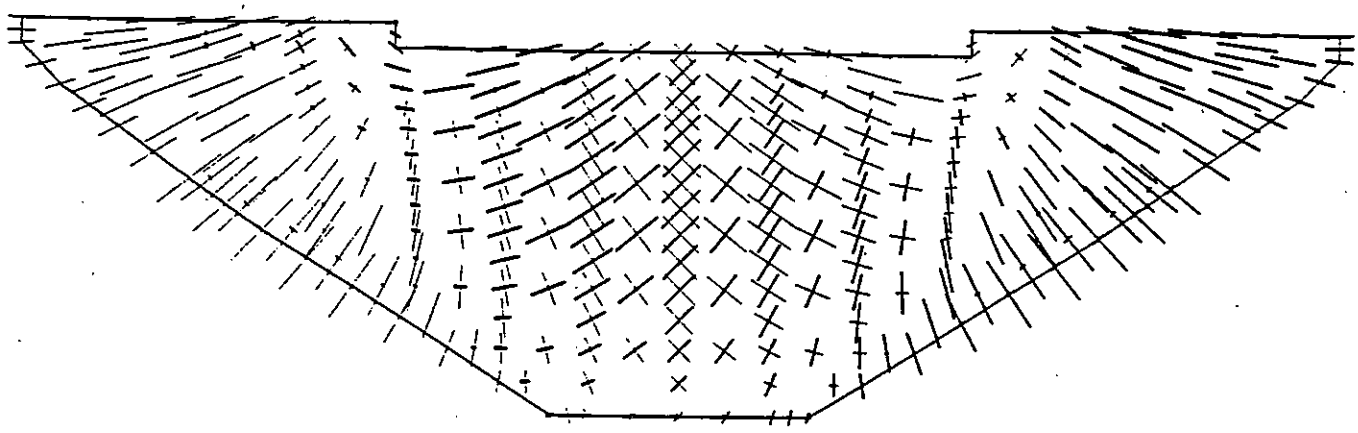

Principal Stress : Downstream Face

Figure 4: Results for Mode Shape 1 : Full Reservoir

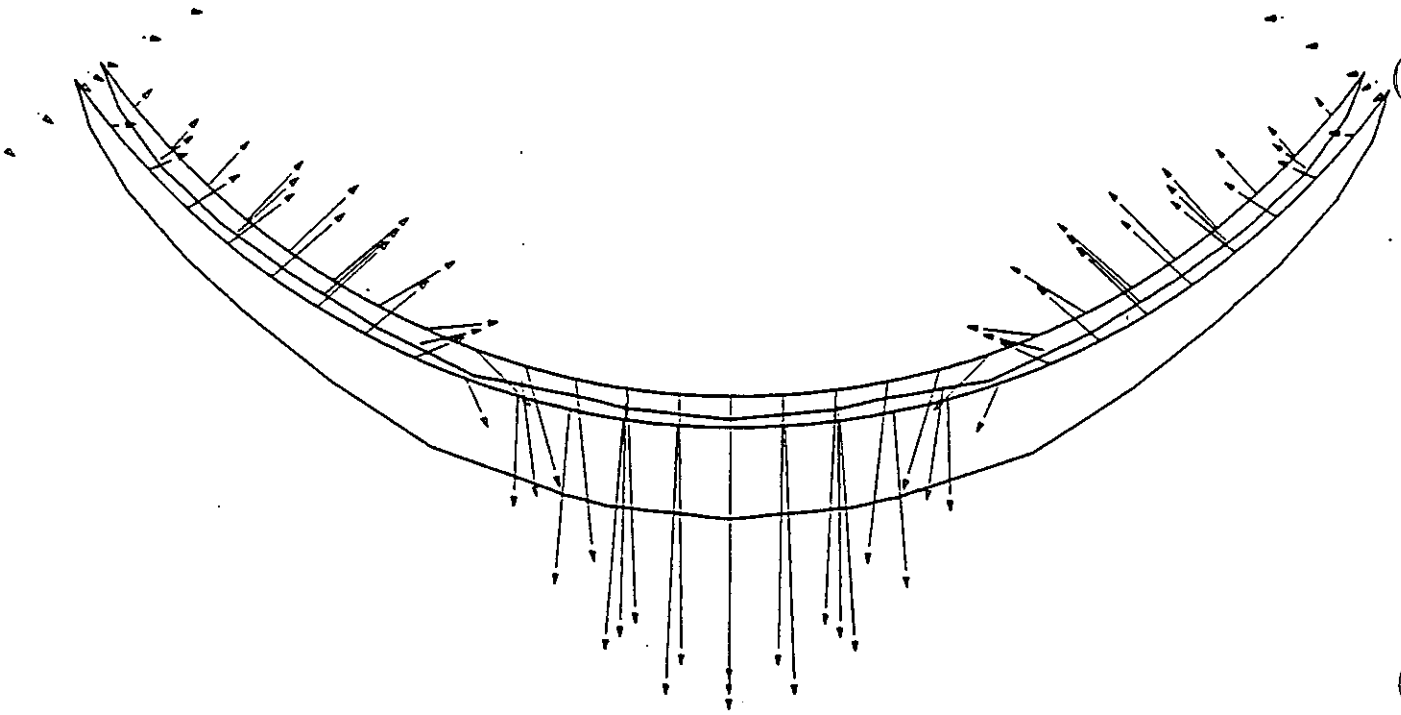

Displaced Section

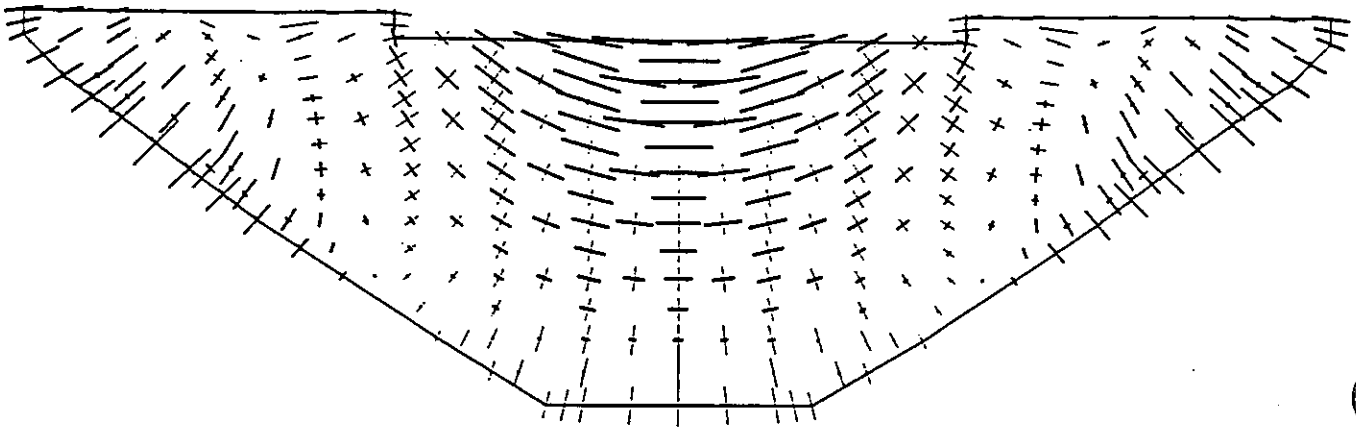

Principal Stress : Upstream Face

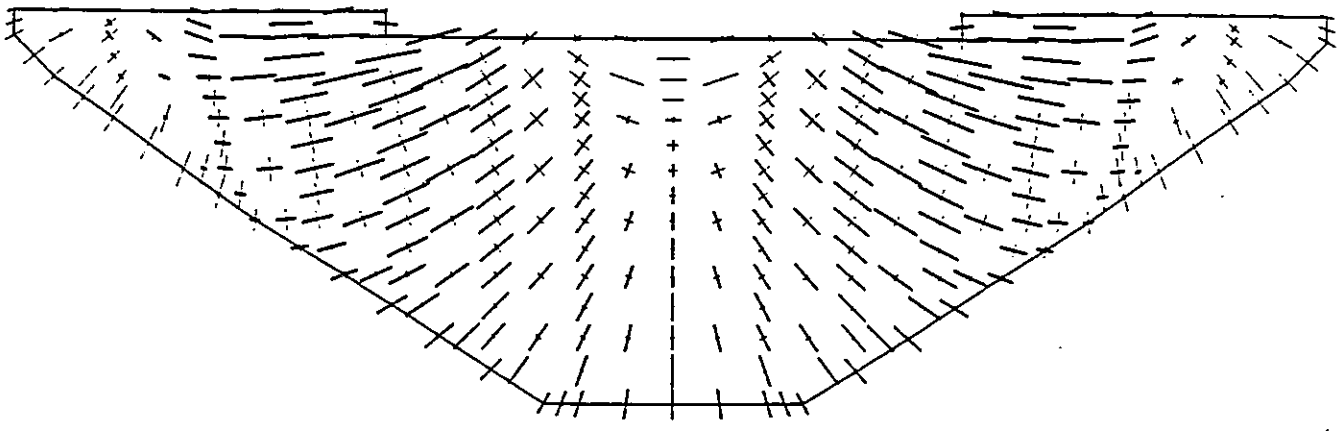

Principal Stress : Downstream Face

Figure 5: Results for Mode Shape 2 : Full Reservoir

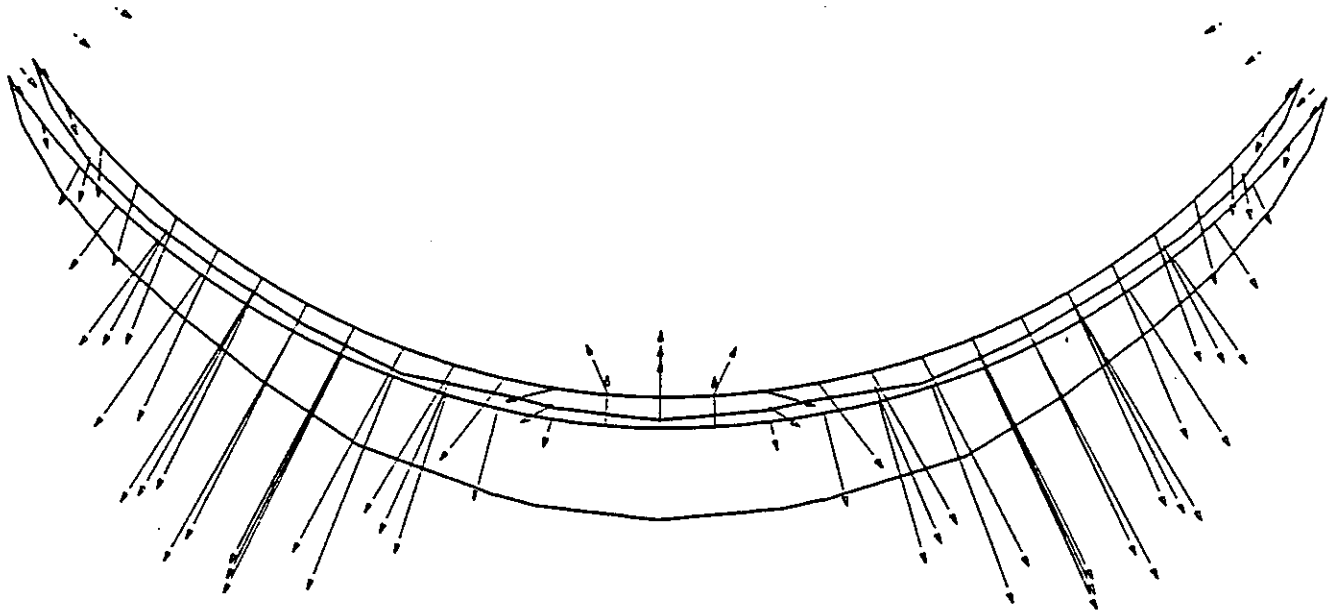

Displaced Section

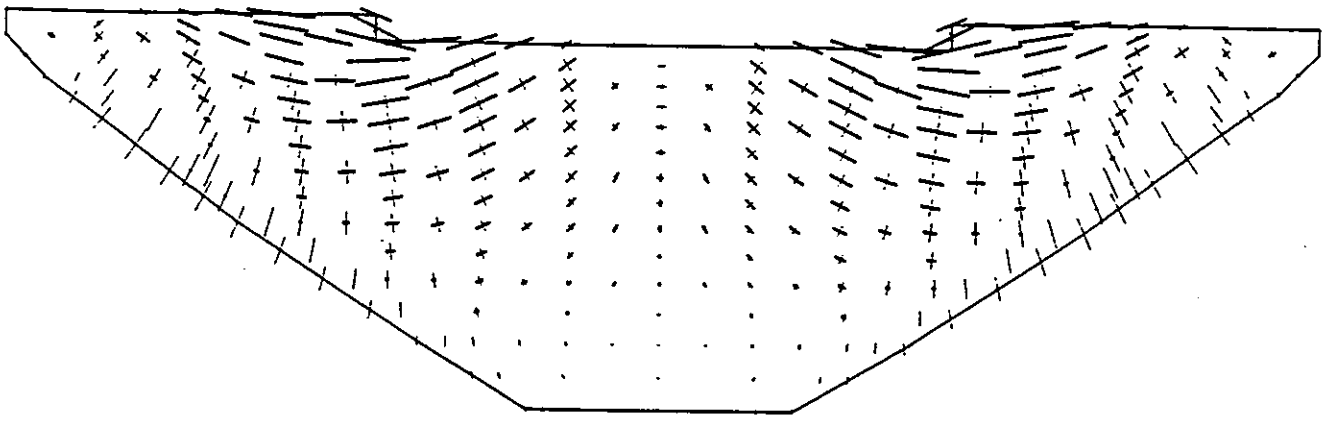

Principal Stress : Upstream Face

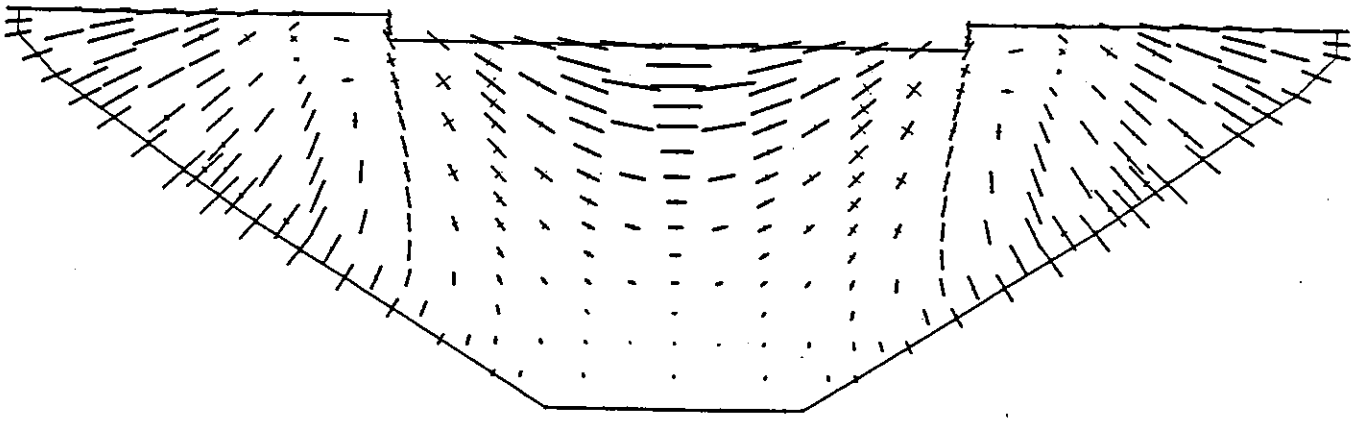

Principal Stress : Downstream Face

Figure 6: Results for Mode Shape 3 : Full Reservoir

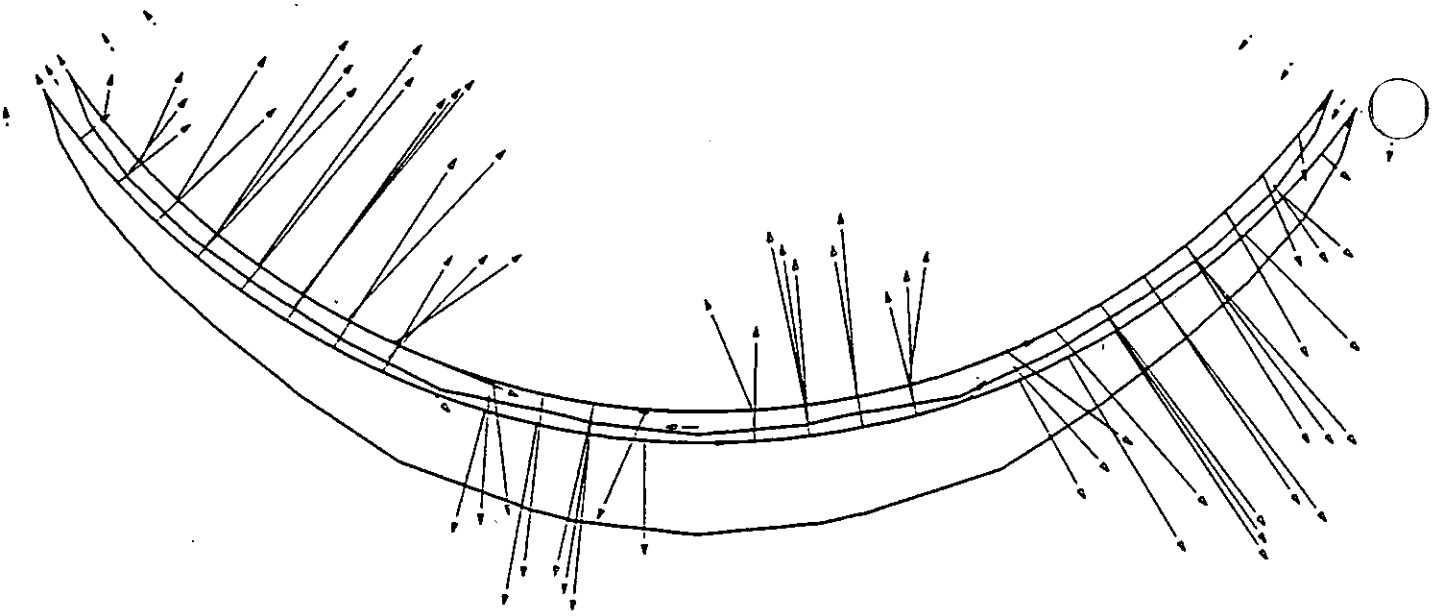

Displaced Section

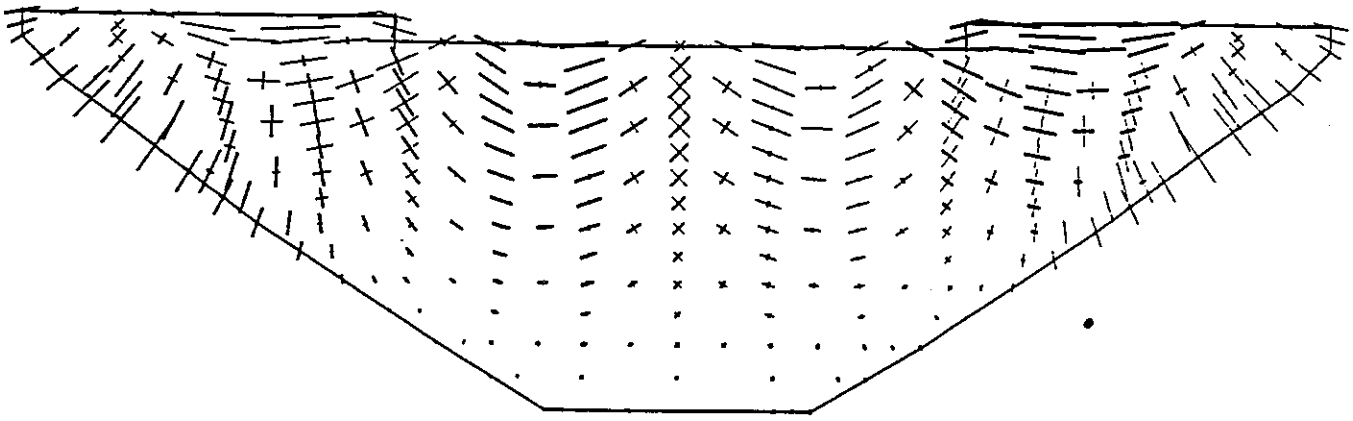

Principal Stress : Upstream Face

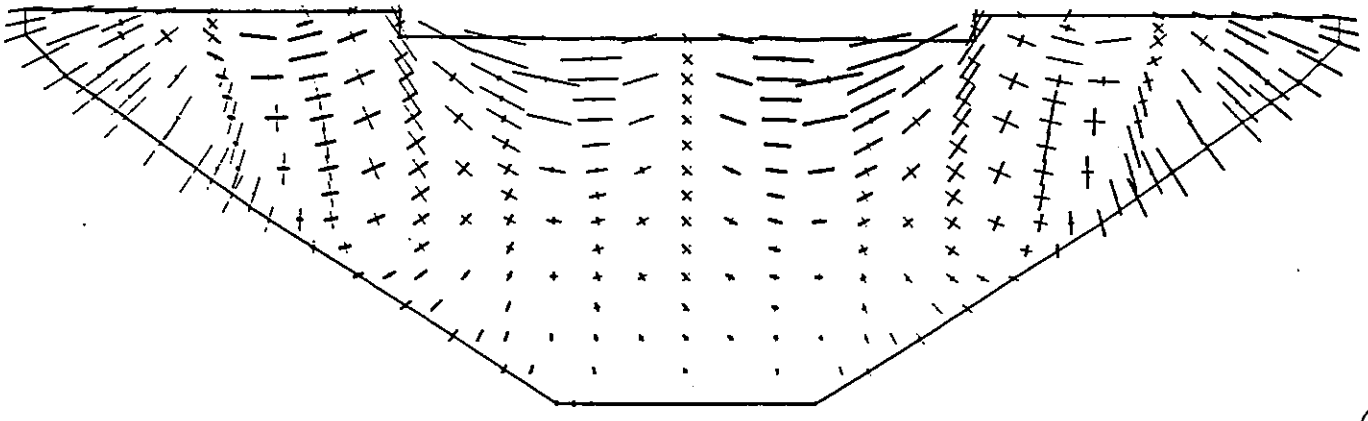

Principal Stress : Downstream Face

Figure 7: Results for Mode Shape 4 : Full Reservoir

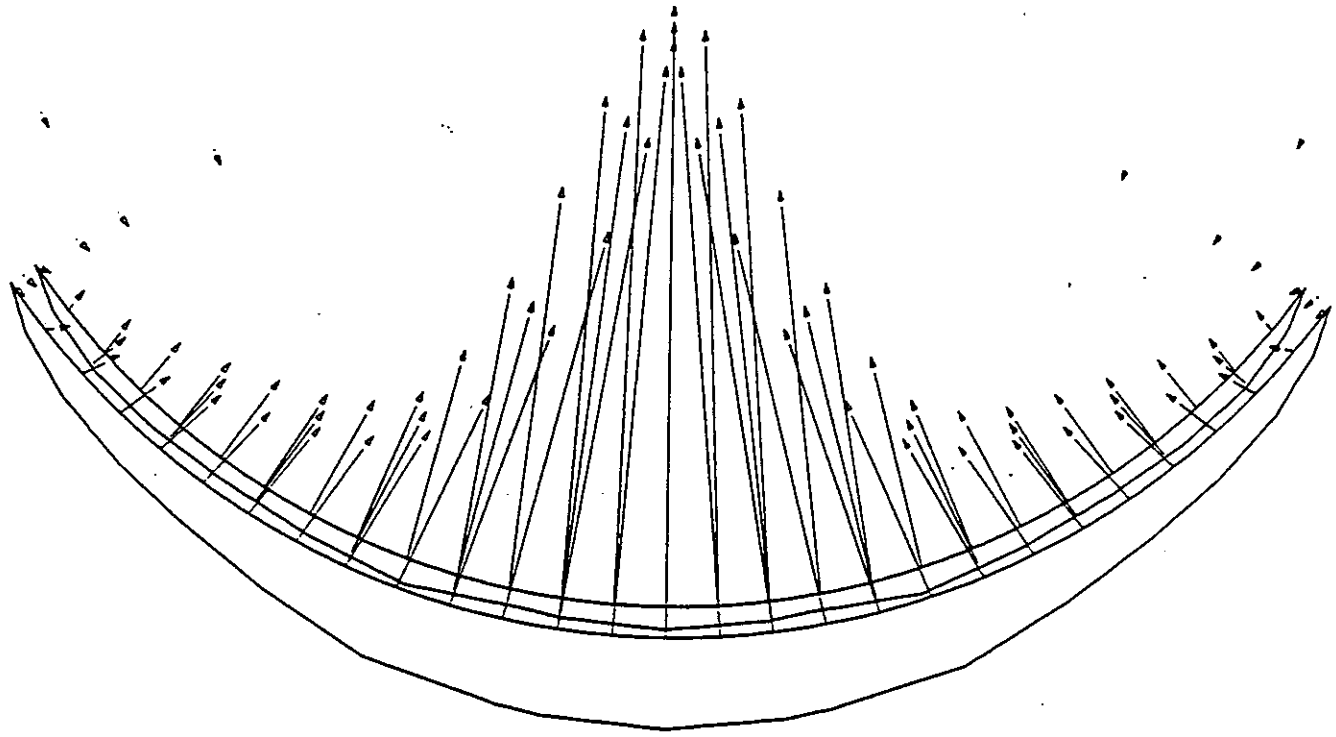

Displaced Section

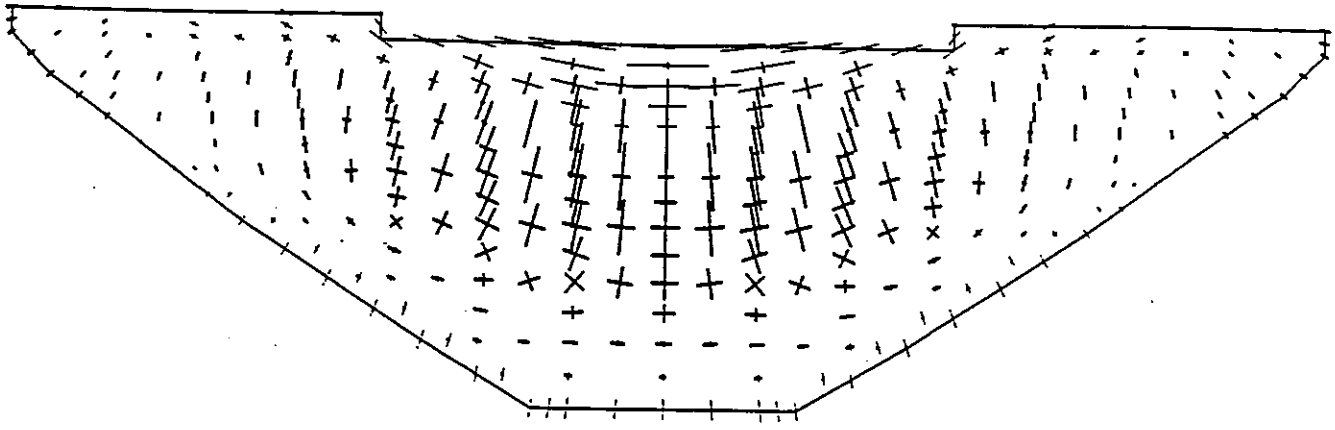

Principal Stress : Upstream Face

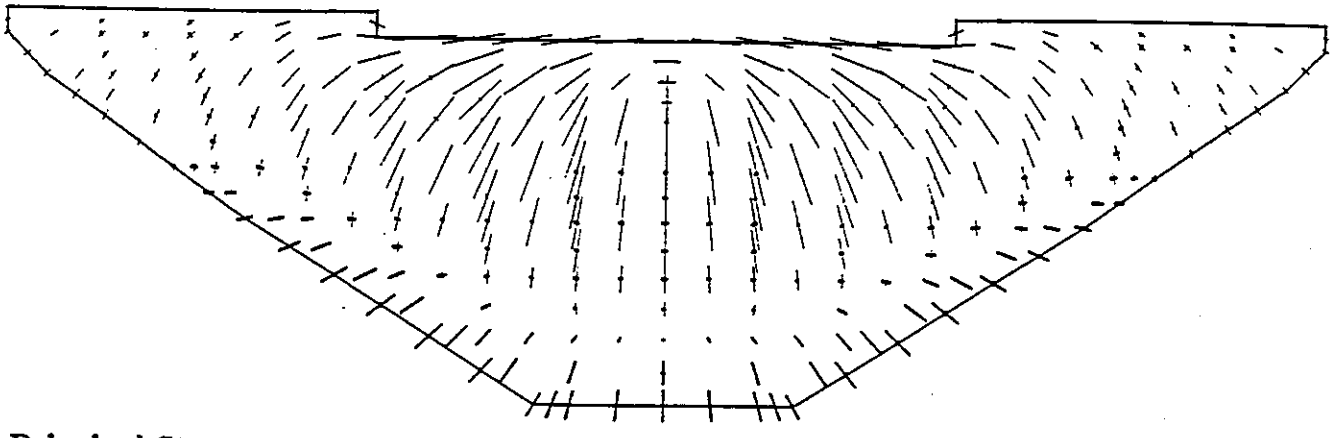

Principal Stress : Downstream Face

Figure 8: Results for Mode Shape 5 : Full Reservoir

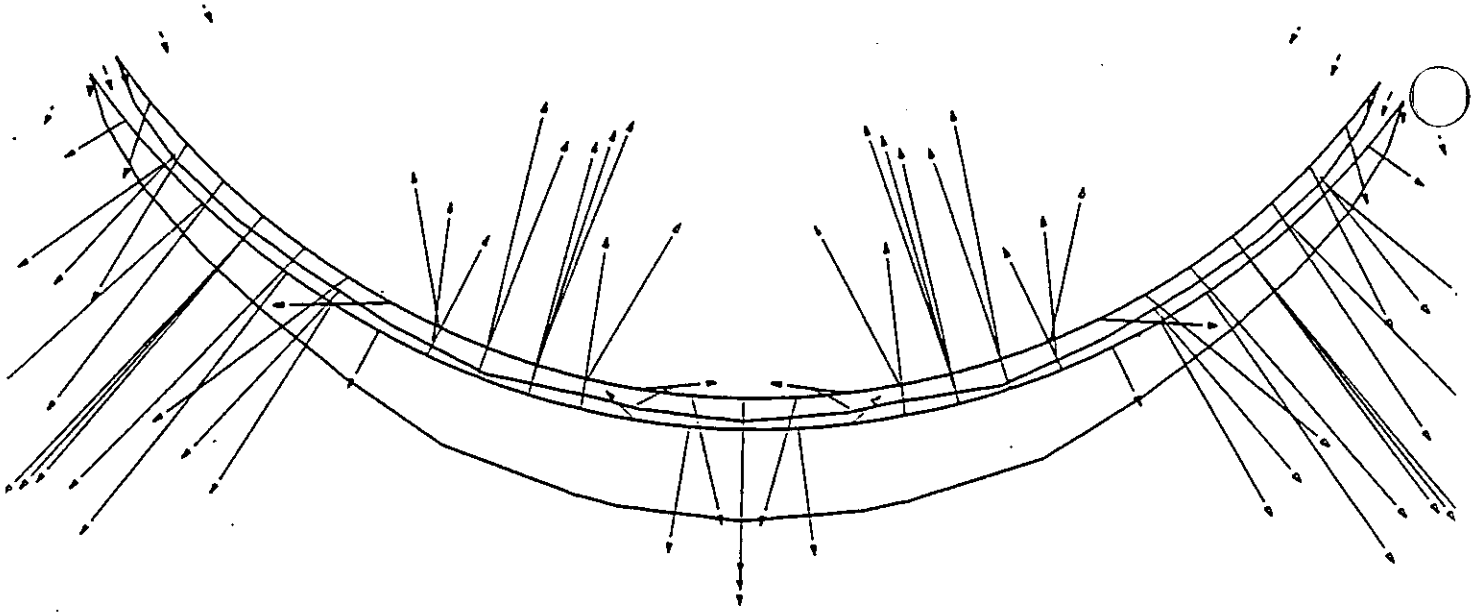

Displaced Section

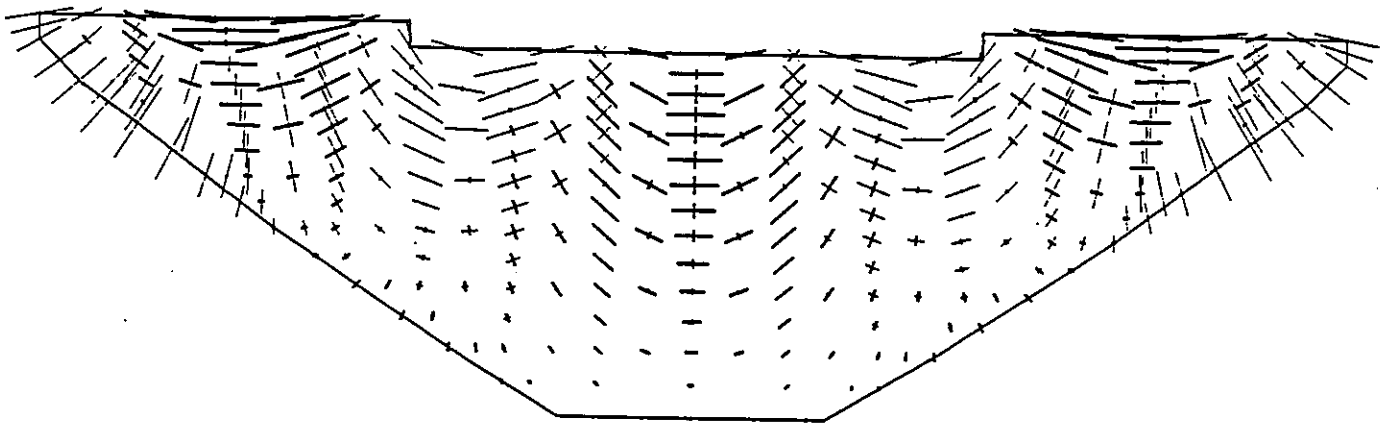

Principal Stress : Upstream Face

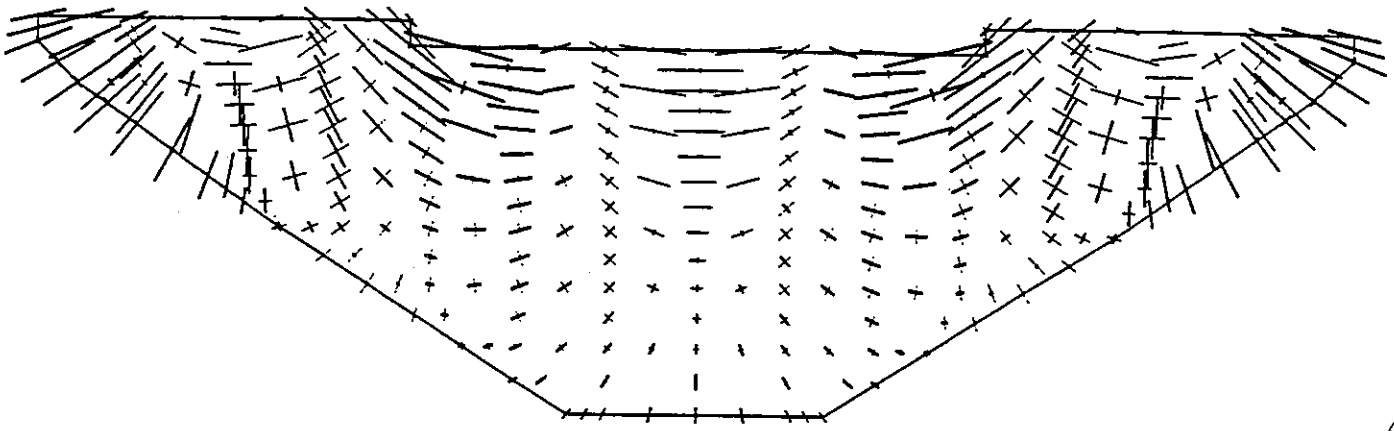

Principal Stress : Downstream Face

Figure 9: Results for Mode Shape 6 : Full Reservoir

Loc Num	Node Num	δ_x	δ_y	δ_z	P_1	P_2	P_3
1	103	0.00000	-0.25994	0.00000	71.5550	0.0000	-71.5551
2	104	0.67723	-0.31745	-0.17379	26.3726	-3.1049	-101.0229
3	106	0.86045	-0.41558	-0.20356	4.8011	-15.8966	-120.5585
4	108	0.16483	-0.07693	-0.02548	3.8923	-1.9712	-71.6236
5	110	0.00000	0.00000	0.00000	4.7555	-5.2613	-31.0622
6	304	0.00000	-0.17252	0.00000	27.4548	0.0000	-27.4549
7	305	0.37115	-0.20145	-0.06146	10.0642	2.4122	-43.9384
8	307	0.44994	-0.23162	-0.04944	17.9313	-13.6309	-53.3000
9	309	0.05953	-0.03475	0.00411	22.3829	0.8460	-14.9879
10	310	0.00000	0.00000	0.00000	9.6548	0.1399	-26.6343
11	477	0.00000	-0.06851	0.00000	27.7622	0.0000	-27.7622
12	478	0.12843	-0.07935	0.00551	25.6868	1.6247	-27.0249
13	480	0.10442	-0.06470	0.01317	32.1989	2.2046	-16.7036
14	482	0.00000	0.00000	0.00000	12.8492	-0.5689	-15.0482
15	603	0.00000	-0.01365	0.00000	16.1553	0.0000	-16.1553
16	604	0.01455	-0.01361	0.00546	25.3482	-0.4657	-5.7506
17	606	0.00000	0.00000	0.00000	20.0094	3.9411	0.9905
18	645	0.00000	0.00000	0.00000	11.5180	0.0000	-11.5181
19	646	0.00000	0.00000	0.00000	15.1842	2.5698	-2.3351
20	647	0.00000	0.00000	0.00000	9.4747	1.3071	-2.9390

Table 13: Results for Eigenvector 1: Empty Reservoir/Fixed Foundation

Loc Num	Node Num	δ_x	δ_y	δ_z	P_1	P_2	P_3
1	103	-0.99937	0.00000	0.23584	128.2272	1.9262	0.3425
2	104	-0.78829	0.02887	0.17710	120.0602	-0.1556	-13.2371
3	106	0.10125	-0.15358	-0.05232	34.1621	-2.6796	-20.4684
4	108	0.14188	-0.13009	-0.04208	13.3509	-0.3322	-11.2863
5	110	0.00000	0.00000	0.00000	7.8817	0.6321	-4.7211
6	304	-0.57758	0.00000	0.08517	70.5015	10.5311	-10.3752
7	305	-0.46404	0.01644	0.06233	65.7481	6.5801	-9.0632
8	307	0.00849	-0.06997	-0.01358	29.0442	-0.3239	-4.8838
9	309	0.03957	-0.04929	-0.00248	40.3137	0.6010	-4.9095
10	310	0.00000	0.00000	0.00000	38.4032	7.0597	-4.6212
11	477	-0.21426	0.00000	-0.01132	31.5824	1.7132	-14.9880
12	478	-0.17114	0.00903	-0.01105	31.6476	-0.7454	-13.0218
13	480	-0.00850	-0.01847	-0.00296	28.4006	-0.6259	-9.5985
14	482	0.00000	0.00000	0.00000	32.0801	4.7640	-4.4701
15	603	-0.02852	0.00000	-0.00947	1.4750	-0.2554	-20.8926
16	604	-0.02038	0.00040	-0.00695	3.6106	-1.1097	-15.2828
17	606	0.00000	0.00000	0.00000	18.8102	3.1257	-3.7572
18	645	0.00000	0.00000	0.00000	-2.5606	-3.5424	-15.1514
19	646	0.00000	0.00000	0.00000	-2.1964	-2.6105	-10.8561
20	647	0.00000	0.00000	0.00000	0.3252	-1.1464	-6.0572

Table 14: Results for Eigenvector 2: Empty Reservoir/Fixed Foundation

Loc Num	Node Num	δ_x	δ_y	δ_z	P_1	P_2	P_3
1	103	-0.07671	0.00000	0.01414	132.9942	7.7035	-3.1530
2	104	-0.25839	0.08459	0.06683	164.5608	9.0863	-11.8972
3	106	-0.82415	0.40961	0.22608	219.5282	27.6204	-1.4085
4	108	-0.28625	0.16907	0.06118	100.2532	5.4850	-7.1429
5	110	0.00000	0.00000	0.00000	41.2760	6.7196	-7.6779
6	304	-0.03321	0.00000	0.00782	63.6097	4.0057	-4.3869
7	305	-0.11596	0.04017	0.02410	70.2924	0.6987	-3.4921
8	307	-0.34653	0.16268	0.05021	75.4869	9.4896	-9.3085
9	309	-0.08614	0.05270	-0.00182	31.6511	-2.8605	-28.6333
10	310	0.00000	0.00000	0.00000	26.7019	2.5017	-16.4086
11	477	-0.00561	0.00000	0.00192	10.2488	3.7100	-1.7393
12	478	-0.02633	0.00774	0.00119	13.0486	0.3495	-2.2945
13	480	-0.05774	0.02634	-0.00502	16.3746	-2.6714	-10.0637
14	482	0.00000	0.00000	0.00000	27.3277	3.5237	-6.9393
15	603	0.00139	0.00000	0.00057	2.7897	-0.7321	-1.1825
16	604	-0.00049	-0.00010	-0.00016	1.3990	-0.2334	-2.0725
17	606	0.00000	0.00000	0.00000	5.1829	1.2975	-3.3131
18	645	0.00000	0.00000	0.00000	2.4907	0.3146	-0.9177
19	646	0.00000	0.00000	0.00000	2.5638	0.0884	-2.1218
20	647	0.00000	0.00000	0.00000	4.4718	0.5016	-1.9639

Table 15: Results for Eigenvector 3: Empty Reservoir/Fixed Foundation

Loc Num	Node Num	δ_x	δ_y	δ_z	P_1	P_2	P_3
1	103	0.00000	-0.07519	0.00000	124.4473	0.0000	-124.4473
2	104	0.64862	-0.11451	-0.17898	29.9652	14.8936	-60.7355
3	106	-0.39355	0.32902	0.15157	280.9202	27.8765	-33.1222
4	108	-0.55772	0.42981	0.15233	118.3921	7.5043	-17.6643
5	110	0.00000	0.00000	0.00000	43.2845	5.9479	-13.5451
6	304	0.00000	-0.04217	0.00000	54.9366	0.0000	-54.9366
7	305	0.34902	-0.06356	-0.06666	30.6429	-16.5744	-45.3476
8	307	-0.03533	0.07577	0.01710	41.4519	-8.3946	-26.4205
9	309	-0.14149	0.12421	0.00554	38.4709	-7.9954	-66.7457
10	310	0.00000	0.00000	0.00000	41.7607	-13.7405	-84.6816
11	477	0.00000	-0.01168	0.00000	17.1225	0.0000	-17.1225
12	478	0.10991	-0.02206	-0.00003	9.8843	-4.4392	-18.7878
13	480	0.02430	0.00165	0.00061	3.2514	-0.3258	-24.9223
14	482	0.00000	0.00000	0.00000	5.4143	-2.0822	-23.1225
15	603	0.00000	-0.00134	0.00000	0.9753	0.0000	-0.9753
16	604	0.01224	-0.00262	0.00262	5.6152	0.5836	-2.7967
17	606	0.00000	0.00000	0.00000	4.6755	-2.3012	-16.4299
18	645	0.00000	0.00000	0.00000	0.9821	0.0000	-0.9821
19	646	0.00000	0.00000	0.00000	2.3502	0.5782	0.5406
20	647	0.00000	0.00000	0.00000	2.0929	-0.1450	-2.8179

Table 16: Results for Eigenvector 4: Empty Reservoir/Fixed Foundation

Loc Num	Node Num	δ_x	δ_y	δ_z	P_1	P_2	P_3
1	103	-1.00000	0.00000	0.38625	154.3503	6.6934	-18.0642
2	104	-0.33342	-0.01172	0.17777	229.8045	2.9135	-161.9814
3	106	0.30311	-0.01460	-0.01251	261.4821	31.6186	-62.4052
4	108	-0.68177	0.58016	0.21162	118.0260	15.6750	-16.9525
5	110	0.00000	0.00000	0.00000	30.5674	6.0501	-0.3169
6	304	-0.37053	0.00000	0.14924	45.4396	34.8470	-9.5711
7	305	-0.06323	-0.02843	0.07250	66.9737	24.9012	-67.4039
8	307	0.33541	-0.11377	-0.02796	29.4959	-26.0712	-79.7358
9	309	-0.13142	0.13017	0.01203	43.3429	-10.9374	-69.0369
10	310	0.00000	0.00000	0.00000	87.7138	-20.1357	-161.2048
11	477	-0.01512	0.00000	0.02595	16.4815	-0.8402	-10.1853
12	478	0.05647	-0.01702	0.02118	20.2631	6.0372	-28.3287
13	480	0.10820	-0.04613	0.00962	22.4591	-5.0844	-43.1859
14	482	0.00000	0.00000	0.00000	6.7762	-9.4743	-38.8659
15	603	0.00976	0.00000	0.00705	19.3824	-1.8338	-2.3808
16	604	0.01391	-0.00299	0.00732	19.8298	-0.1974	-3.1614
17	606	0.00000	0.00000	0.00000	11.2458	1.1774	-10.7457
18	645	0.00000	0.00000	0.00000	17.3782	3.9141	2.1922
19	646	0.00000	0.00000	0.00000	14.5790	3.6158	3.4999
20	647	0.00000	0.00000	0.00000	8.3285	0.8940	-3.8584

Table 17: Results for Eigenvector 5: Empty Reservoir/Fixed Foundation

Loc Num	Node Num	δ_x	δ_y	δ_z	P_1	P_2	P_3
1	103	-0.99363	0.00000	0.60349	441.2479	55.4943	-9.8523
2	104	-0.96318	0.17696	0.56462	384.4729	46.3695	-9.8039
3	106	-0.21091	0.11423	0.17367	59.2878	-6.4218	-90.3069
4	108	0.25932	-0.17122	-0.05211	5.7711	-3.1589	-85.5200
5	110	0.00000	0.00000	0.00000	-1.8966	-7.5051	-35.6289
6	304	0.26412	0.00000	0.14780	25.3060	-33.1325	-48.9333
7	305	0.18866	-0.00328	0.14655	33.6669	6.3053	-82.6039
8	307	0.06750	-0.00837	0.06960	46.5998	-2.0962	-56.5511
9	309	0.07479	-0.04758	0.00691	38.6429	-2.0546	-38.7403
10	310	0.00000	0.00000	0.00000	42.5516	5.4865	-40.4963
11	477	0.57499	0.00000	0.03175	27.1279	-67.3081	-157.6509
12	478	0.48309	-0.05288	0.03559	31.8894	-53.6916	-143.5607
13	480	0.10596	-0.02555	0.03056	54.7568	-11.5155	-59.0253
14	482	0.00000	0.00000	0.00000	29.7102	1.5352	-22.5474
15	603	0.12849	0.00000	0.02504	71.1339	-22.2067	-42.5225
16	604	0.09839	-0.00788	0.02044	55.9530	-9.0798	-44.4249
17	606	0.00000	0.00000	0.00000	28.9513	-7.0569	-66.3474
18	645	0.00000	0.00000	0.00000	60.0069	6.5132	-27.4411
19	646	0.00000	0.00000	0.00000	38.7698	5.5830	-10.8546
20	647	0.00000	0.00000	0.00000	11.5115	-0.6375	-14.6991

Table 18: Results for Eigenvector 6: Empty Reservoir/Fixed Foundation

STATIC AND VIBRATION FINITE ELEMENT ANALYSIS OF TALVACCHIA DAM

J. Miquel *
J. Buil **
*S. Botello**
*E. Oñate**

* *E.T.S. Ingenieros de Caminos, Canales y Puertos*
Universidad Politécnica de Cataluña
c/ Gran Capitán s/n, 08034 Barcelona, Spain

** *ENHER, Barcelona*

SUMMARY

This paper presents the numerical results obtained in the finite element analysis of Talvacchia dam. The analysis conditions have been the following:

Static analysis:
a) Dead weight
b) Hydrostatic loading

Vibration analysis:
a) Empty reservoir with rigid foundation
b) Full reservoir with flexible foundation

20 node solid isoparametric finite elements have been used in the analysis. Fluid-structure interaction effects have been taken into account in the dynamic case.

1. STATIC ANALYSIS

Figures 1 and 2 show the geometry of the dam and the discretization in 244 twenty node solid isoparametric elements. Note that the dam thickhess has been discretized with a single element as specified. The flexibility of the foundation has been included in the analysis although the soil weight has been neglected as its deformation is considered prior to the actual construction of the dam. The loading conditions have been: a) the dam self weight and b) hydrostatic pressure.

The global stiffness equations $\mathbf{Ka} = \mathbf{f}$ [1] have been solved using a skyline method. This simplifies the solution of the equation system using the standard decomposition

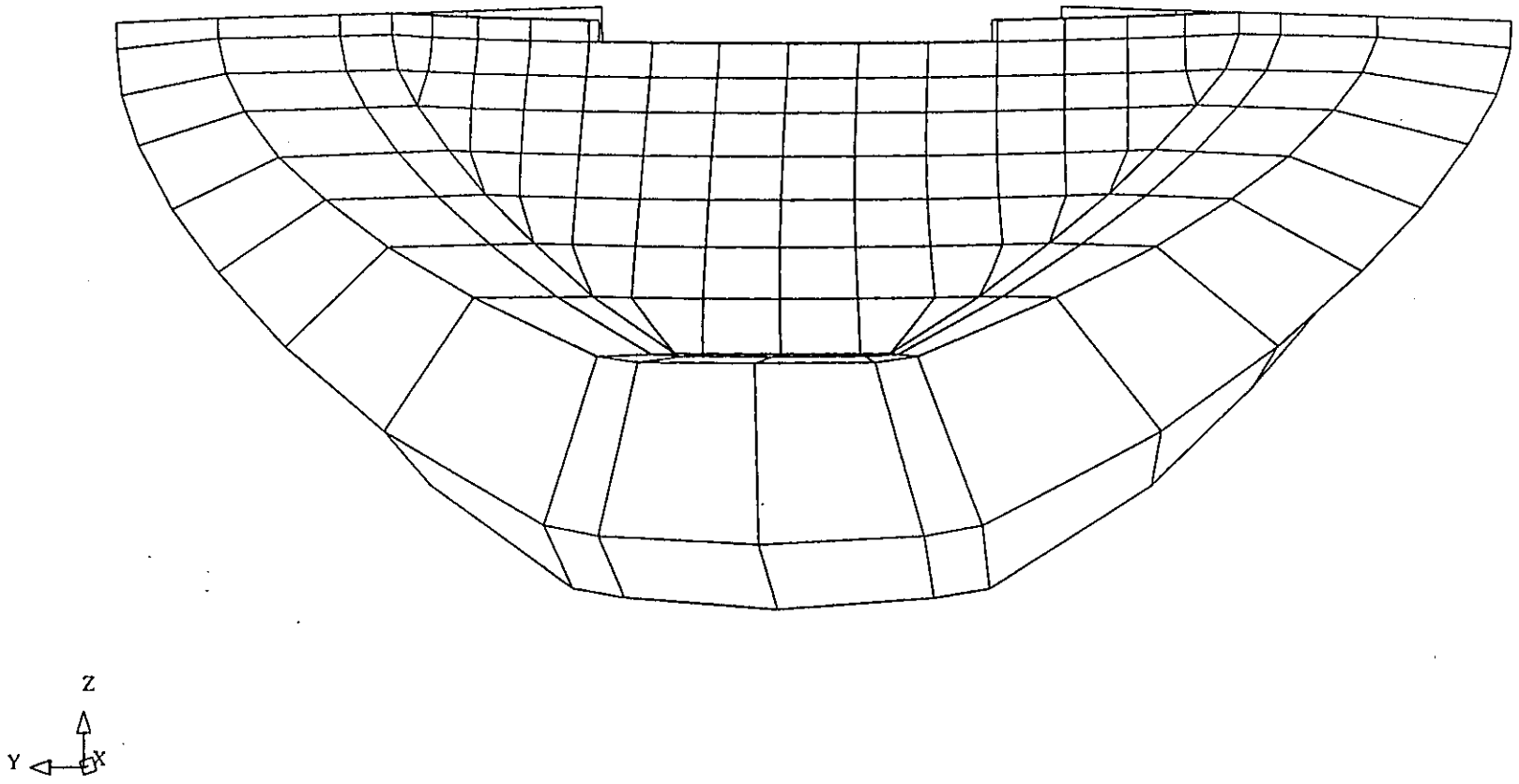

Figure 1. Talvacchia dam. Discretization of dam and foundation with 244 twenty node solid isoparametric elements.

TALVACCHIA Dam

STATIC RESULTS

Reference figure

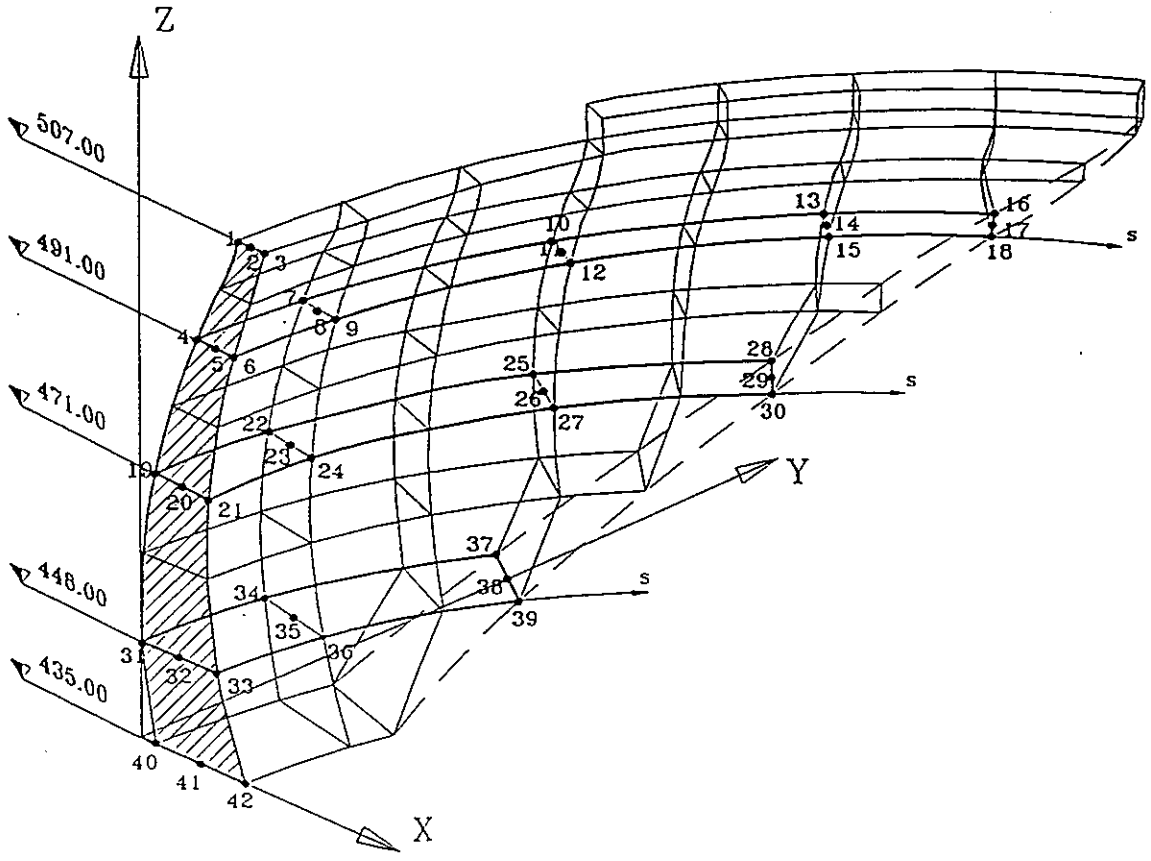

Figure 2

LOADING CONDITION 3.1

DEAD WEIGHT

POINT	S (m)	DISPX (m)	DISPY (m)	DISPZ (m)	P1 (Mpa)	P2 (Mpa)	P3 (Mpa)
1	0.00	0.8020E-03	-0.4098E-06	-0.2919E-02	0.0182	-0.0246	-0.9884
2	0.00	0.8166E-03	-0.5521E-06	-0.3129E-02	0.0177	-0.0242	-1.0098
3	0.00	0.8319E-03	-0.6955E-06	-0.3338E-02	0.0172	-0.0238	-1.0313
4	0.00	-0.5766E-03	-0.1004E-06	-0.2365E-02	0.0934	-0.0111	-0.4296
5	0.00	-0.5678E-03	-0.2368E-06	-0.2595E-02	0.1630	-0.0172	-0.5368
6	0.00	-0.5555E-03	-0.3804E-06	-0.2843E-02	0.2363	-0.0220	-0.6491
7	16.00	-0.5359E-03	-0.1418E-03	-0.2276E-02	0.1069	-0.0326	-0.4033
8	16.00	-0.5297E-03	-0.1567E-03	-0.2507E-02	0.1893	-0.0530	-0.5177
9	16.00	-0.5195E-03	-0.1727E-03	-0.2756E-02	0.2743	-0.0692	-0.6389
10	48.00	-0.2108E-03	-0.4088E-03	-0.1669E-02	0.1529	0.0566	-0.2968
11	48.00	-0.2208E-03	-0.4406E-03	-0.1899E-02	0.3151	0.0111	-0.4628
12	48.00	-0.2239E-03	-0.4754E-03	-0.2158E-02	0.4777	-0.0206	-0.6431
13	80.00	-0.6592E-04	-0.4712E-03	-0.8236E-03	0.2767	0.1370	-0.1929
14	80.00	-0.4755E-04	-0.4422E-03	-0.9810E-03	0.4676	0.1336	-0.4050
15	80.00	-0.1868E-04	-0.4211E-03	-0.1159E-02	0.6587	0.1335	-0.6205
16	99.20	-0.1434E-03	-0.1738E-03	-0.3817E-03	0.3458	0.1674	-0.1848
17	99.20	-0.1332E-03	-0.1416E-03	-0.4522E-03	0.4891	0.1825	-0.3997
18	99.20	-0.1081E-03	-0.1117E-03	-0.4950E-03	0.6438	0.1865	-0.6147
19	0.00	-0.1335E-02	0.1658E-06	-0.2128E-02	0.3620	0.0007	-0.2610
20	0.00	-0.1337E-02	0.5821E-07	-0.2133E-02	0.5202	0.0003	-0.4915
21	0.00	-0.1319E-02	-0.5544E-07	-0.2159E-02	0.6837	-0.0001	-0.7271
22	16.00	-0.1238E-02	0.1077E-03	-0.2063E-02	0.3868	0.0267	-0.2754
23	16.00	-0.1247E-02	0.6655E-04	-0.2061E-02	0.5440	0.0144	-0.5019
24	16.00	-0.8420E-04	0.1001E-03	-0.6994E-03	0.5354	-0.1242	-0.4647
25	48.00	-0.5717E-03	0.1076E-03	-0.1571E-02	0.5240	0.0851	-0.4362
26	48.00	-0.6137E-03	0.2540E-04	-0.1538E-02	0.6547	0.0789	-0.5924
27	48.00	-0.6417E-03	-0.7080E-04	-0.1470E-02	0.7878	0.0716	-0.7499
28	75.00	-0.6471E-04	-0.7255E-04	-0.7915E-03	0.6016	0.1220	-0.5814
29	75.00	-0.9802E-04	-0.9259E-04	-0.8327E-03	0.6539	0.1534	-0.6338
30	75.00	-0.1314E-03	-0.9982E-04	-0.7394E-03	0.7244	0.1681	-0.6876
31	0.00	-0.6267E-03	0.2580E-06	-0.2038E-02	0.7483	0:0000	-0.7740
32	0.00	-0.6111E-03	0.1871E-06	-0.1704E-02	0.7209	0.0000	-0.7930
33	0.00	-0.5893E-03	0.1317E-06	-0.1400E-02	0.6943	0.0000	-0.8129
34	16.00	-0.5198E-03	0.1178E-03	-0.1914E-02	0.7619	0.0141	-0.7869
35	16.00	-0.5163E-03	0.5318E-04	-0.1622E-02	0.7257	0.0137	-0.7957
36	16.00	-0.5053E-03	-0.9385E-05	-0.1329E-02	0.6919	0.0112	-0.8047
37	41.50	0.2225E-05	0.5752E-04	-0.1177E-02	0.8460	0.0476	-0.9934
38	41.50	-0.5284E-04	-0.2123E-04	-0.1163E-02	0.7512	0.0842	-0.8757
39	41.50	-0.1158E-03	-0.6602E-04	-0.9286E-03	0.6743	0.1038	-0.7590
40	0.00	0.7032E-05	0.2020E-06	-0.1456E-02	0.9031	-0.0016	-1.2426
41	0.00	0.1002E-05	0.1906E-06	-0.1292E-02	0.6927	0.0000	-1.0262
42	0.00	-0.5245E-04	0.1471E-06	-0.9582E-03	0.4957	-0.0025	-0.8193

Table I

LOADING CONDITION 3.2

HYDROSTATIC PRESSURE

POINT	S (m)	DISPX (m)	DISPY (m)	DISPZ (m)	P1 (Mpa)	P2 (Mpa)	P3 (Mpa)
1	0.00	0.2205E-01	0.2008E-07	-0.7515E-03	0.0411	-0.1000	-2.2216
2	0.00	0.2208E-01	0.2343E-07	-0.1057E-02	0.0254	-0.0716	-1.8340
3	0.00	0.2209E-01	0.2683E-07	-0.1372E-02	0.0109	-0.0410	-1.4499
4	0.00	0.1968E-01	0.1664E-07	0.3073E-03	0.1630	-0.2860	-3.3036
5	0.00	0.1973E-01	0.1851E-07	-0.3446E-03	0.0576	-0.1819	-2.7683
6	0.00	0.1976E-01	0.2062E-07	-0.9232E-03	0.0036	-0.0526	-2.3097
7	16.00	0.1803E-01	-0.1627E-02	0.3578E-03	-0.0879	-0.5808	-3.1592
8	16.00	0.1815E-01	-0.1103E-02	-0.2428E-03	-0.1514	-0.4585	-2.6946
9	16.00	0.1826E-01	-0.5610E-03	-0.7708E-03	-0.1048	-0.3602	-2.3163
10	48.00	0.8420E-02	-0.1722E-02	0.4589E-03	-0.4299	-0.9321	-2.1122
11	48.00	0.8829E-02	-0.8764E-03	0.1774E-03	-0.5288	-0.9096	-2.0206
12	48.00	0.9245E-02	-0.8374E-05	-0.3917E-04	-0.4153	-0.9281	-2.1006
13	80.00	0.1607E-02	0.7812E-03	0.3683E-04	-0.5490	-0.6092	-1.1270
14	80.00	0.1790E-02	0.9782E-03	0.9507E-04	-0.5238	-0.9136	-1.1529
15	80.00	0.1989E-02	0.1191E-02	0.1754E-03	-0.3993	-1.0855	-1.4107
16	99.20	0.7615E-03	0.7498E-03	-0.1491E-03	-0.4390	-0.5803	-1.1615
17	99.20	0.7822E-03	0.7743E-03	-0.8198E-04	-0.4450	-0.8669	-1.0655
18	99.20	0.7377E-03	0.7403E-03	-0.7923E-05	-0.4071	-1.0021	-1.1648
19	0.00	0.1408E-01	0.1195E-07	0.2564E-02	0.0000	-0.0919	-3.0880
20	0.00	0.1415E-01	0.1577E-07	0.1017E-02	0.0149	-0.1223	-2.5444
21	0.00	0.1420E-01	0.1915E-07	-0.4955E-03	0.0558	-0.1390	-2.0404
22	16.00	0.1273E-01	-0.1590E-02	0.2418E-02	-0.1987	-0.4788	-2.8292
23	16.00	0.1290E-01	-0.1020E-02	0.9483E-03	-0.1818	-0.4372	-2.3772
24	16.00	0.9597E-03	-0.7227E-03	0.3224E-04	0.5423	-0.6016	-0.9081
25	48.00	0.5021E-02	-0.1406E-02	0.1403E-02	-0.4569	-0.9162	-1.2733
26	48.00	0.5512E-02	-0.5302E-03	0.4346E-03	-0.3755	-1.0400	-1.4650
27	48.00	0.6011E-02	0.3256E-03	-0.5699E-03	-0.2710	-1.1037	-1.7400
28	75.00	0.9905E-03	0.6927E-03	0.1132E-03	-0.1868	-0.6296	-0.9761
29	75.00	0.1232E-02	0.9655E-03	-0.1415E-03	-0.2581	-0.9480	-1.2349
30	75.00	0.1285E-02	0.1024E-02	-0.3587E-03	-0.3152	-0.9915	-1.7829
31	0.00	0.5773E-02	-0.7098E-08	0.3176E-02	0.1917	-0.5233	-1.2072
32	0.00	0.5677E-02	0.8202E-08	0.1086E-02	0.3092	-0.6860	-0.8886
33	0.00	0.5685E-02	0.1840E-07	-0.9143E-03	0.5706	-0.3069	-1.2558
34	16.00	0.4888E-02	-0.7378E-03	0.2741E-02	0.0294	-0.4633	-1.1985
35	16.00	0.4907E-02	-0.2283E-03	0.8799E-03	0.1428	-0.6037	-0.9572
36	16.00	0.4998E-02	0.2379E-03	-0.9388E-03	0.3218	-0.0901	-1.4352
37	41.50	0.1080E-02	0.5995E-04	0.8208E-03	0.5899	-0.1983	-1.2801
38	41.50	0.1527E-02	0.6929E-03	-0.8924E-04	0.1689	-0.5251	-1.2465
39	41.50	0.1700E-02	0.9663E-03	-0.7687E-03	0.0788	-0.2911	-2.1044
40	0.00	0.1597E-02	-0.3235E-08	0.1667E-02	1.1345	0.0002	-1.2057
41	0.00	0.1703E-02	-0.7853E-09	0.7968E-04	0.6246	0.0061	-0.9300
42	0.00	0.1702E-02	0.2290E-07	-0.8979E-03	1.0649	0.0060	-1.5985

Table II

LOADING CONDITION

DEAD WEIGHT + HYDROSTATIC PRESSURE

POINT	S (m)	DISPX (m)	DISPY (m)	DISPZ (m)	P1 (Mpa)	P2 (Mpa)	P3 (Mpa)
1	0.00	0.2285E-01	-0.1431E-07	-0.3670E-02	0.0584	-0.1245	-3.2095
2	0.00	0.2290E-01	-0.1647E-07	-0.4185E-02	0.0416	-0.0964	-2.8421
3	0.00	0.2293E-01	-0.1864E-07	-0.4710E-02	0.0255	-0.0672	-2.4764
4	0.00	0.1910E-01	-0.6990E-08	-0.2057E-02	0.2168	-0.2881	-3.7027
5	0.00	0.1916E-01	-0.1017E-07	-0.2940E-02	0.1284	-0.2098	-3.2025
6	0.00	0.1921E-01	-0.1338E-07	-0.3766E-02	0.0496	-0.1184	-2.7250
7	16.00	0.1749E-01	-0.1768E-02	-0.1918E-02	-0.0249	-0.6138	-3.5184
8	16.00	0.1762E-01	-0.1259E-02	-0.2749E-02	-0.0779	-0.5129	-3.0954
9	16.00	0.1774E-01	-0.7334E-03	-0.3526E-02	-0.1075	-0.4085	-2.6993
10	48.00	0.8209E-02	-0.2130E-02	-0.1210E-02	-0.3391	-0.9281	-2.2944
11	48.00	0.8608E-02	-0.1317E-02	-0.1722E-02	-0.4217	-0.9041	-2.2701
12	48.00	0.9021E-02	-0.4834E-03	-0.2197E-02	-0.4486	-0.8816	-2.3000
13	80.00	0.1541E-02	0.3102E-03	-0.7868E-03	-0.3145	-0.4468	-1.3031
14	80.00	0.1742E-02	0.5361E-03	-0.8859E-03	-0.4162	-0.5366	-1.4413
15	80.00	0.1970E-02	0.7697E-03	-0.9840E-03	-0.4197	-0.7058	-1.5983
16	99.20	0.6181E-03	0.5761E-03	-0.5308E-03	-0.2421	-0.2872	-1.3231
17	99.20	0.6490E-03	0.6327E-03	-0.5342E-03	-0.3039	-0.3818	-1.4197
18	99.20	0.6297E-03	0.6286E-03	-0.5030E-03	-0.3196	-0.4947	-1.5442
19	0.00	0.1274E-01	-0.6040E-09	0.4361E-03	0.0594	-0.0092	-3.1285
20	0.00	0.1282E-01	-0.1553E-08	-0.1115E-02	0.1006	-0.0001	-2.7232
21	0.00	0.1288E-01	-0.3074E-08	-0.2655E-02	0.1570	-0.0054	-2.3186
22	16.00	0.1149E-01	-0.1483E-02	0.3550E-03	-0.0420	-0.4413	-2.8853
23	16.00	0.1165E-01	-0.9534E-03	-0.1112E-02	0.0223	-0.3884	-2.5736
24	16.00	0.8766E-03	-0.6232E-03	-0.6638E-03	0.5301	-0.4681	-1.0818
25	48.00	0.4450E-02	-0.1299E-02	-0.1680E-03	-0.3223	-0.5983	-1.5528
26	48.00	0.4898E-02	-0.5047E-03	-0.1103E-02	-0.2593	-0.5555	-1.9245
27	48.00	0.5369E-02	0.2549E-03	-0.2039E-02	-0.1905	-0.4957	-2.3188
28	75.00	0.9258E-03	0.6202E-03	-0.6784E-03	-0.1331	-0.3778	-1.1396
29	75.00	0.1134E-02	0.8730E-03	-0.9742E-03	-0.1486	-0.3924	-1.7265
30	75.00	0.1154E-02	0.9240E-03	-0.1098E-02	-0.1473	-0.4024	-2.3350
31	0.00	0.5146E-02	-0.9490E-08	0.1139E-02	0.1733	-0.4683	-1.2692
32	0.00	0.5066E-02	0.6537E-09	-0.6183E-03	0.5115	-0.2315	-1.6174
33	0.00	0.5096E-02	0.7088E-08	-0.2314E-02	1.0146	-0.1285	-1.9966
34	16.00	0.4369E-02	-0.6202E-03	0.8275E-03	0.0146	-0.4819	-1.1761
35	16.00	0.4391E-02	-0.1753E-03	-0.7423E-03	0.3302	-0.1701	-1.6343
36	16.00	0.4493E-02	0.2284E-03	-0.2268E-02	0.8246	-0.0162	-2.1135
37	41.50	0.1082E-02	0.1174E-03	-0.3561E-03	0.0149	-0.2903	-0.7127
38	41.50	0.1474E-02	0.6716E-03	-0.1252E-02	0.1026	-0.0808	-1.6647
39	41.50	0.1584E-02	0.9003E-03	-0.1697E-02	0.4050	-0.0391	-2.6636
40	0.00	0.1604E-02	-0.4435E-08	0.2108E-03	0.3539	-0.1567	-0.6089
41	0.00	0.1704E-02	0.2575E-09	-0.1212E-02	0.8318	-0.0683	-1.3961
42	0.00	0.1649E-02	0.2082E-07	-0.1856E-02	1.4804	-0.0393	-2.2946

Table III

$$\mathbf{K} = \mathbf{L}^T \mathbf{D} \mathbf{L}$$

Tables I–III show some characteristic results for the nodal displacements and stresses for the two load cases considered.

2. VIBRATION ANALYSIS

Two different cases have been considered. The first case considers an empty reservoir and neglects the soil stiffness. The finite element mesh used coincides with that shown in Figure 1 for the static case. The stiffness matrix is therefore identical to that previously used for the static analysis. The mass matrix [1] has been diagonalized by simply adding the terms of each row.

The eigenvalues and eigenmodes have been obtained using both the subspace Iteration Method [2] and the Determinant Search Method [1,2]. Identical results have been obtained with both procedures.

The second case considered corresponds to full reservoir conditions and including the soil stiffness. The effect of the reservoir water has been taken into account by solving the wave equation

$$\nabla^2 p = \frac{1}{c^2} \frac{\partial^2 p}{\partial t^2}$$

where p is the water pressure and c is the wave speed.

All the analysis has been carried out in the frequency domain.

The finite element discretization of the fluid equation leads to (Figure 3) [3,4,5]

$$\begin{bmatrix} -\omega^2 \mathbf{G}_{11} + \mathbf{H}_{11} & -\omega^2 \mathbf{G}_{12} + \mathbf{H}_{12} \\ -\omega^2 \mathbf{G}_{21} + \mathbf{H}_{21} & -\omega^2 \mathbf{G}_{22} + \mathbf{H}_{22} \end{bmatrix} \begin{bmatrix} \mathbf{P}_1 \\ \mathbf{P}_2 \end{bmatrix} + \begin{bmatrix} \mathbf{0} \\ \int_{S_c} \mathbf{N} \frac{\partial p}{\partial n} dS_c \end{bmatrix} = -\mathbf{S} \ddot{\bar{\mathbf{a}}}^t$$

where w is the eigenvalue (natural frequency), $\mathbf{G}$ and $\mathbf{H}$ the mass and stiffness matrices of the fluid respectively, $\mathbf{P}$ the nodal pressure and $\mathbf{S}$ the fluid structure coupling matrix. The variables $\mathbf{P}_1$ denote the pressures of the nodes in the contact fluid-structure region and $\mathbf{P}_2$ the rest of the fluid nodal pressures.

Taking into account that for the non contact region Ω_2 (Figure 3) the following condition must be satisfied

$$p = P_2 \exp(-kx)$$

and coupling this equation with the discretized decoupled dam equation for each vibration mode, the following equation system is obtained [3,4,5]

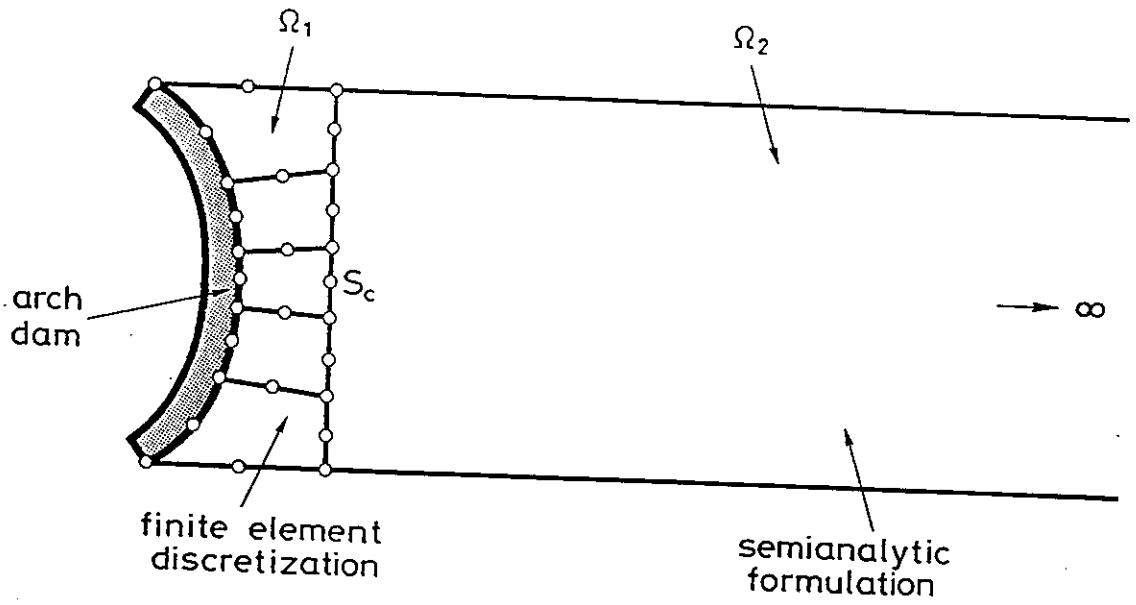

Figure 3. Fluid domain discretization.

$$\begin{bmatrix} -\omega^2\mathbf{G}_{11}+\mathbf{H}_{11} & (-\omega^2\mathbf{G}_{12}+\mathbf{H}_{12})\boldsymbol{\alpha} & -\omega^2\mathbf{S}\boldsymbol{\Phi} \\ \boldsymbol{\alpha}^t(-\omega^2\mathbf{G}_{21}+\mathbf{H}_{21}) & \boldsymbol{\alpha}^t(-\omega^2\mathbf{G}_{22}+\mathbf{H}_{22})\boldsymbol{\alpha}+\boldsymbol{\alpha}^t\boldsymbol{\Psi} & \mathbf{0} \\ \frac{1}{\rho}\boldsymbol{\Phi}^t\mathbf{S}^t & \mathbf{0} & \mathbf{T} \end{bmatrix} \begin{bmatrix} \mathbf{P}_1 \\ \boldsymbol{\gamma} \\ \mathbf{y} \end{bmatrix} = \begin{bmatrix} -\mathbf{S}\mathbf{J}\bar{a}_g \\ \mathbf{0} \\ -\boldsymbol{\Phi}\mathbf{M}\mathbf{J}\bar{a}_g \end{bmatrix}$$

where the elements of $\mathbf{T}$ matrix are

$$T_{ij} = -\omega^2 + i\omega C_i + \omega_i^2 \quad \text{si} \quad i = j$$
$$T_{ij} = 0 \quad \text{si} \quad i \neq j$$

In above $\boldsymbol{\alpha}$ are the eigenvalues of S_c (Figure 3), $\boldsymbol{\Phi}$ the eigenvectors of the dam and $\mathbf{y}$ the generalized coordinates of the dam, $\boldsymbol{\gamma}$ the generalized coordinates of the cross section of the fluid and $\boldsymbol{\alpha}^T\boldsymbol{\Psi}$ is a term taking into account the effect of infinite fluid boundaries [5].

By solving the above matrix equation for different eigenvalues, the peaks in the solution for $\mathbf{y}$ will indicate the resonant frequencies of the dam.

Figure 4 shows a plant of the geometry of the dam,solid and fluid regions used for the analysis.

Figure 5 and Tables IV–VII show results for the first natural frequencies and modal shapes on the dam with rigid foundation for an empty reservoir. Table VIII shows the first 6 natural frequencies including (compressible) water effects.

ACKNOWLEDGEMENTS

The authors are grateful to P.I.E. (Programa de Investigación Electrotécnico) for the economical suppost of this study.

3. REFERENCES

1. A.H. Barbat and J. Miquel Canet, "Structural response computations in earthquake engineering", Pineridge Press, 1989.
2. K.J. Bathe, "Finite Element procedures in Engineering Analysis", Prentice Hall, 1982.
3. K.L. Fox and A.K. Chopra, "Earthquake analysis and response of concrete arch dams", Report No. UCB/EERC-85/07 University of California. Bekeley.
4. J.F. Hall and A.K. Chopra, "Dynamic response of embankment concrete-gravity and arch dams including hydrodynamic interaction. Report No. UCB/EERC–80/39. University of California. Berkeley.
5. J. Miquel, E. Oñate, J. Buil and E. Herrero, "Análisis dinámico de Presas", PIE, Jannuary, 1990.

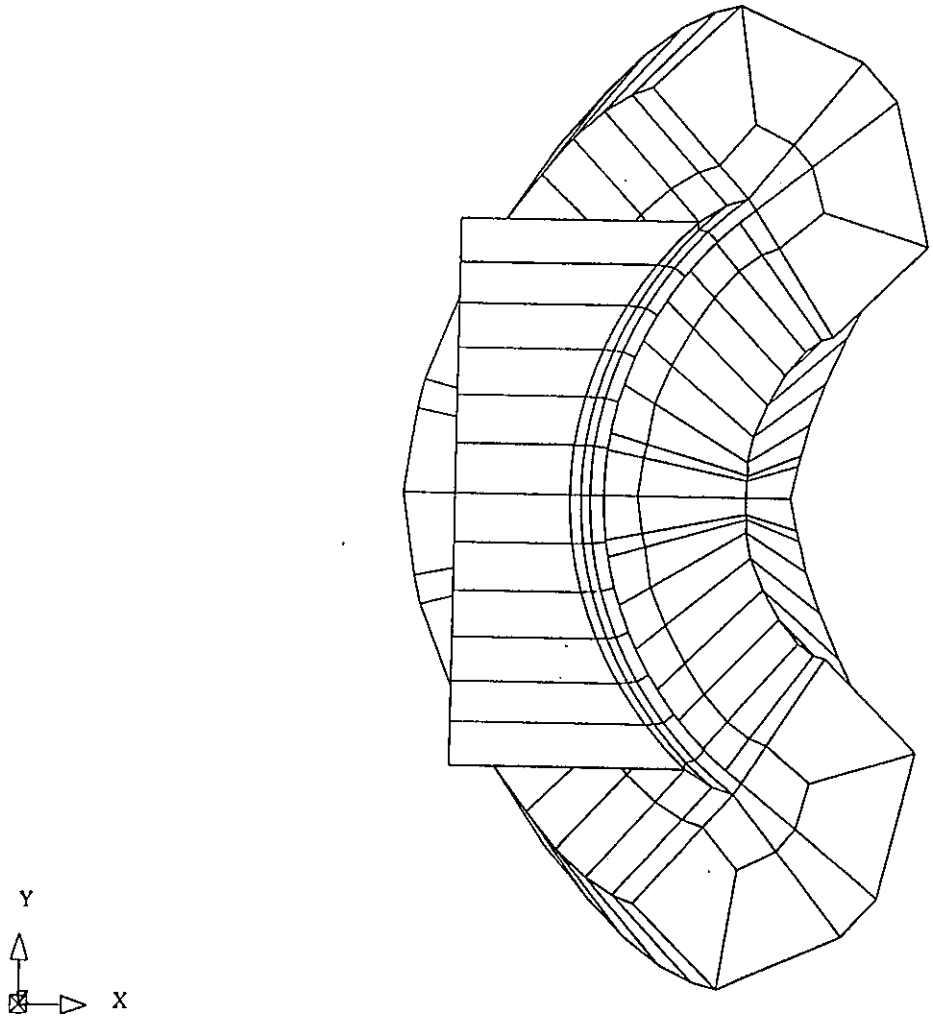

Figure 4. Talvacchia dam. Finite element mesh showing discretization of dam, fluid and foundation.

TALVACCHIA Dam

DINAMIC RESULTS

Reference figure

The modal shapes are normalisated with the Mass Matrix

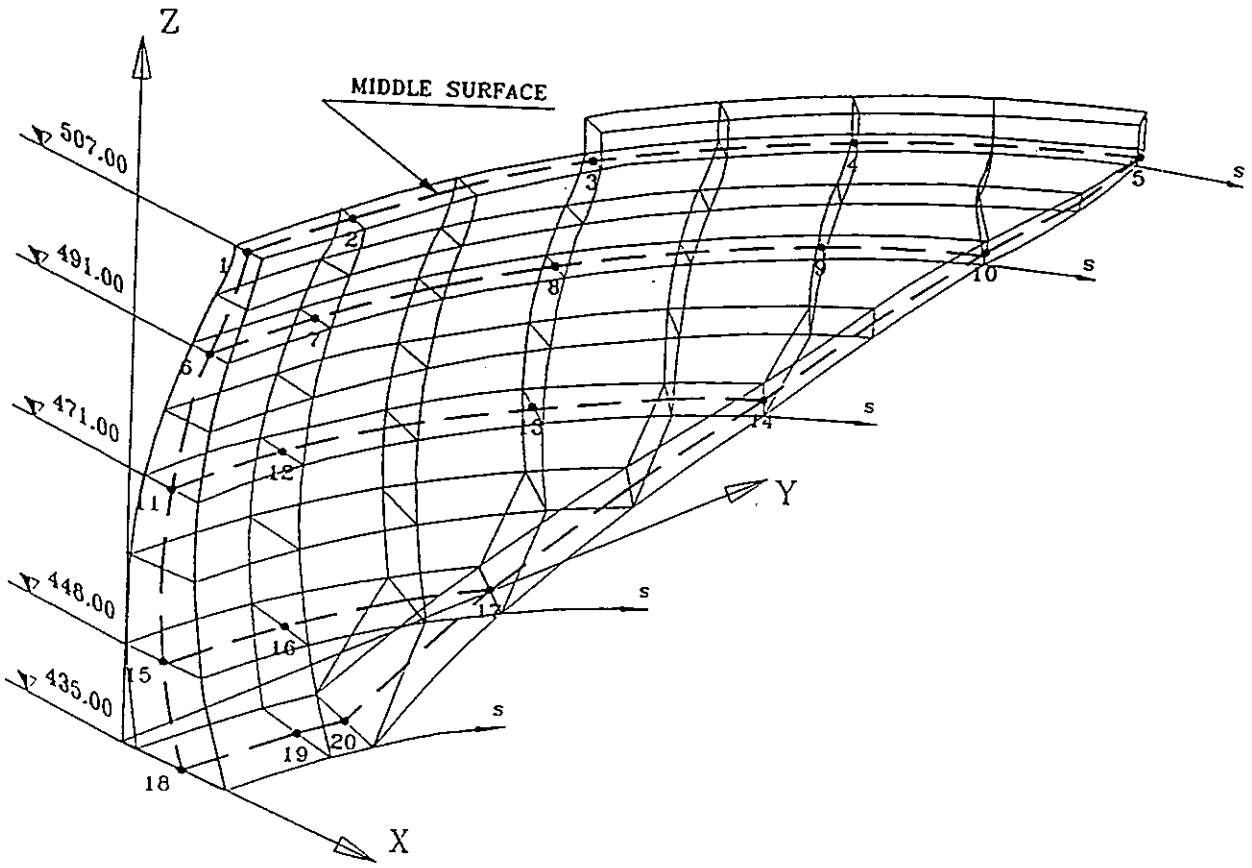

Figure 5

LOADING CONDITION 3.5.1

DAM ON RIGID FOUNDATION WITHOUT WATER

FIRST 6 NATURAL FREQUENCIES

FREQUENCY	VALUE HERTZ
1 st	4.319
2 nd	4.459
3rd	5.752
4 th	6.780
5 th	8.604
6 th	8.868

Table IV

DAM ON RIGID FUNDATION

MODAL SHAPE FOR FREQUENCY= 4.319

POINT	S (m)	DISPX (m)	DISPY (m)	DISPZ (m)
1	0.00	0.9600E-04	-0.1800E-05	-0.3185E-04
2	16.00	0.4551E-04	0.5796E-05	-0.1929E-04
3	48.00	-0.9026E-04	0.4600E-04	0.1317E-04
4	80.00	-0.3355E-04	0.1380E-04	0.1987E-05
5	112.90	-0.2831E-05	-0.2624E-05	-0.2029E-06
6	0.00	0.5251E-04	-0.3893E-05	-0.1445E-04
7	16.00	0.2094E-04	0.1734E-05	-0.9047E-05
8	48.00	-0.6568E-04	0.3079E-04	0.3228E-05
9	80.00	-0.1972E-04	0.8939E-05	-0.2152E-05
10	99.20	-0.3426E-05	-0.2373E-05	-0.7966E-06
11	0.00	0.1781E-04	-0.5693E-05	-0.2238E-05
12	16.00	0.2303E-05	-0.1879E-05	-0.2381E-05
13	48.00	0.1645E-04	-0.4990E-05	0.2429E-05
14	75.00	-0.7527E-05	-0.1071E-05	-0.3196E-06
15	0.00	0.3811E-05	-0.5447E-05	0.4383E-06
16	16.00	-0.1716E-05	-0.2755E-05	-0.5033E-06
17	41.50	-0.4457E-05	0.1888E-06	-0.1009E-05
18	0.00	0.1183E-05	-0.4146E-05	0.2875E-06
19	16.00	-0.5864E-06	-0.2516E-05	0.2049E-06
20	22.00	-0.1741E-05	-0.1967E-05	0.1240E-06

MODAL SHAPE FOR FREQUENCY= 4.459

POINT	S (m)	DISPX (m)	DISPY (m)	DISPZ (m)
1	0.00	0.2227E-03	0.8647E-07	-0.3595E-04
2	16.00	0.1823E-03	-0.2473E-05	-0.2639E-04
3	48.00	-0.2688E-05	0.3735E-04	0.1195E-04
4	80.00	-0.3411E-04	0.4114E-04	0.1043E-04
5	112.90	0.1081E-05	0.1543E-05	0.2483E-07
6	0.00	0.1521E-03	0.2863E-07	-0.1048E-04
7	16.00	0.1276E-03	-0.3561E-05	-0.6870E-05
8	48.00	0.1534E-04	0.1726E-04	0.4546E-05
9	80.00	-0.9290E-05	0.2052E-04	0.3557E-06
10	99.20	0.2008E-05	0.4784E-05	-0.9875E-06
11	0.00	0.7939E-04	-0.4237E-07	0.8664E-05
12	16.00	0.6735E-04	-0.3415E-05	0.8010E-05
13	48.00	0.7566E-04	0.5052E-05	0.2126E-04
14	75.00	0.2952E-05	0.6596E-05	-0.3809E-06
15	0.00	0.2260E-04	-0.1060E-06	0.8492E-05
16	16.00	0.1852E-04	-0.1955E-06	0.6949E-05
17	41.50	0.4646E-05	0.4037E-05	0.1068E-05
18	0.00	0.4617E-05	-0.1235E-06	0.3318E-05
19	16.00	0.3614E-05	0.1211E-05	0.2713E-05
20	22.00	0.2973E-05	0.1677E-05	0.2228E-05

Table V

DAM ON RIGID FUNDATION

MODAL SHAPE FOR FREQUENCY= 5.752

POINT	S (m)	DISPX (m)	DISPY (m)	DISPZ (m)
1	0.00	0.8595E-04	-0.1055E-07	-0.3835E-04
2	16.00	0.2017E-04	0.1508E-04	-0.1948E-04
3	48.00	-0.2011E-03	0.1023E-03	0.4290E-04
4	80.00	-0.9036E-04	0.4842E-04	0.1423E-04
5	112.90	-0.5618E-05	-0.5093E-05	0.1206E-06
6	0.00	0.3417E-04	-0.4731E-07	-0.1702E-04
7	16.00	-0.1046E-05	0.9440E-05	-0.9629E-05
8	48.00	-0.1061E-03	0.5065E-04	0.7696E-05
9	80.00	-0.4025E-04	0.2138E-04	-0.1984E-05
10	99.20	-0.6527E-05	-0.3865E-05	-0.5732E-06
11	0.00	-0.6329E-05	-0.1889E-06	-0.4135E-05
12	16.00	-0.1757E-04	0.4099E-05	-0.3942E-05
13	48.00	-0.9666E-05	0.9500E-06	-0.9297E-06
14	75.00	-0.8392E-05	-0.1364E-05	-0.5749E-06
15	0.00	-0.1053E-04	-0.2189E-06	-0.2394E-05
16	16.00	-0.1112E-04	0.1422E-05	-0.2732E-05
17	41.50	-0.5486E-05	0.1121E-06	-0.1475E-05
18	0.00	-0.4238E-05	-0.1514E-06	-0.5481E-06
19	16.00	-0.3872E-05	-0.1336E-06	-0.6658E-06
20	22.00	-0.3449E-05	-0.2476E-06	-0.7411E-06

MODAL SHAPE FOR FREQUENCY= 6.780

POINT	S (m)	DISPX (m)	DISPY (m)	DISPZ (m)
1	0.00	0.1988E-04	0.1115E-04	-0.4144E-05
2	16.00	-0.3661E-04	0.1753E-04	0.1171E-04
3	48.00	-0.7454E-04	0.3464E-04	0.2840E-04
4	80.00	-0.1906E-04	0.1087E-04	0.7764E-05
5	112.90	-0.1245E-05	-0.1070E-05	0.9775E-07
6	0.00	0.5971E-05	0.5705E-05	0.3012E-05
7	16.00	-0.8198E-05	0.1242E-04	0.1640E-05
8	48.00	-0.1854E-04	0.1034E-04	0.6816E-05
9	80.00	-0.3128E-05	-0.2831E-05	0.2441E-05
10	99.20	-0.2345E-05	-0.2105E-05	0.5482E-06
11	0.00	-0.7037E-05	0.4492E-05	0.1123E-04
12	16.00	0.1120E-05	0.8846E-05	0.1464E-05
13	48.00	-0.6160E-05	-0.7942E-06	0.1198E-04
14	75.00	-0.1336E-04	0.2616E-05	0.1178E-05
15	0.00	-0.6663E-05	0.1020E-04	0.6082E-05
16	16.00	-0.7249E-05	0.1222E-04	0.3120E-05
17	41.50	0.2177E-05	0.7096E-05	-0.7698E-06
18	0.00	-0.5698E-05	0.1084E-04	0.4924E-05
19	16.00	-0.4996E-05	0.1129E-04	0.2958E-05
20	22.00	-0.2269E-05	0.9469E-05	0.2054E-05

Table V (cont.)

DAM ON RIGID FUNDATION

MODAL SHAPE FOR FREQUENCY=8.604

POINT	S (m)	DISPX (m)	DISPY (m)	DISPZ (m)
1	0.00	0.8770E-05	0.5797E-05	-0.3946E-05
2	16.00	0.1140E-03	-0.8972E-05	-0.4355E-04
3	48.00	0.1462E-03	-0.5042E-04	-0.5250E-04
4	80.00	0.1546E-04	0.6742E-05	-0.5425E-05
5	112.90	0.2584E-05	0.3150E-05	-0.3240E-06
6	0.00	0.6409E-05	0.1174E-04	-0.2926E-05
7	16.00	0.2433E-04	0.9025E-05	-0.1209E-04
8	48.00	0.3932E-04	0.6843E-07	-0.1269E-04
9	80.00	-0.1215E-06	0.1726E-04	-0.1388E-05
10	99.20	0.3546E-05	0.6864E-05	-0.1685E-05
11	0.00	0.3753E-05	0.1590E-04	-0.1632E-05
12	16.00	-0.3729E-04	0.2164E-04	0.1711E-05
13	48.00	0.2645E-04	0.8094E-05	-0.4182E-05
14	75.00	-0.9546E-06	0.1036E-04	-0.1038E-05
15	0.00	0.1317E-05	0.1184E-04	-0.8512E-06
16	16.00	-0.2749E-04	0.1751E-04	0.5281E-06
17	41.50	-0.1268E-04	0.1165E-04	0.3249E-05
18	0.00	0.6026E-06	0.1577E-04	-0.7357E-06
19	16.00	-0.9937E-05	0.1466E-04	0.3235E-05
20	22.00	-0.9563E-05	0.1266E-04	0.3748E-05

MODAL SHAPE FOR FREQUENCY= 8.868

POINT	S (m)	DISPX (m)	DISPY (m)	DISPZ (m)
1	0.00	0.1231E-03	-0.2748E-06	-0.3567E-04
2	16.00	0.6409E-05	0.1335E-04	-0.2854E-05
3	48.00	-0.5579E-04	-0.5176E-05	0.4145E-05
4	80.00	0.1876E-03	-0.1574E-03	-0.5096E-04
5	112.90	0.6632E-05	0.2744E-05	-0.8165E-06
6	0.00	0.8380E-04	-0.4330E-06	-0.1827E-04
7	16.00	0.1518E-04	0.7099E-05	-0.4175E-05
8	48.00	-0.7657E-04	0.2585E-04	0.1204E-04
9	80.00	0.4710E-04	-0.4407E-04	-0.4834E-06
10	99.20	0.7282E-05	-0.5529E-05	0.1412E-05
11	0.00	0.4175E-04	-0.6049E-06	0.4148E-06
12	16.00	0.1484E-04	0.1594E-05	-0.9157E-06
13	48.00	0.3309E-04	0.6554E-05	0.4960E-05
14	75.00	-0.3706E-05	-0.1886E-05	0.3196E-05
15	0.00	0.1424E-04	-0.6895E-06	0.1301E-05
16	16.00	0.6122E-05	0.2462E-05	0.4175E-06
17	41.50	-0.3264E-05	0.4278E-05	0.2659E-05
18	0.00	0.3632E-05	-0.6667E-06	-0.4965E-07
19	16.00	0.9124E-06	0.5416E-05	0.4428E-07
20	22.00	0.9245E-06	0.5820E-05	0.7858E-06

Table V (cont.)

LOADING CONDITION

DAM ON FLEXIBLE FOUNDATION WITHOUT WATER

FIRST 6 NATURAL FREQUENCIES

FREQUENCY	VALUE HERTZ
1 st	3.806
2 nd	4.142
3rd	5.331
4 th	6.287
5 th	7.947
6 th	8.405

Table VI

DAM ON FLEXIBLE FUNDATION

MODAL SHAPE FOR FREQUENCY= 3.806

POINT	S (m)	DISPX (m)	DISPY (m)	DISPZ (m)
1	0.0	0.2176E-09	0.6467E-04	0.1499E-09
2	16.0	-0.1348E-03	0.7545E-04	0.3078E-04
3	48.0	-0.1909E-03	0.9638E-04	0.3828E-04
4	80.0	-0.5044E-04	0.2402E-04	0.5579E-05
5	112.0	-0.3178E-05	-0.3064E-05	0.8559E-07
6	0.0	0.1968E-09	0.4415E-04	0.1539E-09
7	16.0	-0.7775E-04	0.4999E-04	0.9707E-05
8	48.0	-0.1073E-03	0.5871E-04	0.6751E-05
9	80.0	-0.2378E-04	0.1410E-04	-0.2669E-05
10	99.2	-0.3195E-05	-0.2231E-05	-0.5572E-06
11	0.0	0.1814E-09	0.2074E-04	0.1364E-09
12	16.0	-0.3105E-04	0.2333E-04	-0.3312E-05
13	48.0	0.1748E-04	0.1342E-04	0.5588E-05
14	75.0	-0.3623E-05	0.1044E-05	-0.1837E-05
15	0.0	0.1075E-09	0.7368E-05	0.1074E-09
16	16.0	-0.5909E-05	0.7670E-05	-0.3583E-05
17	41.5	-0.1824E-05	0.4111E-05	-0.3583E-05
18	0.0	-0.2093E-10	0.3821E-05	0.2430E-10
19	16.0	-0.3020E-06	0.3443E-05	-0.1811E-05
20	22.0	-0.1668E-06	0.3180E-05	-0.2356E-05

MODAL SHAPE FOR FREQUENCY= 4.142

POINT	S (m)	DISPX (m)	DISPY (m)	DISPZ (m)
1	0.0	0.3023E-03	-0.1906E-09	-0.6212E-04
2	16.0	0.2433E-03	-0.5217E-05	-0.4681E-04
3	48.0	-0.2230E-04	0.5390E-04	0.1547E-04
4	80.0	-0.5432E-04	0.5627E-04	0.1415E-04
5	112.9	0.3123E-06	0.1003E-05	-0.2325E-07
6	0.0	0.1847E-03	-0.1358E-09	-0.1965E-04
7	16.0	0.1519E-03	-0.3527E-05	-0.1403E-04
8	48.0	0.5217E-05	0.2612E-04	0.4314E-05
9	80.0	-0.1706E-04	0.2731E-04	-0.3705E-06
10	99.2	0.1262E-05	0.5087E-05	-0.1462E-05
11	0.0	0.8011E-04	-0.5593E-10	0.8556E-05
12	16.0	0.6641E-04	-0.2332E-05	0.7788E-05
13	48.0	0.7599E-04	0.5123E-05	0.2371E-04
14	75.0	0.2051E-05	0.7282E-05	-0.1021E-05
15	0.0	0.1890E-04	-0.1563E-10	0.8752E-05
16	16.0	0.1508E-04	0.3045E-06	0.7032E-05
17	41.5	0.3282E-05	0.4209E-05	0.7636E-06
18	0.0	0.2898E-05	-0.3577E-10	0.3897E-05
19	16.0	0.2166E-05	0.1055E-05	0.3152E-05
20	22.0	0.1684E-05	0.1427E-05	0.2534E-05

Table VII

DAM ON FLEXIBLE FUNDATION

MODAL SHAPE FOR FREQUENCY= 5.331

POINT	S (m)	DISPX (m)	DISPY (m)	DISPZ (m)
1	0.0	-0.1001E-04	-0.6498E-09	-0.5758E-05
2	16.0	-0.6102E-04	0.2216E-04	0.8867E-05
3	48.0	-0.2355E-03	0.1146E-03	0.5751E-04
4	80.0	-0.1023E-03	0.5471E-04	0.1875E-04
5	112.9	-0.6196E-05	-0.5687E-05	0.3977E-06
6	0.0	-0.1174E-04	-0.4394E-09	-0.2401E-05
7	16.0	-0.3564E-04	0.1129E-04	0.2233E-05
8	48.0	-0.1107E-03	0.4891E-04	0.1168E-04
9	80.0	-0.4214E-04	0.2058E-04	-0.6656E-06
10	99.2	-0.7264E-05	-0.4797E-05	0.1546E-06
11	0.0	-0.9721E-05	-0.2211E-09	-0.1974E-05
12	16.0	-0.1616E-04	0.2702E-05	-0.2179E-05
13	48.0	-0.1170E-04	0.5350E-06	-0.3851E-05
14	75.0	-0.7337E-05	-0.2851E-05	0.3396E-06
15	0.0	-0.3022E-05	-0.7902E-10	-0.1885E-05
16	16.0	-0.3702E-05	-0.1428E-06	-0.2101E-05
17	41.5	-0.2426E-05	-0.1139E-05	-0.1175E-05
18	0.0	-0.3767E-06	-0.2826E-10	-0.1093E-05
19	16.0	-0.4587E-06	-0.4512E-06	-0.1122E-05
20	22.0	-0.5041E-06	-0.5478E-06	-0.1096E-05

MODAL SHAPE FOR FREQUENCY= 6.287

POINT	S (m)	DISPX (m)	DISPY (m)	DISPZ (m)
1	0.0	-0.1683E-08	-0.1940E-04	0.6247E-09
2	16.0	0.1726E-03	-0.2970E-04	-0.4736E-04
3	48.0	-0.6794E-04	0.7561E-04	0.2632E-04
4	80.0	-0.1661E-03	0.1316E-03	0.4057E-04
5	112.9	-0.5484E-05	-0.3256E-05	0.5182E-06
6	0.0	-0.8312E-09	-0.9972E-05	0.2496E-09
7	16.0	0.9365E-04	-0.1570E-04	-0.1769E-04
8	48.0	0.2179E-05	0.1881E-04	0.2891E-06
9	80.0	-0.5350E-04	0.4809E-04	0.3016E-06
10	99.2	-0.5812E-05	0.3393E-05	-0.1381E-05
11	0.0	-0.2272E-09	-0.1711E-05	0.3537E-10
12	16.0	0.3212E-04	-0.4659E-05	-0.2774E-06
13	48.0	-0.1905E-04	0.5314E-05	-0.4394E-05
14	75.0	-0.1881E-05	0.4968E-05	-0.1157E-05
15	0.0	-0.5804E-10	0.5411E-06	0.1270E-10
16	16.0	0.6152E-05	-0.5900E-07	0.8426E-06
17	41.5	0.3071E-05	0.1475E-05	-0.1565E-05
18	0.0	0.3271E-11	0.2986E-06	0.5936E-10
19	16.0	0.1125E-05	0.3767E-06	-0.2509E-06
20	22.0	0.1239E-05	0.4595E-06	-0.4495E-06

Table VII (cont.)

DAM ON FLEXIBLE FUNDATION

MODAL SHAPE FOR FREQUENCY= 7.947

POINT	S (m)	DISPX (m)	DISPY (m)	DISPZ (m)
1	0.0	0.3267E-03	-0.3438E-09	-0.1474E-03
2	16.0	0.1825E-03	-0.1501E-04	-0.1007E-03
3	48.0	-0.5470E-04	-0.7521E-05	-0.1698E-04
4	80.0	0.1426E-03	-0.1336E-03	-0.4753E-04
5	112.9	0.2821E-05	-0.3992E-06	-0.1338E-05
6	0.0	0.8967E-04	-0.1778E-09	-0.6014E-04
7	16.0	0.2540E-04	0.2944E-05	-0.4270E-04
8	48.0	-0.8386E-04	0.2498E-04	-0.5843E-05
9	80.0	0.2906E-04	-0.3657E-04	-0.6054E-05
10	99.2	0.3040E-05	-0.7476E-05	-0.5860E-06
11	0.0	-0.3655E-04	-0.4175E-10	-0.1804E-04
12	16.0	-0.4926E-04	0.7106E-05	-0.1662E-04
13	48.0	-0.4004E-04	0.2404E-06	-0.1265E-04
14	75.0	-0.5806E-05	-0.5040E-05	-0.2531E-05
15	0.0	-0.2382E-04	0.3151E-10	-0.1238E-04
16	16.0	-0.2279E-04	0.2092E-05	-0.1167E-04
17	41.5	-0.8940E-05	-0.1191E-05	-0.5091E-05
18	0.0	-0.5757E-05	0.8750E-10	-0.6298E-05
19	16.0	-0.4957E-05	-0.4670E-06	-0.5781E-05
20	22.0	-0.4404E-05	-0.7184E-06	-0.5345E-05

MODAL SHAPE FOR FREQUENCY= 8.405

POINT	S (m)	DISPX (m)	DISPY (m)	DISPZ (m)
1	0.0	-0.9640E-04	0.1468E-09	0.8559E-04
2	16.0	-0.1617E-03	0.3779E-04	0.1007E-03
3	48.0	-0.1127E-03	0.4376E-04	0.5742E-04
4	80.0	0.1360E-03	-0.1024E-03	-0.2646E-04
5	112.9	0.7852E-05	0.4408E-05	0.1680E-06
6	0.0	0.6938E-04	0.7031E-09	0.2709E-04
7	16.0	0.2646E-04	0.5521E-05	0.3372E-04
8	48.0	-0.3149E-04	0.1665E-04	0.2747E-04
9	80.0	0.4364E-04	-0.3069E-04	0.5973E-05
10	99.2	0.8990E-05	-0.1708E-05	0.3269E-05
11	0.0	0.1169E-03	0.1296E-08	0.1176E-04
12	16.0	0.9372E-04	-0.7810E-05	0.1246E-04
13	48.0	0.1084E-03	0.1029E-04	0.1843E-04
14	75.0	0.5451E-05	0.1076E-05	0.6474E-05
15	0.0	0.4724E-04	0.1032E-08	0.1178E-04
16	16.0	0.3836E-04	-0.1834E-05	0.1027E-04
17	41.5	0.9301E-05	0.4890E-05	0.5129E-05
18	0.0	0.1223E-04	0.7738E-09	0.2899E-05
19	16.0	0.9601E-05	0.2104E-05	0.2893E-05
20	22.0	0.7921E-05	0.2894E-05	0.2768E-05

Table VII (cont.)

LOADING CONDITION 3.5.2

)AM ON FLEXIBLE FOUNDATION WATER LEVEL 491 m a. s. l.

FIRST 6 NATURAL FREQUENCIES

Analysis with compresible fluid

FREQUENCY	VALUE HERTZ
1 st	3.621
2 nd	3.812
3rd	5.165
4 th	6.167
5 th	6.764
6 th	7.950

Table VIII

First Benchmark Workshop
on
Numerical Analysis of Dams

Theme A
Benchmark Analysis of a Double Curvature Concrete Arch Dam

By A. L. Mee, D. D. Curtis and Z. Wozniak
Acres International Limited
Niagara Falls, Ontario, Canada

Theme A - Benchmark Analysis of a Double Curvature Concrete Arch Dam

by Allen L. Mee, Dan D. Curtis and Z. Wozniak
Acres International Limited
Niagara Falls, Ontario, Canada

1 Introduction

The purpose of this paper is to contribute results of well defined arch dam computations as part of the first ICOLD Benchmark Workshop. Some results of complementary analyses obtained using Acres' arch dam software will also be presented for comparison. In order to provide a link with older methods some arch cantilever analysis results will also be provided.

2 Acres Arch Dam Analysis Software

Acres arch dam analysis software will be briefly described under the following categories

- dam model generation
- static stress analysis
- dynamic stress analysis
- thermal analysis
- processing of results.

2.1 Dam Model Generation

The initial finite element mesh for the dam and foundation is generated using a mesh generator from the Enhanced Arch Dam Analysis Program (EADAP, Ghannat and Clough, 1989). The finite element mesh from EADAP can be refined in the preprocessor program Display-II, for example by adding additional solid elements through the thickness of the dam and replacing EADAP elements with 20-noded and 15-noded solid elements. A generic finite element model is output which is used for load generation, finite element analysis and post-processing of results.

2.2 Static Stress Analysis

At present, the Acres arch dam analysis program considers the following static loads: gravity, hydrostatic, thermal and pore pressure.

Gravity loading is available in the three dimensional analysis programs, however there are drawbacks to using a one step (gravity turn-on) or two step (independent alternate cantilevers) approach. The gravity turn-on approach considers the dam as monolithic and gravity is 'turned-on' after complete construction. The approximations in this approach are obvious. The independent alternate cantilever approach assumes the cantilevers are ungrouted over the full height of the dam. The results from this analysis are sensitive to geometry of the finite element mesh. Acres tends to use trial load methods and 2D finite element models of cantilevers to determine dead load stresses, in addition to the above methods.

Hydrostatic forces on the upstream and downstream face of the dam are computed by numerically integrating the linear hydrostatic pressure distribution over the surface of each pressure-exposed element face.

Temperatures at nodal points are determined directly using Acres HEAT3D program with a finite element mesh compatible with the static analyses. In a similar fashion, the pore pressure distribution in the dam foundation may be determined using the HEAT3D program and the pore pressure loads may be simulated in a static analysis.

The static finite element analysis is performed using 20-noded solid hexahedron and 15-noded solid pentahedron (wedge) elements. These 20-noded and 15-noded elements were added to EADAP for the following reasons.

- The 20-noded solid element represents a distinct improvement over the 8-noded solid with incompatible deformation modes incorporated in EADAP. The foundation elements are distorted from rectangular and the above 8-noded element performs poorly under these conditions (Strang and Fix, 1973).

- the 15-noded wedge element replaces a collapsed hexahedron. The interpolation functions for a collapsed hexadron are poor approximations of a true wedge element (Newton, 1973).

- Solid elements were selected over shell elements in order to allow refined analyses to be undertaken. If elements are added through the thickness of the dam then the

no-tension stress transfer technique can be applied directly to these elements--in both the dam and foundation. Also, additional elements may be required through the thickness of the dam in areas where shear stresses are large i.e., at the base of a dam in a wide valley.

- The thermal, pore pressure and stress analysis programs use compatible elements.

A subprogram was developed by Acres to perform a no-tension stress analysis which interactively applies nodal forces (based on principal tensile stress) to redistribute tensile stresses. The procedure may be applied to any initial stress configuration provided the final stress-state represents a stable compressive stress configuration.

The output from the static stress analysis includes displacements at nodes and stresses a the element reduced integration points i.e., optimal stress points (Barlow, 1976). The element stresses are extrapolated to element nodal points using a trilinear extrapolation procedure (Hinton and Campbell, 1979). The processing of stresses is discussed further in Section 2.5.

2.3 Dynamic Stress Analysis

The dynamic analysis is performed assuming linear elastic material behavior. A time history analysis is performed using mode superposition techniques. The mode shapes and frequencies are determined by the subspace iteration technique.

The added-mass of the incompressible water is obtained by solving the Helmholtz pressure wave equation (Ghannat and Clough, 1989). The solution is based on a finite-element formulation which takes account of the effects resulting from the geometry and flexibility of the dam as well as the natural topography of the reservoir. The finite-element formulation for the added-mass calculation is given in Kuo, 1982.

The following description of the INCRES added-mass program was extracted from Ghannat and Clough, 1989. The reservoir water is descretized by 2D and 3D liquid elements and is bounded on the upstream by a vertical plane located at a distance from the dam of about three times the dam height. The bottom and side walls of the incompressible reservoir and the vertical plane at the upstream end are assumed to be rigid. The hydrodynamic pressures at nodal points on the reservoir free surface are set to zero, and thus the effects of surface waves are neglected. Furthermore, the pressures along the dam-reservoir interface are related to the total nodal accelerations in the direction normal to the dam face. The calculated hydrodynamic pressures on the face

of the dam are then converted into equivalent nodal forces using a consistent lumping process. Since the hydrodynamic forces, like the pressures, are proportional to the accelerations at nodal degrees of freedom on the face of the dam, this conversion leads to the added-mass coefficient matrix.

The output from the dynamic analysis includes mode shapes, natural frequencies, time histories of displacements and stresses. A snapshot of stresses at key points in time is also an option. The stresses are output at the optimal stress points. Further post-processing is described in Section 2.5.

2.4 Thermal Analysis

Acres has developed a finite element program to analyze three-dimensional heat transfer problems. The program, HEAT3D, has a variety of elements including 20-noded hexahedrons and 15-noded wedges. An infinite element is also available to effectively model an unbounded exterior problem (based on an approach by Zienkiewicz et al, 1983). The program is used to solve steady-state, periodic or transient heat transfer problems. The periodic solution is performed in the frequency domain using the complex form of the heat transfer equation.

2.5 Processing of Results

The output from a static or dynamic stress analysis includes displacements at nodes and element stresses at optimal stress points. The element stresses are extrapolated to the element nodes using a trilinear extrapolation procedure (Hinton and Campbell, 1979). Stresses from all dam elements adjacent to a node are then averaged to obtain a single value for contouring and display. It is important to note that the trilinear extrapolation procedure computes direct bending stresses (σ_{xx}, σ_{yy}, σ_{zz}) quite accurately, however shear stress is also extrapolated linearly to the nodes, although in beam bending the shear stress actually varies parabolically. The stress extrapolation procedure is approximate in areas where shear stresses are large and only one element is used in the thickness direction, however this may be overcome by adding additional elements in the thickness direction of the dam.

Stresses at the upstream heel of the dam are influenced by including the foundation element in the averaging procedure. There is a significant change if the upstream foundation element is included in particular. The stresses presented herein are obtained by averaging stresses from dam elements only.

The six global stress components are transformed into stress component directions which are useful for arch dam design. In addition to the six global stress components and three principal stresses, the following local stress components are computed

$\{\sigma_a, \sigma_c, \tau_{ac}, \sigma_1, \sigma_2, \theta\}$ --on the upstream and downstream faces

$\{\sigma_r, \sigma_v, \tau_{rv}, \sigma_1, \sigma_2, \theta\}$ --on vertical planes through the dam

where

σ_a	is an arch stress parallel to the dam face
σ_c	is a cantilever stress parallel to the dam face
τ_{ac}	is the shear stress in the arch-cantilever plane
σ_r	is the horizontal "radial" stress perpendicular to the dam face
σ_v	is the vertical stress
τ_{rv}	is the shear stress in the radial-vertical plane
σ,σ_2,θ	are corresponding principal stresses and directions.

The results plotted in the form of deformed shapes, color-fill or line contours and stress vectors. The results are processed such that views of the upstream face, downstream face, arches, cantilevers and isolated crown cantilever are automatically generated.

3 Results of Analyses

The loading conditions and assumptions suggested by the workshop organizing committee were analyzed by Acres using the computer programs described in Section 2. It is noted that the analyses have been performed using single precision arithmetic and the results of double precision analyses will be discussed at the workshop.

The workshop finite element mesh denoted MESH-ONE was used for the dead weight, hydrostatic pressure and dynamic analyses. The workshop mesh denoted MESH-TWO was used for the thermal and thermal stress analyses.

3.1 Dead Weight

The dead weight stress analysis was performed by applying body loads to the dam elements only and the dam was assumed to be a three-dimensional monolithic structure.

Arch and cantilever stress contours on the upstream face are presented in Figures 3.1 and 3.2, respectively. The results of the analysis are generally produced in color. In this paper, the color fill patterns are replaced with various black and white fill patterns. The arch stress distribution suggests that the dam is supporting dead weight by spanning the valley--which is not realistic. For comparison purposes the dead load stresses on the crown cantilever from an ADSAS trial load and the finite element benchmark analysis are presented in Table 3.1.

3.2 Hydrostatic Pressure

The hydrostatic pressure was applied to the upstream dam element faces only. A water level of 507 m asl was assumed. Arch and cantilever stress contours on the upstream face are presented in Figures 3.3 and 3.4. For comparison purposes, the hydrostatic loading calculations were varied as follows

(a) using the workshop criteria
(b) eliminating the foundation elements upstream of the dam and applying hydrostatic pressure to the dam only
(c) as in (b), but applying hydrostatic pressure to the dam and foundation upstream face
(d) ADSAS trail load analysis.

The crown cantilever results of each analysis are presented in Table 3.2.

3.3 Thermal Analyses

The thermal analyses were performed using Acres 3D heat transfer finite element programs and the workshop finite element mesh (MESH-TWO).

3.3.1 Steady-State Analysis

The steady-state temperature distribution through the crown cantilever section is shown in Figure 3.5.

3.3.2 Periodic Analysis

The periodic thermal analysis was performed by solving the heat transfer equation in the frequency domain. The temperature is represented by temperature amplitude and temperature phase. The temperature variation in the time domain may be computed using

$$T(t) = A \sin(\omega t + \emptyset)$$

where

$T(t)$	is the temperature at time t
A	is the temperature amplitude
$\emptyset$	is the temperature phase
ω	is the frequency of the oscillation ($\omega=2\pi/365$ for an annual cycle and t is given in days).

Amplitude and phase contours through crown cantilever sections are presented in Figures 3.6 and 3.7.

3.4 Stress Analysis Under Thermal Loading

The thermal stress analysis was performed using the steady-state temperature distribution and the dam-rock interface was restrained to zero displacement. Cantilever stresses on the crown cantilever section are presented in Figure 3.8 and arch stresses on the upper arches (top surface of dam elements) are presented in Figure 3.9.

3.5 Dynamic Analysis

The dynamic analyses were performed using the programs described in Section 2.

3.5.1 Dam on Rigid Foundation Without Water

The first six natural frequencies from the analysis are presented in Table 3.3. The modes are normalized such that the largest modal amplitude in any global direction is set to unity. The first two mode shapes are illustrated in Figures 3.10 and 3.11.

3.5.2 Dam on Flexible Foundation with Water Level at 491 m asl

The reservoir mesh supplied by the workshop committee was not used in this analysis. The reservoir mesh required by INCRES was generated using fluid elements which have linear interpolation functions in the upstream-downstream direction. The reservoir mesh contains 652 nodes, 144 3D fluid elements and 48 2D interface elements. It is noted that the fluid mesh contains less degrees-of-freedom than the mesh provided by the workshop committee and a comparison of this effect will be presented at the workshop.

The first six natural frequencies from the analysis are presented in Table 3.3.

4 Conclusions and Recommendations

Talvacchia dam was analyzed using the finite element model data and analysis assumptions provided by the benchmark workshop committee. It is understood that the analysis assumptions are somewhat crude and further workshops may investigate the effects of more realistic design assumptions.

References

J. Barlow, "Optimal Stress Locations in Finite Element Models", Int. J. Num. Meth. Eng., Col. 10, 1976, pp 243 - 251.

Yusof Ghannat, Ray W. Clough, "EADAP Enhanced Arch Dam Analysis Program, User's Manual," Earthquake Engineering Research Center, Report No. UCB/EERC-89/07, November 1989.

E. Hinton and J. S, Campbell, "Local and Global Smoothening of Discontinuous Finite Element Functions Using Least Squares Method," Int. J. Num. Meth. in Eng., Vol. 8, 1979, pp 461 - 480.

J. S.-H. Kuo, "Fluid-Structure Interactions: Added-Mass Computations for Incompressible Fluid," Report No. UCB/EERC 82/09, Earthquake Engineering Research Center, University of California, Berkeley, August 1982.

R. E. Newton, "Degeneration of Brick-Type Isoparametric Elements," Int. J. Num. Meth. Eng., Vol. 7, 1973, pp 579 - 581.

G. Strang and G. J. Fix, An Analysis of the Finite Element Method, Prentice-Hall, Inc., Englewood Cliffs, N.J., 1973.

O. C. Zienkiewicz, The Finite Element Method Third Edition, McGraw-Hill, 1977.

O. C. Zienkiewicz, C. Emson, and P. Bettess, "A Novel Boundary Infinite Element", Int. J. Num. Meth. Eng., Vol 19, No. 3, pp 393 - 404 (March 1983).

Table 3.1

Dead Load Cantilever Stresses on the Crown Cantilever

Elevation (m)	Cantilever Stress (MPa) Upstream Face			Downstream Face		
	Finite Element Analysis	ADSAS Grouted	ADSAS Ungrouted	Finite Element Analysis	ADSAS Grouted	ADSAS Ungrouted
507	-0.02	0.0	0.0	0.02	0.0	0.0
499	-0.15	-0.08	0.11	-0.22	-0.31	-0.47
491	-0.03	0.12	0.56	-0.56	-0.81	-1.20
481	0.10	0.43	1.15	-0.92	-1.45	-2.16
471	0.13	0.48	1.29	-1.14	-1.72	-2.57
460	-0.07	-0.20	0.88	-1.18	-1.72	-2.40
448	-0.59	-0.37	-0.02	-0.83	-1.46	-1.76
435	-1.86	-1.95	-1.67	-1.84	-0.42	-0.46

Table 3.2

Crown Cantilever Results from Various Hydrostatic Load Analyses

Elevation (m)	Stress Direction	Upstream Face Stress (MPa) FEM (a)	FEM (b)	FEM (c)	ADSAS	Downstream Face Stress (MPa) FEM (a)	FEM (b)	FEM (c)	ADSAS
507	A[1]	-2.68	-2.55	-2.38	-3.56	-0.52	0.03	0.13	-1.66
	C[1]	0.06	0.06	0.05	0.0	0.01	0.02	0.02	0.0
499	A	-3.50	-3.48	-3.31	-3.75	-0.95	-0.53	-0.47	-1.54
	C	-0.72	-0.68	-0.64	-0.72	0.48	-0.45	0.42	0.63
491	A	-4.30	-4.41	-4.23	-4.08	-1.44	-1.22	-1.20	-1.45
	C	-1.42	-1.32	-1.21	-1.50	0.99	0.86	0.77	1.25
481	A	-4.59	-4.84	-4.69	-4.33	-1.54	-1.50	-1.56	-1.32
	C	-1.66	-1.58	-1.39	-1.89	1.08	0.88	0.71	1.45
471	A	-4.24	-4.66	-4.57	-4.40	-1.25	-1.31	-1.48	-1.00
	C	-1.37	-1.42	-1.21	-1.59	0.75	0.60	0.36	1.05
460	A	-3.31	-3.96	-4.01	-4.01	-0.72	-0.80	-1.11	-0.57
	C	-0.66	-0.97	-0.79	-0.96	0.10	0.14	-0.12	0.41
448	A	-1.97	-2.81	-3.11	-2.46	-0.11	-0.04	-0.46	0.26
	C	0.76	-0.07	-0.11	0.18	-1.43	-0.71	-0.76	-0.75
435	A	0.99	-0.57	-1.58	-	-0.27	0.01	-0.77	-
	C	3.92	2.57	2.20	3.37	-4.83	-4.05	-3.71	-4.09

Notes

FEM(a) - FEM hydrostatic load analysis using workshop criteria.
FEM(b) - FEM hydrostatic load analysis with upstream foundation elements eliminated.
FEM(c) - FEM hydrostatic load analysis as in (b), but hydrostatic pressure also applied to foundation.

[1] A = arch stress, C = cantilever stress

Table 3.3

Natural Frequencies from Dynamic Analyses 3.5.1 and 3.5.2

Mode Number	Natural Frequency (H_z)	
	Analysis 3.5.1	Analysis 3.5.2
1	4.30	3.67
2	4.58	3.91
3	5.70	5.19
4	6.72	6.17
5	8.59	7.14
6	9.38	8.01

EMRC - DISPLAY II POST-PROCESSOR VER 90.0 Feb/23/91

Upstream Face
File: MSH1-DL1
VIEW : -1.08E+00
RANGE: 1.09E+00

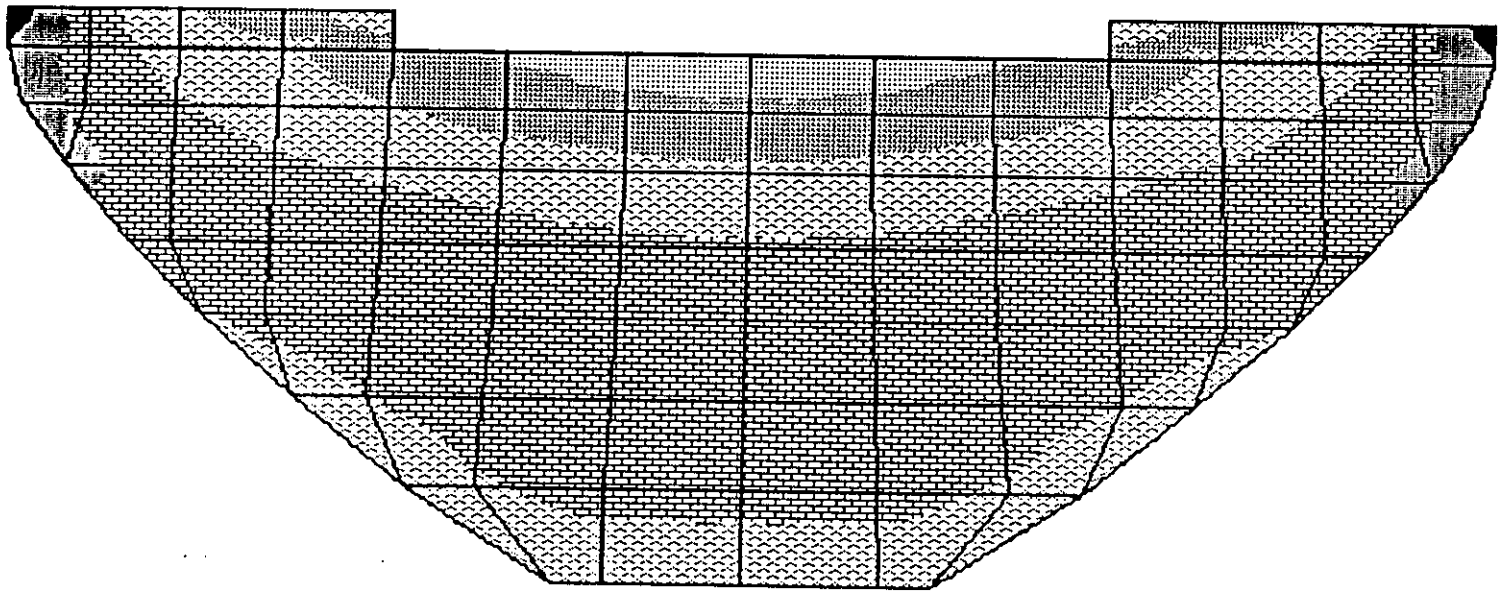

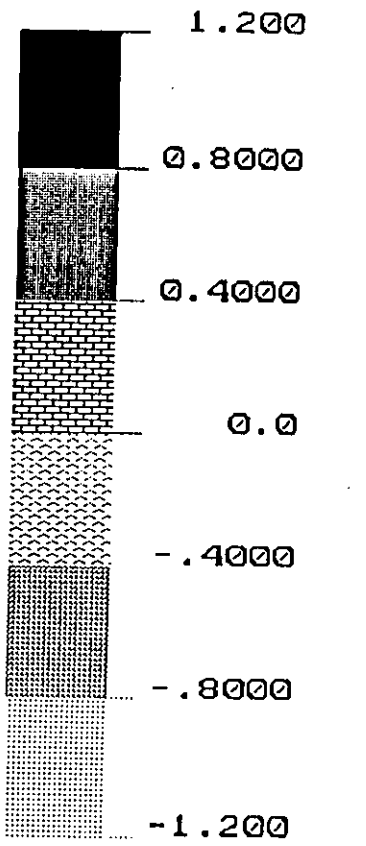

LOAD CONDITION 3.1 DEAD WEIGHT. ARCH STRESS (MPA)

First Benchmark Workshop on Numerical Analysis of Dams

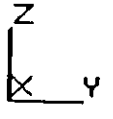

RX= -90
RY= 0
RZ= -90

EMRC - DISPLAY II POST-PROCESSOR VER 90.0 Feb/23/91

Upstream Face
File: MSH1-DL1
VIEW : -1.86E+00
RANGE: 3.36E-01

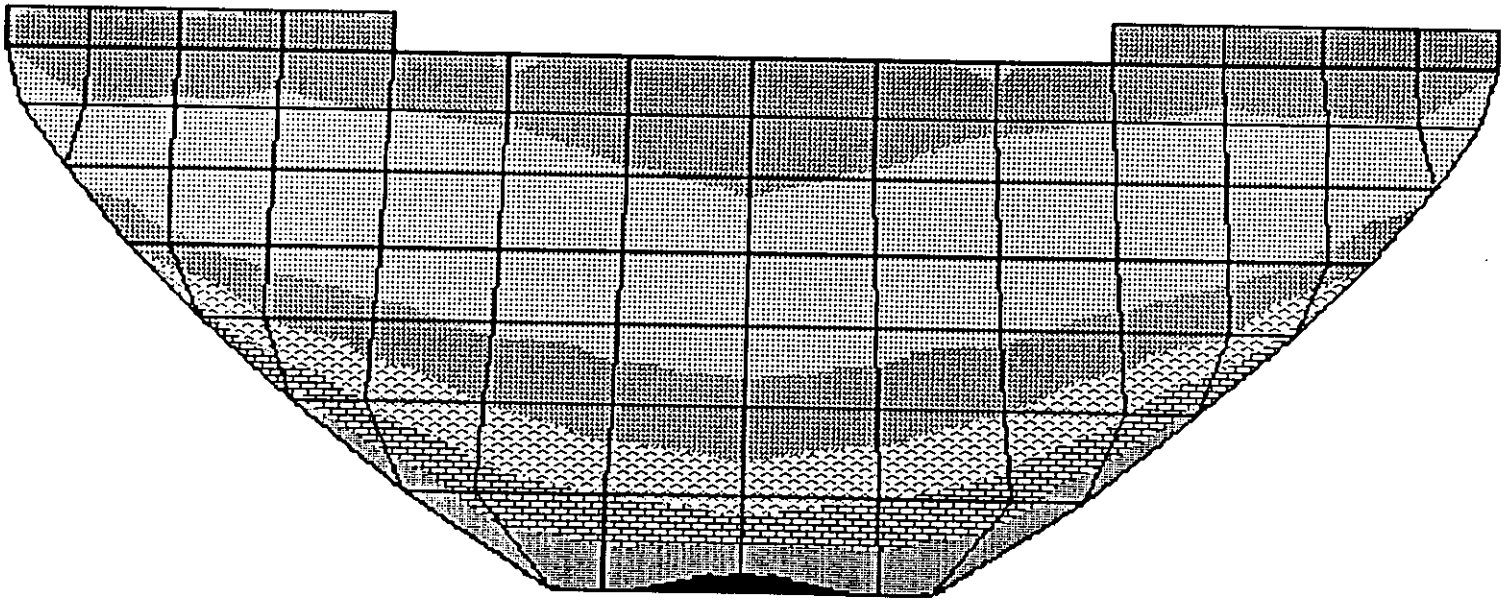

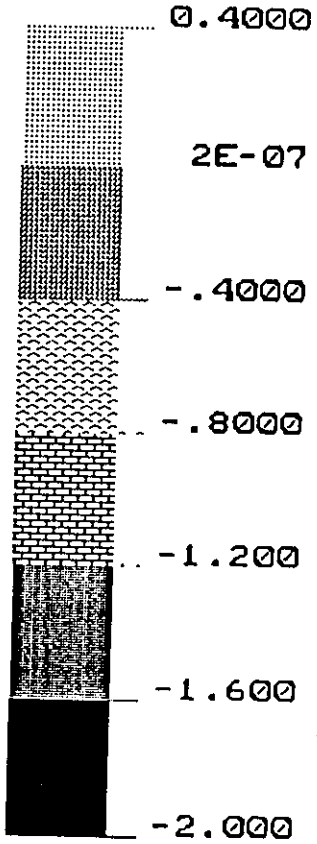

LOAD CONDITION 3.1 DEAD WEIGHT. CANT. STRESS (MPA)

First Benchmark Workshop on Numerical Analysis of Dams

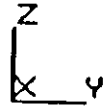

RX= -90
RY= 0
RZ= 90

EMRC - DISPLAY II POST-PROCESSOR VER 90.0 Feb/23/91

Upstream Face
File: MSH1-HY1
VIEW : -4.59E+00
RANGE: 1.14E+00

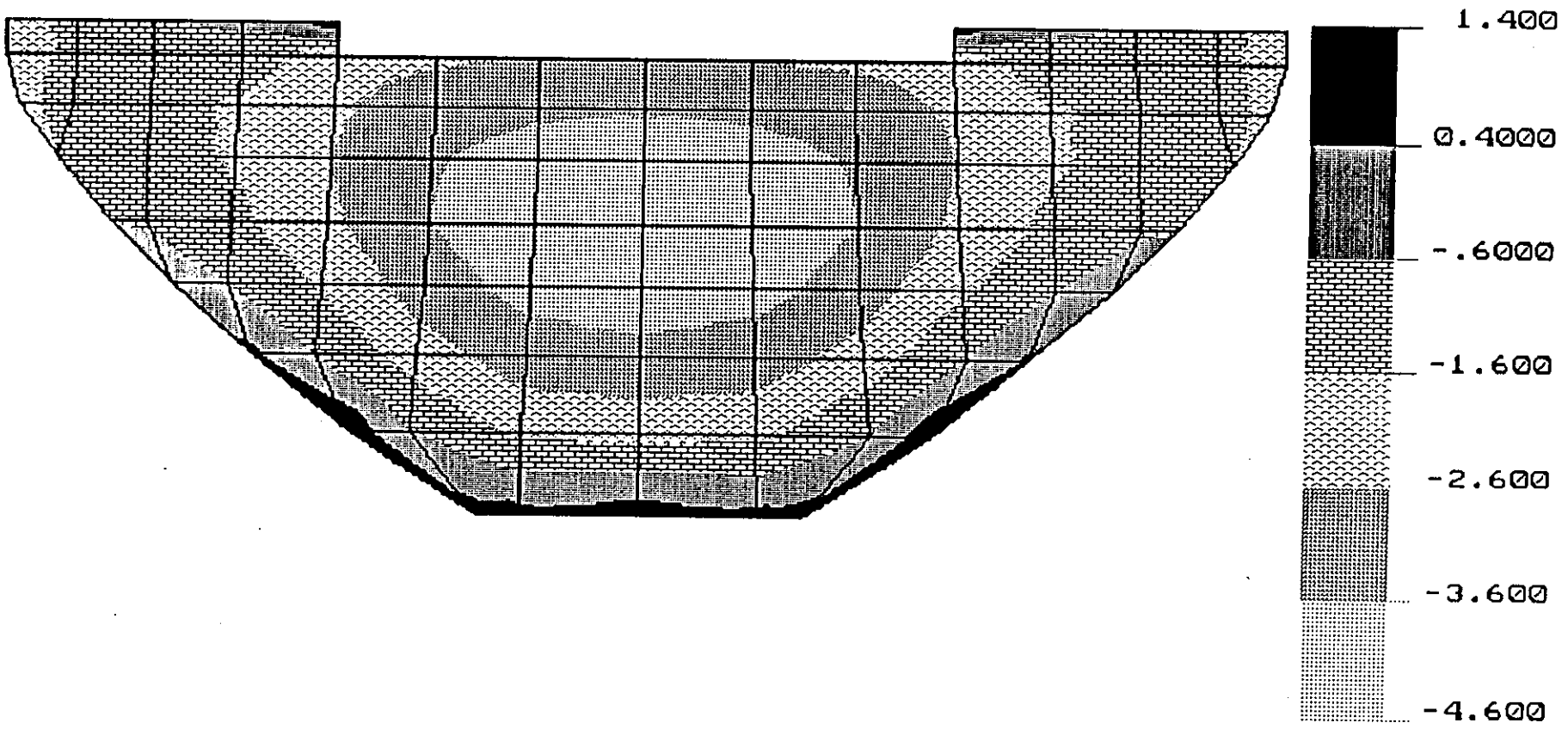

LOAD CONDITION 3.2 HYDROSTATIC. ARCH STRESS (MPA)

First Benchmark Workshop on Numerical Analysis of Dams

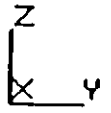

RX= -90
RY= 0
RZ= -90

EMRC - DISPLAY II POST-PROCESSOR VER 90.0 Feb/23/91

Upstream Face
File: MSH1-HY1
VIEW : -1.68E+00
RANGE: 3.92E+00

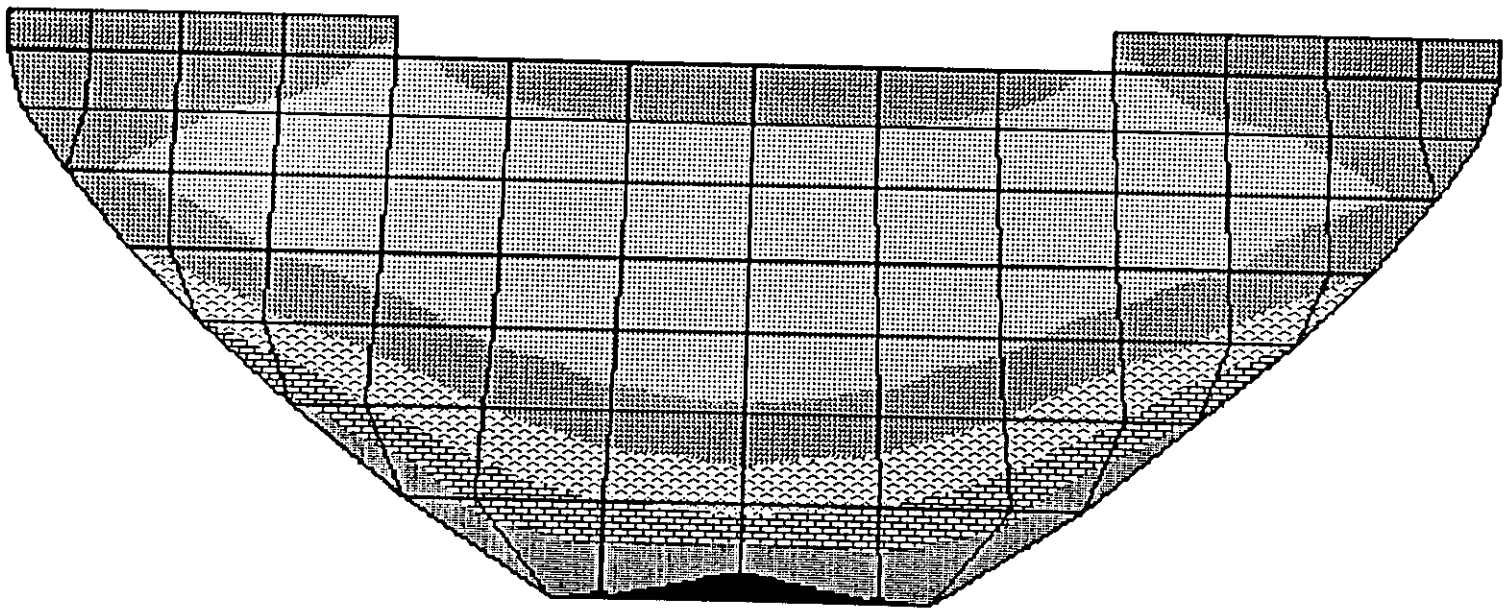

4.000
3.050
2.100
1.150
0.2000
-.7500
-1.700

LOAD CONDITION 3.2 HYDROSTATIC. CANT. STRESS (MPA)

First Benchmark Workshop on Numerical Analysis of Dams

RX= -90
RY= 0
RZ= -90

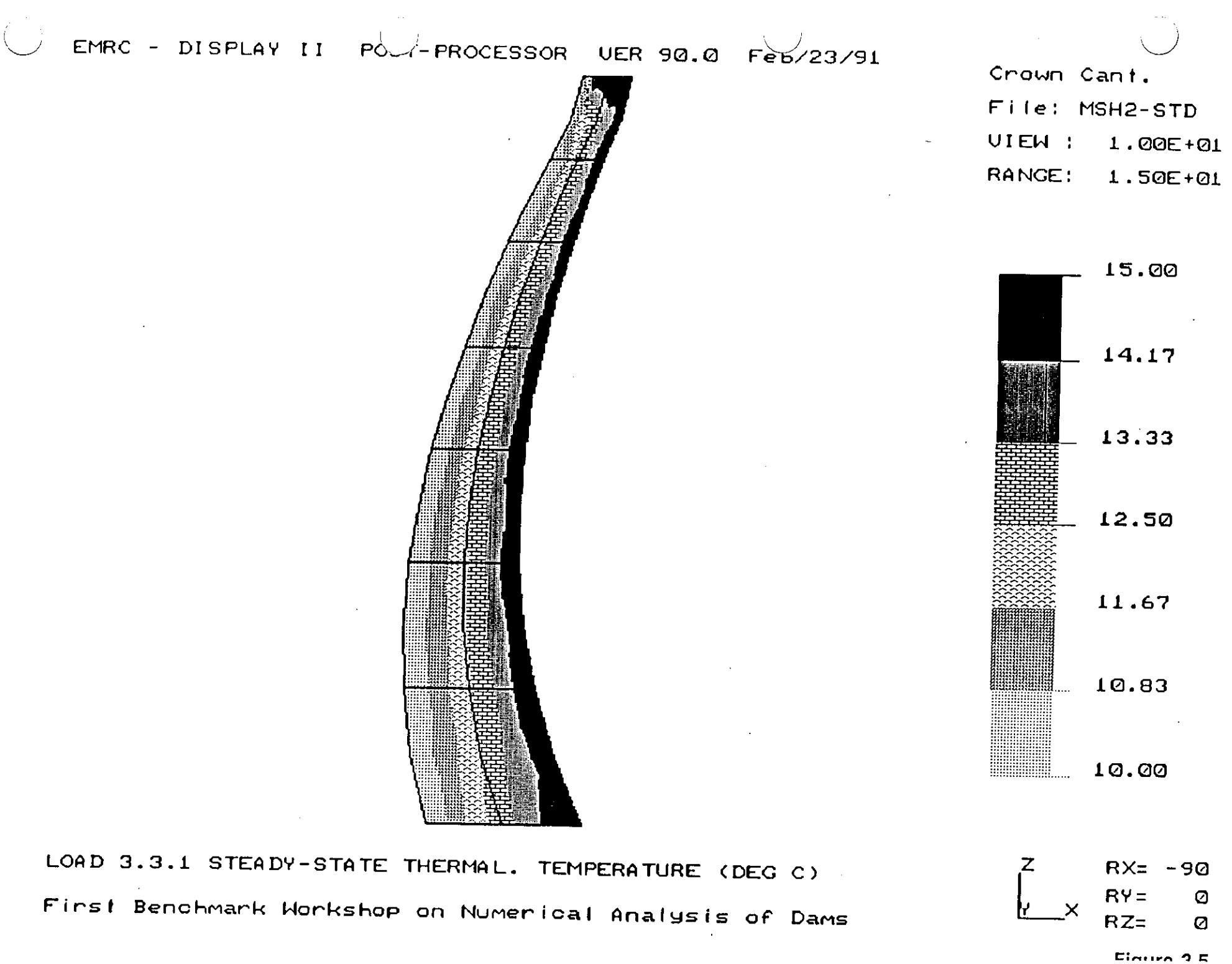
EMRC - DISPLAY II POST-PROCESSOR VER 90.0 Feb/23/91
Crown Cant.
File: MSH2-STD
VIEW : 1.00E+01
RANGE: 1.50E+01
15.00
14.17
13.33
12.50
11.67
10.83
10.00
LOAD 3.3.1 STEADY-STATE THERMAL. TEMPERATURE (DEG C)
First Benchmark Workshop on Numerical Analysis of Dams
Z
Y
X
RX= -90
RY= 0
RZ= 0

Figure 2.5

EMRC - DISPLAY II POST-PROCESSOR VER 90.0 Feb/23/91

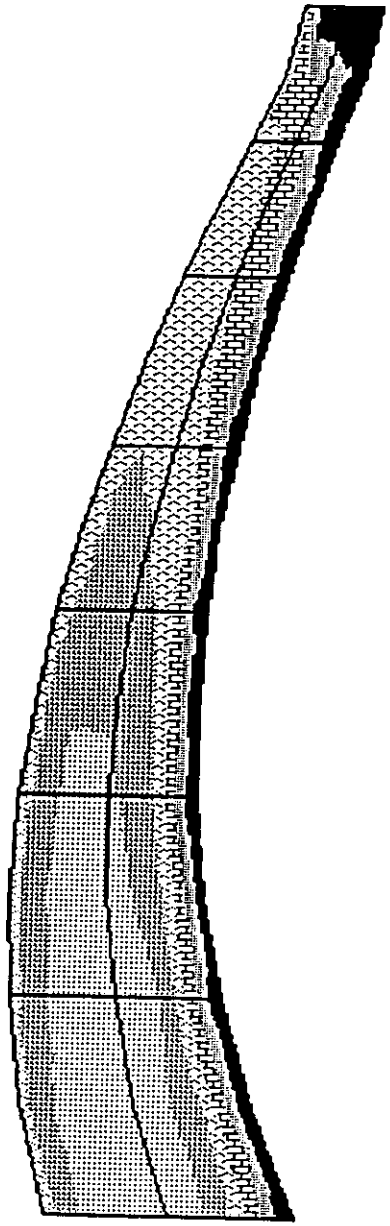

Crown Cant.
File: MSH2-PER
VIEW : 1.67E+00
RANGE: 1.00E+01

10.00
8.600
7.200
5.800
4.400
3.000
1.600

LOAD 3.3.2 PERIODIC THERMAL. AMPLITUDE (DEG C)

First Benchmark Workshop on Numerical Analysis of Dams

Z
Y X

RX= -90
RY= 0
RZ= 0

EMRC - DISPLAY II POST-PROCESSOR VER 90.0 Feb/23/91

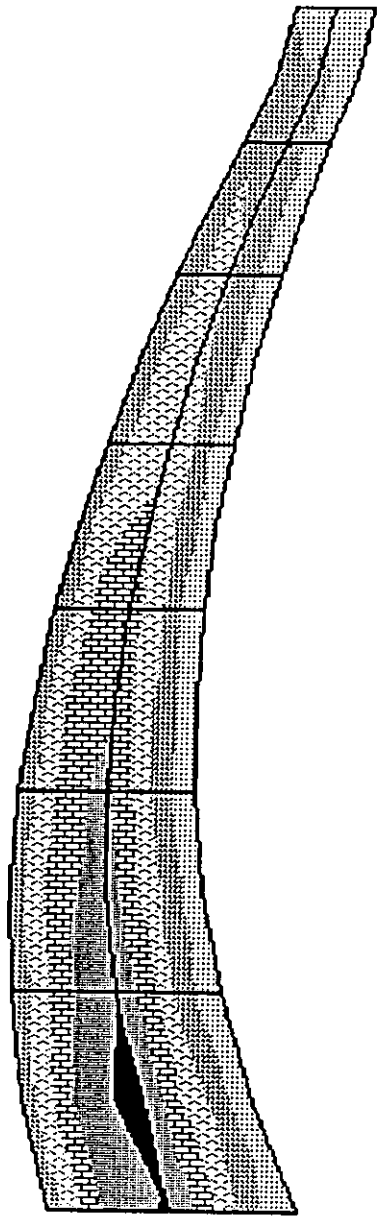

Crown Cant.
File: MSH2-PER
VIEW : -2.50E+00
RANGE: 0.00E+00

0.0
-.4500
-.9000
-1.350
-1.800
-2.250
-2.700

LOAD 3.3.2 PERIODIC THERMAL. PHASE (RADIANS)

First Benchmark Workshop on Numerical Analysis of Dams

Z
Y
X
RX= -90
RY= 0
RZ= 0

Figure 3.7

EMRC - DISPLAY II POST-PROCESSOR VER 90.0 Mar/ 2/91

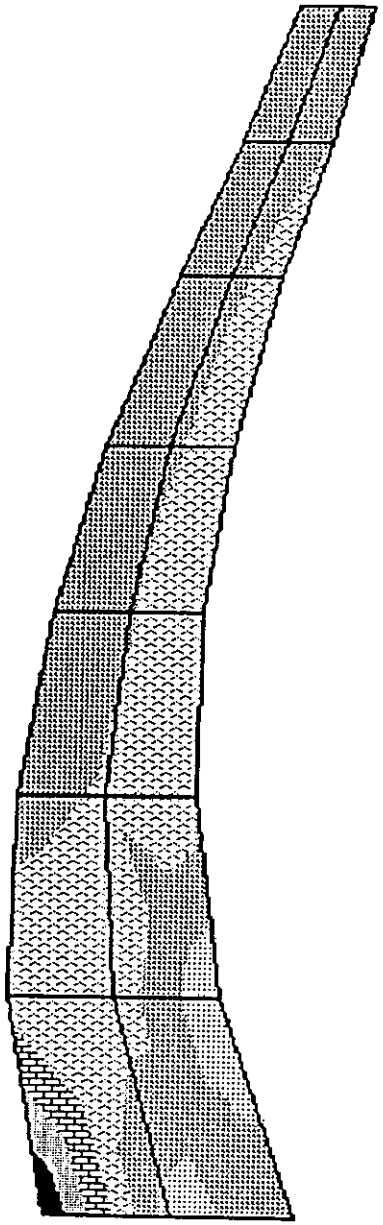

Crown Cant.
File: MSH2-TMP
VIEW : -5.24E+00
RANGE: 2.03E+00

2.250
1.000
-.2500
-1.500
-2.750
-4.000
-5.250

LOAD 3.4 THERMAL STRESS. CANTILEVER STRESS (MPA)

First Benchmark Workshop on Numerical Analysis of Dams

Z
Y X

RX= -90
RY= 0
RZ= 0

EMRC - DISPLAY II POST-PROCESSOR VER 90.0 Mar 2/91

Arches
File: MSH2-TMP
VIEW : -1.14E+01
RANGE: 2.05E+00

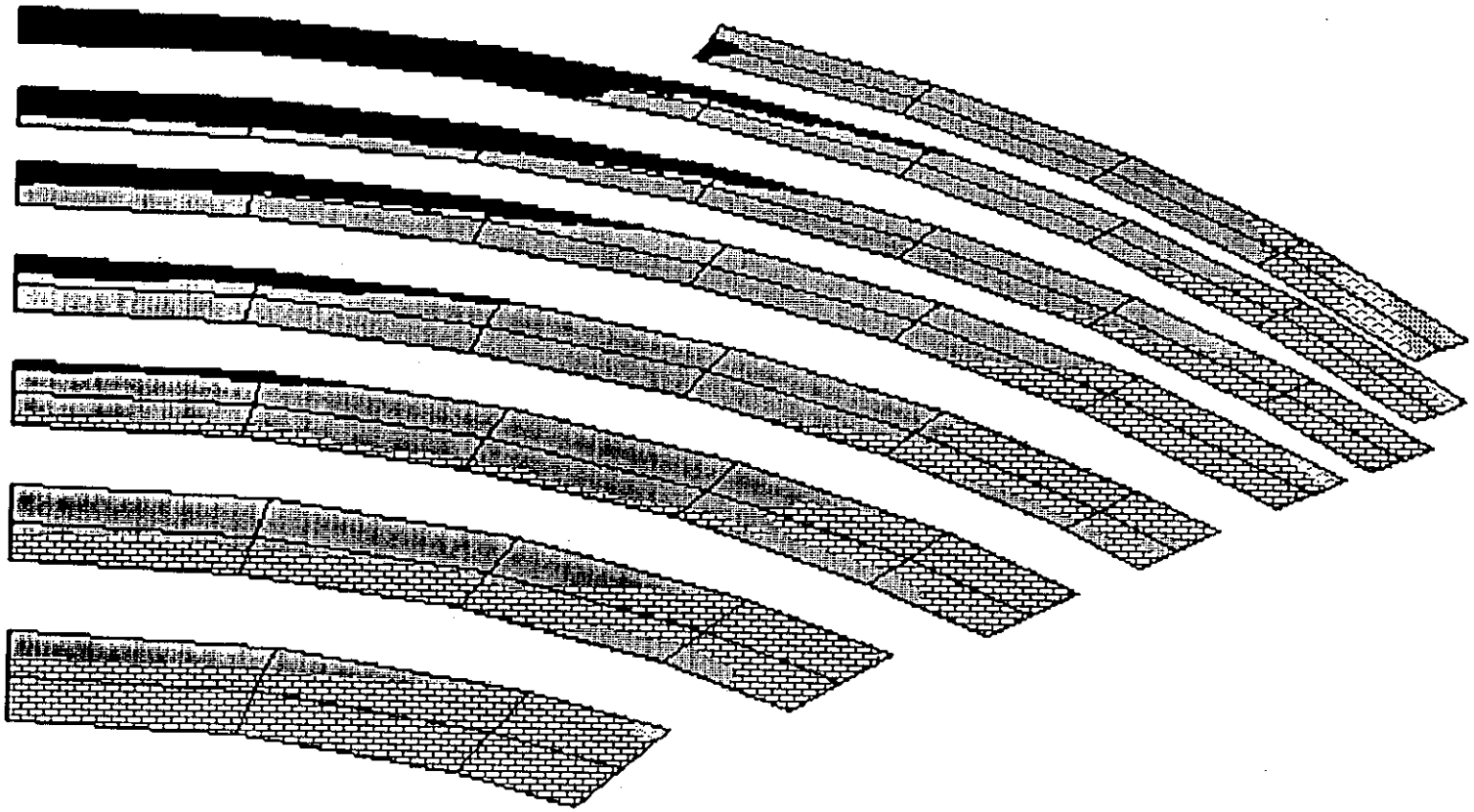

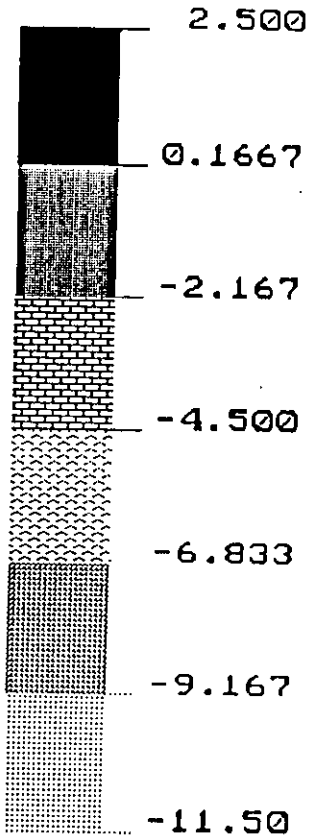

LOAD 3.4 THERMAL STRESS. ARCH STRESS (MPA)

First Benchmark Workshop on Numerical Analysis of Dams

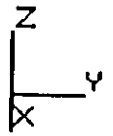

RX= -60
RY= 0
RZ= -90

EMRC - DISPLAY II POST-PROCESSOR VER 90.0 Mar/13/91

DISPLACED-SHAPE
MX.DEF= 1.14E+00
NODE NO= 1115
SCALE = 1.0
(MAPPED SCALING)

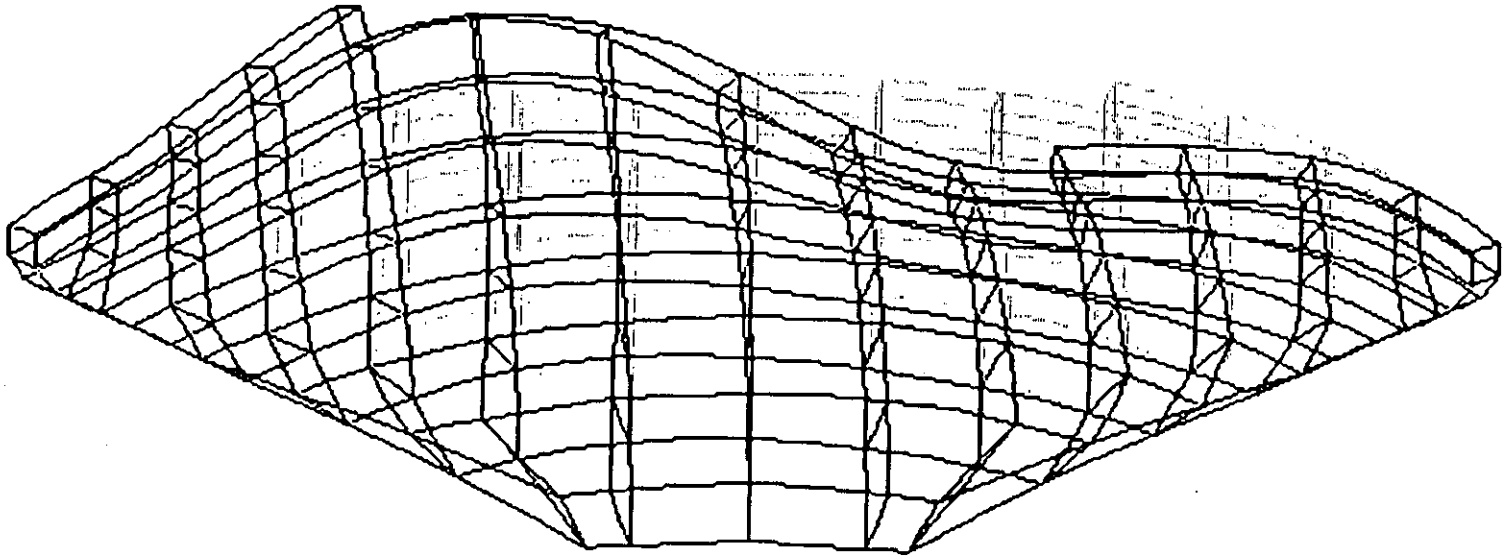

DYNAMIC ANALYSIS 3.5.1: Fn(1) = 4.30 Hz

First Benchmark Workshop on Numerical Analysis of Dams

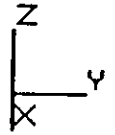

RX= -60
RY= 0
RZ= 90

EMRC - DISPLAY II POST-PROCESSOR VER 90.0 Mar/13/91

DISPLACED-SHAPE
MX.DEF= 1.04E+00
NODE NO= 725
SCALE = 1.0
(MAPPED SCALING)

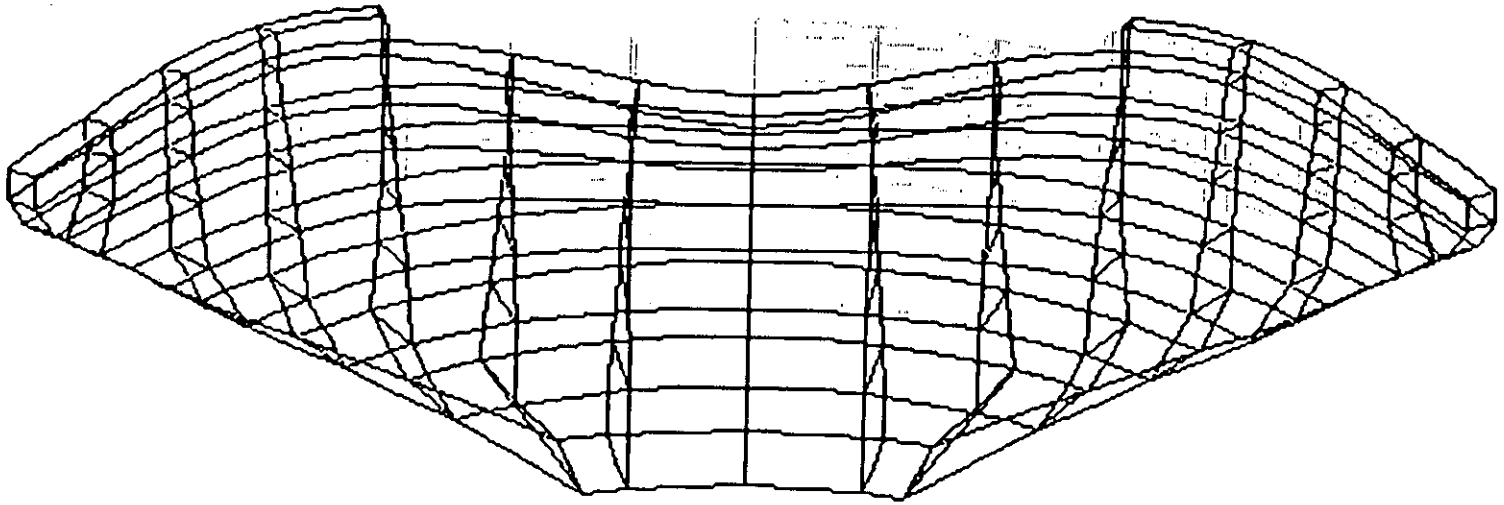

DYNAMIC ANALYSIS 3.5.1: Fn(2) = 4.58 Hz

First Benchmark Workshop on Numerical Analysis of Dams

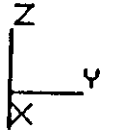

RX= -60
RY= 0
RZ= -90

Appendix A

Results at Key Locations from Workshop Guidelines

Table A.1

Load Condition 3.1 Dead Weight

Points	s (m)	Displ.x (mm)	Displ.y (mm)	Displ.z (mm)	P1 (MPa)	P2 (MPa)	P3 (MPa)
1	0.0	0.819	0.000	-2.975	0.010	-0.015	-1.089
2	0.0	0.834	0.000	-3.189	0.003	0.002	-1.143
3	0.0	0.849	0.000	-3.402	0.020	-0.004	-1.197
4	0.0	-0.586	0.000	-2.410	0.011	-0.046	-0.336
5	0.0	-0.577	0.000	-2.645	0.002	-0.299	-0.421
6	0.0	-0.565	0.000	-2.897	0.003	-0.506	-0.560
7	16.0	-0.546	-0.144	-2.320	0.036	-0.019	-0.304
8	16.0	-0.539	-0.159	-2.555	0.002	-0.256	-0.429
9	16.0	-0.529	-0.176	-2.809	0.003	-0.445	-0.635
10	48.0	-0.215	-0.416	-1.702	0.298	-0.013	-0.113
11	48.0	-0.226	-0.449	-1.936	0.008	-0.04	-0.449
12	48.0	-0.229	-0.484	-2.200	0.003	-0.171	-0.968
13	80.0	-0.067	-0.480	-0.840	0.339	0.188	-0.022
14	80.0	-0.049	-0.451	-1.000	0.212	0.019	-0.511
15	80.0	-0.019	-0.429	-1.182	0.214	0.04	-1.319
16	99.2	-0.146	-0.177	-0.389	0.562	0.241	-0.268
17	99.2	-0.136	-0.145	-0.461	0.320	-0.156	-0.542
18	99.2	-0.110	-0.114	-0.505	0.189	-0.154	-1.325
19	0.0	-1.360	0.000	-2.169	0.278	0.129	-0.023
20	0.0	-1.361	0.000	-2.173	0.061	-0.021	-0.512
21	0.0	-1.343	0.000	-2.201	-0.022	-0.155	-1.15
22	16.0	-1.261	0.110	-2.103	0.293	0.104	-0.023
23	16.0	-1.270	0.068	-2.101	0.077	-0.02	-0.534
24	16.0	-1.259	0.023	-2.115	-0.018	-0.138	-1.172
25	48.0	-0.583	0.110	-1.602	0.255	0.073	-0.229
26	48.0	-0.626	0.026	-1.567	0.156	0.01	-0.678
27	48.0	-0.654	-0.072	-1.498	0.065	0.034	-1.219
28	75.0	-0.066	-0.074	-0.807	0.174	-0.036	-1.28
29	75.0	-0.100	-0.094	-0.849	0.180	-0.205	-0.722
30	75.0	-0.134	-0.101	-0.754	0.330	0.179	-0.859
31	0.0	-0.638	0.000	-2.076	0.190	0.072	-0.587
32	0.0	-0.622	0.000	-1.737	0.022	0.004	-0.759
33	0.0	-0.600	0.000	-1.427	-0.012	-0.183	-0.947
34	16.0	-0.530	0.120	-1.950	0.167	0.023	-0.823
35	16.0	-0.526	0.054	-1.654	0.017	-0.032	-0.828
36	16.0	-0.515	-0.010	-1.355	-0.002	-0.203	-0.849
37	41.5	0.002	0.058	-1.198	-0.015	-0.278	-1.963
38	41.5	-0.054	-0.022	-1.186	-0.015	-0.284	-0.862
39	41.5	-0.118	-0.067	-0.948	0.476	0.232	-0.772
40	0.0	0.007	0.000	-1.484	-0.191	-0.399	-2.241
41	0.0	0.001	0.000	-1.317	-0.234	-0.318	-0.952
42	0.0	-0.053	0.000	-0.977	0.509	-0.07	-0.619

Table A.2

Load Condition 3.2 Hydrostatic Pressure

Points	s (m)	Displ.x (mm)	Displ.y (mm)	Displ.z (mm)	P1 (MPa)	P2 (MPa)	P3 (MPa)
1	0.0	22.170	0.001	-0.566	0.077	0.010	-2.696
2	0.0	22.202	0.001	-0.843	0.046	0.020	-1.610
3	0.0	22.219	0.000	-1.131	0.076	-0.031	-0.524
4	0.0	19.965	0.001	0.426	-0.100	-1.420	-4.315
5	0.0	20.020	0.000	-0.203	-0.019	-0.235	-2.880
6	0.0	20.051	0.000	-0.756	0.996	0.015	-1.444
7	16.0	18.364	-1.661	0.468	-0.101	-1.373	-4.148
8	16.0	18.487	-1.154	-0.110	-0.017	-0.225	-2.881
9	16.0	18.592	-0.629	-0.614	1.002	0.013	-1.639
10	48.0	8.895	-1.892	0.524	-0.112	-1.264	-2.739
11	48.0	9.305	-1.048	0.257	-0.017	-0.193	-2.579
12	48.0	9.720	-0.182	0.057	1.102	0.009	-2.576
13	80.0	1.822	0.648	0.074	-0.123	-0.942	-1.199
14	80.0	2.030	0.873	0.133	0.169	-0.049	-1.947
15	80.0	2.252	1.114	0.215	1.317	0.043	-2.749
16	99.2	0.840	0.723	-0.132	-0.106	-0.582	-2.053
17	99.2	0.869	0.757	-0.075	0.033	-0.300	-1.818
18	99.2	0.831	0.733	-0.012	0.712	-0.046	-2.094
19	0.0	14.427	0.000	2.670	-0.318	-1.387	-4.262
20	0.0	14.503	0.000	1.115	-0.099	-0.323	-2.758
21	0.0	14.548	0.000	-0.402	0.769	0.092	-1.254
22	16.0	13.134	-1.629	2.518	-0.293	-1.252	-4.022
23	16.0	13.298	-1.085	1.044	-0.105	-0.293	-2.682
24	16.0	13.433	-0.521	-0.407	0.754	0.052	-1.398
25	48.0	5.526	-1.628	1.488	0.040	-0.457	-1.781
26	48.0	6.030	-0.744	0.503	0.132	-0.215	-2.223
27	48.0	6.526	0.124	-0.510	0.618	-0.156	-2.876
28	75.0	1.199	0.547	0.170	1.222	0.747	-0.993
29	75.0	1.478	0.868	-0.119	0.224	-0.522	-1.797
30	75.0	1.547	0.964	-0.370	-0.321	-0.590	-4.256
31	0.0	5.981	0.000	3.299	0.750	-1.352	-1.967
32	0.0	5.881	0.000	1.150	0.129	-0.937	-1.040
33	0.0	5.894	0.000	-0.909	0.588	-0.113	-1.601
34	16.0	5.170	-0.758	2.875	1.212	-1.029	-1.913
35	16.0	5.181	-0.287	0.950	0.134	-0.667	-1.200
36	16.0	5.260	0.144	-0.935	0.513	0.002	-2.249
37	41.5	1.400	-0.097	0.939	3.367	1.464	0.517
38	41.5	1.866	0.573	-0.051	0.628	0.106	-1.489
39	41.5	2.021	0.867	-0.791	-0.283	-1.372	-5.203
40	0.0	1.668	0.000	1.742	4.305	1.281	0.979
41	0.0	1.780	0.000	0.096	0.991	0.362	-1.066
42	0.0	1.789	0.000	-0.924	-0.255	-0.879	-4.857

Table A.3

Loading 3.3.1 and 3.3.2 Steady-State and Periodic Thermal Analysis

Points	s (m)	Steady State Analysis Temperature (°C)	Periodic Analysis	
			Amplitude A (°C)	Phase φ (rad)
1	0.0	15.000	10.000	0.000
2	16.0	15.000	10.000	0.000
3	48.0	15.000	10.000	0.000
4	80.0	13.550	7.630	-0.547
5	112.9	13.569	7.646	-0.552
6	0.0	12.346	5.856	-0.958
7	16.0	12.346	5.841	-0.961
8	48.0	12.348	5.728	-0.981
9	80.0	12.361	5.630	-1.013
10	99.2	12.311	5.682	-1.007
11	0.0	12.347	3.752	-1.567
12	16.0	12.349	3.740	-1.572
13	48.0	12.364	3.683	-1.592
14	75.0	12.673	4.134	-1.467
15	0.0	12.377	1.853	-2.250
16	16.0	12.387	1.895	-2.254
17	41.5	12.658	2.224	-2.128
18	0.0	13.028	1.733	-2.289
19	16.0	13.009	1.674	-2.342
20	22.0	13.042	1.698	-2.291

Table A.4

Load Condition 3.4 Stress Anslysis Under Thermal Loadings

Points	s (m)	Displ.x (mm)	Displ.y (mm)	Displ.z (mm)	P1 (MPa)	P2 (MPa)	P3 (MPa)
1	0.0	-17.724	-0.001	8.696	2.056	0.148	-0.006
2	0.0	-17.510	-0.003	9.575	0.765	-0.023	-0.119
3	0.0	-17.279	-0.006	10.425	0.446	0.106	0.013
4	0.0	-13.245	-0.001	5.461	1.631	0.752	-0.039
5	0.0	-13.013	-0.002	6.322	0.279	0.098	-0.104
6	0.0	-12.701	-0.003	7.169	0.004	-0.704	-1.207
7	16.0	-12.333	1.765	5.173	1.462	0.618	-0.037
8	16.0	-12.141	1.439	6.049	0.236	0.051	-0.142
9	16.0	-11.872	1.107	6.915	-0.004	-0.681	-1.221
10	48.0	-6.806	3.237	3.210	0.532	-0.029	-0.635
11	48.0	-6.806	2.598	4.144	0.220	0.021	-1.133
12	48.0	-6.743	1.938	5.093	-0.021	-0.166	-1.833
13	80.0	-1.380	1.582	0.953	0.391	-0.708	-2.432
14	80.0	-1.445	1.072	1.554	0.657	0.013	-2.912
15	80.0	-1.498	0.499	2.227	1.353	0.528	-3.518
16	99.2	0.000	0.000	0.000	-1.084	-3.779	-5.775
17	99.2	-0.469	0.367	0.813	0.330	-0.639	-3.888
18	99.2	0.000	0.000	0.000	3.219	-2.861	-4.731
19	0.0	-8.468	0.000	1.862	0.746	0.717	-0.029
20	0.0	-8.127	-0.001	3.081	-0.074	-0.214	-0.917
21	0.0	-7.647	-0.001	4.289	-0.004	-1.293	-2.782
22	16.0	-7.578	1.364	1.740	0.635	0.340	-0.045
23	16.0	-7.299	0.921	2.912	-0.004	-0.196	-1.117
24	16.0	-6.888	0.455	4.085	-0.054	-1.083	-2.842
25	48.0	-2.543	1.660	0.777	0.020	-0.903	-2.112
26	48.0	-2.469	0.907	1.640	0.586	-0.018	-2.538
27	48.0	-2.315	0.153	2.491	0.908	-0.211	-3.171
28	75.0	0.000	0.000	0.000	-0.695	-3.812	-6.133
29	75.0	0.000	0.000	0.000	1.493	-2.673	-3.584
30	75.0	0.000	0.000	0.000	2.123	-3.958	-4.574
31	0.0	-2.768	0.000	-0.302	1.479	-1.048	-1.264
32	0.0	-2.169	0.000	0.914	0.911	-1.599	-2.799
33	0.0	-1.417	0.000	2.130	2.406	0.126	-3.625
34	16.0	-2.320	0.553	-0.143	0.866	-1.231	-1.645
35	16.0	-1.781	0.207	0.892	0.957	-1.522	-3.071
36	16.0	-1.103	-0.146	1.941	1.809	0.042	-4.088
37	41.5	0.000	0.000	0.000	-1.050	-4.388	-8.427
38	41.5	0.000	0.000	0.000	1.837	-2.873	-3.498
39	41.5	0.000	0.000	0.000	2.528	-3.968	-4.629
40	0.0	0.000	0.000	0.000	-1.663	-4.729	-8.306
41	0.0	0.000	0.000	0.000	1.380	-2.850	-3.901
42	0.0	0.000	0.000	0.000	2.217	-3.564	-4.421

Table A.5

Dynamic Analysis 3.5.1
Dam on Rigid Foundation Without Water

Points	s (m)	Mode 1 Displ.x	Mode 1 Displ.y	Mode 1 Displ.z	Mode 2 Displ.x	Mode 2 Displ.y	Mode 2 Displ.z	Mode 3 Displ.x	Mode 3 Displ.y	Mode 3 Displ.z
1	0.0	0.0009	-0.2599	-0.0002	0.9994	0.0001	-0.2358	0.0772	0.0000	-0.0142
2	16 0	0.6777	-0.3174	-0.1739	0.7879	-0.0287	-0.1770	0.2586	-0.0845	-0.0669
3	48.0	0.8605	-0.4155	-0.2035	-0.1020	0.1540	0.0525	0.8239	-0.4095	-0.2260
4	80.0	0.1648	-0.0769	-0.0255	-0.1421	0.1302	0.0421	0.2862	-0.1690	-0.0612
5	112.9	0.0000	0.0000	0.0000	0.0000	0.0000	0.0000	0.0000	0.0000	0.0000
6	0 0	0.0006	-0.1725	-0.0001	0.5777	0.0001	-0.0852	0.0335	0.0000	-0.0079
7	16.0	0.3715	-0.2015	-0.0615	0.4639	-0.0163	-0.0623	0.1161	-0.0401	-0.0241
8	48.0	0.4500	-0.2316	-0.0494	-0.0088	0.0702	0.0136	0.3465	-0.1626	-0.0502
9	80.0	0.0595	-0.0347	0.0041	-0.0397	0.0494	0.0025	0.0861	-0.0527	0.0018
10	99.2	0.0000	0.0000	0.0000	0.0000	0.0000	0.0000	0.0000	0.0000	0.0000
11	0.0	0.0002	-0.0685	0.0000	0.2143	0.0000	0.0113	0.0057	0.0000	-0.0019
12	16 0	0.1286	-0.0794	0.0055	0.1711	-0.0090	0.0110	0.0264	-0.0077	-0.0012
13	48.0	0.1044	-0.0647	0.0132	0.0084	0.0185	0.0029	0.0577	-0.0263	0.0050
14	75.0	0.0000	0.0000	0.0000	0.0000	0.0000	0.0000	0.0000	0.0000	0.0000
15	0.0	0.0000	-0.0137	0.0000	0.0285	0.0000	0.0095	-0.0014	0.0000	-0.0006
16	16.0	0.0146	-0.0136	0.0055	0.0204	-0.0004	0.0069	0.0005	0.0001	0.0002
17	41.5	0.0000	0.0000	0.0000	0.0000	0.0000	0.0000	0.0000	0.0000	0.0000
18	0.0	0.0000	0.0000	0.0000	0.0000	0.0000	0.0000	0.0000	0.0000	0.0000
19	16.0	0.0000	0.0000	0.0000	0.0000	0.0000	0.0000	0.0000	0.0000	0.0000
20	22.0	0.0000	0.0000	0.0000	0.0000	0.0000	0.0000	0.0000	0.0000	0.0000

Points	s (m)	Mode 4 Displ.x	Mode 4 Displ.y	Mode 4 Displ.z	Mode 5 Displ.x	Mode 5 Displ.y	Mode 5 Displ.z	Mode 6 Displ.x	Mode 6 Displ.y	Mode 6 Displ.z
1	0.0	0.0002	0.0752	-0.0001	1.0000	0.0000	-0.3863	0.9936	-0.0001	-0.6039
2	16.0	-0.6485	0.1145	0.1789	0.3335	0.0117	-0.1778	0.9652	-0.1774	-0.5658
3	48.0	0.3934	-0.3289	-0.1515	-0.3033	0.0146	0.0126	0.2104	-0.1143	-0.1735
4	80.0	0.5578	-0.4299	-0.1524	0.6819	-0.5804	-0.2117	-0.2599	0.1715	0.0524
5	112.9	0.0000	0.0000	0.0000	0.0000	0.0000	0.0000	0.0000	0.0000	0.0000
6	0.0	0.0000	0.0422	0.0000	0.3707	0.0000	-0.1493	-0.2638	-0.0001	-0.1482
7	16.0	-0.3490	0.0636	0.0667	0.0633	0.0284	-0.0725	-0.1889	0.0033	-0.1469
8	48.0	0.0352	-0.0757	-0.0171	-0.3355	0.1138	0.0280	-0.0671	0.0080	-0.0698
9	80.0	0.1415	-0.1242	-0.0055	0.1315	-0.1302	-0.0120	-0.0744	0.0472	-0.0069
10	99.2	0.0000	0.0000	0.0000	0.0000	0.0000	0.0000	0.0000	0.0000	0.0000
11	0.0	0.0000	0.0117	0.0000	0.0152	0.0000	-0.0260	-0.5749	0.0001	-0.0320
12	16.0	-0.1099	0.0221	0.0000	-0.0565	0.0170	-0.0212	-0.4841	0.0531	-0.0357
13	48.0	-0.0243	-0.0016	-0.0006	-0.1082	0.0461	-0.0096	-0.1063	0.0256	-0.0306
14	75.0	0.0000	0.0000	0.0000	0.0000	0.0000	0.0000	0.0000	0.0000	0.0000
15	0.0	0.0000	0.0013	0.0000	-0.0097	0.0000	-0.0070	-0.1285	0.0000	-0 0251
16	16.0	-0.0122	0.0026	-0.0026	-0.0139	0.0030	-0.0073	-0.0986	0.0080	-0.0205
17	41.5	0.0000	0.0000	0.0000	0.0000	0.0000	0.0000	0.0000	0.0000	0.0000
18	0.0	0.0000	0.0000	0.0000	0.0000	0.0000	0.0000	0.0000	0.0000	0.0000
19	16.0	0.0000	0.0000	0.0000	0.0000	0.0000	0.0000	0.0000	0.0000	0.0000
20	22.0	0.0000	0.0000	0.0000	0.0000	0.0000	0.0000	0.0000	0.0000	0 0000

Table A.6

Dynamic Analysis
Dam on Flexible Foundation With Water Level at 491 m

Points	s (m)	Mode 1 Displ.x	Displ.y	Displ.z	Mode 2 Displ.x	Displ.y	Displ.z	Mode 3 Displ.x	Displ.y	Displ.z
1	0 0	-0.0022	-0.3024	0.0004	0.9997	-0.0004	-0.1901	-0.1224	0.0000	0.0706
2	16.0	0.6192	-0.3510	-0.1393	0.8115	-0.0162	-0.1427	0.0901	-0.0717	0.0094
3	48.0	0.8712	-0.4394	-0.1708	-0.0458	0.1716	0.0506	0.8384	-0.4205	-0.1996
4	80.0	0.2263	-0.1058	-0.0233	-0.1684	0.1849	0.0465	0.3800	-0.2088	-0.0681
5	112.9	0.0145	0.0140	-0.0003	0.0025	0.0047	0.0000	0.0225	0.0204	-0.0012
6	0.0	-0.0014	-0.2068	0.0001	0.6380	-0.0003	-0.0597	-0.0268	0.0000	0.0262
7	16.0	0.3635	-0.2340	-0.0446	0.5300	-0.0139	-0.0420	0.0747	-0.0395	0.0060
8	48.0	0.4995	-0.2733	-0.0304	0.0397	0.0814	0.0157	0.4049	-0.1875	-0.0399
9	80.0	0.1091	-0.0645	0.0127	-0.0501	0.0905	-0.0003	0.1588	-0.0829	0.0038
10	99.2	0.0147	0.0103	0.0027	0.0061	0.0186	-0.0047	0.0262	0.0160	0.0005
11	0 0	-0.0006	-0.0981	-0.0001	0.3016	-0.0001	0.0304	0.0288	0.0000	0.0064
12	16.0	0.1509	-0.1109	0.0149	0.2533	-0.0110	0.0279	0.0572	-0.0118	0.0072
13	48.0	0.1637	-0.1076	0.0317	0.0433	0.0303	0.0070	0.1161	-0.0444	0.0135
14	75.0	0.0181	-0.0052	0.0085	0.0096	0.0261	-0.0029	0.0287	0.0079	-0.0003
15	0 0	-0.0002	-0.0353	-0.0001	0.0793	0.0000	0.0313	0.0169	0.0000	0 0054
16	16 0	0.0306	-0.0371	0.0166	0.0644	0.0001	0.0252	0.0198	-0.0007	0.0065
17	41.5	0.0109	-0.0199	0.0160	0.0156	0.0155	0.0026	0.0126	0.0029	0 0038
18	0.0	0.0000	-0.0187	0.0000	0.0148	0.0000	0.0125	0.0045	0.0000	0.0021
19	16.0	0.0023	-0.0169	0.0081	0.0115	0.0041	0.0101	0.0046	0.0015	0 0025
20	22.0	0.0019	-0.0156	0.0105	0.0093	0.0056	0.0080	0.0046	0.0018	0 0026

		Mode 4			Mode 5			Mode 6		
1	0.0	0.0003	0.0704	-0.0002	0.9971	-0.0002	-0.4592	0.5029	-0.0001	-0.1310
2	16.0	-0.6438	0.1066	0.1745	0.7970	-0.1010	-0.3868	-0.0422	0.0714	0.0280
3	48 0	0.3086	-0.3165	-0.1157	0.1669	-0.1030	-0.1384	-0.4486	0.0853	0.1024
4	80.0	0.6573	-0.5176	-0.1599	0.0950	-0.1003	-0.0539	0.7678	-0.6539	-0.2053
5	112.9	0.0218	0.0133	-0.0021	-0.0027	-0.0035	-0.0032	0.0285	0.0105	-0.0031
6	0.0	0.0001	0.0361	-0.0001	0.1960	-0.0002	-0.1708	0.3919	-0.0001	-0.0814
7	16.0	-0.3601	0.0578	0.0673	0.1219	-0.0095	-0.1441	0.1035	0.0261	-0.0175
8	48.0	0.0062	-0.0809	-0.0036	-0.0682	0.0206	-0.0525	-0.3256	0.1132	0.0585
9	80.0	0.2132	-0.1901	-0.0013	0.0009	-0.0178	-0.0198	0.1990	-0.1873	-0.0006
10	99 2	0.0232	-0.0127	0.0052	-0.0032	-0.0062	-0.0070	0.0320	-0.0260	0.0074
11	0 0	-0.0001	0.0071	0.0000	-0.2323	-0.0002	-0.0380	0.2433	-0.0001	-0.0241
12	16.0	-0.1332	0.0195	0.0023	-0.2271	0.0280	-0.0370	0.1373	-0.0036	-0.0170
13	48.0	-0.0438	-0.0072	0.0080	-0.1243	0.0391	-0.0300	-0.0883	0.0452	0.0049
14	75 0	0.0076	-0.0197	0.0044	-0.0189	-0.0057	-0.0137	-0.0025	-0.0114	0.0109
15	0 0	0.0000	-0.0011	0.0000	-0.1408	-0.0001	-0.0289	0.0874	-0.0001	-0.0060
16	16.0	-0.0285	0.0016	-0.0029	-0.1241	0.0103	-0.0264	0.0607	-0.0005	-0.0079
17	41.5	-0.0149	-0.0053	0.0073	-0.0419	-0.0071	-0.0101	0.0043	0.0118	-0.0020
18	0.0	0.0000	0.0000	0.0000	-0.0440	-0.0001	-0.0041	0.0280	-0.0001	-0.0152
19	16.0	-0.0059	-0.0005	0.0017	-0.0369	-0.0038	-0.0042	0.0208	0.0054	-0 0130
20	22.0	-0.0065	-0.0010	0.0026	-0.0320	-0.0057	-0.0039	0.0163	0.0073	-0.0117

FIRST BENCHMARK WORKSHOP

ON

NUMERICAL ANALYSIS OF DAMS

IBERDUERO'S PACKAGE FOR PRELIMINARY STATIC, THERMAL AND DYNAMIC ANALYSYS OF ARCH DAMS

by

Antonio J. Salmonte

IBERDUERO S.A.

Avda. de America 32

28028 Madrid (Spain)

1.-INTRODUCTION

Undoubtedly, for a given finite element mesh, and using elements of identical robustness, under identical loads, identical results are obtained.

Once this statement is established, we will set up our aim in participating in this workshop: the project of an arch dam has several phases, the most sensitive being that of its insertion in the site and its geometric definition. In addition to geometrical and topographic considerations to be solved at the drawing desk, the designer must have a tool at his disposal, both economical and quick, to allow him to judge about the stress adequacy of the different solutions analyzed throughout the process.

The finite element method is deemed to be the adequate tool, together with a software fulfilling the aforementioned conditions: swiftness and economy.

From the accuracy point of view, both conditions are counteractive. It is well known that for well formulated finite elements, quality of the results improves by

-decreasing the mesh size (i.e. increasing the number of nodes)

-using more robust elements, with more complex formulation

but, unfortunately, this two conditions are opposed to the declared objective:they imply higher CPU time and, consequently, higher price.

A balance has to be reached, in the sense that the designer has to get the certainty, at this stage, that any further analysis by means of a more refined and detailed model, will not be likely to impair the design acceptability, although as a matter of fact, it will improve the accuracy of the results.

This is the aim of the software (Refs. 1-3) that we are submitting to the Workshop: providing a tool to carry out quick and economic but accurate enough analisys of each one of the several trials that have to be made in order to reach a final design, without having to rely solely on intuition.

2.-STATIC ANALYSIS

The Organizing Committee has proposed a mesh with the following characteristics. (Given the symmetry of the model, only half dam has been considered, with symmetry boundary conditions imposed on the nodes lying on the simmetry plan).

	Nodes	Elements(*)	D.O.F's
Dam	347	42	1022
Foundation	472	80	1218
Total	819	122	2240

Our proposed model (Fig. 1), however, consists of

	Nodes	Elements(*)	D.O.F's
Dam	212	126	604
Foundation	264	200	594
Total	476	336	1198

(*): The elements in the Committee's model are 20-node isoparametric whereas ours are 8-node isoparametric as will be discussed later.

The relation between the number of nodes and dof's in both models warrants a saving in CPU of about 75% in favour of the proposed model, besides the much smaller storage capacity required. Given the size and complexity of the formulation of the 20-nodes element against that of the BRICK as we will call our element from now on, the time consumed in forming the element stiffnesses is not higher with the BRICKS that it would have been with the others, in spite of the bigger number of them required. Finally, the smaller amount of data, makes much faster the unavoidable checking process.

Of course, all this savings result from the use of a finite element of less quality: the 8-node isoparametric element with incompatible modes. This element has been profusely described in the literature(Ref. 4), its main inconvenient being its bad behaviour whenever its shape degenerates into a wedge (six nodes instead of eight).

We have analyzed this behaviour thoroughly,reaching the following conclusions:

a) The presence of incompatible modes artificially stiffens the element as it becomes more and more degenerated, i.e. when its shape becomes less and less parallelepipedic, leading to stresses in the element which are up to 50% over-valued.

b) Selective suppression of one or more of the three incompatible modes (at least the one corresponding to bending of the faces which degenerate into triangles), leads to much more accurate stresses, even a little smaller than the actual ones in the faces of the element, but good enough at the centroid.

Therefore, this is the element chosen, keeping in mind that unless the selective suppression of some of the incompatible modes is performed, the results would be bad, mainly for the 6-node wedges present at the dam-foundation interfaces which are moreover the most sensitive elements in a stress analysis. A provision was made in our software to automatically suppress these offending modes when the finite element mesh is generated.

There is an additional limitation implied by the use of BRICKs, which we consider as a minor one, given the objective of the model we have developed: its inability to get accurate stresses at the nodes. However, with the contribution of the incompatible modes, stresses are good enough at centroids both of the element and of each of its faces.

Any trial to evaluate them at the nodes would therefore be useless. This is the reason why we were bound to evaluate stresses at points slightly different from those required by the Committee. Figure 2 illustrates the locations chosen for stress evaluation.

Regarding stresses, values shown in Annex II are computed at three points for each selected (s,z) location, two of them lying on the dam surfaces. For this two, one principal stress is known beforehand: the one that has to be either zero or, on occasion, the applied hydrostatic pressure. No attempt has been made to adjust the stresses in this direction even though our software also includes the capability of producing and plotting in-plane surface stresses, obtained by neglecting three out of plane components of the computed stress tensor.

We want to point out two special features of our dead load analysis.

1) Soil mass is assumed to be zero, since displacements and stresses we are looking for are due to the weight of concrete. Otherwise, we will be also considering the effects of soil-settlement which has happened before construction and has no effect whatsoever in the dam body.

2) The analysis is carried out in two steps. The first one, with only the even cantilevers been active both in weight and stiffness and the second where the odd cantilevers are active. Stresses are obtained by adding up the two cases. Nodal displacements are the average of those obtained for each case, since each node belongs to two cantilevers, one even and the other odd. In this way, the dam does not bear the gravity load as a monolithic body as we consider it is really the case. (See Fig. 3 for definition of even and odd cantilevers)

To comply with the Committee's requirements, we have also carried out the dead load case considering the dam as a monolithic body. Results corresponding to both cases are included in annexes I (displacements)and II (stresses).

3.-THERMAL STRESS ANALYSIS

Again, our aim was to provide a suitable tool with the capability of helping the designer and fulfilling both conditions to make it attractive: swiftness and economy.

The reasons outlined in the former paragraph did lean us towards the 8-node isoparametric element with incompatible modes. Once again, an analysis of its behaviour, this time under thermal loads, was made. The BRICK proved to be successful under uniform temperature increases. However, under non-uniform temperature increases, we had to introduce some modifications in the stress-recovery matrix formulation to get the right stresses at the element faces. To get this, the element has to have zero average temperature. This being rarely the case, the inconvenient is overcome by means of a duplication of the loading case, the first one with the elements under fictitious nodal temperatures equal to the actual ones minus the element average and the second with the elements subjected to an uniform temperature increment equal to the average temperature subtracted before.

Let us point out that our approach allowed us to carry out the required analysis with the following features:

	Nodes	Elements	D.O.F's
IBERDUERO	212	126	476
Committee's	347	42	966

(Since the dam was to be considered as clamped to the soil, all foundation elements and nodes were suppressed from the static analysis model).

We think it is out of discussion that the clamped interface between dam and foundation plus the absence of soil expansions severely distorts the results. Coming back to our even-odd cantilever approach, nodal temperatures at the moment of joint injection represent a stress free state.

Variations around this state into either the warmer or the colder side give rise to thermal stresses which have to be analized.

Results of this run are also included in annexes I (displacements), and II (stresses). Temperatures at the required nodes are tabulated in Annex III.

Computation of the temperature distribution was made by means of ADINA-T (Ref. 5), using the same mesh and elements as for the stress analysis.

4.-DYNAMIC ANALISIS

There is no special feature in the first case (Dam on rigid foundation without water), except for the use, once again of the BRICK element.

Since we were interested in simultaneously getting symmmetric and antisymmetric modes, the model included the whole body of the dam, with clamped nodes all along the dam-foundation interface, resulting in the following model characteristics:

Nodes	Elements	D.O.F's
392	252	924

The orthonormalization criteria adopted for the adimensional mode--shapes was the following:

$$\Phi^T M \Phi = I$$

Mode-shape frequencies are, expressed in hertzs (see figs. 4-6):

Mode	Freq. (Hz.)	Mode	Freq. (Hz.)
1	4.320	4	6.870
2	4.609	5	8.770
3	5.692	6	9.194

The required modal coordinates are tabulated in Annex IV.

In the second case, (dam on flexible foundation with a water level of 491 m. asl), we have used a special compressible water element (Ref. 6) which incorporates the following novel ideas:

-Reduced integration to avoid artificial stiffening of the water, resulting in an element that has to be held on some kind of container as fluids have. In other words, an element unable to hold itself without essential boundary conditions applied to all but one of its external surfaces.

-Inclusion of some kind of geometric stiffness to take into account the effect that its own hydrostatic pressure has on deformability.

-Introduction of an additional rank deficient stiffness matrix, multiplied by an infinitesimal, to prevent some elemental deformation modes (shear deformation modes), to pollute the solution.

-Introduction of two underintegrated stiffnes matrices multiplied by adequate penalty factors to yield an irrotational displacement field within the fluid domain.

With use of this element, we developed a model consisting of:

Nodes.....		1360
-Dam.....	392	
-Water.....	464	
-Soil.....	504	
8-node elements.....		1040
-BRICK (Dam).....	252	
(Foundation)	452	
-WAT3D (Water).....	336	
Auxiliary elements....		138
-BOUNDARY.....	80	
-RIGID LINKS.....	58	
D.O.F.'s.....		3567

A length of about 430 m. was taken, measured alog the river axis from the upstream face of the dam. Nodes at the reservoir boundary farther removed from the dam were considered free to move side to side and upwards down (two degrees of freedom each), but they do not have freedom to move in the upstream-downstream direction.

Two details of the reservoir model are shown in fig. 7

Boundary elements are to fix the water nodes to the lateral surfaces of the reservoir , leaving them free to slide on a tangent plane to this surface. Rigid links play a similar role at the dam-water interface.

Mode-shape frequencies are, expressed in hertzs (see figs 8-10):

Mode	Freq. (Hz.)	Mode	Freq. (Hz.)
1	3.179	4	5.390
2	3.446	5	5.757
3	4.694	6	6.034

The required modal coordinates are tabulated in Annex V.

5.-REFERENCES

1. SAP-ID General purpose finite element program of IBERDUERO. Report K1-INCENIA-003; Rev 4 (1987)
2. PRESAP-ID Mesh generator for arch dams. Report K1-INCENIA-014; Rev 2 (1988)
3. POSAP-ID Postprocessor for SAP-ID Report K1-INCENIA-010; Rev 2 (1987)
4. E. L. Wilson. "SOLID SAP. A static analysis program for three dimensional solid structures. Report UC-SESM-71-19 (1972).
5. K. J. Bathe. "A Finite element program for dynamic incremental nonlinear analysis of temperatures". Report ARD 87-2 (1987).
6. A. J. Salmonte. "Elementos fluidos en 2D y 3D para analisis dinamico con interacción fluido-estructura". Rev. Internacional de Metodos Numéricos para Calculo y Diseño en ingeniería. Vol. 4, #3, pp. 313-347 (1988)

ANNEX I

Displacements at selected nodes

Load case 3.1: Dead load (Dam acting as a vault)

Points	s (m)	z (m)	Dx (m)	Dy (m)	Dz (m)
1	0.0	507.0	0.25E-03	0.00E+00	-0.31E-02
2	0.0	507.0	0.27E-03	0.00E+00	-0.34E-02
3	0.0	507.0	0.28E-03	0.00E+00	-0.35E-02
4	0.0	491.0	-0.98E-03	0.00E+00	-0.27E-02
5	0.0	491.0	-0.97E-03	0.00E+00	-0.29E-02
6	0.0	491.0	-0.95E-03	0.00E+00	-0.31E-02
7	16.0	491.0	-0.89E-03	0.12E-03	-0.26E-02
8	16.0	491.0	-0.89E-03	0.15E-03	-0.27E-02
9	16.0	491.0	-0.88E-03	0.18E-03	-0.30E-02
10	48.0	491.0	-0.35E-03	0.42E-03	-0.19E-02
11	48.0	491.0	-0.38E-03	0.47E-03	-0.21E-02
12	48.0	491.0	-0.38E-03	0.52E-03	-0.24E-02
13	80.0	491.0	-0.98E-04	0.55E-03	-0.93E-03
14	80.0	491.0	-0.77E-04	0.52E-03	-0.11E-02
15	80.0	491.0	-0.43E-04	0.49E-03	-0.13E-02
16	99.2	491.0	-0.18E-03	0.23E-03	-0.42E-03
17	99.2	491.0	-0.14E-03	0.18E-03	-0.53E-03
18	99.2	491.0	-0.10E-03	0.14E-03	-0.61E-03
19	0.0	471.0	-0.16E-02	0.00E+00	-0.25E-02
20	0.0	471.0	-0.16E-02	0.00E+00	-0.24E-02
21	0.0	471.0	-0.15E-02	0.00E+00	-0.24E-02
22	16.0	471.0	-0.14E-02	-0.13E-03	-0.24E-02
23	16.0	471.0	-0.14E-02	-0.77E-04	-0.24E-02
24	16.0	471.0	-0.14E-02	-0.20E-04	-0.23E-02
25	48.0	471.0	-0.64E-03	-0.12E-03	-0.18E-02
26	48.0	471.0	-0.68E-03	-0.25E-04	-0.18E-02
27	48.0	471.0	-0.73E-03	0.82E-04	-0.17E-02
28	75.0	471.0	-0.78E-04	0.79E-04	-0.94E-03
29	75.0	471.0	-0.12E-03	0.10E-03	-0.95E-03
30	75.0	471.0	-0.15E-03	0.11E-03	-0.87E-03
31	0.0	448.0	-0.69E-03	0.00E+00	-0.25E-02
32	0.0	448.0	-0.64E-03	0.00E+00	-0.20E-02
33	0.0	448.0	-0.60E-03	0.00E+00	-0.17E-02
34	16.0	448.0	-0.55E-03	-0.14E-03	-0.23E-02
35	16.0	448.0	-0.53E-03	-0.56E-04	-0.19E-02
36	16.0	448.0	-0.52E-03	0.24E-04	-0.16E-02
37	41.5	448.0	0.22E-04	-0.72E-04	-0.15E-02
38	41.5	448.0	-0.60E-04	0.15E-04	-0.14E-02
39	41.5	448.0	-0.12E-03	0.73E-04	-0.11E-02
40	0.0	435.0	0.60E-04	0.00E+00	-0.18E-02
41	0.0	435.0	0.20E-04	0.00E+00	-0.16E-02
42	0.0	435.0	-0.19E-04	0.00E+00	-0.13E-02

ANNEX I

Displacements at selected nodes

Load case 3.1.bis: Dead load (Cantilevered Dam)

Points	s (m)	z (m)	Dx (m)	Dy (m)	Dz (m)
1	0.0	507.0	0.16E-01	0.00E+00	-0.60E-02
2	0.0	507.0	0.16E-01	0.00E+00	-0.72E-02
3	0.0	507.0	0.16E-01	0.00E+00	-0.84E-02
4	0.0	491.0	0.77E-02	0.00E+00	-0.28E-02
5	0.0	491.0	0.77E-02	0.00E+00	-0.42E-02
6	0.0	491.0	0.77E-02	0.00E+00	-0.55E-02
7	16.0	491.0	0.68E-02	0.16E-02	-0.28E-02
8	16.0	491.0	0.68E-02	0.16E-02	-0.41E-02
9	16.0	491.0	0.68E-02	0.16E-02	-0.54E-02
10	48.0	491.0	0.44E-02	0.80E-03	-0.17E-02
11	48.0	491.0	0.44E-02	0.80E-03	-0.25E-02
12	48.0	491.0	0.44E-02	0.81E-03	-0.35E-02
13	80.0	491.0	0.12E-02	0.22E-03	-0.91E-03
14	80.0	491.0	0.13E-02	0.19E-03	-0.12E-02
15	80.0	491.0	0.13E-02	0.18E-03	-0.17E-02
16	99.2	491.0	-0.53E-04	0.90E-04	-0.16E-03
17	99.2	491.0	-0.38E-04	0.73E-04	-0.23E-03
18	99.2	491.0	-0.21E-04	0.61E-04	-0.28E-03
19	0.0	471.0	0.15E-02	0.00E+00	-0.14E-02
20	0.0	471.0	0.15E-02	0.00E+00	-0.22E-02
21	0.0	471.0	0.15E-02	0.00E+00	-0.30E-02
22	16.0	471.0	0.11E-02	0.69E-03	-0.15E-02
23	16.0	471.0	0.11E-02	0.66E-03	-0.22E-02
24	16.0	471.0	0.12E-02	0.63E-03	-0.30E-02
25	48.0	471.0	0.87E-03	-0.51E-04	-0.12E-02
26	48.0	471.0	0.89E-03	-0.83E-04	-0.16E-02
27	48.0	471.0	0.94E-03	-0.11E-03	-0.20E-02
28	75.0	471.0	-0.49E-04	0.11E-03	-0.43E-03
29	75.0	471.0	-0.36E-04	0.11E-03	-0.52E-03
30	75.0	471.0	-0.22E-04	0.93E-04	-0.51E-03
31	0.0	448.0	-0.19E-03	0.00E+00	-0.17E-02
32	0.0	448.0	-0.17E-03	0.00E+00	-0.17E-02
33	0.0	448.0	-0.13E-03	0.00E+00	-0.16E-02
34	16.0	448.0	-0.23E-03	0.90E-04	-0.17E-02
35	16.0	448.0	-0.19E-03	0.97E-04	-0.16E-02
36	16.0	448.0	-0.14E-03	0.10E-03	-0.15E-02
37	41.5	448.0	-0.20E-04	0.13E-03	-0.73E-03
38	41.5	448.0	-0.30E-04	0.14E-03	-0.80E-03
39	41.5	448.0	-0.31E-04	0.12E-03	-0.73E-03
40	0.0	435.0	0.53E-04	0.00E+00	-0.15E-02
41	0.0	435.0	0.36E-04	0.00E+00	-0.15E-02
42	0.0	435.0	0.17E-04	0.00E+00	-0.12E-02

Displacements at selected nodes

Load case 3.2: Hydrostatic pressure

Points	s (m)	z (m)	Dx (m)	Dy (m)	Dz (m)
1	0.0	507.0	0.23E-01	0.00E+00	-0.50E-03
2	0.0	507.0	0.23E-01	0.00E+00	-0.65E-03
3	0.0	507.0	0.23E-01	0.00E+00	-0.90E-03
4	0.0	491.0	0.21E-01	0.00E+00	0.60E-03
5	0.0	491.0	0.21E-01	0.00E+00	-0.10E-03
6	0.0	491.0	0.21E-01	0.00E+00	-0.60E-03
7	16.0	491.0	0.19E-01	0.18E-02	0.60E-03
8	16.0	491.0	0.19E-01	0.12E-02	0.00E+00
9	16.0	491.0	0.20E-01	0.67E-03	-0.50E-03
10	48.0	491.0	0.95E-02	0.20E-02	0.60E-03
11	48.0	491.0	0.98E-02	0.11E-02	0.25E-03
12	48.0	491.0	0.10E-01	0.24E-03	0.20E-03
13	80.0	491.0	0.21E-02	-0.69E-03	0.50E-04
14	80.0	491.0	0.23E-02	-0.89E-03	0.13E-03
15	80.0	491.0	0.25E-02	-0.11E-02	0.20E-03
16	99.2	491.0	0.95E-03	-0.86E-03	-0.17E-03
17	99.2	491.0	0.99E-03	-0.89E-03	-0.10E-03
18	99.2	491.0	0.97E-03	-0.84E-03	-0.10E-04
19	0.0	471.0	0.16E-01	0.00E+00	0.29E-02
20	0.0	471.0	0.16E-01	0.00E+00	0.12E-02
21	0.0	471.0	0.16E-01	0.00E+00	-0.30E-03
22	16.0	471.0	0.14E-01	0.17E-02	0.27E-02
23	16.0	471.0	0.14E-01	0.12E-02	0.12E-02
24	16.0	471.0	0.14E-01	0.55E-03	-0.40E-03
25	48.0	471.0	0.60E-02	0.18E-02	0.16E-02
26	48.0	471.0	0.65E-02	0.85E-03	0.55E-03
27	48.0	471.0	0.71E-02	-0.92E-04	-0.50E-03
28	75.0	471.0	0.14E-02	-0.62E-03	0.21E-03
29	75.0	471.0	0.17E-02	-0.96E-03	-0.14E-03
30	75.0	471.0	0.19E-02	-0.11E-02	-0.53E-03
31	0.0	448.0	0.68E-02	0.00E+00	0.38E-02
32	0.0	448.0	0.66E-02	0.00E+00	0.13E-02
33	0.0	448.0	0.65E-02	0.00E+00	-0.10E-02
34	16.0	448.0	0.58E-02	0.93E-03	0.32E-02
35	16.0	448.0	0.58E-02	0.33E-03	0.95E-03
36	16.0	448.0	0.58E-02	-0.23E-03	-0.10E-02
37	41.5	448.0	0.18E-02	0.13E-03	0.11E-02
38	41.5	448.0	0.23E-02	-0.59E-03	-0.10E-03
39	41.5	448.0	0.24E-02	-0.12E-02	-0.11E-02
40	0.0	435.0	0.21E-02	0.00E+00	0.19E-02
41	0.0	435.0	0.22E-02	0.00E+00	0.15E-03
42	0.0	435.0	0.20E-02	0.00E+00	-0.13E-02

ANNEX I

Displacements at selected nodes

Load case 3.3.1: Thermal (Steady state)

Points	s (m)	z (m)	Dx (m)	Dy (m)	Dz (m)
1	0.0	507.0	-0.18E-01	0.00E+00	0.90E-02
2	0.0	507.0	-0.18E-01	0.00E+00	0.98E-02
3	0.0	507.0	-0.18E-01	0.00E+00	0.11E-01
4	0.0	491.0	-0.13E-01	0.00E+00	0.56E-02
5	0.0	491.0	-0.13E-01	0.00E+00	0.65E-02
6	0.0	491.0	-0.13E-01	0.00E+00	0.74E-02
7	16.0	491.0	-0.12E-01	-0.18E-02	0.52E-02
8	16.0	491.0	-0.12E-01	-0.15E-02	0.62E-02
9	16.0	491.0	-0.12E-01	-0.11E-02	0.71E-02
10	48.0	491.0	-0.67E-02	-0.33E-02	0.32E-02
11	48.0	491.0	-0.67E-02	-0.26E-02	0.42E-02
12	48.0	491.0	-0.67E-02	-0.19E-02	0.52E-02
13	80.0	491.0	-0.12E-02	-0.16E-02	0.11E-02
14	80.0	491.0	-0.13E-02	-0.98E-03	0.17E-02
15	80.0	491.0	-0.12E-02	-0.33E-03	0.24E-02
16	99.2	491.0	0.00E+00	0.00E+00	0.00E+00
17	99.2	491.0	0.00E+00	0.00E+00	0.00E+00
18	99.2	491.0	0.00E+00	0.00E+00	0.00E+00
19	0.0	471.0	-0.85E-02	0.00E+00	0.19E-02
20	0.0	471.0	-0.82E-02	0.00E+00	0.32E-02
21	0.0	471.0	-0.77E-02	0.00E+00	0.44E-02
22	16.0	471.0	-0.75E-02	-0.14E-02	0.18E-02
23	16.0	471.0	-0.73E-02	-0.94E-03	0.30E-02
24	16.0	471.0	-0.68E-02	-0.44E-03	0.42E-02
25	48.0	471.0	-0.23E-02	-0.17E-02	0.88E-03
26	48.0	471.0	-0.23E-02	-0.95E-03	0.17E-02
27	48.0	471.0	-0.22E-02	-0.17E-03	0.26E-02
28	75.0	471.0	0.00E+00	0.00E+00	0.00E+00
29	75.0	471.0	0.00E+00	0.00E+00	0.00E+00
30	75.0	471.0	0.00E+00	0.00E+00	0.00E+00
31	0.0	448.0	-0.29E-02	0.00E+00	-0.50E-03
32	0.0	448.0	-0.21E-02	0.00E+00	0.11E-02
33	0.0	448.0	-0.12E-02	0.00E+00	0.21E-02
34	16.0	448.0	-0.24E-02	-0.60E-03	-0.15E-03
35	16.0	448.0	-0.16E-02	-0.15E-03	0.12E-02
36	16.0	448.0	-0.82E-03	0.30E-03	0.21E-02
37	41.5	448.0	0.00E+00	0.00E+00	0.00E+00
38	41.5	448.0	0.00E+00	0.00E+00	0.00E+00
39	41.5	448.0	0.00E+00	0.00E+00	0.00E+00
40	0.0	435.0	0.00E+00	0.00E+00	0.00E+00
41	0.0	435.0	0.00E+00	0.00E+00	0.00E+00
42	0.0	435.0	0.00E+00	0.00E+00	0.00E+00

ANNEX II

Stresses at selected points

Load case 3.1: Dead load (Dam acting as a vault)

Points	s (m)	z (m)	P1 (MPa)	P2 (MPa)	P3 (Mpa)
1	8.0	503.0	-0.005	-0.099	-0.844
2	8.0	503.0	-0.004	-0.097	-0.940
3	8.0	503.0	-0.005	-0.112	-1.045
4	8.0	486.0	0.059	-0.020	-0.086
5	8.0	486.0	-0.007	-0.216	-0.377
6	8.0	486.0	-0.012	-0.391	-0.793
7	24.0	486.0	0.163	-0.017	-0.087
8	24.0	486.0	-0.009	-0.115	-0.439
9	24.0	486.0	-0.015	-0.308	-0.908
10	40.0	486.0	0.276	-0.009	-0.056
11	40.0	486.0	0.014	-0.031	-0.482
12	40.0	486.0	-0.012	-0.164	-1.070
13	72.0	486.0	0.255	0.052	-0.009
14	72.0	486.0	0.189	-0.009	-0.543
15	72.0	486.0	0.196	-0.001	-1.239
16	86.9	486.0	0.306	-0.033	-0.164
17	86.9	486.0	0.270	-0.097	-0.570
18	86.9	486.0	0.218	-0.117	-1.307
19	8.0	465.5	0.301	-0.012	-0.125
20	8.0	465.5	0.105	-0.019	-0.519
21	8.0	465.5	-0.036	-0.190	-1.257
22	24.0	465.5	0.288	-0.006	-0.200
23	24.0	465.5	0.123	-0.015	-0.589
24	24.0	465.5	-0.032	-0.120	-1.218
25	40.0	465.5	0.237	0.017	-0.314
26	40.0	465.5	0.151	-0.004	-0.702
27	40.0	465.5	0.060	-0.016	-1.061
28	61.5	467.3	0.018	-0.237	-1.209
29	61.5	467.3	0.160	-0.170	-0.704
30	61.5	467.3	0.277	-0.118	-0.950
31	8.0	441.5	-0.101	-0.212	-1.466
32	8.0	441.5	-0.070	-0.162	-0.786
33	8.0	441.5	-0.135	-0.153	-0.571
34	21.9	441.5	-0.099	-0.204	-1.500
35	21.9	441.5	-0.082	-0.189	-0.857
36	21.9	441.5	-0.084	-0.166	-0.681
37	35.5	443.7	-0.324	-0.446	-2.076
38	35.5	443.7	-0.085	-0.296	-0.826
39	35.5	443.7	0.047	-0.146	-0.741

ANNEX II

Stresses at selected points

Load case 3.1.bis: Dead load (Cantilevered Dam)

Points	s (m)	z (m)	P1 (MPa)	P2 (MPa)	P3 (Mpa)
1	8.0	503.0	0.111	0.008	-0.129
2	8.0	503.0	0.043	-0.018	-0.112
3	8.0	503.0	0.072	0.023	-0.224
4	8.0	486.0	1.038	0.020	-0.035
5	8.0	486.0	0.055	0.007	-0.457
6	8.0	486.0	0.000	-0.020	-1.870
7	24.0	486.0	0.984	0.017	-0.035
8	24.0	486.0	0.043	0.000	-0.452
9	24.0	486.0	0.000	-0.020	-1.815
10	40.0	486.0	0.828	0.031	-0.032
11	40.0	486.0	0.019	0.009	-0.439
12	40.0	486.0	-0.002	-0.019	-1.667
13	72.0	486.0	0.611	0.080	0.003
14	72.0	486.0	0.094	-0.002	-0.479
15	72.0	486.0	0.042	-0.018	-1.683
16	86.9	486.0	0.155	0.058	-0.025
17	86.9	486.0	0.068	-0.062	-0.381
18	86.9	486.0	-0.047	-0.093	-0.978
19	8.0	465.5	0.887	0.035	-0.016
20	8.0	465.5	0.017	-0.023	-0.641
21	8.0	465.5	-0.038	-0.108	-2.716
22	24.0	465.5	0.744	0.004	-0.005
23	24.0	465.5	0.011	-0.018	-0.663
24	24.0	465.5	-0.024	-0.055	-2.452
25	40.0	465.5	0.421	0.075	0.023
26	40.0	465.5	0.082	0.001	-0.710
27	40.0	465.5	0.072	-0.001	-1.903
28	61.5	467.3	0.219	-0.005	-0.411
29	61.5	467.3	-0.055	-0.255	-0.752
30	61.5	467.3	-0.289	-0.340	-1.932
31	8.0	441.5	-0.152	-0.223	-1.105
32	8.0	441.5	-0.102	-0.124	-0.954
33	8.0	441.5	-0.109	-0.139	-1.230
34	21.9	441.5	-0.155	-0.195	-1.199
35	21.9	441.5	-0.089	-0.144	-1.078
36	21.9	441.5	-0.114	-0.139	-1.317
37	35.5	443.7	-0.210	-0.224	-1.299
38	35.5	443.7	-0.170	-0.243	-0.923
39	35.5	443.7	-0.181	-0.261	-1.653

ANNEX II

Stresses at selected points

Load case 3.2: Hydrostatic pressure

Points	s (m)	z (m)	P1 (MPa)	P2 (MPa)	P3 (Mpa)
1	8.0	503.0	0.073	-0.396	-3.250
2	8.0	503.0	0.137	-0.062	-2.060
3	8.0	503.0	0.303	0.099	-0.832
4	8.0	486.0	-0.079	-1.506	-4.421
5	8.0	486.0	0.060	-0.302	-3.041
6	8.0	486.0	1.186	0.099	-1.523
7	24.0	486.0	-0.099	-1.418	-3.995
8	24.0	486.0	0.021	-0.264	-2.967
9	24.0	486.0	1.184	0.055	-1.898
10	40.0	486.0	-0.162	-1.287	-3.149
11	40.0	486.0	-0.061	-0.214	-2.780
12	40.0	486.0	1.213	0.004	-2.424
13	72.0	486.0	-0.251	-0.863	-1.169
14	72.0	486.0	0.074	-0.188	-2.092
15	72.0	486.0	1.279	-0.031	-2.854
16	86.9	486.0	-0.127	-0.563	-1.367
17	86.9	486.0	0.338	-0.430	-1.650
18	86.9	486.0	0,903	-0.271	-2.649
19	8.0	465.5	-0.233	-0.813	-3.697
20	8.0	465.5	-0.110	-0.403	-2.464
21	8.0	465.5	0.621	0.051	-0.989
22	24.0	465.5	-0.228	-0.562	-3.126
23	24.0	465.5	-0.062	-0.311	-2.293
24	24.0	465.5	0.620	0.015	-1.471
25	40.0	465.5	-0.071	-0.493	-1.978
26	40.0	465.5	0.099	-0.412	-2.173
27	40.0	465.5	0.425	-0.053	-2.545
28	61.5	467.3	1.302	0.046	-0.448
29	61.5	467.3	0.256	-0.538	-1.616
30	61.5	467.3	-0.407	-0.929	-4.872
31	8.0	441.5	2.457	0.007	-0.702
32	8.0	441.5	0.538	-0.312	-0.835
33	8.0	441.5	0.257	-0.017	-3.256
34	21.9	441.5	2.539	0.026	-0.586
35	21.9	441.5	0.439	0.089	-0.949
36	21.9	441.5	0.331	-0.068	-3.371
37	35.5	443.7	3.753	0.811	0.164
38	35.5	443.7	0.528	0.421	-1.195
39	35.5	443.7	-0.115	-0.615	-5.221

ANNEX II

Stresses at selected points

Load case 3.3.1: Thermal (Steady state)

Points	s (m)	z (m)	P1 (MPa)	P2 (MPa)	P3 (Mpa)
1	8.0	503.0	1.990	0.248	-0.100
2	8.0	503.0	0.897	0.008	-0.072
3	8.0	503.0	0.063	0.001	-0.084
4	8.0	486.0	1.374	0.549	-0.101
5	8.0	486.0	0.088	-0.037	-0.183
6	8.0	486.0	0.013	-0.838	-1.697
7	24.0	486.0	1.008	0.184	-0.095
8	24.0	486.0	0.123	0.000	-0.562
9	24.0	486.0	0.046	-0.623	-1.737
10	40.0	486.0	0.498	-0.057	-0.558
11	40.0	486.0	0.140	-0.022	-1.225
12	40.0	486.0	0.202	-0.160	-1.955
13	72.0	486.0	0.414	-0.380	-1.966
14	72.0	486.0	0.525	0.270	-2.630
15	72.0	486.0	1.786	0.553	-3.019
16	86.9	486.0	-0.405	-1.869	-3.658
17	86.9	486.0	0.721	-1.573	-3.559
18	86.9	486.0	2.550	-1.382	-3.813
19	8.0	465.5	0.068	-0.121	-0.449
20	8.0	465.5	0.024	-0.154	-1.377
21	8.0	465.5	-0.103	-1.520	-3.430
22	24.0	465.5	-0.068	-0.485	-0.835
23	24.0	465.5	0.188	-0.207	-1.766
24	24.0	465.5	-0.028	-0.722	-3.432
25	40.0	465.5	0.203	-0.601	-1.745
26	40.0	465.5	0.506	-0.212	-2.443
27	40.0	465.5	1.477	0.190	-3.111
28	61.5	467.3	-0.905	-3.555	-4.730
29	61.5	467.3	0.802	-2.779	-3.703
30	61.5	467.3	2.298	-2.755	-3.986
31	8.0	441.5	-1.800	-2.903	-3.474
32	8.0	441.5	0.103	-2.006	-3.352
33	8.0	441.5	1.150	-1.657	-4.201
34	21.9	441.5	-1.862	-2.993	-3.411
35	21.9	441.5	-0.563	-2.165	-3.752
36	21.9	441.5	0.383	-1.747	-4.333
37	35.5	443.7	-1.663	-4.295	-7.328
38	35.5	443.7	0.423	-3.163	-3.943
39	35.5	443.7	2.238	-3.154	-4.181

ANNEX III

Temperatures at selected nodes

Steady state thermal load

Points	s (m)	z (m)	T (^{o}C)
1	0.0	507.0	15.000
2	16.0	507.0	15.000
3	48.0	507.0	15.000
4	80.0	507.0	13.980
5	112.9	507.0	13.951
6	0.0	491.0	12.400
7	16.0	491.0	12.399
8	48.0	491.0	12.392
9	80.0	491.0	12.371
10	99.2	491.0	12.295
11	0.0	471.0	12.366
12	16.0	471.0	12.368
13	48.0	471.0	12.392
14	75.0	471.0	12.625
15	0.0	448.0	12.288
16	16.0	448.0	12.339
17	41.5	448.0	12.696
18	0.0	435.0	12.850
19	16.0	435.0	12.781
20	22.0	435.0	12.909

ANNEX IV

Dynamic case: Dam on rigid foundation without water

Mode number = 1 Freq. = 4.31 hz

Points	s (m)	z (m)	Dx	Dy	Dz
1	0.0	507.0	-0.4927E-13	0.5836E-04	0.1646E-13
2	16.0	507.0	0.1553E-03	0.7166E-04	-0.3933E-04
3	48.0	507.0	0.1969E-03	0.9449E-04	-0.4552E-04
4	80.0	507.0	0.3719E-04	0.1738E-04	-0.5470E-05
5	112.9	507.0	0.0000E+00	0.0000E+00	0.0000E+00
6	0.0	491.0	-0.1881E-13	0.3765E-04	0.4883E-14
7	16.0	491.0	0.8467E-04	0.4466E-04	-0.1335E-04
8	48.0	491.0	0.1009E-03	0.5239E-04	-0.9936E-05
9	80.0	491.0	0.1207E-04	0.7010E-05	0.1239E-05
10	99.2	491.0	0.0000E+00	0.0000E+00	0.0000E+00
11	0.0	471.0	-0.1248E-13	0.1491E-04	0.1612E-14
12	16.0	471.0	0.2908E-04	0.1751E-04	0.1772E-05
13	48.0	471.0	0.2224E-04	0.1409E-04	0.3472E-05
14	75.0	471.0	0.0000E+00	0.0000E+00	0.0000E+00
15	0.0	448.0	-0.3837E-14	0.3092E-05	0.1418E-15
16	16.0	448.0	0.3098E-05	0.3056E-05	0.1572E-05
17	41.5	448.0	0.0000E+00	0.0000E+00	0.0000E+00
18	0.0	435.0	0.0000E+00	0.0000E+00	0.0000E+00
19	16.0	435.0	0.0000E+00	0.0000E+00	0.0000E+00
20	22.0	435.0	0.0000E+00	0.0000E+00	0.0000E+00

Mode number = 2 Freq. = 4.60 hz.

Points	s (m)	z (m)	Dx	Dy	Dz
1	0.0	507.0	-0.3306E-03	-0.1105E-13	0.7607E-04
2	16.0	507.0	-0.2623E-03	-0.1054E-04	0.5735E-04
3	48.0	507.0	0.2400E-04	0.4496E-04	-0.1501E-04
4	80.0	507.0	0.4170E-04	0.3968E-04	-0.1220E-04
5	112.9	507.0	0.0000E+00	0.0000E+00	0.0000E+00
6	0.0	491.0	-0.1901E-03	-0.9723E-14	0.2595E-04
7	16.0	491.0	-0.1530E-03	-0.6656E-05	0.1883E-04
8	48.0	491.0	-0.2370E-07	0.2067E-04	-0.4150E-05
9	80.0	491.0	0.1014E-04	0.1412E-04	-0.3265E-06
10	99.2	491.0	0.0000E+00	0.0000E+00	0.0000E+00
11	0.0	471.0	-0.7061E-04	-0.4947E-14	-0.4977E-05
12	16.0	471.0	-0.5625E-04	-0.3385E-05	-0.4658E-05
13	48.0	471.0	-0.3127E-05	0.5744E-05	-0.9180E-06
14	75.0	471.0	0.0000E+00	0.0000E+00	0.0000E+00
15	0.0	448.0	-0.9449E-05	-0.1776E-14	-0.3443E-05
16	16.0	448.0	-0.6356E-05	-0.3308E-07	-0.2478E-05
17	41.5	448.0	0.0000E+00	0.0000E+00	0.0000E+00
18	0.0	435.0	0.0000E+00	0.0000E+00	0.0000E+00
19	16.0	435.0	0.0000E+00	0.0000E+00	0.0000E+00
20	22.0	435.0	0.0000E+00	0.0000E+00	0.0000E+00

Dynamic case: Dam on rigid foundation without water

Mode number = 3 Freq. = 5.69 hz.

Points	s (m)	z (m)	Dx	Dy	Dz
1	0.0	507.0	0.1035E-04	0.4273E-12	-0.2765E-05
2	16.0	507.0	0.6940E-04	0.2571E-04	-0.1943E-04
3	48.0	507.0	0.2494E-03	0.1242E-03	-0.6769E-04
4	80.0	507.0	0.8488E-04	0.5045E-04	-0.1774E-04
5	112.9	507.0	0.0000E+00	0.0000E+00	0.0000E+00
6	0.0	491.0	-0.3420E-06	0.1706E-12	-0.1713E-05
7	16.0	491.0	0.2709E-04	0.1111E-04	-0.6826E-05
8	48.0	491.0	0.1023E-03	0.4884E-04	-0.1392E-04
9	80.0	491.0	0.2302E-04	0.1440E-04	0.1357E-05
10	99.2	491.0	0.0000E+00	0.0000E+00	0.0000E+00
11	0.0	471.0	-0.2596E-05	0.1920E-13	-0.1168E-05
12	16.0	471.0	0.4390E-05	0.1790E-05	-0.7260E-06
13	48.0	471.0	0.1578E-04	0.7490E-05	0.1886E-05
14	75.0	471.0	0.0000E+00	0.0000E+00	0.0000E+00
15	0.0	448.0	-0.7966E-06	-0.4113E-13	-0.4447E-06
16	16.0	448.0	-0.2054E-06	-0.1101E-06	-0.7398E-07
17	41.5	448.0	0.0000E+00	0.0000E+00	0.0000E+00
18	0.0	435.0	0.0000E+00	0.0000E+00	0.0000E+00
19	16.0	435.0	0.0000E+00	0.0000E+00	0.0000E+00
20	22.0	435.0	0.0000E+00	0.0000E+00	0.0000E+00

Mode number = 4 Freq. = 6.86 hz.

Points	s (m)	z (m)	Dx	Dy	Dz
1	0.0	507.0	0.5482E-12	-0.2131E-04	0.2606E-11
2	16.0	507.0	-0.1756E-03	-0.3161E-04	0.4723E-04
3	48.0	507.0	0.1054E-03	0.8679E-04	-0.4095E-04
4	80.0	507.0	0.1486E-03	0.1145E-03	-0.3986E-04
5	112.9	507.0	0.0000E+00	0.0000E+00	0.0000E+00
6	0.0	491.0	0.5303E-11	-0.9436E-05	0.7053E-12
7	16.0	491.0	-0.9388E-04	-0.1604E-04	0.1629E-04
8	48.0	491.0	0.9988E-05	0.1887E-04	-0.4879E-05
9	80.0	491.0	0.3330E-04	0.3004E-04	0.3476E-07
10	99.2	491.0	0.0000E+00	0.0000E+00	0.0000E+00
11	0.0	471.0	-0.5781E-12	-0.2117E-05	0.1405E-11
12	16.0	471.0	-0.2863E-04	-0.5163E-05	-0.9557E-06
13	48.0	471.0	-0.6275E-05	0.3572E-06	-0.1661E-06
14	75.0	471.0	0.0000E+00	0.0000E+00	0.0000E+00
15	0.0	448.0	-0.1109E-11	-0.1457E-06	0.4175E-12
16	16.0	448.0	-0.2803E-05	-0.5004E-06	-0.9470E-06
17	41.5	448.0	0.0000E+00	0.0000E+00	0.0000E+00
18	0.0	435.0	0.0000E+00	0.0000E+00	0.0000E+00
19	16.0	435.0	0.0000E+00	0.0000E+00	0.0000E+00
20	22.0	435.0	0.0000E+00	0.0000E+00	0.0000E+00

ANNEX IV

Dynamic case: Dam on rigid foundation without water

Mode number = 5 Freq. = 8.77 hz.

Points	s (m)	z (m)	Dx	Dy	Dz
1	0.0	507.0	-0.2944E-03	0.3832E-09	0.1202E-03
2	16.0	507.0	-0.1210E-03	-0.3220E-05	0.6551E-04
3	48.0	507.0	0.7308E-04	0.6907E-06	0.2929E-05
4	80.0	507.0	-0.1646E-03	-0.1417E-03	0.5169E-04
5	112.9	507.0	0.0000E+00	0.0000E+00	0.0000E+00
6	0.0	491.0	-0.7914E-04	0.1518E-09	0.3963E-04
7	16.0	491.0	-0.4763E-05	0.5416E-05	0.2174E-04
8	48.0	491.0	0.8733E-04	0.3024E-04	-0.3430E-05
9	80.0	491.0	-0.2599E-04	-0.2765E-04	0.1655E-05
10	99.2	491.0	0.0000E+00	0.0000E+00	0.0000E+00
11	0.0	471.0	0.2201E-04	-0.2415E-10	0.6424E-05
12	16.0	471.0	0.3444E-04	0.5897E-05	0.6294E-05
13	48.0	471.0	0.2878E-04	0.1175E-04	0.4239E-05
14	75.0	471.0	0.0000E+00	0.0000E+00	0.0000E+00
15	0.0	448.0	0.8605E-05	-0.5668E-10	0.2497E-05
16	16.0	448.0	0.7337E-05	0.8606E-06	0.2660E-05
17	41.5	448.0	0.0000E+00	0.0000E+00	0.0000E+00
18	0.0	435.0	0.0000E+00	0.0000E+00	0.0000E+00
19	16.0	435.0	0.0000E+00	0.0000E+00	0.0000E+00
20	22.0	435.0	0.0000E+00	0.0000E+00	0.0000E+00

Mode number = 6 Freq. = 9.19 hz.

Points	s (m)	z (m)	Dx	Dy	Dz
1	0.0	507.0	-0.1936E-03	-0.1245E-09	0.1252E-03
2	16.0	507.0	-0.2110E-03	-0.4224E-04	0.1238E-03
3	48.0	507.0	-0.5607E-04	-0.2607E-04	0.3910E-04
4	80.0	507.0	0.9017E-04	0.6388E-04	-0.2077E-04
5	112.9	507.0	0.0000E+00	0.0000E+00	0.0000E+00
6	0.0	491.0	0.8737E-04	-0.3250E-10	0.2428E-04
7	16.0	491.0	0.5722E-04	0.2196E-05	0.2696E-04
8	48.0	491.0	0.9146E-05	-0.1685E-06	0.1525E-04
9	80.0	491.0	0.2051E-04	0.1424E-04	0.1738E-05
10	99.2	491.0	0.0000E+00	0.0000E+00	0.0000E+00
11	0.0	471.0	0.1381E-03	0.4105E-10	0.6095E-05
12	16.0	471.0	0.1129E-03	0.1283E-04	0.7168E-05
13	48.0	471.0	0.2022E-04	0.4657E-05	0.6761E-05
14	75.0	471.0	0.0000E+00	0.0000E+00	0.0000E+00
15	0.0	448.0	0.3023E-04	0.3553E-10	0.5560E-05
16	16.0	448.0	0.2172E-04	0.1420E-05	0.4287E-05
17	41.5	448.0	0.0000E+00	0.0000E+00	0.0000E+00
18	0.0	435.0	0.0000E+00	0.0000E+00	0.0000E+00
19	16.0	435.0	0.0000E+00	0.0000E+00	0.0000E+00
20	22.0	435.0	0.0000E+00	0.0000E+00	0.0000E+00

ANNEX V

Dynamic case: Dam on flexible foundation with water (w.l. 491 m.)

Mode number = 1 Freq. = 3.179 hz

Points	s (m)	z (m)	Dx	Dy	Dz
1	0.0	507.0	-3.61837D-08	3.78087D-03	1.31641D-08
2	16.0	507.0	-8.15269D-03	5.11708D-03	1.85625D-03
3	48.0	507.0	-1.13387D-02	5.47885D-03	2.18326D-03
4	80.0	507.0	-2.98859D-03	1.12513D-03	2.72612D-04
5	112.9	507.0	-2.21022D-04	-2.16586D-04	1.66839D-05
6	0.0	491.0	-2.31264D-08	3.18652D-03	9.36407D-09
7	16.0	491.0	-5.11949D-03	3.49803D-03	7.32650D-04
8	48.0	491.0	-7.01386D-03	3.68412D-03	6.07719D-04
9	80.0	491.0	-1.58238D-03	7.72235D-04	-8.37125D-05
10	99.2	491.0	-2.33769D-04	-1.81575D-04	-2.01328D-05
11	0.0	471.0	-1.05984D-08	1.61037D-03	4.72769D-09
12	16.0	471.0	-2.31506D-03	1.75754D-03	-6.53459D-05
13	48.0	471.0	-2.60646D-03	1.51319D-03	-1.98842D-04
14	75.0	471.0	-2.57978D-04	1.75100D-04	-2.53780D-04
15	0.0	448.0	-2.57143D-09	6.09174D-04	2.39837D-09
16	16.0	448.0	-5.26553D-04	6.02731D-04	-1.62896D-04
17	41.5	448.0	-2.79563D-04	2.81311D-04	-1.03231D-04
18	0.0	435.0	-1.68494D-09	2.63479D-04	2.30698D-09
19	16.0	435.0	-5.00402D-05	2.65615D-04	-2.02143D-04
20	22.0	435.0	-3.80932D-05	2.44128D-04	-2.34229D-04

Mode number = 2 Freq. = 3.446 hz

Points	s (m)	z (m)	Dx	Dy	Dz
1	0.0	507.0	-1.90157D-02	-1.74905D-08	2.88835D-03
2	16.0	507.0	-1.55684D-02	-7.25217D-05	2.59987D-03
3	48.0	507.0	2.34453D-04	-3.42070D-03	-1.04780D-03
4	80.0	507.0	3.12974D-03	-3.48578D-03	-9.98046D-04
5	112.9	507.0	-3.33787D-05	-9.44187D-05	-2.62715D-05
6	0.0	491.0	-1.30407D-02	-1.52716D-08	1.39521D-03
7	16.0	491.0	-1.09240D-02	1.06989D-04	1.00447D-03
8	48.0	491.0	-1.20325D-03	-1.71555D-03	-3.56667D-04
9	80.0	491.0	9.39839D-04	-1.73784D-03	-1.36034D-04
10	99.2	491.0	-7.79247D-05	-4.08694D-04	3.01653D-05
11	0.0	471.0	-6.55901D-03	-1.09281D-08	-2.81574D-04
12	16.0	471.0	-5.57126D-03	1.21311D-04	-2.80437D-04
13	48.0	471.0	-1.12294D-03	-7.11749D-04	-1.08999D-04
14	75.0	471.0	-2.26536D-04	-6.24996D-04	1.44299D-04
15	0.0	448.0	-1.73325D-03	-5.57142D-09	-4.22697D-04
16	16.0	448.0	-1.42505D-03	-8.04799D-05	-3.11485D-04
17	41.5	448.0	-4.44830D-04	-4.08367D-04	5.59607D-05
18	0.0	435.0	-3.15448D-04	-1.06656D-08	-5.00325D-04
19	16.0	435.0	-2.21882D-04	-5.48127D-05	-3.96945D-04
20	22.0	435.0	-2.03874D-04	-7.97921D-05	-3.08686D-04

ANNEX V

Dynamic case: Dam on flexible foundation with water (w.l. 491 m.)

Mode number = 3 Freq. = 4.694 hz

Points	s (m)	z (m)	Dx	Dy	Dz
1	0.0	507.0	-4.15599D-03	2.18403D-09	1.78146D-03
2	16.0	507.0	8.79548D-04	-2.08206D-03	6.08418D-04
3	48.0	507.0	1.78086D-02	-8.97764D-03	-4.30398D-03
4	80.0	507.0	8.28650D-03	-3.93982D-03	-1.52683D-03
5	112.9	507.0	5.97041D-04	5.38633D-04	-7.70925D-05
6	0.0	491.0	-1.41851D-03	2.24274D-08	8.42123D-04
7	16.0	491.0	1.26310D-03	-1.21829D-03	2.17684D-04
8	48.0	491.0	9.81044D-03	-4.65081D-03	-1.34055D-03
9	80.0	491.0	3.91894D-03	-1.77558D-03	-2.06750D-04
10	99.2	491.0	7.34972D-04	4.38081D-04	-7.29077D-05
11	0.0	471.0	1.64173D-04	1.38131D-08	1.63121D-04
12	16.0	471.0	1.07775D-03	-4.30760D-04	9.55169D-05
13	48.0	471.0	3.28376D-03	-1.31400D-03	-5.12370D-05
14	75.0	471.0	7.80675D-04	-1.43028D-05	1.98088D-04
15	0.0	448.0	1.16036D-04	5.92845D-09	6.19850D-05
16	16.0	448.0	2.73361D-04	-4.57723D-05	6.87500D-05
17	41.5	448.0	3.16767D-04	3.66919D-05	-4.04884D-05
18	0.0	435.0	-1.85540D-05	6.38207D-09	8.17487D-05
19	16.0	435.0	-5.79690D-06	2.86991D-05	1.05300D-04
20	22.0	435.0	7.29192D-07	4.68864D-05	9.28756D-05

Mode number = 4 Freq. = 5.390 hz

Points	s (m)	z (m)	Dx	Dy	Dz
1	0.0	507.0	4.11457D-03	6.24851D-07	-1.24918D-03
2	16.0	507.0	3.80508D-03	-4.18234D-04	-1.38129D-03
3	48.0	507.0	1.45848D-03	-3.20557D-04	-5.01290D-04
4	80.0	507.0	-1.63317D-04	3.10211D-04	1.85613D-05
5	112.9	507.0	-4.22472D-07	1.32873D-05	-4.83569D-06
6	0.0	491.0	1.40920D-03	-6.22220D-09	-5.97192D-04
7	16.0	491.0	1.39327D-03	-1.34788D-04	-5.56875D-04
8	48.0	491.0	6.38120D-04	-6.35796D-05	-2.20256D-04
9	80.0	491.0	-7.40555D-05	1.82783D-04	-2.84661D-05
10	99.2	491.0	-6.21590D-07	5.99114D-05	-2.22793D-05
11	0.0	471.0	-6.17023D-04	-6.03438D-08	1.49521D-05
12	16.0	471.0	-4.02802D-04	3.36345D-05	-1.59630D-05
13	48.0	471.0	6.72627D-05	2.42412D-05	-7.30367D-05
14	75.0	471.0	-2.38453D-06	6.59342D-05	-5.46802D-05
15	0.0	448.0	-4.76742D-04	-1.61770D-08	7.90968D-05
16	16.0	448.0	-3.84843D-04	1.41237D-05	6.73808D-05
17	41.5	448.0	-1.03071D-04	-3.06796D-05	1.10785D-05
18	0.0	435.0	-1.64087D-04	-4.58323D-08	4.55076D-05
19	16.0	435.0	-1.35669D-04	-9.88267D-06	3.52864D-05
20	22.0	435.0	-1.25189D-04	-1.60892D-05	3.59406D-05

ANNEX V

Dynamic case: Dam on flexible foundation with water (w.l. 491 m.)

Mode number = 5 Freq. = 5.757 hz

Points	s (m)	z (m)	Dx	Dy	Dz
1	0.0	507.0	1.06549D-05	2.89627D-04	-1.68741D-05
2	16.0	507.0	-1.13218D-02	1.76006D-03	3.17159D-03
3	48.0	507.0	7.29398D-03	-7.78946D-03	-2.97732D-03
4	80.0	507.0	1.40712D-02	-1.03596D-02	-3.79979D-03
5	112.9	507.0	7.16381D-04	4.54259D-04	-1.75688D-04
6	0.0	491.0	-1.70197D-05	8.58831D-04	-9.35257D-06
7	16.0	491.0	-7.13101D-03	1.00195D-03	1.53208D-03
8	48.0	491.0	8.38491D-04	-2.61770D-03	-3.43287D-04
9	80.0	491.0	5.04643D-03	-4.05792D-03	-5.65609D-04
10	99.2	491.0	8.60419D-04	-2.16525D-04	-1.44174D-04
11	0.0	471.0	-1.52462D-05	2.45748D-04	-6.10022D-06
12	16.0	471.0	-2.86339D-03	3.85394D-04	2.98209D-04
13	48.0	471.0	-9.07053D-04	-5.11265D-04	2.60133D-04
14	75.0	471.0	2.34917D-04	-5.83532D-04	3.50502D-04
15	0.0	448.0	1.71518D-06	3.20947D-08	-5.12009D-06
16	16.0	448.0	-5.68008D-04	3.03597D-06	6.45017D-05
17	41.5	448.0	-4.27413D-04	-1.77343D-04	3.13080D-04
18	0.0	435.0	3.73756D-06	-6.85819D-05	-4.86743D-06
19	16.0	435.0	-9.63232D-05	-5.25019D-05	-2.26128D-06
20	22.0	435.0	-1.26734D-04	-5.65346D-05	2.60023D-05

Mode number = 6 Freq. = 6.034 hz

Points	s (m)	z (m)	Dx	Dy	Dz
1	0.0	507.0	1.63750D-02	-3.19706D-06	-6.03345D-03
2	16.0	507.0	1.43116D-02	-1.62295D-03	-6.42780D-03
3	48.0	507.0	5.36773D-03	-2.14493D-03	-2.75335D-03
4	80.0	507.0	1.05291D-03	-6.15977D-04	-6.64328D-04
5	112.9	507.0	9.41579D-06	1.67755D-05	-5.59401D-05
6	0.0	491.0	4.59261D-03	-4.91047D-06	-3.09146D-03
7	16.0	491.0	3.75354D-03	-2.74284D-04	-2.71162D-03
8	48.0	491.0	7.62271D-04	-9.90669D-05	-1.11512D-03
9	80.0	491.0	9.45700D-05	-3.40280D-07	-3.24444D-04
10	99.2	491.0	2.94342D-05	5.45349D-05	-1.45364D-04
11	0.0	471.0	-3.17603D-03	-4.57209D-06	-4.96267D-04
12	16.0	471.0	-3.07750D-03	4.07875D-04	-4.59929D-04
13	48.0	471.0	-1.49980D-03	4.86802D-04	-3.55974D-04
14	75.0	471.0	-1.51012D-04	5.69257D-05	-2.55494D-04
15	0.0	448.0	-2.77836D-03	-2.91603D-06	4.51461D-06
16	16.0	448.0	-2.42709D-03	1.54694D-04	1.46789D-05
17	41.5	448.0	-9.01841D-04	-1.74794D-04	7.41270D-05
18	0.0	435.0	-1.11141D-03	-1.88145D-06	-7.72066D-05
19	16.0	435.0	-8.98782D-04	-2.07688D-05	-9.21131D-05
20	22.0	435.0	-7.86195D-04	-6.45398D-05	-5.08002D-05

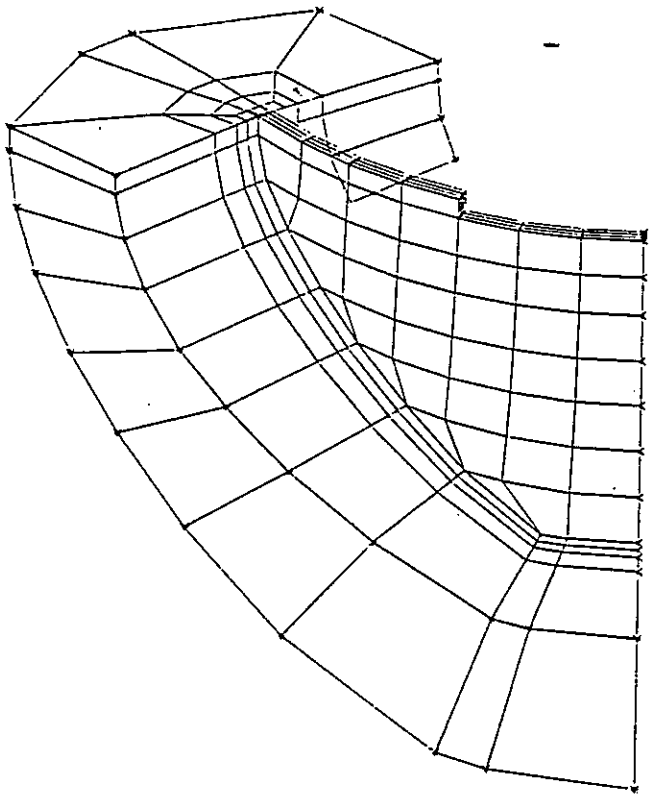

Dam and foundation (Static model)

IBERDUERO S.A. DEPARTAMENTO INGEN

22/03/91

FIGURA NO 1

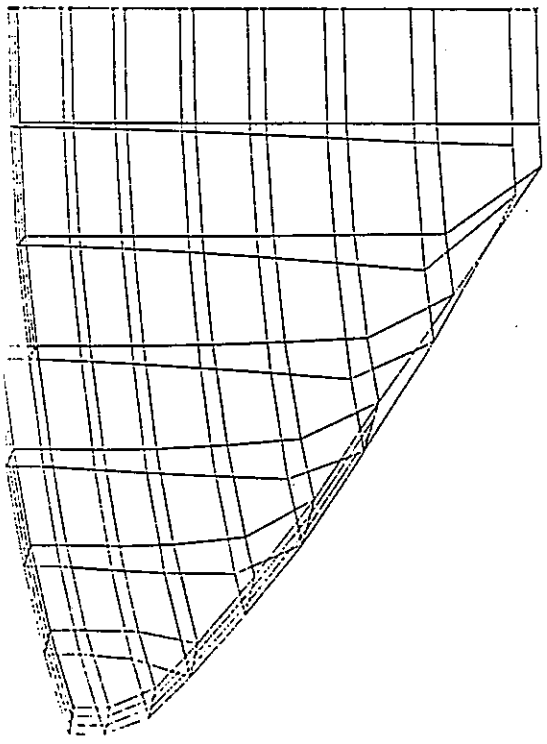

DAM BODY (Sym.)

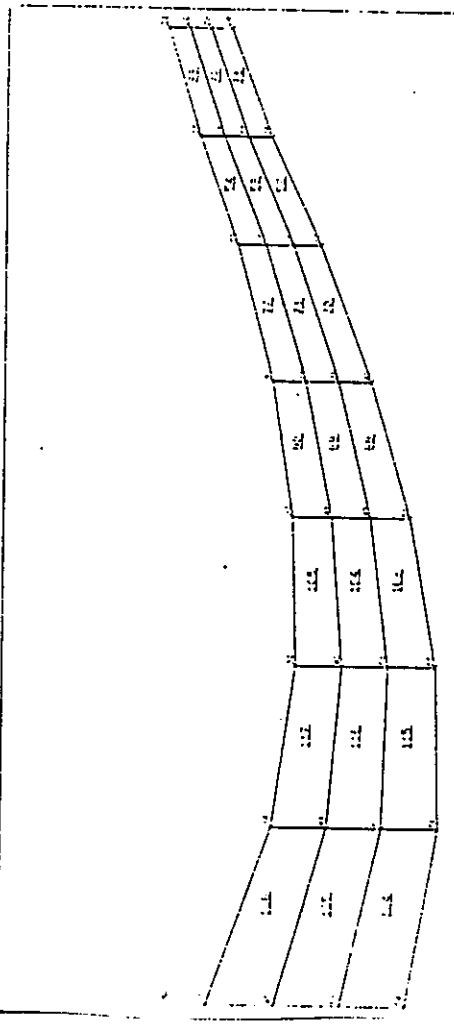

CROWN CANTILEVER

. 1.- Static model: a) Upstream view; b) Dam body; c) Crown cantilever

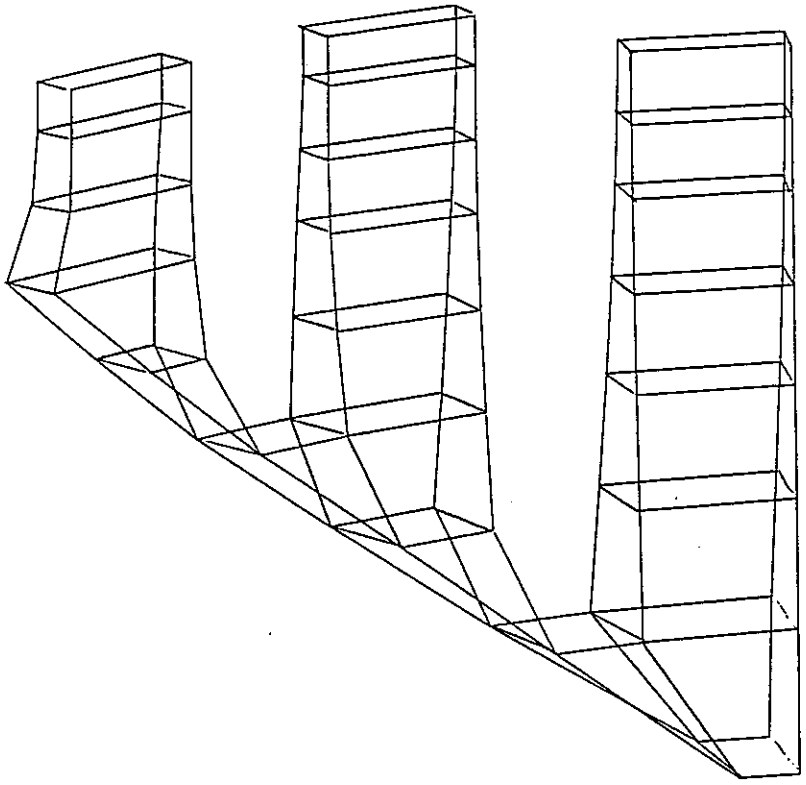

presa de TALVACCIA modelo estatico (simetria central)

IBERDUERO S.A.
DEPARTAMENTO INCEN
16/02/91
ESCALA-1: 521.08
FIGURA NO. 1

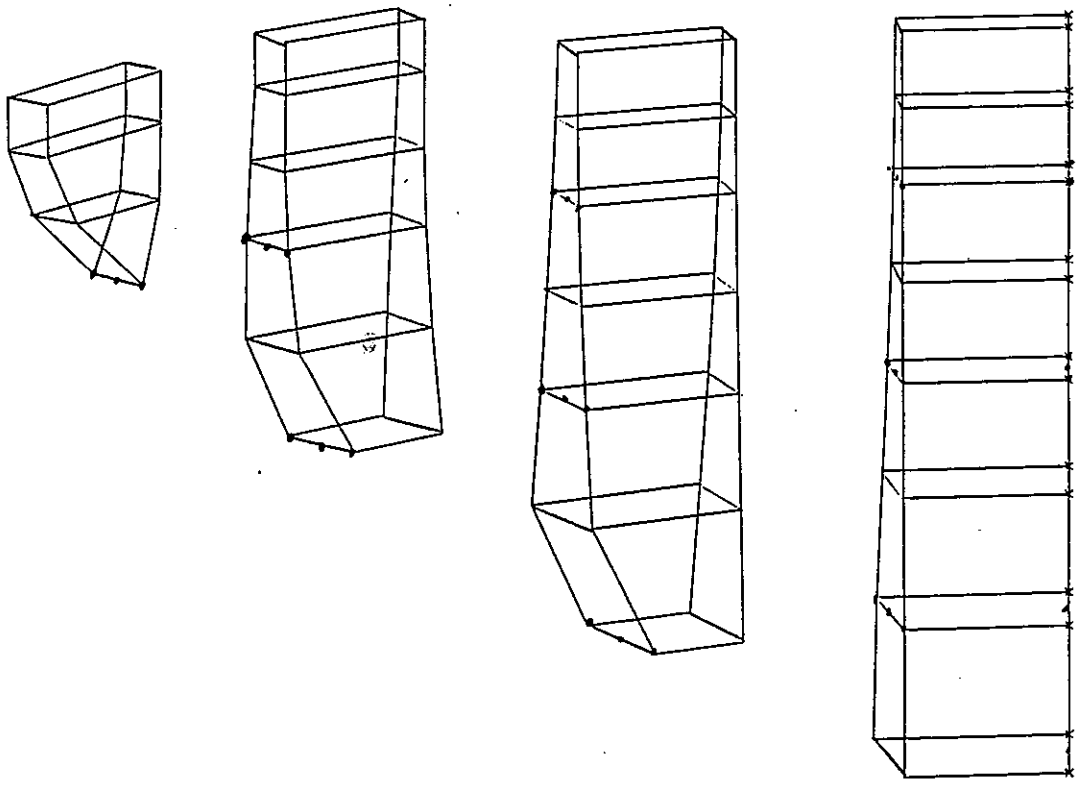

presa de TALVACCIA modelo completo (simetr.a central)

IBERDUERO S.A.
DEPARTAMENTO INCEN
16/02/91
ESCALA-1: 505.71
FIGURA NO. 1

Fig. 2.- Dead load analysis: Definition of even and odd cantilevers.

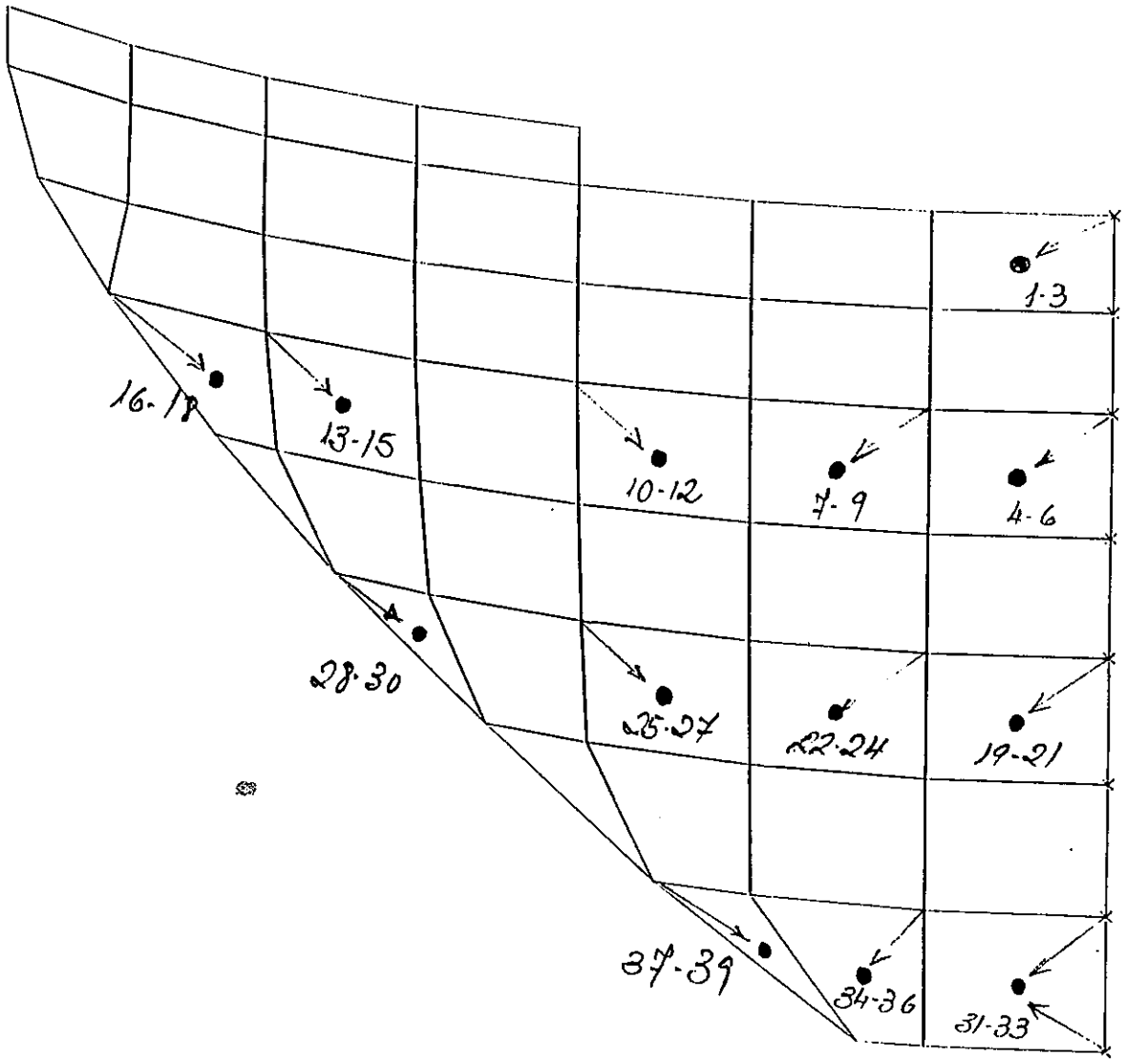

Fig. 3.- Stress output locations

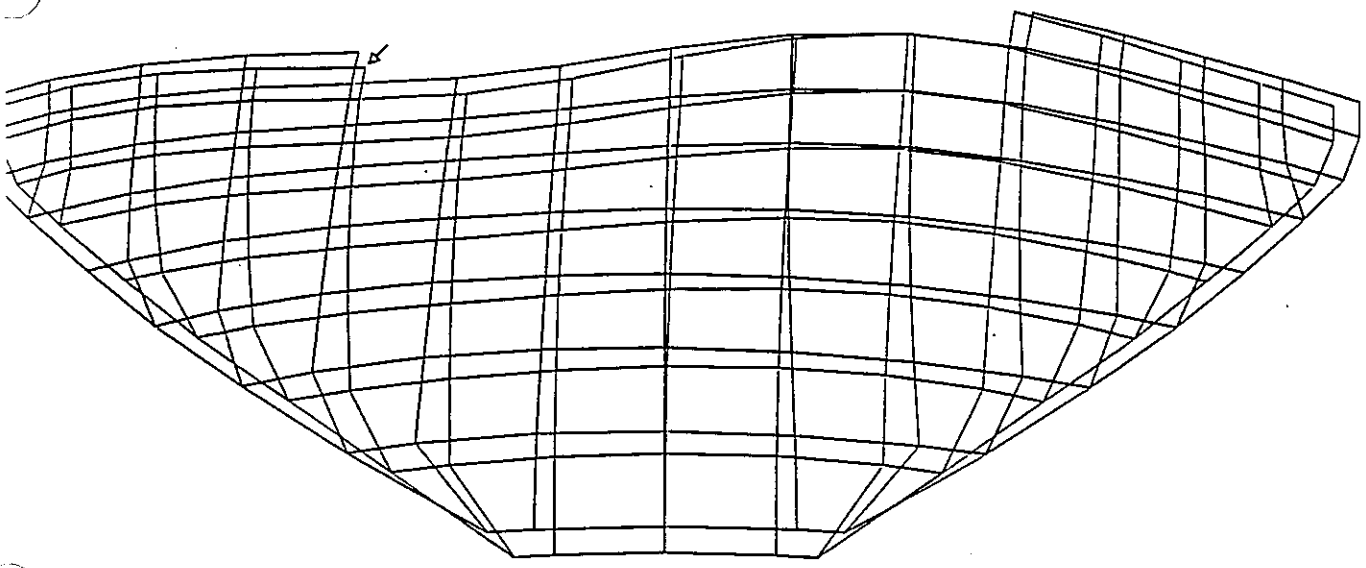

Talvaccia Dam (Dynamic model)
MODO NO. 1 FREQUENCY = 4.31 CPS

Y

IBERDUERO S.A.
DEPARTAMENTO INCEN

22/03/91

LA DE LAS DEFORMACIONES=1: 0.02312

ESCALA=1: 773.11

FIGURA NO. 1

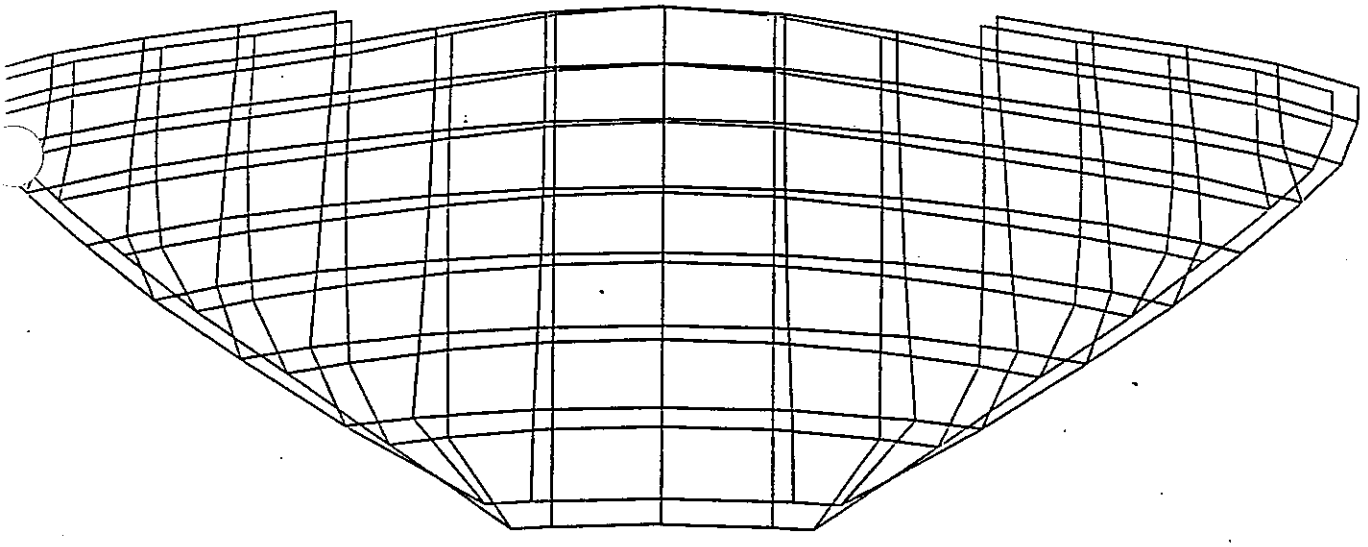

Talvaccia Dam (Dynamic model)
MODO NO. 2 FREQUENCY = 4.60 CPS

Y

IBERDUERO S.A.
DEPARTAMENTO INCEN

22/03/91

LA DE LAS DEFORMACIONES=1.0.03306

ESCALA=1: 773.11

FIGURA NO. 2

Fig. 4.- Dynamic analysis without water: Mode shapes 1 & 2

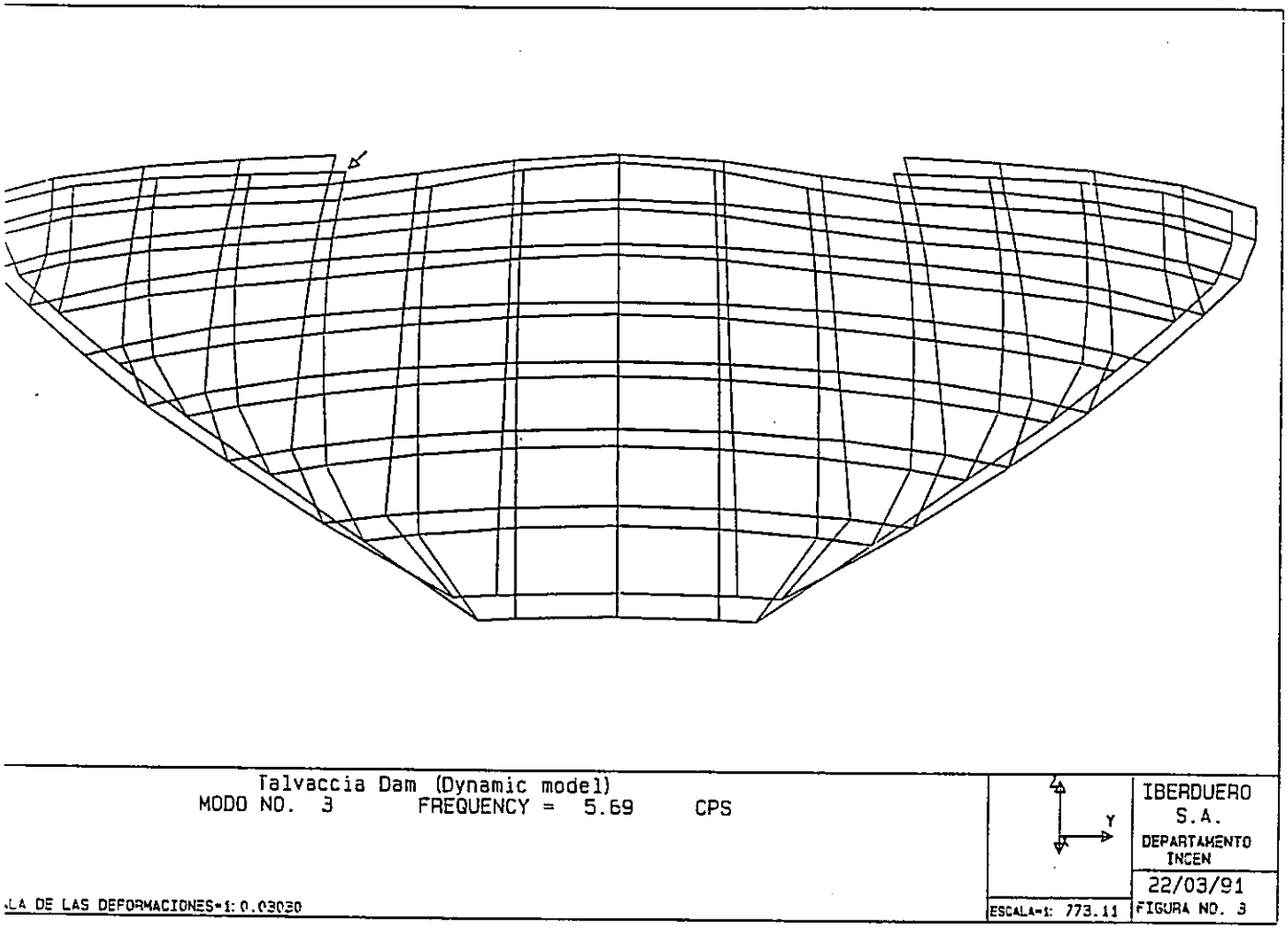

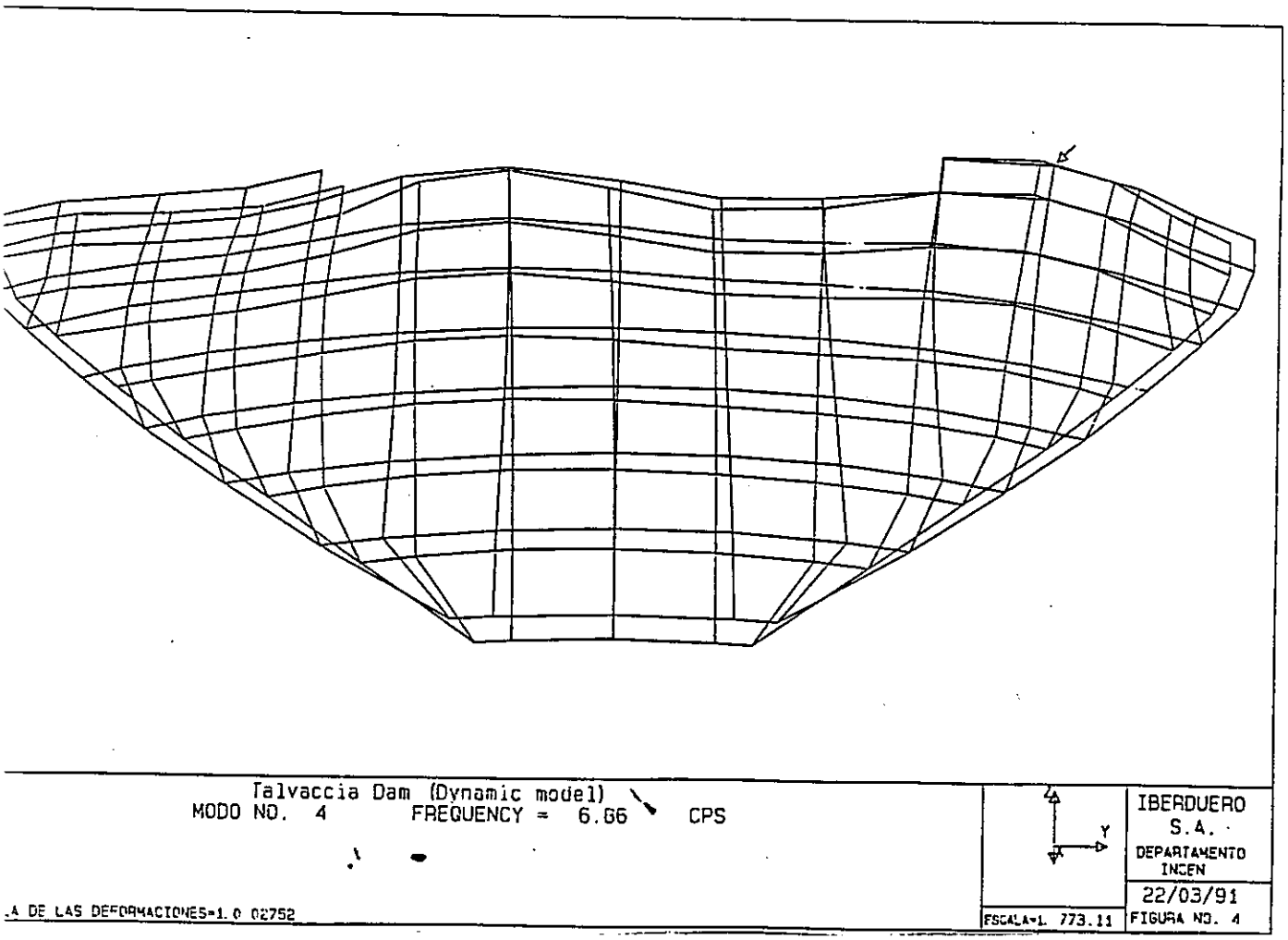

Fig. 5.- Dynamic analysis without water: Mode shapes 3 & 4

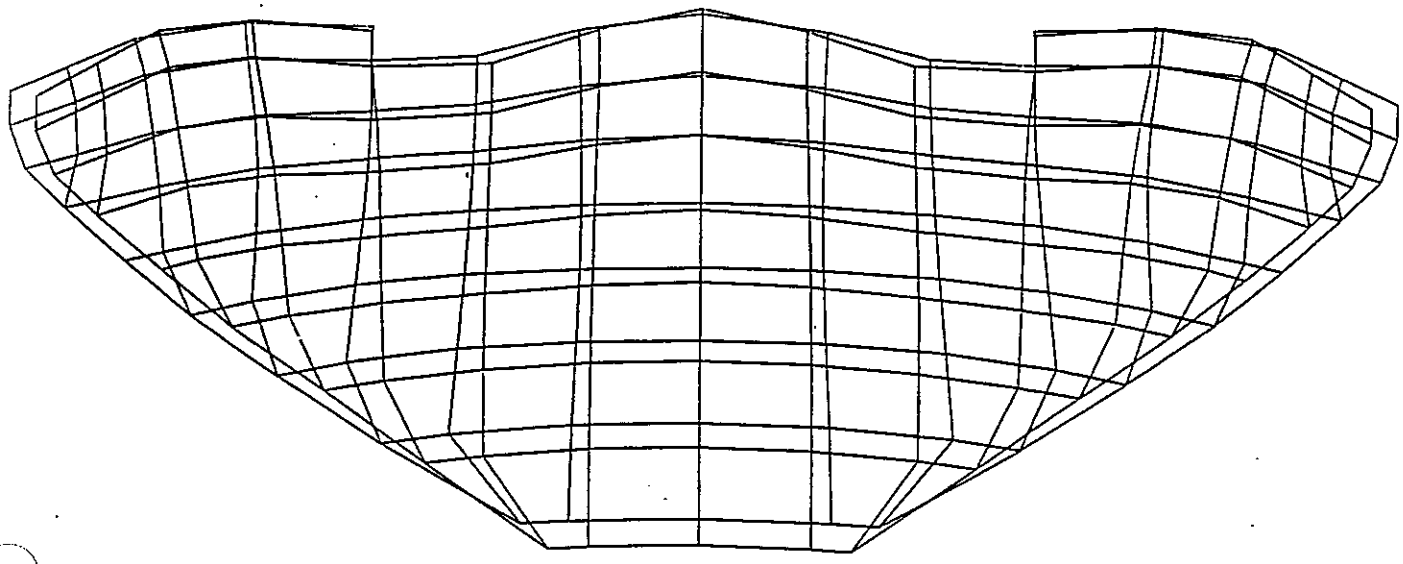

Talvaccia Dam (Dynamic model)
MODO NO. 5 FREQUENCY = 8.77 CPS

ESCALA DE LAS DEFORMACIONES=1: 0.02947

Y

IBERDUERO S.A.
DEPARTAMENTO INCEN
22/03/91
ESCALA=1. 773.11 FIGURA NO. 5

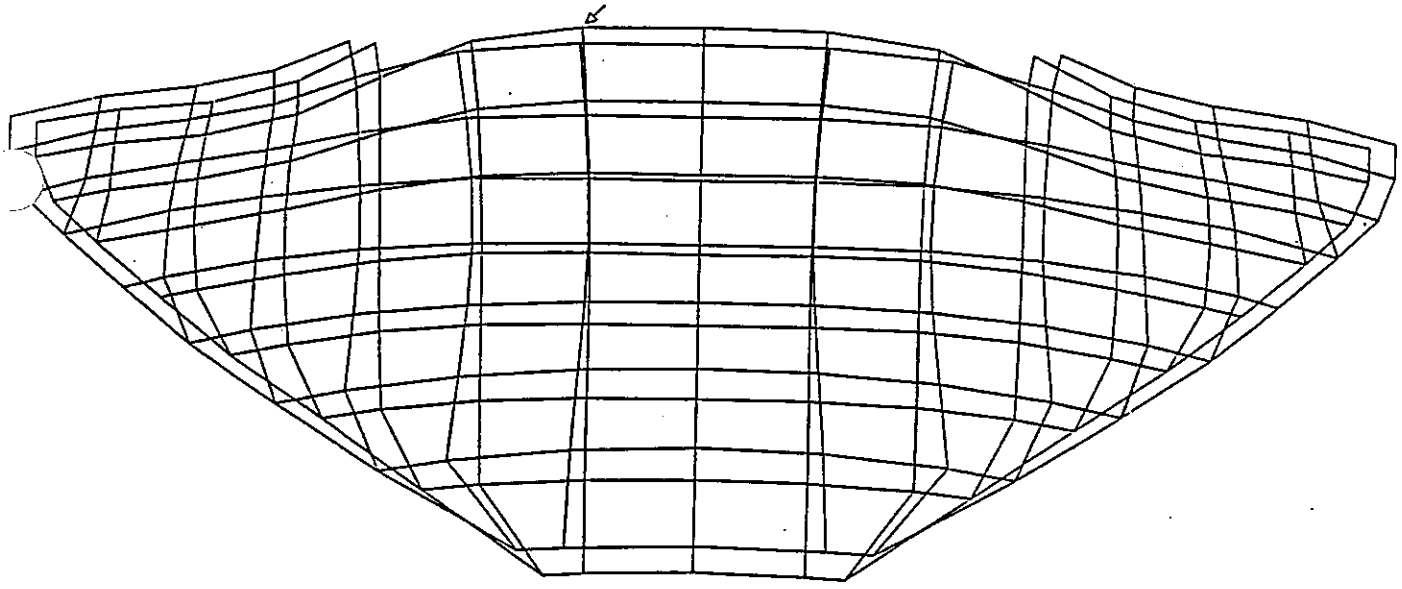

Talvaccia Dam (Dynamic model)
MODO NO. 6 FREQUENCY = 9.19 CPS

ESCALA DE LAS DEFORMACIONES=1.0.02116

Y

IBERDUERO S.A.
DEPARTAMENTO INCEN
22/03/91
ESCALA=1: 773.11 FIGURA NO. 6

Fig. 6.- Dynamic analysis without water: Mode shapes 5 & 6

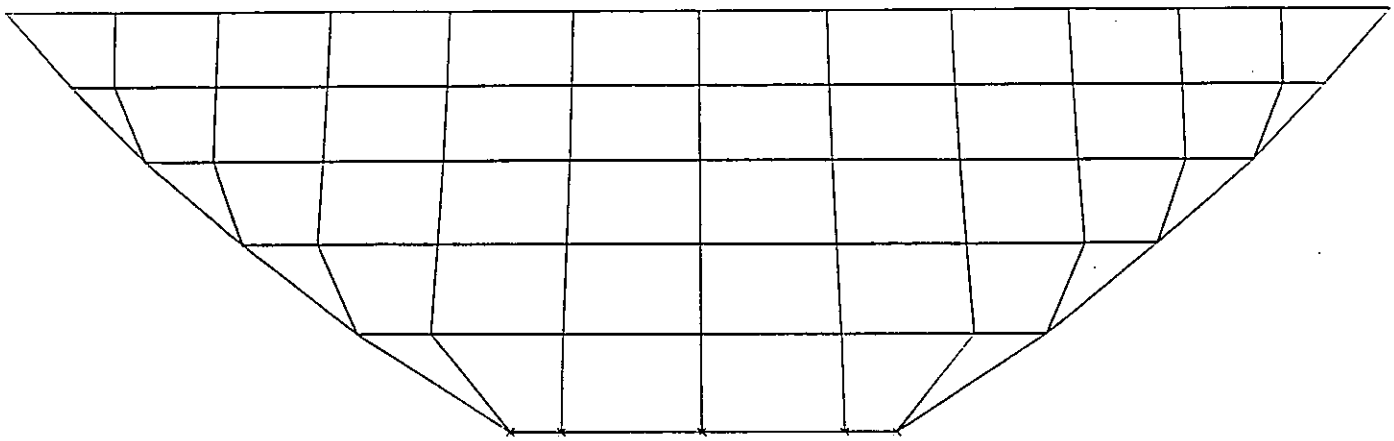

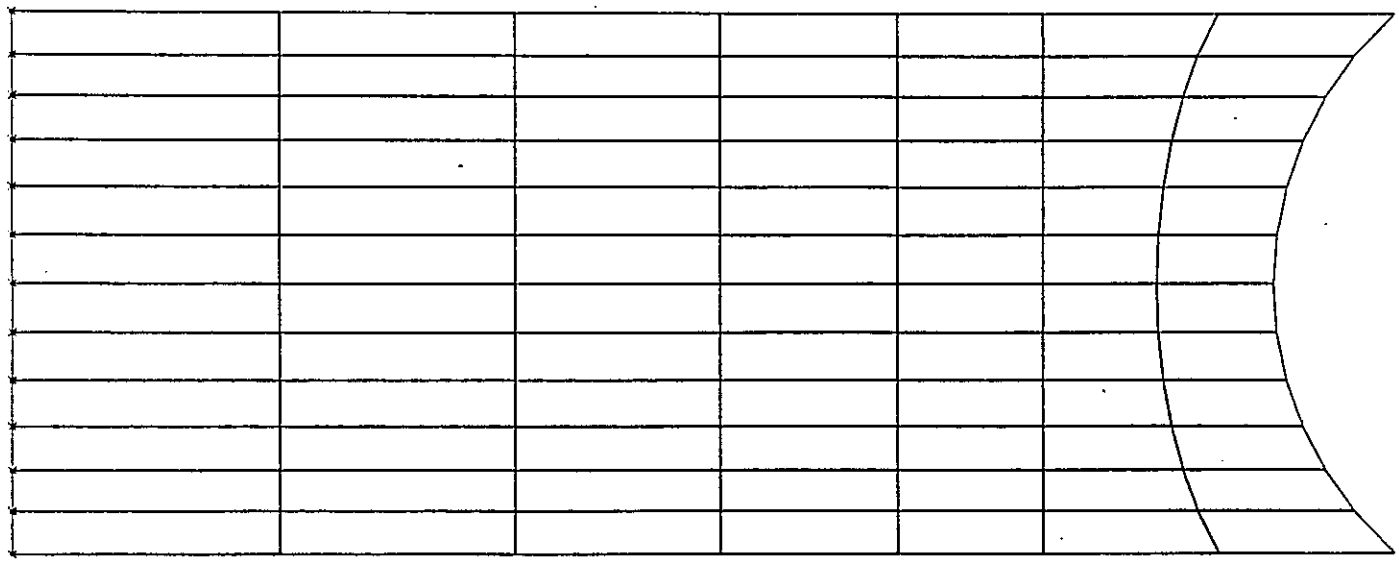

Fig. 7.- Dynamic analysis with water: a) Orthogonal view of dam-water interface; b) Plan view of reservoir surface.

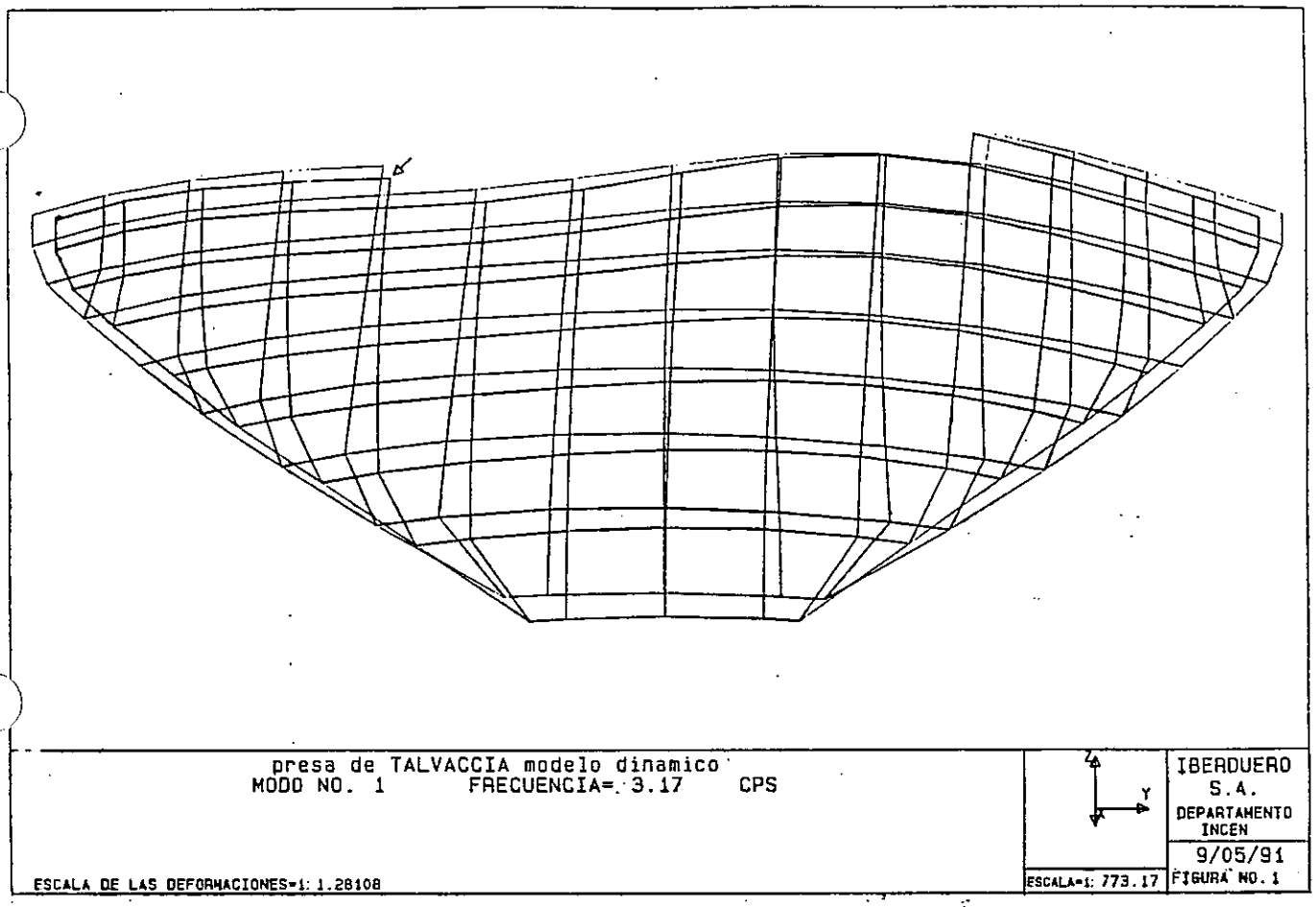

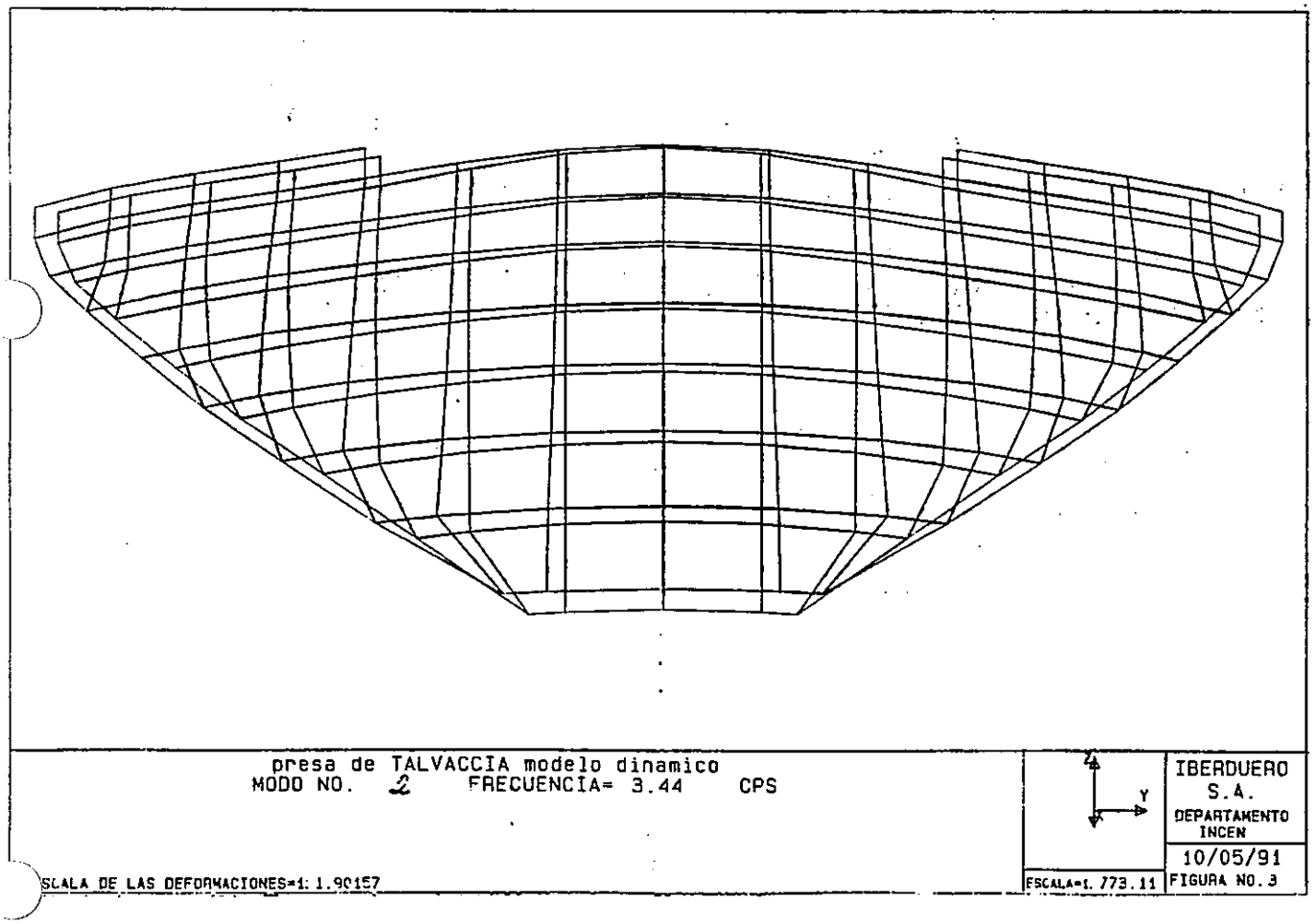

Fig. 8.- Dynamic analysis with water: Mode shapes 1 & 2

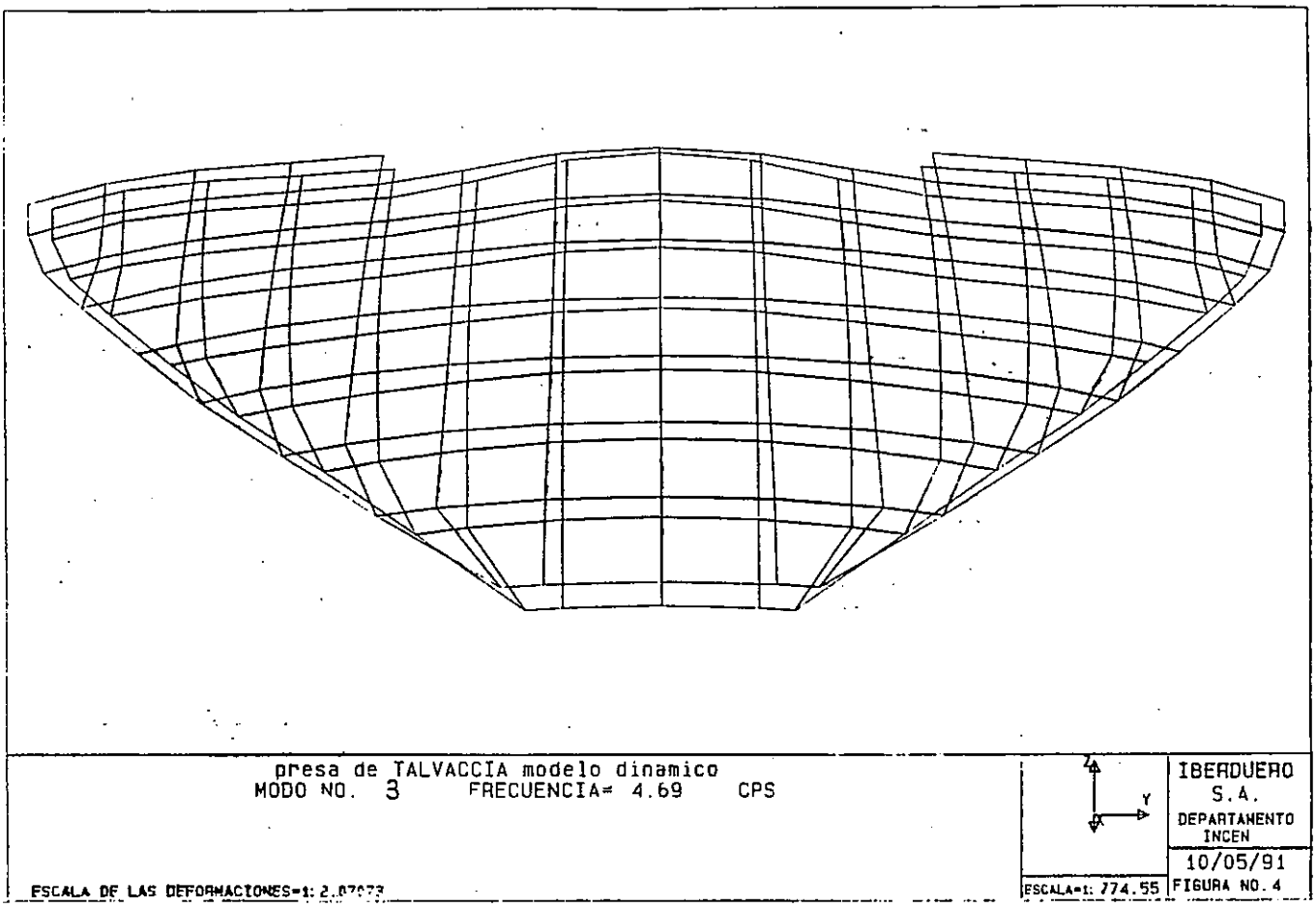

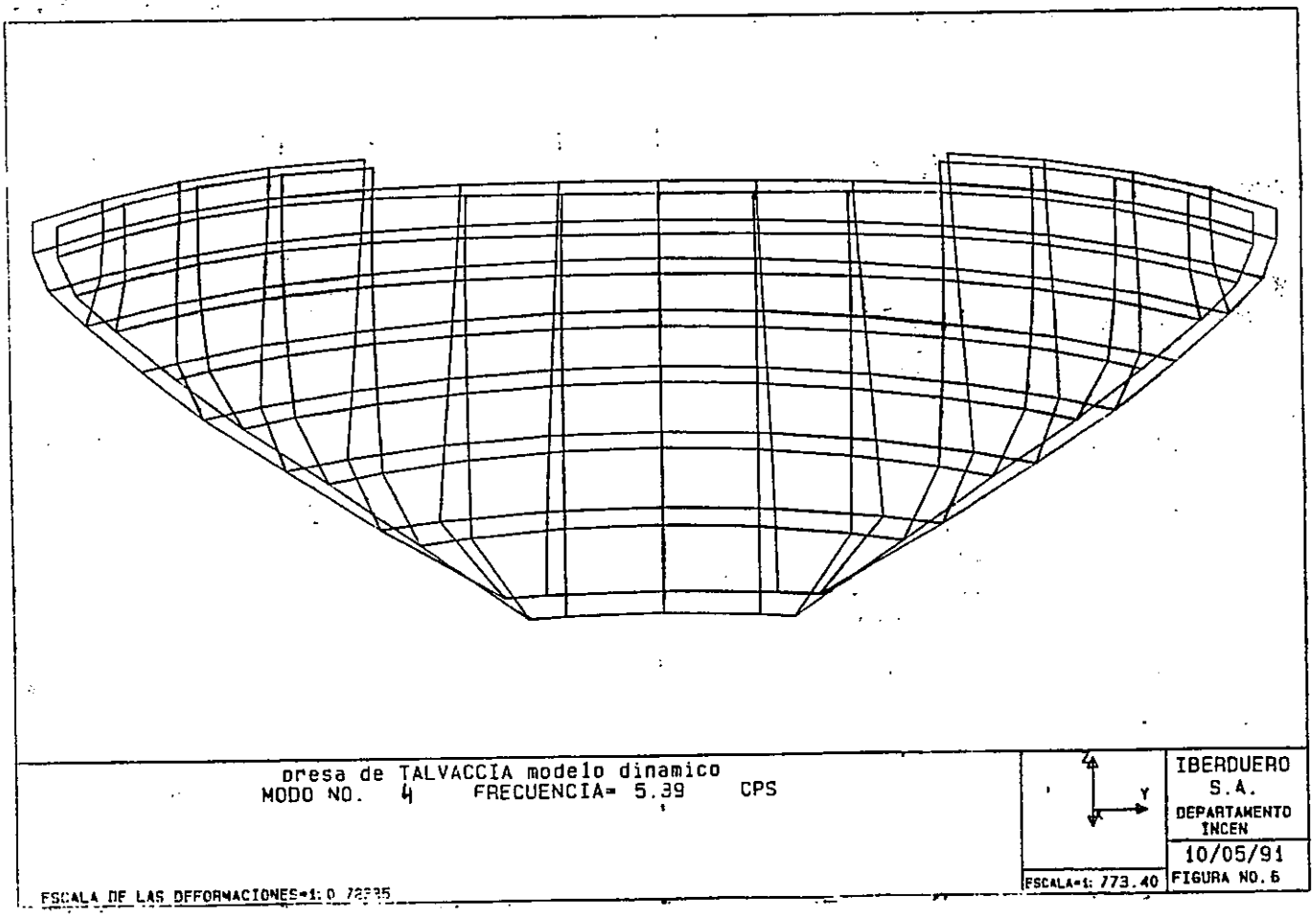

Fig. 9.— Dynamic analysis with water: Mode shapes 3 & 4

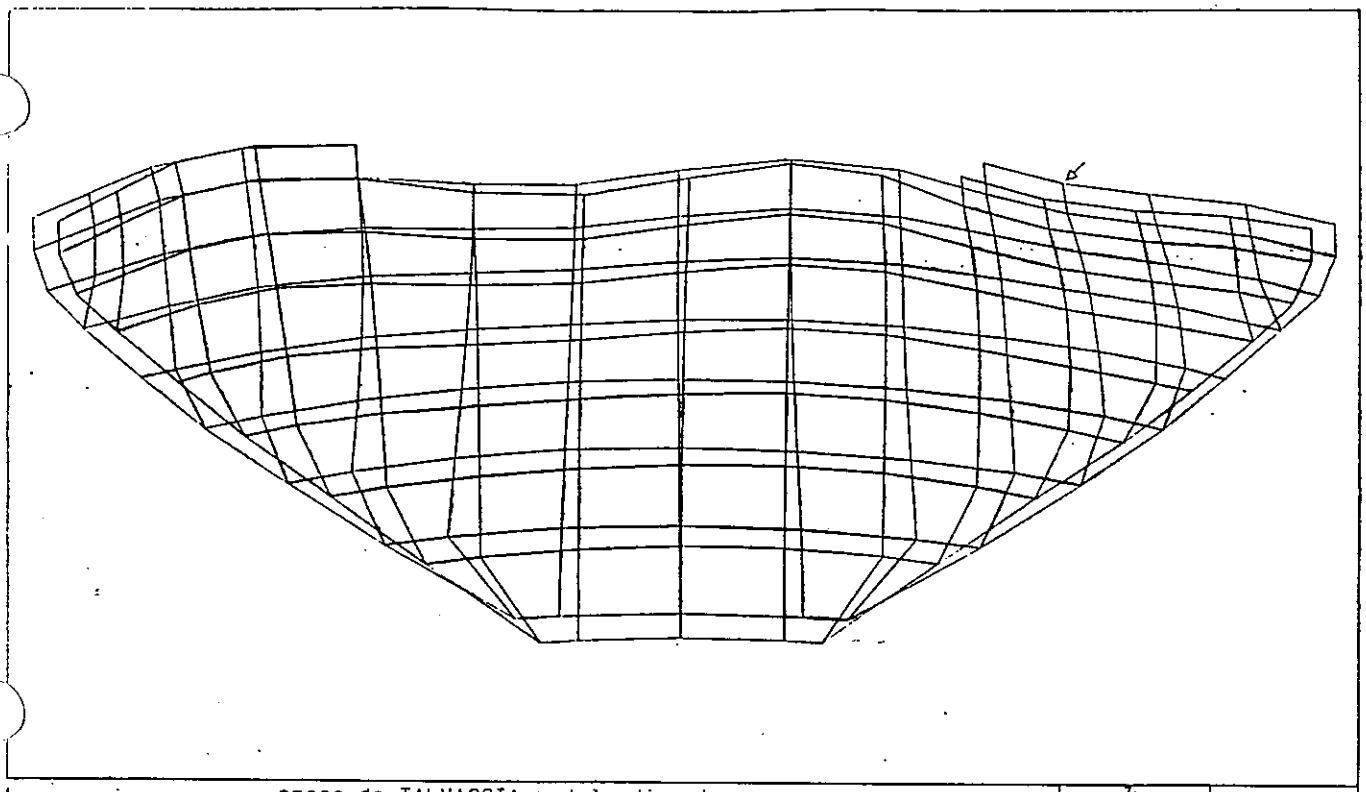

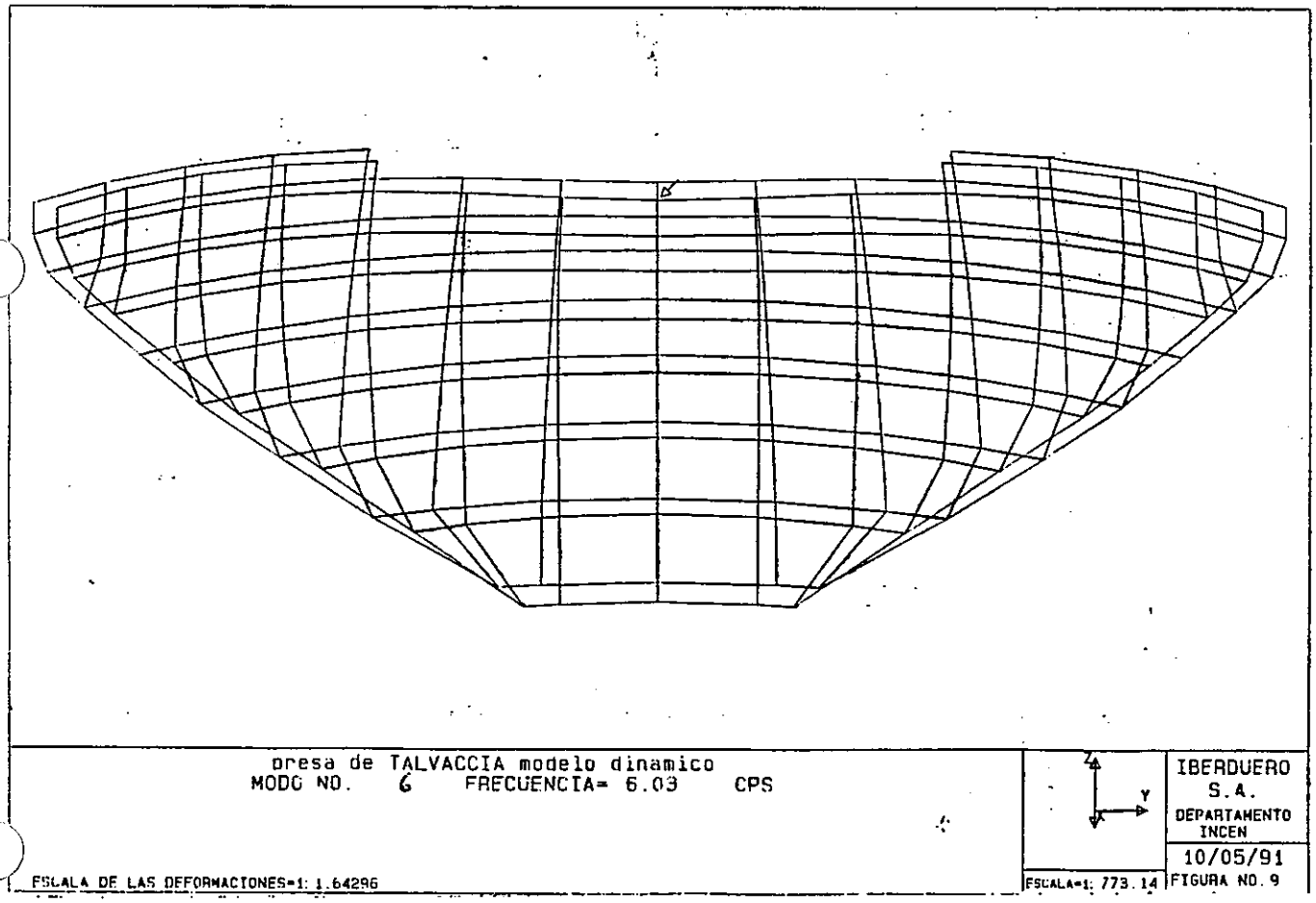

Fig. 10.- Dynamic analysis with water: Mode shapes 5 & 6

COYNE ET BELLIER
BUREAU D'INGENIEURS CONSEIL
5, rue d'Heliopolis, 75017 PARIS
Tel 40546869 - Télex COYBE 280177 f
FAX 46223874

FIRST BENCHMARK WORKSHOP ON NUMERICAL ANALYSIS OF DAMS

THEME A : DOUBLE CURVATURE CONCRETE ARCH DAM

DYNAMIC AND STATIC STUDY REPORT

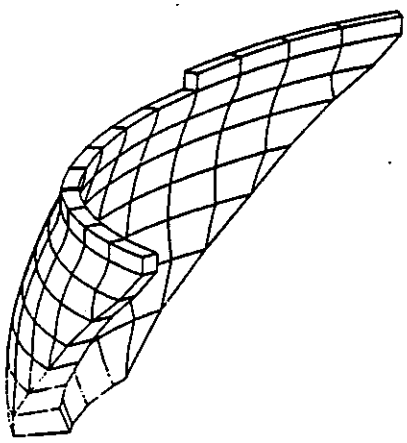

TALVACCHIA DAM ITALY

MARCH 1991

PRESENTATION

This document is the final report of the Talvacchia dam study. This study is for the "First Benchmark Workshop on Numerical Analysis of Dams" with, for theme, "Double Curvature Concrete Arch Dams."

The first part of this document presents the assumptions adopted for the numerical analyses. The second part presents the results requested by the authors.

The appendixes are divided up as follows:

Appendix 1: The Meshes of the Dam and Reservoir

Appendix 2: Tables of Results

Appendix 3: Deformed Shapes, Eigen Modes of the Dam and Drawings of Stresses on the Dam Faces for Different Cases of Loads

Appendix 4: Frequency Response of Some Points of the Dam for the Dynamic Study of the Dam with Water Supply

I. GENERAL ASSUMPTIONS

1. GEOMETRICAL PARAMETERS

The dam model adopted is a model with thick shell elements. The foundation was modeled using so-called Vogt elements.

Vogt's theory (1) and subsequent work by Mladyenovitch (2) state the relationship between forces and moments at the dam/foundation contact and the corresponding displacements and rotations in terms of the deformation modulus and Poisson's ratio of the foundation rock, and the aspect ratio describing the type of dam/foundation contact (producing an "equivalent rectangle" (3)). Once these values are known , the contact can be modelled as a set of independent springs whose individual stiffnesses take into account the total effect.

Vogt's foundation modelling has been widely used in the "trial load" method (3) and is therefore still considered as a reference method by many Engineers, despite its evident simplification assumption.

The mesh which has been used in our calculation for the dam is directly derived from the one suggested by the Author, for easier comparison with other results. It should be noted that its design may be criticized mainly regarding the shapes of the elements close to the foundation.

This mesh has been modified for thick shell analysis by removing the intermediate nodes between the arch faces (Appendix 1).

The length of the reservoir is equal to five times the height of the dam. It does not have any boundary parallel to the upstream face of the dam, which indicates the semi-infinite aspect of the reservoir.

---

(1)F. Vogt "Uber die berechnung der fundament deformation".
Der Norske Videnskaps Akademi, Oslo , 1925
(2) V. Mladyenovitch "Déformation des fondations de barrages"
Travaux, November-December 1966
(3)Usbr. "Trial load method of analyzing arch dams".
Denver , 1938

The program used to perform the calculation in static analysis is COQEF3. It is a finite element program based on quadratic isoparametric thick shell elements . The program itself, together with its pre- and post-processors, is designed especially for analysis of arch dams, to replace the "trial load" method. In addition to the fact that it is easier to used COQEF3, this program provides an FEM approach that is more rigorous than the one mentioned above.

The program used to perform the calculation in dynamic analysisis I.F.S.S.(Soil-Structure-fluid interaction)(4). This program has been especially developed to take into account the dynamic response of the dam with reservoir coupling at reasonable cost, which means that some simplifying assumptions (elastic behaviour) has been adopted. Each domain is analysed with specific tools (for example thick-shell dam modelling or boundary elements for the fluid domain), and only during the last stage are various components linked together.

2. PHYSICAL PARAMETERS

The data used for numerical analysis is as follows:

- Young's static modulus (concrete) $E_c = 3.00\ 10^{10}\ Nm^{-2}$
- Young's dynamic modulus (concrete) (5) $E_{cd} = 2 * E_c$
- Young's static modulus (rock) $E_r = 1.20\ 10^{10}\ Nm^{-2}$
- Young's dynamic modulus (rock) (5) $E_{cr} = 2 * E_r$
- Poisson's ratio (concrete) $V_c = 0.20$
- Poisson's ratio (rock) $V_r = 0.16$
- Thermal diffusion coefficient (concrete) $a = 1.0\ 10^{-6}\ m\ s^{-1}$
- Conductivity coefficient (concrete) $\lambda = 2\ w/m°C$

(4)B. Tardieu, A. Carrère, J.-M. Crépel "Computational and engineering aspects of the aseismic design of arch dams" Dam Engineering Vol. 1 Issue 1

(5) Assumption not provided by the author

-	Coefficient of dilatation (concrete)	$\alpha = 0.7\ 10^{-5}\ C^{-1}$
-	Unit weight (concrete)	$\gamma_c = 24{,}000\ Nm^{-3}$
-	Unit weight (rock)	$\gamma_r = 20{,}000\ Nm^{-3}$
-	Unit weight (water)	$\gamma_w = 10{,}000\ Nm^{-3}$
-	Wave celerity (water)	$e = 1440\ ms^{-1}$

3. THERMAL ANALYSIS

The thermal analysis consisted of evaluating the range of temperature only in the dam. The dam/foundation interface was considered to be an adiabatic surface. The water level is 507.0 m above sea level.

As indicated by the telefax (SGE/REL 1624), the reference temperature of dam at joint grouting is to be 0° C.

The transmission of heat through a rockmass without heat emission follows Fourier's general equation:

$$\frac{\partial T}{\partial t} = a \left(\frac{\partial^2 T}{\partial x^2} + \frac{\partial^2 T}{\partial y^2} + \frac{\partial^2 T}{\partial z^2} \right)$$

where T is the temperature in °C at a given point at a given time,

t: time,

x, y, z: coordinates of the point considered,

a: thermal diffusivity coefficient of the material.

For transient analysis, the temperature of the faces of the dam are sinusoidal functions of time:

$$T_1 = A_1 \sin (\omega t + \phi_1)$$

$$T_2 = A_2 \sin (\omega t + \phi_2)$$

Temperature T of any point whatsoever at a distance a from the original face (downstream face) and at each moment t is given by the formula:

$$T = f \cos(\omega t) + \Psi \sin(\omega t) + C_1 + C_2 x$$

where:

$$f = a \cos(\mu x)\,Ch(\mu x) + b \cos(\mu x)Sh(\mu x) + c \sin(\mu x)Ch(\mu x) + d \sin(\mu x)Sh(\mu x)$$

$$\Psi = -a \sin(\mu x)Sh(\mu x) - b \sin(\mu x)Ch(\mu x) + c \cos(\mu x)Sh(\mu x) + d \cos(\mu x)Ch(\mu x)$$

with

$$\mu = \sqrt{\frac{\omega}{2a}}$$

a: thermal diffusivity coefficient

ω: frequency of the waves.

Should the joint grouting temperature be 0°C, the expression of temperature becomes:

$$T = f \cos(\omega t) + \Psi \sin(\omega t) = A \sin(\omega t + \phi)$$

$$A = \sqrt{f^2 + \Psi^2}$$

$$\phi = \arctan\left(\frac{\Psi}{f}\right)$$

3–1 Steady–state analysis

The air temperature was presumed to be constant and equal to T_1 = 15°C. The free surface of the water was at the same temperature. Between levels 435.0 and 492.0 m, water temperature was constant. It was equal to T_2 = 10°C. In order to ensure temperature continuity, the temperature is presumed to vary in linear terms between level 492.00 m and the free surface of the water (507.0 m).

3–2 Periodic analysis

The amplitudes and range of temperatures taken into account in the computations are as follows:

$A_1 = 10°C$ $\phi_1 = 0$ rad for air.

$A_2 = 5°C$ $\phi_2 = -0.52$ rad for water.

4. STATIC ANALYSES

Three types of load were taken into account:

- Dead Load
- Hydrostatic Pressure
- Thermal Loading.

4.1. Dead Load

The dam was considered to be a monolithic solid to which dead load was applied after construction, as stipulated in the terms of reference. Such an approach is generally considered irrealistic and is often replaced by a simulation of a layer-by-layer construction, with or without considering the transient thermal effect and Noten

4.2. Hydrostatic Pressure

Hydrostatic pressure was applied to the upstream face of the dam only (not to the foundation). The water level is 507.0 m ASL.

4.3. Thermal Loading

The distribution of temperature that was evaluated in the thermal steady-state analysis was taken as the loading condition. The mesh used for this numerical analysis is the same as the one used above. The dam/foundation interface nodes were clamped.

5. DYNAMIC ANALYSES

This involved evaluating the first six eigen frequencies of the dam as well as the associated eigen modes in two situations:

- dam on a rigid foundation without water supply.
- dam on a flexible foundation with water supply.

The criteria for normalization chosen for the eigen modes is the following:

where (ϕ_i) represents all of the eigen modes
and M is the mass matrix

$${}^t\phi_i \, M \, \phi_j = \delta_{ij} \qquad \delta_{ii} = 1, \; \delta_{ij} = 0, \text{ if } i \neq j$$

Young's dynamic modulus (for the concrete as well as for the foundation) is taken as being equal to two times Young's static modulus.

5.1. Dam on Rigid Foundation without Water Supply

In this particular case, the foundation was considered as being rigid, and the dam/foundation interface nodes were clamped.

5.2. Dam on Flexible Foundation with Water Supply

The water supply level is 491.0 m ASL. Only fluid/structure interaction was taken into account in these analyses. The mass of the foundation was neglected.

Water was considered as an incompressible fluid.

Due to the fact that the reservoir does not have any boundary parallel to the upstream face, we have Sommerfeld radiation conditions in which the waves from the dam or the reservoir towards this boundary are absorbed.

II. PRESENTATION OF THE RESULTS

The mesh proposed by the author shows some shortcomings, but we used it in order to respect the imposed degrees of freedom.

The first one is the alignment of the intermediate nodes on the foundation surface, which gives a shape in discordance with the general shape of the dam faces (Appendix 1-5).

The second is the sharp shaping of the prismatic elements in the lower part of the dam mesh, which gives bad jacobien determinant values and reduces the general model quality.

Nevertheless the results that were obtained generally correspond to what we expected.

Note: Because the model on which we performed numerical analyses was a shell model, no normal principal stresses were available.

1. THERMAL ANALYSIS

1.1. Steady-state analysis

The value of nodal temperatures relevant to the middle interal surface are presented in Appendix 2-2.

1.2. Periodic analysis

The value of amplitudes A (°C) and phase (radian) are shown in Appendix 2-2.

2. STATIC ANALYSIS

2.1. Dead load

Displacements as well as principal stresses are shown in the table in Appendix 2–4. A drawing of the principal stresses on the faces can be found in Appendixes 3–1 and 3–2.

2.2. Hydrostatic pressure

Displacements as well as principal stresses are presented in the table in Appendix 2–5. The deformed shape of the dam is presented in Appendix 3–3. A drawing of the principal stresses on the faces is presented in Appendixes 3–4 and 3–5.

2.3. Thermal load

Displacements as well as principal stresses are shown in the table in Appendix 2–6. The deformed shape of the dam is presented in Appendix 3–6. A drawing of the principal stresses on the faces can be found in Appendixes 3–7 and 3–8. What draws our attention is the fact that there are high tensile stresses on the spillway.

Appendix 3–9 to 3–13 present deformed shapes and drawings of the principal stresses resulting from the superposition of some or all of the three precedent loads.

3. DYNAMIC ANALYSIS

3.1. Dam on a Rigid Foundation without Water Supply

The eigen modes for the first six eigen frequencies are presented in the tables in Appendixes 2–7 to 2–12. Eigen modes are presented in Appendixes 3–14 to 3–19.

3.2. Dam on a Flexible Foundation with Water Supply

The frequency response of the dam for the points chosen is presented in Appendixes 4. The response enabled us to calculate the eigen frequencies of the dam. The associated eigen modes are presented in Tables 2-13 to 2-18, and drawings are presented in Appendixes 3-20 to 3-25.

APPENDIX 1

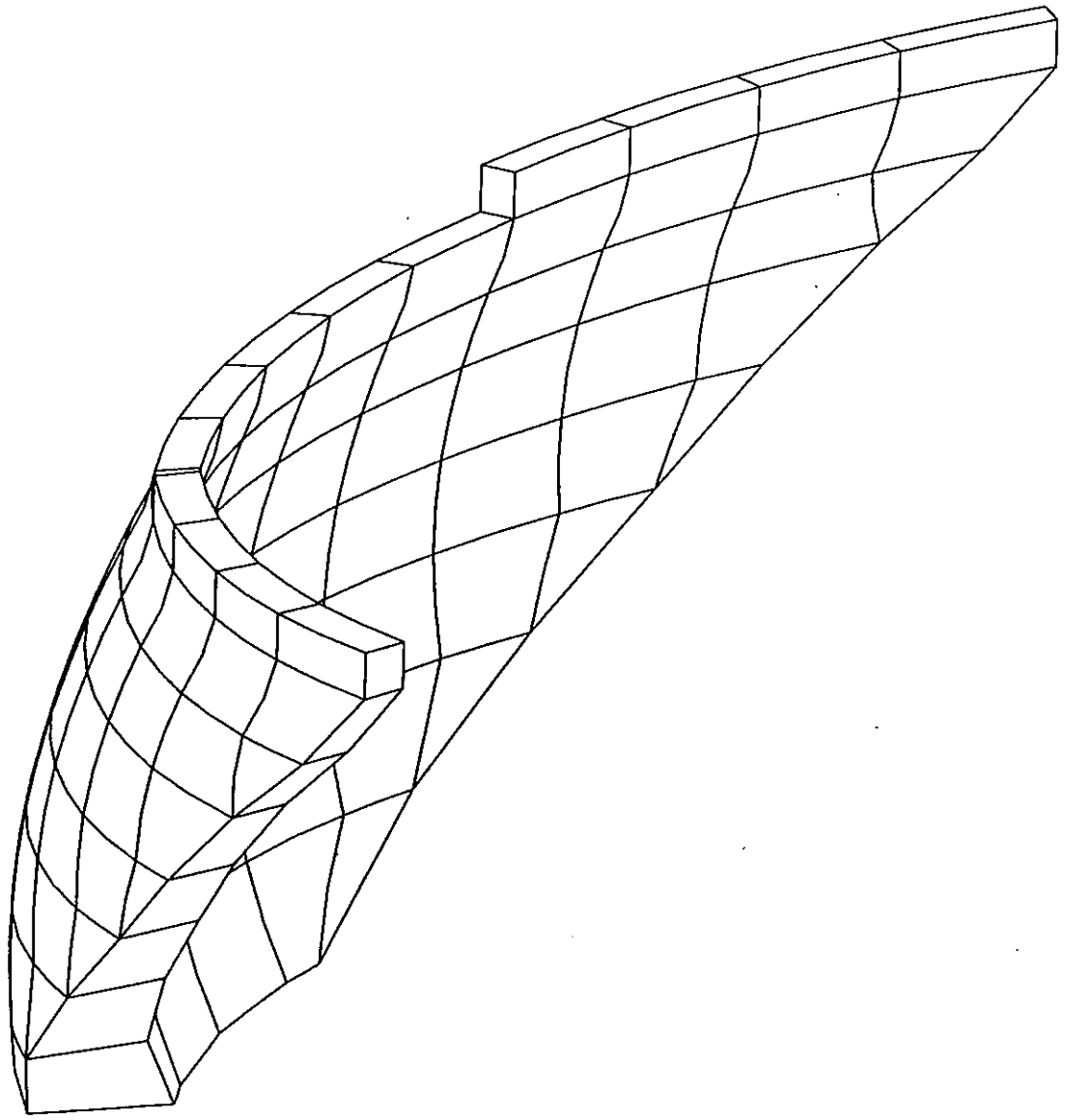

0 10

TALVACCHIA DAM

VIEW FROM RIGHT BANK

SCALE : 1.312E-03

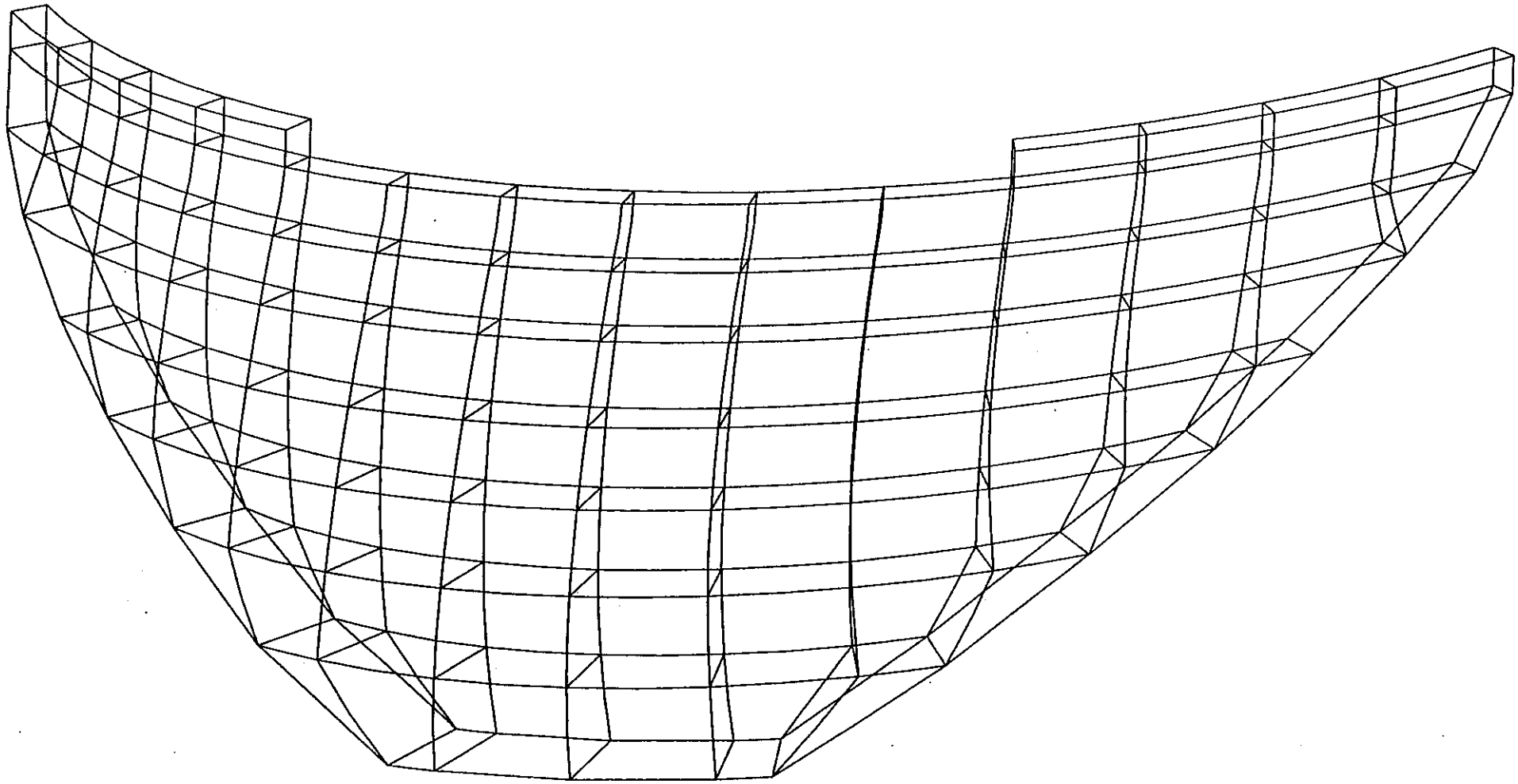

0 10

TALVACCHIA DAM

UPSTREAM VIEW

SCALE : 1.286E-03

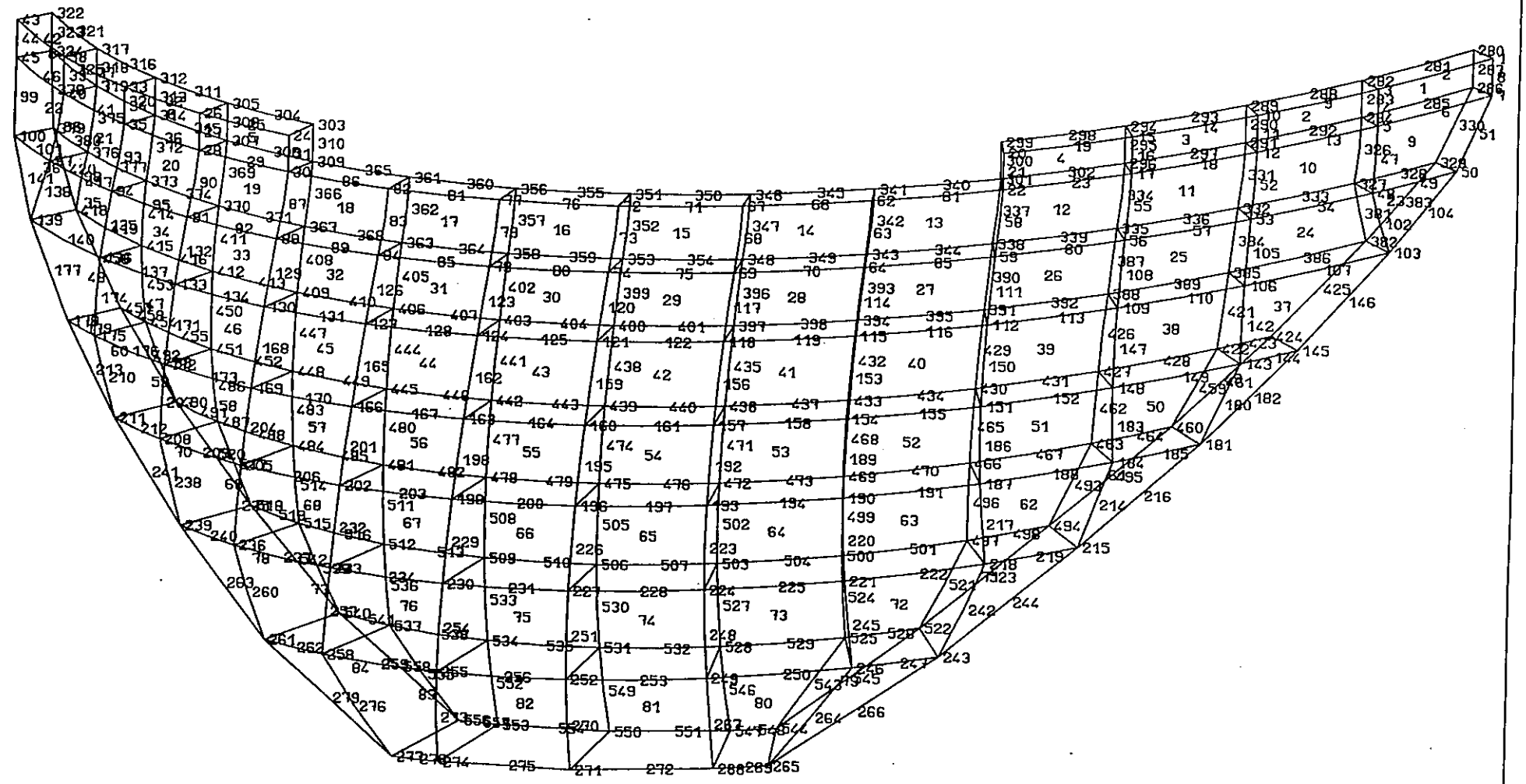

TALVACCHIA DAM

UPSTREAM VIEW

SCALE : 1.286E-03

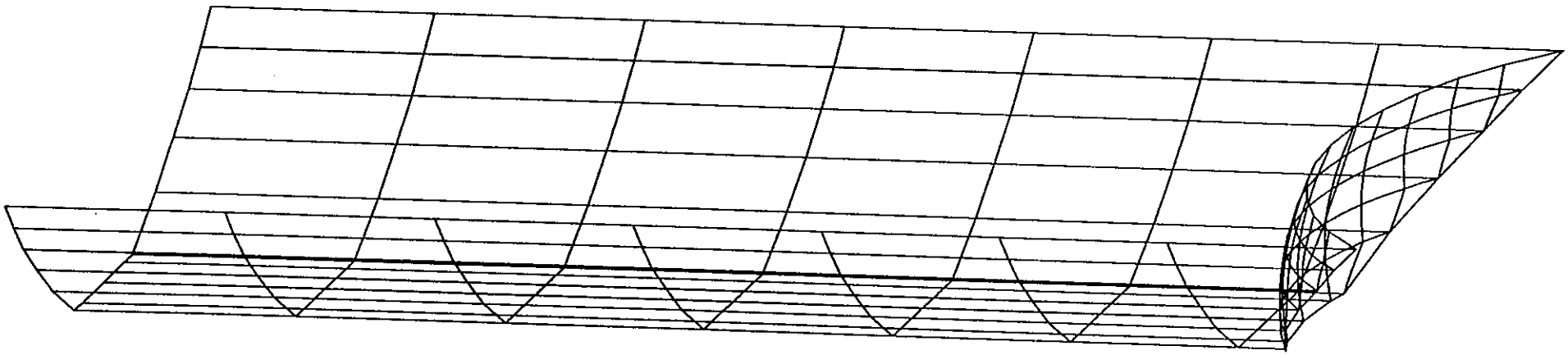

0 20

MESH OF RESERVOIR

WATER LEVEL 491 M A.S.L.

SCALE : 5.204E-04

COYNE ET BELLIER | COQEF3

APPENDIX 1-5

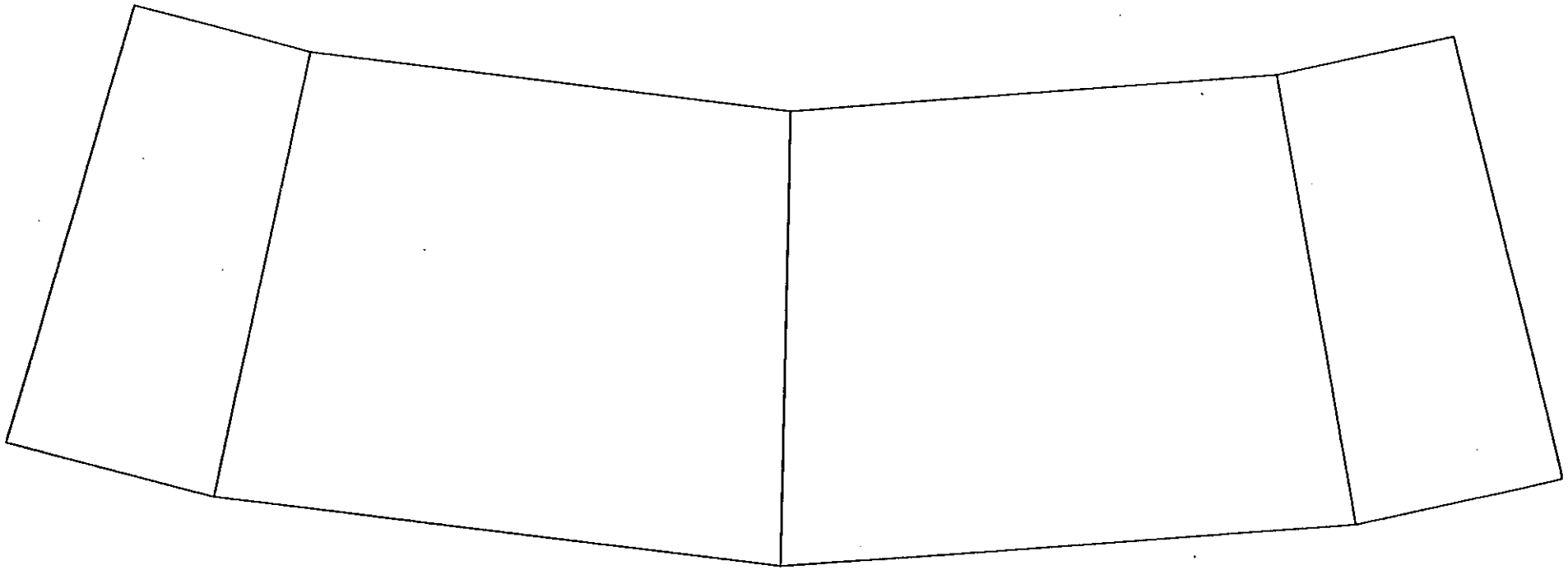

0 2

TALVACCHIA DAM

ARC OF THE FOUNDATION

SCALE : 5.027E-03

APPENDIX 2

APPENDIX 2-1

Selected points for thermal and dynamic analysis

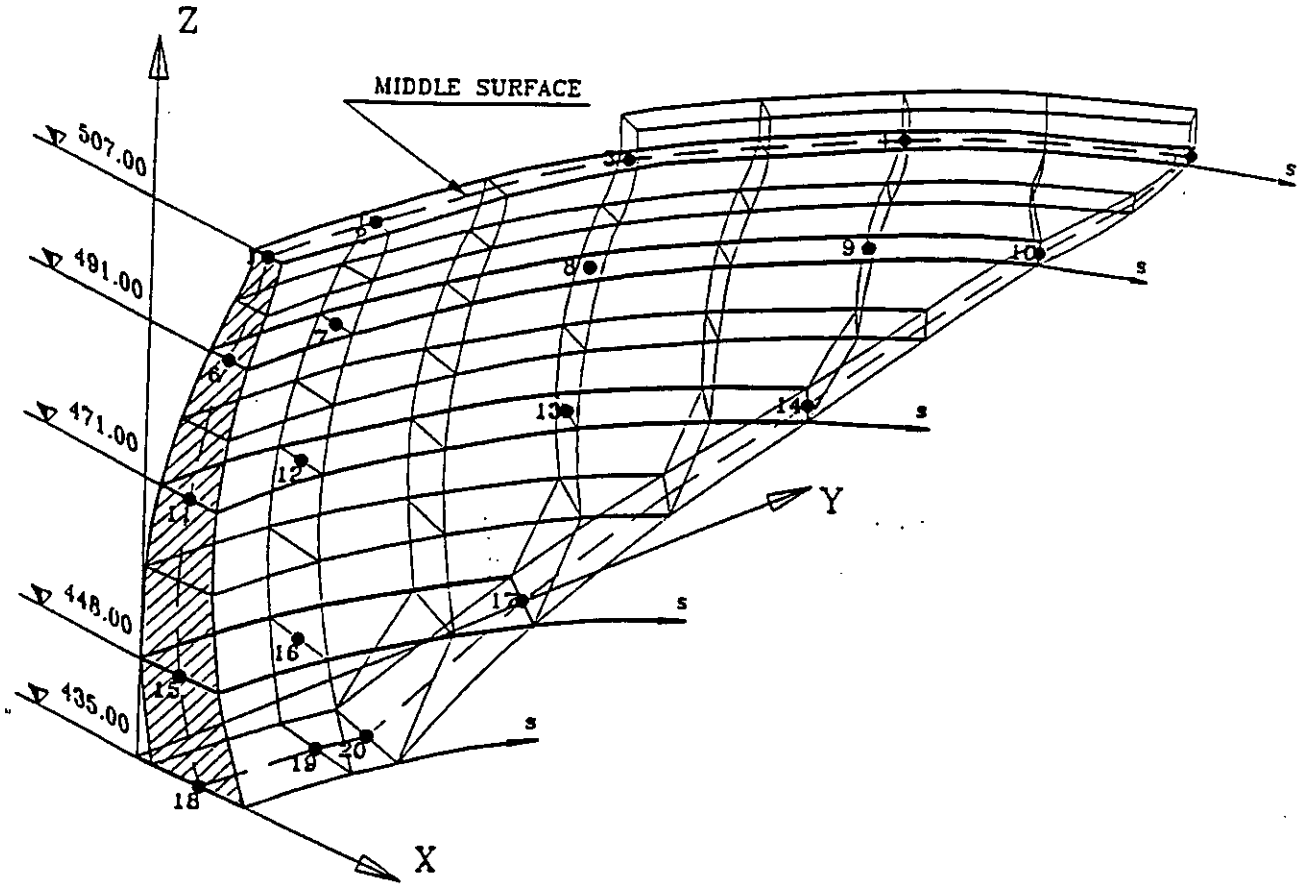

APPENDIX 2-2

Thermal analysis

Points	s (m)	Steady state analysis temperature T (°C)	Periodic analysis Amplitude(°C)	Phase (rad)
1	0,0	12,5	6,9	0,35
2	16,0	12,5	6,9	0,35
3	48,0	12,5	6,9	0,35
4	80,0	12,5	6,9	0,35
5	112,9	12,5	6,9	0,35
6	0,0	12,5	5,9	0,35
7	16,0	12,5	5,9	0,71
8	48,0	12,5	5,9	0,71
9	80,0	12,5	5,9	0,71
10	99,2	12,5	5,9	0,71
11	0,0	12,5	3,9	1,54
12	16,0	12,5	3,9	1,54
13	48,0	12,5	3,9	1,54
14	75,0	12,5	3,9	1,54
15	0,0	12,5	2,1	1,99
16	16,0	12,5	2,1	1,99
17	41,5	12,5	2,1	1,99
18	0,0	12,5	1,4	2,20
19	16,0	12,5	1,4	2,20
20	22,0	12,5	1,4	2,20

APPENDIX 2-3

Selected points for static analysis

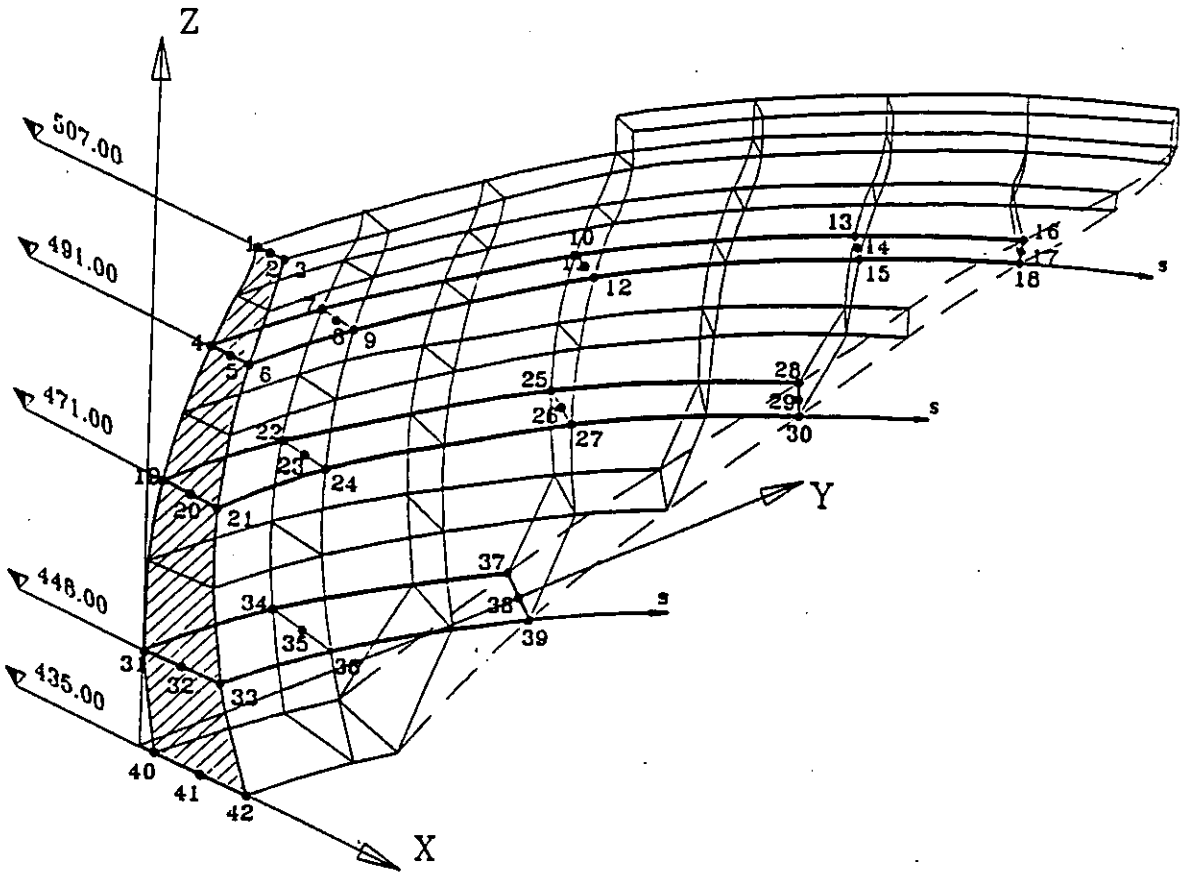

P1 > P2 > P3

APPENDIX 2-4

LOADING : Dead weight

Points	s (m)	Displ. x (m)	Displ. y (m)	Displ. z (m)	P1 (MPa)	P2 (Mpa)	P3 (Mpa)
1	0,0	0,000	0,000	-0,004	-0,09	-1,22	0/-0,09
2	0,0	0,000	0,000	-0,004	0,00	-1,33	
3	0,0	0,000	0,000	-0,005	0,03	-1,44	-1,44
4	0,0	-0,001	0,000	-0,004	-0,10	-0,35	0/-0,10
5	0,0	-0,001	0,000	-0,004	-0,28	-0,45	
6	0,0	-0,001	0,000	-0,004	-0,51	-0,51	-0,56
7	16,0	-0,001	0,000	-0,004	0,00	-0,33	
8	16,0	-0,001	0,000	-0,004	-0,23	-0,45	
9	16,0	-0,001	0,000	-0,004	-0,47	-0,61	
10	48,0	0,000	0,000	-0,003	0,42	-0,15	
11	48,0	0,000	0,000	-0,003	0,07	-0,47	
12	48,0	0,000	0,000	-0,003	-0,12	-0,97	
13	80,0	0,000	0,000	-0,001	0,45	0,17	
14	80,0	0,000	0,000	-0,001	0,37	-0,50	
15	80,0	0,000	0,000	-0,002	0,44	-1,33	
16	99,2	0,000	0,000	0,000	0,63	0,17	
17	99,2	0,000	0,000	0,000	0,53	-0,48	
18	99,2	0,000	0,000	0,000	0,49	-1,19	
19	0,0	-0,002	0,000	-0,004	0,34	0,10	0
20	0,0	-0,002	0,000	-0,004	0,14	-0,47	
21	0,0	-0,002	0,000	-0,004	-0,06	-1,06	-1,06
22	16,0	-0,002	0,000	-0,004	0,40	0,08	
23	16,0	-0,002	0,000	-0,004	0,18	-0,51	
24	16,0	-0,002	0,000	-0,004	-0,04	-1,11	
25	48,0	0,000	0,000	-0,003	0,49	-0,09	
26	48,0	0,000	0,000	-0,003	0,35	-0,67	
27	48,0	0,000	0,000	-0,003	0,21	-1,26	
28	75,0	0,000	0,000	-0,001	0,32	-0,80	
29	75,0	0,000	0,000	-0,001	0,43	-0,77	
30	75,0	0,000	0,000	-0,001	0,57	-0,66	
31	0,0	0,000	0,000	-0,004	0,41	0 -0,38	-0,38
32	0,0	0,000	0,000	-0,003	0,20	-0,68	
33	0,0	0,000	0,000	-0,003	0,00	-0,96	-0,96
34	16,0	0,000	0,000	-0,004	0,39	-0,53	
35	16,0	0,000	0,000	-0,003	0,18	-0,70	
36	16,0	0,000	0,000	-0,003	-0,03	-0,85	
37	41,5	0,000	0,000	-0,003	0,19	-1,27	
38	41,5	0,000	0,000	-0,002	0,26	-0,88	
39	41,5	0,000	0,000	-0,002	0,38	-0,44	
40	0,0	0,000	0,000	-0,003	0,09	0 -1,46	-1,46
41	0,0	0,000	0,000	-0,003	0,11	-0,85	
42	0,0	0,000	0,000	-0,002	0,13	-0,11	-0,11

APPENDIX 2-5

LOADING : Hydrostatic pressure

Points	s (m)	Displ. x (m)	Displ. y (m)	Displ. z (m)	P1 (MPa)	P2 (Mpa)	P3 (Mpa
1	0,0	0,026	0,000	0,000	0,08	-2,85	
2	0,0	0,026	0,000	0,000	0,03	-1,53	
3	0,0	0,026	0,000	0,000	-0,03	-0,21	
4	0,0	0,024	0,000	0,000	-1,37	-4,50	
5	0,0	0,024	0,000	0,000	-0,19	-2,99	
6	0,0	0,024	0,000	0,000	0,94	-1,69	
7	16,0	0,021	-0,018	0,000	-1,31	-4,41	
8	16,0	0,022	0,012	0,000	-0,17	-3,03	
9	16,0	0,023	0,000	0,000	0,94	-1,69	
10	48,0	0,011	0,002	0,000	-1,25	-3,19	
11	48,0	0,012	0,000	0,000	-0,11	-2,90	
12	48,0	0,012	0,000	0,000	1,19	-2,84	
13	80,0	0,003	0,001	0,000	-1,04	-1,18	
14	80,0	0,003	0,002	0,000	0,18	-2,10	
15	80,0	0,003	0,002	0,000	1,54	-3,15	
16	99,2	0,001	0,002	0,000	-0,56	-1,84	
17	99,2	0,001	0,001	0,000	0,01	-1,94	
18	99,2	0,001	0,001	0,000	0,75	-2,19	
19	0,0	0,018	0,000	0,003	-1,60	-4,53	
20	0,0	0,018	0,000	0,000	-0,44	-3,02	
21	0,0	0,018	0,000	0,000	0,76	1,51	
22	16,0	0,017	0,002	0,003	-1,49	-4,37	
23	16,0	0,017	-0,001	0,001	-0,39	-2,95	
24	16,0	0,017	0,000	0,000	0,79	-1,57	
25	48,0	0,008	-0,002	0,002	-0,60	-2,20	
26	48,0	0,009	0,000	0,000	0,08	-2,39	
27	48,0	0,009	0,000	0,000	0,95	2,76	
28	75,0	0,002	0,001	0,000	0,75	-0,56	
29	75,0	0,003	0,002	0,000	0,22	-1,85	
30	75,0	0,003	0,002	0,000	-0,22	-3,51	
31	0,0	0,009	0,000	0,004	0,04	-2,19	
32	0,0	0,009	0,000	0,002	-0,28	-1,16	
33	0,0	0,009	0,000	0,000	-0,14	-0,77	
34	16,0	0,008	0,000	0,004	0,29	-2,11	
35	16,0	0,008	0,000	0,002	-0,17	-1,09	
36	16,0	0,008	0,000	0,000	0,53	-1,40	
37	41,5	0,003	0,000	0,001	2,31	0,20	
38	41,5	0,003	0,000	0,000	0,68	-0,93	
39	41,5	0,004	0,002	-0,001	0,51	-4,03	
40	0,0	0,003	0,000	0,003	2,80	0,17	
41	0,0	0,003	0,000	0,000	0,41	-0,01	
42	0,0	0,003	0,000	-0,002	0,66	-3,63	

APPENDIX 2-6

LOADING : Thermal loading

Points	s (m)	Displ. x (m)	Displ. y (m)	Displ. z (m)	P1 (MPa)	P2 (Mpa)	P3 (Mpa
1	0,0	-0,017	0,000	0,008	2,26	-0,02	
2	0,0	-0,017	0,000	0,009	1,22	0,00	
3	0,0	-0,017	0,000	0,010	0,19	0,02	
4	0,0	-0,013	0,000	0,005	1,44	0,67	
5	0,0	-0,013	0,000	0,006	0,10	-0,03	
6	0,0	-0,013	0,000	0,007	-0,65	-1,24	
7	16,0	-0,012	0,002	0,005	1,28	0,56	
8	16,0	-0,012	0,001	0,006	0,08	-0,03	
9	16,0	-0,012	0,001	0,007	-1,26	-0,62	
10	48,0	-0,006	0,003	0,003	0,37	-0,62	
11	48,0	-0,007	0,003	0,004	0,15	-1,19	
12	48,0	-0,007	0,002	0,005	-0,06	-1,81	
13	80,0	-0,001	0,001	0,000	-0,92	-2,37	
14	80,0	-0,001	0,001	0,002	0,17	-2,79	
15	80,0	-0,002	0,001	0,002	1,18	-3,25	
16	99,2	0,000	0,000	0,000	-2,06	-4,31	
17	99,2	0,000	0,000	0,000	0,16	-3,64	
18	99,2	0,000	0,000	0,000	2,88	-3,52	
19	0,0	-0,008	0,000	0,002	0,58	0,49	
20	0,0	-0,008	0,000	0,003	-0,20	-0,97	
21	0,0	-0,008	0,001	0,004	-0,94	-2,51	
22	16,0	-0,007	0,001	0,002	0,46	,19	
23	16,0	-0,007	0,001	0,003	-0,20	-0,97	
24	16,0	-0,007	0,001	0,004	-0,76	-2,59	
25	48,0	-0,002	0,002	0,00	-0,90	-2,08	
26	48,0	-0,003	0,000	0,002	-0,18	-1,14	
27	48,0	-0,003	0,000	0,002	1,07	-2,84	
28	75,0	0,000	0,000	0,000	-1,70	-3,56	
29	75,0	0,000	0,000	0,000	0,10	-2,45	
30	75,0	0,000	0,000	0,000	2,56	-3,37	
31	0,0	-0,003	0,000	0,000	-1,44	-1,66	
32	0,0	-0,003	0,000	0,000	0,23	-3,26	
33	0,0	-0,003	0,000	0,002	0,76	-3,50	
34	16,0	-0,002	0,001	0,000	-1,43	-1,87	
35	16,0	-0,002	0,000	0,000	-0,73	-2,57	
36	16,0	-0,002	0,000	0,002	0,35	-3,62	
37	41,5	0,000	0,000	0,000	-2,65	-4,34	
38	41,5	0,000	0,000	0,000	-0,15	-3,13	
39	41,5	0,000	0,000	0,000	3,20	-3,06	
40	0,0	0,000	0,000	0,000	-3,26	-3,84	
41	0,0	0,000	0,000	0,000	-0,48	-3,15	
42	0,0	0,000	0,000	0,000	-3,04	3,73	

APPENDIX 2-7

Dynamic analysis: Modal shapes

Dam on rigid foundation (without water)

Natural frequency No : 1

f= 4,34 HZ

Points	s (m)	Displ. x	Displ y	Displ. z
1	0,0	0,00	-0,06	0,00
2	16,0	-0,15	-0,07	0,04
3	48,0	-0,20	-0,10	0,05
4	80,0	-0,04	-0,02	0,01
5	112,9	0,00	0,00	0,00
6	0,0	0,00	-0,04	0,00
7	16,0	-0,09	-0,05	0,01
8	48,0	-0,11	-0,05	0,01
9	80,0	-0,01	0,00	0,00
10	99,2	0,00	0,00	0,00
11	0,0	0,00	-0,02	0,00
12	16,0	-0,03	-0,02	0,00
13	48,0	-0,03	-0,02	0,00
14	75,0	0,00	0,00	0,00
15	0,0	0,00	0,00	0,00
16	16,0	0,00	0,00	0,00
17	41,5	0,00	0,00	0,00
18	0,0	0,00	0,00	0,00
19	16,0	0,00	0,00	0,00
20	22,0	0,000	0,00	0,00

APPENDIX 2-8

Dynamic analysis: Modal shapes

Dam on rigid foundation (without water)

Natural frequency No : 2

f= 4,62 HZ

Points	s (m)	Displ. x	Displ y	Displ. z
1	0,0	0,33	0,00	-0,08
2	16,0	0,26	0,01	-0,06
3	48,0	-0,04	-0,05	0,02
4	80,0	-0,05	-0,04	0,01
5	112,9	0,00	0,00	0,00
6	0,0	0,19	0,00	-0,03
7	16,0	0,16	0,01	-0,02
8	48,0	0,00	-0,02	0,00
9	80,0	-0,01	-0,02	0,00
10	99,2	0,00	0,00	0,00
11	0,0	0,07	0,00	0,00
12	16,0	0,06	0,00	0,00
13	48,0	0,00	0,00	0,00
14	75,0	0,00	0,00	0,00
15	0,0	0,01	0,00	0,00
16	16,0	0,01	0,00	0,00
17	41,5	0,00	0,00	0,00
18	0,0	0,00	0,00	0,00
19	16,0	0,00	0,00	0,00
20	22,0	0,00	0,00	0,00

APPENDIX 2-9

Dynamic analysis: Modal shapes

Dam on rigid foundation (without water)

Natural frequency No : 3

f= 5,75 HZ

Points	s (m)	Displ. x	Displ y	Displ. z
1	0,0	-0,03	0,00	0,00
2	16,0	-0,08	-0,03	0,02
3	48,0	-0,25	-0,12	0,07
4	80,0	-0,09	-0,05	0,02
5	112,9	0,00	0,00	0,00
6	0,0	-0,01	0,00	0,00
7	16,0	-0,04	-0,01	0,01
8	48,0	-0,11	-0,05	0,02
9	80,0	-0,03	-0,02	0,00
10	99,2	0,00	0,00	0,00
11	0,0	0,00	0,00	0,00
12	16,0	-0,01	0,00	0,00
13	48,0	-0,02	-0,01	0,00
14	75,0	0,00	0,00	0,00
15	0,0	0,00	0,00	0,00
16	16,0	0,00	0,00	0,00
17	41,5	0,00	0,00	0,00
18	0,0	0,00	0,00	0,00
19	16,0	0,00	0,00	0,00
20	22,0	0,00	0,00	0,00

APPENDIX 2-10

Dynamic analysis: Modal shapes

Dam on rigid foundation (without water)

Natural frequency No : 4

f= 6,73 HZ

Points	s (m)	Displ. x	Displ y	Displ. z
1	0,0	0,00	0,02	0,00
2	16,0	0,18	0,03	-0,05
3	48,0	-0,11	-0,09	0,04
4	80,0	-0,15	-0,12	0,04
5	112,9	0,00	0,00	0,00
6	0,0	0,00	0,01	0,00
7	16,0	0,10	0,02	-0,02
8	48,0	-0,01	-0,02	0,05
9	80,0	-0,04	-0,04	0,00
10	99,2	0,00	0,00	0,00
11	0,0	0,00	0,00	0,00
12	16,0	0,00	0,00	0,00
13	48,0	0,03	0,00	0,00
14	75,0	0,00	0,00	0,00
15	0,0	0,00	0,00	0,00
16	16,0	0,00	0,00	0,00
17	41,5	0,00	0,00	0,00
18	0,0	0,00	0,00	0,00
19	16,0	0,00	0,00	0,00
20	22,0	0,00	0,00	0,00

APPENDIX 2-11

Dynamic analysis: Modal shapes

Dam on rigid foundation (without water)

Natural frequency No : 5

f= 8,56 HZ

Points	s (m)	Displ. x	Displ y	Displ. z
1	0,0	-0,25	0,00	0,10
2	16,0	-0,08	0,01	0,04
3	48,0	0,08	0,01	-0,01
4	80,0	-0,19	-0,16	0,06
5	112,9	0,00	0,00	0,00
6	0,0	-0,11	0,00	0,04
7	16,0	-0,02	0,01	0,02
8	48,0	-0,09	0,03	-0,01
9	80,0	-0,04	-0,04	0,00
10	99,2	0,00	0,00	0,00
11	0,0	-0,01	0,00	0,01
12	16,0	0,01	0,00	0,01
13	48,0	0,03	0,01	0,00
14	75,0	0,00	0,00	0,00
15	0,0	0,00	0,00	0,00
16	16,0	0,00	0,00	0,00
17	41,5	0,00	0,00	0,00
18	0,0	0,00	0,00	0,00
19	16,0	0,00	0,00	0,00
20	22,0	0,00	0,00	0,00

APPENDIX 2-12

Dynamic analysis: Modal shapes

Dam on rigid foundation (without water)

Natural frequency No : 6

f= 9,53 HZ

Points	s (m)	Displ. x	Displ y	Displ. z
1	0,0	0,25	0,00	-0,15
2	16,0	0,23	0,04	-0,14
3	48,0	0,05	0,03	-0,04
4	80,0	-0,05	-0,03	0,01
5	112,9	0,00	0,00	0,00
6	0,0	-0,05	0,00	-0,05
7	16,0	-0,04	0,00	-0,04
8	48,0	-0,02	0,00	-0,02
9	80,0	-0,02	-0,01	0,00
10	99,2	0,00	0,00	0,00
11	0,0	-0,14	0,00	-0,01
12	16,0	-0,12	-0,01	-0,01
13	48,0	-0,03	-0,01	-0,01
14	75,0	0,00	0,00	0,00
15	0,0	-0,04	0,00	-0,01
16	16,0	-0,03	0,00	0,00
17	41,5	0,00	0,00	0,00
18	0,0	0,00	0,00	0,00
19	16,0	0,00	0,00	0,00
20	22,0	0,00	0,00	0,000

APPENDIX 2-13

Dynamic analysis: Modal shapes

Dam on flexible foundation water level 491 m a.s.l.

Natural frequency No : 1

f= 3,46 HZ

Points	s (m)	Displ. x	Displ y	Displ. z
1	0,0	0,27	0,00	-0,04
2	16,0	0,22	0,01	-0,03
3	48,0	0,01	-0,04	0,01
4	80,0	-0,05	-0,06	0,01
5	112,9	0,00	0,00	0,00
6	0,0	0,18	0,00	-0,01
7	16,0	0,15	0,00	0,00
8	48,0	0,03	-0,02	0,00
9	80,0	-0,01	-0,03	0,00
10	99,2	0,00	-0,01	0,00
11	0,0	0,09	0,00	0,01
12	16,0	0,08	0,00	0,01
13	48,0	0,02	-0,01	0,00
14	75,0	0,00	-0,01	0,00
15	0,0	0,03	0,00	0,01
16	16,0	0,02	0,00	0,01
17	41,5	0,01	-0,01	0,00
18	0,0	0,01	0,00	0,01
19	16,0	0,01	0,00	0,01
20	22,0	0,00	0,00	0,00

APPENDIX 2-14

Dynamic analysis: Modal shapes

Dam on flexible foundation water level 491 m a.s.l.

Natural frequency No : 2

f= 4,74 HZ

Points	s (m)	Displ. x	Displ y	Displ. z
1	0,0	-0,02	0,00	0,02
2	16,0	0,00	0,01	0,00
3	48,0	0,13	0,07	-0,03
4	80,0	0,07	0,04	-0,01
5	112,9	0,01	-0,01	0,00
6	0,0	-0,01	0,00	0,01
7	16,0	0,01	0,01	0,00
8	48,0	0,07	0,03	-0,01
9	80,0	0,04	0,02	0,00
10	99,2	0,01	0,00	0,00
11	0,0	0,00	0,00	0,00
12	16,0	0,01	0,00	0,00
13	48,0	0,02	0,00	0,00
14	75,0	0,01	0,00	0,00
15	0,0	0,00	0,00	0,00
16	16,0	0,00	0,00	0,00
17	41,5	0,00	0,00	0,00
18	0,0	0,00	0,00	0,00
19	16,0	0,00	0,00	0,00
20	22,0	0,00	0,00	0,00

APPENDIX 2-15

Dynamic analysis: Modal shapes

Dam on flexible foundation water level 491 m a.s.l.

Natural frequency No : 3

f= 7,20 HZ

Points	s (m)	Displ. x	Displ y	Displ. z
1	0,0	-0,26	0,00	0,11
2	16,0	-0,13	0,00	0,07
3	48,0	0,07	0,00	0,01
4	80,0	-0,17	-0,02	0,05
5	112,9	-0,01	0,00	0,00
6	0,0	-0,11	0,00	0,06
7	16,0	-0,04	0,00	0,04
8	48,0	0,08	0,03	0,00
9	80,0	-0,04	-0,05	0,01
10	99,2	-0,01	-0,01	0,00
11	0,0	-0,01	0,00	0,02
12	16,0	0,01	0,00	0,02
13	48,0	0,04	0,02	0,01
14	75,0	0,01	0,00	0,00
15	0,0	0,01	0,00	0,02
16	16,0	0,01	0,00	0,03
17	41,5	0,08	0,03	0,01
18	0,0	0,00	0,00	0,01
19	16,0	0,00	0,00	0,01
20	22,0	0,00	0,00	0,01

APPENDIX 2-16

Dynamic analysis: Modal shapes

Dam on flexible foundation water level 491 m a.s.l.

Natural frequency No : 4

f= 7,48 HZ

Points	s (m)	Displ. x	Displ y	Displ. z
1	0,0	0,07	0,00	-0,06
2	16,0	0,14	0,03	-0,08
3	48,0	0,14	0,05	-0,06
4	80,0	-0,16	-0,12	0,03
5	112,9	-0,01	0,01	0,00
6	0,0	-0,05	0,00	-0,02
7	16,0	0,00	0,01	-0,03
8	48,0	-0,06	0,02	-0,03
9	80,0	-0,05	-0,04	-0,01
10	99,2	-0,01	-0,01	0,00
11	0,0	-0,09	0,00	-0,01
12	16,0	-0,07	0,00	-0,01
13	48,0	-0,01	0,00	-0,01
14	75,0	0,00	0,00	-0,01
15	0,0	-0,05	0,00	-0,01
16	16,0	-0,04	0,00	-0,01
17	41,5	-0,01	0,08	-0,01
18	0,0	-0,02	0,00	0,00
19	16,0	-0,02	0,00	0,00
20	22,0	-0,01	0,00	0,00

APPENDIX 2-17

Dynamic analysis: Modal shapes

Dam on flexible foundation water level 491 m a.s.l.

Natural frequency No : 5

f= 8,54 HZ

Points	s (m)	Displ. x	Displ y	Displ. z
1	0,0	0,08	0,01	-0,10
2	16,0	0,03	0,02	-0,08
3	48,0	-0,06	0,00	-0,02
4	80,0	-0,04	0,00	0,00
5	112,9	-0,01	0,01	0,00
6	0,0	-0,02	0,01	-0,01
7	16,0	-0,02	0,01	-0,06
8	48,0	-0,01	0,02	-0,04
9	80,0	-0,02	0,01	-0,01
10	99,2	-0,01	0,01	0,00
11	0,0	-0,07	0,01	-0,05
12	16,0	-0,04	0,01	-0,05
13	48,0	0,00	0,01	-0,03
14	75,0	0,00	0,01	-0,01
15	0,0	-0,04	0,01	-0,05
16	16,0	-0,02	0,01	-0,04
17	41,5	0,00	0,01	-0,03
18	0,0	-0,01	0,01	-0,04
19	16,0	0,00	0,01	-0,03
20	22,0	0,00	0,01	-0,03

APPENDIX 2-18

Dynamic analysis: Modal shapes

Dam on flexible foundation water level 491 m a.s.l.

Natural frequency No : 6

f= 8,92 HZ

Points	s (m)	Displ. x	Displ y	Displ. z
1	0,0	-0,01	0,05	0,04
2	16,0	0,01	0,04	0,04
3	48,0	0,20	-0,07	0,10
4	80,0	0,11	0,12	-0,02
5	112,9	0,01	0,00	0,00
6	0,0	0,00	0,05	0,04
7	16,0	0,05	0,04	0,03
8	48,0	-0,05	0,00	0,04
9	80,0	0,02	0,04	0,02
10	99,2	0,08	0,02	0,01
11	0,0	0,02	0,04	0,03
12	16,0	0,06	0,04	0,03
13	48,0	0,02	0,03	0,03
14	75,0	-0,01	0,01	0,02
15	0,0	0,01	0,03	0,03
16	16,0	0,03	0,03	0,03
17	41,5	0,01	0,02	0,02
18	0,0	0,00	0,02	0,02
19	16,0	0,01	0,02	0,02
20	22,0	0,00	0,02	0,02

APPENDIX 3

APPENDIX 3-1

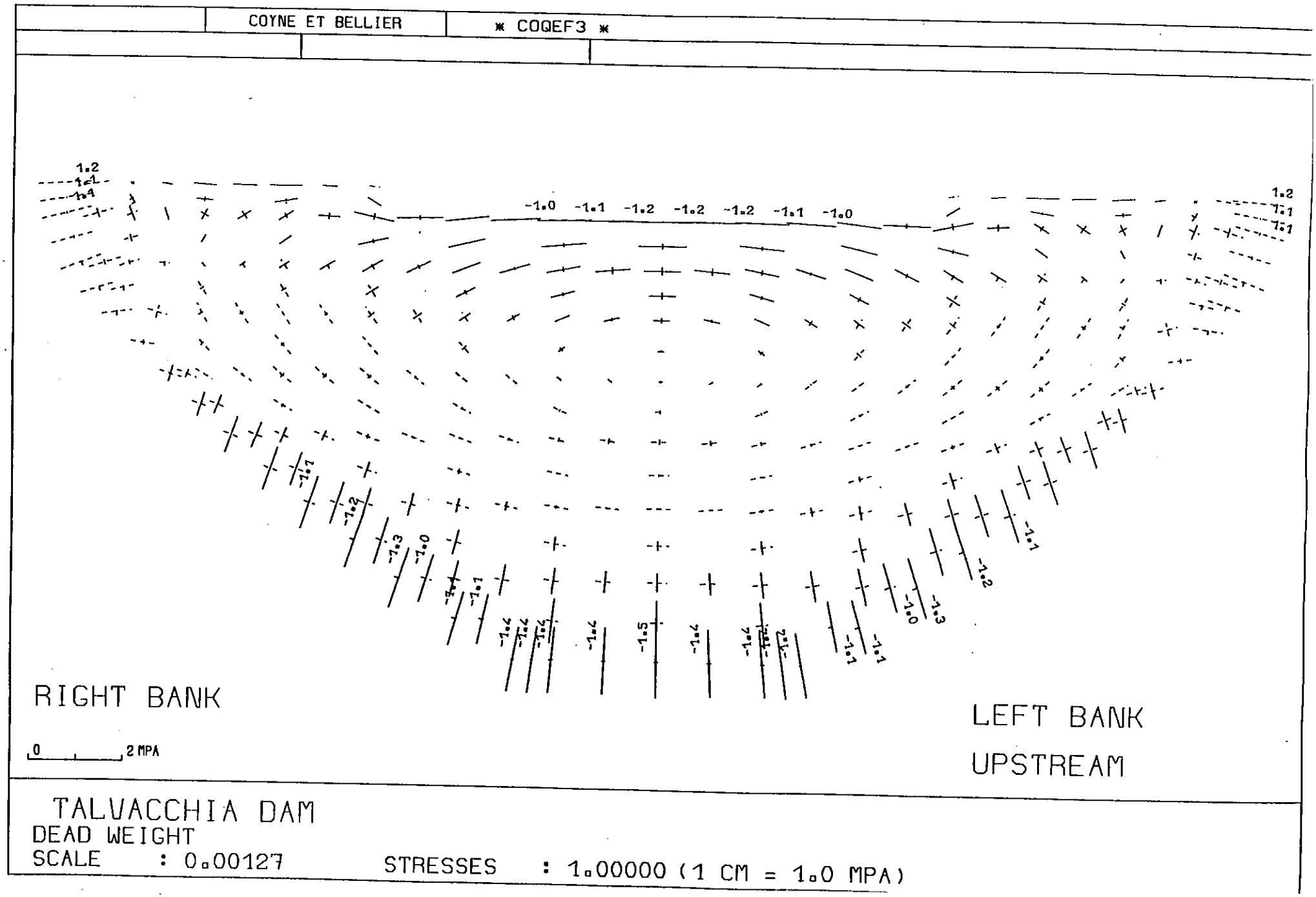
COYNE ET BELLIER
* COQEF3 *
RIGHT BANK
LEFT BANK
UPSTREAM
0
2 MPA
TALVACCHIA DAM
DEAD WEIGHT
SCALE : 0.00127
STRESSES : 1.00000 (1 CM = 1.0 MPA)

APPENDIX 3-2

COYNE ET BELLIER | * COQEF3 *

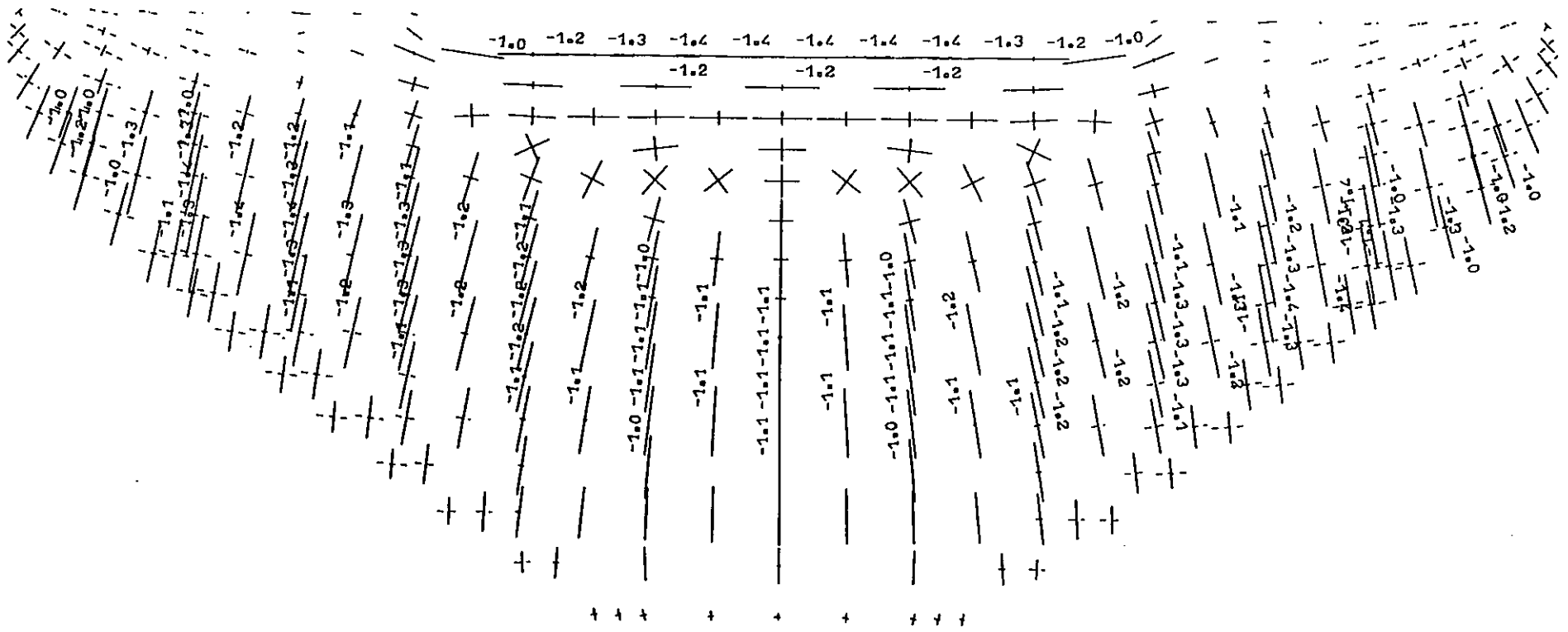

TALVACCHIA DAM
DEAD WEIGHT
SCALE : 0.00127 STRESSES : 1.00000 (1 CM = 1.0 MPA)

APPENDIX 3-3

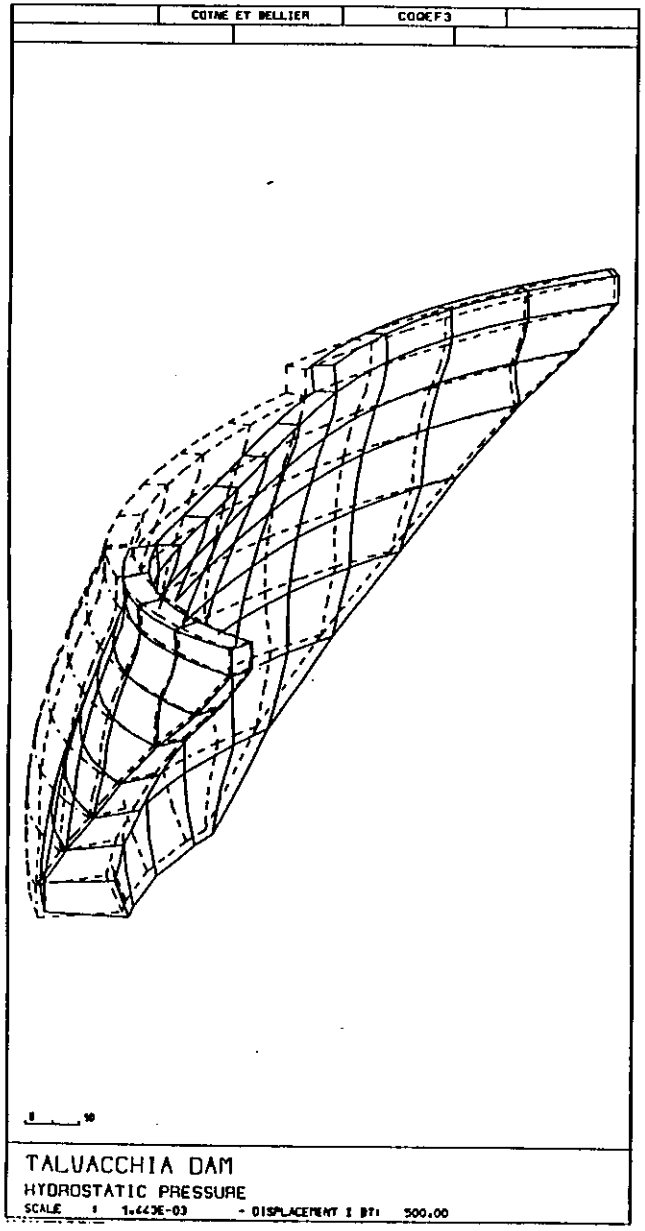
COYNE ET BELLIER
CODEF3
TALVACCHIA DAM
HYDROSTATIC PRESSURE
SCALE : 1.443E-03 - DISPLACEMENT I BT: 500.00

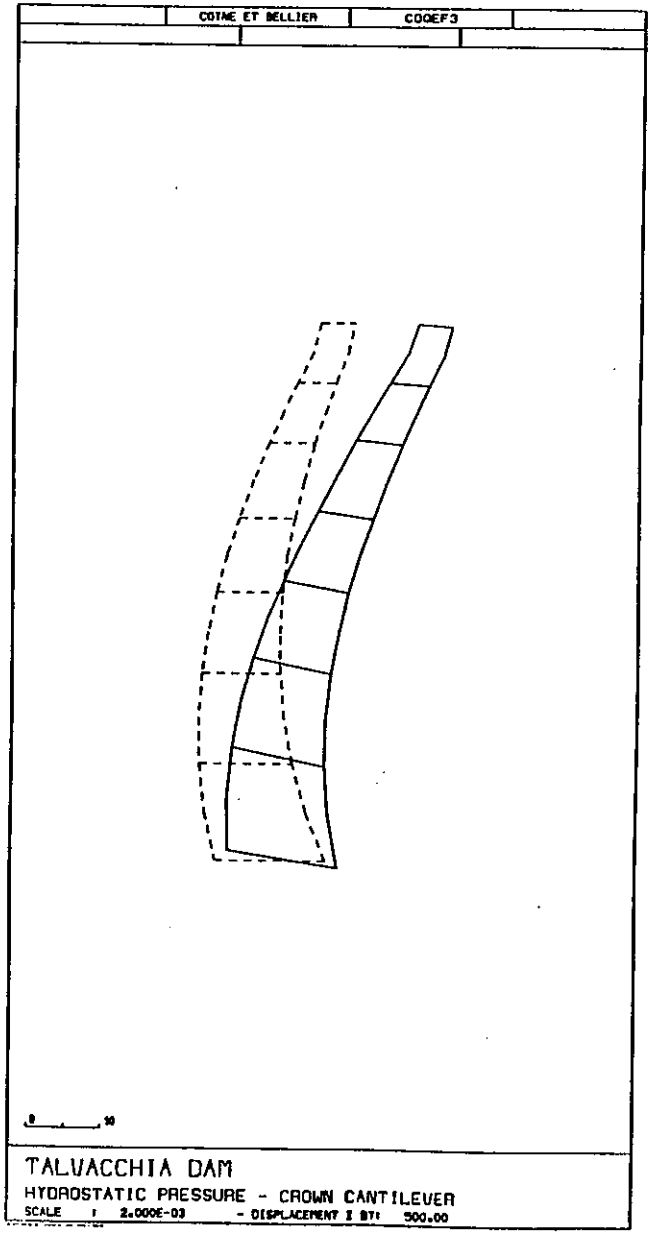
COYNE ET BELLIER
CODEF3
TALVACCHIA DAM
HYDROSTATIC PRESSURE - CROWN CANTILEVER
SCALE : 2.000E-03 - DISPLACEMENT I BT: 500.00

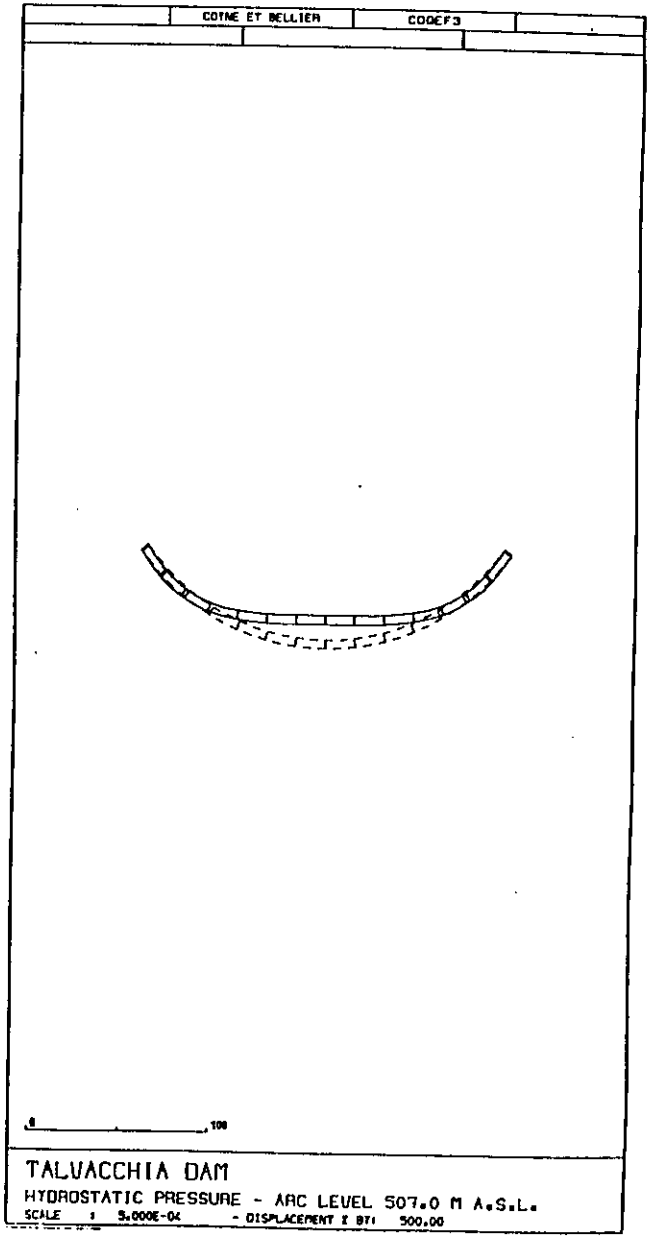
COYNE ET BELLIER
CODEF3
TALVACCHIA DAM
HYDROSTATIC PRESSURE - ARC LEVEL 507.0 M A.S.L.
SCALE : 5.000E-04 - DISPLACEMENT I BT: 500.00

APPENDIX 3-4

COYNE ET BELLIER | * COQEF3 *

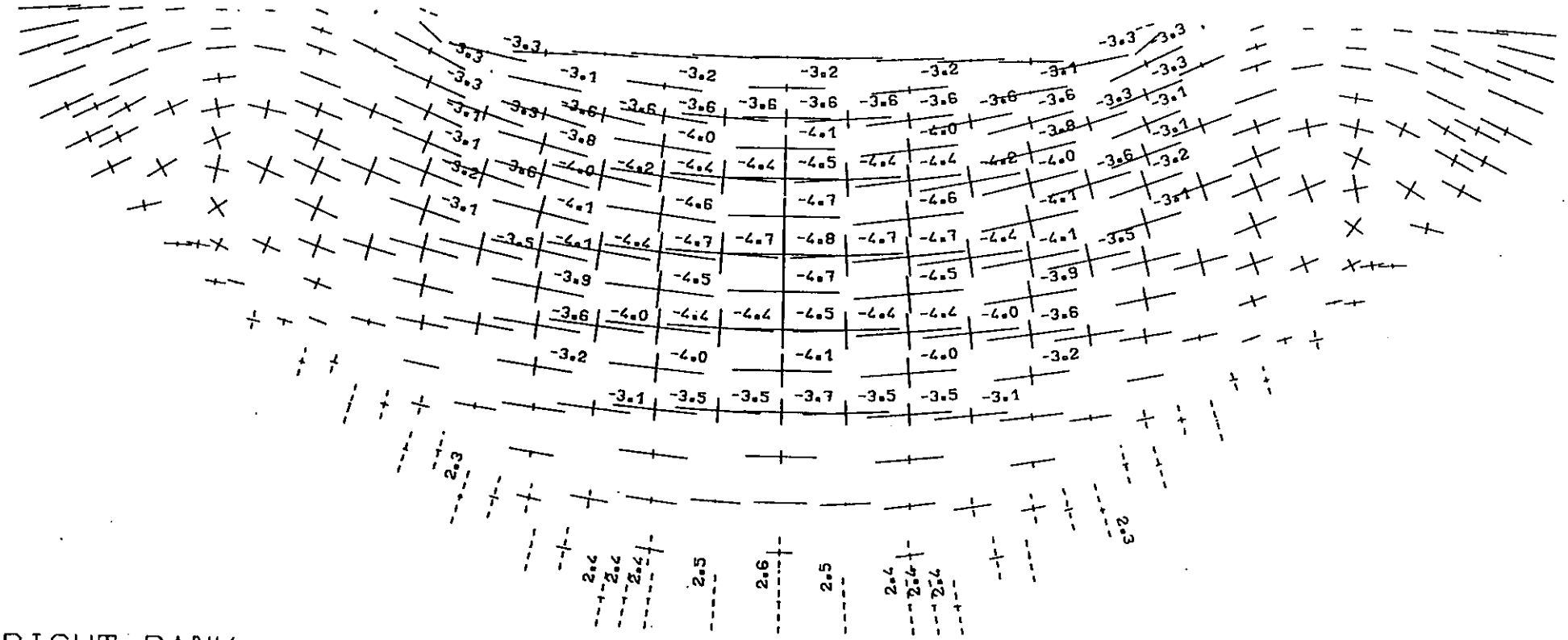

TALVACCHIA DAM
HYDROSTATIC PRESSURE
SCALE : 0.00125 STRESSES : 0.40000 (1 CM = 2.5 MPA)

APPENDIX 3-5

COYNE ET BELLIER | * COQEF3 *

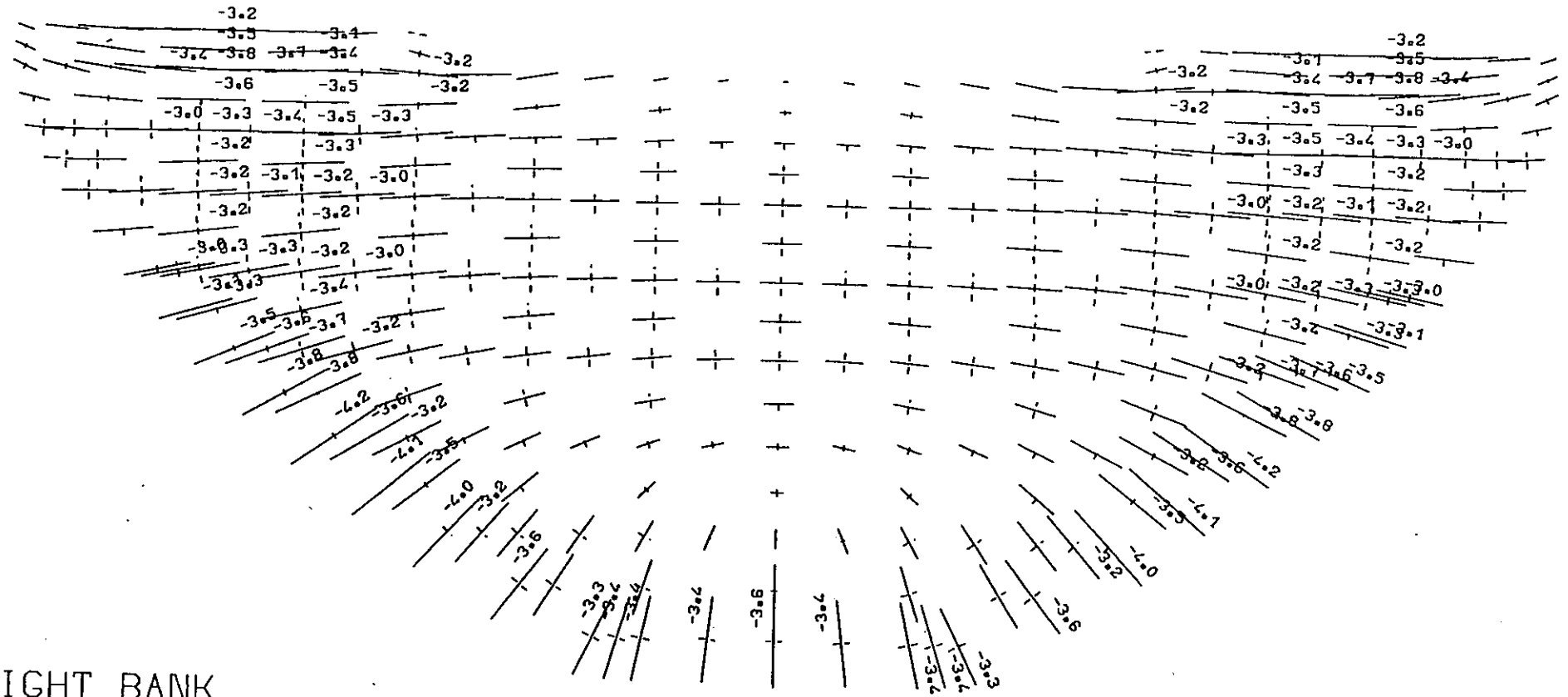

TALVACCHIA DAM
HYDROSTATIC PRESSURE
SCALE : 0.00125 STRESSES : 0.40000 (1 CM = 2.5 MPA)

APPENDIX 3-6

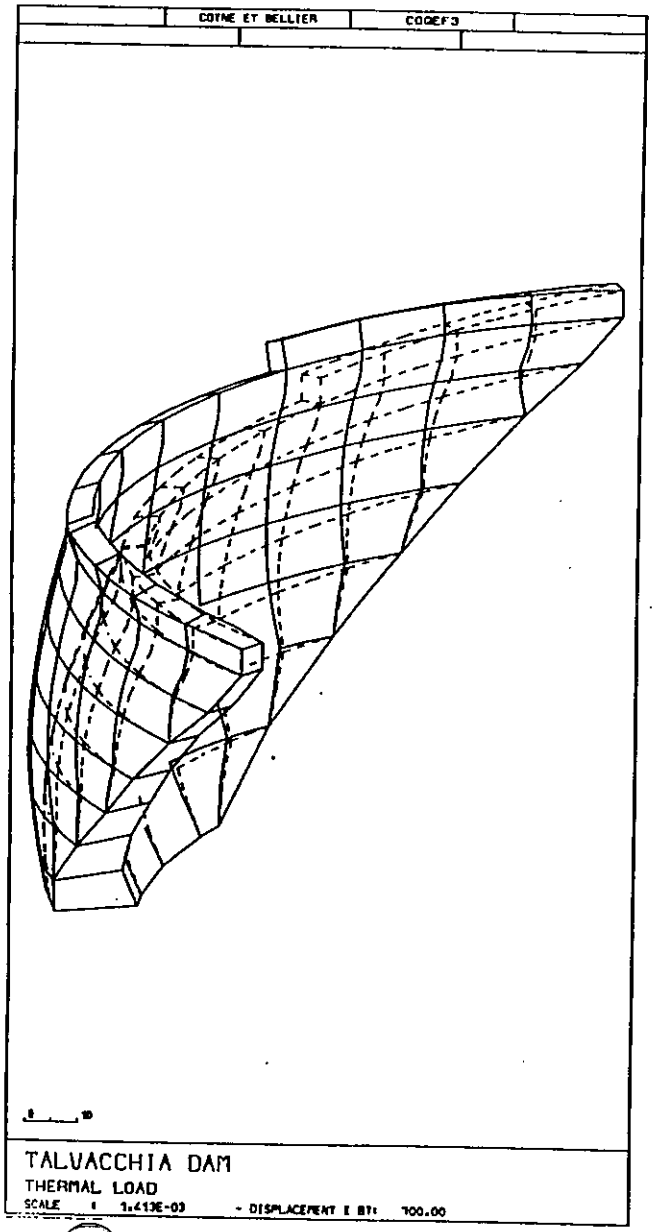
COYNE ET BELLIER
COQEF3
TALVACCHIA DAM
THERMAL LOAD
SCALE 1 1.413E-03 - DISPLACEMENT X BY: 100.00

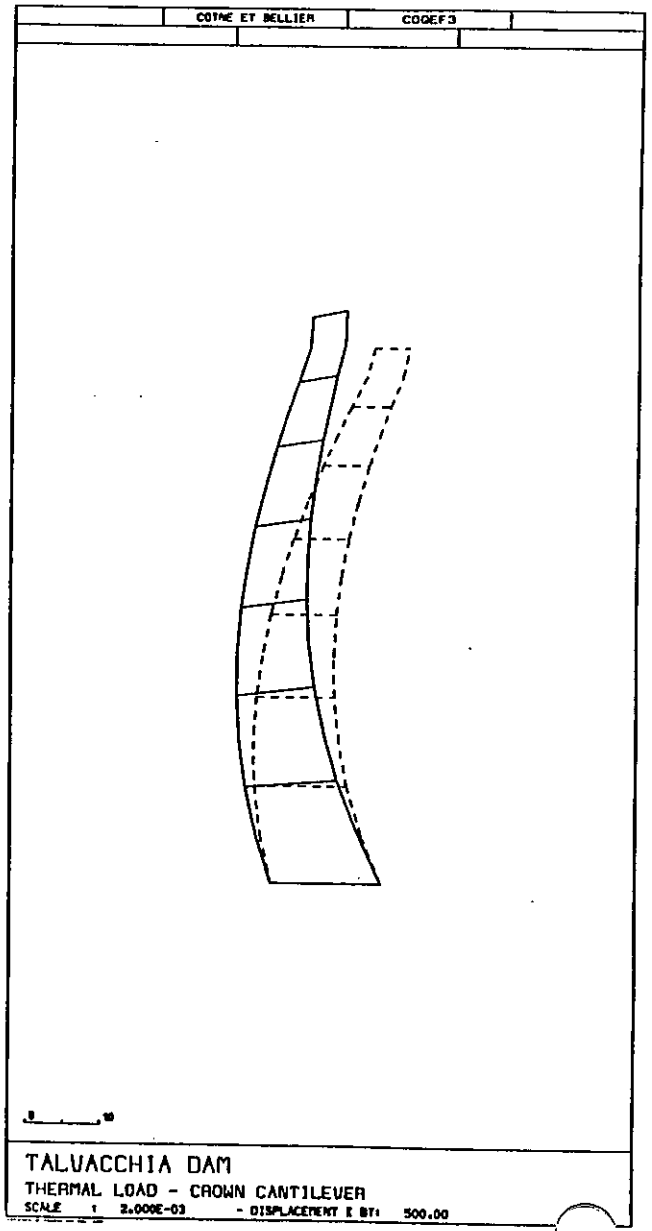
COYNE ET BELLIER
COQEF3
TALVACCHIA DAM
THERMAL LOAD - CROWN CANTILEVER
SCALE 1 2.000E-03 - DISPLACEMENT X BY: 500.00

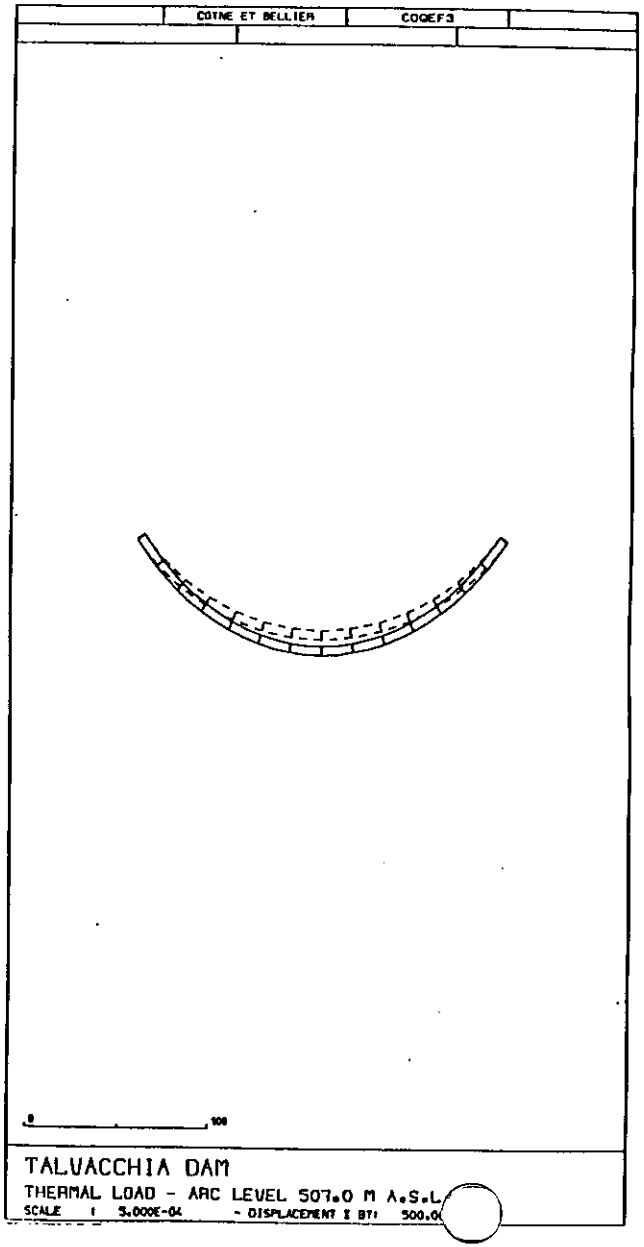
COYNE ET BELLIER
COQEF3
TALVACCHIA DAM
THERMAL LOAD - ARC LEVEL 507.0 M A.S.L.
SCALE 1 5.000E-04 - DISPLACEMENT X BY: 500.0

APPENDIX 3-7

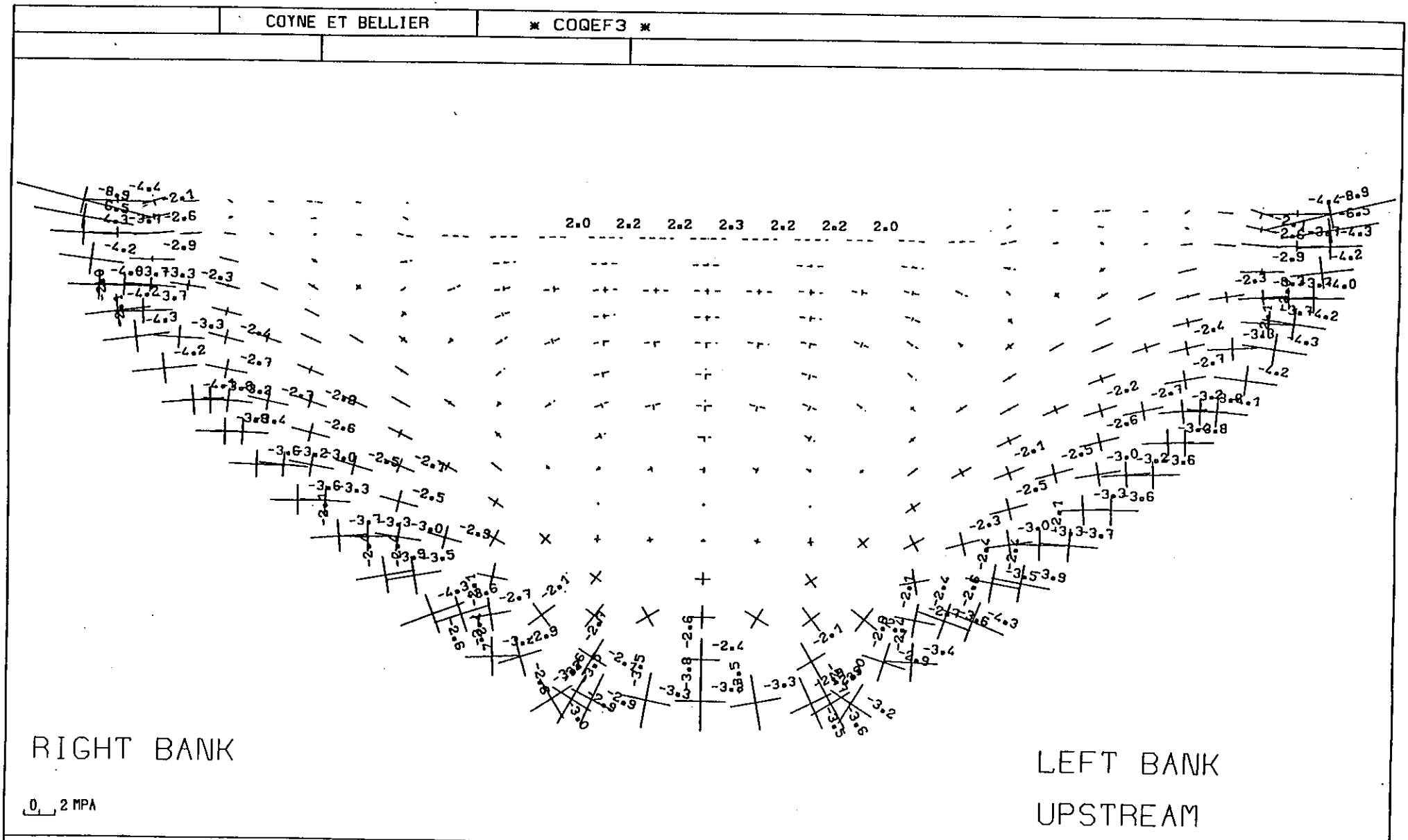
COYNE ET BELLIER
* COQEF3 *
RIGHT BANK
LEFT BANK
UPSTREAM
0 2 MPA
TALVACCHIA DAM
THERMAL LOAD
SCALE : 0.00124
STRESSES : 0.30000 (1 CM = 3.3 MPA)

APPENDIX 3-8

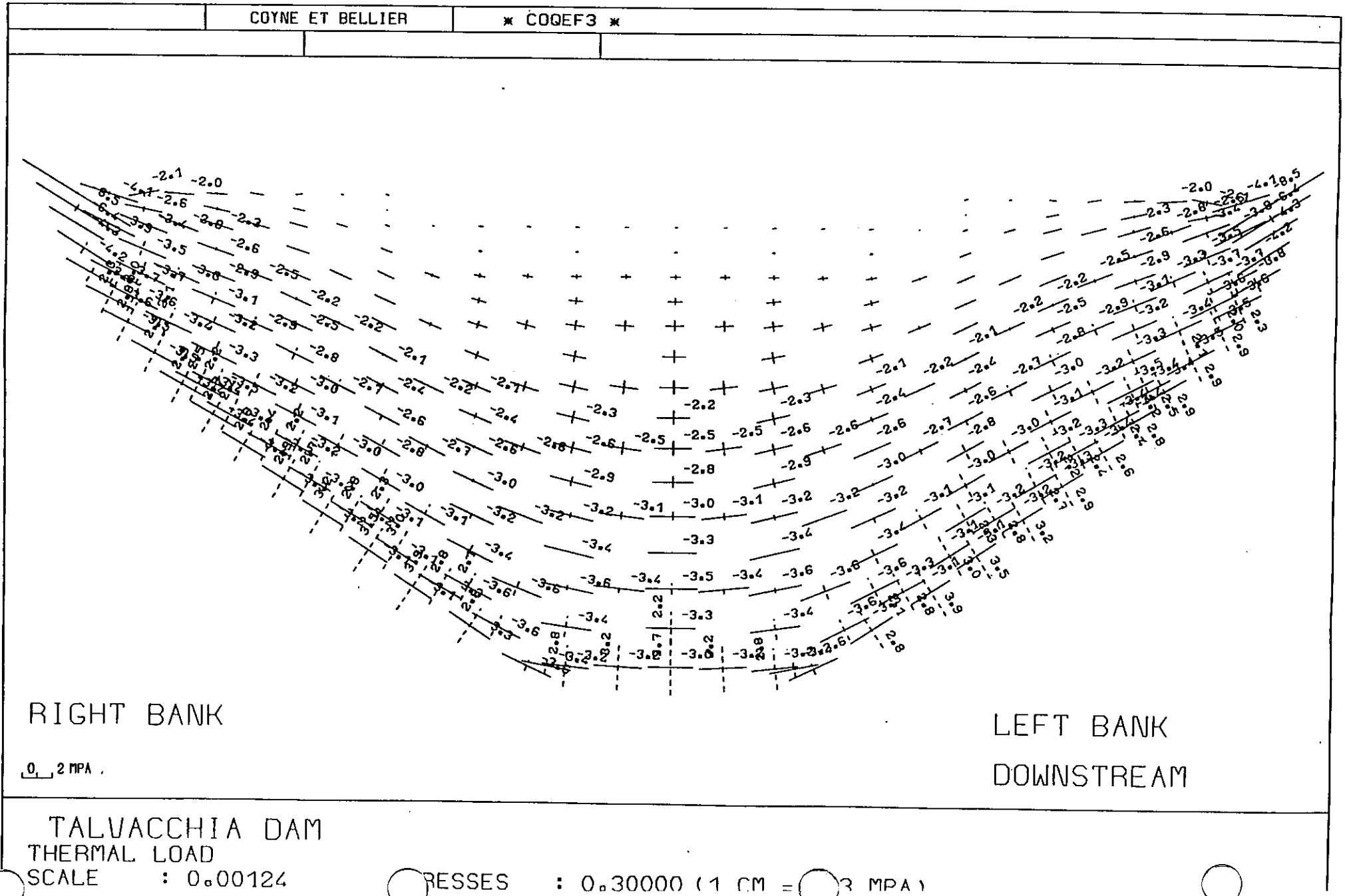
COYNE ET BELLIER
* COQEF3 *
RIGHT BANK
LEFT BANK
DOWNSTREAM
0 2 MPA .
TALVACCHIA DAM
THERMAL LOAD
SCALE : 0.00124
RESSES : 0.30000 (1 CM =
MPA)

APPENDIX 3-9

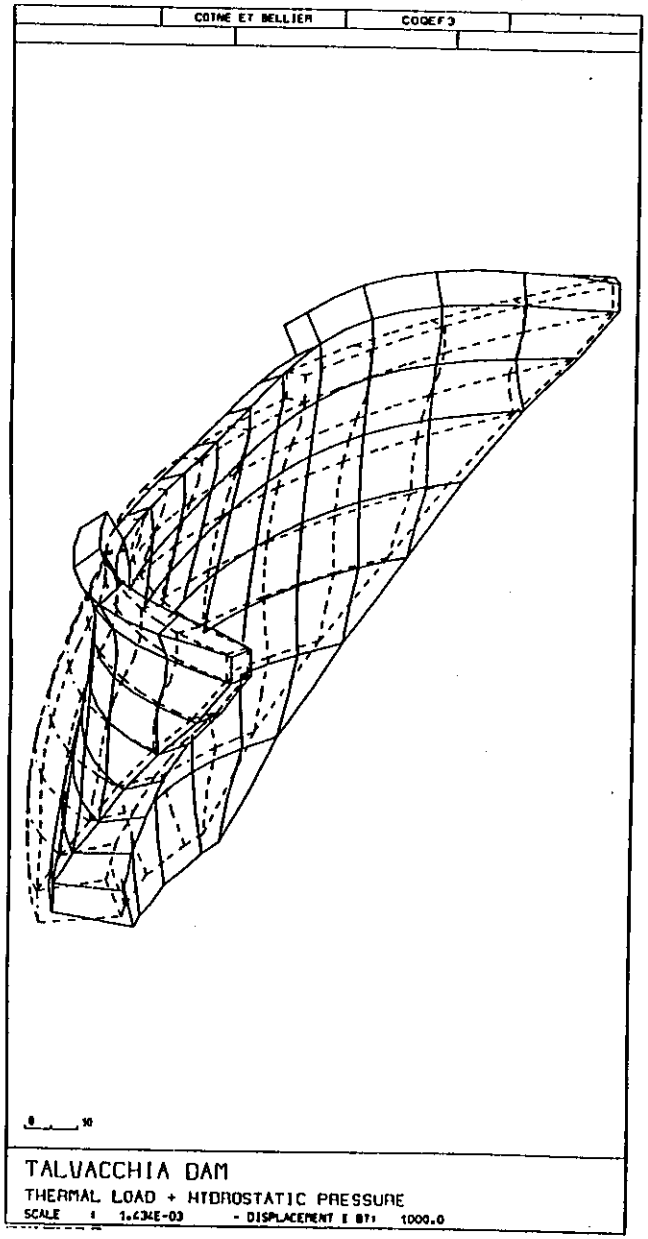
COYNE ET BELLIER
COQEF3
0
10
TALVACCHIA DAM
THERMAL LOAD + HYDROSTATIC PRESSURE
SCALE : 1.634E-03 - DISPLACEMENT X BY: 1000.0

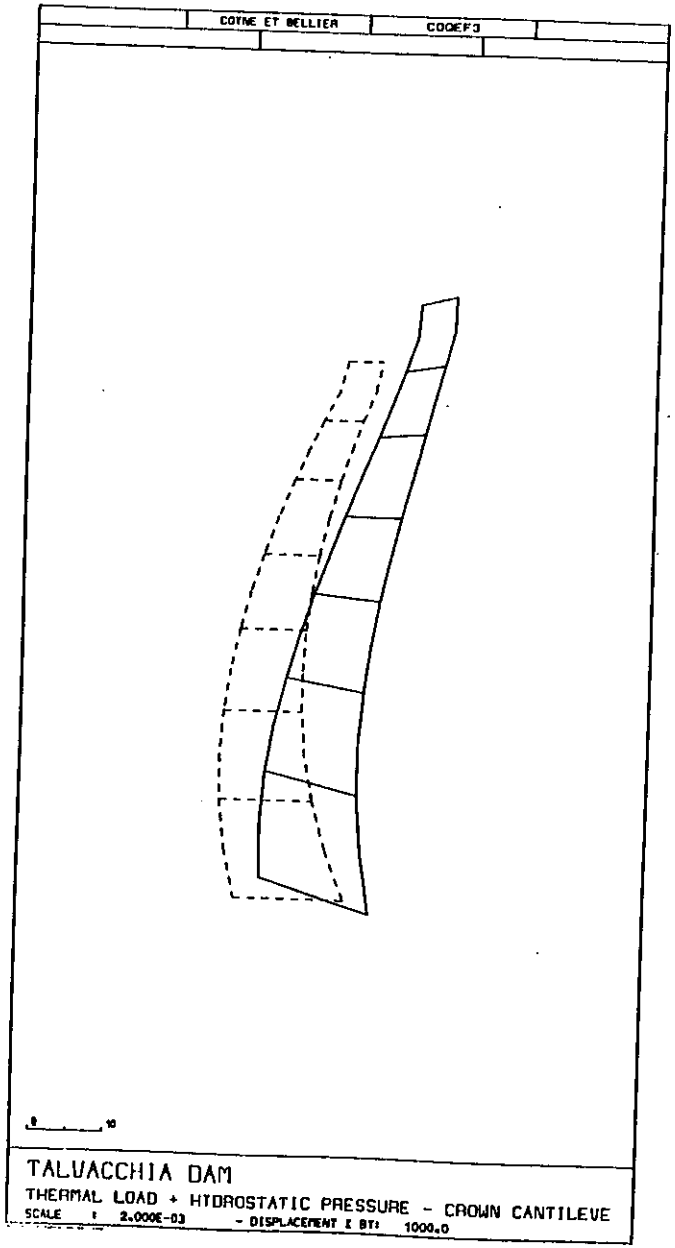
COYNE ET BELLIER
COQEF3
0
10
TALVACCHIA DAM
THERMAL LOAD + HYDROSTATIC PRESSURE - CROWN CANTILEVE
SCALE : 2.000E-03 - DISPLACEMENT X BY: 1000.0

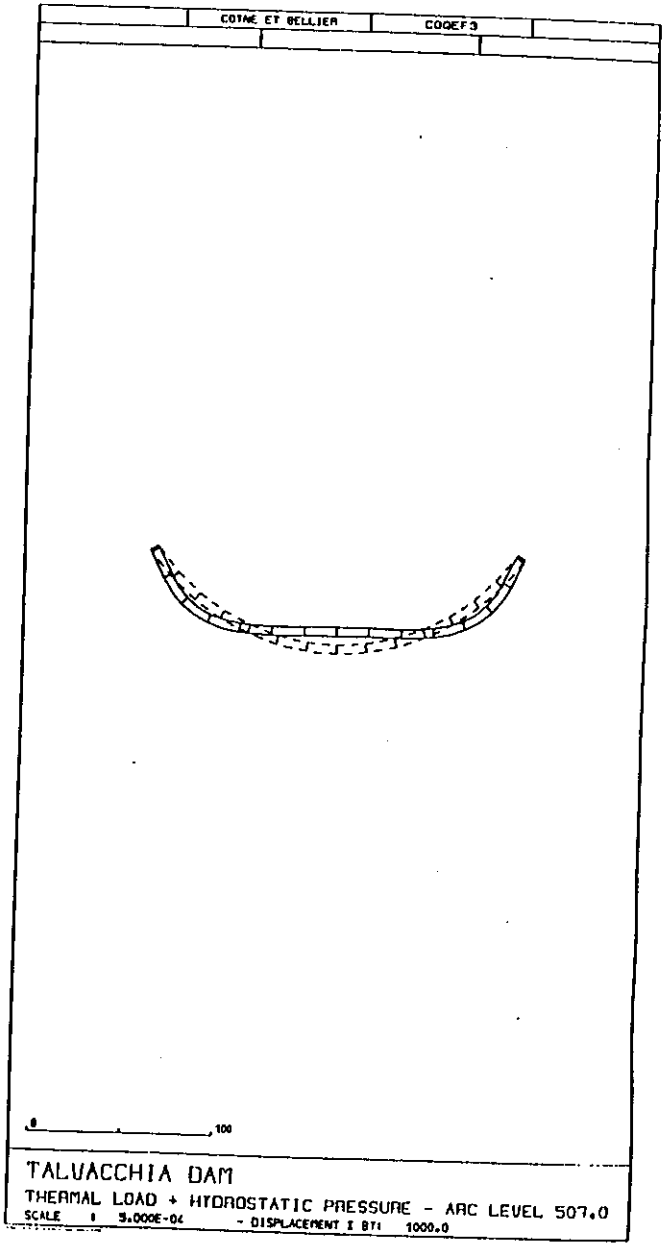
COYNE ET BELLIER
COQEF3
0
100
TALVACCHIA DAM
THERMAL LOAD + HYDROSTATIC PRESSURE - ARC LEVEL 507.0
SCALE : 5.000E-04 - DISPLACEMENT X BY: 1000.0

COYNE ET BELLIER | * COQEF3 *

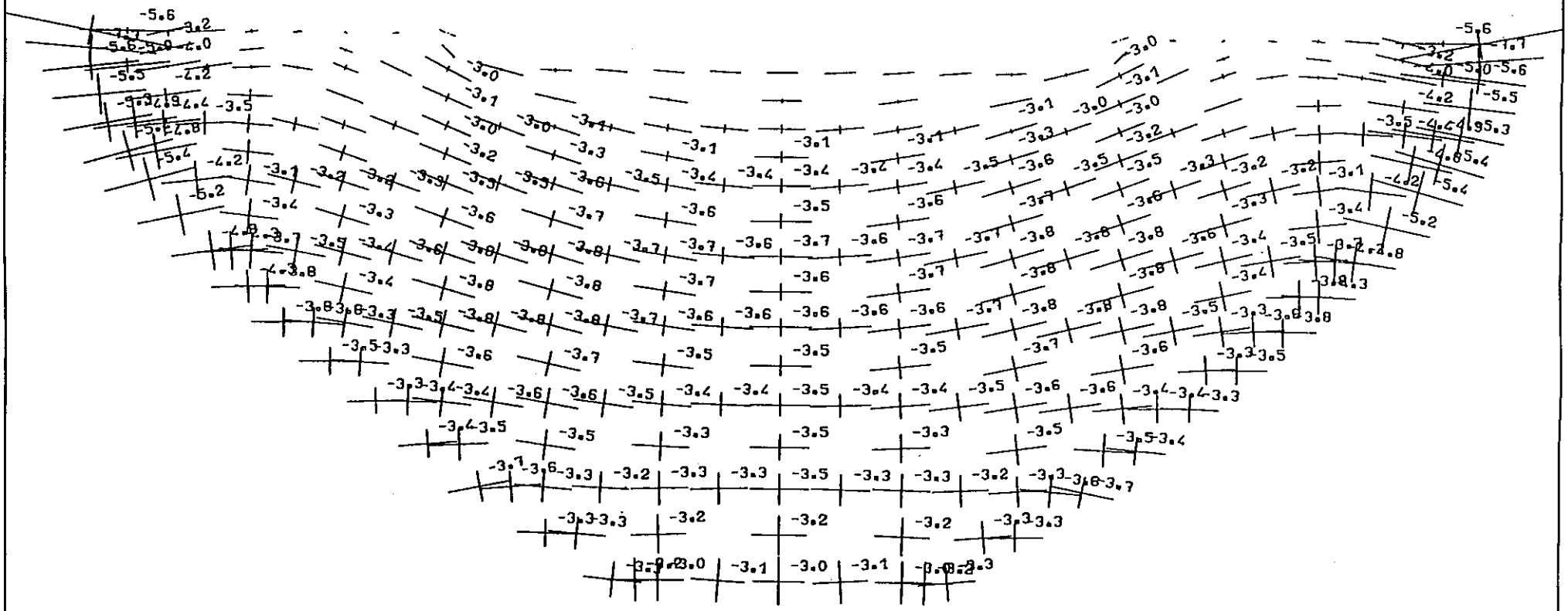

TALVACCHIA DAM
DEAD WEIGHT + THERMAL LOAD + HYDROSTATIC PRESSURE
SCALE : 0.00123 STRESSES : 0.30000 (1 CM = 3.3 MPA)

COYNE ET BELLIER | * COQEF3 *

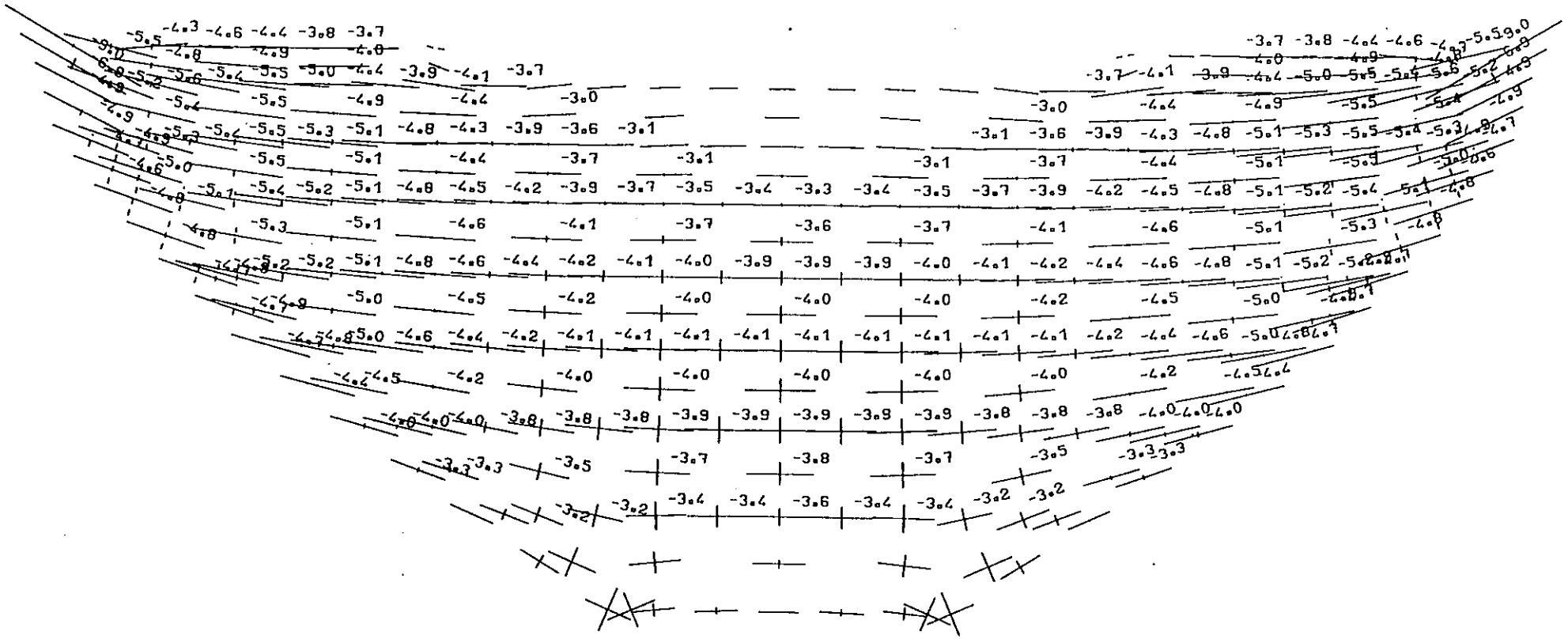

TALVACCHIA DAM
DEAD WEIGHT + THERMAL LOAD + HYDROSTATIC PRESSURE
SCALE : 0.00123 STRESSES : 0.30000 (1 CM = 3.3 MPA)

COYNE ET BELLIER | * COQEF3 *

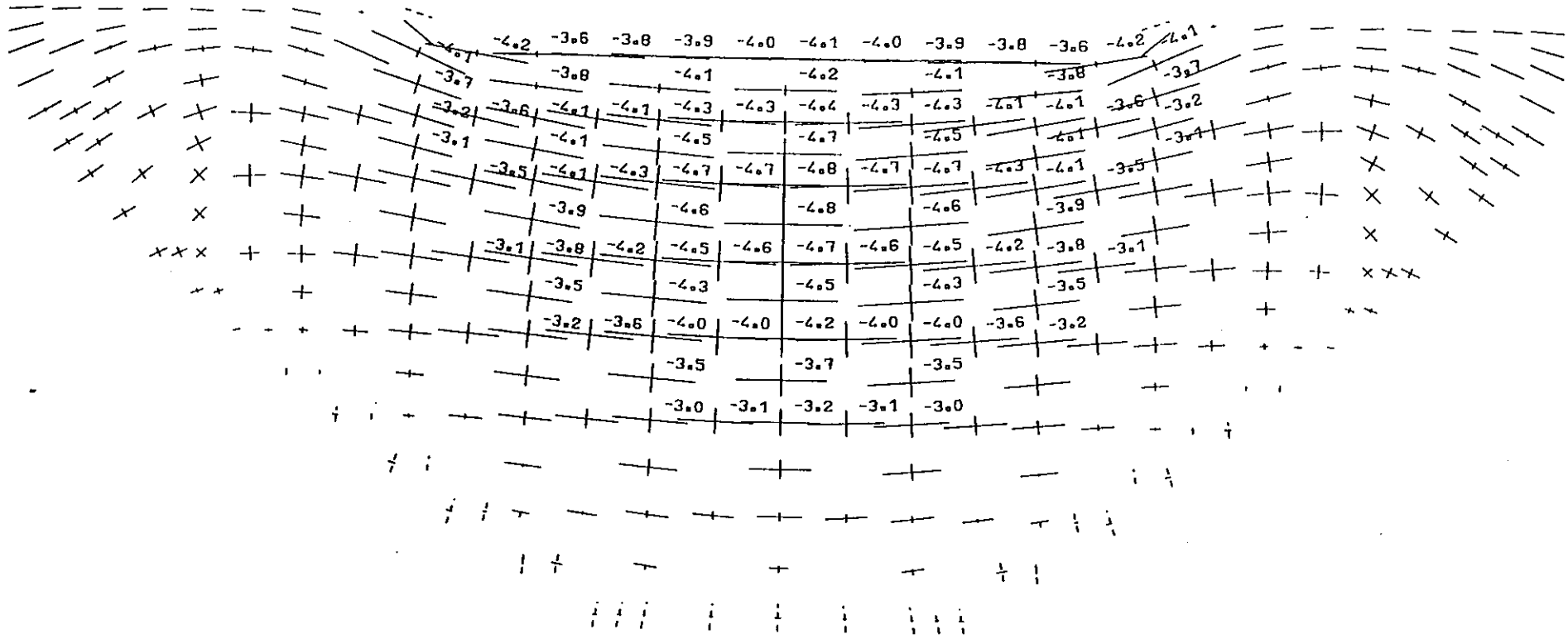

TALVACCHIA DAM
DEAD WEIGHT + HYDROSTATIC PRESSURE
SCALE : 0.00125 STRESSES : 0.40000 (1 CM = 2.5 MPA)

COYNE ET BELLIER | * COQEF3 *

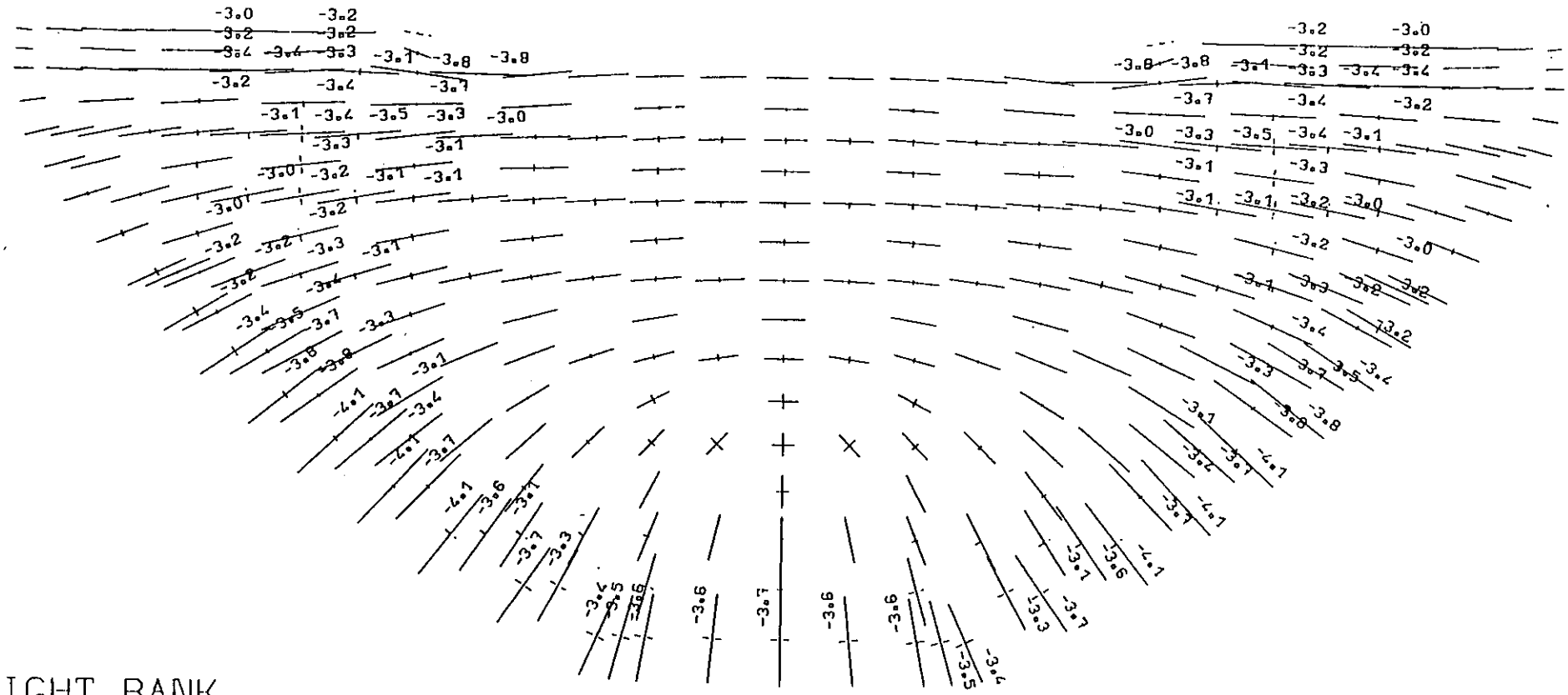

TALVACCHIA DAM
DEAD WEIGHT + HYDROSTATIC PRESSURE
SCALE : 0.00125 STRESSES : 0.40000 (1 CM = 2.5 MPA)

APPENDIX 3-14

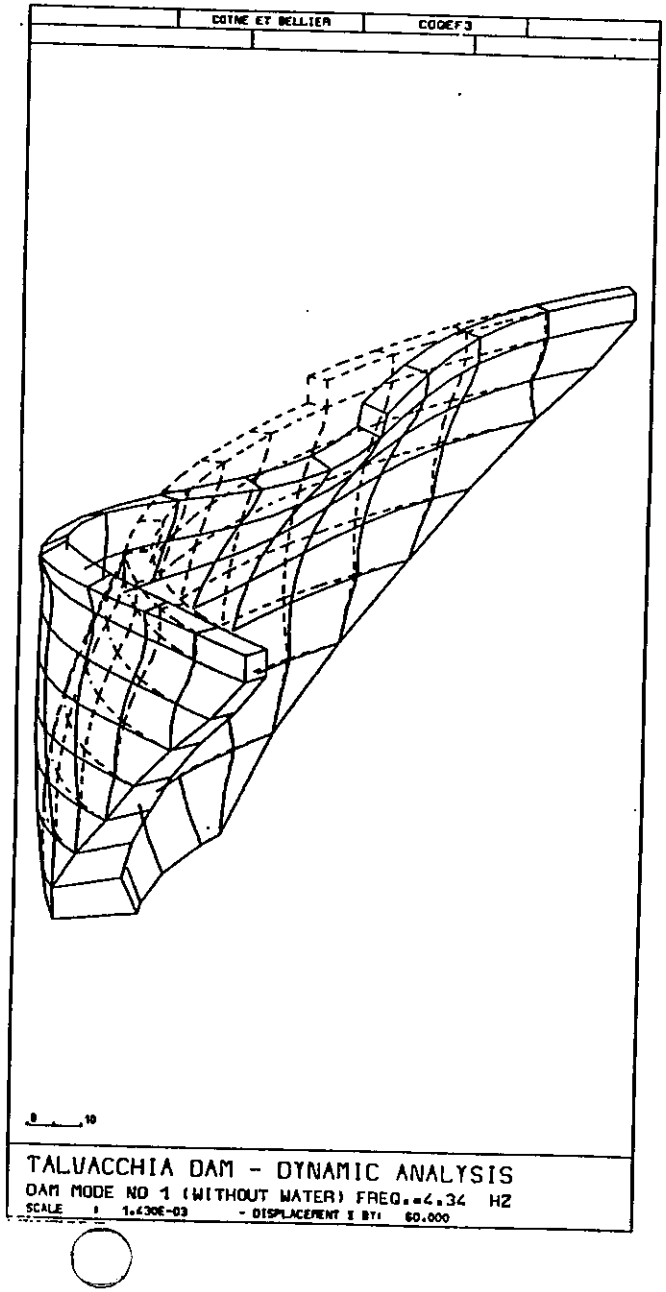

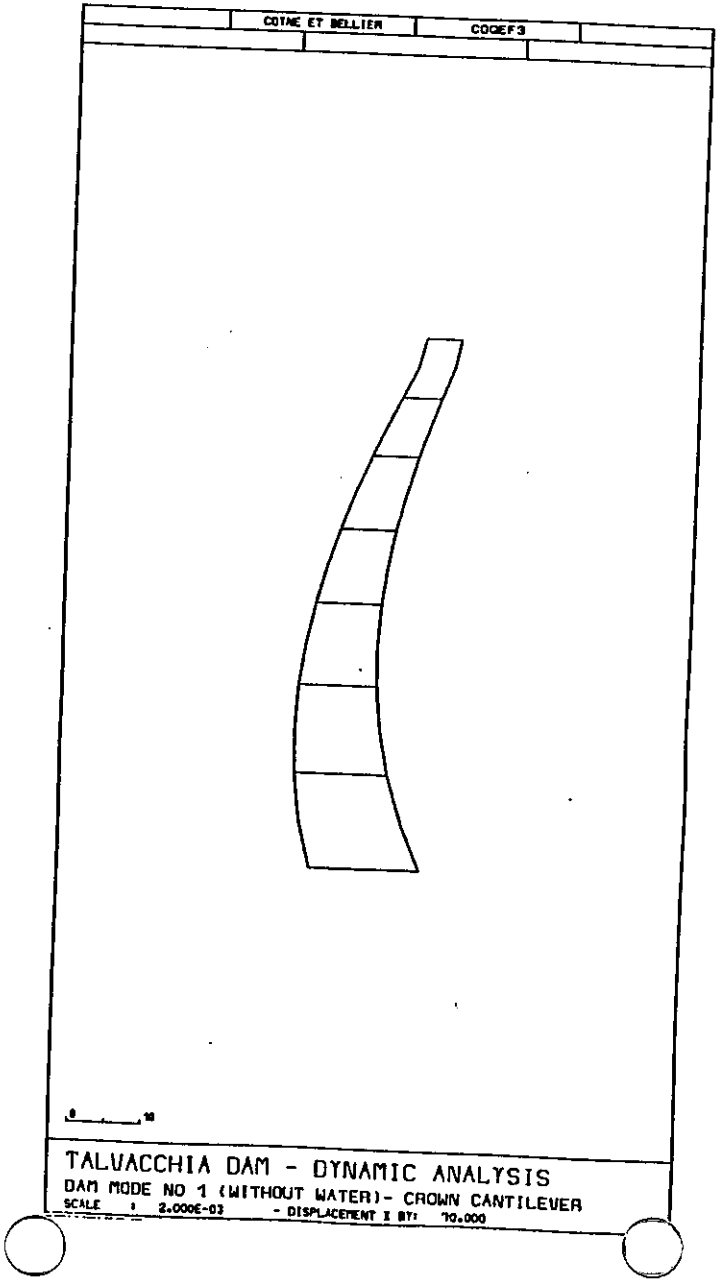

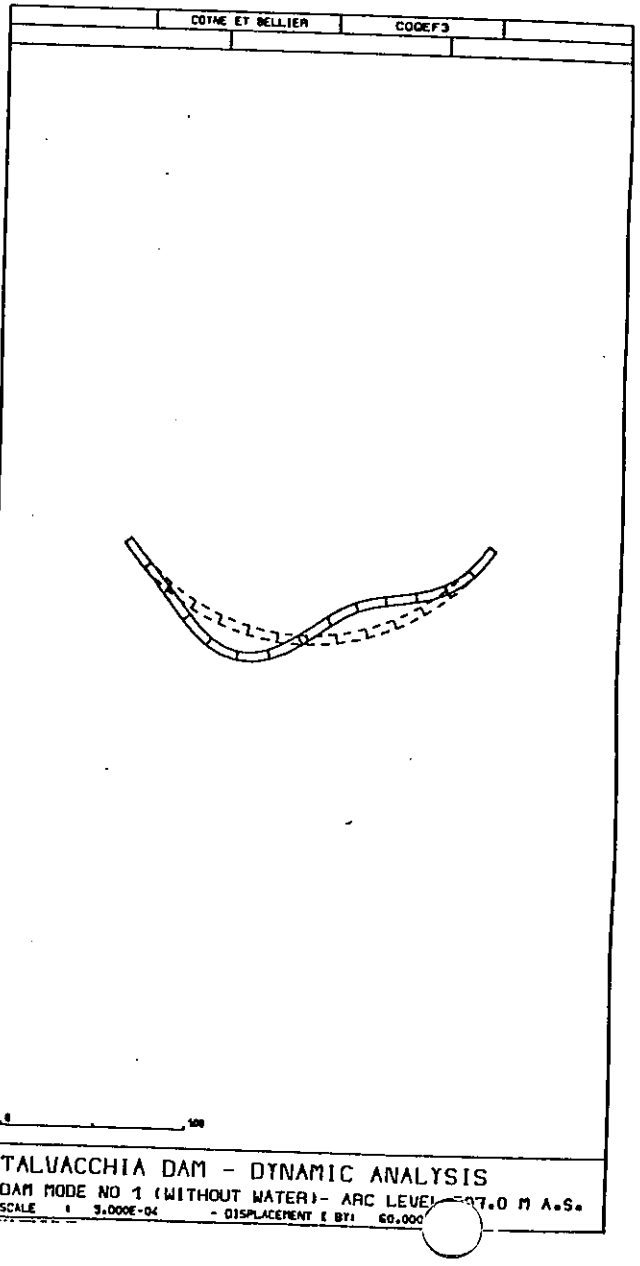

COYNE ET BELLIER | COGEF3

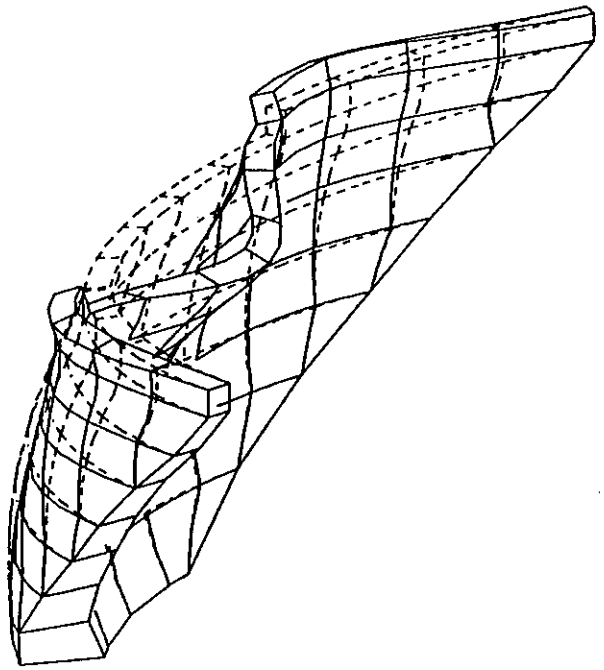

TALVACCHIA DAM - DYNAMIC ANALYSIS
DAM MODE NO 2 (WITHOUT WATER) FREQ.= 4.62 HZ
SCALE : 1.451E-03 - DISPLACEMENT (BT) 70.000

COYNE ET BELLIER | COGEF3

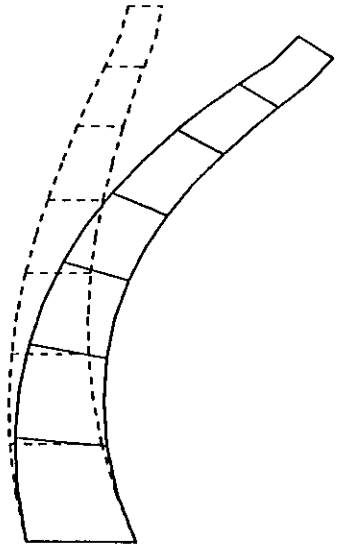

TALVACCHIA DAM - DYNAMIC ANALYSIS
DAM MODE NO 2 (WITHOUT WATER)- CROWN CANTILEVER
SCALE : 2.000E-03 - DISPLACEMENT (BT) 70.000

COYNE ET BELLIER | COGEF3

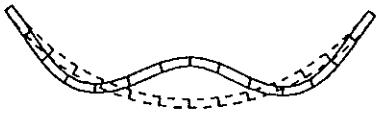

TALVACCHIA DAM - DYNAMIC ANALYSIS
DAM MODE NO 2 (WITHOUT WATER)- ARC LEVEL 507.0 M A.S.
SCALE : 5.000E-04 - DISPLACEMENT (BT) 70.000

APPENDIX 3-16

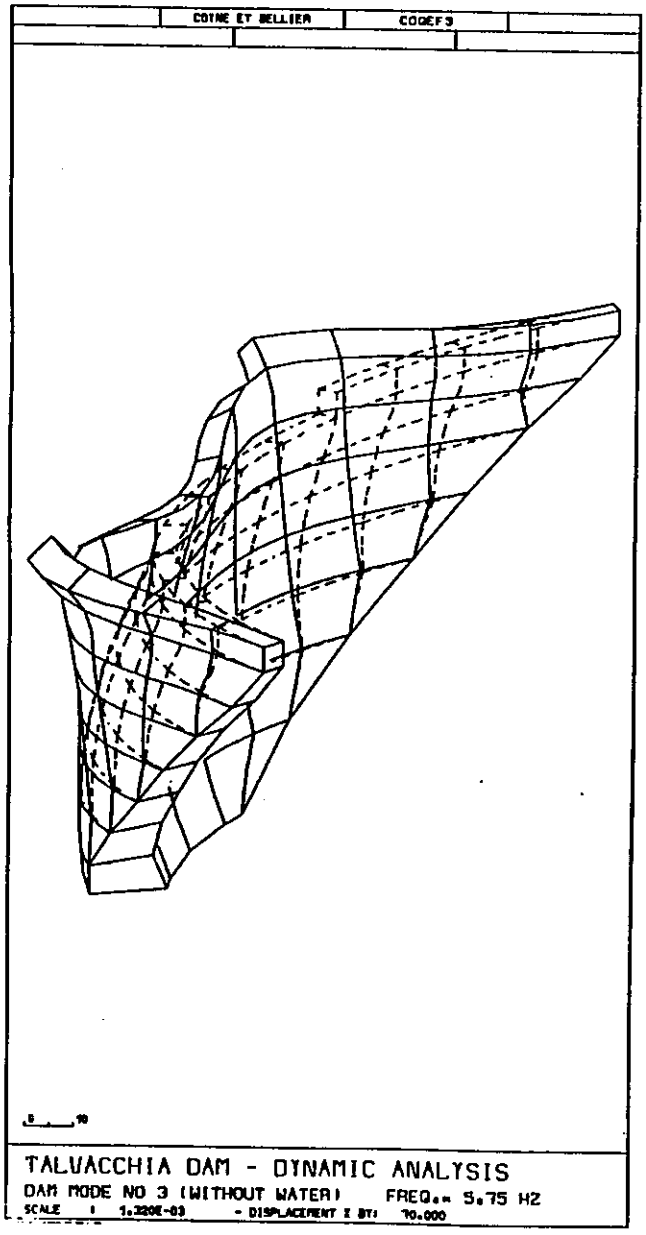

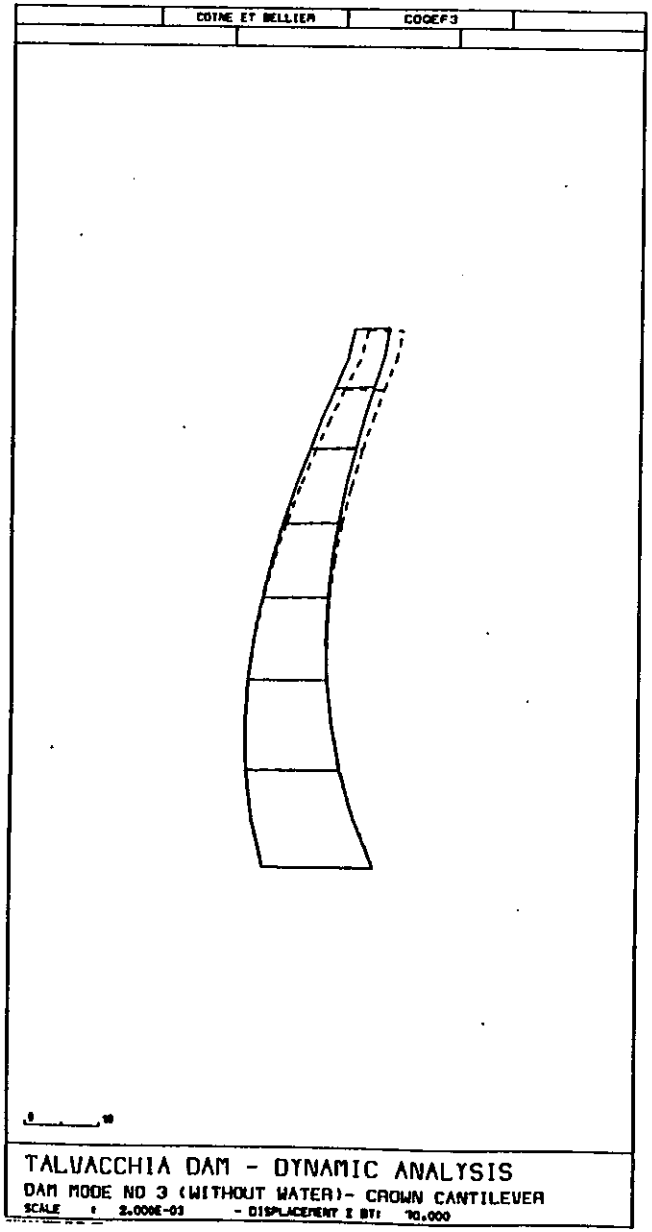

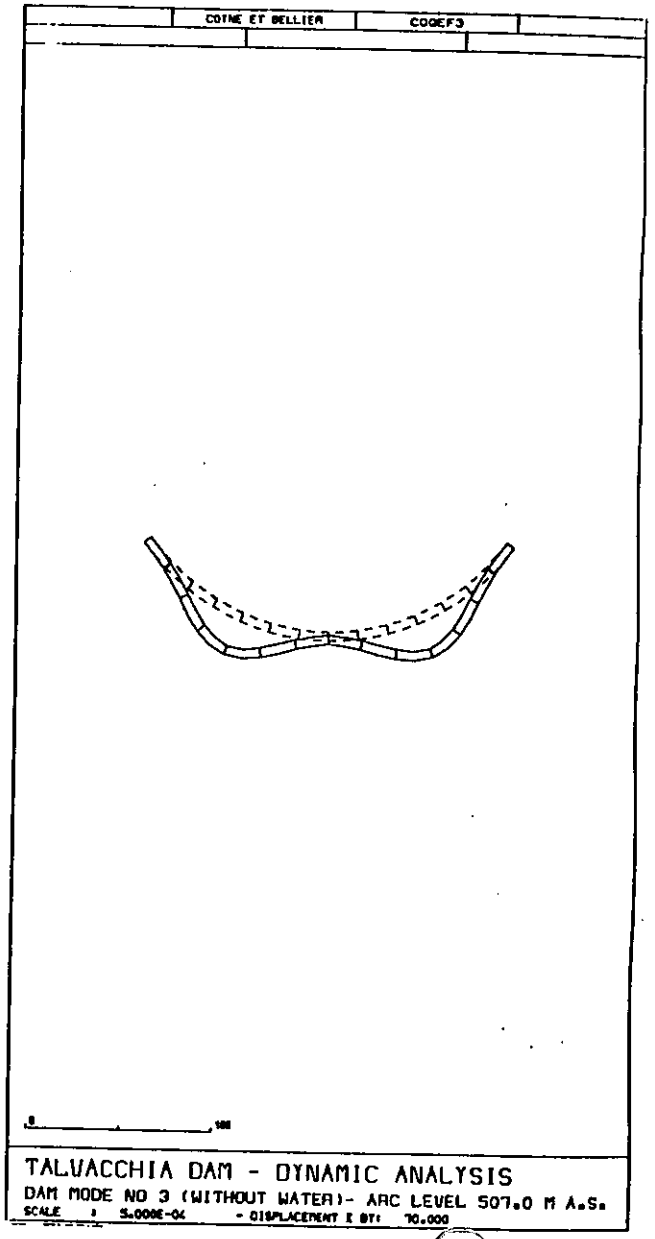

COYNE ET BELLIER | COQEF3

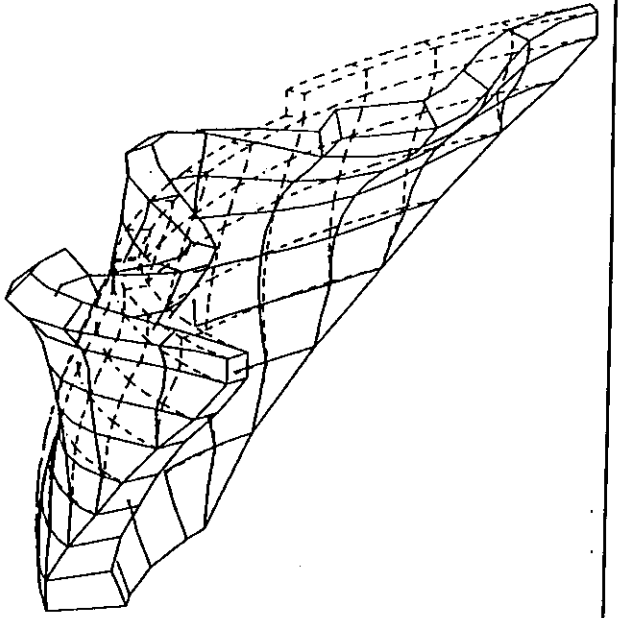

TALVACCHIA DAM - DYNAMIC ANALYSIS
DAM MODE NO 4 (WITHOUT WATER) FREQ.= 6.73 HZ
SCALE : 1.364E-03 - DISPLACEMENT : BY: 70.000

COYNE ET BELLIER | COQEF3

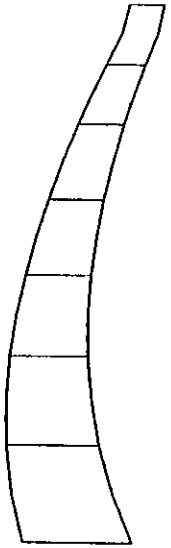

TALVACCHIA DAM - DYNAMIC ANALYSIS
DAM MODE NO 4 (WITHOUT WATER)- CROWN CANTILEVER
SCALE : 2.000E-03 - DISPLACEMENT : BY: 70.000

COYNE ET BELLIER | COQEF3

TALVACCHIA DAM - DYNAMIC ANALYSIS
DAM MODE NO 4 (WITHOUT WATER) - ARC LEVEL 507.0 M A.S
SCALE : 5.000E-04 - DISPLACEMENT : BY: 70.000

APPENDIX 3-18

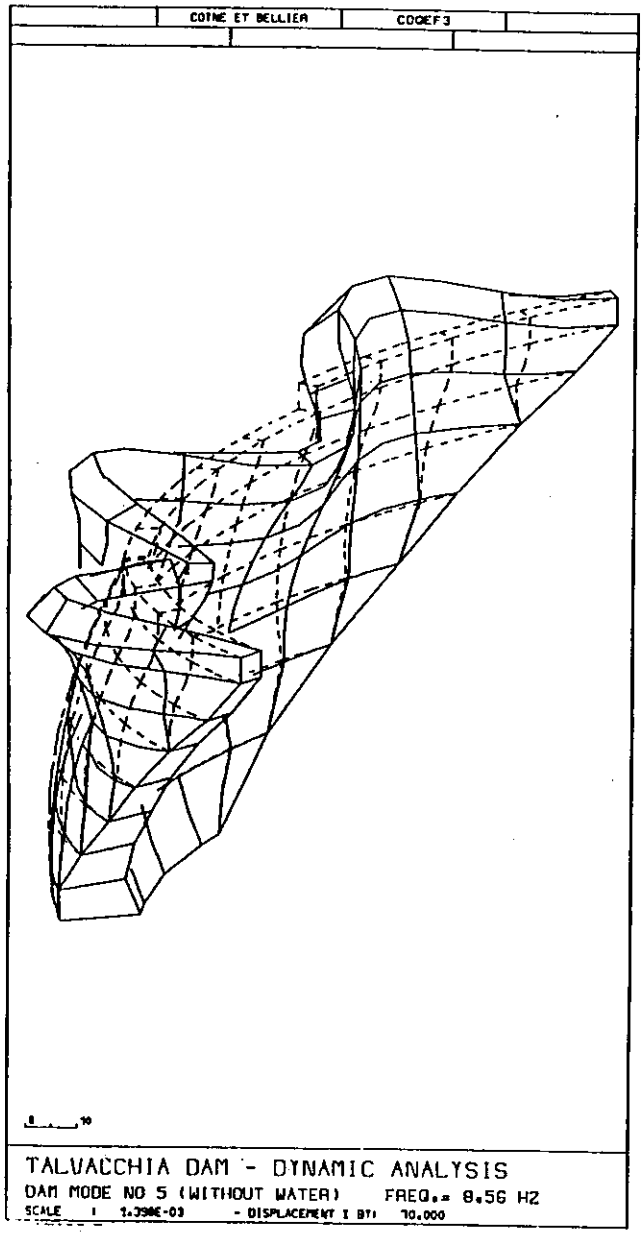

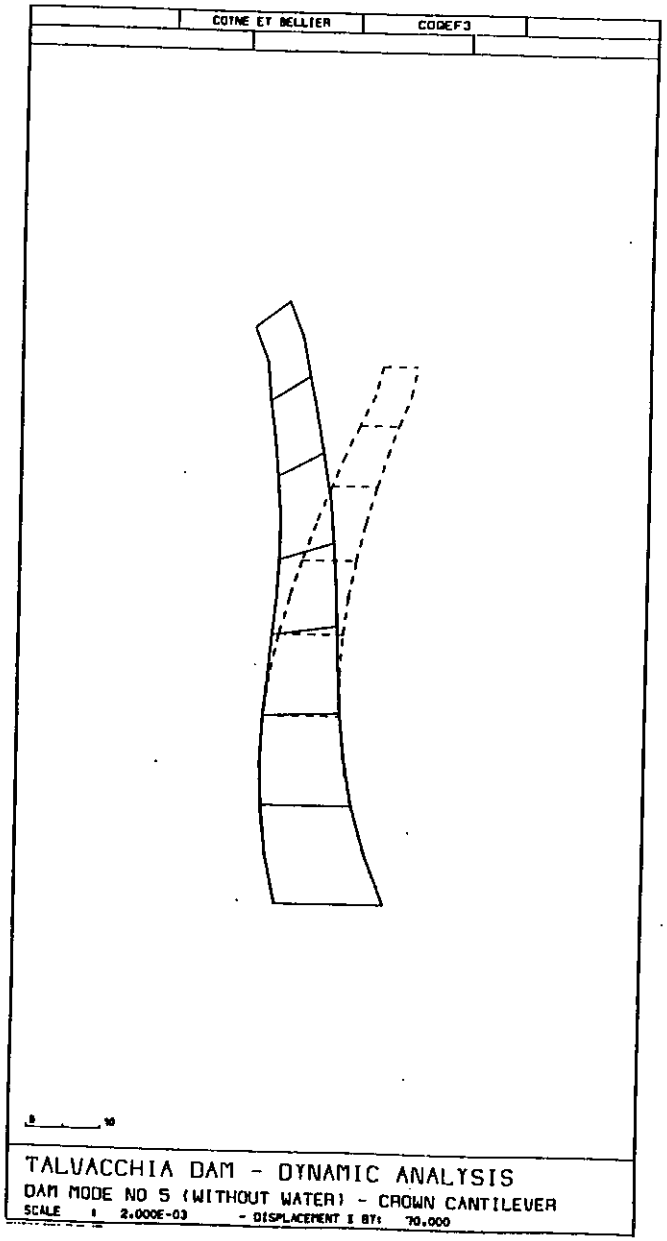

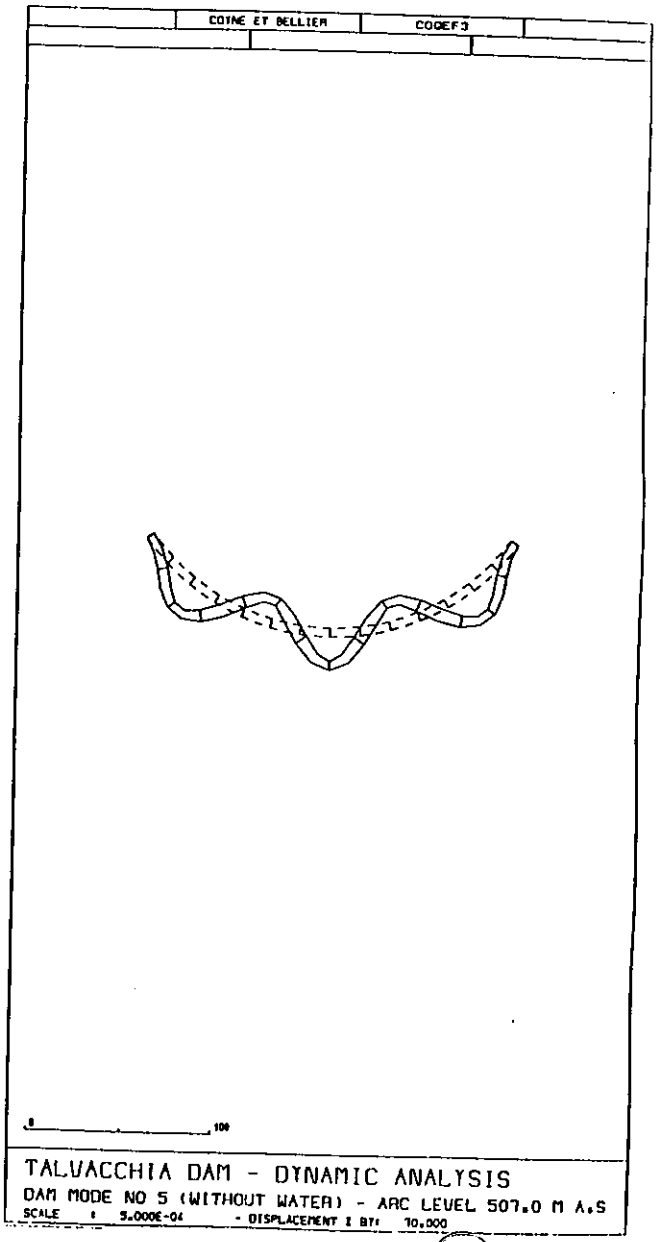

COYNE ET BELLIER | CODEF3

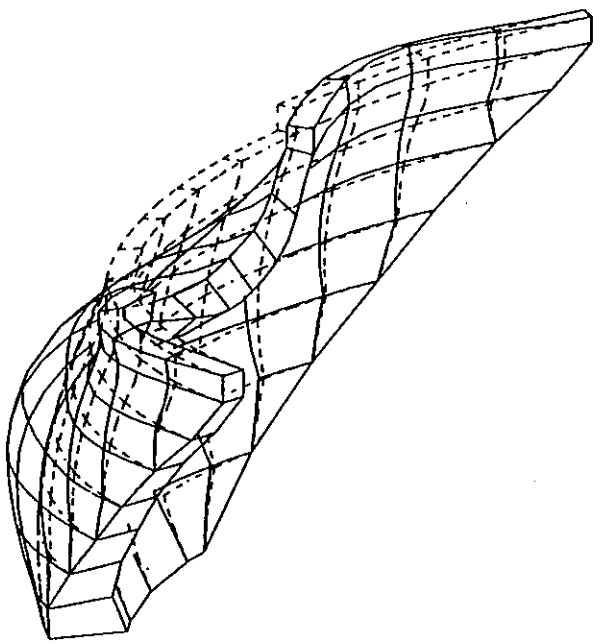

TALVACCHIA DAM - DYNAMIC ANALYSIS
DAM MODE NO 6 (WITHOUT WATER) FREQ.= 9.53 HZ
SCALE : 1.371BE-03 - DISPLACEMENT X BY: 70.000

COYNE ET BELLIER | CODEF3

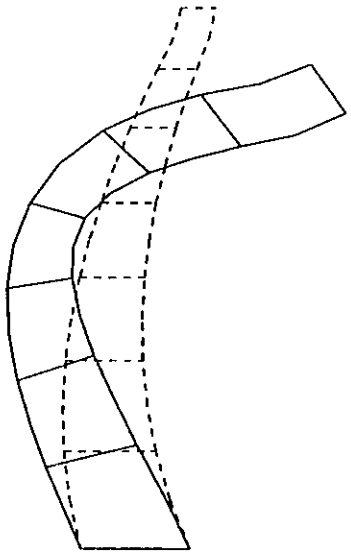

TALVACCHIA DAM - DYNAMIC ANALYSIS
DAM MODE NO 6 (WITHOUT WATER) - CROWN CANTILEVER
SCALE : 2.000E-03 - DISPLACEMENT X BY: 70.000

COYNE ET BELLIER | CODEF3

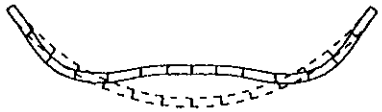

TALVACCHIA DAM - DYNAMIC ANALYSIS
DAM MODE NO 6 (WITHOUT WATER) - ARC LEVEL 507.0 M A.S
SCALE : 5.000E-04 - DISPLACEMENT X BY: 70.000

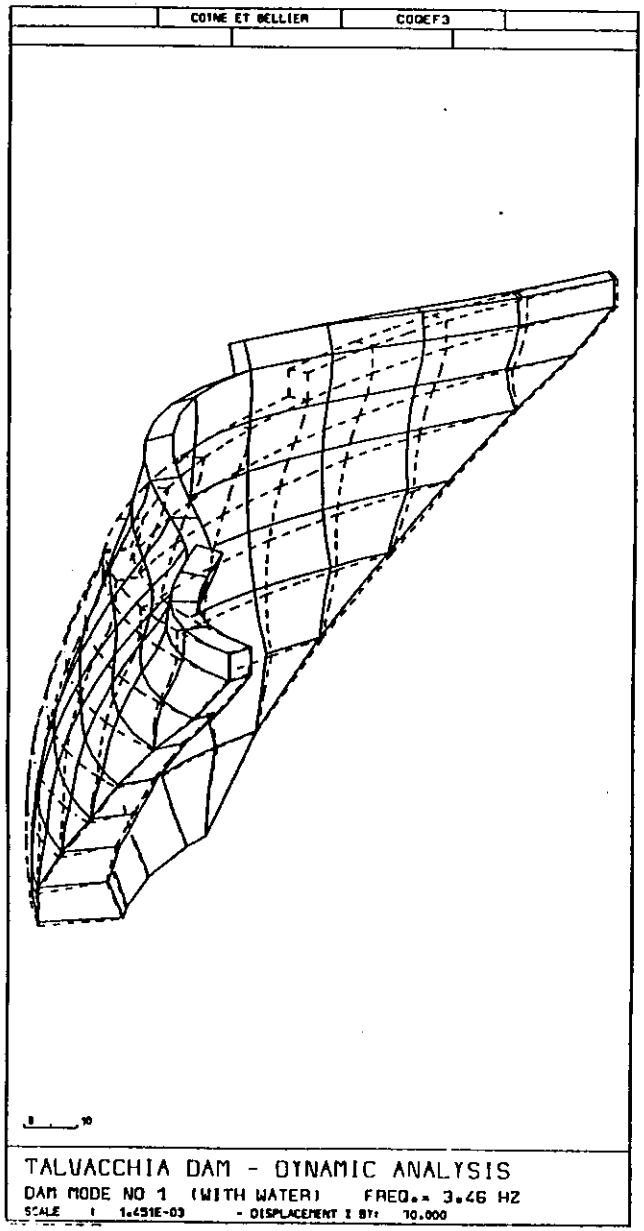
COYNE ET BELLIER
CODEF3
0
10
TALVACCHIA DAM - DYNAMIC ANALYSIS
DAM MODE NO 1 (WITH WATER) FREQ.= 3.46 HZ
SCALE : 1.451E-03 - DISPLACEMENT X 8Y: 70.000

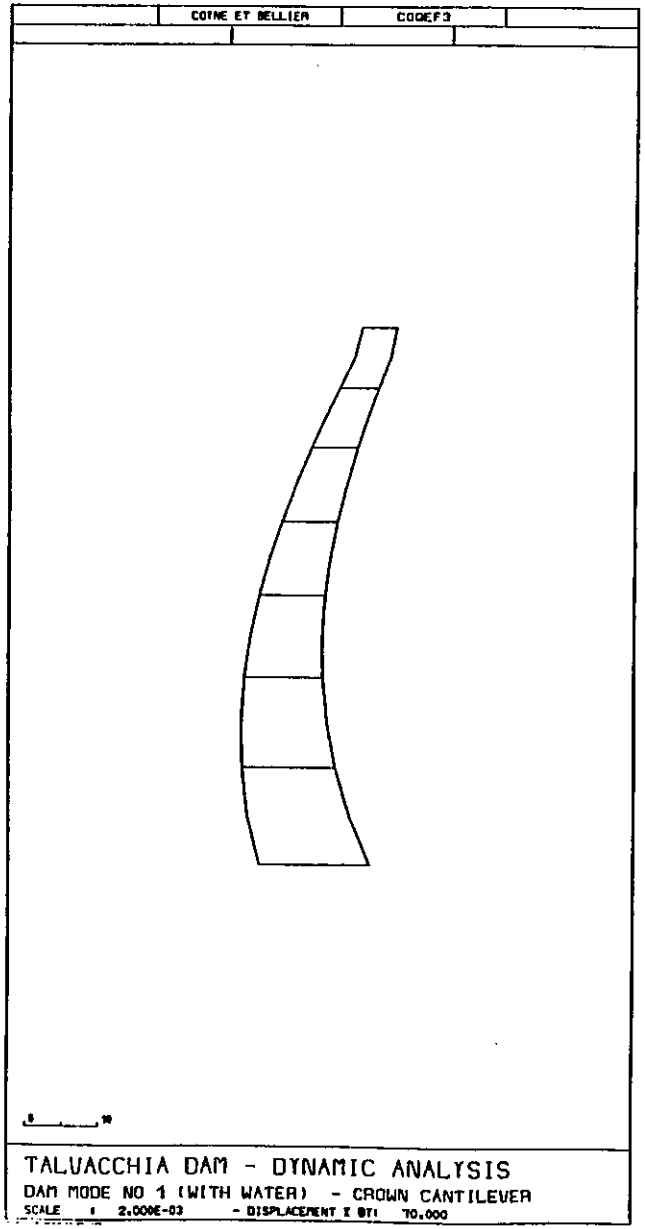
COYNE ET BELLIER
CODEF3
0
10
TALVACCHIA DAM - DYNAMIC ANALYSIS
DAM MODE NO 1 (WITH WATER) - CROWN CANTILEVER
SCALE : 2.000E-03 - DISPLACEMENT X BY: 70.000

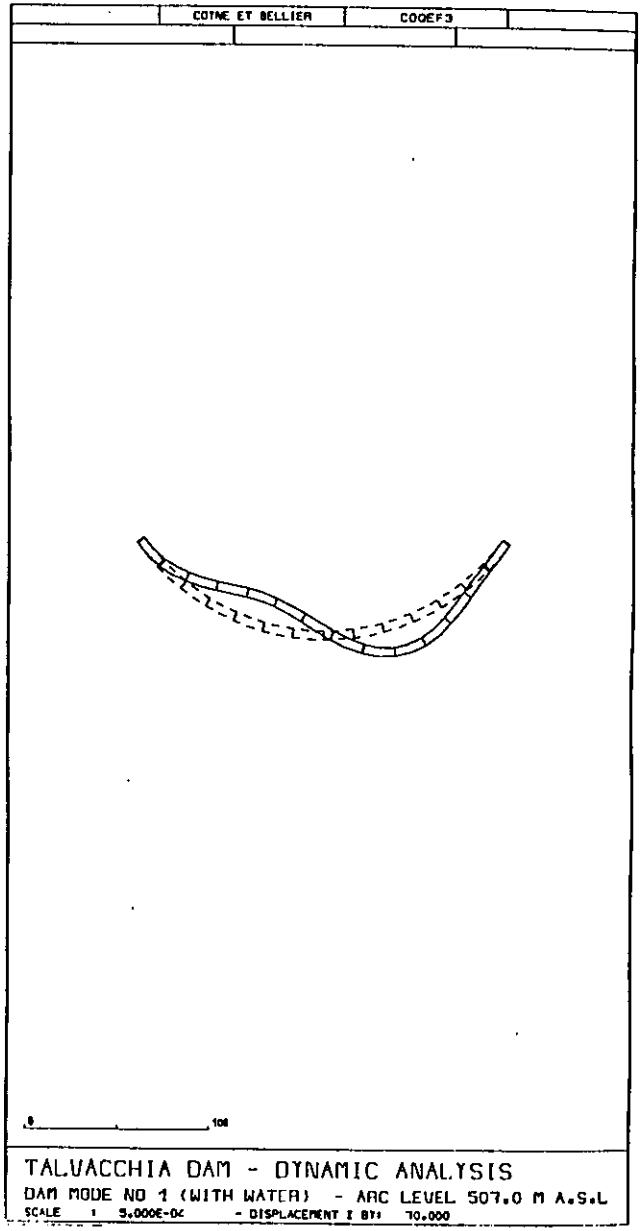
COYNE ET BELLIER
CODEF3
0
100
TALVACCHIA DAM - DYNAMIC ANALYSIS
DAM MODE NO 1 (WITH WATER) - ARC LEVEL 507.0 M A.S.L
SCALE : 5.000E-02 - DISPLACEMENT X BY: 70.000

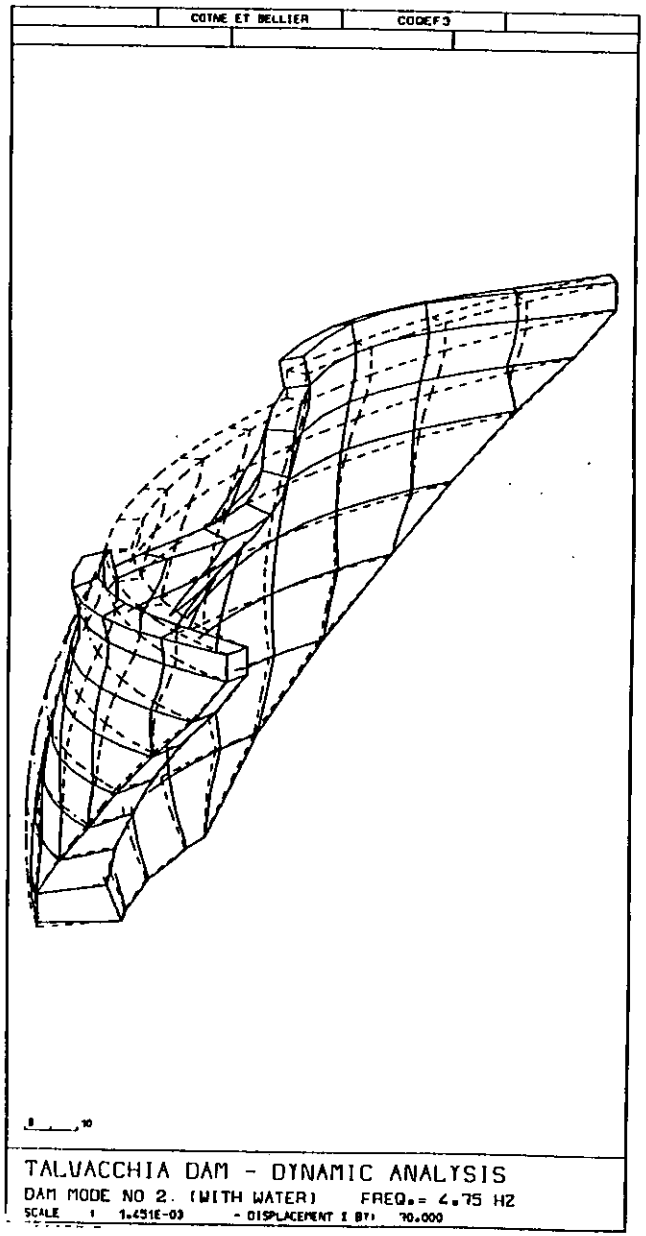
COYNE ET BELLIER
CODEF3
TALVACCHIA DAM - DYNAMIC ANALYSIS
DAM MODE NO 2. (WITH WATER) FREQ.= 4.75 HZ
SCALE : 1.451E-03 - DISPLACEMENT X BY: 70.000

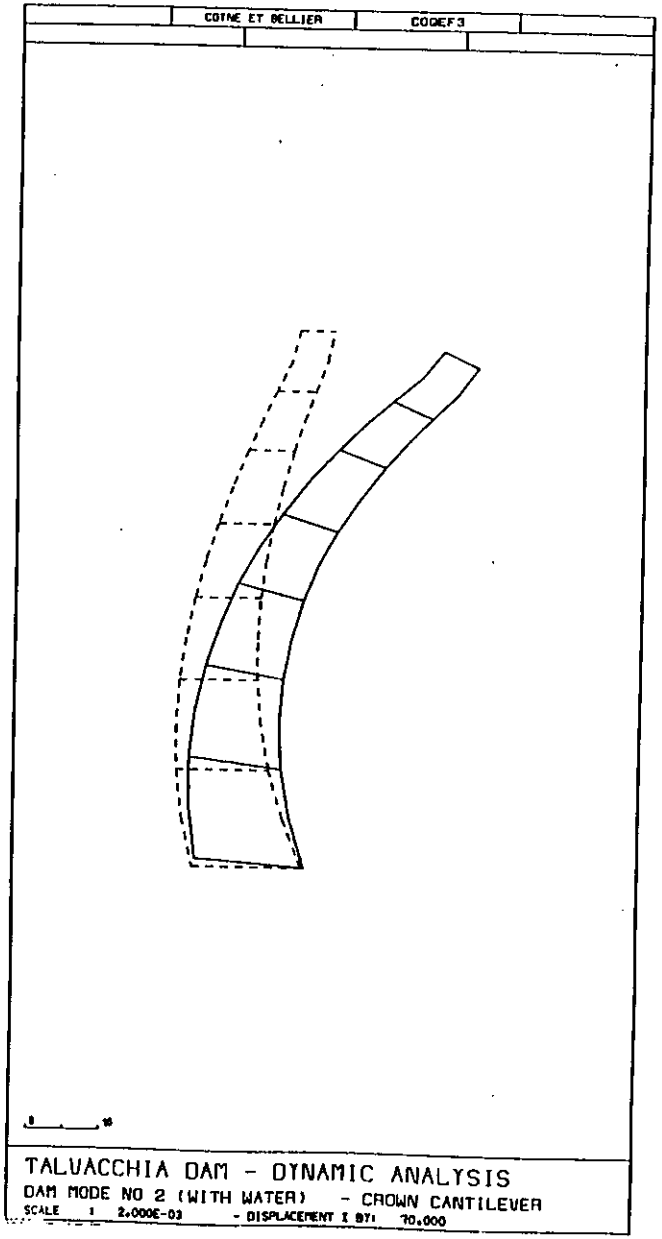
COYNE ET BELLIER
CODEF3
TALVACCHIA DAM - DYNAMIC ANALYSIS
DAM MODE NO 2 (WITH WATER) - CROWN CANTILEVER
SCALE : 2.000E-03 - DISPLACEMENT X BY: 70.000

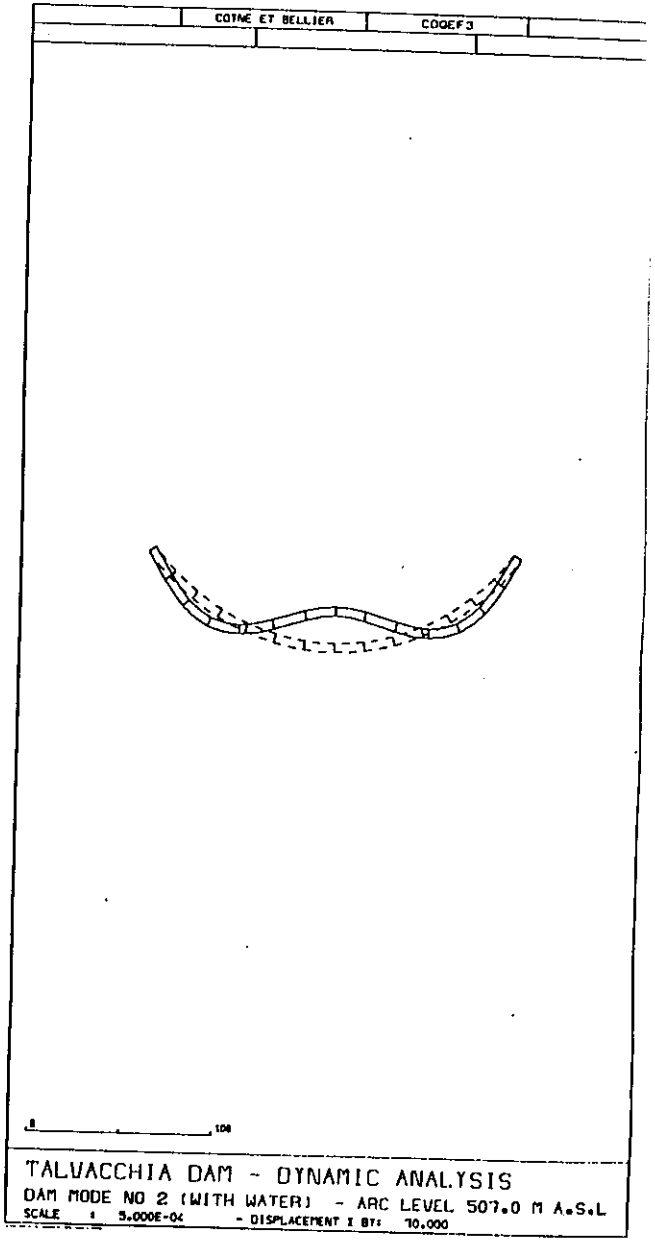
COYNE ET BELLIER
CODEF3
TALVACCHIA DAM - DYNAMIC ANALYSIS
DAM MODE NO 2 (WITH WATER) - ARC LEVEL 507.0 M A.S.L
SCALE : 5.000E-04 - DISPLACEMENT X BY: 70.000

APPENDIX 3-22

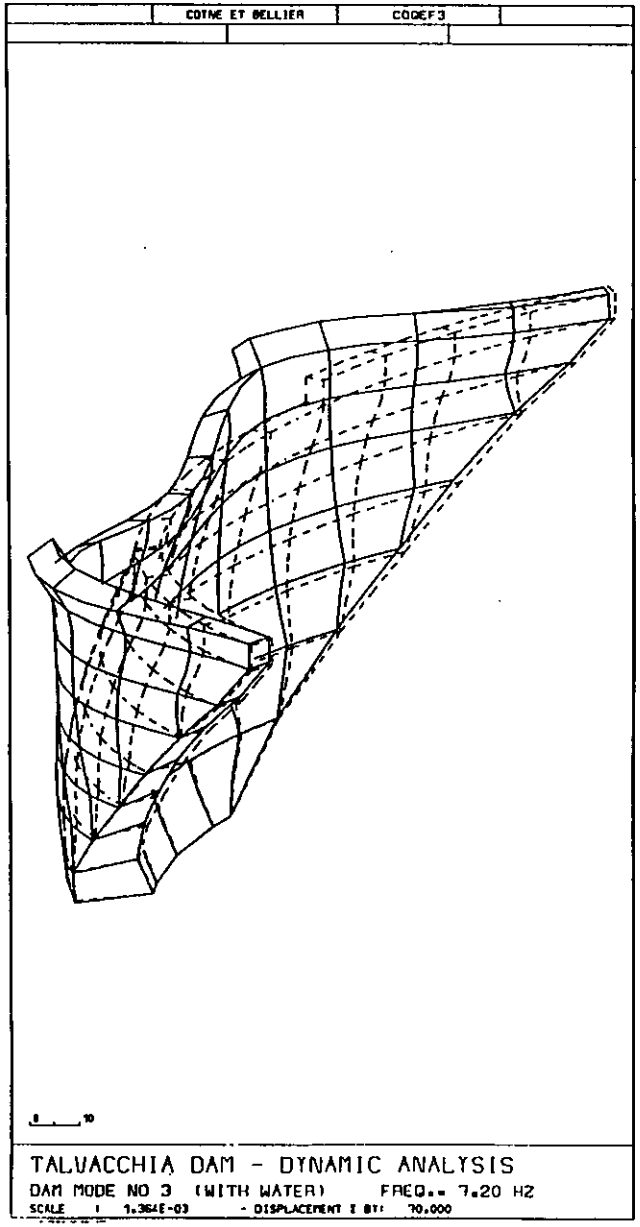

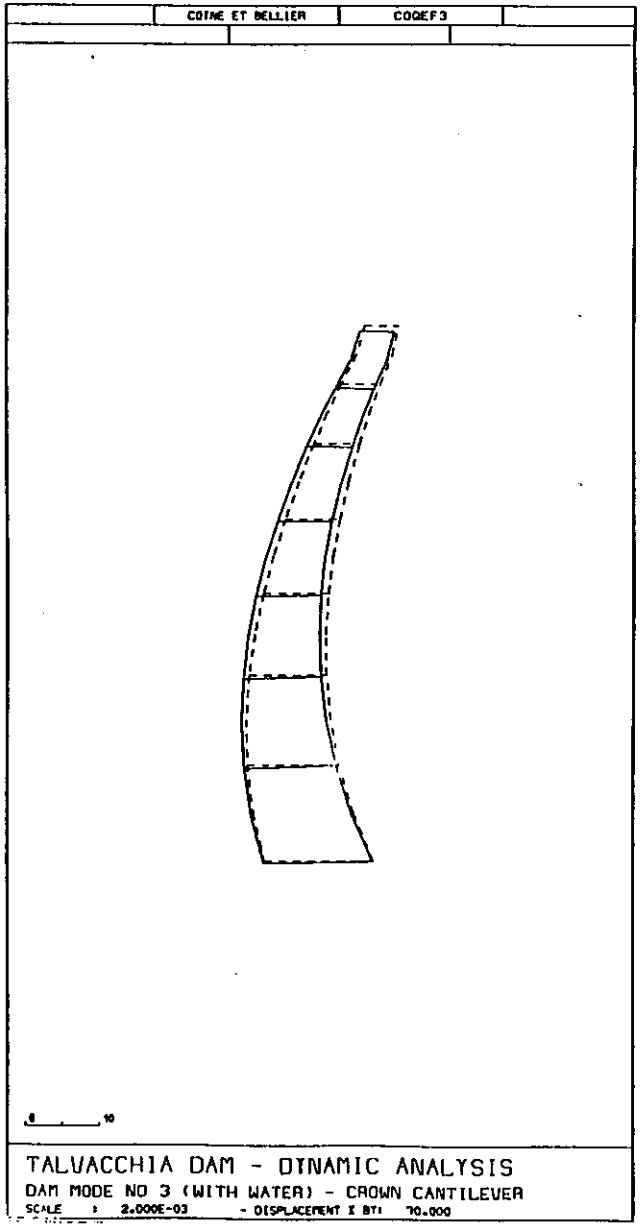

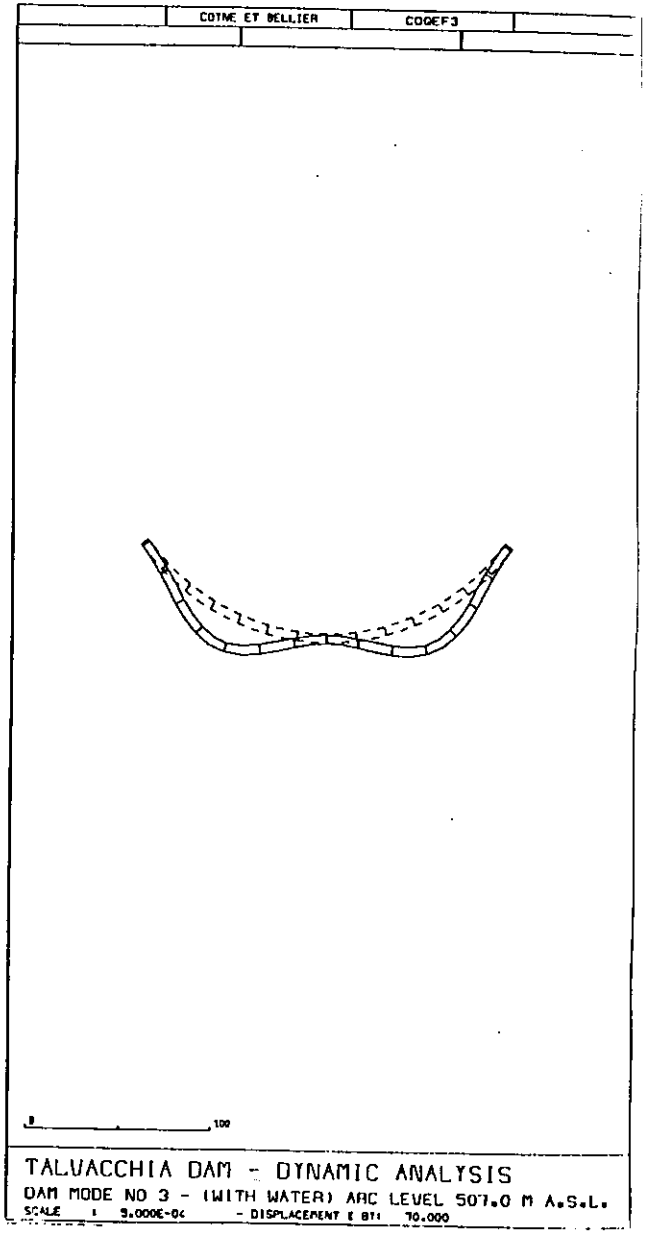

COYNE ET BELLIER | CODEF3

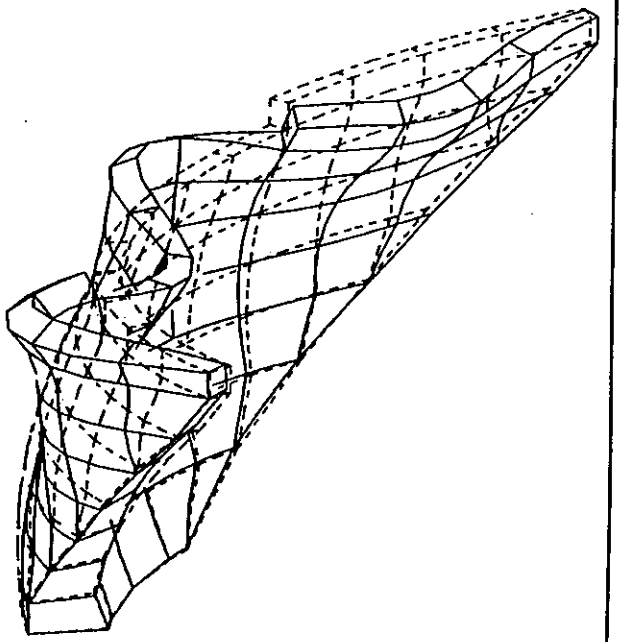

TALVACCHIA DAM - DYNAMIC ANALYSIS
DAM MODE NO 4 (WITH WATER) FREQ.= 7.48 HZ
SCALE : 1.402E-03 - DISPLACEMENT I BT: 70.000

COYNE ET BELLIER | CODEF3

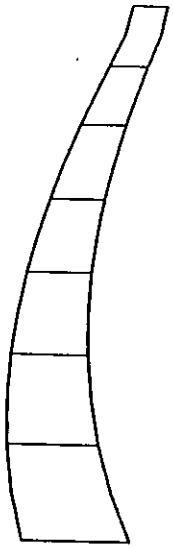

TALVACCHIA DAM - DYNAMIC ANALYSIS
DAM MODE NO 4 (WITH WATER) - CROWN CANTILEVER
SCALE : 2.000E-03 - DISPLACEMENT I BT: 70.000

COYNE ET BELLIER | CODEF3

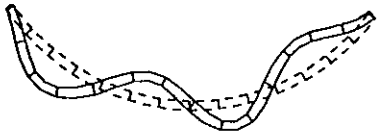

TALVACCHIA DAM - DYNAMIC ANALYSIS
DAM MODE NO 4 (WITH WATER) - ARC LEVEL 507.0 M A.S.L
SCALE : 5.000E-04 - DISPLACEMENT I BT: 70.000

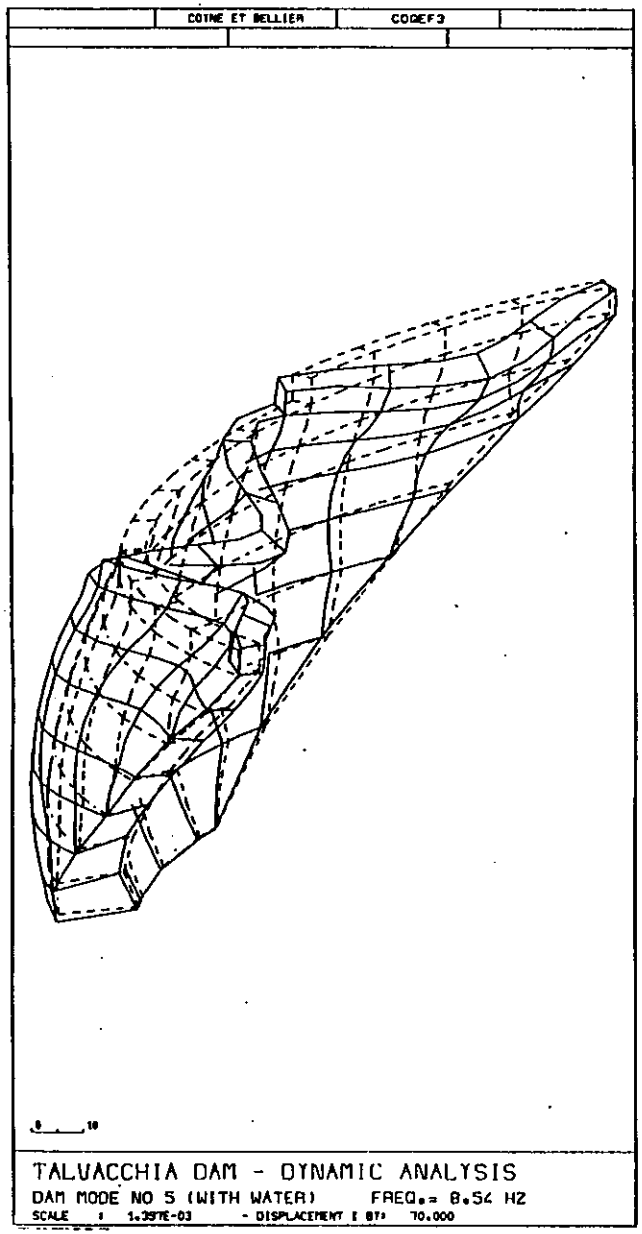
COYNE ET BELLIER
CODEF3
0 10
TALVACCHIA DAM - DYNAMIC ANALYSIS
DAM MODE NO 5 (WITH WATER) FREQ.= 8.54 HZ
SCALE : 1.39TE-03 - DISPLACEMENT X 8T: 70.000

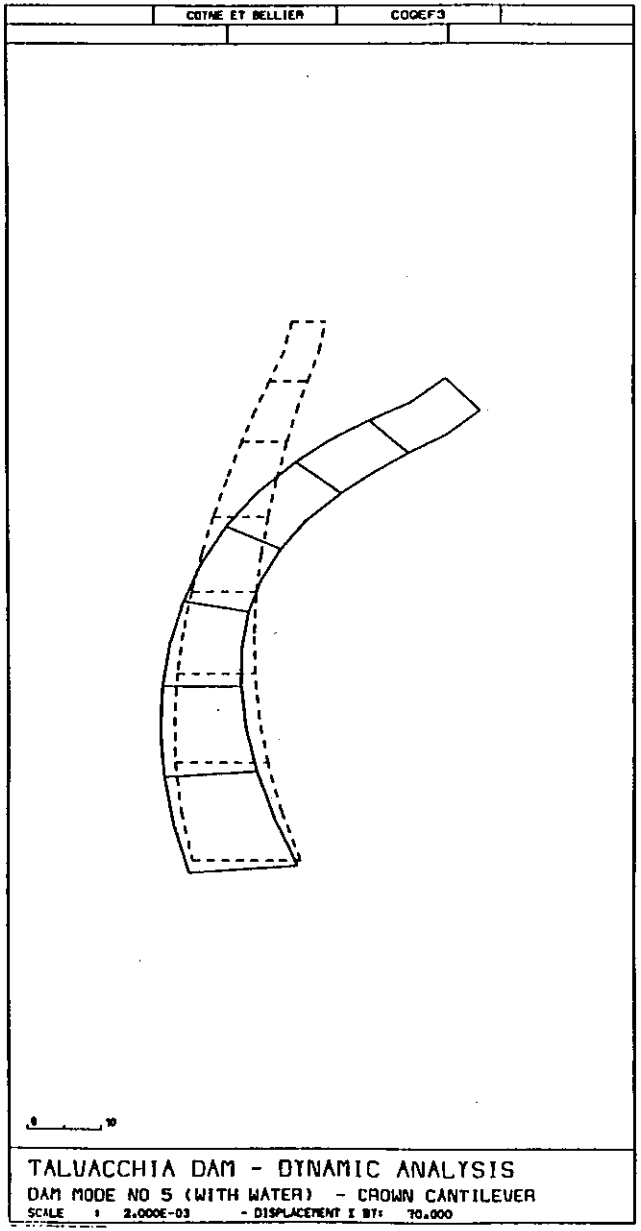
COYNE ET BELLIER
CODEF3
0 10
TALVACCHIA DAM - DYNAMIC ANALYSIS
DAM MODE NO 5 (WITH WATER) - CROWN CANTILEVER
SCALE : 2.000E-03 - DISPLACEMENT X 8T: 70.000

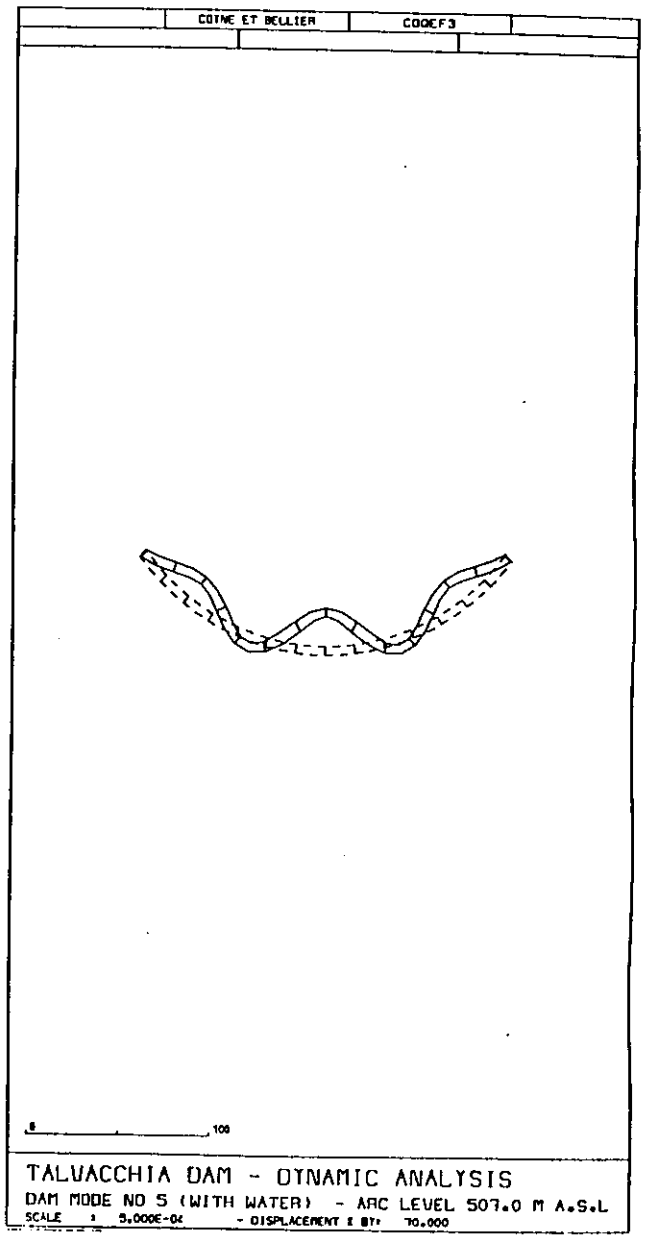
COYNE ET BELLIER
CODEF3
0 100
TALVACCHIA DAM - DYNAMIC ANALYSIS
DAM MODE NO 5 (WITH WATER) - ARC LEVEL 507.0 M A.S.L
SCALE : 5.000E-0 - DISPLACEMENT X 8T: 70.000

APPENDIX 3-25

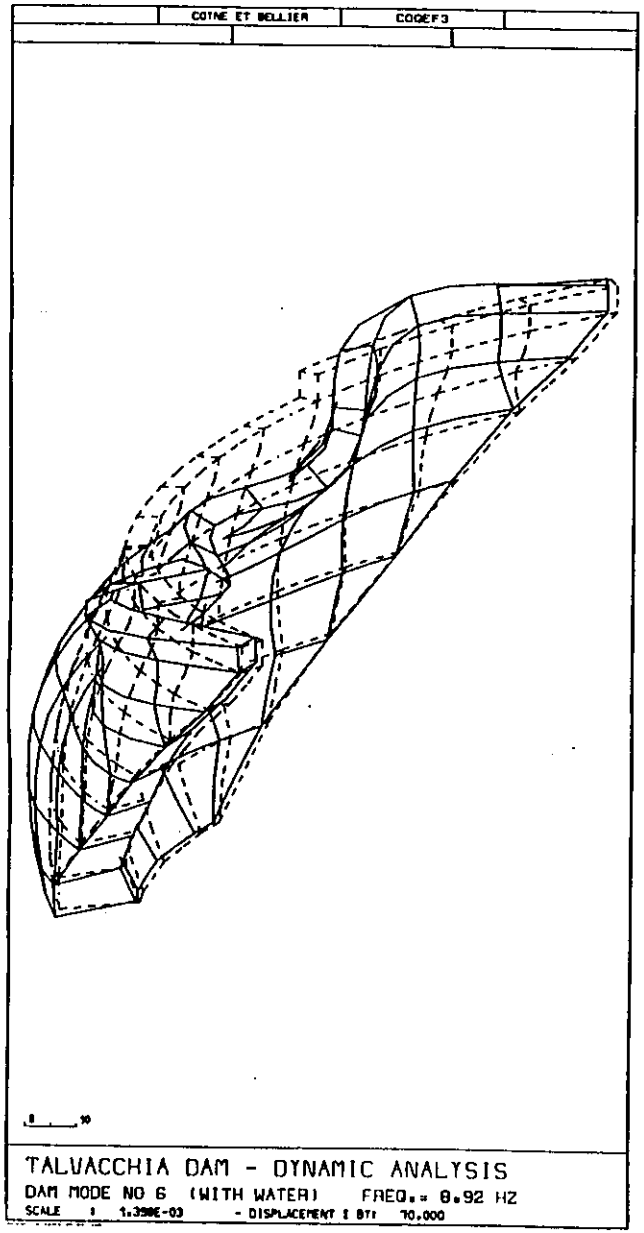

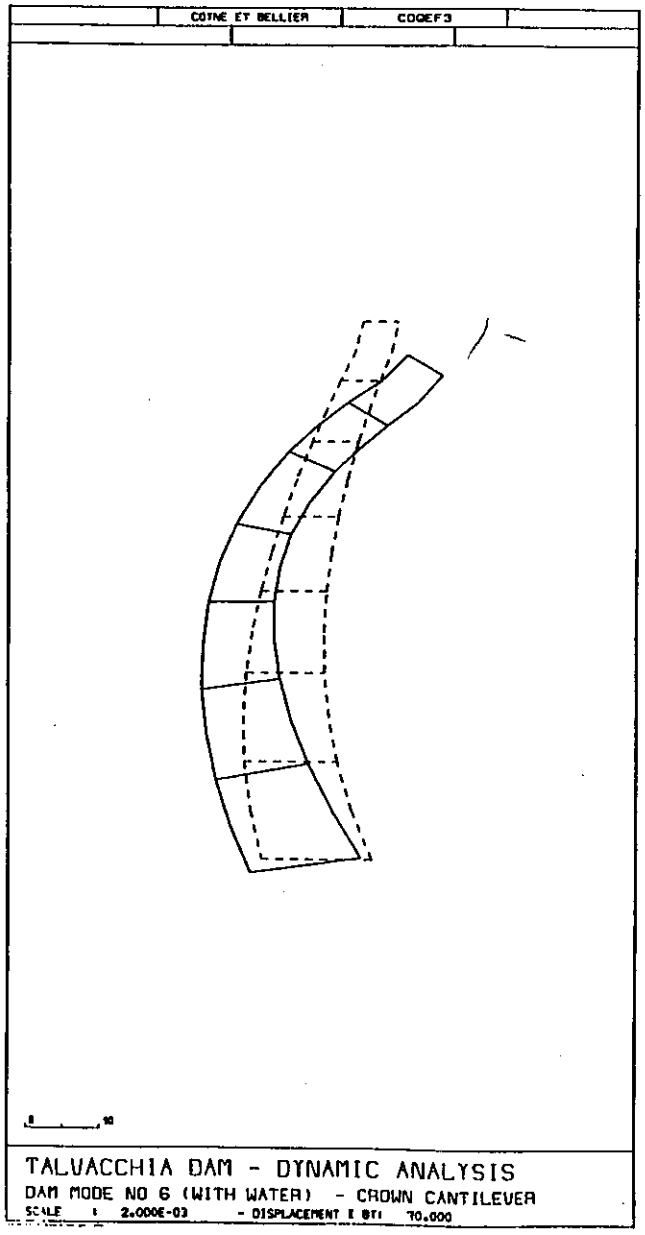

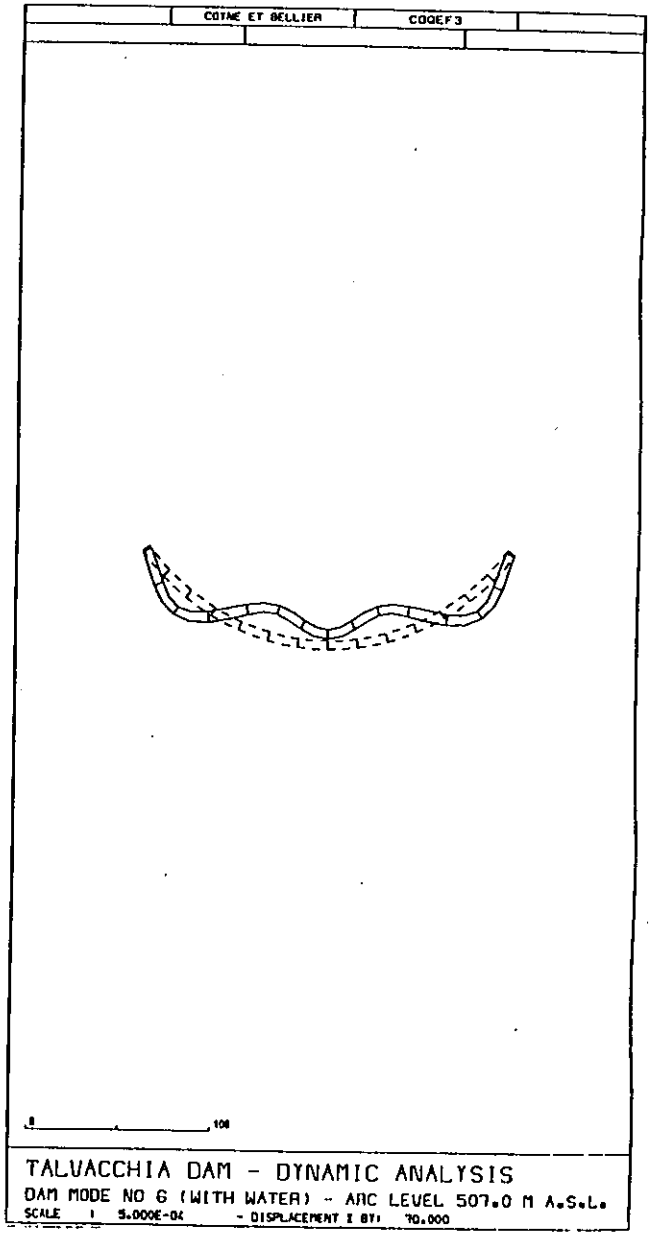

APPENDIX 4

COYNE ET BELLIER | GRAPHIX

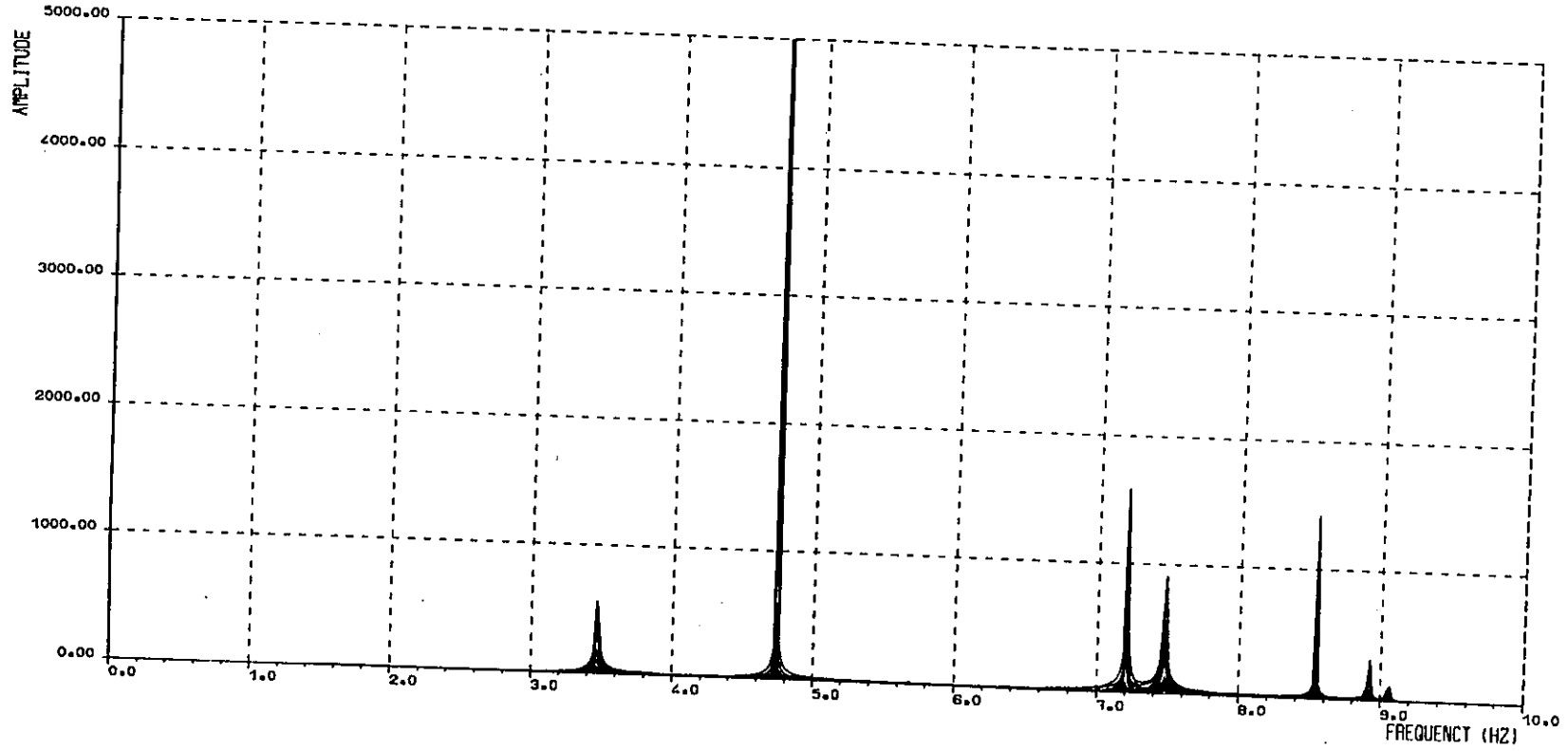

TALVACCHIA DAM - DYNAMIC ANALYSIS (WITH WATER)

FREQUENCY RESPONSE AT DIFFERENT POINTS OF THE DAM

BENCHMARK ANALYSIS OF TALVACCHIA DAM USING EACD-3D PROGRAM

by

Hanchen Tan[1] and Anil K. Chopra[2]

Introduction

Presented in this report are the results of the benchmark analysis of Talvacchia Dam using the computer program Earthquake Analysis of Concrete Dams--Three Dimensional--EACD-3D [1]. The program was developed in 1986 under research grants from the U.S. National Science Foundation and is available at nominal cost from the National Information Service for Earthquake Engineering, admistered by the Earthquake Engineering Research Center of the University of California at Berkeley.

In this report a brief description of the EACD-3D program is presented, followed by the various results specified in the benchmark workshop instructions.

EACD-3D Program

EACD-3D is a special purpose finite element program developed for three-dimensional static and dynamic analysis of concrete dams supported by flexible foundation rock in a canyon and impounding a reservoir of water (Fig. 1). Thus, arch dams which must be treated as three-dimensional systems can be analyzed. Similarly, the program can be useful for analysis of gravity dams located in narrow canyons or with keyed contraction points--situations where two-dimensional analyses may be inappropriate.

The EACD-3D program implements a procedure for three-dimensional analysis of earthquake response of concrete dams [2] considering the following effects:

- Dam-water interaction--with water compressibility considered or neglected
- Hydrodynamic wave absorptive effects of the rock and overlying sediments at the reservoir bottom and sides
- Foundation flexibility.

However, the inertial and damping effects (material and radiation) of the foundation rock are ignored in the present version of the program

The static analysis considers only the effects of the weight of the dam and hydrostatic pressures, not the thermal effects in the concrete or construction sequence of the dam. Three components of ground motion can be specified as spatially-uniform excitation at the interface between the dam and supporting foundation rock.

The analysis procedure implemented by the EACD-3D program is based on a substructure method (Fig. 2). This procedure is formulated in the frequency domain in order to represent the

---

[1]Graduate Student, Department of Civil Engineering, University of California, Berkeley, California.

[2]Professor of Civil Engineering, University of California, Berkeley, California.

frequency-dependent hydrodynamic interaction and loading terms in the governing equations. The frequency dependence of these terms arises from water compressibility and hydrodynamic wave absorption at the reservoir bottom and sides. Similarly, full consideration of dam-foundation rock interaction, including inertial and damping (material and radiation) effects, would lead to additional frequency-dependent terms. Extension of the program along these lines is currently in progress.

An arch dam is idealized in the EACD-3D program as an asssemblage of finite elements with the main part of the dam represented by thick-shell finite elements, and the portion of the dam at its junction with foundation rock represented by transition elements, designed to connect thick-shell elements in the dam to three-dimensional solid elements employed in idealizing the foundation rock (Fig. 2). A shell element mesh employs one element in the thickness direction of the dam. Nodes are located at the mid-surface of the shell, each with five degrees of freedom (three translational and two rotational), with the change in thickness being neglected. Two types of isoparametric elements can be used: the rectangular 4-to-8-node element in which any or all of nodes 5, 6, 7, and 8 can be omitted; and the triangular 3-to-6-node element in which any or all of nodes 4, 5, and 6 can be omitted. The transition element transforms the five degrees of freedom for each shell mid-surface node on the dam-foundation interface to six translational degrees of freedom at the corresponding two auxiliary nodes on the dam faces. Transition elements are automatically formed from shell elements by the program where needed. The Talvacchia Dam is idealized as an assemblage of these thick shell and transition elements consistent with the mesh geometry specified in the workshop instructions. The shell idealization was prepared because it is more efficient in representing dam behavior. (However, essentially identical results were obtained by using the 3-D solid idealization of the dam specified in the workshop instructions.)

In the EACD-3D program two types of isoparametric solid elements can be used to discretize the foundation (Fig. 2): the rectangular prism 8-to-20-node element in which any or all of nodes 9, 10, . . . , 20 can be omitted; and the triangular prism 6-to-15-node element in which any or all of nodes 7, 8, . . . , 15 can be omitted. Each node has three degrees of freedom. In this analysis the finite element mesh used for the foundation is the same as in the workshop instructions.

In the EACD-3D program the water impounded behind the dam is idealized as a combination of two regions (Fig. 2). A region of irregular geometry starting at the dam face and extending a minimal distance in the upstream direction is connected to a uniform cross-section channel extending to infinity along the upstream direction. The restriction of uniform cross-section makes it possible to efficiently recognize the hydrodynamic wave propagation in the upstream direction of a long reservoir, an important factor if water compressibility is considered in the analysis.

The irregular region is idealized as an assemblage of three-dimensional elements with the water nodes in contact with the dam matching those on the dam face. The hydrodynamic pressure at each node is the only degree of freedom. For the infinitely long channel of uniform cross-section, a finite element discretization of the cross-section, compatible with the discretization of the irregular region over the common cross-section--the transmitting plane in Fig. 2c--combined with a continuum representation in the upstream direction provides for transmission of pressure waves. Physically, this treatment can be interpreted as a discretization of the fluid domain into subchannels of infinite length (Fig. 2c). For Talvacchia Dam the impounded water was idealized as described in Fig. 2c with the irregular region defined as the assemblage of the first layer of finite elements specified in the workshop instructions. (The vibration properties of the dam obtained with this idealization of the reservoir water were essentially identical to the results using the idealization extending to five times the water depth in the upstream direction, as specified in the workshop instructions.)

Static Analysis

Talvacchia Dam, idealized as described in the preceding section, is analyzed for two loading conditions: dead weight, and hydrostatic pressures with water level at 507.0 m above sea level. The EACD-3D program computes the static displacements in all the degrees of freedom in the dam idealization; however, only the translations at the nodes on the mid-surface of the shell in the three global coordinates are printed by the program. Such results are presented in Tables 1 and 2, only for the mid-surface nodes specified in the workshop instructions.

The EACD-3D program evaluates the stresses at the four Gauss quadrature points in the interior of each element, which are linearly extrapolated to determine the stresses on the upstream and downstream faces of the dam. At each stress point for both types of elements, the program provides the surface stresses defined with respect to a local axis normal to the dam face, together with two axes tangent to the face in the arch and cantilever directions; the surface principal stresses and their orientation are also computed by the program.

The stresses due to the two static loading conditions are presented in Figs. 3 and 4 and Tables 3 and 4. Contour plots of the arch and cantilever stresses on the upstream and downstream faces due to the dead weight of the dam are shown in Fig. 3, and those due to hydrostatic pressures are presented in Fig. 4, and the combined stresses in Fig. 5. Tables 3 and 4 list the two surface principal stresses at selected locations which are not coincident with the surface nodes specified in the workshop instructions, but are close to them. The locations for which surface stresses are available are shown (+) in Fig. 6 on the dam faces, and are identified in Tables 3 and 4 as location points 2', 5', etc., where 2' indicates the location closest to node 2. The program does not provide stresses at the mid-surface nodes.

Vibration Frequencies and Mode Shapes

The EACD-3D program determines the frequencies and mode shapes of the dam supported on flexible foundation rock with no impounded water; the foundation rock is assumed to be massless in the dynamic analysis. These mode shapes are used as generalized coordinates to reduce the number of degrees of freedom in the frequency domain analysis of dam response.

The vibration properties of the Talvacchia dam-water-foundation rock system were evaluated by the EACD-3D program for four cases: rigid foundation without water, flexible foundation without water, rigid foundation with water impounded to elevation 491 m above sea level, and flexible foundation with water. For the first two cases the results were directly provided by the program output. For the third and fourth cases, with impounded water but neglecting water compressibility effects, the results were obtained by a supplementary solution of a small eigenproblem in the generalized coordinate domain.

The first six frequencies of the dam are listed in Table 5 for the four cases. The first six vibration mode shapes are plotted in Fig. 7 for three of the aforementioned cases. In addition, the global coordinate displacements of these mode shapes for the two cases specified in the workshop instructions are listed in Tables 6a through 6f and 7a through 7f, respectively. These are displacements at the mid-surface nodes specified in the workshop instructions. Each mode shape has been normalized to a unit value for the largest nodal displacement component.

Concluding Remarks

It is evident from Table 5 that the impounded water has a relatively small influence on the vibration frequencies because the water level is well below the crest of Talvacchia Dam. As a result, water compressibility or hydrodynamic wave absorption at the reservoir boundary would be

expected to have even smaller influence on the vibration frequencies. Analyses including these effects were therefore not carried out. However, these factors may have significant influence on the earthquake response of the dam because of additional damping arising from radiation of hydrodynamic waves in the upstream direction and their absorption at the reservoir boundary.

References

1. K-L. Fok, J. F. Hall, and A. K. Chopra, *EACD-3D: A Computer Program for Three-Dimensional Earthquake Analysis of Concrete Dams*, Report No. UCB/EERC-86/09, Earthquake Engineering Research Center, University of California at Berkeley, July, 1986, 144 pages.

2. K-L. Fok and A. K. Chopra, "Earthquake Analysis of Arch Dams including Dam-Water Interaction, Reservoir Boundary Absorption, and Foundation Flexibility," *Earthquake Engineering and Structural Dynamics*, Vol. 14, 1986, pp. 155-184.

Table 1 — Displacements (in meter) of the Dam due to Dead Weight

Node	Displ.x	Displ.y	Displ.z
2	0.7483E−03	0.0000E+00	−0.3207E−02
5	−0.6135E−03	0.0000E+00	−0.2684E−02
8	−0.5747E−03	−0.1608E−03	−0.2589E−02
11	−0.2485E−03	−0.4501E−03	−0.1951E−02
14	−0.5051E−04	−0.4546E−03	−0.9961E−03
17	−0.1360E−03	−0.1958E−03	−0.3910E−03
20	−0.1430E−02	0.0000E+00	−0.2204E−02
23	−0.1339E−02	0.7512E−04	−0.2125E−02
26	−0.6743E−03	0.4409E−04	−0.1561E−02
29	−0.2979E−04	−0.1125E−03	−0.8314E−03
32	−0.7258E−03	0.0000E+00	−0.1764E−02
35	−0.6171E−03	0.6950E−04	−0.1670E−02
38	0.7865E−04	0.1041E−04	−0.1256E−02
41	0.1655E−03	0.0000E+00	−0.1522E−02

Table 2 — Displacements (in meter) of the Dam due to Hydrostatic Pressure

Node	Displ.x	Displ.y	Displ.z
2	0.2347E−01	0.0000E+00	−0.1212E−02
5	0.2048E−01	0.0000E+00	−0.2693E−03
8	0.1892E−01	−0.1195E−02	−0.1694E−03
11	0.9520E−02	−0.1110E−02	0.2307E−03
14	0.2072E−02	0.8522E−03	0.1034E−03
17	0.8914E−03	0.6986E−03	−0.1507E−03
20	0.1440E−01	0.0000E+00	0.1218E−02
23	0.1320E−01	−0.1074E−02	0.1136E−02
26	0.5965E−02	−0.7476E−03	0.5320E−03
29	0.1274E−02	0.5468E−03	0.1446E−03
32	0.5837E−02	0.0000E+00	0.1314E−02
35	0.5134E−02	−0.3138E−03	0.1094E−02
38	0.1410E−02	−0.8370E−05	0.9025E−03
41	0.1456E−02	0.0000E+00	0.1624E−02

Table 3 — Surface Principal Stresses (in Megapascal) in the Dam due to Dead Weight

Stress Point*	Principal Stresses	
	P_1	P_2
1′	−0.5530E−01	−0.1026E+01
3′	−0.3277E−01	−0.1154E+01
4′	−0.7419E−01	−0.4020E+00
6′	−0.4809E+00	−0.5680E+00
7′	−0.4657E−01	−0.3842E+00
9′	−0.4662E+00	−0.5840E+00
10′	0.1884E+00	−0.1971E+00
12′	−0.2380E+00	−0.8246E+00
13′	0.2592E+00	0.9649E−01
15′	0.1757E+00	−0.1101E+01
16′	0.5967E+00	0.9922E−01
18′	0.1616E+00	−0.1074E+01
19′	0.2456E+00	0.1206E+00
21′	−0.1486E+00	−0.1114E+01
22′	0.2616E+00	0.1090E+00
24′	−0.1362E+00	−0.1137E+01
25′	0.2579E+00	−0.9370E−01
27′	0.1536E+00	−0.1061E+01
28′	0.1541E+00	−0.5966E+00
30′	0.3110E+00	−0.7505E+00
31′	0.2371E+00	−0.4261E+00
33′	−0.1325E+00	−0.9841E+00
34′	0.2064E+00	−0.5765E+00
36′	−0.1283E+00	−0.8908E+00
37′	−0.3472E−01	−0.1307E+01
39′	0.2244E+00	−0.4539E+00
40′	−0.1550E+00	−0.1480E+01
42′	−0.5449E−01	−0.1118E+00

* n' indicates stress point closest to nodal point no. n for which stresses were available.

Table 4 — Surface Principal Stresses (in Megapascal) in the Dam due to Hydrostatic Pressure

Stress Point*	Principal Stresses	
	P_1	P_2
1′	−0.1225E+00	−0.3264E+01
3′	0.1118E+00	−0.9650E+00
4′	−0.1151E+01	−0.4209E+01
6′	0.8079E+00	−0.1537E+01
7′	−0.1132E+01	−0.4157E+01
9′	0.8121E+00	−0.1621E+01
10′	−0.1038E+01	−0.2980E+01
12′	0.8045E+00	−0.2581E+01
13′	−0.8231E+00	−0.1177E+01
15′	0.1114E+01	−0.2739E+01
16′	−0.3558E+00	−0.1759E+01
18′	0.5957E+00	−0.1493E+01
19′	−0.1117E+01	−0.4034E+01
21′	0.5655E+00	−0.1408E+01
22′	−0.1058E+01	−0.3926E+01
24′	0.5723E+00	−0.1475E+01
25′	−0.6903E−01	−0.1446E+01
27′	0.1380E+00	−0.3304E+01
28′	0.7920E+00	−0.4139E+00
30′	−0.7574E−01	−0.3498E+01
31′	0.8587E+00	−0.1770E+01
33′	−0.3506E+00	−0.1381E+01
34′	0.1131E+01	−0.1520E+01
36′	0.1267E+00	−0.1993E+01
37′	0.2677E+01	0.6184E−01
39′	−0.2445E+00	−0.4016E+01
40′	0.2989E+01	0.8963E−01
42′	−0.9496E−01	−0.3737E+01

* n' indicates stress point closest to nodal point no. n for which stresses were available.

Table 5 — Natural Vibration Frequencies (Hz) of the Dam

Mode	Type	Rigid Fdn. w/o Water	Flex. Fdn. w/o Water	Rigid Fdn. w/ Water	Flex. Fdn. w/ Water
1	antisym.	4.31	3.78	4.13	3.58
2	sym.	4.59	4.13	4.30	3.79
3	sym.	5.72	5.31	5.62	5.14
4	antisym.	6.75	6.26	6.63	6.12
5	sym.	8.61	7.92	8.06	7.03
6	sym.	9.46	8.36	8.50	7.89

Table 6a — First Vibration Mode Shape of Dam on Rigid Foundation without Water

Node	Displ.x	Displ.y	Displ.z
1	0.0000E+00	−0.2685E+00	0.0000E+00
2	0.6755E+00	−0.3249E+00	−0.1713E+00
3	0.8730E+00	−0.4233E+00	−0.2040E+00
4	0.1713E+00	−0.8046E−01	−0.2633E−01
5	0.0000E+00	0.0000E+00	0.0000E+00
6	0.0000E+00	−0.1798E+00	0.0000E+00
7	0.3788E+00	−0.2090E+00	−0.6234E−01
8	0.4654E+00	−0.2402E+00	−0.5127E−01
9	0.6363E−01	−0.3760E−01	0.3819E−02
10	0.0000E+00	0.0000E+00	0.0000E+00
11	0.0000E+00	−0.7215E−01	0.0000E+00
12	0.1344E+00	−0.8335E−01	0.5372E−02
13	0.1111E+00	−0.6855E−01	0.1360E−01
14	0.0000E+00	0.0000E+00	0.0000E+00
15	0.0000E+00	−0.1400E−01	0.0000E+00
16	0.1689E−01	−0.1443E−01	0.6761E−02
17	0.0000E+00	0.0000E+00	0.0000E+00
18	0.0000E+00	0.0000E+00	0.0000E+00
19	0.0000E+00	0.0000E+00	0.0000E+00
20	0.0000E+00	0.0000E+00	0.0000E+00

Table 6b — Second Vibration Mode Shape of Dam on Rigid Foundation without Water

Node	Displ.x	Displ.y	Displ.z
1	0.1000E+01	0.0000E+00	−0.2321E+00
2	0.7929E+00	−0.2753E−01	−0.1751E+00
3	−0.9253E−01	0.1529E+00	0.5048E−01
4	−0.1436E+00	0.1327E+00	0.4242E−01
5	0.0000E+00	0.0000E+00	0.0000E+00
6	0.5921E+00	0.0000E+00	−0.8656E−01
7	0.4776E+00	−0.1647E−01	−0.6363E−01
8	−0.5128E−02	0.7130E−01	0.1365E−01
9	−0.4207E−01	0.5196E−01	0.3003E−02
10	0.0000E+00	0.0000E+00	0.0000E+00
11	0.2247E+00	0.0000E+00	0.1121E−01
12	0.1799E+00	−0.9362E−02	0.1109E−01
13	0.8885E−02	0.1917E−01	0.3171E−02
14	0.0000E+00	0.0000E+00	0.0000E+00
15	0.3264E−01	0.0000E+00	0.1189E−01
16	0.2326E−01	−0.9932E−03	0.8589E−02
17	0.0000E+00	0.0000E+00	0.0000E+00
18	0.0000E+00	0.0000E+00	0.0000E+00
19	0.0000E+00	0.0000E+00	0.0000E+00
20	0.0000E+00	0.0000E+00	0.0000E+00

Table 6c — Third Vibration Mode Shape of Dam on Rigid Foundation without Water

Node	Displ.x	Displ.y	Displ.z
1	0.7114E−01	0.0000E+00	−0.1263E−01
2	0.2527E+00	−0.8634E−01	−0.6494E−01
3	0.8330E+00	−0.4164E+00	−0.2273E+00
4	0.2957E+00	−0.1751E+00	−0.6295E−01
5	0.0000E+00	0.0000E+00	0.0000E+00
6	0.2926E−01	0.0000E+00	−0.7406E−02
7	0.1149E+00	−0.4204E−01	−0.2437E−01
8	0.3594E+00	−0.1702E+00	−0.5344E−01
9	0.9230E−01	−0.5715E−01	0.8846E−03
10	0.0000E+00	0.0000E+00	0.0000E+00
11	0.3325E−02	0.0000E+00	−0.2100E−02
12	0.2568E−01	−0.8261E−02	−0.1556E−02
13	0.6138E−01	−0.2827E−01	0.4884E−02
14	0.0000E+00	0.0000E+00	0.0000E+00
15	−0.2067E−02	0.0000E+00	−0.7119E−03
16	0.1861E−03	0.1854E−03	0.1606E−03
17	0.0000E+00	0.0000E+00	0.0000E+00
18	0.0000E+00	0.0000E+00	0.0000E+00
19	0.0000E+00	0.0000E+00	0.0000E+00
20	0.0000E+00	0.0000E+00	0.0000E+00

Table 6d — Fourth Vibration Mode Shape of Dam on Rigid Foundation without Water

Node	Displ.x	Displ.y	Displ.z
1	0.0000E+00	0.7789E−01	0.0000E+00
2	−0.6465E+00	0.1153E+00	0.1775E+00
3	0.3888E+00	−0.3316E+00	−0.1507E+00
4	0.5699E+00	−0.4401E+00	−0.1550E+00
5	0.0000E+00	0.0000E+00	0.0000E+00
6	0.0000E+00	0.4550E−01	0.0000E+00
7	−0.3583E+00	0.6637E−01	0.6896E−01
8	0.3655E−01	−0.7995E−01	−0.1874E−01
9	0.1519E+00	−0.1327E+00	−0.7728E−02
10	0.0000E+00	0.0000E+00	0.0000E+00
11	0.0000E+00	0.1339E−01	0.0000E+00
12	−0.1162E+00	0.2395E−01	0.8501E−03
13	−0.2519E−01	−0.1673E−02	−0.6965E−03
14	0.0000E+00	0.0000E+00	0.0000E+00
15	0.0000E+00	0.1283E−02	0.0000E+00
16	−0.1386E−01	0.2969E−02	−0.3422E−02
17	0.0000E+00	0.0000E+00	0.0000E+00
18	0.0000E+00	0.0000E+00	0.0000E+00
19	0.0000E+00	0.0000E+00	0.0000E+00
20	0.0000E+00	0.0000E+00	0.0000E+00

Table 6e — Fifth Vibration Mode Shape of Dam on Rigid Foundation without Water

Node	Displ.x	Displ.y	Displ.z
1	0.1000E+01	0.0000E+00	−0.3839E+00
2	0.3173E+00	0.1940E−01	−0.1708E+00
3	−0.3305E+00	0.1921E−01	0.1842E−01
4	0.7270E+00	−0.6192E+00	−0.2246E+00
5	0.0000E+00	0.0000E+00	0.0000E+00
6	0.4106E+00	0.0000E+00	−0.1608E+00
7	0.8161E−01	0.3162E−01	−0.7798E−01
8	−0.3530E+00	0.1187E+00	0.3008E−01
9	0.1502E+00	−0.1466E+00	−0.1572E−01
10	0.0000E+00	0.0000E+00	0.0000E+00
11	0.3842E−01	0.0000E+00	−0.3033E−01
12	−0.4375E−01	0.1759E−01	−0.2377E−01
13	−0.1154E+00	0.5007E−01	−0.9520E−02
14	0.0000E+00	0.0000E+00	0.0000E+00
15	−0.8537E−02	0.0000E+00	−0.7739E−02
16	−0.1419E−01	0.3272E−02	−0.8312E−02
17	0.0000E+00	0.0000E+00	0.0000E+00
18	0.0000E+00	0.0000E+00	0.0000E+00
19	0.0000E+00	0.0000E+00	0.0000E+00
20	0.0000E+00	0.0000E+00	0.0000E+00

Table 6f — Sixth Vibration Mode Shape of Dam on Rigid Foundation without Water

Node	Displ.x	Displ.y	Displ.z
1	0.1000E+01	0.0000E+00	−0.6211E+00
2	0.9519E+00	−0.1754E+00	−0.5757E+00
3	0.1990E+00	−0.1147E+00	−0.1782E+00
4	−0.2420E+00	0.1545E+00	0.4522E−01
5	0.0000E+00	0.0000E+00	0.0000E+00
6	−0.2208E+00	0.0000E+00	−0.1823E+00
7	−0.1591E+00	0.2872E−03	−0.1753E+00
8	−0.7340E−01	0.1030E−01	−0.7727E−01
9	−0.7528E−01	0.4636E−01	−0.6921E−02
10	0.0000E+00	0.0000E+00	0.0000E+00
11	−0.5859E+00	0.0000E+00	−0.4466E−01
12	−0.4956E+00	0.5431E−01	−0.4669E−01
13	−0.1152E+00	0.2896E−01	−0.3355E−01
14	0.0000E+00	0.0000E+00	0.0000E+00
15	−0.1490E+00	0.0000E+00	−0.3581E−01
16	−0.1144E+00	0.1109E−01	−0.2845E−01
17	0.0000E+00	0.0000E+00	0.0000E+00
18	0.0000E+00	0.0000E+00	0.0000E+00
19	0.0000E+00	0.0000E+00	0.0000E+00
20	0.0000E+00	0.0000E+00	0.0000E+00

Table 7a — First Vibration Mode Shape of Dam on Flexible Foundation with Water Level 491m a.s.l.

Node	Displ.x	Displ.y	Displ.z
1	0.0000E+00	−0.3240E+00	0.0000E+00
2	0.6329E+00	−0.3714E+00	−0.1371E+00
3	0.8940E+00	−0.4514E+00	−0.1680E+00
4	0.2324E+00	−0.1069E+00	−0.2211E−01
5	0.1639E−01	0.1399E−01	−0.9771E−03
6	0.0000E+00	−0.2231E+00	0.0000E+00
7	0.3890E+00	−0.2517E+00	−0.4637E−01
8	0.5315E+00	−0.2910E+00	−0.3089E−01
9	0.1154E+00	−0.6839E−01	0.1355E−01
10	0.1227E−01	0.5583E−02	0.6469E−02
11	0.0000E+00	−0.1070E+00	0.0000E+00
12	0.1681E+00	−0.1212E+00	0.1570E−01
13	0.1791E+00	−0.1168E+00	0.3432E−01
14	0.7314E−02	−0.1750E−01	0.2958E−01
15	0.0000E+00	−0.3789E−01	0.0000E+00
16	0.3528E−01	−0.4010E−01	0.1901E−01
17	0.2920E−02	−0.2731E−01	0.4119E−01
18	0.0000E+00	−0.1503E−01	0.0000E+00
19	0.1080E−02	−0.1596E−01	0.2001E−01
20	−0.2116E−03	−0.1608E−01	0.2406E−01

Table 7b — Second Vibration Mode Shape of Dam on Flexible Foundation with Water Level 491m a.s.l.

Node	Displ.x	Displ.y	Displ.z
1	0.1000E+01	0.0000E+00	−0.1789E+00
2	0.8158E+00	−0.1248E−01	−0.1340E+00
3	−0.3032E−01	0.1712E+00	0.4912E−01
4	−0.1635E+00	0.1857E+00	0.4531E−01
5	0.4965E−02	0.7180E−02	−0.1039E−02
6	0.6654E+00	0.0000E+00	−0.5829E−01
7	0.5549E+00	−0.1408E−01	−0.4082E−01
8	0.5021E−01	0.8245E−01	0.1607E−01
9	−0.4918E−01	0.9331E−01	−0.4208E−03
10	0.1237E−01	0.2391E−01	−0.1277E−01
11	0.3272E+00	0.0000E+00	0.3210E−01
12	0.2748E+00	−0.1191E−01	0.2960E−01
13	0.4760E−01	0.3155E−01	0.7590E−02
14	0.1420E−01	0.2820E−01	−0.1193E−01
15	0.8845E−01	0.0000E+00	0.3517E−01
16	0.7139E−01	−0.3388E−03	0.2818E−01
17	0.1236E−01	0.8333E−02	0.1154E−01
18	0.1188E−01	0.0000E+00	0.3707E−01
19	0.8769E−02	0.4321E−03	0.2975E−01
20	0.7038E−02	0.1035E−02	0.2375E−01

Table 7c — Third Vibration Mode Shape of Dam on Flexible Foundation with Water Level 491m a.s.l.

Node	Displ.x	Displ.y	Displ.z
1	−0.1798E+00	0.0000E+00	0.8785E−01
2	0.4542E−01	−0.7403E−01	0.2416E−01
3	0.8476E+00	−0.4324E+00	−0.1954E+00
4	0.3934E+00	−0.2178E+00	−0.6787E−01
5	0.2409E−01	0.1870E−01	−0.1434E−02
6	−0.6246E−01	0.0000E+00	0.3484E−01
7	0.5197E−01	−0.4212E−01	0.1211E−01
8	0.4301E+00	−0.2048E+00	−0.4196E−01
9	0.1713E+00	−0.9305E−01	0.4189E−02
10	0.2149E−01	0.5895E−02	0.9995E−02
11	0.1770E−01	0.0000E+00	0.7102E−02
12	0.5199E−01	−0.1308E−01	0.7646E−02
13	0.1266E+00	−0.5125E−01	0.1468E−01
14	0.2120E−01	−0.5108E−02	0.2281E−01
15	0.1600E−01	0.0000E+00	0.4908E−02
16	0.1976E−01	−0.8380E−03	0.6535E−02
17	0.1046E−01	−0.2471E−03	0.1656E−01
18	0.3635E−02	0.0000E+00	0.6224E−02
19	0.3797E−02	0.1709E−02	0.7731E−02
20	0.3930E−02	0.1676E−02	0.8094E−02

Table 7d — Fourth Vibration Mode Shape of Dam on Flexible Foundation with Water Level 491m a.s.l.

Node	Displ.x	Displ.y	Displ.z
1	0.0000E+00	0.6455E−01	0.0000E+00
2	−0.5975E+00	0.9334E−01	0.1587E+00
3	0.3495E+00	−0.3395E+00	−0.1255E+00
4	0.6632E+00	−0.5191E+00	−0.1580E+00
5	0.1932E−01	0.6920E−02	−0.9622E−04
6	0.0000E+00	0.3442E−01	0.0000E+00
7	−0.3597E+00	0.5465E−01	0.6727E−01
8	0.2781E−01	−0.9506E−01	−0.6968E−02
9	0.2252E+00	−0.1987E+00	−0.2014E−02
10	0.9776E−02	−0.3000E−01	0.2988E−01
11	0.0000E+00	0.8429E−02	0.0000E+00
12	−0.1445E+00	0.2144E−01	0.4353E−02
13	−0.4248E−01	−0.9338E−02	0.9517E−02
14	0.2801E−02	−0.2504E−01	0.2814E−01
15	0.0000E+00	−0.6244E−03	0.0000E+00
16	−0.3249E−01	0.2682E−02	−0.3169E−02
17	−0.1261E−01	0.1059E−02	−0.1169E−02
18	0.0000E+00	−0.4119E−02	0.0000E+00
19	−0.6366E−02	−0.1860E−02	−0.5455E−02
20	−0.6827E−02	−0.6342E−03	−0.5066E−02

Table 7e — Fifth Vibration Mode Shape of Dam on Flexible Foundation with Water Level 491m a.s.l.

Node	Displ.x	Displ.y	Displ.z
1	0.1000E+01	0.0000E+00	−0.4543E+00
2	0.8157E+00	−0.1020E+00	−0.3869E+00
3	0.2094E+00	−0.1152E+00	−0.1487E+00
4	0.8898E−01	−0.8907E−01	−0.5201E−01
5	−0.3351E−02	−0.4042E−02	−0.2659E−02
6	0.2422E+00	0.0000E+00	−0.1833E+00
7	0.1667E+00	−0.1381E−01	−0.1555E+00
8	−0.4521E−01	0.1547E−01	−0.5659E−01
9	−0.1187E−02	−0.1215E−01	−0.1976E−01
10	−0.3784E−02	−0.6299E−02	−0.3906E−02
11	−0.2179E+00	0.0000E+00	−0.4153E−01
12	−0.2128E+00	0.2643E−01	−0.3959E−01
13	−0.1156E+00	0.3671E−01	−0.2964E−01
14	−0.1188E−01	−0.3311E−03	−0.1726E−01
15	−0.1450E+00	0.0000E+00	−0.2948E−01
16	−0.1256E+00	0.1033E−01	−0.2666E−01
17	−0.2856E−01	0.4461E−02	−0.2996E−01
18	−0.3759E−01	0.0000E+00	−0.3724E−01
19	−0.3025E−01	0.1671E−02	−0.3321E−01
20	−0.2526E−01	0.1521E−02	−0.2882E−01

Table 7f — Sixth Vibration Mode Shape of Dam on Flexible Foundation with Water Level 491m a.s.l.

Node	Displ.x	Displ.y	Displ.z
1	0.4636E+00	0.0000E+00	−0.1260E+00
2	−0.5761E−01	0.7403E−01	0.2433E−01
3	−0.3776E+00	0.4765E−01	0.6707E−01
4	0.7824E+00	−0.6626E+00	−0.2146E+00
5	0.2047E−01	−0.1861E−02	0.8228E−03
6	0.3788E+00	0.0000E+00	−0.8399E−01
7	0.8692E−01	0.3090E−01	−0.1942E−01
8	−0.3333E+00	0.1152E+00	0.5264E−01
9	0.2031E+00	−0.1893E+00	−0.6246E−02
10	0.1284E−01	−0.4675E−01	0.4178E−01
11	0.2421E+00	0.0000E+00	−0.2772E−01
12	0.1295E+00	−0.1715E−03	−0.1983E−01
13	−0.1048E+00	0.5360E−01	0.2052E−02
14	−0.2410E−02	−0.4797E−02	0.1752E−01
15	0.8637E−01	0.0000E+00	−0.7124E−02
16	0.5754E−01	−0.1241E−04	−0.9696E−02
17	0.1075E−02	0.8366E−02	−0.1113E−01
18	0.2538E−01	0.0000E+00	0.2411E−02
19	0.1796E−01	−0.5951E−03	−0.2130E−02
20	0.1317E−01	0.7303E−03	−0.4806E−02

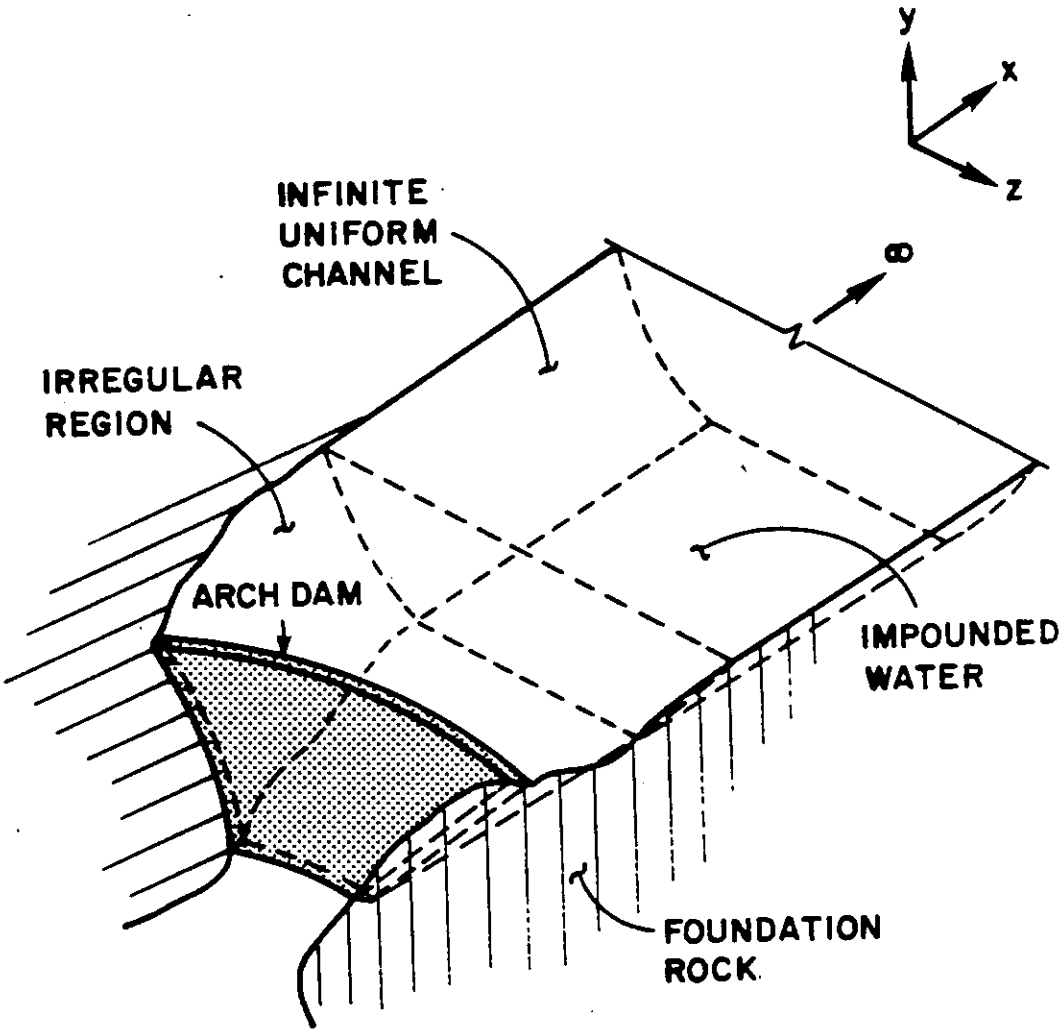

Fig. 1 -- Arch Dam-Water-Foundation Rock System

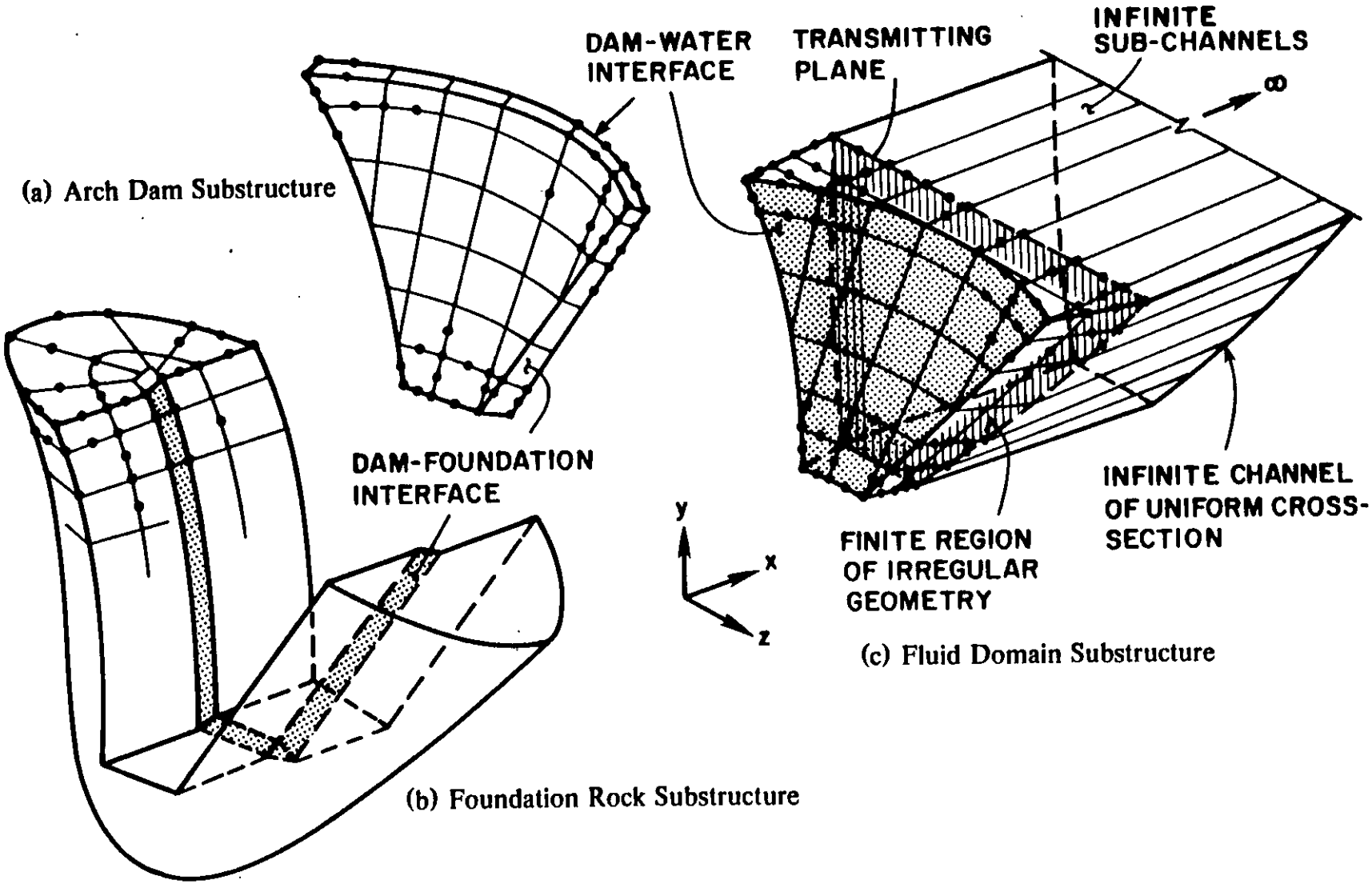

Fig. 2 -- Finite Element Models of Dam, Foundation Rock, and Fluid Domain Substructures

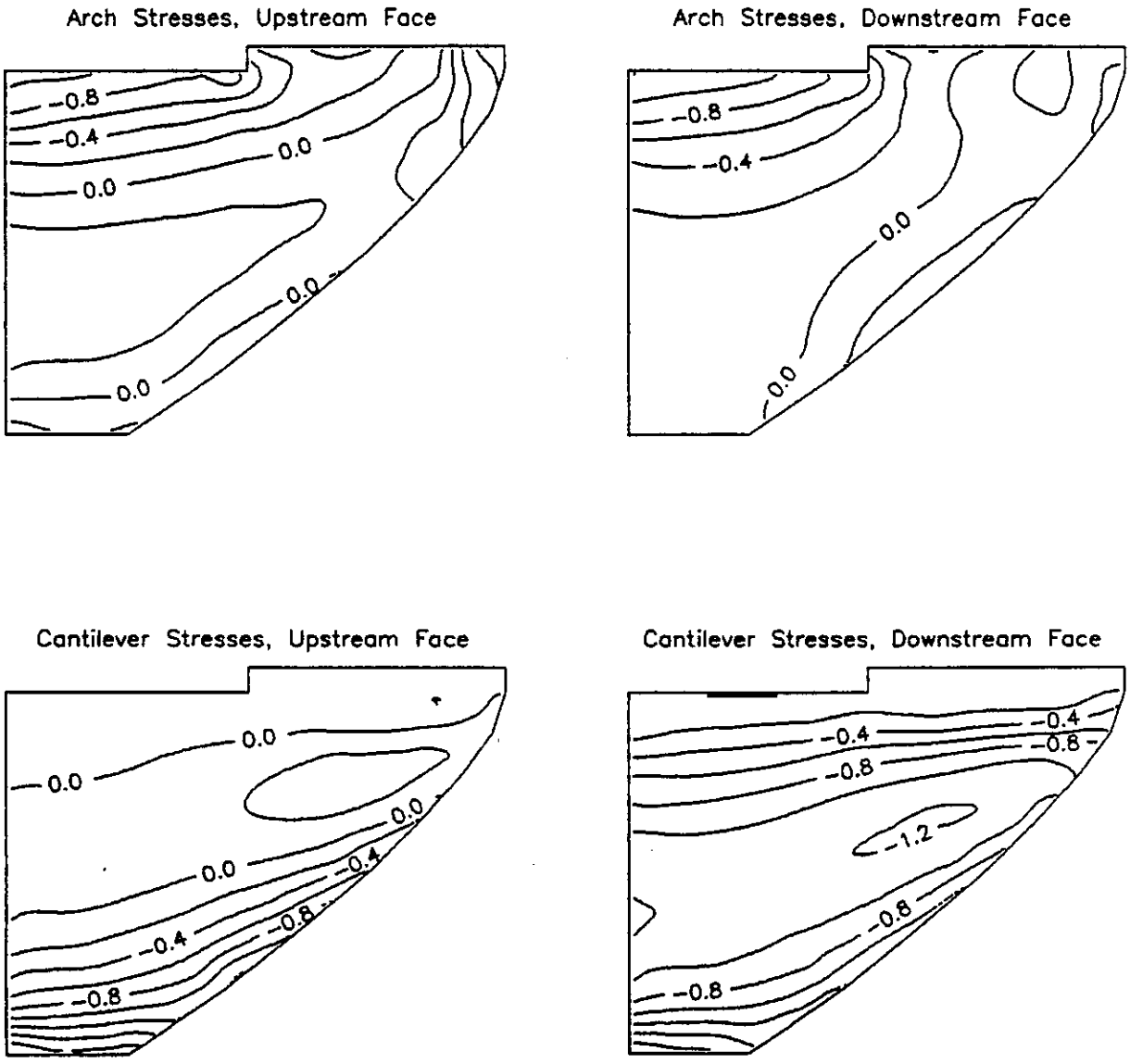

Fig. 3 — Arch and Cantilever Stresses (in Megapascal) on Upstream and Downstream Faces of the Dam due to Dead Weight

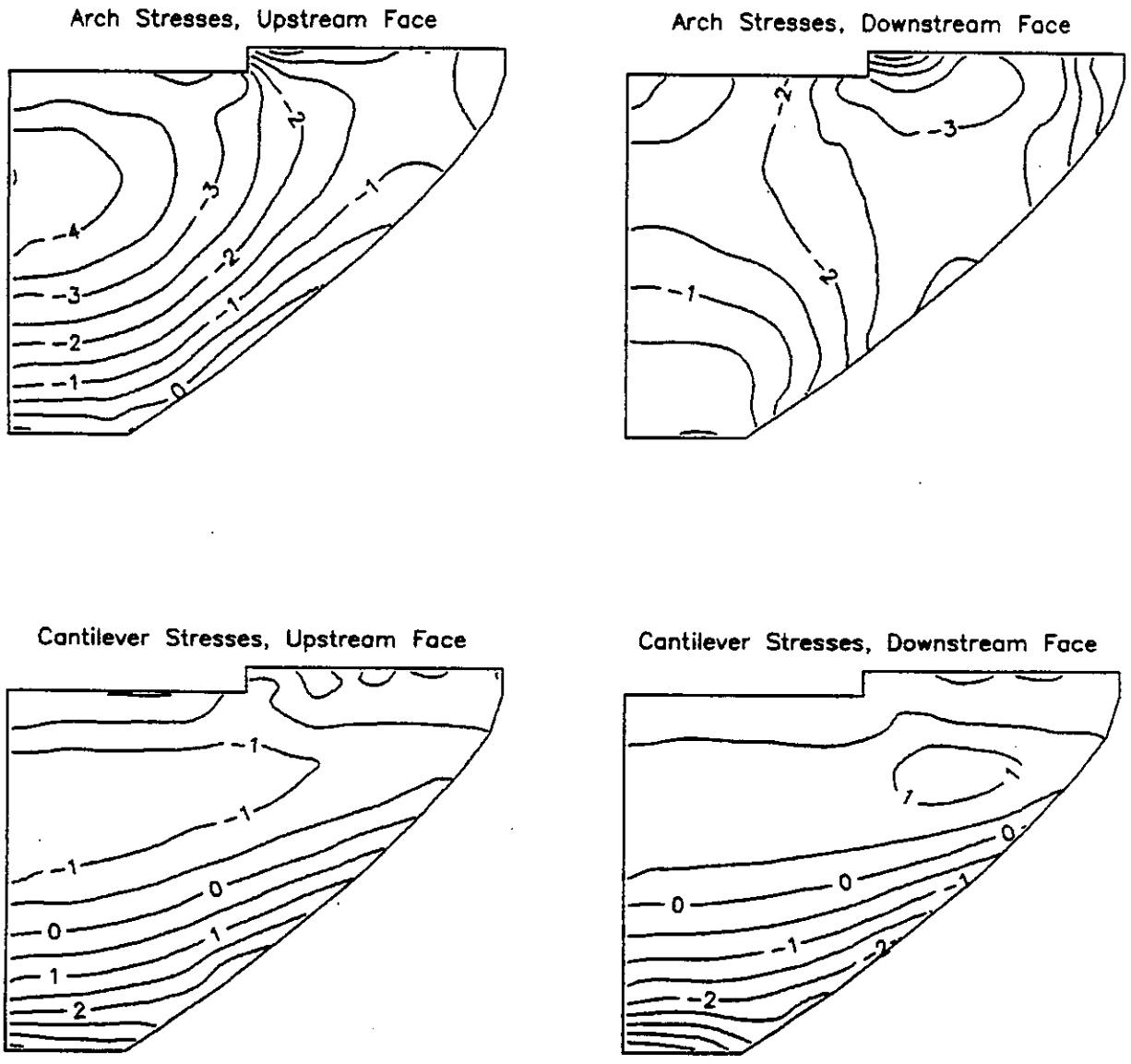

Fig. 4 — Arch and Cantilever Stresses (in Megapascal) on Upstream and Downstream Faces of the Dam due to Hydrostatic Pressure

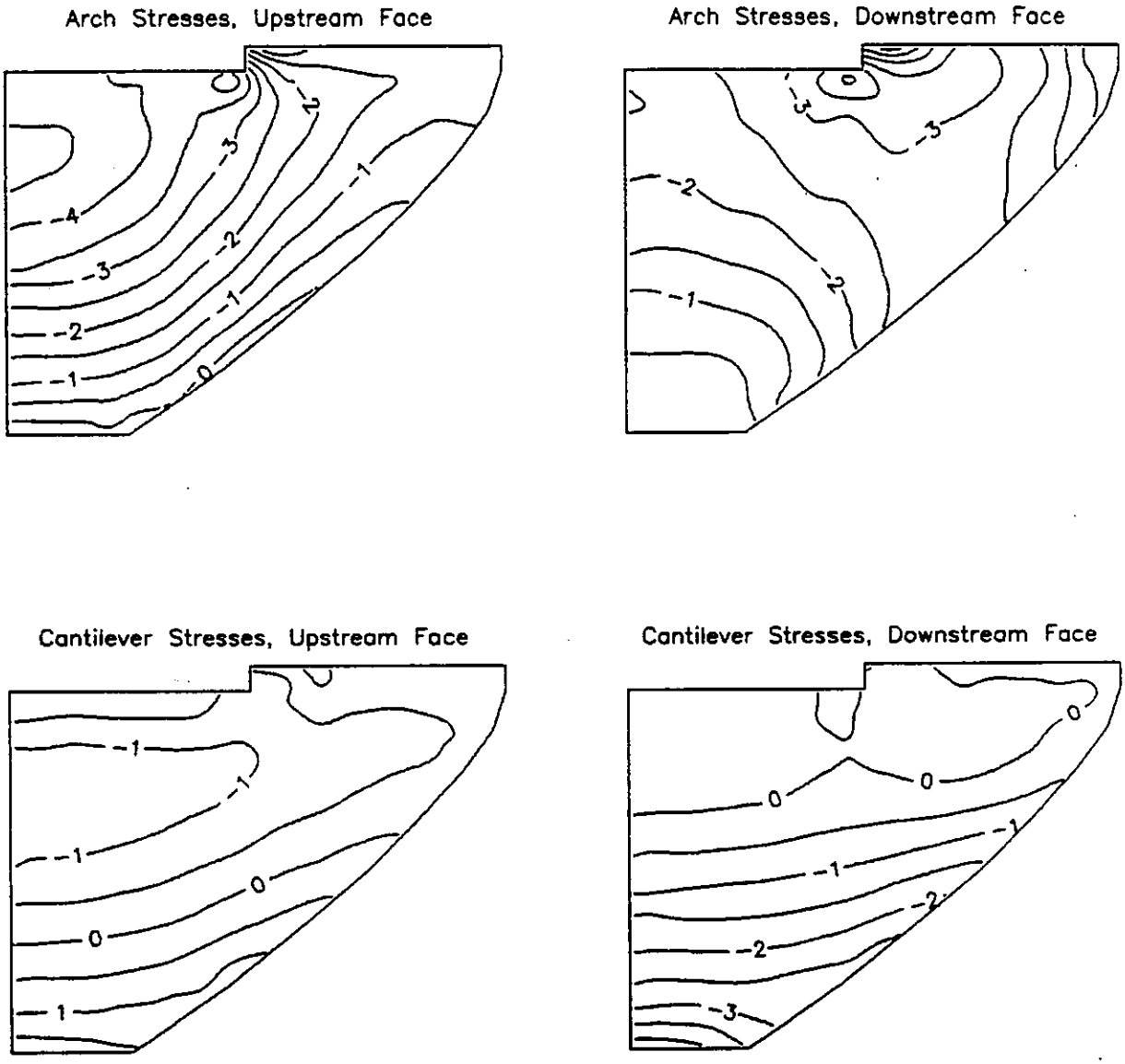

Fig. 5 — Arch and Cantilever Stresses (in Megapascal) on Upstream and Downstream Faces of the Dam due to Combined Dead Weight and Hydrostatic Pressure

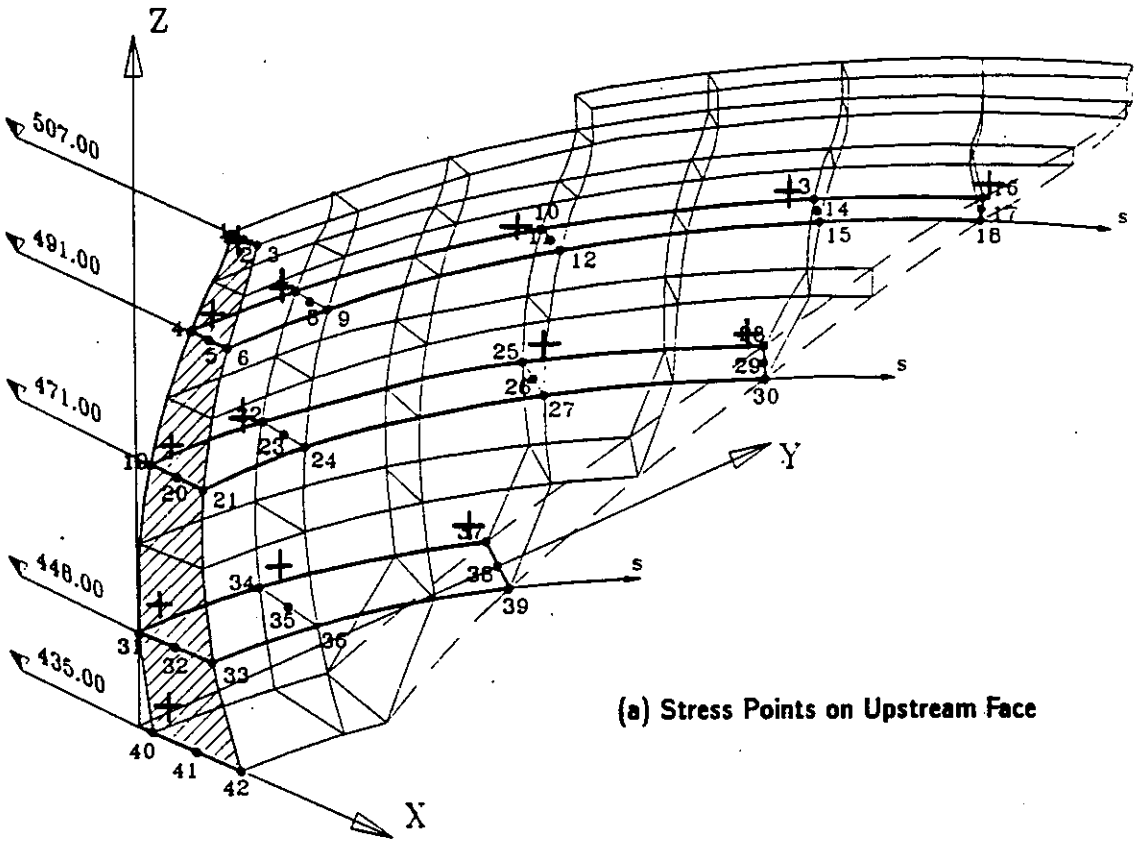

(a) Stress Points on Upstream Face

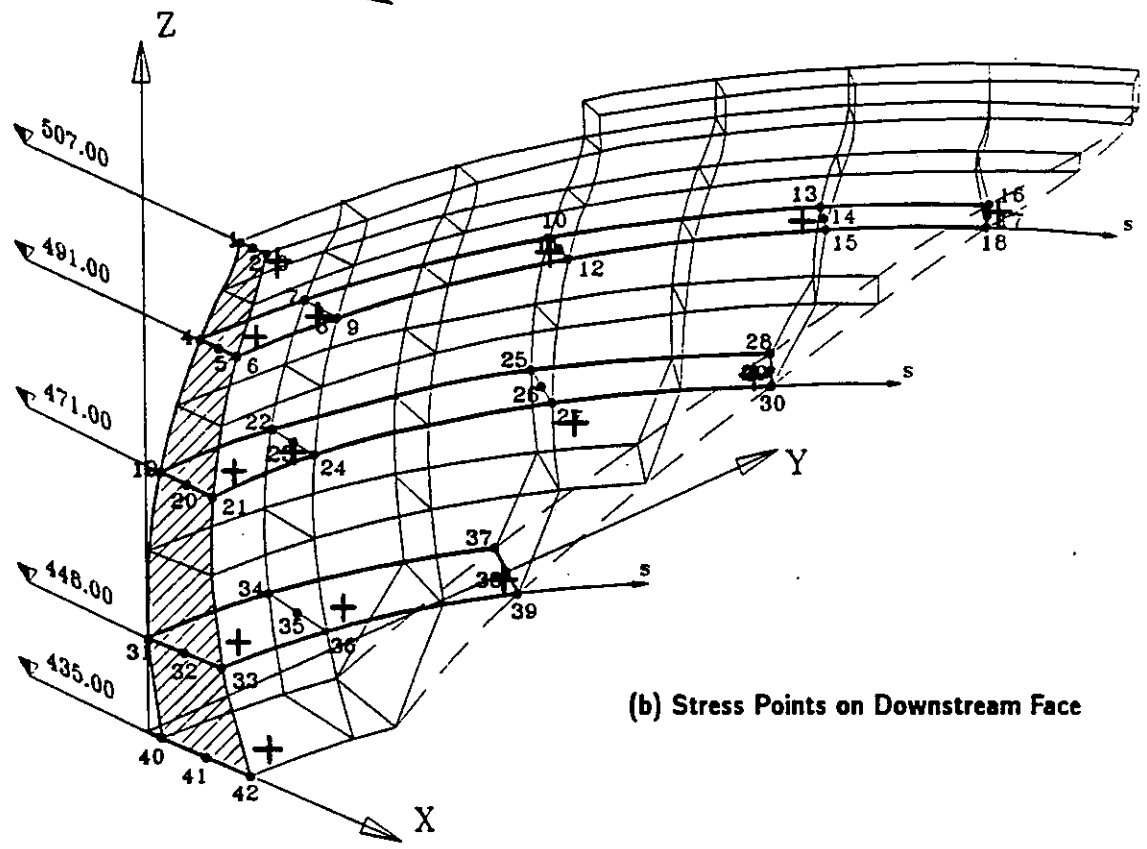

(b) Stress Points on Downstream Face

Fig. 6 — Locations of Stress Points for Which Stresses Are Listed in Tables 3 and 4

Arch at 507.00 m a.s.l.

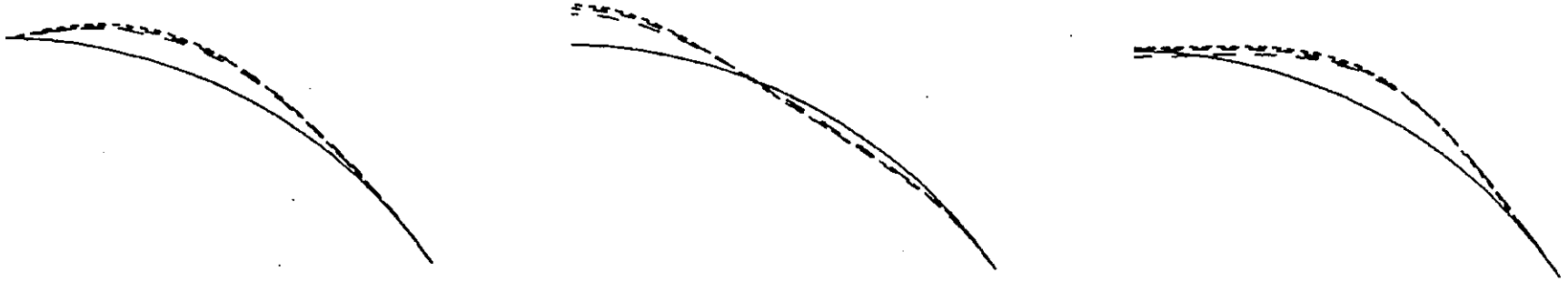

Cantilever at s=0 (Symm. Mode) or s=16m (Antisymm. Mode)

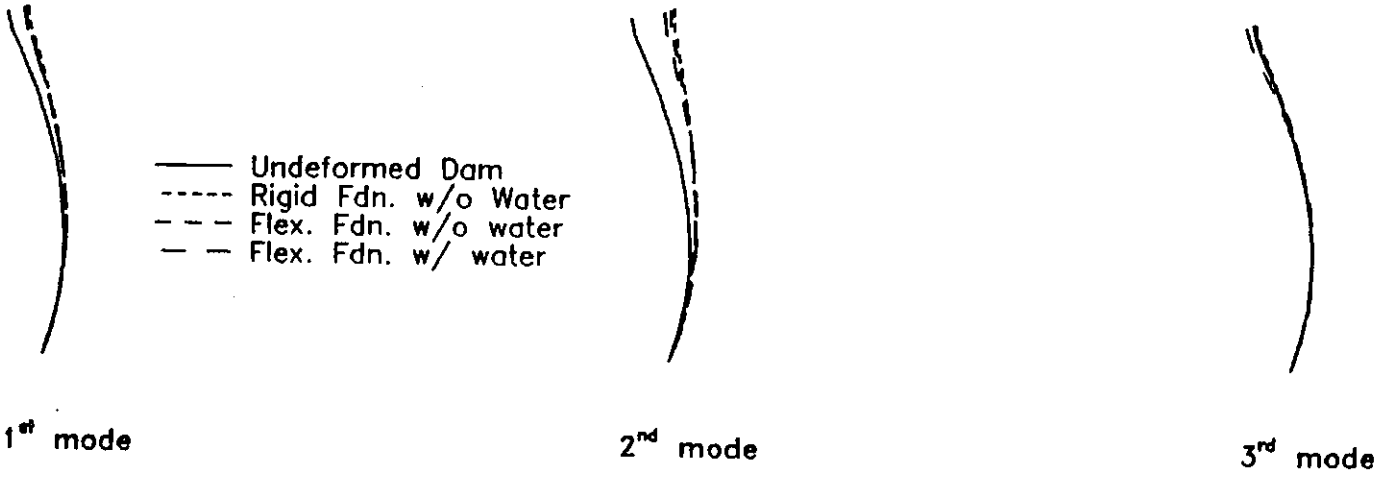

Fig. 7a -- Shapes of the First Three Vibration Modes of Dam

Arch at 507.00 m a.s.l.

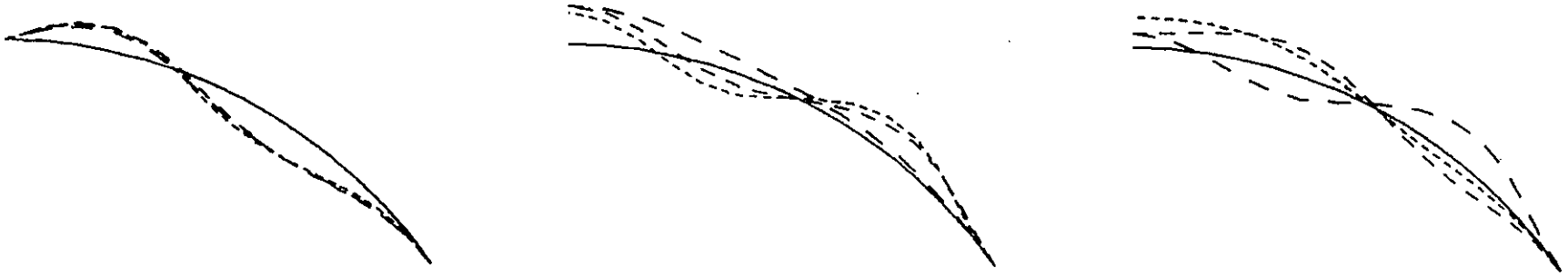

Cantilever at s=0 (Symm. Mode) or s=16m (Antisymm. Mode)

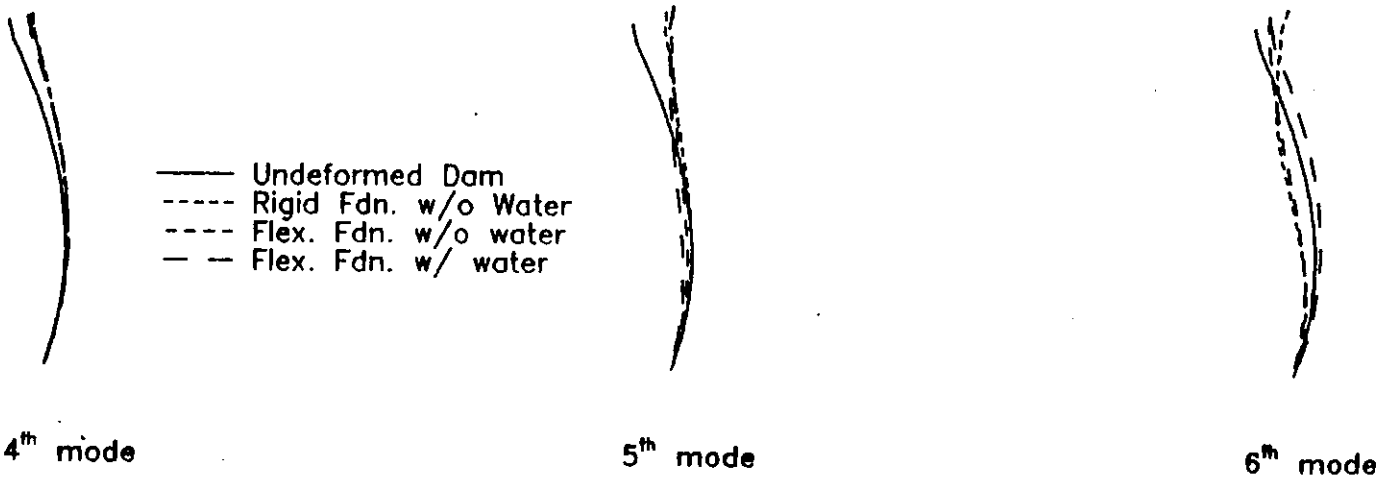

Fig. 7b -- Shapes of the 4th 5th and 6th Vibration Modes of Dam

WORKSHOP ON NUMERICAL ANALYSIS OF DAMS

G. Ruggeri (*), P. Palumbo (*), G. Mazza'(**)
(*) ISMES S.p.A. Bergamo -(**) ENEL CRIS Milano

LINEAR-ELASTIC ANALYSIS OF A DOUBLE CURVATURE ARCH DAM: THE TALVACCHIA DAM (Italy)

1.0 INTRODUCTION

This report describes the benchmark analysis of the Talvacchia Dam and summarizes the essential results obtained.

The analyses were carried out using the finite element program FIESTA.

FIESTA is a computer program for the analysis of solid structures based on the p-version of the finite element method.

This report starts with a brief description of FIESTA and then presents the various results specified for the Benchmark Workshop.

Geometrical, physical and mechanical parameters supplied for the benchmark solution will not be repeated here. It is assumed that the benchmark requirements are well known to the reader. The finite element models that were adopted are represented in figure 4.

2.0 FIESTA DESCRIPTION

2.1 Theoretical background

There are two versions of the finite element method, the h-version and the p-version. Most of the current finite element programs are based on the h-version. FIESTA, on the other hand, is based on the p-version.

The goal of the computation, for either the h-version or p-version, is to produce an approximate solution so that the error between the computed results from the finite element analysis and the exact solution is within acceptable bounds.

The error of approximation can be made arbitrarily small by increasing the

number of degrees of freedom. Depending on whether the degrees of freedom are increased by mesh refinement or by increased sophistication of elements, we speak of h-convergence or p-convergence, respectively.

In the conventional convergence process, called h-convergence, the number and type of shape functions are fixed for each element and the finite element mesh is refined in such a way that the maximum diameter of the element "h" becomes smaller and smaller. Thus, the error of approximation is controlled by the size of the elements (see figure 1).

The p-version of the finite element method offers a more efficient convergence process that has been investigated in theoretical studies, tested in numerical experiments and applied to the solution of large practical problems.
The distinguishing feature of this convergence process is that the number and distribution of finite element is fixed, while the number of shape functions, which are complete polynomials of order p, are progressively increased over some or all elements (see figure 1).
Each level of approximation is obtained by adding higher order shape functions to the ones used in the previous level. Therefore the stiffness matrices of lower order elements are embedded in the stiffness matrices of higher order elements (hierarchical property).
Because of the hierarchical character of the FIESTA shape functions, important computational reductions are achieved in the numerical integration process: the stiffness terms corresponding to low p values are not changed when p is increased. Consequently, low order integration rules are used for the low order terms of the stiffness matrix and progressively higher order rules are employed for the higher order terms.

It has been established that the rate of p-convergence is twice as fast (on a logarithmic scale) as the rate of h-convergence when uniform mesh refinement is used (see figure 2).

2.2 Type of elements

The element library of FIESTA is comprised of solid elements of various shapes including hexahedra (bricks), triangular prisms (wedges), tetrahedra and pyramids. The element shapes can have either straight or curved edges. The

element shapes and their nodal numbering schemes are shown in figure 3.
All element types can be used within the same model. Additionally, the joining of elements with different polynomial orders is permitted.

2.3 Type of materials

The current release of FIESTA is capable of representing the behavior of linear elastic materials. The material may be isotropic, transversely isotropic, orthotropic as well as generally anisotropic.

2.4 Solution techniques

A frontal solver method is used in FIESTA. Nodes can be numbered arbitrarily with any gap in the sequence; the element ordering, as it was input, can be easily redesignated manually and repeated for a minimum wave front size.
All changes to the model are therefore accomplished with few difficulties.

2.5 Thermal analysis with cyclic boundary conditions

The approach used in FIESTA, for the mathematical modeling of structures subject to periodic boundary conditions, is based on the assumption that the variable temperature can be obtained by superimposing the first few harmonics of a truncated Fourier series, of period T.

Denoting the 3D coordinates of a point in the domain of analysis by x, y, and z, the related temperature $\theta(x,y,z,t)$ can be expressed as:

$$\theta = \theta_0 + \Sigma_n \, [A_n \sin(n\omega t) + B_n \cos(n\omega t)] \qquad (1)$$

where θ_0 is the average value of the temperature, and

$$\begin{aligned} A_n &= A_n(x,y,z) \\ B_n &= B_n(x,y,z) \\ \omega &= 2\pi/T \end{aligned} \qquad (2)$$

Disregarding the mean temperature θ_0 (the effect of which can be considered by a separate computation and then added to the other partial results) the substitution of the periodic part of equation (1) into the heat conduction equation :

$$c\rho \, \partial\theta/\partial t = \lambda \, \nabla^2\theta + Q \qquad (3)$$

leads to a system of coupled equations. For each harmonic we can in fact write:

$$\begin{aligned} -c\rho \, n\omega A_n + \lambda \, \nabla^2 B_n &= Q_c \\ \lambda \, \nabla^2 A_n + c\rho \, n\omega B_n &= Q_s \end{aligned} \qquad (4)$$

where Q_s and Q_c indicate the sine and cosine components of internal heat generated per unit volume.

By applying the finite element solution technique, equations (4) can be expressed in a matrix form as:

$$\left|\begin{array}{c|c} -n\omega C & H \\ \hline H & n\omega C \end{array}\right| \left|\frac{A_n}{B_n}\right| = \left|\frac{Q_{1c}}{Q_{1s}}\right| \qquad (5)$$

where [C] denotes the heat capacity matrix and [H] the heat transfer matrix.

Equation (5) is solved for each individual sinusoidal component. Partial results of the various computations can then be added together so as to obtain the response of structure.

3.0 PRESENTATION OF RESULTS

3.1 Static analysis

Calculations were carried out discretizing dam and foundation using both p-level=2 and p-level=6. Presented results are grouped as follows:

a) Dead weight, in table 1 (p-level=6); 1.1 (p-level=2) and figures 5.1; 5.2; 5.3;

b) Hydrostatic pressure, in table 2 (p-level=6); 2.1 (p-level=2) and figures 6.1; 6.2; 6.3;

c) Thermal analysis with steady-state boundary conditions, in tables 3.1-a, 3.2 and figure 7.1; 7.2; 7.3;

d) Thermal analysis with periodic boundary conditions, in table 3.1-b.

3.2 Dynamic analysis

The finite element equations of motion of the dam and incompressible reservoir may be expressed as follows:

$$[M_s + M_f]\{\ddot{u}\} + [K]\{u\} = \{0\}$$

where $[M_s]$ and $[K]$ are the mass and stiffness matrices of the dam structures and $[M_f]$ is the added mass of the incompressible reservoir.

The vibration mode shapes $\{\Phi\}$ of the incompressible reservoir-dam system were calculated by solving the eigenproblem:

$$[K - \omega^2 M]\{\Phi\} = 0$$

in which $[M] = [M_s] + [M_f]$ is the combined mass of the dam-reservoir system. The mass matrix of the fluid $[M_f]$ was determined using an approach based on Laplace's equation with assigned boundary conditions; the method used is an approximate integral method which employs the superposition of fundamental solutions. These fundamental solutions are harmonic functions representing potential functions generated by a distribution of point sources.

The modal vectors are normalized such that the largest component is unity.

The first 6 natural frequencies and the corresponding modal shapes are presented for:

a) Dam on a rigid foundation without water, in tables 4.1; 4.2 and figure 8;

b) Dam on a flexible foundation, water level 491 m a.s.l, in tables 4.1; 4.3 and figure 9.

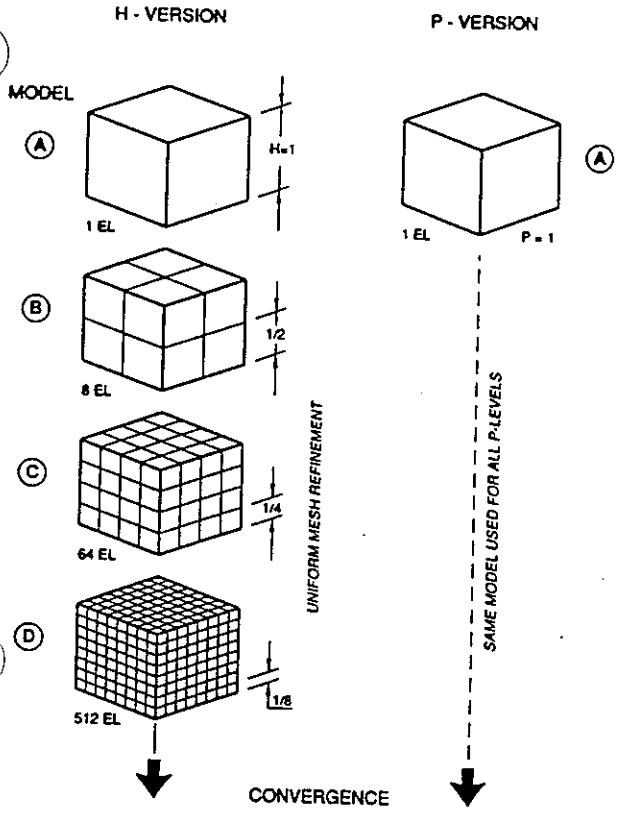

Fig. 1

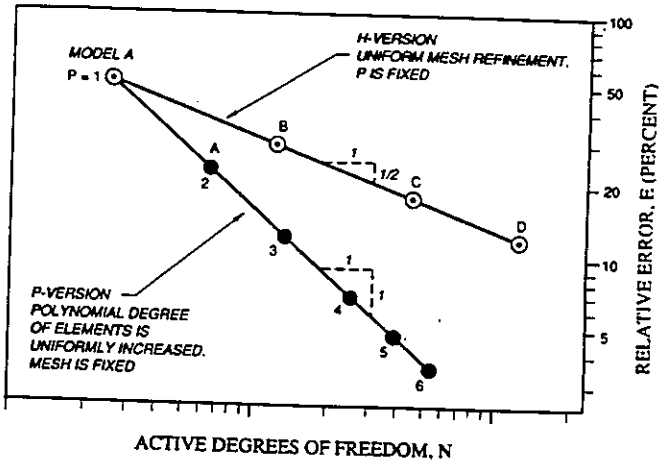

Fig. 2

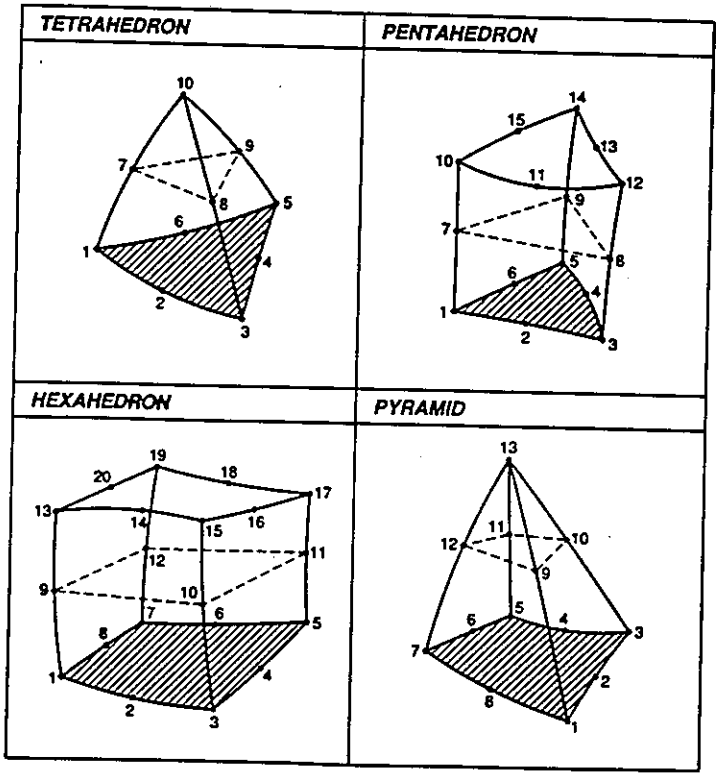

Fig. 3

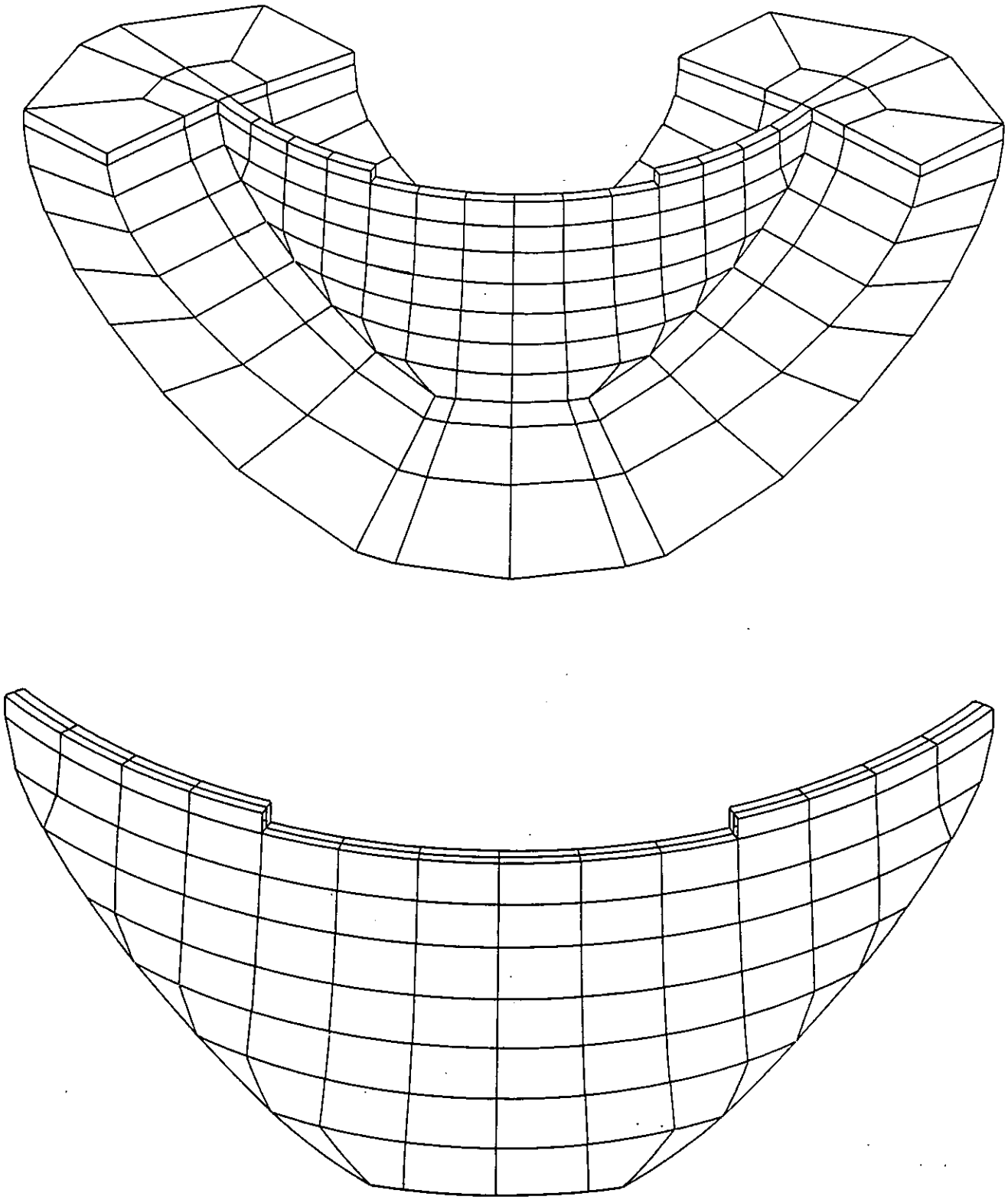

Finite element models of Talvacchia dam

Fig. 4

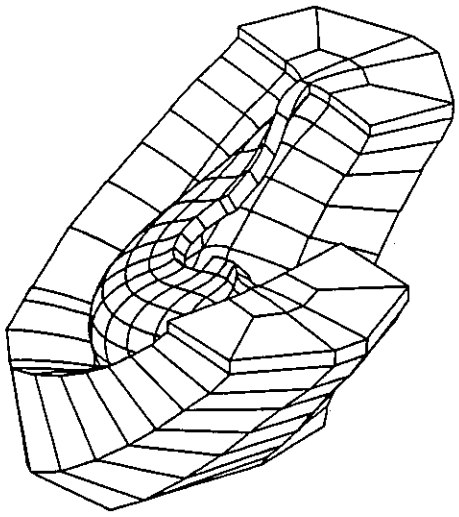

Deformed shape for dead weight

Fig. 5.1

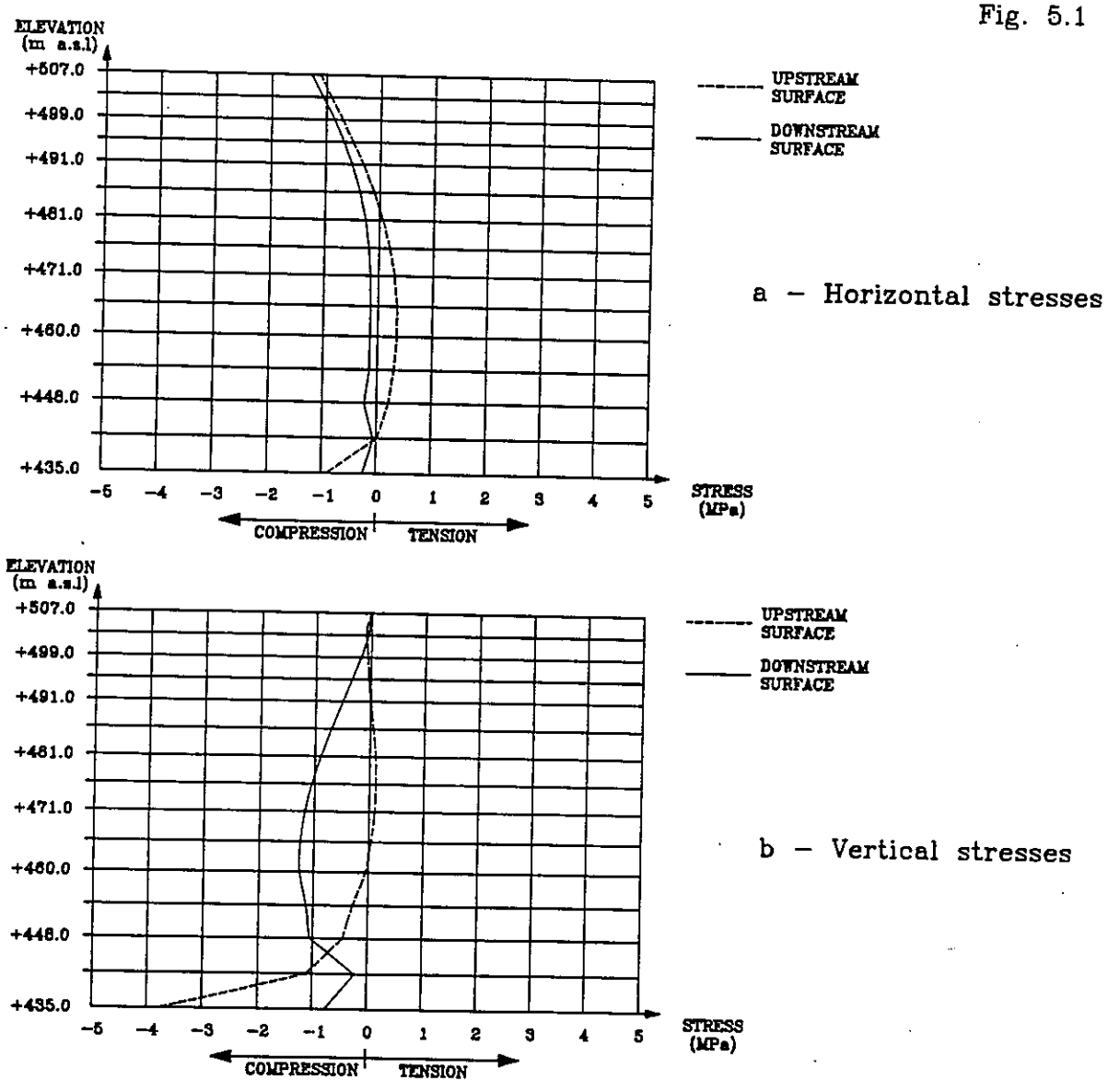

Dead weight : horizontal and vertical stresses in central cantilever

Fig. 5.2

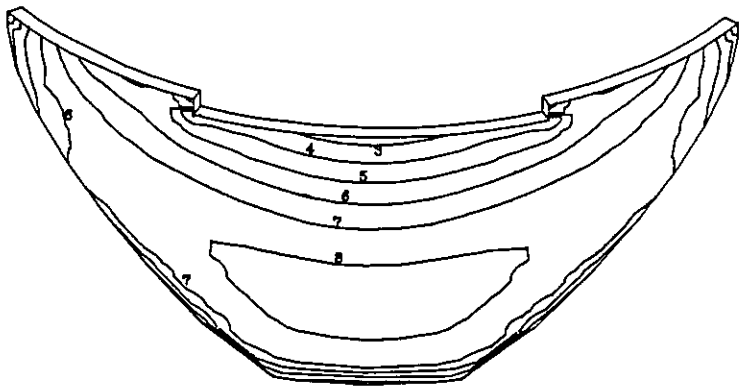

a – Arch stresses – Upstream Surface

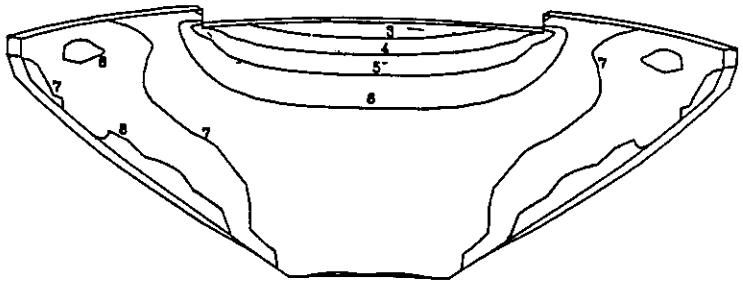

b – Arch stresses – Downstream surface

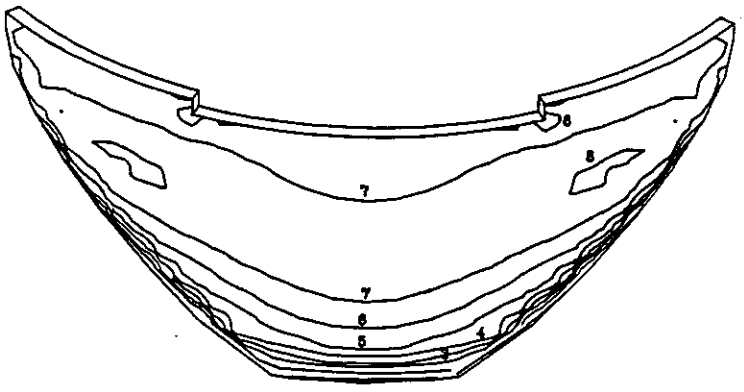

c – Cantilever stresses – Upstream Surface

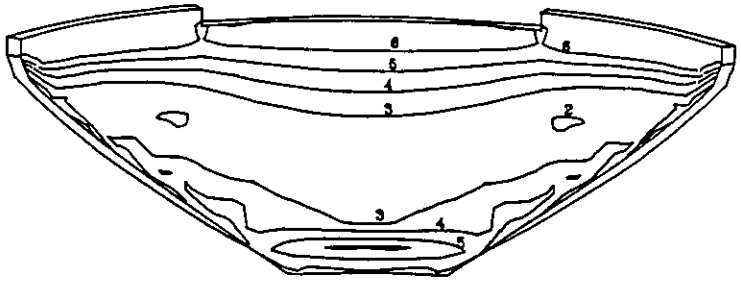

d – Cantilever stresses – Downstream surface

9	0.50
8	0.25
7	0.00
6	−0.25
5	−0.50
4	−0.75
3	−1.00
2	−1.25
1	−1.50 MPa

Dead weight – Arch and cantilever stresses

Fig. 5.3

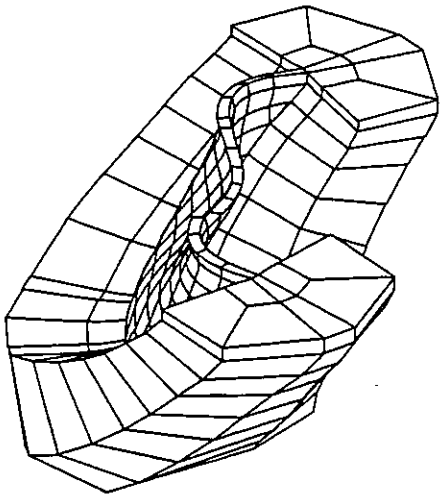

Deformed shape for hydrostatic pressure

Fig. 6.1

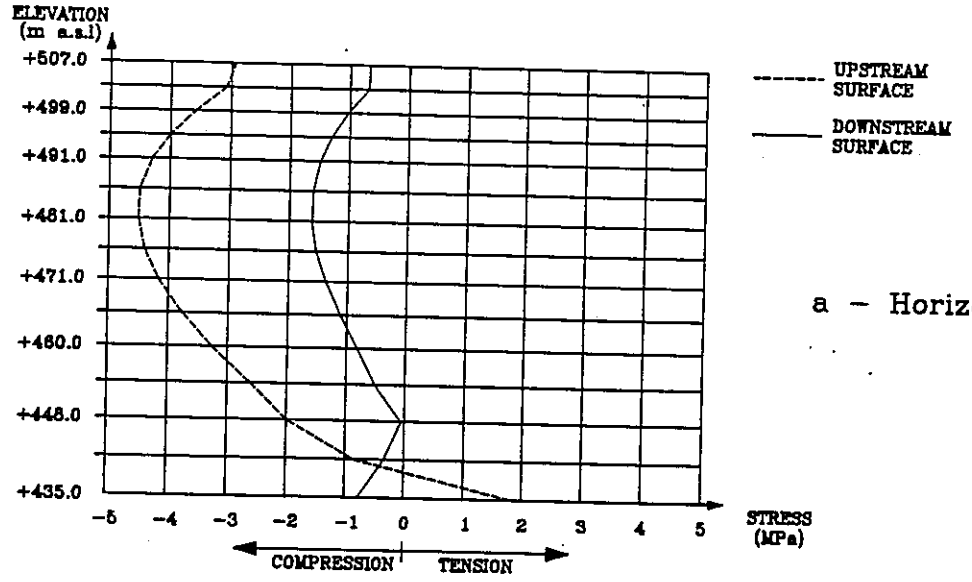

a – Horizontal stresses

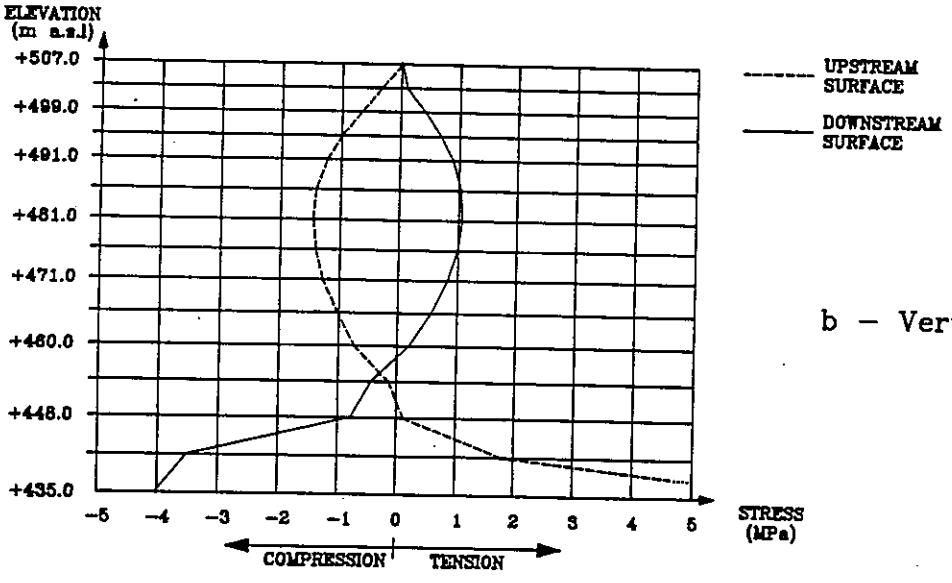

b – Vertical stresses

Hydrostatic pressure : horizontal and vertical stresses in central cantilever

Fig. 6.2

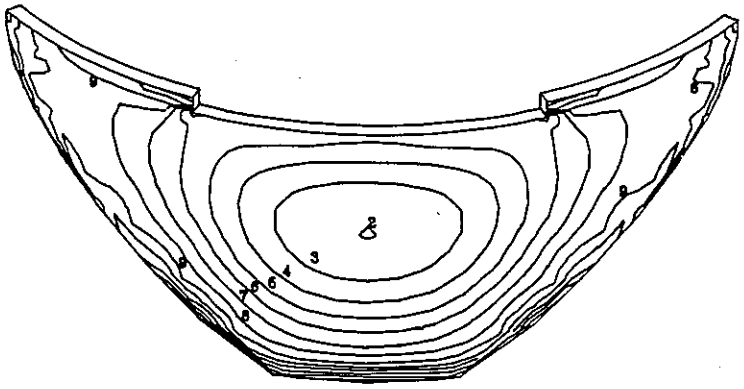

a – Arch stresses – Upstream Surface

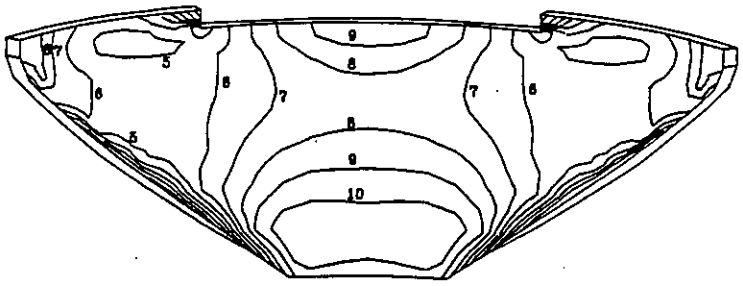

b – Arch stresses – Downstream surface

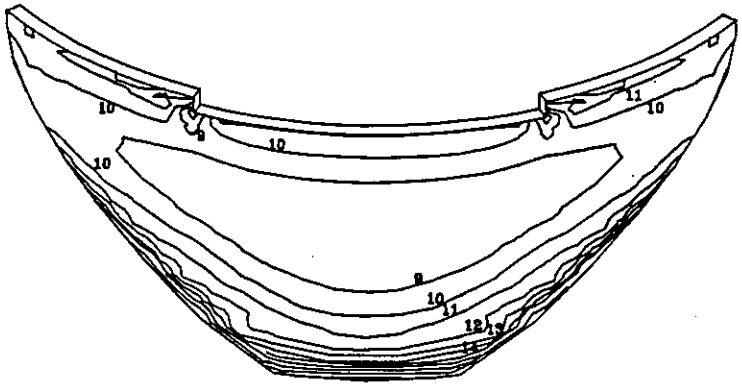

c – Cantilever stresses – Upstream Surface

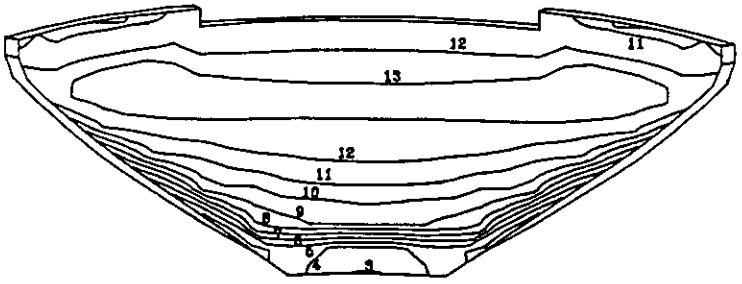

d – Cantilever stresses – Downstream surface

14	1.5
13	1.0
12	0.5
11	0.0
10	-0.5
9	-1.0
8	-1.5
7	-2.0
6	-2.5
5	-3.0
4	-3.5
3	-4.0
2	-4.5
1	-5.0 MPa

Hydrostatic pressure – Arch and cantilever stresses

Fig. 6.3

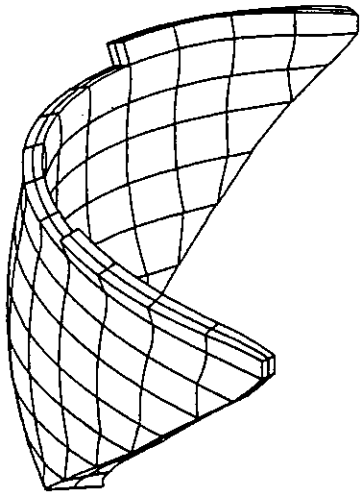

Deformed shape for thermal loading

Fig. 7.1

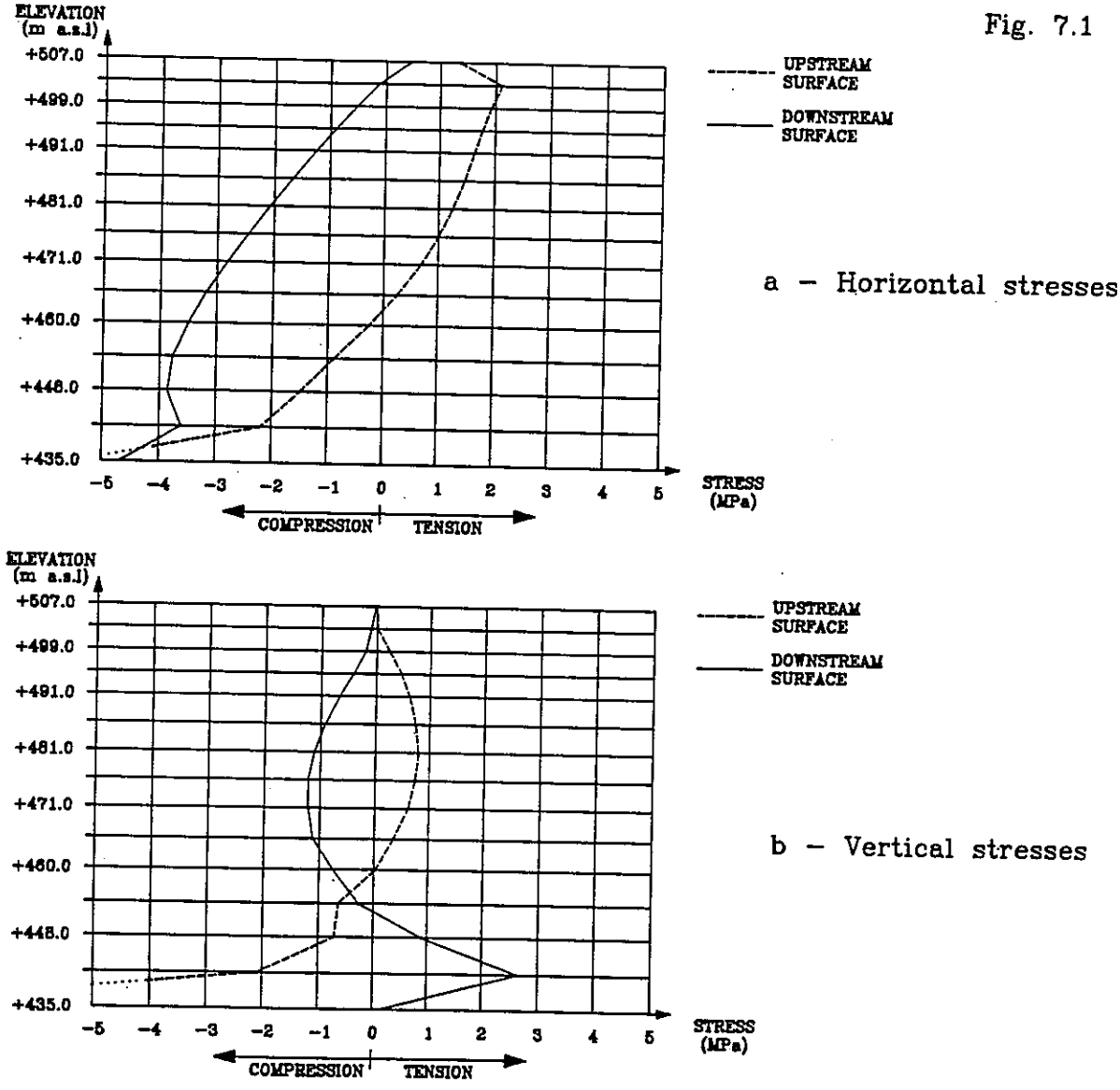

Thermal loading : horizontal and vertical stresses in central cantilever

Fig. 7.2

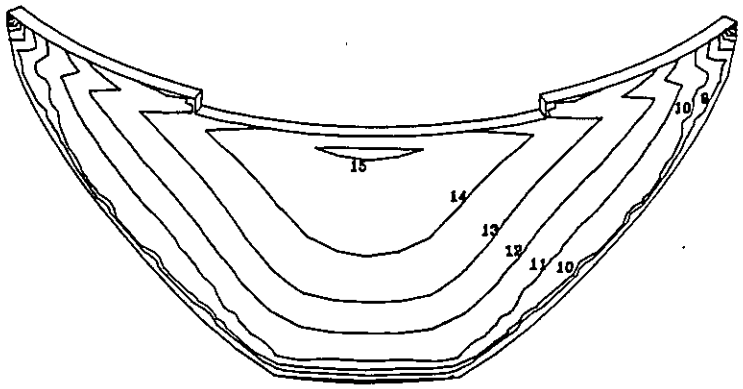

a – Arch stresses – Upstream Surface

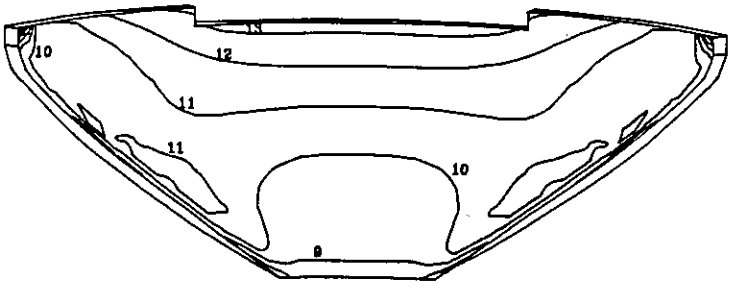

b – Arch stresses – Downstream surface

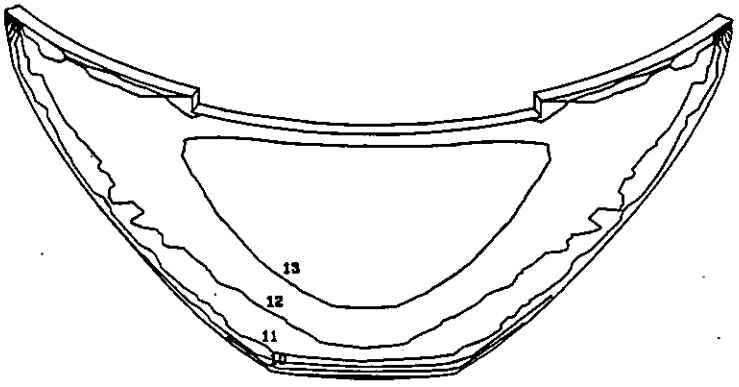

c – Cantilever stresses – Upstream Surface

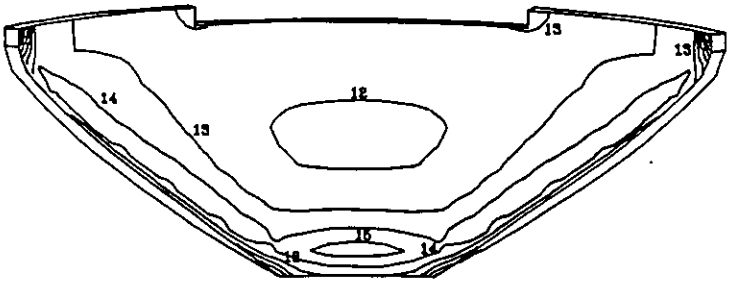

d – Cantilever stresses – Downstream surface

15	2.0
14	1.0
13	0.0
12	−1.0
11	−2.0
10	−3.0
9	−4.0
8	−5.0
7	−6.0
6	−7.0
5	−8.0
4	−9.0
3	−10.0
2	−11.0
1	−12.0 MPa

Thermal loading – Arch and cantilever stresses

Fig. 7.3

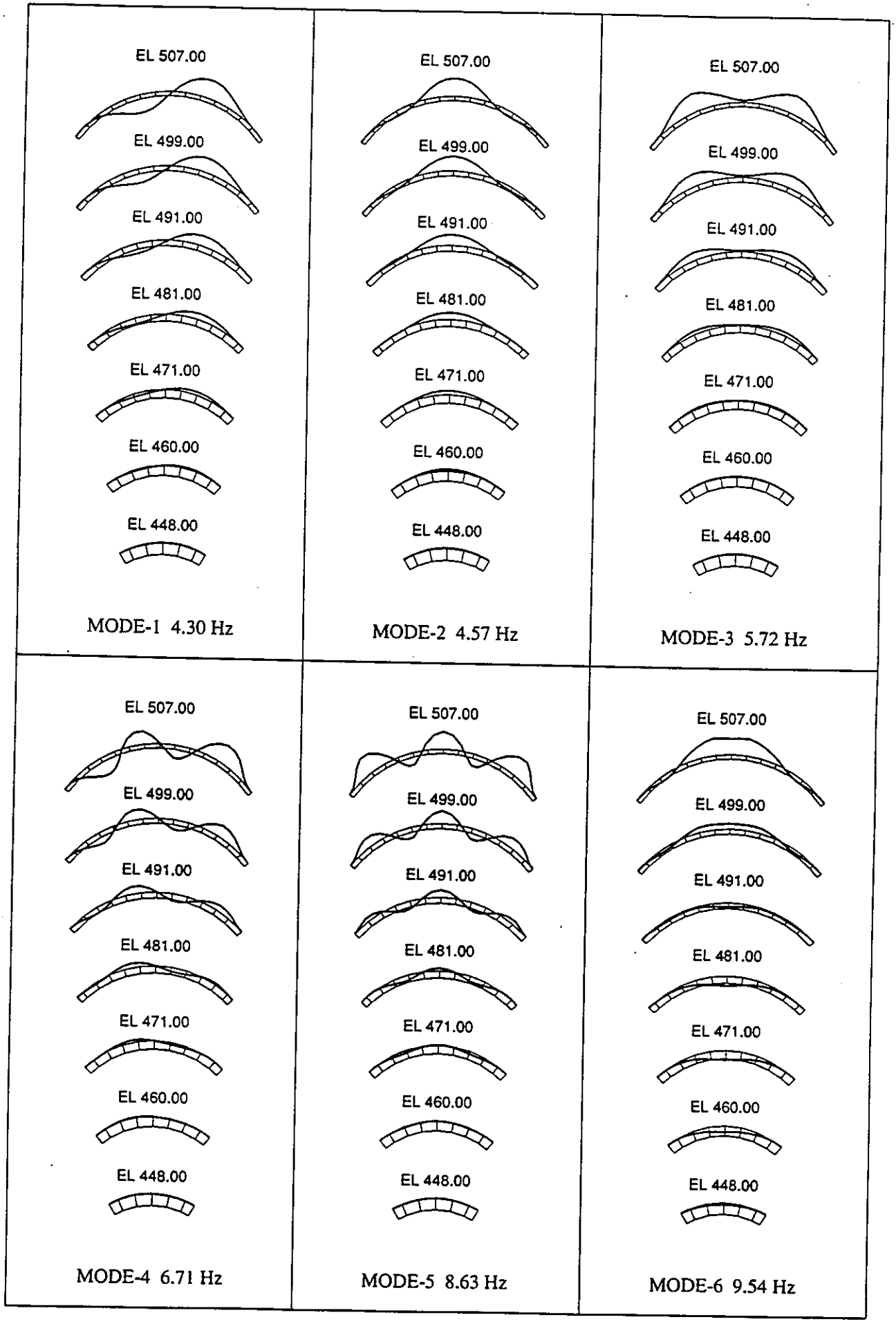

Fig. 8 : Vibration shapes for rigid foundation; no water.

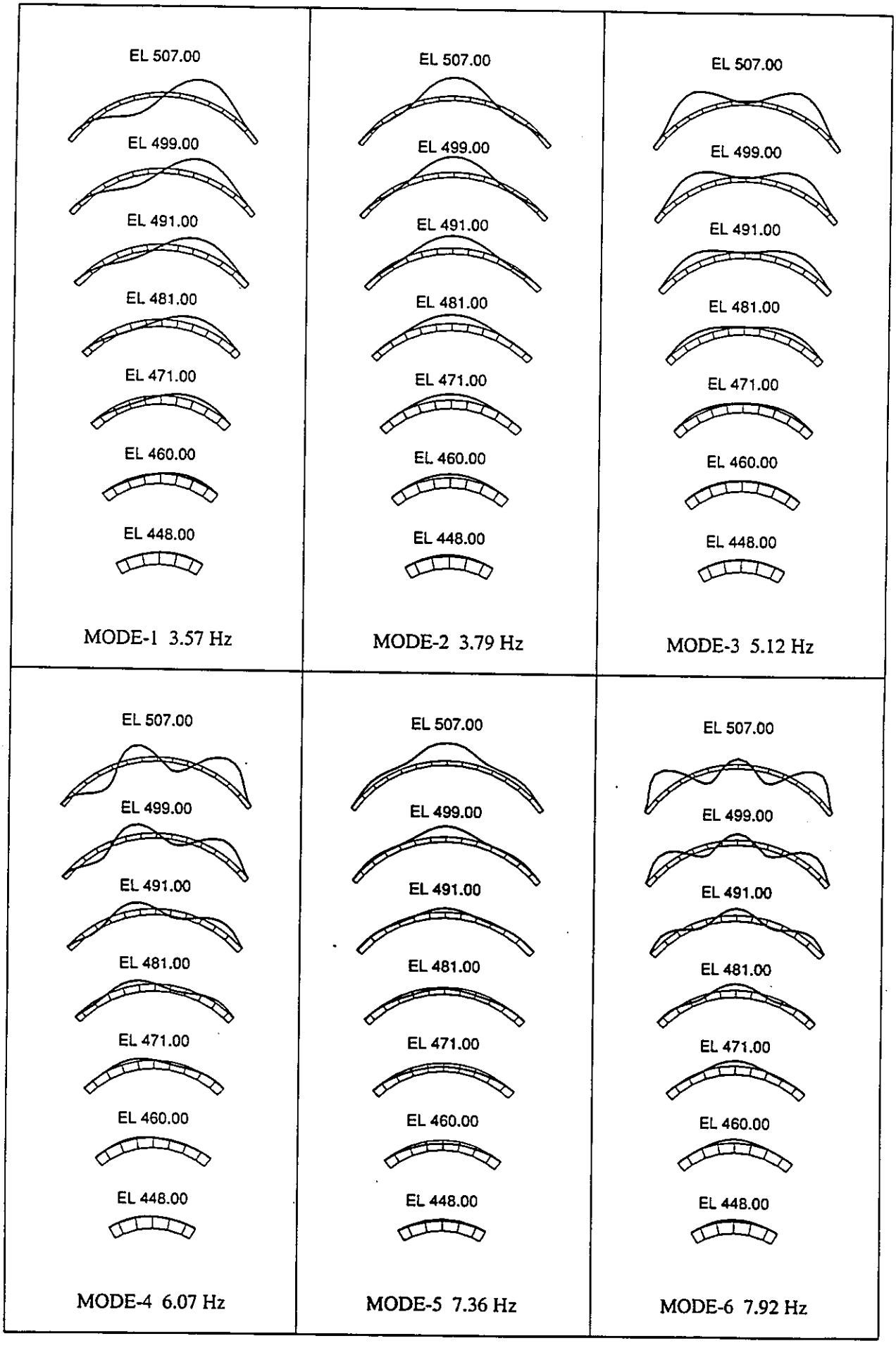

Fig. 9 : Vibration shapes for flexible foundation; water level 491m a.s.l.

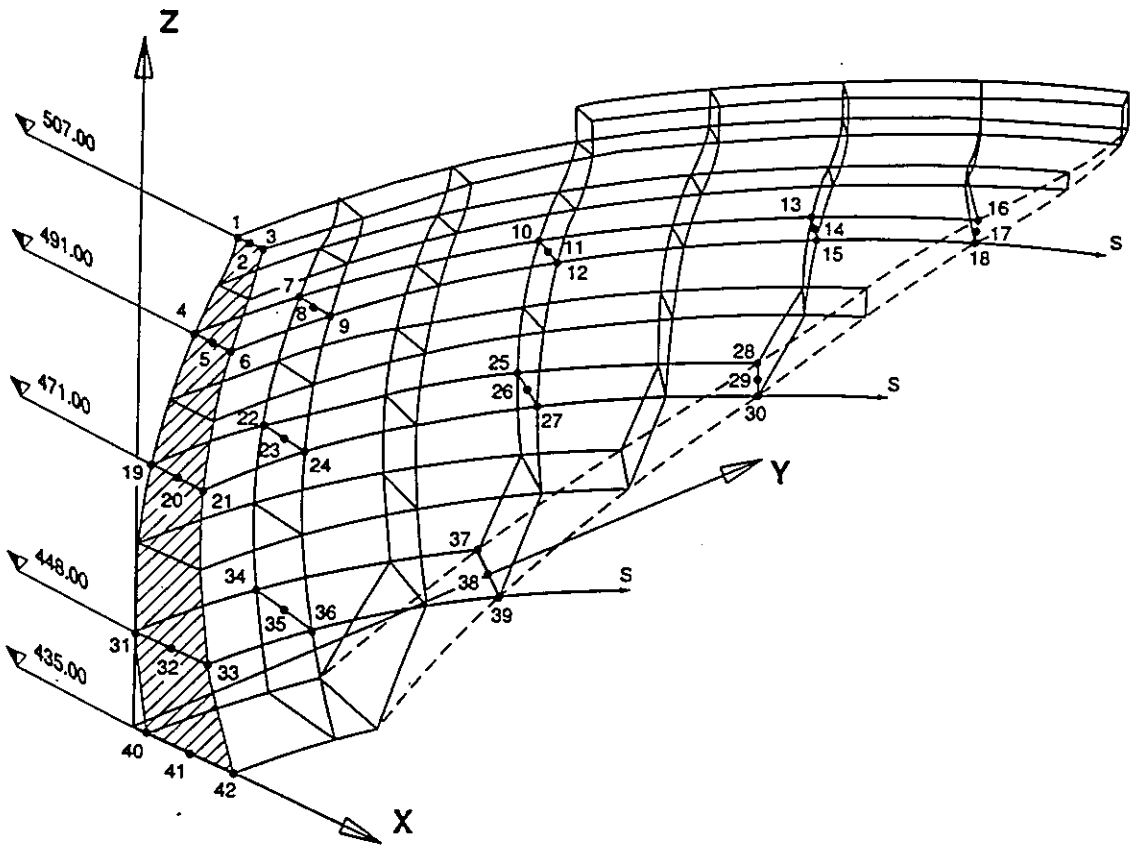

DEAD WEIGHT

Points	s (m)	Displ. x (mm)	Displ. y (mm)	Displ. z (mm)	P1 (MPa)	P2 (MPa)	P3 (MPa)
1	0.0	0.6	0.0	-3.1	0.01	0.00	-1.11
2	0.0	0.7	0.0	-3.3	0.00	-0.01	-1.19
3	0.0	0.7	0.0	-3.5	0.00	-0.01	-1.27
4	0.0	-0.7	0.0	-2.5	0.00	-0.01	-0.31
5	0.0	-0.7	0.0	-2.8	0.00	-0.31	-0.41
6	0.0	-0.7	0.0	-3.0	0.00	-0.51	0.57
7	16.0	-0.7	-0.1	-2.4	0.04	0.00	-0.27
8	16.0	-0.7	-0.2	-2.7	0.00	-0.26	-0.42
9	16.0	-0.7	-0.2	-2.9	0.00	-0.45	-0.64
10	48.0	-0.3	-0.4	-1.8	0.30	0.01	-0.09
11	48.0	-0.3	-0.5	-2.0	0.01	-0.04	-0.45
12	48.0	-0.3	-0.5	-2.3	0.01	-0.16	-0.99
13	80.0	-0.1	-0.5	-0.9	0.30	0.14	-0.03
14	80.0	0.0	-0.5	-1.1	0.19	-0.01	-0.45
15	80.0	0.0	-0.5	-1.2	0.25	0.02	-1.20
16	99.2	-0.2	-0.2	-0.4	0.66	0.02	-0.38
17	99.2	-0.1	-0.2	-0.5	0.30	-0.08	-0.37
18	99.2	-0.1	-0.1	-0.5	0.13	-0.14	-1.69
19	0.0	-1.5	0.0	-2.3	0.30	0.12	-0.01
20	0.0	-1.5	0.0	-2.3	0.09	-0.02	-0.50
21	0.0	-1.5	0.0	-2.3	-0.01	-0.15	-1.19
22	16.0	-1.4	0.1	-2.2	0.31	0.09	0.00
23	16.0	-1.4	0.1	-2.2	0.10	-0.03	-0.52
24	16.0	-1.4	0.0	-2.2	0.01	-0.13	-1.22
25	48.0	-0.7	0.1	-1.7	0.25	0.01	-0.19
26	48.0	-0.7	0.0	-1.6	0.17	-0.03	-0.64
27	48.0	-0.8	-0.1	-1.6	0.10	0.06	-1.21
28	75.0	-0.1	-0.1	-0.8	-0.04	-0.47	-2.39
29	75.0	-0.1	-0.1	-0.9	0.21	-0.12	-0.28
30	75.0	-0.2	-0.1	-0.8	0.44	-0.18	-1.60
31	0.0	-0.8	0.0	-2.2	0.21	-0.03	-0.45
32	0.0	-0.7	0.0	-1.9	0.07	0.03	-0.76
33	0.0	-0.7	0.0	-1.5	-0.24	-0.25	-1.05
34	16.0	-0.6	0.1	-2.1	0.18	-0.05	-0.62
35	16.0	-0.6	0.1	-1.8	0.06	0.01	-0.78
36	16.0	-0.6	0.0	-1.4	-0.15	-0.22	-0.92
37	41.5	0.0	0.1	-1.3	-0.53	-0.76	-3.93
38	41.5	-0.1	0.0	-1.3	0.03	-0.17	-0.32
39	41.5	-0.1	-0.1	-1.0	0.41	-0.16	-1.25
40	0.0	0.0	0.0	-1.6	-0.85	-0.90	-4.06
41	0.0	0.0	0.0	-1.4	-0.10	-0.19	-0.45
42	0.0	-0.1	0.0	-1.0	-0.13	-0.25	-1.02

Tab. 1

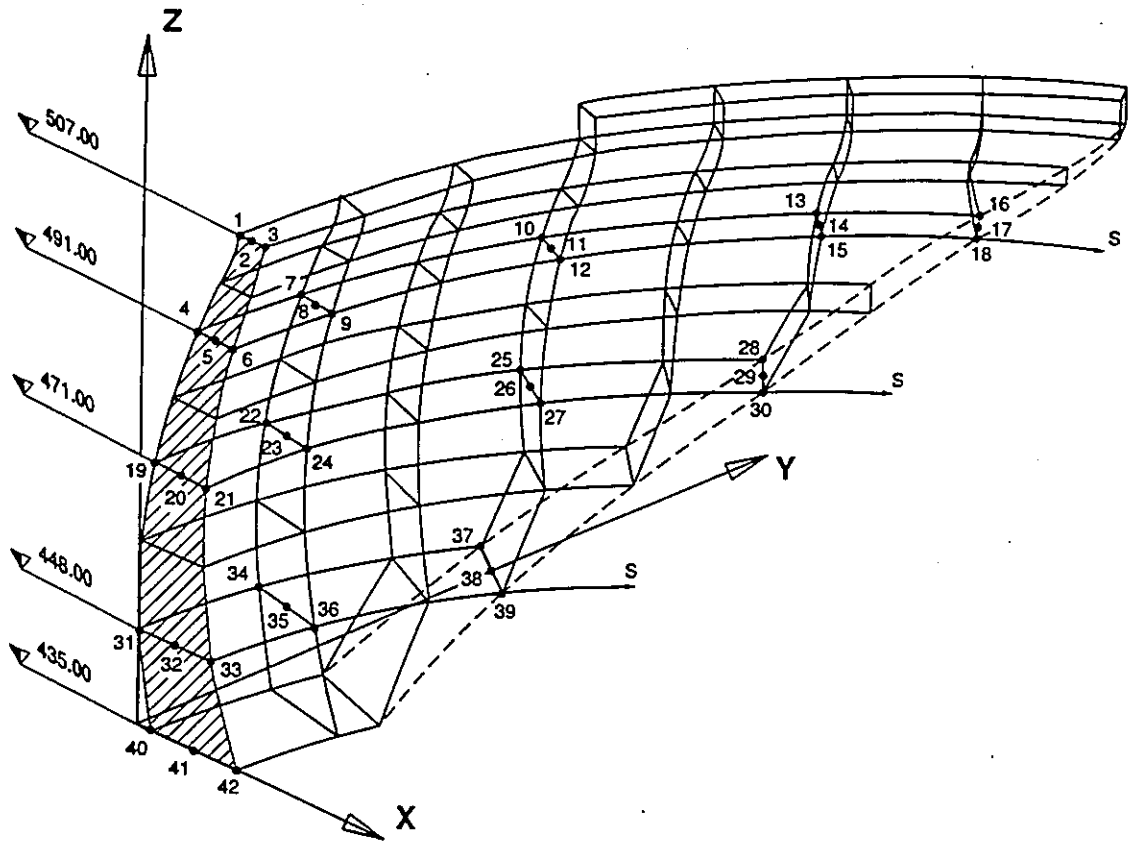

HYDROSTATIC PRESSURE

Points	s (m)	Displ. x (mm)	Displ. y (mm)	Displ. z (mm)	P1 (MPa)	P2 (MPa)	P3 (MPa)
1	0.0	22.9	0.0	-0.4	0.04	-0.01	-2.93
2	0.0	22.9	0.0	-0.6	0.01	-0.02	-1.83
3	0.0	22.9	0.0	-0.9	0.03	-0.02	-0.67
4	0.0	20.7	0.0	0.6	-0.16	-1.43	-4.28
5	0.0	20.8	0.0	0.0	-0.02	-0.25	-2.94
6	0.0	20.8	0.0	-0.6	1.00	0.00	-1.49
7	16.0	19.1	-1.7	0.6	-0.16	-1.39	-4.14
8	16.0	19.2	-1.2	0.1	-0.02	-0.24	-2.94
9	16.0	19.3	-0.7	-0.4	1.01	0.00	-1.69
10	48.0	9.4	-1.9	0.6	-0.12	-1.25	-2.79
11	48.0	9.8	-1.1	0.4	-0.04	-0.21	-2.66
12	48.0	10.2	-0.2	0.2	1.14	-0.01	-2.67
13	80.0	2.0	0.7	0.1	-0.18	-0.92	-1.25
14	80.0	2.2	1.0	0.2	0.12	-0.07	-1.84
15	80.0	2.4	1.2	0.3	1.26	-0.07	-2.75
16	99.2	0.9	0.8	-0.2	-0.27	-0.56	-3.50
17	99.2	1.0	0.9	-0.1	0.04	-0.45	-1.31
18	99.2	0.9	0.8	0.0	0.64	-0.23	-2.67
19	0.0	15.2	0.0	2.9	-0.38	-1.34	-4.18
20	0.0	15.3	0.0	1.3	-0.10	-0.39	-2.85
21	0.0	15.3	0.0	-0.2	0.83	0.02	-1.36
22	16.0	13.9	-1.7	2.7	-0.35	-1.21	-3.96
23	16.0	14	-1.1	1.2	-0.09	-0.37	-2.77
24	16.0	14.2	-0.6	-0.2	0.82	-0.02	-1.48
25	48.0	6.0	-1.7	1.6	-0.06	-0.24	-1.75
26	48.0	6.5	-0.8	0.6	0.19	-0.33	-2.24
27	48.0	7.0	0.1	-0.5	0.63	-0.17	-2.92
28	75.0	1.3	0.6	0.2	2.19	-0.28	-1.31
29	75.0	1.6	1.0	-0.1	0.10	-0.19	-0.98
30	75.0	1.7	1.1	-0.4	-0.81	-1.07	-7.64
31	0.0	6.5	0.0	3.6	0.12	-0.99	-2.01
32	0.0	6.4	0.0	1.3	0.19	-0.88	-1.06
33	0.0	6.4	0.0	-0.9	0.85	-0.06	-1.19
34	16.0	5.6	-0.8	3.2	0.54	-0.83	-1.89
35	16.0	5.6	-0.3	1.1	0.21	-0.65	-1.13
36	16.0	5.7	0.1	-0.9	0.53	0.26	-1.77
37	41.5	1.5	-0.1	1.0	7.55	1.15	0.36
38	41.5	2.0	0.6	0.0	0.64	0.29	-0.69
39	41.5	2.1	1.0	-0.9	-1.36	-1.43	-9.93
40	0.0	1.7	0.0	1.9	9.08	1.83	1.09
41	0.0	2.0	0.0	0.2	0.81	0.49	-0.45
42	0.0	-1.8	0.0	-1	-0.78	-0.85	-6.66

Tab. 2

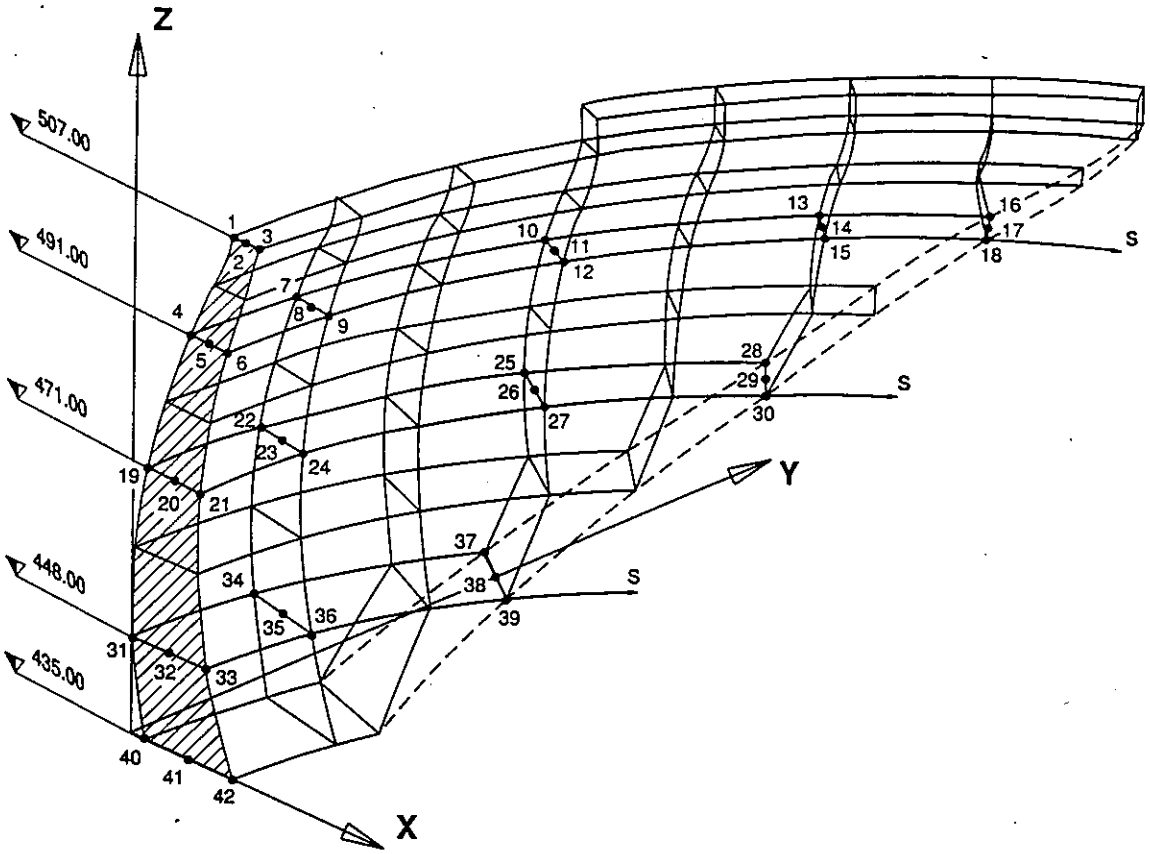

DEAD WEIGHT(P-LEVEL 2)

Points	s (m)	Displ.x (mm)	Displ.y (mm)	Displ.z (mm)	P1 (MPa)	P2 (MPa)	P3 (MPa)
1	0.0	0.8	0.0	-3.0	0.00	-0.02	-1.11
2	0.0	0.8	0.0	-3.2	0.00	-0.01	-1.18
3	0.0	0.8	0.0	-3.4	0.02	-0.01	-1.25
4	0.0	-0.6	0.0	-2.4	0.03	-0.04	-0.32
5	0.0	-0.6	0.0	-2.6	-0.01	-0.31	-0.42
6	0.0	-0.6	0.0	-2.9	-0.01	-0.52	-0.58
7	16.0	-0.5	-0.1	-2.3	0.06	-0.02	-0.28
8	16.0	-0.5	-0.2	-2.6	-0.01	-0.26	-0.43
9	16.0	-0.5	-0.2	-2.8	-0.01	-0.45	-0.65
10	48.0	-0.2	-0.4	-1.7	0.32	-0.02	-0.10
11	48.0	-0.2	-0.4	-1.9	0.02	-0.04	-0.44
12	48.0	-0.2	-0.5	-2.2	0.00	-0.17	-0.97
13	80.0	-0.1	-0.5	-0.8	0.36	0.17	-0.05
14	80.0	0.0	-0.5	-1.0	0.19	-0.01	-0.39
15	80.0	0.0	-0.4	-1.2	0.21	0.01	-1.15
16	99.2	-0.1	-0.2	-0.4	0.47	0.13	-0.29
17	99.2	-0.1	-0.1	-0.5	0.29	-0.16	-0.37
18	99.2	-0.1	-0.1	-0.5	0.15	-0.17	-1.18
19	0.0	-1.4	0.0	-2.2	0.27	0.12	-0.02
20	0.0	-1.4	0.0	-2.2	0.08	0.00	-0.46
21	0.0	-1.3	0.0	-2.2	-0.02	-0.16	-1.18
22	16.0	-1.3	0.1	-2.1	0.29	0.10	-0.02
23	16.0	-1.3	0.1	-2.1	0.10	0.00	-0.48
24	16.0	-1.3	0.0	-2.1	-0.02	-0.14	-1.19
25	48.0	-0.6	0.1	-1.6	0.24	0.11	-0.21
26	48.0	-0.6	0.0	-1.6	0.15	0.01	-0.65
27	48.0	-0.7	-0.1	-1.5	0.08	0.03	-1.14
28	75.0	-0.1	-0.1	-0.8	0.10	-0.13	-1.54
29	75.0	-0.1	-0.1	-0.8	0.18	-0.20	-0.63
30	75.0	-0.1	-0.1	-0.8	0.30	0.00	-1.04
31	0.0	-0.6	0.0	-2.1	0.12	-0.05	-0.74
32	0.0	-0.6	0.0	-1.7	0.00	-0.04	-0.78
33	0.0	-0.6	0.0	-1.4	-0.09	-0.20	-1.07
34	16.0	-0.5	0.1	-2.0	0.12	-0.06	-0.82
35	16.0	-0.5	0.1	-1.7	-0.01	-0.05	-0.78
36	16.0	-0.5	0.0	-1.4	-0.06	-0.21	-0.93
37	41.5	0.0	0.1	-1.2	-0.13	-0.39	-2.42
38	41.5	-0.1	0.0	-1.2	0.00	-0.24	-0.73
39	41.5	-0.1	-0.1	-0.9	0.17	0.10	-1.04
40	0.0	0.0	0.0	-1.5	-0.30	-0.47	-2.41
41	0.0	0.0	0.0	-1.3	-0.25	-0.37	-0.97
42	0.0	-0.1	0.0	-1.0	0.18	-0.13	-0.70

Tab. 1.1

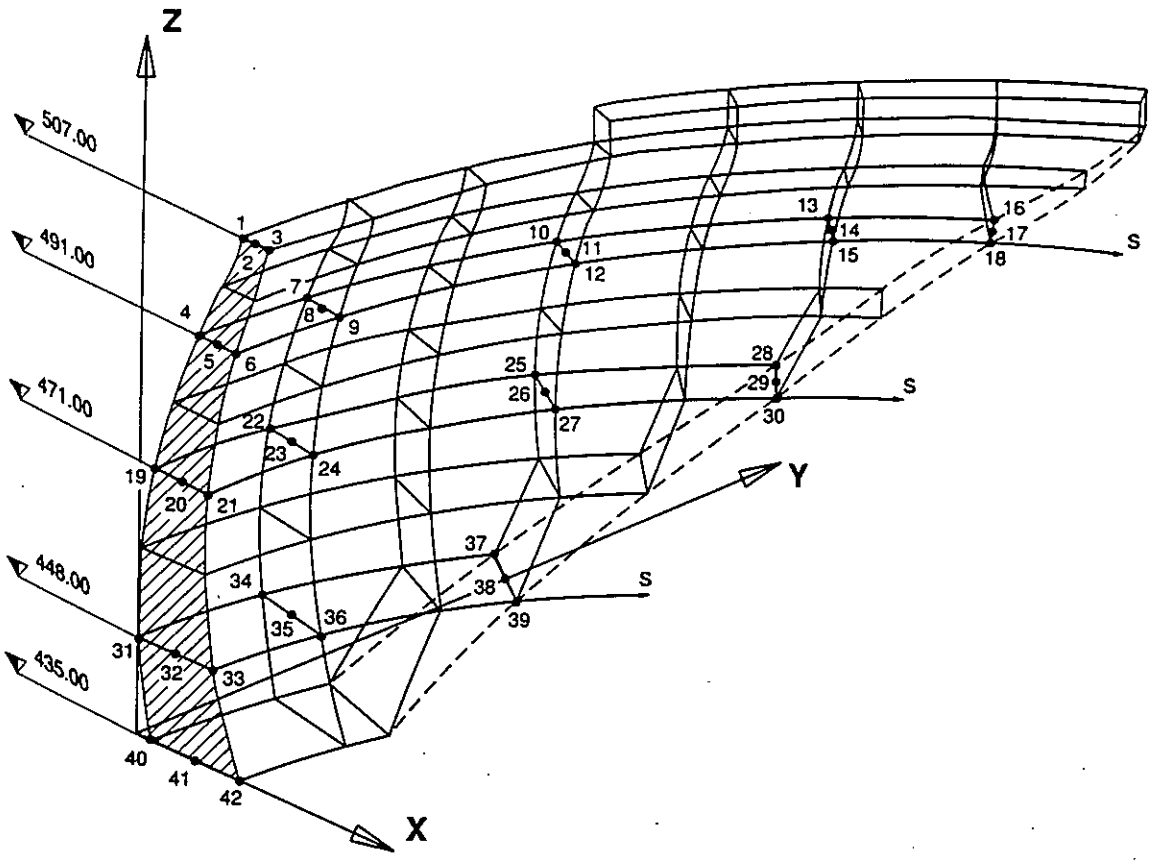

HYDROSTATIC PRESSURE (P-LEVEL 2)

Points	s (m)	Displ.x (mm)	Displ.y (mm)	Displ.z (mm)	P1 (MPa)	P2 (MPa)	P3 (MPa)
1	0.0	22.2	0.0	-0.6	0.05	-0.03	-3.12
2	0.0	22.2	0.0	-0.8	0.14	-0.05	-2.01
3	0.0	22.2	0.0	-1.1	0.08	-0.16	-0.90
4	0.0	20.0	0.0	0.4	-0.12	-1.50	-4.38
5	0.0	20.0	0.0	-0.2	-0.05	-0.31	-3.05
6	0.0	20.1	0.0	-0.8	0.96	0.00	-1.60
7	16.0	18.4	-1.7	0.5	-0.13	-1.44	-4.21
8	16.0	18.5	-1.2	-0.1	-0.06	-0.29	-3.03
9	16.0	18.6	-0.6	-0.6	0.97	0.00	-1.78
10	48.0	8.9	-1.9	0.5	-0.14	-1.27	-2.70
11	48.0	9.3	-1.0	0.3	-0.10	-0.24	-2.59
12	48.0	9.7	-0.2	0.1	1.05	-0.03	-2.63
13	80.0	1.8	0.6	0.1	-0.17	-0.93	-1.05
14	80.0	2.0	0.9	0.1	0.02	-0.12	-1.70
15	80.0	2.3	1.1	0.2	1.14	-0.05	-2.50
16	99.2	0.8	0.7	-0.1	-0.18	-0.55	-1.99
17	99.2	0.9	0.8	-0.1	-0.07	-0.37	-1.52
18	99.2	0.8	0.7	0.0	0.54	-0.24	-1.80
19	0.0	14.4	0.0	2.7	-0.35	-1.32	-4.20
20	0.0	14.5	0.0	1.1	-0.17	-0.48	-2.91
21	0.0	14.6	0.0	-0.4	0.76	0.03	-1.39
22	16.0	13.1	-1.6	2.5	-0.32	-1.20	-3.96
23	16.0	13.3	-1.1	1.0	-0.15	-0.44	-2.80
24	16.0	13.4	-0.5	-0.4	0.73	-0.01	-1.53
25	48.0	5.5	-1.6	1.5	0.10	-0.50	-1.60
26	48.0	6.0	-0.7	0.5	0.20	-0.30	-2.10
27	48.0	6.5	0.1	-0.5	0.54	-0.22	-2.84
28	75.0	1.2	0.5	0.2	0.97	0.44	-1.23
29	75.0	1.5	0.9	-0.1	0.37	-0.43	-1.43
30	75.0	1.5	1.0	-0.4	-0.50	-0.64	-4.87
31	0.0	6.0	0.0	3.3	0.81	-1.12	-1.87
32	0.0	5.9	0.0	1.2	0.73	-0.73	-0.95
33	0.0	5.9	0.0	-0.9	0.92	-0.21	-1.76
34	16.0	5.2	-0.8	2.9	1.03	-0.87	-1.79
35	16.0	5.2	-0.3	1.0	0.57	-0.51	-1.04
36	16.0	5.3	0.1	-0.9	0.54	0.10	-2.22
37	41.5	1.4	-0.1	0.9	3.25	1.17	0.37
38	41.5	1.9	0.6	0.0	0.94	0.39	-0.96
39	41.5	2.0	0.9	-0.8	-0.43	-1.21	-6.05
40	0.0	1.7	0.0	1.7	4.42	1.60	1.03
41	0.0	1.8	0.0	0.1	1.85	0.70	-0.46
42	0.0	1.8	0.0	-0.9	-0.13	-0.23	-4.54

Tab. 2.1

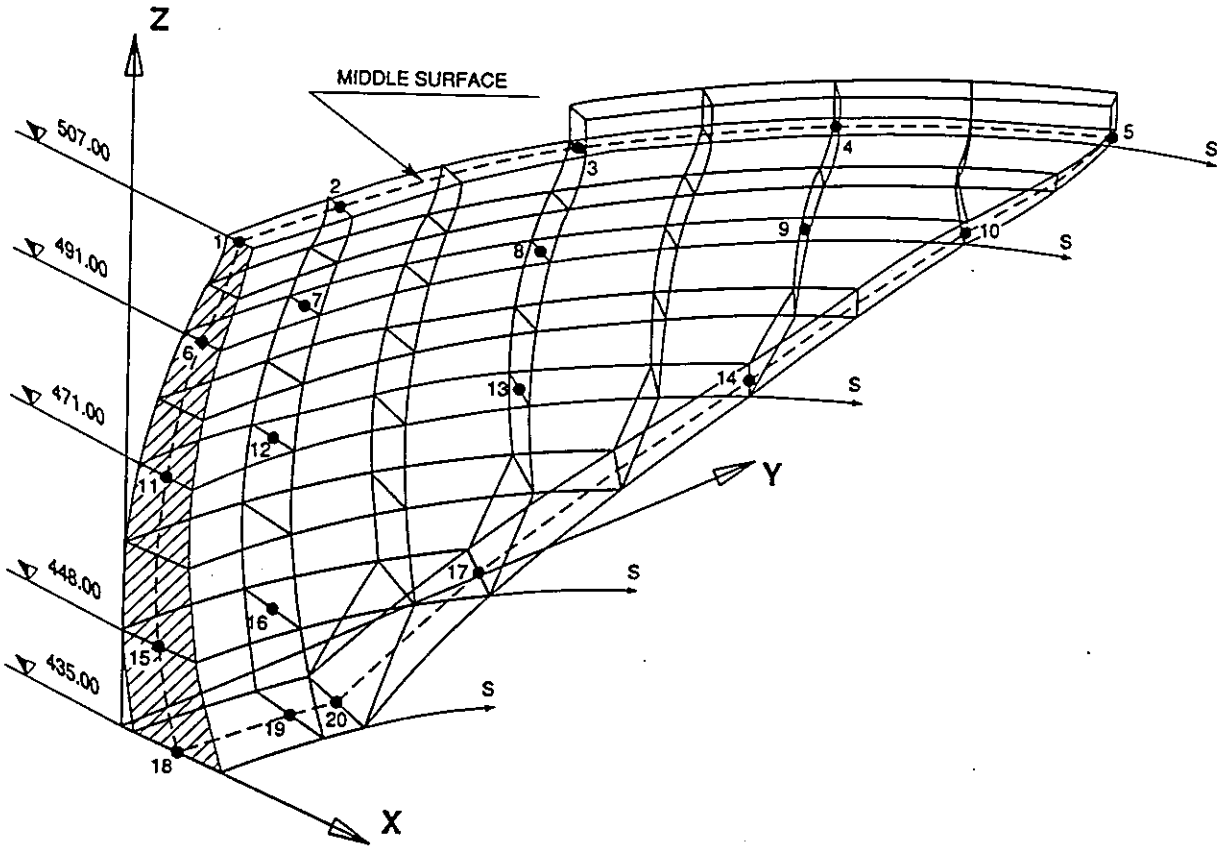

Points	s (m)	Steady state analysis temperature T (°C)
1	0.0	15.00
2	16.0	15.00
3	48.0	15.00
4	80.0	14.62
5	112.9	14.79
6	0.0	12.44
7	16.0	12.43
8	48.0	12.43
9	80.0	12.42
10	99.2	12.38
11	0.0	12.40
12	16.0	12.40
13	48.0	12.41
14	75.0	12.60
15	0.0	12.36
16	16.0	12.37
17	41.5	12.56
18	0.0	12.86
19	16.0	12.84
20	21.0	12.84

Tab. 3.1/a

Points	Periodic analysis	
	Amplitude A (°C)	Phase φ (rad)
1	10.00	0.0
2	10.00	0.0
3	10.00	0.0
4	8.79	-0.5
5	9.09	-0.5
6	5.89	-1.0
7	5.87	-1.0
8	5.76	-1.0
9	5.64	-1.0
10	5.74	-1.0
11	3.79	-1.6
12	3.78	-1.6
13	3.71	-1.6
14	4.15	-1.5
15	2.08	-2.2
16	2.05	-2.2
17	2.28	-2.1
18	1.87	-2.2
19	1.83	-2.2
20	1.90	-2.2

Tab. 3.1/b

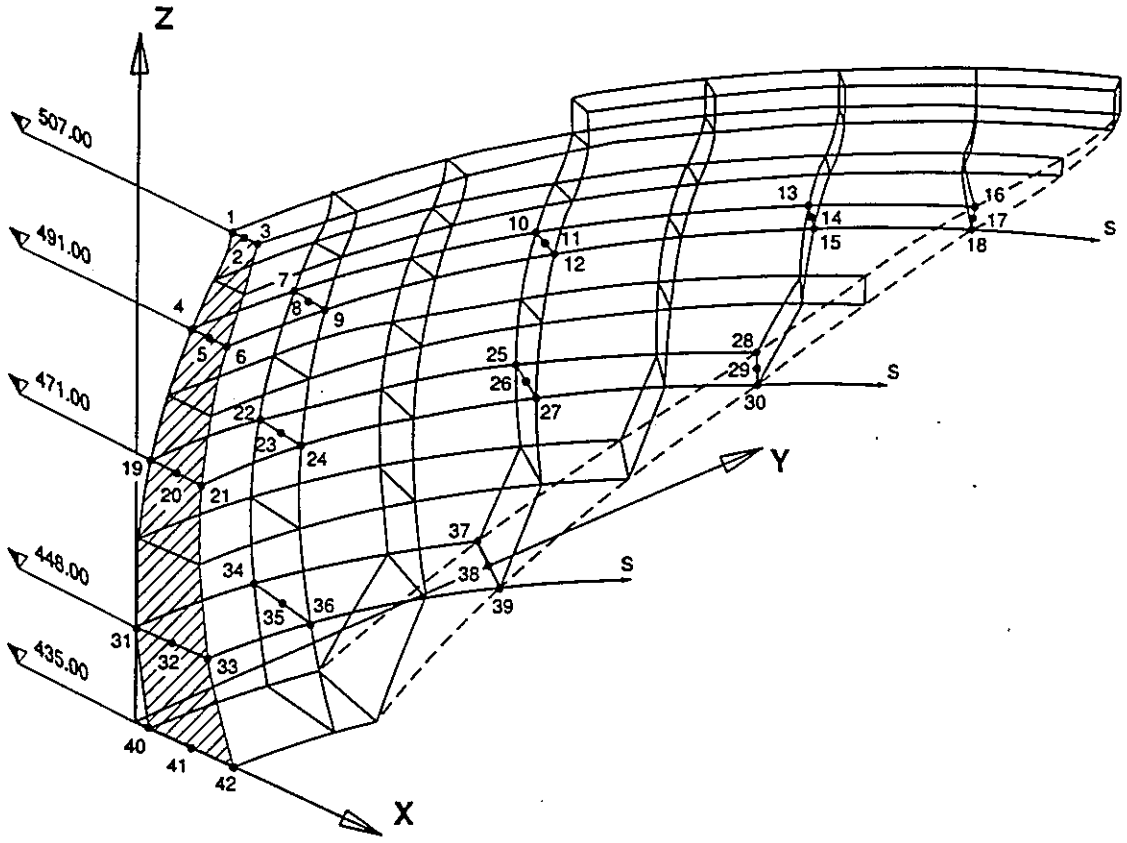

THERMAL LOADING

Points	s (m)	Displ. x (mm)	Displ. y (mm)	Displ. z (mm)	P1 (MPa)	P2 (MPa)	P3 (MPa)
1	0.0	-17.9	0.0	8.7	1.35	0.02	-0.15
2	0.0	-17.7	0.0	9.6	0.91	0.01	-0.07
3	0.0	-17.4	0.0	10.4	0.46	0.01	-0.03
4	0.0	-13.4	0.0	5.4	1.64	0.75	0.00
5	0.0	-13.1	0.0	6.3	0.22	0.07	-0.10
6	0.0	-12.8	0.0	7.2	0.00	-0.72	-1.26
7	16.0	-12.4	1.8	5.2	1.47	0.62	0.00
8	16.0	-12.2	1.4	6.0	0.19	0.01	-0.16
9	16.0	-12.0	1.1	6.9	0.00	-0.68	-1.28
10	48.0	-6.8	3.2	3.2	0.47	0.01	-0.63
11	48.0	-6.8	2.6	4.1	0.17	-0.05	-1.19
12	48.0	-6.8	1.9	5.1	0.02	-0.11	-1.84
13	80.0	-1.4	1.6	0.9	0.19	-0.91	-2.31
14	80.0	-1.5	1.1	1.6	0.39	0.02	-2.64
15	80.0	-1.5	0.5	2.2	1.35	0.24	-3.25
16	99.2	0.0	0.0	0.0	-1.38	-4.25	-7.15
17	99.2	0.0	0.0	0.0	0.39	-3.90	-4.23
18	99.2	0.0	0.0	0.0	2.77	-4.31	-5.00
19	0.0	-8.6	0.0	1.8	0.69	0.65	-0.02
20	0.0	-8.2	0.0	3.1	-0.02	-0.23	-0.96
21	0.0	-7.8	0.0	4.3	-0.01	-1.25	-2.82
22	16.0	-7.7	1.4	1.7	0.57	0.29	0.02
23	16.0	-7.4	0.9	2.9	-0.03	-0.25	-1.17
24	16.0	-7.0	0.5	4.1	0.01	-1.04	-2.89
25	48.0	-2.6	1.7	0.8	0.04	-0.73	-2.00
26	48.0	-2.5	0.9	1.6	0.18	-0.43	-2.54
27	48.0	-2.4	0.2	2.5	1.04	0.05	-3.05
28	75.0	0.0	0.0	0.0	-1.10	-4.44	-8.59
29	75.0	0.0	0.0	0.0	1.73	-3.57	-3.70
30	75.0	0.0	0.0	0.0	1.46	-4.81	-6.67
31	0.0	-2.9	0.0	-0.3	-0.29	-0.74	-1.49
32	0.0	-2.3	0.0	1.0	0.94	-0.28	-2.48
33	0.0	-1.5	0.0	2.1	0.93	-0.25	-3.86
34	16.0	-2.4	0.6	-0.2	-0.13	-1.11	-1.68
35	16.0	-1.9	0.2	0.9	0.72	-0.36	-2.51
36	16.0	-1.2	-0.2	2.0	0.85	-0.15	-4.08
37	41.5	0.0	0.0	0.0	-1.88	-5.11	-11.18
38	41.5	0.0	0.0	0.0	1.42	-3.63	-3.78
39	41.5	0.0	0.0	0.0	1.59	-4.79	-6.70
40	0.0	0.0	0.0	0.0	-2.68	-5.43	-11.85
41	0.0	0.0	0.0	0.0	1.56	-3.68	-3.77
42	0.0	0.0	0.0	0.0	1.37	-4.69	-5.92

Tab. 3.2

NATURAL FREQUENCIES

MODE NO	RIGID FOUNDATION NO RESERVOIR	FLEXIBLE FOUNDATION WITH RESERVOIR
1	4.302	3.57
2	4.578	3.798
3	5.728	5.123
4	6.711	6.075
5	8.633	7.365
6	9.548	7.926

Tab. 4.1

VIBRATION SHAPES FOR RIGID FOUNDATION; NO WATER

		Mode 1 Freq=4.302 Hz			Mode 2 Freq=4.578 Hz			Mode 3 Freq=5.728 Hz		
Pt.	s (m)	Displ.x	Displ.y	Displ.z	Displ.x	Displ.y	Displ.z	Displ.x	Displ.y	Displ.z
1	0.0	0.0048	0.2568	-0.0009	-1.0000	0.0006	0.2368	-0.0911	0.0000	0.0173
2	16.0	-0.6758	0.3167	0.1741	-0.8082	0.0290	0.1817	-0.2687	0.0834	0.0684
3	48.0	-0.8589	0.4139	0.2038	0.1201	-0.1650	-0.0583	-0.8170	0.4021	0.2243
4	80.0	-0.1591	0.0727	0.0241	0.1481	-0.1345	-0.0436	-0.2733	0.1593	0.0580
5	112.9	0.0000	0.0000	0.0000	0.0000	0.0000	0.0000	0.0000	0.0000	0.0000
6	0.0	0.0030	0.1723	-0.0003	-0.5936	0.0004	0.0875	-0.0458	0.0000	0.0093
7	16.0	-0.3691	0.2006	0.0619	-0.4756	0.0168	0.0643	-0.1241	0.0396	0.0252
8	48.0	-0.4479	0.2306	0.0501	0.0146	-0.0742	-0.0148	-0.3412	0.1586	0.0503
9	80.0	-0.0578	0.0334	-0.0040	0.0415	-0.0509	-0.0025	-0.0823	0.0494	-0.0017
10	99.2	0.0000	0.0000	0.0000	0.0000	0.0000	0.0000	0.0000	0.0000	0.0000
11	0.0	0.0013	0.0684	0.0002	-0.2205	0.0001	-0.0117	-0.0110	0.0000	0.0016
12	16.0	-0.1276	0.0790	-0.0053	-0.1756	0.0093	-0.0113	-0.0302	0.0078	0.0009
13	48.0	-0.1038	0.0644	-0.0130	-0.0075	-0.0193	-0.0029	-0.0569	0.0255	-0.0049
14	75.0	0.0000	0.0000	0.0000	0.0000	0.0000	0.0000	0.0000	0.0000	0.0000
15	0.0	0.0003	0.0135	0.0001	-0.0289	0.0000	-0.0097	0.0006	0.0000	0.0003
16	16.0	-0.0145	0.0135	-0.0054	-0.0209	0.0004	-0.0071	-0.0010	-0.0001	-0.0003
17	41.5	0.0000	0.0000	0.0000	0.0000	0.0000	0.0000	0.0000	0.0000	0.0000
18	0.0	0.0000	0.0000	0.0000	0.0000	0.0000	0.0000	0.0000	0.0000	0.0000
19	16.0	0.0000	0.0000	0.0000	0.0000	0.0000	0.0000	0.0000	0.0000	0.0000
20	21.0	0.0000	0.0000	0.0000	0.0000	0.0000	0.0000	0.0000	0.0000	0.0000

		Mode 4 Freq=6.711 Hz			Mode 5 Freq=8.633 Hz			Mode 6 Freq=9.548 Hz		
Pt.	s (m)	Displ.x	Displ.y	Displ.z	Displ.x	Displ.y	Displ.z	Displ.x	Displ.y	Displ.z
1	0.0	0.0008	-0.0729	-0.0004	-0.9509	0.0000	0.3726	-0.9321	0.0004	0.5874
2	16.0	0.6542	-0.1149	-0.1819	-0.3187	-0.0199	0.1682	-0.9881	0.1769	0.5672
3	48.0	-0.4064	0.3312	0.1548	0.3361	-0.0229	-0.0221	-0.1891	0.1074	0.1658
4	80.0	-0.5447	0.4191	0.1486	-0.7387	0.6266	0.2276	0.2252	-0.1434	-0.0424
5	112.9	0.0000	0.0000	0.0000	0.0000	0.0000	0.0000	0.0000	0.0000	0.0000
6	0.0	0.0003	-0.0422	-0.0002	-0.4080	0.0000	0.1565	0.2390	0.0004	0.1542
7	16.0	0.3482	-0.0632	-0.0680	-0.0717	-0.0301	0.0719	0.1756	-0.0032	0.1491
8	48.0	-0.0392	0.0762	0.0178	0.3568	-0.1218	-0.0344	0.0779	-0.0130	0.0661
9	80.0	-0.1385	0.1214	0.0058	-0.1445	0.1419	0.0134	0.0678	-0.0416	0.0066
10	99.2	0.0000	0.0000	0.0000	0.0000	0.0000	0.0000	0.0000	0.0000	0.0000
11	0.0	-0.0001	-0.0116	-0.0001	-0.0350	0.0000	0.0269	0.5669	0.0004	0.0322
12	16.0	0.1088	-0.0218	-0.0003	0.0446	-0.0162	0.0212	0.4731	-0.0521	0.0350
13	48.0	0.0225	0.0021	0.0005	0.1102	-0.0479	0.0088	0.1050	-0.0267	0.0295
14	75.0	0.0000	0.0000	0.0000	0.0000	0.0000	0.0000	0.0000	0.0000	0.0000
15	0.0	-0.0001	-0.0013	0.0000	0.0059	0.0000	0.0066	0.1161	0.0002	0.0238
16	16.0	0.0120	-0.0026	0.0026	0.0115	-0.0029	0.0070	0.0943	-0.0078	0.0203
17	41.5	0.0000	0.0000	0.0000	0.0000	0.0000	0.0000	0.0000	0.0000	0.0000
18	0.0	0.0000	0.0000	0.0000	0.0000	0.0000	0.0000	0.0000	0.0000	0.0000
19	16.0	0.0000	0.0000	0.0000	0.0000	0.0000	0.0000	0.0000	0.0000	0.0000
20	21.0	0.0000	0.0000	0.0000	0.0000	0.0000	0.0000	0.0000	0.0000	0.0000

VIBRATION SHAPES FOR FLEXIBLE FOUNDATION; FULL WATER

		Mode 1 Freq=3.57 Hz			Mode 2 Freq=3.798 Hz			Mode 3 Freq=5.123 Hz		
Pt.	s (m)	Displ.x	Displ.y	Displ.z	Displ.x	Displ.y	Displ.z	Displ.x	Displ.y	Displ.z
1	0.0	0.0000	0.3037	0.0000	1.0000	0.0000	-0.1901	0.1214	0.0000	-0.0701
2	16.0	-0.6282	0.3543	0.1408	0.8242	-0.0148	-0.1452	-0.0859	0.0710	-0.0106
3	48.0	-0.8711	0.4369	0.1691	-0.0576	0.1798	0.0535	-0.8320	0.4149	0.1976
4	80.0	-0.2175	0.0982	0.0207	-0.1728	0.1882	0.0470	-0.3635	0.1967	0.0639
5	112.9	-0.0144	-0.0139	0.0003	0.0025	0.0043	-0.0001	-0.0217	-0.0200	0.0011
6	0.0	0.0000	0.2093	0.0000	0.6578	0.0000	-0.0636	0.0259	0.0000	-0.0254
7	16.0	-0.3729	0.2367	0.0464	0.5445	-0.0141	-0.0454	-0.0765	0.0396	-0.0047
8	48.0	-0.5061	0.2755	0.0316	0.0354	0.0852	0.0158	-0.4071	0.1883	0.0421
9	80.0	-0.1077	0.0628	-0.0126	-0.0530	0.0932	-0.0004	-0.1555	0.0807	-0.0032
10	99.2	-0.0143	-0.0107	-0.0027	0.0063	0.0183	-0.0049	-0.0249	-0.0163	-0.0003
11	0.0	0.0000	0.0992	0.0000	0.3117	0.0000	0.0292	-0.0267	0.0000	-0.0059
12	16.0	-0.1565	0.1123	-0.0146	0.2601	-0.0112	0.0268	-0.0560	0.0118	-0.0065
13	48.0	-0.1679	0.1093	-0.0314	0.0413	0.0321	0.0063	-0.1175	0.0455	-0.0124
14	75.0	-0.0174	0.0041	-0.0081	0.0092	0.0263	-0.0031	-0.0271	-0.0087	0.0011
15	0.0	0.0000	0.0352	0.0000	0.0767	0.0000	0.0307	-0.0124	0.0000	-0.0048
16	16.0	-0.0313	0.0371	-0.0167	0.0634	0.0005	0.0248	-0.0165	0.0004	-0.0061
17	41.5	-0.0102	0.0193	-0.0156	0.0141	0.0162	0.0021	-0.0106	-0.0031	-0.0033
18	0.0	0.0000	0.0186	0.0000	0.0124	0.0000	0.0119	-0.0022	0.0000	-0.0021
19	16.0	-0.0021	0.0168	-0.0079	0.0099	0.0044	0.0096	-0.0028	-0.0014	-0.0024
20	21.0	-0.0014	0.0154	-0.0103	0.0077	0.0059	0.0076	-0.0029	-0.0018	-0.0025

		Mode 4 Freq=6.075 Hz			Mode 5 Freq=7.365 Hz			Mode 6 Freq=7.926 Hz		
Pt.	s (m)	Displ.x	Displ.y	Displ.z	Displ.x	Displ.y	Displ.z	Displ.x	Displ.y	Displ.z
1	0.0	0.0001	-0.0623	0.0000	-0.9987	0.0000	0.4682	-0.2963	-0.0001	0.0447
2	16.0	0.6278	-0.0985	-0.1713	-0.8174	0.0989	0.3959	0.2032	-0.0924	-0.0996
3	48.0	-0.3395	0.3269	0.1217	-0.1335	0.0985	0.1323	0.4535	-0.0837	-0.1157
4	80.0	-0.6420	0.5028	0.1545	-0.1571	0.1541	0.0706	-0.7937	0.6693	0.2066
5	112.9	-0.0208	-0.0142	0.0018	0.0007	0.0024	0.0033	-0.0281	-0.0142	0.0025
6	0.0	0.0001	-0.0322	0.0000	-0.2212	0.0000	0.1799	-0.3759	-0.0001	0.0603
7	16.0	0.3550	-0.0533	-0.0685	-0.1212	0.0066	0.1469	-0.0831	-0.0280	-0.0043
8	48.0	-0.0225	0.0878	0.0050	0.0993	-0.0309	0.0471	0.3217	-0.1101	-0.0693
9	80.0	-0.2136	0.1893	0.0019	-0.0176	0.0339	0.0201	-0.2146	0.1979	-0.0008
10	99.2	-0.0213	0.0104	-0.0053	0.0009	0.0080	0.0062	-0.0309	0.0227	-0.0088
11	0.0	0.0000	-0.0055	0.0000	0.2267	0.0000	0.0392	-0.2983	0.0000	0.0231
12	16.0	0.1333	-0.0180	-0.0038	0.2256	-0.0288	0.0372	-0.1788	0.0080	0.0142
13	48.0	0.0379	0.0101	-0.0090	0.1301	-0.0422	0.0294	0.0785	-0.0430	-0.0105
14	75.0	-0.0077	0.0184	-0.0040	0.0161	0.0076	0.0125	0.0001	0.0109	-0.0129
15	0.0	0.0000	0.0016	0.0000	0.1159	0.0000	0.0282	-0.0963	0.0000	0.0034
16	16.0	0.0278	-0.0011	0.0023	0.1112	-0.0094	0.0271	-0.0748	0.0013	0.0046
17	41.5	0.0130	0.0061	-0.0078	0.0327	0.0081	0.0100	-0.0066	-0.0133	0.0000
18	0.0	0.0000	0.0003	0.0000	0.0294	0.0000	0.0055	-0.0260	0.0000	0.0148
19	16.0	0.0053	0.0008	-0.0021	0.0267	0.0038	0.0055	-0.0209	-0.0065	0.0125
20	21.0	0.0056	0.0013	-0.0031	0.0223	0.0057	0.0052	-0.0158	-0.0087	0.0109

ANALYSIS OF TALVACCHIA ARCH DAM

V. LOTFI, N. NAJI-MAHALLEH, A. MOKHTAR-ZADEH, A. OROOMCHI.

STRUCTURAL DIVISION OF DAM DEPARTMENT
MAHAB GHODSS CONSULTING ENGS. TEHRAN 19 ,IRAN.

INTRODUCTION

This paper presents the computational results obtained for Talvacchia Arch Dam concerning participation on theme A of First Benchmark Workshop on Numerical Analysis of Dams. Both the static and dynamic analysis are performed using a finite element program named "MADAP". The finite element meshes used in different analysis are similar to suggested meshes with some modifications for taking advantage of geometric symmetry in reducing the number of equations.

The loading cases for static analysis include dead weight, hydrostatic pressure, and thermal loading. The temperature field in dam body is computed by "MHEAT" program for both steady state and periodic analysis. The first 6 natural frequencies and corresponding mode shapes are obtained for the dam on rigid foundation with empty reservoir.

The results are presented as suggested tables and also in the form of cross of principal stresses. Also plots of first 6 mode shapes using post processing program "PLADAP" which easily links to "MADAP" program are presented.

FINITE ELEMENT MESHES

Three different finite element meshes are used in this analysis. In all of these meshes 3-D 20-noded elements are used for both dam body and foundation.

MESH A - This finite element mesh is obtained from MESH ONE with one row of elements in thickness, in which the numbering of elements and nodes are changed in order to take advantage of symmetry and

reduce the bandwidth. Therefore , the nodes and the elements in the right part of dam body are omitted and the displacements in cross-canyon direction for the nodal points on the reference plane are set to zero. The order of node numbering is also changed.This mesh is used for static analysis concerning dead weight and hydrostatic pressure load cases.

MESH B - MESH TWO is also modified to reduce the number of equations. The elements in right part of dam body are omitted but the node numbering of MESH TWO is maintained . However, the boundary conditions of the nodes are changed and the nodes in right part of the dam are fixed, while the displacement in cross-canyon direction for the nodal points in reference plane are set to zero. MESH B is used for thermal stress analysis, while original mesh two is used for temperature distribution analysis.

MESH C - This mesh is used for dynamic analysis of dam on rigid foundation without water. This is a part of MESH ONE in which the nodal points and the elements of the foundation are omitted and the boundary conditions are modified for the nodal points on dam-foundation contact surface.

SOFTWARES

The general flowchart of analysis and post processing of the results is shown in Fig. 1. In this figure circles represent the computer programs and rectangles represent the input or output files. The following softwares are used in this process.

"MHEAT" program [Ref.2] is developed for steady state and also periodic heat transfer analysis of three dimensional continuum systems. The program is written by applying Finite Element procedure in solving Laplace equation in the case of steady state , and Helmholtz equation for periodic thermal analysis.

"MADAP" program [Ref.3] is a modified version of original "ADAP" program [Ref.1] for static and dynamic anaysis of arch dams.The program

is executable on personal computers due to extensive modifications made specially in the eigenvalue solver overlay.The element library is also extended to include 20-noded isoparametric shell elements.

"PLADAP" program [Ref.4] is developed for drawing suitable plots of dam body model, it's deflected shape and , mode shapes obtained from dynamic analysis. It also plots the cross of principal stresses obtained from "MADAP" program in the middle of upstream and downstream faces of each element.

RESULTS

In summary , the values of displacements at the dam crest , and the maximum tensile and compressive principal stresses are shown in table-1 , for all three cases of static loadings considered. More extensive results for each individual static analysis,thermal analysis and mode shapes are given below for a few selective points which are shown in Figs.2-3 ,respectively.

DEAD WEIGHT - Dam is considered as a 3-D monolitic body to which it's dead weight is applied after construction. Displacements and principal stresses for requested points are presented in table-2.
It should be noticed that values are obtained by taking average of stresses calculated from different elements connected to a node. Cross of principal stresses for upstream and downstream faces are shown in Fig.4 .

HYDROSTATIC PRESSURE - The water surface is assumed to be at elevation 507.0 m above sea level . results of displacements and principal stresses are presented in table-3 and plot for cross of principal stresses are shown in Fig. 5.

THERMAL ANALYSIS - The temperature field in dam body is caculated by "MHEAT" program for both steady state and periodic analysis. The results are given in table-5.

STRESS ANALYSIS UNDER THERMAL LOADING - Stress analysis is performed for temperature distribution obtained from steady state thermal analysis. It should be noticed that stress free tempreture is taken as 0 C . Displacements, and principal stresses are presented in table-4, and cross of principal stresses are shown in Fig.6 .

DYNAMIC ANALYSIS - The first 6 natural frequencies and the corresponding mode shapes are calculated for dam on rigid foundation with empty reservior. The values of natural frequencies are summarized in table-6.

Displacements corresponding to modal shapes normalized with respect to mass matrix are presented in table 7-12 , the corresponding plots are shown in Figs 7-12.

REFRENCES

1. R.W. Clough, J.M. Raphael, S. Mojtahedi,"ADAP- A computer program for static and dynamic analysis of arch dams", Report NO. UCB/EERC 73/14 , Earthquake Engineering Research Center , University of California, Berkeley, June 1973.

2. V. Lotfi , N. Naji-Mahalleh , "MHEAT: A computer program for heat transfer analysis of three dimensional continuum systems", Mahab Ghodss Co., Tehran 19, Dec. 1990.

3. V. Lotfi , N. Naji-Mahalleh , "MADAP: Modified Version of ADAP " , Mahab Ghodss Co. Tehran 19, July 1989.

4. A. Mokhtar-Zadeh , "PLADAP: Post-processing program of MADAP" , Mahab Ghodss Co. Tehran 19, June 1990.

Loading		Dead Weight	Hydrostatic Pressure	Temperature Field
Displ.X (m)		0.000821	0.022190	-0.016184
Displ.Z (m)		-0.002974	-0.000570	0.009478
Max. Tensile Stress (MPA)	U/S	0.605270	1.998100	1.241600
	D/S	0.367000	1.332600	2.694800
Max. Compressive Stress (MPA)	U/S	-1.567200	-4.247500	-4.997900
	D/S	-1.298800	-5.997800	-4.542200

TABLE-1 DISPLACEMENTS AT THE DAM CREST & THE MAXIMUM PRINCIPAL STRESSES ON DAM FACES.

Points	S (m)	Displ.X (m)	Displ.Y (m)	Displ.Z (m)	P1 (MPA)	P2 (MPA)	P3 (MPA)
1	0.0	0.00082101	0.00000000	-0.00297430	0.00235470	-0.01644000	-1.11040000
2	0.0	0.00083595	0.00000000	-0.00318810	0.00242300	-0.01100800	-1.18010000
3	0.0	0.00085149	0.00000000	-0.00340200	0.02102200	-0.01050300	-1.25020000
4	0.0	-0.00058465	0.00000000	-0.00240920	0.02647900	-0.03730600	-0.31704000
5	0.0	-0.00057565	0.00000000	-0.00264440	-0.00811140	-0.30692000	-0.41763000
6	0.0	-0.00056311	0.00000000	-0.00289660	-0.00900740	-0.51568000	-0.57592000
7	16.0	-0.00054391	-0.00014444	-0.00231870	0.06386000	-0.02094300	-0.28498000
8	16.0	-0.00053758	-0.00015954	-0.00255400	-0.00624710	-0.25606000	-0.43088000
9	16.0	-0.00052722	-0.00017567	-0.00280820	-0.00788220	-0.45256000	-0.65247000
10	48.0	-0.00021395	-0.00041650	-0.00170100	0.32274000	-0.01651500	-0.10250000
11	48.0	-0.00022405	-0.00044878	-0.00193540	0.01618800	-0.03868800	-0.44014000
12	48.0	-0.00022709	-0.00048405	-0.00219910	-0.00258280	-0.16682000	-0.97457000
13	80.0	-0.00006809	-0.00047911	-0.00084010	0.35815000	0.17214000	-0.04657100
14	80.0	-0.00004941	-0.00044956	-0.00099983	0.19341000	-0.00795700	-0.39040000
15	80.0	-0.00002003	-0.00042787	-0.00118080	0.20707000	0.01263900	-1.15190000
16	99.2	-0.00014607	-0.00017675	-0.00038981	0.42135000	0.09042600	-0.29869000
17	99.2	-0.00013583	-0.00014412	-0.00046119	0.29436000	-0.16477000	-0.38948000
18	99.2	-0.00011052	-0.00011374	-0.00050414	0.16146000	-0.16294000	-1.20910000
19	0.0	-0.00135870	0.00000000	-0.00216800	0.27166000	0.12006000	-0.02265600
20	0.0	-0.00136040	0.00000000	-0.00217260	0.08075800	-0.00289710	-0.45889000
21	0.0	-0.00134240	0.00000000	-0.00220020	-0.02311200	-0.15922000	-1.17500000
22	16.0	-0.00126000	0.00010960	-0.00210160	0.28600000	0.09847200	-0.02356500
23	16.0	-0.00126900	0.00006771	-0.00209970	0.09516700	-0.00224680	-0.48342000
24	16.0	-0.00125750	0.00002289	-0.00211440	-0.01674400	-0.13973000	-1.19100000
25	48.0	-0.00058227	0.00010963	-0.00160120	0.24592000	0.11203000	-0.21146000
26	48.0	-0.00062486	0.00002603	-0.00156680	0.14737000	0.00557840	-0.64942000
27	48.0	-0.00065320	-0.00007157	-0.00149790	0.07278300	0.02650300	-1.14390000
28	75.0	-0.00006538	-0.00007401	-0.00080737	0.10041000	-0.12516000	-1.51210000
29	75.0	-0.00009976	-0.00009442	-0.00084868	0.16518000	-0.19942000	-0.64829000
30	75.0	-0.00013399	-0.00010141	-0.00075344	0.27735000	-0.02962100	-1.04760000
31	0.0	-0.00063803	0.00000000	-0.00207530	0.12352000	-0.04889700	-0.73953000
32	0.0	-0.00062219	0.00000000	-0.00173590	0.00118180	-0.03983900	-0.77604000
33	0.0	-0.00059988	0.00000000	-0.00142640	-0.08775800	-0.19892000	-1.06720000
34	16.0	-0.00052937	0.00011985	-0.00194960	0.11822000	-0.06281400	-0.82169000
35	16.0	-0.00052572	0.00005409	-0.00165270	-0.00695160	-0.05270000	-0.77890000
36	16.0	-0.00051450	-0.00000951	-0.00135430	-0.05962000	-0.21415000	-0.93122000
37	41.5	0.00000192	0.00005859	-0.00119980	-0.12044000	-0.37004000	-2.39070000
38	41.5	-0.00005397	-0.00002162	-0.00118520	-0.01316000	-0.25375000	-0.74736000
39	41.5	-0.00011778	-0.00006678	-0.00094676	0.13812000	0.04407300	-1.05920000
40	0.0	0.00000731	0.00000000	-0.00148280	-0.30099000	-0.46580000	-2.41500000
41	0.0	0.00000119	0.00000000	-0.00131550	-0.25144000	-0.37384000	-0.97534000
42	0.0	-0.00005330	0.00000000	-0.00097574	0.17628000	-0.12632000	-0.70409000

TABLE-2 Displacements & Principal Stresses for Dead Weight Loading.

Points	S (m)	Displ.X (m)	Displ.Y (m)	Displ.Z (m)	P1 (MPA)	P2 (MPA)	P3 (MPA)
1	0.0	0.02219000	0.00000000	-0.00057066	0.05369200	-0.02995500	-3.11700000
2	0.0	0.02222200	0.00000000	-0.00085005	0.14176000	-0.04433500	-2.01010000
3	0.0	0.02223900	0.00000000	-0.00113960	0.07843300	-0.15606000	-0.90210000
4	0.0	0.01997500	0.00000000	0.00042393	-0.12436000	-1.49710000	-4.38280000
5	0.0	0.02002900	0.00000000	-0.00020612	-0.05393200	-0.31241000	-3.04680000
6	0.0	0.02006100	0.00000000	-0.00076042	0.96165000	0.00115720	-1.59990000
7	16.0	0.01837300	-0.00166280	0.00046618	-0.12870000	-1.44370000	-4.20590000
8	16.0	0.01849700	-0.00115500	-0.00011340	-0.05790300	-0.29237000	-3.02520000
9	16.0	0.01860200	-0.00062997	-0.00061821	0.96811000	-0.00209300	-1.77770000
10	48.0	0.00889970	-0.00189390	0.00052386	-0.13931000	-1.26730000	-2.69420000
11	48.0	0.00931000	-0.00105000	0.00025626	-0.09731400	-0.24413000	-2.58590000
12	48.0	0.00972500	-0.00018291	0.00005557	1.04780000	-0.02809800	-2.63700000
13	80.0	0.00182800	0.00064300	0.00007576	-0.17063000	-0.93240000	-1.05320000
14	80.0	0.00203610	0.00086926	0.00013285	0.02049700	-0.12807000	-1.69720000
15	80.0	0.00225810	0.00111080	0.00021431	1.13830000	-0.05063900	-2.49510000
16	99.2	0.00084067	0.00072230	-0.00013167	-0.08157500	-0.47668000	-1.87310000
17	99.2	0.00086933	0.00075774	-0.00007478	-0.04088000	-0.34962000	-1.49240000
18	99.2	0.00083150	0.00073413	-0.00001205	0.54662000	-0.26515000	-1.81750000
19	0.0	0.01442900	0.00000000	0.00267020	-0.35039000	-1.32240000	-4.19340000
20	0.0	0.01450600	0.00000000	0.00111430	-0.16651000	-0.48073000	-2.90400000
21	0.0	0.01455100	0.00000000	-0.00040426	0.76103000	0.02767400	-1.39130000
22	16.0	0.01313600	-0.00162960	0.00251850	-0.32079000	-1.20090000	-3.95270000
23	16.0	0.01329900	-0.00108470	0.00104230	-0.15164000	-0.44255000	-2.80200000
24	16.0	0.01343500	-0.00052118	-0.00040896	0.73196000	-0.00986250	-1.53080000
25	48.0	0.00553080	-0.00162990	0.00148840	0.10911000	-0.49612000	-1.60940000
26	48.0	0.00603480	-0.00074695	0.00050325	0.21198000	-0.30418000	-2.10520000
27	48.0	0.00653020	0.00011925	-0.00051080	0.57519000	-0.21459000	-2.84310000
28	75.0	0.00119600	0.00054530	0.00017220	0.98463000	0.32407000	-1.13940000
29	75.0	0.00147650	0.00087016	-0.00012081	0.43649000	-0.41026000	-1.47070000
30	75.0	0.00154610	0.00096849	-0.00037489	-0.44733000	-0.49900000	-4.86920000
31	0.0	0.00598150	0.00000000	0.00329880	0.80621000	-1.12560000	-1.86430000
32	0.0	0.00588040	0.00000000	0.00114980	0.72649000	-0.72679000	-0.94775000
33	0.0	0.00589380	0.00000000	-0.00091032	0.91966000	-0.21454000	-1.75750000
34	16.0	0.00516680	-0.00075739	0.00287380	1.03280000	-0.87172000	-1.78880000
35	16.0	0.00517910	-0.00028568	0.00094907	0.57708000	-0.51216000	-1.03780000
36	16.0	0.00525890	0.00014412	-0.00093499	0.55266000	0.09915000	-2.21710000
37	41.5	0.00140400	-0.00010210	0.00094178	3.46850000	1.19110000	0.26964000
38	41.5	0.00186580	0.00057194	-0.00005261	1.11850000	0.38164000	-0.79329000
39	41.5	0.00201570	0.00086935	-0.00079349	-0.33107000	-1.02310000	-5.82820000
40	0.0	0.00166820	0.00000000	0.00174180	4.42630000	1.60460000	1.02570000
41	0.0	0.00177980	0.00000000	0.00009595	1.85700000	0.69916000	-0.45953000
42	0.0	0.00178840	0.00000000	-0.00092366	-0.09344000	-0.26542000	-4.53550000

TABLE-3 Displacements & Principal Stresses for Hydrostatic Presure Loading.

Points	S (m)	Displ.X (m)	Displ.Y (m)	Displ.Z (m)	P1 (MPA)	P2 (MPA)	P3 (MPA)
1	0.0	-0.01618400	0.00021365	0.00947840	1.13730000	0.96395000	0.82190000
2	0.0	-0.01594500	-0.00010174	0.01045700	0.21145000	-0.03447300	-0.32051000
3	0.0	-0.01570000	-0.00040011	0.01140000	0.20237000	-0.00705750	-0.04661900
4	0.0	-0.01081600	-0.00088411	0.00575430	0.69716000	0.02979700	-0.11426000
5	0.0	-0.01057900	-0.00121320	0.00675510	0.44610000	0.01931600	-0.15007000
6	0.0	-0.01028700	-0.00156490	0.00776220	0.23533000	-0.00023147	-0.23065000
7	16.0	-0.00936020	0.00032850	0.00469920	0.79578000	0.02066100	-0.11201000
8	16.0	-0.00914530	0.00011967	0.00560710	0.19410000	0.00351370	-0.31236000
9	16.0	-0.00886900	-0.00011127	0.00653150	-0.02347700	-0.28712000	-0.65489000
10	48.0	-0.00592830	0.00236260	0.00308870	0.57872000	0.00942050	-0.54462000
11	48.0	-0.00585160	0.00190640	0.00396190	0.15262000	0.00367930	-1.06730000
12	48.0	-0.00571140	0.00142660	0.00485680	-0.03825500	-0.14015000	-1.87060000
13	80.0	-0.00136420	0.00148330	0.00095777	-0.41951000	-0.97816000	-2.32070000
14	80.0	-0.00141450	0.00100740	0.00153710	0.07667200	-0.59505000	-2.88210000
15	80.0	-0.00145760	0.00046151	0.00219330	0.79505000	-0.48952000	-3.57780000
16	99.2	0.00000000	0.00000000	0.00000000	-1.56750000	-4.11600000	-6.21500000
17	99.2	0.00000000	0.00000000	0.00000000	-0.20996000	-4.07940000	-4.57200000
18	99.2	0.00000000	0.00000000	0.00000000	1.95310000	-4.42830000	-4.80260000
19	0.0	-0.00598890	-0.00200180	0.00204780	0.85098000	0.02194100	-0.09322300
20	0.0	-0.00566620	-0.00229440	0.00305930	0.89255000	0.11279000	-0.15270000
21	0.0	-0.00526440	-0.00261960	0.00406590	0.91843000	0.07332400	-0.07238700
22	16.0	-0.00511410	-0.00071900	0.00178020	0.57779000	-0.02115900	-0.37372000
23	16.0	-0.00479630	-0.00094014	0.00265480	0.12671000	-0.23154000	-0.49856000
24	16.0	-0.00438120	-0.00118830	0.00355240	-0.03822700	-0.43106000	-1.15420000
25	48.0	-0.00221610	0.00092081	0.00090069	0.09941700	-0.54591000	-1.65560000
26	48.0	-0.00205000	0.00037767	0.00158850	0.55743000	0.04458100	-2.19620000
27	48.0	-0.00179600	-0.00017649	0.00227600	0.58780000	-0.21075000	-3.04960000
28	75.0	0.00000000	0.00000000	0.00000000	-0.86775000	-3.91960000	-6.67880000
29	75.0	0.00000000	0.00000000	0.00000000	0.91976000	-3.74200000	-3.94560000
30	75.0	0.00000000	0.00000000	0.00000000	1.37840000	-4.75340000	-5.55480000
31	0.0	-0.00188100	-0.00193910	-0.00037967	0.61128000	0.17145000	-0.83437000
32	0.0	-0.00139690	-0.00206330	0.00035677	0.60691000	-0.10487000	-1.36180000
33	0.0	-0.00076172	-0.00214840	0.00115830	1.68150000	0.45534000	-0.36556000
34	16.0	-0.00171700	-0.00070210	0.00032176	-0.09194100	-0.26958000	-2.04680000
35	16.0	-0.00117630	-0.00083645	0.00089834	-0.22145000	-0.73949000	-3.17120000
36	16.0	-0.00050176	-0.00097330	0.00153940	0.79505000	-0.59799000	-3.47190000
37	41.5	0.00000000	0.00000000	0.00000000	-0.53692000	-3.92530000	-7.11620000
38	41.5	0.00000000	0.00000000	0.00000000	1.36650000	-3.55620000	-3.72220000
39	41.5	0.00000000	0.00000000	0.00000000	1.10760000	-4.98460000	-6.02340000
40	0.0	0.00000000	0.00000000	0.00000000	-1.62800000	-5.22050000	-11.87400000
41	0.0	0.00000000	0.00000000	0.00000000	-0.33502000	-4.96170000	-8.04200000
42	0.0	0.00000000	0.00000000	0.00000000	-0.04401600	-5.43210000	-8.21650000

TABLE-4 Displacements & Principal Stresses for Thermal Loading.

Points	S (m)	Steady state analysis temperature T (C)	Periodic analysis	
			Amplitude (C)	Phase (rad)
1	0.0	15.00000	10.00000	0.00000
2	16.0	15.00000	10.00000	0.00000
3	48.0	15.00000	10.00000	0.00000
4	80.0	13.54900	7.62870	-0.54674
5	112.9	13.55200	7.63330	-0.55343
6	0.0	12.34600	5.85570	-0.95811
7	16.0	12.34600	5.84060	-0.96098
8	48.0	12.34800	5.72790	-0.98062
9	80.0	12.35700	5.63000	-1.01250
10	99.2	12.31900	5.69330	-1.00470
11	0.0	12.34800	3.75030	-1.56750
12	16.0	12.34800	3.74220	-1.57110
13	48.0	12.36300	3.68090	-1.59040
14	75.0	12.68800	4.12090	-1.46170
15	0.0	12.39100	1.85150	-2.26160
16	16.0	12.40000	1.87300	-2.19890
17	41.5	12.61800	2.20860	-2.03110
18	0.0	13.05400	1.70190	-2.30010
19	16.0	13.07300	1.67620	-2.28880
20	22.0	13.30100	2.22510	-2.39730

TABLE-5: TEMPRETURE DISTRIBUTION FOR STEADY STATE & PERIODIC ANALYSIS

Mode	Natural Circular Freq. w (rad/sec)	Natural Freq. f (hz)	Periods T (sec)
1	27.0144	4.2995	0.2326
2	28.7823	4.5808	0.2183
3	35.8198	5.7009	0.1754
4	42.2517	6.7246	0.1487
5	54.0188	8.5974	0.1163
6	58.9234	9.3780	0.1066

TABLE-6: FIRST SIX NATURAL FREQUENCIES & PERIODS OF TALVACCHIA ARCH DAM

Points	S (m)	Displ.X	Displ.Y	Displ.Z
1	0.0	-0.00000374	0.00060000	0.00000086
2	16.0	-0.00157000	0.00073300	0.00040200
3	48.0	-0.00199000	0.00095900	0.00047000
4	80.0	-0.00037900	0.00017600	0.00005850
5	112.9	0.00000000	0.00000000	0.00000000
6	0.0	-0.00000218	0.00039800	0.00000031
7	16.0	-0.00085900	0.00046500	0.00014200
8	48.0	-0.00104000	0.00053400	0.00011400
9	80.0	-0.00013700	0.00008000	-0.00000953
10	99.2	0.00000000	0.00000000	0.00000000
11	0.0	-0.00000080	0.00015800	-0.00000004
12	16.0	-0.00029700	0.00018300	-0.00001270
13	48.0	-0.00024100	0.00014900	-0.00003030
14	75.0	0.00000000	0.00000000	0.00000000
15	0.0	-0.00000010	0.00003150	-0.00000003
16	16.0	-0.00003360	0.00003130	-0.00001260
17	41.5	0.00000000	0.00000000	0.00000000
18	0.0	0.00000000	0.00000000	0.00000000
19	16.0	0.00000000	0.00000000	0.00000000
20	22.0	0.00000000	0.00000000	0.00000000

TABLE-7 MODE-1 (NORMALIZED WITH RESPECT TO MASS MATRIX)

Points	S (m)	Displ.X	Displ.Y	Displ.Z
1	0.0	-0.00332000	-0.00000070	0.00078300
2	16.0	-0.00261000	0.00009520	0.00058700
3	48.0	0.00033700	-0.00051000	-0.00017400
4	80.0	0.00046900	-0.00043000	-0.00013900
5	112.9	0.00000000	0.00000000	0.00000000
6	0.0	-0.00192000	-0.00000047	0.00028300
7	16.0	-0.00154000	0.00005410	0.00020700
8	48.0	0.00002860	-0.00023200	-0.00004520
9	80.0	0.00013100	-0.00016300	-0.00000823
10	99.2	0.00000000	0.00000000	0.00000000
11	0.0	-0.00071100	-0.00000018	-0.00003750
12	16.0	-0.00056800	0.00002970	-0.00003660
13	48.0	-0.00002820	-0.00006130	-0.00000983
14	75.0	0.00000000	0.00000000	0.00000000
15	0.0	-0.00009460	-0.00000003	-0.00003140
16	16.0	-0.00006760	0.00000128	-0.00002300
17	41.5	0.00000000	0.00000000	0.00000000
18	0.0	0.00000000	0.00000000	0.00000000
19	16.0	0.00000000	0.00000000	0.00000000
20	22.0	0.00000000	0.00000000	0.00000000

TABLE-8 MODE-2 (NORMALIZED WITH RESPECT TO MASS MATRIX)

Points	S (m)	Displ.X	Displ.Y	Displ.Z
1	0.0	-0.00022900	0.00000009	0.00004200
2	16.0	-0.00078400	0.00025800	0.00020300
3	48.0	-0.00251000	0.00125000	0.00068900
4	80.0	-0.00086900	0.00051300	0.00018600
5	112.9	0.00000000	0.00000000	0.00000000
6	0.0	-0.00009830	0.00000005	0.00002350
7	16.0	-0.00035100	0.00012200	0.00007320
8	48.0	-0.00106000	0.00049500	0.00015300
9	80.0	-0.00026200	0.00016000	-0.00000556
10	99.2	0.00000000	0.00000000	0.00000000
11	0.0	-0.00001600	0.00000001	0.00000591
12	16.0	-0.00007940	0.00002350	0.00000370
13	48.0	-0.00017600	0.00008020	-0.00001520
14	75.0	0.00000000	0.00000000	0.00000000
15	0.0	0.00000438	0.00000000	0.00000178
16	16.0	-0.00000139	-0.00000032	-0.00000043
17	41.5	0.00000000	0.00000000	0.00000000
18	0.0	0.00000000	0.00000000	0.00000000
19	16.0	0.00000000	0.00000000	0.00000000
20	22.0	0.00000000	0.00000000	0.00000000

TABLE-9: MODE-3 (NORMALIZED WITH RESPECT TO MASS MATRIX)

Points	S (m)	Displ.X	Displ.Y	Displ.Z
1	0.0	0.00000021	−0.00020500	−0.00000007
2	16.0	0.00177000	−0.00031200	−0.00048800
3	48.0	−0.00108000	0.00089800	0.00041500
4	80.0	−0.00152000	0.00117000	0.00041400
5	112.9	0.00000000	0.00000000	0.00000000
6	0.0	0.00000008	−0.00011500	−0.00000001
7	16.0	0.00095100	−0.00017300	−0.00018200
8	48.0	−0.00009790	0.00020700	0.00004690
9	80.0	−0.00038500	0.00033800	0.00001510
10	99.2	0.00000000	0.00000000	0.00000000
11	0.0	0.00000000	−0.00003180	0.00000000
12	16.0	0.00030000	−0.00006010	−0.00000012
13	48.0	0.00006610	0.00000445	0.00000165
14	75.0	0.00000000	0.00000000	0.00000000
15	0.0	0.00000000	−0.00000364	0.00000000
16	16.0	0.00003330	−0.00000711	0.00000713
17	41.5	0.00000000	0.00000000	0.00000000
18	0.0	0.00000000	0.00000000	0.00000000
19	16.0	0.00000000	0.00000000	0.00000000
20	22.0	0.00000000	0.00000000	0.00000000

TABLE-10: MODE-4 (NORMALIZED WITH RESPECT TO MASS MATRIX)

Points	S (m)	Displ.X	Displ.Y	Displ.Z
1	0.0	-0.00267000	-0.00000014	0.00103000
2	16.0	-0.00089400	-0.00003020	0.00047600
3	48.0	0.00080400	-0.00003730	-0.00003270
4	80.0	-0.00181000	0.00154000	0.00056200
5	112.9	0.00000000	0.00000000	0.00000000
6	0.0	-0.00098500	-0.00000021	0.00039700
7	16.0	-0.00016600	-0.00007610	0.00019300
8	48.0	0.00089200	-0.00030200	-0.00007450
9	80.0	-0.00035000	0.00034700	0.00003200
10	99.2	0.00000000	0.00000000	0.00000000
11	0.0	-0.00003700	-0.00000026	0.00006870
12	16.0	0.00015400	-0.00004580	0.00005600
13	48.0	0.00028800	-0.00012300	0.00002550
14	75.0	0.00000000	0.00000000	0.00000000
15	0.0	0.00002640	-0.00000010	0.00001870
16	16.0	0.00003740	-0.00000804	0.00001940
17	41.5	0.00000000	0.00000000	0.00000000
18	0.0	0.00000000	0.00000000	0.00000000
19	16.0	0.00000000	0.00000000	0.00000000
20	22.0	0.00000000	0.00000000	0.00000000

TABLE-11: MODE-5 (NORMALIZED WITH RESPECT TO MASS MATRIX)

Points	S (m)	Displ.X	Displ.Y	Displ.Z
1	0.0	0.00244000	0.00000033	-0.00148000
2	16.0	0.00237000	-0.00043500	-0.00139000
3	48.0	0.00051900	-0.00028100	-0.00042700
4	80.0	-0.00064000	0.00042200	0.00012900
5	112.9	0.00000000	0.00000000	0.00000000
6	0.0	-0.00065100	0.00000033	-0.00036400
7	16.0	-0.00046300	0.00000795	-0.00036100
8	48.0	-0.00016500	0.00002020	-0.00017100
9	80.0	-0.00018500	0.00011800	-0.00001700
10	99.2	0.00000000	0.00000000	0.00000000
11	0.0	-0.00141000	0.00000020	-0.00007880
12	16.0	-0.00119000	0.00013000	-0.00008810
13	48.0	-0.00026000	0.00006280	-0.00007520
14	75.0	0.00000000	0.00000000	0.00000000
15	0.0	-0.00031600	0.00000006	-0.00006180
16	16.0	-0.00024200	0.00001940	-0.00005050
17	41.5	0.00000000	0.00000000	0.00000000
18	0.0	0.00000000	0.00000000	0.00000000
19	16.0	0.00000000	0.00000000	0.00000000
20	22.0	0.00000000	0.00000000	0.00000000

TABLE-12: MODE-6 (NORMALIZED WITH RESPECT TO MASS MATRIX)

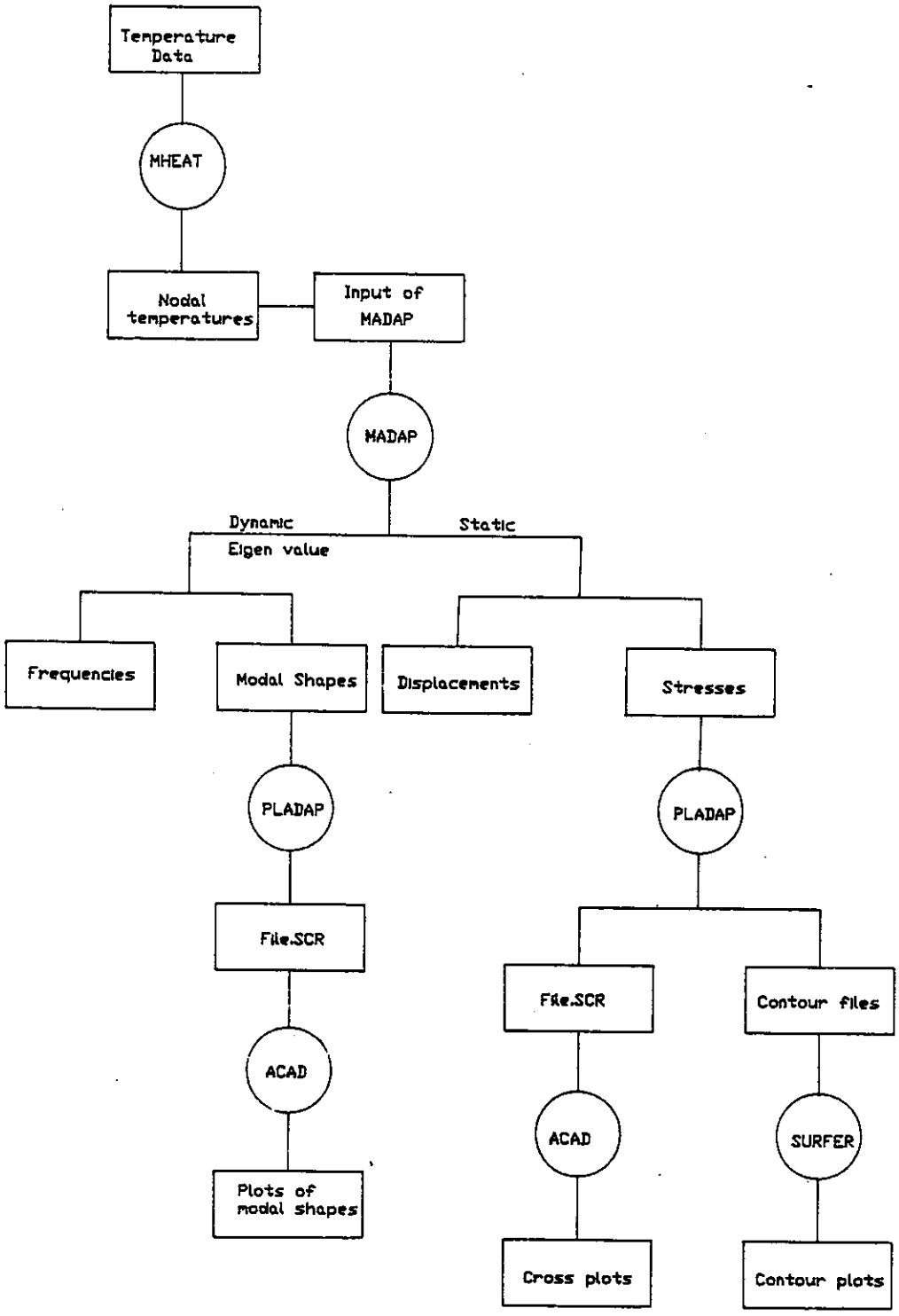

Fig. 1 - Flowchart of Analysis.

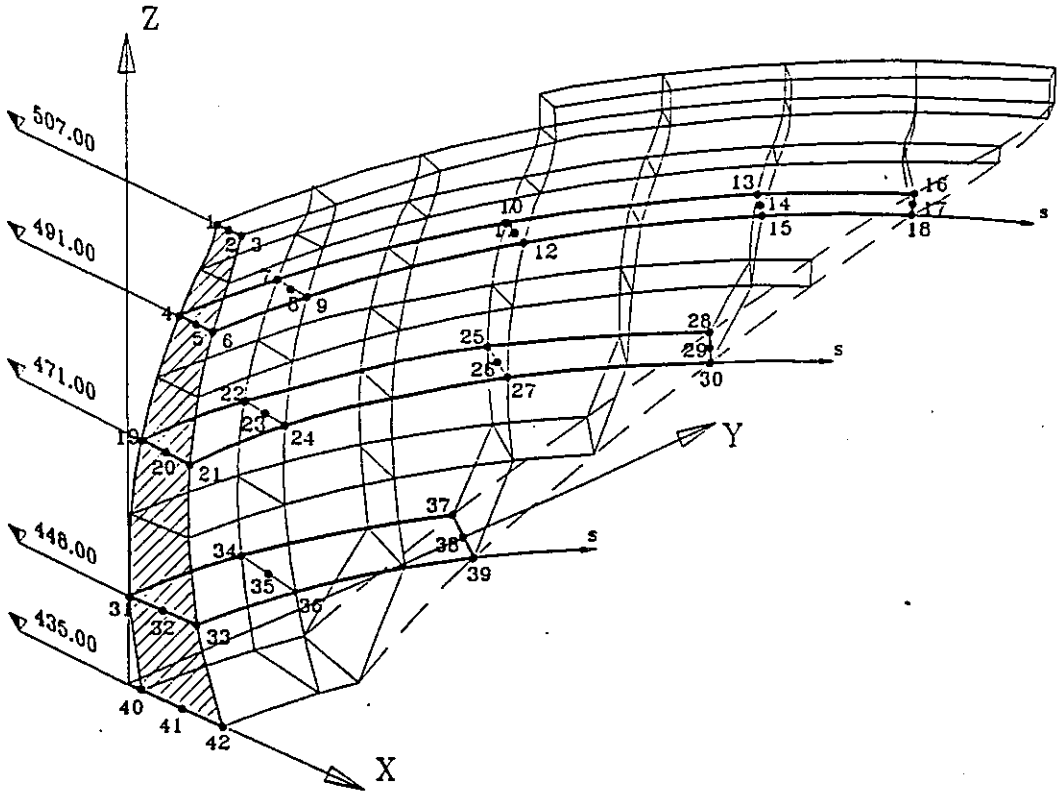

Fig. 2

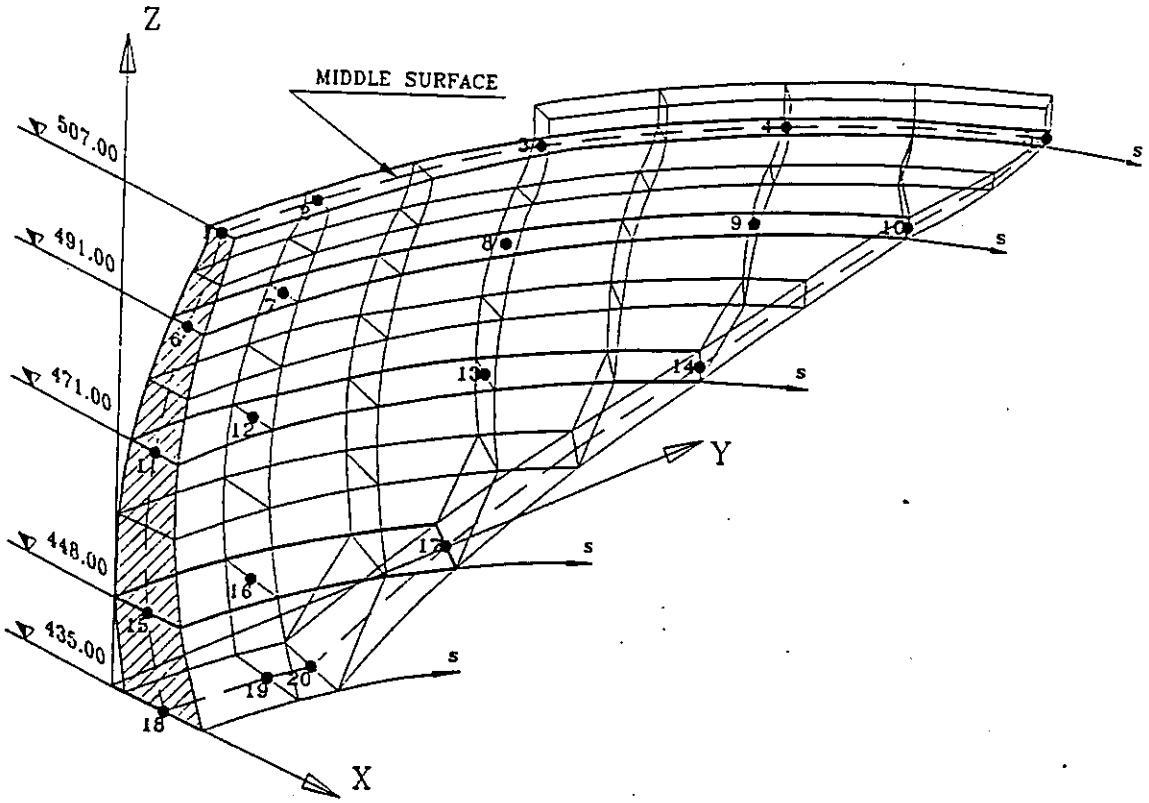

Fig. 3

1st Benchmark Workshop on

"Numerical Analysis of Dams"

Bergamo (Italy) - May 28-29, 1991

E. BOURDAROT, V. MILOVANOVITCH

E.D.F.-C.N.E.H., Le Bourget du Lac, France

"Analysis of Talvacchia Arch Dam" *

* The colour meshes sent by the Authors and concerning the results cannot be published on this B/W Preprint volume. Therefore please refer to the oral presentation.

EDF
Electricité de France

Centre National d'Equipement Hydraulique

SAVOIE TECHNOLAC – 73373 LE BOURGET DU LAC CEDEX tél : 79 60 60 60

Benchmark Workshop on numerical analysis of dam

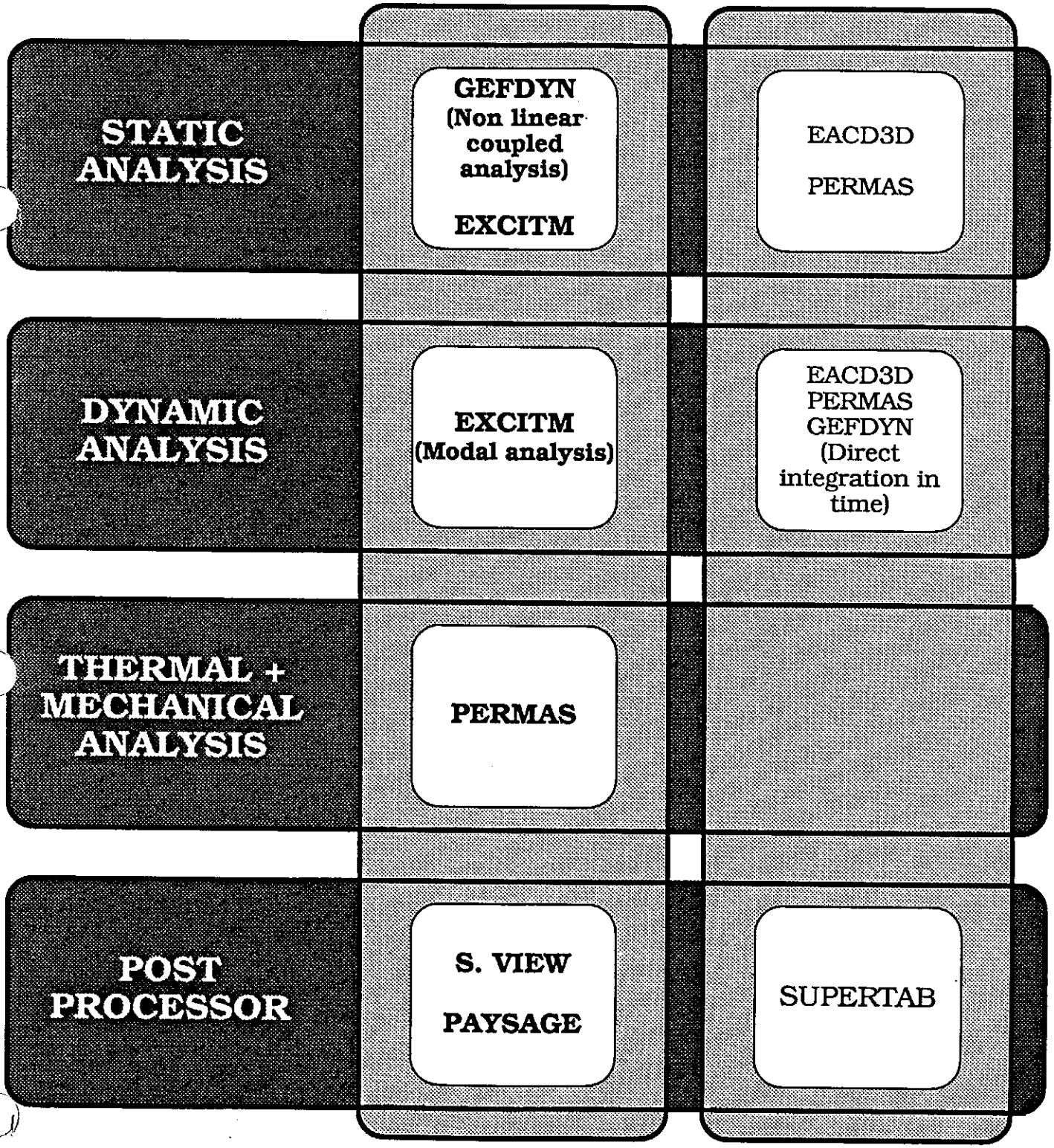

3.1

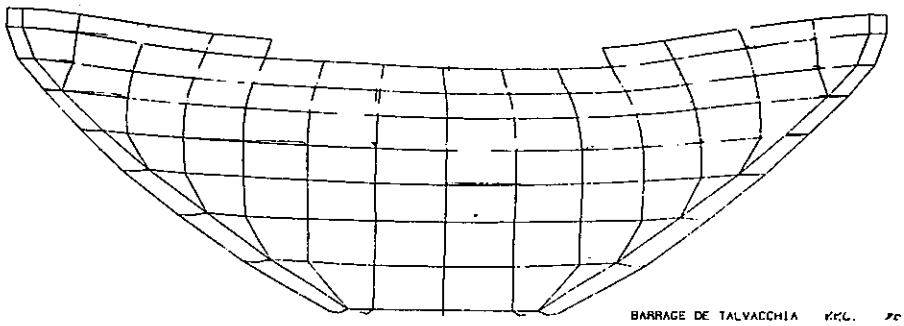

BARRAGE DE TALVACCHIA
CONTRAINTE SOLIDE PRINCIPALE SIGMA 1 T = 0.1000E+01
VUE PERSPECTIVE
BARRAGE DE TALCACCHIA

EDF

MAXIMUM 0.168E6
0.324E6
0.114E6
0.950E5
-0.304E6
-0.514E6
-0.723E6
-0.933E6
-0.114E7
-0.135E7
-0.156E7
-0.177E7
MINIMUM -0.155E7

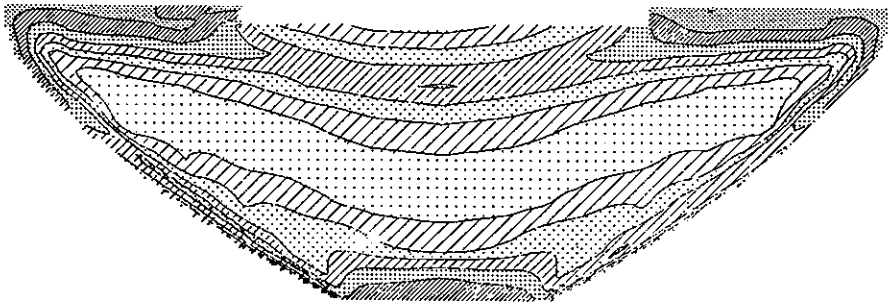

VISUALISATION DE LA DEFORMEE AMPLITUDE MUL
DEPLACEMENTS TOTAUX DATE = 0.20
BARRAGE DE TALCACCHIA

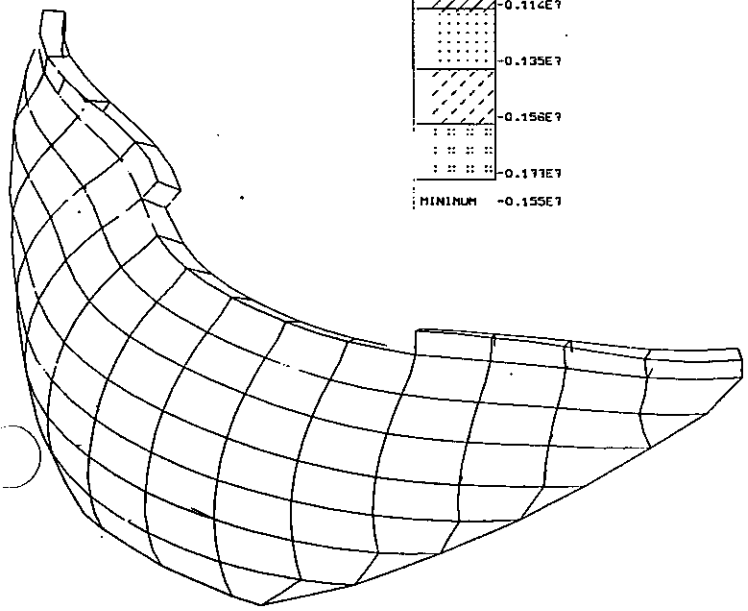

BARRAGE DE TALVACCHIA
CONTRAINTE SOLIDE PRINCIPALE SIGMA 1 T = 0.1000E+01
VUE PERSPECTIVE
BARRAGE DE TALCACCHIA

EDF

FIDER NOVE 1985 24/MAI /91

MAXIMUM 0.308E6
0.324E6
0.114E6
0.950E5
-0.304E6
-0.514E6
-0.723E6
-0.933E6
-0.114E7
-0.135E7
-0.156E7
-0.177E7
MINIMUM -0.178E7

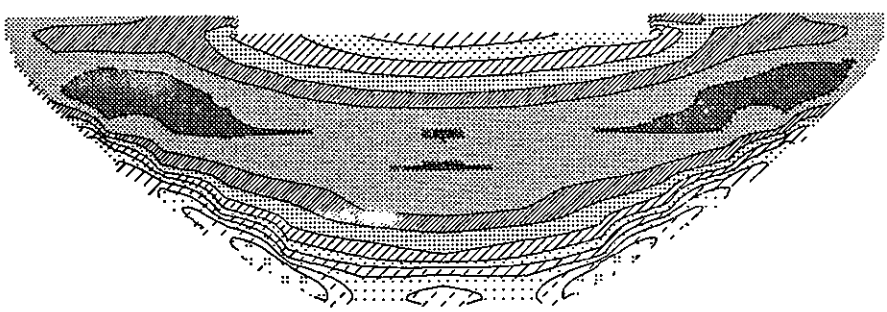

VISUALISATION DE LA DEFORMEE AMPLITUDE MULTIPLIEE PAR 0.1000+04
DEPLACEMENTS TOTAUX DATE = 0.3000E+01
BARRAGE DE TALCACCHIA

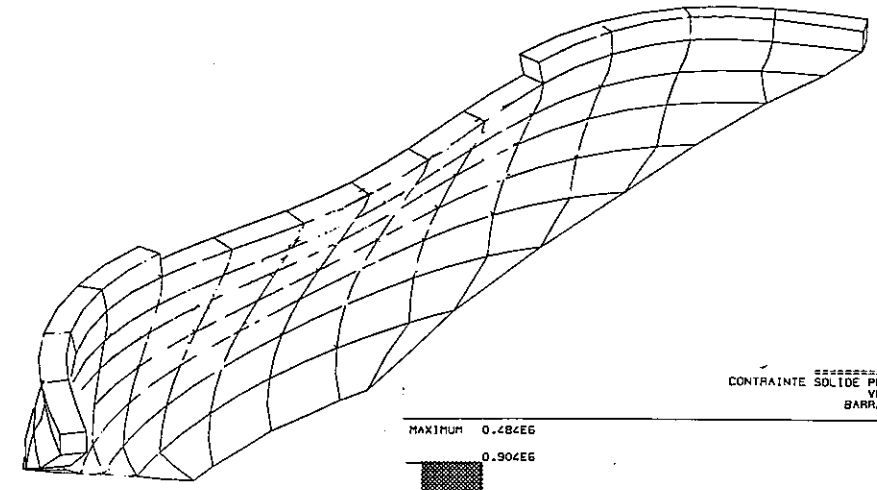

PAYSAGE (C) EDF/DER MVMS 1985 23/MAI /91

CONTRAINTE SOLIDE PRINCIPALE SIGMA 1 T = 0.3000E+01
VUE PERSPECTIVE
BARRAGE DE TALCACCHIA

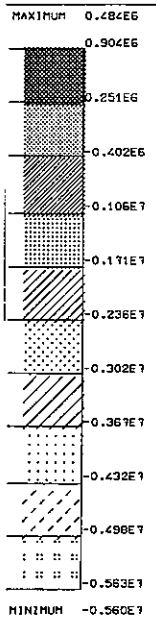

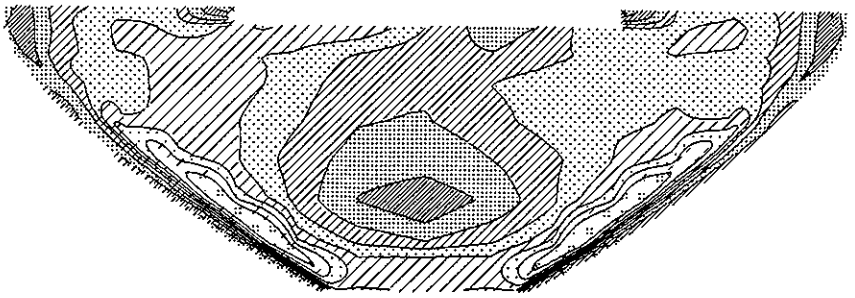

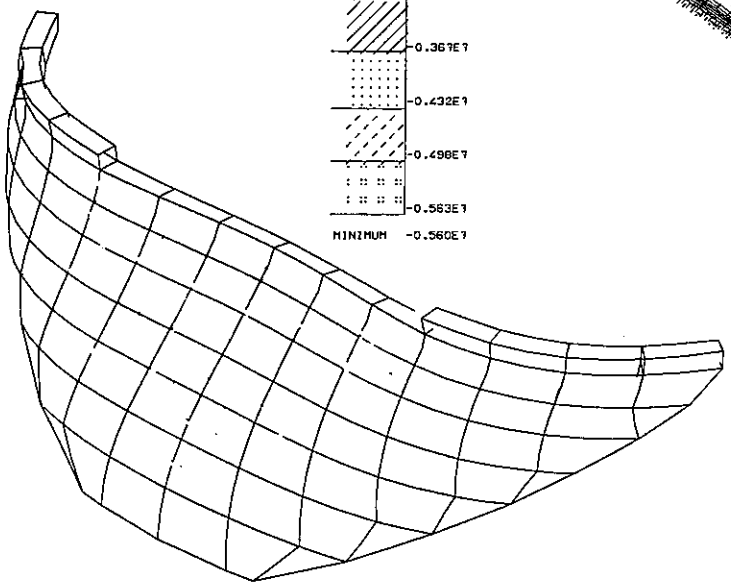

PAYSAGE (C) EDF/DER MVMS 1985 23/MAI /91

X 2000.

CONTRAINTE SOLIDE PRINCIPALE SIGMA 1 T = 0.3000E+01
VUE PERSPECTIVE
BARRAGE DE TALCACCHIA

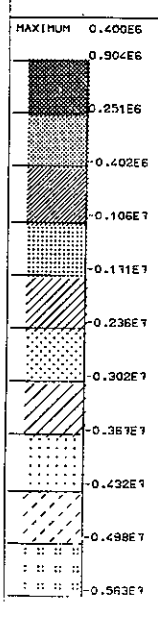

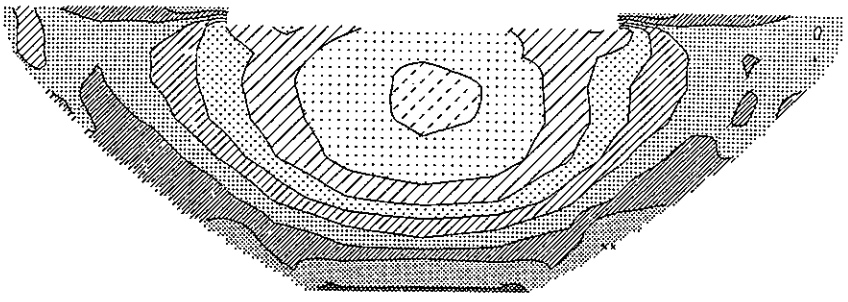

EDF Electricité de France

Centre National d'Equipement Hydraulique

SAVOIE TECHNOLAC – 73373 LE BOURGET DU LAC CEDEX tél : 79 60 60 60

Theme A

Benchmark Workshop on numerical analysis of dam

Thermal steady state & periodic analysis
Boundary conditions

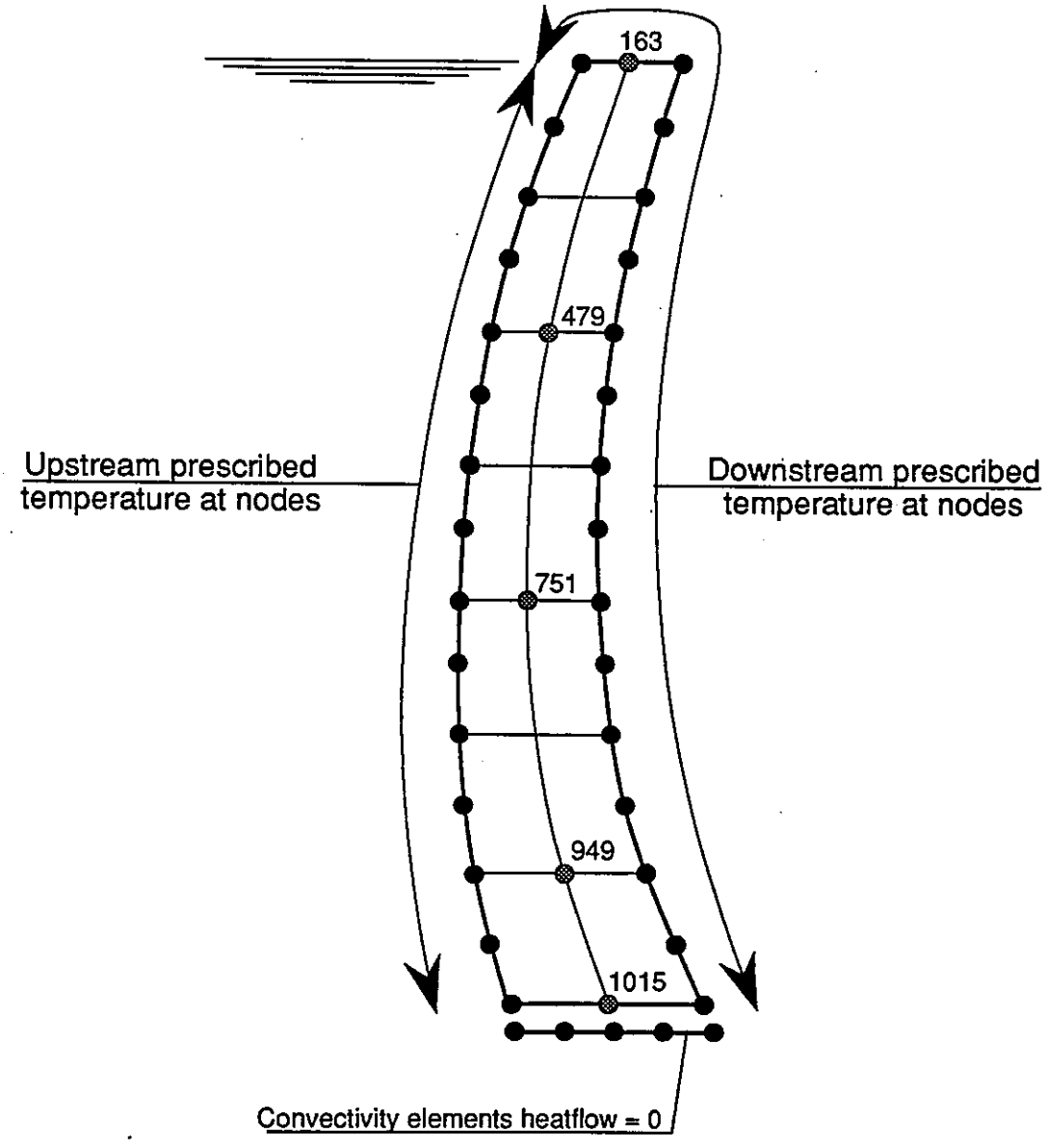

TALVACCHIA DAM THERMAL PERIODIC ANALYSIS

EDF-CNEH

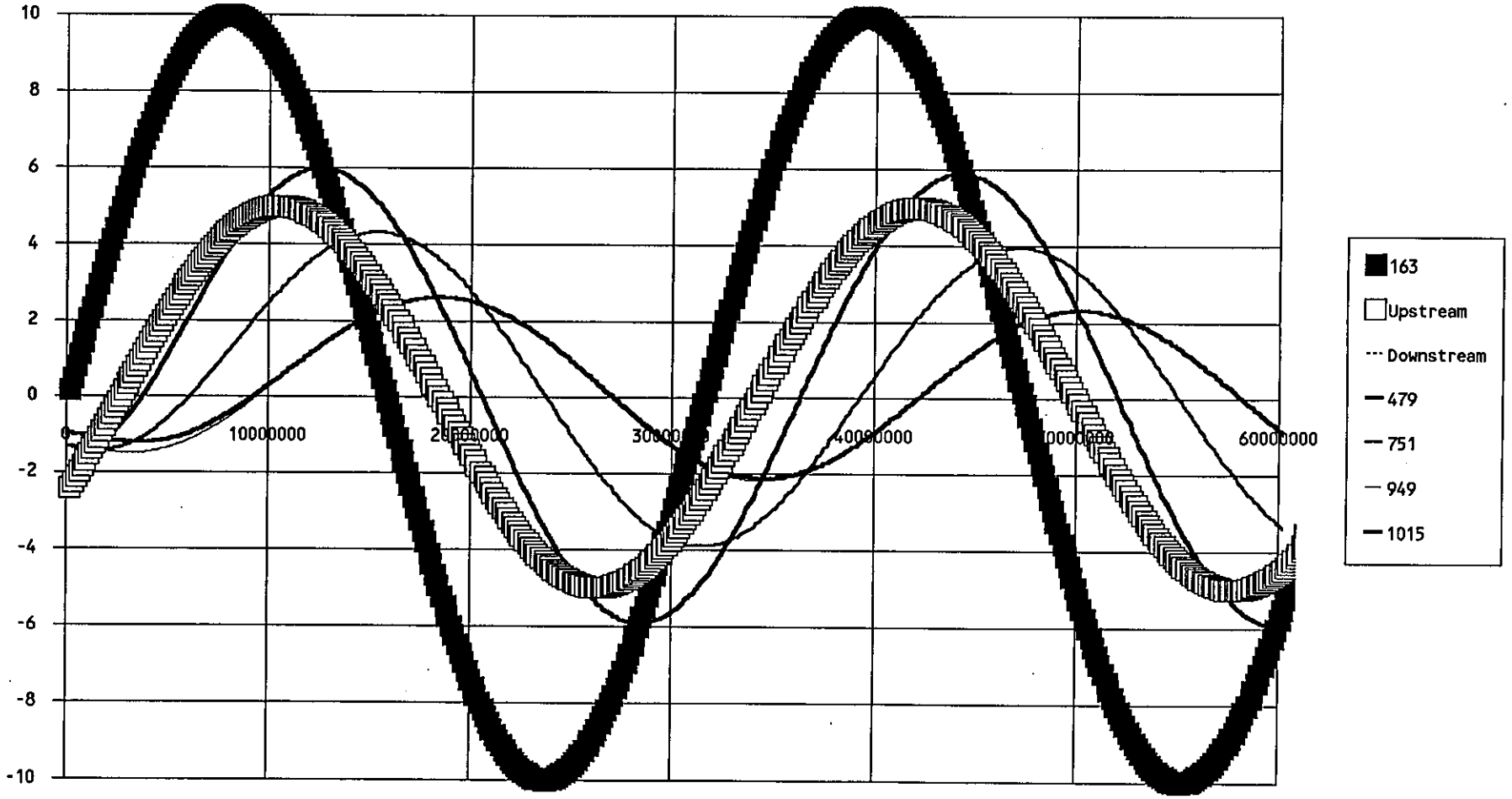

FIRST BENCHMARK WORKSHOP ON NUMERICAL ANALYSIS OF DAMS

THEME A: Double curvature concrete arch dam

ANALYSIS RESULTS

All analysis were performed on the suggested model. The HEXA20 and PENTA15 elements were transformed in 8HEXA8 and 4HEXA8 + 4PENTA6 isoparametric elements respectivly. The HEXA8 elements used to discretize the dam with its foundation are the elements with incompatible modes (internal degrees of freedom). It means that the mesh used here had 27 instead of 20 nodes for hexahedral volume and 21 instead of 15 nodes for pentahedral volume. All physical-mechanical parameters were used as suggested.

STATIC ANALYSIS

LOADING CONDITION 3.1 - Dead wieght

The suggested loading was applied on the dam-foundation system. We considered the dead weight of the dam only. The obtained results are presented in the annex. The nodal stresses are calculated as the average of all stresses obtained for that node.

LOADING CONDITION 3.2. - Hydrostatic pressure

As suggested, the hydrostatic pressure was applied on the upstream face of the dam only. The dam-foundation system was considered in the analysis. The obtained results are presented in the annex. The nodal stresses are calculated as the average of all stresses obtained for that node.

DYNAMIC ANALYSIS

LOADING CONDITION 3.5.1.

The eigenvalue analysis was performed for dam on rigid foundation without water. The results are presented in the annex. The eigenvectors are normalized with the regard of the greatest value of each eigenvector separately.

The symetric modes are : 2, 3, 5, 8, 9, 10.
The antisymetric modes are : 1, 4, 6, 7.

LOADING CONDITION 3.5.2.

The dynamic modal analysis was performed on the complete model that contains the concrete dam with its foundation and the reservoir with the impounded water. The damping is not included in the analysis that means that all modes have real values. The formulation of the fluid-structure coupling eigenvalue problem treated here contains two types of degrees of freedom. The first is associated with the dam and its foundations and the second with the impounded water. The dam with its foundation is discretized with solid elements that have three displacement degrees of freedom per node. The impounded water was discretized with fluid elements that have two degrees of freedom per node. These are the pressure and the potential of displacement. The coupling elements contain four degrees of freedom per node. These are three displacements and one potential of displacement. The free surface elements contain two degrees of freedom with one potential of displacement and one displacement of free surface in the vertical direction.

The analysis, carried out here, supposed the dam-water coupling only ie.without foundation-water coupling. The boundary conditions adopted are:

(a) The fixed nodes at the foundation boundary as suggested

(b) The fixed nodes at the fluid boundary on the fluid-foundation contact and at the fluid boundary farther removed from upstream dam face without absorption. For free surface boundary conditions we adopted the pressure equal zero which means that the potential of displacement and the vertical displacement of free surface are zero too.

The free surface elements permit the calculation of sloshing modes. These modes are neglected in this analysis because of fact that below the frequency of, for example, 1 Hz there are the hundreds of sloshing modes. In general, there is a great density of sloshing modes and it means that to reach the first dam mode we need to calculate several hundreds of sloshing modes that makes the eigenvalue analysis almost impossible.

In the eigenvalue analysis of solid-fluid coupling problem with the fluid compressible, we have different types of modes . To define which of them is in question we calculate the potential and the kinetic energy of solid and fluid. These energies are normalized with the regard of coupling energy. This permits of to distinguish the dam mode (with or without the added mass of water) from the acoustic mode or from the dam-fluid coupling mode. In general, the first few modes are the modes of the dam (with or without the added mass of water) and after that come the acoustic modes and the coupling modes (because of boundary conditions at the free surface). The frequencies of coupled problem with compressible fluid are less separated (after the first acoustic mode) than frequencies of the problem without coupling or with empty reservoir. The accuracy of higher acoustic modes depend on the mesh density in fluid.

If we consider the fluid incompressible there is no acoustic and coupling modes but only modes of the dam with or without the added mass of fluid.

Both analysis are performed here, with fluid compressible and incompressible. The results are presented in the annex.

The eigenvectors are normalized with the regard of the greatest displacement value of each eigenvector separately.

COMPRESSIBLE FLUID

MODE	MODE TYPE	DAM	FLUID
1	dam mode with the added mass of water	antisymetric	antisymetric
2	dam mode with the added mass of water	symetric	symetric
3	dam mode with the added mass of water	symetric	symetric
4	dam mode with the added mass of water	antisymetric	antisymetric
5	dam-water coupling mode	symetric	symetric
6	dam and acoustic mode equal frequencies - no coupling	symetric	symetric
7	dam and acoustic mode equal frequencies - no coupling	symetric	symetric
8	dam-water coupling mode	---	---
9	dam and acoustic mode equal frequencies - no coupling	---	---
10	dam and acoustic mode equal frequencies - no coupling	---	symetric

The analysis with incompressible fluid shows for all calculated modes that the coupling energy is equal to the kinetic energy of fluid and the potential energy of fluid is zero.

All modes are the dam modes with the added mass of water.

INCOMPRESSIBLE FLUID

MODE	DAM	FLUID
1	antisymetric	antisymetric
2	symetric	symetric
3	symetric	symetric
4	antisymetric	antisymetric
5	symetric	symetric
6	symetric	symetric
7	antisymetric	antisymetric
8	antisymetric	antisymetric
9	symetric	symetric
10	symetric	---

THERMAL ANALYSIS

3D thermal finite element analysis was performed on the 3D suggested model keeping into account the dam only (mesh 2 with two rows of elements in thickness).

For steady-state and periodic analyses following conditions was assumed :

- Prescribed temperature conditions on upstream and downstream faces as suggested in annexes 4 and 5 .

- Adiabatic conditions at dam-fondation interface.

Loading conditions 3.3.1. and 3.3.2.

Temperatures at selected nodes are given in the annex .

For periodic analysis,initial temperature conditions are given by a preliminarly steady-state analysis.Amplitude and phases are calculated at the two extremum of temperature curves.

Loading condition 3.4

Cartesian displacements (dx,dy,dz) at selected points are given in the annex .

LOADING CONDITION 3.1

	DISPLACEMENTS			STRESSES		
	X (m)	Y (m)	Z (m)	P1 (MPa)	P2 (MPa)	P3 (MPa)
1	0.57133E-03	-0.18108E-08	-0.30070E-02	-0.56926E-03	-0.64954E-01	-0.11017E+01
2	0.58636E-03	-0.19590E-08	-0.32065E-02	-0.65329E-03	-0.49465E-01	-0.11803E+01
3	0.60236E-03	-0.21076E-08	-0.34069E-02	-0.79819E-03	-0.42440E-01	-0.12663E+01
4	-0.75200E-03	-0.13133E-09	-0.24666E-02	0.28574E-01	-0.40123E-01	-0.29003E+00
5	-0.74335E-03	0.82597E-10	-0.26923E-02	0.20853E-02	-0.30049E+00	-0.40319E+00
6	-0.73077E-03	0.23163E-09	-0.29327E-02	0.13078E-02	-0.48802E+00	-0.59184E+00
7	-0.69533E-03	-0.13424E-03	-0.23738E-02	0.56777E-01	-0.17538E-01	-0.26416E+00
8	-0.69003E-03	-0.15446E-03	-0.26004E-02	0.22232E-02	-0.25029E+00	-0.41906E+00
9	-0.68044E-03	-0.17606E-03	-0.28436E-02	0.13521E-02	-0.44350E+00	-0.64980E+00
10	-0.26902E-03	-0.41406E-03	-0.17353E-02	0.28735E+00	-0.68099E-02	-0.10297E+00
11	-0.28317E-03	-0.45551E-03	-0.19694E-02	0.88116E-02	-0.36197E-01	-0.43790E+00
12	-0.29071E-03	-0.50043E-03	-0.22298E-02	-0.78070E-02	-0.16158E+00	-0.97425E+00
13	-0.54943E-04	-0.51315E-03	-0.84497E-03	0.25193E+00	0.13610E+00	-0.19495E-01
14	-0.37051E-04	-0.48698E-03	-0.10180E-02	0.21909E+00	-0.13724E-01	-0.40066E+00
15	-0.10120E-04	-0.46507E-03	-0.12042E-02	0.22691E+00	-0.22404E-01	-0.11313E+01
16	-0.15269E-03	-0.18930E-03	-0.38076E-03	0.32677E+00	0.19685E-01	-0.14187E+00
17	-0.13469E-03	-0.15686E-03	-0.47614E-03	0.24828E+00	-0.44754E-01	-0.25876E+00
18	-0.10235E-03	-0.11921E-03	-0.52549E-03	0.12156E+00	-0.13857E+00	-0.75204E+00
19	-0.14744E-02	0.17896E-08	-0.22428E-02	0.29622E+00	0.11078E+00	-0.16089E-01
20	-0.14761E-02	0.25206E-08	-0.22397E-02	0.88744E-01	-0.13804E-01	-0.47670E+00
21	-0.14578E-02	0.31744E-08	-0.22544E-02	-0.13583E-01	-0.15530E+00	-0.11676E+01
22	-0.13633E-02	0.12433E-03	-0.21739E-02	0.30446E+00	0.77127E-01	-0.17323E-01
23	-0.13728E-02	0.77513E-04	-0.21635E-02	0.10314E+00	-0.14471E-01	-0.49838E+00
24	-0.13625E-02	0.27282E-04	-0.21674E-02	-0.13963E-01	-0.13457E+00	-0.11857E+01
25	-0.61481E-03	0.12666E-03	-0.16590E-02	0.24347E+00	-0.94040E-03	-0.20208E+00
26	-0.66257E-03	0.33700E-04	-0.16075E-02	0.17316E+00	-0.97375E-02	-0.62095E+00
27	-0.69882E-03	-0.69304E-04	-0.15443E-02	0.92145E-01	-0.17414E-01	-0.11578E+01
28	-0.59226E-04	-0.80257E-04	-0.82732E-03	0.65373E-01	-0.17615E+00	-0.79632E+00
29	-0.10504E-03	-0.99572E-04	-0.87288E-03	0.16205E+00	-0.56303E-01	-0.43094E+00
30	-0.13667E-03	-0.10415E-03	-0.77907E-03	0.20934E+00	-0.11030E+00	-0.69154E+00
31	-0.69614E-03	0.18684E-07	-0.21614E-02	0.17456E+00	0.76725E-02	-0.59567E+00
32	-0.67460E-03	0.23439E-07	-0.18243E-02	0.60814E-01	-0.12875E-04	-0.85760E+00

33	-0.62188E-03	0.30382E-07	-0.14383E-02	0.13767E+00	-0.11942E+00	-0.77424E+00
34	-0.57850E-03	0.13303E-03	-0.20375E-02	0.19361E+00	0.18733E-01	-0.65752E+00
35	-0.56962E-03	0.60369E-04	-0.17264E-02	0.73161E-01	0.33625E-02	-0.80685E+00
36	-0.53837E-03	-0.13526E-04	-0.13766E-02	0.10995E+00	-0.11201E+00	-0.70199E+00
37	0.34954E-04	0.59437E-04	-0.12616E-02	-0.14407E+00	-0.35292E+00	-0.13790E+01
38	-0.66372E-04	-0.20861E-04	-0.12288E-02	0.70198E-01	-0.11023E+00	-0.57089E+00
39	-0.12403E-03	-0.73689E-04	-0.98429E-03	0.14356E+00	-0.77468E-01	-0.61616E+00
40	0.51353E-04	0.67340E-08	-0.15707E-02	-0.22958E+00	-0.35007E+00	-0.12666E+01
41	-0.15689E-04	0.31456E-06	-0.14020E-02	-0.93831E-01	-0.22860E+00	-0.66666E+00
42	-0.60555E-04	0.10732E-05	-0.10326E-02	-0.80085E-01	-0.13824E+00	-0.47710E+00

LOADING CONDITION 3.2

	DISPLACEMENTS			STRESSES		
	X (m)	Y (m)	Z (m)	P1 (MPa)	P2 (MPa)	P3 (MPa)
1	0.22374E-01	0.63957E-07	-0.42138E-03	-0.20645E-01	-0.15461E+00	-0.28850E+01
2	0.22401E-01	0.80038E-07	-0.68434E-03	0.28365E-01	-0.46703E-01	-0.17593E+01
3	0.22412E-01	0.96336E-07	-0.95206E-03	0.86480E-01	-0.43787E-01	-0.59664E+00
4	0.20257E-01	0.38842E-07	0.53339E-03	-0.14324E+00	-0.14581E+01	-0.42670E+01
5	0.20307E-01	0.57097E-07	-0.80918E-04	-0.10513E+00	-0.25937E+00	-0.29352E+01
6	0.20335E-01	0.75383E-07	-0.62119E-03	0.99526E+00	-0.76539E-01	-0.14956E+01
7	0.18636E-01	-0.16863E-02	0.56449E-03	-0.13669E+00	-0.14069E+01	-0.41041E+01
8	0.18756E-01	-0.11732E-02	0.11878E-05	-0.97659E-01	-0.24457E+00	-0.29324E+01
9	0.18858E-01	-0.64350E-03	-0.48909E-03	0.10040E+01	-0.69823E-01	-0.16951E+01
10	0.90592E-02	-0.19278E-02	0.55547E-03	-0.10116E+00	-0.12434E+01	-0.26885E+01
11	0.94726E-02	-0.10775E-02	0.30182E-03	-0.57995E-01	-0.20256E+00	-0.26003E+01
12	0.98903E-02	-0.20738E-03	0.11350E-03	0.10986E+01	-0.26033E-01	-0.26452E+01
13	0.18551E-02	0.64473E-03	0.64652E-04	-0.40170E-01	-0.79571E+00	-0.11008E+01
14	0.20936E-02	0.89566E-03	0.12175E-03	0.84675E-01	-0.29746E-01	-0.18531E+01
15	0.23204E-02	0.11256E-02	0.21200E-03	0.11560E+01	0.22249E-01	-0.25736E+01
16	0.86100E-03	0.75001E-03	-0.15704E-03	-0.12482E+00	-0.31579E+00	-0.14762E+01
17	0.91884E-03	0.80705E-03	-0.95726E-04	0.78579E-01	-0.19670E+00	-0.12140E+01
18	0.85882E-03	0.75110E-03	-0.19096E-04	0.34361E+00	-0.17996E+00	-0.13467E+01
19	0.14743E-01	-0.39565E-08	0.28031E-02	-0.25166E+00	-0.12856E+01	-0.40953E+01
20	0.14817E-01	0.35221E-07	0.12420E-02	-0.13845E+00	-0.43499E+00	-0.28231E+01
21	0.14856E-01	0.72556E-07	-0.28313E-03	0.74130E+00	-0.99904E-01	-0.13600E+01
22	0.13428E-01	-0.16776E-02	0.26420E-02	-0.24626E+00	-0.11452E+01	-0.38567E+01
23	0.13590E-01	-0.11220E-02	0.11576E-02	-0.12589E+00	-0.39304E+00	-0.27311E+01
24	0.13724E-01	-0.55070E-03	-0.29918E-03	0.74029E+00	-0.96555E-01	-0.15050E+01
25	0.56765E-02	-0.17004E-02	0.15603E-02	-0.14733E-01	-0.39763E+00	-0.17178E+01
26	0.61854E-02	-0.79745E-03	0.54929E-03	0.12754E+00	-0.23767E+00	-0.21387E+01
27	0.67133E-02	0.92887E-04	-0.47451E-03	0.58763E+00	-0.99587E-01	-0.28900E+01
28	0.12147E-02	0.56812E-03	0.17910E-03	0.63050E+00	0.26761E-01	-0.71765E+00
29	0.15380E-02	0.90433E-03	-0.12025E-03	0.22896E+00	-0.24159E+00	-0.12178E+01
30	0.16042E-02	0.10354E-02	-0.42672E-03	-0.16742E+00	-0.59317E+00	-0.29727E+01
31	0.61649E-02	-0.70457E-07	0.34801E-02	0.80677E+00	-0.52756E+00	-0.17471E+01
32	0.61038E-02	0.27749E-07	0.12877E-02	0.38276E+00	-0.70230E+00	-0.98178E+00

33	0.60143E-02	0.13145E-06	-0.92366E-03	-0.58247E-01	-0.45377E+00	-0.22215E+01
34	0.53257E-02	-0.81135E-03	0.30551E-02	0.96562E+00	-0.51275E+00	-0.16580E+01
35	0.53618E-02	-0.31013E-03	0.10552E-02	0.28271E+00	-0.54115E+00	-0.10319E+01
36	0.53864E-02	0.14658E-03	-0.93394E-03	0.24977E+00	-0.36405E+00	-0.24467E+01
37	0.14017E-02	-0.86360E-04	0.98987E-03	0.23186E+01	0.66576E+00	0.20492E+00
38	0.19461E-02	0.56936E-03	0.97941E-05	0.68390E+00	0.91899E-01	-0.10649E+01
39	0.20485E-02	0.10264E-02	-0.90575E-03	-0.31698E+00	-0.75217E+00	-0.36373E+01
40	0.16550E-02	-0.86153E-07	0.18378E-02	0.24357E+01	0.96063E+00	0.46214E+00
41	0.18855E-02	0.50745E-06	0.17941E-03	0.81715E+00	0.22120E+00	-0.59031E+00
42	0.17527E-02	0.18928E-05	-0.11189E-02	-0.29605E-01	-0.27150E+00	-0.24076E+01

LOADING CONDITIONS 3.3

Points	Steady-state analysis temperature T°C	Periodic analysis amplitude °C	phase (rad)
1	15.00	10.0	0.
2	15.00	10.0	0.
3	15.00	10.0	0.
4	13.51	8.83	-0.50
5	13.56	9.05	-0.50
6	12.39	5.91	-0.94
7	12.39	5.90	-0.94
8	12.36	5.81	-0.97
9	12.37	5.69	-1.01
10	12.30	5.76	-1.01
11	12.35	3.95	-1.54
12	12.35	3.94	-1.57
13	12.37	3.90	-1.57
14	12.68	4.31	-1.45
15	12.38	2.32	-2.14
16	12.39	2.35	-2.14
17	12.65	2.65	-2.04
18	13.03	2.28	-2.14
19	13.01	2.22	-2.17
20	13.04	2.26	-2.17

LOADING CONDITION 3.4
****

DISPLACEMENTS (M)

	X	Y	Z
1	-0.0179	0.0000	0.0089
2	-0.0177	0.0000	0.0097
3	-0.0175	0.0000	0.0105
4	-0.0134	0.0000	0.0055
5	-0.0132	0.0000	0.0064
6	-0.0128	0.0000	0.0072
7	-0.0125	0.0018	0.0052
8	-0.0123	0.0015	0.0061
9	-0.0120	0.0011	0.0070
10	-0.0069	0.0033	0.0032
11	-0.0069	0.0026	0.0042
12	-0.0068	0.0020	0.0051
13	-0.0014	0.0016	0.0010
14	-0.0014	0.0011	0.0016
15	-0.0015	0.0005	0.0022
16	0.0000	0.0000	0.0000
17	0.0000	0.0000	0.0000
18	0.0000	0.0000	0.0000
19	-0.0085	0.0000	0.0019
20	-0.0082	0.0000	0.0031
21	-0.0077	0.0000	0.0043
22	-0.0076	0.0014	0.0017
23	-0.0073	0.0009	0.0029
24	-0.0069	0.0005	0.0041
25	-0.0025	0.0017	0.0008
26	-0.0025	0.0009	0.0016
27	-0.0023	0.0002	0.0025
28	0.0000	0.0000	0.0000
29	0.0000	0.0000	0.0000
30	0.0000	0.0000	0.0000
31	-0.0028	0.0000	-0.0003
32	-0.0022	0.0000	0.0009
33	-0.0014	0.0000	0.0021
34	-0.0023	0.0006	-0.0001
35	-0.0018	0.0002	0.0009
36	-0.0011	-0.0001	0.0019
37	0.0000	0.0000	0.0000
38	0.0000	0.0000	0.0000
39	0.0000	0.0000	0.0000
40	0.0000	0.0000	0.0000
41	0.0000	0.0000	0.0000
42	0.0000	0.0000	0.0000

→

LOADING CONDITION 3.5.1

MODE	FREQUENCY (Hz)	(rad/s)	PERIOD (s)	GENERALIZED MASS
1	4.3122	27.0944	0.2319	0.185370E+02
2	4.5936	28.8623	0.2177	0.912544E+01
3	5.7059	35.8511	0.1753	0.106958E+02
4	6.7437	42.3717	0.1483	0.131117E+02
5	8.6594	54.4084	0.1155	0.133029E+02
6	9.4161	59.1634	0.1062	0.166572E+02
7	10.8052	67.8910	0.0925	0.115937E+02
8	11.4731	72.0875	0.0872	0.117768E+02
9	13.0749	82.1521	0.0765	0.107081E+02
10	14.2405	89.4758	0.0702	0.124257E+02

LOADING CONDITION 3.5.1

MODE SHAPE 1

1	-0.13626E-10	-0.26442E+00	0.31820E-11
2	0.67066E+00	-0.31971E+00	-0.16977E+00
3	0.86035E+00	-0.41415E+00	-0.20058E+00
4	0.16596E+00	-0.77050E-01	-0.24696E-01
5			
6	-0.77919E-11	-0.17075E+00	0.10685E-11
7	0.36999E+00	-0.20014E+00	-0.58863E-01
8	0.44938E+00	-0.23305E+00	-0.45941E-01
9	0.59288E-01	-0.35381E-01	0.46549E-02
10			
11	-0.28836E-11	-0.67898E-01	-0.20465E-12
12	0.12938E+00	-0.79205E-01	0.70189E-02
13	0.10463E+00	-0.65334E-01	0.14526E-01
14			
15	-0.39388E-12	-0.14070E-01	-0.14455E-12
16	0.14839E-01	-0.13894E-01	0.61477E-02
17			
18			
19			
20			

MODE SHAPE 2

1	0.99996E+00	-0.21487E-11	-0.23111E+00
2	0.78913E+00	-0.25404E-01	-0.17311E+00
3	-0.10502E+00	0.15726E+00	0.54197E-01
4	-0.14486E+00	0.13239E+00	0.42083E-01
5			
6	0.58179E+00	-0.14375E-11	-0.81128E-01
7	0.46720E+00	-0.17376E-01	-0.58905E-01
8	-0.99031E-02	0.70542E-01	0.13912E-01
9	-0.40073E-01	0.50369E-01	0.20215E-02
10			
11	0.21887E+00	-0.61571E-12	0.14230E-01
12	0.17467E+00	-0.98136E-02	0.13424E-01
13	0.85168E-02	0.18721E-01	0.29642E-02
14			
15	0.30555E-01	-0.14082E-12	0.10946E-01
16	0.21555E-01	-0.43942E-03	0.79059E-02
17			
18			
19			
20			

MODE SHAPE 3

1	0.76836E-01	0.89664E-12	-0.14620E-01
2	0.25409E+00	-0.86703E-01	-0.65465E-01
3	0.82438E+00	-0.41036E+00	-0.22526E+00
4	0.28998E+00	-0.17130E+00	-0.60603E-01
5			
6	0.32154E-01	0.58747E-12	-0.82507E-02
7	0.11372E+00	-0.39106E-01	-0.23533E-01
8	0.34456E+00	-0.16249E+00	-0.47064E-01
9	0.86702E-01	-0.54408E-01	0.27811E-02
10			
11	0.53516E-02	0.23021E-12	-0.22736E-02
12	0.25999E-01	-0.74146E-02	-0.11615E-02
13	0.57391E-01	-0.26324E-01	0.58952E-02
14			
15	-0.13126E-02	0.41289E-13	-0.72645E-03
16	0.49176E-03	0.14727E-03	0.74320E-04
17			
18			
19			
20			

MODE SHAPE 4

1	0.75238E-12	-0.86682E-01	0.66494E-12
2	0.64787E+00	-0.12108E+00	-0.17667E+00
3	-0.38622E+00	0.32910E+00	0.15314E+00
4	-0.56097E+00	0.43254E+00	0.15080E+00
5			
6	0.24190E-11	-0.41632E-01	0.62719E-13
7	0.35025E+00	-0.64499E-01	-0.63652E-01
8	-0.29497E-01	0.70145E-01	0.16146E-01
9	-0.14160E+00	0.12591E+00	0.37647E-02
10			
11	0.20312E-11	-0.11156E-01	0.11637E-12
12	0.11061E+00	-0.22211E-01	0.18999E-02
13	0.25784E-01	0.44010E-03	0.91344E-03
14			
15	0.42614E-12	-0.14515E-02	0.98750E-13
16	0.12303E-01	-0.26808E-02	0.31605E-02
17			
18			
19			
20			

MODE SHAPE 5

1	0.10000E+01	0.95321E-09	-0.38414E+00
2	0.34154E+00	0.24325E-01	-0.17878E+00
3	-0.31966E+00	0.18558E-01	0.12515E-01
4	0.67624E+00	-0.57758E+00	-0.20824E+00
5			
6	0.36979E+00	0.11311E-08	-0.14416E+00
7	0.65752E-01	0.25278E-01	-0.71059E-01
8	-0.33981E+00	0.11976E+00	0.25800E-01
9	0.12954E+00	-0.12931E+00	-0.10048E-01
10			
11	0.12044E-01	0.46199E-09	-0.23518E-01
12	-0.57645E-01	0.16157E-01	-0.20551E-01
13	-0.10814E+00	0.46738E-01	-0.11393E-01
14			
15	-0.11559E-01	0.17094E-09	-0.72680E-02
16	-0.14782E-01	0.29539E-02	-0.76550E-02
17			
18			
19			
20			

MODE SHAPE 6

1	-0.99402E+00	0.62439E-08	0.60435E+00
2	-0.97054E+00	0.17934E+00	0.56736E+00
3	-0.21979E+00	0.11341E+00	0.17474E+00
4	0.27413E+00	-0.18354E+00	-0.55034E-01
5			
6	0.26597E+00	0.74333E-08	0.14612E+00
7	0.18792E+00	-0.33586E-02	0.14516E+00
8	0.64581E-01	-0.67804E-02	0.69775E-01
9	0.77803E-01	-0.50383E-01	0.76000E-02
10			
11	0.58286E+00	0.31622E-08	0.34504E-01
12	0.48904E+00	-0.54782E-01	0.37935E-01
13	0.10625E+00	-0.26624E-01	0.31655E-01
14			
15	0.13689E+00	0.11696E-08	0.29763E-01
16	0.10363E+00	-0.82677E-02	0.23340E-01
17			
18			
19			
20			

LOADING CONDITION 3.5.2 (compressible fluid)

MODE	FREQUENCY (Hz)	(rad/s)	PERIOD (s)	GENERALIZED MASS
1	3.5531	22.3246	0.2814	0.254711E+02
2	3.7555	23.5964	0.2663	0.163873E+02
3	5.0801	31.9190	0.1968	0.151914E+02
4	6.0739	38.1636	0.1646	0.158404E+02
5	6.4526	40.5428	0.1550	0.141066E+02
6	7.4304	46.6866	0.1346	0.104184E+04
7	7.7775	48.8675	0.1286	0.658886E+02
8	8.2411	51.7804	0.1213	0.154419E+02
9	8.4293	52.9627	0.1186	0.441145E+02
10	9.3340	58.6471	0.1071	0.666273E+02

MODE	FREQUENCY (Hz)	EPS	ECS	EPF	ECF
1	3.5531	0.94522E+01	0.84522E+01	0.38557E-01	0.10386E+01
2	3.7555	0.56125E+01	0.46125E+01	0.96564E-01	0.10966E+01
3	5.0801	0.13310E+02	0.12310E+02	0.17623E+00	0.11762E+01
4	6.0739	0.22152E+02	0.21152E+02	0.10280E+00	0.11028E+01
5	6.4526	0.37912E+01	0.27912E+01	0.12511E+01	0.22511E+01
6	7.4304	0.74976E+01	0.64951E+01	0.82259E+03	0.82359E+03
7	7.7775	0.18550E+02	0.17775E+02	0.82843E+02	0.83618E+02
8	8.2411	0.43255E+01	0.33399E+01	0.12365E+01	0.22222E+01
9	8.4293	0.64277E+01	0.55205E+01	0.26016E+02	0.26923E+02
10	9.3340	0.24496E+02	0.26322E+02	0.12248E+03	0.12066E+03

EPS - Potential energy of the structure

ECS - Kinetic energy of the structure

EPF - Potential energy of the fluid

ECF - Kinetic energy of the fluid

All energies are normalized with the regard of coupling energy

LOADING CONDITION 3.5.2 (compressible fluid)

MODE SHAPE 1

1	0.62366E+00	-0.36175E+00	-0.13467E+00
3	0.87491E+00	-0.43974E+00	-0.16294E+00
4	0.22795E+00	-0.10427E+00	-0.20395E-01
5	0.16344E-01	0.15170E-01	-0.86294E-03
6	0.29611E-02	-0.21178E+00	-0.67992E-04
7	0.37600E+00	-0.24011E+00	-0.42347E-01
8	0.51314E+00	-0.28200E+00	-0.25835E-01
9	0.11331E+00	-0.67802E-01	0.14011E-01
10	0.15535E-01	0.10662E-01	0.31379E-02
11	0.16664E-02	-0.10161E+00	0.26328E-03
12	0.16320E+00	-0.11597E+00	0.17096E-01
13	0.17659E+00	-0.11534E+00	0.34920E-01
14	0.20798E-01	-0.62721E-02	0.92063E-02
15	0.50761E-03	-0.37878E-01	0.25364E-03
16	0.34834E-01	-0.39850E-01	0.18631E-01
17	0.13740E-01	-0.21967E-01	0.17803E-01
18	0.10603E-03	-0.20569E-01	0.12591E-03
19	0.32018E-02	-0.18475E-01	0.92810E-02
20	0.25163E-02	-0.16976E-01	0.11643E-01

MODE SHAPE 2

1	0.10000E+01	0.97612E-03	-0.17491E+00
2	0.81179E+00	-0.91205E-02	-0.12920E+00
3	-0.44684E-01	0.17923E+00	0.54778E-01
4	-0.17269E+00	0.19261E+00	0.47408E-01
5	0.28319E-02	0.53777E-02	0.20734E-03
6	0.66158E+00	0.67625E-03	-0.52439E-01
7	0.54995E+00	-0.14466E-01	-0.35469E-01
8	0.45401E-01	0.83131E-01	0.17628E-01
9	-0.51308E-01	0.95737E-01	-0.53268E-03
10	0.72236E-02	0.20894E-01	-0.55423E-02
11	0.33133E+00	0.34558E-03	0.35174E-01
12	0.27868E+00	-0.13150E-01	0.32125E-01
13	0.50192E-01	0.30602E-01	0.79816E-02
14	0.10937E-01	0.28730E-01	-0.30667E-02
15	0.92404E-01	0.14348E-03	0.35629E-01
16	0.75167E-01	-0.34041E-03	0.28466E-01
17	0.19082E-01	0.16689E-01	0.32835E-02
18	0.18914E-01	0.86331E-04	0.14378E-01
19	0.14704E-01	0.45037E-02	0.11482E-01
20	0.12128E-01	0.59136E-02	0.87015E-02

MODE SHAPE 3

1	-0.23917E+00	0.11514E-02	0.10611E+00
2	-0.10784E-01	-0.69047E-01	0.41237E-01
3	0.83978E+00	-0.43275E+00	-0.19357E+00
4	0.40367E+00	-0.22679E+00	-0.69109E-01
5	0.25973E-01	0.22183E-01	-0.21634E-02
6	-0.80958E-01	0.80227E-03	0.38132E-01
7	0.31467E-01	-0.37392E-01	0.16483E-01
8	0.41649E+00	-0.19999E+00	-0.35866E-01
9	0.17290E+00	-0.96603E-01	0.58048E-02
10	0.28131E-01	0.15028E-01	0.17470E-02
11	0.21482E-01	0.45608E-03	0.52781E-02
12	0.54720E-01	-0.12699E-01	0.65534E-02
13	0.12958E+00	-0.53573E-01	0.15760E-01
14	0.32858E-01	0.55454E-02	0.60023E-03
15	0.20962E-01	0.23653E-03	0.42684E-02
16	0.24337E-01	-0.15189E-02	0.58853E-02
17	0.15874E-01	0.19662E-02	0.43339E-02
18	0.69164E-02	0.16773E-03	0.84213E-03
19	0.67663E-02	0.15031E-02	0.15727E-02
20	0.63746E-02	0.19375E-02	0.17176E-02

MODE SHAPE 4

1	0.38626E-02	0.70873E-01	-0.12776E-02
2	-0.58365E+00	0.97381E-01	0.15344E+00
3	0.33301E+00	-0.32792E+00	-0.12497E+00
4	0.65572E+00	-0.51425E+00	-0.15591E+00
5	0.25605E-01	0.14737E-01	-0.37843E-02
6	0.18208E-02	0.30269E-01	-0.44813E-03
7	-0.34244E+00	0.51988E-01	0.60314E-01
8	0.15432E-01	-0.81249E-01	-0.49696E-02
9	0.21691E+00	-0.19298E+00	0.16209E-03
10	0.24245E-01	-0.13754E-01	0.66028E-02
11	0.34033E-03	0.61399E-02	0.24710E-04
12	-0.13917E+00	0.19969E-01	0.20926E-02
13	-0.48042E-01	-0.52268E-02	0.88217E-02
14	0.77913E-02	-0.20284E-01	0.48066E-02
15	-0.38819E-04	-0.13876E-03	0.55963E-04
16	-0.32764E-01	0.30760E-02	-0.31475E-02
17	-0.18414E-01	-0.42985E-02	0.77716E-02
18	-0.34188E-04	0.11505E-02	0.57281E-04
19	-0.73200E-02	0.49136E-03	0.19081E-02
20	-0.80821E-02	-0.27497E-04	0.30518E-02

MODE SHAPE 5

1	-0.99734E+00	0.32382E-04	0.40364E+00
2	-0.85755E+00	0.10167E+00	0.35244E+00
3	-0.29412E+00	0.12210E+00	0.14279E+00
4	-0.60205E-01	0.38574E-01	0.33660E-01
5	-0.68937E-03	-0.10314E-02	0.29580E-02
6	-0.27734E+00	0.64902E-05	0.14626E+00
7	-0.22422E+00	0.19644E-01	0.12680E+00
8	-0.35406E-01	0.21704E-02	0.49264E-01
9	-0.47129E-02	-0.18945E-02	0.15806E-01
10	-0.14139E-02	-0.31795E-02	0.74722E-02
11	0.16525E+00	-0.54109E-05	0.18662E-01
12	0.15906E+00	-0.22660E-01	0.18929E-01
13	0.81982E-01	-0.33867E-01	0.20472E-01
14	0.10545E-01	-0.30109E-02	0.12917E-01
15	0.13474E+00	-0.49250E-05	0.15313E-01
16	0.11788E+00	-0.11773E-01	0.13840E-01
17	0.39996E-01	0.29034E-02	0.53830E-02
18	0.49712E-01	0.13628E-04	-0.47941E-02
19	0.41658E-01	0.26248E-02	-0.37047E-02
20	0.35891E-01	0.42224E-02	-0.37672E-02

MODE SHAPE 6

1	0.99768E+00	0.11842E-02	-0.46878E+00
2	0.79678E+00	-0.98013E-01	-0.39829E+00
3	0.19669E+00	-0.12603E+00	-0.16096E+00
4	0.10855E+00	-0.11477E+00	-0.60226E-01
5	-0.32066E-02	-0.40447E-02	-0.34715E-02
6	0.16998E+00	0.97147E-03	-0.16806E+00
7	0.86424E-01	-0.51564E-02	-0.14121E+00
8	-0.92768E-01	0.27790E-01	-0.54202E-01
9	-0.13487E-02	-0.19233E-01	-0.20379E-01
10	-0.43852E-02	-0.71636E-02	-0.69382E-02
11	-0.23505E+00	0.12862E-02	-0.41143E-01
12	-0.24338E+00	0.31883E-01	-0.39410E-01
13	-0.14671E+00	0.49235E-01	-0.31854E-01
14	-0.23852E-01	-0.52405E-02	-0.13912E-01
15	-0.12313E+00	0.93307E-03	-0.33440E-01
16	-0.11428E+00	0.10546E-01	-0.30267E-01
17	-0.42789E-01	-0.55740E-02	-0.11981E-01
18	-0.33899E-01	0.80075E-03	-0.93286E-02
19	-0.29912E-01	-0.26772E-02	-0.84083E-02
20	-0.26335E-01	-0.42596E-02	-0.69643E-02

LOADING CONDITION 3.5.2 (incompressible fluid)

MODE	FREQUENCY (Hz)	(rad/s)	PERIOD (s)	GENERALIZED MASS
1	3.5598	22.3670	0.2809	0.251866E+02
2	3.7819	23.7622	0.2644	0.155626E+02
3	5.1031	32.0637	0.1960	0.146533E+02
4	6.0851	38.2338	0.1643	0.158601E+02
5	6.9329	43.5604	0.1442	0.993496E+01
6	7.8969	49.6174	0.1266	0.157439E+02
7	8.6897	54.5992	0.1151	0.152691E+02
8	9.8563	61.9292	0.1015	0.143183E+02
9	10.8510	68.1785	0.0922	0.926526E+01
10	11.7713	73.9611	0.0850	0.275389E+02

MODE	FREQUENCY (Hz)	EPS	ECS	EPF	ECF
1	3.5598	0.98125E+01	0.88125E+01	0.72442E-15	0.10000E+01
2	3.7819	0.61503E+01	0.51503E+01	0.14852E-14	0.10000E+01
3	5.1031	0.15374E+02	0.14374E+02	0.20720E-14	0.10000E+01
4	6.0851	0.24443E+02	0.23443E+02	0.15080E-14	0.10000E+01
5	6.9329	0.44987E+01	0.34987E+01	0.75399E-14	0.10000E+01
6	7.8969	0.17257E+02	0.16257E+02	0.33880E-14	0.10000E+01
7	8.6897	0.46699E+01	0.36699E+01	0.59140E-14	0.10000E+01
8	9.8563	0.25663E+02	0.24663E+02	0.25496E-14	0.10000E+01
9	10.8510	0.49942E+01	0.39942E+01	0.59306E-14	0.10000E+01
10	11.7713	0.24951E+02	0.23951E+02	0.18412E-13	0.10000E+01

EPS - Potential energy of the structure

ECS - Kinetic energy of the structure

EPF - Potential energy of the fluid

ECF - Kinetic energy of the fluid

All energies are normalized with the regard of coupling energy

LOADING CONDITION 3.5.2 (compressible fluid)

MODE SHAPE 1

1	0.41272E-02	-0.31523E+00	-0.46903E-03
2	0.62366E+00	-0.36175E+00	-0.13467E+00
3	0.87491E+00	-0.43974E+00	-0.16294E+00
4	0.22795E+00	-0.10427E+00	-0.20395E-01
5	0.16344E-01	0.15170E-01	-0.86294E-03
6	0.29611E-02	-0.21178E+00	-0.67992E-04
7	0.37600E+00	-0.24011E+00	-0.42347E-01
8	0.51314E+00	-0.28200E+00	-0.25835E-01
9	0.11331E+00	-0.67802E-01	0.14011E-01
10	0.15535E-01	0.10662E-01	0.31379E-02
11	0.16664E-02	-0.10161E+00	0.26328E-03
12	0.16320E+00	-0.11597E+00	0.17096E-01
13	0.17659E+00	-0.11534E+00	0.34920E-01
14	0.20798E-01	-0.62721E-02	0.92063E-02
15	0.50761E-03	-0.37878E-01	0.25364E-03
16	0.34834E-01	-0.39850E-01	0.18631E-01
17	0.13740E-01	-0.21967E-01	0.17803E-01
18	0.10603E-03	-0.20569E-01	0.12591E-03
19	0.32018E-02	-0.18475E-01	0.92810E-02
20	0.25163E-02	-0.16976E-01	0.11643E-01

MODE SHAPE 2

1	0.10000E+01	0.84495E-03	-0.17742E+00
2	0.81112E+00	-0.95205E-02	-0.13131E+00
3	-0.48059E-01	0.17969E+00	0.54507E-01
4	-0.17399E+00	0.19245E+00	0.47307E-01
5	0.25891E-02	0.51531E-02	0.19824E-03
6	0.65767E+00	0.58738E-03	-0.53500E-01
7	0.54607E+00	-0.14295E-01	-0.36388E-01
8	0.42209E-01	0.83699E-01	0.17287E-01
9	-0.52191E-01	0.95608E-01	-0.69842E-03
10	0.69218E-02	0.20601E-01	-0.55667E-02
11	0.32549E+00	0.30187E-03	0.34699E-01
12	0.27334E+00	-0.12684E-01	0.31668E-01
13	0.47790E-01	0.31006E-01	0.76463E-02
14	0.10443E-01	0.28401E-01	-0.31443E-02
15	0.89265E-01	0.12637E-03	0.35143E-01
16	0.72451E-01	-0.16355E-03	0.28065E-01
17	0.18166E-01	0.16449E-01	0.32418E-02
18	0.17831E-01	0.76261E-04	0.14401E-01
19	0.13796E-01	0.44066E-02	0.11510E-01
20	0.11344E-01	0.57743E-02	0.87547E-02

MODE SHAPE 3

1	-0.17860E+00	0.11592E-02	0.88194E-01
2	0.38682E-01	-0.71770E-01	0.26555E-01
3	0.84122E+00	-0.42789E+00	-0.19500E+00
4	0.39692E+00	-0.22021E+00	-0.68143E-01
5	0.25851E-01	0.22195E-01	-0.22344E-02
6	-0.52438E-01	0.80612E-03	0.31789E-01
7	0.54181E-01	-0.38094E-01	0.11403E-01
8	0.41533E+00	-0.19587E+00	-0.36549E-01
9	0.16993E+00	-0.92778E-01	0.52724E-02
10	0.28125E-01	0.15646E-01	0.13289E-02
11	0.25232E-01	0.45607E-03	0.58184E-02
12	0.56699E-01	-0.12146E-01	0.70046E-02
13	0.12651E+00	-0.50777E-01	0.15358E-01
14	0.32344E-01	0.64970E-02	0.15639E-03
15	0.18228E-01	0.23548E-03	0.49254E-02
16	0.21621E-01	-0.10097E-02	0.63620E-02
17	0.14509E-01	0.24208E-02	0.43902E-02
18	0.53060E-02	0.16576E-03	0.16356E-02
19	0.53310E-02	0.15598E-02	0.22305E-02
20	0.50934E-02	0.19731E-02	0.22904E-02

MODE SHAPE 4

1	-0.28200E-02	-0.73282E-01	0.88653E-03
2	0.59903E+00	-0.10127E+00	-0.15827E+00
3	-0.32246E+00	0.32438E+00	0.12194E+00
4	-0.65848E+00	0.51736E+00	0.15663E+00
5	-0.25671E-01	-0.14690E-01	0.37759E-02
6	-0.14814E-02	-0.31449E-01	0.30629E-03
7	0.34825E+00	-0.53654E-01	-0.61681E-01
8	-0.11199E-01	0.79862E-01	0.42312E-02
9	-0.21769E+00	0.19413E+00	-0.22874E-03
10	-0.24299E-01	0.14070E-01	-0.67312E-02
11	-0.46070E-03	-0.61086E-02	-0.35842E-04
12	0.13842E+00	-0.19816E-01	-0.18213E-02
13	0.47182E-01	0.57366E-02	-0.86325E-02
14	-0.79617E-02	0.20510E-01	-0.48774E-02
15	-0.86647E-04	0.46926E-03	-0.63842E-04
16	0.31452E-01	-0.26024E-02	0.32358E-02
17	0.17483E-01	0.45838E-02	-0.75273E-02
18	-0.15718E-04	-0.75524E-03	-0.47766E-04
19	0.67919E-02	-0.13973E-03	-0.17252E-02
20	0.74998E-02	0.33739E-03	-0.28252E-02

MODE SHAPE 5

1	-0.99756E+00	0.72170E-04	0.43908E+00
2	-0.81871E+00	0.98474E-01	0.37441E+00
3	-0.20785E+00	0.10741E+00	0.14028E+00
4	-0.80011E-01	0.77181E-01	0.46545E-01
5	0.15287E-02	0.21293E-02	0.32548E-02
6	-0.22295E+00	0.61637E-04	0.15975E+00
7	-0.15508E+00	0.12644E-01	0.13590E+00
8	0.37624E-01	-0.15685E-01	0.50812E-01
9	-0.69313E-03	0.98884E-02	0.18442E-01
10	0.16770E-02	0.31699E-02	0.71793E-02
11	0.21067E+00	0.46034E-04	0.30368E-01
12	0.20596E+00	-0.26896E-01	0.30037E-01
13	0.11310E+00	-0.39803E-01	0.27210E-01
14	0.16705E-01	0.22467E-02	0.13724E-01
15	0.13850E+00	0.29411E-04	0.25001E-01
16	0.12178E+00	-0.11033E-01	0.22642E-01
17	0.41701E-01	0.53389E-02	0.92131E-02
18	0.45752E-01	0.34624E-04	0.17275E-02
19	0.38209E-01	0.34073E-02	0.21600E-02
20	0.32906E-01	0.50873E-02	0.15062E-02

MODE SHAPE 6

1	-0.49215E+00	0.39222E-03	0.13983E+00
2	0.17576E-01	-0.76002E-01	-0.71422E-02
3	0.40919E+00	-0.59277E-01	-0.73834E-01
4	-0.76975E+00	0.65950E+00	0.20744E+00
5	-0.33224E-01	-0.11368E-01	0.59004E-02
6	-0.37922E+00	0.15042E-03	0.87340E-01
7	-0.97570E-01	-0.23636E-01	0.26933E-01
8	0.33442E+00	-0.11903E+00	-0.49586E-01
9	-0.19663E+00	0.18716E+00	0.75813E-03
10	-0.31945E-01	0.28632E-01	-0.87827E-02
11	-0.23616E+00	0.24265E-04	0.29254E-01
12	-0.12492E+00	0.23558E-02	0.22247E-01
13	0.11164E+00	-0.55221E-01	-0.84828E-03
14	0.84103E-02	0.10741E-01	-0.10661E-01
15	-0.86052E-01	-0.20828E-04	0.91037E-02
16	-0.57254E-01	-0.33686E-03	0.11362E-01
17	0.20609E-03	-0.13192E-01	0.39408E-02
18	-0.28790E-01	-0.88965E-05	0.17276E-01
19	-0.21100E-01	-0.59354E-02	0.15033E-01
20	-0.16571E-01	-0.75349E-02	0.13910E-01

Loading condition 3.5.2 (incompressible fluid)

mode shapes

1. Dam mode shapes
2. Modal pressures in water
3. Modal pressures on the upstream dam face

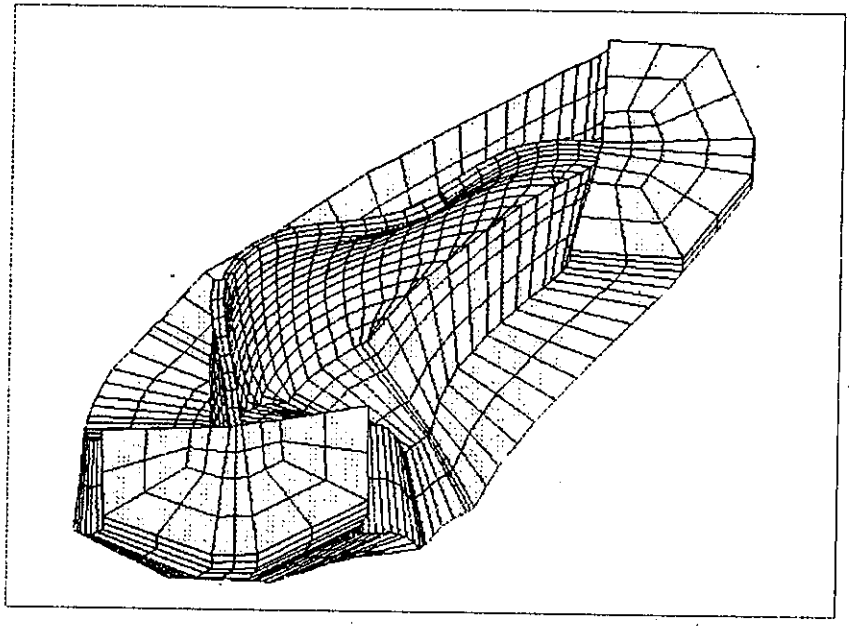

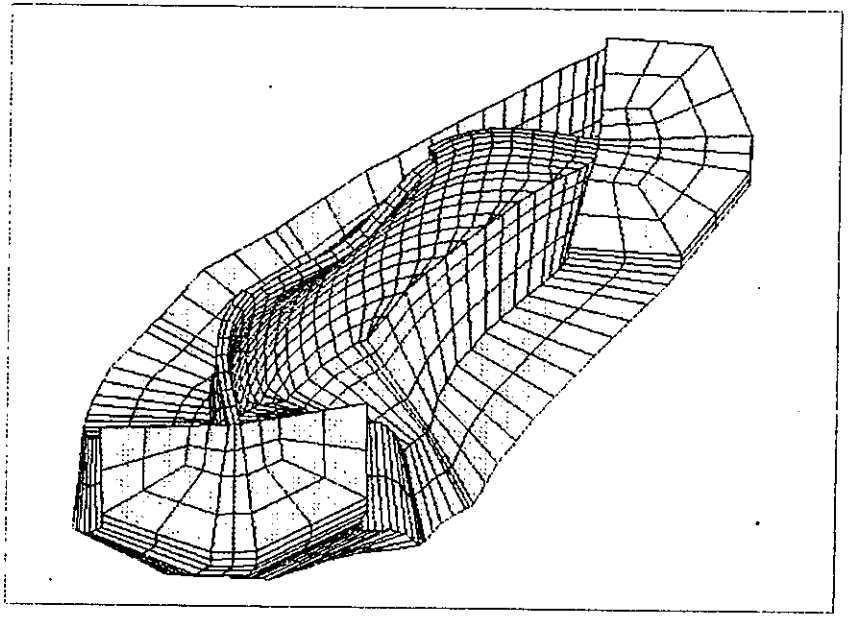

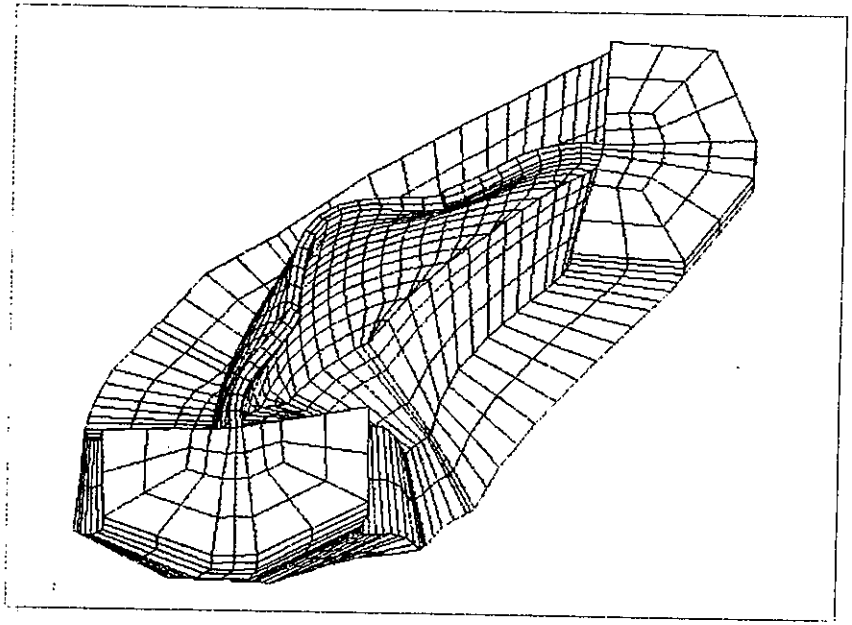

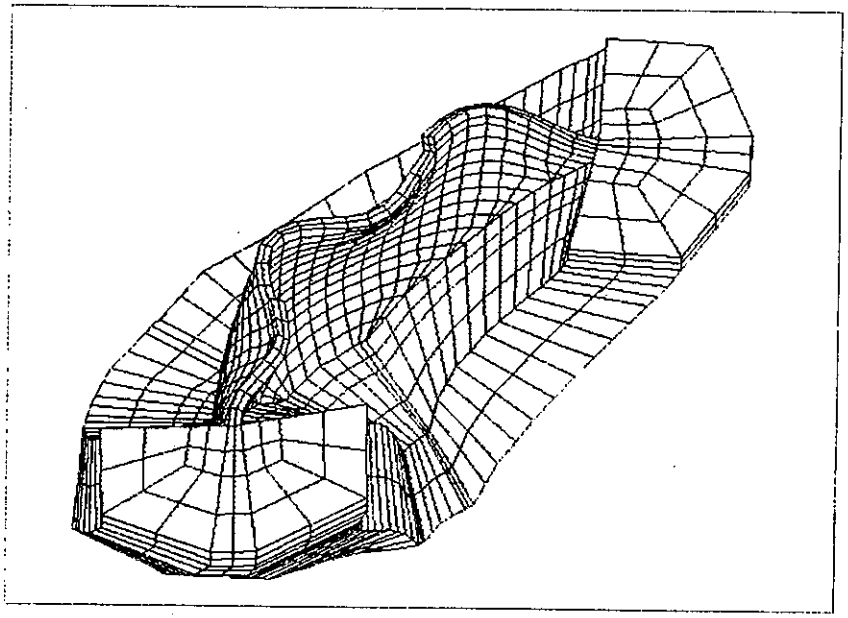

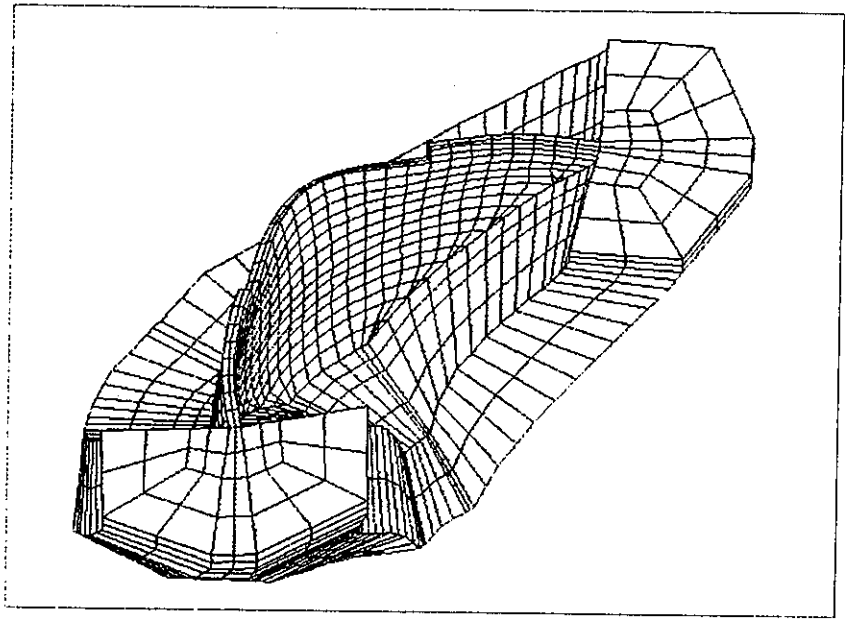

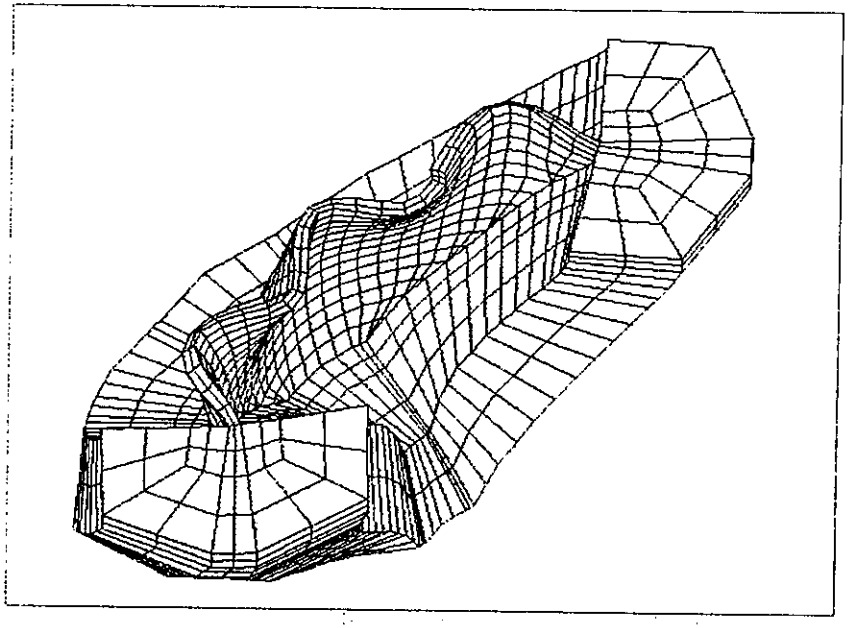

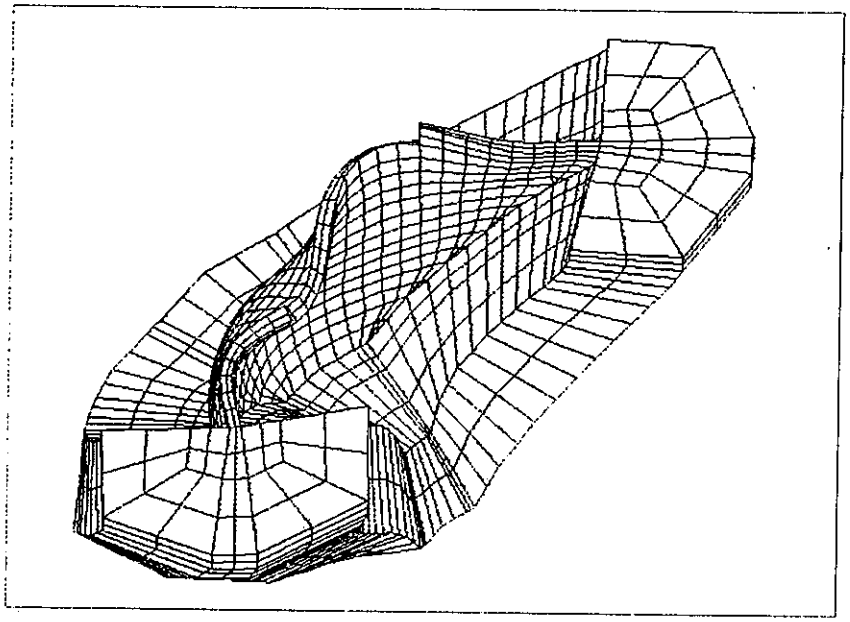

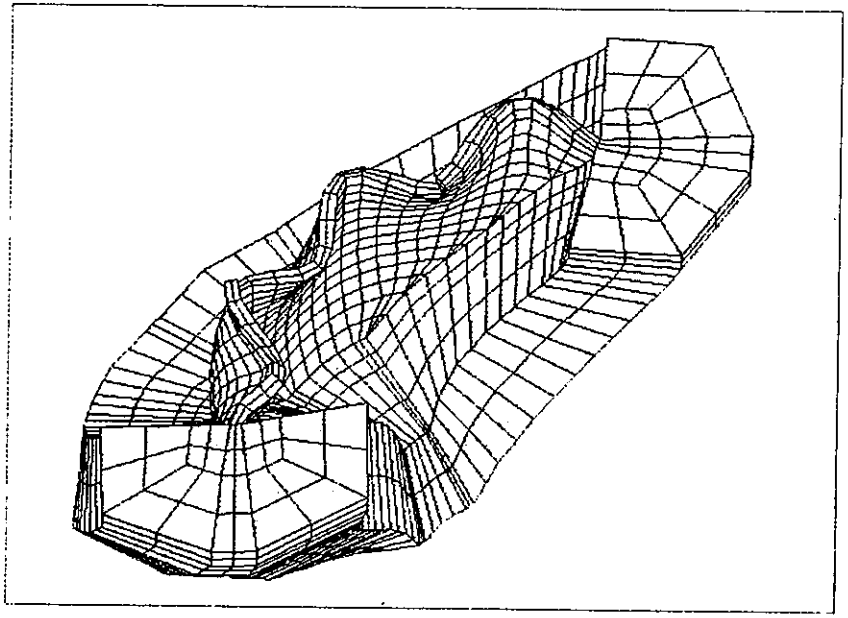

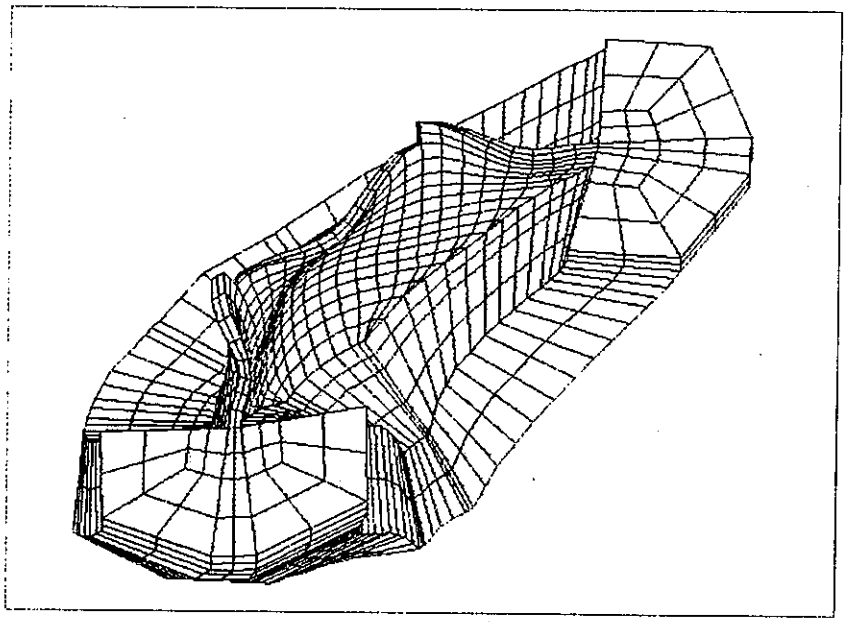

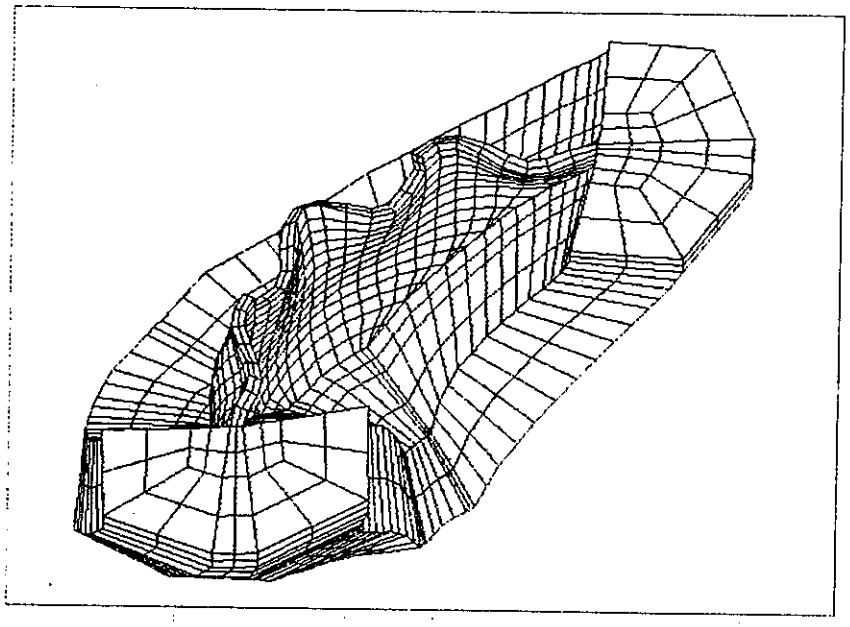

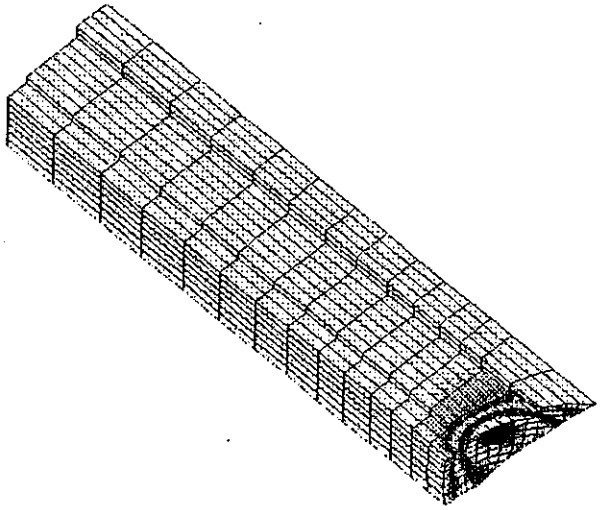

mode shape 2

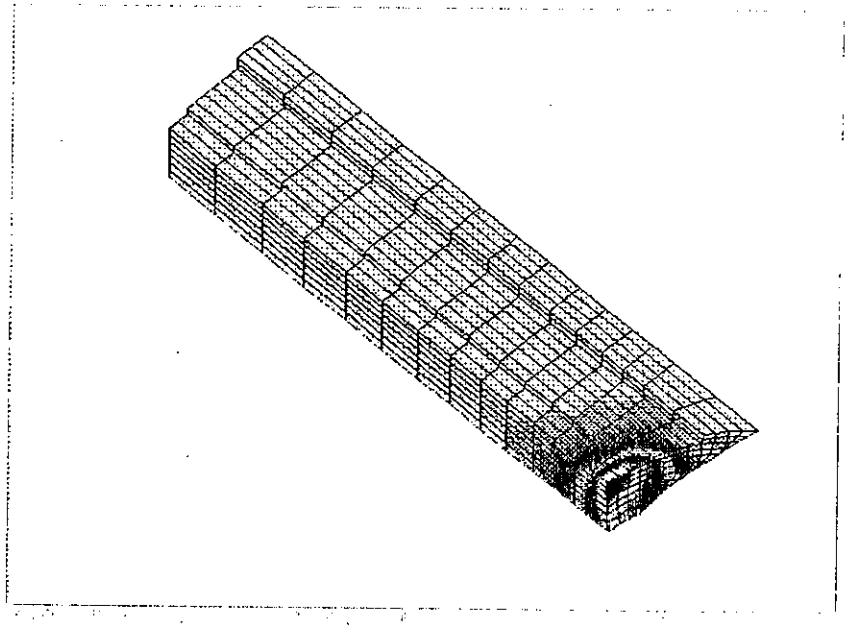

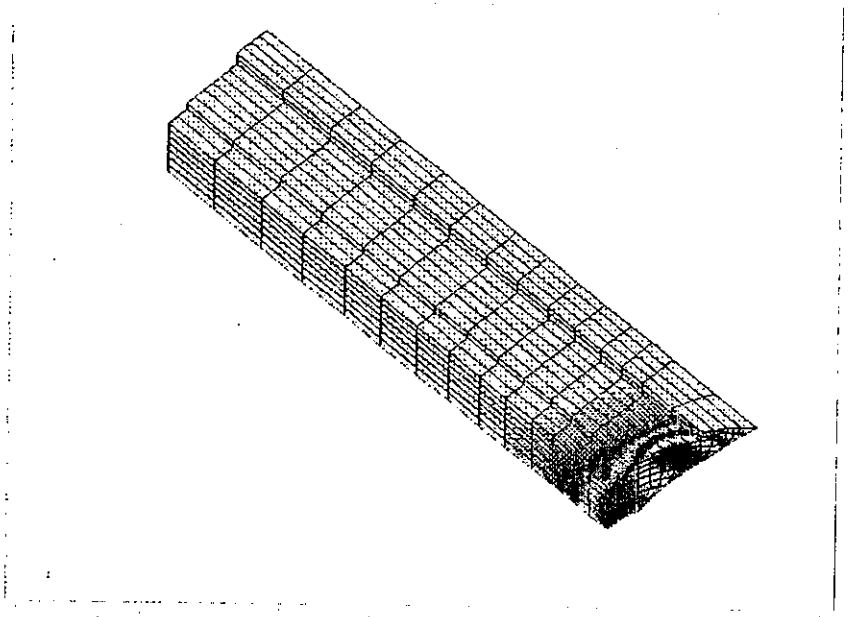

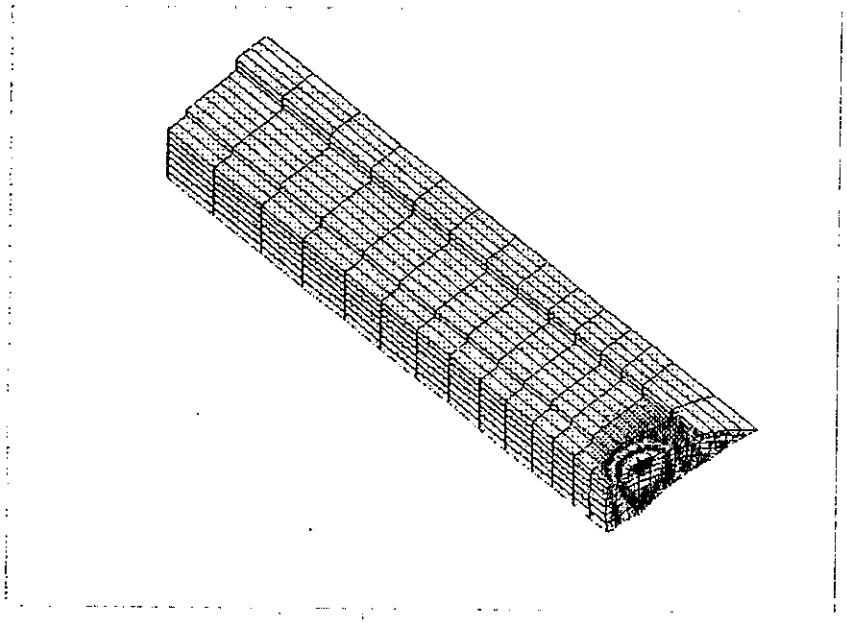

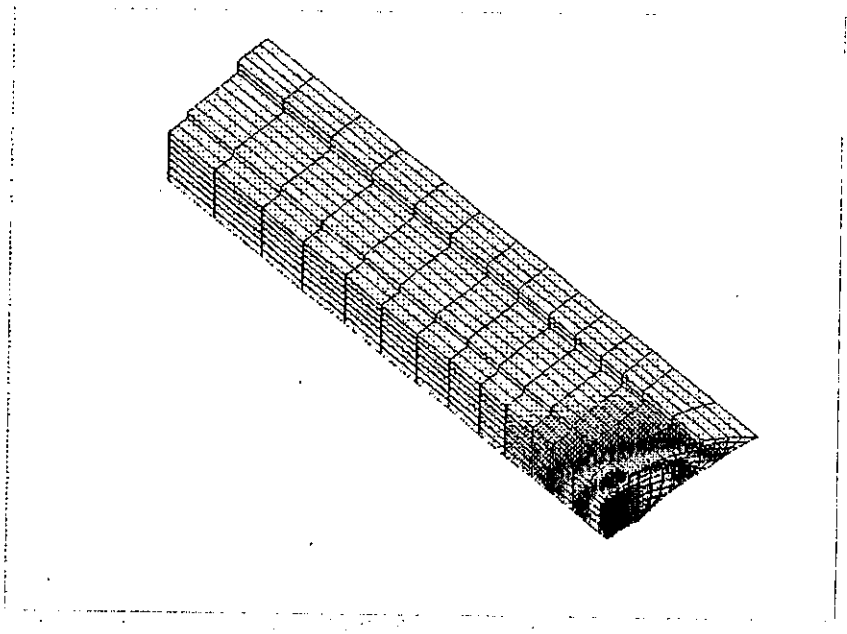

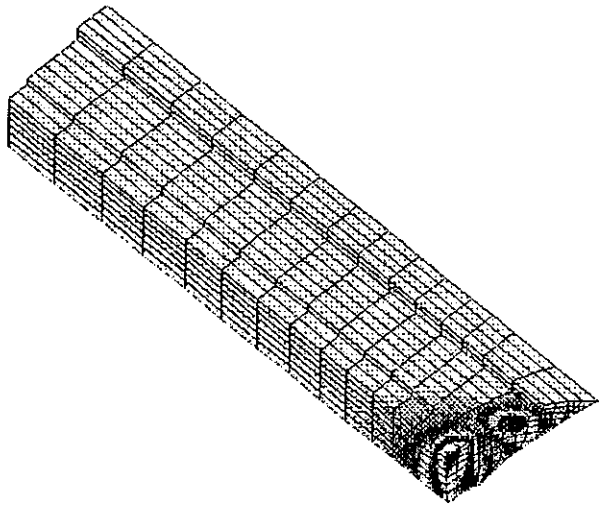

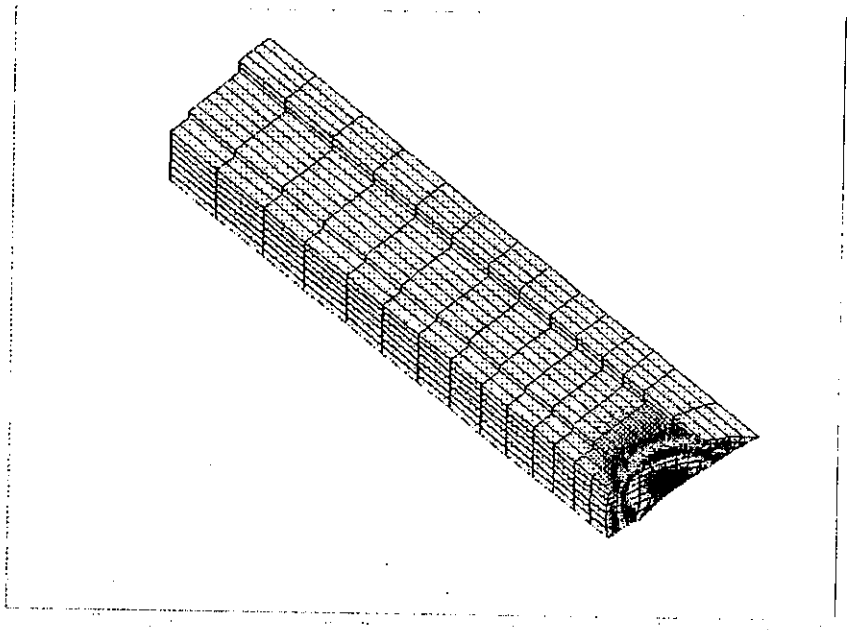

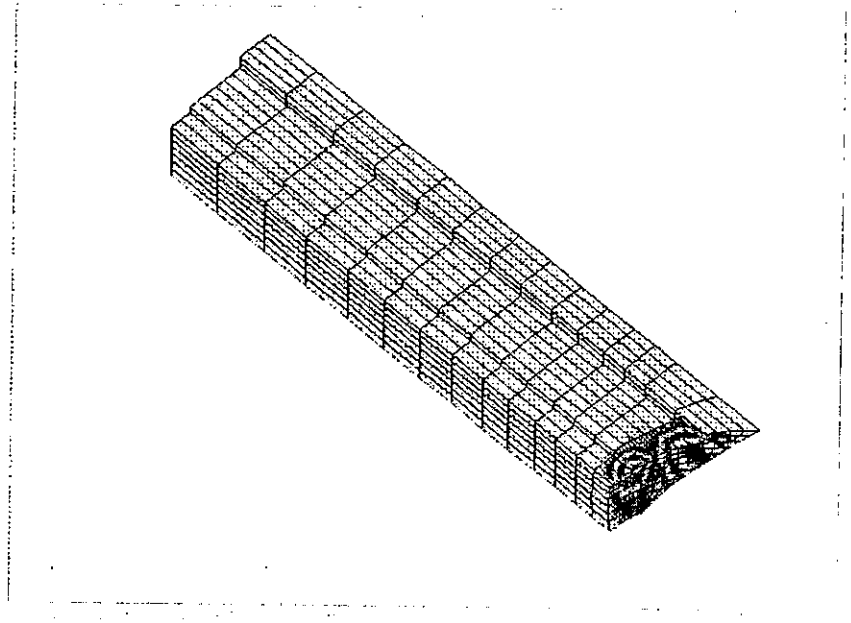

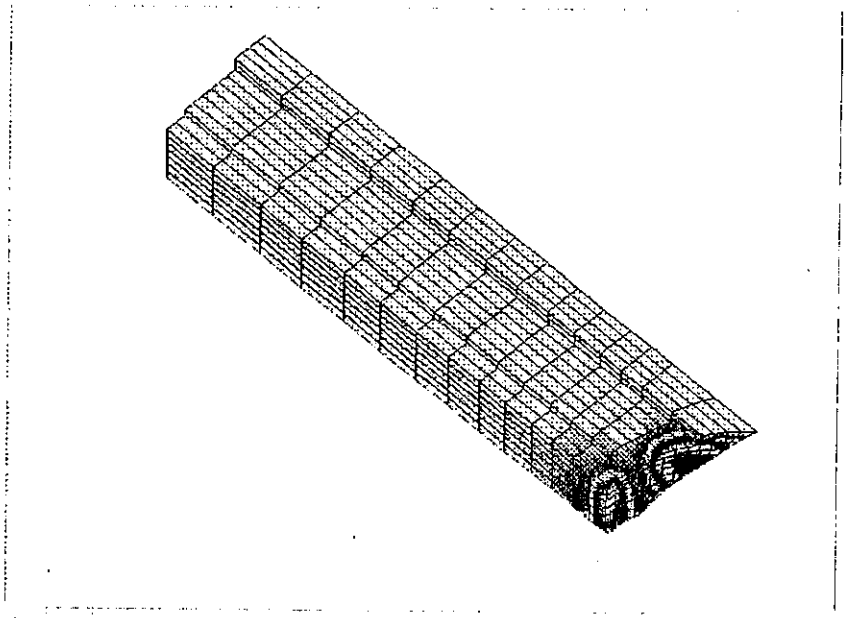

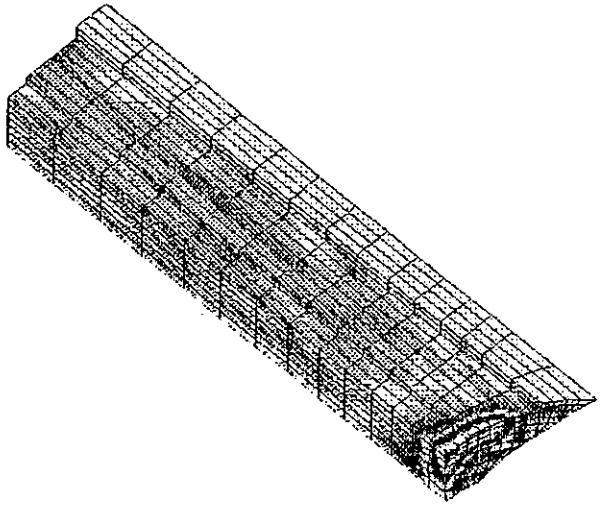

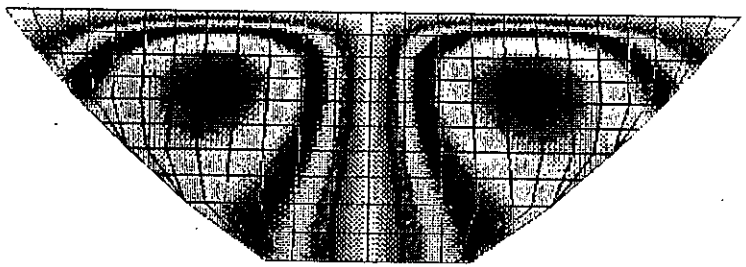

mode shape 2

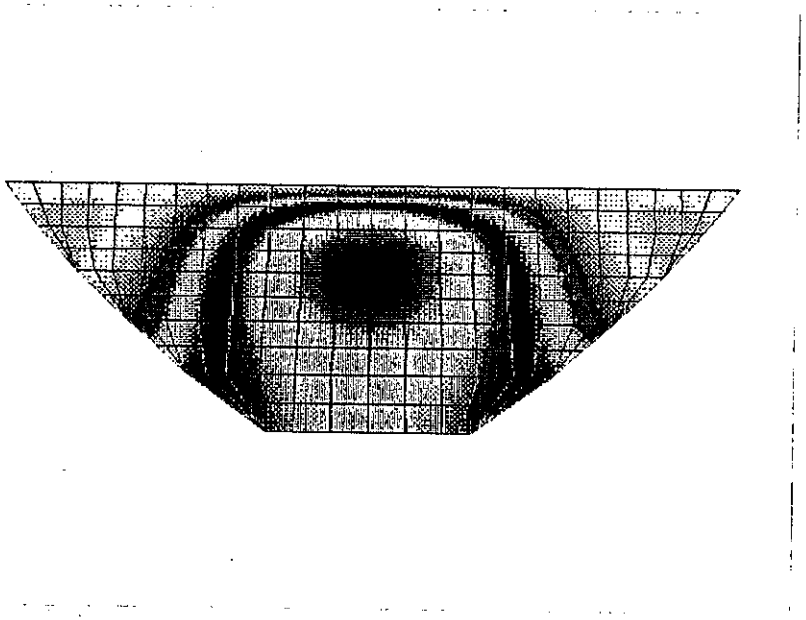

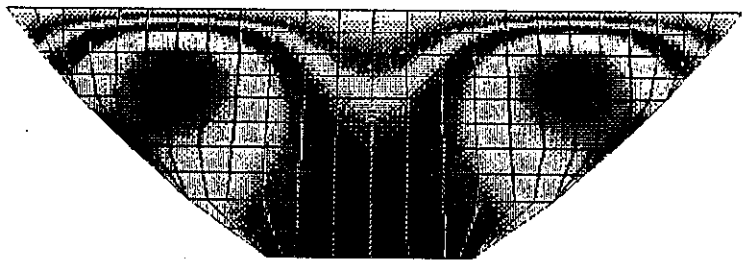

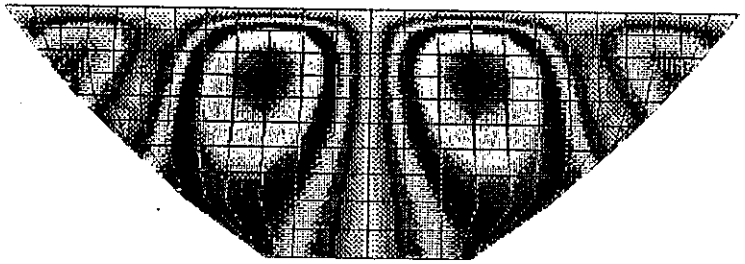

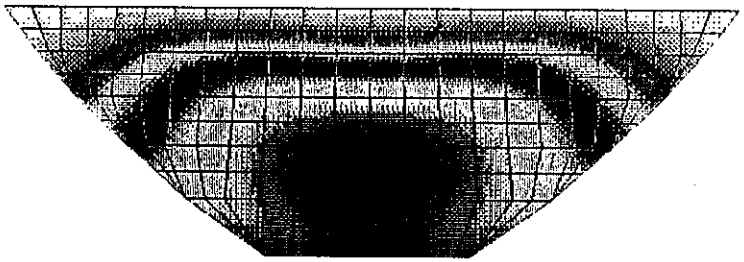

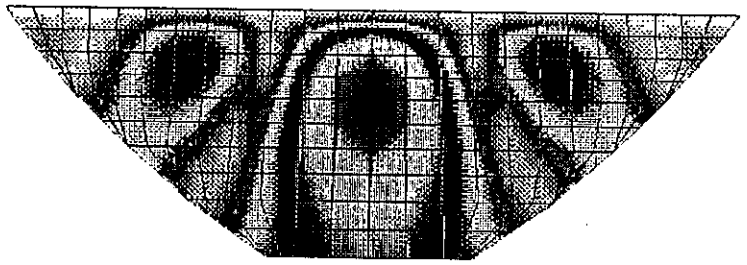

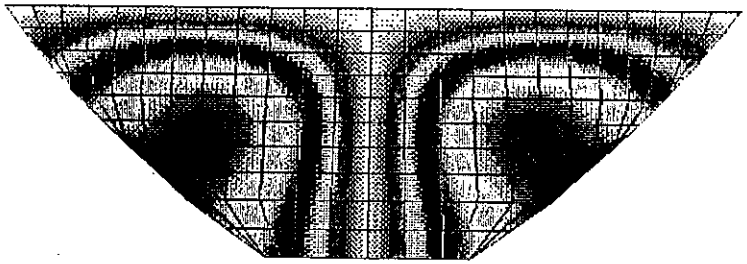

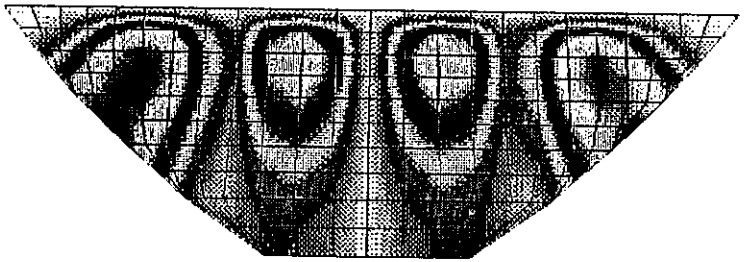

mode 8

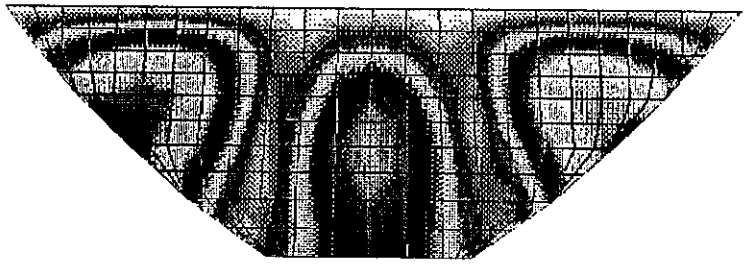

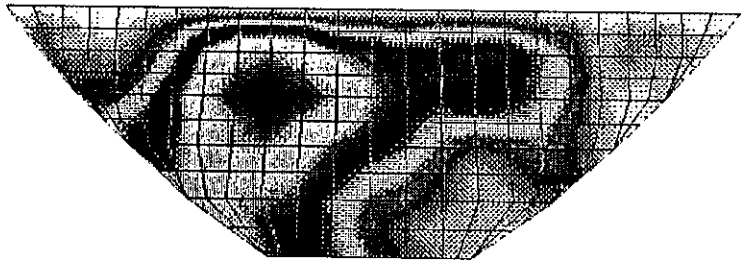

Loading condition 3.5.2 (compressible fluid)

mode shapes

1. Dam mode shapes
2. Modal pressures in water
3. Modal pressures on the upstream dam face

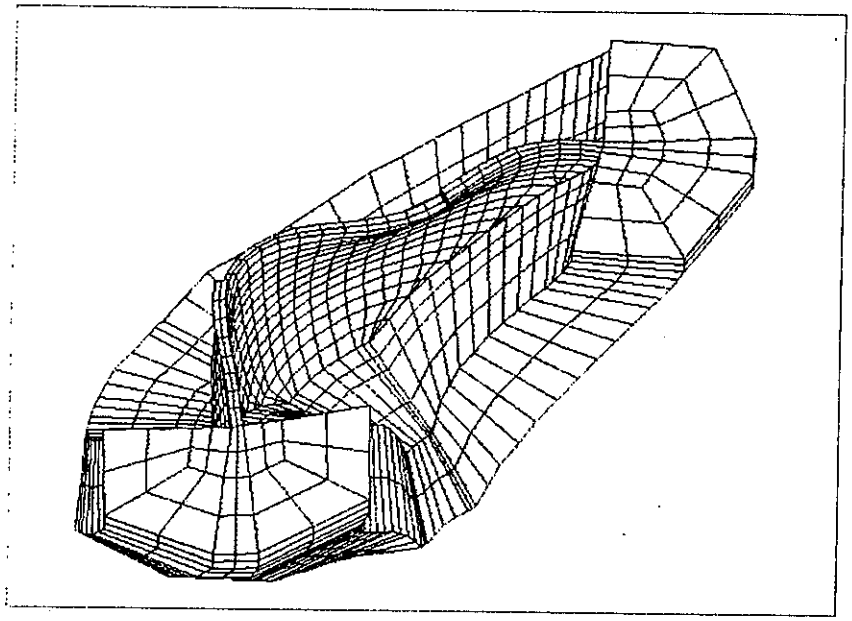

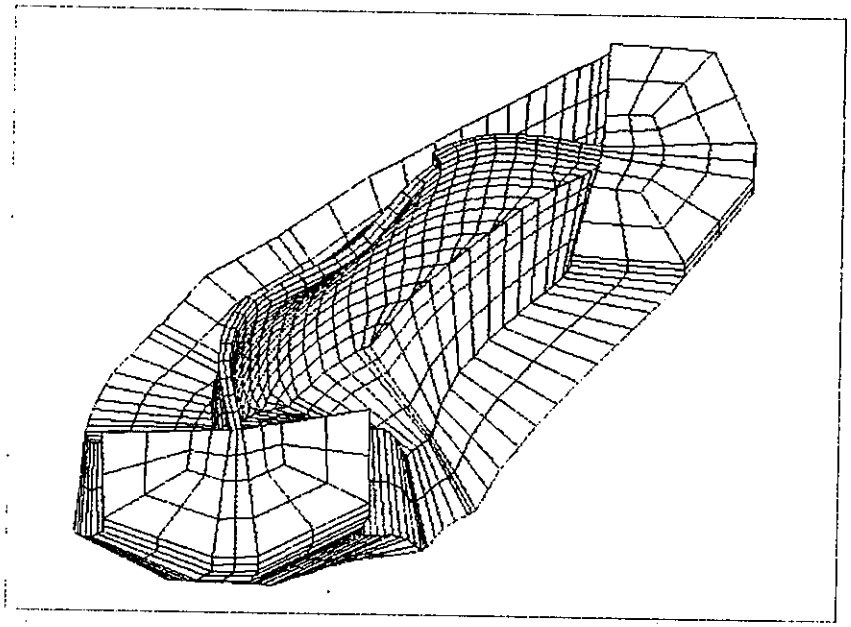

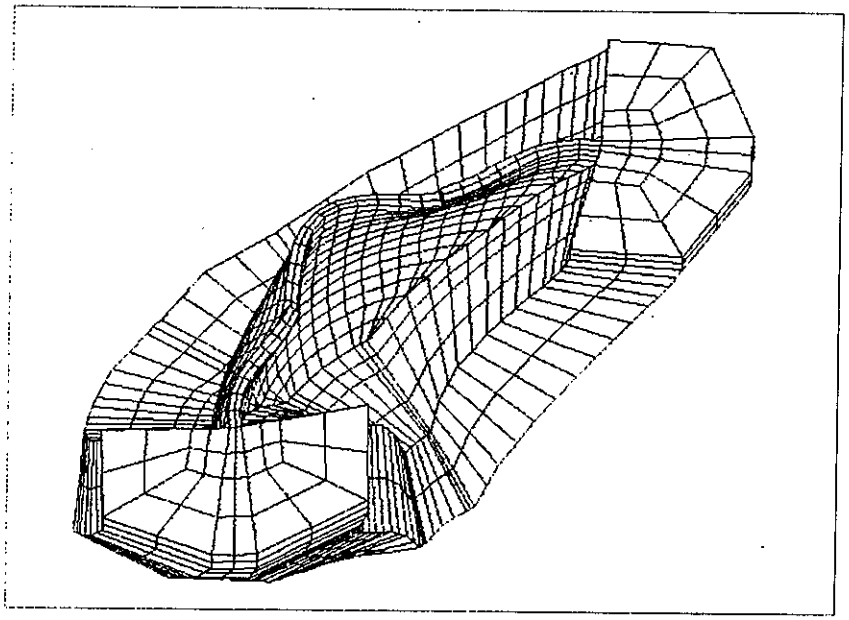

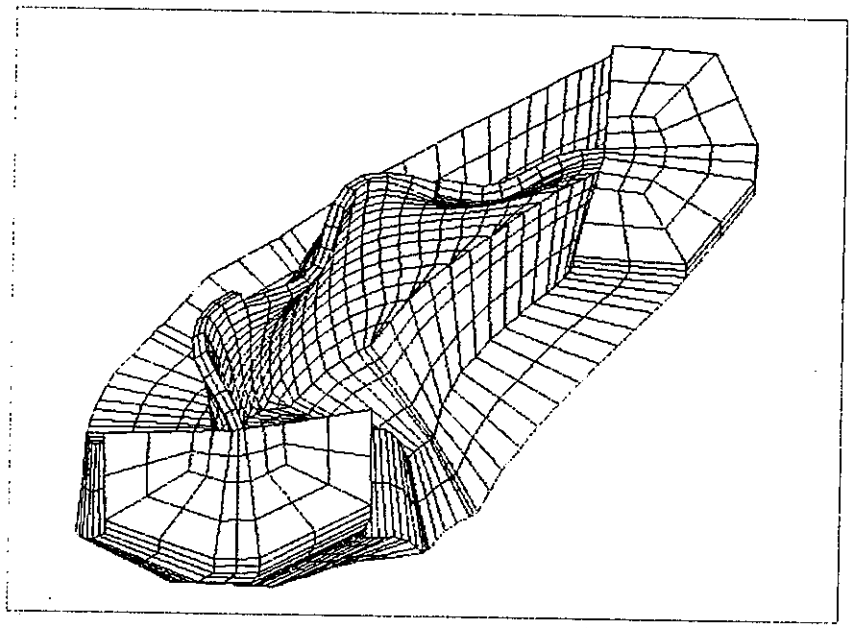

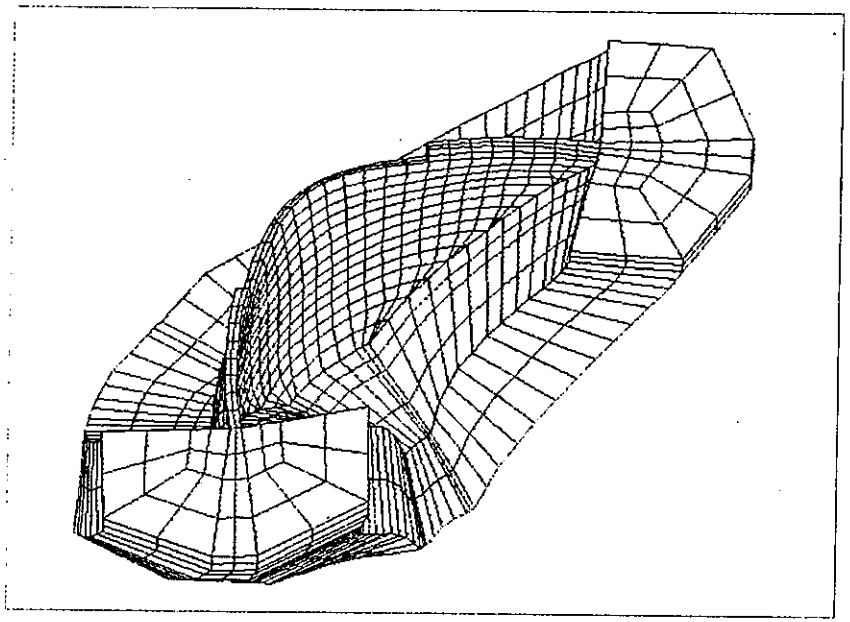

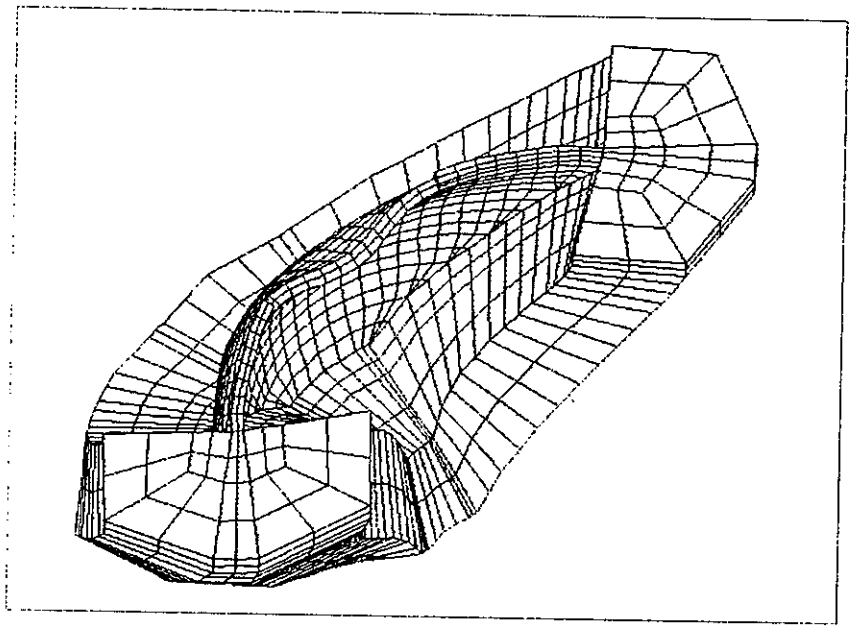

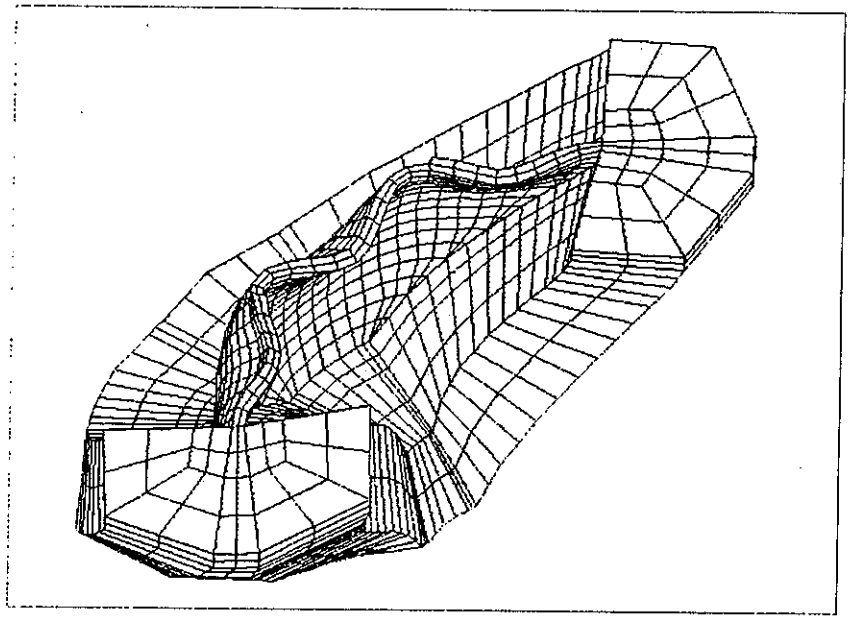

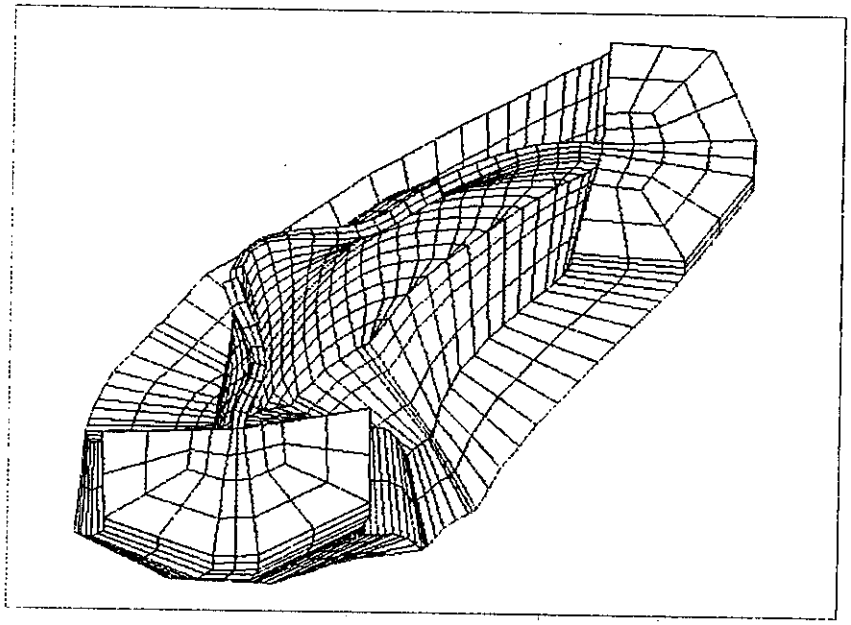

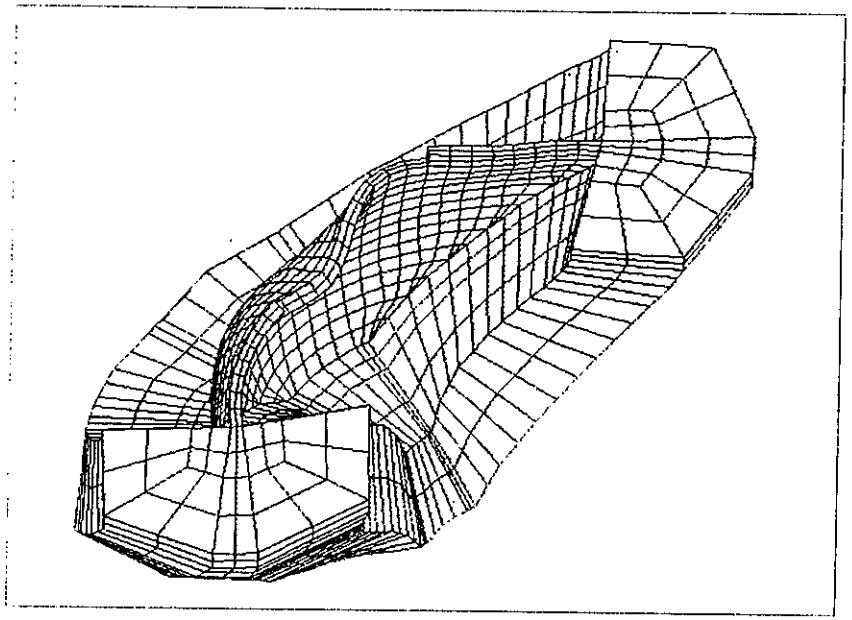

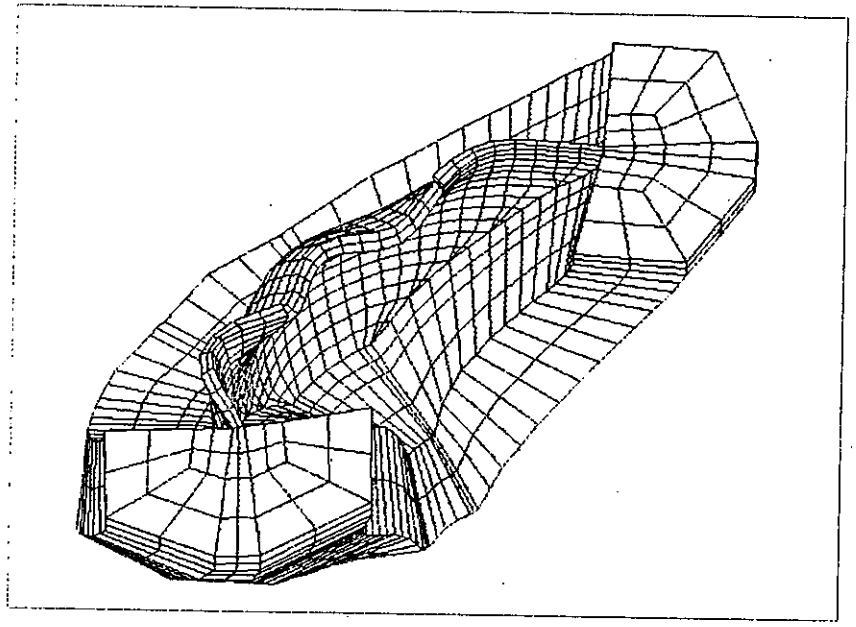

mold shape

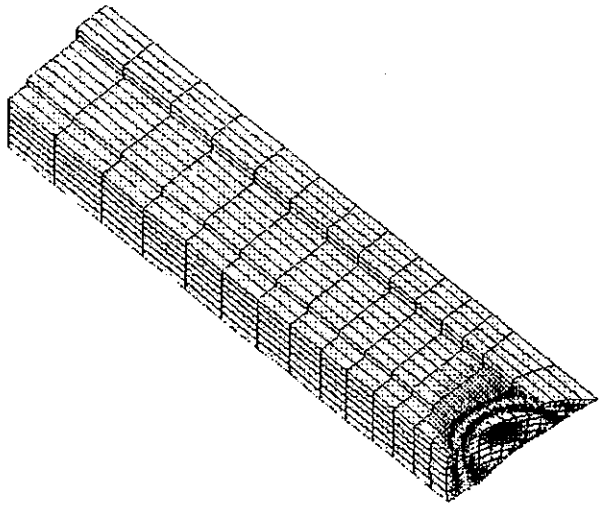

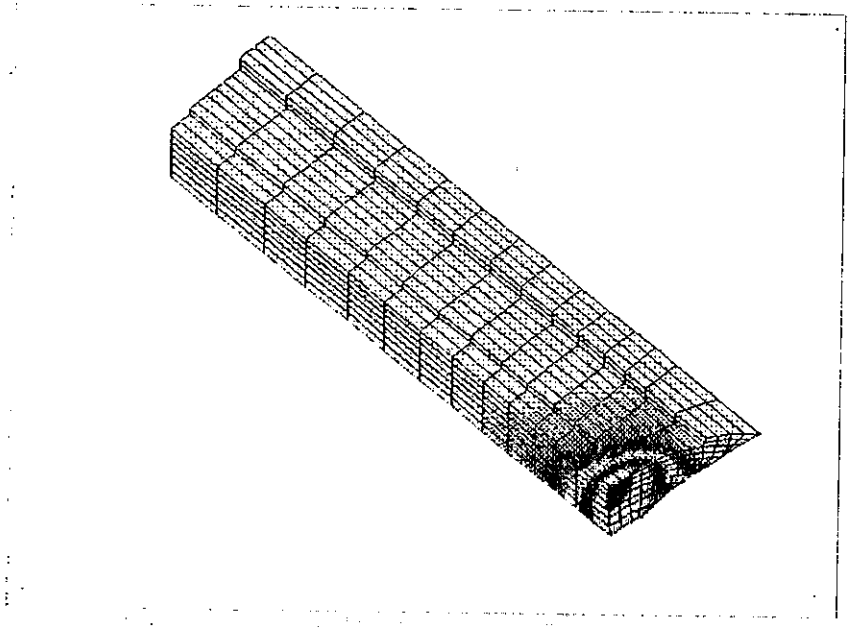

mode shape 3

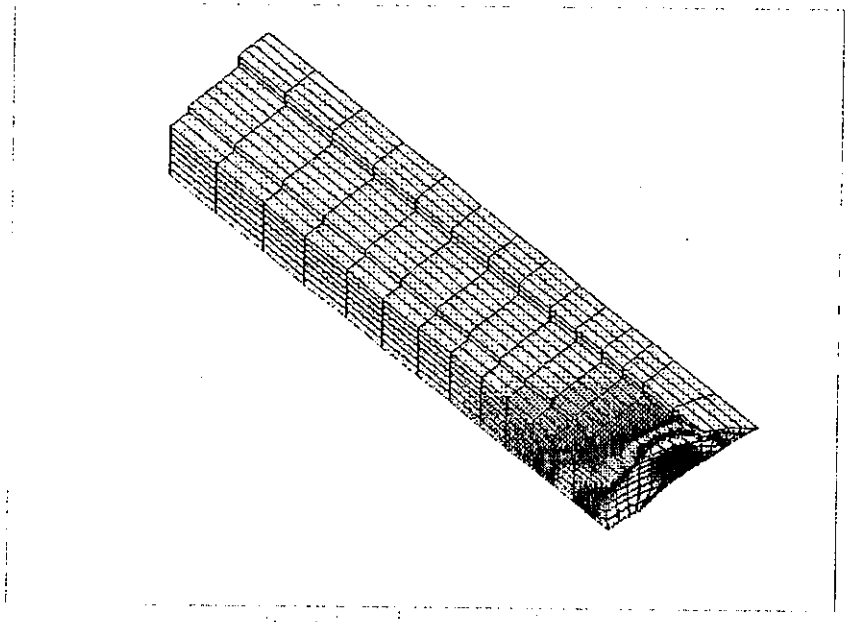

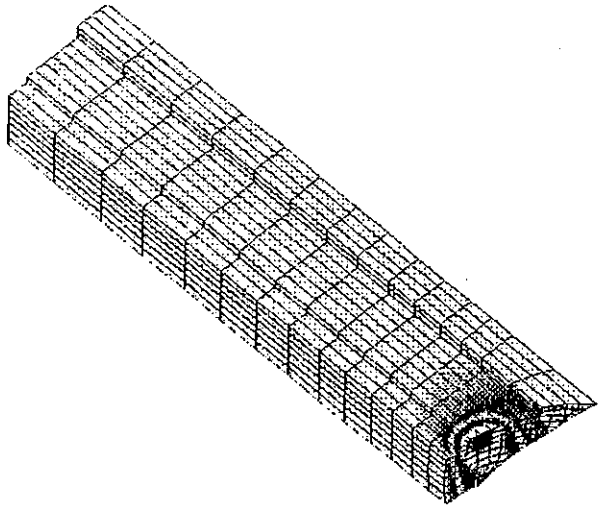

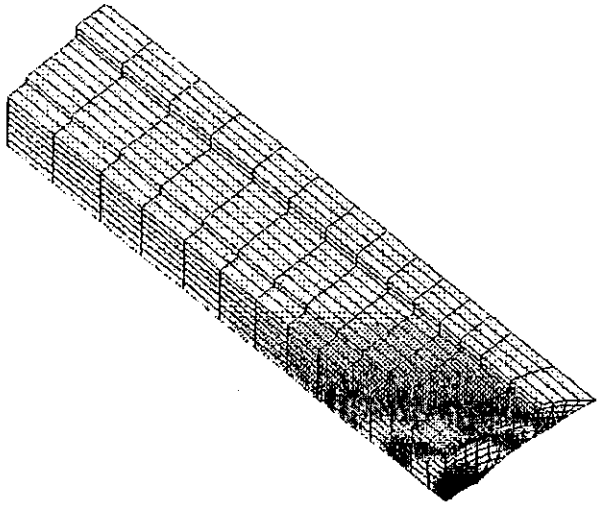

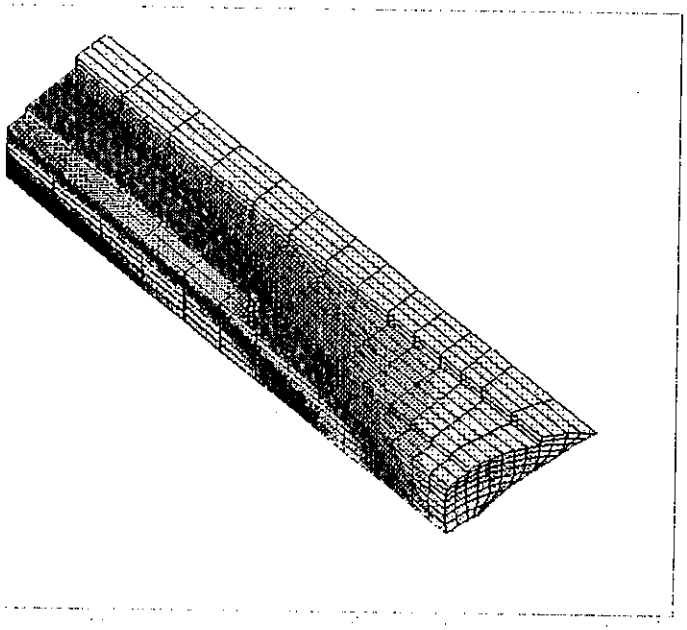

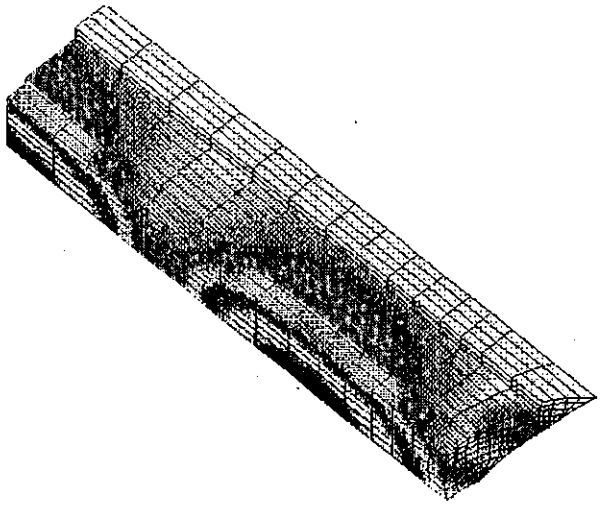

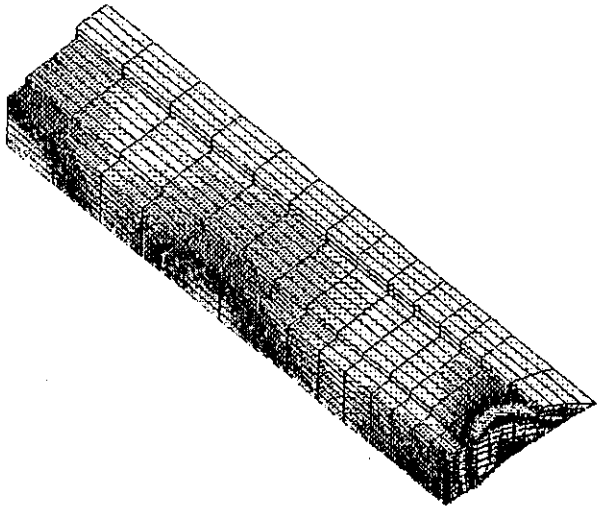

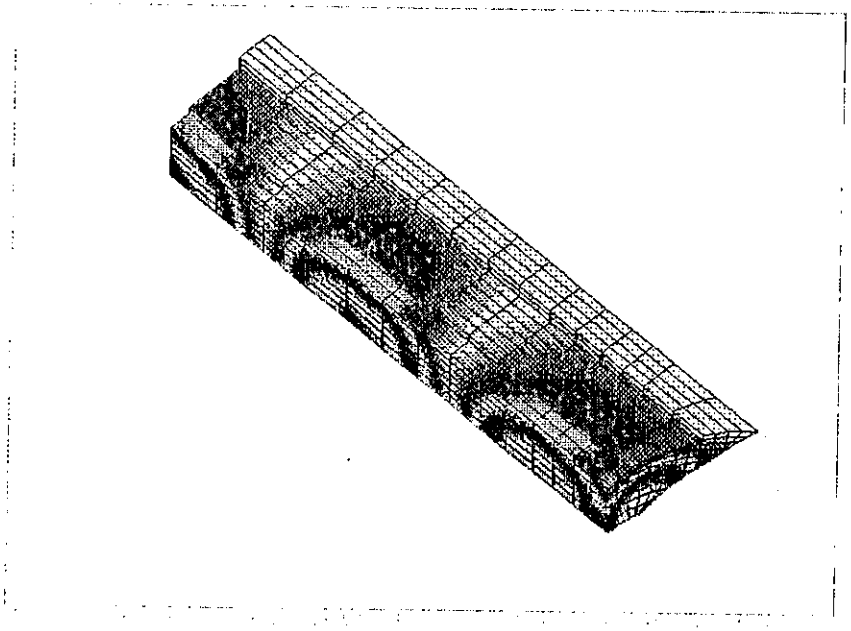

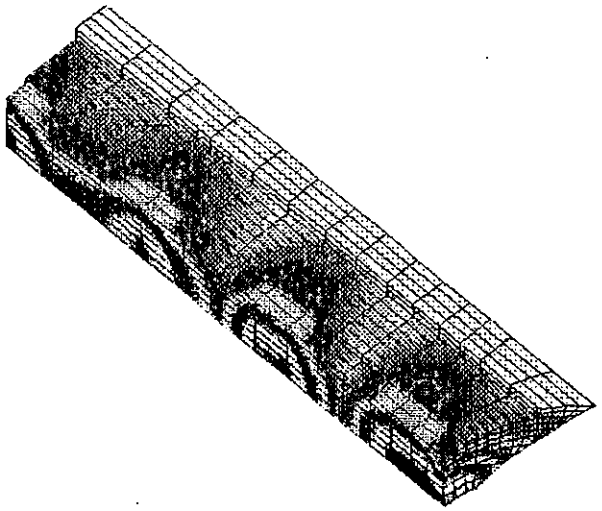

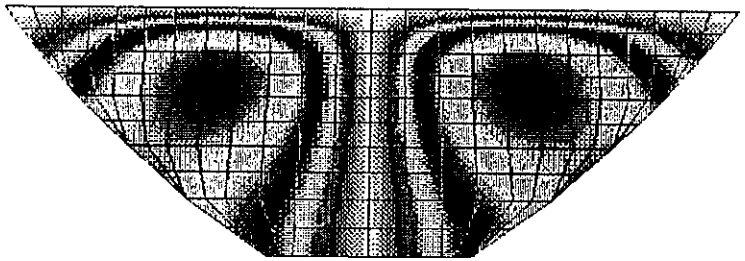

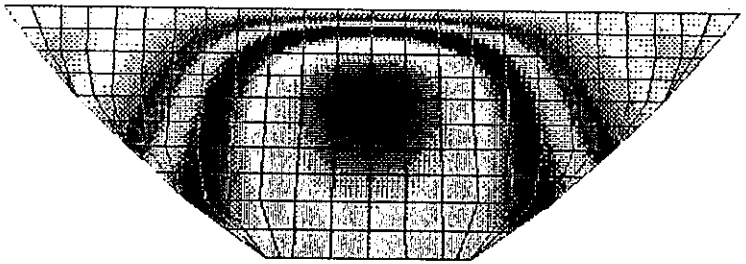

mode shape 3

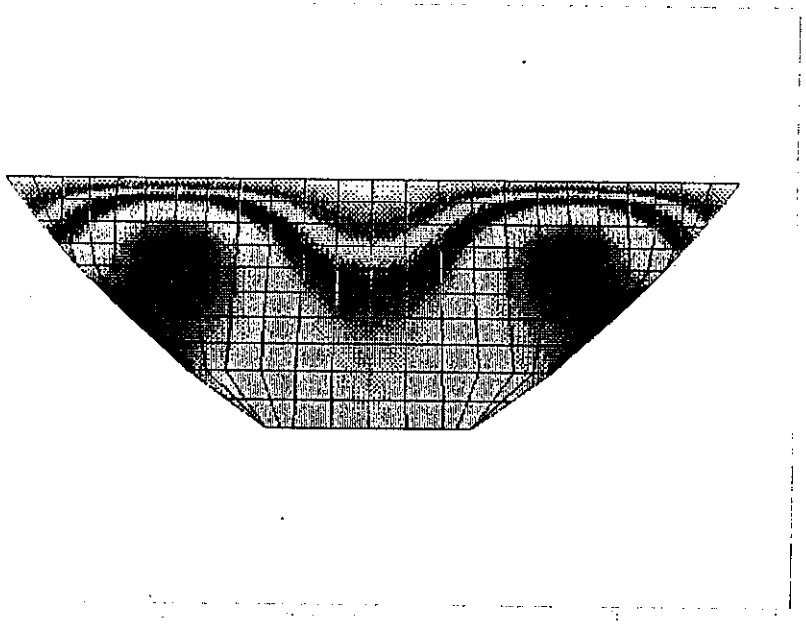

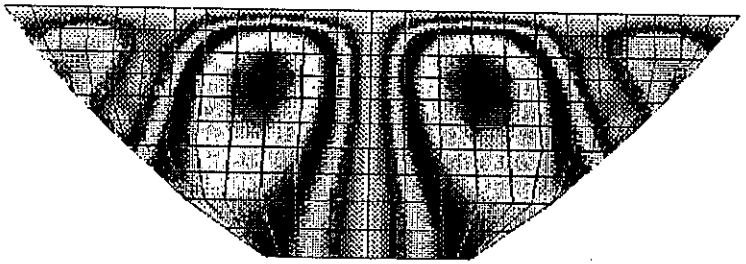

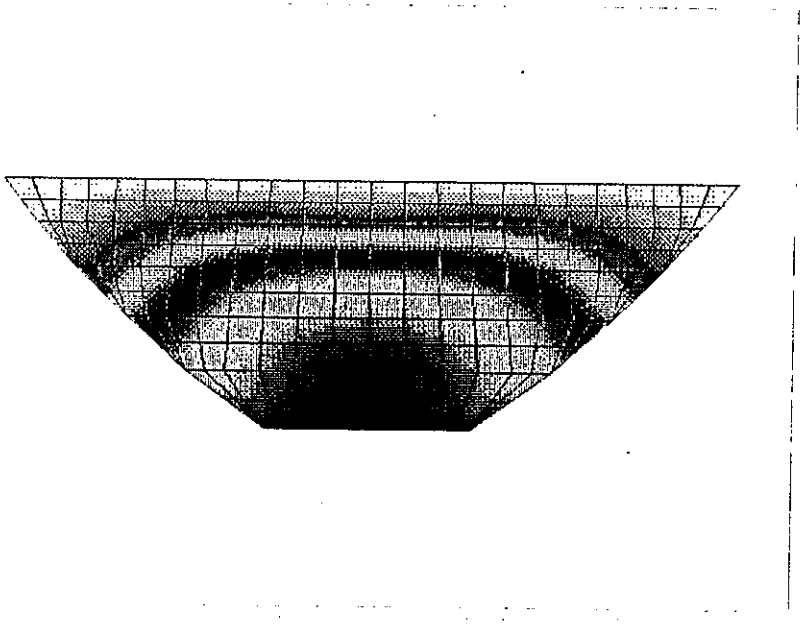

mode shape 6

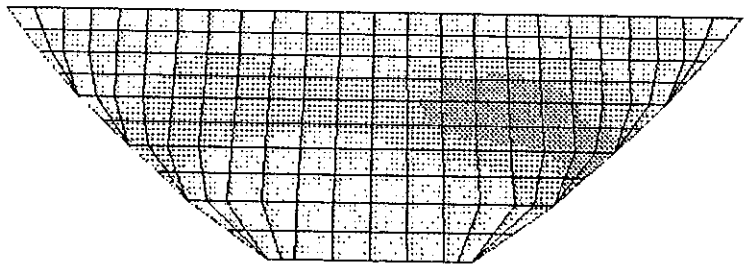

mode 7

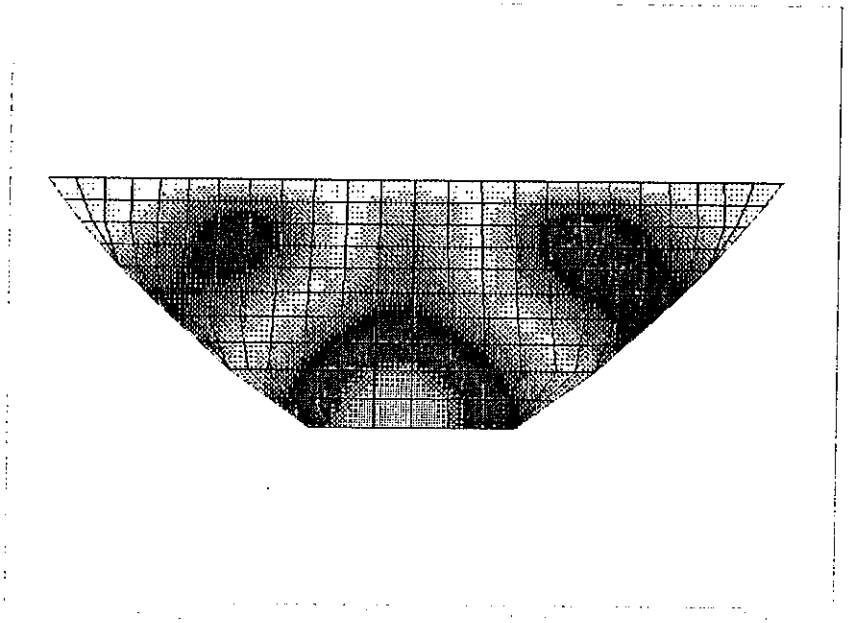

mode shape 5

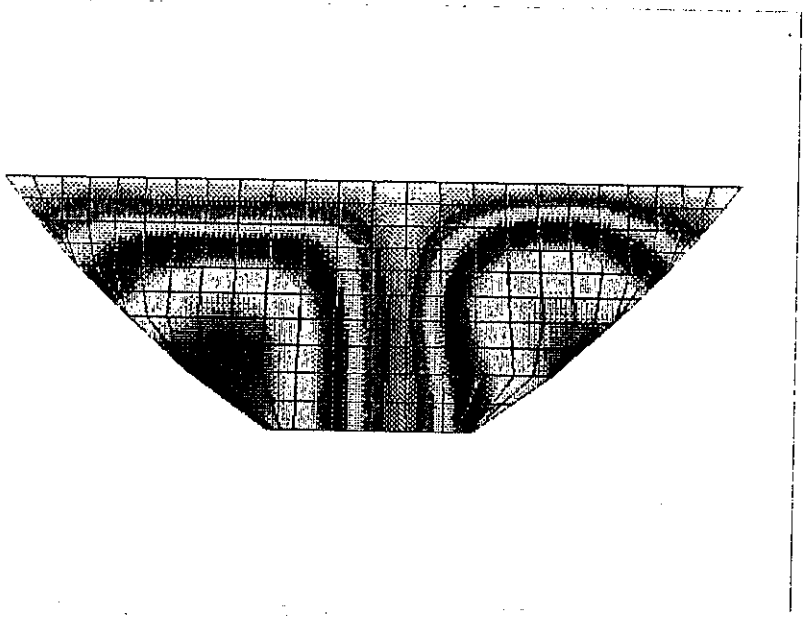

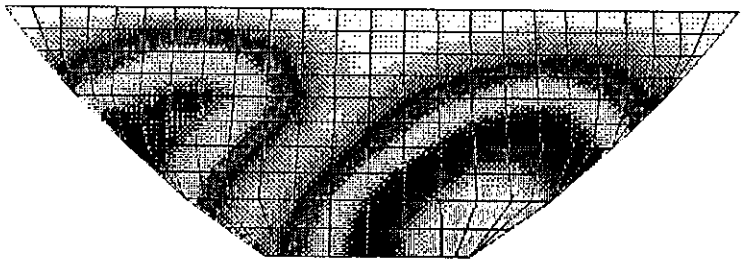

mode shape 10

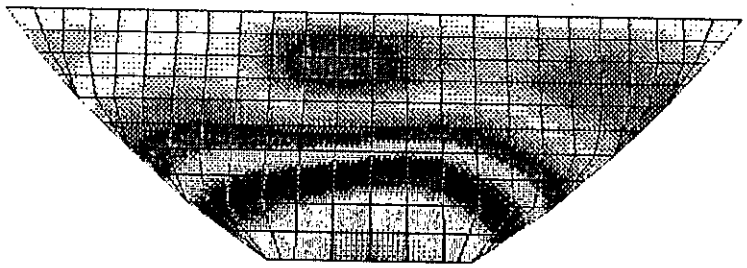

LOADING CONDITION 3.5.2 (compressible fluid)

MODE SHAPE 1

1	0.41272E-02	-0.31523E+00	-0.46903E-03
2	0.62366E+00	-0.36175E+00	-0.13467E+00
3	0.87491E+00	-0.43974E+00	-0.16294E+00
4	0.22795E+00	-0.10427E+00	-0.20395E-01
5	0.16344E-01	0.15170E-01	-0.86294E-03
6	0.29611E-02	-0.21178E+00	-0.67992E-04
7	0.37600E+00	-0.24011E+00	-0.42347E-01
8	0.51314E+00	-0.28200E+00	-0.25835E-01
9	0.11331E+00	-0.67802E-01	0.14011E-01
10	0.15535E-01	0.10662E-01	0.31379E-02
11	0.16664E-02	-0.10161E+00	0.26328E-03
12	0.16320E+00	-0.11597E+00	0.17096E-01
13	0.17659E+00	-0.11534E+00	0.34920E-01
14	0.20798E-01	-0.62721E-02	0.92063E-02
15	0.50761E-03	-0.37878E-01	0.25364E-03
16	0.34834E-01	-0.39850E-01	0.18631E-01
17	0.13740E-01	-0.21967E-01	0.17803E-01
18	0.10603E-03	-0.20569E-01	0.12591E-03
19	0.32018E-02	-0.18475E-01	0.92810E-02
20	0.25163E-02	-0.16976E-01	0.11643E-01

THEME B

"The seismic response of an embankment dam under conditions of both low and medium levels of seismic loading"

Analyses non-linéaires statique et dynamique du barrage d'El Infiernillo

D. AUBRY [1], A. MODARESSI [1] & I. BENZENATI [1,2]

1. Ecole Centrale de Paris

2. Bureau de Recherches Géologiques et Minières

Résumé

Des résultats de simulation numérique du comportement du barrage d'El Infiernillo sont présentés dans ce présent rapport. L'étude a été effectuée dans le cadre du premier Benchmark du calcul numérique organisé par " International Commission on Large Dams (ICOLD) " et ISMES. Le barrage d'El Infiernillo représente un cas de validation de codes de calcul assez intéressant puisqu'il s'agit d'un ouvrage équipé d'instruments de mesures tels que des piézomètres, des inclinomètres, des accéléromètres et des jauges de déformations [1,4]. C'est ainsi que depuis le début de la construction du barrage en 1960, des mesures de l'évolution des pressions interstitielles, des tassements, des et déformations ont été effectuées à divers profils du barrage. De plus, des mesures de tassements et d'accélérations ont été enregistrés durant les différents séismes qui ont secoué le barrage. Plusieurs études utilisant différentes méthodes de stabilité ont été menées sur ce barrage et ont fait l'object de publications [2,3]. La présente analyse a été effectuée en déformations planes à l'aide du code de calculs GEFDYN qui s'appuie sur un modèle de milieu poreux couplant déformations et pressions interstitielles et utilisant une méthode d'éléments finis. Le modèle de comportement élastoplasique cyclique multimécanismes de Hujeux a été adopté pour décrire le comportement rhéologique des matériaux constituant l'ouvrage [5,14].

INTRODUCTION

Dans les barrages en remblais, les contraintes et les les pressions interstitielles suivent des chemins complexes depuis la période de leur construction et durant la phase de leur exploitation. On ne se limitera pas donc dans cette étude seulement à la réponse sismique du barrage puisque cette dernière est liée à toute l'histoire du barrage avant l'arrivée du tremblement de terre. Trois phases principales sont souvent distinguées dans les études de stabilité de ce type d'ouvrages:

- Phase de construction qui consiste à modéliser la mise en place des matériaux et la consolidation qui se produit durant la montée du niveau du remblai.
- Phase de mise en eau qui représente l'étape de remplissage du réservoir et le régime d'écoulement stationnaire qui s'établit ainsi de l'amont vers l'aval.
- Phase de fonctionnement et d'exploitation du barrage durant laquelle des phénomènes aléatoires de fluctuations du niveaux d'eau et de tremblements de terre peuvent se produire.

Les travaux de construction du barrage d'El Infiernillo ont débuté en 1960, la capacité totale du réservoir est d'environ 12 10^9 m^3. Il est constitué essentiellement de matériaux en enrochements compactés et d'un noyau argileux (Figure 1). La hauteur de sa section la plus profonde est de 150m. Le barrage est également muni dans sa partie avale de galeries ayant une capacité de décharge de 13400m^3/s permettant le drainage de l'ouvrage[1,4].

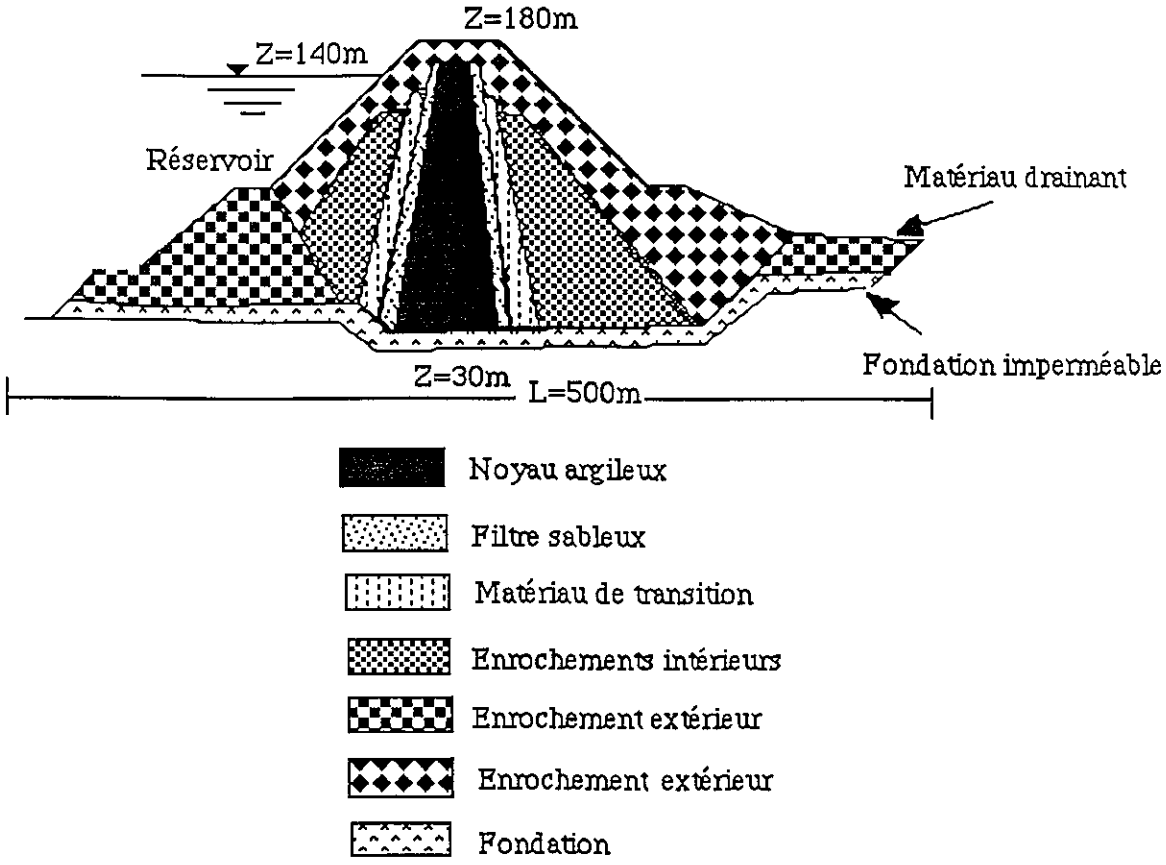

Figure 1: Coupe transversale du barrage et hypothèses du calcul

Plusieurs tremblements de terre ont secoué le barrage depuis son achèvement dont les plus violents sont:
- Le séisme du 14 mars 1979 où l'accélération maximale à la base a atteint 0.1g.

- Le séisme du 19 septembre 1985 où l'accélération maximale à la base est de 0.3g.

HYPOTHESES DES CALCULS

Les simulations numériques ont été menées en adoptant un certain nombre d'hypothèses concernant à la fois le comportement rhéologique des matériaux du barrage, les conditions initiales ainsi que les conditions aux limites mécaniques et hydrauliques en régimes statique et dynamique.

1) Modèle éléments finis

Un maillage assez similaire à celui proposé par les organisateurs du benchmark a été utilisé pour l'ensemble des analyses statiques et dynamiques effectuées. Ce maillage est constitué d'un domaine correspondant aux matériaux solides (enrochements, noyau argileux et le filtre) et d'un domaine représentant la partie fluide correspondant au réservoir du barrage (figure 2a). Cependant, un certain nombre de modifications de ce maillage ont été effectuées:

- les éléments correspondant au réservoir ont été éliminés du maillage utilisé dans les calculs puisque l'eau du réservoir n'est prise en compte que par son action mécanique et hydraulique extérieure sur le domaine du sol modélisé.
- Afin de pouvoir effectuer correctement les calculs dynamiques en utilisant des frontières absorbantes, la fondation du barrage doit être assimilée à un matériau soit imperméable soit perméable. Car nous ne disposons pas à l'heure actuelle de frontières absorbantes en milieux biphasiques. Le choix d'une fondation imperméable qui est le plus raisonnable a été effectué. Une rangée d'éléments traités seulement en monophasique et d'éléments paraxiaux activés seulement en dynamique ont été alors superposés à la base du maillage proposé (figure 2b).
- L'action du réservoir est supposée extérieure au modèle, des éléments de chargement de surface sur le parement amont du barrage sont alors à prévoir lors de la mise en eau. A noter que durant la construction par couches du barrage ces éléments restent non chargés.
- Le barrage d'El Infiernillo comporte dans sa partie avale des galeries pour lesquelles les dimensions et la position exacte dans la structure n'ont pas été fournies. Des conditions de drainage sont alors imposées dans une zone arbitraire à l'aval du modèle.

Le problème est considéré couplé dans sa globalité où l'eau est supposée compressible et occupe tous les vides intergranulaires. Les perméabilités sont considérées isotropes pour tous les matériaux.

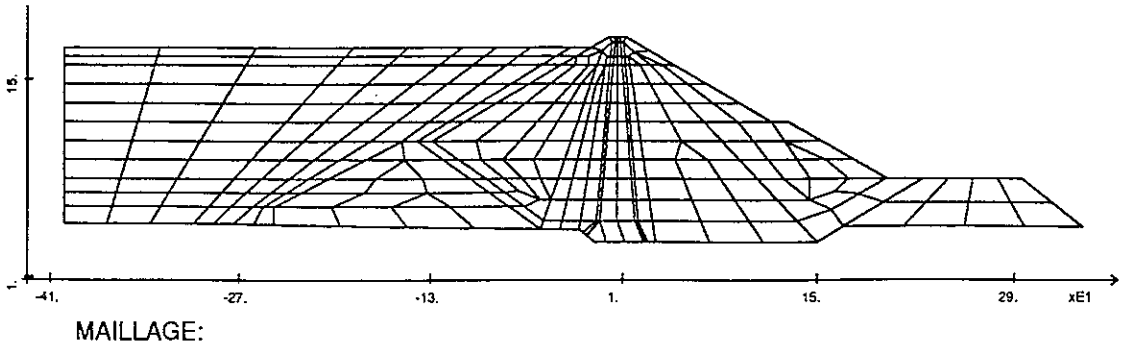

Figure 2a: Maillage proposé par les organisateurs du benchmark

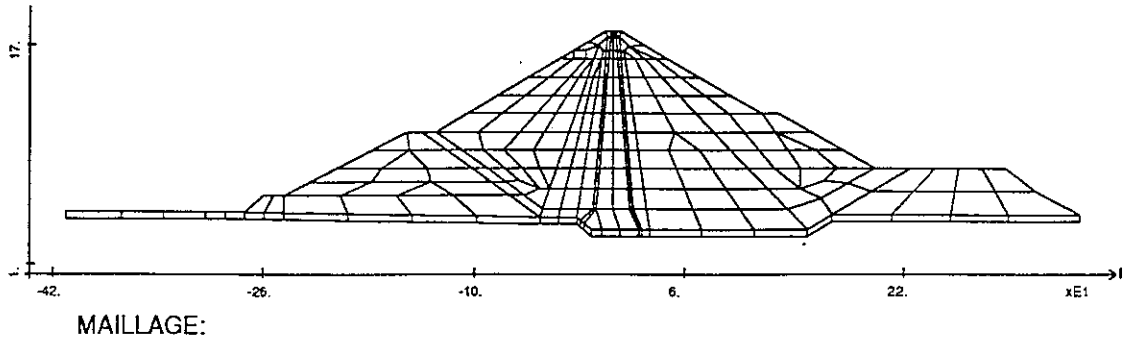

Figure 2b: Maillage utilisé pour l'analyse

2) Calage des paramètres de la lois de Hujeux:

En l'absence de courbes d'essais triaxiaux, les paramètres de la loi de Hujeux ont été choisis pour mieux approcher les courbes G-γ (figure 3) fournies par les organisateurs du benchmark. Les jeux de paramètres initiaux sont celui du sable d'Hostûn dense pour les enrochements et celui de la Kaolinite pour le noyau argileux. Par ailleurs, les valeurs des perméabilités publiées dans la littérature sont utilisées dans la simulation [1]. La fondation est modélisée par un matériau élastique linéaire imperméable.

Paramètres des matériaux	Symboles	Enrochement	Noyau	Filtre	Fondation
Paramètres élastiques	n K_i G_i P_{ref}	0.5 65. Mpa 50. MPa 1. MPa	0.7 25 MPa 10. MPa 1. MPa	0.5 90. MPa 50. MPa 1. MPa	E= 800 MPa ν = 0.3
Paramètres d'état Critique	P_{co} β ϕ ψ	1.2 MPa 30 30° 30°	0.5 MPa 13 22° 20°	40. MPa 32 35° 35°	35. MPa 30 40° 37°
Paramètres d'écrouissage déviatoire	a_m a_c b	0.006 0.003 0.12	0.006 0.004 0.9	0.006 0.002 0.12	0.003 0.003 0.5
Paramètres d'écrouissage volumique	c_m c_c d	0.004 0.002 2	0.1 0.05 1.6	0.005 0.0025 2	0.005 0.001 5
paramètres des domaines de comportement	r^e r^{hys} r^{mob} m α	0.02 0.04 0.8 2.4 1	0.001 0.002 0.05 2.4 1	0.02 0.04 0.8 2.4 1	0.02 0.04 0.8 2.4 1
Perméabilités (m/s)	K	10^{-6}	10^{-8}	?	10^{-4}

Table 1: Les paramètres des matériaux utilisés pour l'analyse

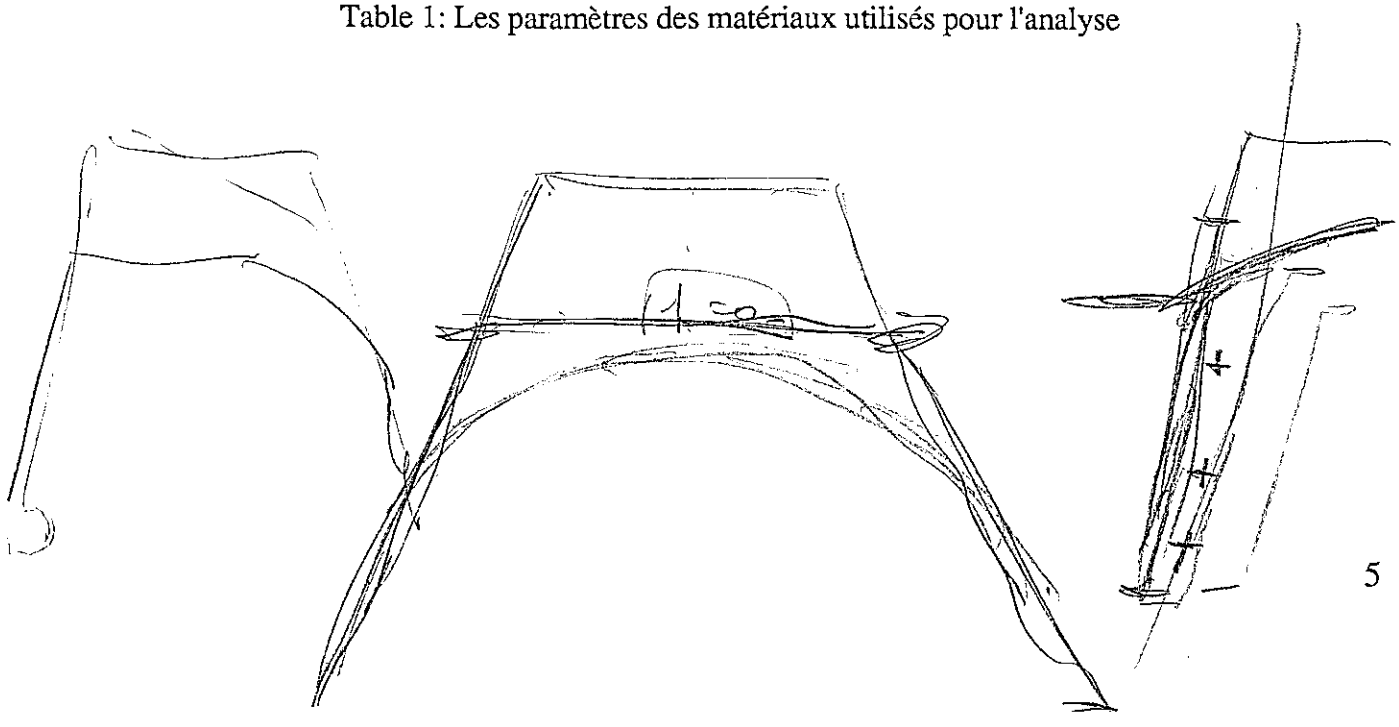

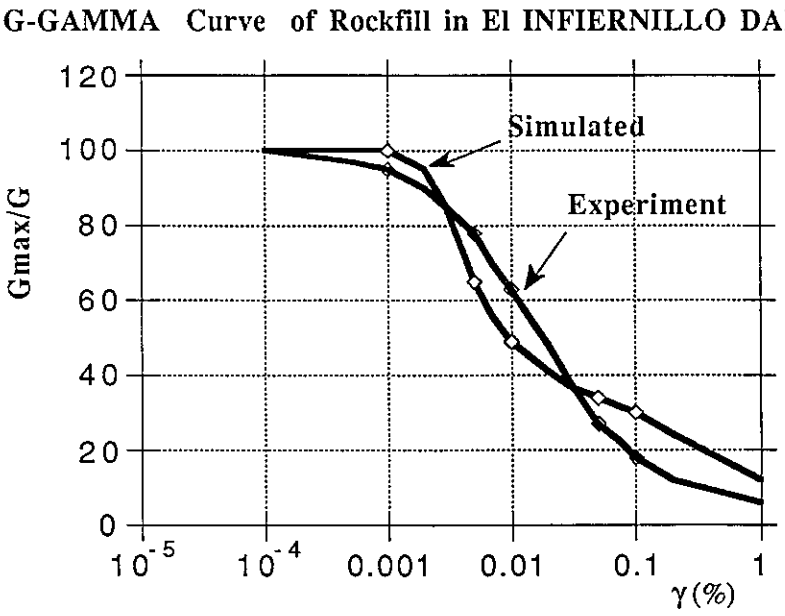

Figure 3: Calage des paramètres de la loi Hujeux sur les courbes G-γ
Cas des enrochements

3) Construction par couches du barrage

La couche de la fondation est supposée présente initialement et ne rentre donc pas dans le scénario de la simulation numérique de la construction du barrage. La mise en place des couches du remblai est modélisée par une courbe linéaire et monotone de la côte de ce dernier en fonction du temps. La vitesse de construction est d'environ 8m par mois. Les phases éventuelles de l'arrêt des travaux pendant les saisons de pluies ne sont pas simulées. Cependant, la durée totale de la pose des mailles correspond à celle de la construction de l'ouvrage qui est de 18 mois[1]. Les contraintes, les pressions et les tassements calculés sont alors comparables aux valeurs mesurées en fin de construction.

4) Remplissage de la retenue

La durée de remplissage des réservoirs de barrages en terre s'étale en général sur plusieurs années. Elle dépend étroitement de l'hydrologie des bassins versant environnants, de leur topographie et des caractéristiques géométriques et mécaniques du barrage en question. Pour simuler la mise en eau du barrage, on considère que le niveau du réservoir augmente d'une façon linéaire et monotone. On ne s'intéressera pas aux fluctuations saisonnières que subit le niveau d'eau du barrage. La modélisation numérique consiste à appliquer sur le parement amont du barrage des forces de surface correspondant au poids de l'eau du réservoir et d'imposer simultanément les pressions interstitielles correspondantes sur les nœuds concernés. La vitesse de montée du niveau d'eau du réservoir est 8m par mois. On signale qu'une période de consolidation a été effectuée à l'issu du remplissage pour que le régime d'écoulement stationnaire soit établi.

On suppose alors que l'état de contrainte et de pression obtenu reste inchangé jusqu'à l'arrivée du séisme.

4) Simulation dynamique

On s'intéresse maintenant à la réponse du barrage au séisme du 14 mars 1979. Les déformations et les déplacements sont remis à zéro; les variables d'histoires, les contraintes et les pressions interstitielles de l'étude statique précédente sont prises comme conditions initiales du problème dynamique. L'action sismique est introduite sous forme d'accélérogramme à partir de la fondation du barrage par l'intermédiaire des éléments de frontières absorbantes. La transformée de Fourier de l'accélérogramme figure 4 montre que le contenu fréquentiel du mouvement sismique est riche dans la gamme de fréquences comprise entre 4 et 8 Hertz. Pour éviter le filtrage numérique de ces fréquences, la plus grande dimension d'un élément du maillage ΔH, est prise telle que :

$$\Delta H < C / 5 F$$

Où C est la vitesse de propagation des ondes sismiques dans le milieu et F la fréquence du mouvement.

La plus faible vitesse de propagation est: C= 300m/s

Pour une fréquence F = 8Hertz, la plus grande dimension du maillage doit être telle que: $\Delta H < 7.5$m.

Or dans le sens vertical correspondant à la direction de la propagation, la plus grande dimension du maillage utilisé est de 12m. Un filtrage de fréquence dû au maillage est alors possible lors des simulations dynamiques.

Les calculs ont été effectués en utilisant le schéma implicite de Newmark avec les paramètres standards suivants:

$\beta = 0.5$ et $\gamma = 0.25$

Le pas de temps du calcul est de 0.001s.

L'angle d'incidence du mouvement sismique est supposé nul et le point de contrôle est situé sur la surface libre à l'aval du barrage. (où ?) à la surface du sol.

implicite / explicite ?

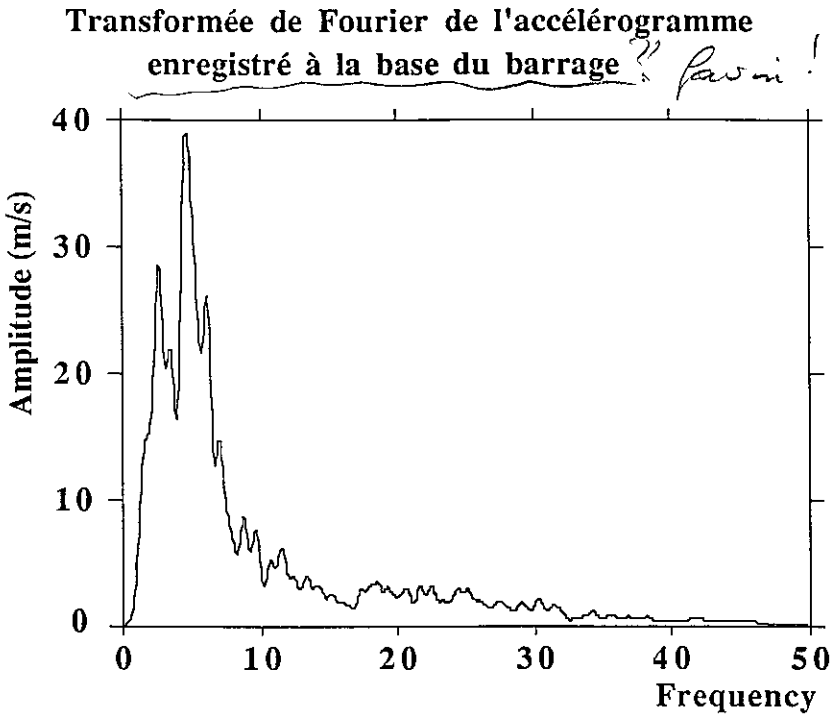

Figure 4: Transformée de Fourier du mouvement sismique

ANALYSE DES RESULTATS

Analyses statiques:

En fin de construction du barrage, on constate que les déplacements mesurés par les inclinomètres situés dans le noyau et les enrochements sont du même ordre de grandeur[1]. Cette déformation régulière et homogène du barrage montre le bon choix des granulométries et des rigidités des matériaux constituant chaque zone de l'ouvrage. Les résultats du tassement dûs au poids propre du barrage obtenus par le calcul statique de la construction par couches sont présentés sur la figure 5. On remarque, comme dans le cas des mesures, que l'ordre de grandeur des tassements dans le noyau est le même que dans les enrochements. Par contre, les résultats numériques semblent plus faibles que les mesures réelles effectuées (Tableau 2).

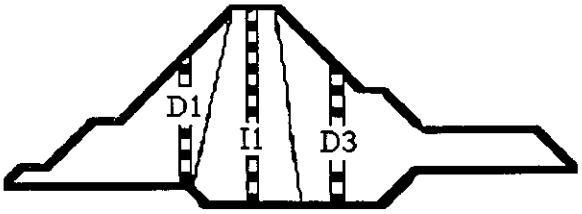

Inclinomètres	Tassement maximal mesuré (m)	Tassement maximal calculé (m)
D1 (Amont)	1.40 à Z=100m	0.75 à Z=80m
I1 (Noyau)	1.60 à Z=110m	1.00 à Z=90m
D3 (Aval)	1.10 à Z=100m	0.50 à Z=50m

Tableau 2: Tassements en fin de construction

Dans le plan horizontal, les différentes mesures des déplacements réalisées montrent que la partie centrale du profil longitudinal du barrage a tendance à se déplacer plus vers la vallée (aval)[1,4]. Les déplacements mesurés dans la direction longitudinale sont relativement faibles. Les valeurs maximales de ces mesures ne dépassent pas 2cm au centre du profil longitudinal du barrage. Par contre, dans la direction transversale, les mesures sont plus importantes et montrent une tendance de glissement du remblai plus marquée vers l'aval. En fin de construction, les valeurs des déplacements transversaux maximaux enregistrés sont de l'ordre de 20cm sur le talus aval à l'élévation Z=130m.

Les résultats des calculs numériques semblent en bonne concordance avec les mesures réelles obtenues. En effet, la composante horizontale du champ de déplacement est plus importante dans la partie avale du barrage. La valeur maximale calculée est de 19 cm, elle est obtenue au nœud situé sur le talus aval à l'élévation Z=130m.

Les phases de consolidation et d'arrêt des travaux qui peuvent être importantes n'ont pas été modélisées dans le calcul, les pressions et les contraintes n'ont donc pas évolué exactement de la même façon. A la fin de la construction, les distributions des pressions interstitielles (Figures 6) et des contraintes (Figures 7a et 7b) sont relativement proches entre le calcul et les observations expérimentales. Les mesures et les résultats des calculs des pressions interstitielles dans le noyau en fin de construction sont résumés dans le tableau 3.

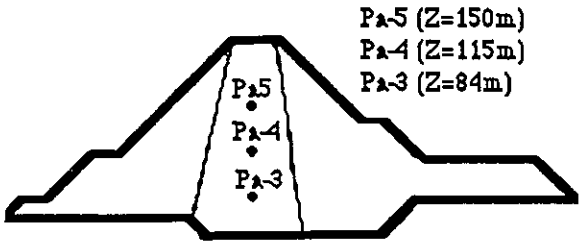

Piézomètres	Elévation (m)	Nœuds correspondants	Pressions d'eau Mesurées (Bars)	Pressions d'eau Calculées
Pa-3	Z=84m	N745 (Z=86m)	6.7	6.1
Pa-4	Z=115m	N650 (Z=113)	3.6	3.5
Pa-5	Z=150m	N533 (Z=146)	1.	1.3 ?

fin de construction

Remplissage du réservoir

A la fin de la phase de remplissage du réservoir effectuée en deux ans, la distribution des pressions interstitielles est représentée sur la figure (8). Des calculs de consolidations (2ans) ont été effectués afin d'obtenir le régime d'écoulement stationnaire du modèle. L'état de pressions interstitielles obtenu (figure 9) est supposé être l'état initial pour les calculs dynamiques.

Durant la phase de mise en eau, des mesures de pressions interstitielles ont été obtenues par l'intermédiaires des piézomètres. On note que lorsque le niveau d'eau était à sa côte maximale (Z=160m), les piézomètres installés dans la fondation indiquaient des pressions de l'ordre de la hauteur du niveau d'eau dans le réservoir c'est à dire 130m. Le calcul numérique aboutit à des résultats similaires qui sont de l'ordre de 14 Bars à la fin du remplissage et 13.3 Bars durant le régime stationnaire.

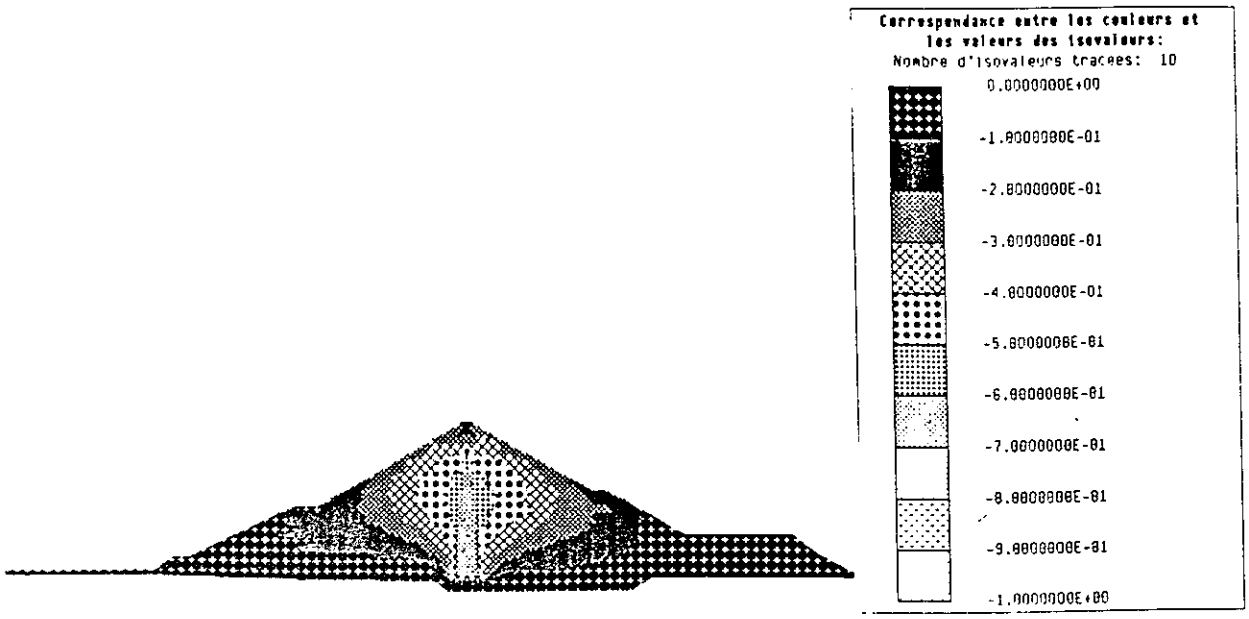

Figure 5: Isovaleurs des tassements en fin de construction du barrage

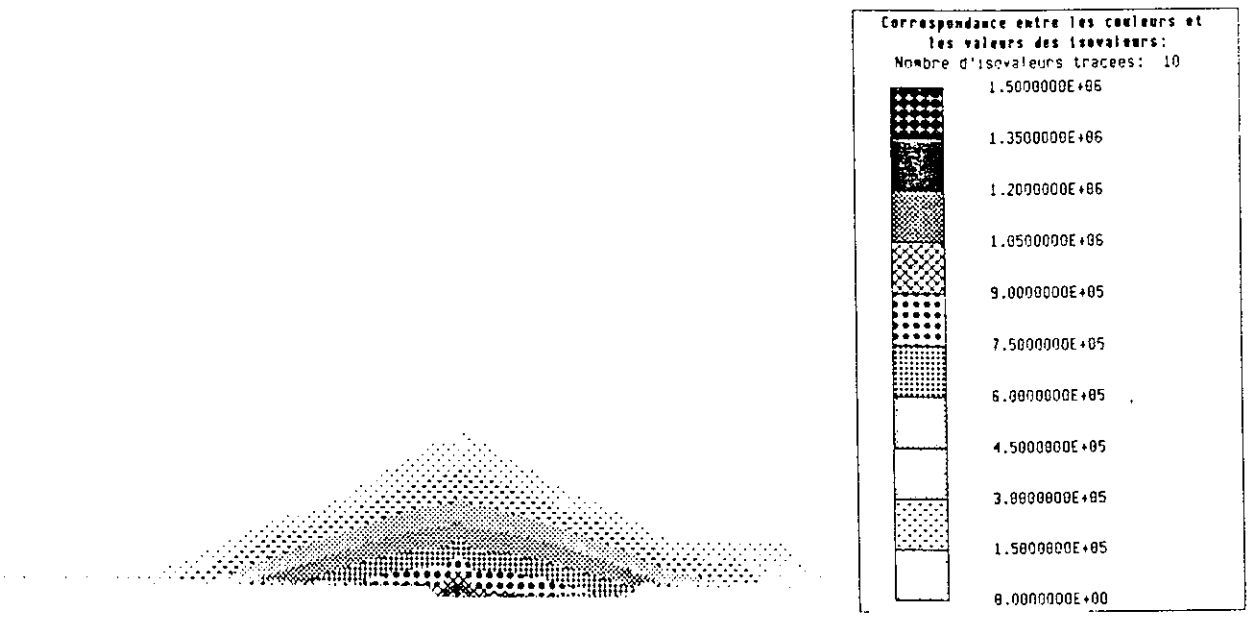

Figure 6: Isovaleurs des pressions interstitielles en fin de construction du barrage

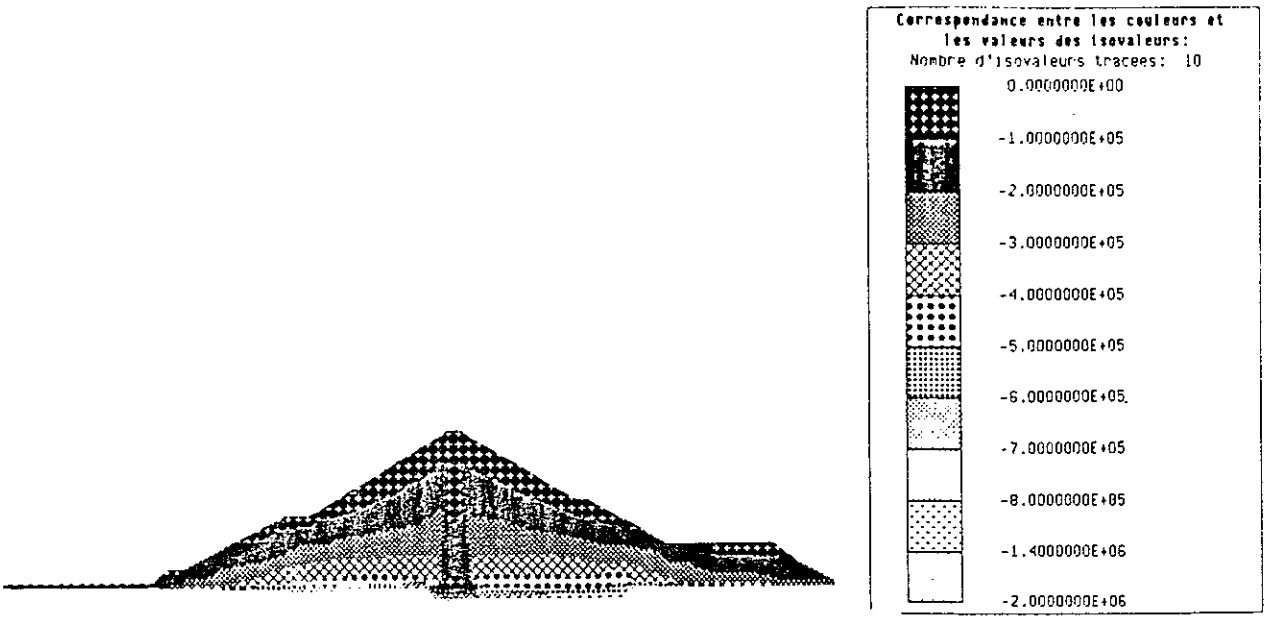

Figure 7a: Isovaleurs des contraintes horizontales en fin de construction du barrage

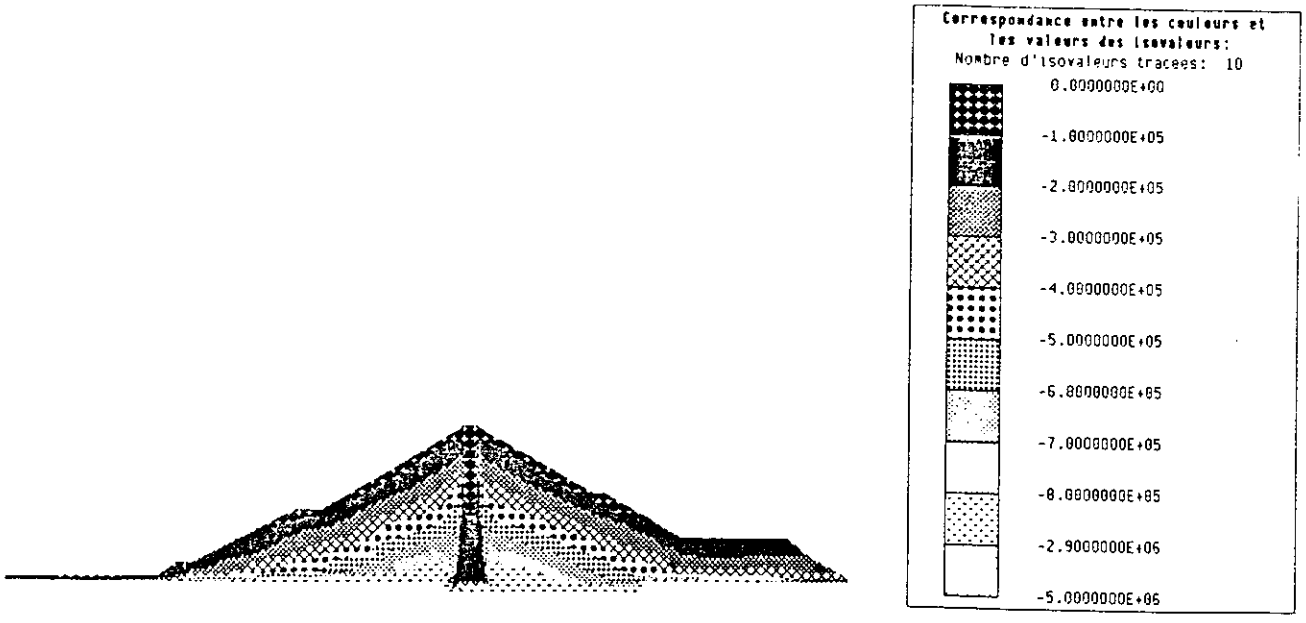

Figure 7b: Isovaleurs des contraintes verticales en fin de construction du barrage

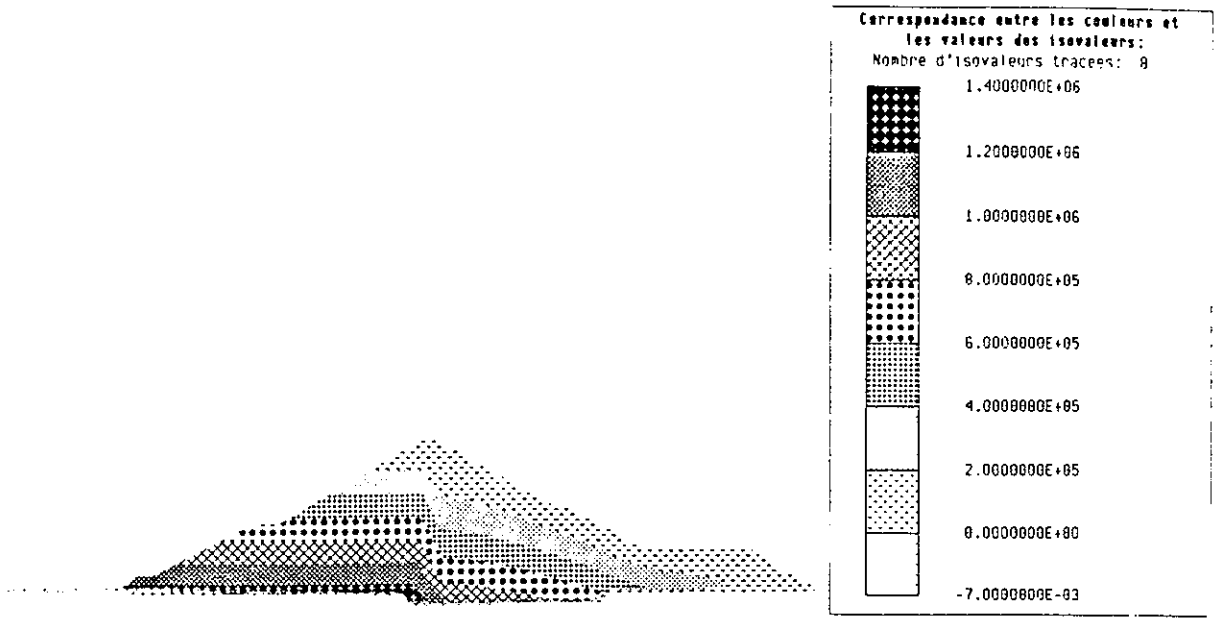

Figure 8: Isovaleurs des pressions interstitielles en fin de remplissage du du réservoir

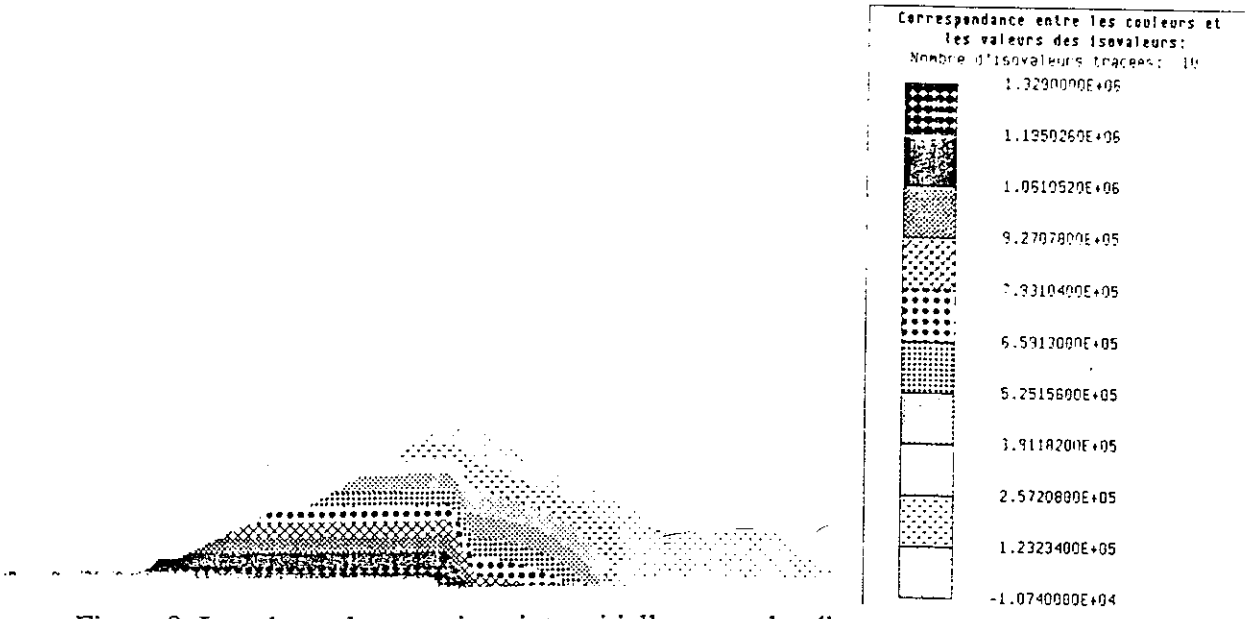

Figure 9: Isovaleurs des pressions interstitielles avant le séisme

Analyse dynamique

Les résultats de mesures pendant le séisme du 14 mars 1979 sont essentiellement les déplacements dans le noyau et les accélérations en crête du barrage. Les piézomètres ne sont pas suffisamment performants pour suivre l'évolution des pressions interstitielles pendant le séisme du fait de la rapidité du mouvement. On présente dans ce qui suit les résultats des calculs numériques effectués qu'on comparera aux mesures réelles disponibles.

Une simulation numérique du comportement sismique du barrage a été effectuée sur une durée de séisme de 10 secondes et les résultats sont présentés aux nœuds indiqués sur la figure 10. (correspondent-il à des point de mesure?)

De légères amplifications d'accélérations sont constatées en crête et sur les surfaces libres amont et avale du barrage (figures 11a;11e). Les accéléromètres installés le long de la crête du barrage ont enregistré une accélération maximale de l'ordre de 3.55 m/s2 alors que le calcul donne une accélération maximale de 1.9m/s2. On note toutefois que la valeur maximale des accélérations calculées est atteinte en crête. Par ailleurs, on ne dispose pas des mesures obtenus par les autres accéléromètres. lesquels ?

Les évolutions des tassements sont présentés sur les figures 12a et 12b. On constate que des déplacements verticaux permanents apparaissent notamment sur la partie supérieure du noyau du barrage.

Sur les figures 13a et 13b sont présentés les résultats des déplacements horizontaux des parements amont et aval ainsi du noyau. On remarque que ces courbes ont pratiquement les mêmes allures que celles des tassements; les déplacements permanents se produisent surtout sur la partie supérieure de l'ouvrage.

(ces évidents après la lecture)

Les comparaisons entre les résultats des déplacements permanents du calcul et les mesures expérimentales (figures 14 et 15) montrent que la simulation numérique est satisfaisante.

Des résultats des augmentations des pressions interstitielles sont représentés sur les figures 16a, 16b et 16c. On constate que l'augmentation des pressions se produit seulement sur la partie supérieure, à partir environ de l'élévation Z=100m.

Le maillage déformé du barrage en fin du séisme est représenté sur la figure 17.

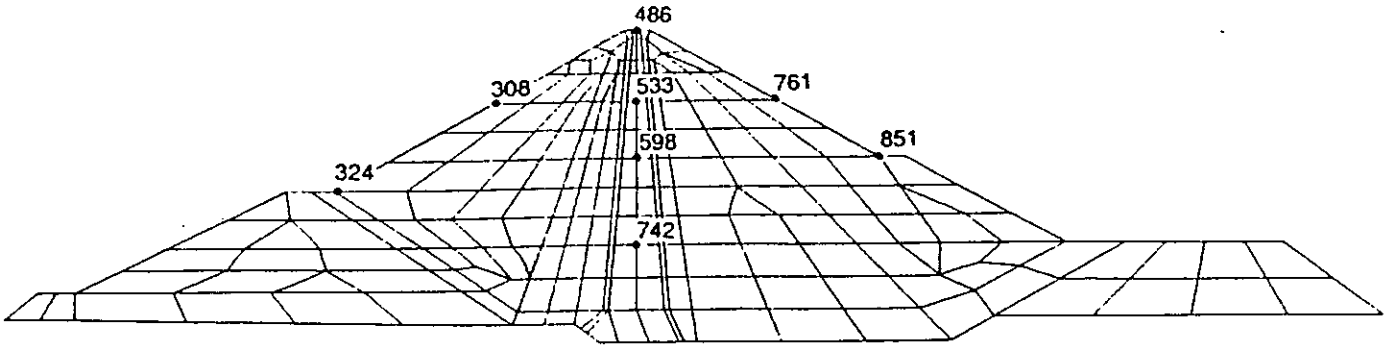

Figure 10: Nœuds choisis pour les résultats dynamiques

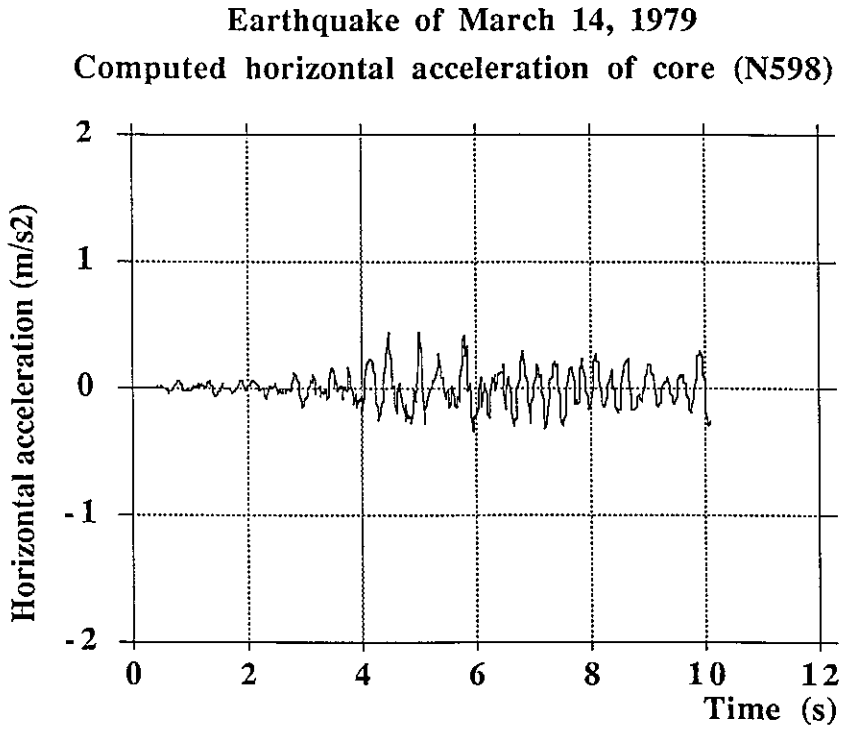

Figure 11: Evolution de l'accélération horizontale au nœud 598 pendant le séisme

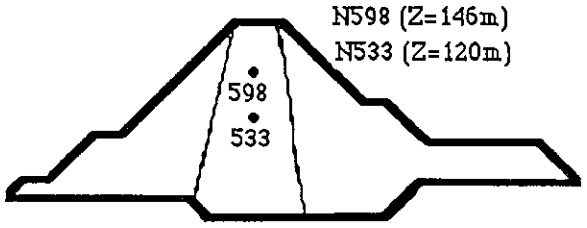

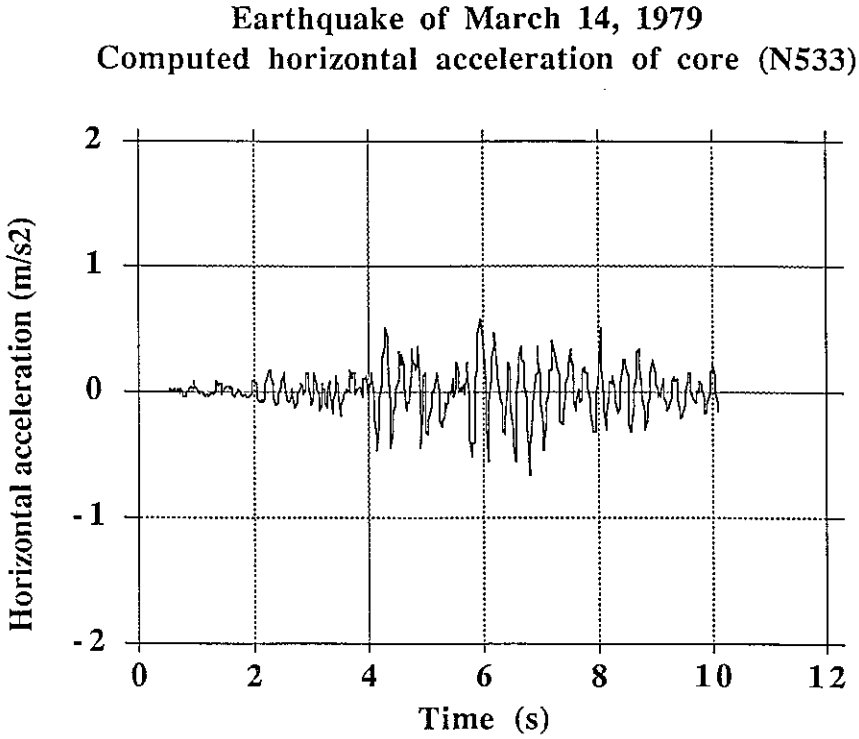

Figure 11b: Evolution de l'accélération horizontale au nœud 533 pendant le séisme

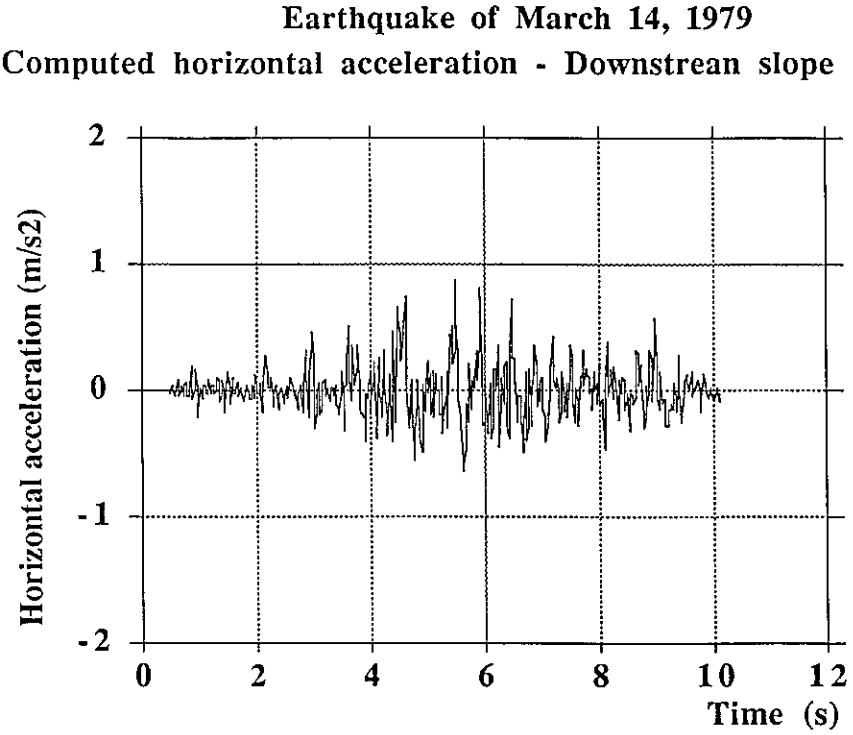

Figure 11c: Evolution de l'accélération horizontale au nœud 761 pendant le séisme

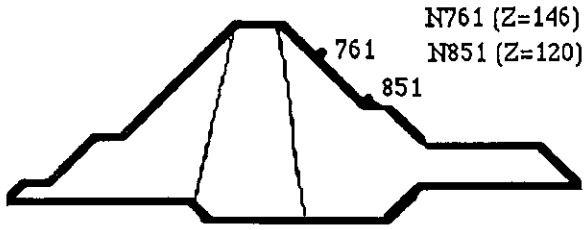

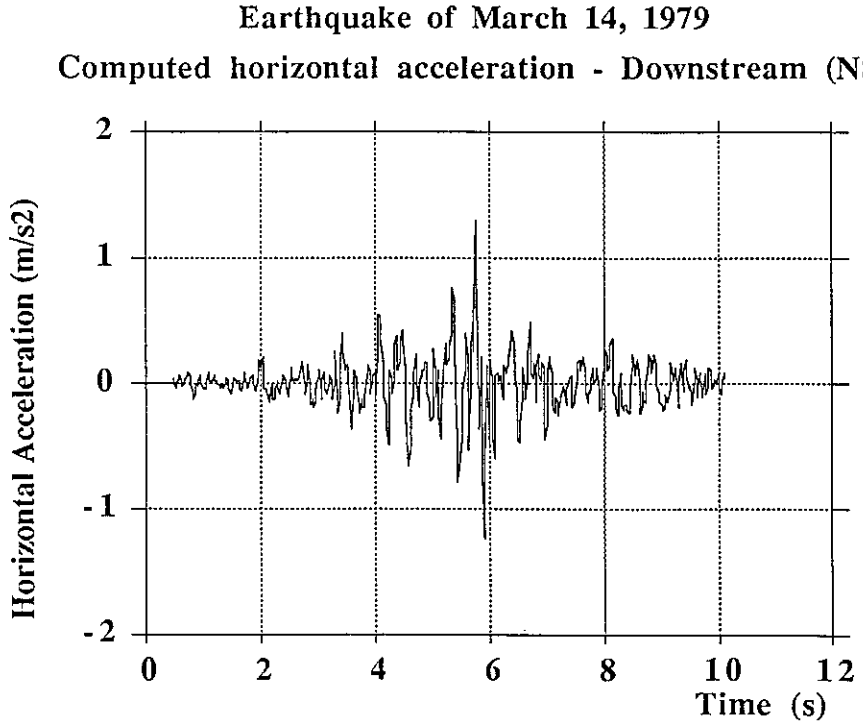

Figure 11d: Evolution de l'accélération horizontale au nœud 851 pendant le séisme

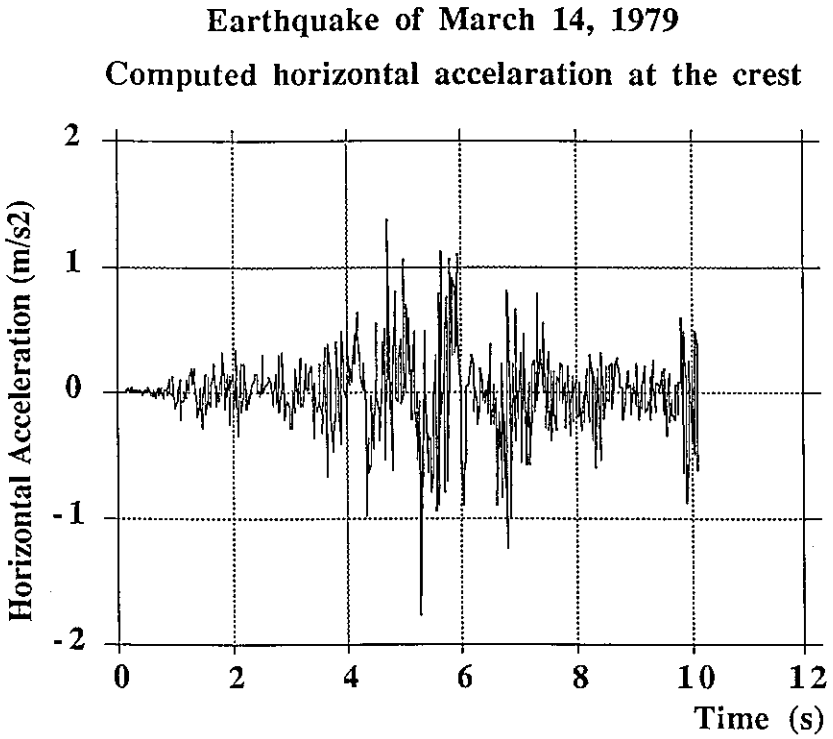

Figure 11e: Evolution de l'accélération horizontale en crête pendant le séisme

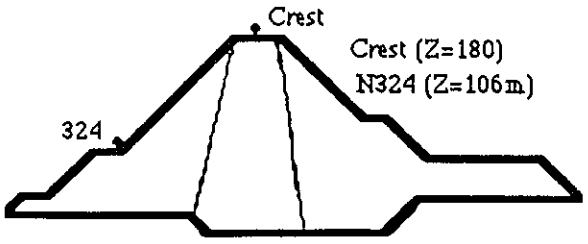

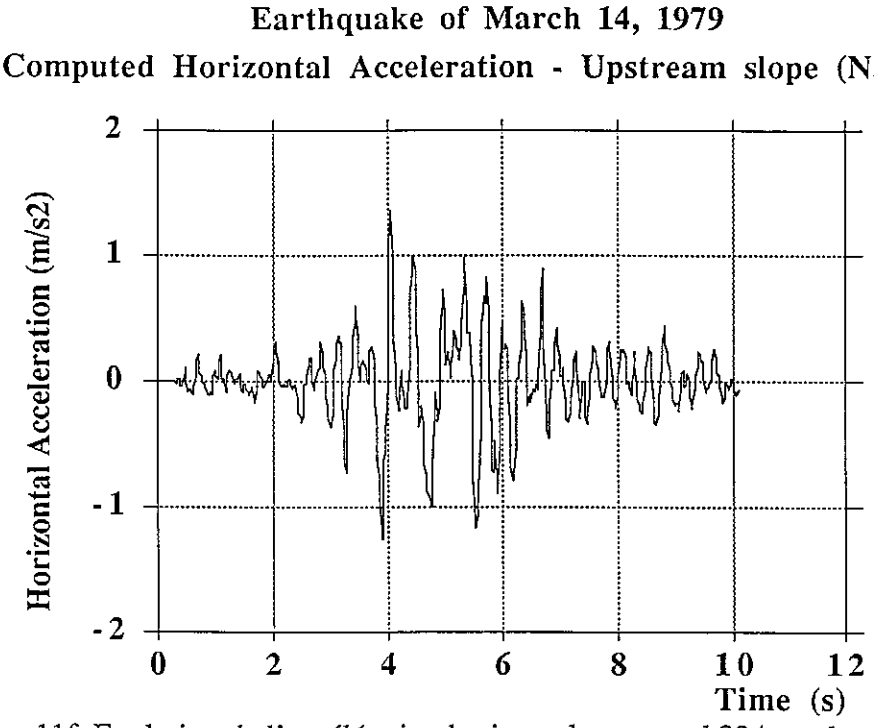

Figure 11f: Evolution de l'accélération horizontale au nœud 324 pendant le séisme

Earthquake of March 14, 1979
Computed Settlements of Downstream and Upstream Slope

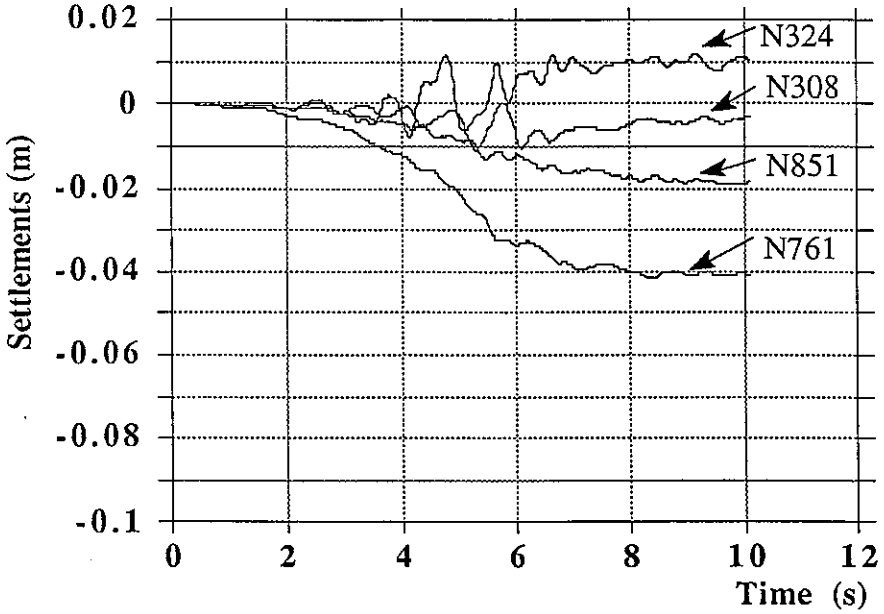

Figure 12a: Tassement des nœuds amont et aval durant le séisme

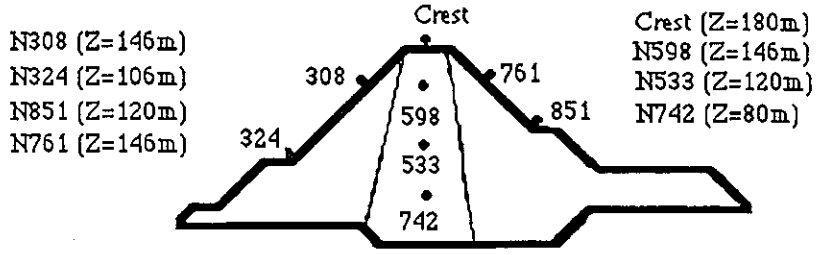

Earthquake of March 14, 1979
Computed settlements of core

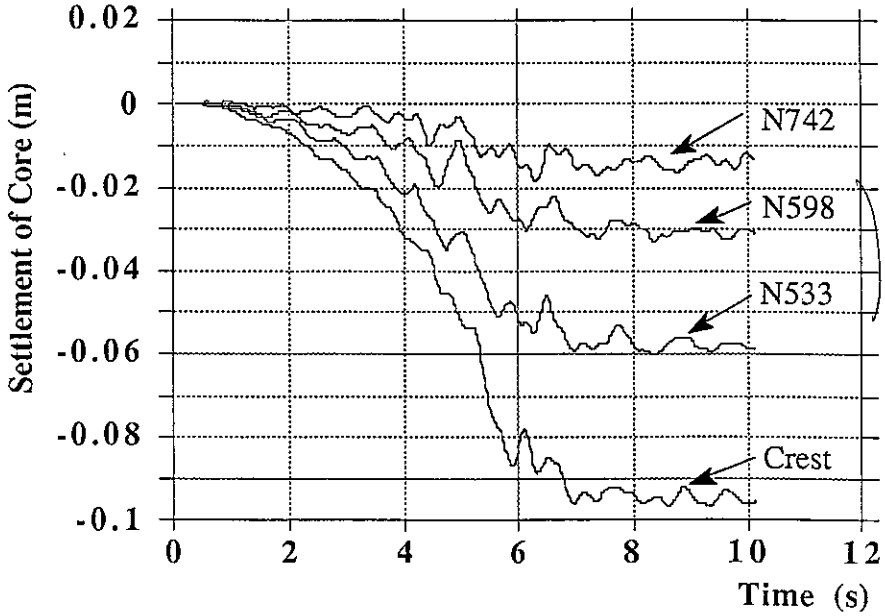

Figure 12b: Tassement du noyau durant le séisme

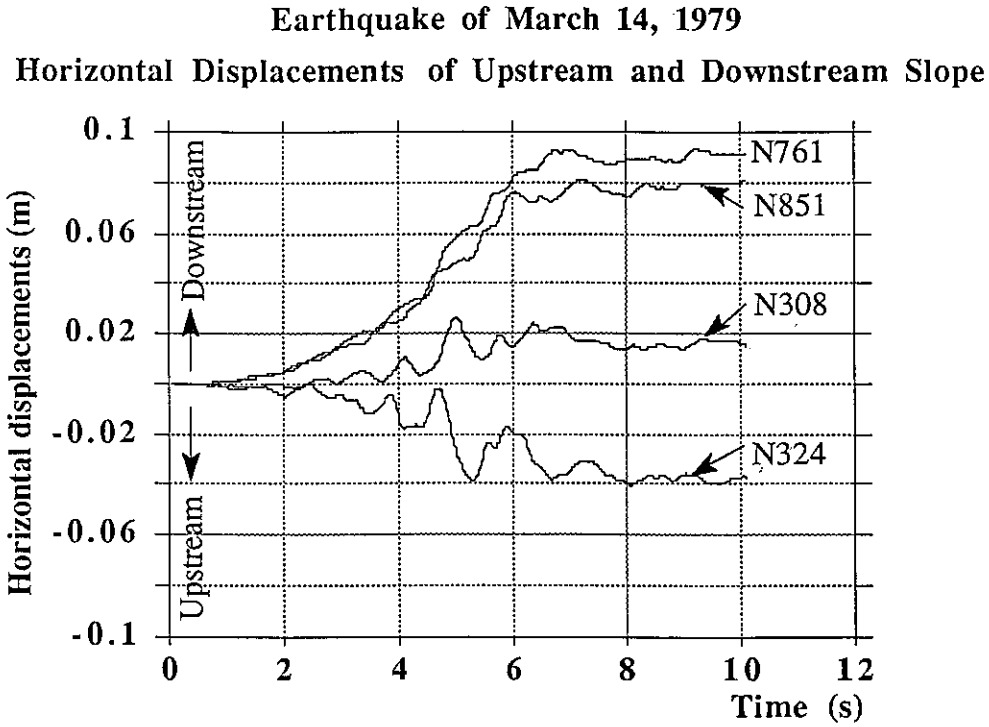

Figure 13a: Déplacements horizontaux des parements amont et aval durant le séisme

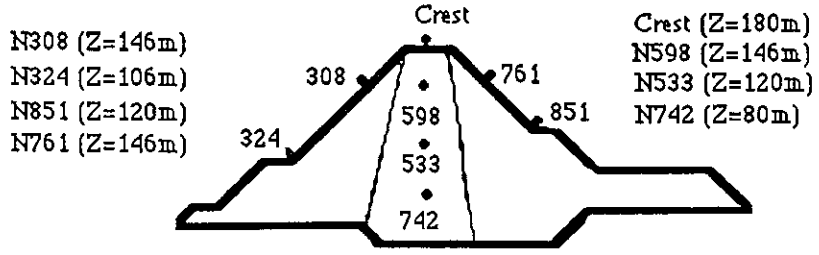

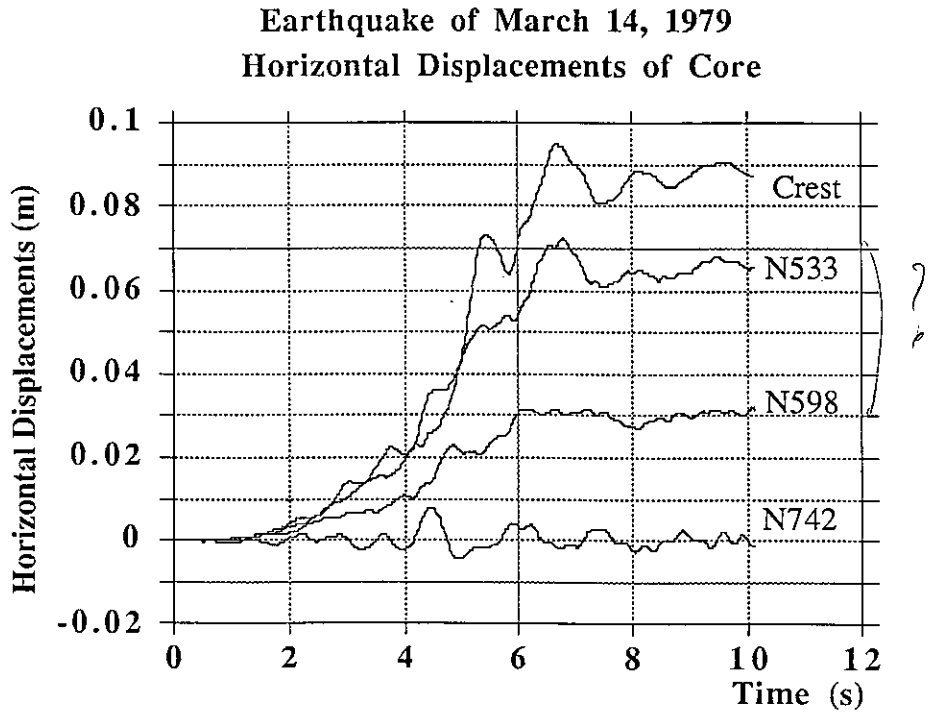

Figure 13b: Déplacements horizontaux du noyau durant le séisme

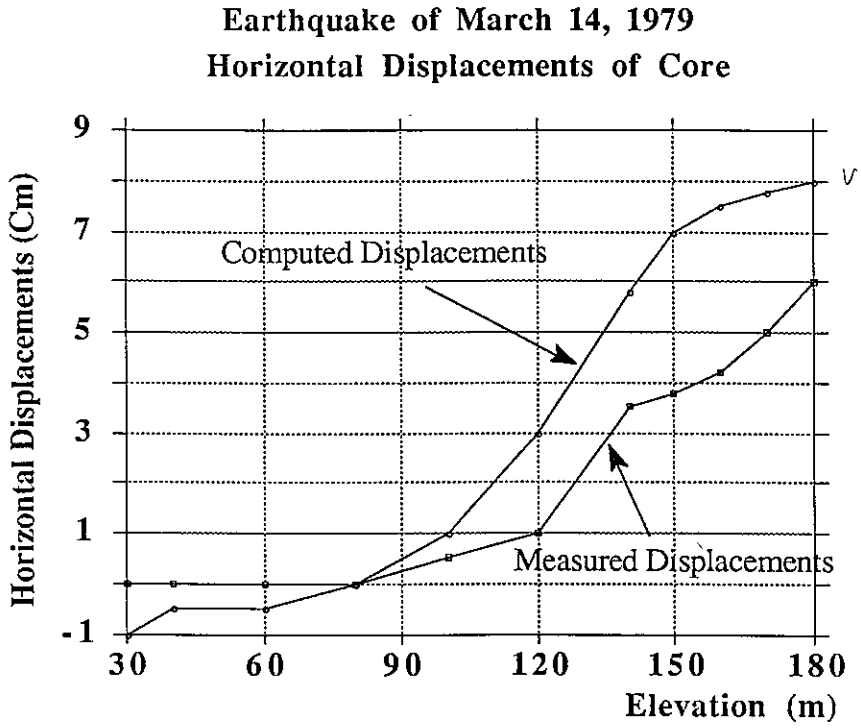

Figure 14: Composante horizontale des déplacements parements dûs au séisme le long de la hauteur du noyau

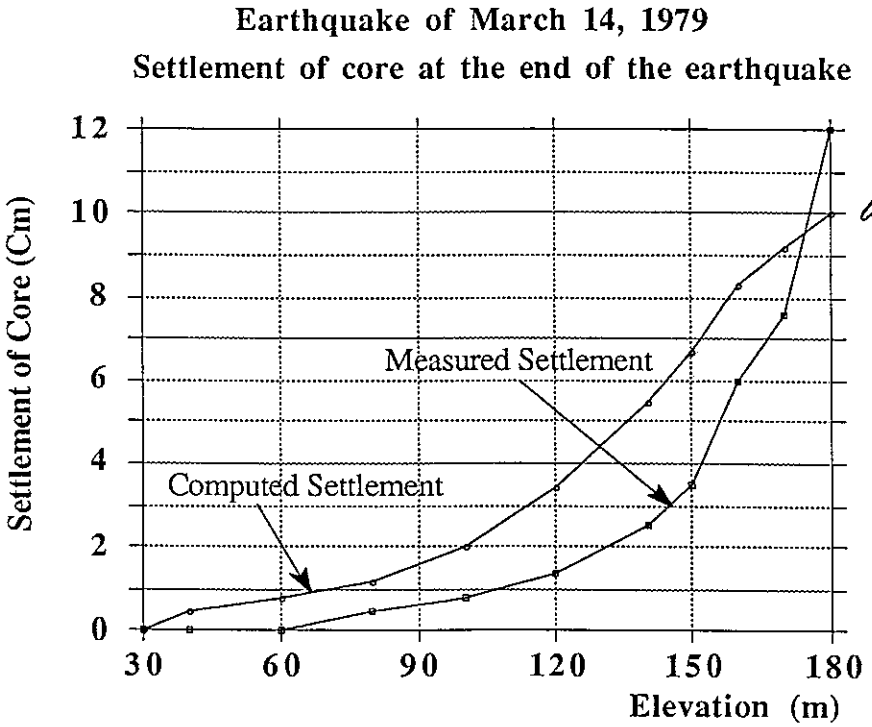

Figure 15: Composante Verticale des déplacements permanents dûs au séisme le long de la hauteur du noyau

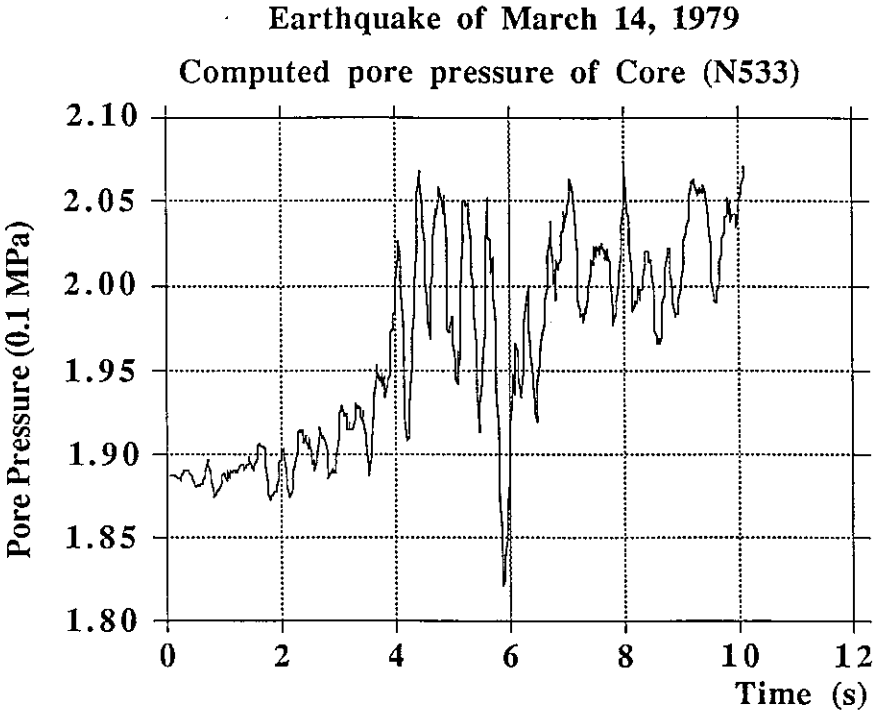

Figure 16a: Evolution de la pression interstitielle au nœud 533 durant le séisme

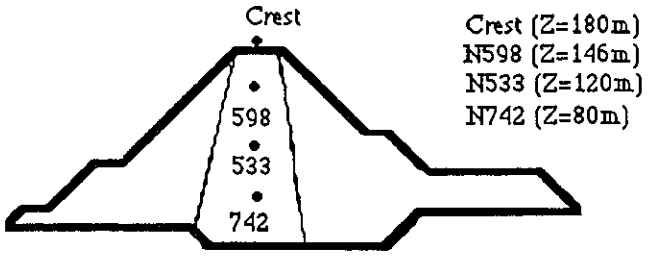

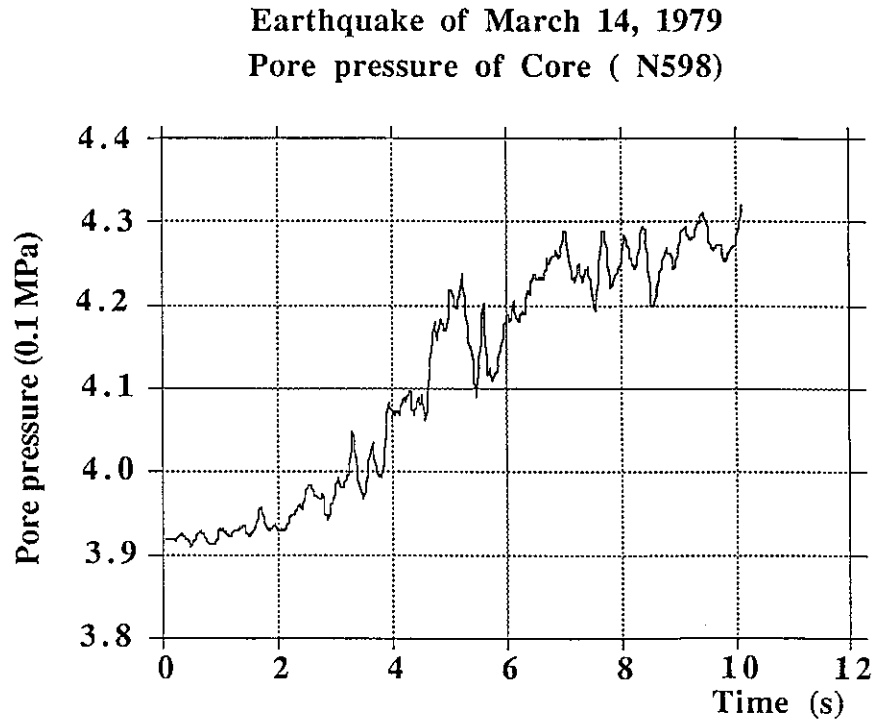

Figure 16b: Evolution de la pression interstitielle au nœud 598 durant le séisme

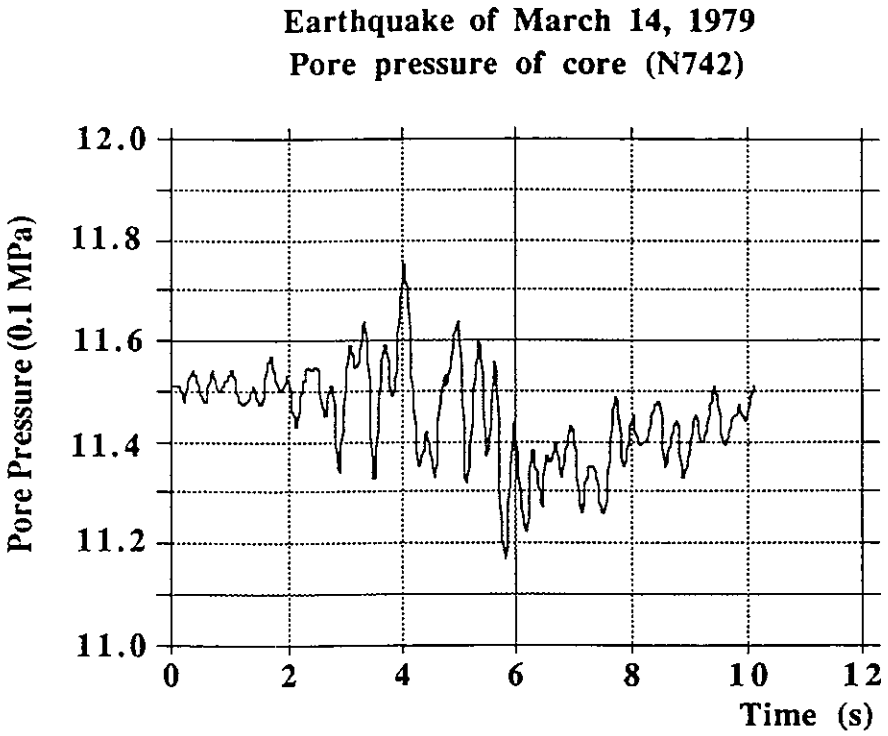

Figure 16c: Evolution de la pression interstitielle au nœud 742 durant le séisme

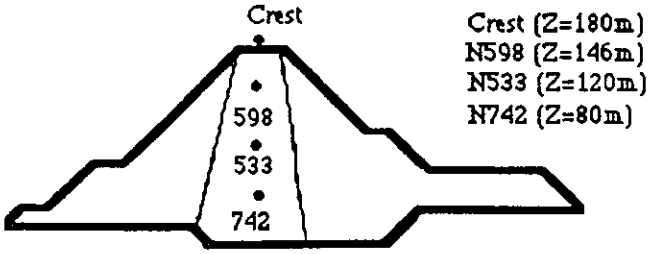

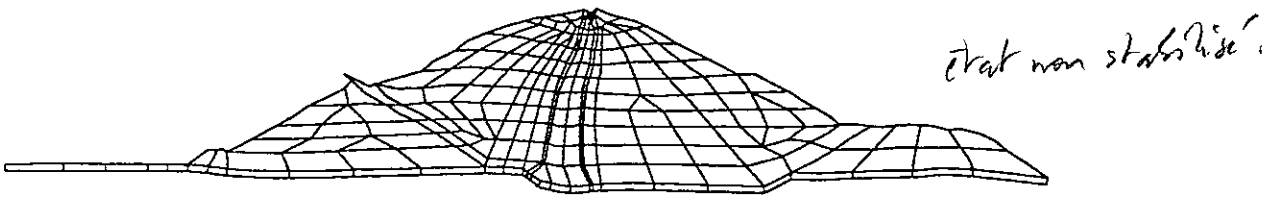

Figure 17: Maillage Déformé à la fin du séisme

CONCLUSIONS

Dans cette étude, une modélisation numérique complète simulant les étape les plus importantes de la vie d'un barrage a été effectuée. Le but principal de l'étude qui consistait à confronter les résultats des simulations numériques à la fois statique et dynamiques aux mesures réelles existantes a été atteint. Les résultats obtenus en statique ou en dynamique semblent proches des mesures réelles, ils sont donc très encourageants. L'étude a montré que les calculs sont en très bonne concordance avec les mesures réelles et aboutissent à des conclusions similaires quant à la stabilité de l'ouvrage en fin de construction et durant le séisme. Quelques différences de résultats avec l'expérience sont constatées en statiques surtout en ce qui concerne les valeurs des tassements en fin de construction. Cet écart peut être attribué à deux facteurs essentiels; l'imprécision des paramètres de comportement des matériaux d'une part et l'hypothèse des déformations planes adoptée d'autre part.

Par ailleurs, on note l'absence de résultats de mesures des contraintes qui reste un élément fondamental pour la compréhension du comportement de ce type d'ouvrage.

Cependant, en dynamique le calcul ne donne pas des amplifications d'accélérations équivalentes à celles observées pendant le séisme. Cette différence peut être dûe aux dimensions trop importantes des éléments du maillage qui filtrent vraisemblablement les grandes fréquences du mouvement (F > 8Hertz). Notons en plus, que la précision des résultats des calculs est meilleure en termes de déplacements qu'en accélérations puisque ces dernières sont calculées à partir des déplacements par dérivation. Des erreurs supplémentaires numériques peuvent éventuellement s'accumuler lors de ces opérations.

Malgré les problèmes de convergences des algorithmes numériques liés aux maillage, on peut dire que les résultats des calculs statiques sont de bonne qualité.

Ce premier benchmark a été d'une grande réussite puisque plusieurs modèles et méthodes ont été confrontés pour essayer de modéliser le plus correctement possible le comportement de ce type d'ouvrage. Néanmoins, le manque de données sur le comportement des matériaux de l'ouvrage reste un problème auquel il faudrait trouver une solution pour le prochain benchmark. Par ailleurs, il serait important dans l'avenir de s'intéresser, en plus de la réponse sismique, au comportement statique du barrage.

Nous comptons pour la prochaine participation, améliorer les paramètres de comportement des matériaux et utiliser un maillage plus fin.

REMERCIEMENTS

Nous tenons à remercier vivement Mr H. Modaressi pour ses aides et ses conseils le long de toute l'étude.

REFERENCES

1. Comisiòn Federal de Electricidad, Department of experimental Studies. Several reports related to the measurements undertaken at El Infiernillo Dam

2. M. P. Romo, D. Resendiz; " Computed and observed deformation of two embankment dams under seismic loading" Desing of dams to resist earthquake, ICE, London, 1980

3. D. Resendiz, M .P Romo, E. Moreno; " El Infiernillo and La Villita Dams: Dams behavior " Journal of the Geotechnical Engineering Division, ASCE, Vol. 108, No. GT1, January 1982

4. R. J. Marsal, L. R. Arellano; " Performance of the El Infiernillo Dam, 1963-1966 "; Journal of the soil Mechanics and Fondations Division, ASCE, Vol. 93, No SM4, Proc. Paper 5318, July, 1967, pp 265-298

5. Aubry D., Chouvet D., Modaressi A. & Modaressi H. (1985) *GEFDYN_5* : Logiciel d'analyse du comportement statique et dynamique des sols par éléments finis avec prise en compte du couplage sol-eau-air. Rapport Scientifique Ecole Centrale de Paris.

6. Aubry D., Hujeux J.C., Lassoudière F. & Meimon Y. (1982) A double memory model with multiple mechanisms for cyclic soil behaviour, Int. Symp. Num. Mod. Geomech., Balkema,pp 3-13.

7. Aubry D., Modaressi H. (1988) Numerical modelling of the dynamics of saturated anelastic soils, Seismic hazards in Mediterranean regions (Ed. J. Bonnin, M. Cara, A. Cisternas) Kluwer, Dordrecht, pp 151-172.

8. Aubry D., Modaressi H. (1990) Numerical Modelling in Soil Dynamics, Geomaterials, Constitutive equations and modelling, (Ed. F.Darve), Elsevier Applied Science.

9. Aubry D., Modaressi H. (1990) Dynamic analysis of saturated non linear media, Numerical Methods and Constitutive Modelling in Geomechanics, CISM Courses and lectures no. 311 Udine, (Ed.C.S.Desai & G.Gioda).

10. Hujeux J.C. (1985) Une loi de comportement pour le chargement cyclique des sols, Génie Parasismique, (Ed. V. Davidovici), Presses Ponts et Chaussées, Paris, pp 287-302.

11. Modaressi-Farahmand Razavi A. (1989) Modélisation mécanique des bétons bitumineux; Applications aux barrages en remblais, Doctoral Dissertation, Ecole Centrale de Paris.

12. Modaressi H. (1987) Modélisation numérique de la propagation des ondes dans les milieux poreux anélastiques, Doctoral Dissertation , Ecole Centrale de Paris.

13. Ozanam O.(1988), Modélisaion numérique des sols élastoplastiques non-saturés; Application aux barrages en remblais, Doctoral Dissertation , Ecole Centrale de Paris.

14. Zienkiewicz O.C.& Shiomi T. (1984) Dynamic behaviour of saturated porous media ; The generalized Biot formulation and its numerical solution. Int. Jour. Num. and Anal. Meth. Geomech. vol 8, pp71-96.

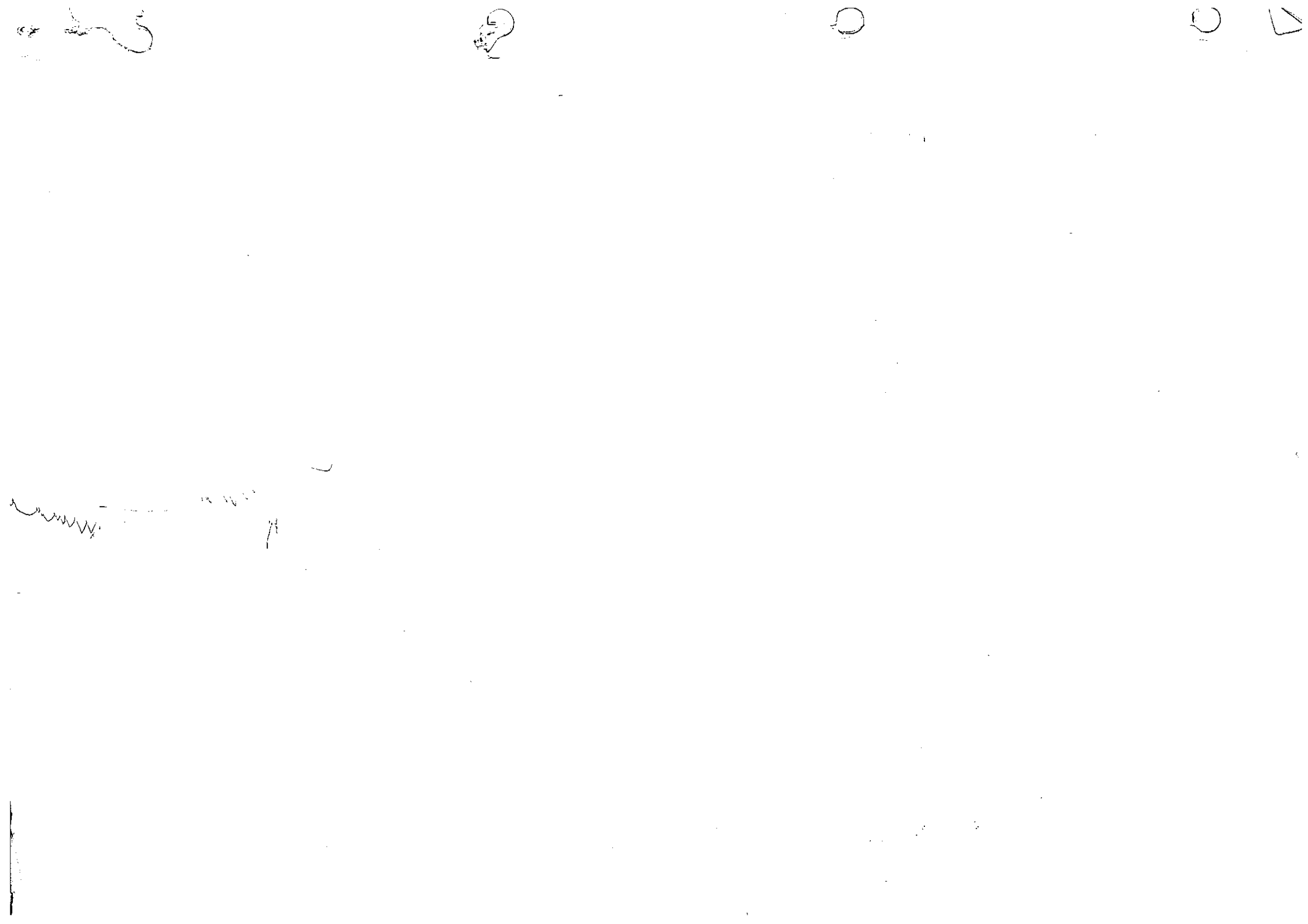

The Seismic Response of the Infiernillo Embankment Dam: Effective Elasto-plastic Stress Analysis

A. Fusco, A. De Crescenzo, G. La Barbera- ISMES S.p.A, Bergamo, Italy;
M. Cervera - Universitat Politecnica de Catalunya, Barcelona, Spain;
G. Mazzà, F. Bettinali - ENEL/CRIS, Milano, Italy

May 28, 1991

1 Introduction

The common engineering practice approaches the analysis of an embankment dam subjected to seismic loads according to the so-called *Total Stress Theory*. It is known that this theory is based on several semplifying assumptions, most of them deriving from the fact that the contribution of the fluid phase to the equilibrium is not explicitely taken into account.

A more rigorous analysis may be obtained following the so-called *Coupled Solid-Fulid Theory* where both the solid and the fluid phases in the soil are explicitely taken into account in the equilibrium equations, Ref. [1,2,3,4,5 and 6].

For the Benchmarck analysis of El Infernillo Embankment Dam, two jointed contributions have been presented. The first one in Ref. [7] reports a complete set of results obtained according to the total stress theory. This is the second contribution reporting the main results obtained according to the complete coupled-theory, restricted to the case of low excitation (earthquake accelerogram EQ1.DAT). The aim is to propose a useful comparison, both in terms of results and computational costs, between the two approaches.

The computer program used for the analysis is called OMEGA; this is a FE code developed for the numerical solution of non-linear analysis of both one-phase solid and two-phases solid-fluid medium subjected to static and dynamic loading conditions. The code version used for the seismic analysis presented in this paper has been jointly developed by ISMES S.p.A

(Bergamo, Italy) and CIMNE (Barcellona, Spain). Although this version covers already a wide range of important applications, it has to be considered only as a first release. In fact, its peculiarity is the finite element formulation and the informatic structure, which makes it easy to extend to many other types of engineering problems.

The different material property zones and the mesh employed for the analysis are those proposed in the technical specifications, Figs. 1 and 2. The numerical computations have been carried out in an ALLIANT FX80 at the ISMES computer facilities in Bergamo.

2 Principle of Effective Stress

In a fully saturated soil, because of the fluid component, only part of the total stress $\boldsymbol{\sigma}$ in equilibrium with the applied external forces is carried by the solid phase (soil skelecton). Since fluid cannot support shear, its presence affects only the normal stress component. In mathematical form, this concept, known as Terzaghi's *Principle of Effective Stress*, is expressed by

$$\boldsymbol{\sigma} = \boldsymbol{\sigma}' - \pi \widehat{\mathbf{m}} \tag{1}$$

where $\boldsymbol{\sigma}'$ is the *effective stress* due to the solid skelecton, π is the hydrostatic pressure due to the fluid phase and

$$\widehat{\mathbf{m}} = \{1, 1, 0, 1, 0, 0\}^T \tag{2}$$

The negative signe has been introduced since π acts in compression.

3 Stress-Strain Relationship

The rate of change of the total strain $\delta\boldsymbol{\epsilon}$ of the solid skelecton in a saturated soil may be viewed as the result of two distinct contributions

$$\delta\boldsymbol{\epsilon} = \delta\boldsymbol{\epsilon}^{(\sigma')} + \delta\boldsymbol{\epsilon}^{(\pi)} \tag{3}$$

The first term $\delta\boldsymbol{\epsilon}^{(\sigma')}$ is the strain rate caused by a variation of the effective stress and it may be expressed as

$$\delta\boldsymbol{\epsilon}^{(\sigma')} = \mathbf{C}^{-1}\delta\boldsymbol{\sigma}' \tag{4}$$

where $\mathbf{C}$ is the tangent constitutive matrix. This constitutive relationship is not affected by the fluid phase and consequently it may be determined experimentally in dry conditions.

The second term $\delta\epsilon^{(\pi)}$ is the strain rate caused by a variation of the pore pressure. Since π acts on the single grain with an hydrostatic compression, the relative strain rate may be expressed as:

$$\delta\epsilon^{(\pi)} = -\frac{\delta\pi}{3\mathcal{B}_m}\widehat{\mathbf{m}} \tag{5}$$

where $\mathcal{B}_m$ is the bulk modulus of the mineral particles.

From the above positions and the Principle of effective stress in Eq. 1, it follows that the relationship between the total strain rate of the solid skelecton and the rate of change of the stress is given by

$$\delta\sigma' = \mathbf{C}\delta\epsilon + \mathbf{r}\delta\pi \tag{6}$$

$$\delta\sigma = \mathbf{C}\delta\epsilon - \mathbf{q}\delta\pi \tag{7}$$

where

$$\mathbf{r} = \frac{\mathbf{C}\widehat{\mathbf{m}}}{3\mathcal{B}_m}$$

$$\mathbf{q} = \widehat{\mathbf{m}} - \mathbf{r}$$

4 Elasto-Plastic Constitutive Equations

The most popular constitutive theory to account for irreversible plastic deformations is the so-called *Incremental Theory of Plasticity.* According to this theory, under *loading condition* the strain increment $\delta\epsilon$ results to be the sum of an elastic (fully recoverable) component $\delta\epsilon^{(e)}$ and a plastic (irreversable) component $\delta\epsilon^{(p)}$, namely

$$\delta\epsilon = \delta\epsilon^{(e)} + \delta\epsilon^{(p)} \tag{8}$$

These two strain vectors are respectively defined as

$$\delta\epsilon^{(e)} = \mathbf{D}^{(e)}\delta\sigma' = \left(\mathbf{C}^{(e)}\right)^{-1}\delta\sigma' \tag{9}$$

$$\delta\epsilon^{(p)} = \delta\lambda\mathbf{b} \tag{10}$$

where $\mathbf{C}^{(e)}$ is the elastic (symmetric) constitutive matrix while

$$\delta\lambda = \frac{1}{A}\mathbf{a}^T\delta\sigma' = -\frac{1}{A}\frac{\partial F}{\partial k}\delta k \geq 0$$

$$\mathbf{a} = \frac{\partial F}{\partial\sigma'}$$

$$\mathbf{b} = \frac{\partial G}{\partial\sigma'}$$

The functions

$$A = A(\sigma', k) \tag{11}$$
$$F = F(\sigma', k) \tag{12}$$
$$G = G(\sigma', k) \tag{13}$$

are known respectively as the *plastic modulus*, the *yield* and the *potential* functions. If $G \equiv F$ the constitutive model is said to obey an *associative flow rule*. The parameter k, known as the *hardening parameter*, is in general some function of the plastic deformations $\epsilon^{(p)}$.

According to the above strain increment definitions, the elasto-plastic constitutive equation results to be defined as

$$\delta\sigma' = \mathbf{C}\delta\epsilon \tag{14}$$

where

$$\begin{aligned} \mathbf{C} &= \mathbf{C}^{(e)} - \mathbf{C}^{(p)} \\ \mathbf{C}^{(p)} &= \frac{\mathbf{c}^{(G)}\mathbf{c}^{(F)T}}{A + \mathbf{c}^{(F)T}\mathbf{b}} \\ \mathbf{c}^{(F)} &= \mathbf{C}^{(e)}\mathbf{a} \\ \mathbf{c}^{(G)} &= \mathbf{C}^{(e)}\mathbf{b} \end{aligned}$$

If the constitutive model obeys associative flow rule, the elasto-plastic matrix $\mathbf{C}^{(p)}$, and thus the constitutive matrix $\mathbf{C}$, are symmetric.

5 Constitutive Equations for Soils

Traditionally, geotechnical engineers are accustomed to model the soil response by an elastic-perfectly plastic constitutive equation. The yield and the potential functions are assumed to coincide (associative flow rule) with the Mohr-Coulomb surface type, Fig. 3, of equation

$$F = q + Mp - N \tag{15}$$

where

$$\begin{aligned} M &= \frac{3\sin\phi}{\sqrt{3}\cos\theta - \sin\theta\sin\phi} \\ N &= \frac{3c\cos\phi}{\sqrt{3}\cos\theta - \sin\theta\sin\phi} \end{aligned}$$

and c and ϕ are two material parameters.

This constitutive model has proved to be sufficiently useful for estimating the ultimate static load of a geotechnical structure. However, it does not estimate satisfactorily displacement and excess pore water pressure. In dynamics its predictions are not realistic.

More realistic soil response prediction under static loading conditions may be obtained using the so-called Cam-Clay model, which assumes a yield surface of the type shown in Fig. 4. This model however does not give satisfactory results when dynamic loadings are considered.

For the dynamic analysis required in this workshop, we have then used the ECAM model Ref. [8], which may be viewed as an extension of the Cam-Clay model. This extension tries to overcome the limit of the Cam-Clay by improving the mathematical description of the soil when it is in a state of overconsolidation. In order to assess the material parameters required by ECAM, it is necessary a number of triaxial tests, namely:

1. An isotropic drained triaxial test. This test allows to determine the vergin and swelling lines shown in Fig. 5a.

2. A number of undrained triaxial tests on the soil with various degrees of overconsolidation. These tests allow to determine the critical state, the elastic and the bounding surfaces shown in Fig. 5b. Moreover they allow to determine the q *vs.* ϵ_a soil response shown in Fig. 5c.

6 Governing Field Equations

According to the Coupled Solid-Fluid Theory, the complete solution of a stress analysis problem in a saturated porous medium may be obtained solving contemporaneously the *Equilibrium Equations* and the *Flow Continuity Equation*, namely

$$\begin{cases} \int_\Gamma \delta \mathbf{u}^T \mathbf{t}\, d\Gamma + \int_\Omega \varrho \delta \mathbf{u}^T \mathbf{f}\, d\Omega = \int_\Omega \delta \epsilon^T \sigma\, d\Omega \\ \\ \operatorname{div} \mathcal{P} \operatorname{grad} \frac{\pi_e}{\gamma_f} = \mathbf{q}^T \dot{\epsilon} + \frac{\dot{\pi}_e}{\mathcal{B}_\pi} \end{cases} \tag{16}$$

where

$\mathbf{u}$ = displacement of the solid skelecton

π_e = excess pore pressure in the fluid phase

while

$$\begin{aligned} \varrho &= (1-n)\varrho_m + n\varrho_f \\ \gamma_f &= g\varrho_f \\ g &= \text{acceleration gravity} \\ \varrho_m &= \text{density of the solid skelecton} \\ \varrho_f &= \text{density of the fluid phase} \\ n &= \text{porosity} \end{aligned}$$

Finally

$$\begin{aligned} \mathbf{f} &= \mathbf{b} - \frac{c}{\varrho}\dot{\mathbf{u}} - \ddot{\mathbf{u}} \\ \mathbf{b} &= \text{body forces} \\ \mathbf{t} &= \text{tractions} \\ c &= \text{viscosity coefficient} \end{aligned}$$

and

$$\delta\boldsymbol{\sigma} = \mathbf{C}\delta\boldsymbol{\epsilon} - \mathbf{q}\delta\pi_e \tag{17}$$

where $\mathbf{C}$ is the constitutive matrix of the soil skelecton in dry conditions.

In case of dry conditions, where $\delta\pi_e = 0$, the above system of equations reduces to

$$\int_\Gamma \delta\mathbf{u}^T\mathbf{t}\,d\Gamma + \int_\Omega \varrho\delta\mathbf{u}^T\mathbf{f}\,d\Omega = \int_\Omega \delta\boldsymbol{\epsilon}^T\boldsymbol{\sigma}\,d\Omega \tag{18}$$

where

$$\delta\boldsymbol{\sigma} \equiv \delta\boldsymbol{\sigma}' = \mathbf{C}\delta\boldsymbol{\epsilon} \tag{19}$$

Similar semplified formulation may be applied as well for the case of saturated materials in undrained conditions, i.e. when the fluid phase is not allowed to escape from the porous of the solid material. In this case, in fact, the $2nd$ equation in Eq. 16 can be solve explicity and find that the excess pore pressure value is related to the volumetric strain as

$$\dot{\pi}_e = -\mathcal{B}_\pi\mathbf{q}^T\dot{\boldsymbol{\epsilon}} \tag{20}$$

Consequently, from Eq. 7, the total stress rate may be directly related to the soil deformation as

$$\delta\boldsymbol{\sigma} = \overline{\mathbf{C}}\delta\boldsymbol{\epsilon} \tag{21}$$

where $\overline{\mathbf{C}}$ is the *Undrained Constitutive Matrix* defined as

$$\overline{\mathbf{C}} = [\mathbf{C} + \mathcal{B}_\pi \mathbf{q}\mathbf{q}^T]$$

In dynamics, such undrained formulation may be applied to those soils whose permeability is sufficiently high, so that the fluid stored in the porous of these materials has not sufficient time to escape during the short period of an earthquake excitation.

In case of an earthquake excitation, the displacement field may be decomposed as

$$\mathbf{u} = \mathbf{u}^{(g)} + \mathbf{u}^{(r)} \tag{22}$$

where

$$\begin{aligned} \mathbf{u}^{(g)} &= \text{rigid (ground) displacement field} \\ \mathbf{u}^{(r)} &= \text{relative displacement field} \end{aligned}$$

Accordingly, the acceleration field can be decomposed as

$$\ddot{\mathbf{u}} = \ddot{\mathbf{u}}^{(g)} + \ddot{\mathbf{u}}^{(r)} \tag{23}$$

where $\ddot{\mathbf{u}}^{(g)}$ represents the seismic excitation. The equilibrium equations may then be solved in terms of $\mathbf{u}^{(r)}$, the relative displacement field due to the application of the seismic load, proportional to $\rho\ddot{\mathbf{u}}^{(g)}$.

7 Evaluation of the Initial Stress Distribution

In an elasto-plastic effective stress approach, it is of crucial importance to evaluate the initial state variables, such as effective stress and plastic variables of the material, from which to start the dynamic analysis. The numerical evaluation of these quantities requires an accurate simulation of the loading history which the structure has been subjected to.

Unfortunaly, the loading history of the Infernillo embankment dam is not reported in the technical specifications. Consequently, a drastically semplified analysis has been carried out assuming an elastic-perfectly plastic constitutive model; the yield (potential) function has been assumed to be of Mohr-Coulomb type. The material parameters used for the analysis are reported in Table 1.

The analyses performed consist of:

Table 1: Material properties assumed for the initial stress analysis

Mat.No.	Young (ton/m^2)	Poisson	c (ton/m^2)	ϕ	γ_{wet} (ton/m^3)	γ_{sat} (ton/m^3)
1	25 000	0.30	0	24.	1.94	2.00
2	31 500	0.33	0	36.	1.85	2.16
3	31 500	0.33	0	42.	1.85	2.16
4	31 500	0.33	0	42.	1.85	2.16
5	15 000	0.33	0	42.	1.76	2.10
6	15 000	0.33	0	42.	1.76	2.10

1. Evaluation of the stress distribution at the end of the construction stage. In this analysis, only the body forces due to the wet weight of the materials have been considered. These body forces have been simply linearly increased up to reach the actual weight of the materials. The stress and the displacement fields resulting from this analysis are reported in Figs. 6, 7, 8 and 9.

2. Evaluation of the stress distribution at the end of the water filling of the reservoir. In this analysis, only the buoyant forces due to the pore pressure distribution shown in Fig. 10 have been considered. Starting from the initial stress distribution determined by the first analysis, these buoyant forces have been simply linearly increased up to reach their actual value. The effective stress and the displacement fields resulting from this analysis are reported in Figs. 11, 12, 13, 14 and 15.

8 Seismic Response

The dynamic response of El Infernillo embankment dam has been calculated for the earthquake accelerograms EQ1.DAT. For the numerical calculations the following assumptions have been made:

1. The effective stress obtained from the *2nd* analysis reported in the previous Section 7, has been taken as the initial effective stress distri-

bution.

2. The materials have been assumed to responde according to the ECAM model. The additional parameter values required by the model which have been used for the analysis are reported in Table 2. They have been estimated in order to be as close as possible to the soil behaviour resulting from the eodometer tests reported in the technical specifications.

3. The core and the filter (materials 1, 2 and 3 in Fig. 2) have been analysed assuming undrained conditions. In other terms, it has been assumed that the permeability values of these materials are sufficiently low, so that the fluid stored in them has not the possibility to escape during the short time of the earthquake excitation.

4. The rockfill (materials 4,5 and 6 in Fig. 2) in the upper stream of the embankment, have been analysed assuming fully drained conditions. In other terms, it has been assumed that the permeability values of these materials are sufficiently high, so that no significant excess pore pressure is built up in them during the earthquake excitation.

Table 2: Additional material properties assumed for the ECAM model

Mat.No.	λ	χ	$\frac{\bar{p}_y}{p_y}$	$\frac{\bar{p}_y}{\bar{p}_c}$	*ovcor*
1	0.0977	0.0147	1.10	2.0	1.1
2,3,4,5,6	0.1670	0.0043	1.01	2.0	1.2

The accelerations, displacements and excess pore pressures response calculated during the earthquake excitations for the points shown in Fig. 1, are reported in Figs. 16, 17, 18 and 19.

9 Conclusions

The results reported in this paper only indicate the potentiality of the mathematical approach and of the OMEGA code. It is evident in fact that a more

accurate modelling of the construction stages and of the actual mechanical material properties would certainly modify the numerical results.

In terms of computational cost, it has been experimented that the seismic analysis is rather costly. The results shown in this paper have been obtained over a time period of 10 sec. and with a time step size Δt of 2.5E-4, for a total amount of 40 000 steps. The total CPU time required by the ALLIANT FX80 has been of 43h 20min, for an average cost of 3.9 sec for each time step.

It is our opinion that, for a more accurate analysis, an even smaller Δt is required. We expect in fact that, with a sufficiently smaller Δt, the acceleration diagram in Fig. 16 should become smoother and the peaks should decrease their values; however, the final value of the permanent deformations should not change much.

References

[1] BIOT M. A., "General theory of three dimensional consolidation", *Journal of Applied Physic*, Vol.12, pp 155-164, 1941.

[2] SANDHU R.S. and WILSON E.L., "Finite element analysis of seepage in elastic media", *proceeding ASCE, Mechanics Division*, Vol.95, No. EM3., 1969

[3] ZIENKIEWICZ O.C. and SHIOMI T., "Dynamic behaviour of saturated porous media: The generalized Biot formulation and its numerical solution", *International Journal of Numerical and Analytical Methods in Geomechanics*, Vol.8, pp 71-96, 1984

[4] FUSCO A., "Continuum mechanics and finite element numerical solutions in geomechanics", *Ph.D. Thesis*, University of Ottawa; 1985

[5] FUSCO A., "Mechanics of two phases solid-fluid medium", *to be published*

[6] FUSCO A., "The finite element method applied to coupled solid-fluid problems", *to be published*

[7] RUGGERI G., PALUMBO P., LA BARBERA G., MAZZA' G., BETTINALI F., "The Seismic Response of the Infiernillo Embankment

Dam: Equivalent linear approach and Newmark method for the evaluation of permanent displacements", *First ICOLD Benchmark Workshop*, Bergamo (Italy), May 28-29, 1991.

[8] DE CRESCENZO A. and FUSCO A., "A unified constitutive equation for isotropic soils under monotonic and cyclic loading", *to be published.*

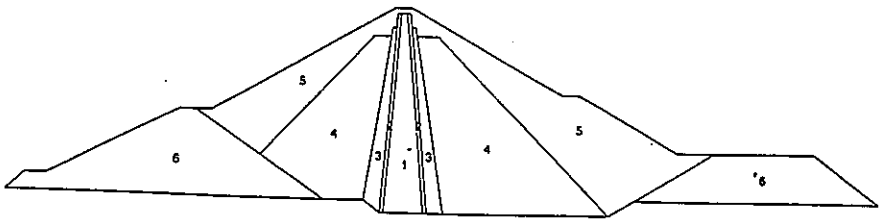

Figure 1: The material property zones

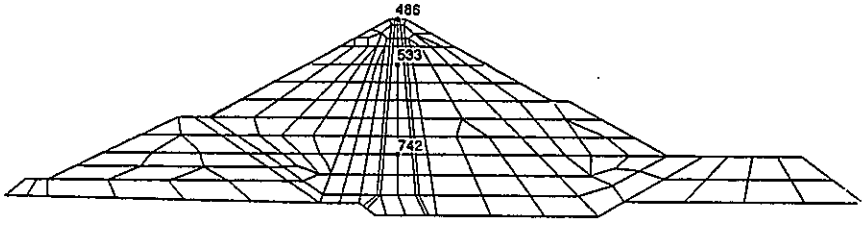

Figure 2: The finite element mesh

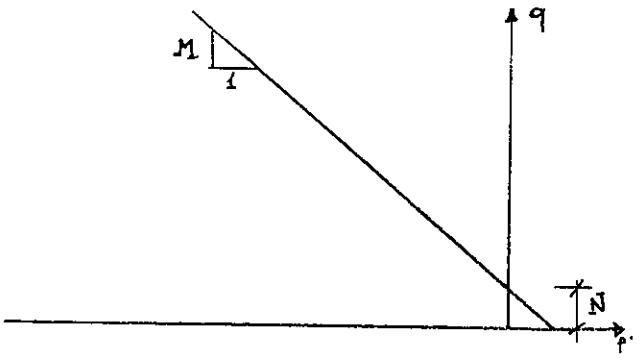

Figure 3: The Mohr-Coulomb yield surface

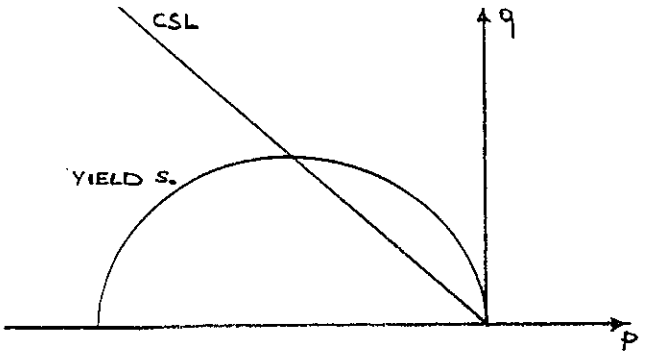

Figure 4: The Cam-Clay yield surface

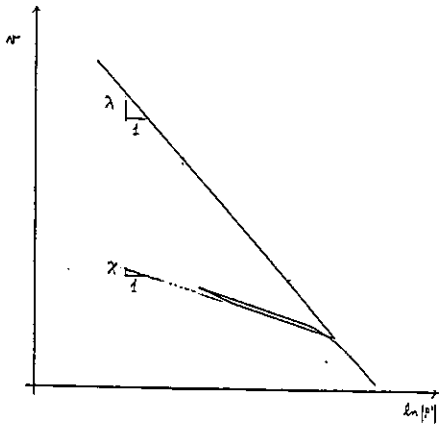

a) Isotropic triaxial drained test

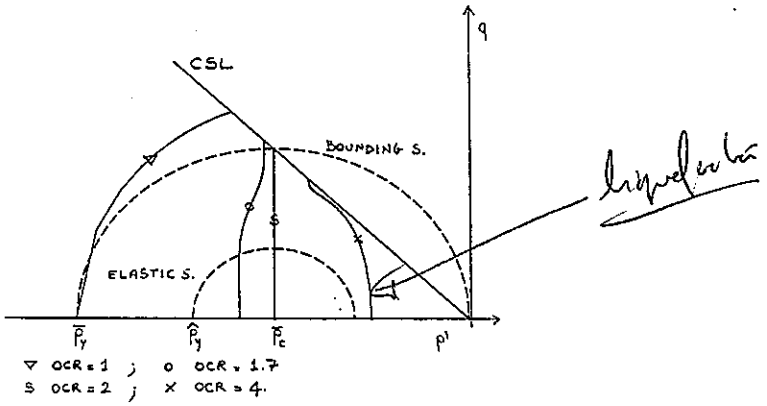

b) Undrained triaxial tests in the p *vs.* q plane

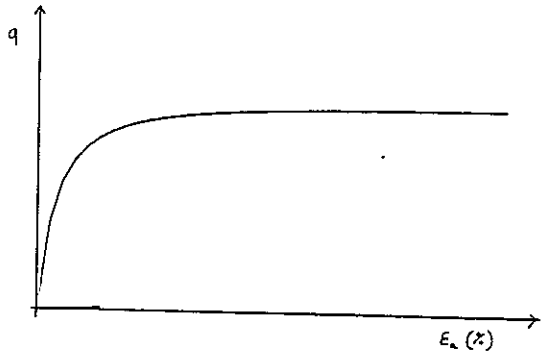

c) Undrained triaxial test in the ϵ_a *vs.* q plane, initial ocr=2.

Figure 5: Experimental tests for the parameter assessment of the ECAM model

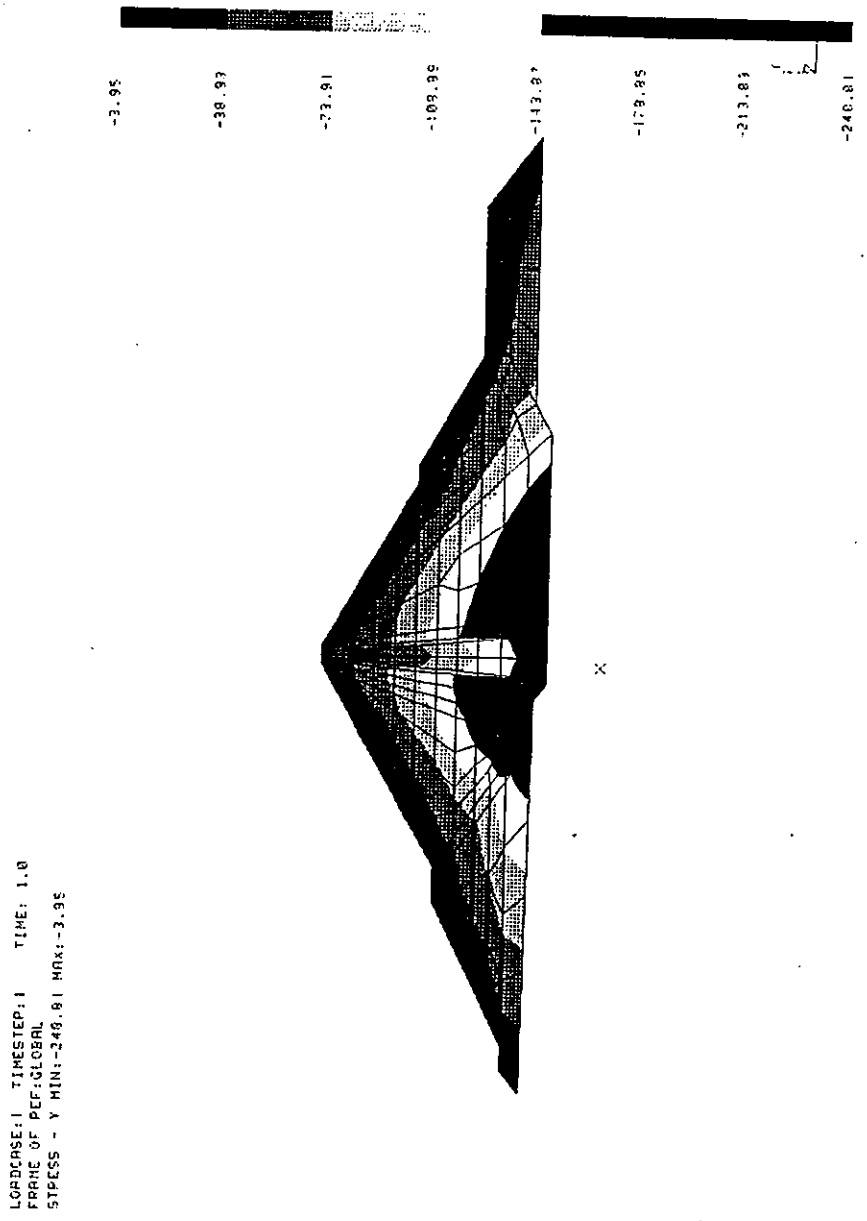

Figure 6: Vertical stress distribution at the end of the construction stage

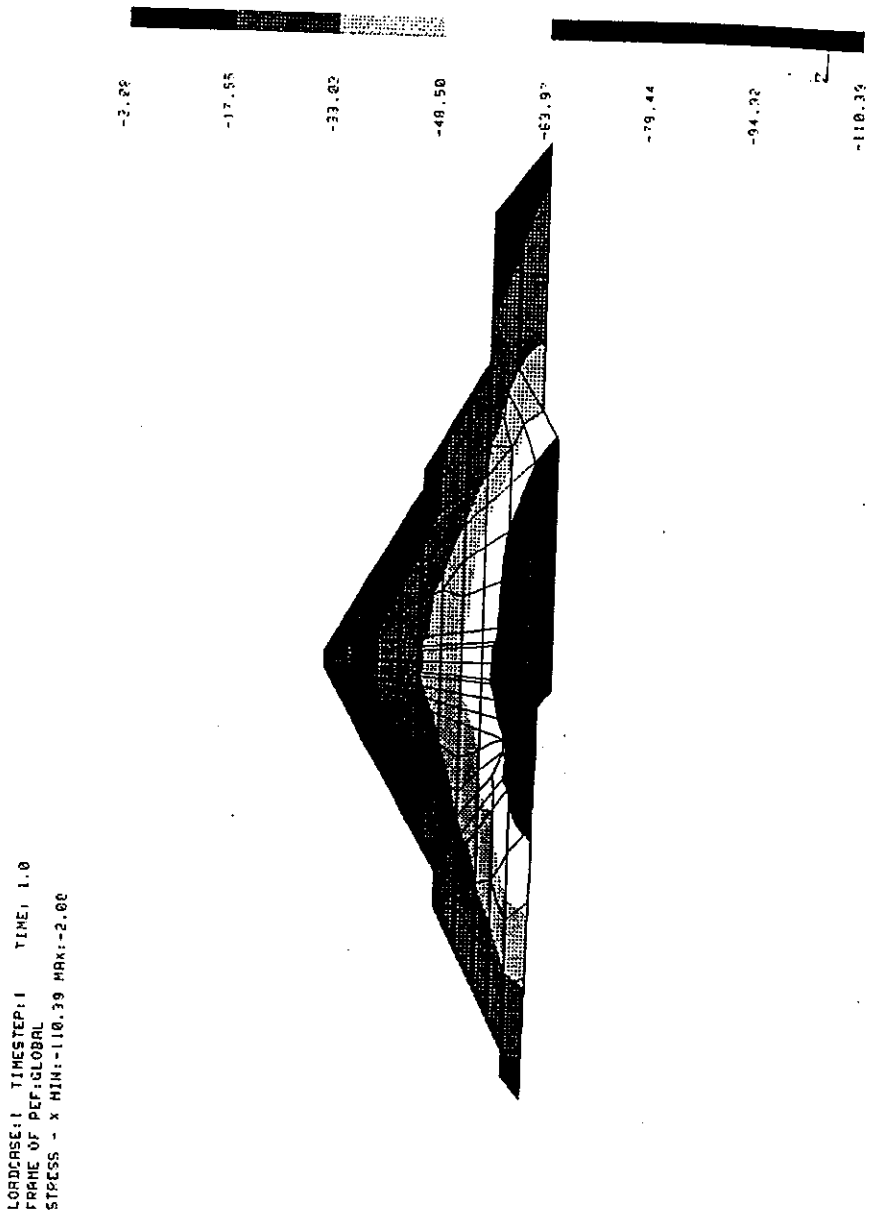

Figure 7: Horizontal stress distribution at the end of the construction stage

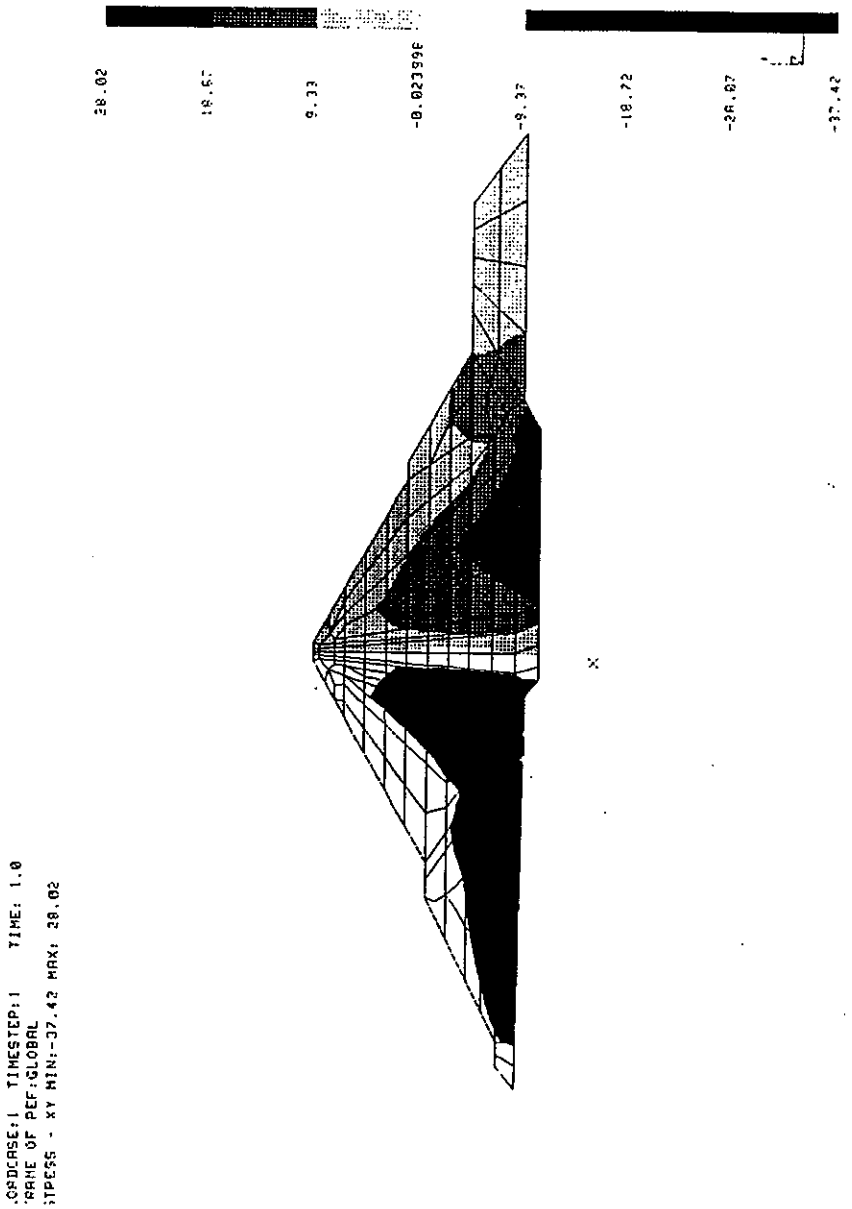

Figure 8: Shear stress distribution at the end of the construction stage

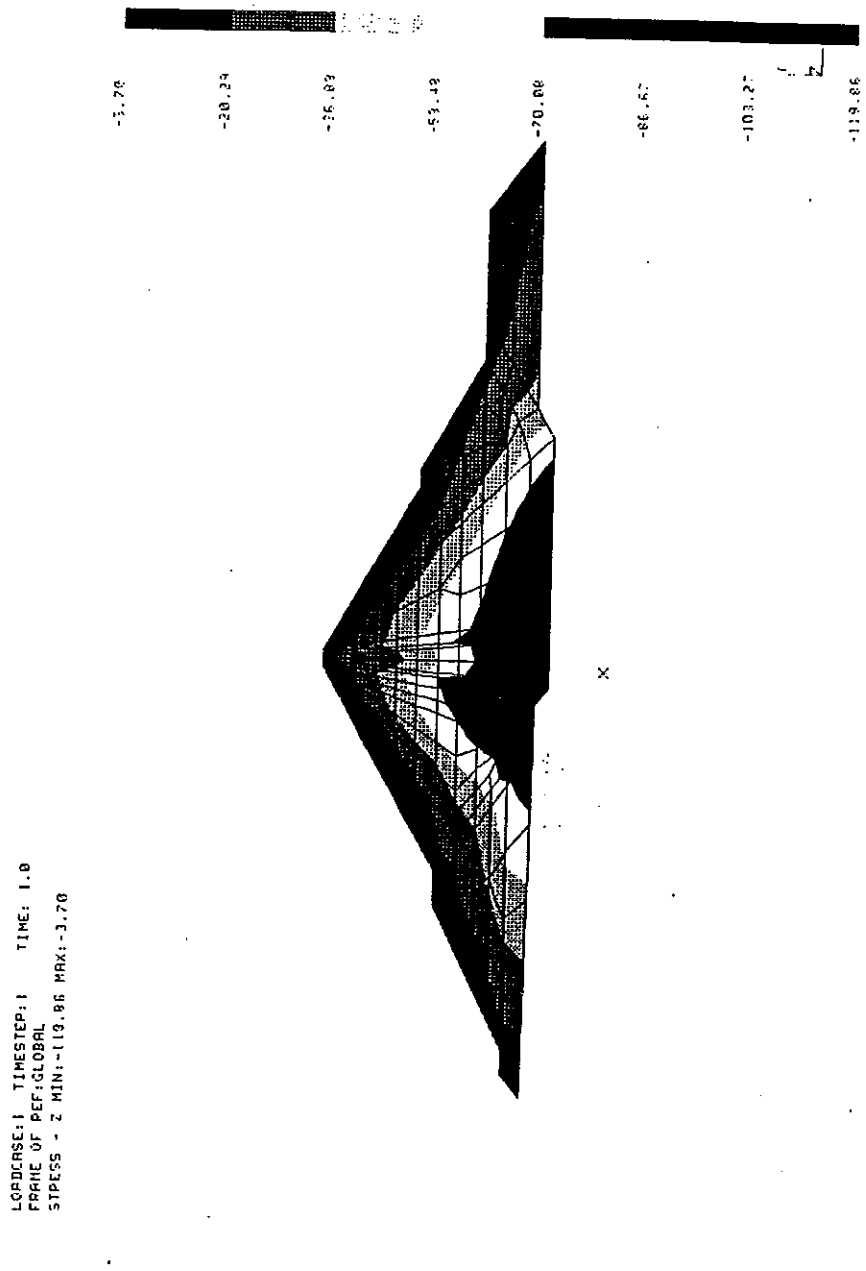

Figure 9: Normal stress distribution at the end of the construction stage

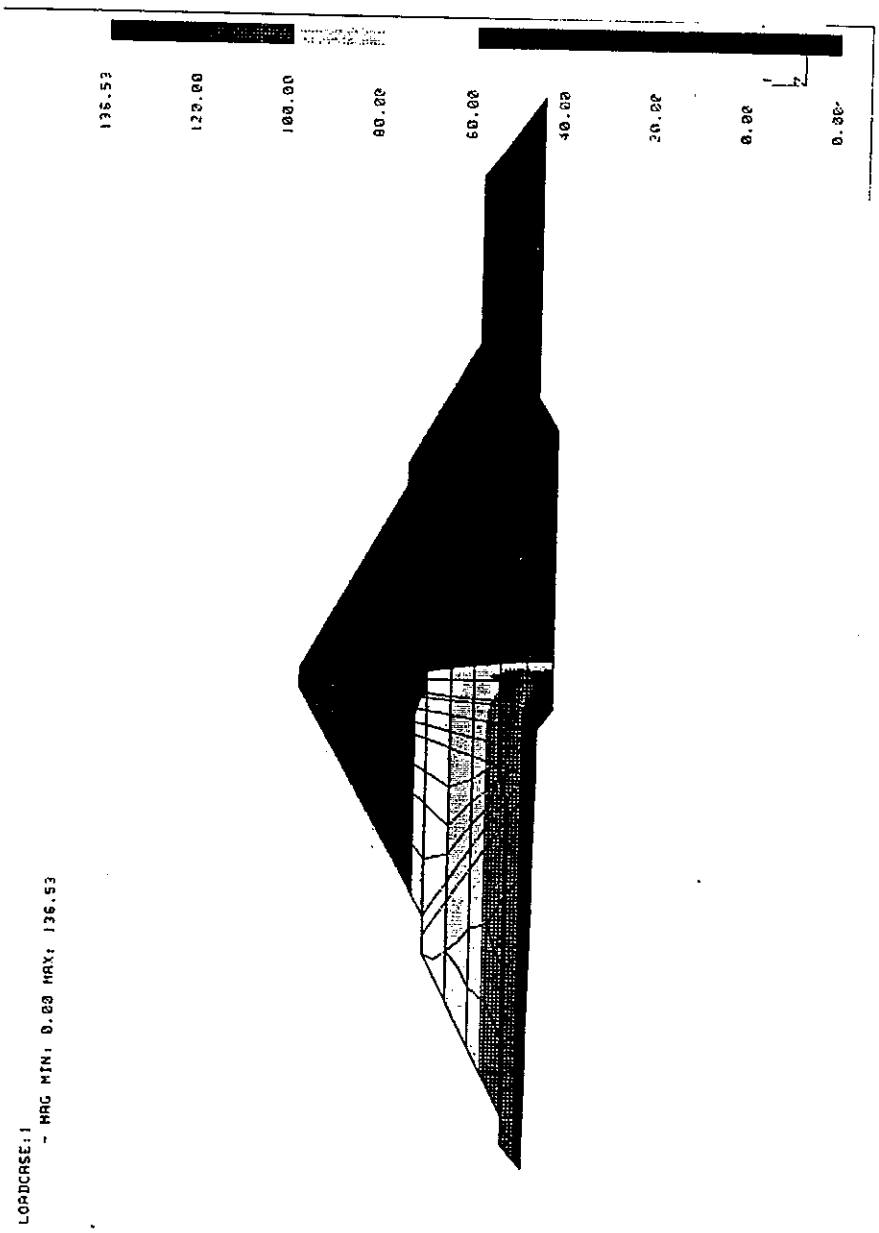

Figure 10: Pore pressure distribution

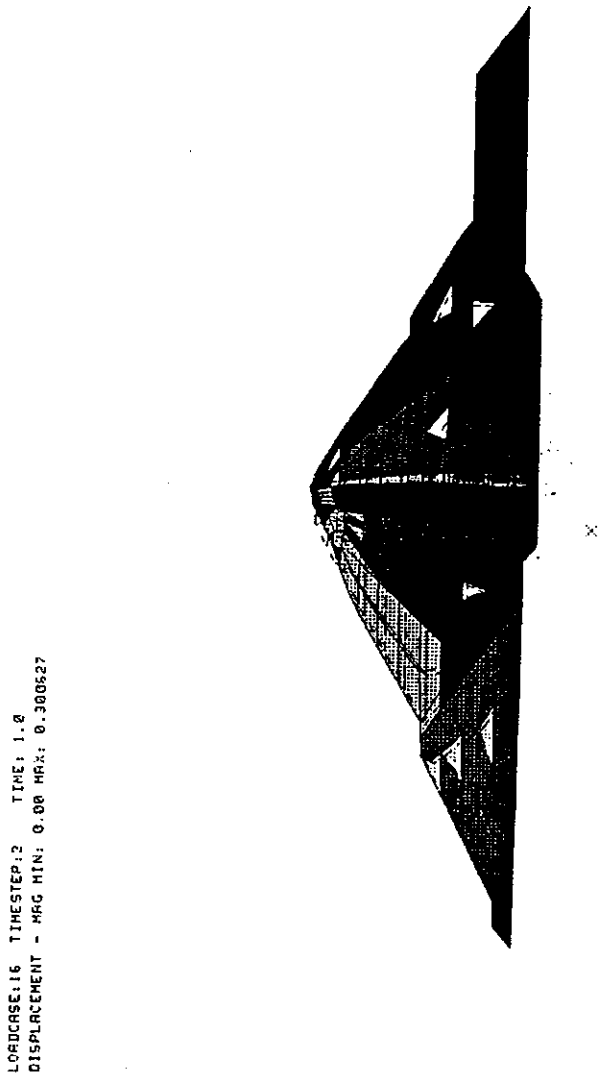

Figure 11: Displacement field mobilized by the water filling of the reservoir

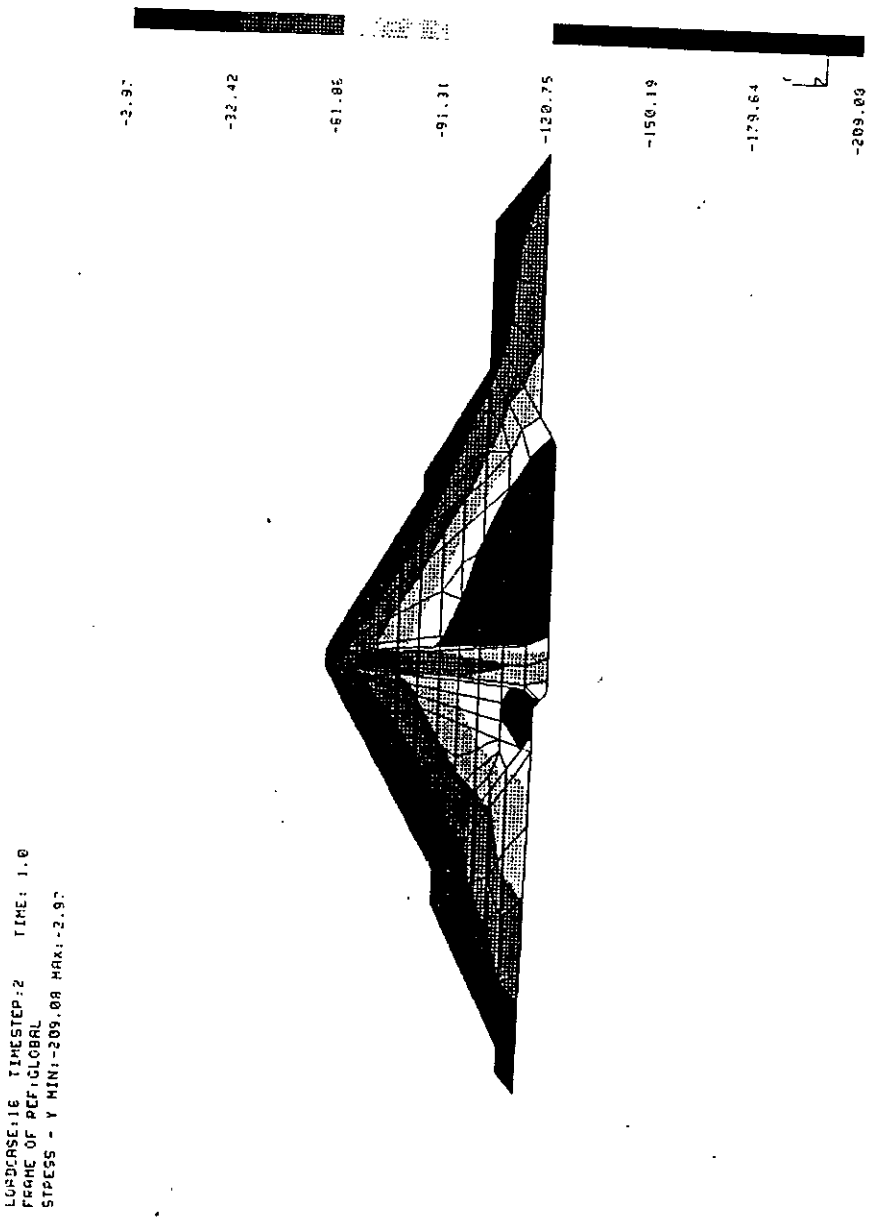

Figure 12: Vertical stress distribution at the end of the water filling of the reservoir

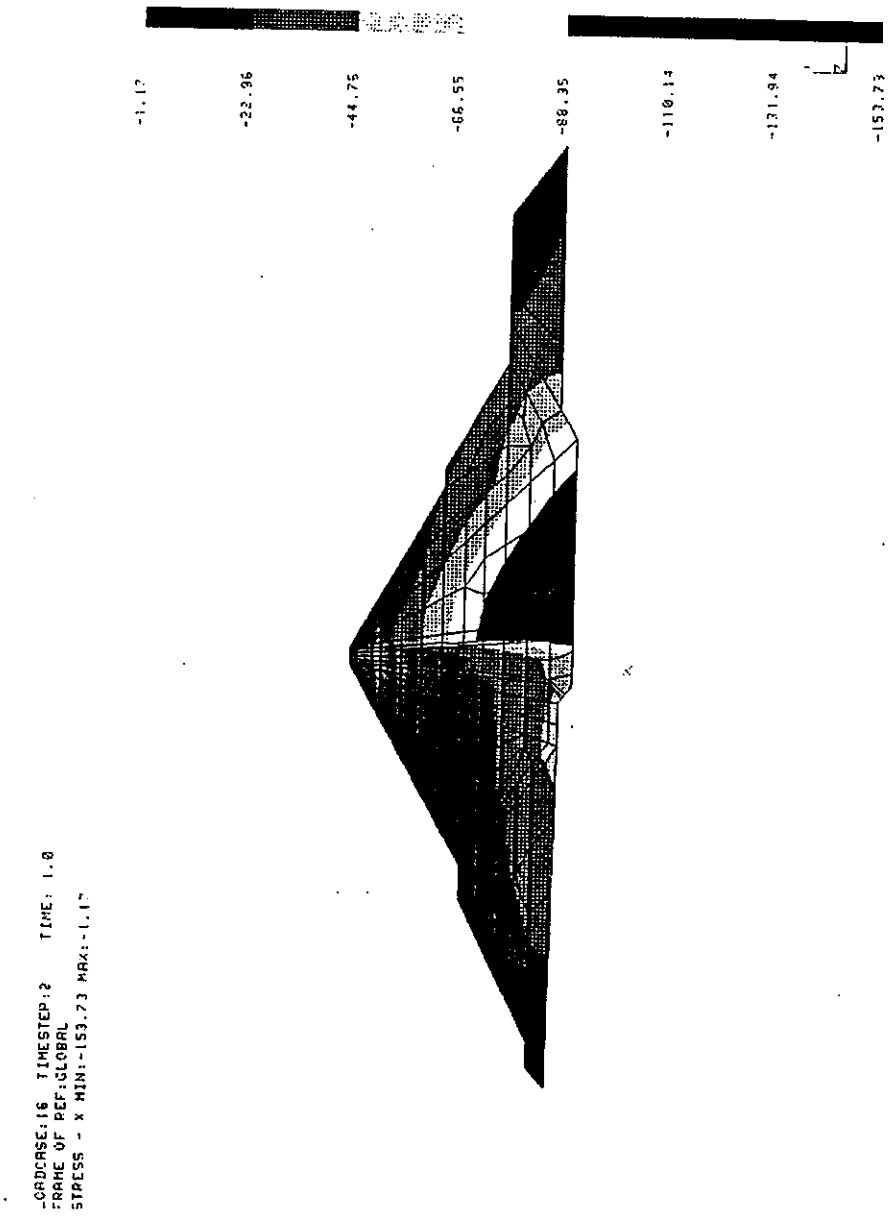

Figure 13: Horizontal stress distribution at the end of the water filling of the reservoir

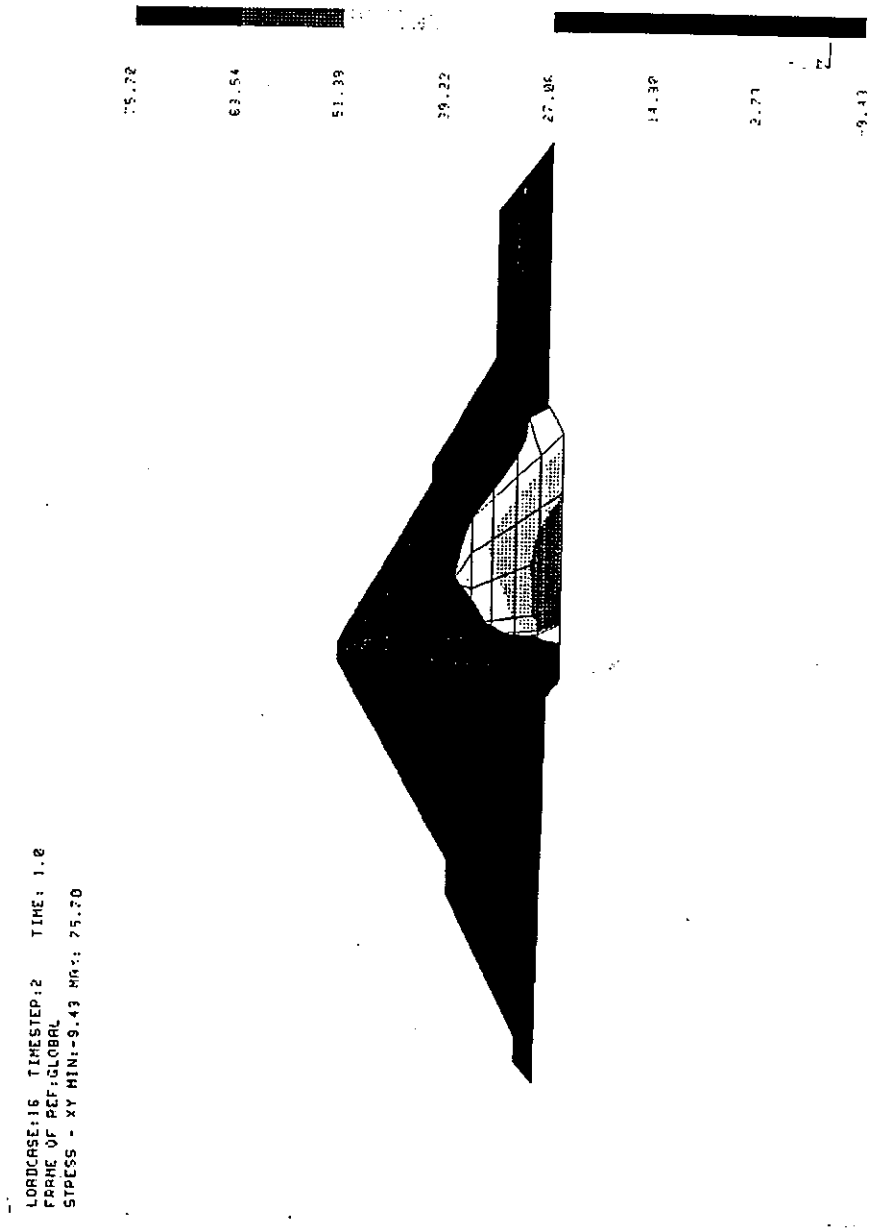

Figure 14: Shear stress distribution at the end of the water filling of the reservoir

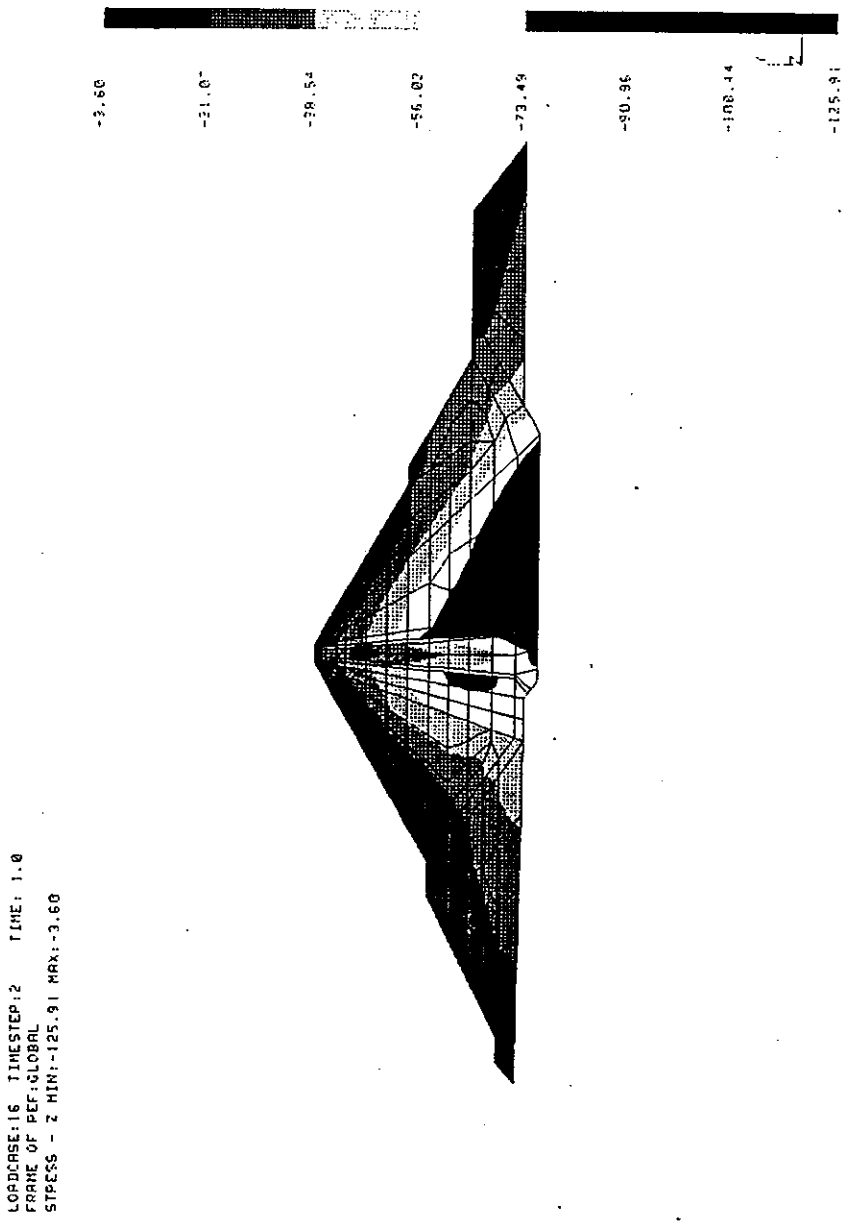

Figure 15: Normal stress distribution at the end of the water filling of the reservoir

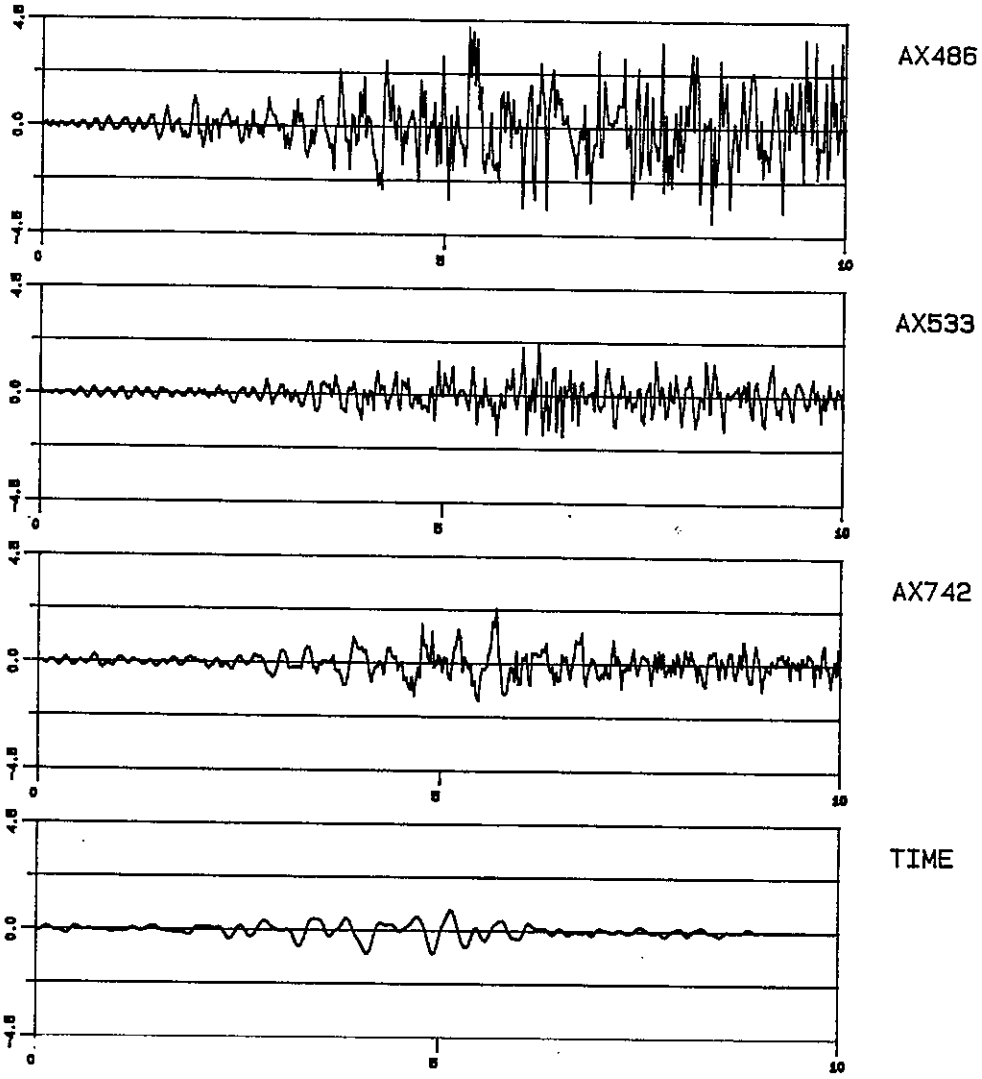

Figure 16: Horizontal component of the total acceleration

séisme EQ1

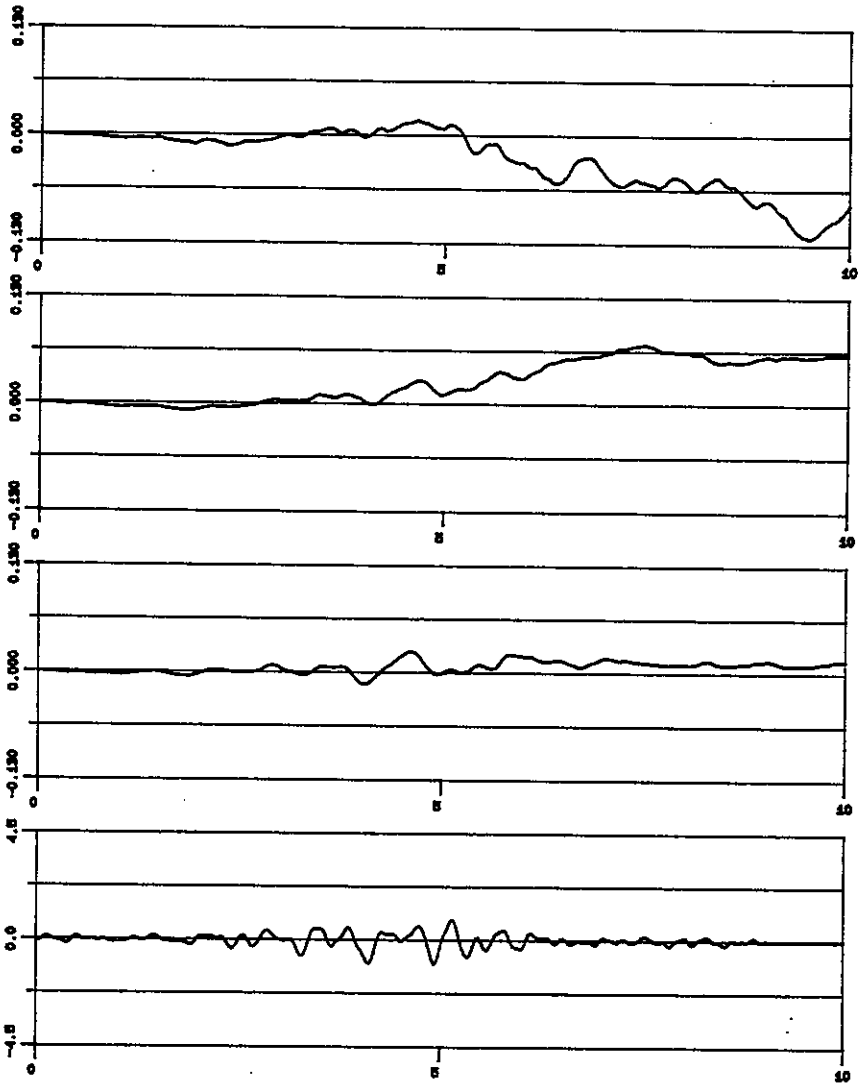

Figure 17: Horizontal component of the displacement

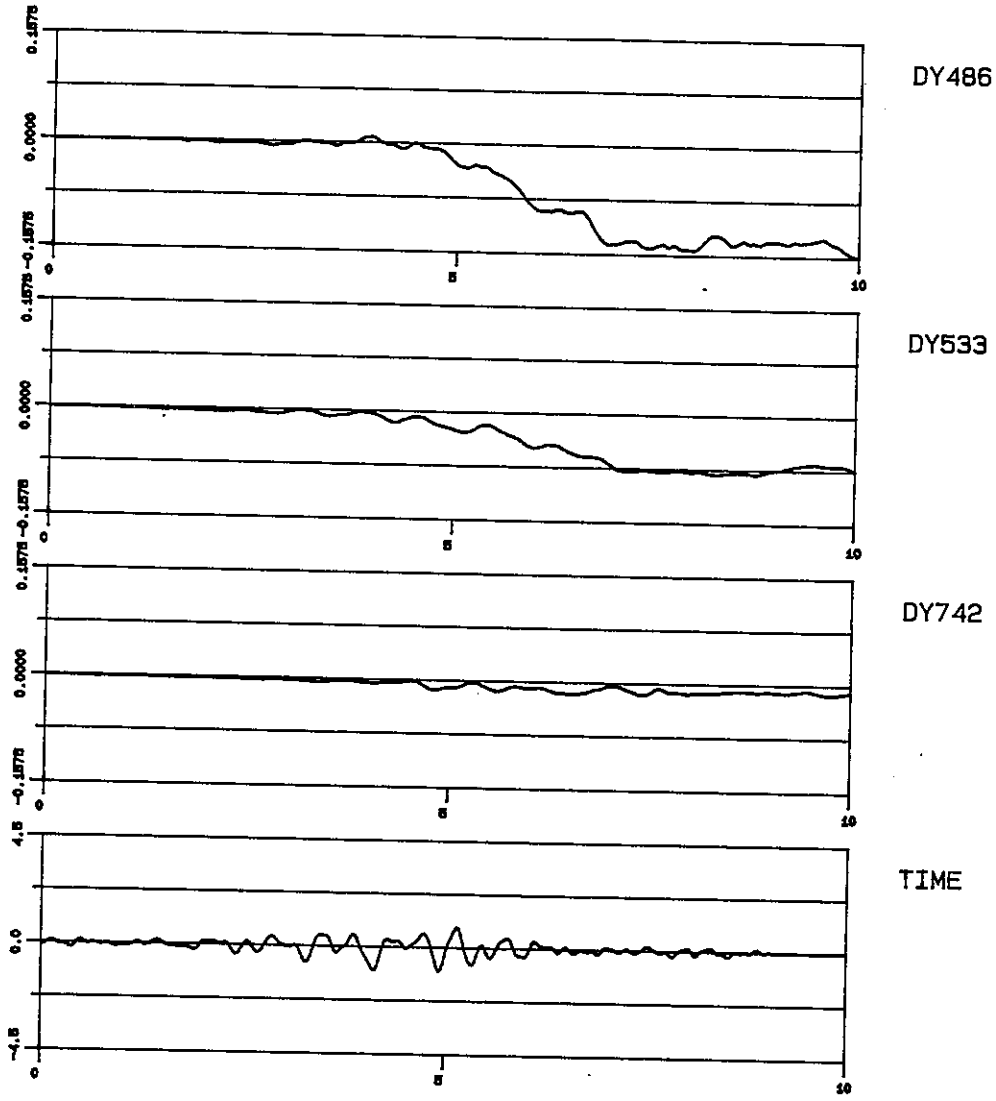

Figure 18: Vertical component of the displacement

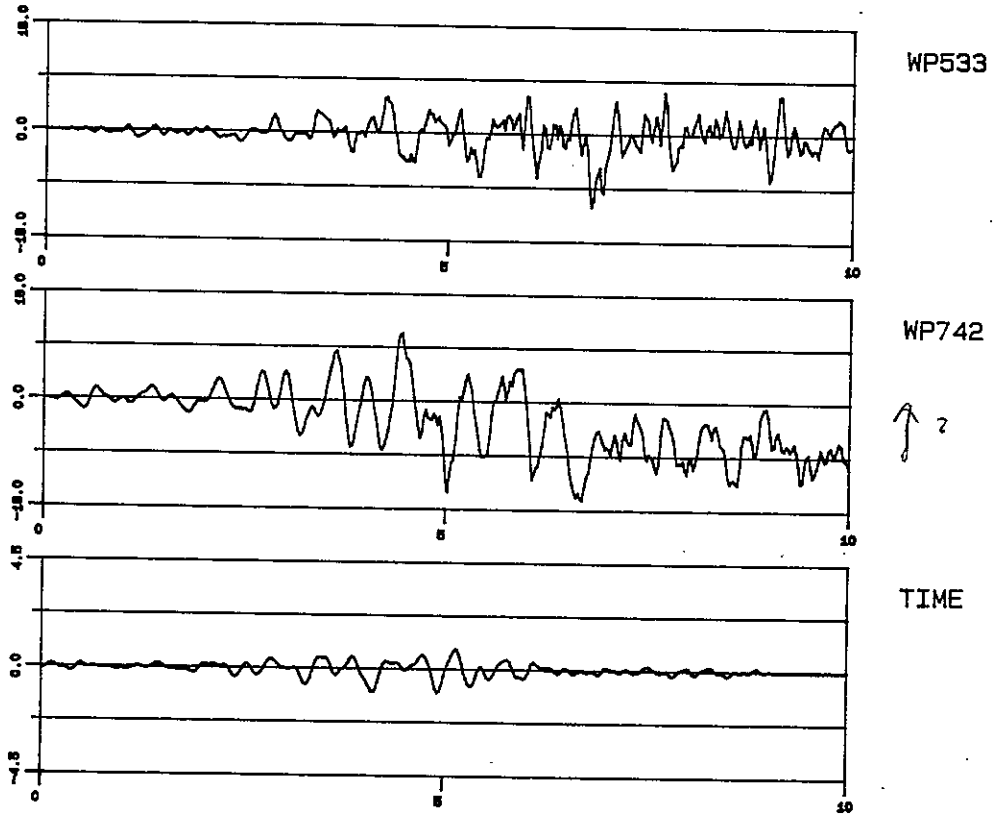

Figure 19: Excess pore pressure

First Benchmark Workshop

on

NUMERICAL ANALYSIS OF DAMS

Seriate (Bergamo - Italy)
May 28-29, 1991

WORKSHOP ON NUMERICAL ANALYSIS OF DAMS

The seismic response of El Infiernillo Embankment Dam: equivalent linear approach and Newmark method for evaulation of permanent displacements

G.Ruggeri(*), P.Palumbo(*), G.La Barbera(*), G.Mazza'(**), F.Bettinali(**)
(*) ISMES Spa Bergamo - (**) ENEL CRIS Milano

1.0 INTRODUCTION

This report describes the benchmark analysis of El Infiernillo Embankment Dam and summarizes the essential results obtained, following option 1 among those specified in chapter 1 of the benchmark inputs.
The principal steps of the analyses are shown in the flow chart illustrated in figure 1.
The analyses were carried out using the following codes: NASTRAN for finite element dynamic analysis; STABL2 for slope stability analysis and NEWDISP for the evaluation of permanent displacements.
Geometrical, physical and mechanical parameters supplied for the benchmark solution are reported in the workshop input specification. It is assumed here that the benchmark requirements are well known to the reader. The finite element model that was adopted is represented in figure 2.

2.0 LINEAR STATIC ANALYSIS

The main purposes of the linear static analysis consist in defining the mean effective stress distribution through the embankment considering the self weight, hydrostatic pressure on the upstream slope and the buoyancy effect on the submerged zone. An illustrative scheme of the loads considered in the analysis is reported in figure 3.

3.0 GENERAL CONSIDERATION ON DYNAMIC ANALYSIS

In earthquake response evaluations, the following set of equations are solved:

$$[M]\{\ddot{u}\} + [C]\{\dot{u}\} + [K]\{u\} = \{F(t)\} \qquad (1)$$

in which:

[M] = mass matrix for the assemblage of elements

[C] = damping matrix for the assemblage of elements

[K] = stiffness matrix for the assemblage of elements

{u} = nodal displacement vector

{F(t)} = earthquake load vector

The equations of motion are solved directly as set of simultaneous equations. Such a solution would require that the damping matrix [C] be known.
For this reason a damping submatrix is formulated for each individual element and all element submatrices are added to obtain the damping matrix for the entire assemblage of elements.

The formulation of such a submatrix is executed adopting the following relationship for each element "e":

$$[c]_e = \gamma_e [k]_e$$

in which $[c]_e$ and $[k]_e$ are the damping and stiffness submatrices for element "e" and γ_e is a parameter that is function of the damping value of element "e". The parameter γ_e is given by:

$$\gamma_e = \lambda_e/\omega_1$$

The value of λ_e, which represent the damping ratio for element "e", is chosen based on the strain developed in the element. The parameter ω_1 is the fundamental frequency of the system and is obtained from the solution of eigenproblem associated to equation (1) with [C] = 0. The damping matrix for the entire assemblage of elements is obtained by addition of the damping submatrices of all the elements in the assemblage.

4.0 SEISMIC RESPONSE OF THE EMBANKMENT

The dynamic response of the embankment is computed using an equivalent linear method that involves:

1) performing static analysis to estimate the initial mean effective stress state due to self weight and hydrostatic load;

2) performing dynamic analysis assigning initial values of shear modulus and damping to each element and iterating then the linear elastic dynamic analysis to make the values of modulus and damping strain-compatible.

Using the computed values of average shear strain developed in each element, new values of shear modulus and damping factor are determined from appropriate data, trough a relationship respect to shear strain. This way, a solution is obtained incorporating modulus and damping values, for each element, which are compatible with the average shear strain developed.
In this type of analysis the seismically induced porewater pressures are not taken into account.

It should be noted that the linear equivalent method provides conservative values of acceleration due to the fact that it does not consider the effect of soil plasticity which imposes a threshold value to the accelerations.

4.1 Input ground motion

Two inputs accelerograms have been considered in the present analysis, namely EQ1 and EQ3, among those specified in the benchmark inputs.

For the given finite element discretization (fig. 2), the maximum frequency content of the motion which can be accurately reproduced is around 8 Hz. For this reason the given accelerograms have been filtered with a cut-off frequency of 8 Hz.

5.0 EVALUATION OF PERMANENT DEFORMATIONS

Equivalent linear method described above is used only to get the distribution of induced acceleration time histories in the dam. Also, since the model is elastic, it cannot predict permanent deformations directly. Further analysis are required as described in the following.

5.1 Description of the method

The analytical approach adopted for estimating the permanent deformations of El Infiernillo Dam is based on the concept outlined by Newmark (1965) in which the displaced part of an embankment is modelled as a rigid block on an horizontal or inclined plane, subjected to induced earthquake motion which causes the block to slide on the plane.

This type of approach does not predict change in strength due to shaking, and therfore is not generally appropriate where liquefaction induced failure must be addressed. On the other hand if limited loss of shear strength due to shaking is anticipated the Newmark approach can be used by a suitable choise of strength parameters. The material types constituting El Infiernillo Dam, while variable, have good compaction characteristics and static strength. Materials of this nature have not been known to liquefy during earthquakes.

A conventional limit equilibrium analysis, or slope stability analysis, provides the critical (limiting) accelerations for fixed potential sliding masses. Because base motion usually is amplified upon being propagated upward through an embankment, an analysis of the amplification response is incorporated to account for that aspect of the embankment behaviour.

The major steps of a permanent displacement analysis of Newmark type are shown in the flow chart reported in figure 1.

5.1.1 Evaluation of critical accelerations

Critical horizontal acceleration K_{hc} is defined as the level of average acceleration induced in the potential sliding mass that will make sliding imminent, reducing the factor of safety to sliding to unity. The value of K_{hc} which is expressed as a fraction of the gravitational acceleration g , is obtained through a conventional pseudostatic analysis. For the present analysis the computer code STABL2 has been used analising, with the simplified Janbu method, circular sliding surfaces stability conditions. The analysis has been performed on effective stresses basis. In table 1 the strength parameters used for the analysis are reported. Based on previous static analyses four sliding surfaces have been chosen in the upstream slope and three in the downstream slope. The critical horizontal acceleration has been determined by a pseudostatic analysis performed on each sliding surface.

5.1.2 Deformations from acceleration data : sliding block analysis

The principal elements of the sliding block analysis are shown in figure 4 (Finn 1990). This method of analysis was pioneered by Newmark (1965). The version adopted for the present analysis was developed by Makdisi and Seed (1978) and differs from the Newmark approach in generating relative displacements by the net acceleration above the sliding surface, whereas Newmark used the net acceleration below the sliding surface.

The potential sliding mass shown in figure 4 is in a condition of impending failure, so that the factor of safety to sliding equals unity. This is attributed to the sliding mass accelerating towards the right with an acceleration a_y. The acceleration in the sliding mass is limited to this value by the limit of the shear stresses that can be exerted across the contact, in a way that if the base acceleration were to increase, the result would be that the mass would move downhill relative to the base. Following D'Alembert principle, the limiting critical acceleration is represented by an inertia force $K_{hc} \cdot W$ applied pseudostatically to the mass in a direction opposite to the acceleration. In the present work the average acceleration time histories for different potential sliding masses have been obtained from a previous NASTRAN iterative analysis.

6.0 PRESENTATION OF RESULTS

6.1 Static analysis

The representative results are reported in figure 5.

6.2 Pseudo static analysis and critical accelerations

The results are summarized in figure 12 and 19 respectively for the upstream and downstream slope

6.3 Dynamic response and calculated permanent displacements

From figure 20 to 26 the results obtained for the input ground motion EQ1 are illustrated. Namely: in figure 20 and 21 the acceleration time histories for various nodal points; in figure 22 and 23 the Fourier spectrum of nodal accelerations; in figure 24 and 25 the time histories of average accelerations for different potential sliding masses both in upstream and downstream slope

respectively; in figure 26 the calculated permanent displacements for different sliding masses are reported for both upstream and downstream slope.

From figure 27 to 33 the results obtained for the input ground motion EQ3 are illustrated. The contents of the figures are the same as those for the previous case EQ1 and they follow exactly the same ordering

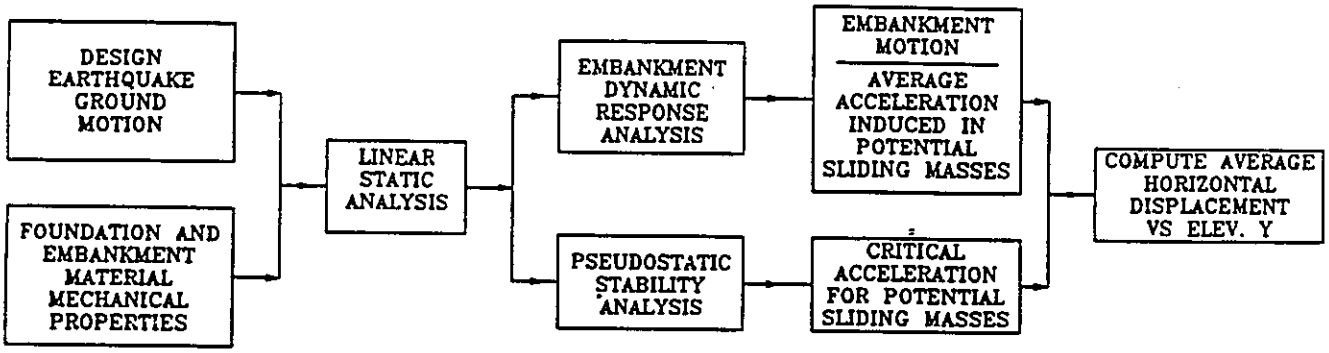

Flow chart representing the main steps of seismic analysis

Figure 1

FINITE ELEMENT MODEL

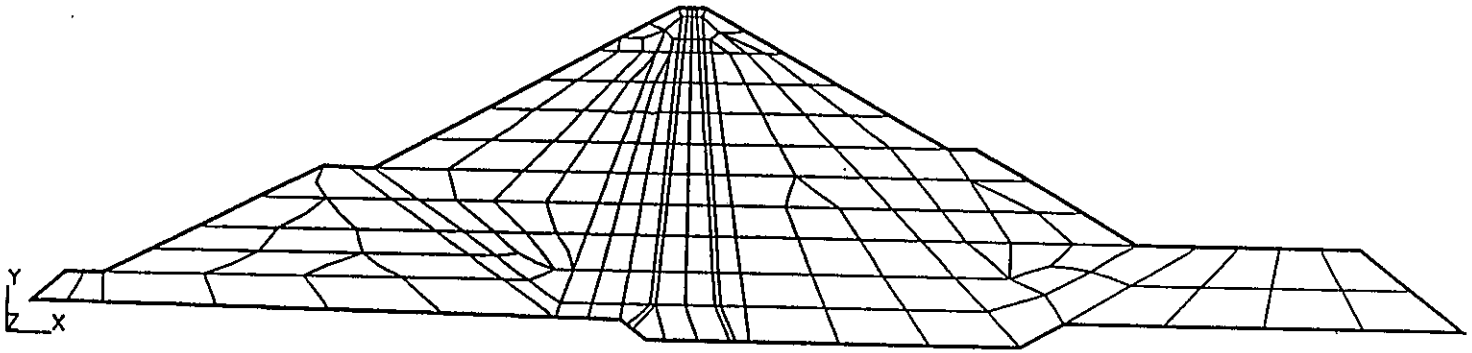

Figure 2

EL INFIERNILLO DAM

LOADS CONSIDERED FOR LINAR STATIC ANALYSIS

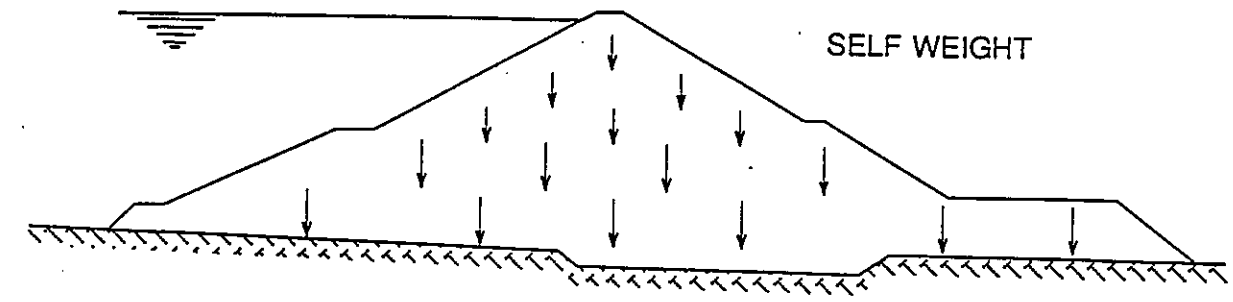

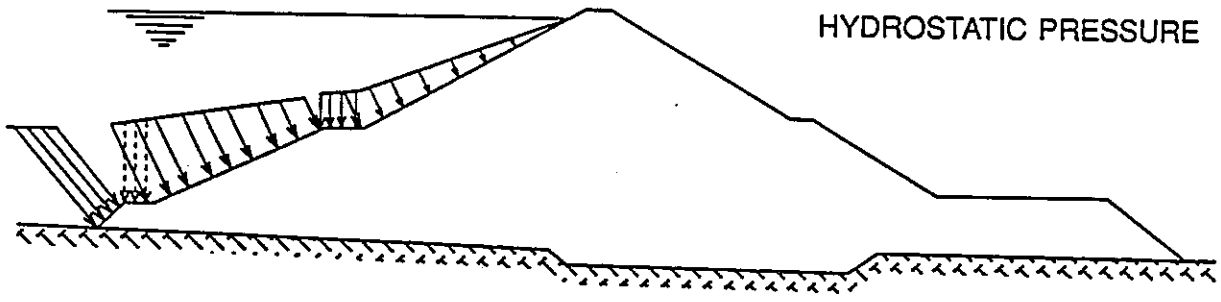

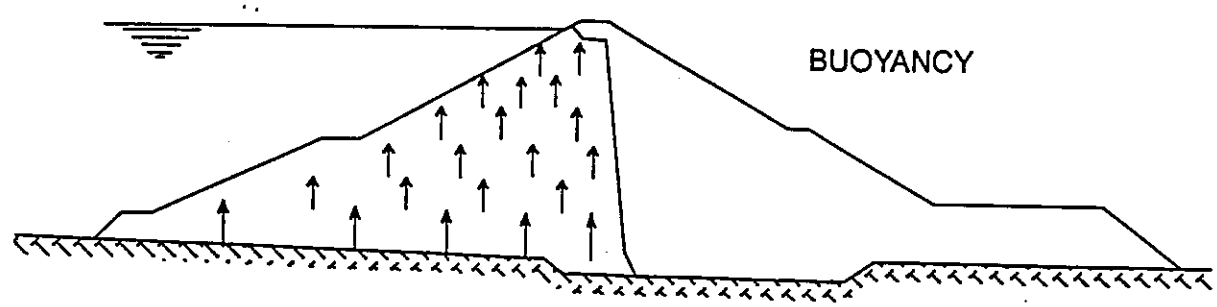

Figure 3

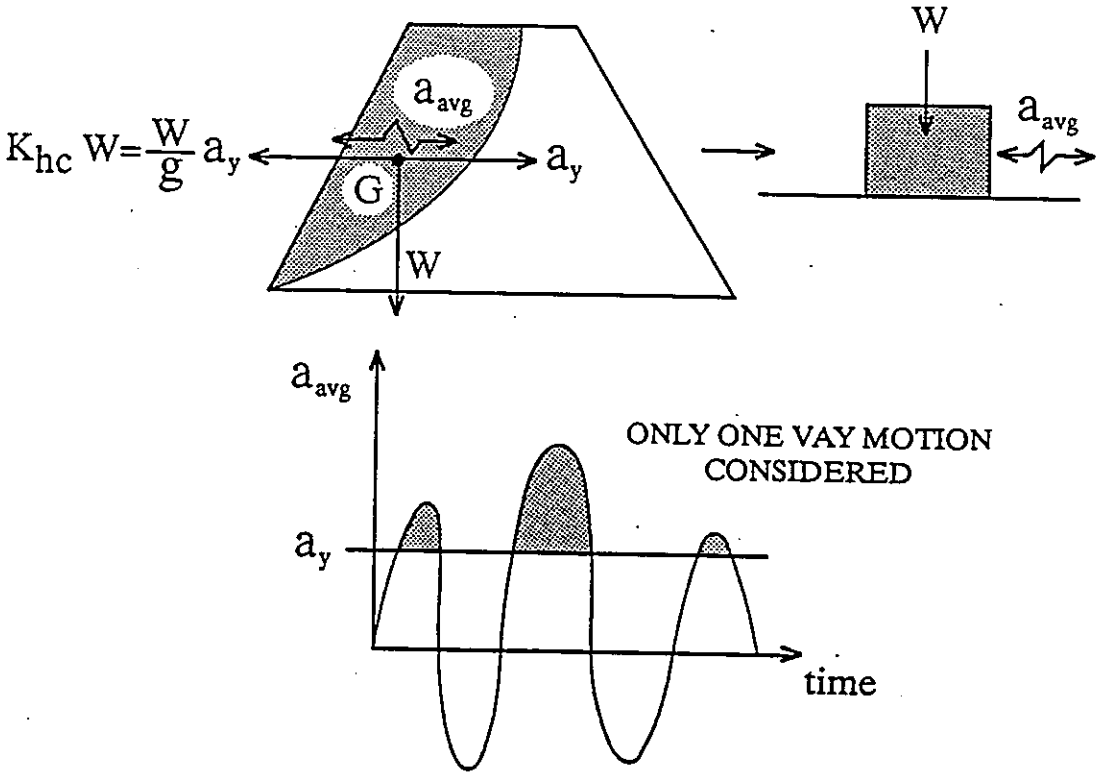

The estimation of oeformation using Newmark's method (Finn, 1990)

Figure 4

LINEAR STATIC ANALYSIS

COMBINED LOADS : OWN WEIGHT + HYDROSTATIC PRESSURE + BUOYANCY

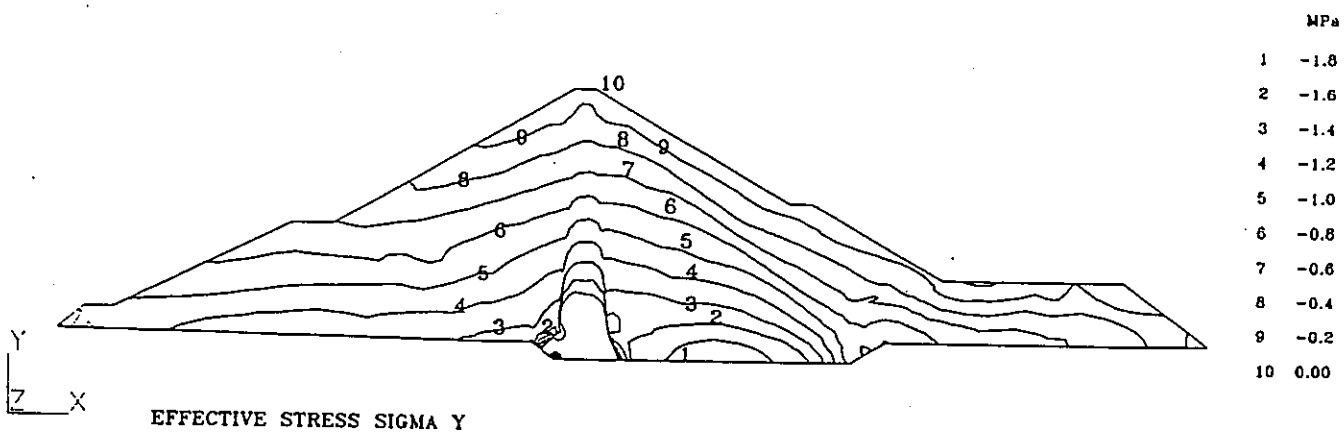

EFFECTIVE STRESS SIGMA Y

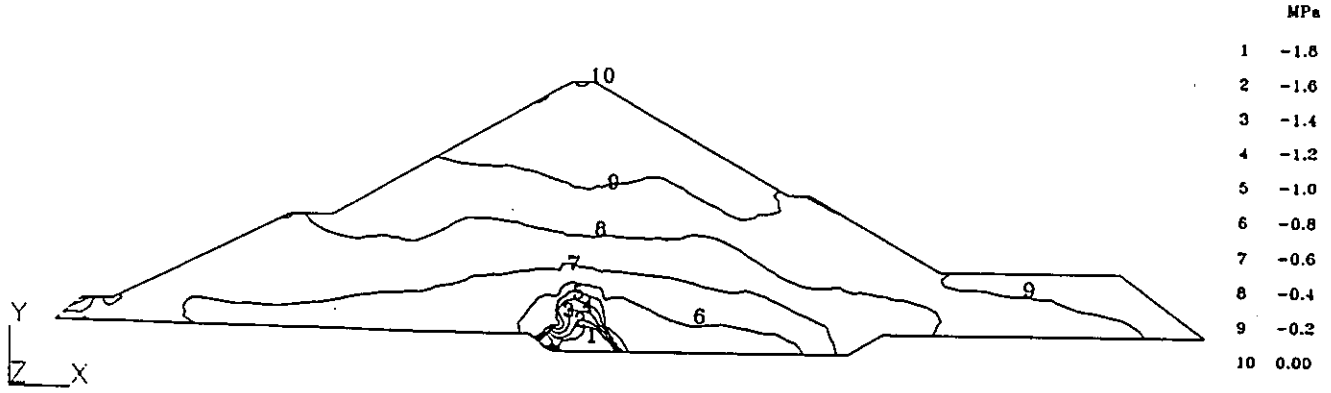

EFFECTIVE STRESS SIGMA X

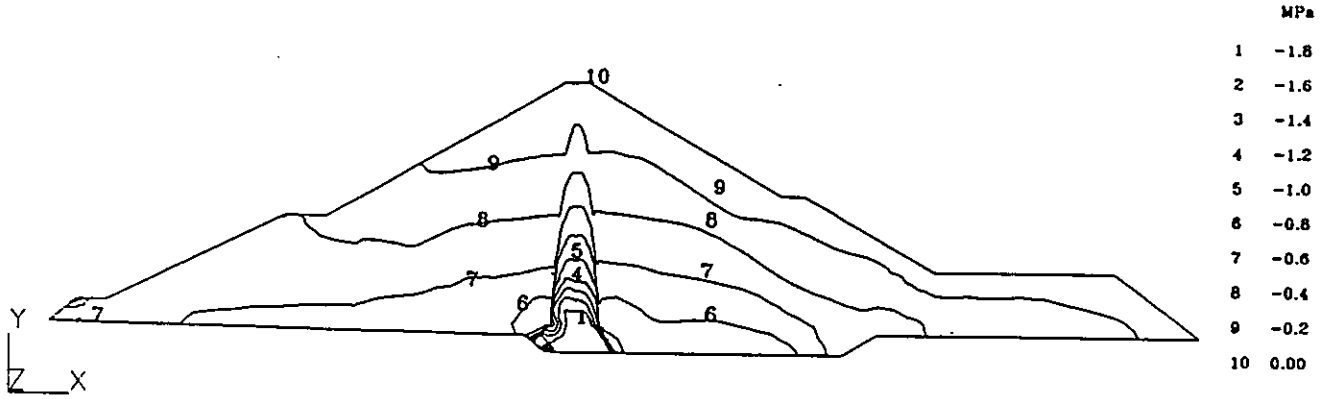

EFFECTIVE MEAN PRESSURE

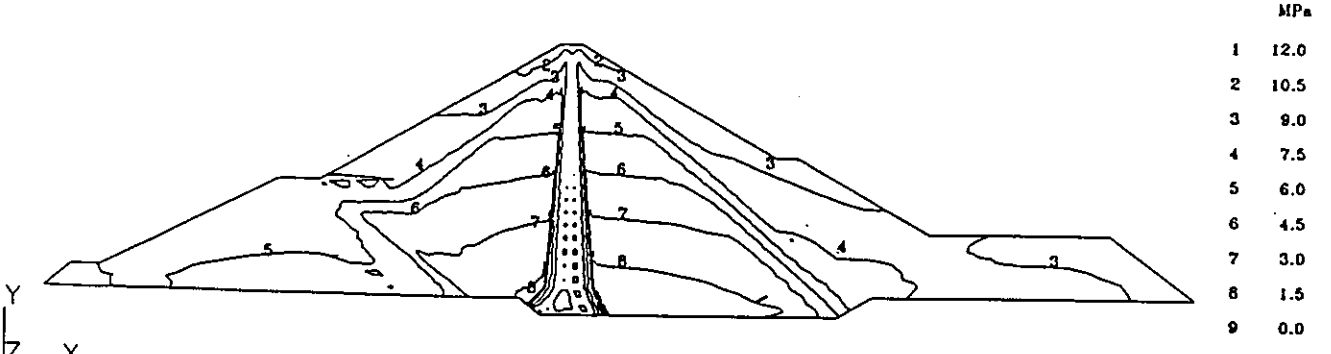

CALCULATED G-MAX DISTRIBUTION BASED ON PREVIOUS STATIC ANALYSIS

Figure 5

EL INFIERNILLO DAM

UPSTREAM SLOPE; SLIDING MASSES EXTENDING AT Y/H = 1/4

100 SURFACES HAVE BEEN GENERATED

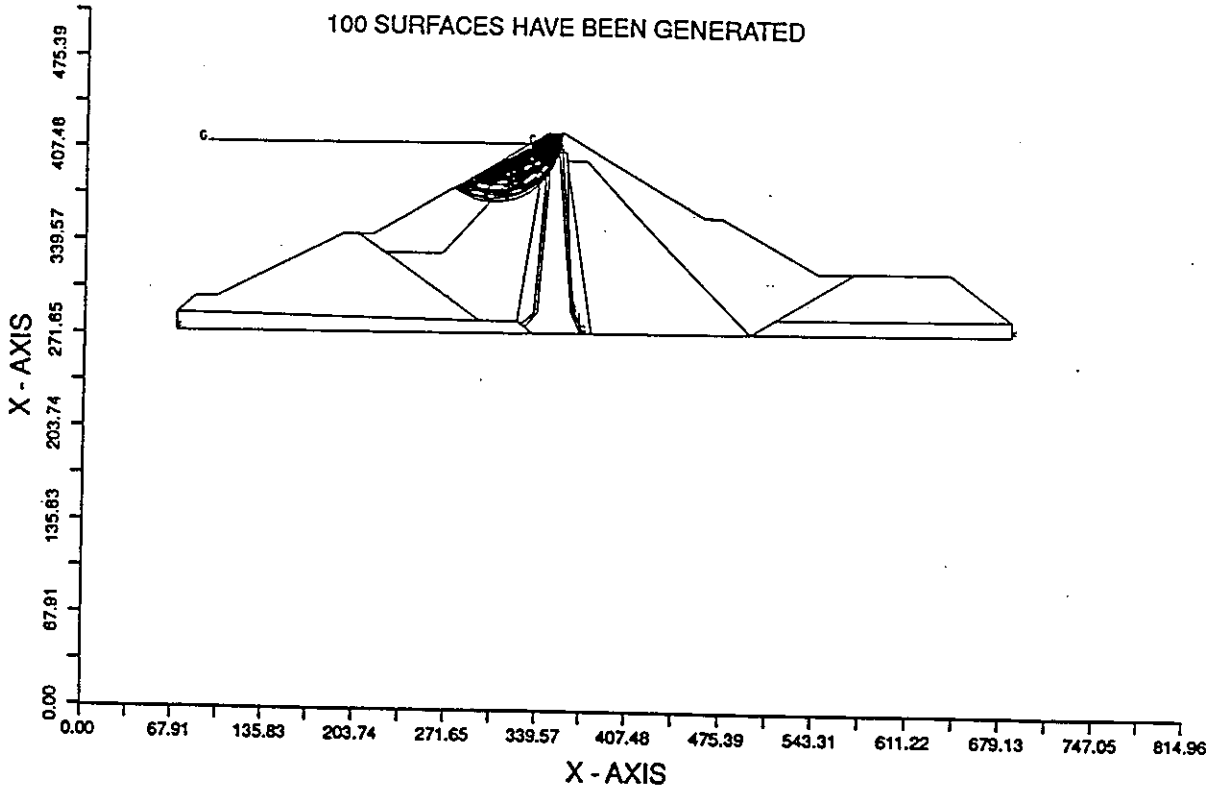

STATIC ANALYSIS

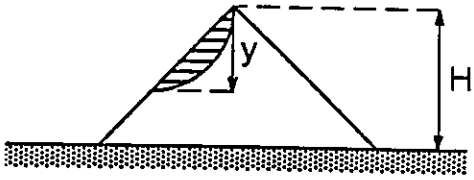

10 MOST CRITICAL OF SURFACES GENERATED
MINIMUM FACTOR OF SAFETY = 1.371

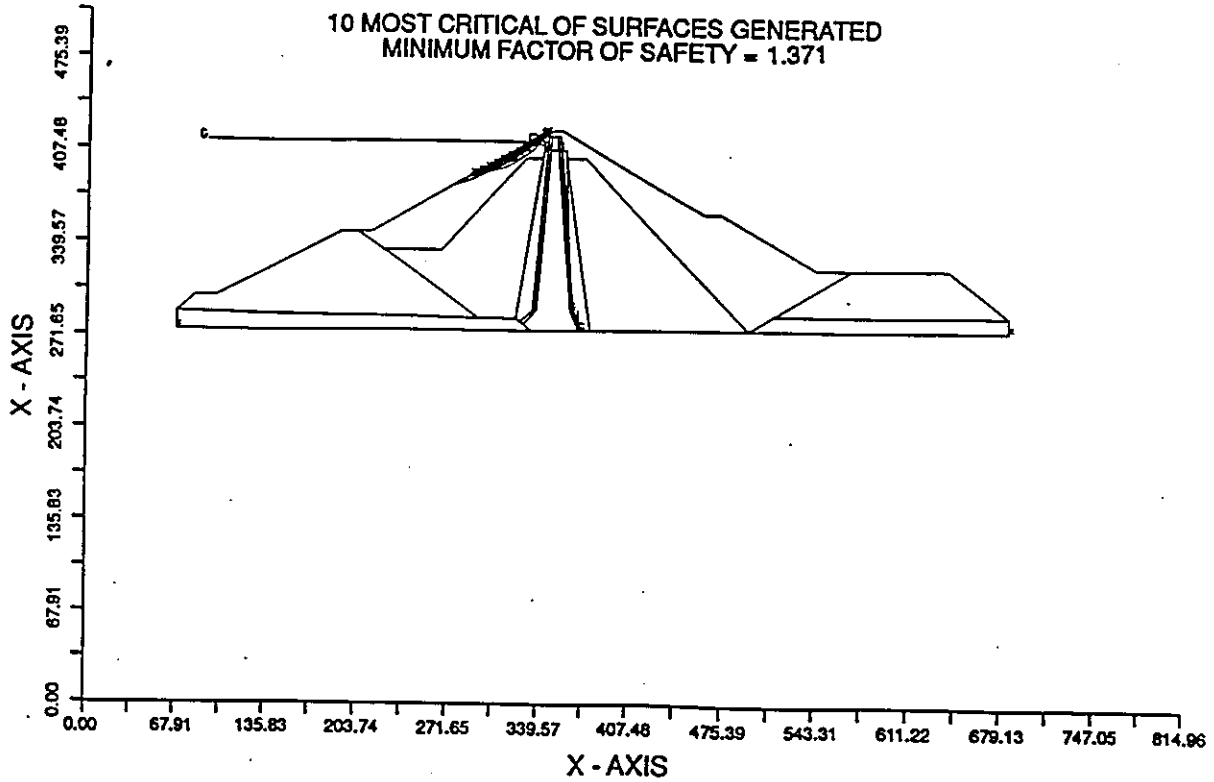

Figure 6

EL INFIERNILLO DAM

UPSTREAM SLOPE; SLIDING MASSES EXTENDING AT Y/H = 1/2

100 SURFACES HAVE BEEN GENERATED

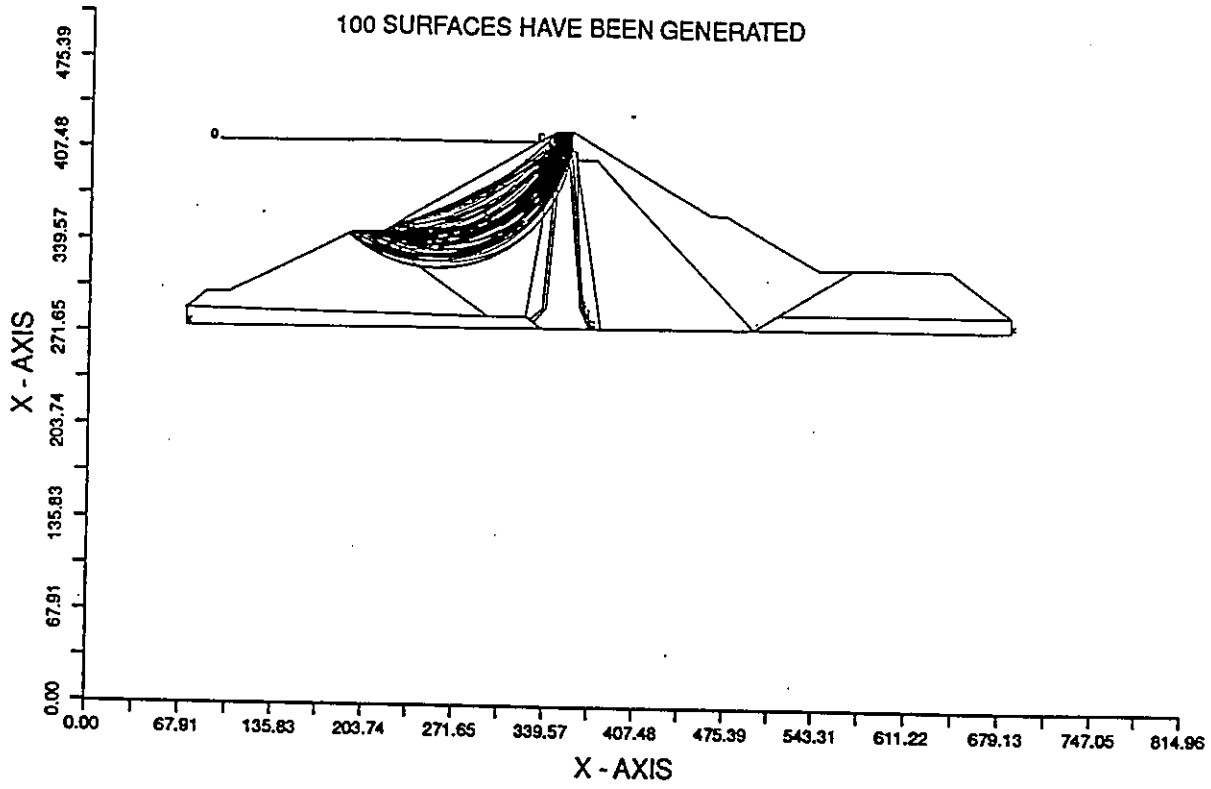

STATIC ANALYSIS

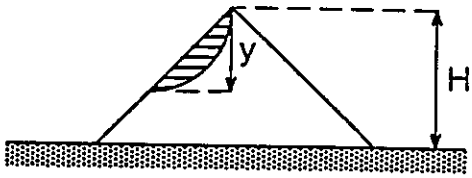

10 MOST CRITICAL OF SURFACES GENERATED
MINIMUM FACTOR OF SAFETY = 1.394

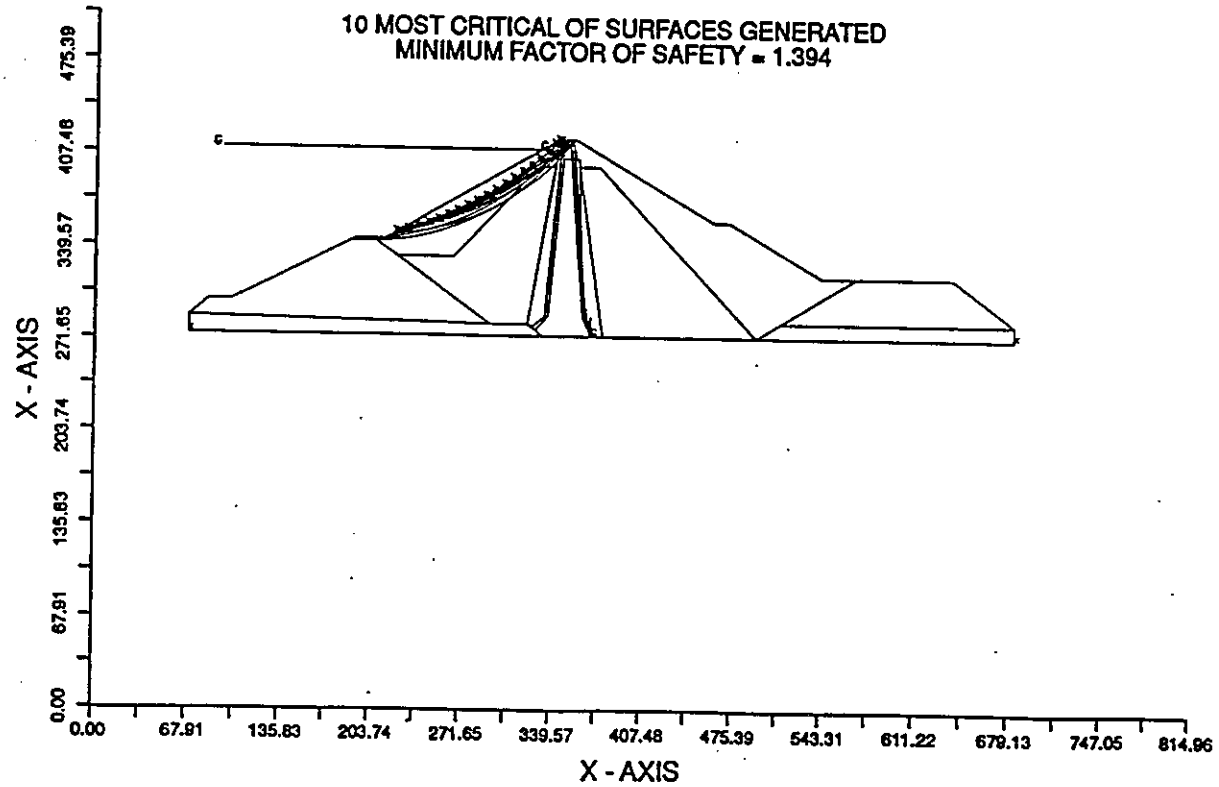

Figure 7

EL INFIERNILLO DAM

UPSTREAM SLOPE; SLIDING MASSES EXTENDING AT Y/H = 3/4

100 SURFACES HAVE BEEN GENERATED

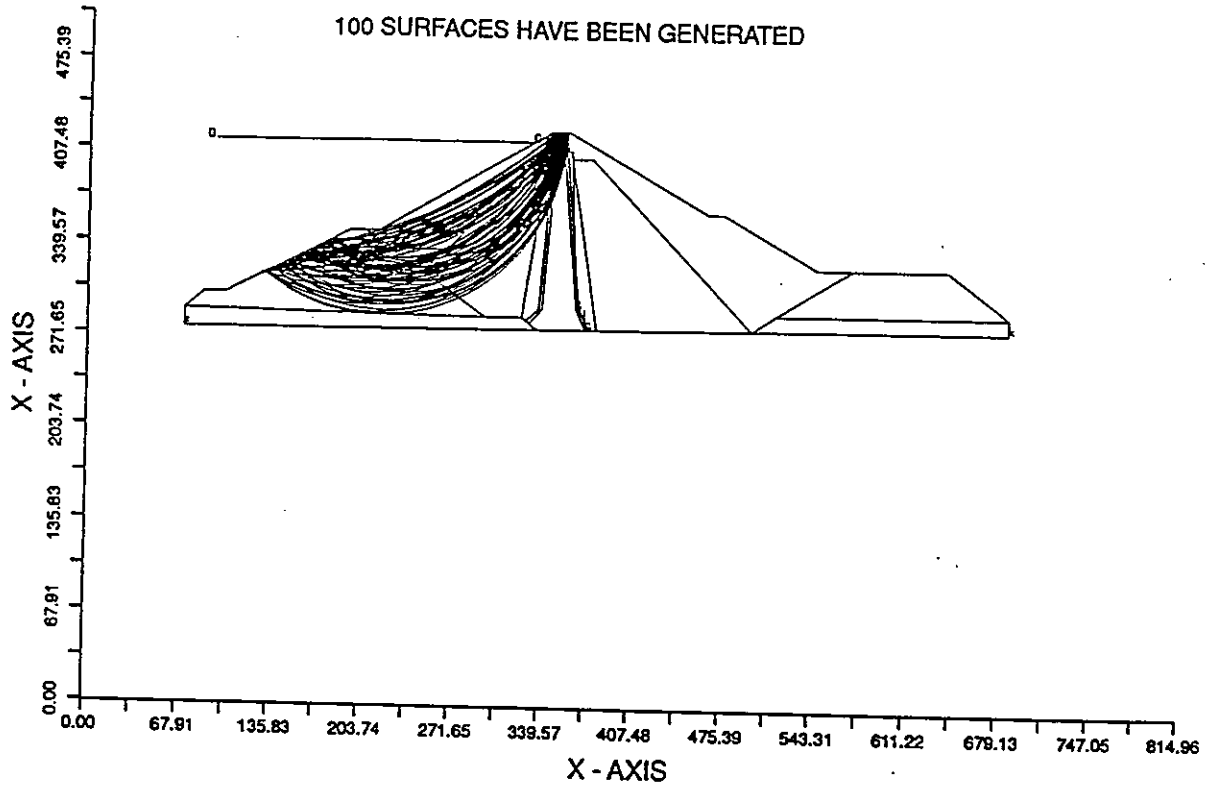

STATIC ANALYSIS

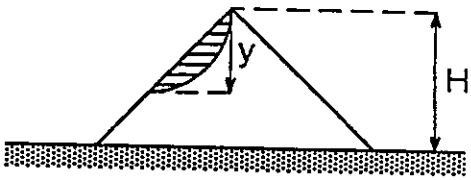

10 MOST CRITICAL OF SURFACES GENERATED
MINIMUM FACTOR OF SAFETY = 1.555

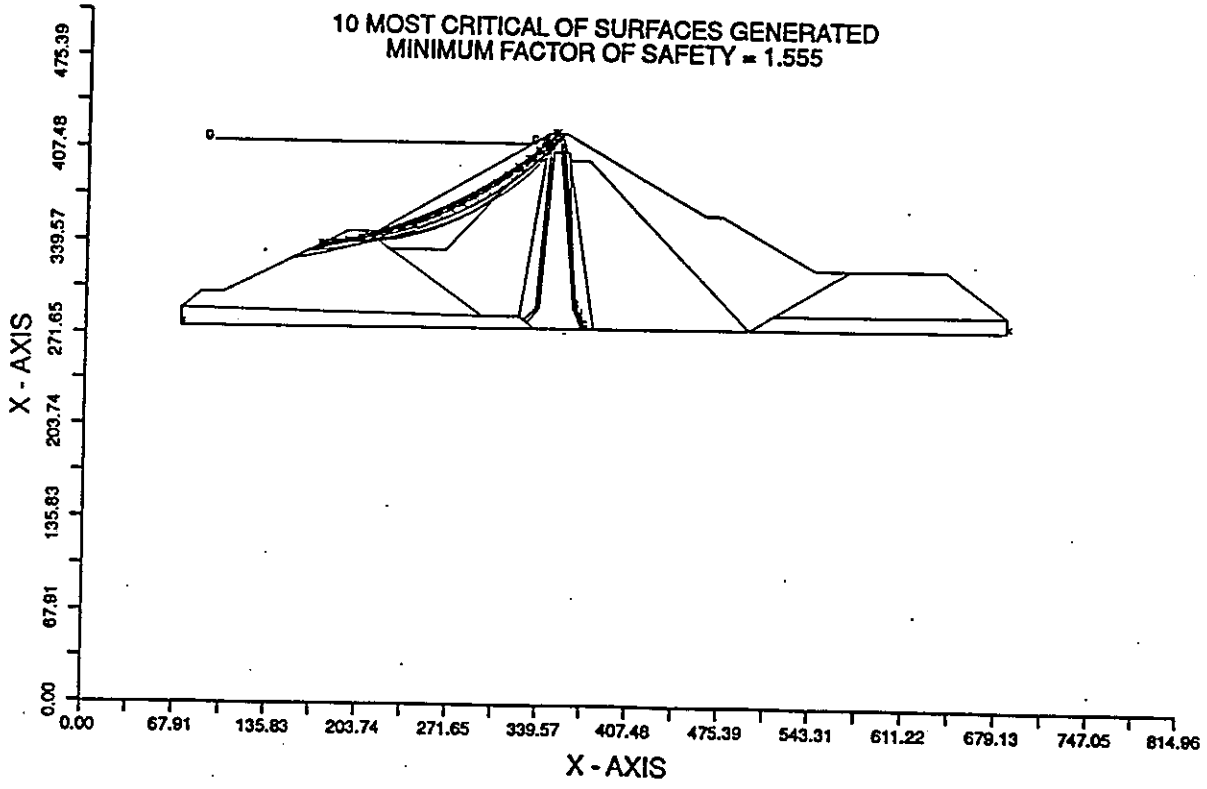

Figure 8

EL INFIERNILLO DAM

UPSTREAM SLOPE; SLIDING MASSES EXTENDING AT Y/H = 1

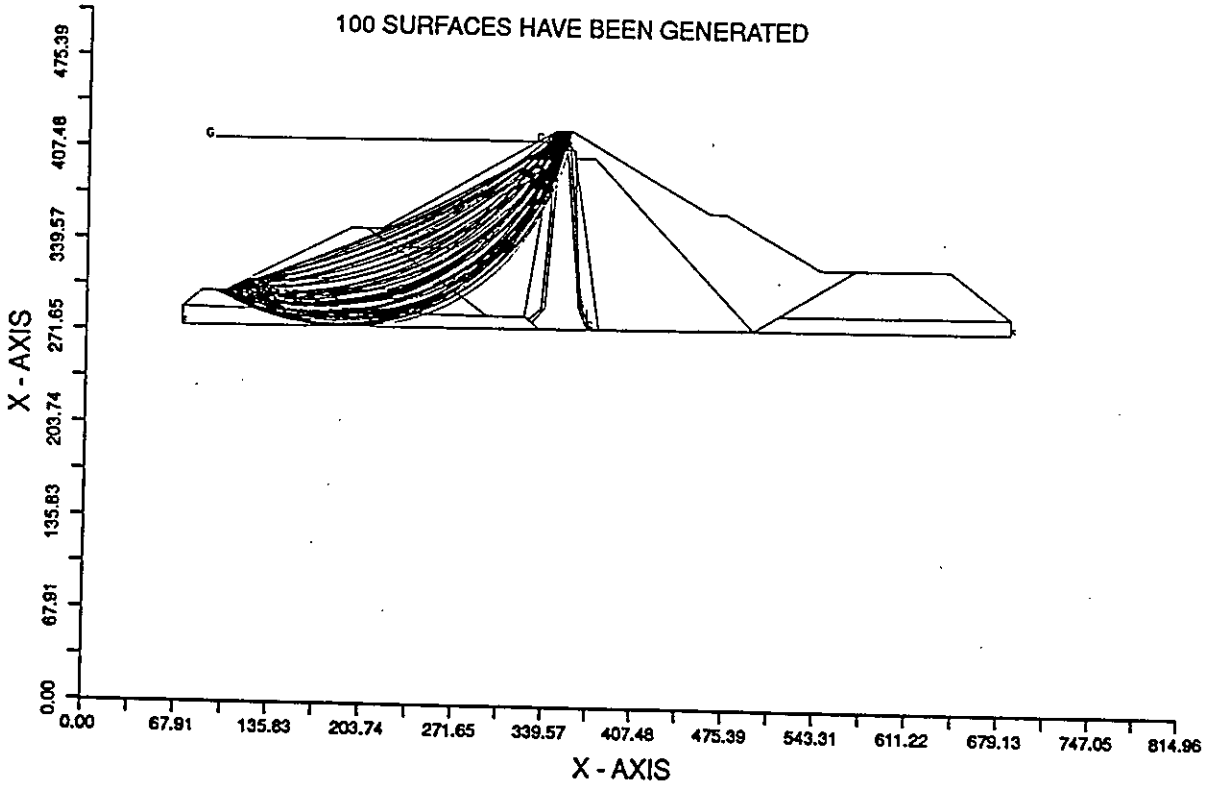

STATIC ANALYSIS

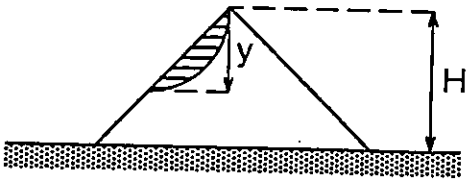

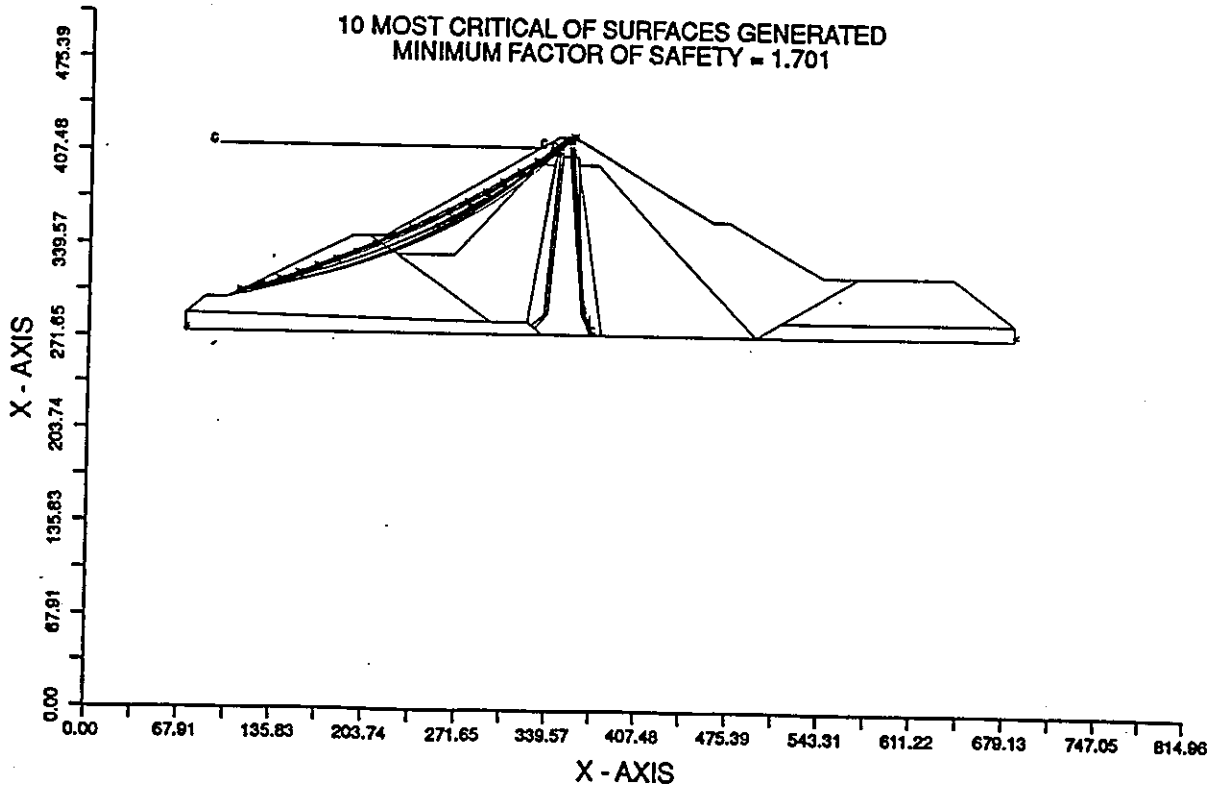

Figure 9

EL INFIERNILLO DAM

UPSTREAM SLOPE

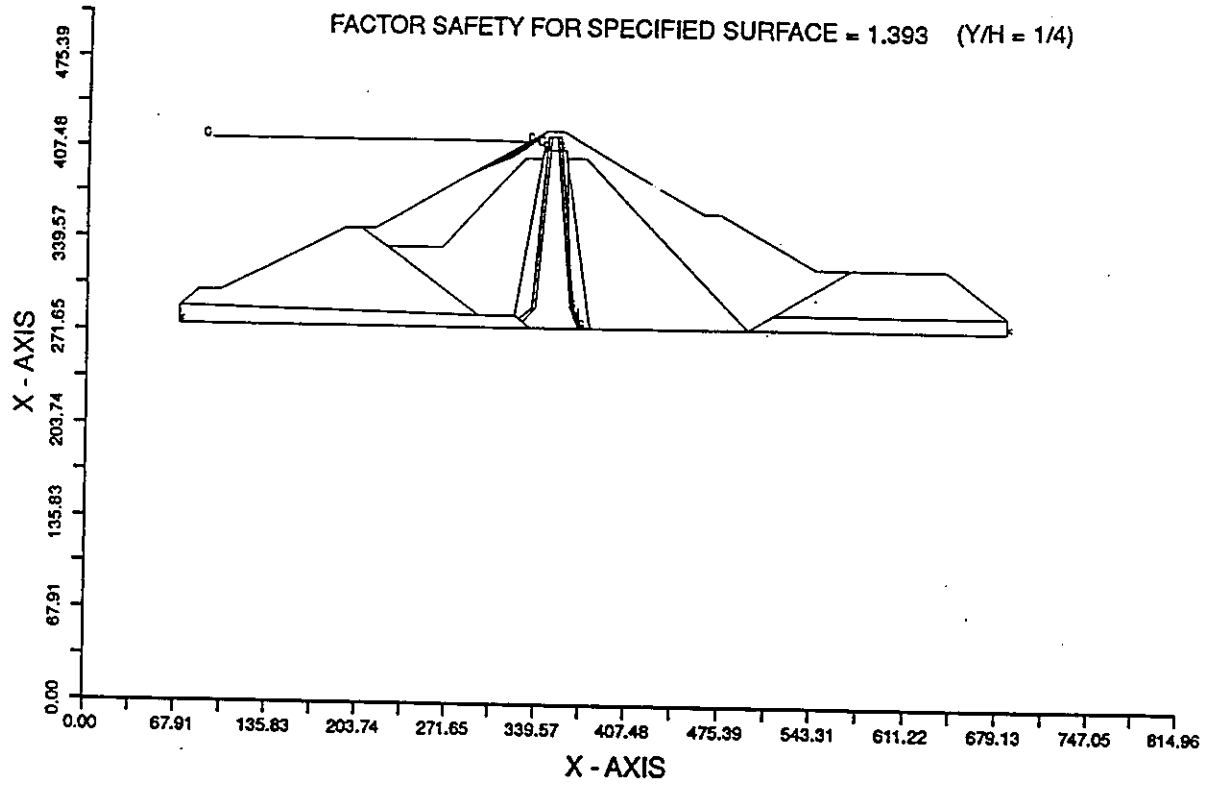

STATIC ANALYSIS

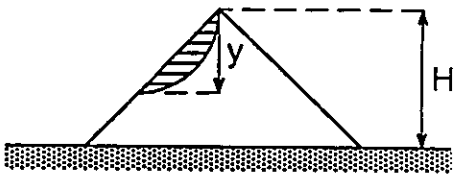

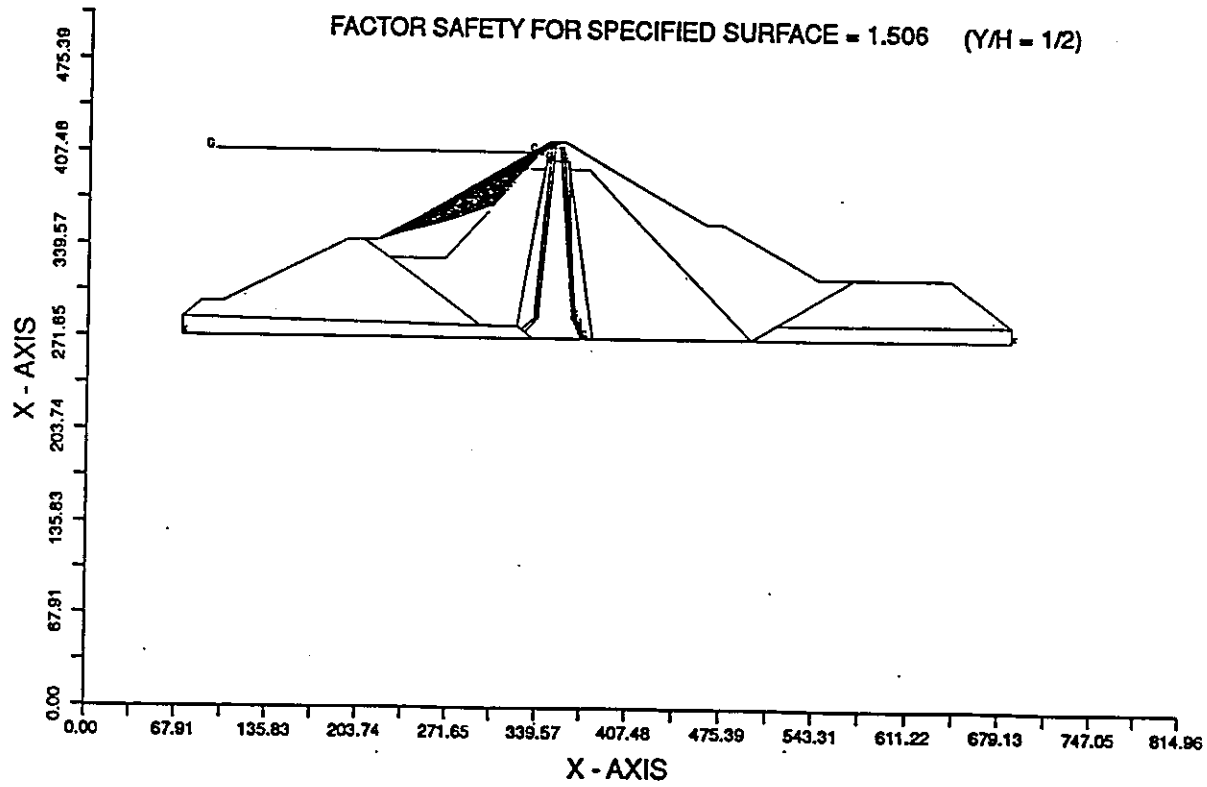

Figure 10

EL INFIERNILLO DAM

UPSTREAM SLOPE

FACTOR SAFETY FOR SPECIFIED SURFACE = 1.705 (Y/H = 3/4)

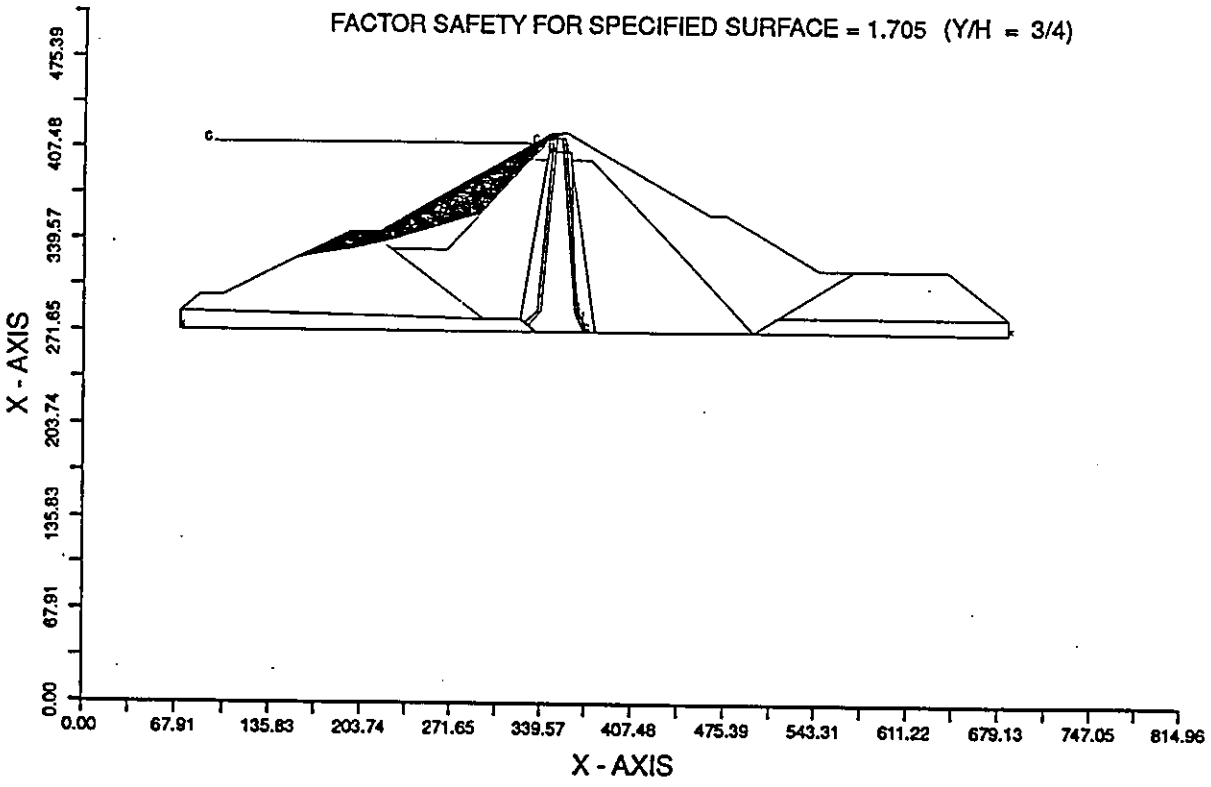

STATIC ANALYSIS

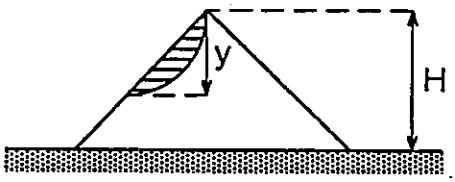

FACTOR SAFETY FOR SPECIFIED SURFACE = 1.838 (Y/H = 1)

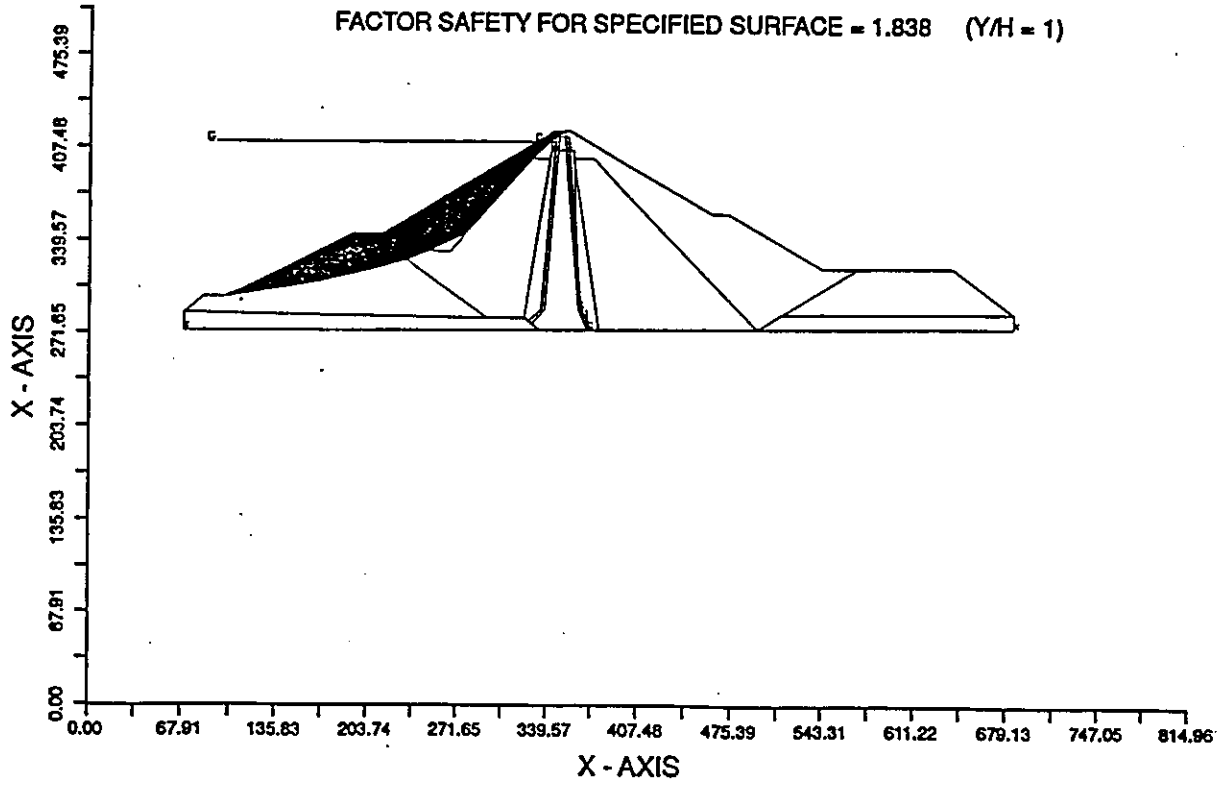

Figure 11

EL INFIERNILLO DAM

UPSTREAM SLOPE
PSEUDOSTATIC ANALYSIS

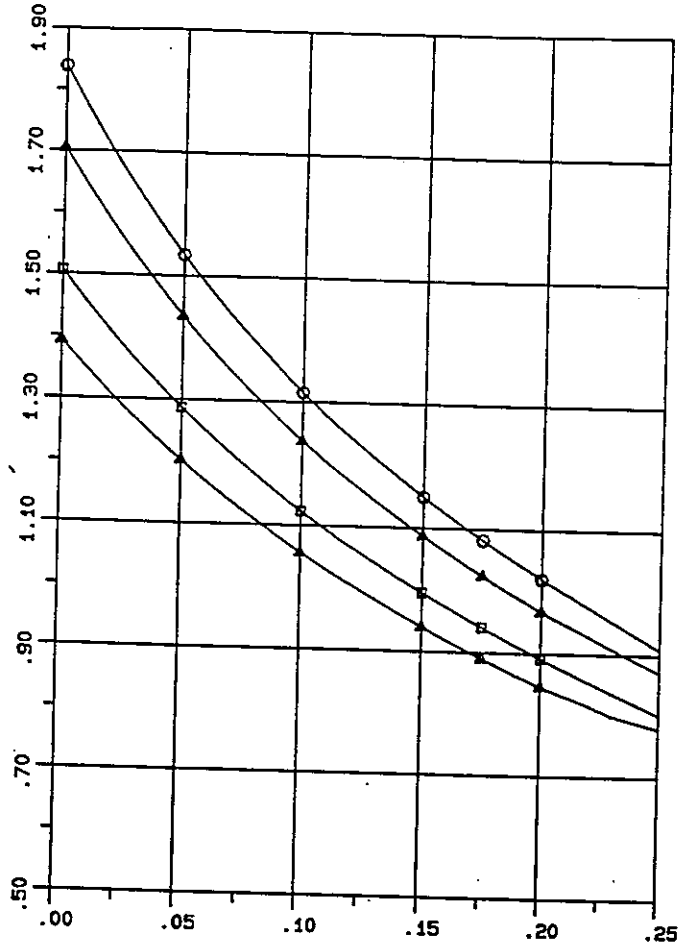

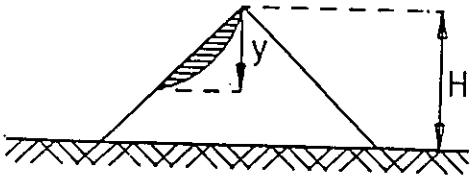

TOE DEPTH OF SLIDING SURFACES:

y/H = 1/4 △

y/H = 1/2 □

y/H = 3/4 ▲

y/H = 1 ○

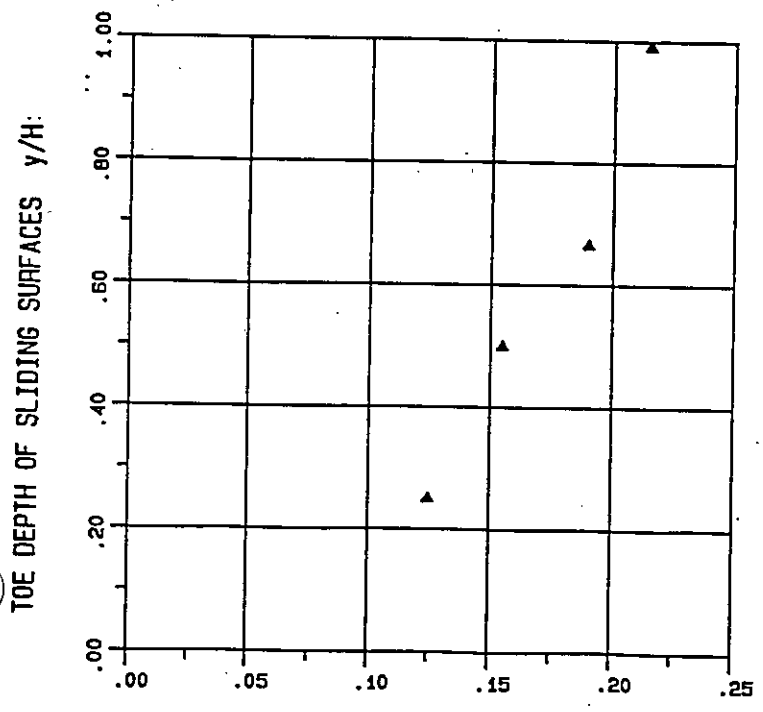

▲ CALCULATED VALUES

Figure 12

EL INFIERNILLO DAM

DOWNSTREAM SLOPE; SLIDING MASSES EXTENDING AT Y/H = 1/4

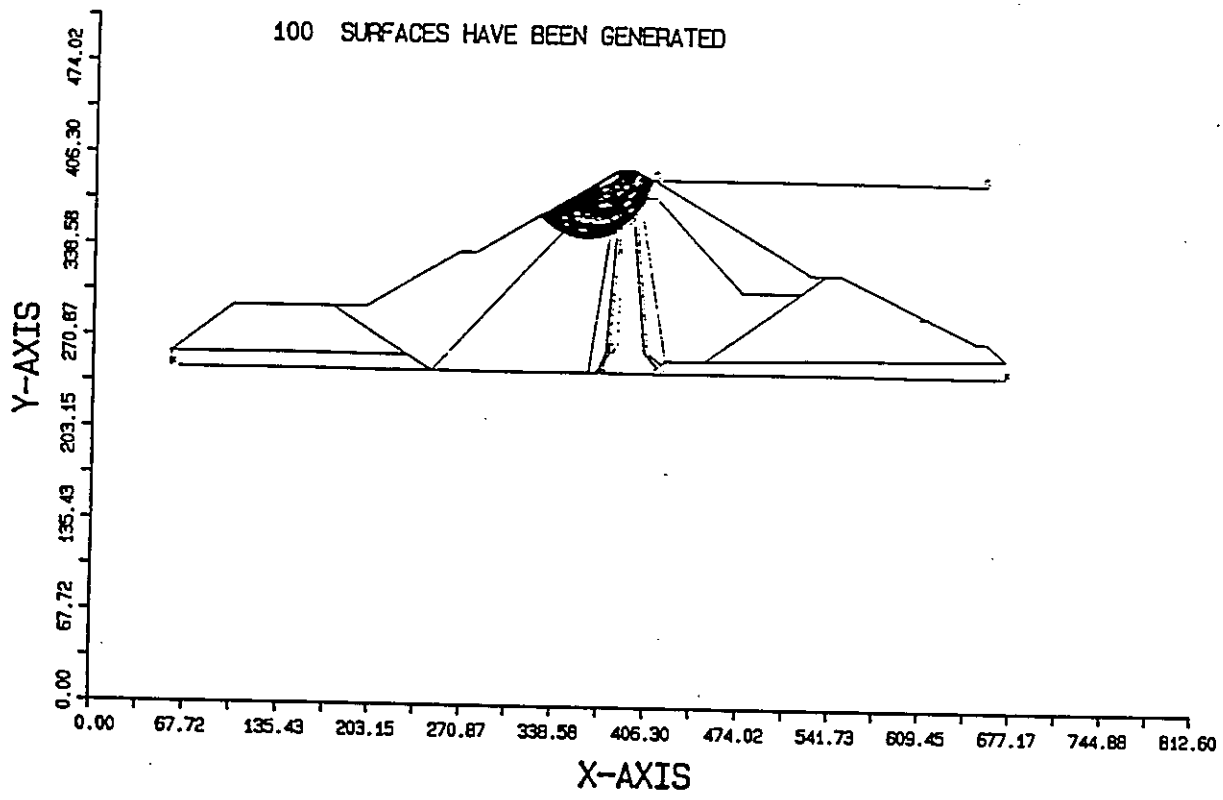

STATIC ANALYSIS

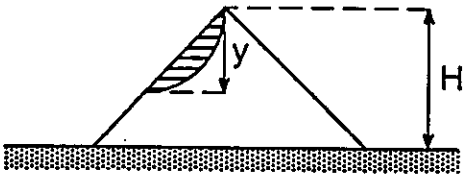

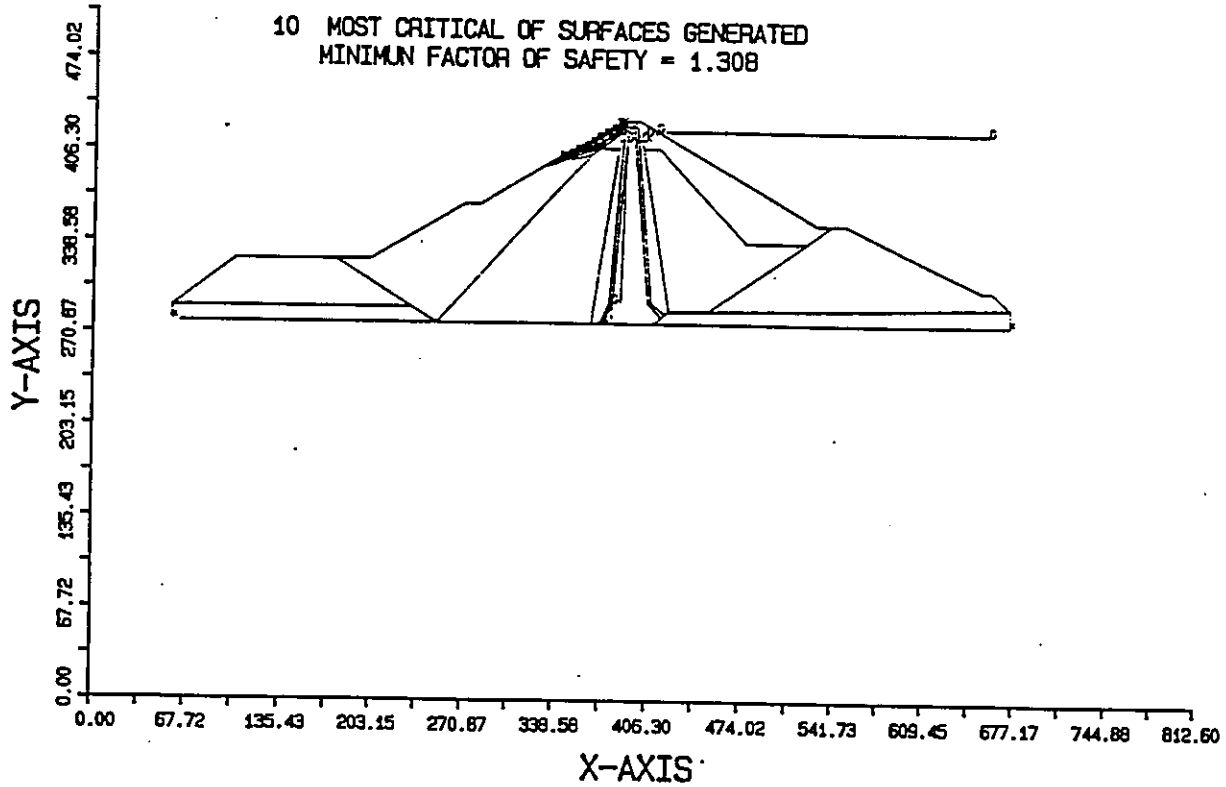

Figure 13

EL INFIERNILLO DAM

DOWNSTREAM SLOPE; SLIDING MASSES EXTENDING AT Y/H = 1/2

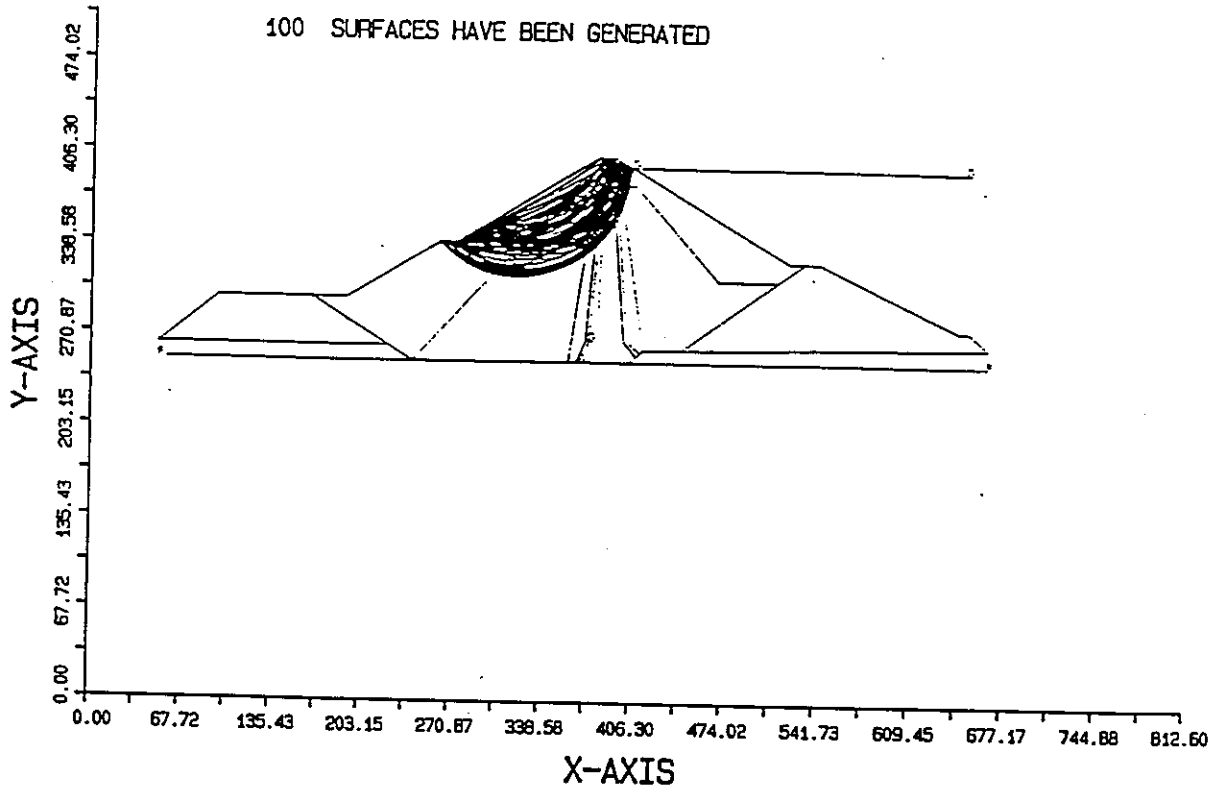

STATIC ANALYSIS

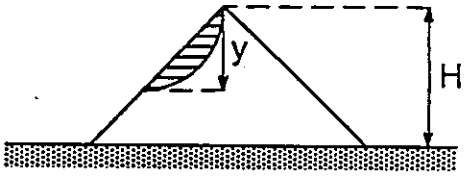

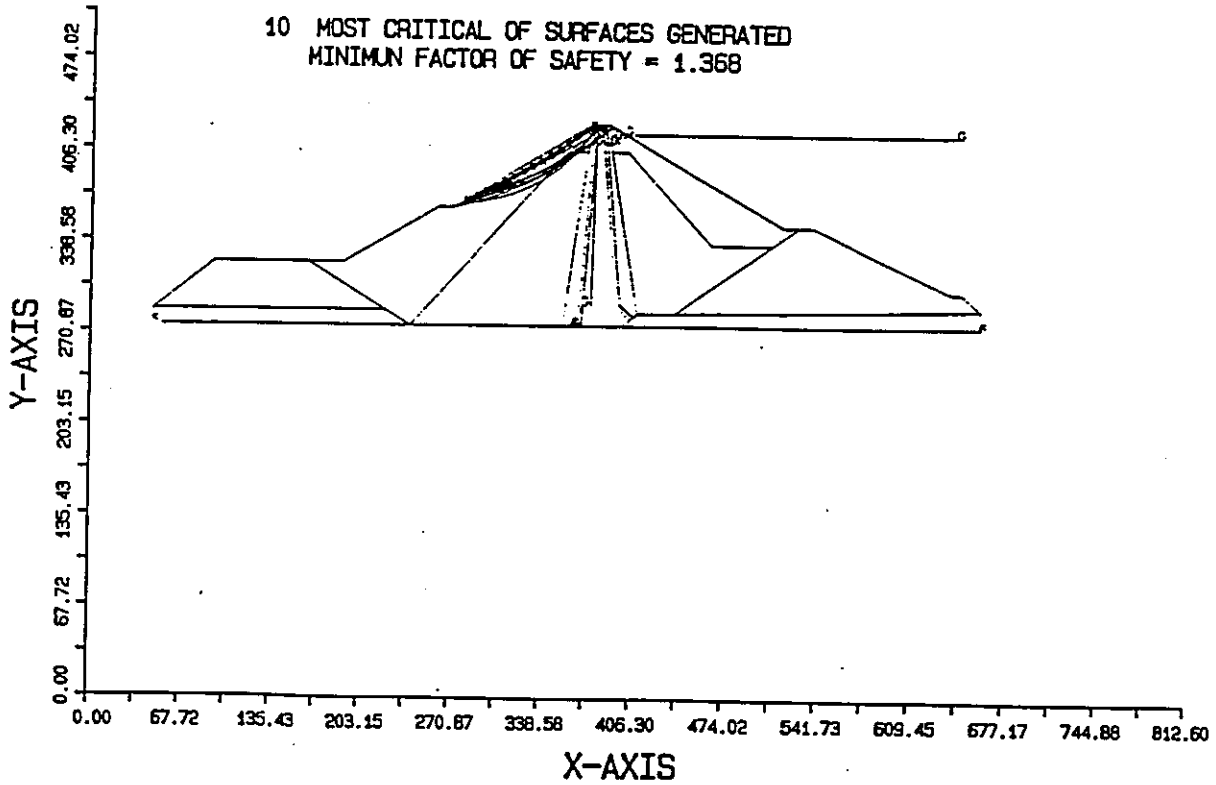

Figure 14

EL INFIERNILLO DAM

DOWNSTREAM SLOPE; SLIDING
MASSES EXTENDING AT Y/H = 3/4

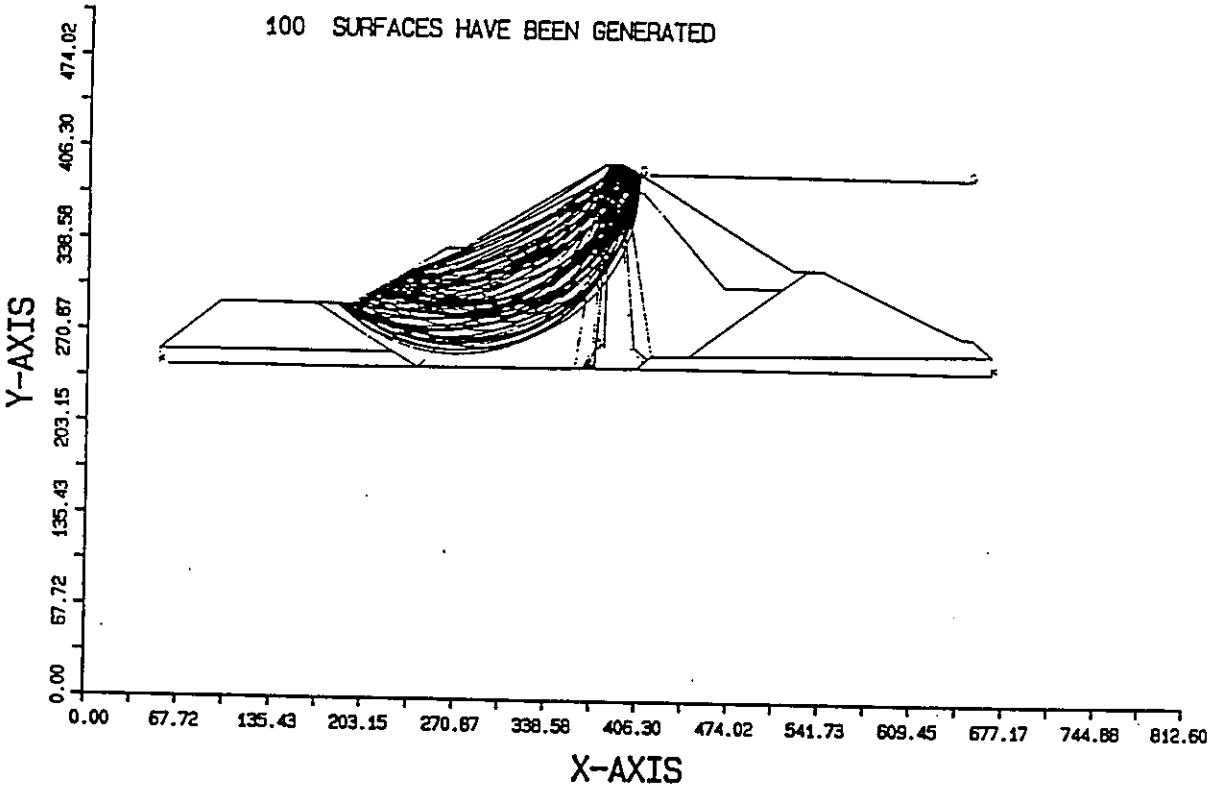

STATIC ANALYSIS

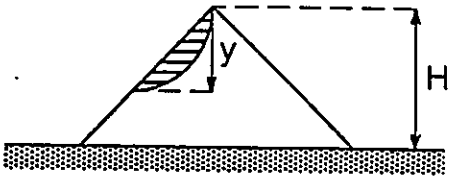

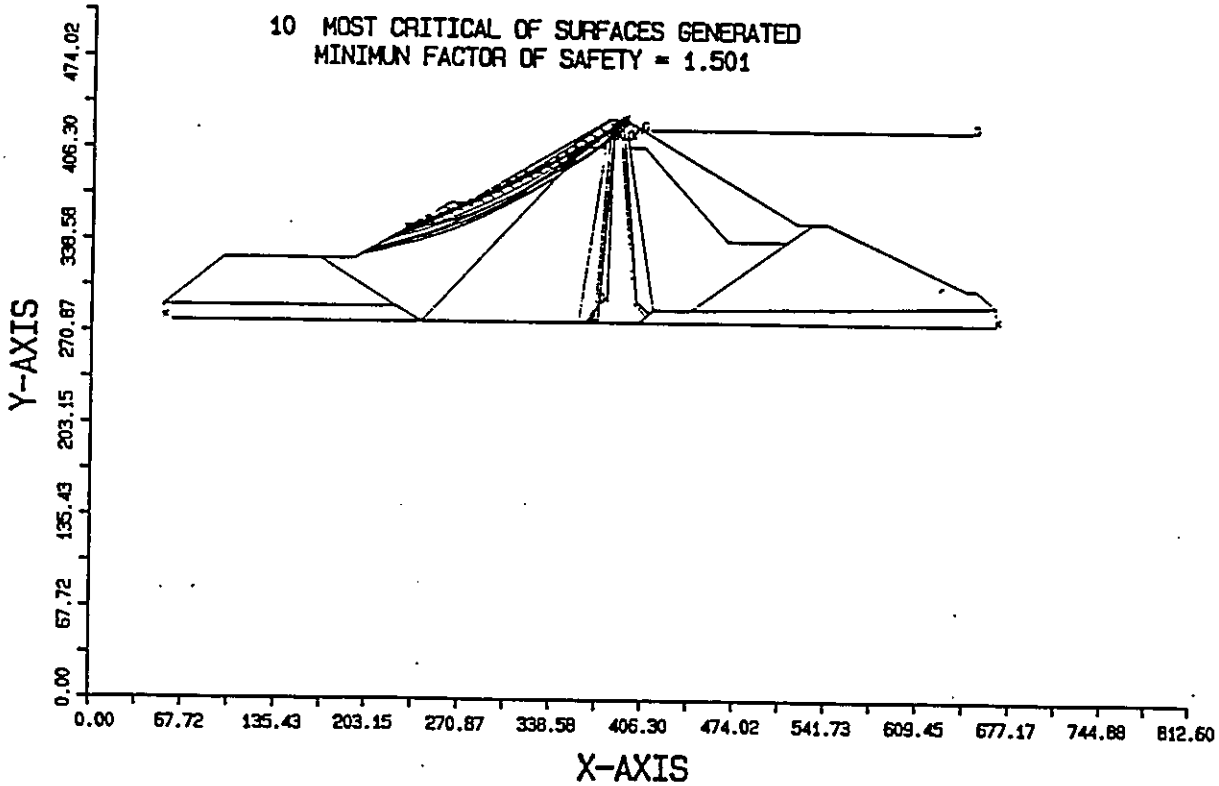

Figure 15

EL INFIERNILLO DAM

DOWNSTREAM SLOPE; SLIDING MASSES EXTENDING AT Y/H = 1

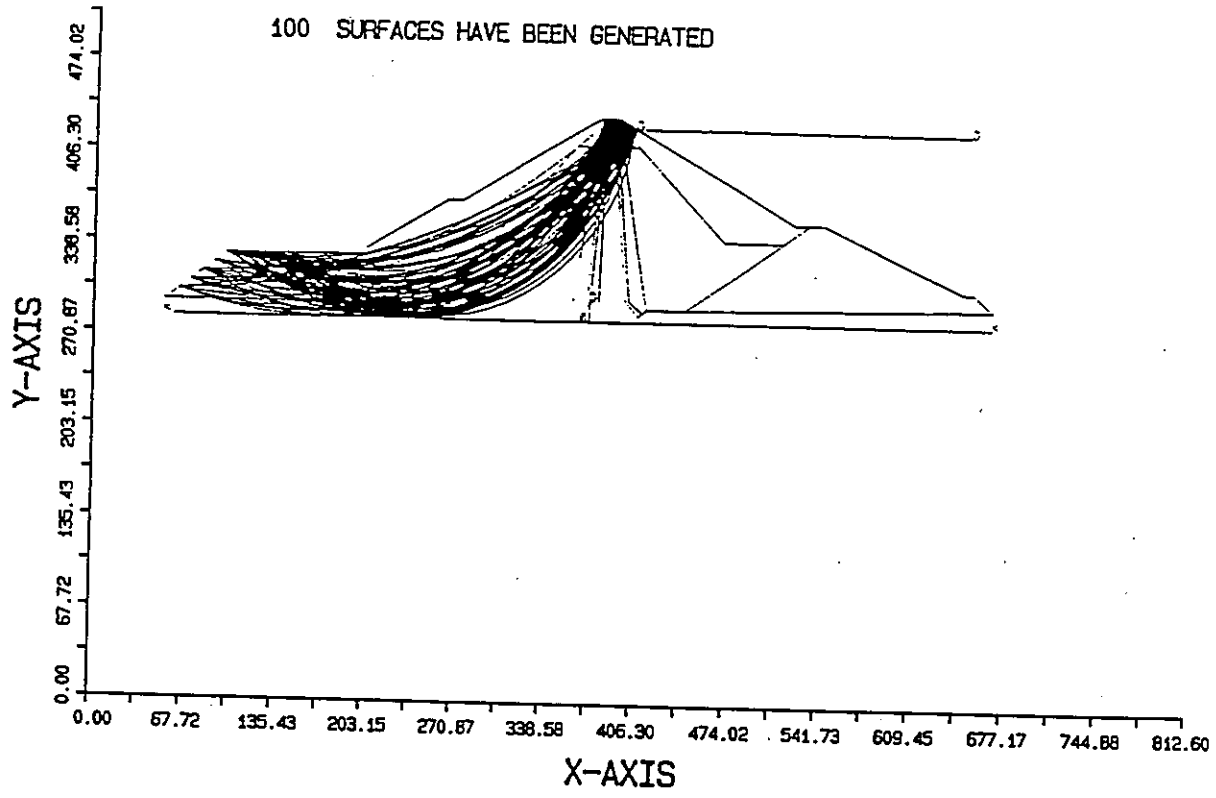

STATIC ANALYSIS

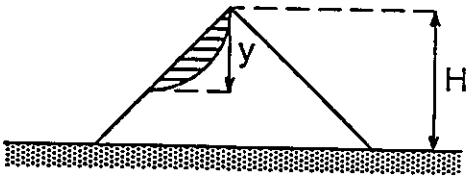

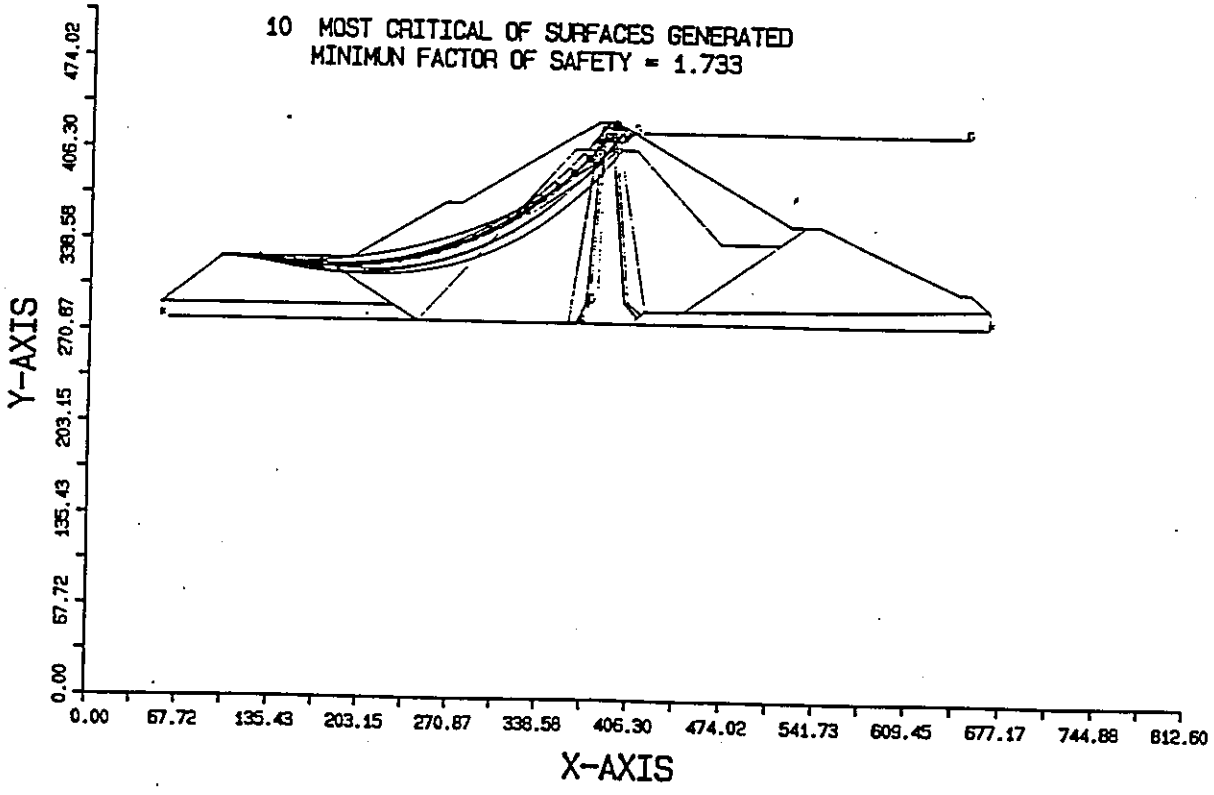

Figure 16

EL INFIERNILLO DAM

DOWNSTREAM SLOPE

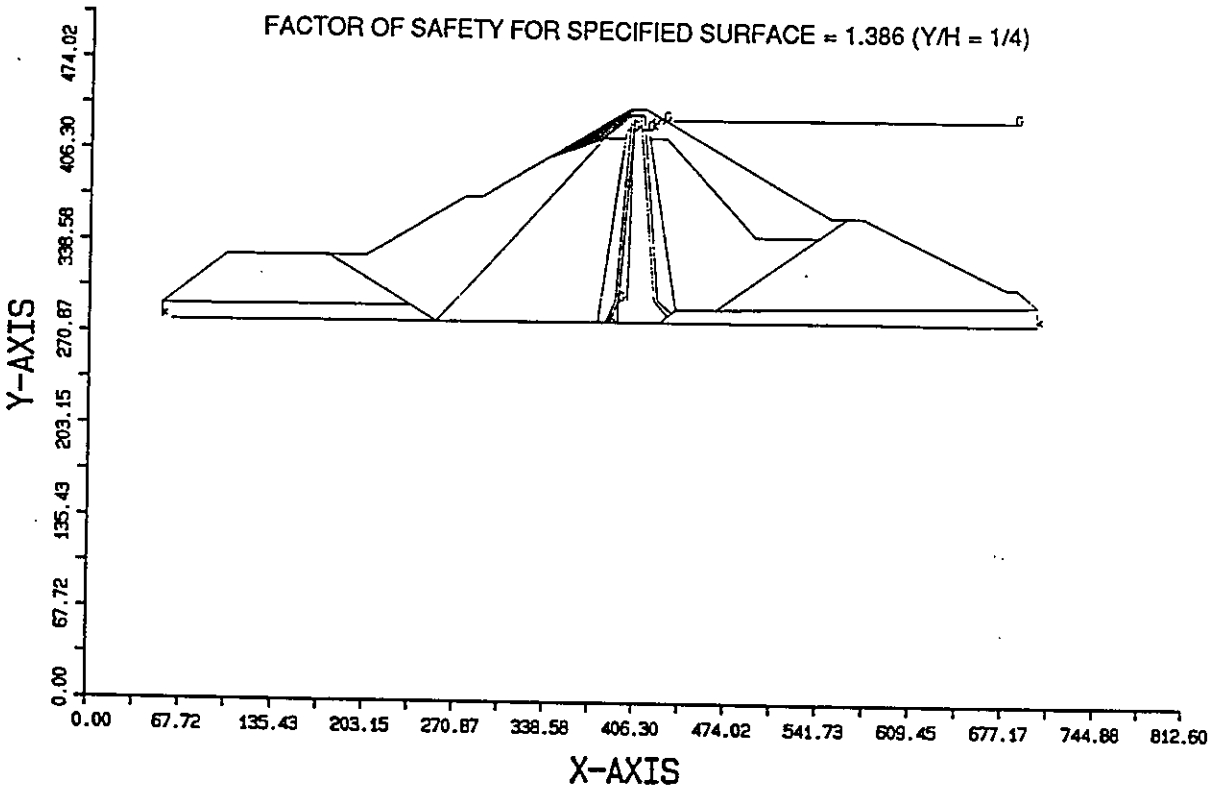

STATIC ANALYSIS

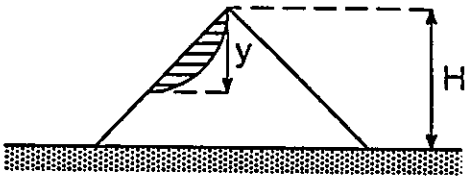

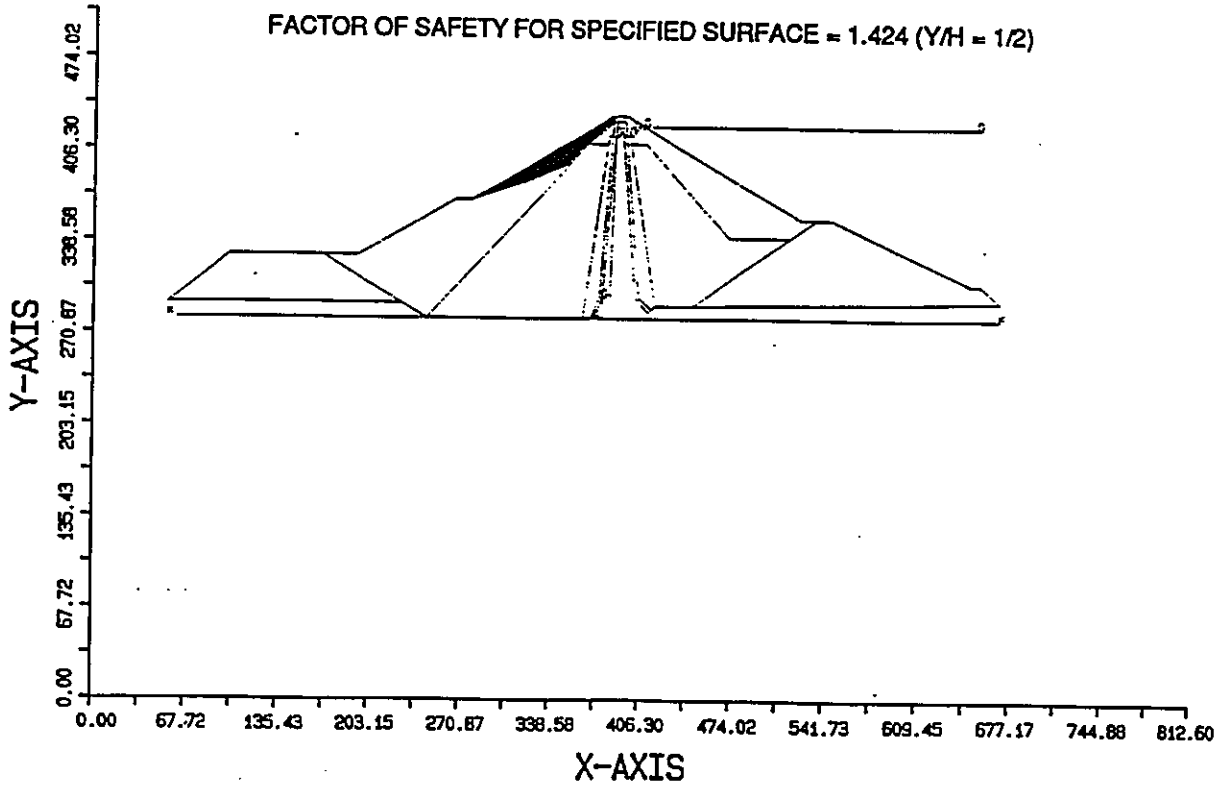

Figure 17

EL INFIERNILLO DAM

DOWNSTREAM SLOPE

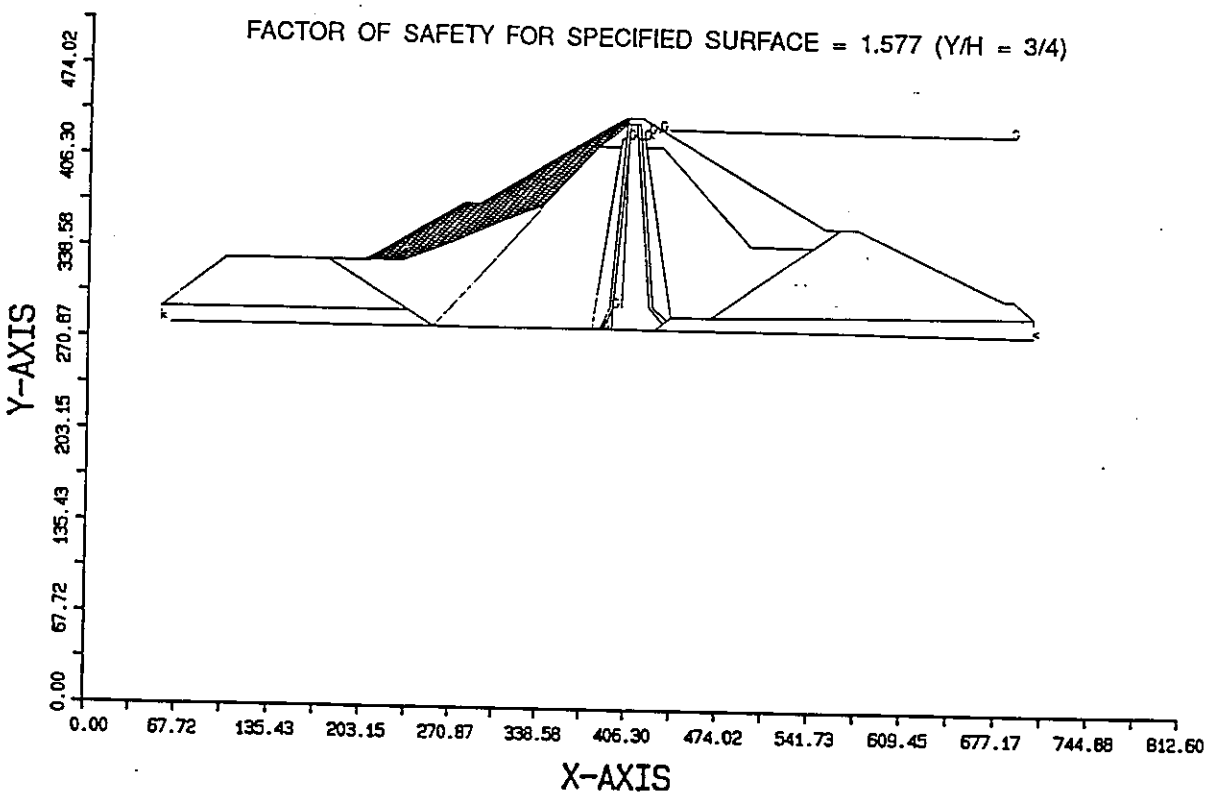

STATIC ANALYSIS

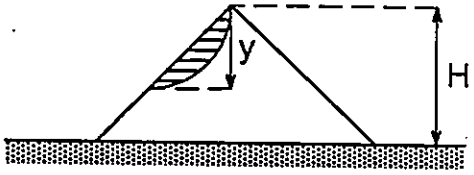

Figure 18

EL INFIERNILLO DAM

DOWNSTREAM SLOPE
PSEUDOSTATIC ANALYSIS:

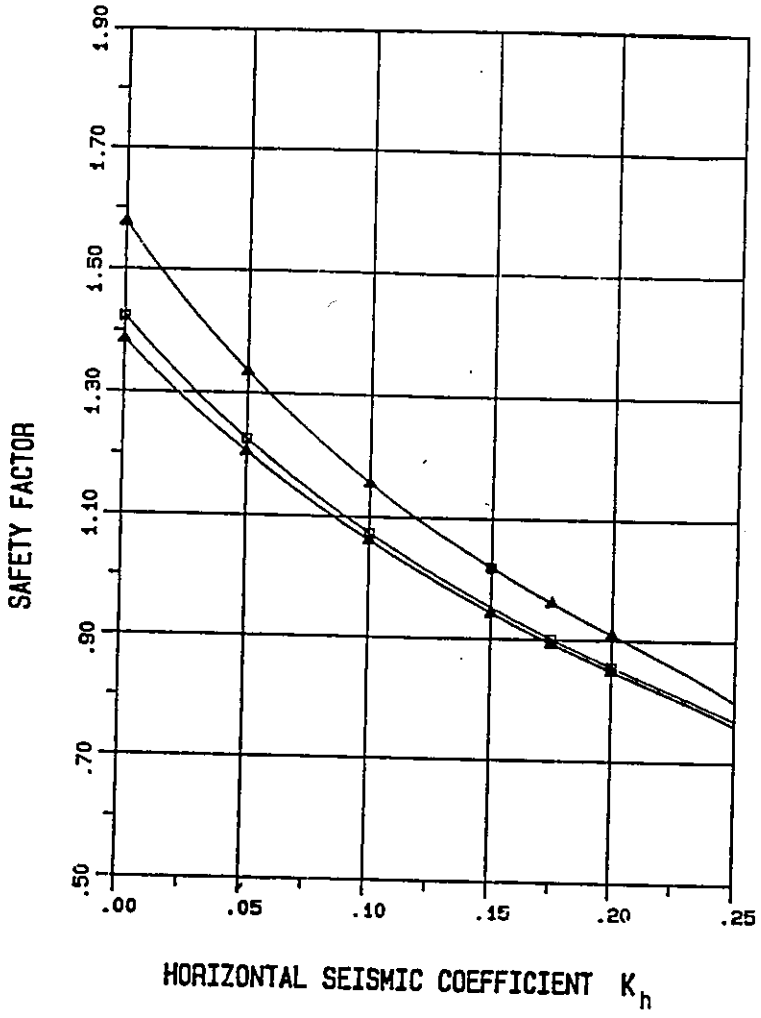

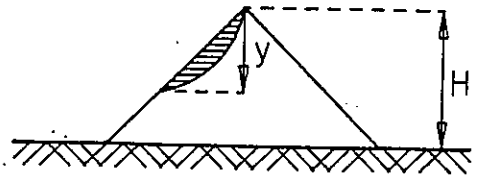

TOE DEPTH OF SLIDING SURFACES:

y/H = 1/4 △

y/H = 1/2 □

y/H = 3/4 ▲

y/H = 1 ○

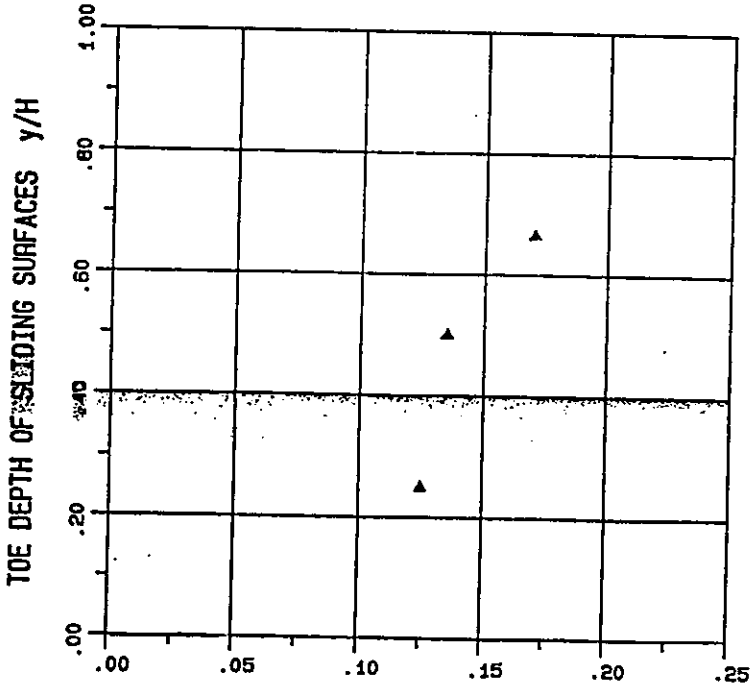

▲ CALCULATED VALUES

Figure 19

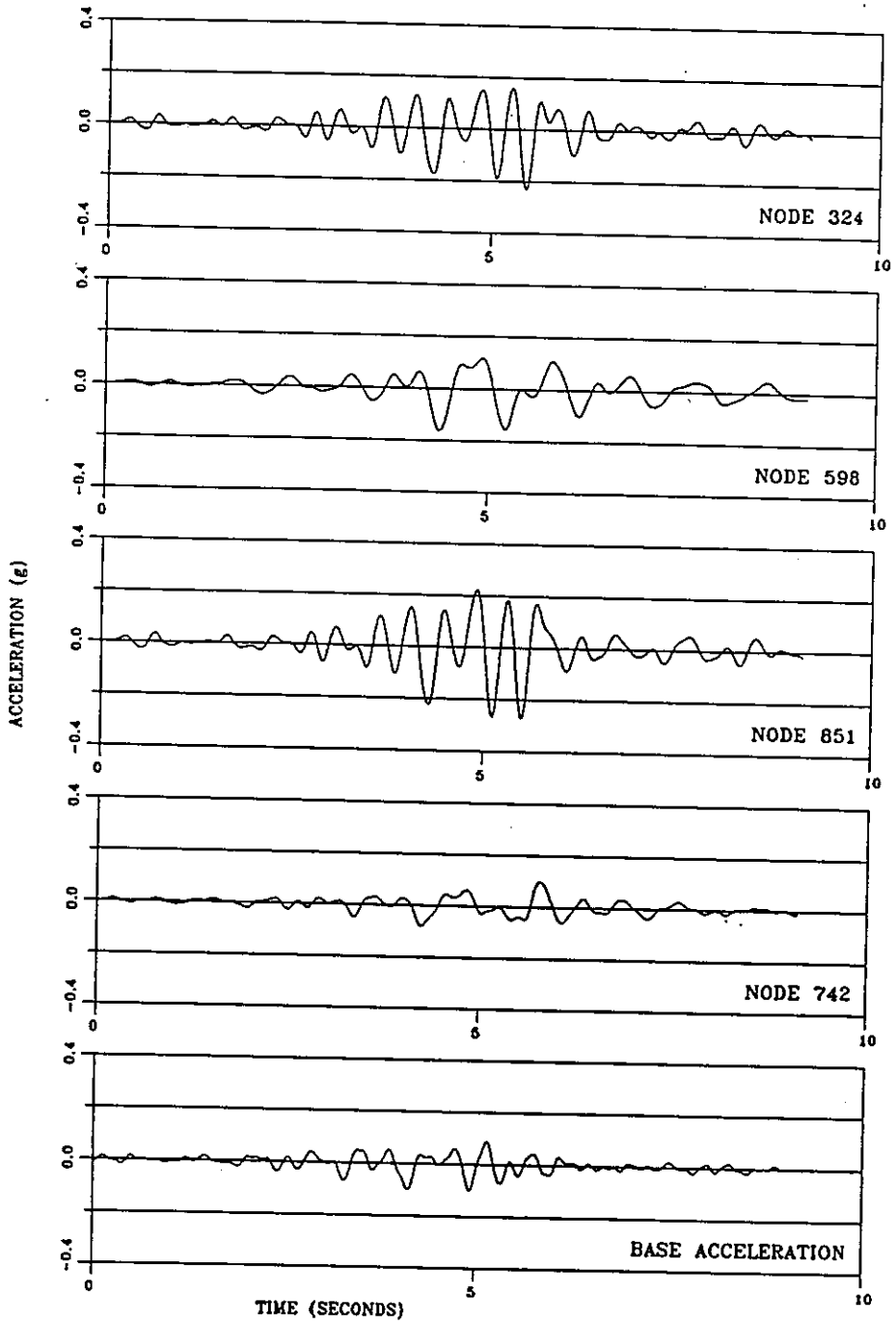

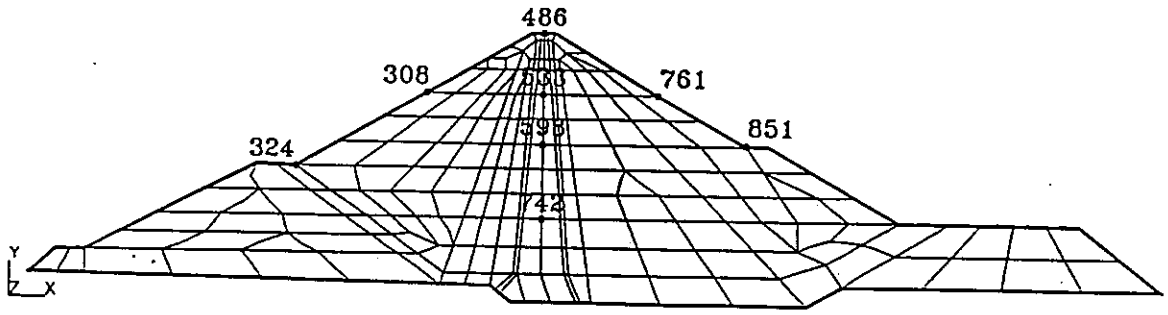

Input ground motion EQ1 – Time histories of accelerations for various selected nodal points

Figure 20

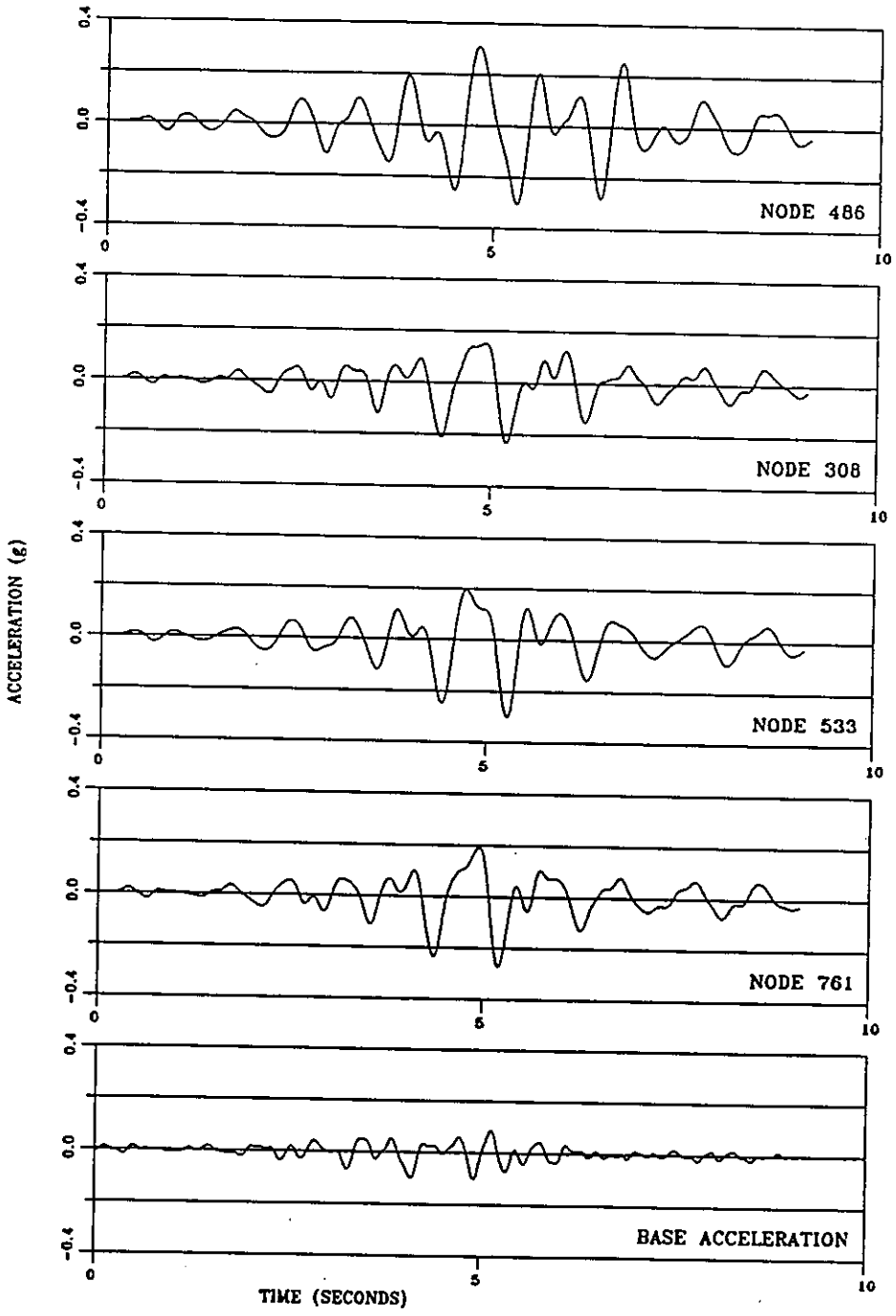

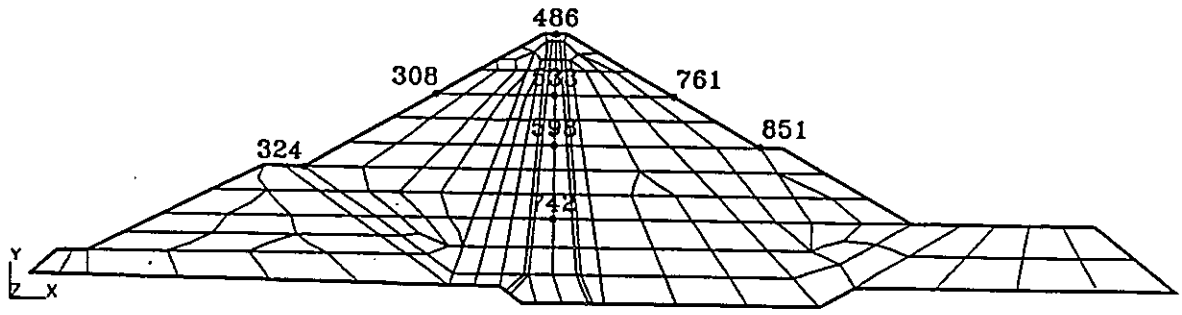

Input ground motion EQ1 – Time histories of accelerations for various selected nodal points

Figure 21

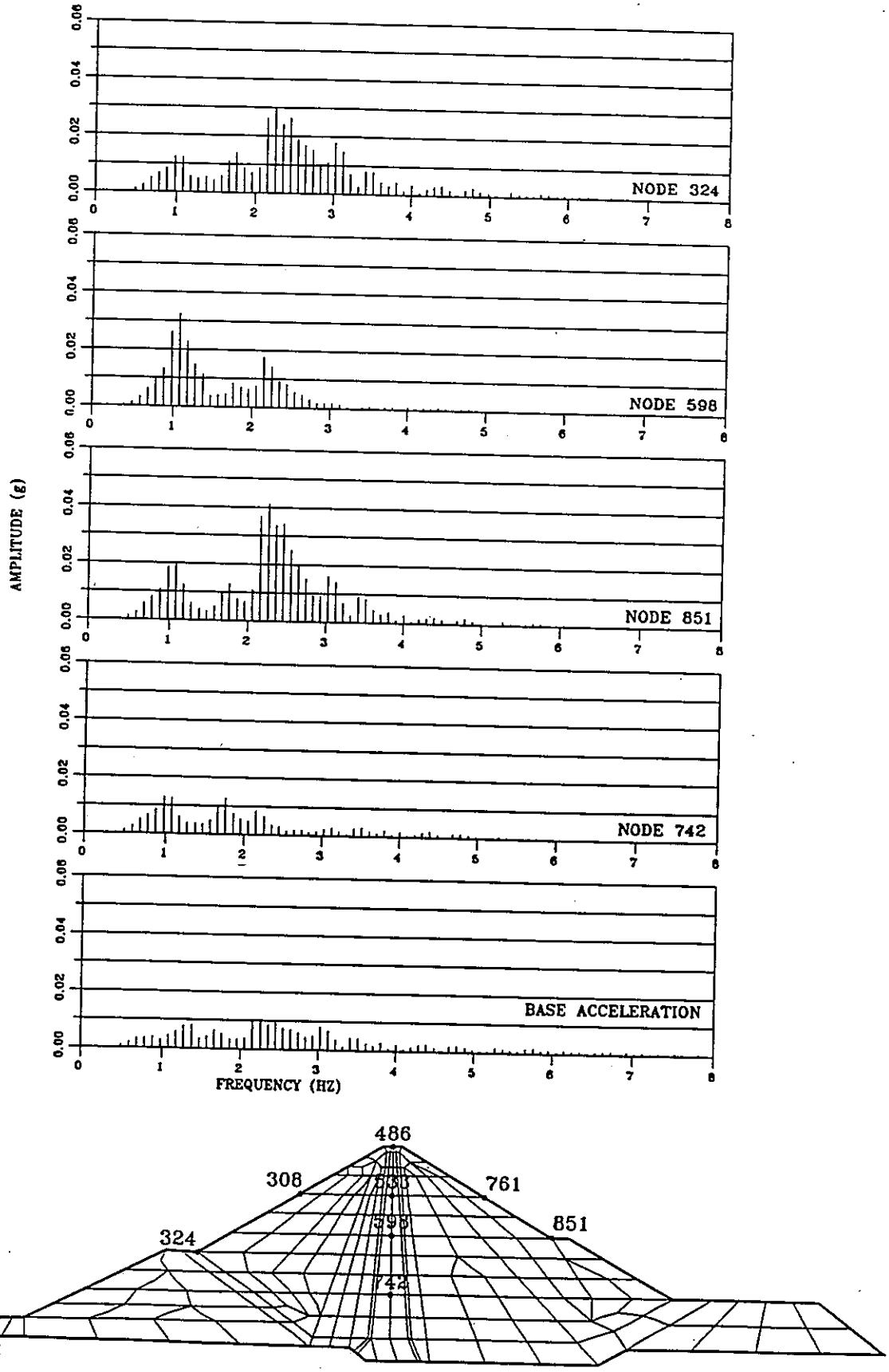

Input ground motion EQ1 – Fourier Spectrum of nodal acceleration time histories

Figure 22

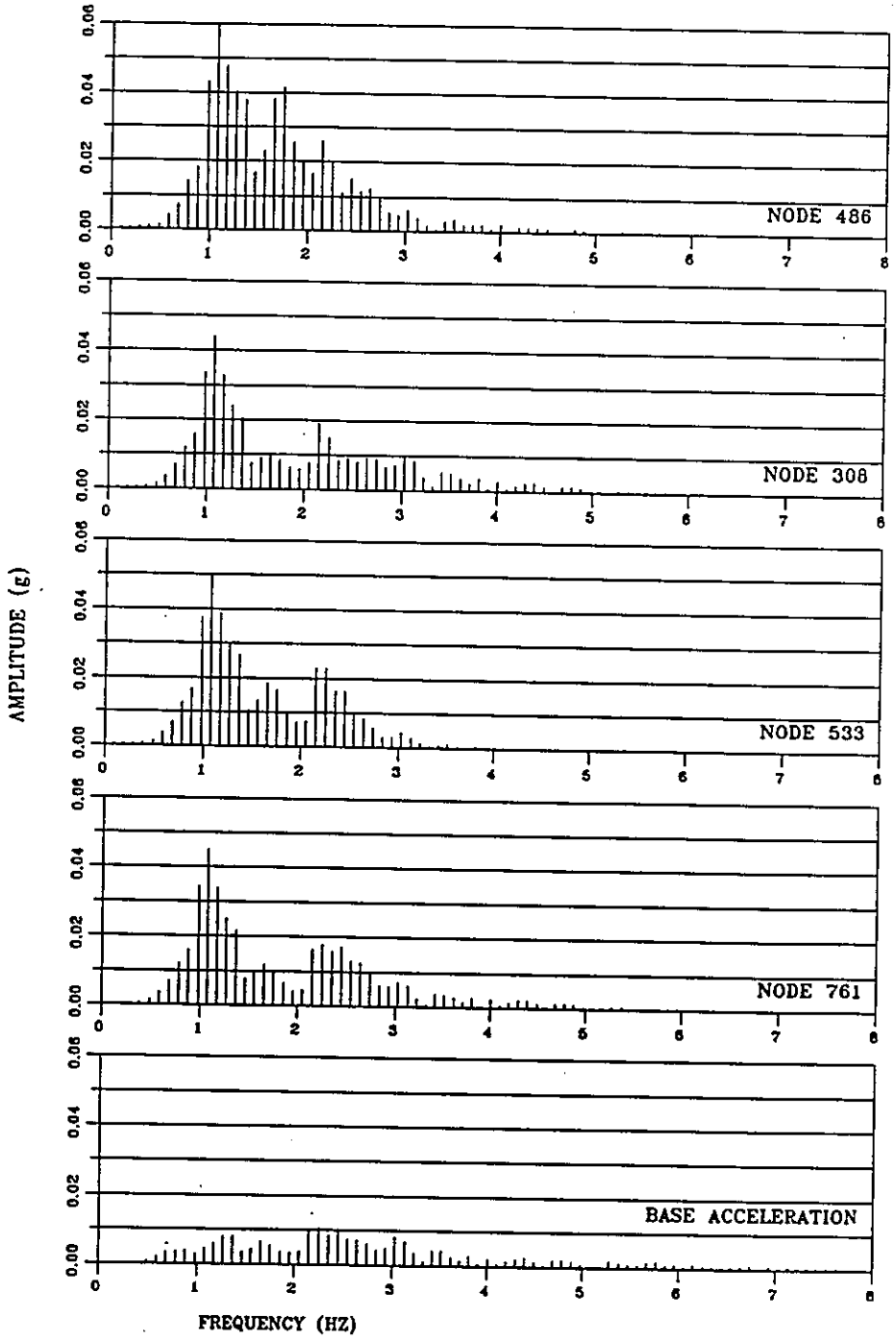

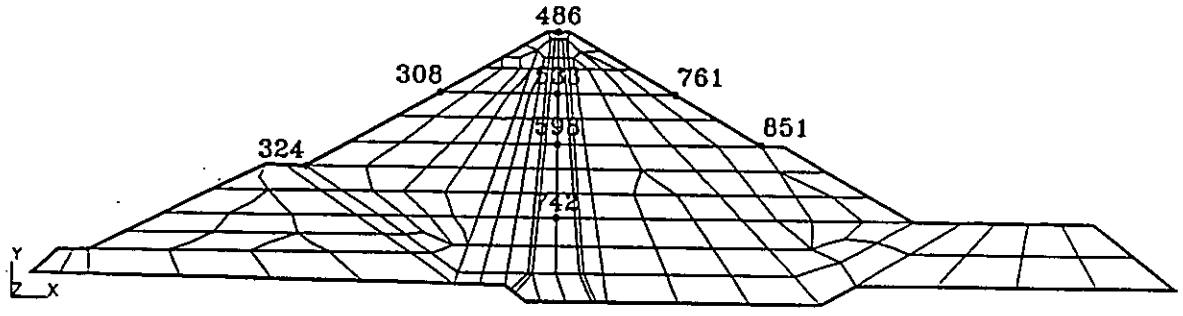

Input ground motion EQ1 – Fourier Spectrum of nodal acceleration time histories

Figure 23

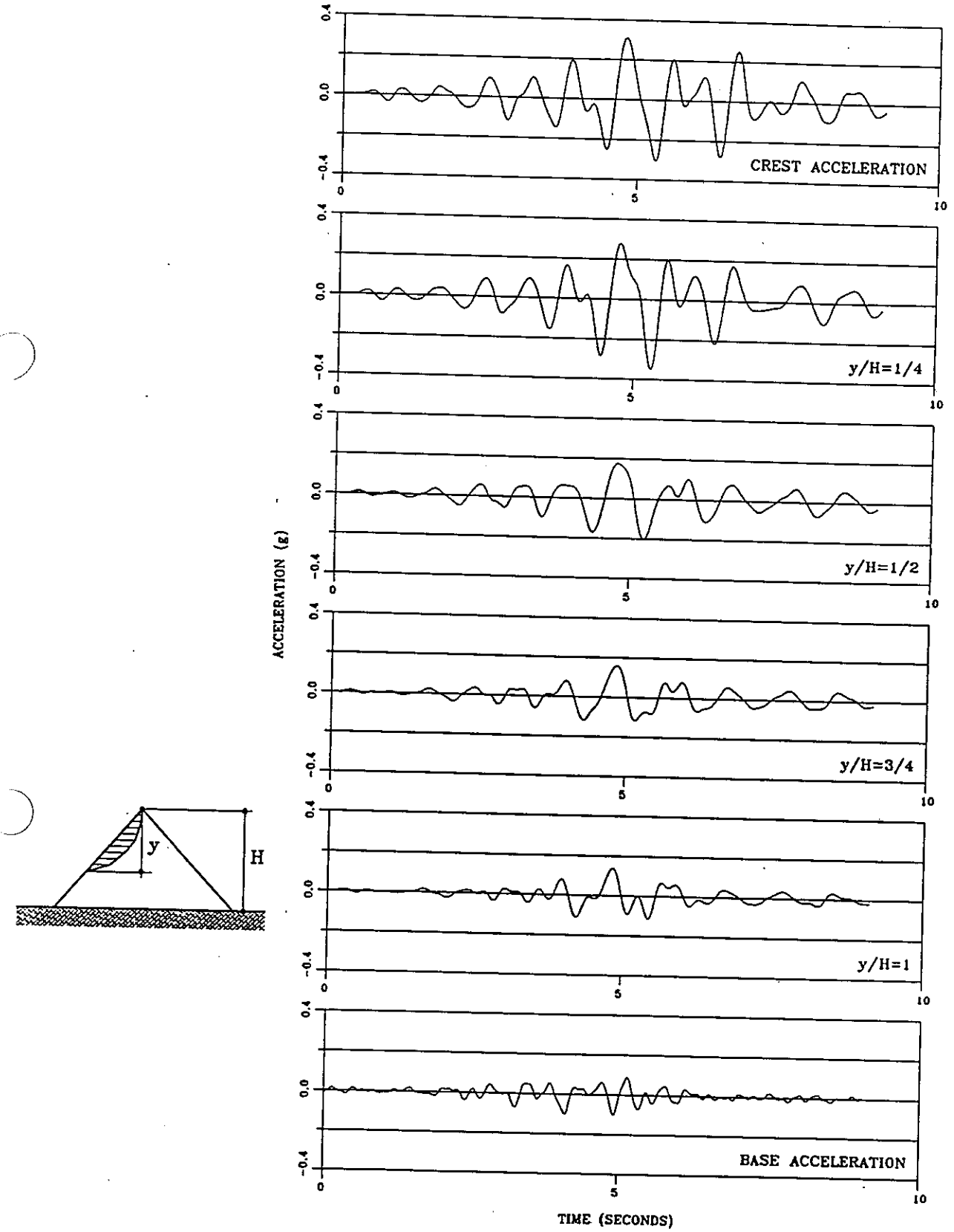

Input ground motion EQ1 – Upstream slope – Time histories of average accelerations for potential sliding masses extending at different depths

Figure 24

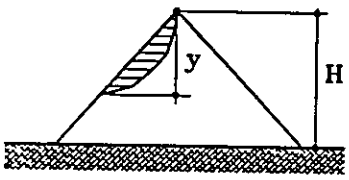

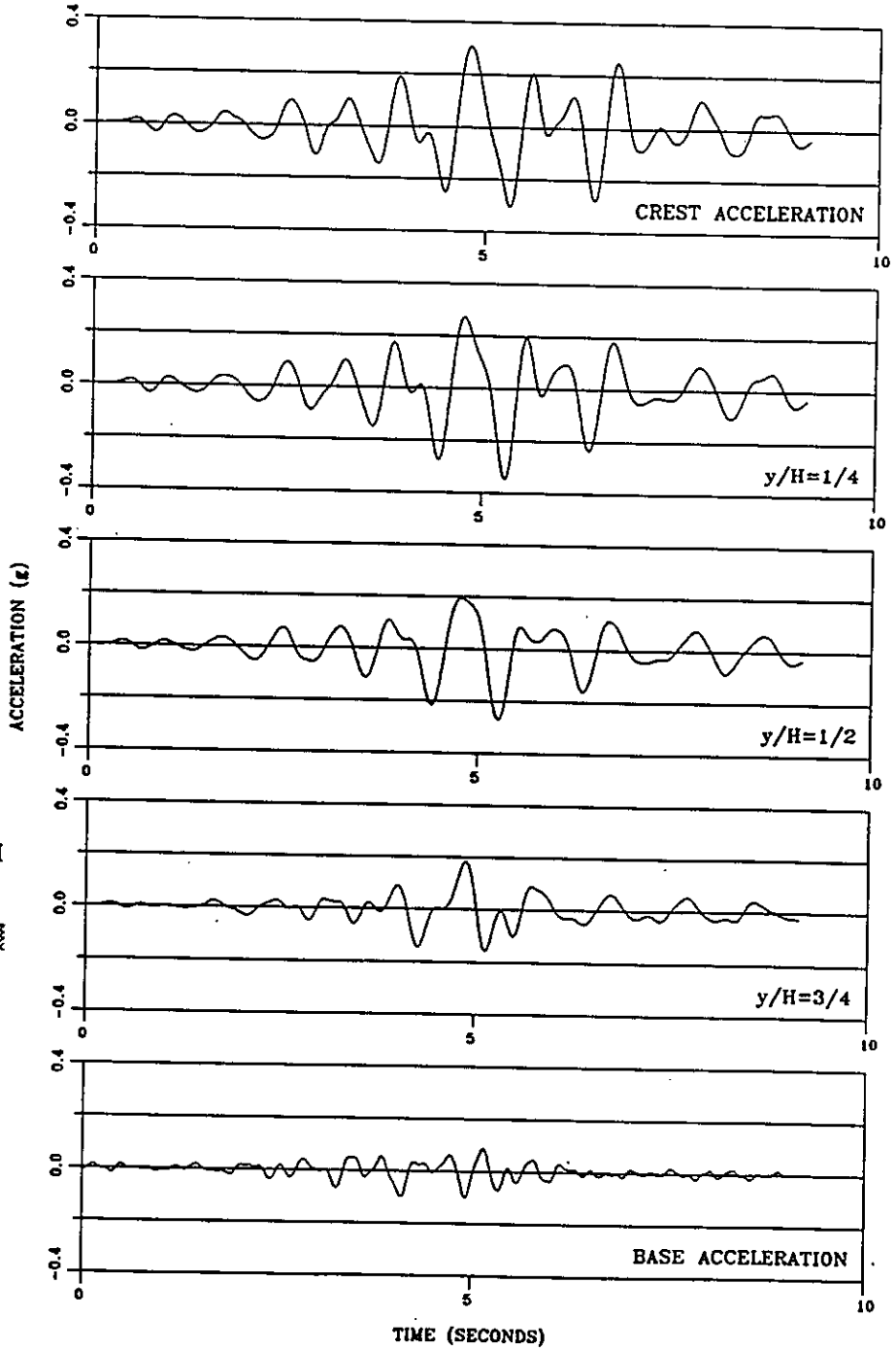

Input ground motion EQ1 – Downstream slope – Time histories of average accelerations for potential sliding masses extending at different depths

Figure 25

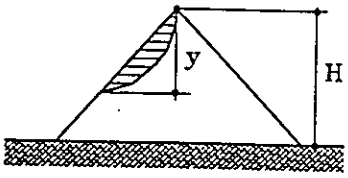

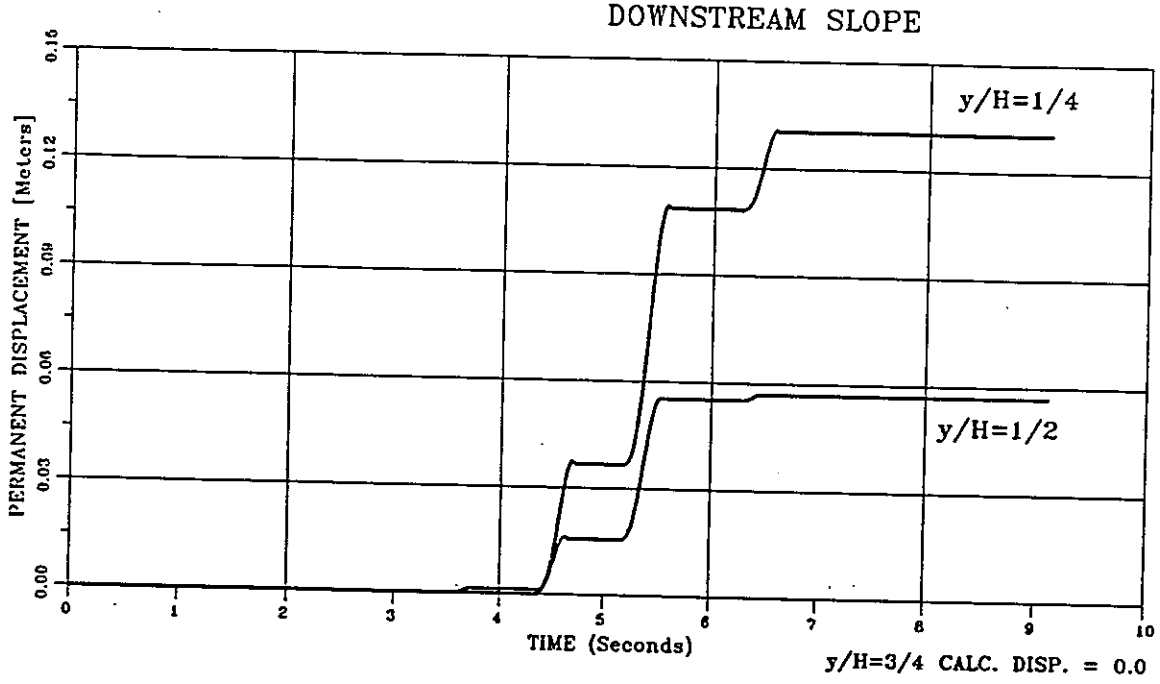

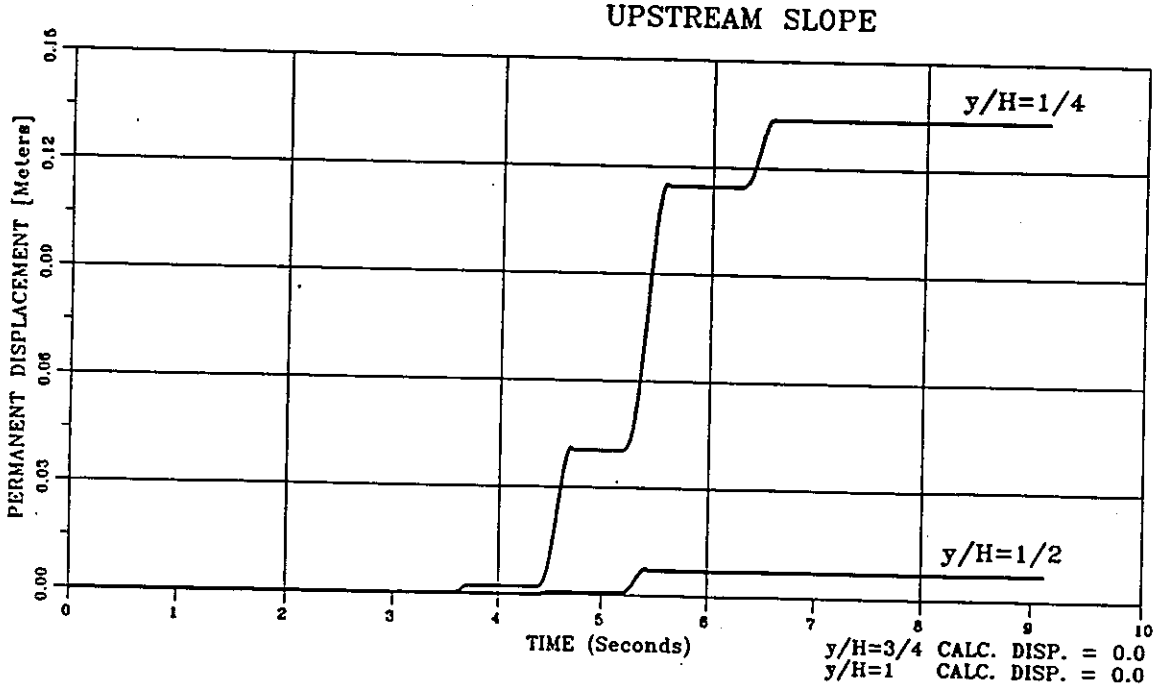

Input ground motion EQ1 – Calculated permanent displacements

FIGURE 26

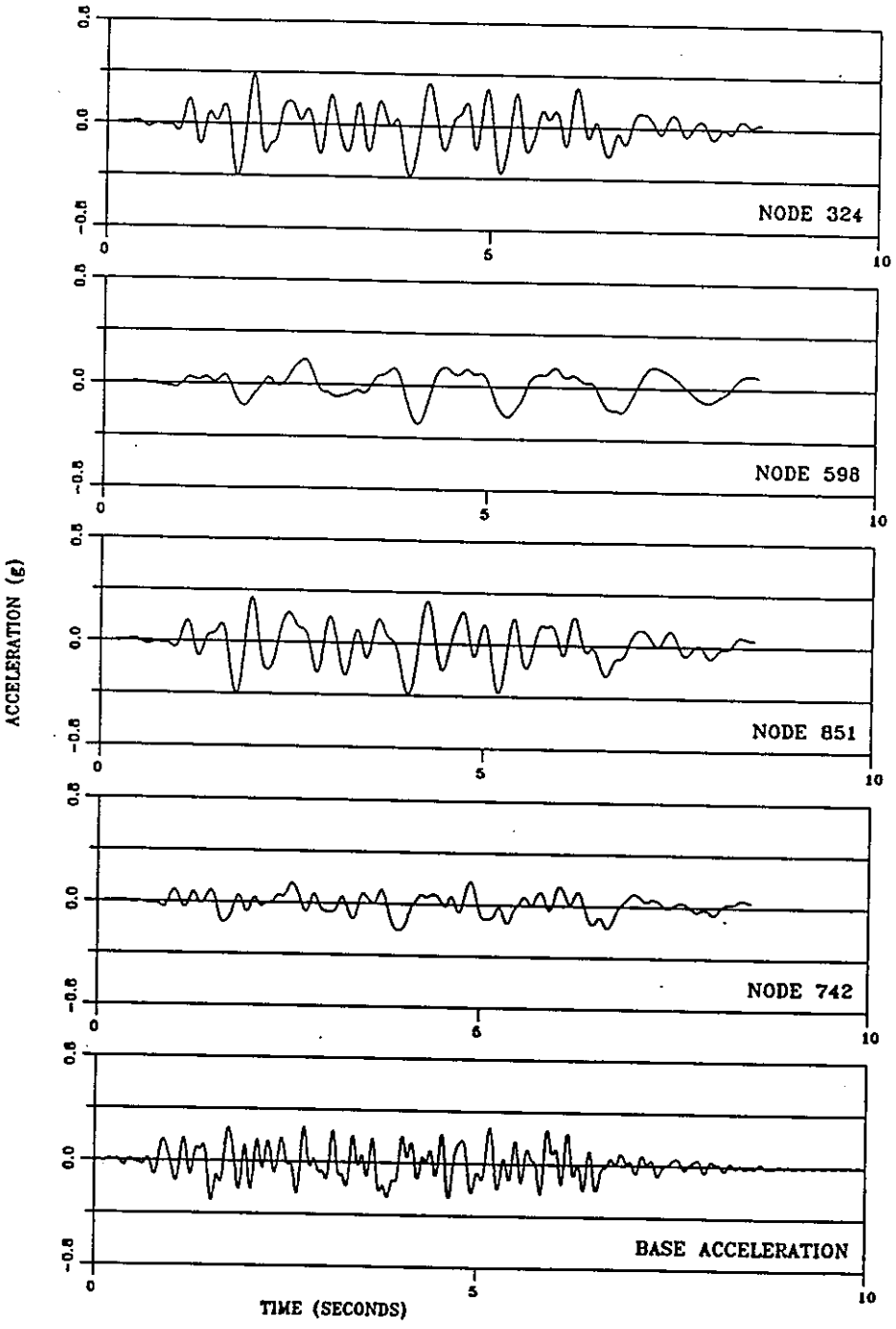

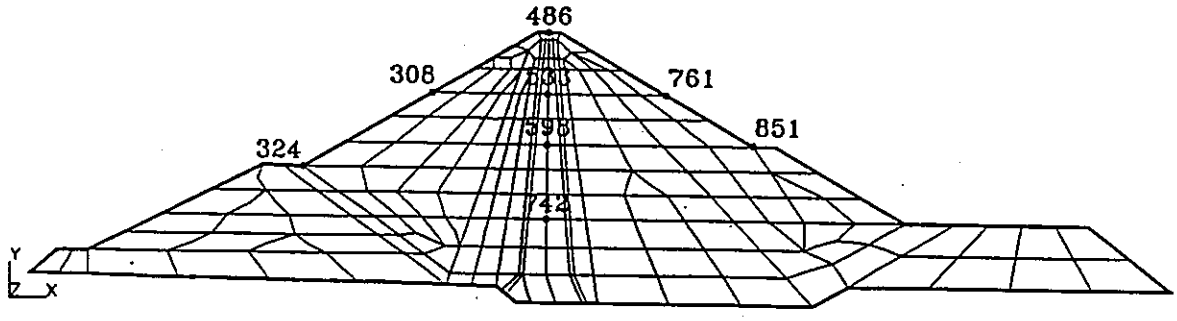

Input ground motion EQ3 – Time histories of accelerations for various selected nodal points

Figure 27

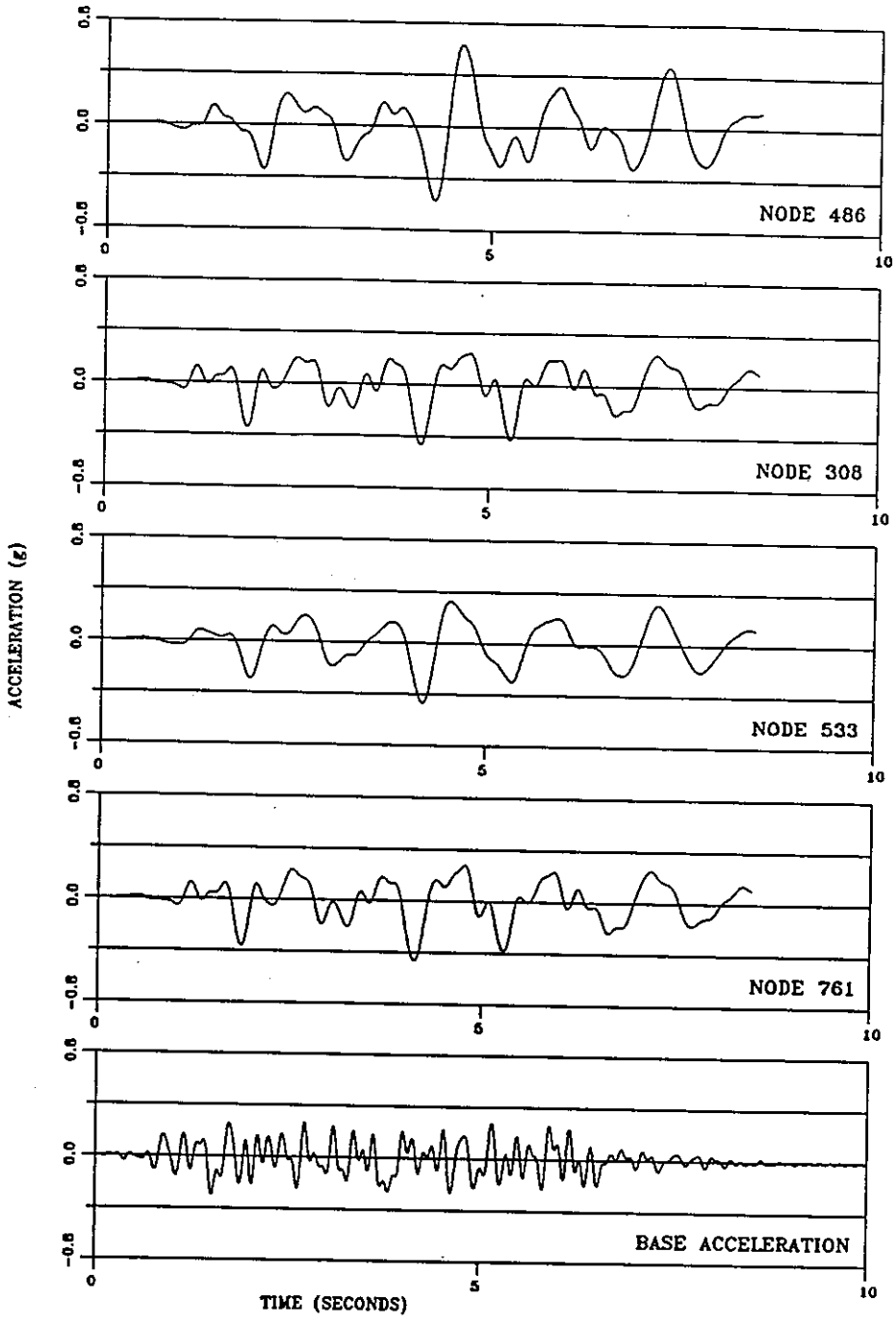

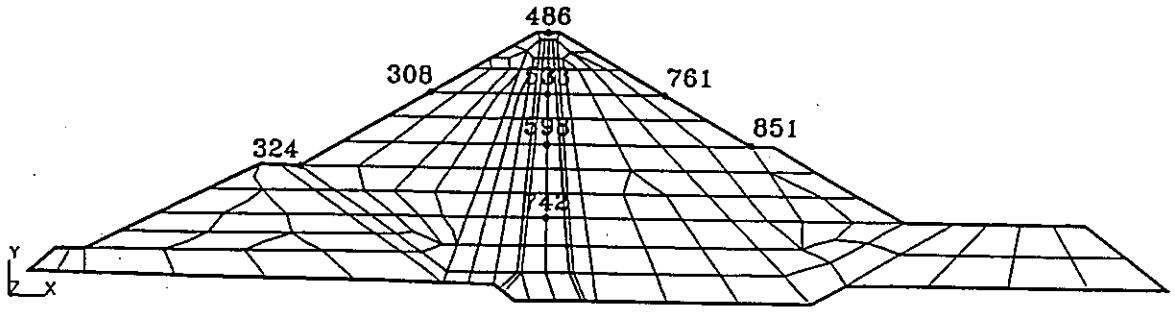

Input ground motion EQ3 – Time histories of accelerations for various selected nodal points

Figure 28

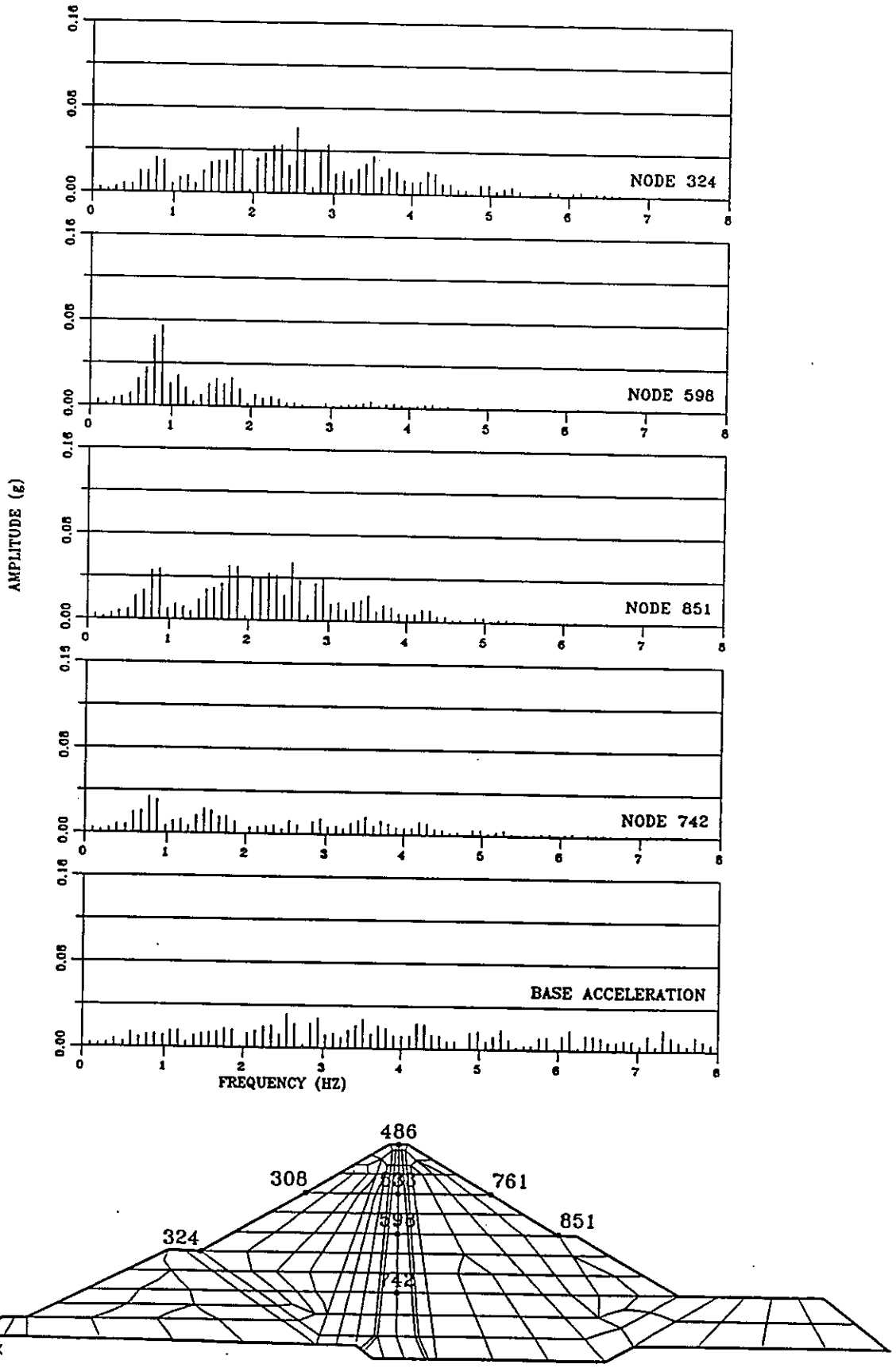

Input ground motion EQ3 – Fourier Spectrum of nodal acceleration time histories

Figure 29

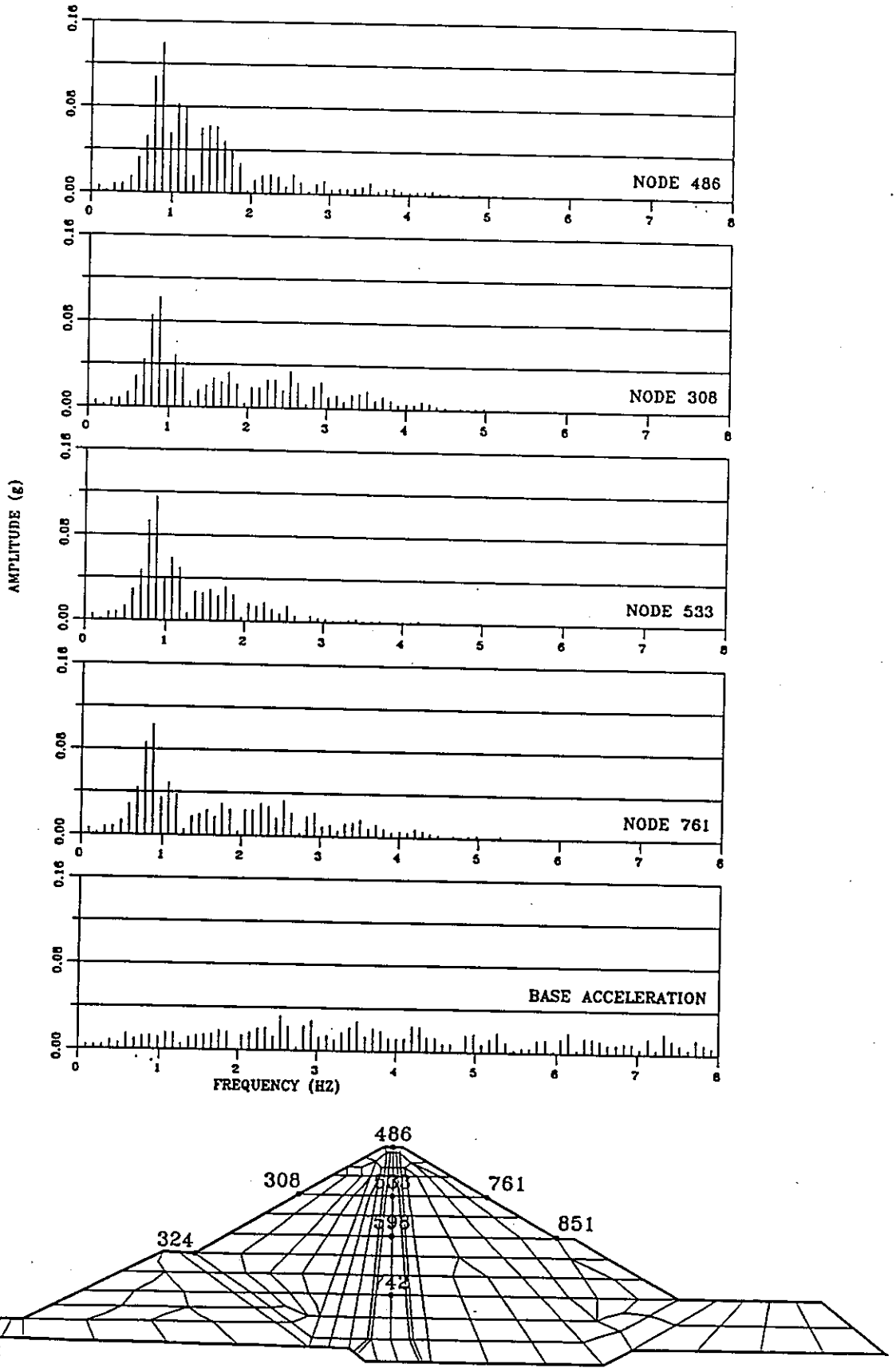

Input ground motion EQ3 – Fourier Spectrum of nodal acceleration time histories

Figure 30

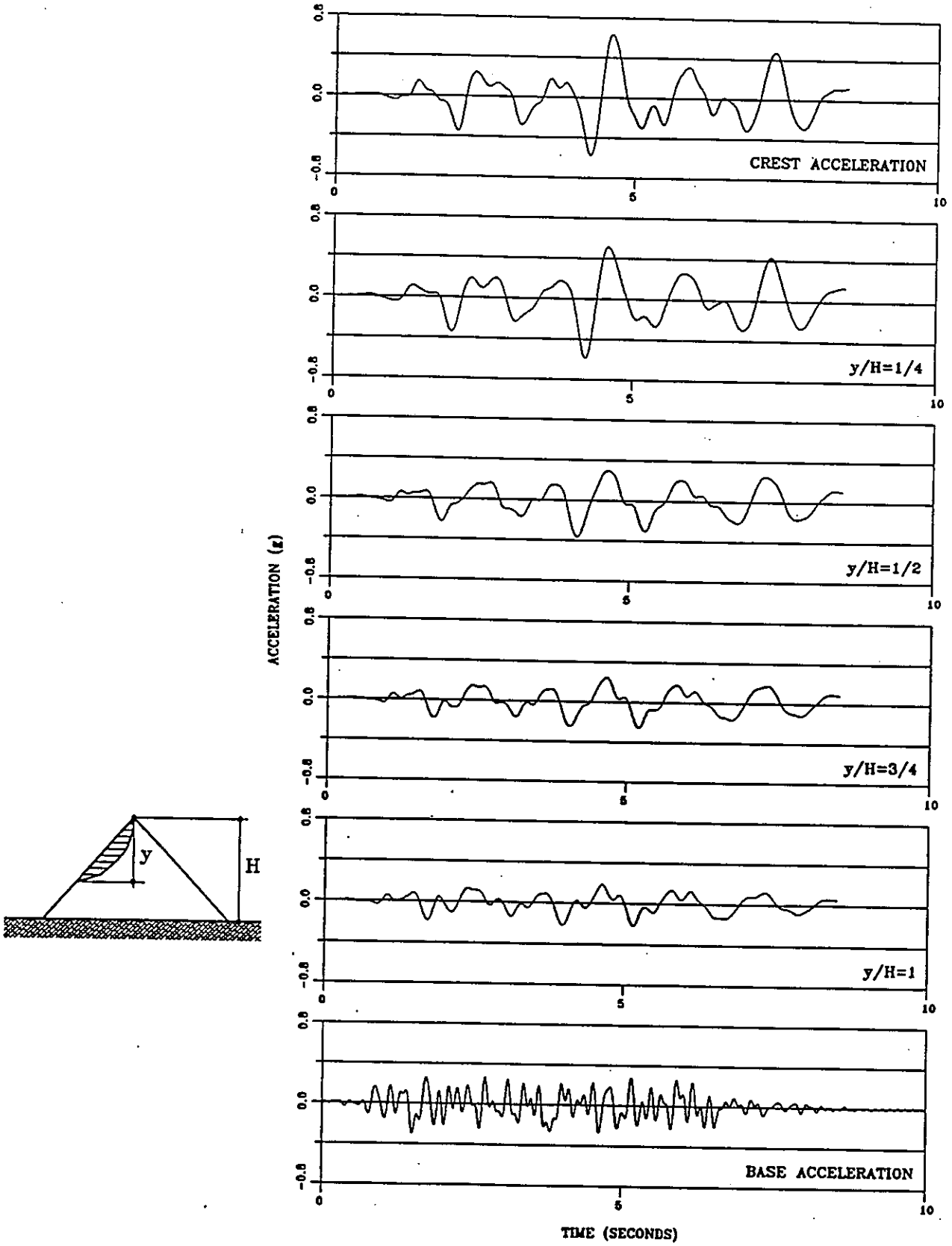

Input ground motion EQ3 – Upstream slope – Time histories of average accelerations for potential sliding masses extending at different depths

Figure 31

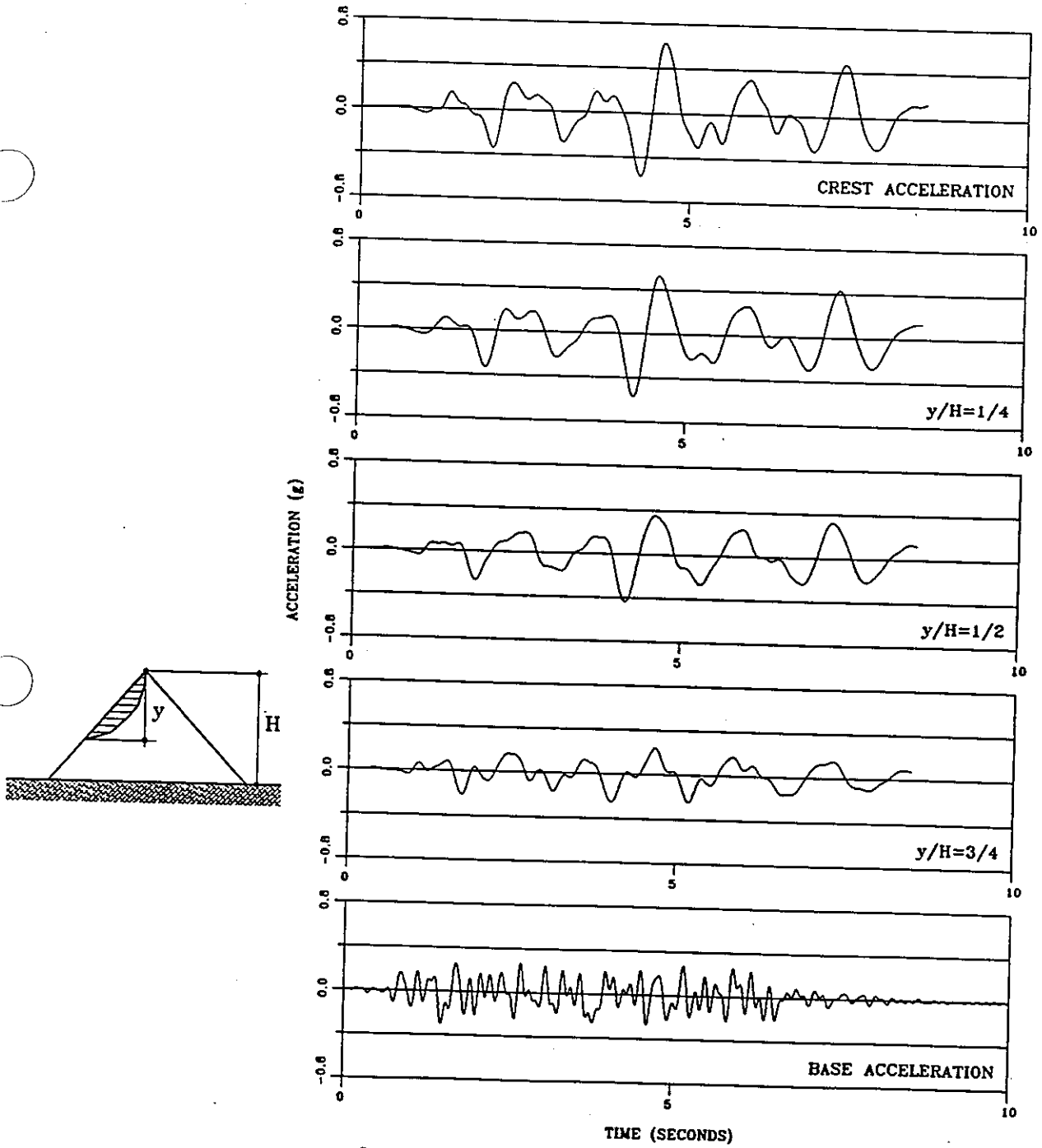

Input ground motion EQ3 – Downstream slope – Time histories of average accelerations for potential sliding masses extending at different depths

Figure 32

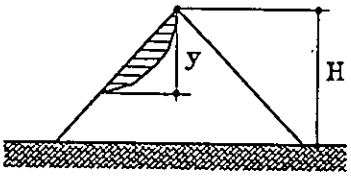

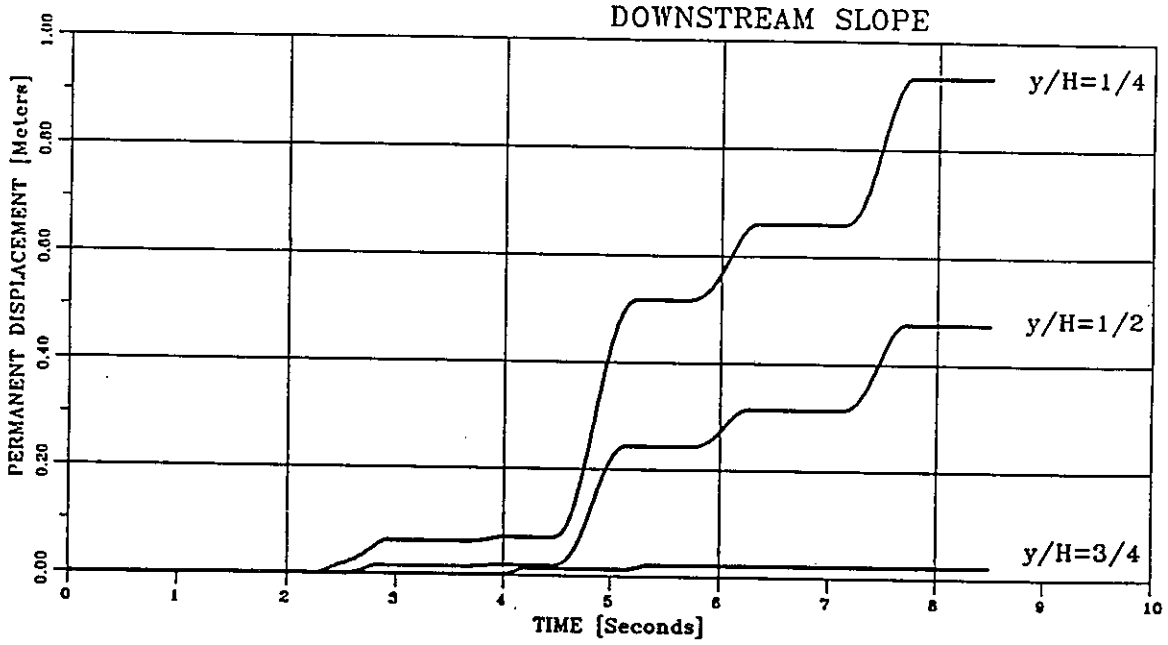

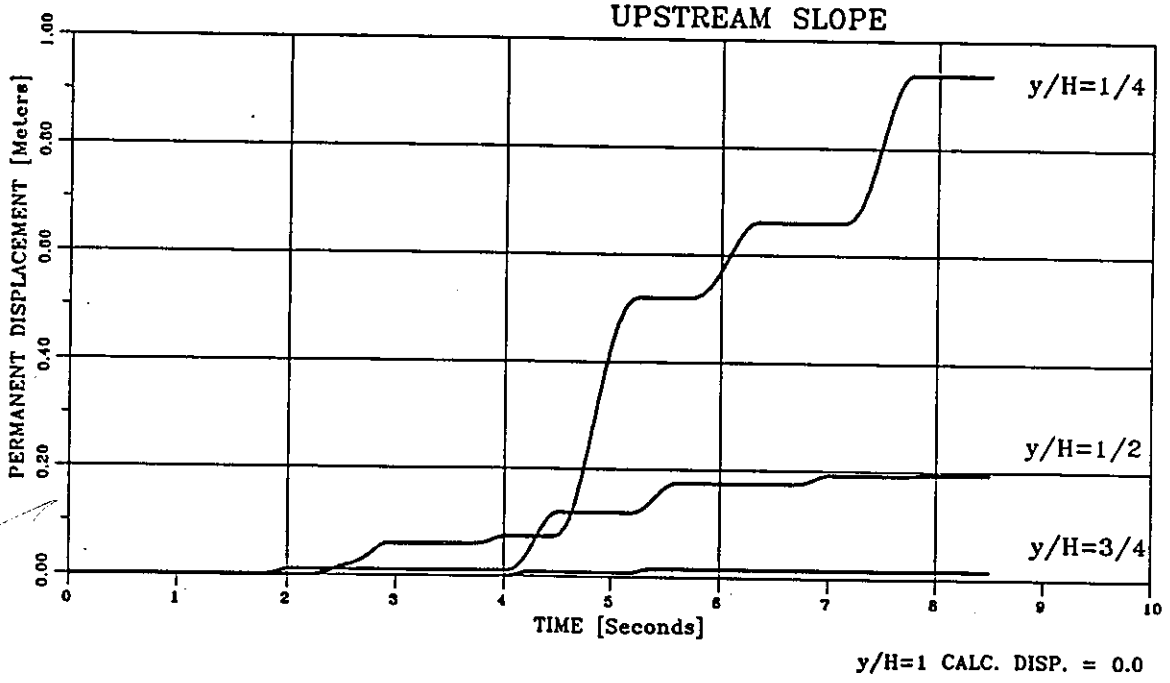

y/H=1 CALC. DISP. = 0.0

Input ground motion EQ3 – Calculated permanent displacements

FIGURE 33

NONLINEAR DYNAMIC RESPONSE OF EL INFIERNILLO DAM

Amjad A. Bangash* and David K. Vaughan**

Introduction

The approach and results of the numerical simulation of earthquake response of El Infiernillo Dam in Mexico are discussed in this paper. The study was part of the "First Benchmark Workshop on Numerical Analysis of Dams," organized by the International Commission on Large Dams (ICOLD) and ISMES S.p.A. El Infiernillo Dam is a well instrumented, 150m high zoned rockfill dam with a central clay core. The response of this dam to the magnitude 7.6 (Richter) earthquake of March 14, 1979 has been presented in detail by Resendiz et al[1]. The predicted response during this earthquake event will be discussed in detail in this paper, followed by a brief summary of results obtained for additional earthquake records provided by ICOLD/ISMES.

A nonlinear dynamic finite element code FLEX[2] was used to perform the analysis. This code was developed to address a number of geotechnical and soil-structure interaction related problems associated with seismic shaking or explosive loading. FLEX uses an explicit second order central difference scheme to perform integration in the time domain. Static loading, including gravity loads, can also be applied within the program using either dynamic relaxation or conjugate gradient techniques.

The constitutive relationships are based on incremental plasticity theory embodied in the

---

* Geotechnical Engineer, Harza Engineering Company
150 S. Wacker Dr., Chicago, IL. 60606, USA.

** Principal, Weidlinger Associates
4410 El Camino Real, Suite 110, Los Altos, Ca. 94022, USA.

cap family of constitutive models[3,4,5]. These models were developed to provide stable, unique and continuous solutions; characteristics which are very important for multi-dimensional dynamic analyses. The specific model selected for this study will be referred to as viscous-cap model since it allows for viscoelastic representation of hysterectic damping for stress states within the yield surface of the model.

Approach

The practical application of a finite element program to conventional design and analysis problems greatly depends on its efficient interaction with the user. The importance of effective pre- and post-processing has already been emphasized over the last few years. In addition, nonlinear analyses impose additional requirements on a program's efficiency. First, the solution scheme should provide the results of desired accuracy in the least amount of clock time. This enables a designer to perform simple parametric studies to evaluate the stability of the solution and the affects of various input parameters. Secondly, the user should be able to define the constitutive model on the basis of conventional testing procedures. The explicit time integration scheme and the cap model employed in FLEX address both these issues.

Solution Scheme

The explicit algorithm is especially suited for nonlinear analysis of large two and three dimensional soil-structure interaction problems since a "stiffness matrix" is never formally assembled. The result is a significant reduction in processing time in comparison to the time associated with the manipulation of large matrices in implicit algorithms. Since nonlinear analyses often require more than one iteration to converge stress strain relationships, an implicit scheme would require a re-assembly of the global stiffness matrix; a very time consuming task. Since the stable time step for explicit schemes is directly proportional to element size and inversely proportional to the material stiffness, thin and stiff elements, such as beams, require very small time steps. Soil-structure

interaction problems are therefore modelled using a mixed implicit-explicit scheme. In FLEX, linear elastic structural components, such as beams, are modeled by an implicit portion which is coupled to the explicit portion representing the relatively softer soil. Additionally, various zones of an explicit model can be assigned different time steps depending on their size and stiffness. In this study a completely explicit scheme is used to model the embankment.

Constitutive Model

The viscous cap model is defined by a modified (curved) Drucker-Prager failure surface and a strain hardening cap. Parameters required to define the failure surface are based on standard Mohr-Coloumb criteria whereas the strain hardening cap parameters are easily determined from the results of one dimensional consolidation tests.

The cap model is based on incremental plasticity theory and satisfies Drucker's postulates of stability, uniqueness, and continuity, Drucker[6,7]. This model was originally developed by DiMaggio and Sandler[3] and later generalized by Sandler et al[4]. The model is defined by a two part yield surface and an associated plastic strain vector normal to this yield surface. This surface is expressed in terms of the hydrostatic pressure, p, and the square root of the second invariant of the deviatoric stress tensor, $\sqrt{J_2}$, where

$$p = \frac{1}{3}(\sigma_1 + \sigma_2 + \sigma_3) \qquad (1)$$

$$J_2 = \frac{1}{6}[(\sigma_1 - \sigma_2)^2 + (\sigma_2 - \sigma_3)^2 + (\sigma_3 - \sigma_1)^2] \qquad (2)$$

In equations (1) and (2), σ_1, σ_2, and σ_3 are the principal stress components (compression assumed negative). Figure 1 shows a typical yield surface represented by

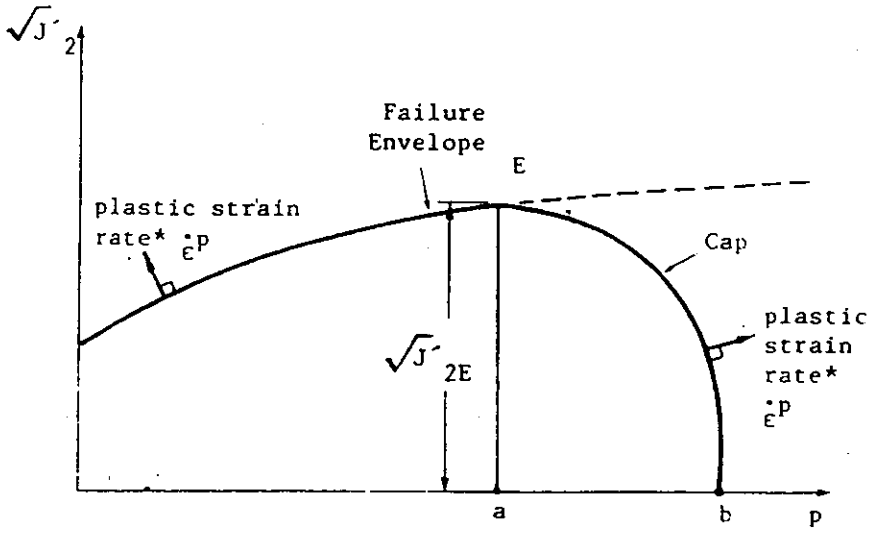

Failure envelope: $\sqrt{J'_2} = A - C \exp(-3Bp)$

cap: $\sqrt{J'_{2E}} = (p_b - p_a)/R = f(\bar{\varepsilon}^p_v)$

Figure 1 The cap model (from Isenberg et al.)[5]

a nonhardening (fixed in stress space), isotropic (third invariant independent) failure surface and an isotropic and hardening cap.

The nonhardening failure surface

This portion of the yield surface is a modified Drucker-Prager surface which transitions into an ideal Von-Mises surface at high hydrostatic pressures. This surface is represented by the equation

$$\sqrt{J_2} = A - C\, e^{3Bp} \tag{3}$$

where A, B, and C are material constants. In order to develop an understanding for this surface in terms of commonly used geotechnical parameters such as cohesion, c, and friction angle, ϕ, equations representing a Drucker-Prager yield surface are:

$$\sqrt{J_2} = 3\alpha p + k \tag{4}$$

where for a conventional triaxial compression stress path

$$\alpha = \frac{2\sin\phi}{\sqrt{3}(3 - \sin\phi)} \tag{5}$$

$$k = \frac{6\, c \cos\phi}{\sqrt{3}(3 - \sin\phi)} \tag{6}$$

Since the cap model was initially developed to study the effects of blast loadings on soil, the current shape of the yield surface was selected to model the fluid-like strength characteristics at large hydrostatic pressures.

Another important feature of the cap model is the use of an associative flow rule, i.e. the plastic strain rate vector is normal to the yield surface. Referring to the plastic strain rate vector in Figure 1, it can be concluded that the plastic strains are composed of a volumetric dilation component (directed horizontally to the left) and a deviatoric

component (directed vertically upwards). Therefore if a stress path lies on the yield surface for a prolonged duration, a large amount of volumetric dilation will result in addition to pure shear flow. Such dilation is shown to be excessive under those circumstances and does not correctly model the behavior of real soils. A means to limit dilation in the cap model is provided by the kinematic cap surface.

The hardening cap surface

An elliptical cap whose position is dependent on strain history is provided to limit the extent of dilation exhibited by the material. The equation representing the cap surface in Figure 1 is

$$(p - p_b)^2 + \frac{1}{9}R^2\hat{J}_2 = (p_b - p_a)^2 \qquad (7)$$

where p_a and p_b are the values of p at points a and b, respectively. The parameter R is a constant representing the ratio of the two principal axes of the elliptical cap. It should be noted that other shapes of the cap and a variable R parameter have been successfully used in other studies. The movement of the cap is controlled by the following hardening rule

$$\overline{\epsilon}_v^p = W\,[1 - e^{3Dp_b}] \qquad (8)$$

where W and D are material constants and $\overline{\epsilon}_v^p$ represents volumetric plastic strain. If a stress path intersects the cap surface the plastic strain rate vector will consist of a volumetric compaction component (directed horizontally to the right) and a deviatoric component (directed vertically upwards). Such a stress path will push the cap surface out resulting in an increase in the value of p_b. Equation (7) will therefore be updated with new values of either or both $\sqrt{J_2}$ and p to keep the final stress state inside the yield surface.

Three modes of behavior

Three modes of behavior are possible for the cap model: elastic, failure, and cap movement. Elastic behavior takes place when the stress state is entirely within the failure surface and the hardening cap. For a given increment of strain rate the corresponding stress rate is given by

$$\dot{p} = K \dot{\epsilon}_{kk} \tag{9}$$

$$\dot{s}_{ij} = 2 G \dot{e}_{ij} \tag{10}$$

where $\dot{\epsilon}_{kk}$, e_{ij}, and s_{ij} are the volumetric strain, deviatoric strain, and deviatoric stress tensors, respectively, and K and G represent the bulk and shear moduli. In the elastic regime, the volumetric and deviatoric components of stress and strain are not coupled, so that a purely volumetric change in strain (perfectly horizontal strain path) does not introduce a deviatoric stress component and a purely deviatoric strain increment (perfectly vertical strain path) does not affect the hydrostatic stress component.

If the stress path intersects the failure surface, deviatoric and volumetric plastic strains occur according to the associative flow rule. The volumetric plastic strain increment is used in the inverse of equation (8) and the cap is moved in (to the left) accordingly. If dilation continues, the cap will recede until the stress state lies at the intersection of the failure surface and the hardening cap. A tangent at this point of intersection is horizontal; therefore, the associative flow rule will dictate only deviatoric strains for such stress point. The recession of the cap limits the total amount of dilative volumetric strains to a reasonable amount.

The cap mode of behavior will take place if the stress point lies on the movable cap surface causing compressive volumetric and deviatoric plastic strains.

Visco-elastoplastic cap model

The visco-elastoplastic cap model (vcap), as used in this study, is identical to the cap model except the behavior in the elastic domain is represented by a viscoelastic model. As mentioned earlier, the cap model was primarily developed for use in blast studies where a strong pulse is imparted to the soil causing a strongly nonlinear but predominantly monotonic response. Since the subsequent cyclic stress cycles are traditionally considered secondary, a nondissipating elastic regime has been considered satisfactory. However, during earthquake loading, material damping at low amplitude stress cycles is considered important; therefore, the elastic regime is replaced by a dissipative viscoelastic regime. In the vcap model a standard solid (a Kelvin unit in series with a spring) was selected to provide a form of linear viscous damping. Although FLEX provides an option to introduce a viscoelastic shear modulus as well as a viscoelastic bulk modulus, only the shear modulus was selected as a viscoelastic parameter. The bulk modulus was kept the same as the elastic bulk modulus. The shear modulus varies from a slow modulus at low frequency ($\omega \rightarrow 0$) to a fast modulus at very high frequencies ($\omega \rightarrow \infty$). The amount of damping diminishes at these two extremes but reaches a maximum value at a "central" frequency depending on the characteristics of the dashpot. Similarly, the amount of dissipation is governed by the difference in the slow and fast shear moduli. It is apparent from this discussion that viscoelastic damping is frequency dependent; however, damping in real soils is frequency independent, Seed and Idriss[8]. But since the viscoelastic damping curve is relatively flat near the "central" damping frequency, therefore, the input parameters could be selected such that they cover a selected range of frequencies. Isenberg[5] et al. show that damping is within 80 percent of maximum for the range $\omega^*/2$ to $2\omega^*$ for properly selected input parameters. In this study a "central" frequency of 6Hz was selected at 10 % damping; therefore for the frequency range of 3Hz to 12Hz the damping is between 8% to 10%.

Details of Input Parameters

Figure 2 shows the results of triaxial and consolidation tests performed on the core and shell materials. The corresponding simulated strength and consolidation curves for the two materials are shown in Figure 2 as dashed lines. Tables 1 and 2 lists the input parameters used in this study. It should be pointed out that the friction angle of the core, based on the results of consolidated undrained tests, varies between 16 and 22 degrees, Figure 2. A friction angle of 20 degrees and no cohesion was assumed for the core materials in this study. Similarly, a friction angle of 46 degrees at low confinement to 34 degrees at high confinement stresses and no cohesion was selected for the rockfill materials.

Table 1

Summary of Cap Parameters

Material Zone	Cap Input					
	A $X 10^7$ Pa	B $X 10^9$ 1/Pa	C $X 10^7$ Pa	D $X 10^7$ 1/Pa	W	R
Core (1)	1.843	9.000	1.843	1.000	0.615	2.500
Filter (2)	1.317	26.00	1.317	1.000	0.615	2.500
Transition (3)	1.317	26.00	1.309	1.000	0.615	2.500
Comp. Rockfill (4)	1.317	26.00	1.309	1.000	0.615	2.500
Dumped Rockfill (5)	1.317	26.00	1.309	1.000	0.615	2.500

The complete procedure for this analysis consists of a static finite element analysis to evaluate the initial stress distribution in the dam, followed by a dynamic analysis. An additional consequence of the static analysis is the proper strain hardening of the

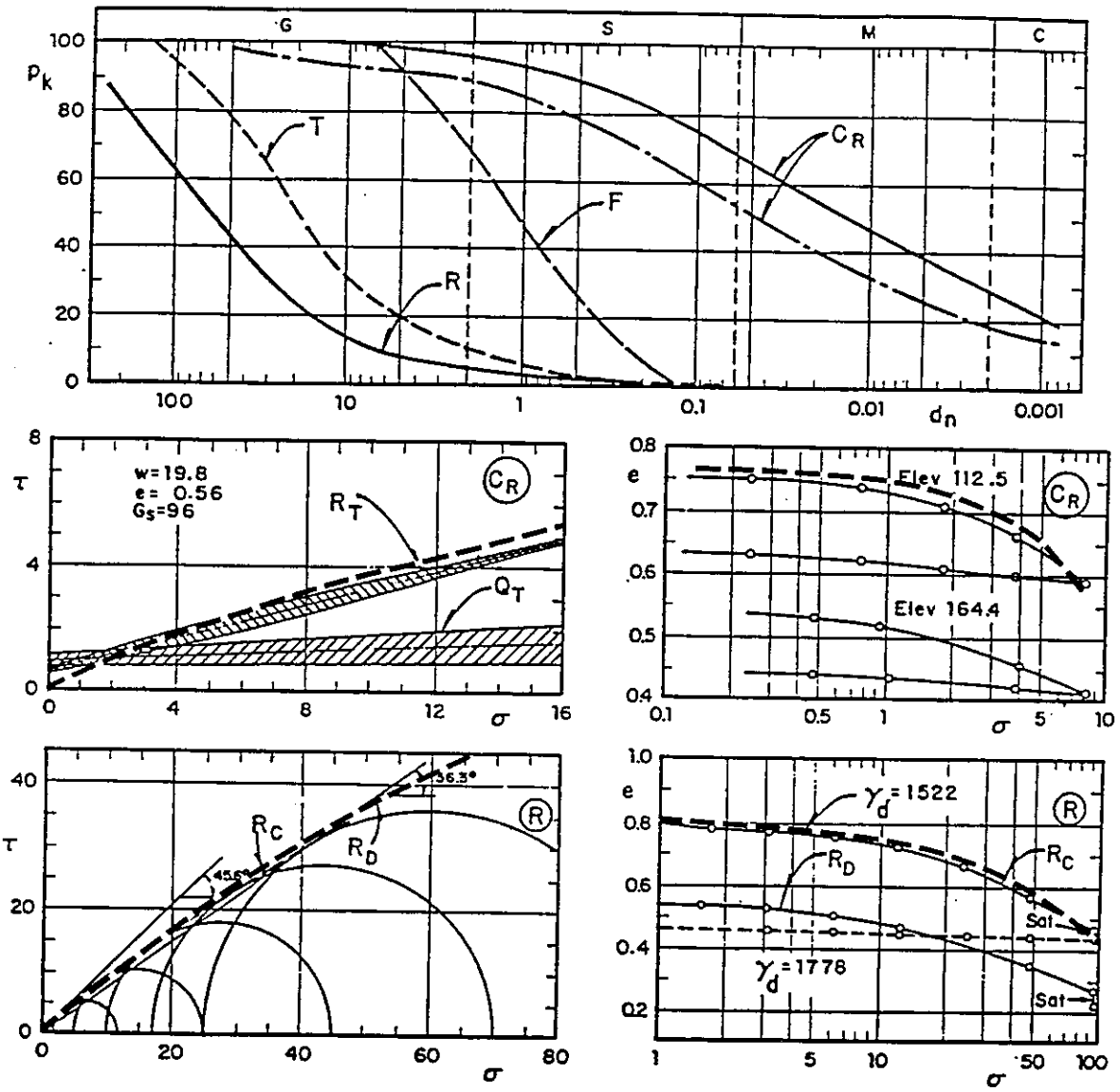

G	Grava *Gravel*	R	Enrocamiento *Rockfill*	Elev	Elevación, en m *Elevation, in m*
S	Arena *Sand*	p_k	Porcentaje que pasa *Per cent finer*		
M	Limo *Silt*	d_n	Diámetro nominal, en mm *Nominal diameter, in mm*		
C	Arcilla *Clay*	w	Contenido de agua, en porcentaje *Water content, in per cent*		
C_R	Núcleo *Core*	e	Relación de vacíos *Void ratio*		
F	Filtros *Filters*	τ	Resistencia al corte, en kg/cm² *Shear strength, in kg/cm²*		
T	Transiciones *Transition zones*	σ	Esfuerzo normal o presión aplicada, en kg/cm² *Normal stress or applied pressure, in kg/cm²*		

γ_d	Peso volumétrico seco, en kg/m³ *Dry unit weight, in kg/m³*
G_s	Grado de saturación, en porcentaje *Degree of saturation, in per cent*
R_T	Pruebas R (consolidada-no drenadas) *R-tests (consolidated-undrained)*
Q_T	Pruebas Q (no consolidada-no drenadas) *Q-tests (unconsolidated-undrained)*
R_C	Conglomerado silicificado *Silicified conglomerate*
R_D	Diorita *Diorite*
Sat	Saturación *Saturation*

Figure 2 Results of triaxial and consolidation tests provided by ICOLD/ISMES.

embankment materials; for example, the elements towards the center and bottom of the embankment are hardened due to the relatively large confinement.

Table 2

Summary of Additional Parameters

Material Zone	Saturated Density Kg/ m^3	Bulk Modulus X 10^9 Pa	Shear Modulus X 10^7 Pa
Core (1)	2000	4.167	8.389
Filter (2)	2160	.3088	11.84
Transition (3)	2160	.3088	11.84
Comp. Rockfill (4)	2160	.3088	11.84
Dumped Rockfill (5)	2100	.1470	5.639
Water (Reservoir)	1000	2.068	0

The hardening is accounted for by "pushing out" of the cap in proportion to the static stress increments. Therefore, for the same material zone the deeper soils exhibit less compaction than the shallower soils during subsequent dynamic excitation. This trend is assumed here on the assumption that the deeper materials have been completely consolidated under the overburden stresses during the post construction years.

It should be noted that since the outer regions of the rockfill shell are under relatively lower confining pressures, they may tend to compact more than the core, under subsequent dynamic loading. This discrepancy in settlement characteristics and the differences in strength and density result in down drag and tensile stresses being applied by the shells to the core. These stresses will influence the final deformed shape of the core.

Results of Dynamic Analyses

The finite element mesh used in the analysis is shown in Figure 3. In addition to the embankment, the reservoir is modelled by a material with a shear modulus set to zero and bulk modulus equal to that of water. An absorbing boundary is used on the upstream side of the reservoir to eliminate any wave reflection. Preliminary dynamic analyses were conducted using the March 14, 1979 earthquake time history as the horizontal base excitation. Permanent horizontal and vertical deformations of the core are shown in Figure 4(a). According to Resendiz et al.[1] the observed horizontal and vertical deformations of the crest during the 1979 event were 5 cm. and 12 cm., respectively. The predicted magnitude of deformations seem to compare well with the observed values. The horizontal displacement of the core seem to follow the deformation characteristics of the shell due to the shell core interaction. The final deformed mesh, scaled by 200 times, is shown in Figure 4(b). As expected, the upstream side of the embankment shows the greatest degree of distress due to relatively smaller confining pressures. Figure 4(b) also shows the influence of upstream slumping on the deformation of the core.

Finally, the results of the dam response to the additional earthquake time histories provided by ICOLD and ISMES are shown in Appendix I through III. All figures shown in the appendices are in accordance with the ICOLD/ISMES guidelines. The predicted permanent displacements at the crest relative to the base are shown in Table 3. Table 3 indicates some interesting results: a) Permanent vertical settlement at the crest for the 0.29g EQ2 are less then those for the 0.1g EQ1; b) Permanent horizontal displacement at the crest for the 0.65g EQ3B event are only 2cm larger than those for the 0.3g EQ3A event. The first observation points out the importance of detailed finite element analysis over simplified pseudo static type of analysis. Pseudo static approaches assume a linear relationship between peak input accelerations and induced stress levels. Here, a transient peak of 0.29g is shown to cause less damage than a cyclic peak of 0.1g. The second observation points out the affect of excessive upstream slumping on the deformation of the core. The top of the core is dragged upstream by the drastically deformed shell, Figure 5.

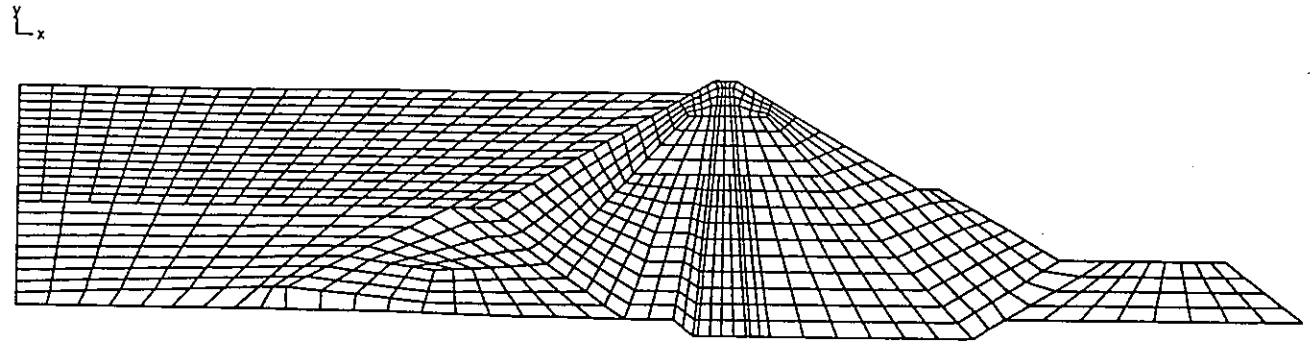

(a) Computational grid

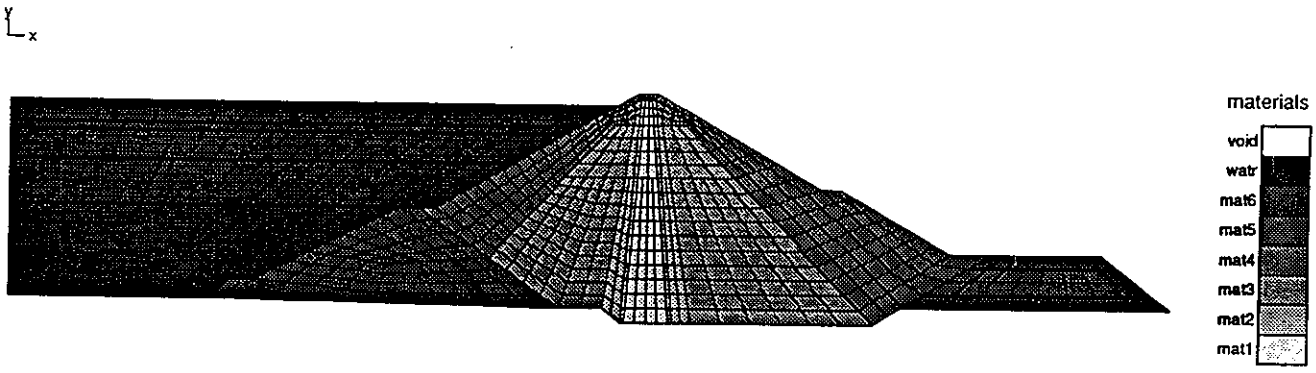

(b) Grid material properties

Figure 3 Finite element mesh and material zones.

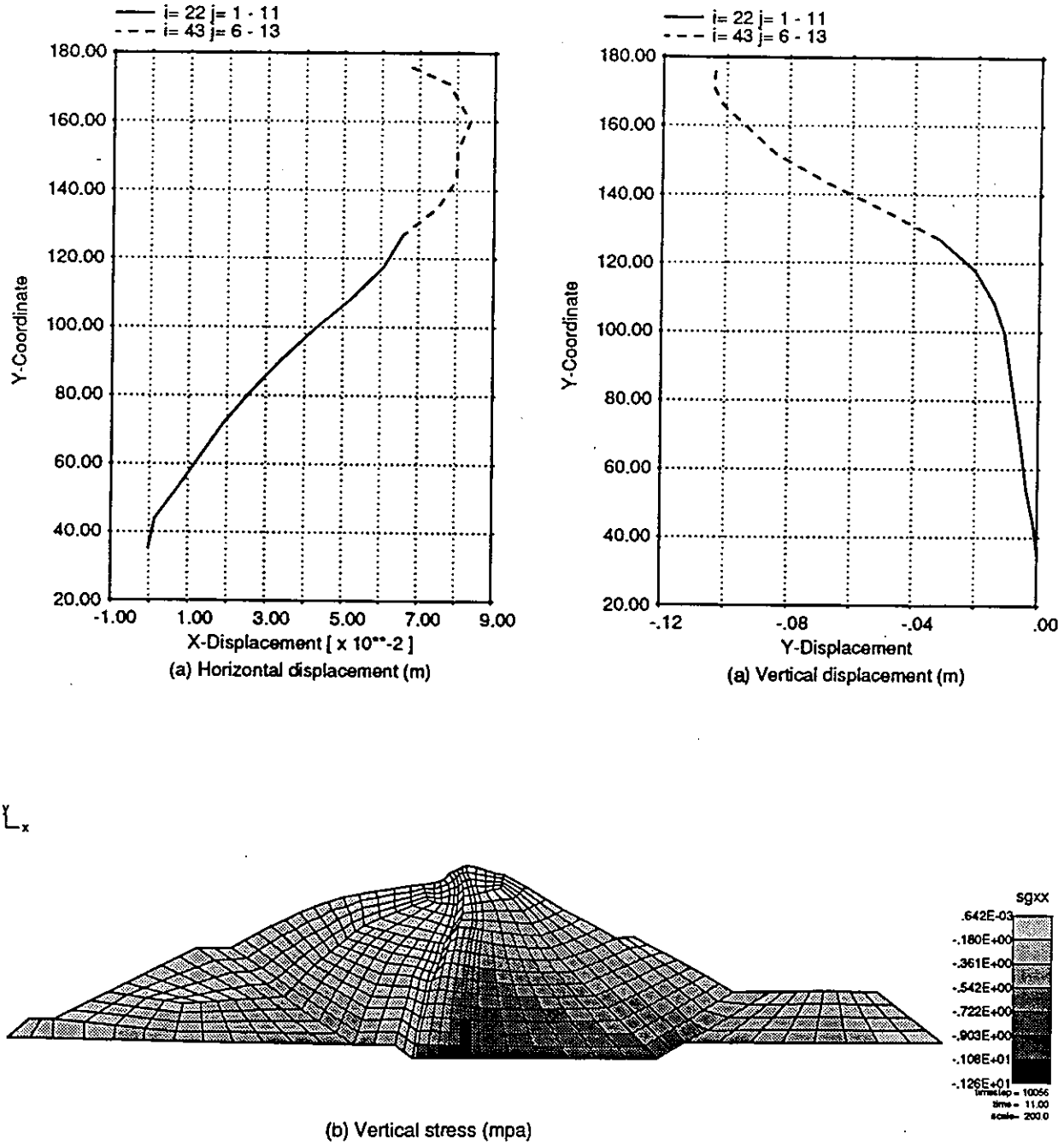

Figure 4 (a) Permanent displacements predicted for the March 14, 1979 earthquake; (b) Deformed mesh scaled by 200 times.

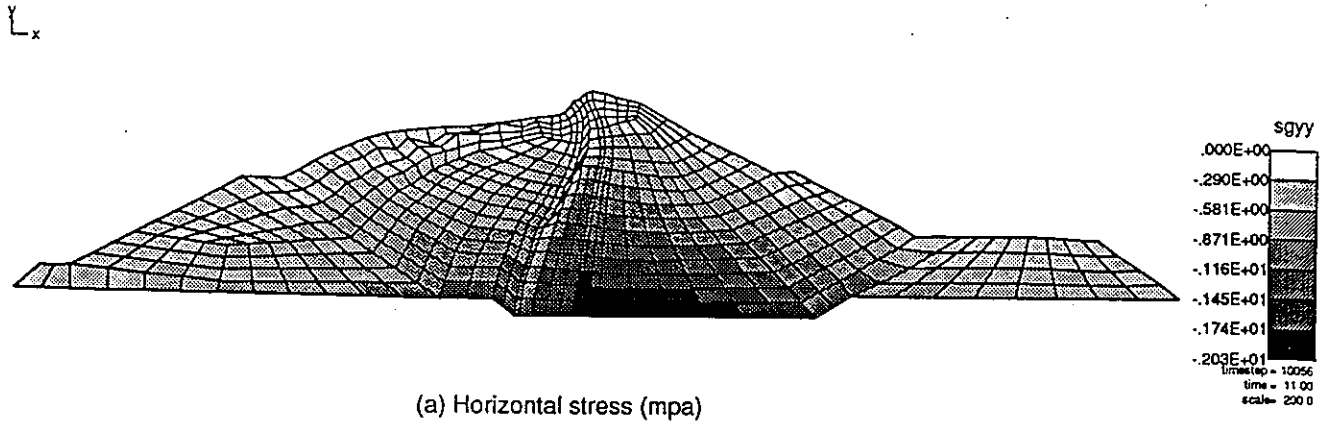

(a) Horizontal stress (mpa)

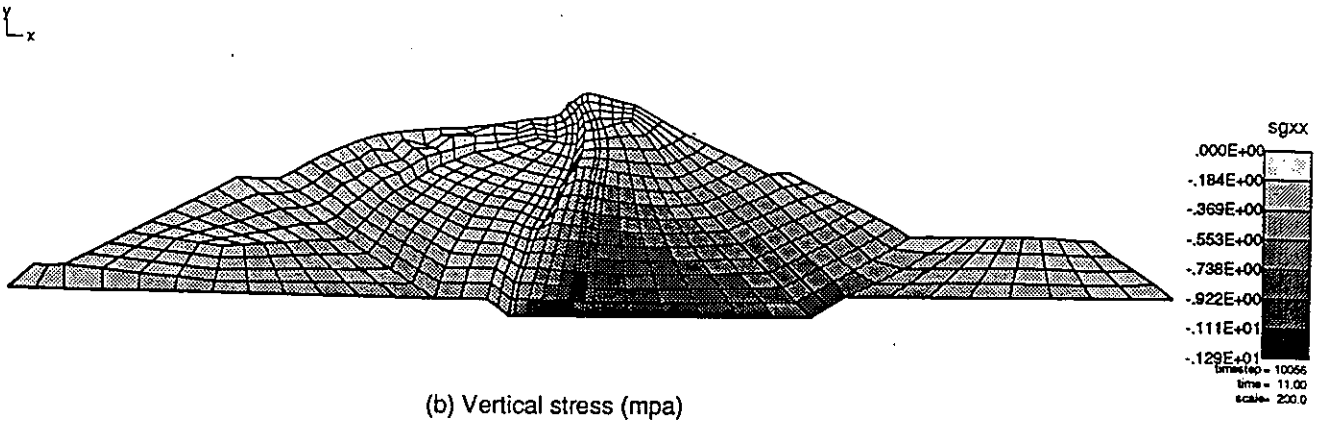

(b) Vertical stress (mpa)

Figure 5 Deformation of the embankment after the 0.65g EQ3B.

Table 3

Predicted Crest Displacements

Earthquake	Acc. (g)	Horiz. (cm)	Vert. (cm)
EQ1 (1979 7.6 Event)	0.10	6	11
EQ2 (1985 8.1 Event)	0.29	4	8
EQ3A (Swiss HSK Rec.)	0.30	7	13
EQ3B (Swiss HSK Rec.)	0.65	9	16

Summary and Conclusions

A nonlinear dynamic finite element program FLEX is used to simulate the response of El Infiernillo Dam under low and medium level seismic excitation. Both static and dynamic analyses were conducted to simulate the field conditions as accurately as possible. The reservoir is also modeled in both the static and dynamic analyses. The efficiency of the code is reflected by the processing time: 1 second of earthquake record utilizes only 1 minute and 15 seconds of cpu time on an IBM RS-6000 workstation.

The plasticity based viscous cap model is used to simulate the nonlinear stress strain characteristics of the embankment materials. The input parameters used to define the constitutive model are based on the results of a limited number of standard geotechnical tests, such as triaxial and one dimensional consolidation tests. Significant uncertainties exist in fitting a nonlinear constitutive model for each material region of the model. It is recommended that a more complete set of soil test data be included in future specifications for a similar benchmark.

The predicted displacements of the embankment during the March 14, 1979 earthquake

seem to follow the deformation pattern observed in the field. Overall, the deformation of the shells control the deformation pattern of the embankment. Upstream shell of the dam shows the greatest amount of movements due to the lower effective confining pressures. The response of the embankment to three other earthquakes is also presented. The deformations and stress levels increase are shown to depend on the frequency and amplitude of input acceleration.

REFERENCES

1. Resendiz, R., M.P. Romo, and E. Moreno. "El Infiernillo and La Villita Dams: Seismic Behavior", Journal of Geotechnical Division, ASCE, Vol. 108, No. GT1, pp. 109-131, January, 1982.

2. Vaughan, D.K., and E. Richardson. FLEX User's Manual, Weidlinger Associates, Los Altos, Ca, 1989.

3. DiMaggio, F.L., I.S. Sandler. "Material Model for Granular Soils", J. Eng. Mech. Div., ASCE, Vol. 97, No. EM3, 1971, pp. 935-950.

4. Sandler, I.S., F.L. DiMaggio, and G.Y. Baladi. "Generalized Cap Model for Geologic Materials", J. Geotech. Eng. Div., ASCE, Vol. 102, No. GT7, July 1976, pp. 683-699.

5. Isenberg, J., D.K. Vaughan and I.S. Sandler. "Nonlinear Soil-Structure Interaction", Weidlinger Associates, Final Report to Electric Power Research Institute (EPRI), Palo Alto, December 1978.

6. Drucker, D.C. "Some Implications of Work Harding and Ideal Plasticity", Quart. Appl. Math., Vol. 7, No. 4, 1950, pp. 411-418.

7. Drucker, D.C., R.E. Gibson, and D.J. Henkel, "Soil Mechanics and Work-Harding Theories of Plasticity," Proceedings, ASCE, Vol. 81, 1955, pp. 1-14.

8. Seed, H.B., and I.M. Idriss (1970). Soil Moduli and Damping Factors for Dynamic Response Analysis, Report No. EERC 70-10, Earthquake Engineering Research Center, University of California, Berkeley.

APPENDIX I

Table of Contents

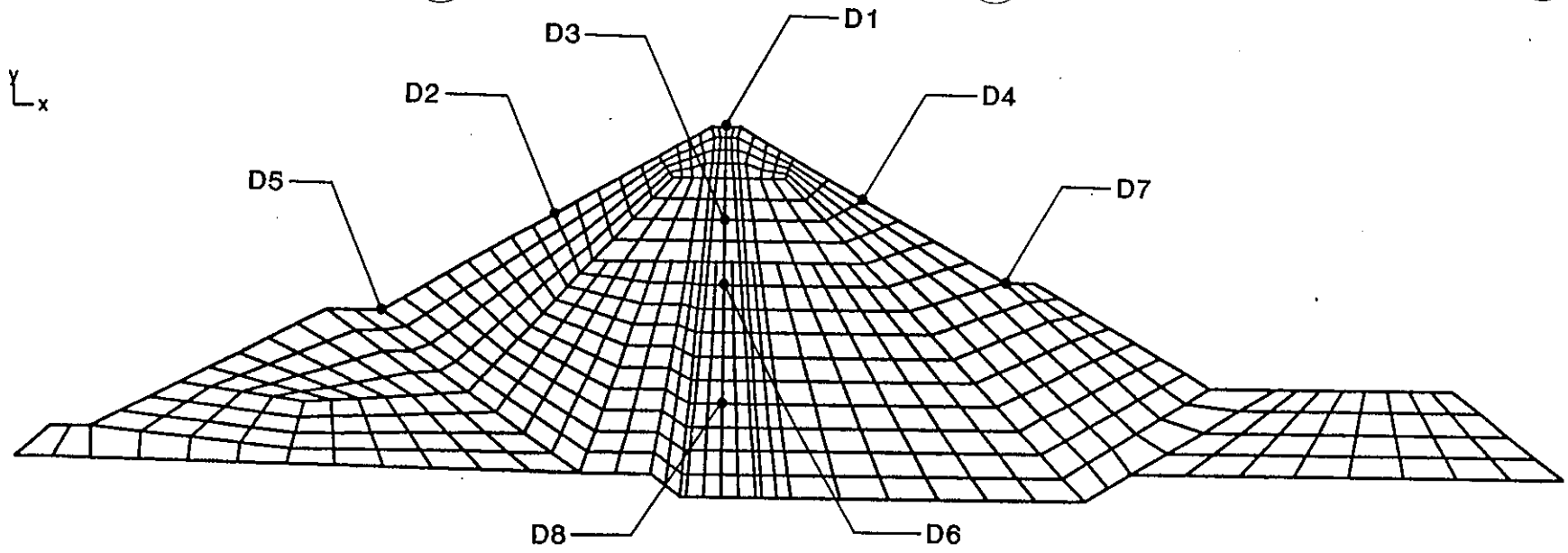

(a) Output points for velocities and displacements

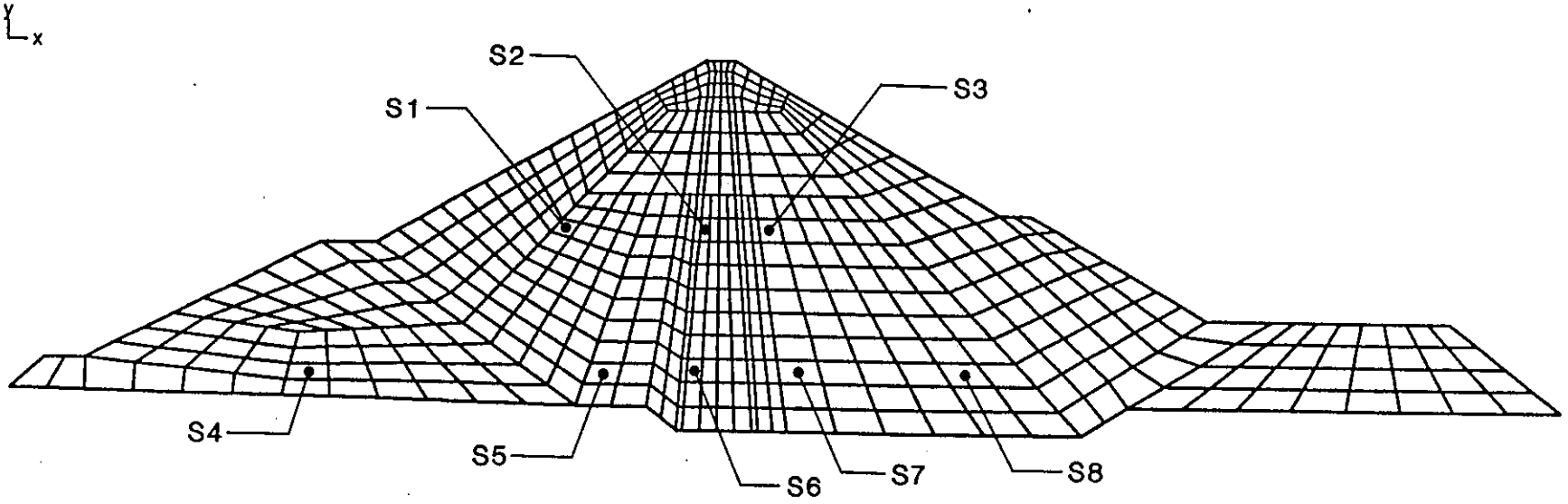

(b) Output points for stresses and strains

EQ1.DAT : Record at base rock, 1979

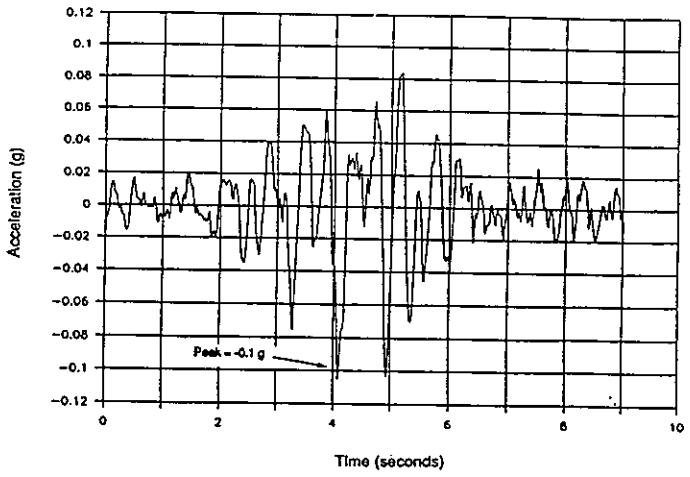

EQ2.DAT : Record at base rock, 1985

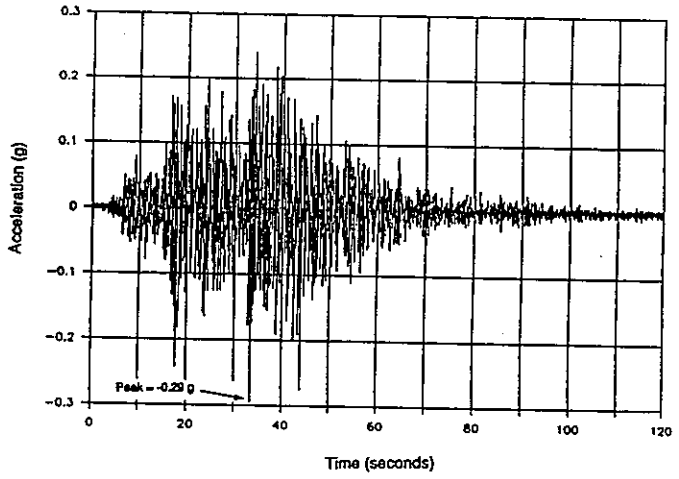

EQ3.DAT : HSK record

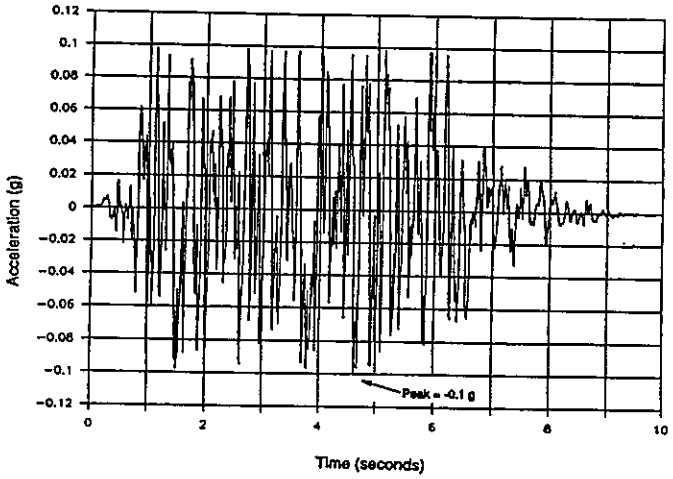

Input Earthquake Time Histories

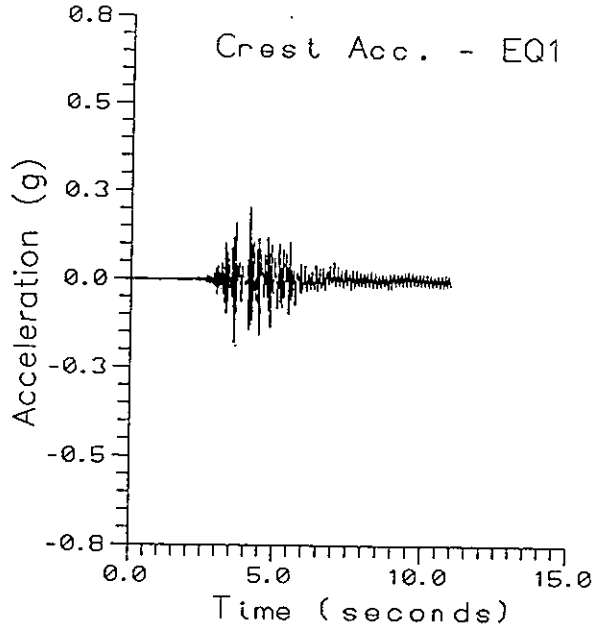

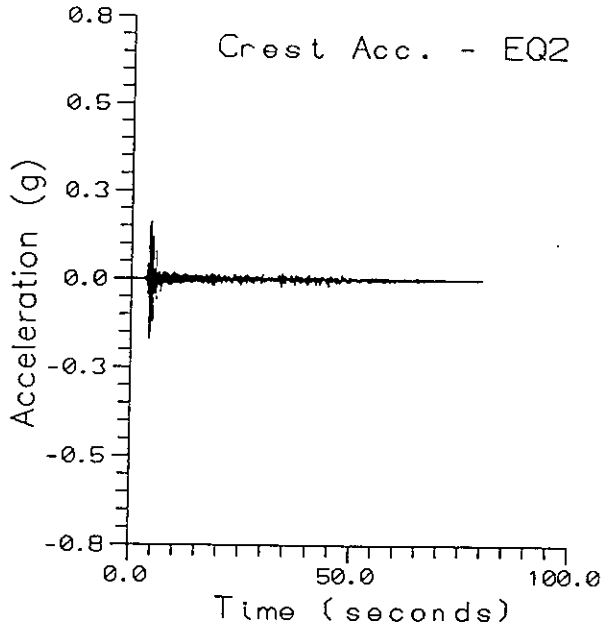

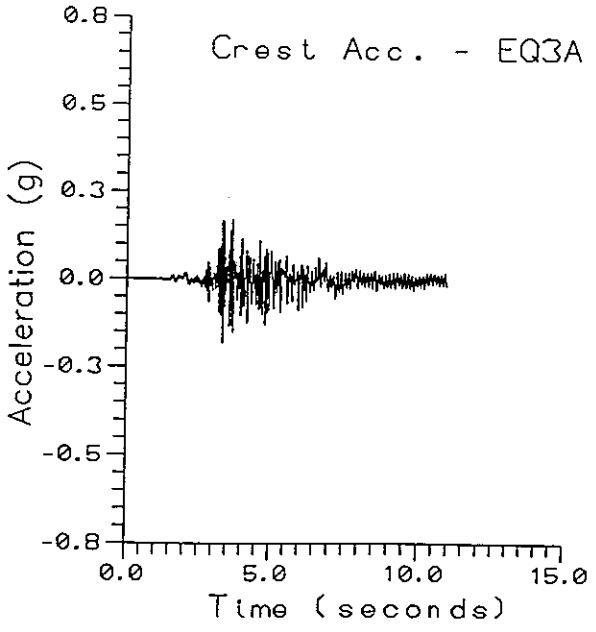

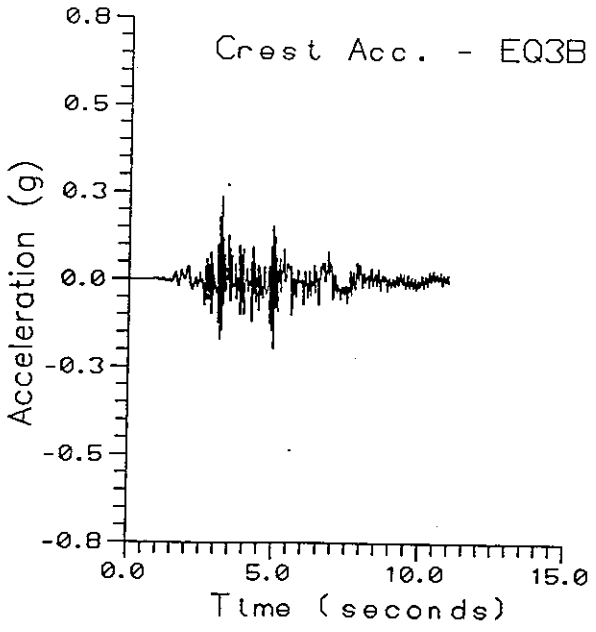

Output Time Histories

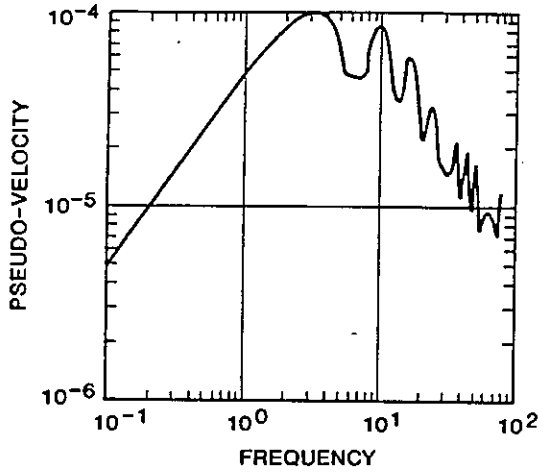

(a) EQ1-0.1g @ Crest (D1)

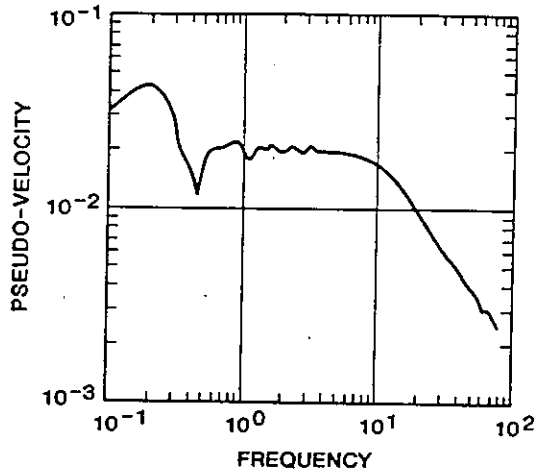

(b) EQ2-0.29g @ D/S Berm (D7)

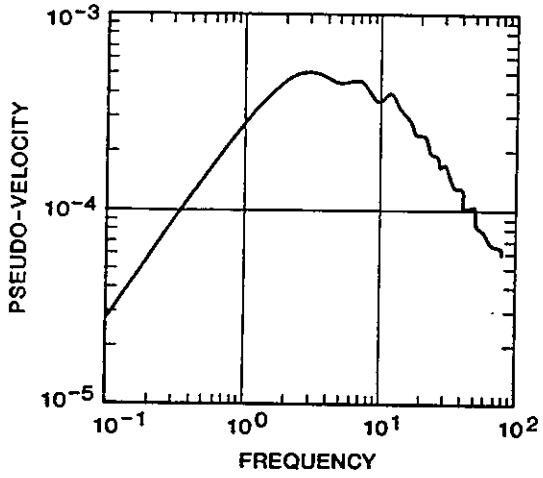

(c) EQ3A-0.3g @ Crest (D1)

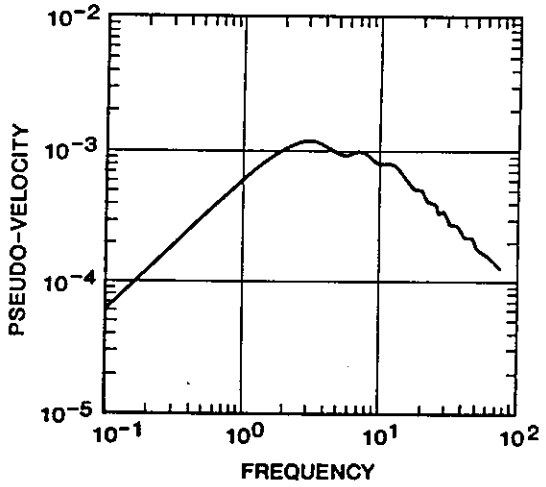

(d) EQ3B-0.65g @ Crest (D1)

Velocity Response Spectra (No Damping)

APPENDIX II

Table of Contents

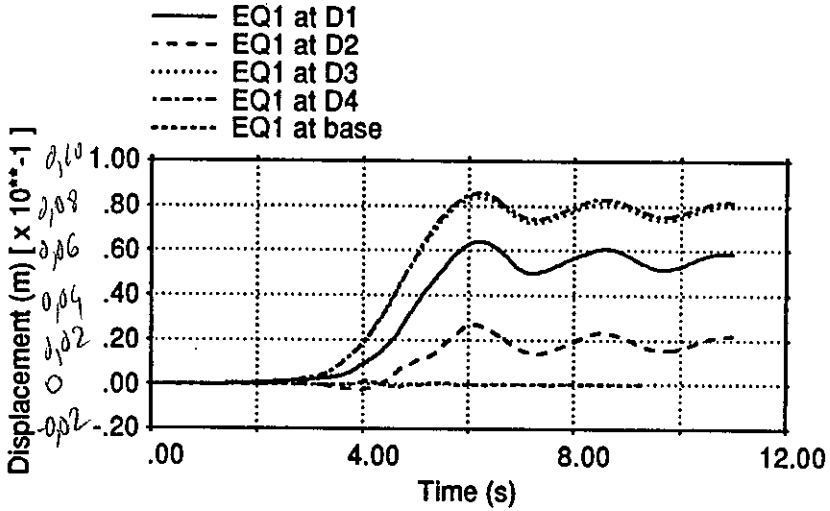

(a) Horizontal (D1 - D4)

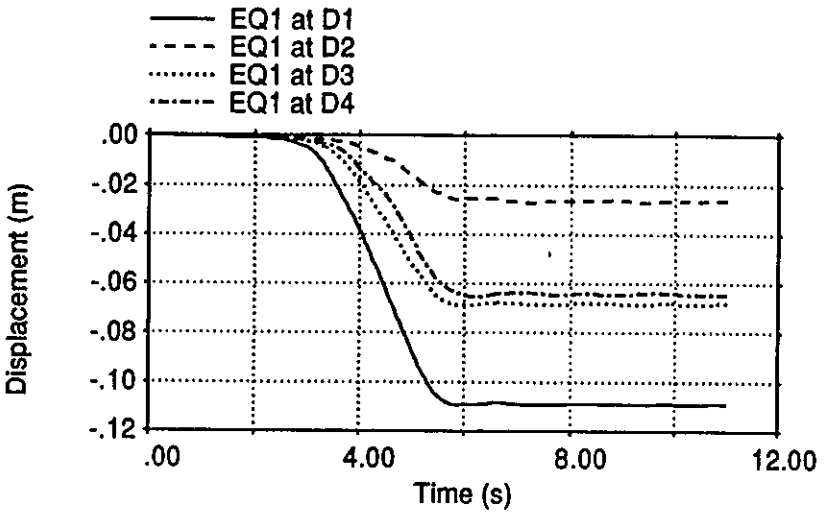

(b) Vertical (D1 - D4)

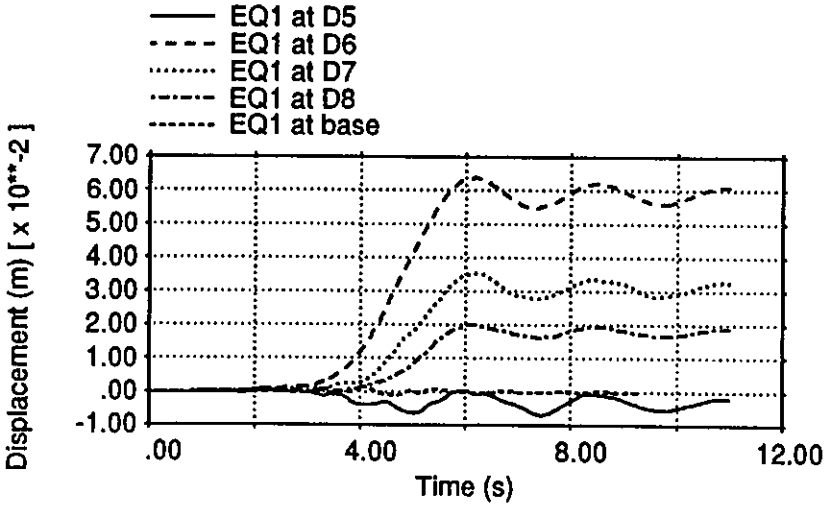

(c) Horizontal (D5 - D8)

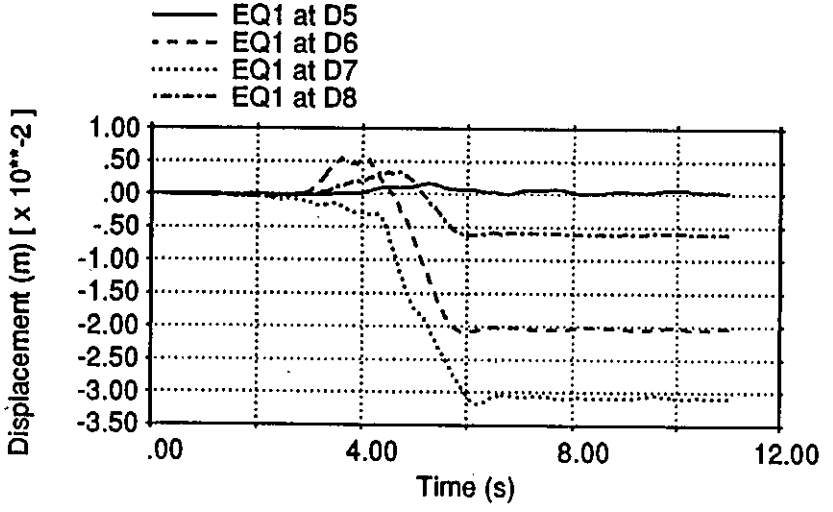

(d) Vertical (D5 - D8)

Displacement quantities for EQ1 (output locations D1 - D8)

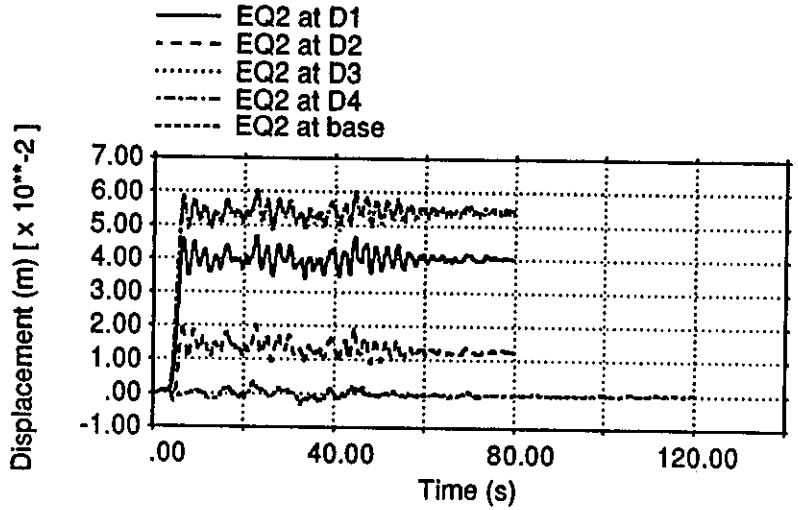

(a) Horizontal (D1 - D4)

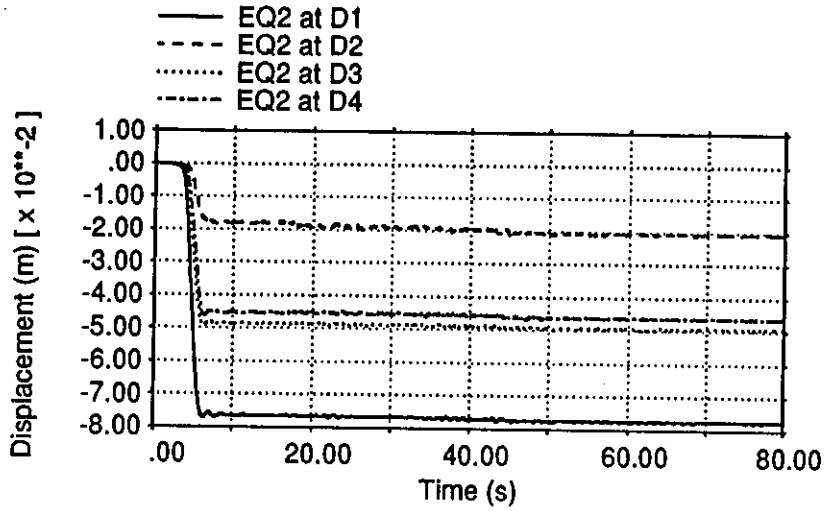

(b) Vertical (D1 - D4)

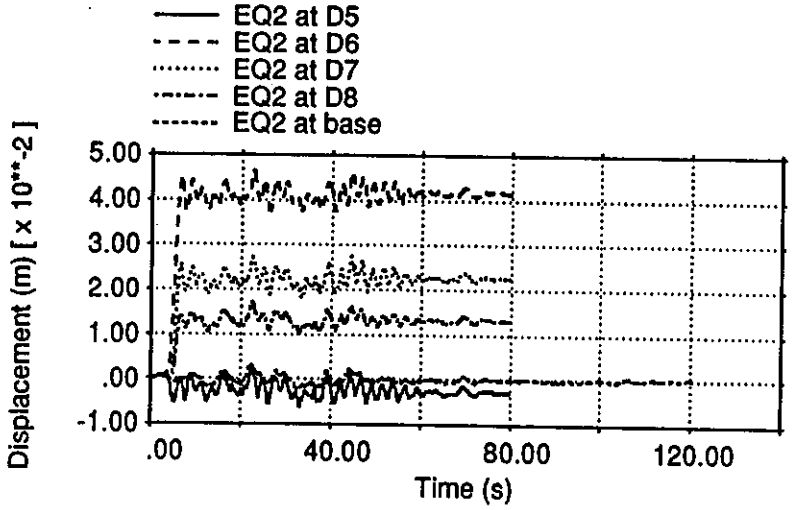

(c) Horizontal (D5 - D8)

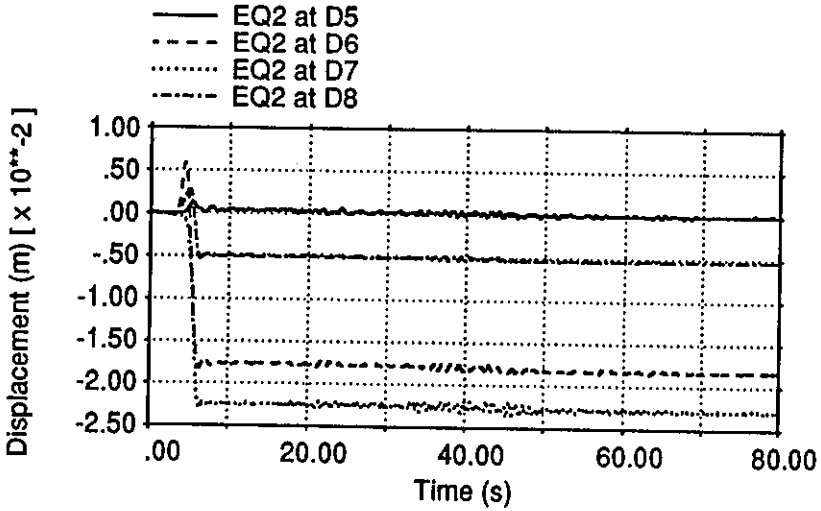

(d) Vertical (D5 - D8)

Displacement quantities for EQ2 (output locations D1 - D8)

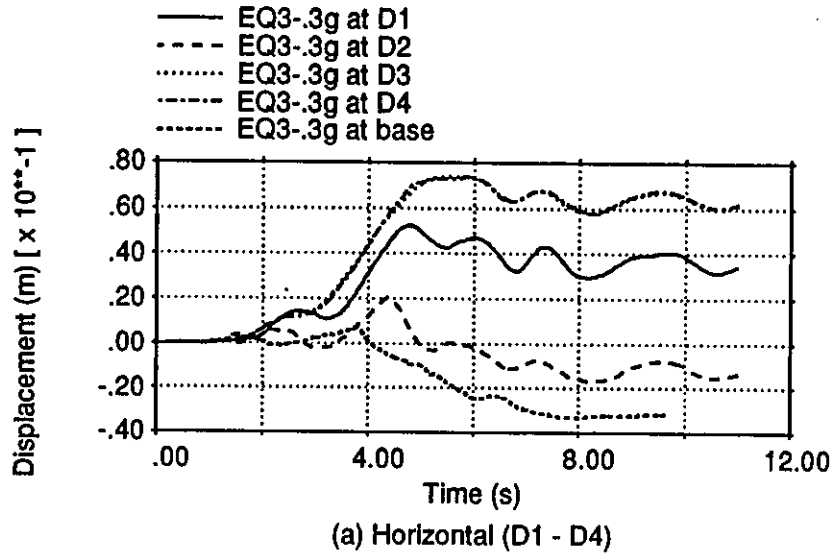

(a) Horizontal (D1 - D4)

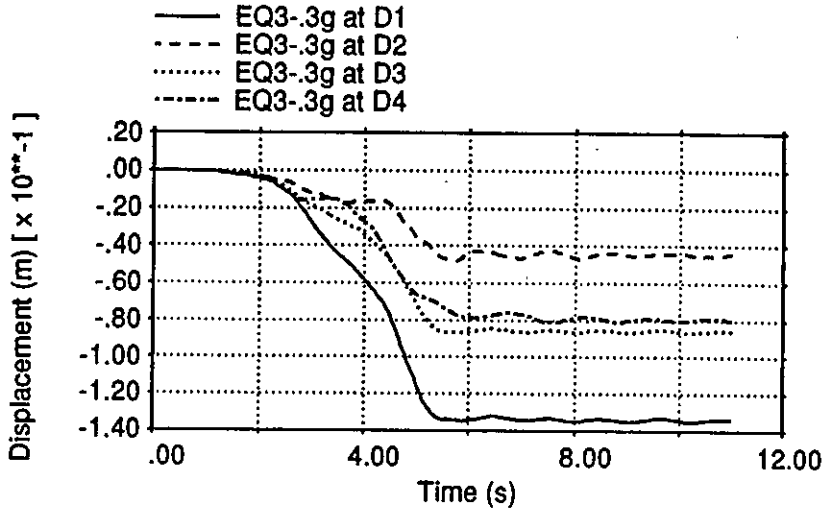

(b) Vertical (D1 - D4)

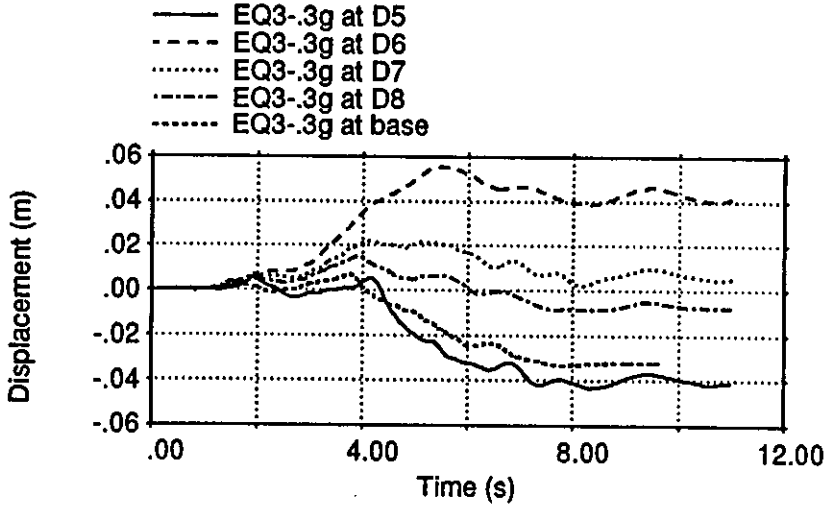

(c) Horizontal (D5 - D8)

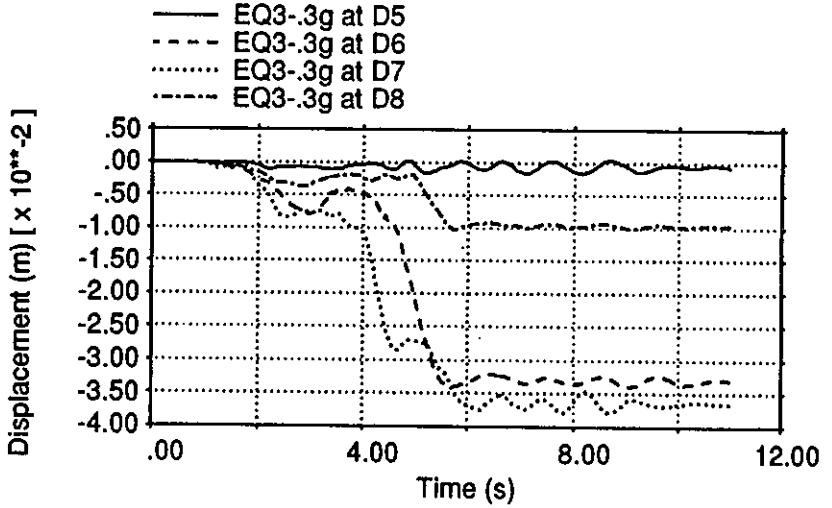

(d) Vertical (D5 - D8)

Displacement quantities for EQ3-.3g (output locations D1 - D8)

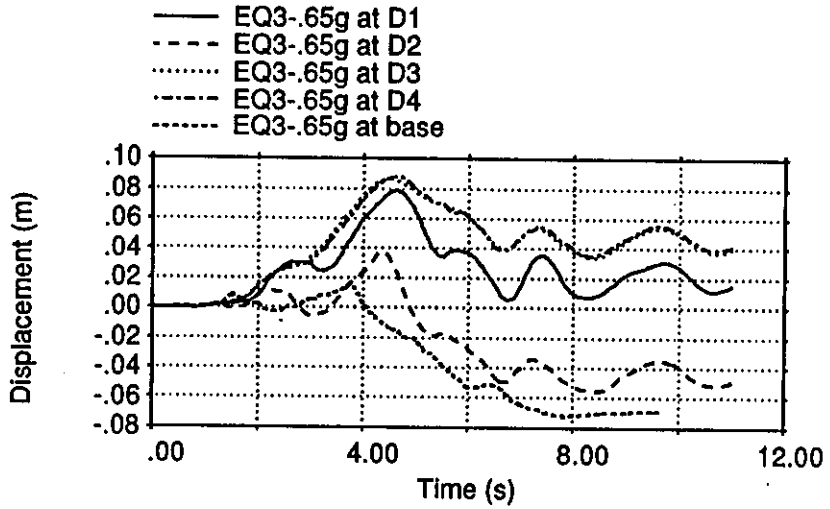

(a) Horizontal (D1 - D4)

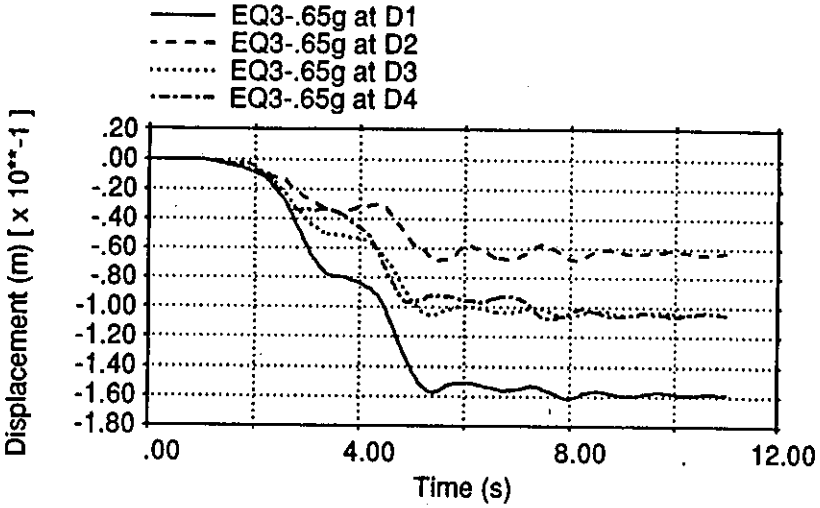

(b) Vertical (D1 - D4)

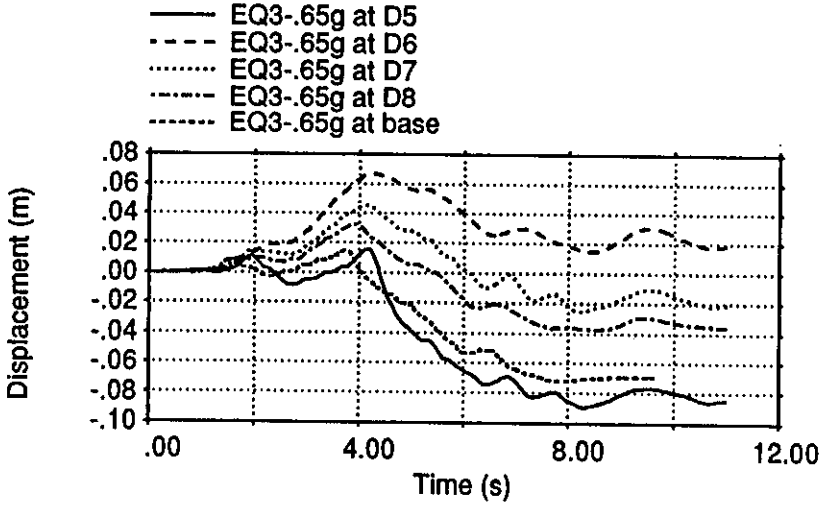

(c) Horizontal (D5 - D8)

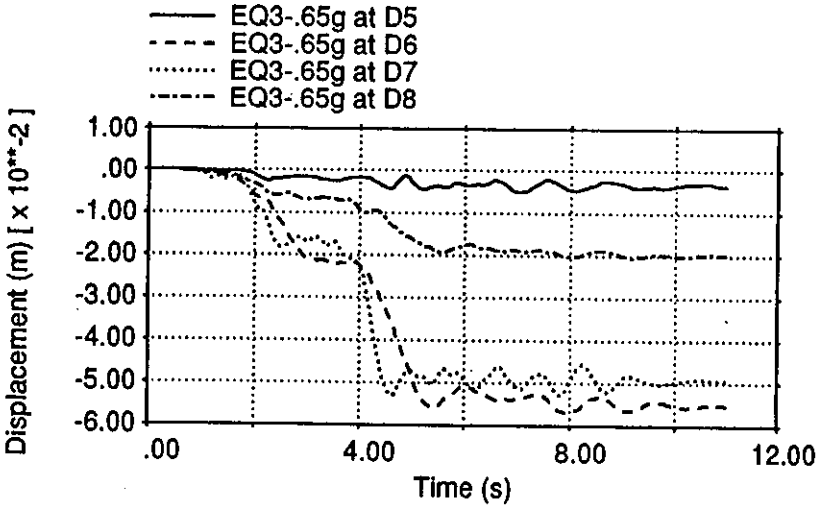

(d) Vertical (D5 - D8)

Displacement quantities for EQ3-.65g (output locations D1 - D8)

APPENDIX III

Table of Contents

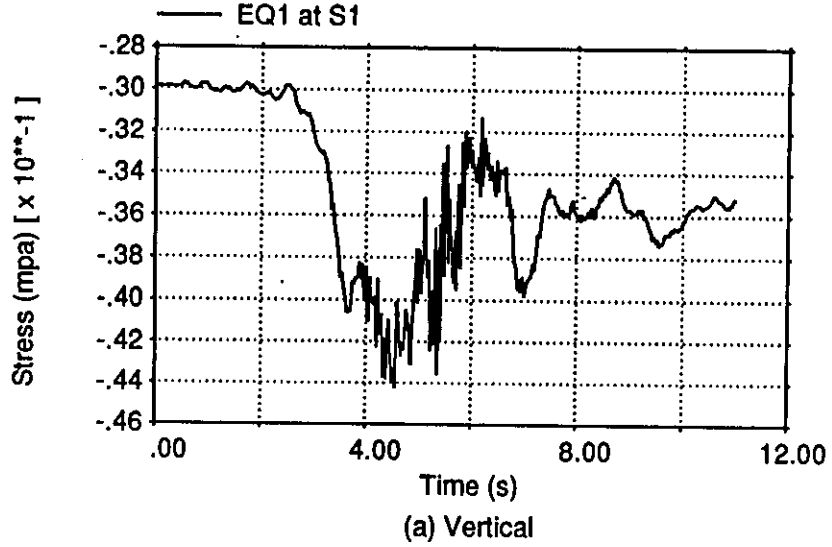

(a) Vertical

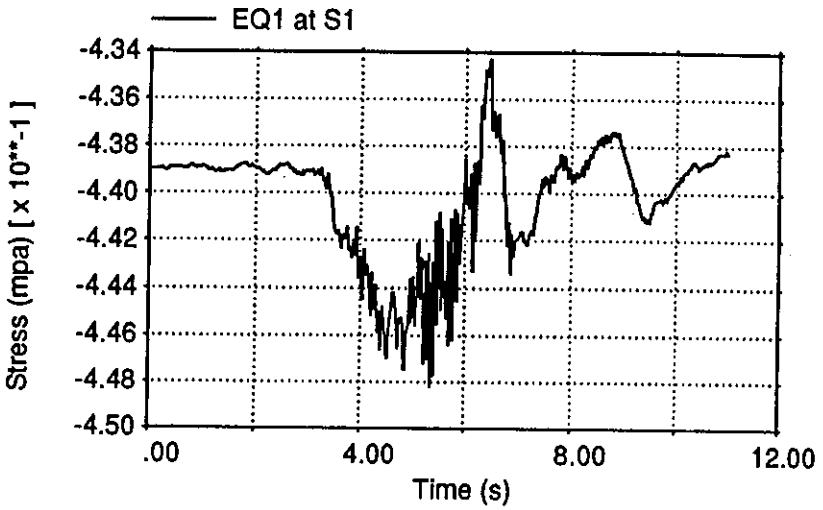

(b) Horizontal

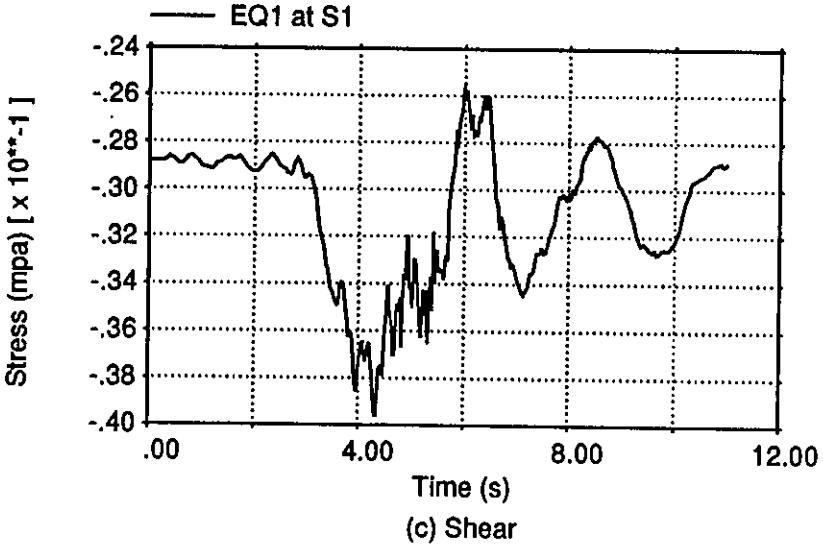

(c) Shear

Stress quantities for EQ1 at output point S1

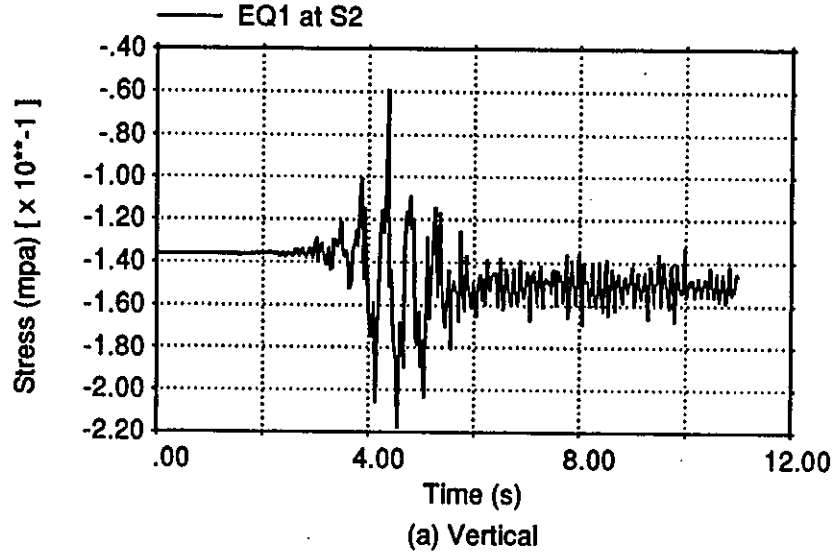

(a) Vertical

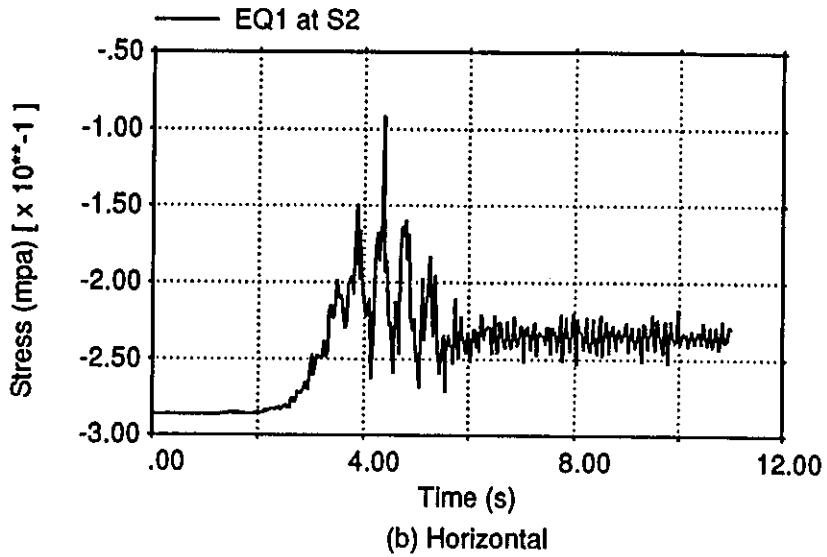

(b) Horizontal

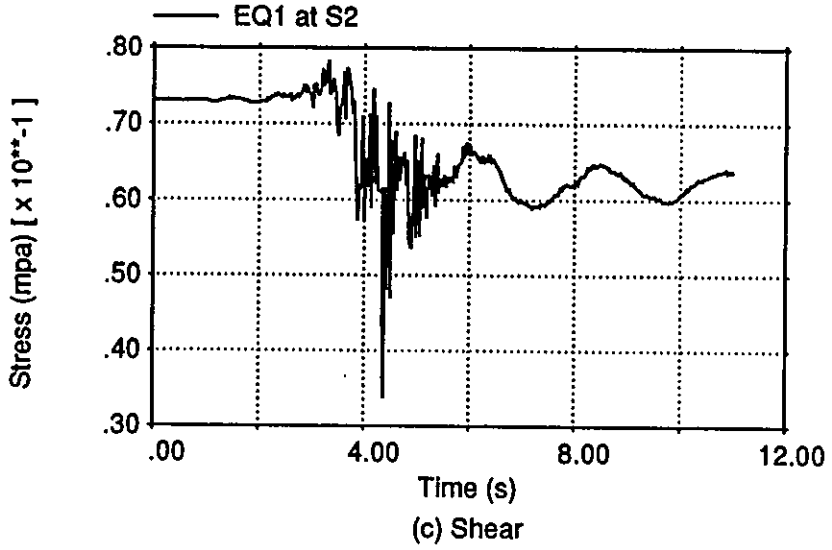

(c) Shear

Stress quantities for EQ1 at output point S2

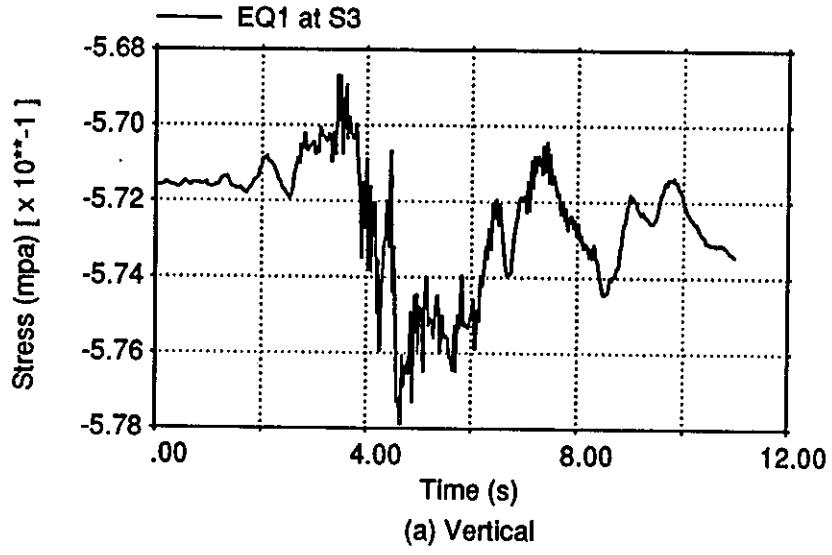

(a) Vertical

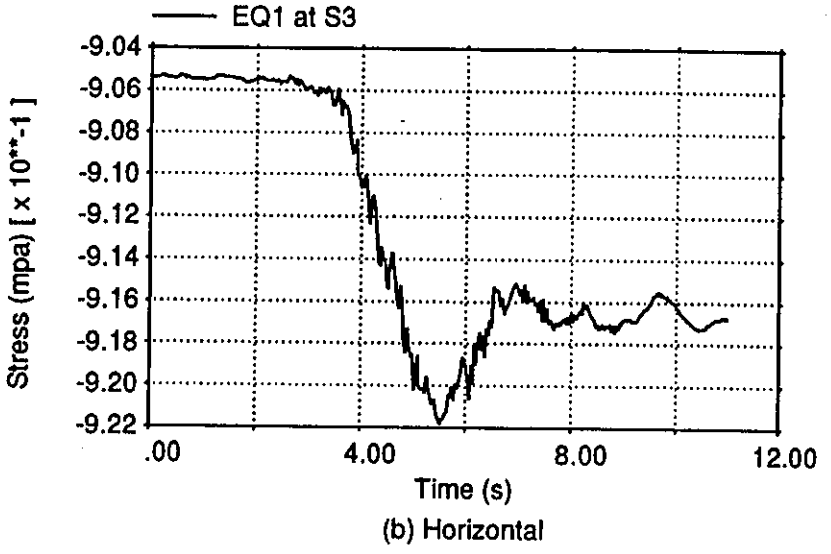

(b) Horizontal

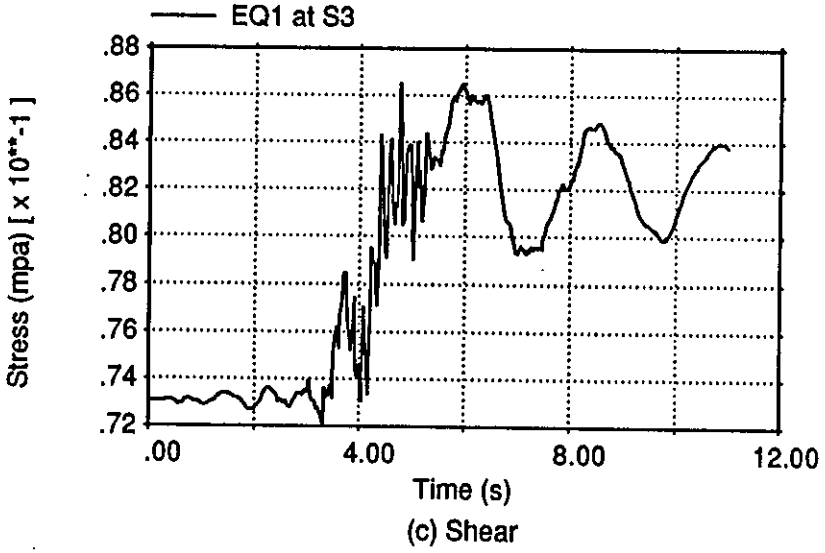

(c) Shear

Stress quantities for EQ1 at output point S3

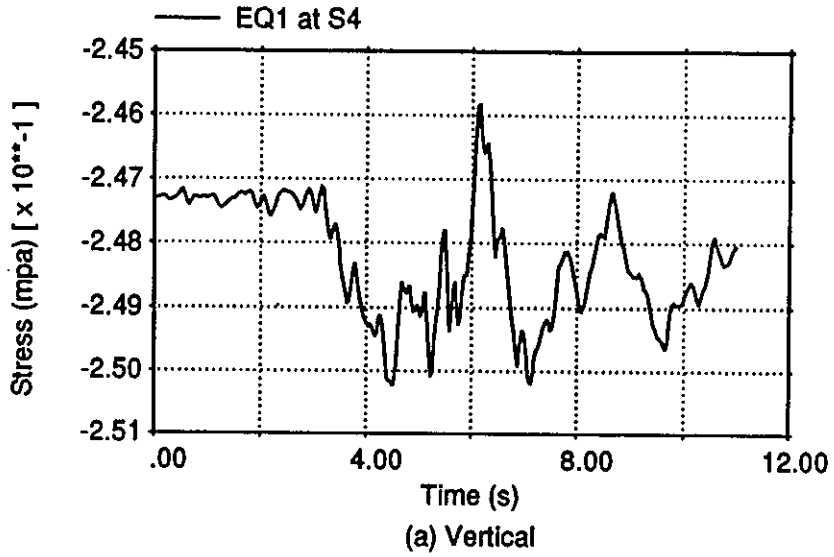

(a) Vertical

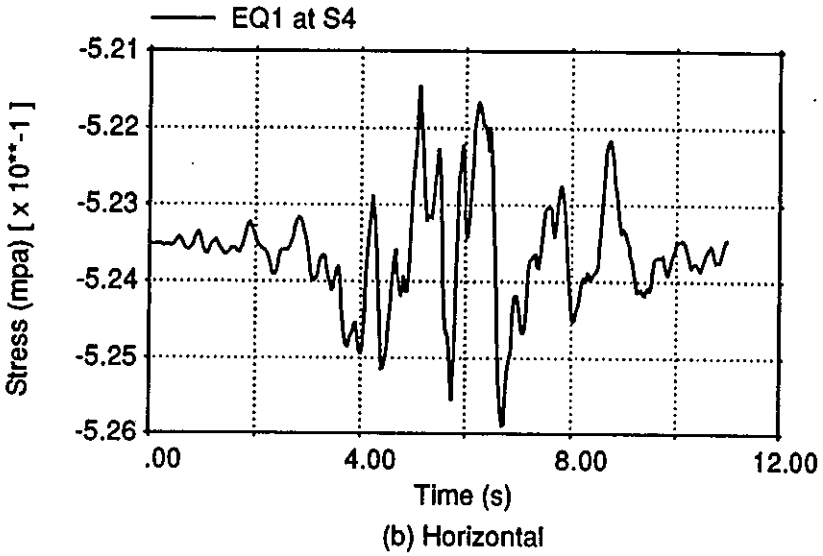

(b) Horizontal

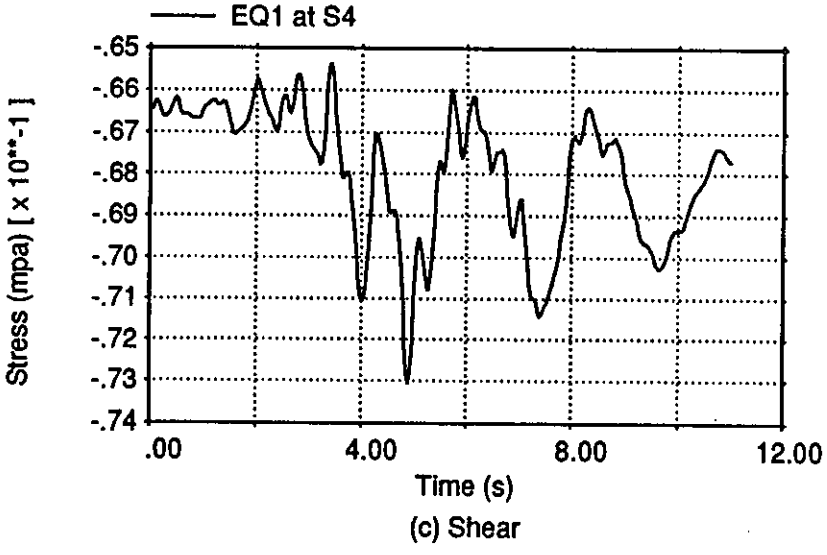

(c) Shear

Stress quantities for EQ1 at output point S4

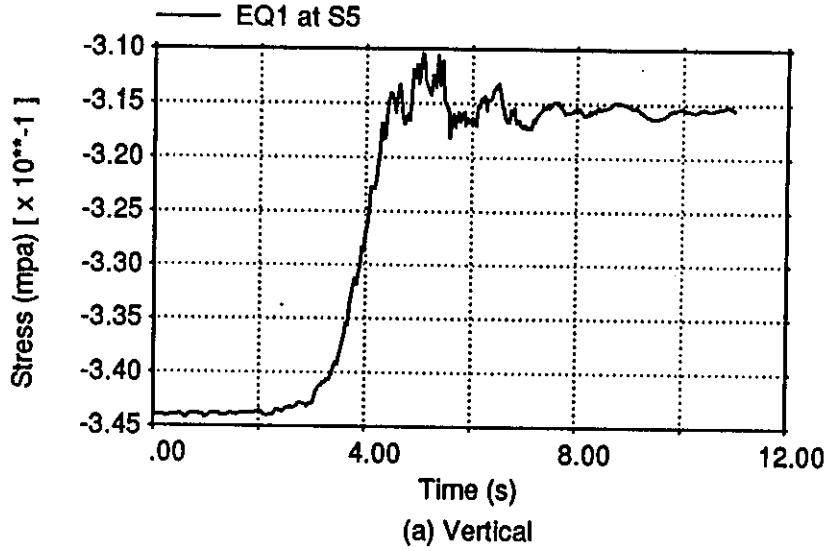

(a) Vertical

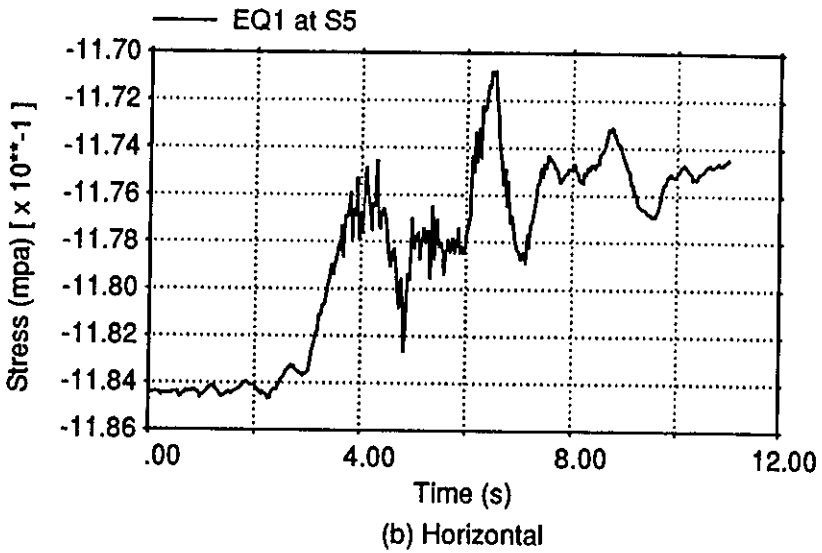

(b) Horizontal

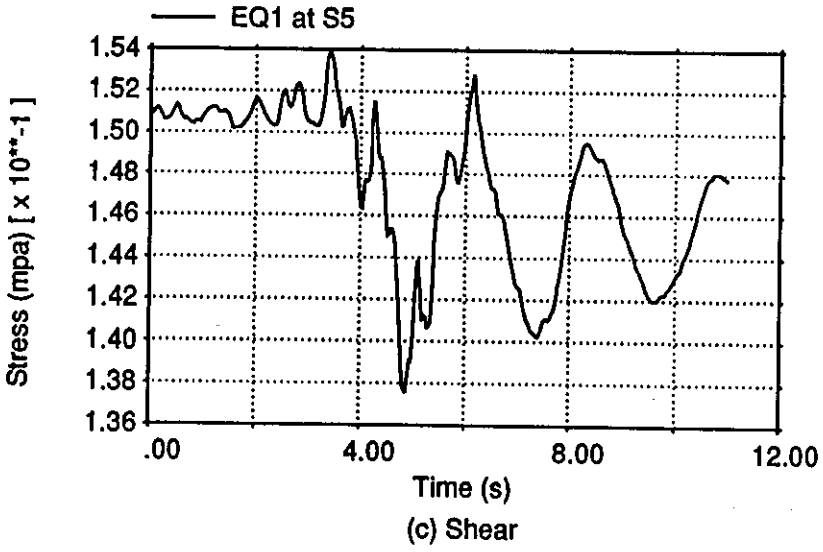

(c) Shear

Stress quantities for EQ1 at output point S5

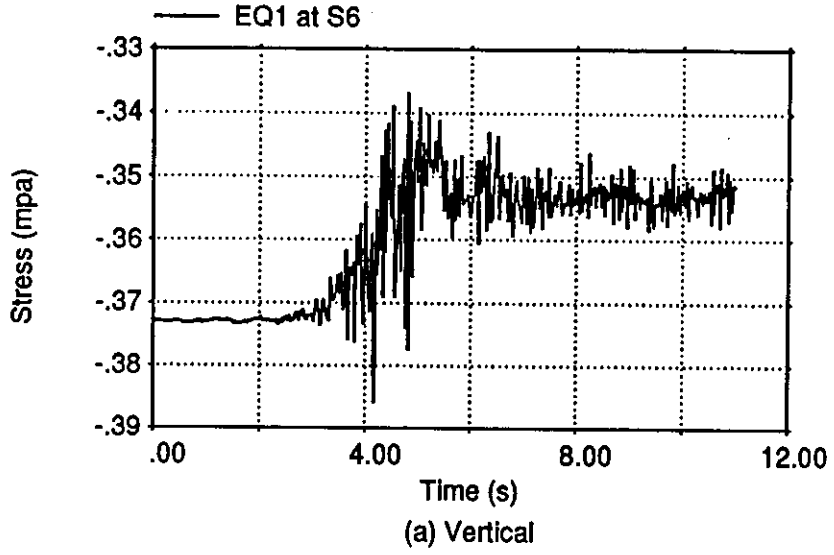

(a) Vertical

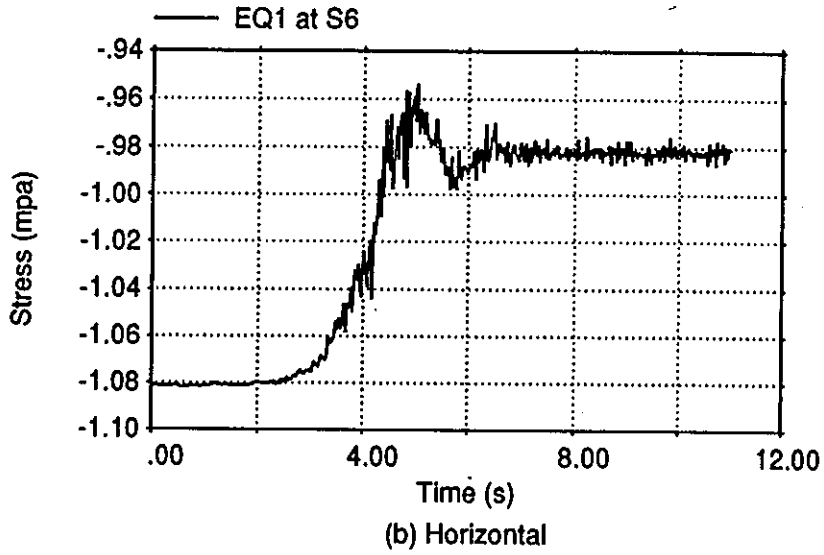

(b) Horizontal

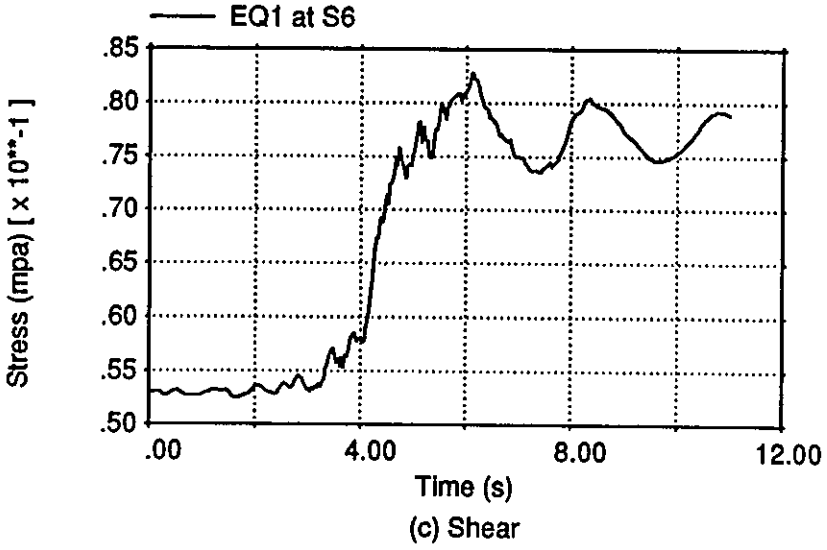

(c) Shear

Stress quantities for EQ1 at output point S6

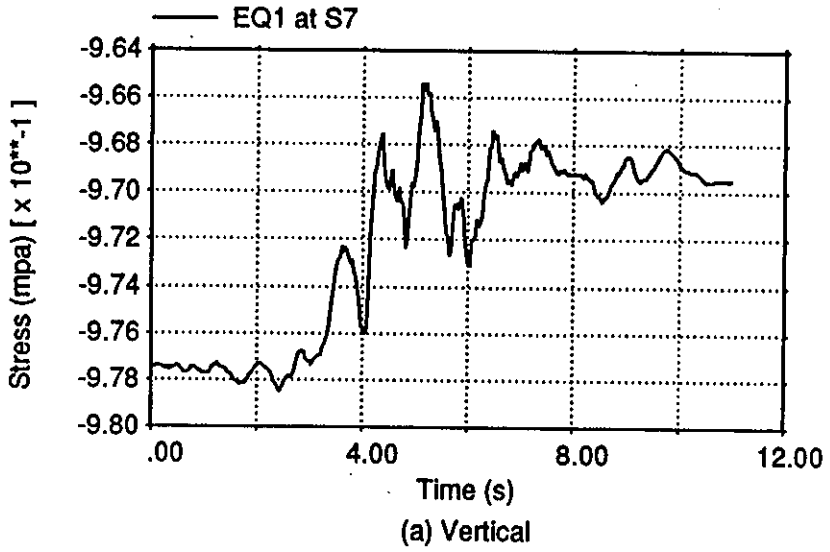

(a) Vertical

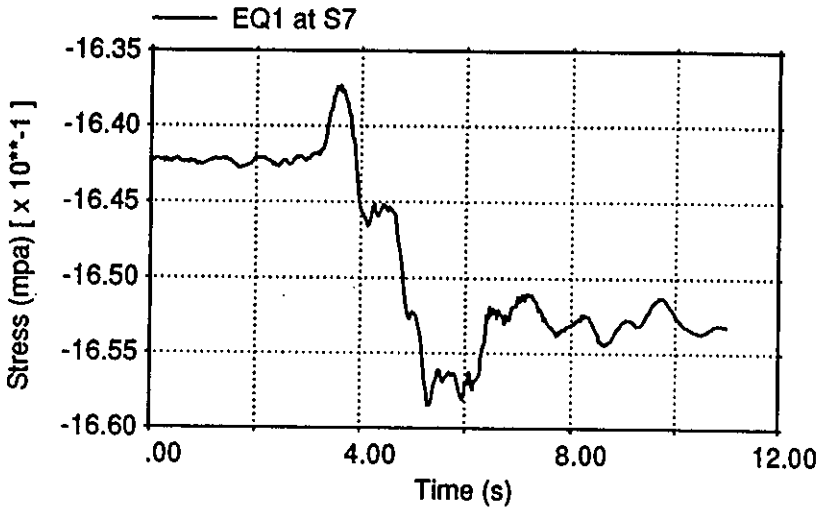

(b) Horizontal

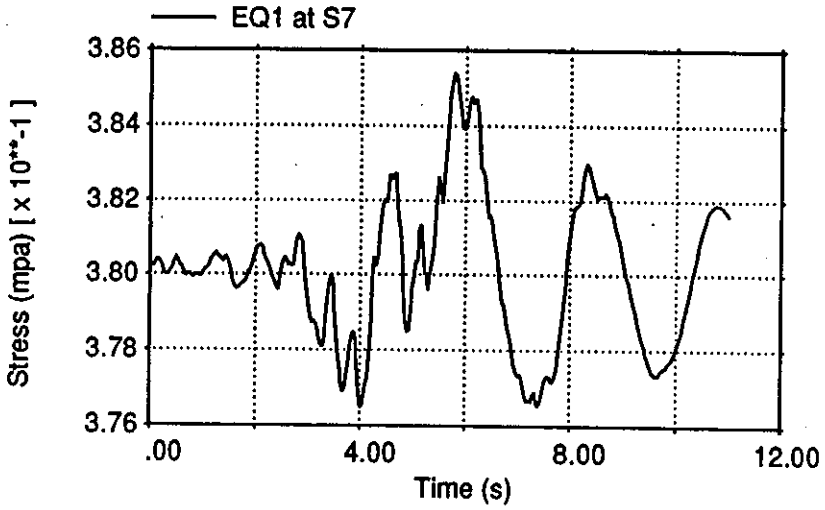

(c) Shear

Stress quantities for EQ1 at output point S7

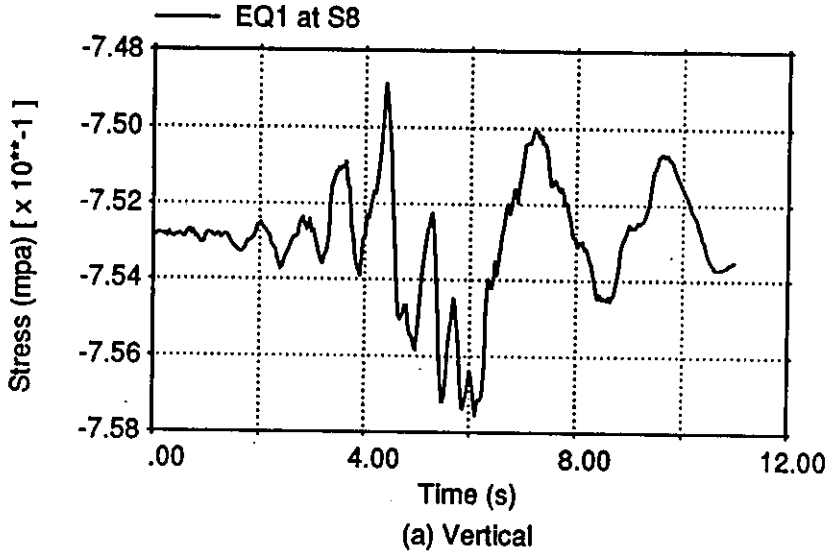

(a) Vertical

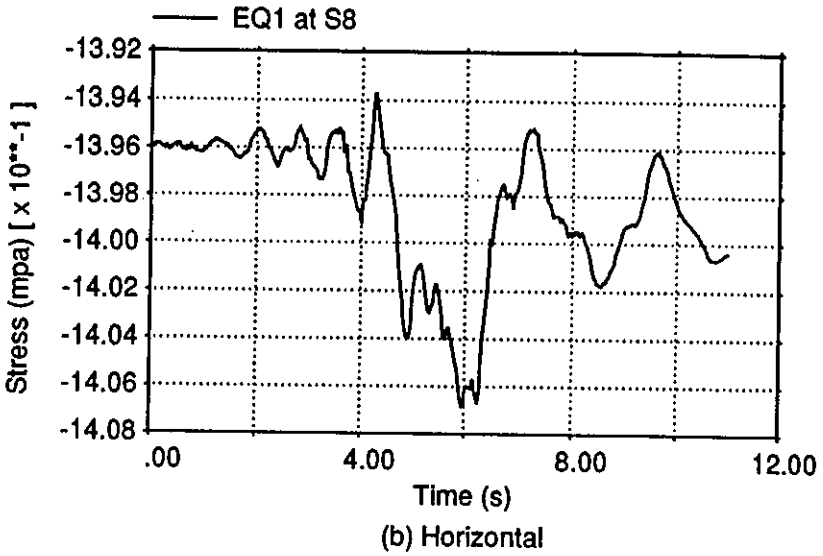

(b) Horizontal

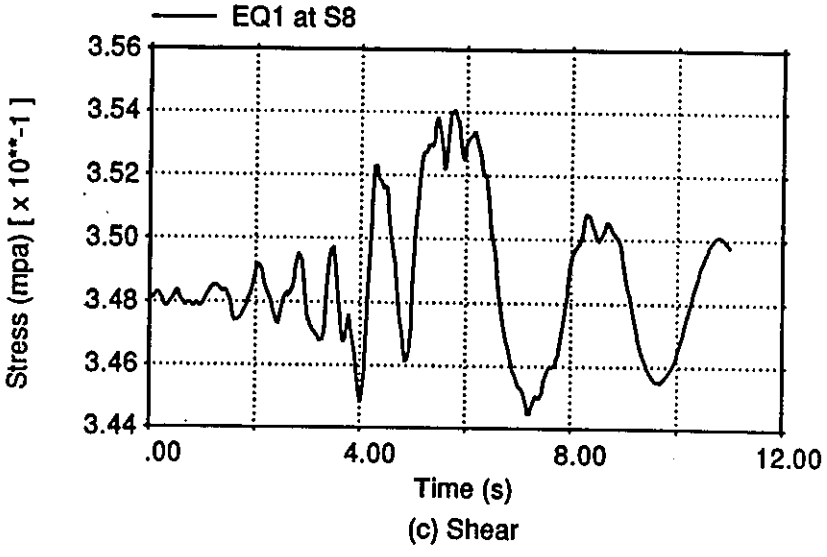

(c) Shear

Stress quantities for EQ1 at output point S8

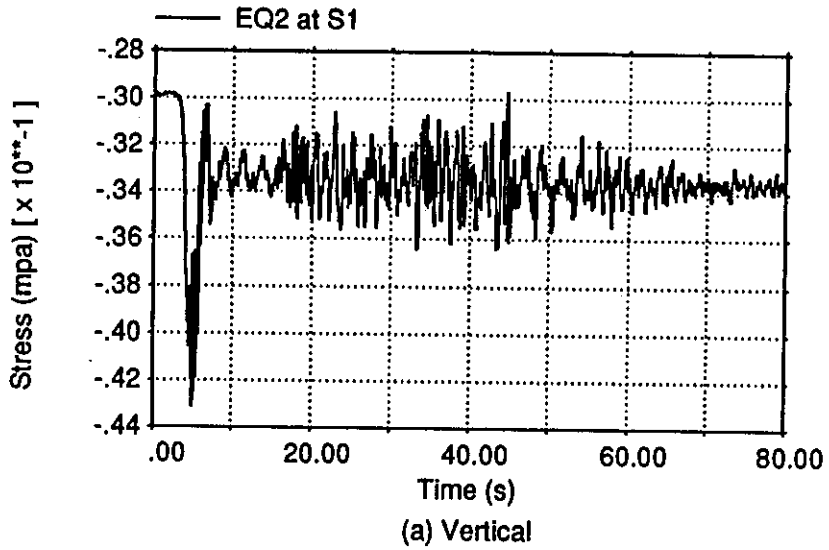

(a) Vertical

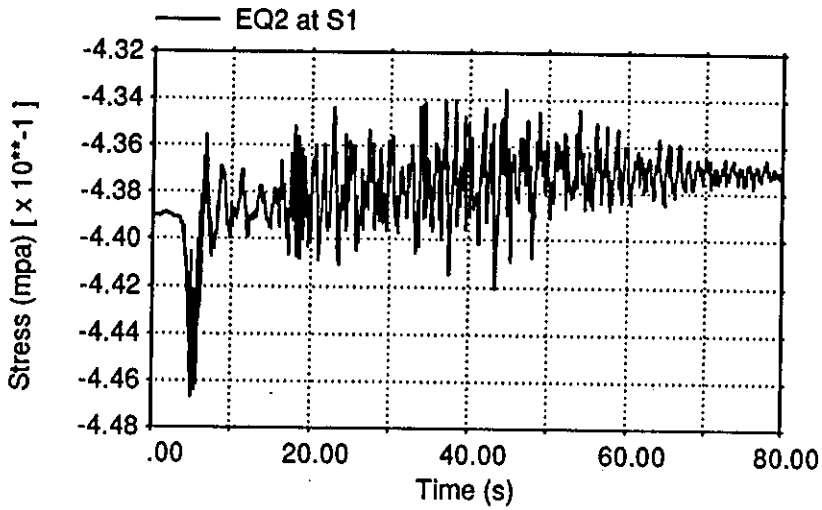

(b) Horizontal

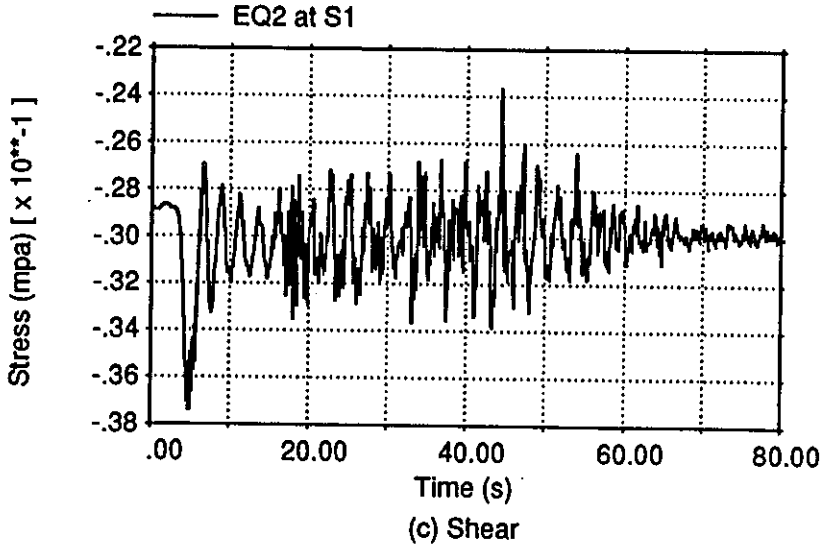

(c) Shear

Stress quantities for EQ2 at output point S1

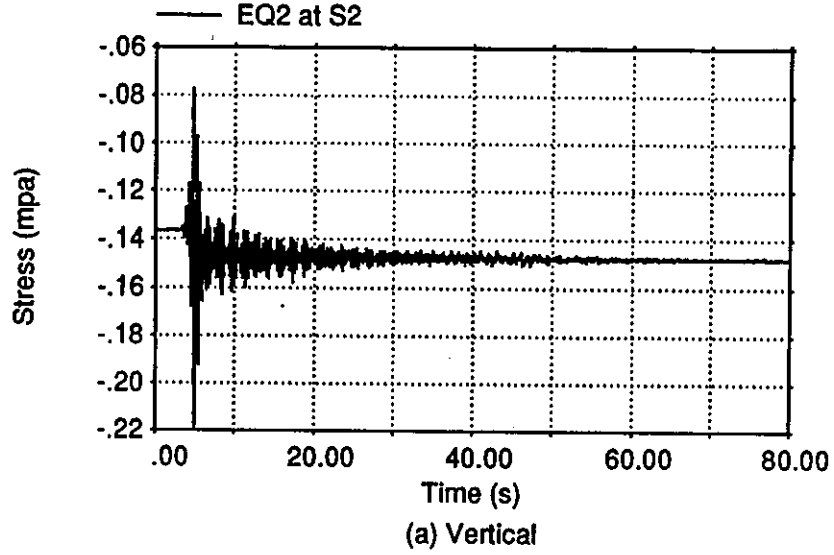

(a) Vertical

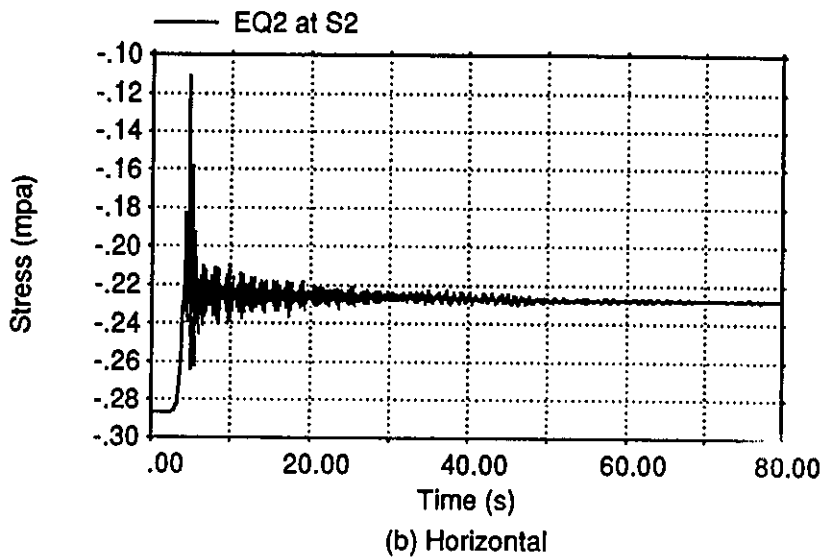

(b) Horizontal

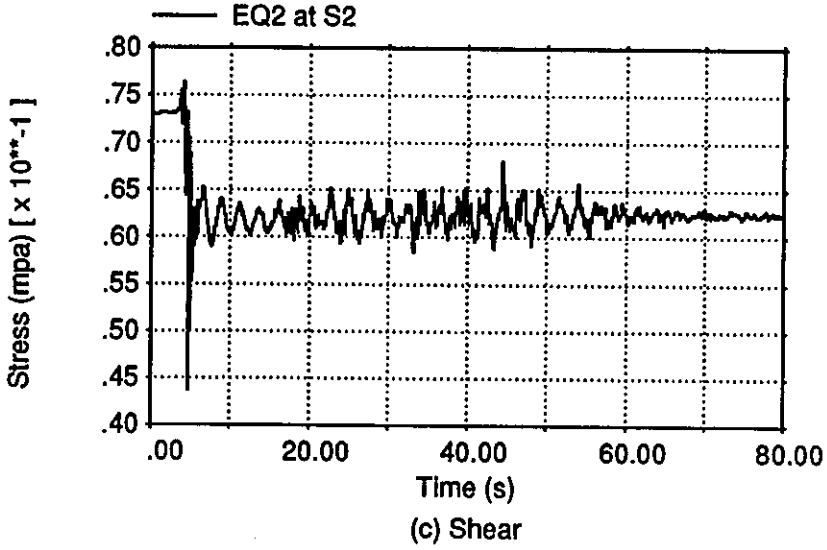

(c) Shear

Stress quantities for EQ2 at output point S2

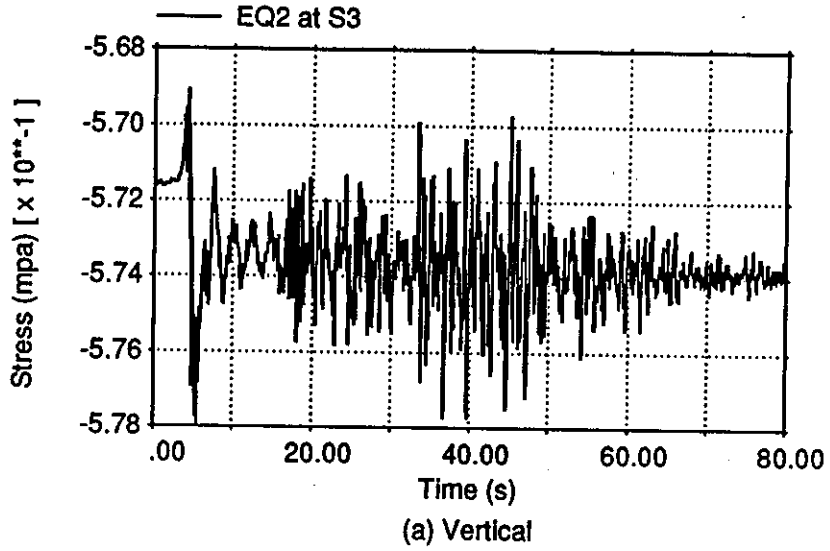

(a) Vertical

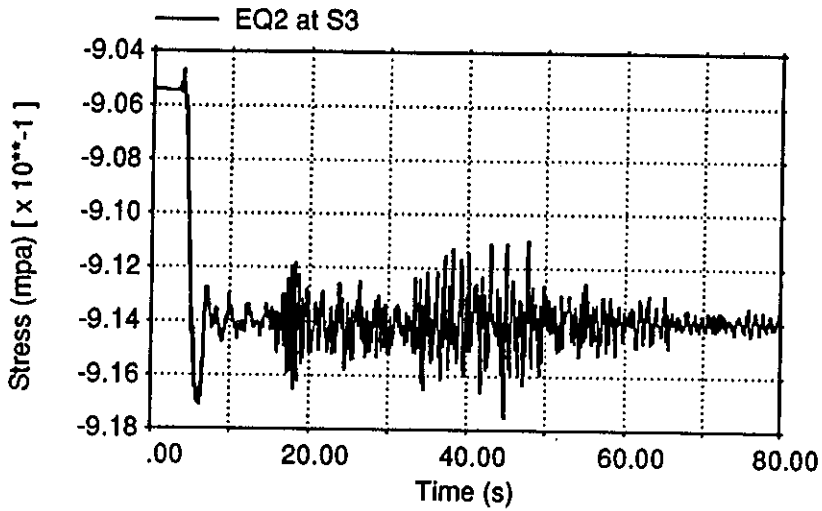

(b) Horizontal

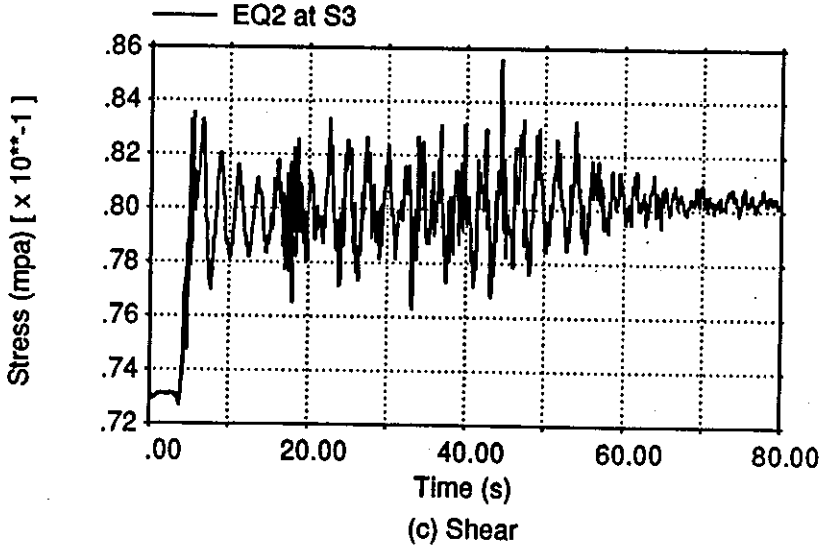

(c) Shear

Stress quantities for EQ2 at output point S3

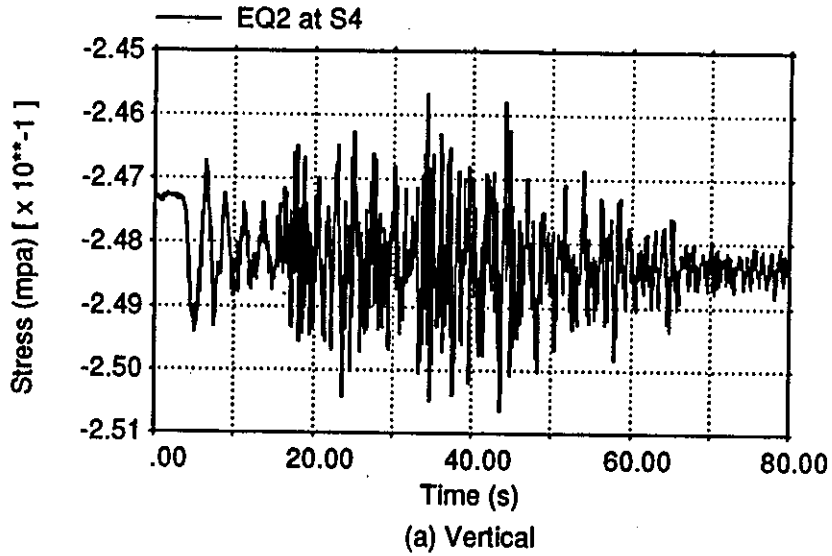

(a) Vertical

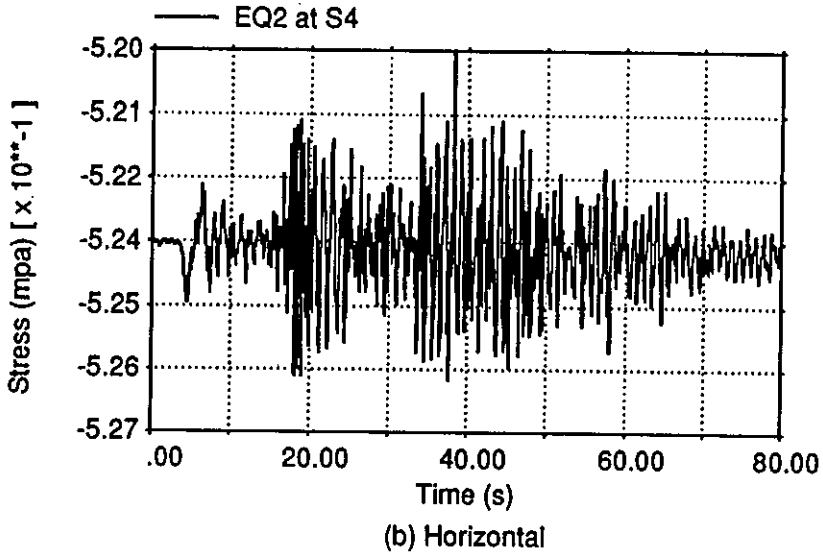

(b) Horizontal

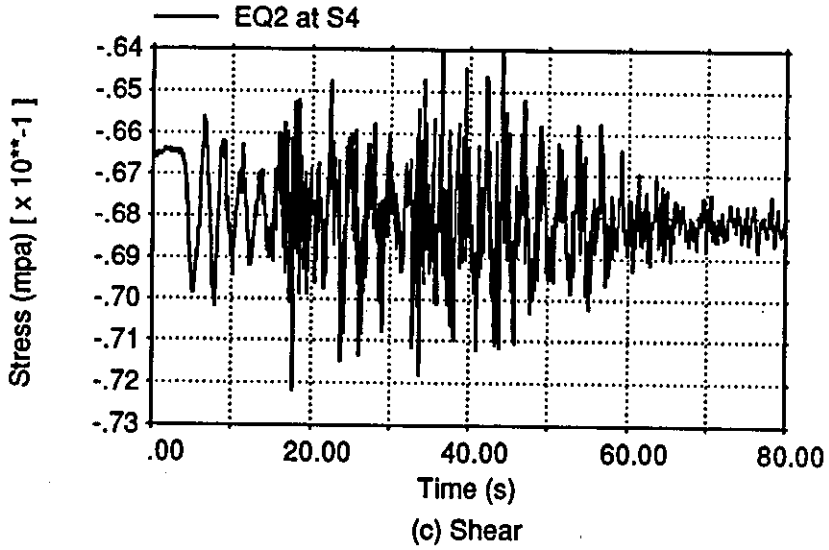

(c) Shear

Stress quantities for EQ2 at output point S4

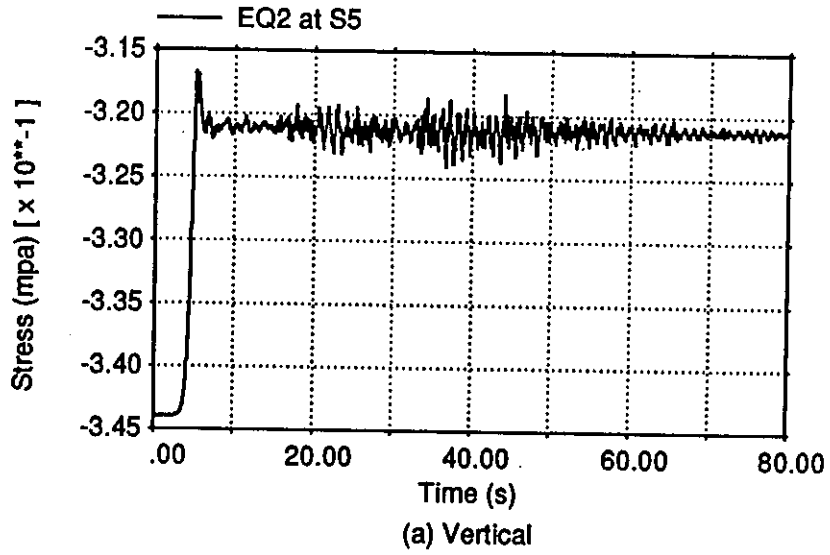

(a) Vertical

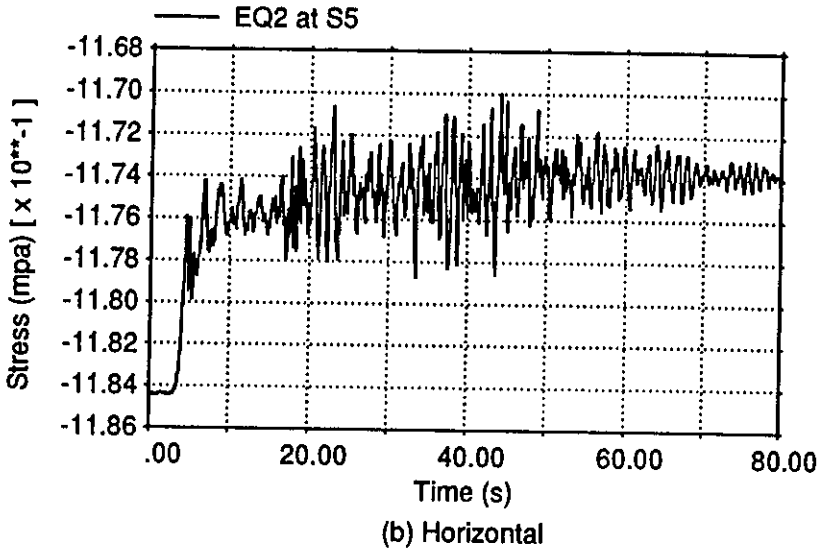

(b) Horizontal

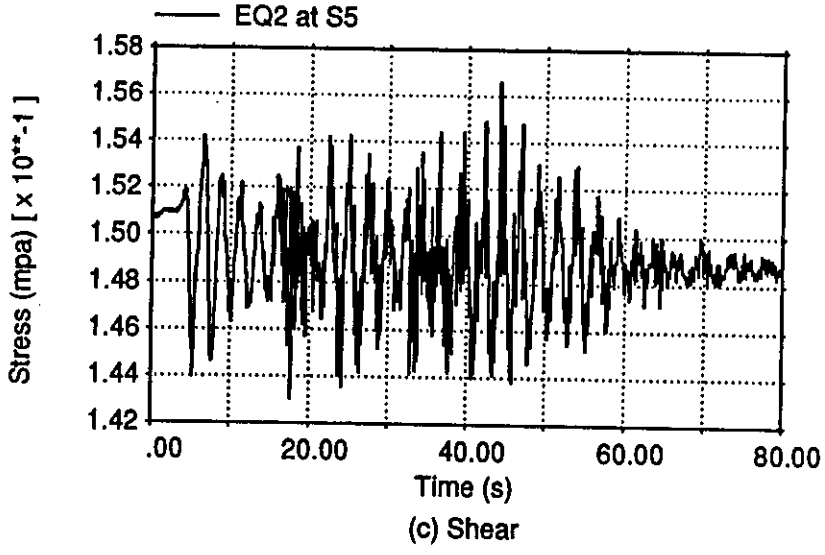

(c) Shear

Stress quantities for EQ2 at output point S5

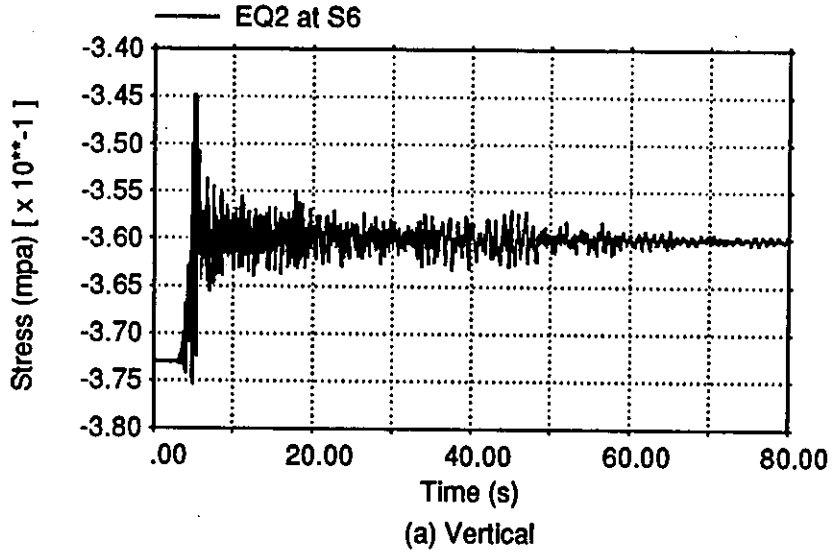

(a) Vertical

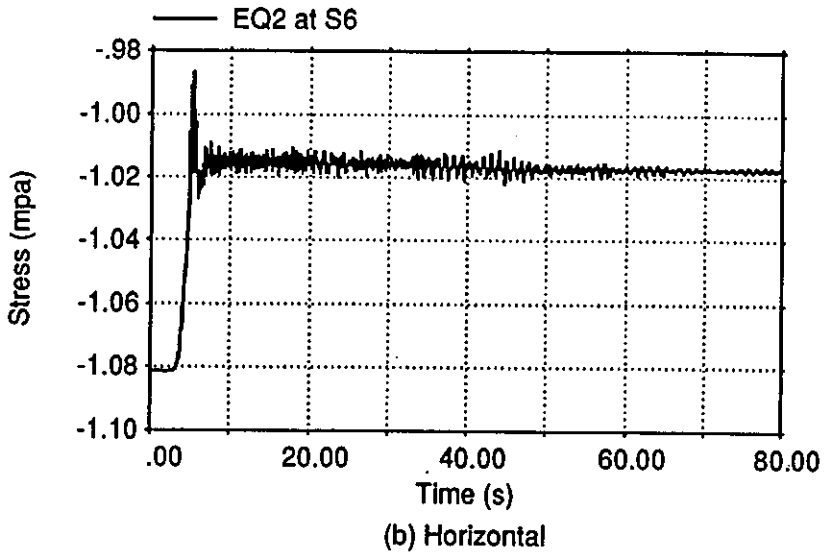

(b) Horizontal

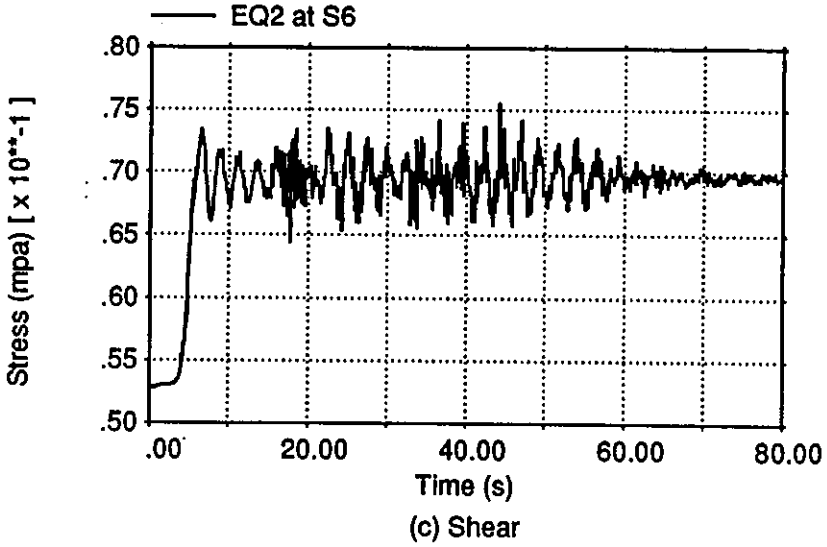

(c) Shear

Stress quantities for EQ2 at output point S6

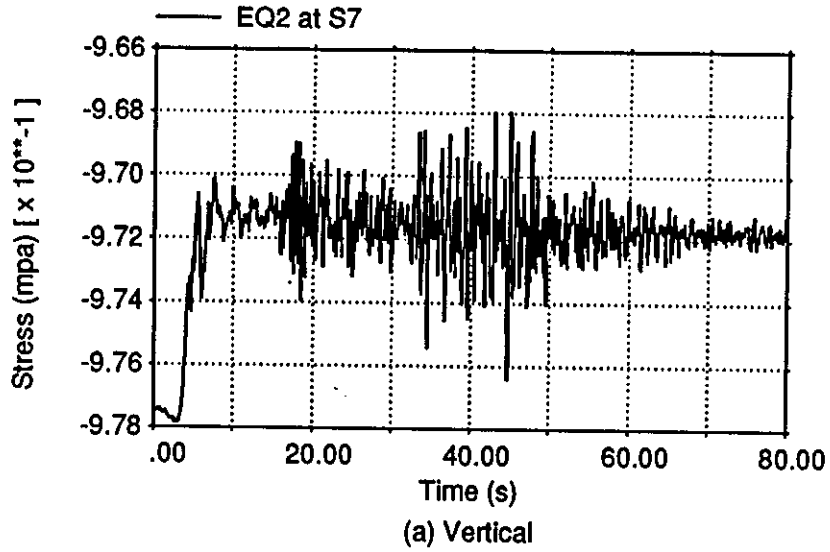

(a) Vertical

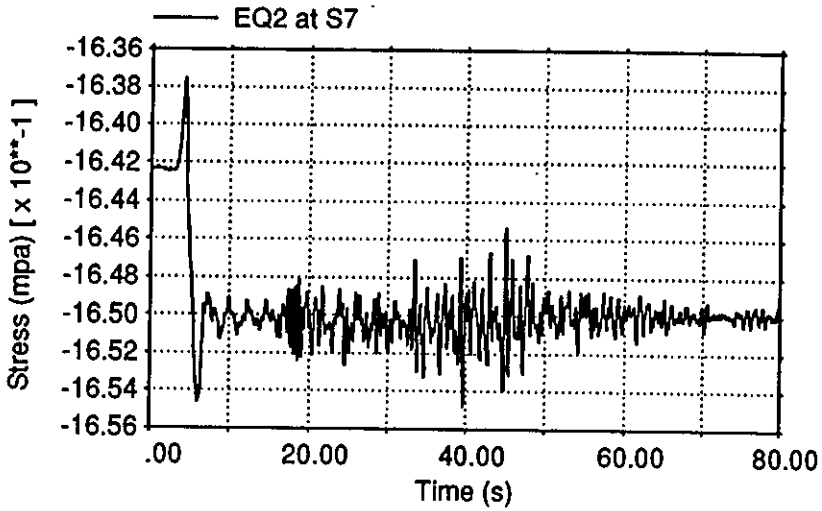

(b) Horizontal

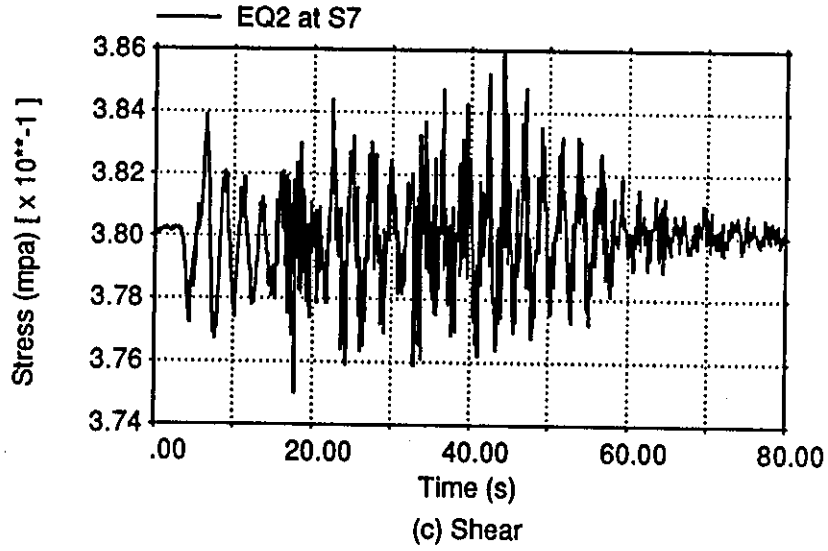

(c) Shear

Stress quantities for EQ2 at output point S7

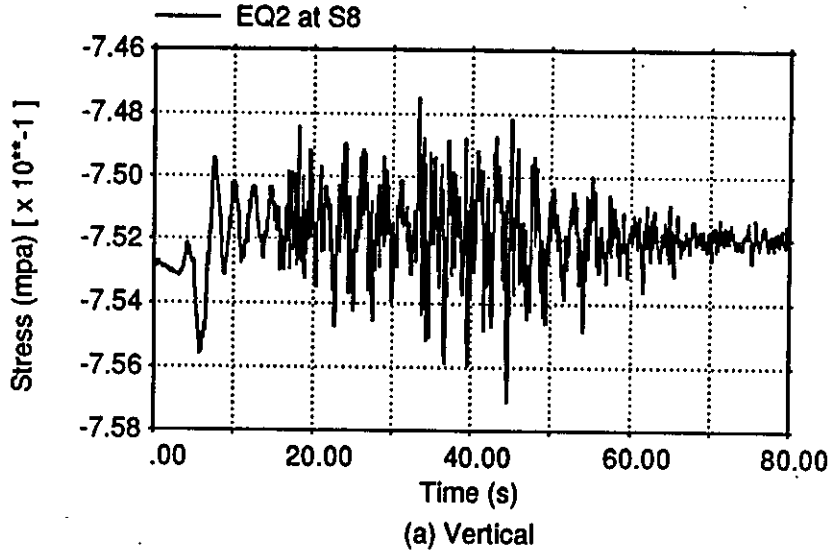

(a) Vertical

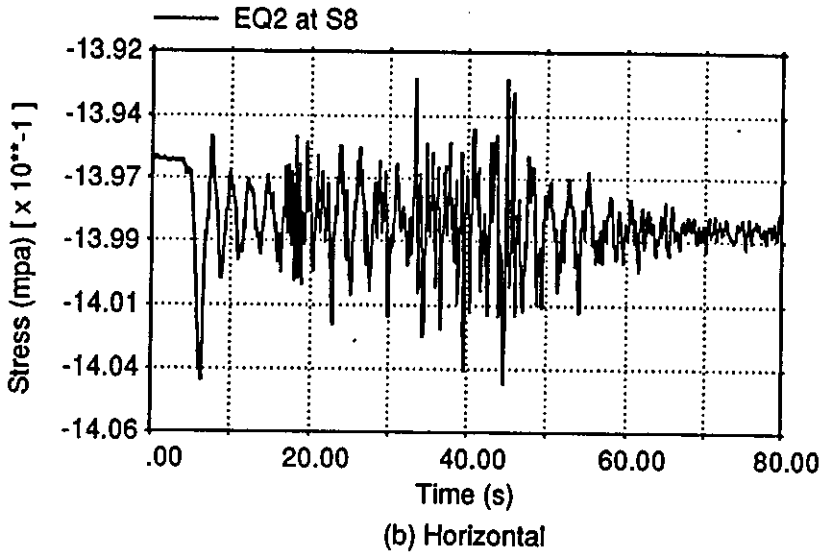

(b) Horizontal

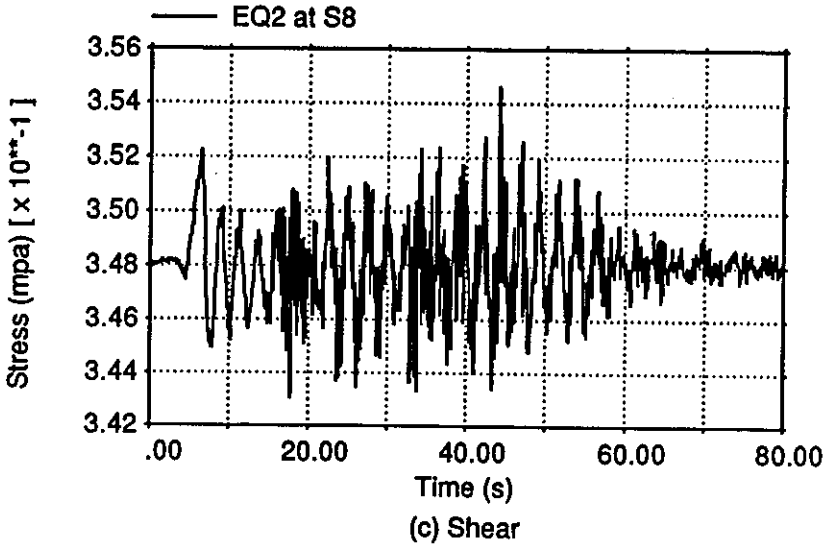

(c) Shear

Stress quantities for EQ2 at output point S8

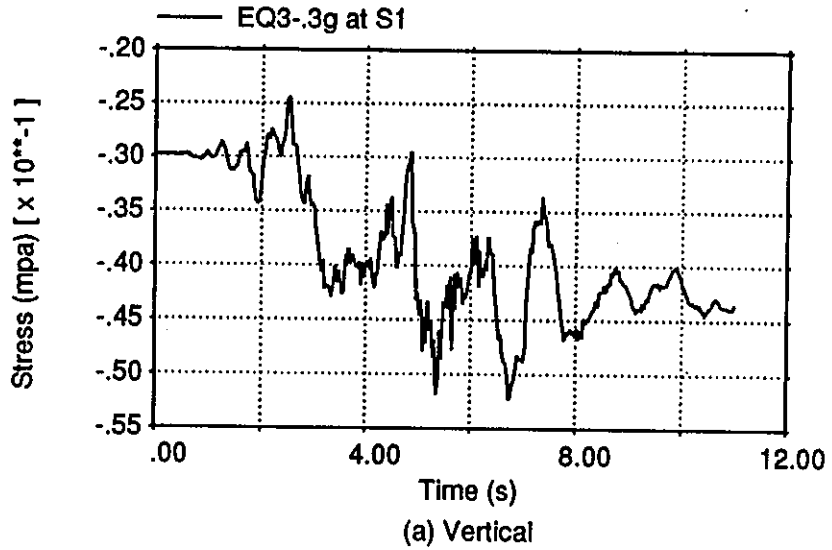

(a) Vertical

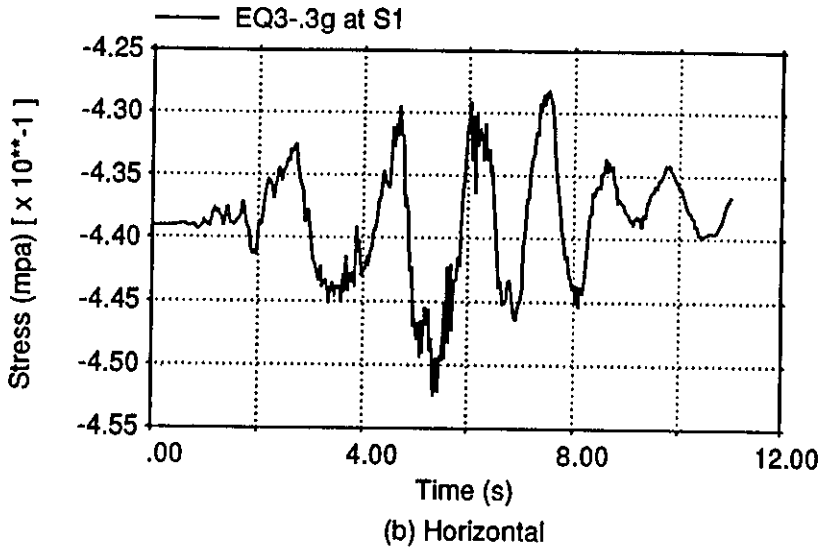

(b) Horizontal

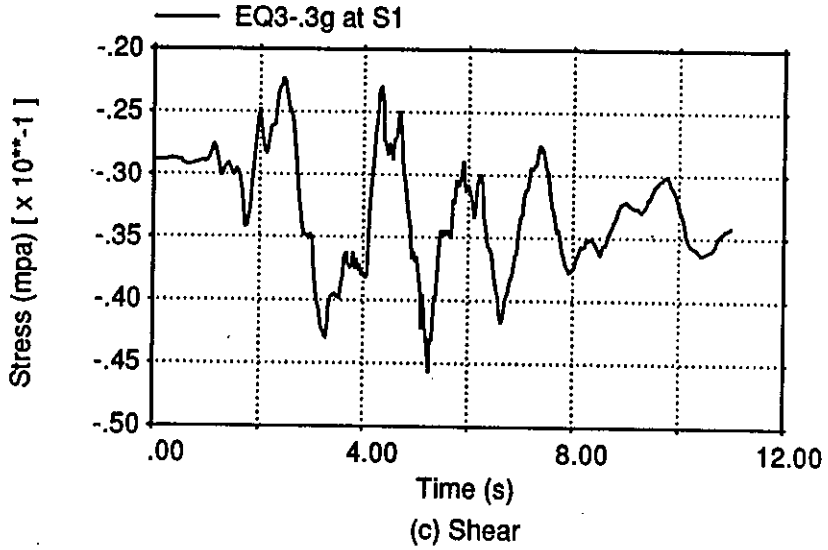

(c) Shear

Stress quantities for EQ3-.3g at output point S1

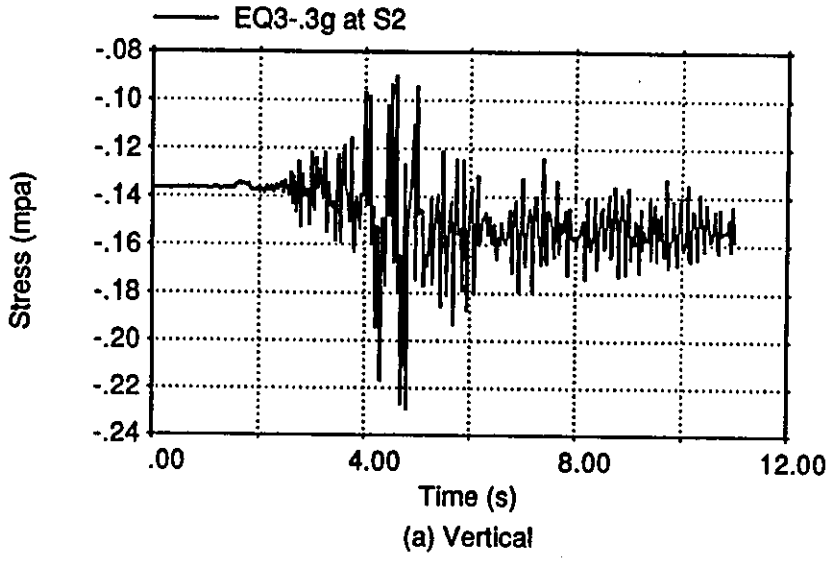

(a) Vertical

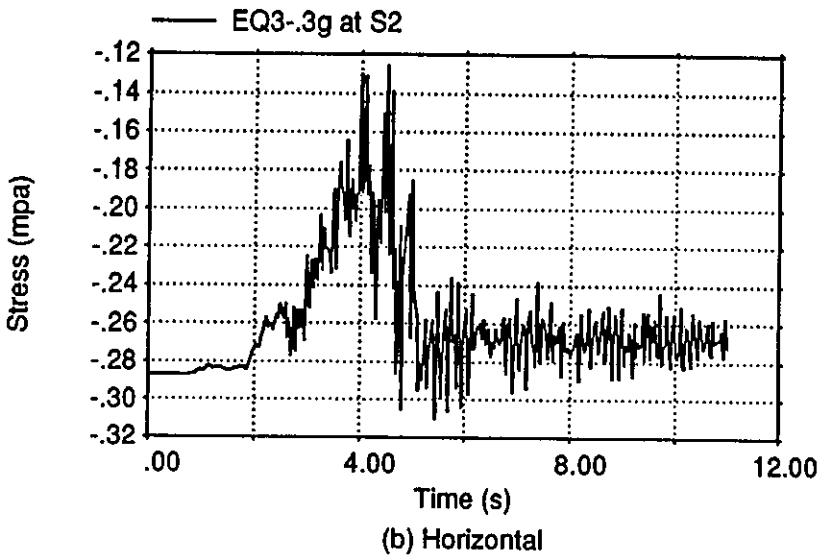

(b) Horizontal

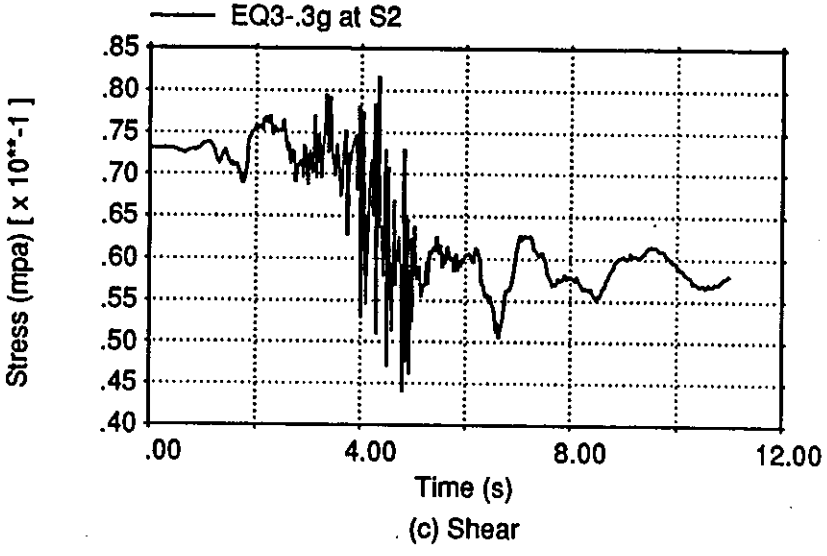

(c) Shear

Stress quantities for EQ3-.3g at output point S2

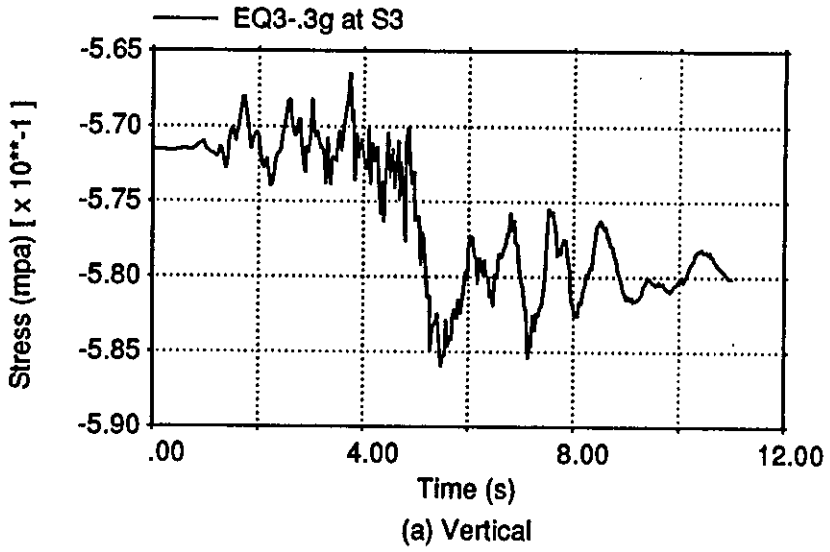

(a) Vertical

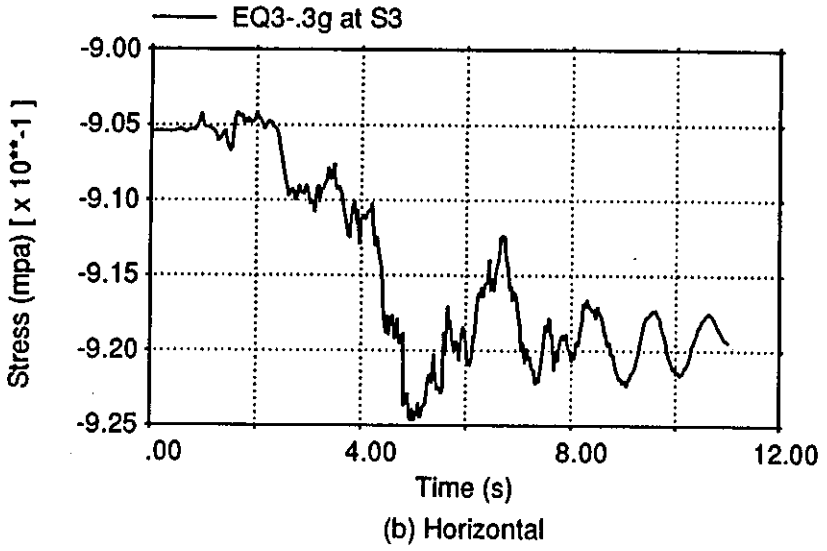

(b) Horizontal

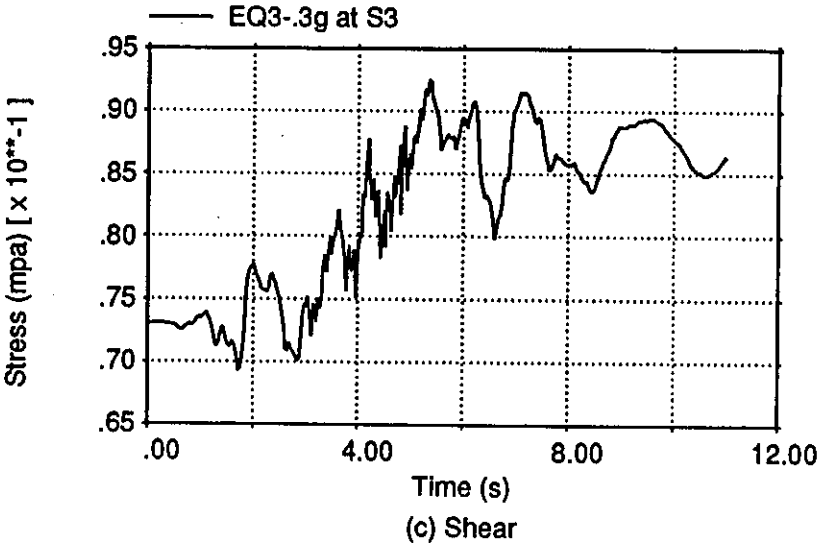

(c) Shear

Stress quantities for EQ3-.3g at output point S3

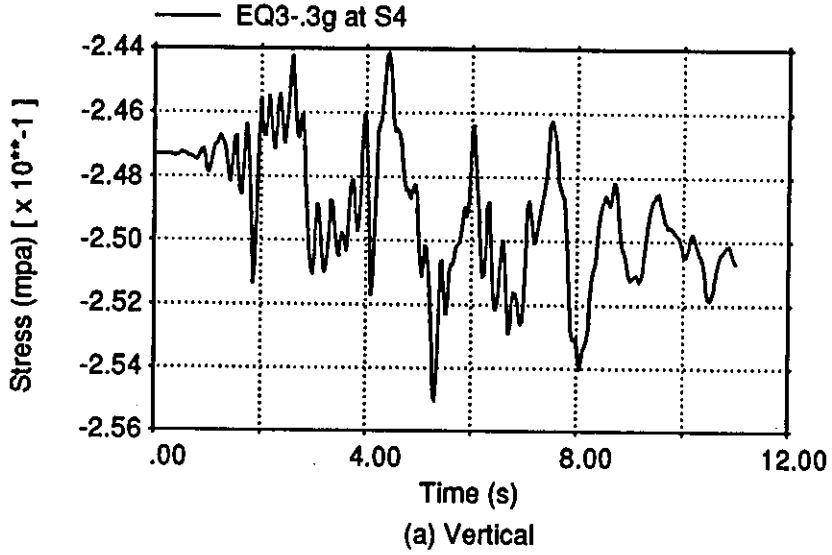

(a) Vertical

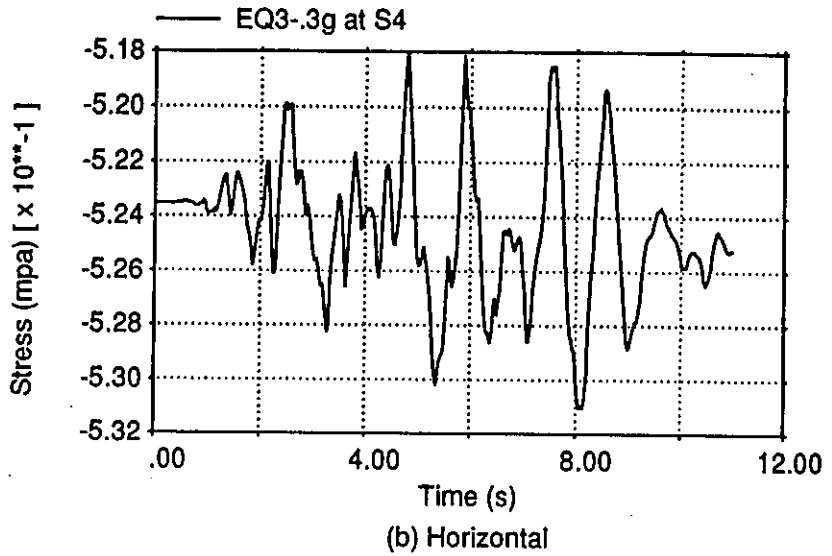

(b) Horizontal

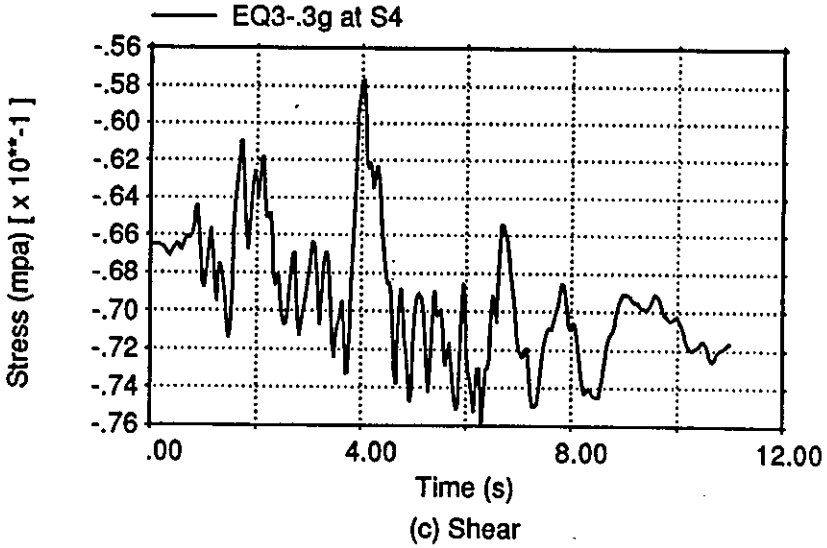

(c) Shear

Stress quantities for EQ3-.3g at output point S4

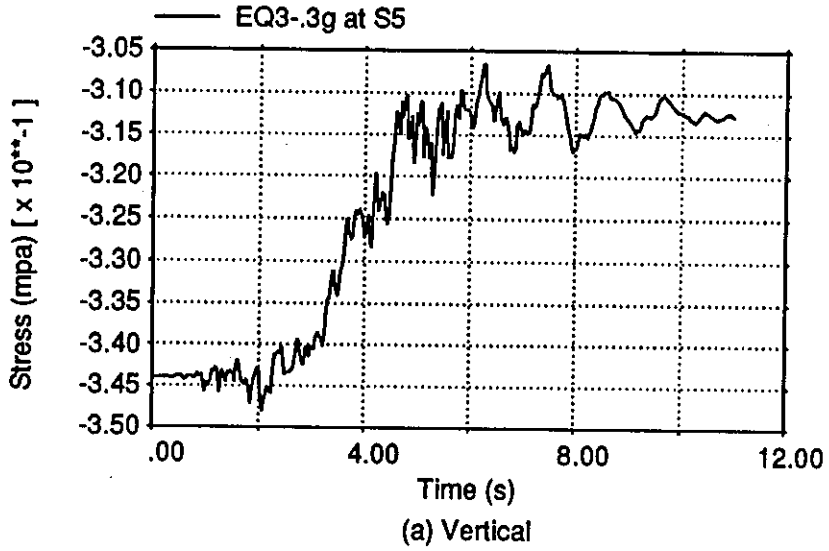

(a) Vertical

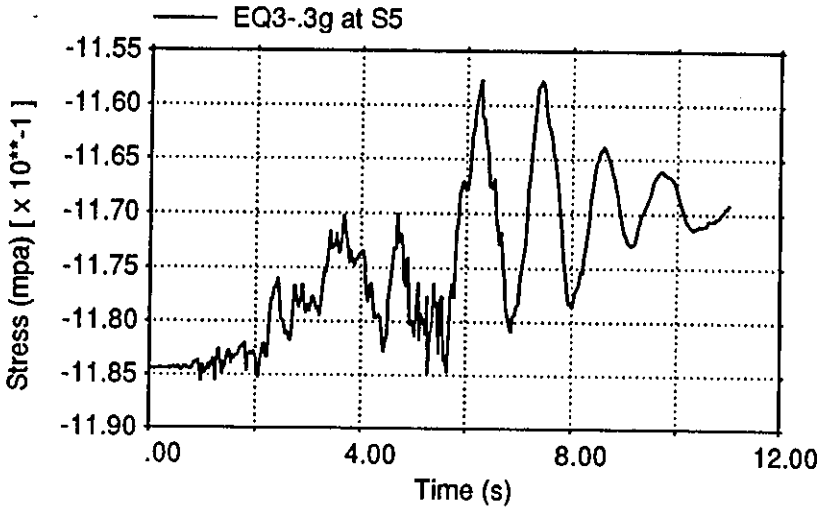

(b) Horizontal

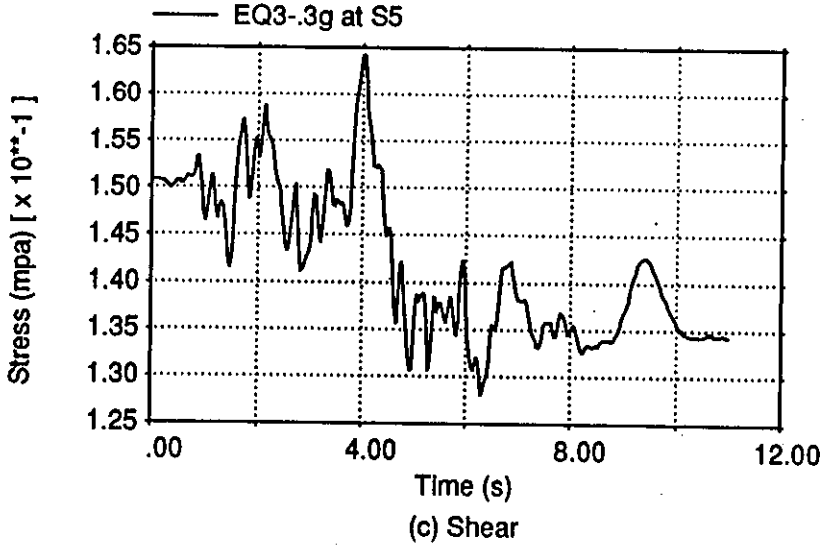

(c) Shear

Stress quantities for EQ3-.3g at output point S5

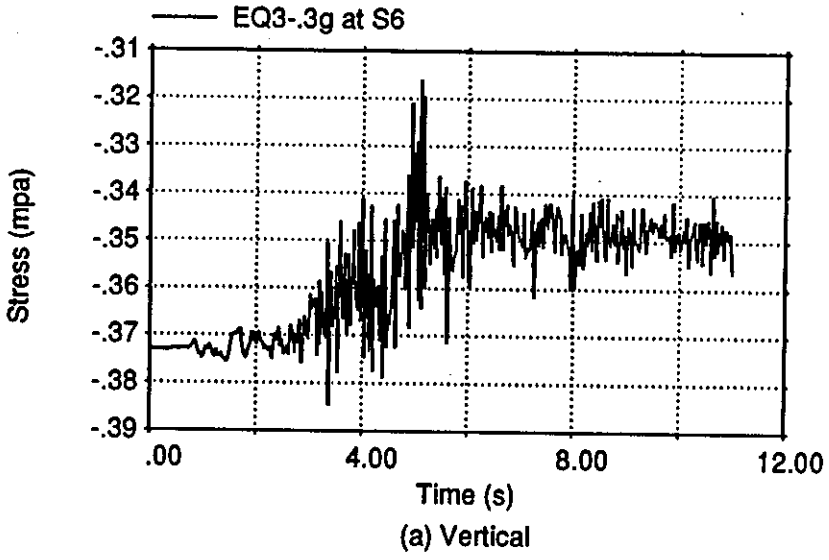

(a) Vertical

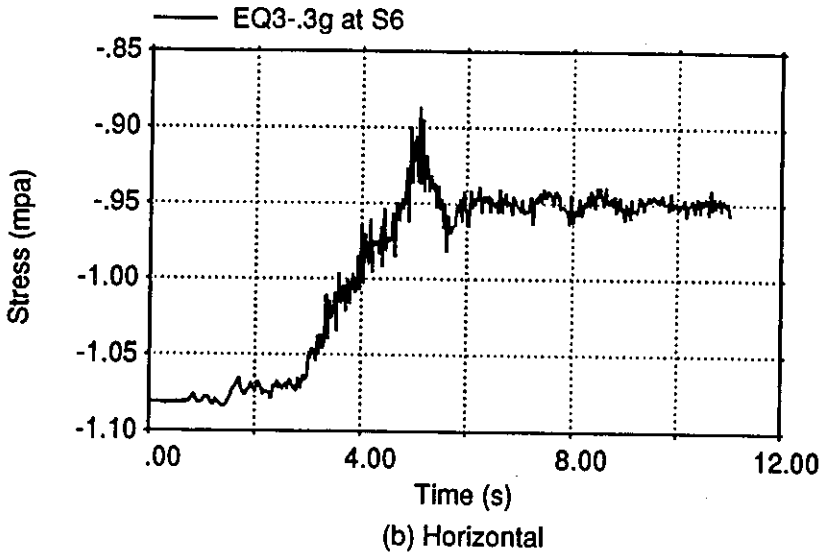

(b) Horizontal

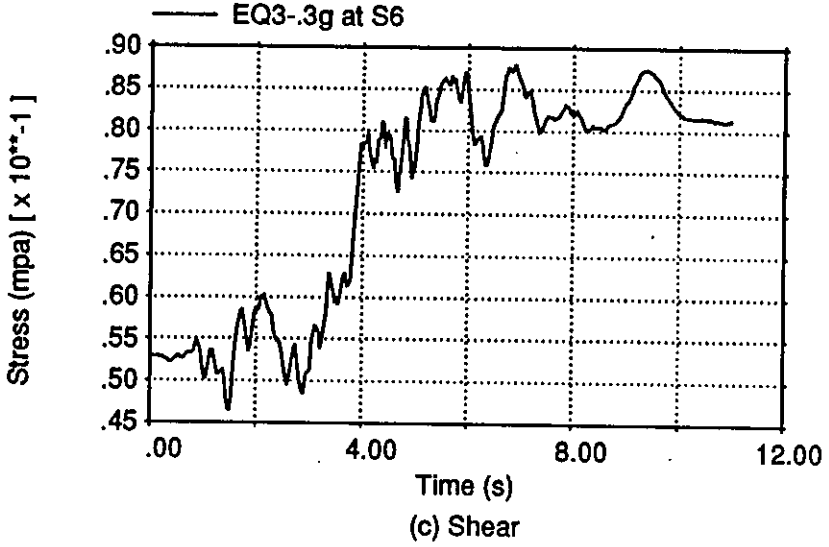

(c) Shear

Stress quantities for EQ3-.3g at output point S6

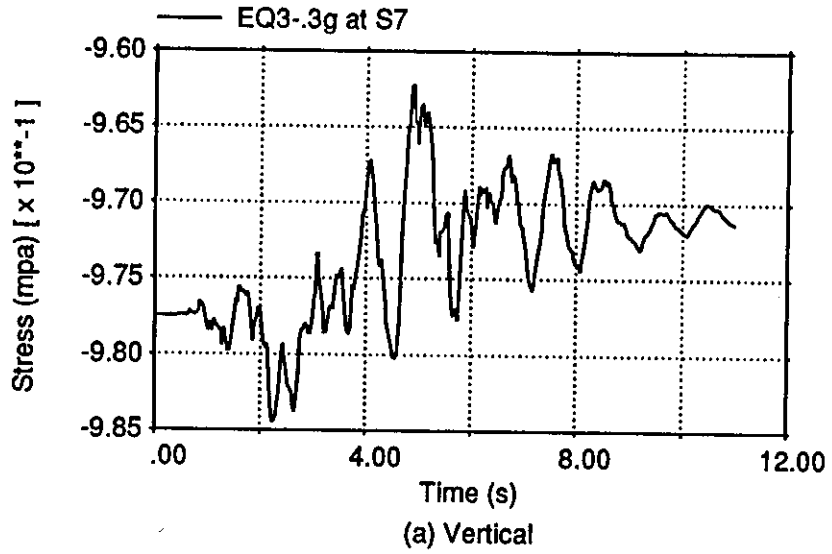

(a) Vertical

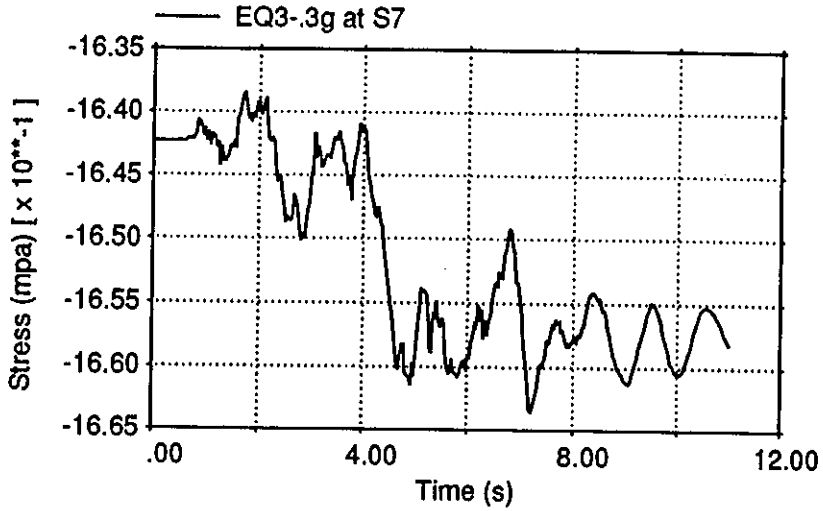

(b) Horizontal

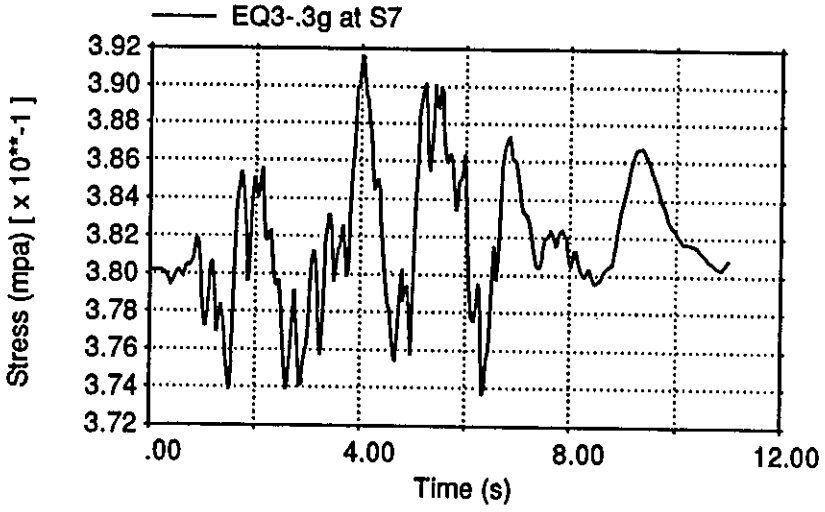

(c) Shear

Stress quantities for EQ3-.3g at output point S7

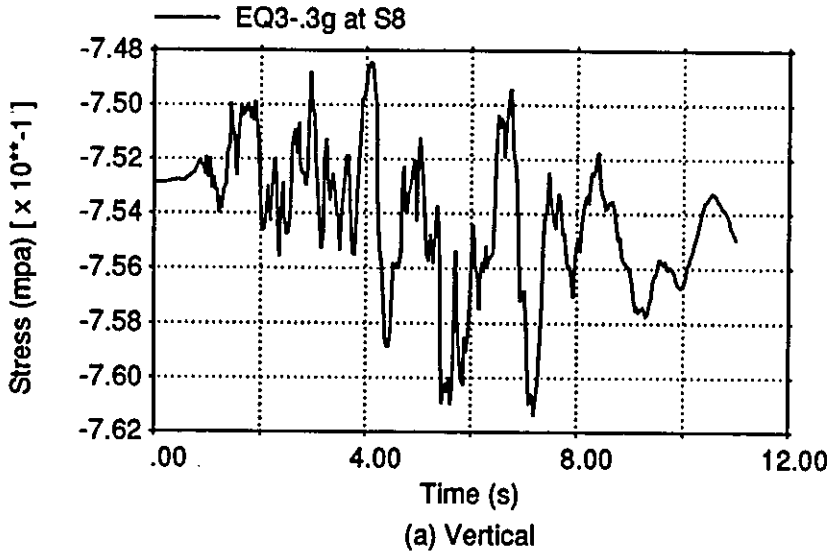

(a) Vertical

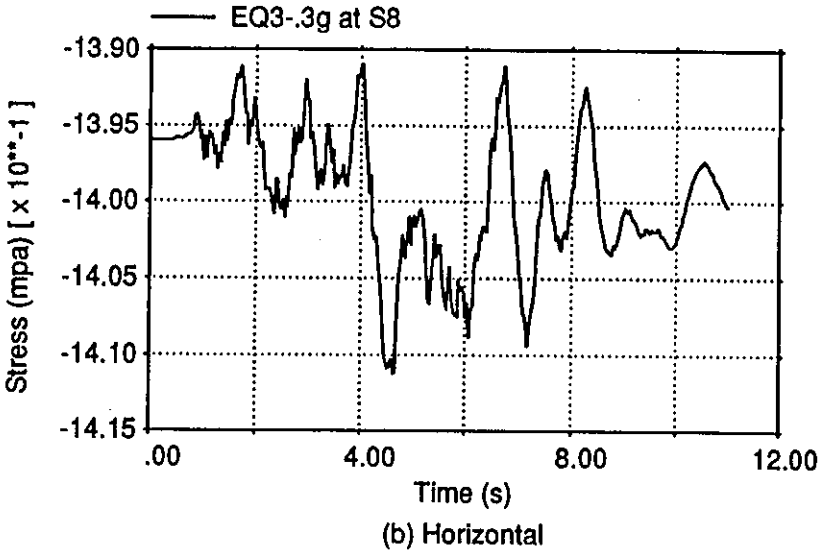

(b) Horizontal

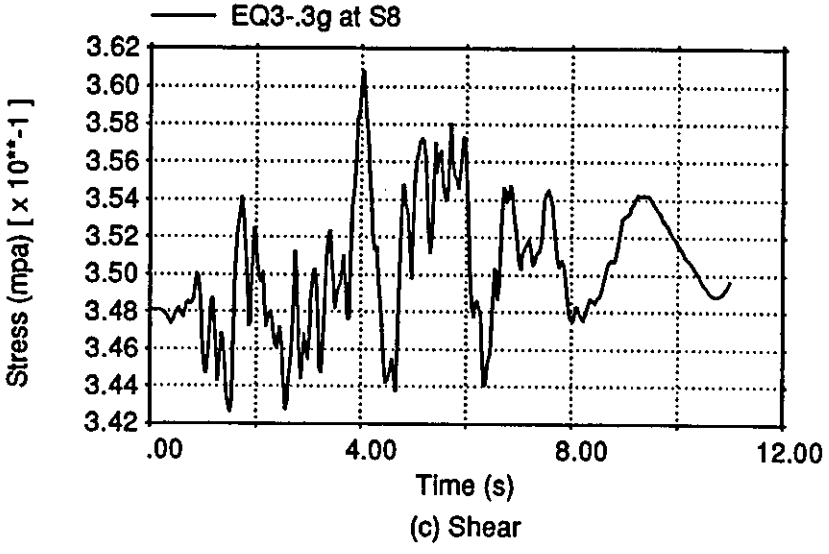

(c) Shear

Stress quantities for EQ3-.3g at output point S8

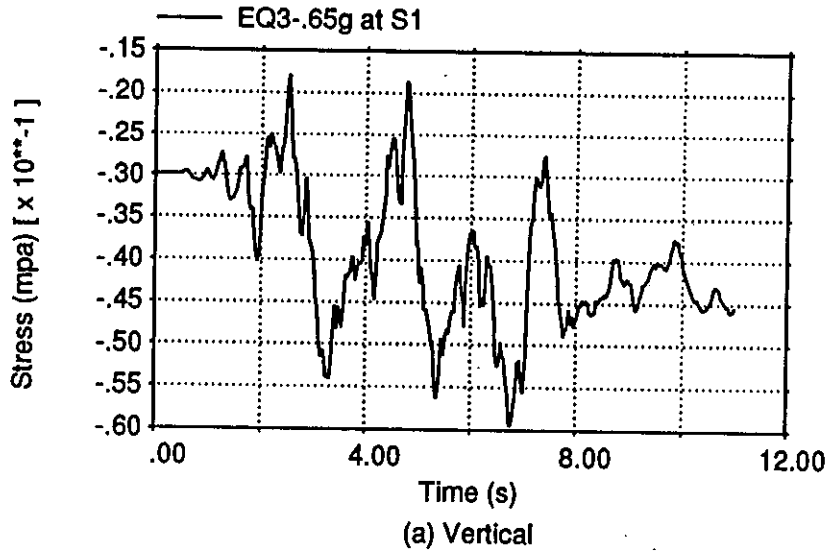

(a) Vertical

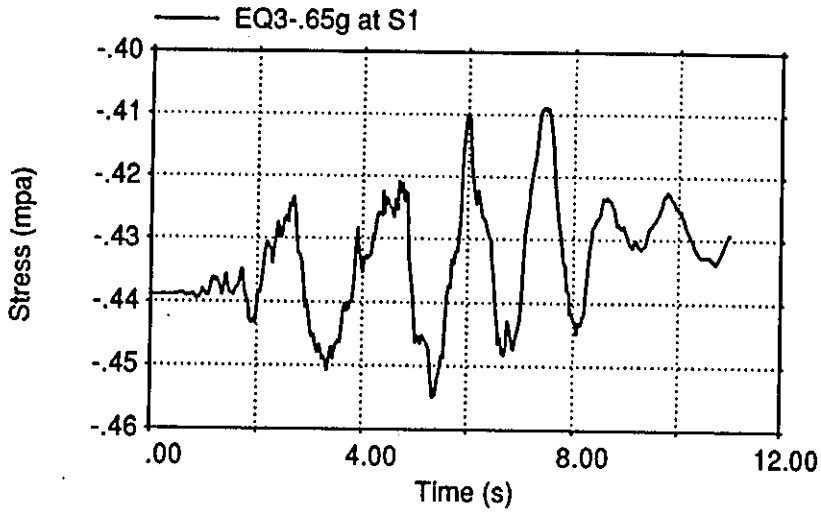

(b) Horizontal

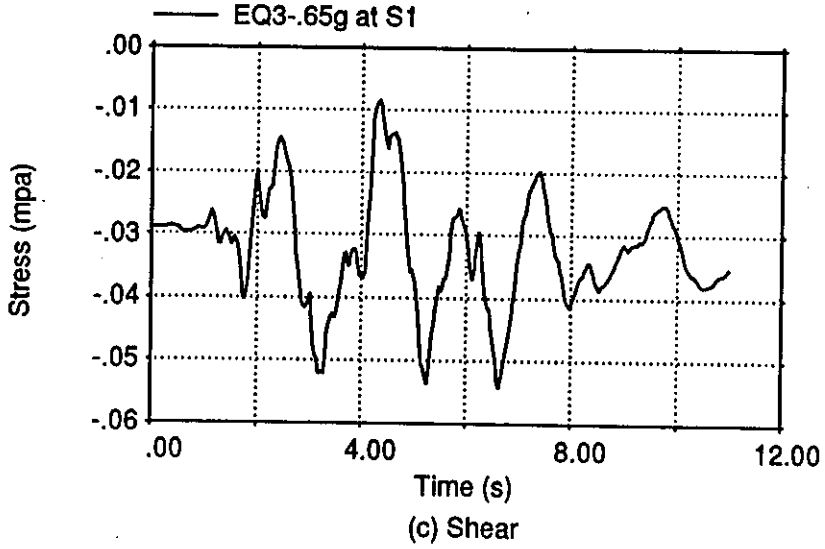

(c) Shear

Stress quantities for EQ3-.65g at output point S1

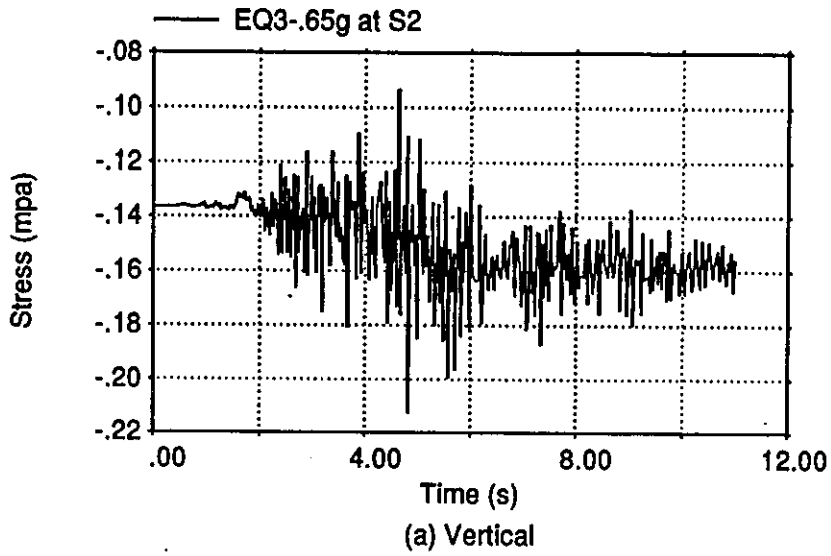

(a) Vertical

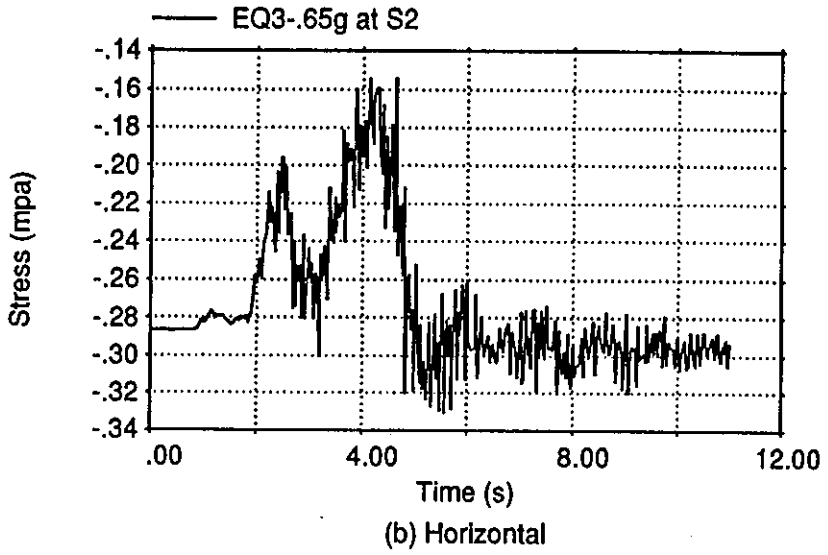

(b) Horizontal

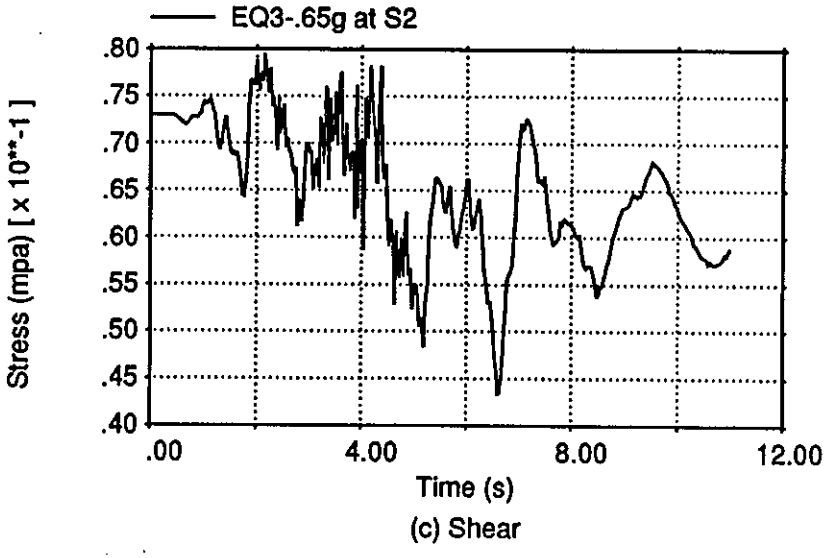

(c) Shear

Stress quantities for EQ3-.65g at output point S2

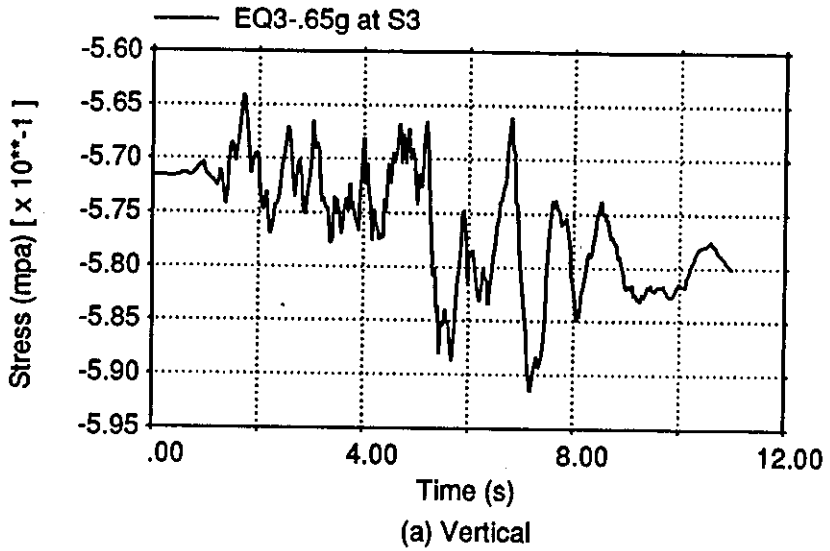

(a) Vertical

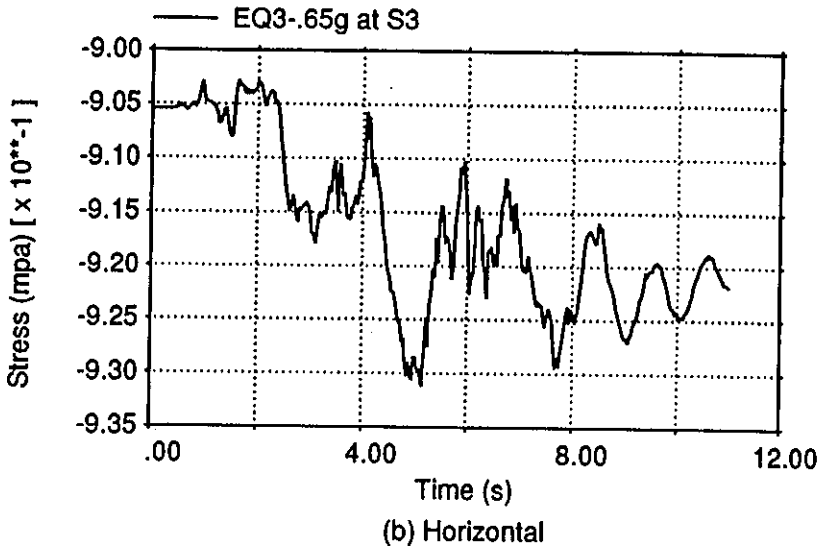

(b) Horizontal

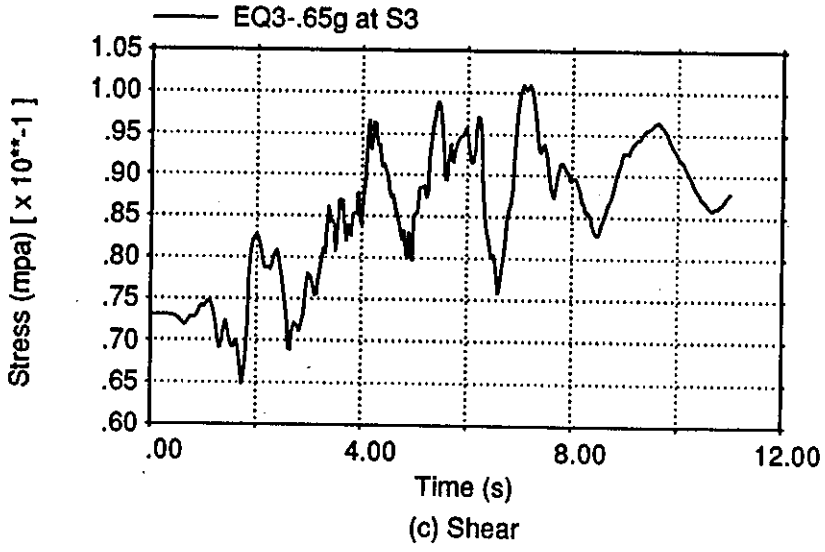

(c) Shear

Stress quantities for EQ3-.65g at output point S3

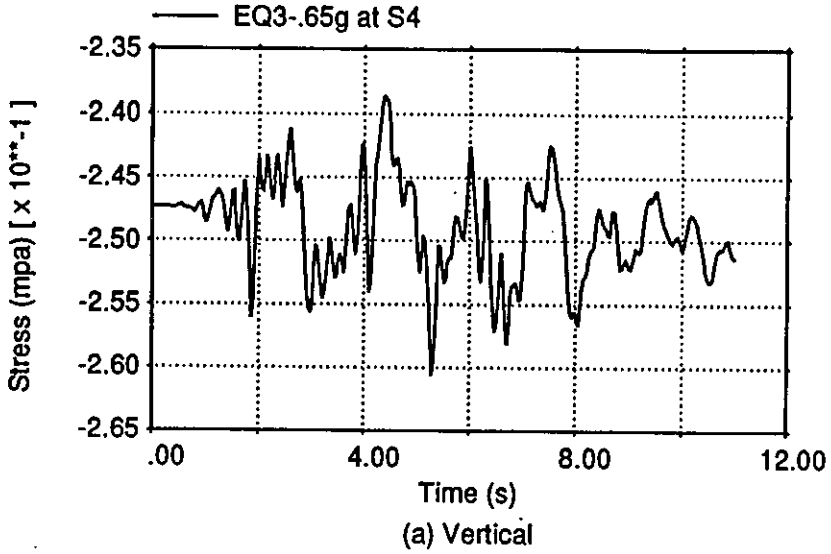

(a) Vertical

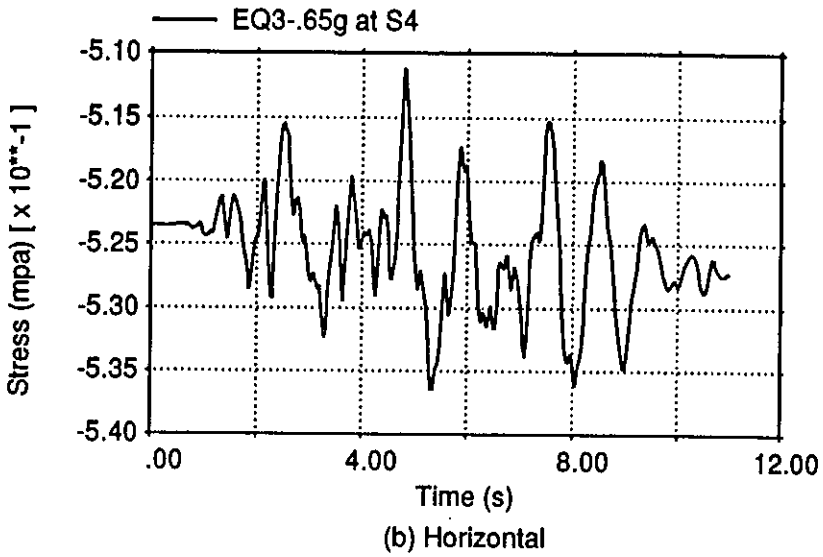

(b) Horizontal

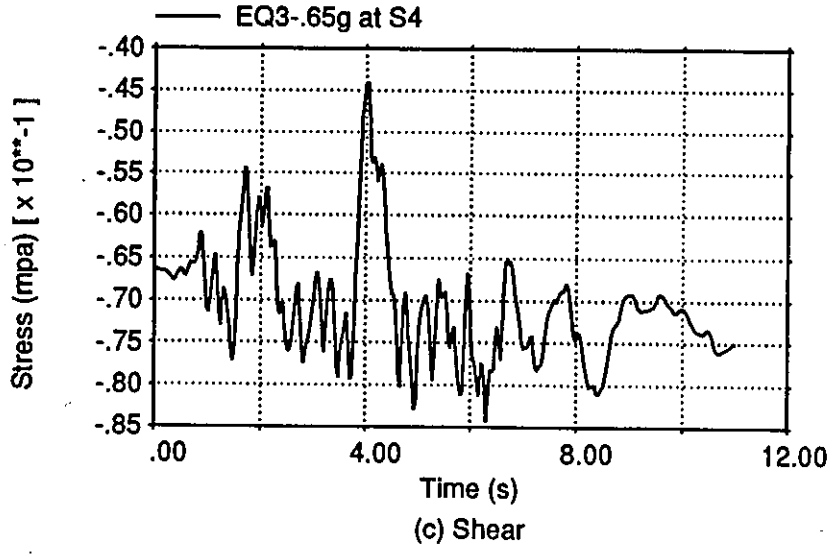

(c) Shear

Stress quantities for EQ3-.65g at output point S4

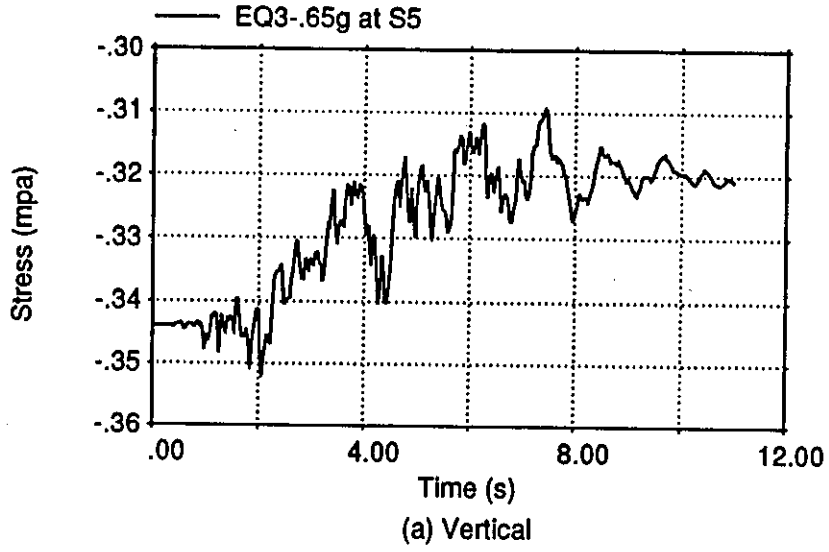

(a) Vertical

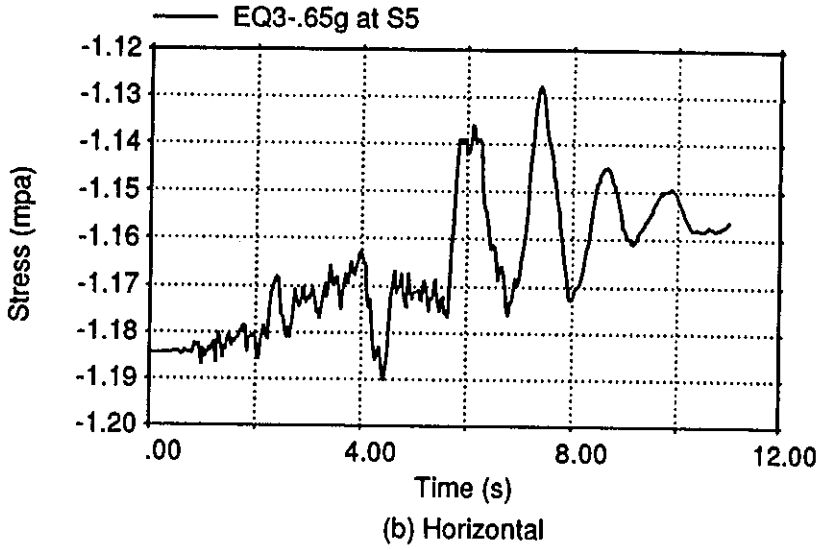

(b) Horizontal

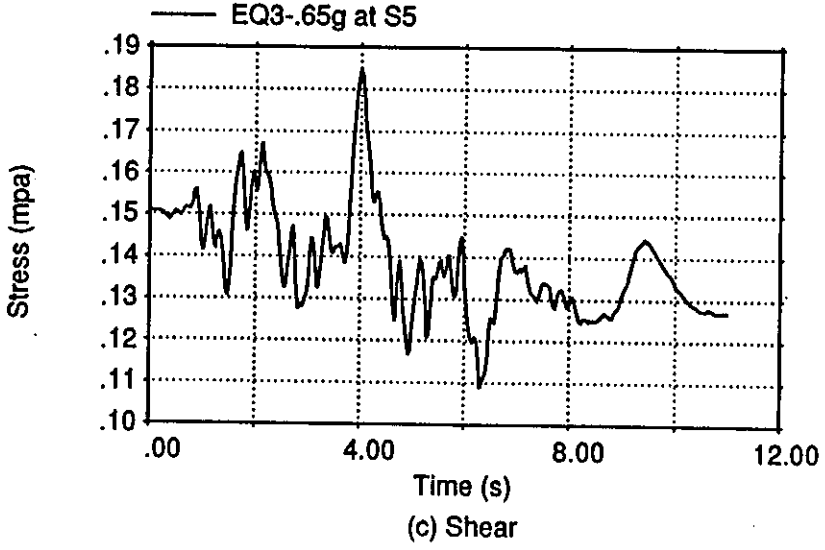

(c) Shear

Stress quantities for EQ3-.65g at output point S5

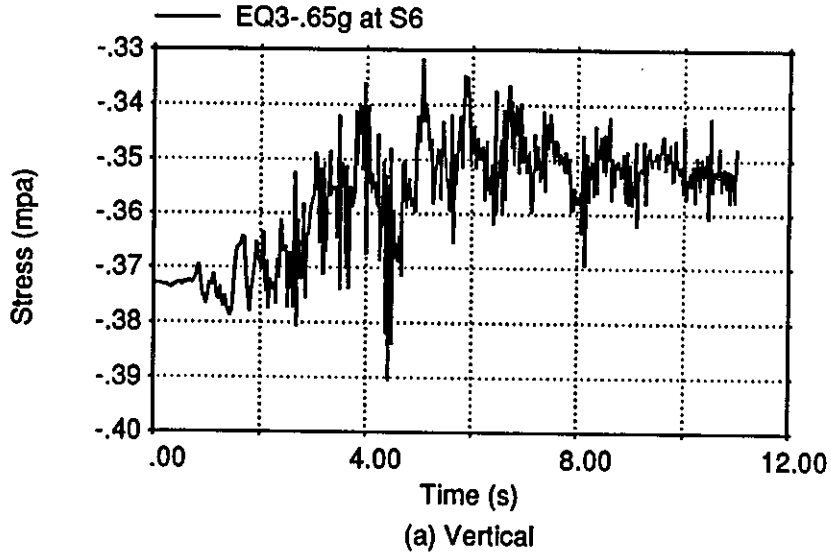

(a) Vertical

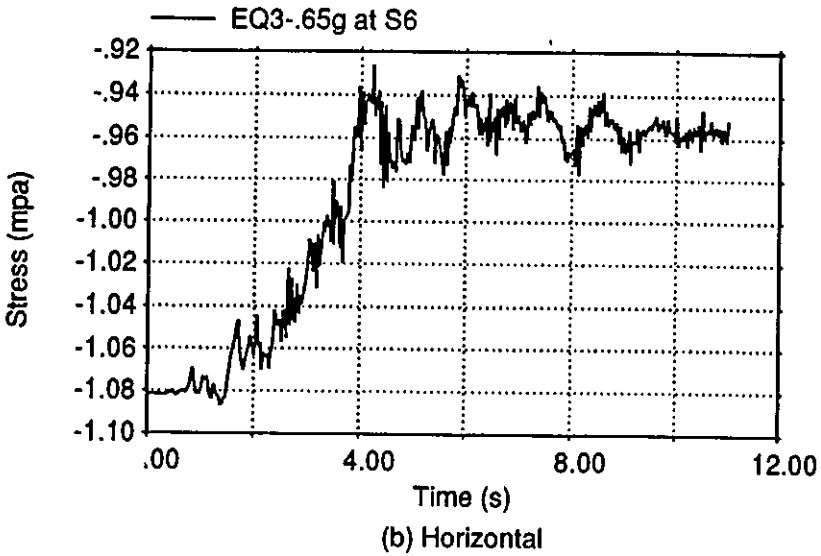

(b) Horizontal

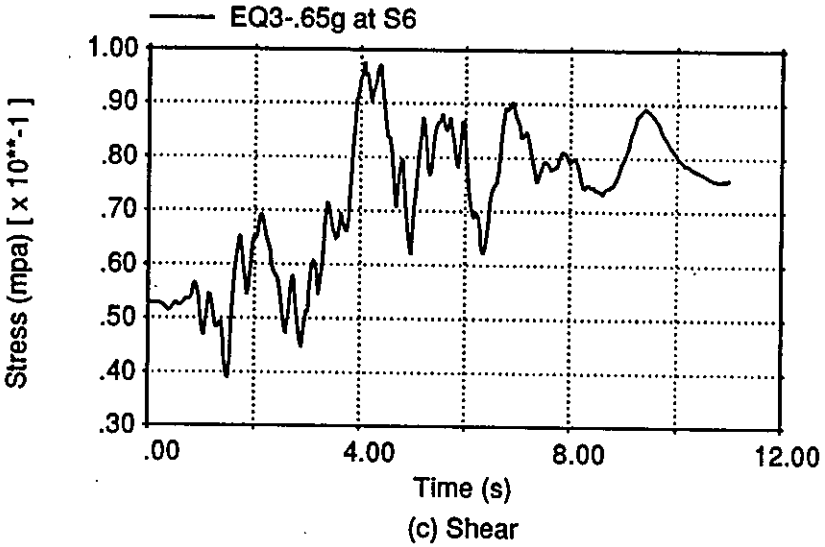

(c) Shear

Stress quantities for EQ3-.65g at output point S6

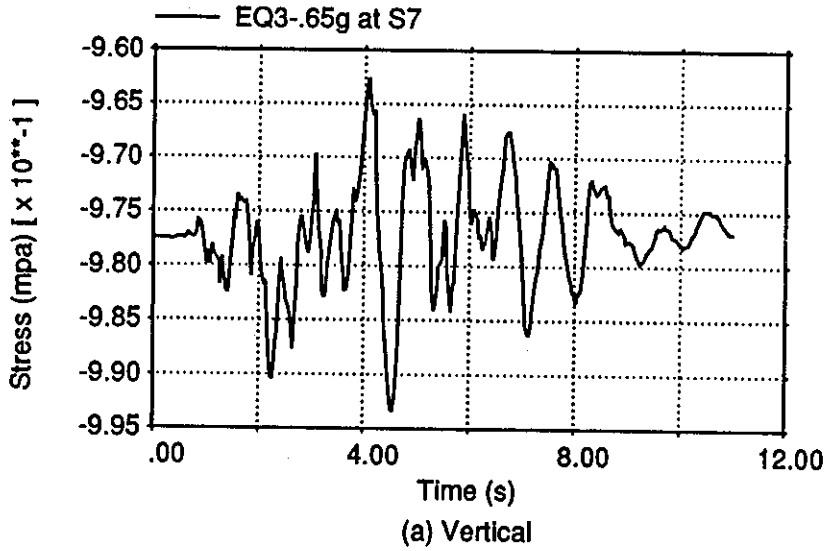

(a) Vertical

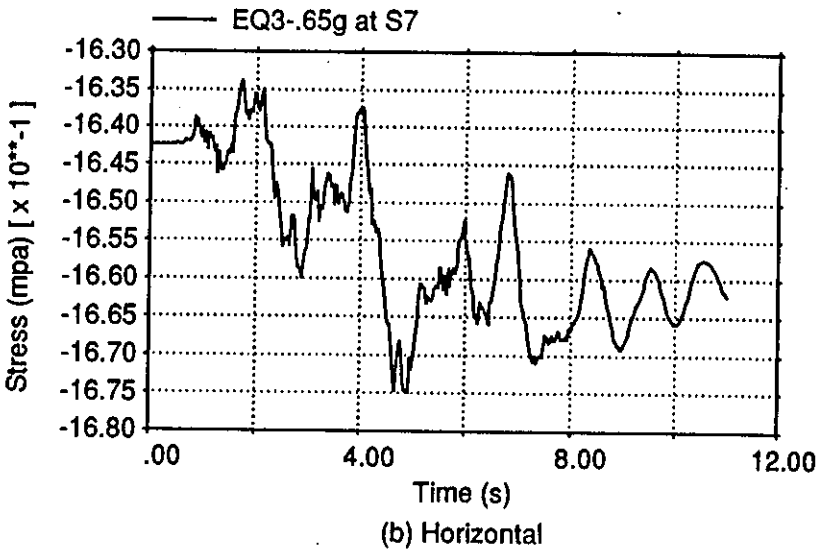

(b) Horizontal

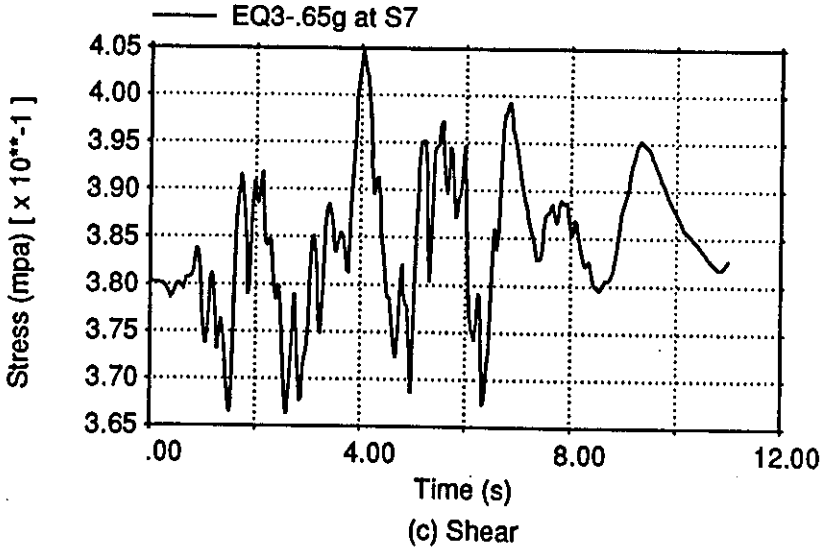

(c) Shear

Stress quantities for EQ3-.65g at output point S7

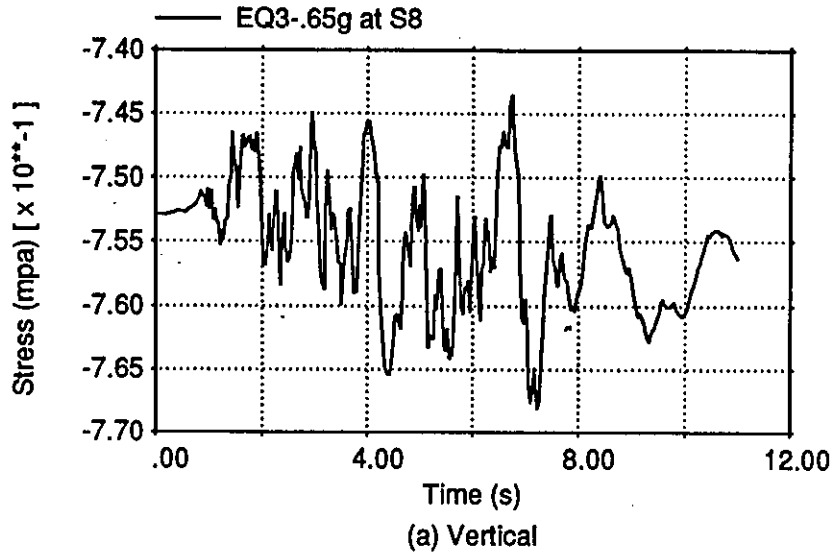

(a) Vertical

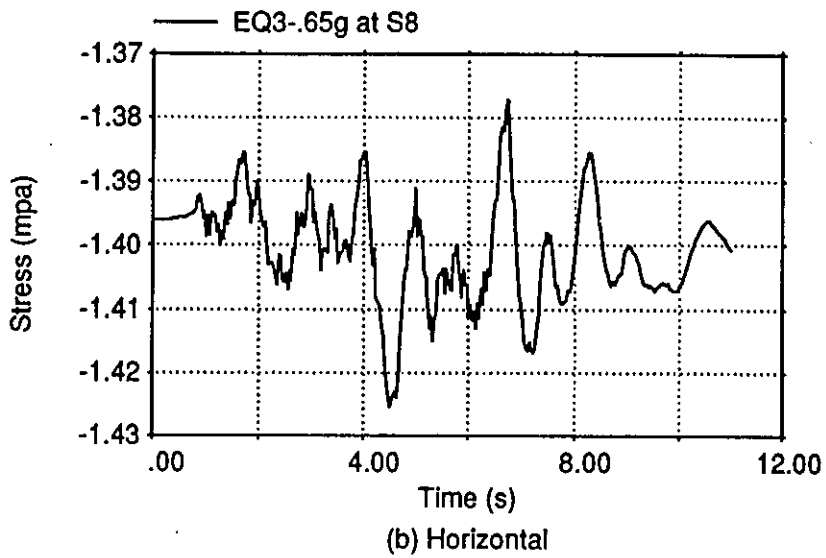

(b) Horizontal

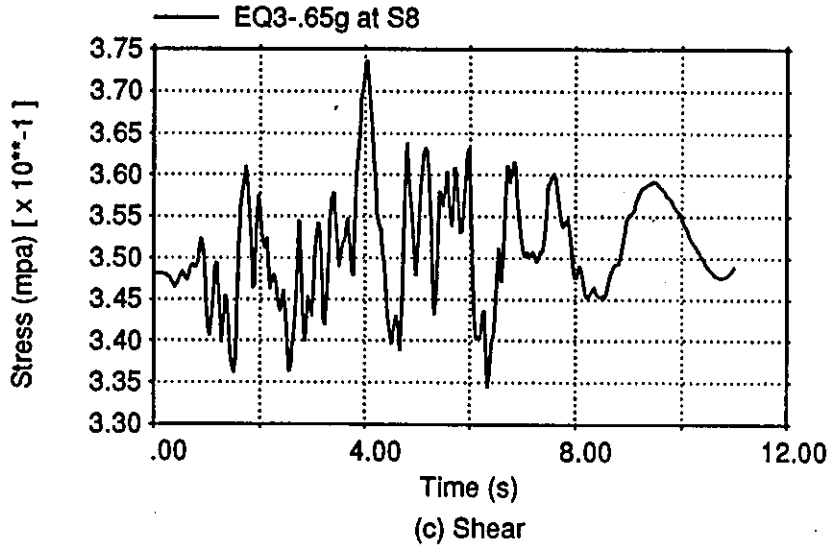

(c) Shear

Stress quantities for EQ3-.65g at output point S8